Synthesis of Helicenes and their Applications in Supramolecular Chemistry

Dissertation

zur

Erlangung des Doktorgrades (Dr. rer. nat.)

der

Mathematisch-Naturwissenschaftlichen Fakultät

der

Rheinischen Friedrich-Wilhelms-Universität Bonn

vorgelegt von

Anh Tu Nguyen

aus Neuwied

Bonn, 2025

Angefertigt mit Genehmigung der Mathematisch-Naturwissenschaftlichen Fakultät der Rheinischen Friedrich-Wilhelms-Universität Bonn.

Gutachter/Betreuer:	Prof. Dr. Arne Lützen
Gutachter:	Prof. Dr. Sigurd Höger
Tag der Promotion:	12.12.2025
Erscheinungsjahr:	2026

Danksagung

An dieser Stelle möchte ich mich bei den vielen Menschen bedanken, die mich bei der Anfertigung dieser Arbeit unterstützt und diese erst ermöglicht haben.

An erster Stelle möchte ich Herrn Prof. Dr. Arne Lützen meinen Dank aussprechen − für die spannende Themenstellung, die gewährte kreative Freiheit sowie seine stets wertvollen Ratschläge und anregenden Diskussionen. Ich hoffe, dass ich mit dieser Arbeit unser gemeinsames Interesse an den Helicenen weiter verstärken konnte.

Herrn Prof. Dr. Sigurd Höger danke ich für die freundliche Übernahme des Zweitgutachtens. Herrn Prof. Dr. Olav Schiemann und Herrn Prof. Dr. Michael Gütschow danke ich für die Teilnahme an meiner Promotionskommission.

Herrn Prof. Dr. Marko Hapke danke ich für die vielen hilfreichen Ratschläge und die freundliche Bereitstellung seiner Katalysatoren.

Bei allen Mitarbeitern der analytischen Abteilung möchte ich mich für die Messung zahlreicher NMR-spektroskopischer-, massenspektrometrischer- und röntgen-kristallographischer Proben bedanken. Insbesondere Frau Dr. Marianne Engeser und Herrn Florian Schäfer danke ich für die Berücksichtigung von Sondermessungen.

Herrn Andreas Schneider danke ich für die oft schwierigen und mühsamen Auftrennungen racemischer Gemische mittels HPLC, welche einen beträchtlichen Anteil an den Ergebnissen dieses Projekts hatten.

Lukas Kunze aus der Arbeitsgruppe von Herrn Prof. Dr. Stefan Grimme danke ich für die Berechnung der ECD-Spektren.

Meinen Bacheloranden Tom Willmer, Sofia Pacino, Teresa Nitschke und Felix Fiete Prümmer danke ich nicht nur für ihr tatkräftiges Mitwirken am Projekt, sondern auch für die gegenseitige Bereicherung darüber hinaus.

Des Weiteren danke ich meinen Freunden aus der Heimat 53 für ihre Unterstützung, die mir half, den Kopf frei zu bekommen und neue Motivation zu finden.

Allen Mitgliedern der Arbeitsgruppe Lützen – sowohl aktive als auch ehemalige – möchte ich ganz herzlich für eine unvergessliche Zeit danken. Sowohl innerhalb als auch außerhalb des Labors war die Atmosphäre immer freundlich und unbeschwert. Besonders möchte ich mich bei meinen Laborpartnern Clemens Hemmann, Sebastian Hütgens, Lukas Glanz, Marvin Schumacher und Hannah Wessely bedanken – für ihre stetige Unterstützung und, allen voran, für die zahlreichen Späße und gegenseitigen Sticheleien. Vor allem die längeren und anstrengenderen Labortage waren dadurch um ein Vielfaches leichter zu bewältigen und bleiben mir so lange wie das eine Lied der Cantina Band in schöner Erinnerung.

Mein größter Dank gilt meiner Familie, die immer an mich geglaubt, mich ständig ermutigt und mich auf meinem langen Weg begleitet hat.

Abstract

The aim of this work was the development of a reliable synthetic route towards functionalized helicenes, their characterization, chiral resolution and application as ligands in supramolecular chemistry.

Using two different strategies, a series of difunctionalized, racemic helicenes were synthesized and largely characterized. These range from racemic penta- to racemic heptahelicenes. The first strategy mainly relied on a nucleophilic addition of benzaldehydes and proved to be the superior one for the synthesis of penta- and heptahelicenes, whereas the second one involving a nucleophilic substitution of toluene derivatives was mandatory for the synthesis of hexahelicenes. The strategies were modular enough for the synthesis of different congeners. The pre-functionalized substrates each carried a methoxy group which guaranteed a late-stage functionalization and the introduction of donor atoms in the final step. A simple change in substitution pattern gave access to different regioisomers and donor angles. At the same time, the methoxy groups increased the solubility of the respective compounds in common organic solvents which was crucial for their chiral resolution by high-performance liquid chromatography.

Following the synthesis of the ligands, investigations were made regarding their ability to form complexes with different metal ions. Out of the investigated helicenes in this work, two bidentate regioisomers based on heptahelicene were able to form polynuclear complexes with tetravalent, square planar Pd^{II}. A subtle change in donor positions had a drastic impact in donor angles which ultimately led to complexes of different compositions. A fixed donor angle of 180° in the first ligand **L¹** made it a suitable candidate as a ditopic rod for the construction of a molecular square $Pd_4(dppp)_4(\mathbf{L^1})_4$, whereas the variable donor angle in the second ligand **L²** facilitated the construction of tri- and tetranuclear complexes $Pd_3(\mathbf{L^2})_6$ und $Pd_4(\mathbf{L^2})_8$ of different architectures, respectively. For each of these structures, a number of stereoisomers came on top as the presence of two enantiomers in each experiment resulted in the formation of different configurational isomers. Finally, the experiments were reiterated with the enantiopure compounds in order to get more insight on the exact processes and potential self-sorting phenomena.

Contents

1 Introduction

The introduction to scientific studies begins in elementary school with the subject of mathematics. Mathematics is a field of study that deals with algebra and geometry. Regarding the latter, a typical task involves the duplication of geometric figures at the same distance from a vertical line using grid paper and a ruler. The student becomes familiar with the terms congruency and symmetry. Although their definitions are taught at the latest then, the intuitive understanding of them is already deeply rooted long before. This is no coincidence, as symmetry plays a fundamental role as a vital element in nature. From plants to animals or even human beings, almost no lifeform exists with a complete lack thereof. While the most occurring form of symmetry stems from the bilaterally symmetrical blueprint for the majority of faunal life, more inconspicuous forms like rotational, translational or point symmetry are imprinted more subtly in our brains from early on. Just thinking about an animal without any form of symmetry is a challenge in itself which speaks volumes about its abundance and importance in our world (**Figure 1**).

Figure 1: Examples of symmetry in nature. Left: Honeycomb (iStock.com/Valengilda); right: peafowl (iStock.com/Peter Takacs).

Its importance is not only reflected in nature, but also in anthropogenic concepts and objects. How could it be otherwise? Throughout human history, the first source of inspiration has always been nature itself. Be it for aesthetic or functional reasons, symmetry has always been an essential building block in engineering, architecture and the likes. This culminated in a peak during the renaissance in which scholars like *Leonardo da Vinci* or *Albrecht Dürer* tried to express perfectionism through both art and science. The *Vitruvian Man*, the archetypical representation of the perfectly

proportional human body remains a popular motive frequently reproduced to this day. Allegorically, the drawing represents harmony and balance. It depicts a human body with outstretched limbs which is encapsulated by a square and a circle (**Figure 2**). Figuratively, all forms of symmetry are cleverly integrated in such a way that the observer instinctively assumes that the human body indeed is the epitome of symmetry and the center of the cosmos.

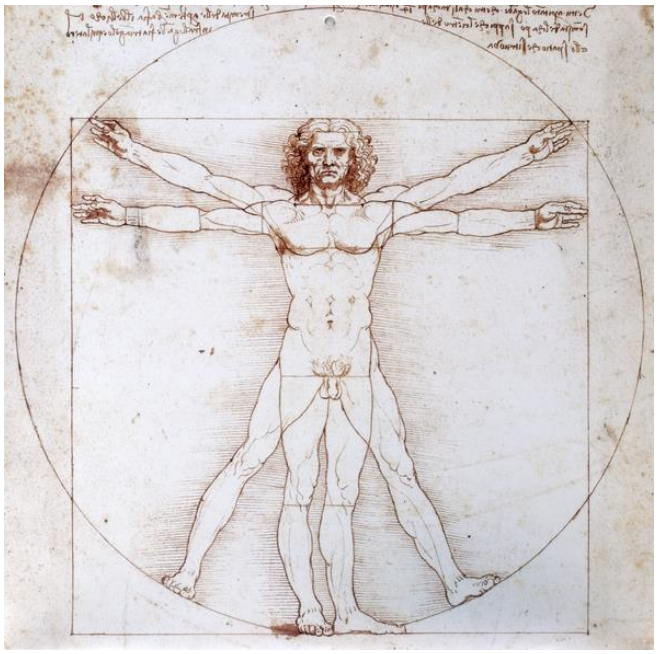

Figure 2: Allegory for harmony – the *Vitruvian Man* (iStock.com/EdnaM).

At that time, little was known about the existence of atoms and molecules. But even on the molecular level not visible to the naked eye, symmetry plays a vital role. Herein, symmetry appears in molecules in the form of chirality. The congruency of molecules is the determining factor in biological mechanisms which rely on the lock and key principle. Like our hands, two mirror-image molecules are similar enough to be confusable on the first glance but at the same time so distinct that they can fulfill different roles. But while the design of scissors or pencils to fit one specific hand is a non-vital design choice, the design of one enantiomer to be active in our body certainly is not. It is safe to say that chemistry and chirality go hand in hand. Almost every biologically functional molecule is chiral, meaning that it is not congruent with its mirror image. For instance, from an evolutionary standpoint, predominantly L-configurated amino acids have prevailed.

Most commonly, chirality in molecules originates from stereogenic centers like asymmetric carbon centers, but chirality is not limited to them. Special cases like axial

chirality (e.g. in BINOLs and allenes) or planar chirality (e.g. in paracyclophanes or metallocenes) also break the identity of image and mirror image. The same goes for structures adopting a helix. The most prominent example is the DNA which consists of 2 complementary helices. But also far less complex molecules can have an intrinsically helical arrangement. As a prototype for helical molecules in the chemical community, one specific class has emerged. Incorporating only carbon and hydrogen atoms,

helicenes

are a class of polycyclic aromatic molecules composed of *ortho*-annulated benzene units. From 4 benzene units onwards, the molecule begins to spiral up like a helix. Thereby, the spiral can turn left or right. Since both can be referred to as image and mirror image, they are a pair of enantiomers, meaning that helicenes are inherently chiral. *Newman* and *Lednicer*, who did intensive research on them and were the eponyms of the term, were also pioneers and influential in their popularity gain in the history of helicene chemistry. Among others, they also proposed a nomenclature which was quickly accepted in literature and replaced the IUPAC one.[1] In this nomenclature, either the amount of benzene units is embedded in squared brackets as numerals or the written-out ancient Greek or Latin numbers are placed as a prefix before the word “helicene”, e.g. [6]helicene and hexahelicene both refer to the same molecule. Regarding the numbering scheme, the innermost carbon atom which is still bound to a hydrogen atom, is always considered 1. Then, the molecule is circumvented and the counting is continued from the inside to the outside with regard to every C-H unit, until the innermost C-H unit from the opposite terminal benzene ring is reached. Carbon atoms not attached to a hydrogen atom share the same number with the preceding carbon atoms, but have additional lowercase Latin letters as suffixes (**Scheme 1**).

Starting the counting at the interior at the same time indirectly underlines the significance of these positions. The positions are located in the so-called fjord region or bay area and numerous studies have shown that functionalization in there not only increases the configurational stability[2,3] but also provides a means to efficiently control regio- and stereoselectivity when used as ligands in catalysis.[4,5] For that reason, a targeted functionalization in this region can be found in a multitude of publications.[6–8]

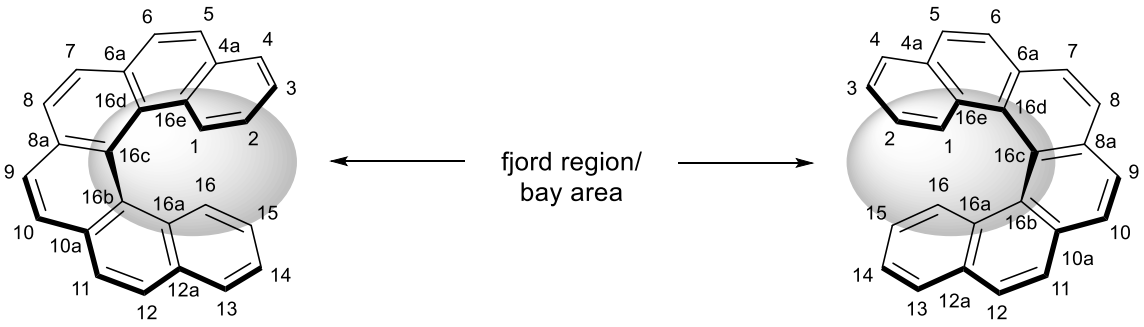

Scheme 1: Numbering scheme for hexahelicene.

Initially only a chemical curiosity, the focus of helicene chemistry has been shifted from general access to physico-chemical properties and applications. With their chirality comes a number of interesting features which led to a significant increase in academic studies. Over time, the family of helicenes has expanded considerably and the boundaries of definitions became blurrier so that not only parent carbohelicenes may be meant when speaking about helicenes. In a broader sense, helicenoides or helicene-like molecules are also member of the same species and can be addressed as helicenes: These include helicenophanes,[9,10] helquats,[11] double helicenes,[12] bihelicenyls[13] etc. (**Figure 3**). While the sheer number of publications is a strong indicator that immense mutual effort has already been put into research, it is undeniable that helicene chemistry is still underdeveloped and far from exhausted in terms of potential and possibilities. If anything, it should rather be seen as an incentive to continue the investigations not only for academic, but also industrial institutions. As of now, helicene chemistry is still growing and currently in its heyday: In the context of modern application-driven research, they are a “hot topic” due to their broad versatility.

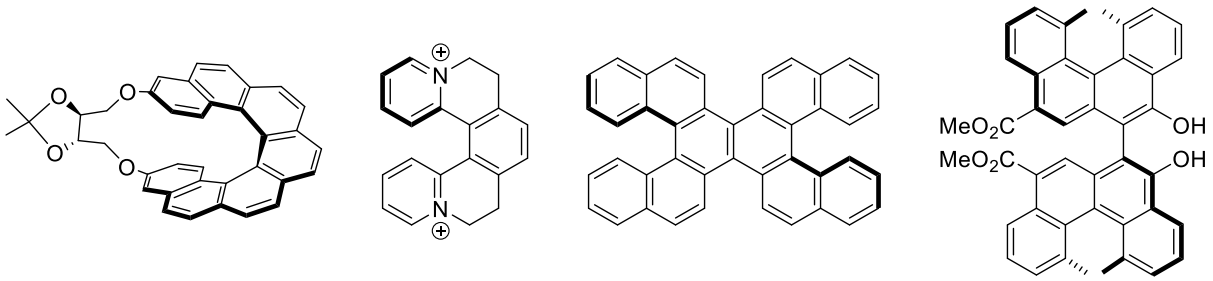

Figure 3: Selection of helicene-like molecules.

2 Motivation and tasks

First and foremost, the universal interest in helicenes certainly comes from the fact that they are aesthetically pleasing. While that alone is a valid reason and molecules sometimes just have to look nice, helicenes offer enormous potential beyond their optical beauty. Due to their inherent chirality, helicenes exhibit a lot of optical properties which are one the main reasons of contemporary studies. Initial investigations were mainly held back by their difficult synthetic access. But with growing synthetic techniques, application-oriented research displayed their use in a wide range of different fields, exploiting their fascinating rigid, curved and chiral structure.

To this day, their synthesis still is anything but trivial and competing reports about their applications scarce. It is debatable if application-oriented research on helicenes is generally in its infancy, but in certain areas, this statement is undoubtedly true. In the framework of this study, the objectives can therefore be formulated as follows: Firstly, a reliable access has to be established. The synthetic route should be versatile enough to enable the synthesis of a wide range of different derivatives. This includes not only the synthesis of a target molecule(s), but also its thorough design beforehand and characterization afterwards. Once the target molecules are in hand, they should be investigated in regard to their possible applications.

For specific applications it is essential to not have a mixture but only one enantiomer in hand. Because of that, a way to separate the racemic mixture needs to be established as well which again includes thorough planning and characterization of the individual isomers. Out of the possible applications, our group is particularly interested in their use as chiral ligands in metallosupramolecular chemistry. Since carbohelicenes do not have any coordinating atoms themselves, it is mandatory to attach donor atoms like nitrogen or phosphorus at some point in the synthetic route which can then coordinate to the metal ions. With the helical backbone, a variety of different dissymmetric ligands can be constructed and different binding modes can be achieved. This can be regulated by means such as denticity, bond angles or bond lengths. Even the backbone itself does not have to stay fixed. Within the homologous series, going from lower to higher congeners should have a drastic impact on their structure.

For one thing, the dihedral angle steadily increases with the number of annulated benzene units before it drops in [7]helicene.[14–18] Altering the framework simply

provides another way to adjust parameters. Of course, this can also be done by other means like substitution pattern, choice of donor atoms or metal ions. If a suitable pattern is paired with suitable metal ions, a cavity with strong π-interactions can be formed for instance. This can in turn be examined in view of host-guest interactions. In general, their coordination behavior can be examined more precisely. This field alone is full of unanswered questions. More often than not, the exact principles and mechanisms of self-sorting phenomena are unknown since they can depend on so many seemingly negligible factors like solvent and temperature. To date, the role of helicenes in metallosupramolecular chemistry is uncharted and the exact dynamics therein are yet to be explored.

3 Synthetic techniques

Looking at a bare helicene from a synthetic point of view, two things immediately stand out. First of all, their unique structure is definitely not something a chemist would refer to as a “natural” conformation. Ever since the advanced chemistry classes in high school, the indoctrination of the planarity of benzene and other aromatic compounds according to Hückel’s rule has been an elemental part of the curriculum. Just by drawing a few *ortho*-annulated benzene rings on a piece of paper, the practicability of such an arrangement is challenged by no later than 6 units if the aim is not to reach a closed ring like in circulenes.

As a logical consequence, both ends have to avoid each other sooner or later, meaning that the molecule spirals up to bypass steric clashes. This leads to involuntary strain within the molecule which in turn translates to a higher energy. In order to compensate for the additional energy, there needs to be a huge driving force to the unfavorable conformation for the synthesis to succeed.

The second noticeable thing is that carbohelicenes merely consist of two atoms − carbons and hydrogens. Even heterohelicenes marginally consist of a negligible number of extra atoms. This means that the main strategy to get helicenes is founded on C-C bond formation which in itself is non-trivial and constrained by a limited number of reactions. This obstacle alone can be seen very distinctly during the slow and moderate beginnings in helicene history. Of course, a lot has changed since then, comparing the possibilities from the past with today’s is misleading and unequal. The upsurge of cross-coupling reactions opened up tremendous possibilities for the buildup of C-C bonds, unsurprisingly and rightfully awarded with the Nobel prize to *Negishi*, *Heck* and *Suzuki* in 2010. Although undoubtedly powerful synthetic tools, these reactions are not a universal panacea. Thus, the preparation of (carbo-) helicenes still remains a great task.

Last but not least, a third reason which can easily be overlooked is the functionalization. In the context of this work, the goal is to get building blocks which can be employed as ligands in supramolecular complexes. For this to be feasible in the first place, donor atoms like nitrogen or phosphorus have to be introduced at some point during the synthetic route. Another valid reason to functionalize them is to separate the enantiomers. Since two enantiomers always have the same physical

properties in an achiral environment, getting the hands on each of them is challenging by conventional methods. The isolation of two diastereomers on the other hand is certainly doable by routine flash chromatography. For this occasion, converting a pair of enantiomers to diastereomers can be beneficial for their separation. For example, the usage of camphor sulfonyl chloride as a chiral auxiliary for exactly these kinds of purposes has more often than not proven to be proficient, not only for helicenes.[19–24]

At first glance, functionalization of the signature aromatic framework *via* electrophilic aromatic substitution seems like a no-brainer. But unlike a simple benzene molecule which has a finite and manageable amount of reactive positions, the much larger helicene framework offers a lot more potential locations for an electrophile to attack. If not, S_EAr reactions on carbohelicenes figuratively cry out for regioselectivity issues. Particularly the crowded bay area is difficult to reach with this method, a location which is lucrative due to several factors mentioned earlier.

Overall, these matters combined make it very clear why there has been an outright discrepancy between the formal interest and the actual research of helicenes. Despite these challenges, a lot of effort has been put towards getting access to them since their discovery. Discussing each strategy would be a journey through the finesse and ingenuity of synthetic problem-solving, but likewise go beyond the scope of this work. Among the numerous different approaches, three methods particularly stand out due to their historic significance and reliability:

- the photoinduced cyclization
- the transition metal catalyzed [2 + 2 + 2] cycloisomerization
- the Diels-Alder reaction.

In view of the other approaches which will be briefly commented on, these methods have prevailed to be the standard for today's procedures to get to helicenes in a still demanding but reliable manner. While the others rather belong to the category "limit testing and eagerness to experiment" especially during the earlier days of helicene chemistry, the three main strategies have stood the test of time. Still, each of them has its own disadvantages, so choosing the right method is dependent on several variables not including subjective preference.

3.1 Photoinduced cyclization

In photoinduced cyclization reactions, light is utilized as an energy source. Starting from 1,2-diarylethylene precursors, in the first step a photochemical excitation induces an equilibrium between the *trans*- and the *cis*-isomers. Compliant with the Woodward-Hoffmann rules, the *cis*-isomer can undergo an intramolecular cyclization *via* a symmetry allowed, conrotatory electrocyclization.[25] This leads to a *trans*-configurated dihydro compound which can be oxidized to the fully aromatic helicene in the attendance of air and catalytic amounts of iodine (Mallory reaction).[26] The reaction happens from the singlet S_1 state, therefore, it is not susceptible to triplet quenchers like oxygen.[27] In absence of an oxidizing agent, the unstable dihydro intermediate relaxes back to the alkene. The resulting hydrogen iodide can cause a photoinduced reduction of double bonds so propylene oxide, cyclohexene or tetrahydrofuran can be added as a scavenger.[28]

Alternatively, an oxidant can be omitted in case of an eliminative photocyclization. Here, the arylethylene needs to contain at least one suitable leaving group in the corresponding positions. The advantage of this more elegant method is that the already mild reaction conditions get even milder since nothing but a light source and a solvent are required, but the presence of a leaving group is a vulnerability for the preparation of the precursors altogether, most notably if the leaving group is a reactive halide. That is why this method is merely convenient for sparsely functionalized carbohelicenes (**Figure 4**). So far, the applicable leaving groups range from halides[29,30] and triflates[31] to methoxides.[32]

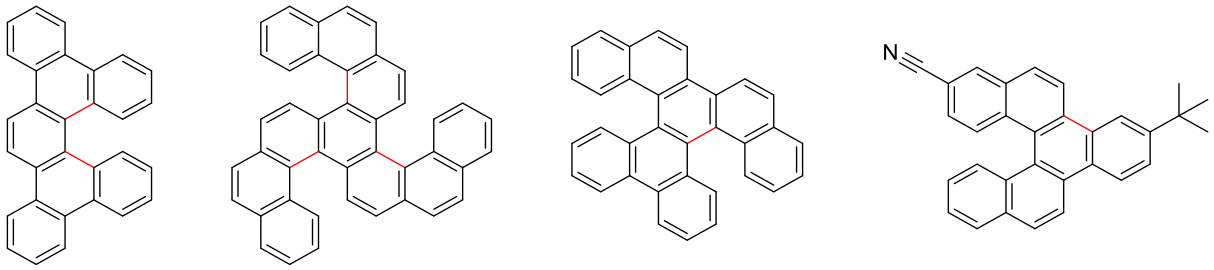

Figure 4: Selection of carbohelicenes prepared *via* eliminative photocyclization (newly formed bond in red).

The first report for a photoinduced cyclization towards a helicene has been made by *Dietz* in 1967, both a [4]helicene and a [5]helicene were synthesized.[33] Therein, the authors also raised questions regarding the regioselectivity of this reaction: Unless pre-

occupied by other atoms bar hydrogen, the cyclization can proceed in both *ortho*-positions relative to the functionalized positions (**Scheme 2**). This means that for every precursor, at least two regioisomers can be expected. Alongside the 1,3-cyclization of β,β′-dinaphthylethylene to the contemplated pentahelicene, their group observed a 1,4- and 2,4-cyclization to the respective dibenzophenanthrene. Furthermore, a second oxidation of the intermediate [5]helicene towards the achiral benzo[*ghi*]perylene was observed.

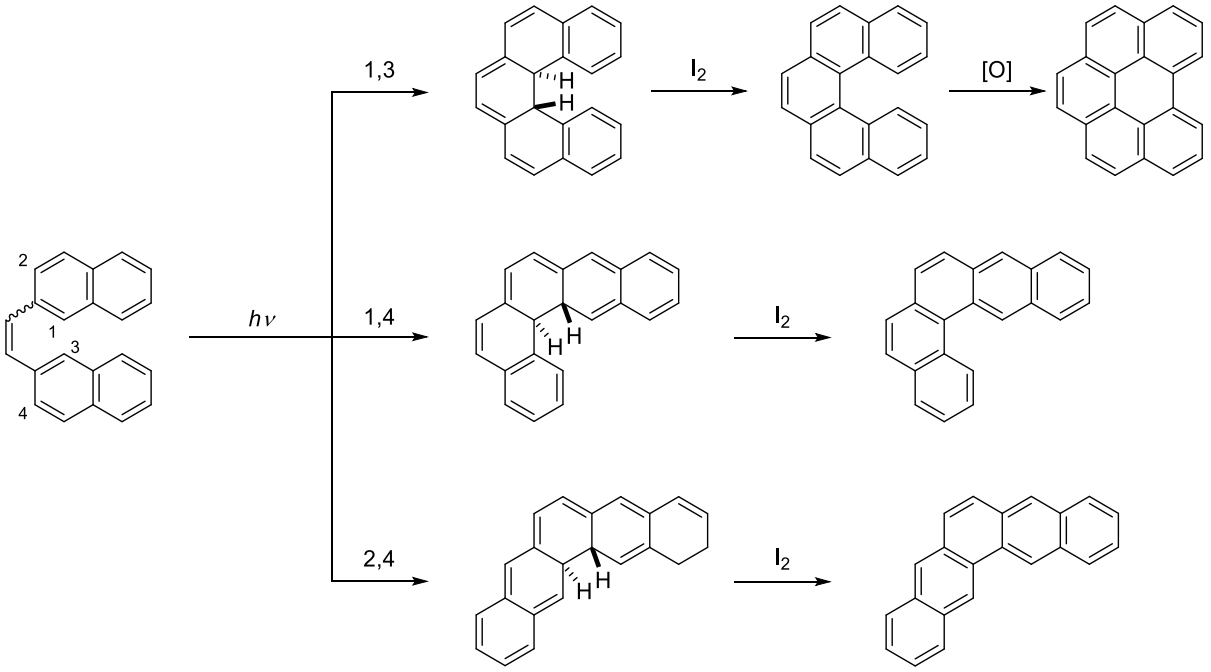

Scheme 2: Photoinduced cyclization of β,β′-dinaphthylethylene.

Being published over 50 years ago, this work highlights key drawbacks of the photocyclization which are still major hindrances to this day: The reaction is very prone to side products which can be tedious to separate. Beside the intramolecular side products, an intermolecular [2 + 2] dimerization of the alkene can occur as well. In order to avoid this, high diluting conditions up to 10^{-4} M are recommended, often in carcinogenic solvents like benzene which make the reaction an economic and safety concern. Typically, a continuous flow reactor (**Figure 5**, (c)) is the most practical setup for this kind of reaction, although the optimizations of flow rate and time of irradiation can be a challenging and protracting task as well. The most common type of photoreactors are immersion wells and external chambers (**Figure 5**, (a) and (b)) due to their easy and quick setup. Commonly, commercially available mercury lamps are used as a UV-light source which produce a lot of heat, making tools to cool the reaction mixture mandatory.[27]

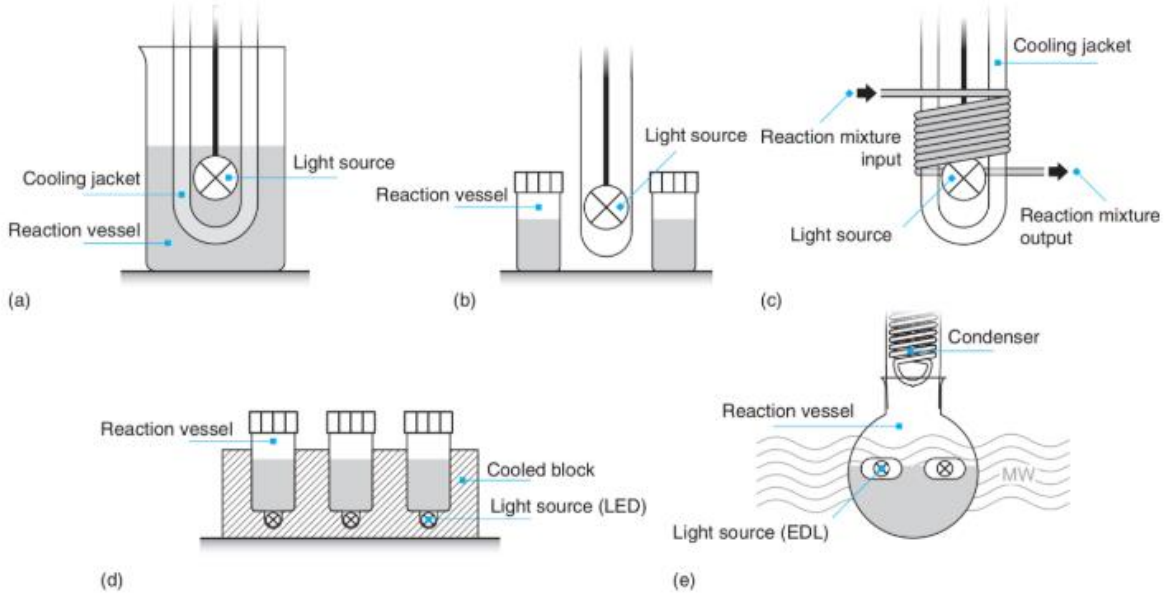

Figure 5: Common photoreactor setups; (a) immersion well, (b) external chamber, (c) continuous flow, (d) LED-type, (e) electrodeless discharge lamps. Reproduced with permission from *John Wiley and Sons*.[34]

Remarkably, a lot of research has been conducted on finding the perfect conditions for the respective setups: The employment of light-emitting diodes for a more effective irradiation,[35] the simultaneous irradiation of the reaction vessel with UV-light and microwaves in EDL-reactors enabling photochemistry at higher temperatures (**Figure 5**, (d) and (e))[36] or changing materials of the reaction vessel to exclusively concentrate light from specific wave length spans[37,38] only scratch the surface of ideal prerequisites and illustrate the popularity of the photochemical pathway among the helicene community.

A famous application of this method was displayed by *Fujita et al.* in 2015 (**Scheme 3**). Therein, they showcased an elaborate substrate design to attain [16]helicene in a single step sextuple oxidative photocyclization, until then the largest congener.[39] The precursor consisted solely of four phenylene and three naphthylene units linked by six vinylene spacers in a [2]+[1]+[1]+[2]+[1]+[1]+[2] manner, with "[n]" denoting *ortho*-fused benzene subunits and "+" denoting the vinylene linkers. This arrangement was selected to keep the precursor design trivial and to minimize the emergence of unwanted side products: Primarily, [1]+[1]+[1] and [2]+[2] sequences would always involve the formation of [5]helicenes which can easily oxidize to benzo[*ghi*]perylene (**Scheme 2**, top),[40] whereas [2]+[1]+[2] sequences are prone to give dinaphthanthracenes instead of desired [7]helicene subunits.[41] Therefore, each

naphthylene unit had to be separated by two phenylene units. Apart from increasing the synthetic aspiration, larger subunits do not necessarily give intended results: Despite favorable theoretical calculations, a [6]+[6] precursor did not give [13]helicene under any circumstances.[42] *Fujita's* precursor was synthesized by a series of Wittig-olefinations, irradiation over 48 h furnished [16]helicene in a 7 % yield. Their sophisticated approach demonstrated a new guideline aiming for higher helicenes.

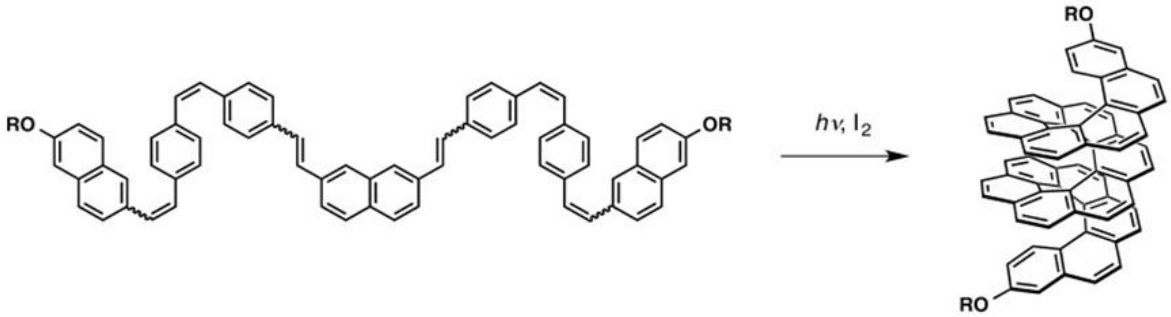

Scheme 3: Sextuple oxidative photocyclization of [16]helicene (R = TIPS). Adapted with permission from *John Wiley and Sons*.[39]

In total, the oxidative photocyclization benefits from a wide variety of easily accessible substrates. As presented, the stilbene-type precursors can be prepared *via* Wittig-type olefinations or cross-coupling reactions, without the need to control diastereoselectivity for *cis*- and *trans*-isomers. As long as these reactions can be executed, the photocyclization has an exceedingly high functional group tolerance due to its mild reaction conditions. This is apparent from the vast number of studies in which helicenes containing other main group elements were obtained. These include aza-,[43,44] thio-[45] and phosphahelicenes[46] for instance (**Figure 6**).

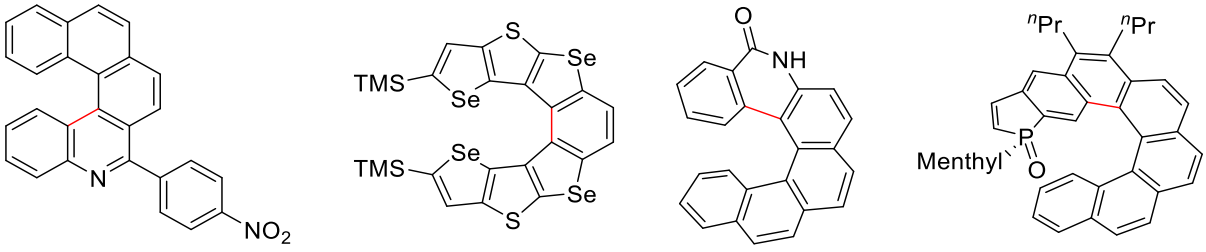

Figure 6: Selection of heterocycles prepared *via* oxidative photocyclization (newly formed bond in red).

As of today, it is hardly surprising that this approach has remained one of the go-to choices for the synthesis of helicenes: The ease of the setup coupled with an easy

entrance to a large inventory of substrates and mild reaction conditions far outweigh the disadvantages in this type of reaction. The minimum requirements are a light source and a way to oxidize the dihydro intermediate, substrates can freely be crafted in a low number of steps. In all fairness, while the mild reaction conditions are definitely a large selling point for this method, it can also be a double-edged sword. In case of poor performance of individual reactions, there are fewer variables which can be changed compared to reactions with more reactants.

3.2 Transition metal catalyzed [2 + 2 + 2] cycloisomerization

In principle, the [2 + 2 + 2] cycloaddition of acetylene to benzene is achievable without the assistance of a catalyst. Thermodynamically, the symmetry allowed reaction is enthalpically favored ($\Delta H = -594\ kJ\ mol^{-1}$).[47] But reality shows that a barrier of about 170 kJ/mol needs to be overcome with temperatures well above 400 °C for the cyclization to occur, attributed to the structural reorganization and entropic penalty. With moderate yields and a bunch of side reactions, this exact approach was *de facto* useless.[48–50]

In 1948, *Reppe's* discovery of a nickel-catalyzed version of the very same reaction kick-started a renaissance on the alkyne trimerization.[51] Changing the narrative from an initially inefficient reaction with little to no practical relevance, the reaction has now become a powerful and reliable tool, flourishing with the help of a myriad of various metals overcoming the kinetic and entropic barriers. By now, over 15 metals have been employed in this reaction: Co, Ni, Ru, Pd, Rh, Ti, Ta, Nb or Ir are most commonly used; but also Fe, Zr or Cr have been shown to be capable of mediating the reaction.[47,52,53] Owing to its high versatility and functional group tolerance, the [2 + 2 + 2] cycloaddition warrants the entry to complex, highly functionalized (hetero-) cycles consisting of unsaturated compounds like alkynes, alkenes, allenes, nitriles, imines, aldehydes, ketones, isocyanates and the like.[47,52–58] The enormous versatility is further amplified by a sheer endless amount of variable ligands attached to the metals. Varying different metal/ligand combinations, chemo-, regio- and enantioselectivity problems can be addressed all at the same time. The reaction also profits from perfect atom-economy, high efficiency and comparably mild reaction conditions, making it in almost no way inferior to the photocyclization.

Because of that, it is no wonder that the transition metal catalyzed [2 + 2 + 2] cycloisomerization has quickly emerged as a competitive rival to the photoisomerization in the context of helicene chemistry as well. Generally, there are many approaches leading to helical structures in literature, but the intramolecular adaption is probably the most prominent one as it solves kinetic and regioselective concerns collectively (**Scheme 4**).[57,59–64] The aromatic triynes required in this take are mainly obtained *via* Sonogashira couplings, although the synthetic effort can be substantially higher for more sophisticated systems. The construction of three cycles in a single operation allows for a rapid enlargement of the helical structure if the concept is scaled up to a multiple cyclization within the same molecule. Using the intramolecular cyclization, an oxa[19]helicene was synthesized by a simultaneous evolution of 12 cycles.[65] On the other hand, the impressive intermolecular cyclization to a [23]helicene proves that this variant is also viable if symmetric considerations prevent the appearance of regioisomers.[62] Despite the buildup of a highly constrained architecture, calculations on a DFT level of theory revealed that this reaction is still a highly exergonic process, although the energy gain can fluctuate heavily depending on the substrates.[63,66]

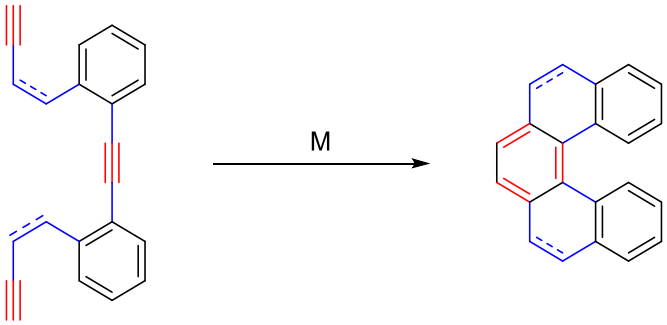

Scheme 4: General scheme of an intramolecular [2 + 2 + 2] cycloisomerization.

The mechanism of the reaction is not unambiguously clear, it relies on the metal catalyst as well as the substrates.[67,68] For late transition metals (Co^{I}, Ni^{0}, Rh^{I}), generally the following mechanism is accepted (**Scheme 5**): In the first step, two alkyne units coordinate to the metal center to form π-complex **A**. Then, an oxidative addition takes place, resulting in metallacyclopentadiene **B**. After complexation of the remaining alkyne moiety to π-complex **C**, either the ring is expanded to metallacycloheptatriene **D**, or an intramolecular Diels-Alder reaction delivers metallanorbornadiene **E**. Either way, a reductive elimination in the last step yields the desired product **F**. In this step, the catalyst also gets regenerated and can re-enter the catalytic cycle.[68]

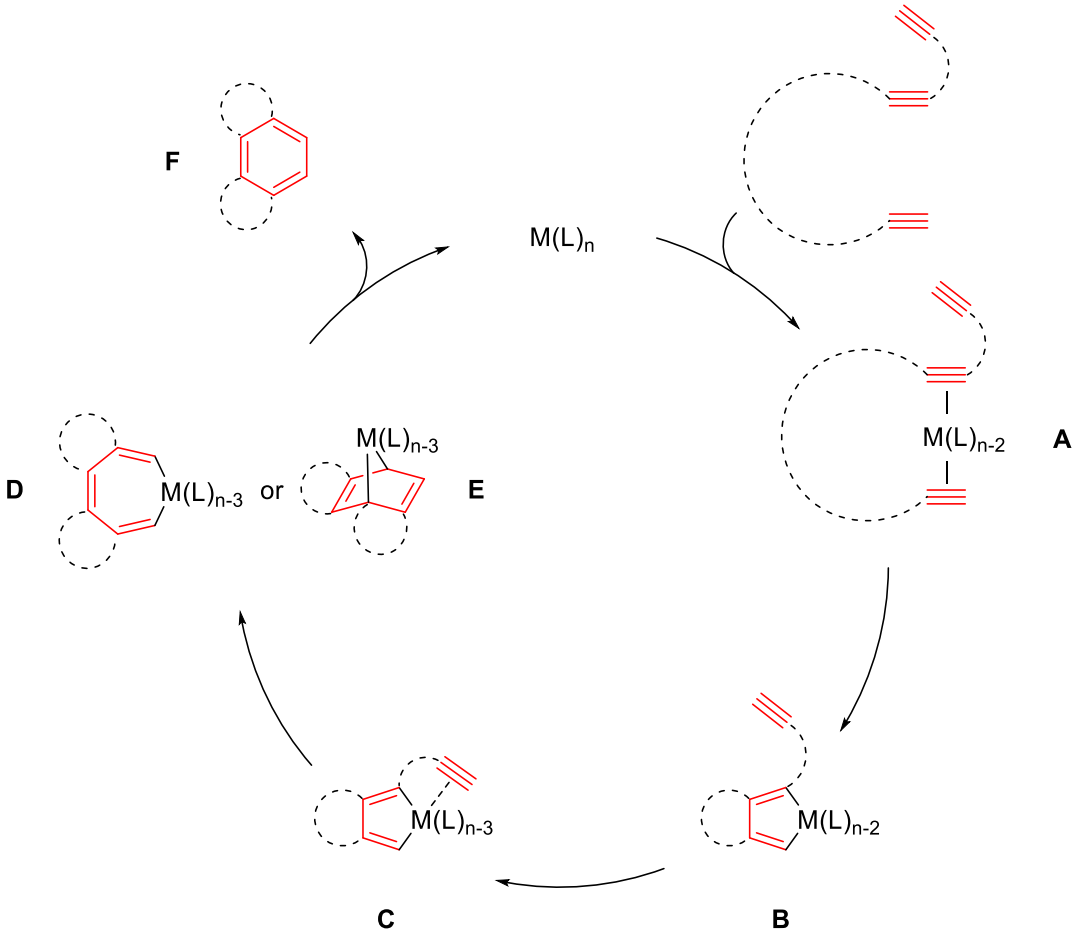

Scheme 5: Proposed mechanism of the intramolecular [2 + 2 + 2] cycloisomerization of triynes.

Even though the substrates are obtainable by conventional aromatic reactions, the vinyl groups (**Scheme 4**, blue) need to be kept in mind. Unlike in the photoinduced cyclization, they have to adopt a *cis*-configuration, otherwise the [2 + 2 + 2] cyclization cannot proceed. These *cis*,*cis*-dienetriyne motifs are difficult to achieve and only stable to a limited extent, so keeping the blue bonds saturated is the most common strategy. But if the system is not entirely unsaturated, a tetrahydrohelicene is formed which has to be oxidized to the fully aromatic helicene. This can be done with oxidizing agents like manganese dioxide,[69] DDQ[70–73] or trityl cations.[63,73–75] The group of *Starý* and *Stará* developed two alternative ways to solve this issue. If the saturated tether bears an oxygen-containing group like an acetoxy or methoxymethyl ether group, the corresponding tetrahydrohelicene derivative can be oxidized by an acid-assisted elimination (**Scheme 6**).[42,76–78]

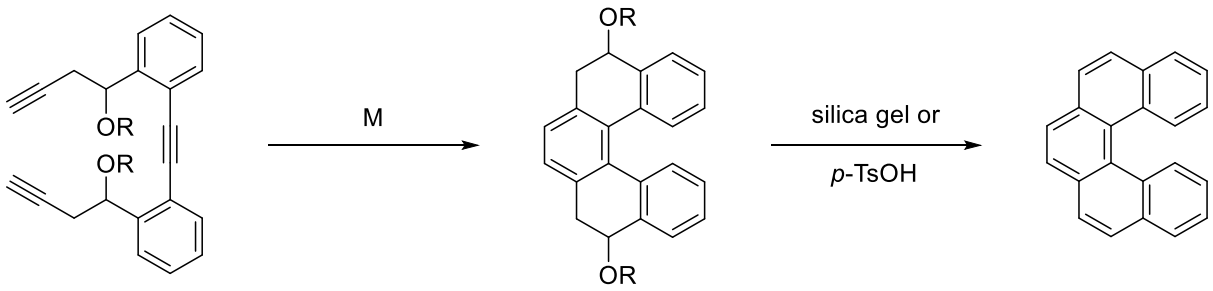

Scheme 6: Acid-assisted aromatization by elimination (R = Ac, MOM).

Also ingenious is the disguise of the rather labile *cis*,*cis*-dienetriynes as *ortho*-phenylenes, increasing their stability and fixing them in the *cis*-configuration (**Scheme 7**).[79,80]

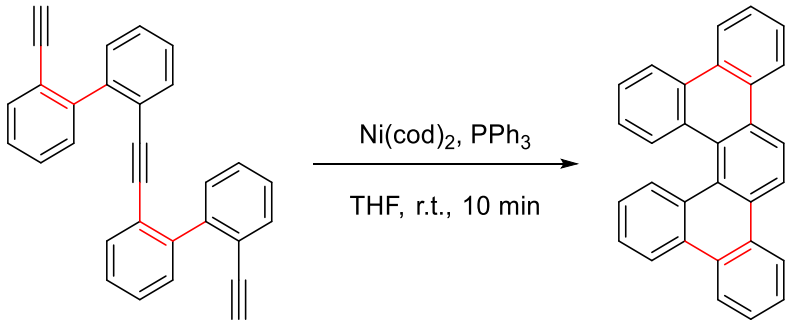

Scheme 7: *Cis*,*cis*-dienetriynes disguised as phenylenes (*cis*-dienes marked in red).

In sum, these methods have also been used to synthesize more complicated molecules like oxa-,[65,81,82] sila-[83,84] and pyridohelicenes.[69,77]

Like previously, the advantages can also be interpreted as downsides. Generally, there is no universal catalyst for the [2 + 2 + 2] cyclization as it depends on many factors. Even if the selection is narrowed down to the most employed metals (Ni, Co, Rh), there is still a myriad of ligands to choose from.[85] As diverse as the reaction can be, the agony of choice can be overwhelming. Many catalysts, especially those based on Ni^0, can oxidize to inactive species which makes working under inert gas obligatory. Air-stable catalysts based on Co^I have been reported by *Hapke* and coworkers, but in contrast to nickel-analogues which often work under room temperature, they need higher temperatures and microwave irradiation for better performances.[86,87]

Moreover, the same side reactions as in the photoinduced method can emerge: Basically, this method is actually further exposed to polymerization as any unsaturated bond within the precursor is a potential weakness, with the terminal alkynes being the most susceptible. To be fair, these trimerizations are less likely than the photoinduced

dimerization because the entropic penalty would be way higher, but a *cis*,*cis*-dienetriynes for illustration has 5 times more reactive sides than a stilbene in their respective reactions. Additionally, while a catalyst in theory cannot turn inactive just like a light source, this is not always the case in reality. Occasionally, a cobaltacyclopentadiene (**Scheme 5**, C) forms a cobaltacyclobutadiene *via* reductive elimination which is barely reactive and can be isolated.[88] For Rh^{I}, *Tanaka et al.* observed an unprecedented [2 + 1 + 2 + 1] cycloaddition *via* a C≡C triple bond cleavage as a side reaction.[89,90] Indicated before, building a triyne framework from scratch is not as plain as a series of Wittig olefinations. As regio- and chemoselectivity are a minor hurdle for the key cyclization, that is not true for the buildup of the substrates. Usually, it makes the most sense to start from halogenated arenes which themselves are not always commercially available or easy to synthesize. On top of that, three alkynes have to be introduced in non-arbitrary positions so that the order of the reaction sequences can be crucial. The synthetic route demands cautious, preliminary planning because there are more competing reactions/reaction sides. It is most reasonable to install the central alkyne first *via* Sonogashira coupling, but even here a Glaser coupling can hamper the construction of the diarylacetylene fragment.

Nonetheless, the benefits also far outweigh the drawbacks of the [2 + 2 + 2] cycloaddition. The versatility cannot be understated. The reaction can infinitely be tailored to the own appeal so that every problem can be tackled individually. As opposed to the photoinduction, the metal catalyzed version can be up-scaled to multigram-dimensions easier since the diluting solvent plays no major role, does not suffer from arbitrary regioselectivity and can be carried out enantio- and diastereoselectively by utilization of chiral ligands. The broad functional group tolerance permits a modular synthetic route and the generation of three concurrent rings is not to be underestimated.

3.3 Diels-Alder reaction

Also being a pericyclic reaction, the Diels-Alder reaction is certainly predestined for the formation of structures composed of 6-membered rings. Due to this, investigations regarding helicene synthesis have been made long before the well-established photocyclization, but it took the reaction over half a century to gain serious attention in the helicene community.[91,92] Originally accompanied with pediatric diseases like harsh reaction conditions, low yields and poor atom economy, it is evident why this method was deterred from. Solely with the optimization of reaction conditions to increase the yields by the group of *Katz*, it became a staple in the synthetic repertoire. Their approach involved a double [4+2] cycloaddition of 1,4-divinylbenzene and 1,4-benzoquinone leading to a [5]helicene derivative with two quinone units at the periphery (**Scheme 8**), soon after they acquired a [6]helicenebisquinone with the same method.[93,94]

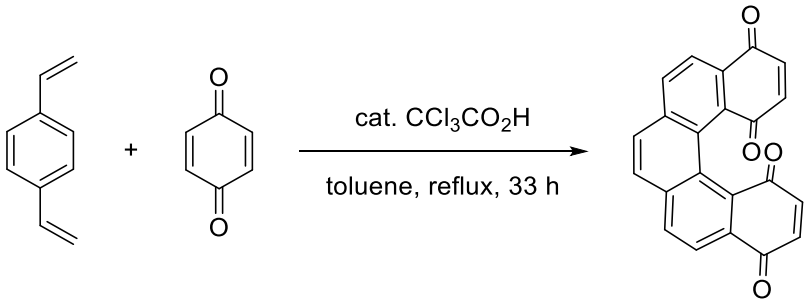

Scheme 8: Diels-Alder reaction to [5]helicenebisquinone.

This method has also been employed to form cycles other than the external ones, but it was always mandatory to have certain functional groups present in the substrates to make these methods word which therefore were also found in the product. On paper, it is possible to specifically target non-functionalized carbohelicenes, but only with inconvenient detours. The usage of benzyne generated *in situ* as a dienophile by *Minuti et al.* (**Scheme 9**) to gain [5]helicene clearly exposes the weakness of the Diels-Alder reaction: The substrate scope is constricted by the demands of diene and dienophile.[95] For the reaction to proceed smoothly, the constellation of an electron-rich diene and an electron-poor dienophile (or *vice versa*) has to be attained by electron-donating and -withdrawing groups. These can rarely be cleaved off from the final helicene so that the amount of potential substrate and product candidates is confined all at once.

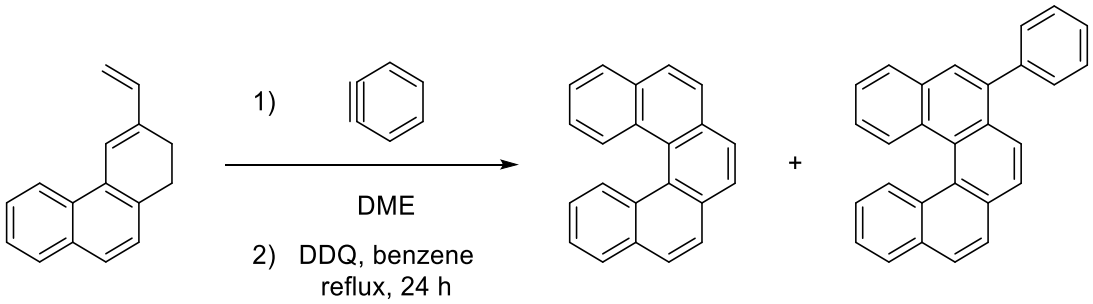

Scheme 9: Diels-Alder with aryne as dienophile.

Because of that, this procedure is primarily viable for the synthesis of quinones. A strong argument for this class of helicene derivatives can be made due to two reasons: Firstly, they are interesting compounds themselves. Helical quinones are prone to assemble in columnar structures by π-stacking which has been exploited to create high-quality Langmuir-Blodgett films.[96] Secondly, they can easily be converted to hydroquinones *via* the Russig-Laatsch reaction.[97,98] The alcohol functions can then be altered according to one's needs. Of course, this method always entails a bilateral hydroxylation which has to be accounted for. But if the quinones are implemented as the exterior cycles, this gives entry to the bay area which is the bulkiest region within the molecule and difficult to access.

Another selling point is the fact that the Diels-Alder reaction can also be modified for enantio- and diastereoselective purposes. The disuse of catalysts and ligands requires more creative sources (chiral auxiliaries or substrate control) for the chiral information which are often more challenging to plan into the synthesis and restricting for the substrate scope in general, but in terms of enantiomeric excesses, they can match the employment of chiral ligands in the asymmetric [2 + 2 + 2] cycloisomerization.

Despite the fact that the Diels-Alder reaction is an obvious choice for the formation of 6-membered rings, publications so far have more or less used the same strategies over and over again. Declaring it as underdeveloped would not be a huge understatement, further research is therefore a vital necessity.

3.4 Miscellaneous approaches

Apart from the three main methods, numerous entries have been added to the synthetic portfolio of helicenes. These include pinacol couplings,[99,100] McMurry couplings,[101,102] ring-closing metathesis or other metal catalyzed non-[2 + 2 + 2] cyclizations,[103,104] radical cyclizations,[105,106] Friedel-Crafts-type cyclizations[107,108] and many more.[109–112] Worth mentioning is the Scholl reaction which is predominant in the field of chiral nanographenes.[113–117] Admittedly niche, a selected report is an oxy-Cope rearrangement by *Karikomi* (**Scheme 10**). Addition of a phenanthrene unit onto a bicyclo[2.2.2]ketone was followed by a 3-oxy-Cope rearrangement after treatment with KHMDS and 18-crown-6. The resulting partly saturated pentahelicene skeleton was turned to 2-acetoxypentahelicene in 4 steps.[118]

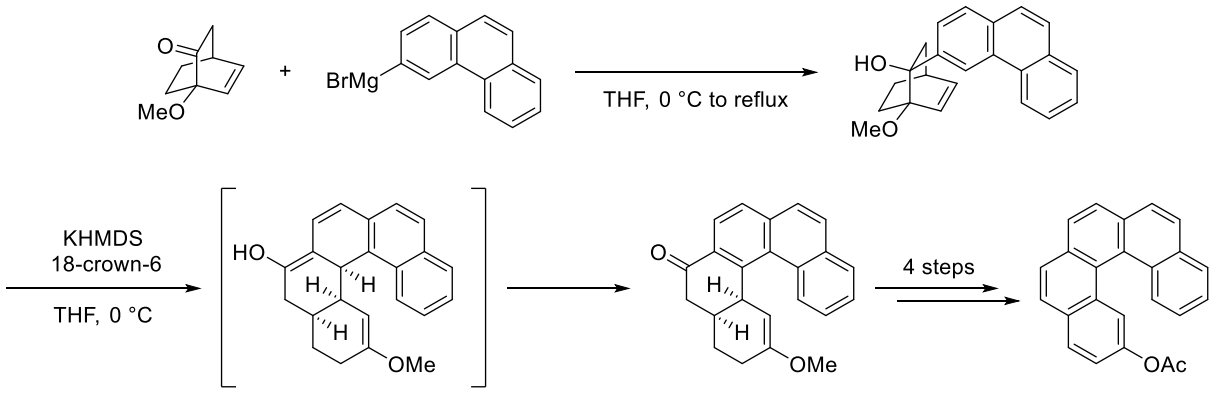

Scheme 10: Synthesis of 2-acetoxy[5]helicene involving oxy-Cope rearrangement.

All these examples have their own pros and cons. As a matter of fact, some are on par with the state-of the art methods. On the other side, some could never gain a foothold due to being special edge scenarios. Still, each one displays the marvelous devoted effort giving today's plethora of options.

3.5 Retrosynthetic analysis

In this section, the three main strategies have to be revisited for the retrosynthetic analysis since the synthetic route heavily relies on the key closing of the helicene. Before this decision can be made, major issues briefly mentioned above have to be addressed first. In the end, the aim is to get functionalized helicenes, so these two questions should be asked in the exact same order:

A) How and with which groups should the functionalization be carried out?
B) Which method serves best for the purposes of A)?

The derivatization of carbohelicenes has caused trouble ever since their discovery. The exclusive existence of sp^2-hybridized carbons offers just about so many possibilities anybody can work with. Naturally, the aromatic scaffold is perfectly suitable for aromatic reactions like electrophilic and nucleophilic aromatic substitutions, but the presence of a range of electronically similar positions in which the substitutions can take place is unsettling. Nonetheless, some studies suggest that these reactions can still be conducted regioselectively. Presumably the most typical and prevalent electrophile is bromine which is a potent functional group for further derivatization. *Usui et al.* demonstrated a bromination at C-6 in a [5]helicene,[24] likewise the same was achieved with a resemblant [6]helicene (**Scheme 11**).[119]

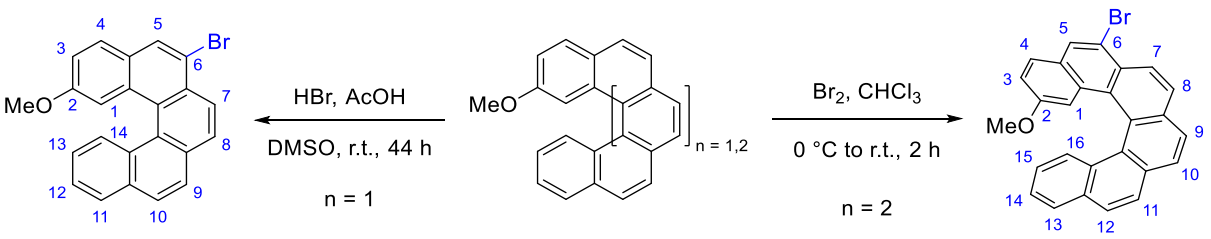

Scheme 11: Bromination of methoxyhelicenes targeting C-6.

The electrophilic aromatic substitution of a benzo[5]helicene[120] (**Scheme 12**, left) and an aza[7]helicene (**Scheme 12**, right)[121] provided the corresponding derivatives brominated at C-5. These instances prove that a selective electrophilic substitution is conceivable in principle, albeit only if directing groups already exist. In contrast, bromination without directing groups is not feasible and underdeveloped.[122] Other publications about derivatization of bare carbohelicenes are scarce and have so far been accomplished by two methods: oxidation and C-H activation.

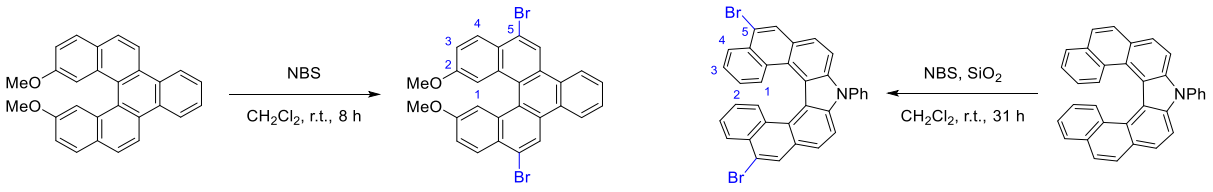

Scheme 12: Bromination of benzo- and azahelicenes targeting C-5.

Targeting C-5 and C-6, *Laarhoven* and coworkers illustrated an oxidation of [6]helicene with Cr^{VI} in acetic acid to the *ortho*-quinone in 70 % yield (**Scheme 13**).[123] Being valuable compounds, this method has been extensively worked on, but meaningful results were continuing to be bound to directing groups.[24,78,119]

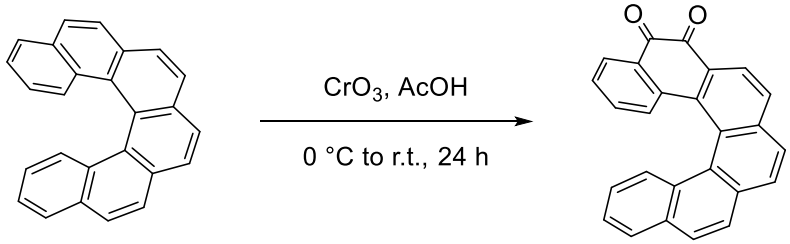

Scheme 13: Oxidation of [6]helicene to 5,6-diketo[6]helicene.

One instance of a C-H activation was given by the group of *Nečas*. A straightforward borylation of [4]helicene led to the pinacol esters at positions 2 and 3 and a combined yield of 74 %.[124] The same procedure for [5]helicene yielded 89 % of the corresponding regioisomers (**Scheme 14**).[125] Their reaction screening specifically aimed for the monoborylated products, but after observation of the remaining chromatographic fractions, they concluded that the symmetric bisborylated species could also be optimized for.

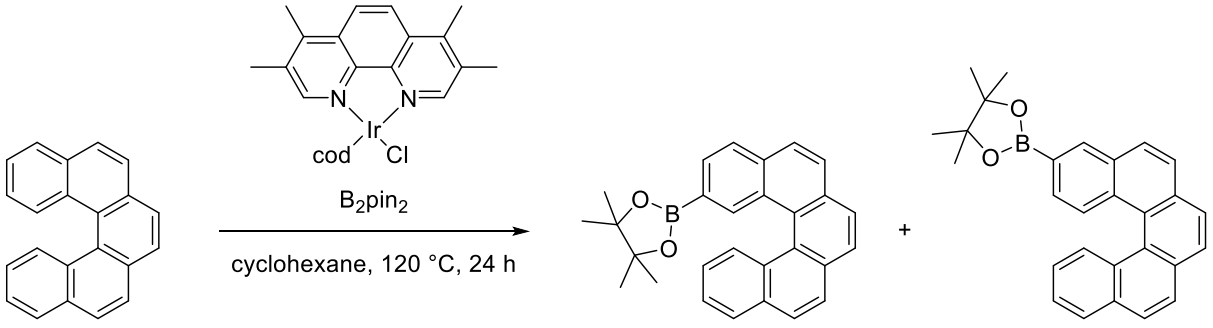

Scheme 14: Selective borylation of [5]helicene.

Other publications on C-H activation exhibited interesting features, but likewise the same flaw in requiring directing groups.[126] To date, late-state modification is lackluster because it is not universally applicable. Its unpredictability makes it an analytic

nightmare and the lucrative position 1 is not accessible with any of the examples given so far. Therefore, starting from pre-functionalized building blocks seems more promising. As long as an appropriate group is chosen, every location can be targeted and (almost) every functionality can be introduced. The single limiting factor is that they must survive all the reactions leading to the helicene which is, to put it lightly, still difficult, but in the long run the most optimal choice.

With this in mind, the Diels-Alder approach can be ruled out. Granted that C-1 is accessible through the quinones, at the same time C-4 is functionalized by doing so which is not always desirable. In addition, the demands for diene and dienophile can make things too convoluted and helicenes higher than [5] are unexplored with this method.

Between the remaining 2 reactions in question, it is more difficult to determine a winner. Each of them has its own strengths and weaknesses which can also be antithetical *à la* one man's joy is another man's sorrow: The ease of the photochemical procedure can be construed as lacking flexibility, the flexibility of the [2 + 2 + 2] cycloaddition can be seen as extra effort. Both allow an incorporation of many functional groups and offer enormous potential in terms of modularity and performance: Practically, every location including the cramped inner territory can be aimed for and a multitude of publications in these fields support their eligibility. Examining and comparing them objectively would probably not be expedient since, depending on who is asked, both are jack-of-all-trades in their own way. And rightfully so, each has their own place within the helicene community.

Eventually, it can be narrowed down to personal concerns. Considering the scope of this work, the [2 + 2 + 2] cycloisomerization is chosen since the opportunities this method provides are valued higher than the convenient setup (which can be deceptively inconvenient). The regio-, chemo- and stereocontrol alongside the vast versatility of metal/ligand-pairings are unmatched and the capability to scale the capacities up is greatly appreciated in the laboratory.

As the metal catalyzed [2 + 2 + 2] cycloaddition of not fully saturated triyne **3** does not necessarily lead to the fully aromatized helicene **1** (**Scheme 15**), the oxidation of the tetrahydrohelicene **2** needs to be dealt with. The synthesis of *cis*,*cis*-dienetriynes is conceptually interesting, but too specific for a general approach and can be ruled out.

The acid-mediated aromatization pioneered by the group of *Starý* and *Stará* introduces an oxygen atom to the system which simplifies the synthesis since it opens up the gateway to carbonyl chemistry.[76,77] Alternatively, a conventional aromatization with oxidizing agents like DDQ is completely viable, too.

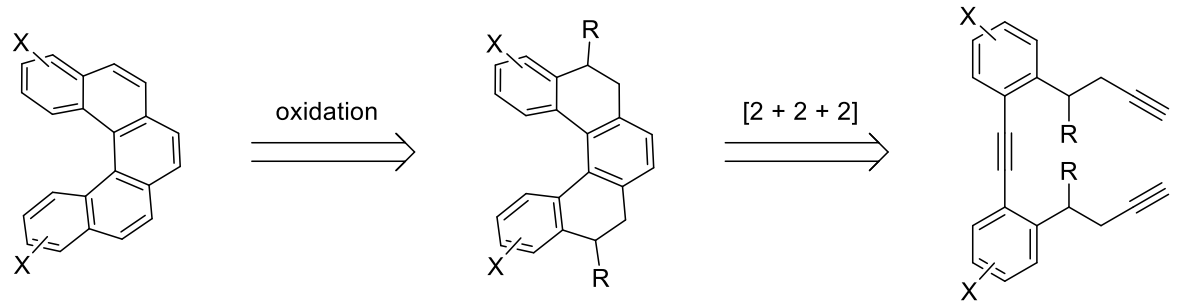

Scheme 15: Retrosynthetic oxidation and [2 + 2 + 2] cycloisomerization of [5]helicene **1** (X = desired functionality; R = OAc, H).

To maximize the effectivity, it is best to install the internal alkyne of triyne **3** in the last step from a retrosynthetic perspective. This ensures the retainment of the C_2 symmetry for the longest amount of time which essentially bisects the number of total reactions. This way, playing out the oxidative scenario involving mild acids, both acetates in **4** can be generated from hydroxy functions (**Scheme 16**). These in turn can be unlocked by the aldehydes/ketones through a formal reduction which comes in handy because the immediate implementation of alcohols is challenging. From here on, the retrosynthetic route can be branched out to multiple ways. Aromatic ketone **6** can be attained by Friedel-Crafts acylation of **8** with the respective acyl chloride bearing the terminal alkyne, but the regioselectivity relies on the desired groups attached on the pre-functionalized benzene core.

Starting from the right regioisomer of a benzaldehyde core **7**, a nucleophilic addition of an organometallic C-nucleophile on the carbonyl function would omit the conventional reduction with reducing agents and lead directly to the alcohol **5**. Presented by the group of *Starý* and *Stará*, a Barbier reaction with propargylic nucleophiles stemming from either magnesium, lithium or gallium created the corresponding alkynes in good to excellent yields. The acquirement of aza- and halogenated helicenes from pre-functionalized starting materials in this manner evidently showcases the proof of concept.[77]

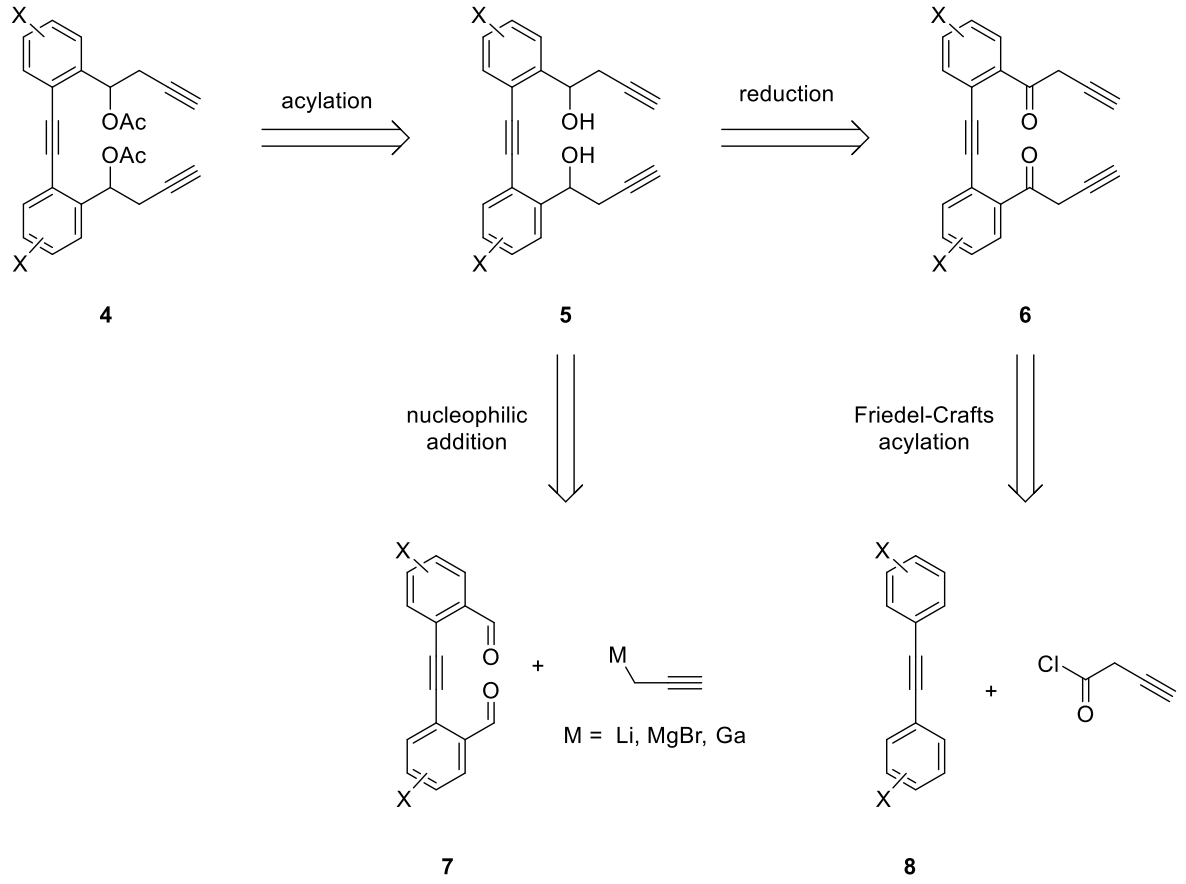

Scheme 16: Retrosynthesis for triyne **4** (X = desired functionality).

In the scenario without oxygen-based substituents, the alkylation of the terminal alkynes is also imaginable *via* Friedel-Crafts alkylation, but a Wagner-Meerwein rearrangement would prevent a simple alkylation. Likewise, a bypass *via* the Friedel-Crafts acylation and a subsequent Wolff-Kishner or Clemmensen reduction of **6** (**Scheme 17**) would be questionable at best because it effectively would be equal to route A. Admittedly, the route is thereby reduced by 1 step (acylation of hydroxides), but trading a fool-proof oxidation with fewer steps might not be the most lucrative deal. Perhaps a more elegant method is the generation of triyne **10** from benzylic (pseudo-) halide **9**. A nucleophilic substitution in this reactive position by the means of Grignard compounds or lithiated reagents evades regioselectivity problems and the workup of aldehydes and alcohols which can sometimes be worrisome. The terminal alkynes may have to be protected *ad hoc* with silyl groups to increase the stability and selectivity. They should not interfere with any reactions and can readily be cleaved off with the addition of fluorides at every stage during the entire route, even after the formation of the helicene.

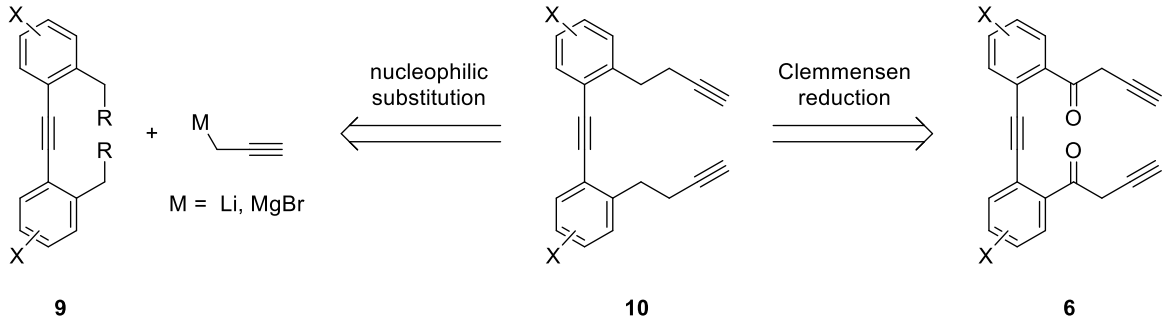

Scheme 17: Retrosynthesis for triyne **10** (X = desired functionality, R = I, Br, Cl, etc.).

The bridging alkyne moiety can be established by a cascade of Sonogashira cross-couplings of silyl-protected acetylene and the respective aryl halide **12** (**Scheme 18**). If the two benzene cores are identical, the C_2 symmetry of the targeted diphenylacetylene permits a two-fold Sonogashira coupling with gaseous acetylene or an *in situ* deprotection.

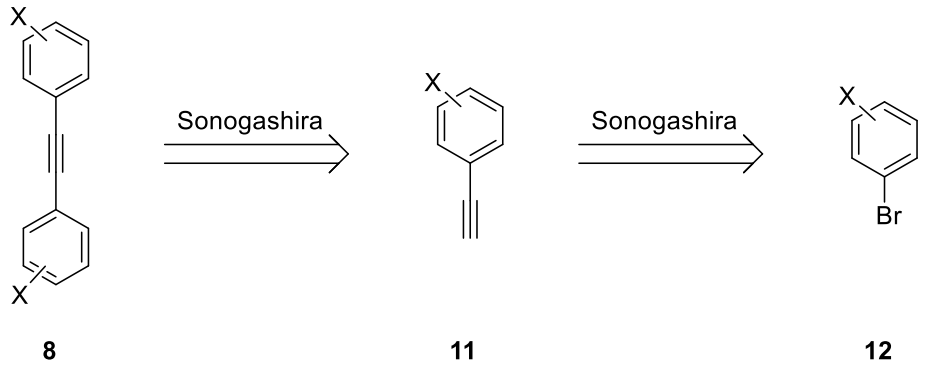

Scheme 18: Retrosynthesis for diphenylacetylene **8** (X = desired functionality).

Regarding the desired functionality X, using heteroaromatics and non-customizable, completed functionalities can be risky due to the unpredictable behavior of individual cases and diminishes the diversity of the strategy. It is smarter to keep all the opportunities until the end and delay their presence for the longest time possible, i.e. X itself should optimally be a versatile reactive center. Deductively, the usage of chemically inert groups, which can be turned to reactive ones after the [2 + 2 + 2] cycloisomerization, is the most sensible choice. This guarantees the success of all the previous steps leading up to the helicene. After the construction of the helix, when all that is left are carbon and hydrogen atoms, harsher conditions can be applied to alter them. Determining the right functional group is crucial for the course of the route since it is grounded on the utilization of pre-functionalized components. Reactive groups like halides and boronic acids can pre-emptively be omitted since they would compete with

the incipient halide in **12**. Exploiting different reaction rates between iodides and bromides can be serviceable, but is not ideal. On the contrary, hydroxy functions can be turned to pseudo halides in a single step and will not hinder a selective cross-coupling reaction. To suppress their nucleophilicity, they can be masked as alkoxides which can also be a lever to enhance the solubility. Alkoxides are inert enough for all the procedures described above and can be cleaved under acidic conditions. The underlying alcohol can be esterified to triflates which opens various doorways to the final ligand.

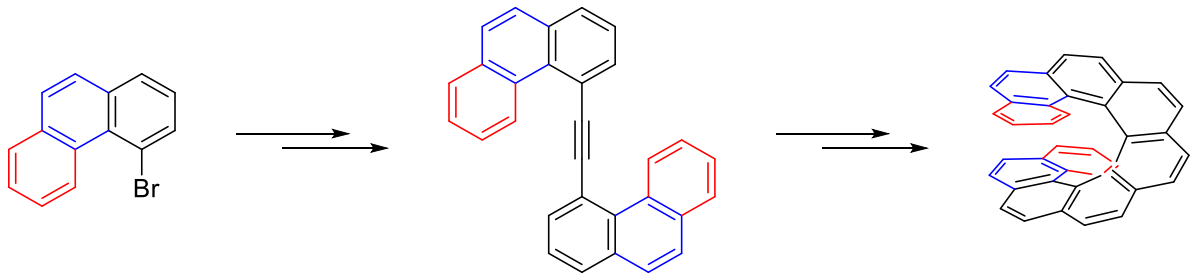

Scheme 19: Schematic synthesis of [n]helicene (n = 5, 6, 7, 8, 9).

No matter where the alkoxy groups are located, since the starting benzene unit ultimately ends up being the outer ring in the helicene, the methoxy groups are always at the rim, too. With this method, the bay positions 1−4 are secured. Whereas strictly starting from benzene blocks generates pentahelicenes exclusively, their application is not compulsory: The application of annulated starting materials should also be feasible by this method, they can even be mixed (which would break the C_2 symmetry up until the cyclization). Accordingly, when pre-functionalized naphthalenes and phenanthrenes are part of the building blocks, higher derivatives ranging from hexa- to nonahelicenes can be crafted (**Scheme 19**).

4 Helicene formation – setting up the scaffold

4.1 [5]Helicene

For the time being, it is sufficient to start humbly with the lowest helicene to keep the synthesis as trivial as possible. Later on, the accumulated experience and information can be used to extend the strategy to higher homologues. Although [4]helicene is the first congener within the series of *ortho*-annulated benzene rings which is non-planar in its lowest energy conformation, the dihedral angle of 26° between the terminal benzene rings only accounts for a racemization barrier of 3−7 kcal/mol.[127] While this barrier can be raised with bulky substituents, a more than triple time elevation needs to be achieved for the helicene to not racemize under ambient temperature. But if one more benzene unit is attached, the landscape changes dramatically: In comparison with its predecessor, the torsion angle in [5]helicene is multiplied by one and a half to 46° and the threshold to form the other enantiomer is multiplied by more than three to about 23 kcal/mol.[14,128] The distinct enantiostability therefore qualifies [5]helicenes for a synthetic first target. The starting materials – phenyl halides – are commercially omnipresent and easier to manage in relation to condensated representatives like naphthalenes.

2,13-Difunctionalized [5]helicene

At the core of the retrosynthetic chapter leading to the diarylacetylene fragment, primarily two pathways came out on top:

- The nucleophilic addition of benzaldehydes (**Scheme 16**)
- The nucleophilic substitution of toluenes (**Scheme 17**)

In case of failure, it is always better to be ahead of schedule and have a fallback option beforehand. For the synthesis of the first helicene of this work, both pathways will be tested to get a better grasp in terms of reaction procedures, performance and workups for future applications.

The pathway of the nucleophilic addition started with a Pd-catalyzed Sonogashira coupling of commercially available 2-bromo-4-methoxybenzaldehyde **13** and trimethylsilylacetylene after a procedure adapted from *Liu* and *Li*.[129] After purification

by column chromatography, aldehyde **14** was isolated in 83 % yield (**Scheme 20**). The good performance of this reaction was pleasant because it established its conditions as a standard instruction for future Sonogashira couplings.

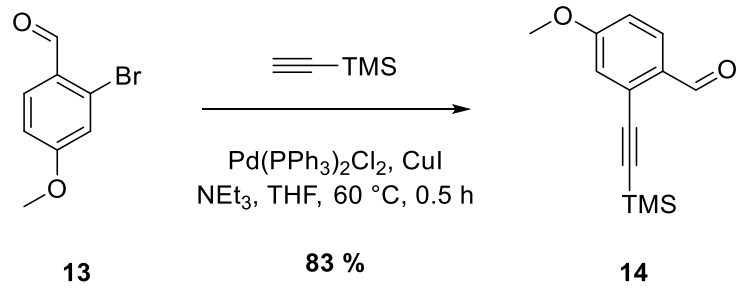

Scheme 20: Sonogashira coupling of **13**.

To arrange the other half of the internal alkyne for a subsequent cross-coupling reaction, it had to be deprotected first. As the most labile protecting group amid the silyl protecting groups, the trimethylsilyl group was cleaved under basic conditions, giving terminal alkyne **15** in almost quantitative yield (**Scheme 21**).

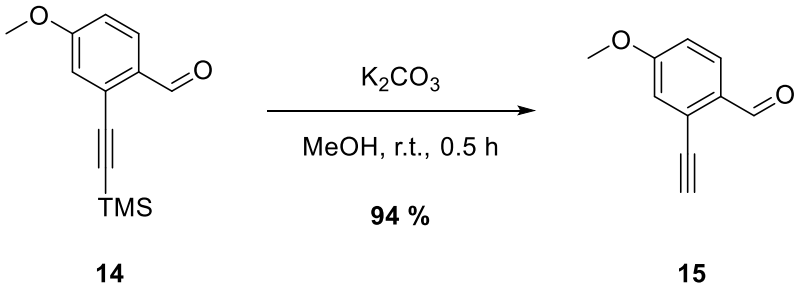

Scheme 21: Deprotection of **14**.

The following Sonogashira coupling was carried out under identical conditions (**Scheme 22**). Unfortunately, the same outcome could not be duplicated.

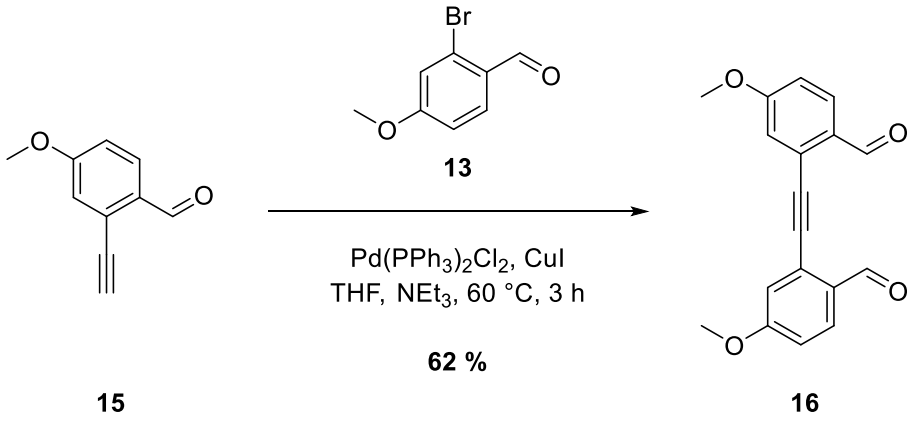

Scheme 22: Sonogashira coupling of **15** with **13**.

The reaction was traced by TLC. Compared to the former Sonogashira cross-coupling, a slight amount of the starting material remained unaffected, even after increase of catalyst load and reaction time. Due to the tailing nature of aldehydes, the purification was accompanied with a sizeable loss of product material. In conjunction, a drop of approximately 25 % in yield was observed. Tolan derivative **16** was isolated in 62 % yield.

Taken together, the buildup of the dialdehyde scaffold was achieved in three steps with an overall yield of 48 %, making it a solid route especially for more complex structures. But since molecule **16** has a C_2 axis, the route can conceivably be shortened by 2 steps if a two-fold Sonogashira cross-coupling is done. To establish such a protocol for symmetric derivatives, this time **16** was targeted in a one-pot double reaction (**Scheme 23**). In a worst-case scenario, only one end would react with **13** which would at least lead to **15**. As a whole, this would render the deprotection of **14** redundant and still decrease the route by 1 step.

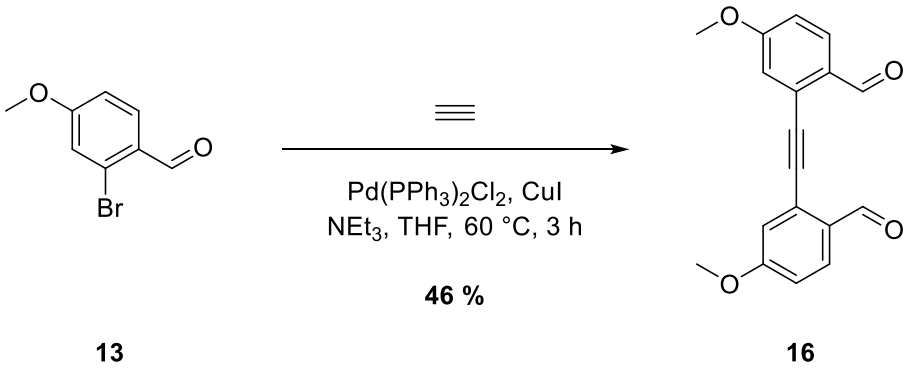

Scheme 23: Two-fold Sonogashira coupling of **13**.

Replacing TMS-acetylene with its unprotected congener was also a transition from a liquid to a gas. Working with gases can be tricky (and dangerous) because the internal pressure, influx and equivalents cannot freely be adjusted, a laboratory compromise is the alienation of balloons to one's own favor. Under the same conditions as the earlier reaction, **16** was treated with gaseous acetylene. After TLC-control, nearly the same observations were made: No total conversion was observed and the workup process was roughly identical as well. In fact, the same was true for the yield: In a single step, symmetric **16** was obtained in 46 % yield. While the initial route is obligatory for non-symmetric molecules, the second variant is a better choice for symmetric ones. Without hesitation, cutting off two percentage points for two reaction steps is a tradeoff

everyone is willing to take. Presumably, an even higher cut for reactions with other substrates would still be a nice tradeoff worth considering. In any case, the bottleneck of this reaction was the workup of the dialdehyde which caused the high material deficit. A workaround could be a temporary modification of the aldehyde functions: For instance, acetals could be introduced with ethylene glycol which could easily be removed under acidic conditions. Of course, this accounts for two more reactions and effectively would only postpone the issue.

The next step according to the strategy is the nucleophilic addition of an organometallic alkyne. Several metals are eligible for this, earlier works by *Starý* and *Stará* highlighted magnesium, lithium, gallium and zinc as the most promising candidates.[77,130] In their studies, the indium-catalyzed organogallium addition exhibited the highest yields, but the unusually employed metals are debatable in two ways. Firstly, accentuated in a publication by *Lee*, a homoallenylation alongside the propargylation can take place depending on the attached residues of the propargyl bromide (**Scheme 24**).[131]

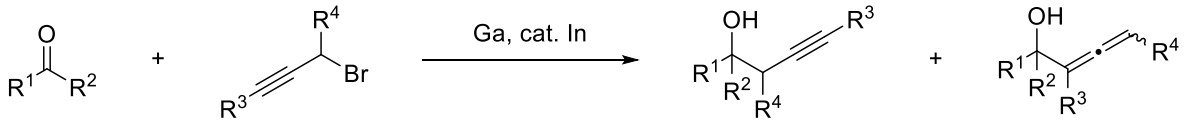

R^1 = *n*-C_8H_{17}, $PhCH_2CH_2$, C_6H_{11}, Ph; R^2 = H, Me

R^3 = Me, Et, Ph, TMS; R^4 = H, Me

Scheme 24: Allenylation and propargylation of carbonyl compounds.

Secondly, in virtue of their rare natural occurrence in the Earth's crust, they are comparably expensive. Since the marginally higher yields are in no way proportional to the costs, alternative options were pursued.

Organolithium compounds are the most potent reagents and do not necessarily require a halide because they can be formed *in situ* by deprotonation. In this case, the alkyne always has to be shielded by protecting groups which in turns adds at least one more reaction to the total balance. Otherwise, the propargylic proton would never be abstracted first. Organolithiums are costlier to manufacture than other organometallic reagents because the molar ratio of metal to organohalide is always twice as much (**Scheme 25**). Also, lithiated compounds have to be handled carefully, particularly *tert*-BuLi is known for its spontaneous ignition on exposure to air. It is known that their aggregation can be manipulated by means of solvent and temperature in effort to

augment their reactivity: Prepackaged *tert*-BuLi is usually dissolved in hydrocarbons. In *n*-hexane, it exists as a tetramer,[132] but in coordinating Lewis bases, the aggregation number can go down to 1 (dimer in Et_2O,[133–135] monomer in THF at <−100 °C[136]) which has a drastic impact on the reactivity.

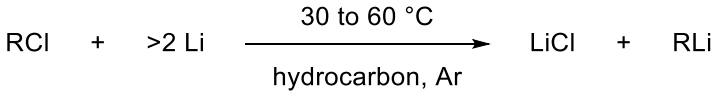

R = *n*-, *s*-, *t*-, *i*-Bu, *n*-Hex

Scheme 25: Commercial preparation of alkyllithiums.

Mandatorily working at low temperatures is a handicap for a universal strategy because it can negatively affect solubility and reaction time. Besides, a high potency does not always translate to outstanding results: Despite their high reactivity, carbanions based on lithium displayed moderate performance during the addition of 2,2′-ethynylenedibenzaldehyde.[77]

Unlike lithium, zinc is abundant and cheap and its lower reactivity is beneficial for a selective addition to the dialdehyde. Organozinc reagents are not sensitive to air and thus do not have to be treated under Schlenk conditions, they are not pyrophoric and several publications demonstrated that the reactions using organozinc compounds can even run in water.[137–139]

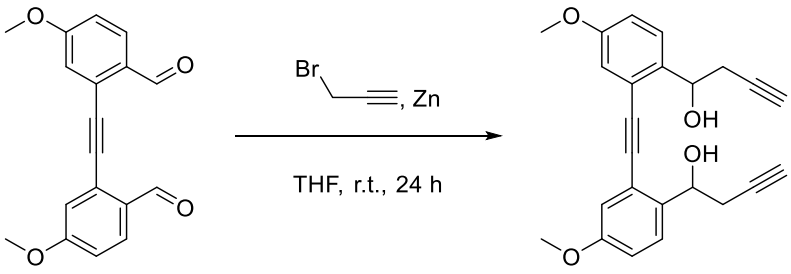

16 mixture of stereoisomers **17**

Scheme 26: Nucleophilic addition of **16**.

Carrying on, aldehyde **16** was thus treated with propargyl bromide and zinc at room temperature (**Scheme 26**). After 24 hours, TLC-control showed no complete conversion. The procedures by *Starý* and *Stará* comprise a one-step propargylation and acylation in the same reaction vessel, but treating **16** with the same reactants did not lead to a replication of their work. The reaction mixture was subjected to flash

chromatography on silica gel, but a meaningful purification of diol **17** could not be achieved. In an attempt to counteract the tailing of the hydroxy groups with small amounts of triethylamine, a second try was carried out. The diol still could not completely be isolated and had some minor impurities presumably stemming from un- and mono-reacted species, nevertheless it was used for the subsequent reaction without further purification. Theoretically, **17** can already undergo the [2 + 2 + 2] cycloisomerization, but the extraction of the hydroxy functions would be problematic.

Opposed to an acylation of triynes in triethylamine done by *Starý* and *Stará*, the solvent was changed to pyridine for a better solubility. With 4-dimethylaminopyridine as a nucleophilic catalyst, the acetylation proceeded smoothly. The change from an alcohol to an ester eliminated any worries during the workup. This was apparent by the circumstance that even the diastereomers could be isolated at this stage, the TLC revealed two distinct spots which were indistinguishable by NMR. Over 2 steps, diacetate **18** was isolated in 61 % yield (**Scheme 27**).

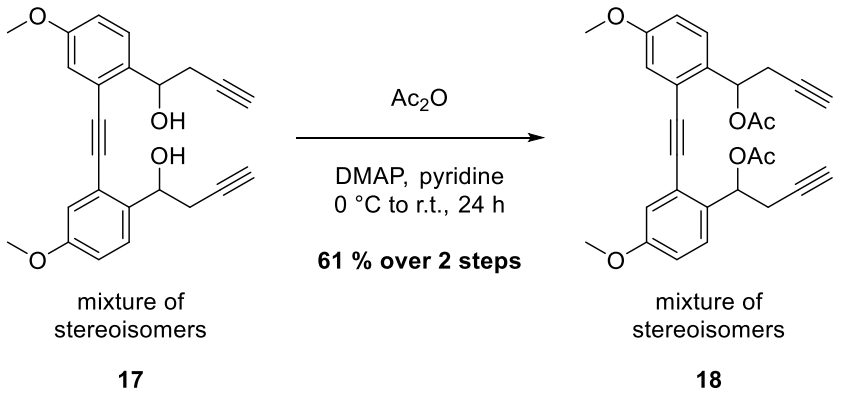

Scheme 27: Acylation of **17**.

With the acylated triyne in hand, the key reaction was ready to start. Continuing from here on, first a reaction screening was conducted to fine-tune the conditions. To begin with, the commercially available half-sandwich complex cyclopentadienylcobalt dicarbonyl merged with phosphine ligands has usually been the catalyst of choice since its employment for the syntheses of indanes, tetralins and estrone by *Vollhardt* in the 70s.[140–143] The dark red liquid decomposes on air and needs higher temperatures of up to 150 °C (conventional heating) or 200 °C (microwave) for activation due to the strong bonding of the carbonyl groups to the Co^{I} center,[87] but featured a high degree of efficiency which *inter alia* has been exploited for the total syntheses of natural products like (±)-allocolchicine or (+)-complanadine.[144–148]

Regarding the reaction conditions, *n*-decane as a high-boiling liquid and stoichiometric amounts of the metal catalyst and the ligand were used (**Scheme 28**). According to the TLC, stirring at 140 °C for 2 hours led to a multiplication of species.

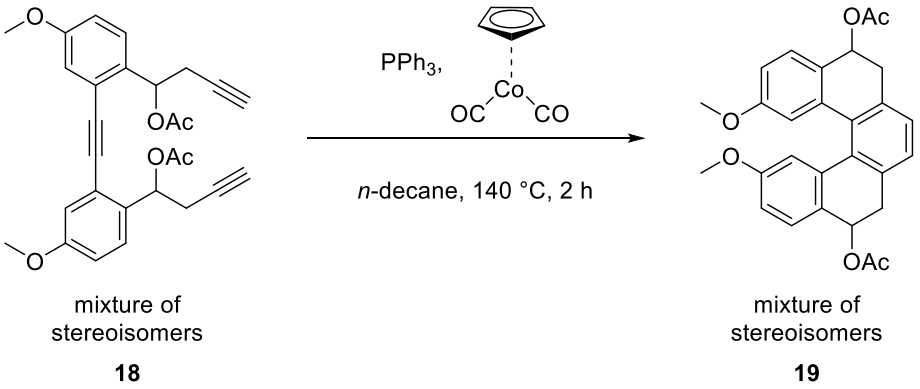

Scheme 28: [2 + 2 + 2] cycloisomerization of **18** mediated by $CpCo(CO)_2$.

This is expected: Respectively, (*P*)- and (*M*)-tetrahydrohelicene **19** originating from (*R*,*R*)-, (*S*,*S*)- and *meso*-**18** can be formed, giving a total of 6 possible stereoisomers or 3 pairs of enantiomers (**Figure 7**).

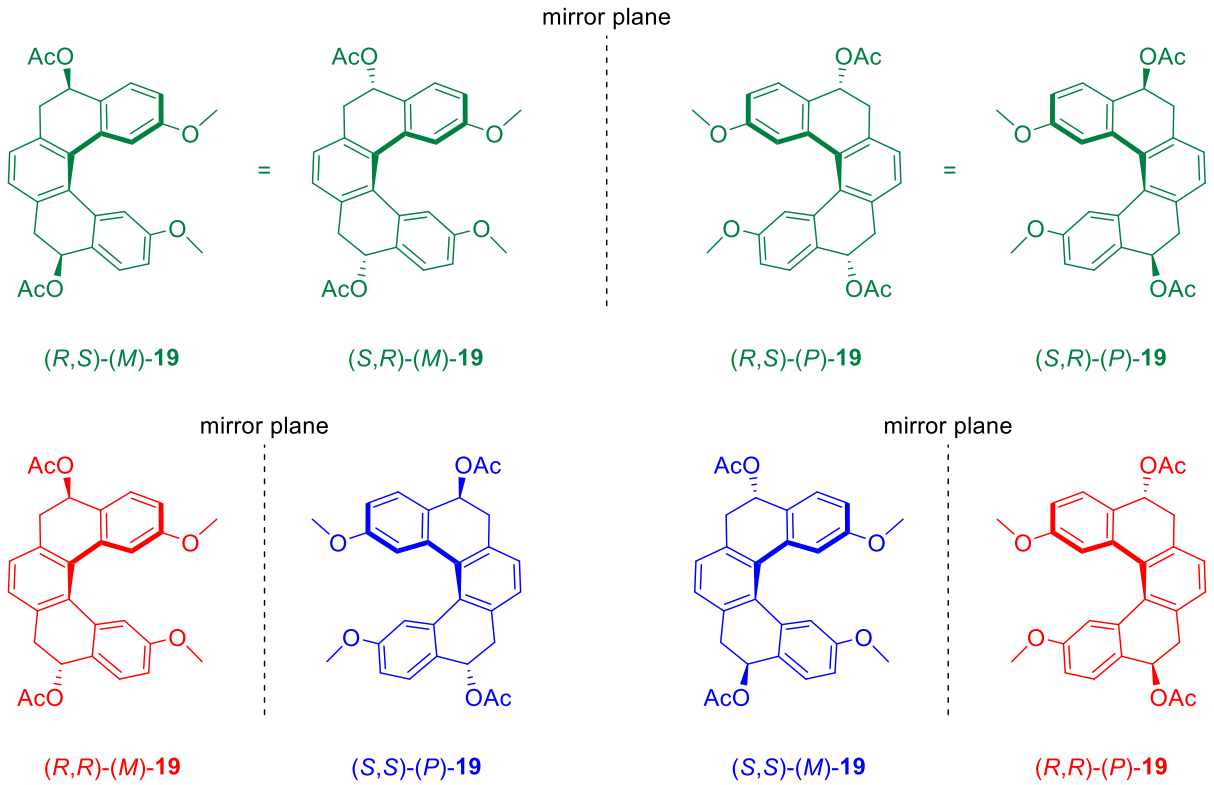

Figure 7: Tetrahydrohelicenes **19** stemming from (*R*,*R*)-**18** (red), (*S*,*S*)-**18** (blue) and *meso*-**18** (green).

Since this reaction had assured the helix formation, this was also the earliest time the relevance of the helical chirality became a major subject. At this stage, a possible chiral

resolution of (*P*)- and (*M*)-enantiomers could be discussed, but a chiral resolution could only be advised against at that point as the presence of 3 enantiomers would make it wasteful and superfluous. It would be wiser to delay the resolution to a point after the detachment of the acetates, when all 6 stereoisomers blend to 2 enantiomers.

Retrospectively, the ^{1}H-NMR spectrum of the crude mixture suggested a partial oxidation to fully aromatic 2,13-dimethoxyhelicene which in turn indicated the huge energy gain arising from the spontaneous aromatization. A black precipitate alluded to the incremental decay of the catalyst from an oxidized species in the form of $Co^{II}(Cp)L_n$ (which might be catalytically active) to $(C_5H_5CoO_3)_x$ (catalytically inactive).[67] A purification of the complex mixture was only successful to some extent, the high number of distinct species prevented a complete separation of each one. One way or the other, since the destruction of both stereogenic centers in the next step was synonymous with a convergence of the diastereomers, their separation was not of interest. More emphasis was put on the separation from the substrates. Every fraction except for those from the substrates was unified and used for the next procedure.

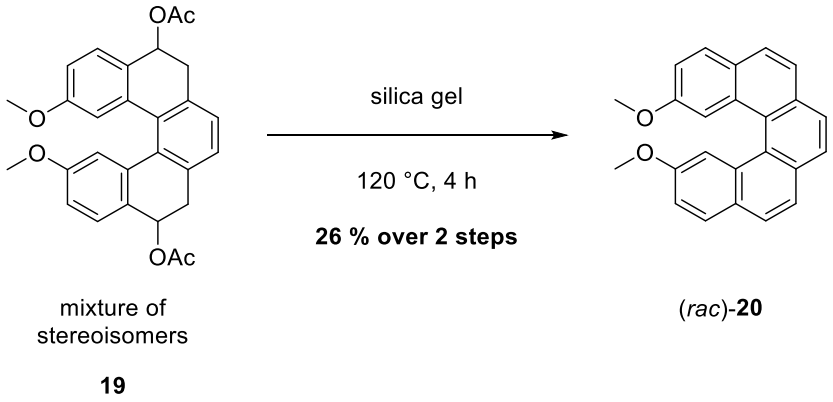

Scheme 29: Silica gel-assisted aromatization of **19**.

Though an aromatization of **19** had occurred in parts, the elimination of the residual acetates had to be ensured. A solution of **19** in dichloromethane was treated with silica gel. After evaporation of DCM under reduced pressure, the solvent-free mixture was stirred at 120 °C for 4 hours (**Scheme 29**). Indeed, TLC-control depicted a substantial diminution of species. The silica gel was put into a plug and extracted with DCM. The mixture was concentrated under vacuum, the ^{1}H-NMR spectrum of the residue unmistakably proved the removal of the acetates and the generation of racemic pentahelicene (*rac*)-**20** (**Figure 8**).

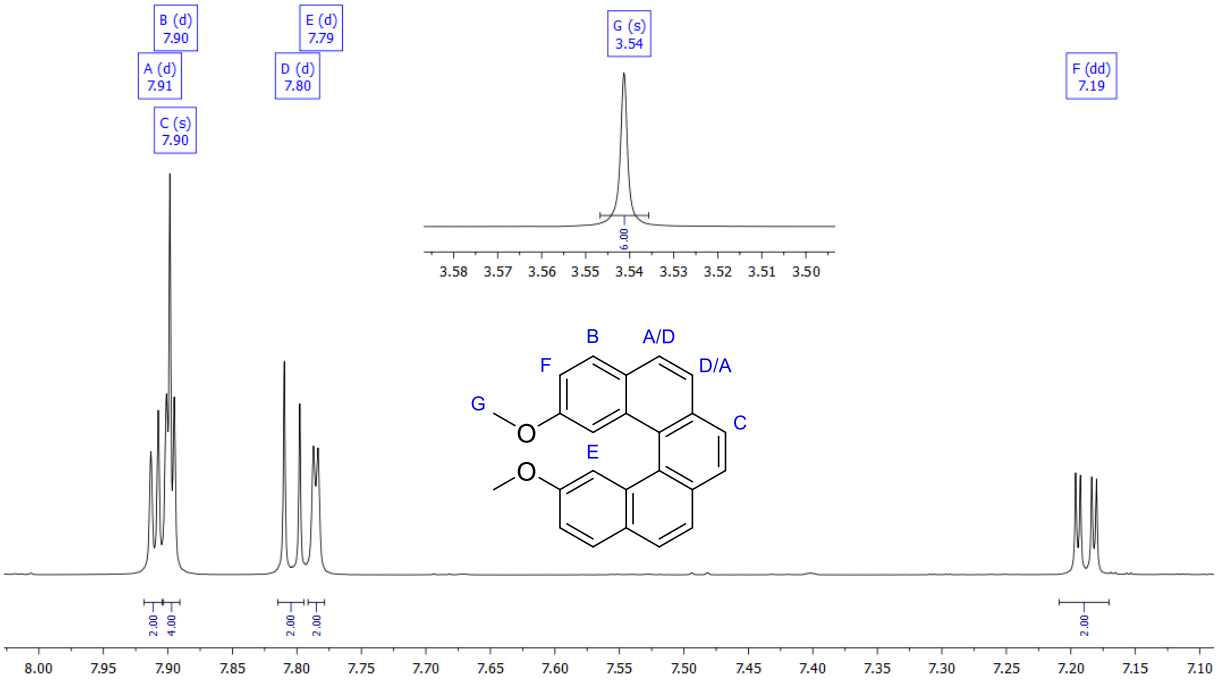

Figure 8: ^{1}H-NMR spectrum and assignment of (*rac*)-**20**.

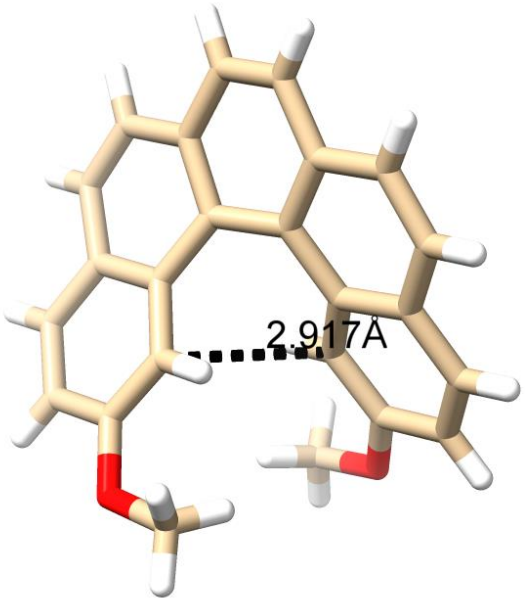

Figure 9: Molecular structure of (*rac*)-**20** as determined by single crystal XRD analysis (carbon in brown, hydrogen in white, oxygen in red).

A solution of (*rac*)-**20** in dichloromethane was layered with *n*-hexane at −10 °C. Overnight, clear yellow plates were collected and subjected to XRD analysis. (*Rac*)-**20** crystallizes in the orthorhombic space group *Pbcn*, the inner helix forms a cavity which has a diagonal of approximately 2.9 Å (**Figure 9**). The methoxy groups point towards each other, the C-C-C-C dihedral angles of the inner helicene rim range from 16−32°.

A non-coplanar conformation of the terminal carbons made a determination of the dihedral angle between the terminal benzene units difficult. Within the accuracy of the experiment, the angles and the distances in large part retain the C_2 symmetry as anticipated.

Unfortunately, only 26 % of (*rac*)-**20** could be retrieved over 2 steps. It was not exactly clear why the efficiency of the catalyst was so poor. But the low yield made a progressive effort in search of superior alternatives evident. Another option based on Co^{I} is its equivalent to Wilkinson's catalyst. While the latter has found much focus in the [2 + 2 + 2] cycloisomerization for years,[149–152] the cobalt analogue is largely unexplored in the field of the trimerization. Aside from scarce reports decades ago,[153] solely the workgroup of *Hapke* has used this catalyst recently.[154] Therein, the catalyst exceeded in the trimerization of triynes under mild conditions.

Head-to-head, both are commercially available or can easily by synthesized from their chlorides with an excess of triphenylphosphine.[155,156] But in contrast to one of the rarest precious metals, there is no shortage for cobalt which has a direct repercussion on its value: The cobalt catalyst is cheaper by a sizable margin. In the face of the fact that yields up to 96 % can be achieved with a variety of ether-bridged alkynes, its tryout was envisaged.

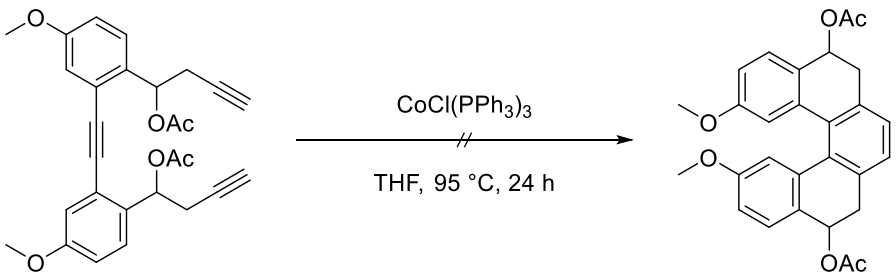

mixture of stereoisomers **18**

mixture of stereoisomers **19**

Scheme 30: [2 + 2 + 2] cycloisomerization of **18** mediated by $CoCl(PPh_3)_3$.

The reaction was monitored by TLC. Stirring **18** in THF at room temperature for 2 hours showed no effect. Even gradual increase of temperature and time up to 95 °C and 24 h had no impact on the mixture (**Scheme 30**). Despite the step backwards, **18** was recovered and other systems were investigated.

At the turn of the decade, powerful, air-stable catalysts have experienced an upsurge for the [2 + 2 + 2] cycloaddition.[157–159] Essentially, they all incorporate some kind of fumarate. Among them, a heteroleptic catalyst integrating a phosphite ligand has been developed by *Hapke et al*.[86,87] The synergy of an electronically rich σ-donor and an electronically poor π-acceptor provided a higher robustness of the precatalyst and excellent results for inter- and intramolecular cyclizations alike. The $CpCo^{I}$-phosphite-fumarate precatalyst can be stored on the bench for months and recycled quantitatively (except in a photochemical cyclization) *via* column chromatography. Interestingly, a re-coordination of the olefin happens as it is unattached during catalysis. In terms of performance and versatility, it surpasses the traditional $CpCo(CO)_2$ complex and can be synthesized from it through ordinary ligand exchange in 2 steps.

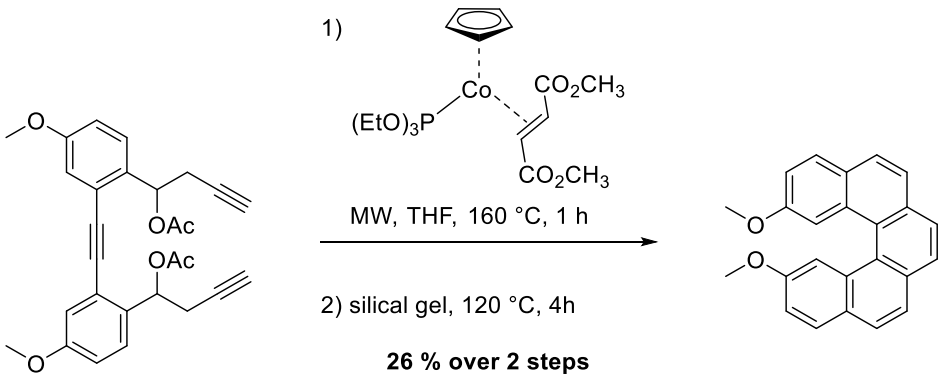

mixture of stereoisomers
18

(*rac*)-**20**

Scheme 31: [2 + 2 + 2] cycloisomerization of **18** mediated by $CpCo[P(OEt)_3]$(*trans*-dimethylfumarate) and subsequent oxidation to (*rac*)-**20**.

Consequently, a procedure adapted from their group was crafted for **18**. The reaction was assisted by microwave irradiation and heated up to 160 °C (**Scheme 31**). Unexpectedly, the air-stable catalyst exhibited the same potency as its predecessor. Although the operation under ambient air was convenient, far better results were hoped for. After the underwhelming outcome, it was concluded to leave the long-standing history of cobalt catalysts behind and change the metal center.

Generally, nickel-based catalysts outperform their cobalt counterparts but are prone to rapid decomposition.[85] From *Reppe's* discovery up to the present day, the $Ni(cod)_2$ catalyst has continued to be a staple in the [2 + 2 + 2] cycloaddition chemistry. The yellow solid is commercially available and the weakly coordinating 1,5-cyclooctadienes

can be replaced with electron rich phosphines to boost its agency.[64,72,79] Outside of the complexes involving phosphines, catalytically active Ni^0 species can be generated *in situ* by treatment of $Ni(acac)_2$ with EtMgBr.[82] If the complex carries no CO ligand, they mostly share the property that they function at room temperature. For that reason, diacetate **18** was stirred in a stock solution of $Ni(cod)_2$ in THF at room temperature overnight. The higher reactivity led to an overall yield gain of only 4 percentage points. It was not until the intermixture with triphenylphosphine that the gap widened as the addition of an electronically rich ligand boosted the performance of the catalytic system significantly (**Scheme 32**).

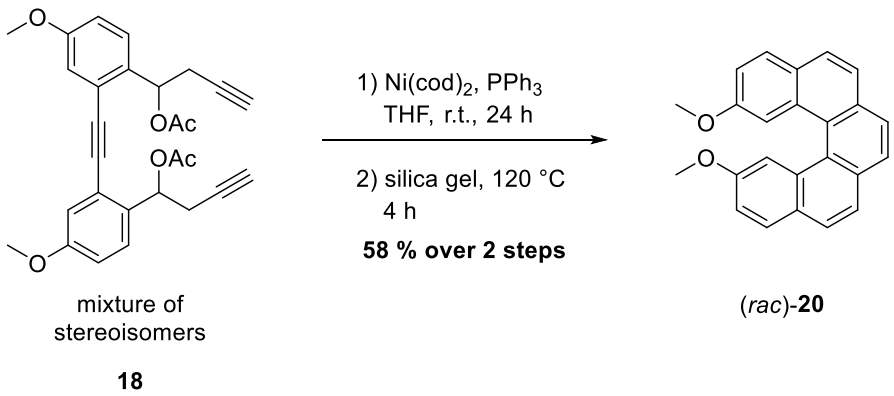

Scheme 32: [2 + 2 + 2] cycloisomerization of **18** mediated by $Ni(cod)_2$ and subsequent oxidation to (*rac*)-**20**.

Fast forward, over 2 steps, the conjunct mixture furnished 58 % of helicene (*rac*)-**20** after purification by column chromatography. In summary, the first half of the retrosynthetic analysis proved itself in praxis. Against all odds, the established, but simpler catalyst, far outshined its new-fashioned, more complex competitors. As expected, working with alcohols and aldehydes caused massive troubles which embodied a major obstacle. The silica-gel assisted aromatization was straightforward, uncomplicated and made up for the previous drawbacks to some degree. In hindsight, the organometallic addition of benzaldehydes prevailed as a useful manual for the accumulation of helicenes, but more insight in respect of the second debated strategy is needed to draw a final résumé.

The nucleophilic substitution of toluenes pre-eminently features the circumvention of aldehydes and alcohols. The lack of oxygen atoms (minus the methoxy group as the key protection group) demands a more creative course of action for the installment of the triyne framework. This strategy is banked on the opposing reactivities of aromatic

and benzylic protons (**c**atalyst, **c**old, **c**ore and **s**earing heat, **s**unlight, **si**de chain rule in basic organic chemistry curriculum). To avoid regioselectivity problems, the former place of the carbonyl function is now occupied by a methyl group. This benzylic position should react in a radical substitution S_R without any complications. But in relation to functionalized benzaldehydes, the selection of functionalized toluenes in commercial catalogues is rather slim. In particular, iodides can have exorbitant price tags. A halogenation/alkylation of disubstituted benzenes would have been feasible, but contained the risk of over-halogenation/alkylation.

The launch of the second strategy was realized with commercially available aniline **21** (**Scheme 33**). Through diazotation, anilines grant access to aryl iodides which are not that easy to get *via* conventional electrophilic aromatic substitution. Comprising the methyl group from its inception, the aniline derivative was altered to the iodide in a Sandmeyer-type reaction. The aqueous workup caused a huge mess due to perpetual salt formation. Between the quantity and the quality of the substance, the latter was given the higher priority. After purification, iodide **22** was isolated in 49 % yield. In light of the inexpensive material and a multigram batch, this was more than tolerable. At a rough estimate, 20−30 % of **22** could have been saved in a scenario of a thorough and extensive workup.

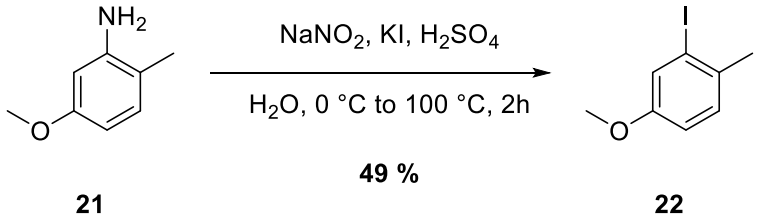

Scheme 33: Sandmeyer-type reaction of **21**.

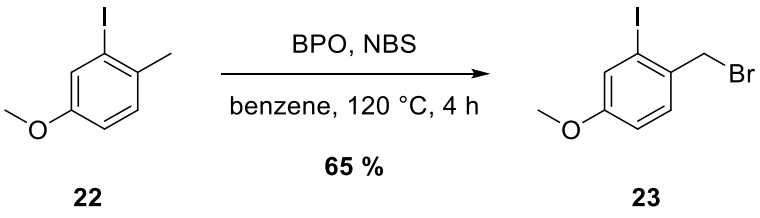

Scheme 34: Radical bromination of **22**.

Next up was the accommodation of another halide. In unison with the SSS-rule, toluene derivative **22** was stirred at 120 °C along with bromide source NBS and radical starter benzoyl peroxide in benzene (**Scheme 34**). The selective bromination at the benzylic

position proceeded smoothly. After purification, 65 % of iodinated benzyl bromide **23** was isolated.

The lateral alkyne fragment was attached through an S_N2 reaction of an *in situ* generated organolithium compound (**Scheme 35**). Surprisingly, the potency of the lithiated alkyne was disappointingly weak. The reaction only gave 14 % of alkyne **24**, side-products arising from metal-halogen exchange were not observed. However, for the most part, substrate **23** could be recycled without a sensible minus past column chromatography. Slowly but steadily, **23** was repeatedly converted to **24**. Following the implementation of the first alkyne, the implementations of the second and third were next in line.

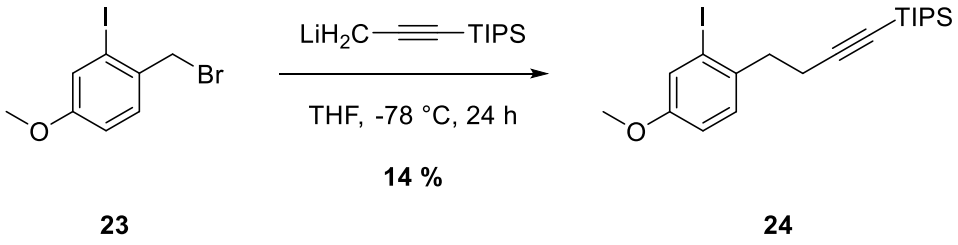

23 **24**

Scheme 35: Nucleophilic substitution of **23**.

Analogously to the initial protocol, **24** was subjected to a sequence of Sonogashira couplings. After evaluation, it was decided to discard the two-fold variant for this occasion. By doing this, a terminal alkyne could be harvested which would be a precious compound for future asymmetric cross couplings. One way or another, having iodide instead of bromide as a leaving group was advantageous for both.

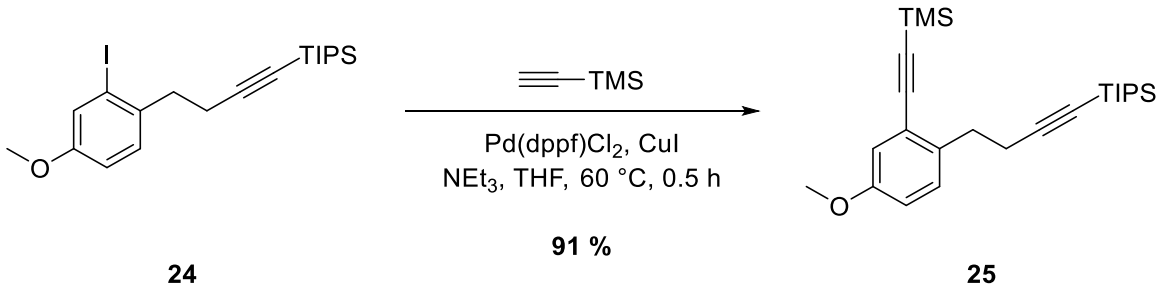

24 **25**

Scheme 36: Sonogashira coupling of **24**.

Accelerated by $Pd(dppf)Cl_2$, coupling of TMS-protected acetylene this time gave 91 % of diyne **25** (**Scheme 36**). Comparing this protocol to the preceding one, their disparities were immediately perceived in the aftermath as the absence of carbonyl

functions made the workups considerably less tedious. Encouragingly, this would not change for the imminent procedures.

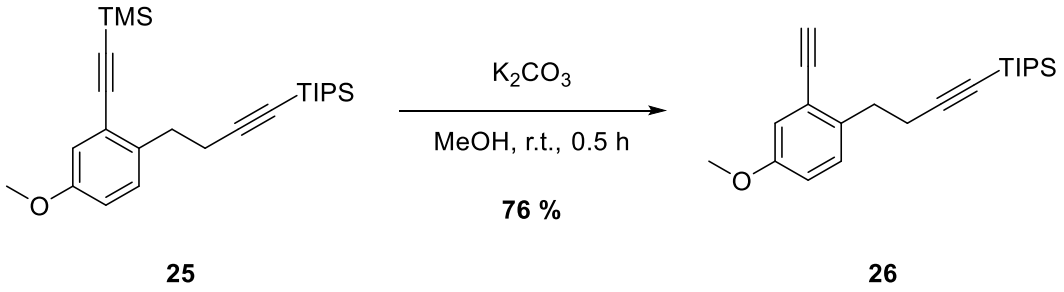

25 **26**

Scheme 37: Deprotection of **25**.

Similar to the first deprotection, the removal of the TMS group was accomplished under basic conditions. The previous almost quantitative reaction could not be replicated for **25**, free alkyne **26** was isolated in 76 % yield (**Scheme 37**).

The consecutive cross-coupling on the other side lived up to the earlier success: Terminal alkyne **26** was matched with iodide **24**, 90 % of TIPS-protected triyne **27** was isolated (**Scheme 38**). With a yield in the upper percentile, the evasion of dicarbonyls excelled to all intents and purposes. For reference, the Sonogashira couplings towards C_2-symmetric dialdehyde **16** in each case entailed roughly a bisection of the material and had a higher chromatographic effort.

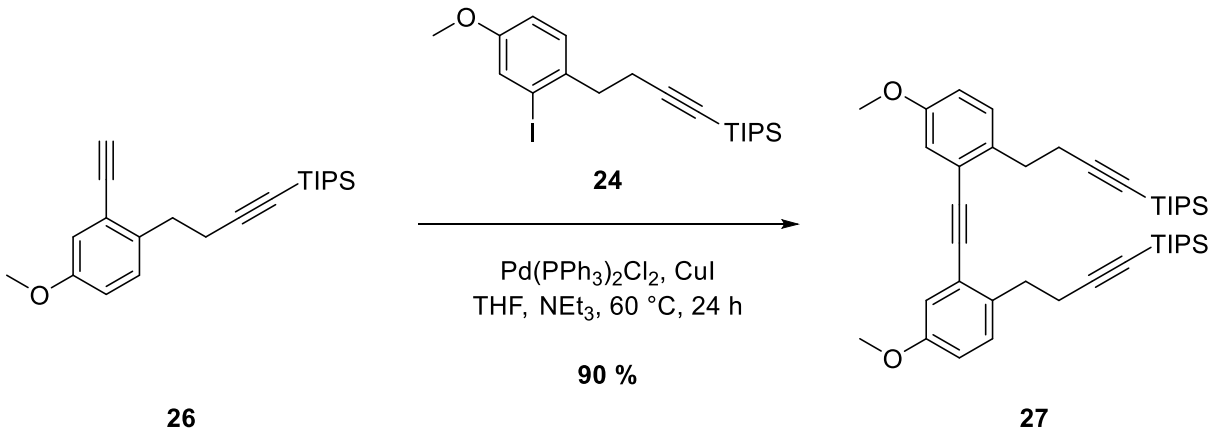

26 **27**

Scheme 38: Sonogashira coupling of **26** with **24**.

In basic media, the relative resistance of the TIPS groups is 100,000 times larger than that of the TMS group, therefore a hydrolysis was not feasible.[160] Exploiting the high affinity of silicium towards fluorides, the cleavage of the silyl group was achieved with a stock solution of tetra-*n*-butylammonium fluoride in anhydrous THF (**Scheme 39**).

After purification by column chromatography, triyne **28** was isolated in 86 % yield. With **28** in hand, next up was the key cyclization.

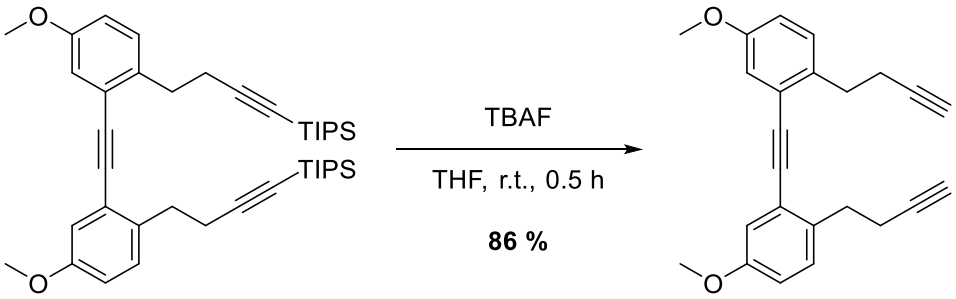

27 **28**

Scheme 39: Deprotection of **27**.

Since the duality of $Ni(cod)_2$ and electron rich PPh_3 tended to be the best system during the screening for the [2 + 2 + 2] cycloisomerization, it was the first choice. The shortage of any stereogenic centers meant no emergence of a complex isomeric mixture. Unfortunately, the high peak efficiency of 58 % could not be reached again, racemic tetrahydrohelicene (*rac*)-**29** was obtained in 38 % yield (**Scheme 40**). Based on these observations, the reaction seemed to be very volatile and unpredictable. From batch to batch, even repetition of the exact same reaction had inconsistent outcomes, possibly arising from dissimilar sizes of the charges.

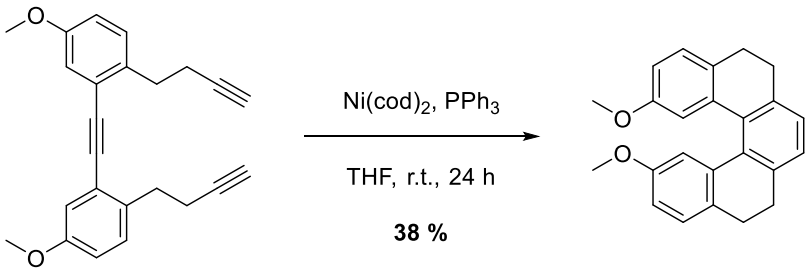

28 (*rac*)-**29**

Scheme 40: [2 + 2 + 2] cycloisomerization of **28**.

For the ensuing step, a suitable oxidizing agent had to be determined. The common denominator of reports by *Crassous*, *Starý* and *Stará* was the ineffectiveness of manganese dioxide, but there was no consensus between the supremacy of either DDQ or tritylium salts.[70,73] Due to present availability, (*rac*)-**29** was refluxed in a solution of DDQ in anhydrous toluene overnight (**Scheme 41**). The oxidation consumed a hyperstoichiometric amount of the oxidant which resulted in a surplus of a black precipitate presumably originating from badly soluble hydroquinone. A basic

filtration facilitated the workup. The tentative ^{1}H-NMR spectrum of the filtrate exhibited the same signals as anticipated (**Figure 8**). With a different strategy, after purification on silica gel, racemic 2,13-dimethoxypentahelicene (*rac*)-**20** was once more isolated in 90 % yield.

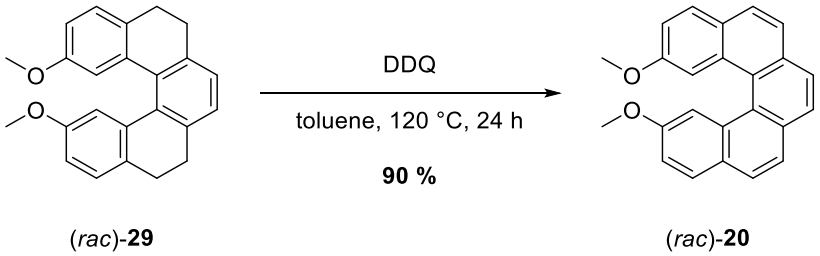

(*rac*)-**29** (*rac*)-**20**

Scheme 41: Aromatization of (*rac*)-**29**.

At large, the nucleophilic substitution strategy also turned out to be a viable pathway to helicenes. The absence of carbonyl functions in this agenda was greatly appreciated as it made the workup considerably less tedious. Between both, individual reactions in this approach had slightly lower yields, although comparing unequal substrates can somewhat be imbalanced and unfair. A larger chokepoint seemed to be the nucleophilic substitution of the alkyne unit which had a poor yield of 14 %, but the fact that the starting material could quantitatively be recovered implied that no side product formation had occurred and that the reaction could be adjusted accordingly. Either way, the methoxy functions each overcame every reaction up until the construction of the helicene. As intended, they were ready for any deliberate functionalization in the bay position.

With two good synthetic procedures in hand, naturally the accumulation of further derivatives was the next objective. Choosing the right one surely depends on many factors like substrates and cost-benefit-balance which can be outside the sphere of influence. Both have shown flaws and leave room for improvement, as well as opportunities for adjustment. The overall better yields in the first route gave it ultimately the upper hand and made it the primary strategy for future derivatives. The reliable installation of the alkynes and the straightforward silica gel assisted elimination to the helicene were vital steps which diminished the difficulties of working with the aldehydes and alcohols. Their absence in the second strategy did not justify the low yields in order to get there in the first place. Still, the nucleophilic substitution strategy is a solid backup plan if the first one fails.

1,14-Difunctionalized [5]helicene

The blueprint for an entry to the 1,14-positions was plainly accomplished by a switch of the methoxy position in the substrate from the *para*- to the *meta*-position (in relation to the aldehyde function). At the time of the contemplated acquirement, 2-bromo-3-methoxybenzaldehyde was up to 10 times more expensive than its 4-methoxy counterpart at various vendors. Thus, the journey this time started with much more affordable 2-bromo-3-hydroxybenzaldehyde **30** (**Scheme 42**). Since the hydroxy groups most likely would hamper or would not withstand certain reactions, their nucleophilicity had to be suppressed by alkylation.

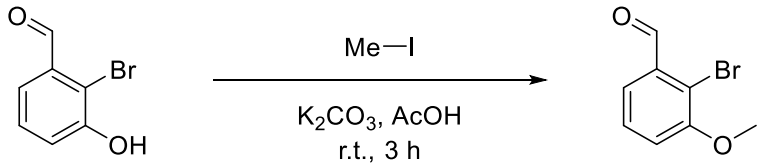

30 **83 %** **31**

Scheme 42: Methylation of **30**.

A swift Williamson ether synthesis of **30** in acetone gave 83 % of 2-bromo-3-methoxybenzaldehyde **31**. With the introduction of the methoxy group, the uniform attainment of the 1,14-difunctionalized helicene was scheduled next. The workup of aldehyde **32** was astonishingly way worse than all the previous times (**Scheme 43**). The two-fold Sonogashira coupling of **31** yielded only 5 % of dialdehyde **32**. Granted that some of **31** could have been recycled, this step still was not sustainable at all on a multigram scale.

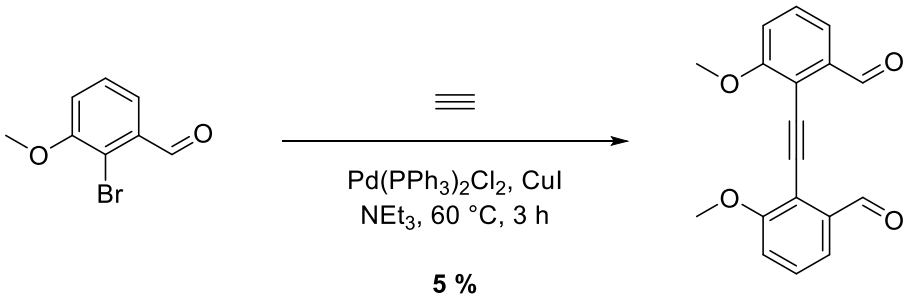

31 **5 %** **32**

Scheme 43: Two-fold Sonogashira coupling of **31**.

Attempts to improve the outcome with better ligands like SPhos brought a relative increase of over 100 %. But in absolute terms, this only translated to a yield of 11 % which can even be attributed to standard deviation. Any efforts to circumvent purification on silica gel by recrystallization failed due to excessive impurity of the mother liquor.

The idea of the sequential Sonogashira couplings was taken up again. The first cross-coupling was executed with near quantitative yield, the difference between working up mono- and dialdehydes could have been hardly more extreme (**Scheme 44**).

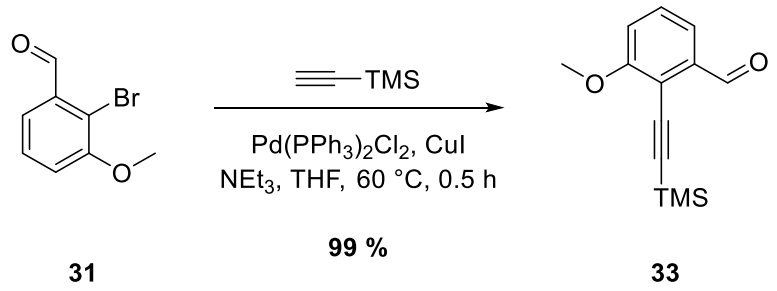

Scheme 44: Sonogashira coupling of **31**.

The deprotection of aldehyde **33** was on par with the one of diyne **25**, free alkyne **34** was obtained in 74 % yield (**Scheme 45**). Over 2 steps, the procedures reached a combined yield of 73 %, i.e. the following reaction had to at least reach an individual yield of 15 % to already secure the superior standing.

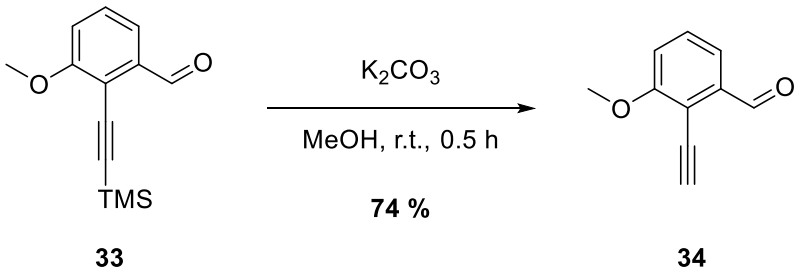

Scheme 45: Deprotection of **33**.

Luckily, the completing “one-fold” Sonogashira coupling surpassed the two-fold coupling by a wide margin. The key distinction was the evasive workup: For one thing, the conversion rate was manyfold higher, for another thing, the crude product could directly be subjected to recrystallization from ethyl acetate. Because of mono- and disubstituted products in addition to the detached ligands, this was not possible before. Omitting any purification by chromatography on silica gel, dialdehyde **32** was isolated

in 71 % yield (**Scheme 46**). With an interrelated yield of 52 % over 3 steps, the detour was more than worth it.

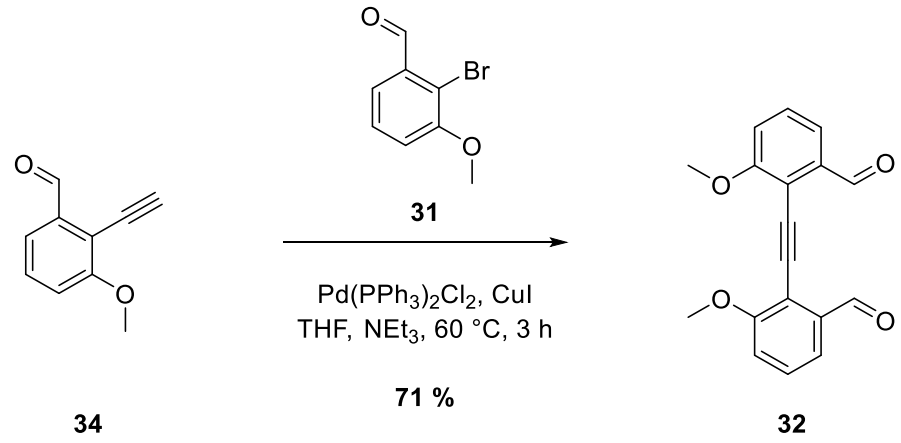

Scheme 46: Sonogashira coupling of **34** with **31**.

The organozinc addition was conducted overnight (**Scheme 47**), TLC-monitoring indicated one major tailing spot in advance. Therefore, the mixture was merely subjected to a quick aqueous workup, the crude white solid was used for the acylation without further purification.

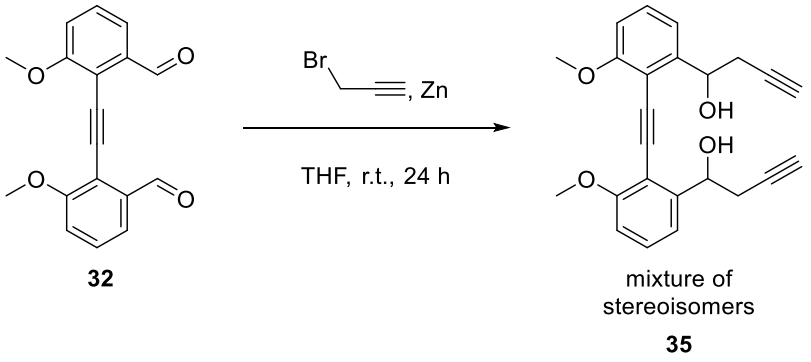

Scheme 47: Nucleophilic addition of **32**.

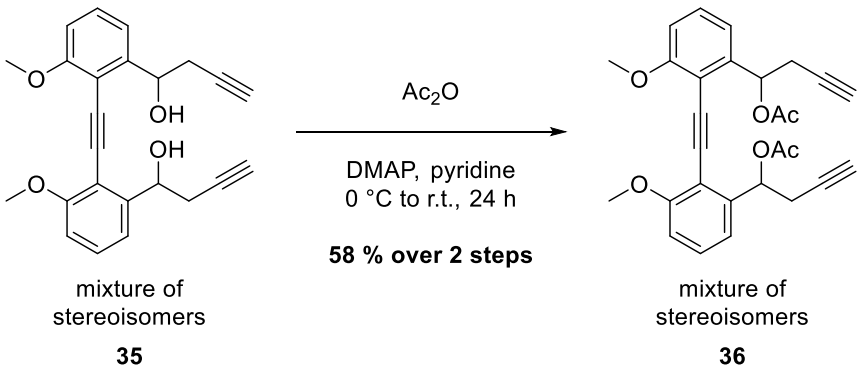

Scheme 48: Acylation of **35**.

Different than before, the mixture displayed a single retention factor for the 3 stereoisomers on the TLC. Nonetheless, since the hydroxy groups had been masked as acetates, the purification could be completed without severe complications. Over 2 steps, nucleophilic addition and acetylation of dialdehyde **32** furnished 58 % of diacetate **36** (**Scheme 48**) which is in line with the former run.

The nickel-catalyzed [2 + 2 + 2] cycloaddition (**Scheme 49**) repeatedly gave a complex mixture of species according to the TLC, probably stemming from the 6 stereoisomers and little amounts of unidentifiable species. After purification by column chromatography, the ^{1}H-NMR spectrum of the fractions did not really provide detailed enlightenment, but ESI-mass spectrometry unmistakenly depicted a prominent peak belonging to **37** in conjunction with a smaller one belonging to the fully aromatized helicene.

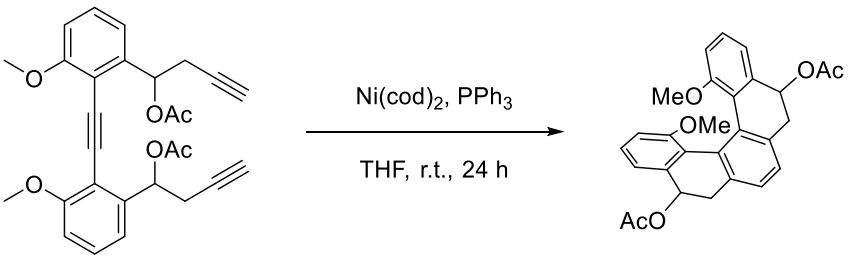

mixture of stereoisomers **36** → mixture of stereoisomers **37**

Scheme 49: [2 + 2 + 2] cycloisomerization of **36**.

Regardless, the unified fractions containing the stereoisomers of **37** and parts of the aromatized helicene were stirred at 120 °C in silica gel. After 4 h, their extraction with DCM converged every species to racemic 1,14-dimethoxypentahelicene (*rac*)-**38** (**Scheme 50**).

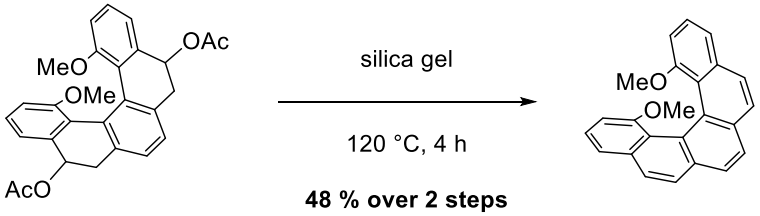

mixture of stereoisomers **37** → (*rac*)-**38**

Scheme 50: Silica gel-assisted Aromatization of **37**.

Its formation was proven by both ^{1}H-NMR (**Figure 10**) and ESI-mass spectrometry. Strangely, in retrospect, the partial existence of helicene **38** after the cyclization towards **37** was not evident by the ^{1}H-NMR alone this time as no fraction unambiguously displayed any traces of **38**. While a minor peak in the ESI(+)-spectrum of **37** could be assigned to protonated **38**, mass spectrometric experiments of pure **38** later on revealed that it is not easily protonated so that the exact mass needed to be recorded by EI-mass spectrometry.

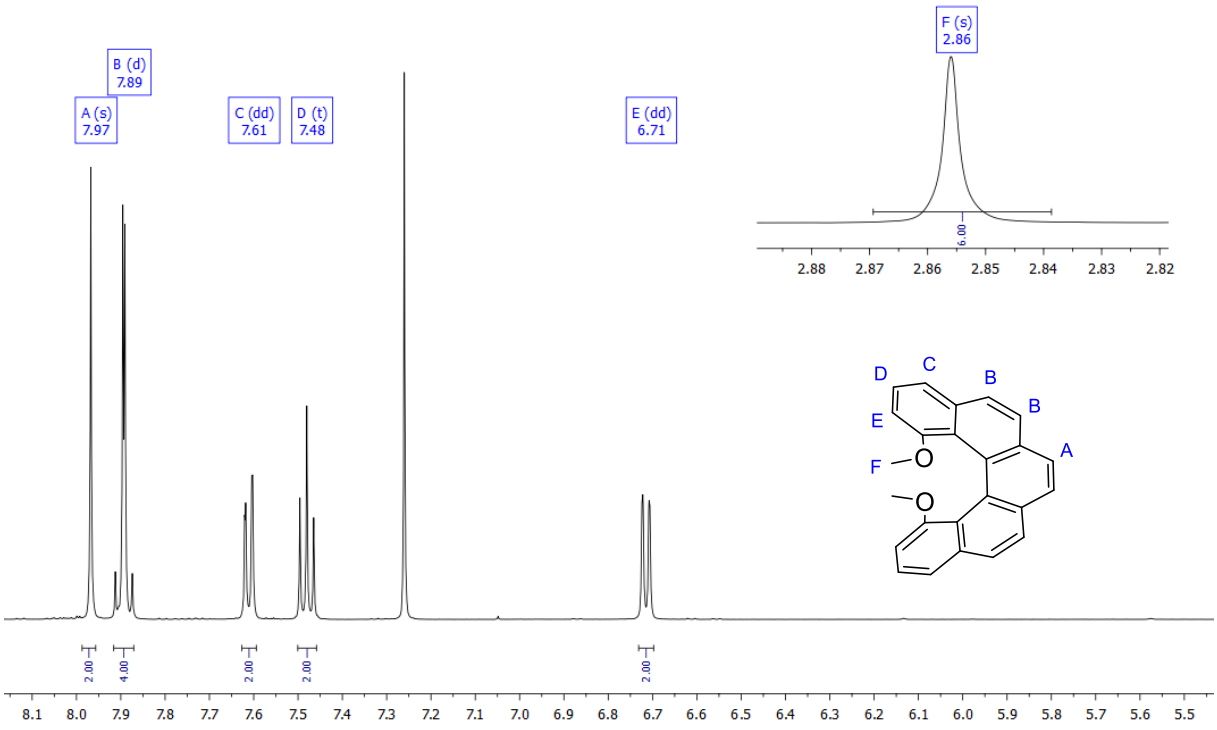

Figure 10: ^{1}H-NMR spectrum and assignment of (*rac*)-**38**.

Over 2 steps, the yield added up to 48 %. For the second time, the reaction was accompanied by reoccurring inconsistency and unpredictability since different batches had a deviation of up to 30 percentage points in yields. On average, this cyclization had a weaker performance than that of the 2,13-difunctionalized helicene. But this can be explained with the rationale that the 1,14-positions are intrinsically more crowded which makes the precursor less likely to cyclize. The favorability of **20** over **38** is further supported by the fact that a non-negligible fraction of **20** could be isolated during the cyclization towards the tetrahydrohelicene. Based on this, it can be assumed that **38** has a higher distortion than 2,13-difunctionalized **20** which results in a higher dihedral angle. But in order to verify this thesis, XRD analysis was required.

1,13-Difunctionalized [5]helicene

So far, the *modus operandi* has been the acquirement of C_2-symmetric building blocks. Of course, this was not done solely for symmetry's sake: Keeping the symmetry persistent throughout the whole operation simplifies the synthesis, characterization and analysis immensely. But asymmetric, polydentate ligands can exhibit interesting phenomena that are not observed in symmetric ones: The higher variety caused by non-equivalent binding sites can lead to different coordination modes and diastereomeric diversity. This along with the proof of concept of the synthetic method, getting hands on a 1,13-difunctionalized [5]helicene was the next target.

Needless to say, the synthesis of non-symmetric molecules is usually more difficult, e.g. the two-fold Sonogashira coupling is not viable here. Fortunately, the components required for the first step were already available prior to their need. Since the asymmetric triyne basically consisted of one half of triyne **16** and another half of triyne **32**, it could be constructed by either Sonogashira coupling of 3-methoxy alkyne **34** and 2-bromo-4-methoxybenzaldehyde **13**; or 4-methoxy alkyne **15** and 2-bromo-3-methoxybenzaldehyde **31**.

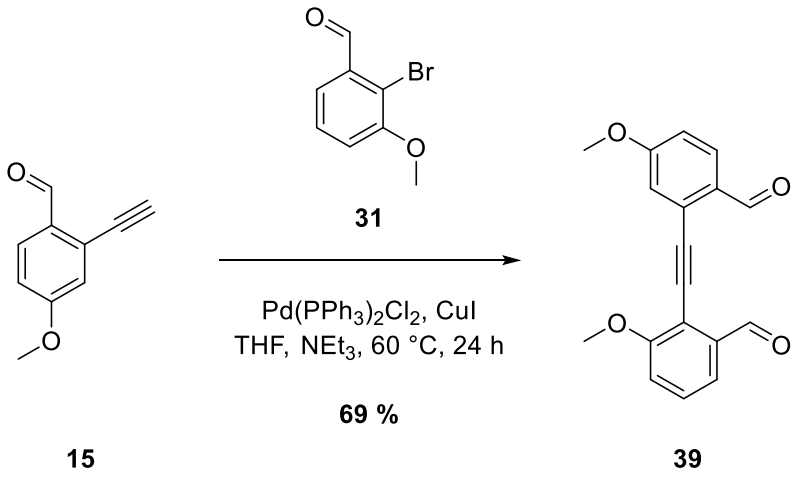

Scheme 51: Sonogashira coupling of **15** with **31**.

Due to present availability, it was opted for the latter. Coupling of **15** with **31** under routine Sonogashira coupling conditions gave rise to non-symmetric dialdehyde **39** (**Scheme 51**). Evaluation of the ^{1}H-NMR spectrum of **39** clearly validated the presence of magnetically dissimilar aldehyde as well as methoxy functions. With 69 %, the reaction had an exceptionally high yield given that the purification of dialdehydes by column chromatography has empirically been nothing but a chore until then.

Dialdehyde **39** was treated with a mixture of propargyl bromide and zinc in THF (**Scheme 52**). According to the TLC, the potential idea of a column chromatographic workup of the diol was quickly omitted once more. The isomeric mixture of **40** was subjected to an aqueous workup and readily used for the subsequent reaction.

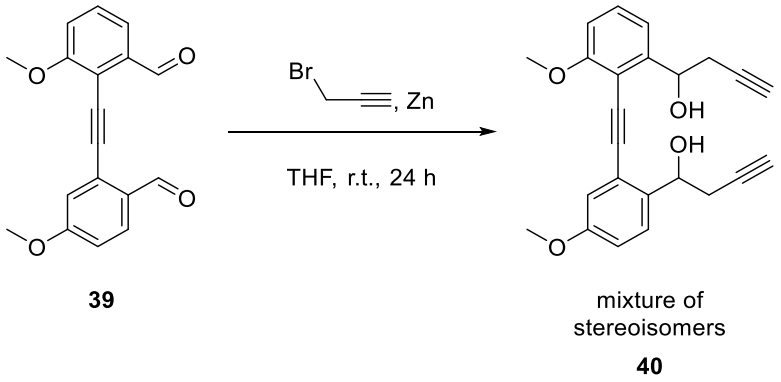

Scheme 52: Nucleophilic addition of **39**.

Luckily, acylation of **40** went smoothly. After purification of the crude mixture by column chromatography, an isomeric mixture of diacetate **41** was gained (**Scheme 53**). Over 2 steps, the yield was 39 %.

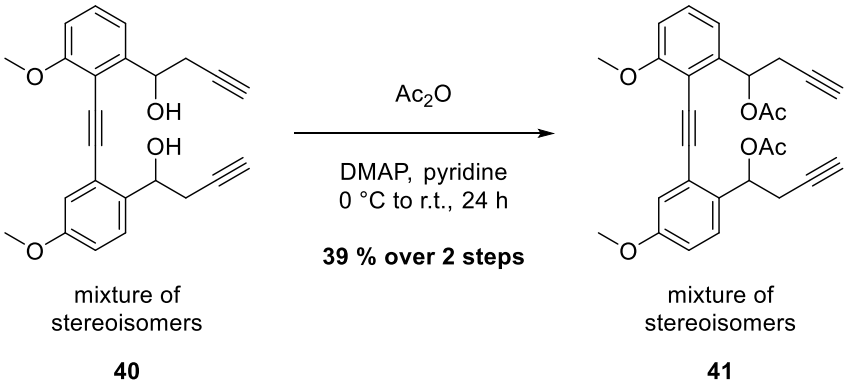

Scheme 53: Acylation of **40**.

Last but not least, diacetate **41** underwent the [2 + 2 + 2] cycloisomerization under Ni^0 catalysis. Over 2 steps, racemic 1,13-dimethoxypentahelicene (*rac*)-**43** was obtained in 68 % yield past oxidative aromatization in silica gel (**Scheme 54**). The surprisingly high yield was puzzling and somehow contradicted the earlier postulated thesis of favorable cyclization in dependence of crowdedness. Ironically, the volatility of the reaction stayed constant. Due to double the amount of signals in the ^{1}H-NMR spectrum caused by the loss of symmetry, an unequivocal identification was more complicated (**Figure 11**). Particularly the clumping of 6 aromatic protons into a large multiplet made

the full characterization awkward, but the unidentical methoxy functions and mass spectrometric experiments supported the presence of (*rac*)-**43**.

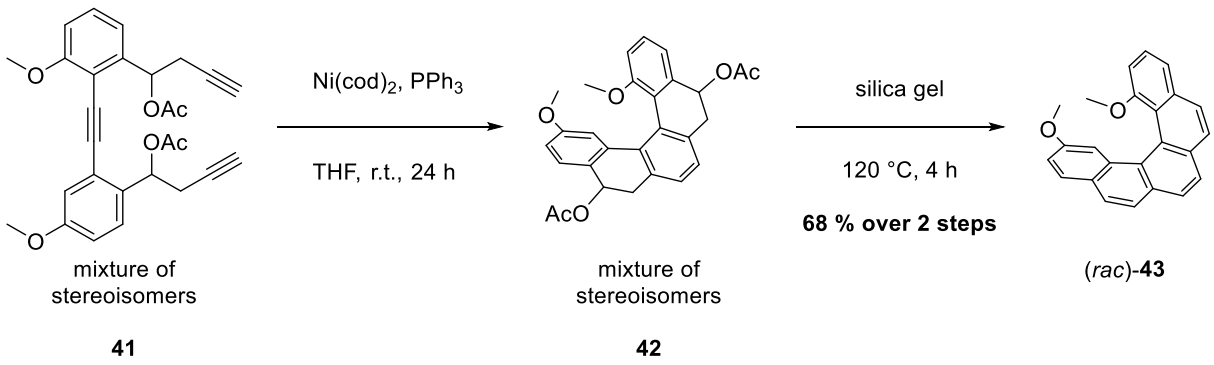

Scheme 54: [2 + 2 + 2] cycloisomerization of **41** and subsequent oxidation to pentahelicene (*rac*)-**43**.

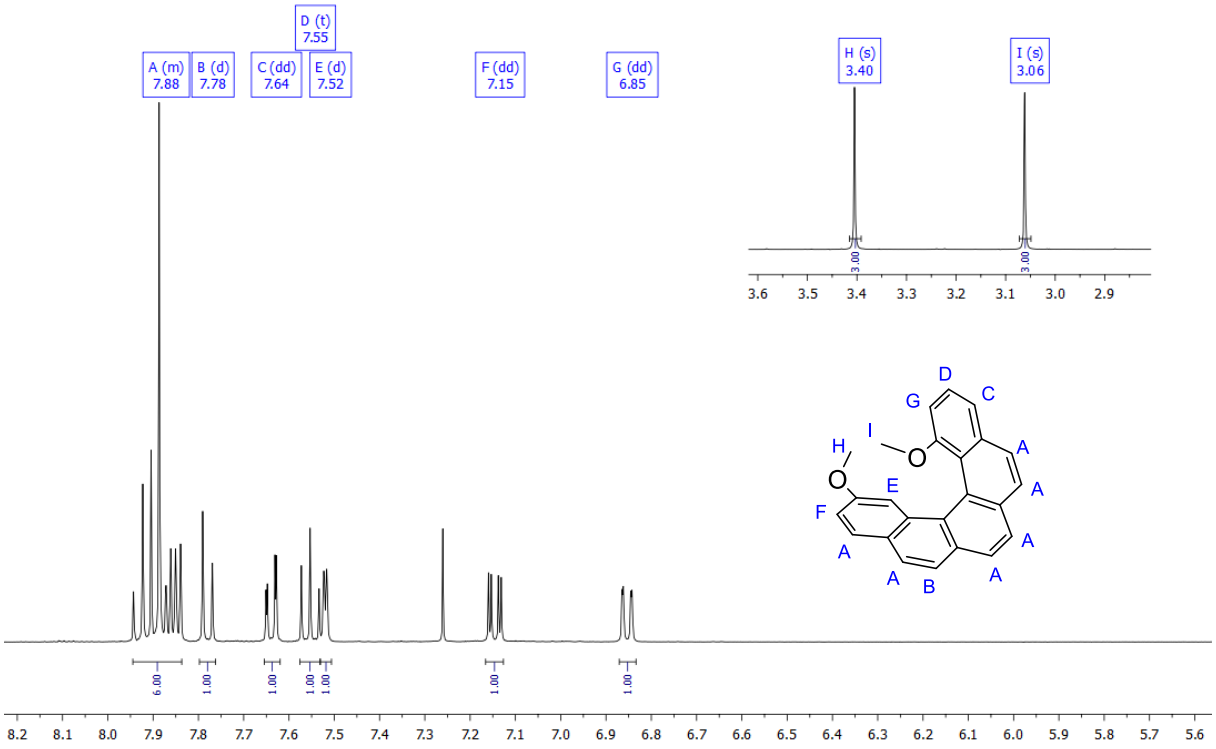

Figure 11: ^{1}H-NMR spectrum and assignment of (*rac*)-**43**.

Concluding with the third attempt towards a difunctionalized pentahelicene, the strategy proved to be efficient and versatile to the utmost satisfaction. The modularity allowed for the access to every proposed constitutional isomer. At no time during each route was there any reason to believe that the remaining isomers are not accessible, as long as the functionalization happens at the termini. Admittedly, the access to the outer positions remains denied, but functionalization in these is of less interest in the context of this work.

4.2 [7]Helicene

At this point, keeping the numerical order would be logical from a narrative point of view. But synthetically and strategically, aiming for heptahelicenes instead of hexahelicenes next was more sensible: In the synthetic route for [7]helicenes, the C_2 symmetry is retained for a longer period of time, whereas the [6]helicene gains its symmetry not until the cyclization which significantly facilitates the characterization of respective species. In light of the practical implementation, the starting piece should be a naphthalene unit. Advantageously, this opened up further locations for functionalization. The switch from pre-modified benzenes to naphthalenes extended the entrance from positions 1−4 to 1−6 on each side of the helicene, respectively (**Scheme 55**).

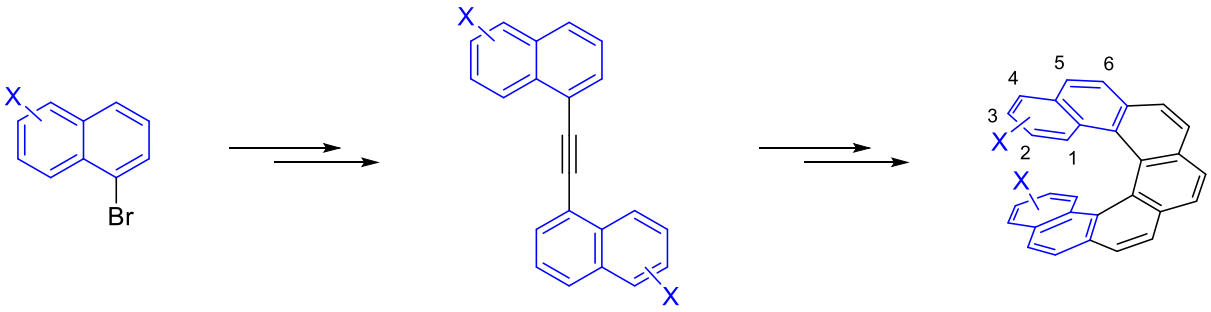

Scheme 55: Access to positions 1−6 in [7]helicene.

As for parent [7]helicene itself, the aromatic hydrocarbon unexpectedly has a dihedral angle that is no more than 4 degrees above that of [4]helicene. This means that the angle increases within the homologous series up until [6]helicene before it is divided in half at [7]helicene.[127] While the sudden bisection can be counterintuitive, the slope of the thermal stability remains consistent. The (*P*)- and (*M*)-enantiomers are disconnected by a kinetic barrier of approximately 40 kcal/mol which is more than enough for the prevention of spontaneous racemization.[15] Altogether, the drastic change in spatial orientation of the outer benzene units from penta- to heptahelicene also includes a change of the donor angle for proposed bidentate ligands.

Mixing penta- and heptahelicenes for the purpose of heteroleptic supramolecular complexes can also be envisaged since it can open up endless capabilities, especially if non-symmetric or unequal donor motifs within the same molecule come into play.

2,17-Difunctionalized [7]helicene

Commercially, trifunctionalized naphthalenes are scarce and consequentially expensive. In fact, not many naphthyl halides bearing a methoxy group are known in literature at all. Principally, an electrophilic aromatic substitution on naphthalene could work, but would likewise be too convoluted, uncertain and inefficient concerning regioselectivity or even reactivity in general. A safer approach would be the usage of its hydrogenated congener tetralin which tends to autoxidize[161] to naturally occurring 1-tetralone.[162] Due to its importance as a key intermediate for the synthesis of (−)-dezocine (Dalgan), an opioid analgesic with a market capacity over 40 % in China,[163] the latter is largely explored in terms of chemical behavior and affordable in large quantities.[164–168]

Starting from 7-methoxy-1-tetralone **44**, several studies showcased a 2-step protocol to the desired trifunctionalized naphthalene **45** (**Scheme 56**).[169–171] Indeed, Vilsmeier-Haack-type reaction of the aldehyde gave rise to vinyl bromide **45**, albeit with very little yield. This was assumedly caused by the size of the batch: The multigram charge resulted in an extraordinary amount of gas, heat and salt formation during the aqueous workup. Cautious treatment of the aqueous phase was required because of the imminent danger of corrosive HBr and sudden pressure build-up in a closed system. As a precautionary measure, a good portion of **45** was preventively discarded over the course of the workup. Relatively, the yield was unsatisfying and left much to be desired, but absolutely, 29 % of a multigram batch was sufficient for the time being.

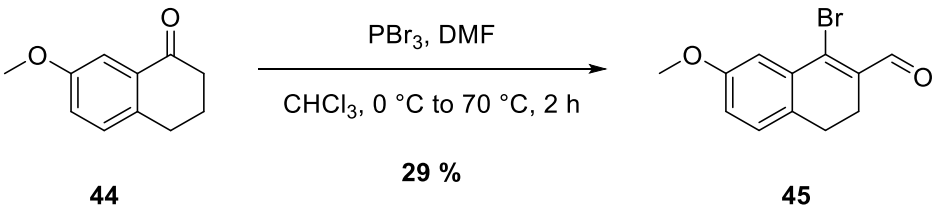

Scheme 56: Vilsmeier-Haack-type reaction of **44**.

Vinyl bromide **45** was then refluxed with DDQ in toluene overnight (**Scheme 57**). The workup was done in the same manner as the oxidation to 2,13-dihydroxypentahelicene **20**, the anticipated filtration of the already familiar hydroquinone facilitated the process immensely. Following the purification on silica gel, with 88 % yield, only a loss of 2 percentage points was recorded in comparison to the aromatization towards the

helicene. From here on, the next step could again be divided into two pathways, namely the one-fold and the two-fold Sonogashira coupling. Experientially, the latter has delivered mixed results so far, but was given the benefit of the doubt. At the very least, 2 steps could be saved that way.

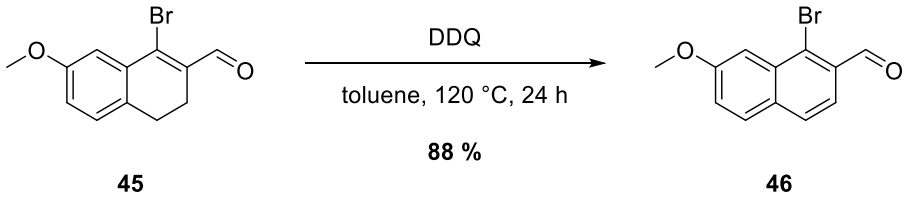

45 **46**

Scheme 57: Oxidation of **45**.

Thus, bromide **46** was subjected to a default Sonogashira procedure (**Scheme 58**). Anticlimactically, the outcome was more underwhelming than before. Granted that the purification of dialdehydes had been the same bad experience, the variances between the ^{1}H-NMR spectra of pre- and post-purification were vanishingly small. The tailing made a meaningful collection of a single fraction impossible. At least 3 distinguishable signals in the down-field region around 11 ppm were assigned to aldehyde functions, 4 signals in the up-field region around 4 ppm were assigned to methoxy functions, signals in the aromatic area and the ratio of the integrals were all over the place (**Figure 12**, middle). Supposedly, homocoupling of 2 identical partners and mono-substitution occurred at different rates. Unfortunately, ESI-mass spectrometry did not provide any clarity.

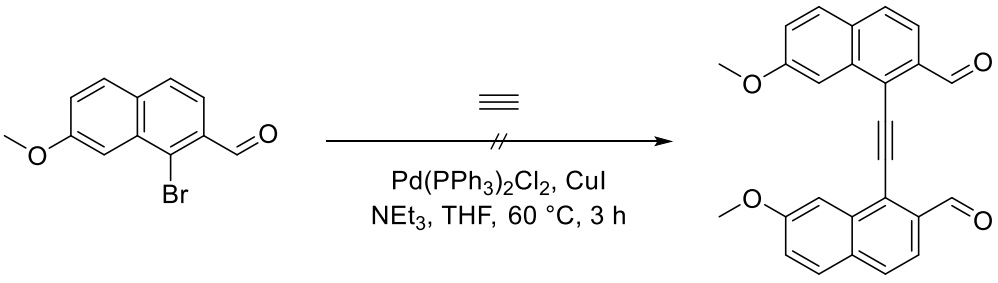

46 **47**

Scheme 58: Two-fold Sonogashira coupling of **46**.

In 2021, the group of *McConnell* demonstrated a copper-free, one-pot Sonogashira coupling for the preparation of symmetric diarylalkynes (**Scheme 59**).[172] In this publication, they overcame usual problems such as the copper-mediated homocoupling of acetylides while maintaining excellent yields. The innovative

exploitation of TBAF as a multifunctional agent made the requirement of a Cu^{I} co-catalyst and an amine base obsolete. Apparently, it was capable of (i) activation of the Pd^{0} species *via* formation of anionic Pd species, (ii) stabilization of low-coordination Pd^{0}, (iii) formation of the acetylide *via* deprotonation, (iv) deprotection of the silyl group *in situ* and (v) phase-transfer catalysis for the inorganic base/substrate/product phases all at once.[173–176] Their work offered a sophisticated way to bipyridine- and benzimidazole-based ligands in just 1 step.

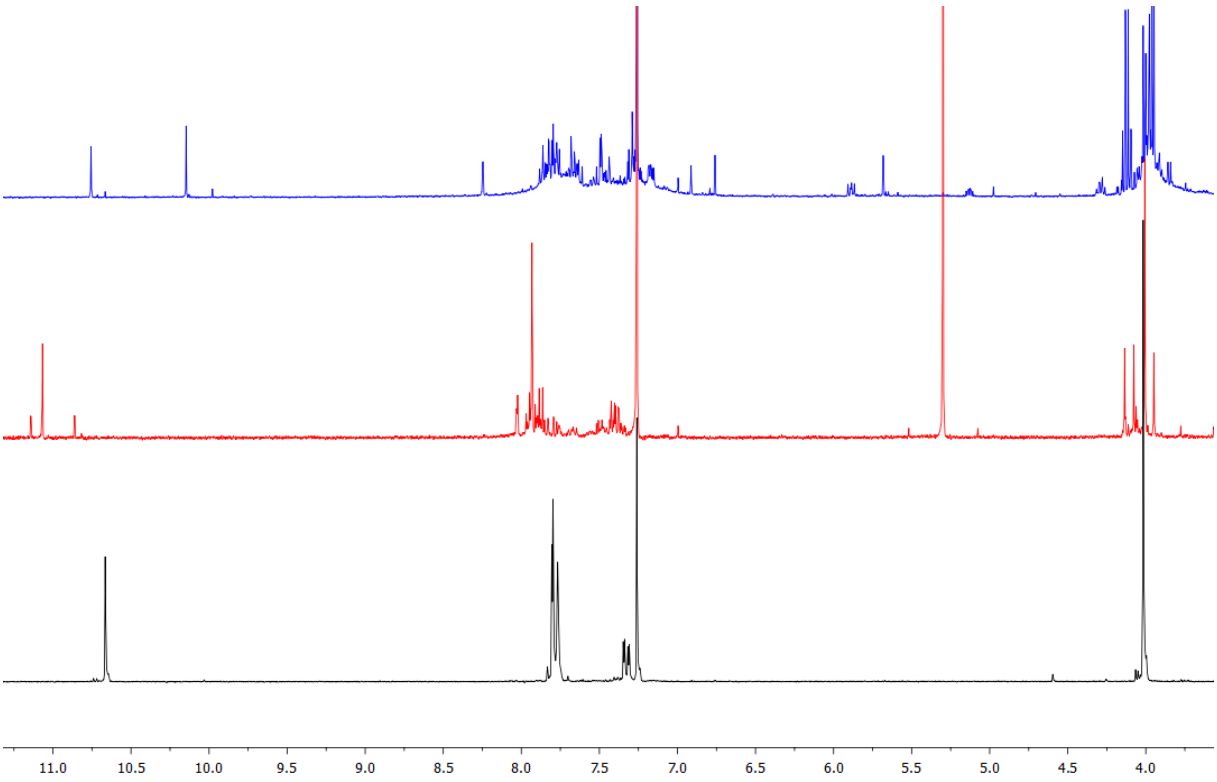

Figure 12: Comparison of ^{1}H-NMR spectra of substrate **46** (bottom), default two-fold Sonogashira coupling of **46** (middle) and copper-free Sonogashira coupling of **46** (top).

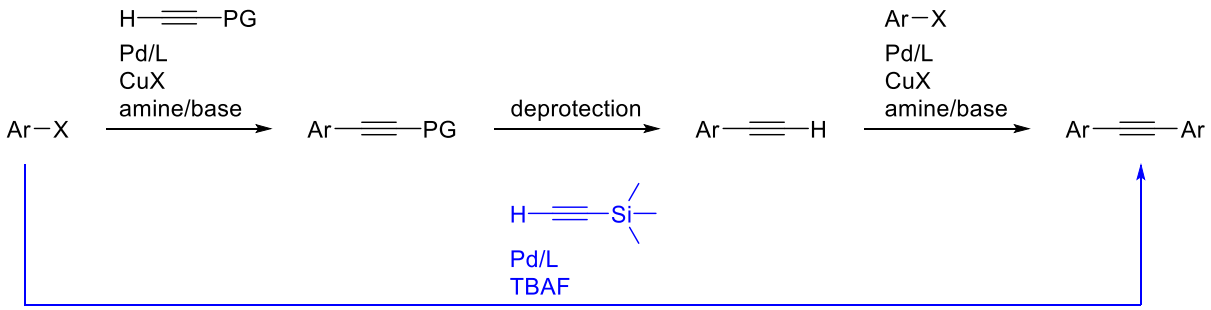

Scheme 59: Synthesis of diarylacetylenes in 3 steps (black) and copper-free method in 1 step (blue).

To counteract the release of gaseous acetylene, the reaction was carried out in a pressure tube. Although only half an equivalent of TMS-acetylene would have been sufficient for the coupling to a symmetric diarylalkyne, the authors observed a better performance when committing to one equivalent. Notably, degassing of the stock solution of TBAF in THF did not bring any advantage. Accordingly, aldehyde **46** was mixed with TMS-acetylene in a 1:1 ratio and stirred at 85 °C in a pressure tube (**Scheme 60**). The workup was reminiscent of the prior Cu^{I}-catalyzed variant, but comparison of the ^{1}H-NMR spectra did not cause a *déjà vu* (**Figure 12**, top). If anything, the new spectrum showed more similarities to that of substrate **46**. Seemingly, a larger amount of the aldehyde remained unreacted as its aldehyde signal was discerned in both. The lack of the same aldehyde signals when compared to the default Sonogashira coupling supported the hypothesis of no Glaser coupling, but for some reason, the reaction was not as selective as hoped for.

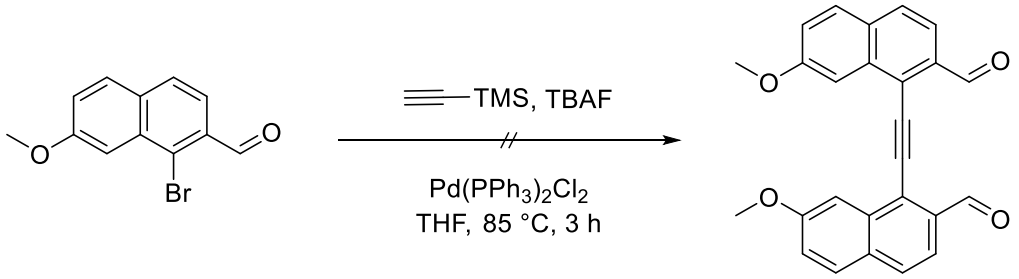

46 **47**

Scheme 60: Copper-free Sonogashira coupling of **46**.

For good measure, the same conditions were applied to the already decoded two-fold coupling of benzaldehyde **13**. This time, only 1 aldehyde signal appeared, but it did align to neither the desired dialdehyde **16** nor to any of the intermediates **14** and **15** (**Scheme 61**).

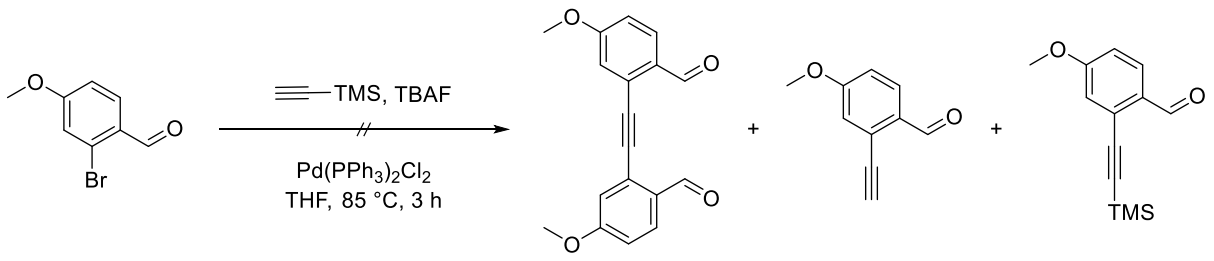

13 **16** **15** **14**

Scheme 61: Copper-free Sonogashira coupling of **13**.

The reaction illustrated the necessary avoidance of any side products which is ensured best by a successive coupling in 3 steps. In a best-case scenario, purification by silica gel can be skipped by recrystallization this way. A synthesis of a [5]helicene from a tetralone derivative by *Usui et al.* suggested a change in the order of the individual steps.[168] Therein, they carried out the cross-coupling reaction with the vinyl halide gained from the Vilsmeier-Haack-type reaction and oxidized it afterwards with DDQ (**Scheme 62**).

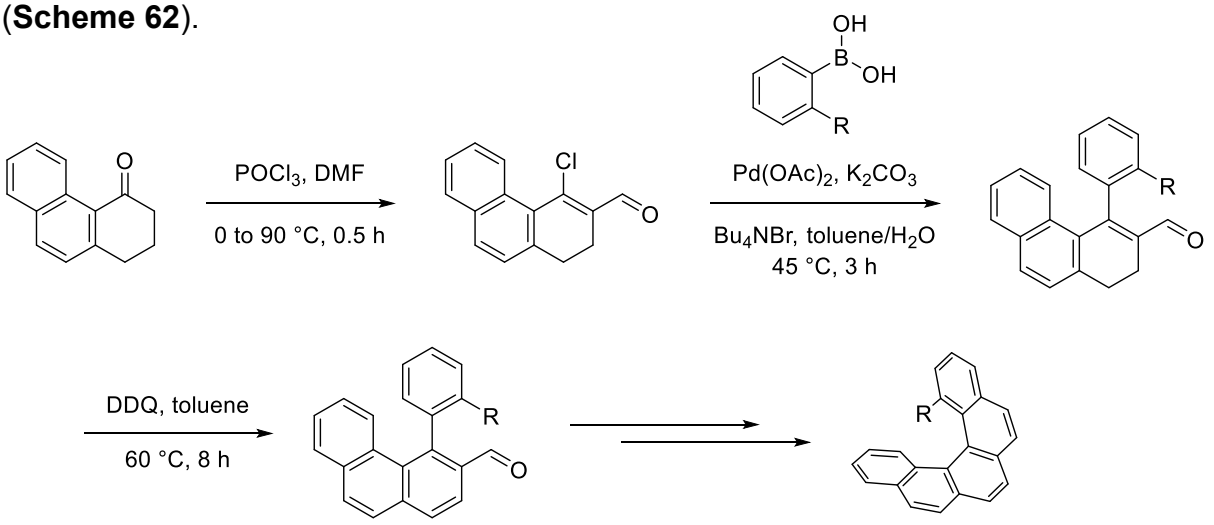

Scheme 62: Synthesis of [5]helicenes by *Usui et al.* (R = OMe, Me).

Following that notion, TMS-acetylene was coupled with vinyl bromide **45** (**Scheme 63**). Fortunately, a quantitative amount of **48** could be accumulated after purification by column chromatography.

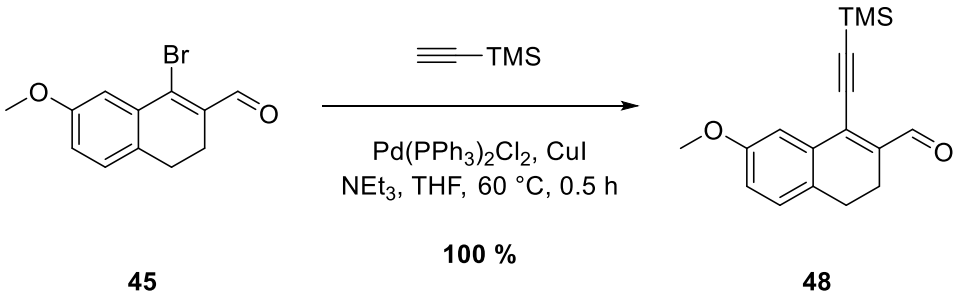

45 **48**

Scheme 63: Sonogashira coupling of **45**.

The deprotection of the TMS group was carried out in basic media. With the complete conversion and isolation from the last reaction in mind, a yield of 77 % during the deprotection of the TMS group was acceptable (**Scheme 64**). A higher value could have likely been achieved by prolonged stirring or usage of more selective fluoride sources like TBAF, but in order to figure out the most optimal synthetic route to the desired, difunctionalized heptahelicene, a quicker experiment was given priority.

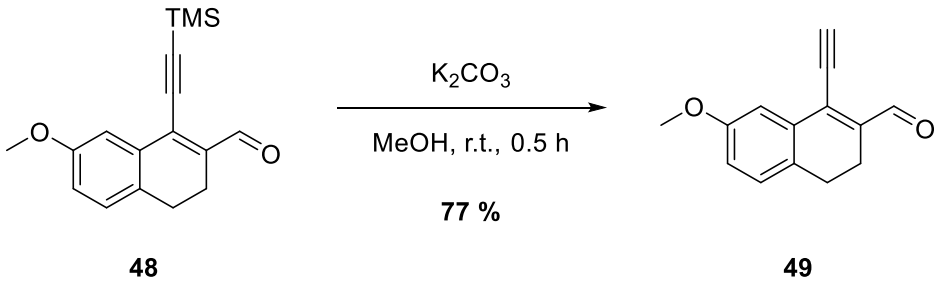

Scheme 64: Sonogashira coupling of **48**

In contrast to the reaction towards bisbenzaldehyde **47**, the excessive and immediate precipitation of a yellow solid within the first seconds of the next reaction was a good sign. As a matter of fact, the solid was easily crystallizable from ethyl acetate, 82 % of bisvinylaldehyde **50** was collected as pure crystals (**Scheme 65**).

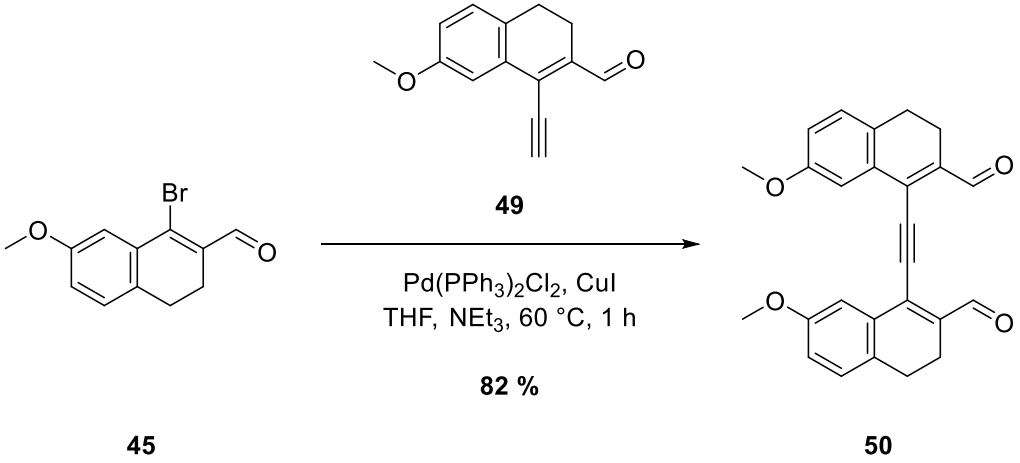

Scheme 65: Sonogashira coupling of **45** with **49**.

The order of the sequences in *Usui's* path may have appeared arbitrary, but it did work out exceedingly well for the purpose of compiling **50**. The ensuing oxidation on the other hand was doubted since dialdehyde **47** is still formed in the end. Expectedly, oxidation of a small sample validated the apprehensions as the same problems arose.

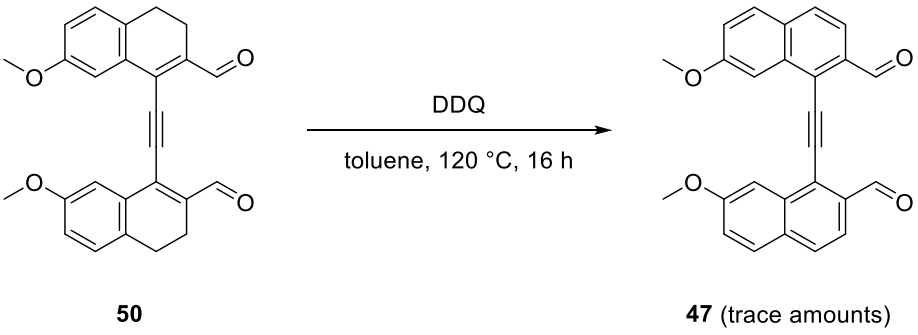

Scheme 66: Oxidation of **50**.

To be fair, mass spectrometric experiments this time showed an infinitesimal signal of **47**, but its isolation remained inconceivable by routine chromatography (**Scheme 66**). Therefore, the order of events was switched around once again.

Compound **47** itself was not a crucial intermediate for the synthetic route, the indispensable sections within the molecule were the already established carbonyl functions which greatly enhanced its reactivity. The retention of the vinyl groups up until the aromatization could very well have a more positive impact on the sequence. If the elimination of the acetates fails for whatever reason, an oxidation with DDQ at that stage would take care of it anyways, killing two birds with one stone.

Proceeding with **50**, the nucleophilic addition was carried out overnight. Surprisingly, the column chromatographic workup of diol **51** was challenging, but feasible. Purification on silica gel got rid of gross impurities like substrates and mono-substituted side products. It is highly doubtful whether the fully unsaturated diol originating from benzaldehyde **47** would have been as easy to clean, but the question “what if” was irrelevant anyways as long as the current pathway was expedient. **51** could be identified in the ^{1}H-NMR spectrum and in mass spectrometric experiments, in total, 45 % was accumulated (**Scheme 67**).

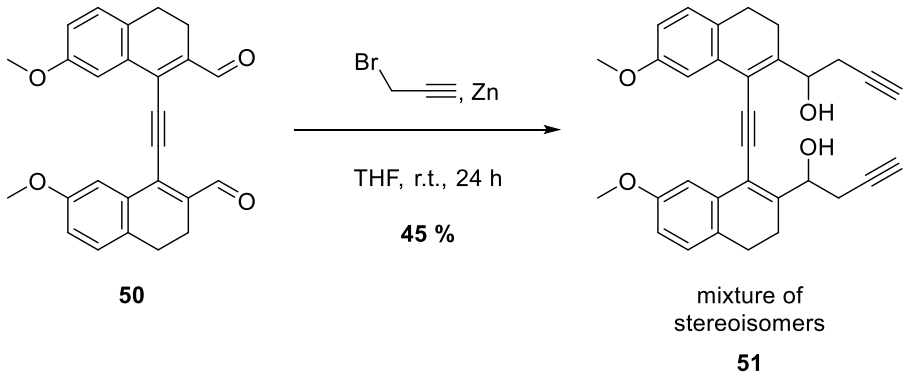

Scheme 67: Nucleophilic addition of **50**.

Leaving the worst chapters in the synthetic route behind, the transformation of the hydroxy groups to the esters was targeted. Stirring diol **51** with acetic anhydride in pyridine overnight led to diacetate **52** in 73 % yield (**Scheme 68**). Mutually, the nucleophilic addition and the acylation delivered a joint yield of roughly 33 % over 2 steps. This is outside of the range of the previous experiments in which the crude diols were directly converted to the respective diacetates. These sequences had a range in

yield of 40 to 60 %, perhaps the same could have been achieved here without the extensive purification of the diol.

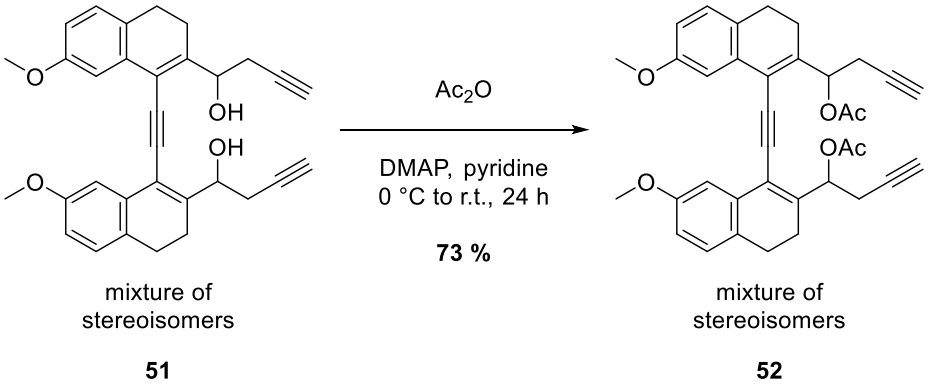

Scheme 68: Acylation of **51**.

At this point, the oxidation of the diacetate was theoretically imaginable as well, but treatment with DDQ was postponed to a later point in which the number of functionalities within the compound were at a minimum. This reduced any risk of unwanted side reactions. Thus, triyne **52** was cyclized under Ni^0 catalysis overnight (**Scheme 69**).

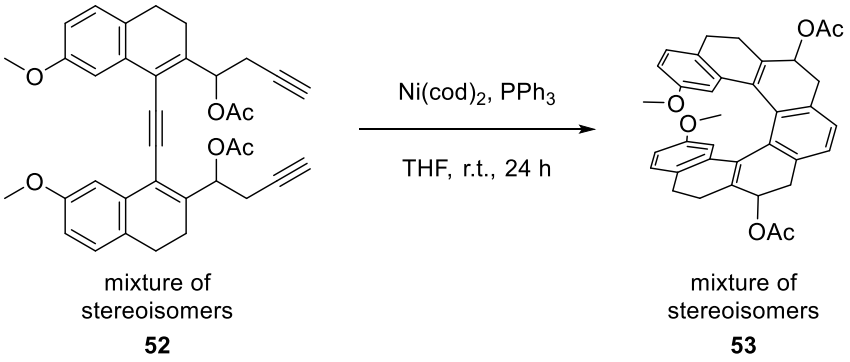

Scheme 69: [2 + 2 + 2] cycloisomerization of **52**.

TLC-monitoring indicated at least three spots which were tentatively assigned to the diastereomers of **53**. As a consequence, the crude mixture was only subjected to filtration over silica gel. Drawing conclusion based on ^{1}H-NMR analysis of the filtrate was unreliable because of heavy overlap of the signals in conjunction to multiple sets of signals induced by the believed diastereomers. APCI-mass spectrometric measurements elucidated a one- and two-fold elimination of the acetates to the tetra- and hexahydrohelicene derivatives. However, a protonated species of **53** itself was not found. This implies that hydrated [7]helicenes are more inclined to spontaneous elimination than the [5]helicene analogues. Presumably, the more compressed

[7]helicene (dihedral angle of [7]- and [5]helicene = 30° vs 54°[127]) causes more tension and a smaller degree of freedom within the system which is expressed in a more improbable maintenance of the tetrahedral angles in the sp^3-centers and an easier elimination at those positions (**Figure 13**). Unfortunately, a low yield was foreseeable during the cyclization: The mixture of mono- and di-eliminated species made a proper determination impossible, but even in a best-case scenario the absolute values forecasted a huge deficit. Again, this can be interpreted as a more unfavorable cyclization towards hydrated [7]helicenes than [5]helicenes. The combination of sp^3- and sp^2-centers demand a cooperative conformation which is not given in the [7]helicene framework. Furthermore, unlike naphthaldehyde **47**, partly saturated **52** comprises two additional "naked" double bonds which are exposed to polymerization.

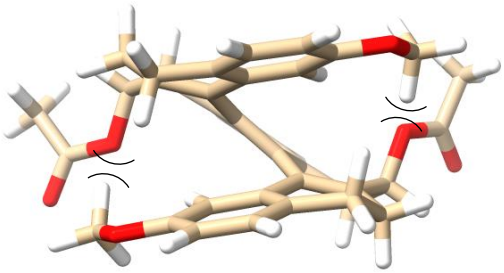

Figure 13: GFN2-xTB[177,178] minimized structure of (*R*,*R*)-(*P*)-**53** (carbon in brown, hydrogen in white, oxygen in red). Turning sp^3- into sp^2-centers could relieve tension due to the changes in orientations, sizes and numbers of the substituents.

Silica gel-assisted elimination confirmed the assumption. Over 2 steps, 10 % of racemic tetrahydroheptahelicene (*rac*)-**54** was gathered (**Scheme 70**). Reiterations of the experiment consistently reassured the hypothesis by giving lower yields than related [5]helicene: The drastic change in torsion angles is reflected by the lower willingness to cyclize as the interior gets too crowded.

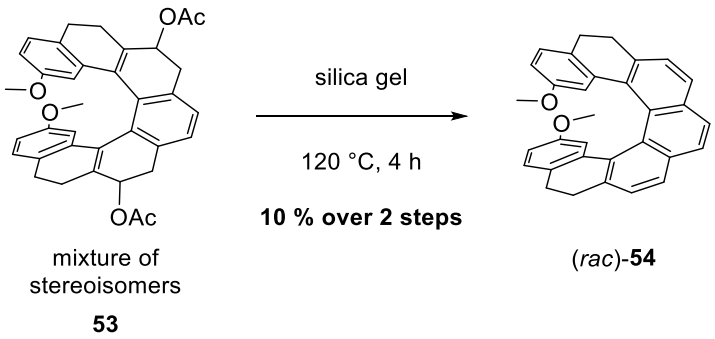

Scheme 70: Silica gel-assisted aromatization of **53**.

(*Rac*)-**54** was characterized by both ^{1}H-NMR and mass spectrometry. While the existence of **54** could already be seen in the mass spectrum of the cyclization towards diacetate **53**, the ^{1}H-NMR spectrum this time showed the prominent signals of the diastereotopic benzylic protons which were the center of attention for the next operation. Since the oxidation of vinyl aldehyde **50** did not occur until that time, it could not be delayed any further. The final reaction was carried out overnight in refluxing toluene. After filtration and purification on silica gel, fully aromatized racemic 2,17-dimethoxyheptahelicene (*rac*)-**55** was acquired in 82 % yield (**Scheme 71**).

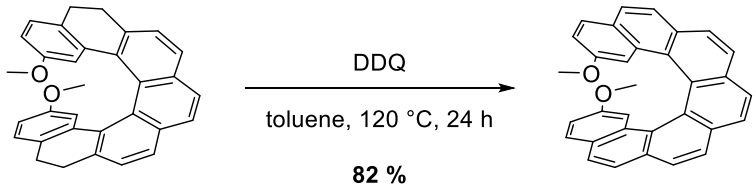

(*rac*)-**54** (*rac*)-**55**

Scheme 71: Oxidation of (*rac*)-**54**.

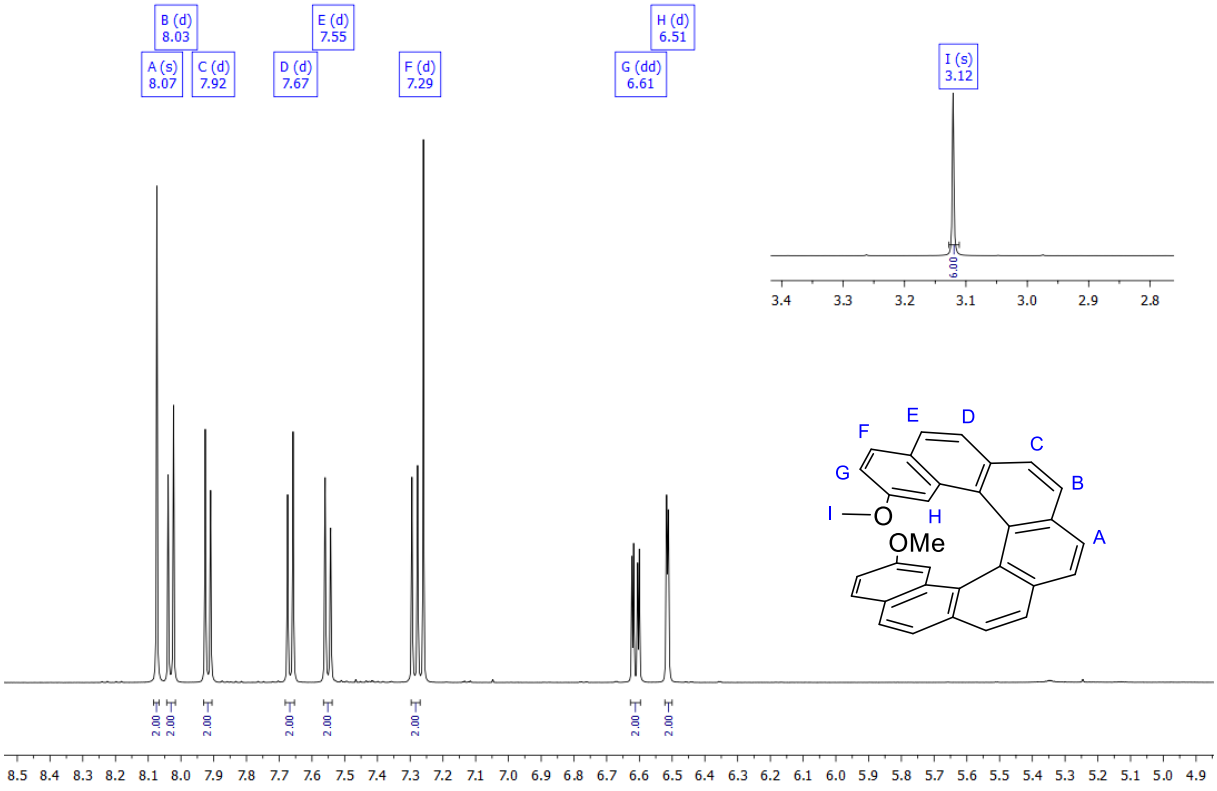

Figure 14: ^{1}H-NMR spectrum and assignment of (*rac*)-**55**.

^{1}H-NMR analysis implied the removal of the diastereotopic benzylic protons at around 2−3 ppm and the presence of a highly symmetric species (**Figure 14**). These observations were consistent with mass spectrometric experiments in which the most

dominant signal matched with the mass of **55**. Curiously, **55** was easier to protonate than the dimethoxypentahelicenes which could not be detected by ESI(+)-spectrometric experiments. A solution of (*rac*)-**55** in dichloromethane was layered with *n*-hexane at −10 °C. Overnight, clear dark yellow plates were collected and subjected to XRD analysis. (*Rac*)-**55** crystallizes in the monoclinic space group *C*2/*c*, the inner helix forms a cavity which is approximately 3.1 Å wide (**Figure 15**). The terminal benzene units overlap and the C-C-C-C dihedral angles of the inner helicene rim range from 17−28° which is in alignment with the observation that the dihedral angle tends to be reduced with substituents.[179,180]

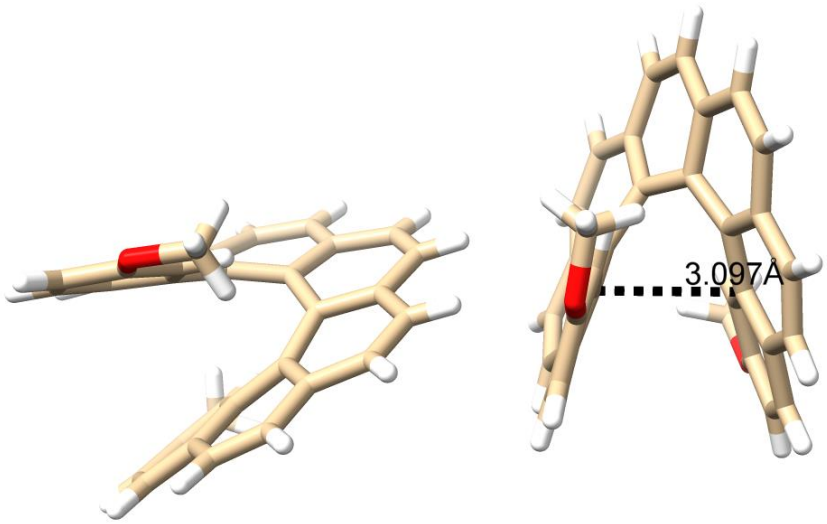

Figure 15: Molecular structures of (*rac*)-**55** as determined by single crystal XRD analysis (carbon in brown, hydrogen in white, oxygen in red).

All things considered, the synthetic strategy has so far been useful for the synthesis of penta- and heptahelicenes. Admittedly, the latter required a change of the sequential order, but in the end, the detour was entirely worth it. The strategy involving the nucleophilic addition of aldehydes was robust enough for the intended purposes and permitted a modular pathway to every contemplated molecule. A few adjustments still have to be made, specifically the [2 + 2 + 2] cycloisomerization has been a let-down. The bottom has been touched with a 10 % yield during the synthesis of [7]helicene derivative **54**, but the problem seemed to be of a rather inherent nature. Nonetheless, the strategy offers enough variables for improvement and gives confidence for the synthesis of hexahelicenes.

4.3 [6]Helicene

Drawing the Lewis structure of [6]helicene immediately reveals that the molecule has to complete a 360° winding one way or another. Indeed, [6]helicene is the first carbohelicene which covers a complete rotation around the helical axis.[181] With a dihedral angle of 58°, it reaches a local extremum before the angle drops in [7]helicene.[127] The enantiomers need to overcome a kinetic barrier of approximately 35 kcal/mol to turn into their mirror images which is large enough to prevent spontaneous racemization at ambient temperature.[14,16] To fill the gap between penta- and heptahelicene narratively, committing to hexahelicene at this point was the next step.

Opposed to a photoinduced approach, a metal catalyzed [2 + 2 + 2] cycloisomerization towards hexahelicenes is only feasible starting from asymmetric precursors. This means that the strategy is not eligible for a bilateral functionalization in either position 5 or 6 (**Scheme 72**). While this circumstance can make planning and interpretation of data more complicated, it should not affect the synthesis itself. Apart from the symmetry breaking, not much changes. Replacing one naphthyl unit by a phenyl unit should already do the job, potentially a workaround *via* the vinyl aldehyde is necessary but all the needed intel has already been gathered. The materials synthesized during both former routes can be reused, otherwise minor tweaks should be sufficient for a big head start.

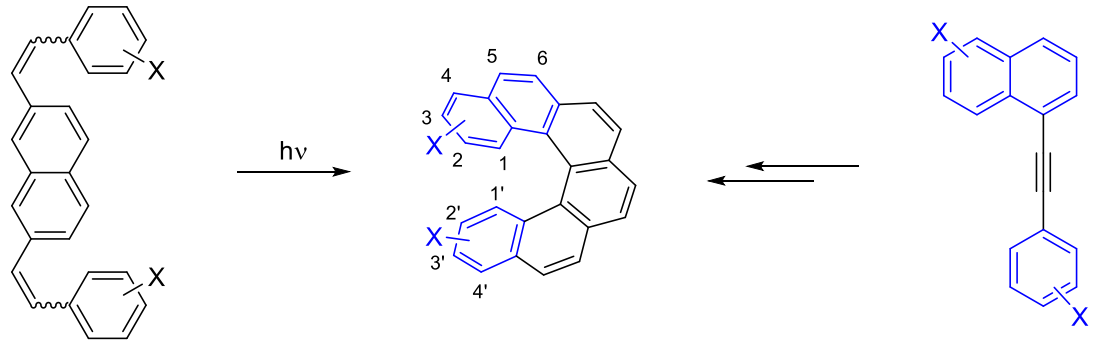

Scheme 72: Photochemical (left) and transition metal catalyzed (right) synthesis of [6]helicene from symmetric and non-symmetric precursors. Positions 5 and 6 are only accessible on one side in the latter method.

2,15-Difunctionalized [6]helicene

Given the available materials, the synthesis of C_2-symmetric 2,15-dimethoxyhexa-helicene started with alkyne **15** and bromide **46**. Under default Sonogashira coupling conditions, they were stirred at 60 °C overnight (**Scheme 73**). Unsurprisingly, the isolation proved to be tedious. After purification on silica gel, a precariously clean fraction of dialdehyde **56** weighing 150 mg (equal to 17 % yield) was collected. The ^{1}H-NMR spectrum showed non-equivalent methoxy and aldehyde signals, but the ratio of the integrals in the aromatic area did not quite match and the appearance of minor side signals prevented a precise characterization (**Figure 16**, bottom). Without further purification, dialdehyde **56** was used for the subsequent reaction.

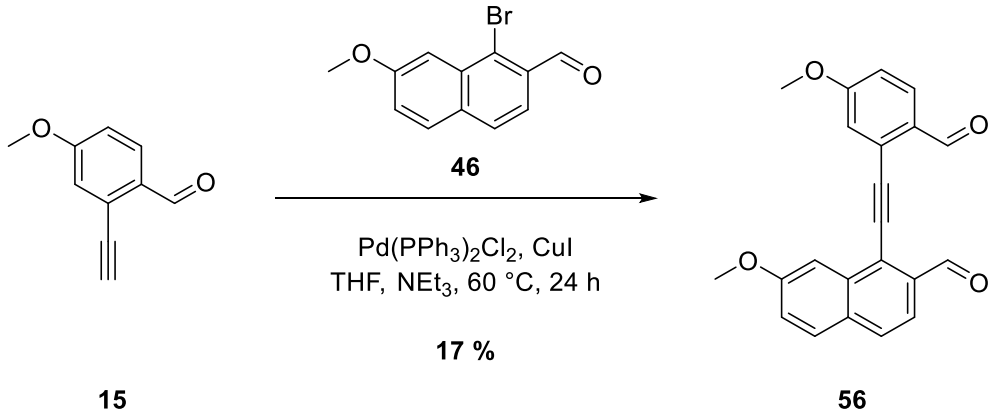

Scheme 73: Sonogashira coupling of **15** with **46**.

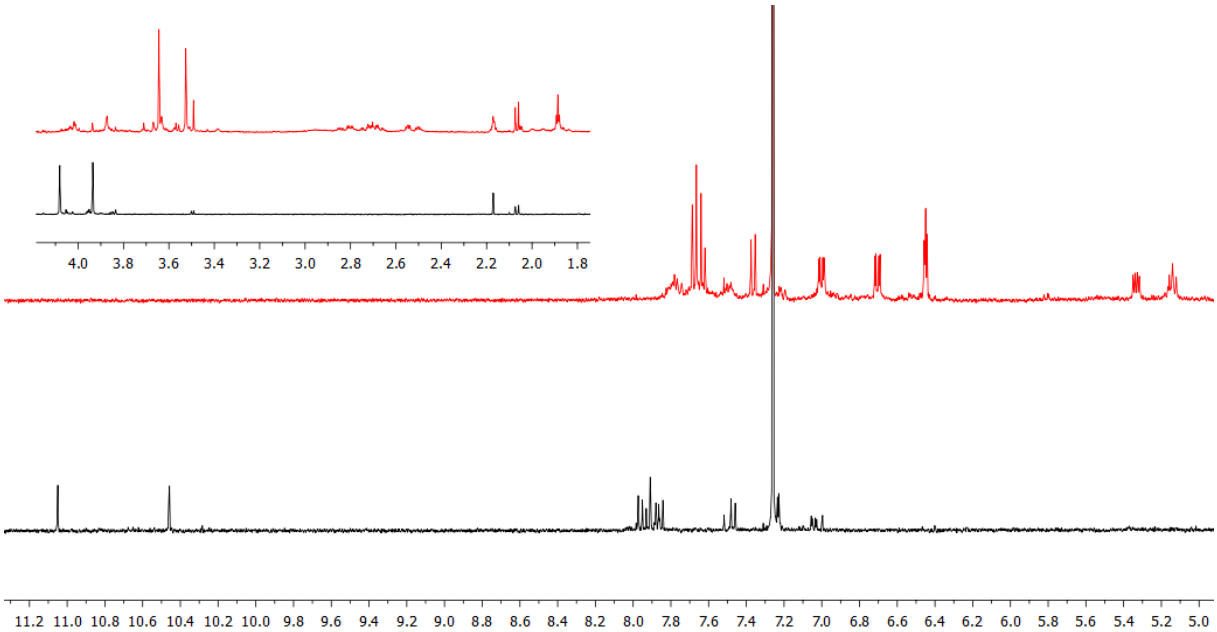

Figure 16: Comparison of presumed ^{1}H-NMR spectra of **56** (bottom) and **57** (top).

With the intention of skipping the workup of the resulting diol, a one-pot procedure of nucleophilic addition and acylation was applied. Over the course of 2 days, dialdehyde **56** was treated with propargyl bromide, zinc and acetic anhydride (**Scheme 74**). The hoped-for result did not really materialize. Purification of the assumed diacetate **57** on silica gel was not accompanied by excessive tailing, but the ^{1}H-NMR spectrum of the main fraction believed to be **57** allowed ambivalent statements about the reaction sequence. The empty space around 10 ppm was a good sign (**Figure 16**, top). Beyond that, the assignment of the present signals was difficult. Two distinct signals around 3.5 ppm would have spoken for the preservation of the methoxy functions, but the adjacent multiplets paired with a turmoil in the aromatic region made an ultimate proposition impossible. It is possible that the impurities from the previous reaction were carried over, a proper isolation of **56** would probably have been better. Either way, a contingent of merely 5 mg of the impure fraction was too little to carry on.

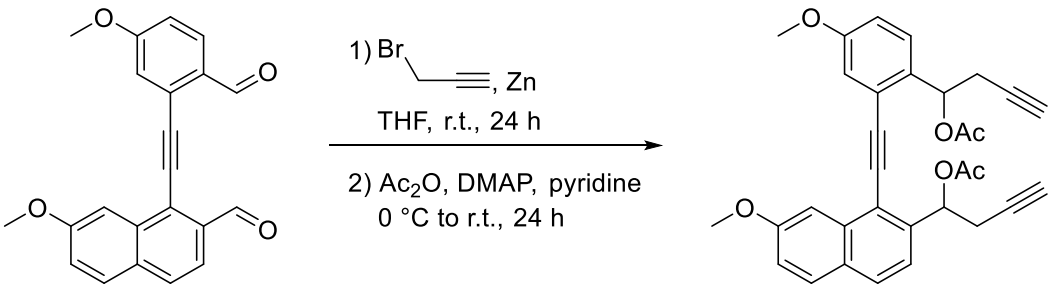

56 **57** (trace amounts)

Scheme 74: One-pot nucleophilic addition and acylation of **56**.

In parallel to the synthesis of [7]helicene, a detour *via* the vinyl compounds was planned. Aryl aldehyde **46** was replaced with vinyl aldehyde **49**, the other half was not tampered with due to three reasons: Firstly, all the starting materials had been available so far, convenience took the upper hand. Furthermore, at that time, the equivalent vinylic component of **13** was not known in literature, so a high stability of substituted cyclohexadienes was uncertain at best. Thirdly, the molecule would stay non-superimposable anyway, so adjusting the other half for the sake of symmetry would have been pointless. Analogously to the Sonogashira coupling towards **56**, terminal alkyne **49** was coupled with **13** (**Scheme 75**). Considering the workup and purification, there was no noticeable difference as the level of difficulty was unchanged. After purification on silica gel, the ^{1}H-NMR spectrum showed up to 6 signals in the range of 10 ppm. Given the fact that the product only exhibits 2 magnetically non-equivalent

aldehyde protons, the 4 additional signals must have originated from other compounds. Since a homocoupling of both **13** and **49** had never been observed until then, it was unlikely that it did suddenly occur this time. 2 of these signals were likely caused by unreacted substrates. The usage of a surplus of 0.1 equivalents of bromide **13** meant that some of it should not have reacted (unless in a homocoupling). The last 2 aldehyde signals could have been the result of the Glaser product. The fact that there were 2 pairs of aldehyde signals with similar integral ratios (one from product **58** itself and one from the Glaser product) as well as a multitude of signals around 3 ppm (where the benzylic/allylic signals are located) supported the theory. Altogether it was difficult to make absolute statements because of the heavy overlap of signals, especially the multiplets around 7 ppm did not provide any clarity. In every case, the purification *via* recrystallization was not successful due to the impurities. Under the assumption that the pair with the higher integral values stemmed from desired **58**, a yield of only 31 % was calculated.

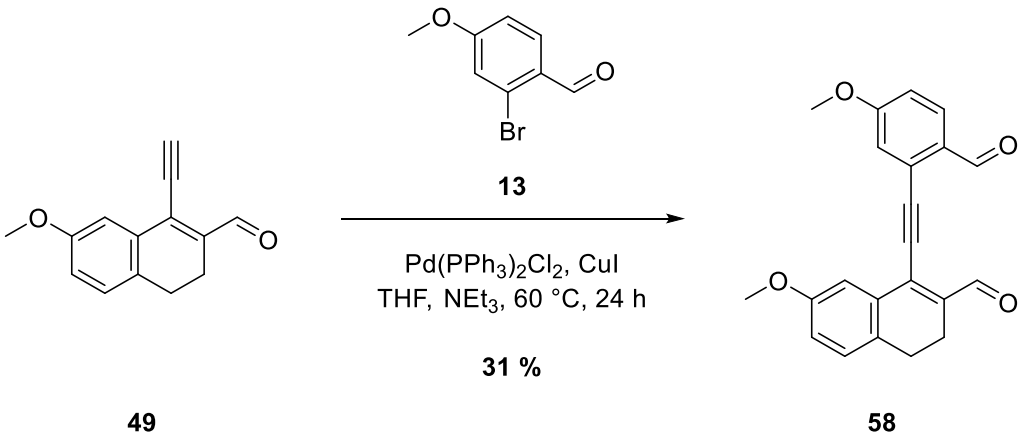

Scheme 75: Sonogashira coupling of **49** with **13**.

In view of the poor yields in both applications of the nucleophilic addition strategy, it was abandoned for good. Evidently, the isolation of the asymmetric dialdehydes was too hard during the synthesis of [6]helicene so a reset for the purpose of reorientation was needed. Luckily, a fallback option was available. The nucleophilic substitution strategy was exactly tailored to circumvent this issue. Unfortunately, on this occasion, no precursors were available which meant that it essentially had to be started from scratch. What was true for naphthaldehydes was true for methylnaphthalenes as well, if not even exacerbated. Supply and demand are not always equal and the former was definitely lower. At the time of this work, only a few suppliers outside the European Union offered naphthalenes with resemblance to the demanded structures at all.

Barring the skyrocketing costs, an intercontinental import was ruled out for time and legal reasons.

After rescheduling, the focus was put on vinyl/aryl aldehydes **45** and **46** once more. Reduction of the aldehydes would give the alcohols which can then be turned to halides or triflates with phosphorus (penta-) tribromide, thionyl chloride or trifluoromethanesulfonic anhydride. Acting as good nucleofuges, they should enable a nucleophilic substitution in the benzylic position. Because of that, aldehyde **46** was subjected to a reduction using a stock solution of LAH in anhydrous THF at 0 °C (**Scheme 76**).

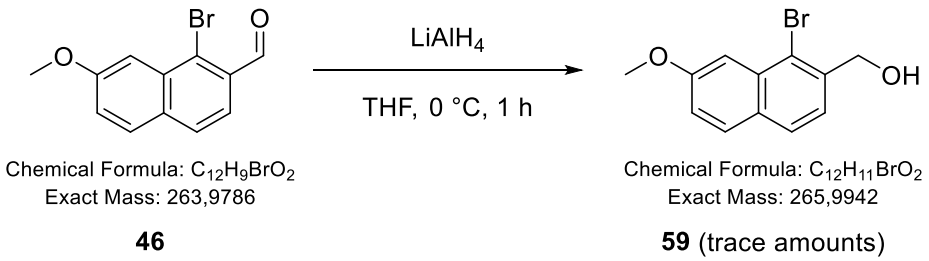

Chemical Formula: $C_{12}H_9BrO_2$
Exact Mass: 263,9786

46

Chemical Formula: $C_{12}H_{11}BrO_2$
Exact Mass: 265,9942

59 (trace amounts)

Scheme 76: Reduction of **46** with $LiAlH_4$.

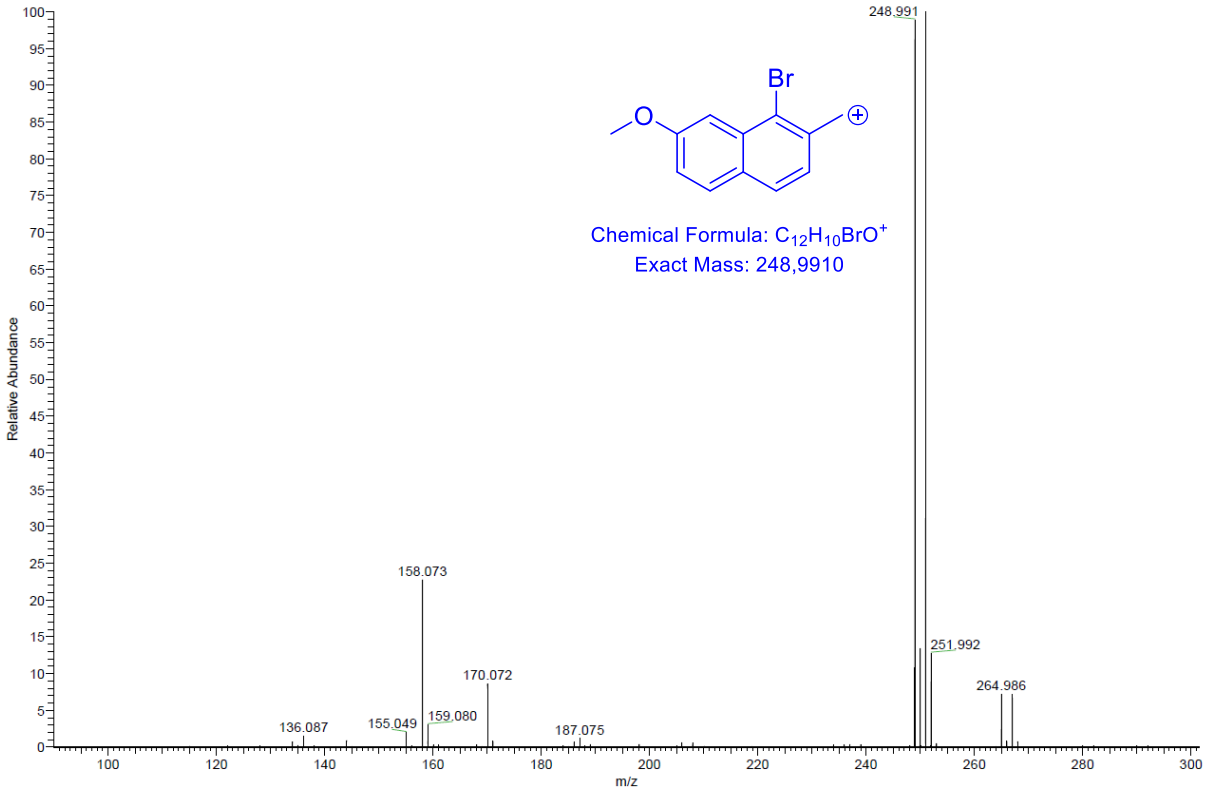

Figure 17: APCI-mass spectrum after reduction of **46** with $LiAlH_4$.

The reaction raised more questions as analytic results contradicted each other. TLC-control showed the formation of a single species. After purification by column chromatography, the ^{1}H-NMR spectrum showed two sets of signals, none of which belonged to the substrate. In the mass spectrum, the most prominent signal at *m*/*z* = 248.991 fitted to a species bearing only 1 oxygen, a smaller signal at *m*/*z* = 264.986 however indicated the protonated substrate (**Figure 17**).

For a better clarification and comparison, vinyl aldehyde **45** was treated under the same conditions as aryl aldehyde **46**. Again, after purification, ^{1}H-NMR analysis revealed 2 sets of signals visible in the range of the expected methoxy protons. ESI(+)-mass spectrometry showed no sensible protonated species, EI-mass spectrometry showed fragments that could have originated from the substrate, the product or intermediates. The impure mixture was used for the next reaction. Treatment with PBr_3 for 2.5 h gave a single species which was identified as allylic bromide **61** by ^{1}H-NMR and mass spectrometry. Apparently, the bromide in vinylic position was too labile to withstand the reduction with LAH (**Scheme 77**).

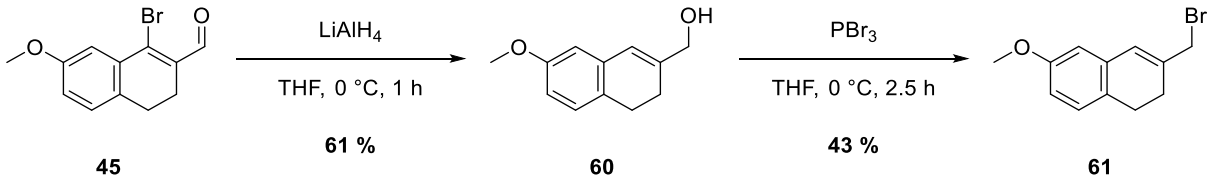

Scheme 77: Reduction of **45** and subsequent bromination.

A third attempt to get to the desired alcohol **59** was made with less reactive reducing agents. Indeed, reduction of **46** with sodium borohydride over 2 h gave **59** in 68 % yield (**Scheme 78**).

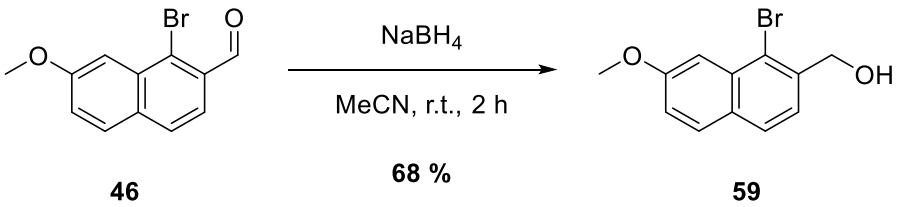

Scheme 78: Reduction of **46** with $NaBH_4$.

In light of the fact that the reaction sequence towards [6]helicene had just begun, the poor yields were demoralizing. Especially the Vilsmeier-Haack formylation towards aldehyde **46** entailed a minus of 74 % of the starting material. Thus, alternative options were looked out for. A publication by *Starý* and *Stará* featured an esterification of

1-bromo-7-methoxy-2-naphthol **63** which was then augmented with a benzylic nucleofuge with alcohol **59** as an intermediate.[64] The regioselective bromination of commercially inexpensive naphthol **62** was adapted from a publication by *Pérez* and *Guitián*.[182]

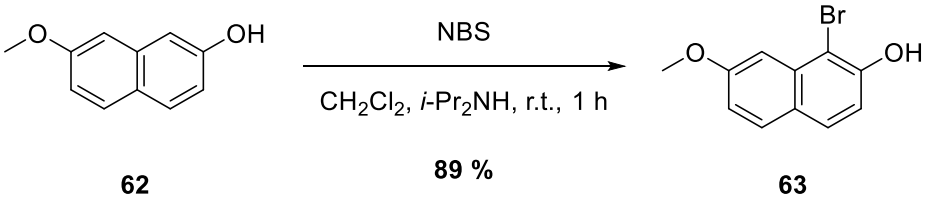

62 **63**

Scheme 79: Bromination of **62**.

With a yield of 89 % for the very first reaction, this was a much better opening (**Scheme 79**). Likewise pleasant, the hydroxy functions on **63** were esterified almost quantitatively (**Scheme 80**).

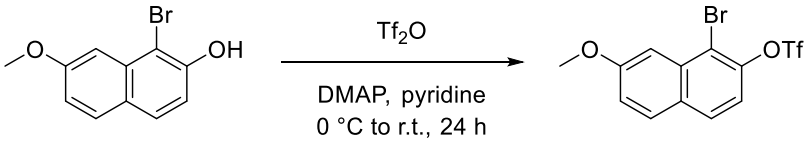

63 **64**

Scheme 80: Triflation of **63**.

Implementing a benzyl moiety by a formal substitution of the triflate by means of aromatic chemistry on the other hand is anything but trivial. One possibility is an alkoxycarbonylation of arenes to benzoate esters which can then be reduced with LAH to get to alcohol **59**.[183] The Pd-catalyzed reaction uses aliphatic alcohols and carbon monoxide as a source for the components of the ester. With the latter being an integral, but also poisonous, odor- and colorless component, special safety measures were taken (**Figure 18**). A direct influx of gaseous CO with a gas cylinder or a balloon would have been the most convenient solution, but this was abolished because it posed a residual risk. A more controlled and safer approach is the indirect influx of the gas. Hereby, carbon monoxide is separately generated *ex situ* by dehydration of formic acid in sulfuric acid (Morgan reaction) in the decarbonylation chamber.[184] The expansion of the gas in the decarbonylation chamber drives it into the carbonylation chamber where the actual reaction takes place. Using a syringe, CO flows directly into the solution of the reactants.

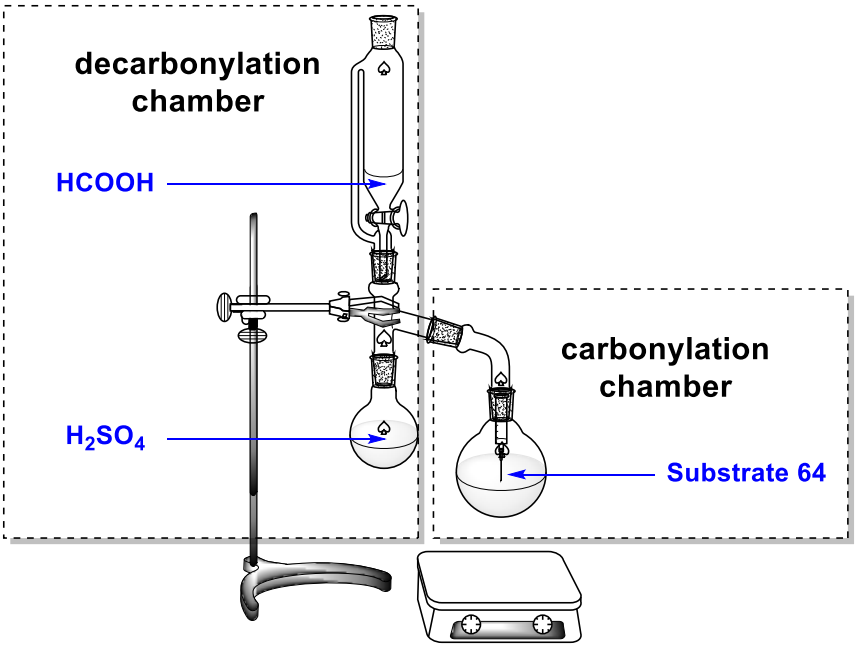

Figure 18: Schematic experimental setup of methoxycarbonylation of **64**.

As described, triflate **64** was mixed with carbon monoxide and methanol in the specific setup, the reaction was stirred for 2 h at 70 °C (**Scheme 81**). Purification went smooth, the appearance of an additional methoxy group in the ^{1}H-NMR spectrum proved the formation of ester **65**. So far, the reactions reached a combined yield of 58 % over 3 steps. For reference, the last sequence towards alcohol **59** had a combined yield of 17 %. Admittedly, 1 extra step was still required in order to turn the ester into the alcohol, but the threshold for the better overall performance was an individual yield of 29 % for the next reaction.

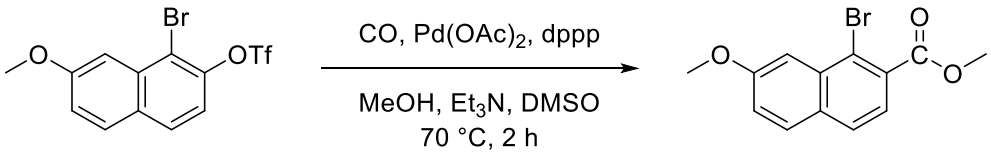

64 **67 %** **65**

Scheme 81: Methoxycarbonylation of **64**.

Over a period of 1 h, ester **65** was stirred with LAH in anhydrous THF (**Scheme 82**). TLC-control falsely predicted a complete conversion. Interestingly, after aqueous workup, the mixture contained the same impurity as in the reductions of aldehydes **45** and **46** with LAH which were inseparable from the product due to identical retention factors. Based on the ^{1}H-NMR spectrum, their ratio was approximately 1:5. Under the

assumption that their masses were equal, this would translate to a yield of 52 % of benzyl alcohol **59** which is well above the threshold of 29 %.

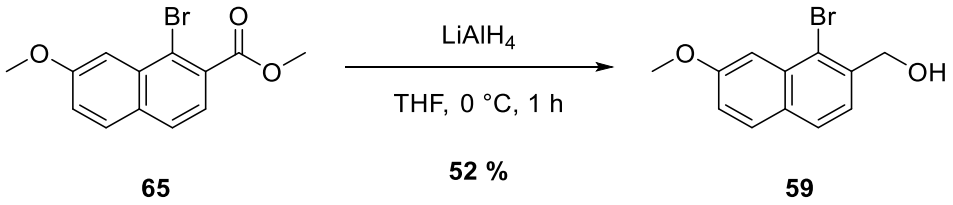

65 **59**

Scheme 82: Reduction of **65**.

Semi-pure alcohol **59** as well as the pure fraction gained from the reduction with $NaBH_4$ were independently altered to the dibromide **66** with phosphorus tribromide within 2.5 h (**Scheme 83**). Regarding the former, the impurity could be separated from the product on this step. Within the measurement accuracy, both had similar performances in the 90 % range. Despite carrying two identical functionalities, the bromides in **66** inherently could not be more different in terms of reactivity. Exploiting the differentiation of aromatic and aliphatic/benzylic positions was the key factor for the following reactions.

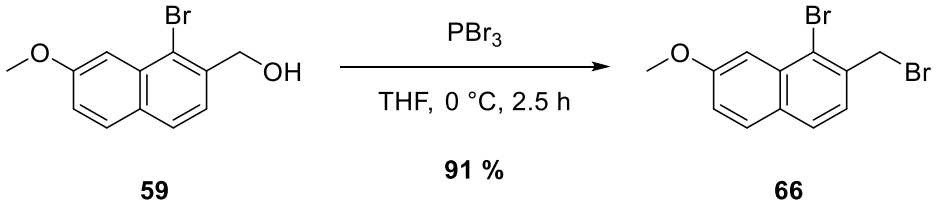

59 **66**

Scheme 83: Bromination of **59**.

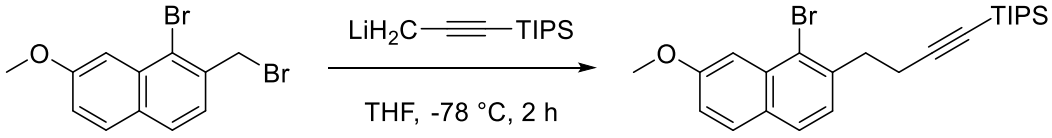

66 **67**

Scheme 84: Nucleophilic substitution of **66**.

Although the retention of C_2 symmetry was redundant during the synthesis of [6]helicene, the installation of the lateral alkyne was done first similar to the synthesis of [5]helicene. Astonishingly, the nucleophilic substitution of dibromide **66** to alkyne **67** (**Scheme 84**) proceeded much better than that of dihalogenide **23** to **24** which had a conversion rate of only 14 % (**Scheme 35**). It was unclear why this molecule had a

roughly six-fold higher conversion under the same conditions, but in view of the better outcome it was gratefully embraced.

To be on the safer side, the bromide was transformed into the iodide. This would increase the overall reactivity and make an unfavorable, intramolecular Heck-type coupling with the internal alkyne less likely. Studies have shown that this special case of the reaction can occur with bromides, chlorides or triflates under rare circumstances, giving dienes as well as allenes *via* an energetically unfavored β-hydride elimination of a vinyl palladium species.[185,186] Conformable to a routine lithiation/iodination protocol, bromide **67** was stirred with *n*-BuLi and iodide over 16 h at −79 °C (**Scheme 85**). During the reaction, minor side product formation was observed by TLC-monitoring, but were not identified as dienes nor allenes. After silica gel purification, 74 % of iodinated naphthalene **68** was obtained as a yellow-brown oil.

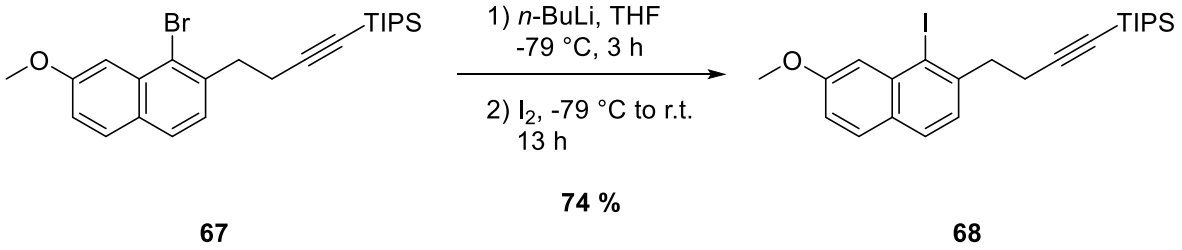

67 **68**

Scheme 85: Iodination of **67**.

The construction of the other half of the desired diarylacetylene had already been accomplished during the synthesis of 2,13-dimethoxypentahelicene **20**. In a Sonogashira cross-coupling, iodide **68** was therefore mixed with diyne **26** at 60 °C overnight (**Scheme 86**). TLC-monitoring indicated the formation of more than one species. After purification by column chromatography a more precise picture emerged. The reaction did not proceed as planned. All the expected proton signals including the benzylic and propargylic ones were visible, but the aromatic ones had a rather moderate agreement concerning their integral ratios. Furthermore, extra signals not attributed to triyne **69** were apparent. Although a surplus of 0.1 equivalents of substrate **26** had been used, the blank area around 2 ppm indicated no presence of a terminal alkyne. As the products arising from homocoupling still had not been observed, they were once again ruled out, shifting the focus to the remaining Glaser byproduct. The area around 4 ppm showed two pairs of signals with the same integral ratio which supported this theory.

Eventually, mass spectrometric experiments confirmed the theory: The APCI-spectrum showed the presence of **69** along with the Glaser byproduct (**Figure 19**), while the substrates or other byproducts originating from homocoupling were not observed. In a second purification attempt, minor successes were achieved. But ultimately, triyne **69** was inseparable from the tetrayne. The impure mixture was used for the subsequent reaction without further purification.

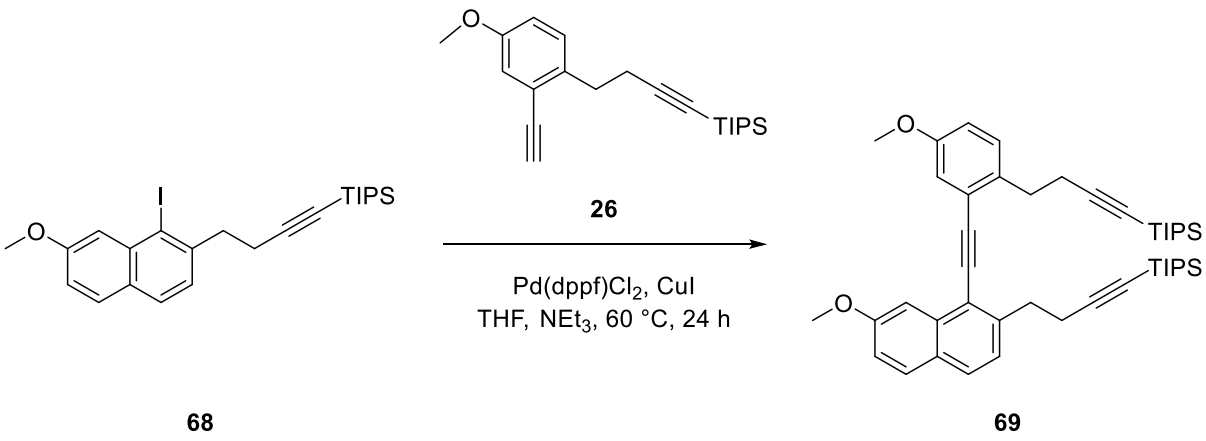

Scheme 86: Sonogashira coupling of **68** with **29**.

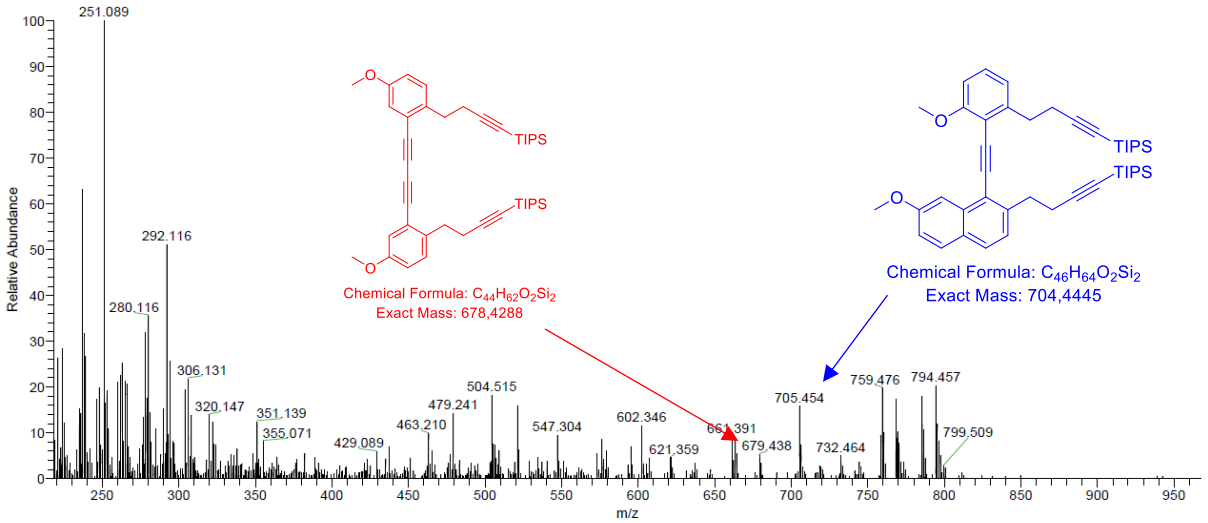

Figure 19: APCI-mass spectrum after Sonogashira coupling of **68** with **26**.

The impure mixture was treated with a stock solution of TBAF in anhydrous THF overnight. After column chromatography, a much cleaner ^{1}H-NMR spectrum was obtained. Minor side signals were present which probably originated from remaining Glaser product. After comparison of the signals with the ones published in literature,[64] the formation of **70** was confirmed. Over 2 steps, a yield of 39 % was calculated (**Scheme 87**).

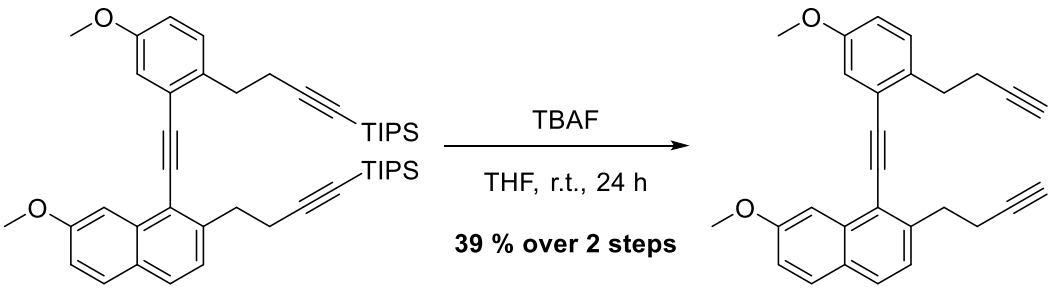

69 **70**

Scheme 87: Deprotection of **69**.

The cyclization of **70** under nickel-catalysis (**Scheme 88**) was accompanied with more troubles than anticipated. After purification, the ^{1}H-NMR spectrum was littered with undefined signals and overlapping multiplets. To be fair, tetrahydrohexahelicene **71** was not yet C_2-symmetric at that time, but its solitary presence was out of the question. A possible explanation for this could be an oligo- or polymerization of the substrate towards varying oligo- and polymers which share similar retention factors, making them impossible to separate by column chromatography. Especially the area around 4 ppm showed the presence of at least 12 magnetically non-equivalent methoxy protons. Since the product only bears 2, this would mean that at least 5 other species were present. Pursuing the same strategy as before, the impure composition was used for the subsequent reaction in hopes of an easier purification after that.

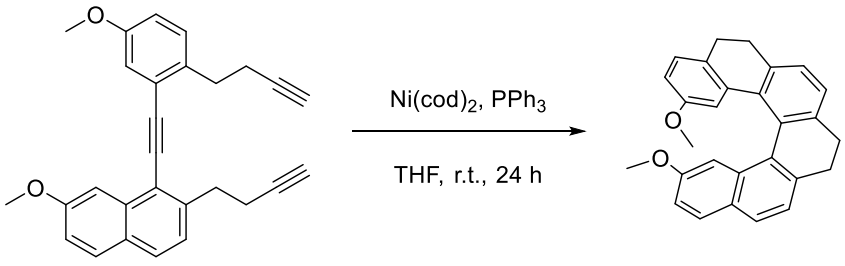

70 (*rac*)-**71**

Scheme 88: [2 + 2 + 2] cycloisomerization of **70**.

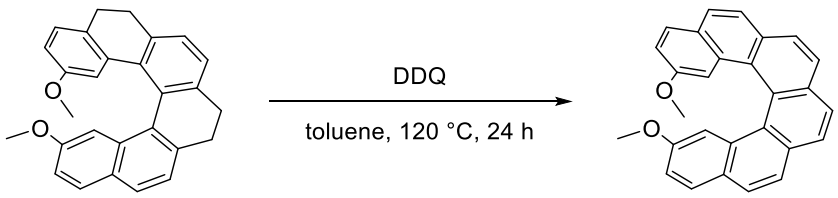

(*rac*)-**71** (*rac*)-**72**

Scheme 89: Aromatization of (*rac*)-**71**.

The mixture was subjected to DDQ in refluxing toluene overnight (**Scheme 89**) and purified under routine workup conditions. Excluding the empty space in the area of the benzylic protons (2−3 ppm), superimposition of pre- and post-reaction ^{1}H-NMR spectra more or less revealed their conformability in terms of multiplicities and chemical shifts. The aromatic as well as the aliphatic area gave no hint to a C_2-symmetrical species, again a multitude of methoxy signals were present which indicated the formation of oligo- and polymers. Unfortunately, this also meant that the isolation was not possible at this stage and probably would not be possible at a later stage either. However, mass spectrometric experiments proved the existence of racemic 2,15-dimethoxy-hexahelicene (*rac*)-**72** in the composition (**Figure 20**). Strangely, the highest signal was shown at *m*/*z* = 415.168.

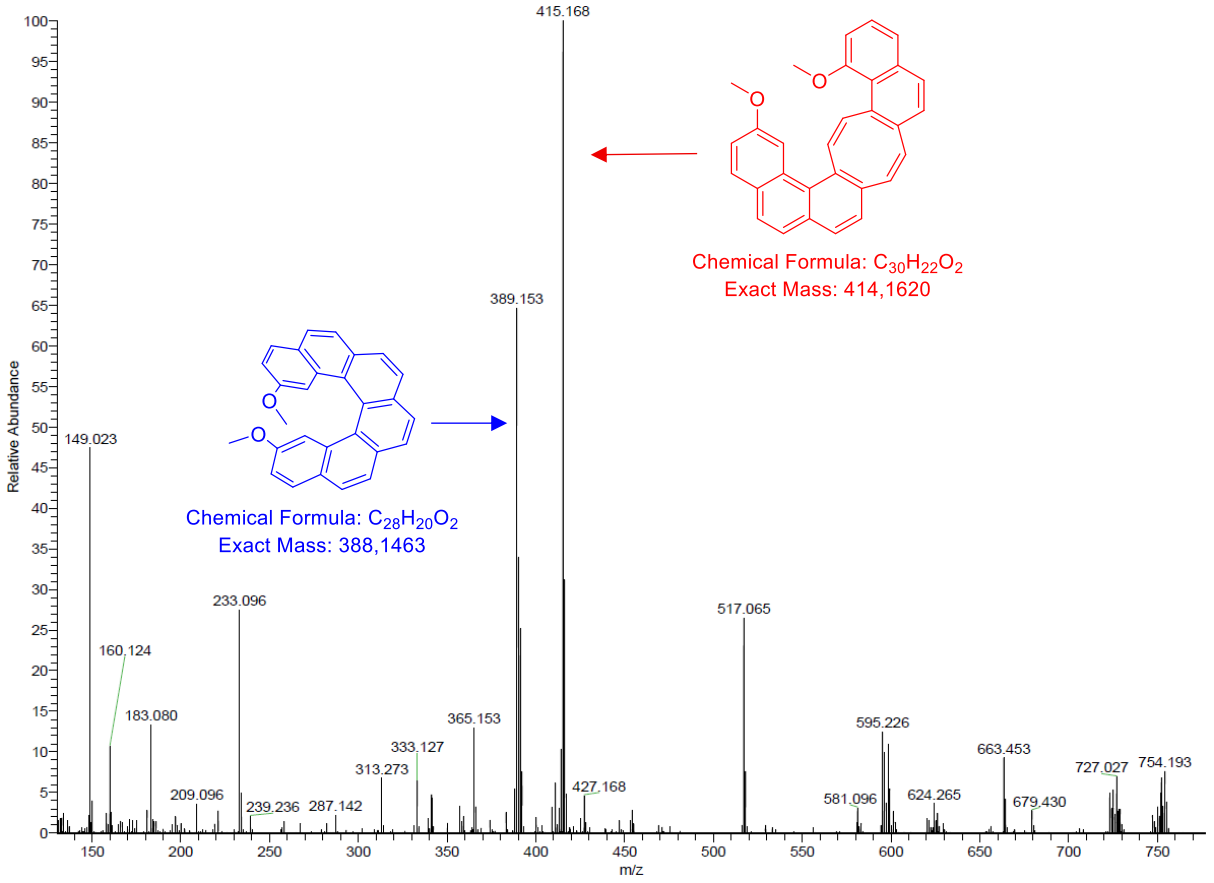

Figure 20: APCI-mass spectrum after aromatization of (*rac*)-**71**.

Under the assumption that this signal belonged to a species containing only carbon, hydrogen and oxygen atoms, a molecule with the constitution of [**72**+C_2H_3]$^+$ or [$C_{30}H_{22}O_2$+H]$^+$ would fit. Since neither C_2H_2 nor C_2H_3 are typical adducts in mass spectrometry, this was very surprising. Two additional carbon atoms could only be explained by the Glaser product which would then not have been separated from

precursor **70** as thoroughly as initially assumed. Indeed, a cyclization of the Glaser product would have the chemical formula of $C_{30}H_{22}O_2$. Although the oligomerization of alkynes to the rather unstable cyclooctatetraene usually needs harsher conditions,[51,187] different products involving a consecutive intramolecular Glaser coupling of the tetrayne formed after the Sonogashira coupling towards **69**, Heck-type coupling of alkynes as described before or something similar, were even more unlikely.

In the end, the evasion maneuver *via* the nucleophilic substitution strategy was not enough to isolate hexahelicene **72**. The marginal deviation of the retention factors of the presumed oligo-/polymers as well as the cyclized Glaser product made their separation impossible. Nonetheless, the route was at least successful up until the cyclization, arguably also after. The side products in the key reaction were a major obstacle, but this can potentially be remedied by further dilution or change in catalyst. Alternatively, other purification methods like crystallization, sublimation etc. can be pursued.

As a whole, the proof of concept still succeeded in the end. The combination of the nucleophilic addition and the nucleophilic substitution strategy proved to be serviceable for a general approach to penta-, hexa- and heptahelicenes. Both displayed their modularity and reliability in the sense that only minor modifications were required in order to get to other constitutional isomers or higher homologues. In direct comparison they are not too different in regard to the expected yields. The nucleophilic addition strategy was wrongly crowned the winner in advance because of the abysmally poor yield during the nucleophilic substitution enroute towards [5]helicene, but the strategy later on redeemed itself with a six-fold higher performance during the synthesis of [6]helicene. With cautious confidence it can be said that they should be eligible for the synthesis of octa- and nonahelicenes by a simple change in substrates (employing at least one phenanthrene unit).

5 Stereochemistry

With the first helicenes set up, this is the very latest point at which their topology has to be addressed and discussed on a stereochemical level. The executed cyclizations forced a special kind of topology on the molecules which unlocked a number of new features. With the adoption of the helical conformation, these features can mainly be traced back to a single element: Although the synthesized helicenes lacked any stereogenic centers, their helical winding induced an unusual form of chirality. Analogously to left- and right-handed screws, helicenes imitate a thread which can run clock- or anti-clockwise.

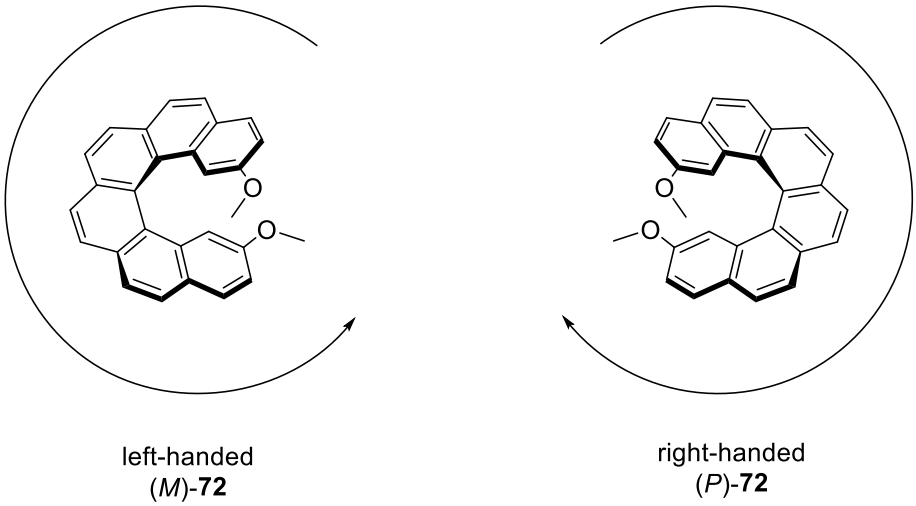

left-handed
(*M*)-**72**

right-handed
(*P*)-**72**

Figure 21: Racemic mixture of **72**.

In relation, they are non-superimposable, mirror-inverted molecules, or in other words, they are enantiomers (**Figure 21**). This means that a non-stereoselective cyclization towards a helicene gives at least two isomers which is typically a pair of enantiomers (diastereomers if other chiral elements were attached to the precursor). As a matter of course, their chirality is one of the reasons why so much research has been done on them. To date, there are numerous applications in which their chirality has been exploited. But in order to exploit their chiral properties, tools to resolve the isomers are needed in the first place.

5.1 Asymmetric synthesis

Strictly speaking not a chiral resolution, the problem can also be addressed preventively with asymmetric synthetic techniques. For this, many entities like reactants, solvents etc. can act as a source for the chiral information. Needless to say, not every method is as effective as others, but a general enrichment of a specific isomer is possible employing different strategies. Since the review of each one would definitely go too far, the selection in this chapter will be restricted to examples categorized by their significance.

Asymmetric photocyclization

Shortly after *Dietz's* first photocyclization of tetra- and pentahelicene, *Kagan et al.* conducted intensive research on an asymmetric variant using circularly polarized light. Depending on the irradiation of the sample with left- or right circularly polarized light, they enriched either (*P*)- or (*M*)-enantiomers of [6]helicene (**Scheme 90**).[188] Four years later, they expanded their series up to [13]helicene, although the chiral induction was unsuccessful in the case of higher helicenes than [10]helicene for unexplained reasons.[189]

For this reaction, three mechanisms were proposed:[190–193]

- The preferential destruction of the disfavored enantiomer (asymmetric photodestruction)
- The preferential ring opening of a dihydrohelicene to the precursor which delays the oxidation of one enantiomer (partial photoresolution)
- Faster cyclization of one enantiomer (asymmetric synthesis)

Independent reports in favor of the third[188,190] and in opposition to the others[180,194] make it the most plausible theory. While the enantioenrichment of helicenes stemming from unequally populated excited states of the involved participants is conceptually fascinating, the absolute values for enantiomeric excesses lag behind. Although the results are consistently reproducible and unlikely to be due to measurement errors, *ee* values below 1 % are rather discouraging. Similar observations were made with the usage of chiral solvents[195,196] or cholesteric liquid crystals.[197,198] The question arises

whether meaningful percentages can be achieved at all. Because of that, asymmetric photocyclizations have remained an interesting concept with little practical relevance.

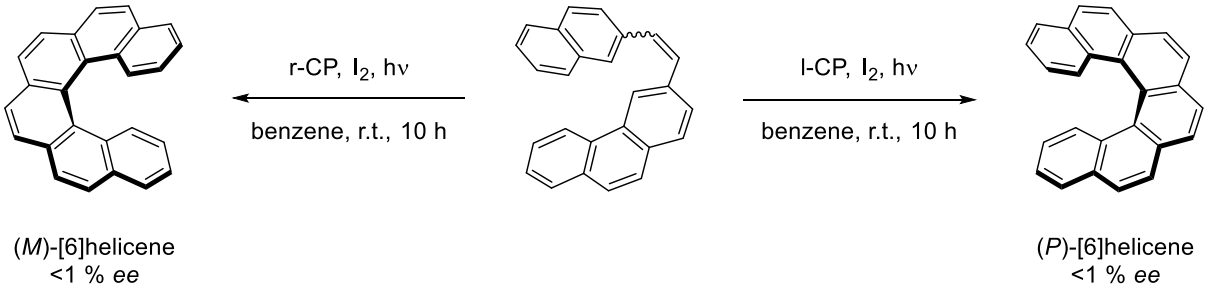

Scheme 90: Asymmetric photocyclization with circularly polarized light.

High enantioselectivity can also be achieved *via* substrate control. The synthesis of a (*M*)-[6]helicene exploited the bulkiness of the [2.2]paracyclophane in the substrate which completely prevented the formation of the (*P*)-isomer (**Scheme 91**). At the same time, the exploitation of the kinetic isotope effect through a deuterium-labelled substrate led to the formation of only one regioisomer.[199] With perfect enantioselectivity, the outlier shows that high values can be achieved, but to be fair, this example is very specific and strictly has little to do with an asymmetric photosynthetic technique itself as the substrate induced strategy would work with every method.

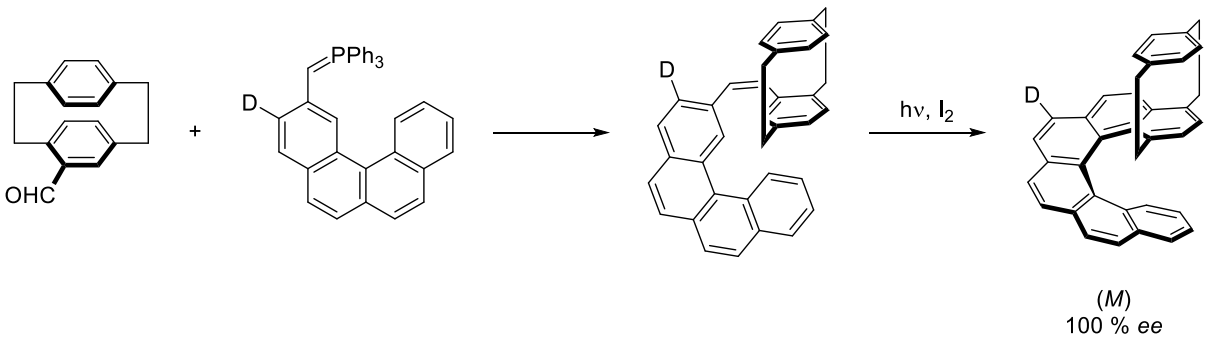

Scheme 91: Substrate-controlled asymmetric photocyclization.

Asymmetric [2 + 2 + 2] cycloisomerization

Obviously, when it comes to asymmetric metal catalyzed reactions, the first thing that comes to mind is the application of chiral ligands. Shortly after establishing the non-asymmetric methodology,[200] the group of *Starý* and *Stará* pioneered the asymmetric one as well. In this, an axially chiral monophospine gave tetrahydro[6]helicene in

48 % *ee*.[72] Since then, the enantioselectivity has steadily been increased with newer ligands.[79,201] Curiously enough, a hopefully temporary peak in terms of asymmetric Ni^0 catalyzed reactions was reached with a novel helicenoidal NHC precursor: Two oxahelicenes linked by an imidazolium salt reached an *ee* of 86 % (**Scheme 92**).[82]

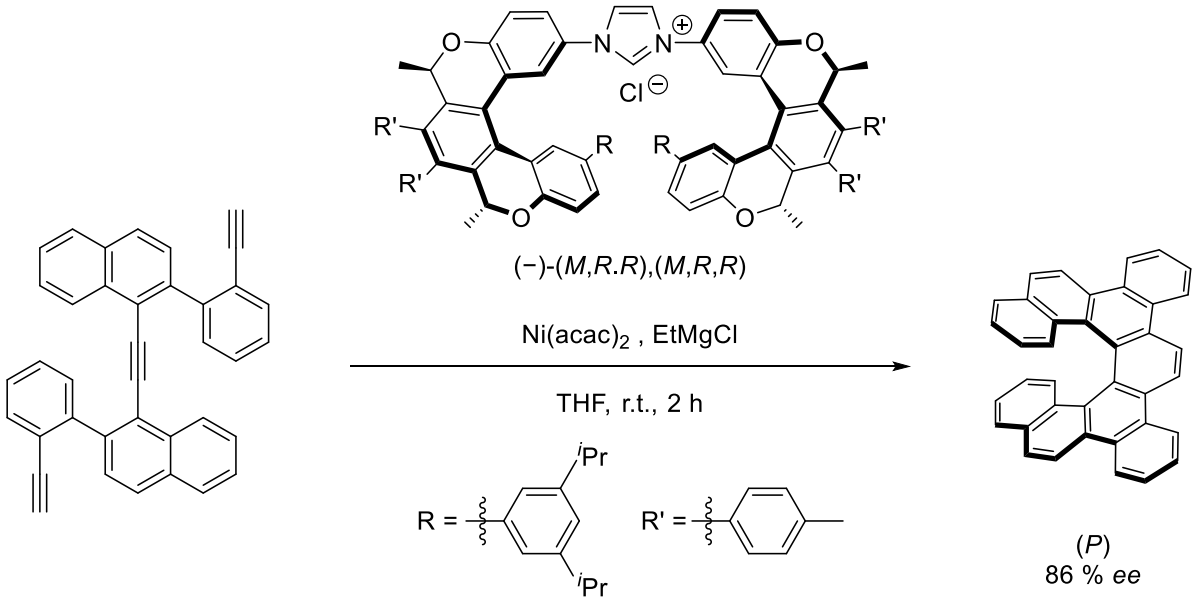

Scheme 92: Enantioselective [2 + 2 + 2] cycloaddition with helical NHC ligand.

Asymmetric catalysis on the basis of Co^I is not as effective, the only permanently bound ligand to the metal center during the catalytic cascade is the Cp moiety, thus, it has to carry the chiral information.[52,201,202] Out of the examined catalysts, the most potent one has reached a moderate *ee* of 25 %.

The highest chirality transfers well over 90 % *ee* have been observed under Rh^I catalysis, but the catch is that the general yields can be low due to incidental [2 + 1 + 2 + 1] cycloaddition. However, out of the three main metals used for the synthesis of helicenes, Rh^I is the only one which is able to promote an intermolecular [2 + 2 + 2] cycloaddition between tetraynes and diynes. Pre-eminent in this field is the group of *Tanaka*. The combination of cationic Rh^I complexes and axially chiral phosphines profits from the latter being largely commercially available, giving consistently high enantiomeric excesses up to virtually enantiopure compunds.[203–205] Curiously, in one instance the enantiomeric excess was retroactively increased from 64 to 99 % by preparative TLC (the racemic product had a lower solubility in the eluent than the enantiopure product).[206]

Aside from these, there are a few instances involving Pd^0 complexes[182,207] or Ir^I complexes.[83] Interestingly, in the single instance employing Ir^I, the system was not able to mediate the intended tandem intermolecular-intramolecular domino sequence of the substrate. While the intermolecular [2 + 2 + 2] cycloaddition succeeded, the intramolecular one was promoted *post hoc* by Ni^0.

Stoichiometrically, a substrate-controlled diastereo- and enantioselective synthesis was elaborately designed by *Starý* and *Stará*. Relying on a 1,3-diaxial interaction, a point to helical chirality transfer was achieved with enantiopure triynes and practically complete diastereo- and enantioselectivity. Initially fixing the absolute configurations of both propargylic centers in the substrate,[158] they later on achieved the same with only one fixed configuration (**Scheme 93**).[76]

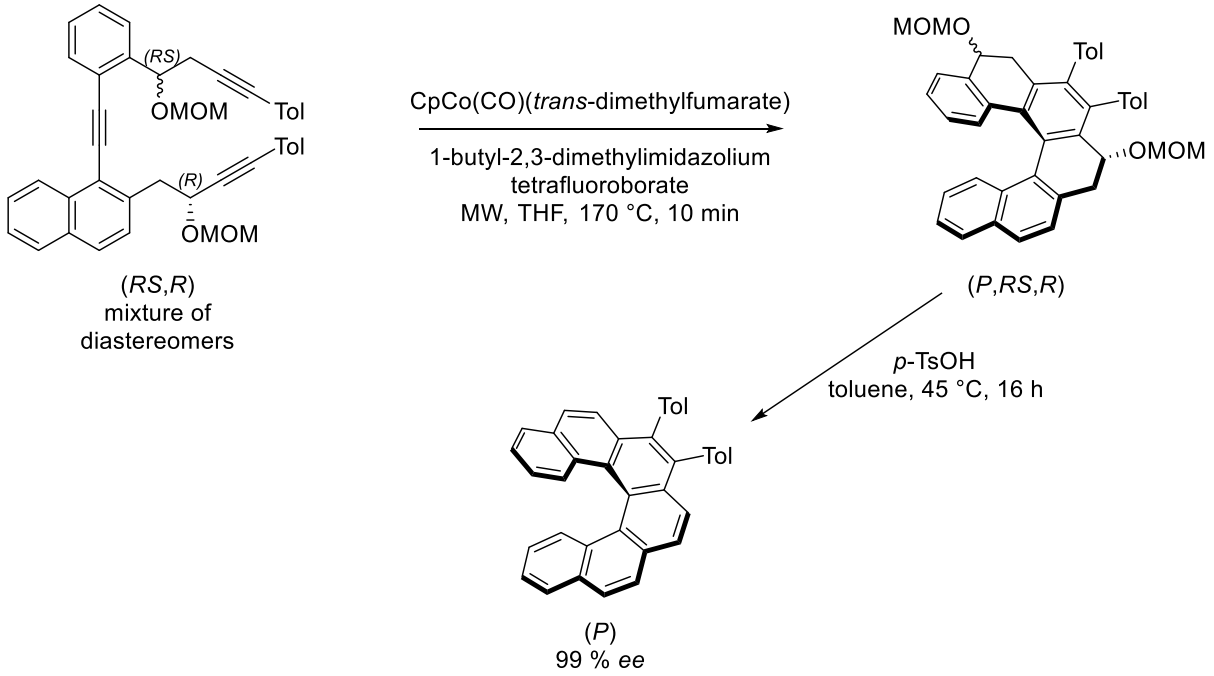

Scheme 93: Asymmetric [2 + 2 + 2] cycloaddition governed by 1,3-allylic-type strain.

By contrast, the benzylic position only had a minor impact on the direction of rotation of the helicene. Theoretical calculations revealed that the stereocontrol stems from the interactions between the functional group in propargylic position and the *p*-tolyl group attached to the alkyne. In the disfavored helicity, both these groups cause an 1,3-allylic-type strain which results in a free energy difference of up to 5.5 kcal/mol (**Figure 22**). Because of that, only one diastereomer is formed. Interestingly, owing to a low epimerization barrier, the outcome is governed by a thermodynamic equilibrium after the cyclization. When methoxymethyl ether groups were used, they could be cleaved

off from the product by an acid-assisted elimination afterwards, highlighting their role as a chiral auxiliary. The proof of concept was shown by alternating the absolute configurations. (*R*)-configurated propargylic MOM groups consistently gave (*P*)-helicenes, while (*S*)-configurated ones gave the (*M*)-antipode. With this strategy, their group managed to synthesize parent penta-, hexa- and heptahelicene as well as functionalized derivatives with high yields and over 99 % *ee* under various reaction conditions. In each case, the stereochemically undefined MOM group in benzylic position was solely used for the mild oxidation towards the final helicene. Apart from the asymmetric Rh^{I}-catalyzed [2 + 2 + 2] cycloisomerization employing chiral ligands, their approach is probably the closest to being a general approach to an asymmetric synthesis with absolute stereocontrol.

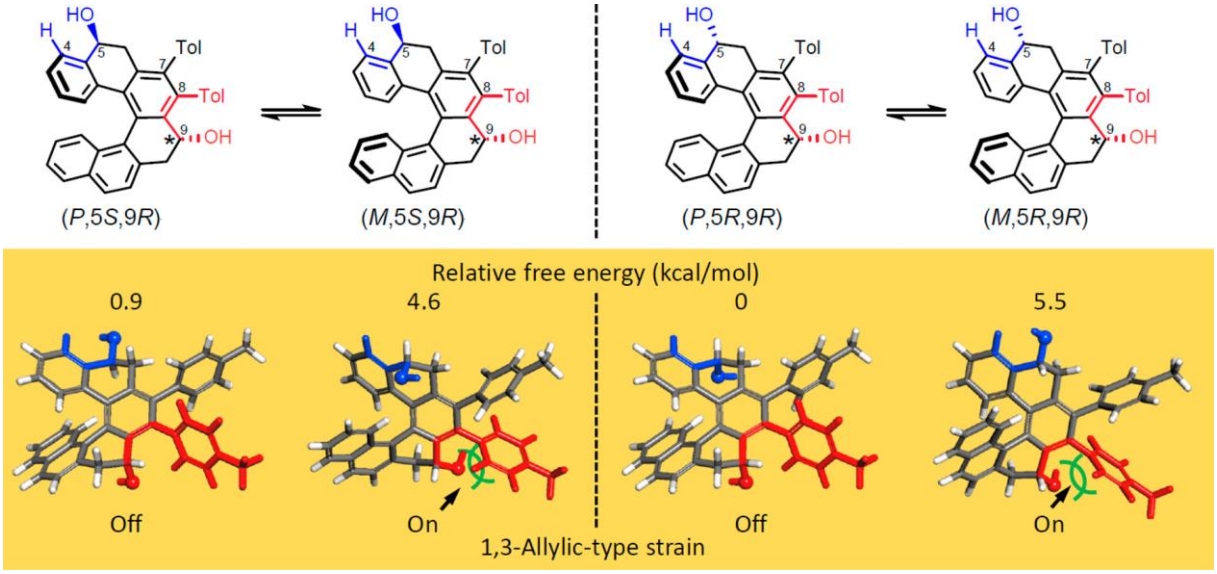

Figure 22: Point to helical chirality transfer. The (*R*)-configurated 9-OH group dictates the helicity, while the configuration of the 5-OH group is insignificant. The fixed absolute configuration in position 9 can cause a 1,3-allylic-type strain between the hydroxy and the *p*-tolyl groups (red). The position 5 does not cause any strain (blue). Adapted with permission from the *American Chemical Society*.[76]

Asymmetric Diels-Alder reaction

Since the non-asymmetric Diels-Alder reaction is already underdeveloped compared to the photosynthetic or metal catalyzed reaction, the same logically holds true for its asymmetric variant. In principle, only the group of *Carreño* has focused on enantio- or diastereoselective Diels-Alder reactions, from which two methods developed. The first clever example is the enrichment of enantiopure helicenes with a homochiral auxiliary carrying a chiral sulfur atom. The usually more stable *s-cis* conformation of the

(*S*)-configurated sulfoxide dictates the *endo*-approach of the diene to the less encumbered side facing the lone pair which leads to the (*M*)-bisquinone in 80 % *ee* (**Scheme 94**).[208] The *s-trans* conformation can be enforced by means of bulky substituents like methoxy groups which would clash with the sulfinylic oxygen of the *s-cis* rotamer, giving (*P*)-handed products up to >98 % *ee*.[209] After the cycloadduct is formed, the sulfoxide moiety undergoes a spontaneous elimination which recovers the quinone backbone.[210]

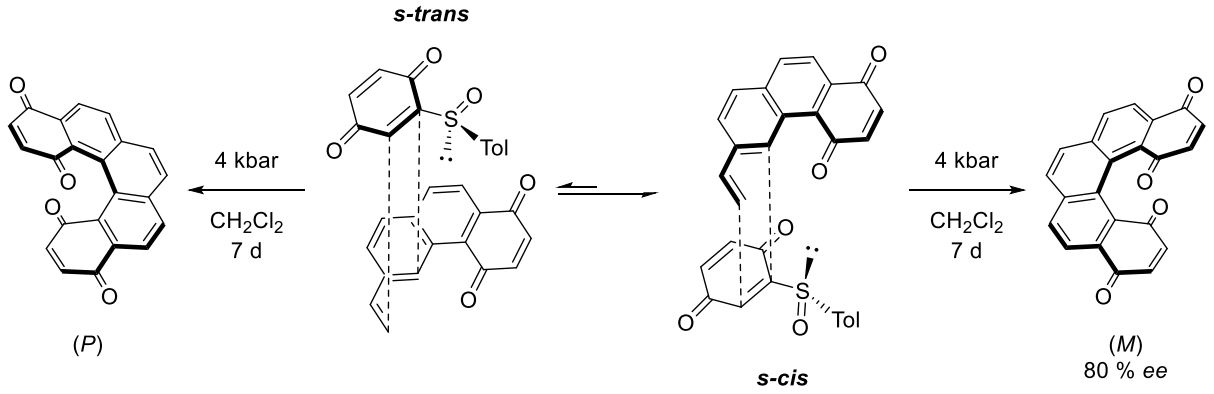

Scheme 94: Regio- and π-facial-selective Diels-Alder reaction.

The second example is a dynamic kinetic resolution (DKR) in a synthesis of [5]helicenic quinones using the same chiral auxiliary. An axially chiral racemic diene underwent [4 + 2] cycloaddition with the chiral sulfoxide, giving a (*P*,S_a)-[5]helicenequinone bearing a biphenyl in 100 % diastereomeric excess (**Scheme 95**).[211] The domino Diels-Alder reaction − sulfoxide elimination − aromatization process resulted in a double asymmetric induction of helical and axial chirality. The stereolabile chiral axis in the substrate allowed an epimerization of the racemate to the one atropisomer which enters the cycloaddition faster. As before, the sulfoxide dictated the helical chirality, but the axial chirality is believed to originate from a contact distance of 3.4−3.6 Å between the biphenyl and the naphthoquinone moiety which is within the range of π-π-interactions.[212] The final product adopts the (S_a)-configuration to maximize π-stacking.

Reports surrounding asymmetric Diels-Alder reactions are scarce articles which involve mainly one group (*Carreño*) as well as one chiral auxiliary for the regulation of the enantioselectivity. Furthermore, the example involving the diastereoselective synthesis is again of substrate-controlled nature. This leaves plenty of room for further research.

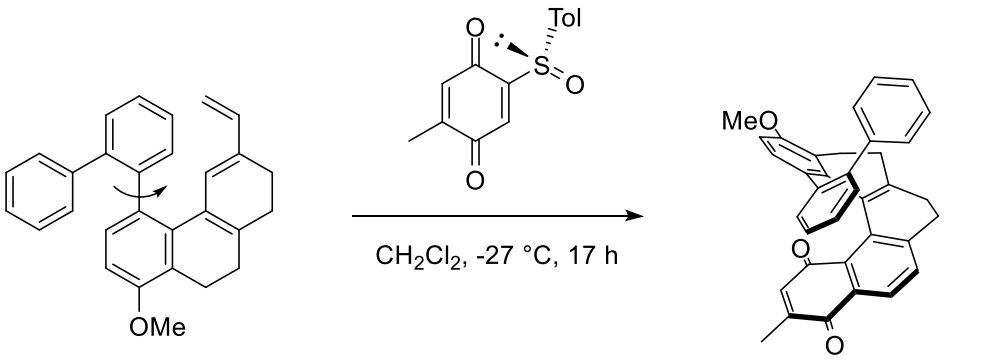

(*rac*) (P,S_a)-[5]helicenequinone
100 % *de*

Scheme 95: Diastereoselective Diels-Alder reaction.

Miscellaneous asymmetric methods

Obviously, other methods each have their own asymmetric version as well. Most of them share the similarity that the chiral information came down to chiral ligands in catalysts (e.g. chiral Grubbs catalyst for asymmetric RCM[213]) or chiral additives (e.g. (−)-sparteine in asymmetric anellation[214]), although most of them are borderline cases between substrate and non-substrate control. *De facto*, all of them are niche solutions providing moderate to low enantioselectivity. As of now, only the [2 + 2 + 2] cycloisomerization and the Diels-Alder addition have consistently been practicable for the efficient enantioselective synthesis of large amounts.

An honorable mention is the predetermined enantioselectivity which is strictly speaking not an asymmetric synthesis *per se* and also falls under the category of substrate-controlled enantioselectivity. This strategy is based on an axial to helical chirality transfer from configurationally defined atropisomers (e.g. benzylic-type coupling of (*S*)-BINOL would give a (*P*)-helicene exclusively). Examples for this are “asymmetric” Wurtz couplings[101,215] or Stevens rearrangements.[110]

5.2 Chiral resolution

Although the asymmetric synthesis is an attractive and powerful approach, not every reaction can be tailored to be enantioselective or diastereoselective. Thus, the manual resolution of racemic mixtures is as important and indispensable. There are several ways to separate a racemate into its components, both classic and old-fashioned as well as modern ones have been used for the resolution of helicenes which will be discussed here.

Recrystallization

Especially in early research when there were no other options, manual crystal picking after *Pasteur* was common practice. Initially, [6]-, [7]-, [8]- and [9]helicenes were resolved that way,[41,216] higher homologues however did not crystallize as conglomerates.[217] Of course, the classic hand-picking is almost obsolete today as it is too tedious and substances crystallize much more frequently as true racemates than conglomerates. The addition of chiral reagents was not new, but unexplored for the optical resolution of helicenes. In 1955, *Newman* and *Lednicer* published the employment of the π-complexing agent 2-(2,4,5,7-tetranitro-9-fluorenylidene-aminooxy)propionic acid (TAPA) in order to get separable diastereomeric charge transfer complexes out of [6]helicene (**Figure 23**).[1,218] Their innovative fractional crystallization was a landmark and opened up new possibilities. Since then, chiral clathrates have been formed from helicenes using silver D-(−)-hydrogendibenzoyl-tartrate,[219] (−)-quinine[220] or (−)-brucine,[221] (±)-*O*,*O*′-dibenzoyl-D-tartaric acid[69] and more.

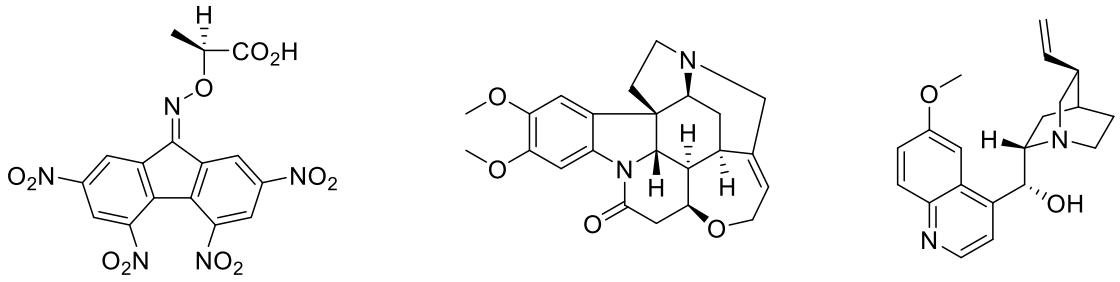

(+)-TAPA (−)-brucine (−)-quinine

Figure 23: Selection of chiral reagents used for optical resolution of helicenes by crystallization.

Enzymatic resolution

Liu and *Katz* achieved a kinetic optical resolution of [5]helicenebisquinone *via* enzymatic hydrolysis (**Scheme 96**).[93] The racemic compound was converted to a hemiketal which in turn was acylated. The acetate was hydrolyzed and resolved with the aid of *bovine pancreas* back to the optically active hemiketal which was oxidized to the original quinone. The enzymatic kinetic resolution yielded an enantiomeric excess of 62 %.

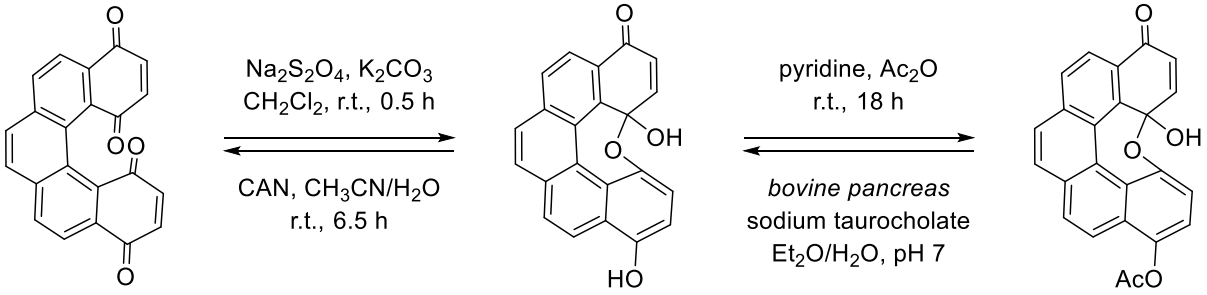

Scheme 96: Enzymatic kinetic resolution of [5]helicenebisquinone.

Using a similar strategy, *Tanaka et al.* achieved a lipase-catalyzed kinetic resolution of a bis(hydroxymethyl)[7]thiahelicene (**Scheme 97**).[222] When treated with *Pseudomonas cepacia* (*PS*) in an acylation, the reaction favorably took place on the (*M*)-enantiomer, leaving the unreacted (*P*)-enantiomer in 98 % *ee*. The reverse phenomenon was observed using *Candida antarctica* (*CA*), leaving the antipode with 92 % *ee*.

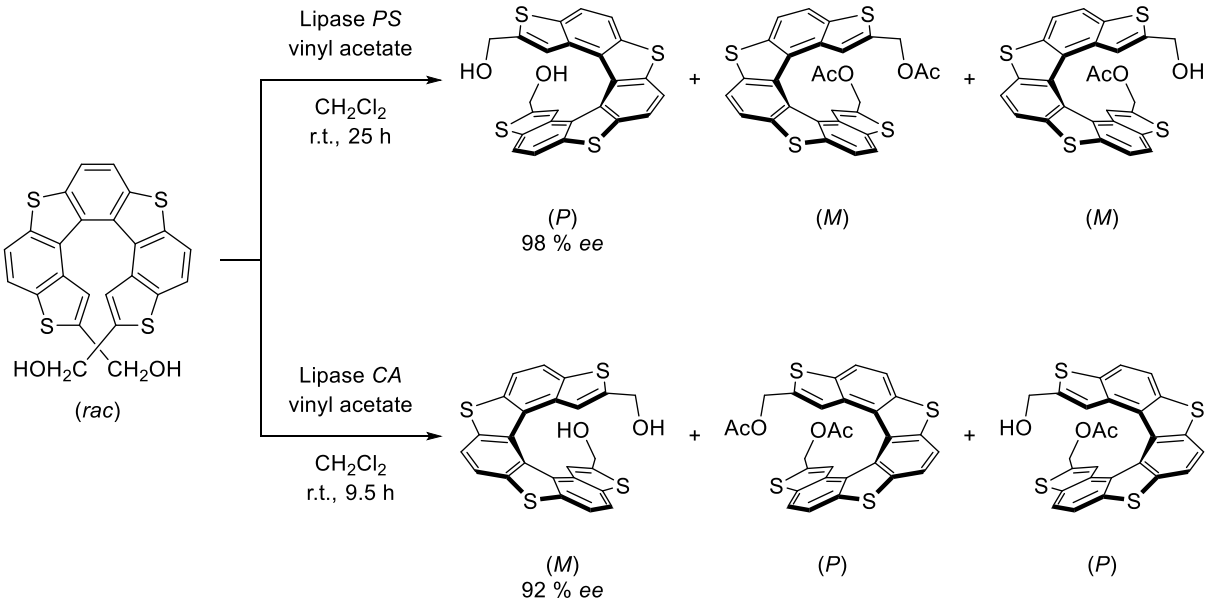

Scheme 97: Lipase-catalyzed resolution of tetrathia[7]helicene.

Capillary electrophoresis

Particularly specific is the optical resolution of charged helicenes by capillary electrophoresis (CE). Randomly sulphated α-, β- and γ-cyclodextrins were used as chiral selectors for the enantioresolution of a series of helical N-heteroaromatic dications (helquats) with 5-, 6- and 7-fused rings.[223] Against slow electro-osmotic flow (EOF), the anions resulting from complex formation of cationic helquats with the sulfated cyclodextrins migrate towards the detector in an electric field, while positively charged unattached helquats migrate to the opposing pole (**Figure 24**). Thereby, the anions resulting from the (*P*)- and (*M*)-enantiomers have a different effective mobility which allowed for their separation. The high polarity resulting from quaternary nitrogen atoms made the helquats reasonably soluble in water. The method benefits from a quick separation with low sample and reagent consumption, but the success of this method relies on the existence of charges and the solubility of the analyte in water.

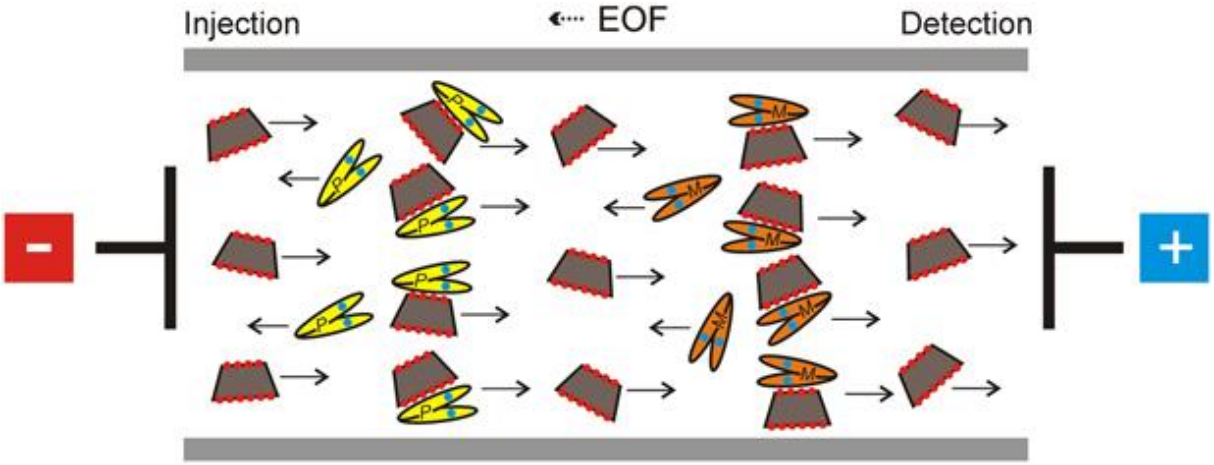

Figure 24: Schematic optical resolution of helquats by CE. Reproduced with permission from *John Wiley and Sons*.[223]

Flash chromatography on achiral phase

The optical resolution by conventional chromatography on an achiral mobile and stationary phase is of course only feasible with chiral auxiliaries. Also addressing charged compounds, *Lacour et al.* managed to separate helicenium cations with enantiopure hexacoordinated BINPHAT anions to achieve a resolution of over 96 % *ee* (**Figure 25**).[224] The diastereomeric salts were subjected to column chromatography on alumina, the absolute configurations were determined by vibrational circular

dichroism spectroscopy (VCD). This approach is noteworthy in the sense that it does not form covalent bonds as the salt formation relies basically on protonation/deprotonation, but again, it stands or falls with the presence of charges.

With aid of (*R*)-(+)-methyl-*p*-tolylsulfoxide, the covalent formation of diastereomers was also done by their group in order to resolve helquats in over 98 % *ee*.[225] With a gap of 0.36 in retention factors, the diastereomers were separated by regular flash chromatography on silica gel. Interestingly, the cleavage of the auxiliary *via* an unprecedented Pummerer-like β-C-C fragmentation was promoted by the electrofugal character of the original helquat.

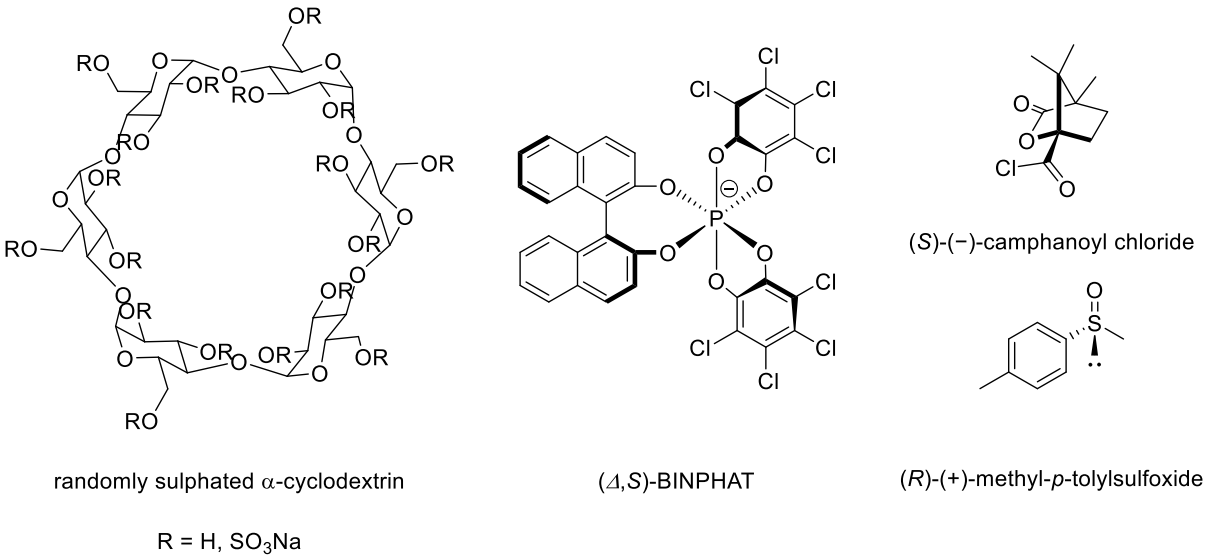

Figure 25: Selection of chiral reagents used for optical resolution of helicenes by CE or column chromatography.

Uncharged enantiomers were separated *via* derivatization to diastereomers by *Katz et al*. The chiral resolution with camphanates in organic chemistry is well known,[19–24] the functional principle involves the pointing direction of the lactone moiety which manipulates the polarity of the diastereomers: In the (*P*)-configurated diastereomer, the lactone points upwards which enhances its polarity, in the (*M*)-diastereomer the sterically favored configuration is the one in which the lactone points downwards, leading to a comparably lower polarity (**Figure 26**). After column chromatography, the auxiliary was cleaved off with methyllithium and chloranil and the enantiomers were retrieved.[226] Because the (*P*)-isomer is usually always more polar as a camphanate compared to its antipode, a quick TLC gives a direct proposition for the absolute configuration as well. The frequency of publications using the same auxiliary confirms

the reliability of this method, in some cases, the favored crystallization of the more polar camphanate was reported, making the resolution even easier.[23,209,227]

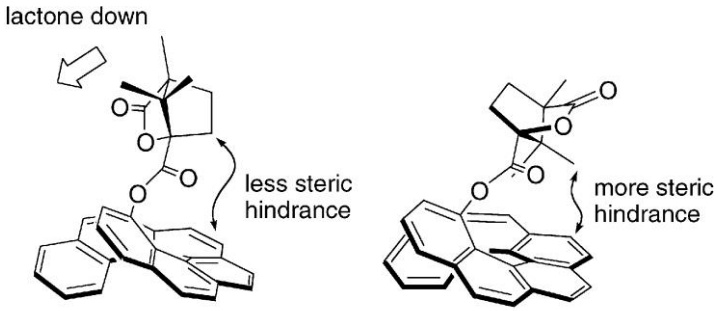

Figure 26: Regulation of the polarity by a lactone moiety in a (*M*)-[6]helicene. Adapted with permission from the *American Chemical Society*.[226]

Flash chromatography on chiral phase

Not every substance crystallizes as a conglomerate (or at all), can be functionalized to diastereomers *ad libitum* or carries charges. Out of the examples mentioned above, probably only the derivatization to diastereomers is versatile enough for a general chiral resolution. But on top of the fact that reactive sides are necessary, this method carries the additional risk that introduction and cleavage could entail a huge deficit in analyte. The ideal solution for this problem would be to make the resolution independent of the analyte, or in other words, relocating the location of the chiral differentiator from the substrate to the external environment.

Undoubtedly the most universal technique for the separation of optically active compounds is the resolution by flash chromatography on a chiral phase. A recurring application is the exploitation of either (+)- or (−)-TAPA to interact better with (*P*)- or (*M*)-helicenes: This time, silica gel columns coated *in situ* with TAPA acted as a chiral stationary phase (CSP).[228,229] For this, eluents had to be carefully selected in which the analytes, but not TAPA, were soluble.

With the exponential technological progress, more refined and more versatile stationary phases and (semi-) automated systems were developed. With the invention of the initially rudimentary high-performance liquid chromatography (HPLC) in the 1970s,[230] it was not a question of if, but when it would become the gold standard for the optical resolution of isomers. Nowadays, powerful systems coming along with a

multitude of CSPs have long since reached the commercial market. This method is practically useful for every kind of isomeric (and non-isomeric) mixture. It stands out due to the fast, efficient and reliable resolution and has surpassed the old-fashioned methods by a wide margin. With low preparative effort, a lot of enantiopure material can be obtained. The only Achilles' heel in this method is the fact that the analyte must be highly soluble in the eluent. Arguably, the acquisition cost of the machine can also be a negative point, but in view of the saved time and effort, the investment quickly pays off.

The strong arguments paired with an established HPLC in-house expertise made it the first choice for the chiral resolution of isomeric mixtures in this work. For that reason, a quick introduction to pivotal technical parameters in HPLC terms is obligatory. When we speak about the elution time, it can mean different things: the elution time of the dead volume t_0 (volume in the chromatographic system which is not swept by the mobile phase) or the elution time of the enantiomers t_n. Furthermore, the individual peak widths of each enantiomer ω_n can be extracted from the chromatogram (**Figure 27**). Indirectly, both provide information about the efficiency of the chromatographic experiment.[231]

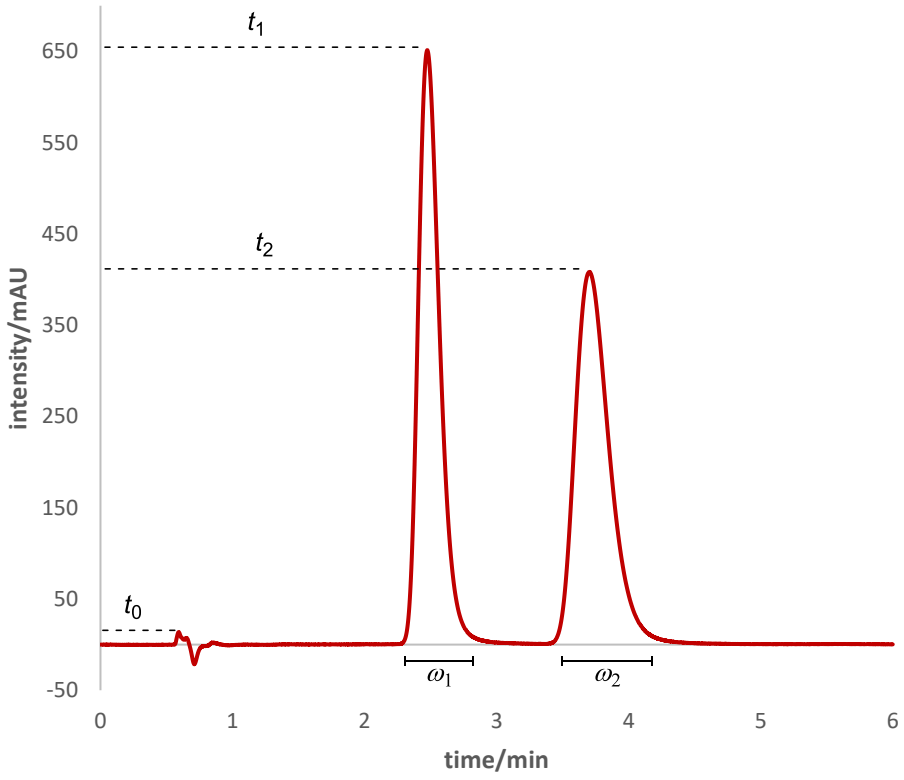

Figure 27: HPLC parameters displayed in a chromatogram.

Given a specific system and experiment, the enantiomers each have a distinct elution time. But as it depends on many variables like eluent, flow rate and column dimensions, it only makes a statement for the one conducted resolution. More generally valid statements can be made with the capacity factor k_n which can be calculated as shown below.

$$k_n = \frac{t_n - t_0}{t_0} \tag{1}$$

The capacity factors are equilibrium constants and give statements for every enantiomer independent of external influences, therefore they are useful for comparing different HPLC systems. The higher the value, the more amount of time the analyte has spent interacting with the stationary phase (and *vice versa*). The value should always lie above 1, otherwise the analyte does not interact with the CSP and may not be resolved at all. The other way around it would be just as bad: If the value is too high, the separation time gets too high as well. As a guideline, the value should be kept around 1 and 10. If statements about the selectivity of the resolution are to be made, the separation factor α can be derived as their quotient.

$$\alpha = \frac{k_2}{k_1} \tag{2}$$

Visually, it represents the difference between both apices of the signals, e.g. the higher the value, the higher the baseline separation. A high selectivity is indicative for a good resolution, but the flaw in this value is that it only accounts for the retention time. For Gaussian curves, this is sufficient enough, but not every chromatographic signal behaves ideally: Dispersion and absorption effects can cause tailing which breaks the symmetry of the signal and decreases the slope towards the end. Oppositely, a high concentration of the analyte can increase the slope in the first half towards the apex. Generally, asymmetric peaks are a bad sign because they make the separation, reproducibility and integration of the signals difficult.

If the sum of the peak widths ω_n is accounted for, the resolution factor R_s can be derived as shown in equation (3).

$$R_s = 2\frac{t_2 - t_1}{\omega_2 + \omega_1} \tag{3}$$

The resolution factor includes the time and width in an inverse manner which means that it should be balanced within a certain range so that the most optimal resolution

can be conducted in the least amount of time. If the value is greater than 1, a separation is occurring to a small degree, but that is not sufficient for a (semi-) preparative resolution without infinite recycling. For a good resolution, the value should be kept around 1.5.

On a practical level, several studies focused on the chiral resolution of helicenes by HPLC. By now, possible CSPs, resolution and separation factors are listed in tabular form and can easily be looked up.[232–236] Out of the sheer infinite pool of CSPs, particularly the ones based on cellulose have shown to be capable of the resolution of helicenes.[237–240] Considering the already available CSPs, the selection was narrowed down to three different ones from three different manufacturers (**Figure 28**). The *CHIRALPAK-IB* (Daicel) and the *CHIRAL ART Cellulose-SC* (*YMC*) each carry a phenylcarbamate on their cellulose backbone, the (*S*,*S*)-*Whelk-O-1* (*Gamma Analysentechnik GmbH*) bears a benzamide and a naphthalene function. All have in common that they provide at least one side for π-π interactions, hydrogen bonds and *van der Waals* forces. Out of the three, the (*S*,*S*)-*Whelk-O-1* offers more sides for π-π interactions which probably is beneficial for the separation of helicene derivative which literally consist of a “π-skeleton”.

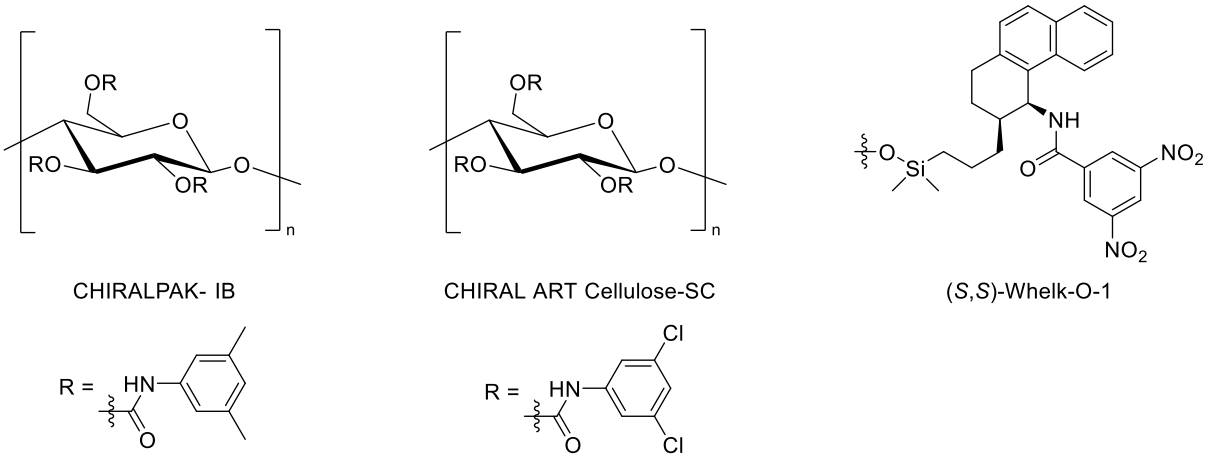

Figure 28: In-house inventory of chiral stationary phases.

5.3 Analysis of structure

After the chiral resolution, the characterization of the fractions is logically the next endeavor. While usual ^{1}H-NMR is perfectly fine for the relative configuration of structures, the measurement of ^{1}H-NMR spectra of two enantiomers would lead to a one-to-one copy. The derivatization to diastereomers along with NMR experiments making use of the nuclear Overhauser effect can be helpful in elucidating the helicity. *Carreño et al.* used NOESY NMR go gain insight on protons in close proximity in order to derive the absolute configuration,[241] a similar practice was done using ROESY.[242] Generally, a series of chiral derivatizing agents have been used for the assignment of absolute configuration by NMR.[243] Above all, the famous mosher ester analysis for alcohols and amides is the most famous one.[244,245]

A pretty safe bet is the prediction or deduction of the absolute configuration from logical conclusions. Some methods have been discussed already, e.g. the predetermined enantioselective synthesis methods with enantiopure BINOL or the diastereoselective point-to-helical chirality transfer of (oxa-) helicenes by *Starý* and *Stará* (*vide supra*). As long as the configurations of the starting materials are defined and known, they should be the same for the product (barring special scenarios like S_N2 or spontaneous epimerization). Analogously, the deduction from the polarity of camphanates by *Katz* can provide information about the absolute configuration as the camphanates of (*P*)-helicenols show a higher polarity than the ones of (*M*)-helicenols. Of course, this only works if both diastereomers are available in the first place, in reactions with absolute enantioselectivity, a quick TLC only gives one retention factor.

Another reliable hint is the algebraic sign of the specific rotation *[α]*. As a rule of thumb, it appears that dextrorotatory helicenes are (*P*)-configurated, levorotatory helicenes appear to be (*M*)-configurated. Other chiroptical techniques are also valid for the assignment. In consequence of their strong π-π* transitions arising from strong dipolar magnetic and electric transition moments, helicenes display intense electronic circular dichroism (ECD) spectra which can be compared to the calculated ones in order to figure out their direction of rotation.[246,247] In dependance of the area of the electromagnetic spectrum, optical rotatory dispersion, vibrational circular dichroism or Raman optical activity have been used especially in the early days of helicene chemistry for their characterization.[248]

But as far as analytical tools go, X-ray crystallography is the most conclusive one. The depiction of atoms in three dimensions allows for the interpretation of their spatial arrangement in terms of locations and distances which can be inaccurate in other methods. However, the determination of the absolute configuration is more complex than a standard XRD experiment.

By definition, an enantiomer possesses a non-centrosymmetric space group (space group without inversion centers), so the determination of the absolute configuration comes down to the assignment of these non-centrosymmetric space groups to one of the two invertible enantiomeric structures. Since the inversion of a crystal structure equals the inversion of its diffraction pattern, matching the experimentally gathered inverted and non-inverted data with the respective calculated data should allow a distinction of the enantiomers. Theoretically, the better fitting data set defines which absolute configuration is the correct one. In practice it is not that simple. According to Friedel's law, X-ray diffraction patterns themselves are approximately centrosymmetric, so an inversion would not do anything and the assignment of the absolute structure remains denied.

When X-rays with the wavelength in the vicinity of the absorption edge of an element is used, the photon gets absorbed by excitation of the electrons of the atom. This leads to anomalous dispersion which does not strictly follow Friedel's law. For the configurational assignment to be feasible, the contribution of the non-anomalous scattering has to be small compared to the contribution of the anomalous one. For heavy atoms like bromine or chlorine, this is the case. For atoms lighter than oxygen, the effects are the smallest which is of course inconvenient for organic molecules.[249]

In 1983, *Flack* described how the anomalous scattering can be used to determine the absolute configuration.[250] The corresponding isolated scattering can be assigned to specific atoms, visually it is noticeable by a change of the structure factor when the incident photon is close to the absorption edge.[251] The sample is considered a reference domain comprising the inverted and non-inverted absolute structures. The relative proportion of the inverted domain is quantified by the Flack parameter *x* which makes a relative statement about the correctness of the absolute configuration. If the parameter gets closer to 0, the current model has the correct absolute structure, likewise an approach towards 1 implies a rising share of the opposing enantiomer in the crystal.

Vital for the quality criterion is its standard uncertainty *u* which is usually attached in brackets after the parameter and refers to the last quoted decimal place, e.g. a value of *x* = 0.1(9) would have such a low precision that neither (+)- nor (−)-configuration can be assumed. Going by a sequential report by *Flack*, *u* should not exceed 0.1 for compounds known to be enantiopure. For compounds with unknown enantiopurity, the value should be below 0.04. Regarding *x* itself, the value should lie within 0±2*u*. Because of random experimental errors, *x* can take negative values. Following a Gaussian probability distribution function, *x* most likely lies somewhere between −3*u* and 1+3*u*. Values far outside are practically unusable und indicate erroneous refinement or data. As already indicated, the uncertainty depends on the wavelengths of the X-ray and the magnitude of the anomalous scattering which in turn relies on the chemical elements in the crystal. This is why the analyte artificially had to be prepared with heavy atoms like chlorine in the past. With better equipment nowadays, this is not mandatory anymore.[252]

Today, his method has become the most common one for the elucidation of the absolute configuration *via* XRD. It stands out from the other methods due to the quickness and inexpensiveness. To be fair, the solid state does not necessarily reflect the situation in solution, but a spontaneous epimerization upon change of aggregate state is doubtful to say the least. One drawback is the fact that not every compound crystallizes and that the resolution of the measurement is dependent on the X-ray source. This can be remedied by synchrotron irradiation for example, but not everyone has access to a particle accelerator.

Therefore, the best method depends on the investigated isomer. If crystals can be grown, XRD is certainly a solid choice, but that does not diminish the importance or accuracy of the other methods. As for almost everything, there is no universal remedy for this problem. Nevertheless, the palette of presented methods gives flexible control over the assignment of the absolute configuration. In fact, the synergy of the techniques is what makes them accurate because the more independent methods agree with the proposed configuration, the more convincing, reliable and definite it becomes in the end.

6 Ligand formation – from scaffold to complete structure

6.1 [5]Helicene

2,13-Difunctionalized [5]helicene

The synthesis of 2,13-dimethoxy [5]helicene (*rac*)-**20** was continued with its chiral resolution. The high solubility facilitated the screening for a suitable mobile phase. Performing a resolution on an analytical scale using a *Daicel CHIRALPAK IB-U* column, the enantiomers eluted after 1.38 and 2.38 min in a mixture of *n*-hexane and isopropanol (**Figure 29**). Considering the elution time of the dead volume t_0 to be 0.63 min, a separation factor of $\alpha = 2.33$ and a resolution factor of $R_s = 2.38$ were achieved which was a promising analytical separation performance.

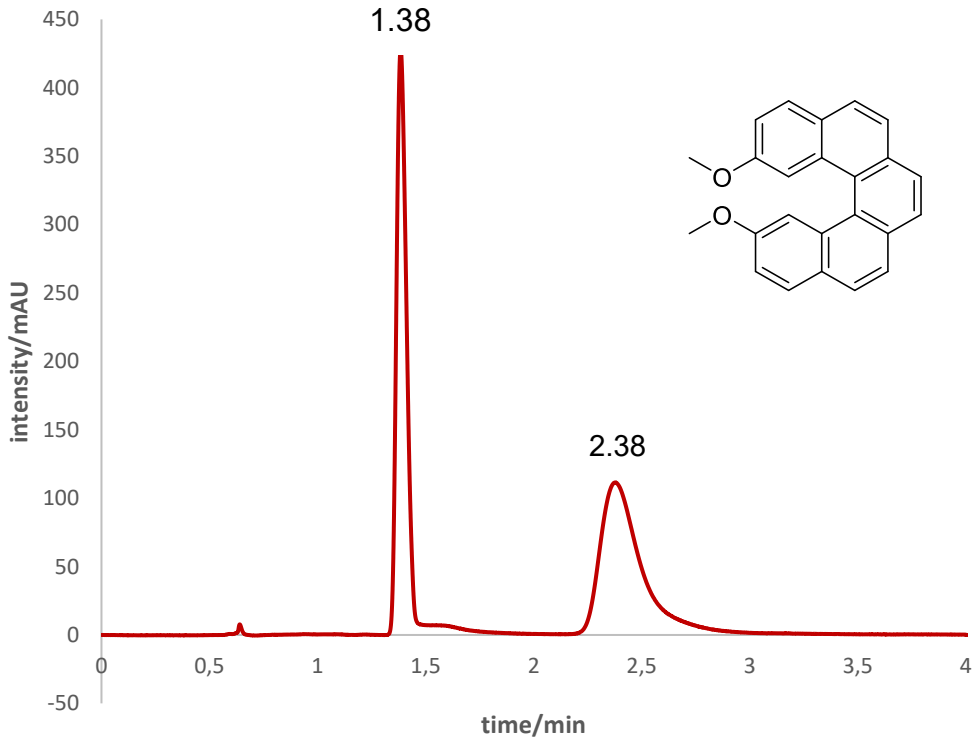

Figure 29: Chiral resolution of (*rac*)-**20** by analytical HPLC (*n*-hexane/^{i}PrOH = 98:2, *Daicel CHIRALPAK IB-U* column, 0.85 mL/min, 235 nm).

Luckily, this performance was transferred to the semipreparative run (**Figure 30**). Under analogous conditions, the enantiomers of (*rac*)-**20** eluted after 6.37 and 7.98 min which results in a separation and resolution factor of $\alpha = 1.42$ and $R_s = 0.88$.

These values are expected to deteriorate from analytical to semipreparative scale, but a slight baseline separation was achieved anyways.

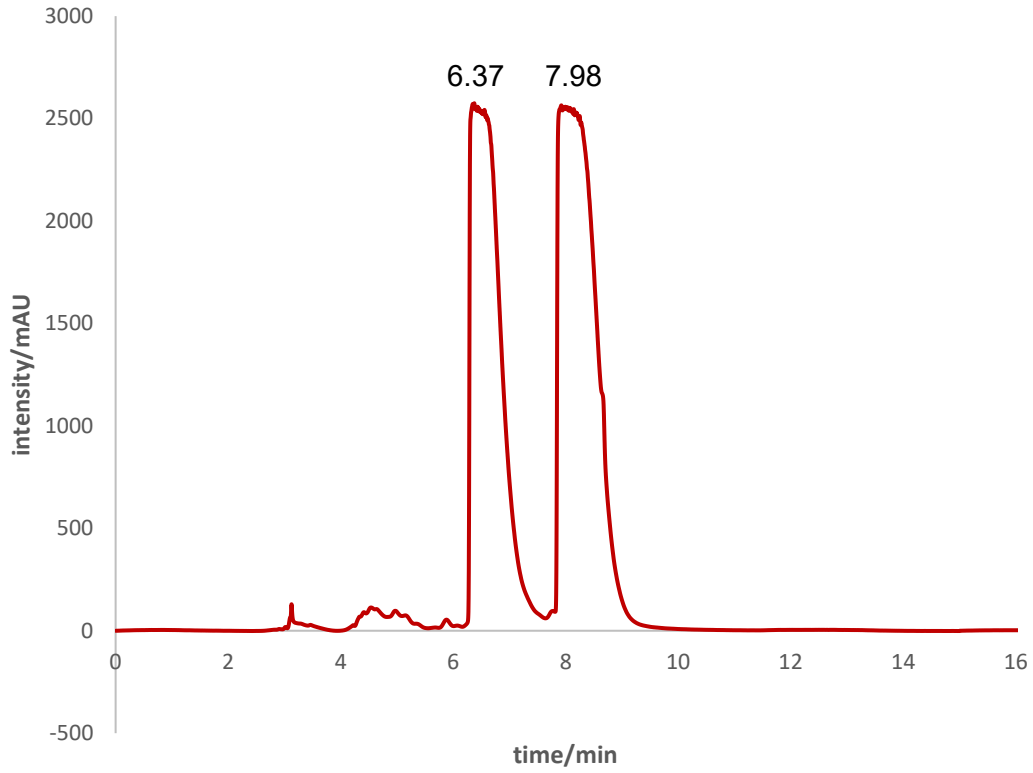

Figure 30: Chiral resolution of (*rac*)-**20** by semipreparative HPLC (*n*-hexane/^{i}PrOH = 98:2, *Daicel CHIRALPAK IB* column, 18 mL/min, 235 nm).

With both enantiomers in hand, the characterization of the obtained fractions was the next objective. As anticipated, both showed the same ^{1}H-NMR and mass spectrum. A first but educated guess was made with the specific rotation *[α]*. Based on their algebraic signs, the first eluting fraction of **20** was tentatively assigned to the (*M*)-isomer, the second eluting fraction to the (*P*)-enantiomer. For some helicenes though, the rule is not rigorously followed and is not regarded as a proof.[253]

Therefore, ECD-spectra were recorded. The emergence of an image − mirror image relationship was a good sign and proved the presence of two enantiomers (**Figure 31**). Theoretical ECD spectra were simulated for each enantiomer *via* simplified time-dependent density functional theory (DFT) by Lukas Kunze from the Grimme group.[254,255] The simulated spectrum had a slight offset to the experimental one which could indicate an incomplete consideration of possible conformers for the calculations. Based on the calculations, a coinciding observation with the optical rotations at the sodium D line was made: The first eluting fraction was assigned to the right-handed

isomer and *vice versa*. The spectra display two distinct bands around λ = 270 and 310 nm of opposite sign, showing a strong resemblance to parent [5]helicene.[247]

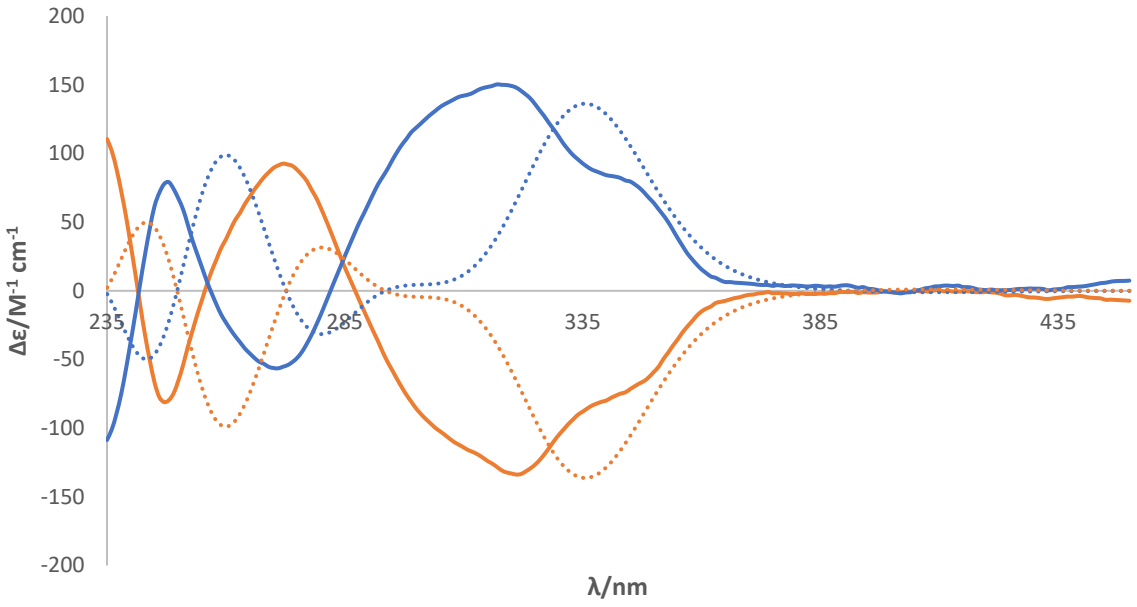

Figure 31: Experimental ECD spectra of (*P*)-**20** (blue solid line, dichloromethane, c = 4.0×10^{-4} g/L), (*M*)-**20** (orange solid line, dichloromethane, c = 4.0×10^{-4} g/L), respectively, and the corresponding calculated ECD spectra (dashed lines).

Single crystals were grown by layering of *n*-hexane on top of a solution of enantiopure **20**, respectively. Since enantiopure compounds can only crystallize in Sohncke space groups, (+)- and (−)-**20** do not crystallize in the same space group like (*rac*)-**20** (*Pbcn*), but in the orthogonal space group $P2_12_12$. Apart from that, the distances and torsional angles were compliant to the racemic compound. Unfortunately, the quality of the crystal was not good enough for a conclusive analysis of the Flack parameter.

The successful optical resolution of (*rac*)-**20** meant that obtaining both enantiomers was possible. Of course, this is not the most optimal stage at which a resolution is sensible: For each past stage a summand of 1 is added to the total sequence of reactions because each reaction from then on must be carried out twice, but in a worst-case scenario in which every following intermediate is irresolvable, the secured resolution was a preliminary solution.

After the assembly of the helix, the focus shifted to the only non-hydrocarbon element left. The methoxy groups survived all the reactions so their purpose was fulfilled. Deprotection of ethers can be done under either Brønsted or Lewis acidic conditions. The former often needs harsher conditions like high temperatures, so it was opted for

the latter. Helicene (*rac*)-**20** was stirred with boron tribromide at −78 °C overnight (**Scheme 98**). The workup was exacerbated by the much lower solubility of the dihydroxy compound.

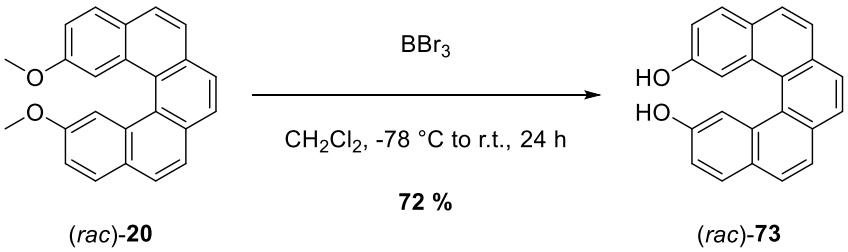

(*rac*)-**20** (*rac*)-**73**

Scheme 98: Deprotection of (*rac*)-**20**.

Contrary to expectation, the newly formed hydrogen bond donors did not provide any benefit for the optical resolution, possibly because of the low solubility in common organic solvents. The resolution showed an overall increase in retention times as well as a higher difference of those (**Figure 32**).

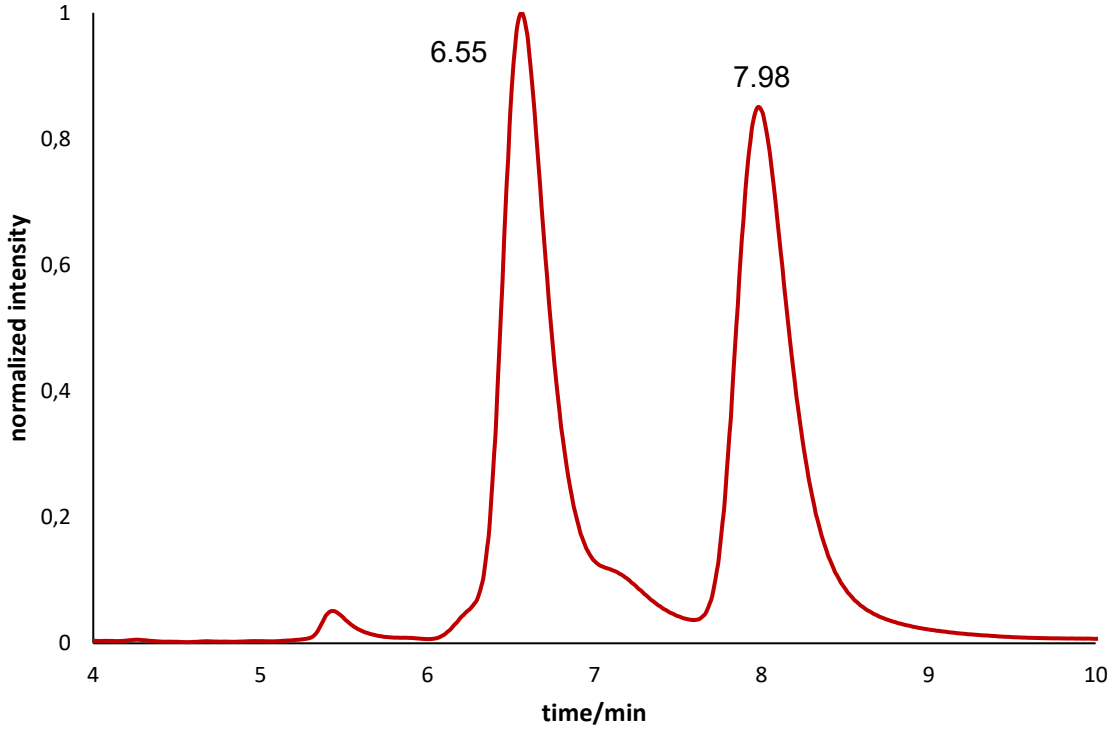

Figure 32: Chiral resolution of (*rac*)-**73** by analytical HPLC (*n*-hexane/^{i}PrOH = 10:1, *(S,S)-Whelk-O-1* column, 1 mL/min, 235 nm).

Both could not be improved by change of eluents without drastically lowering the solubility. On an analytical scale the 5 times higher retention time (compared to **20**) seemed not like a big deal, but could have made a huge difference on a

semipreparative scale. Furthermore, a small shoulder adjacent to the first eluting enantiomer prevented a clean baseline separation, so the idea of a semipreparative resolution was discarded. After purification by column chromatography, 72 % of racemic 2,13-dihydroxy[5]helicene (*rac*)-**73** were accumulated. Byproducts like the mono deprotected alcohol could not be identified, but the yield is in line with the deprotection of 2,15-dimethoxy[6]helicene which in turn seemed to be more difficult to deprotect than the mono functionalized [6]helicene.[64] A harder access to the bay area may be the cause of this.

The penultimate step towards a finished ligand was the esterification of the hydroxy groups so that good nucleofuges were available. Alcohol (*rac*)-**73** was triflated with the corresponding anhydride at 0 °C (**Scheme 99**). In relation to the hydroxy groups, the triflates raised the solubility of the compound enormously which allowed for a smooth purification on silica gel. Racemic triflate (*rac*)-**74** was gained in 80 % yield.

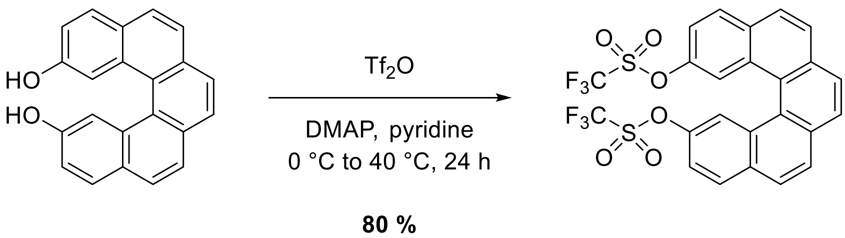

(*rac*)-**73** (*rac*)-**74**

Scheme 99: Triflation of (*rac*)-**73**.

From there on, precursor (*rac*)-**74** paved the way for the synthesis of the final ligands. Various cross-coupling reactions should permit the installation of σ-donors which can then form complexes with various metal centers. For the first donor motif, a 4-pyridinyl moiety was chosen which kept the C_2 symmetry intact. Triflate (*rac*)-**74** was coupled with 4-pyridineboronic acid pinacol ester in a Suzuki-Miyaura cross coupling. Mediated by Pd(dppf)Cl_2, TLC-monitoring did not indicate any transformation. After refluxing for 2 days, the substrate spots still remained (**Scheme 100**, left). The substrate was retrieved by column chromatography without significant deficits. It was unclear why the catalyst was not able to promote the cross-coupling reaction in any way. The system was changed in 2 ways: The catalyst was replaced with $Pd(PPh_3)_4$ and the base was replaced with potassium carbonate (**Scheme 100**, right). Luckily, this time TLC-control indicated a substantially more polar fraction which was assumed to be caused by the newly attached pyridine units. The fraction was isolated by column chromatography on silica gel. ^{1}H-NMR spectroscopy (**Figure 33**) and mass spectrometry proved the

formation of bis(pyridine) (*rac*)-**75**. In total, 54 % was obtained, partly because of the mono functionalized side product. A longer reaction time probably would have given more yield. Nonetheless, the first ligand was ready for complexation attempts.

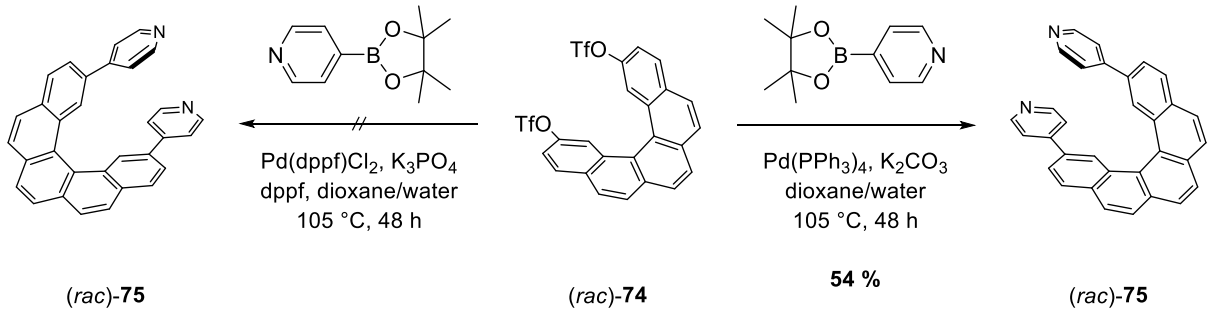

Scheme 100: Suzuki coupling of (*rac*)-**74** to (*rac*)-**75**.

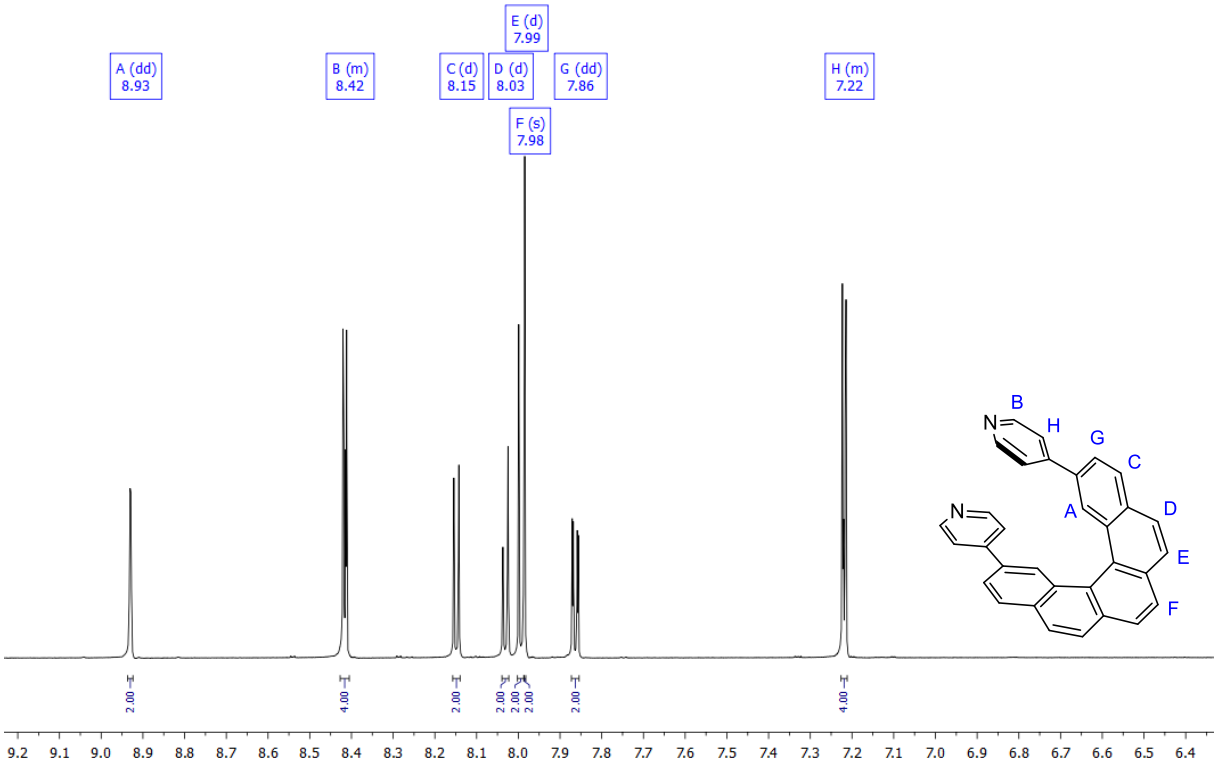

Figure 33: ^{1}H-NMR spectrum and assignment of (*rac*)-**75**.

The racemic mixture was subjected to HPLC resolution. Analytically, the signals were broader than during the resolution of (*rac*)-**20** and the retention times were a bit higher (t_1 = 2.47 min and t_2 = 3.70 min). The basic character of the pyridines had to be counteracted with 3 vol% of diethylamine. A baseline separation was achieved with a separation and a capacity factor of α = 1.67 and R_s = 2.32, respectively (**Figure 34**). Overly optimistic, the assay was resolved by semipreparative HPLC. Hereby, with

retention times of t_1 = 10.58 min and t_2 = 13.59 min, the separation and capacity factors were α = 1.38 and R_s = 1.60 (**Figure 35**).

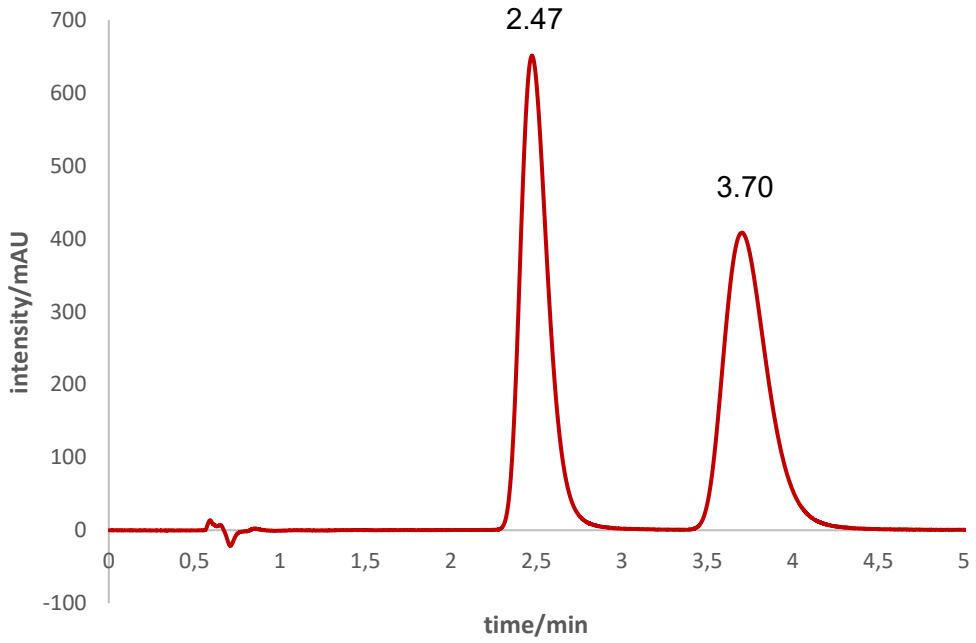

Figure 34: Chiral resolution of (*rac*)-**75** by analytical HPLC (*n*-hexane/EtOH = 7:3 + 0.3 vol% DEA, *Daicel CHIRALPAK IB-U* column, 0.85 mL/min, 235 nm).

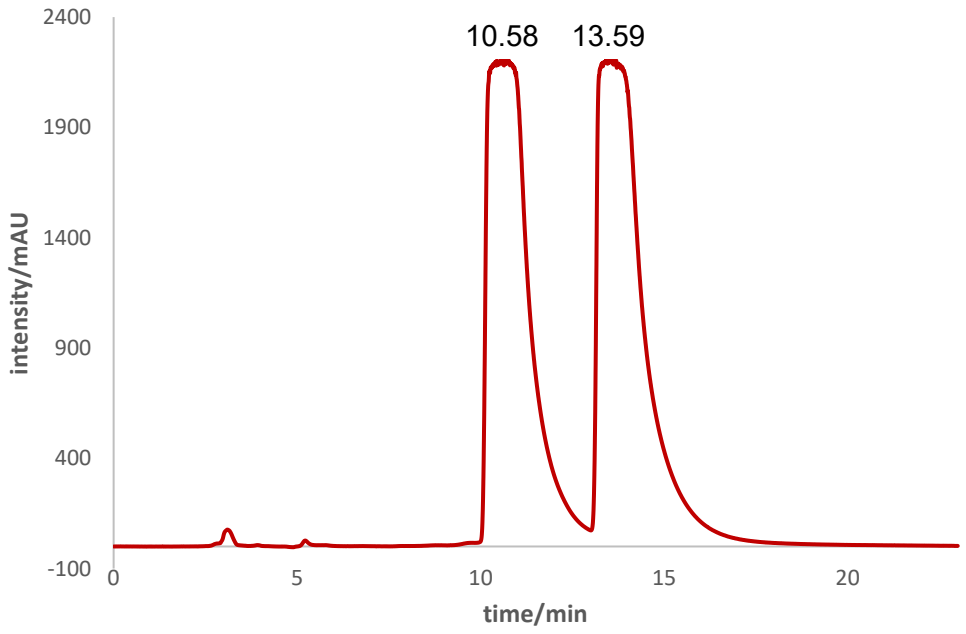

Figure 35: Chiral resolution of (*rac*)-**75** by semipreparative HPLC (*n*-hexane//EtOH = 7:3 + 0.3 vol% DEA, *Daicel CHIRALPAK IB* column, 18 mL/min, 235 nm).

Repeatedly, the characterization routine started with the optical rotations at the sodium D line. According to them, the first eluting enantiomer had to be the right-handed helix.

A first confirmation was made with the ECD spectra which showed the typical image − mirror image relationship (**Figure 36**). The three most prominent bands of the spectra are around λ = 250, 290 and 330 nm. The simulated spectra had a moderate agreement to the experimental ones. The lower similarity between the ECD spectra of (*P*)-**75** and (*M*)-**75** compared to the similarity between those of (*P*)-**20** and (*M*)-**20** indicated a higher number of non-considered conformers which contributed to the final spectrum. In light of the fact that both **20** and **75** should have comparable conformational degrees of freedom, an offset twice as large was unexpected. An alternative or additional explanation could be interfering charge transfer excitations of the molecules which can be difficult to characterize with DFT.[256–258] Still, the moderate agreement was sufficient enough for the confirmation of the previous assignments made on the basis of the optical rotations.

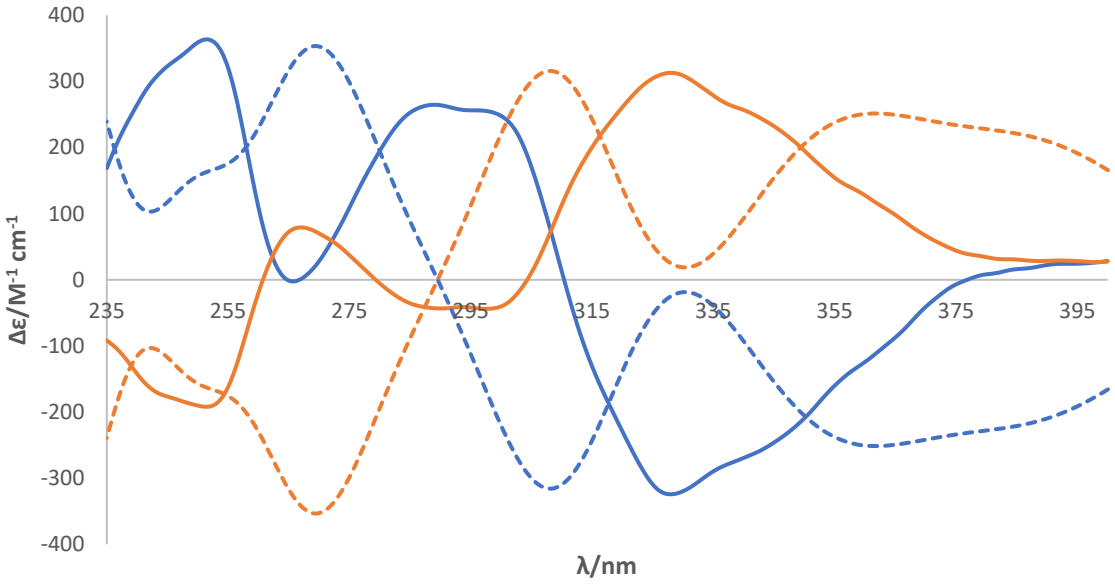

Figure 36: Experimental ECD spectra of (*P*)-**75** (blue solid line, dichloromethane, $c = 5.8\times10^{-4}$ g/L), (*M*)-**75** (orange solid line, dichloromethane, $c = 6.1\times10^{-4}$ g/L), respectively, and the corresponding calculated ECD spectra (dashed lines).

Single crystals for XRD analysis were grown by layering *n*-hexane on top of a solution of enantiopure **75** in dichloromethane overnight at −10 °C. Like enantiopure **20**, (+)- and (−)-**75** crystallize in the orthogonal space group $P2_12_12$. The inner cavity has a diameter of approximately 2.9 Å, the tilt and torsional angles are in the same range of **20** as well (**Figure 37**). The distance of the nitrogen atoms within the 4-pyridinyl moieties accounted for 7.0 Å. Last but not least, Flack parameter analysis reconfirmed the predictions of the absolute configurations.

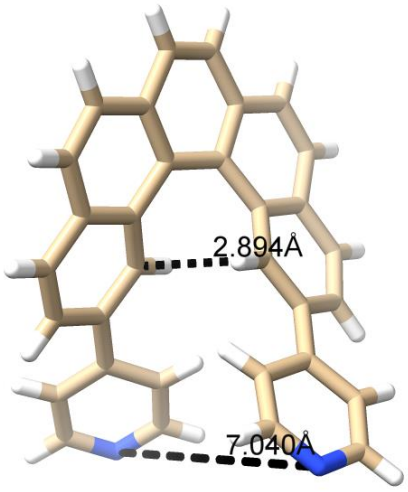

Figure 37: Molecular structure of (*M*)-**75** as determined by single crystal XRD analysis (carbon in brown, hydrogen in white, nitrogen in blue).

With the first bidentate ligand in hand, the preparation of additional ones to fill the assortment was the next aim. Without deviating from the bidentate bis(pyridine) moiety, the keynote for the following building block was the increase of the degrees of freedom in terms of rotation and resulting donor angle. Thus, a lower symmetry was envisaged, caused by a change in position of the donating nitrogen atom from 4 to the 3. Adopting the same procedure of (*rac*)-**75**, triflate (*rac*)-**74** was coupled with 3-pyridineboronic acid. Promoted by $Pd(PPh_3)_4$, the Suzuki coupling of (*rac*)-**74** gave racemic pentahelicene (*rac*)-**76** in 40 % yield (**Scheme 101**). Bis(pyridine) **76** showed a much higher polarity compared to its constitutional isomer **75** which probably caused the lower yield. The ^{1}H-NMR spectrum showed sharp signals with little to no overlap and indicated a species with high symmetry which made the assignment considerably easier (**Figure 38**). Unfortunately, every attempt to resolve the racemate by analytical HPLC or to crystallize the compound was not fruitful. Nonetheless, the second ligand was ready to be complexed with a metal.

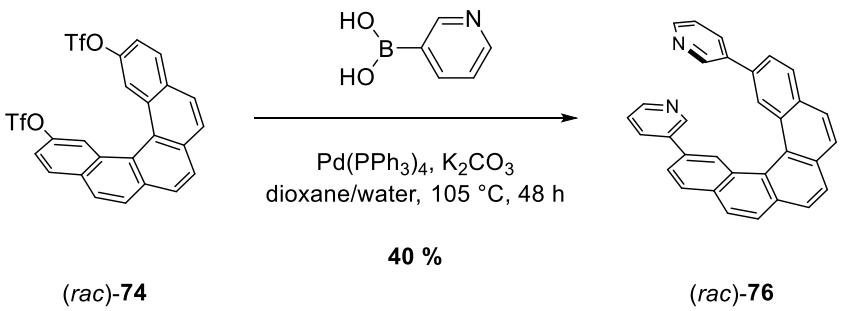

Scheme 101: Suzuki coupling of (*rac*)-**74** to (*rac*)-**76**.

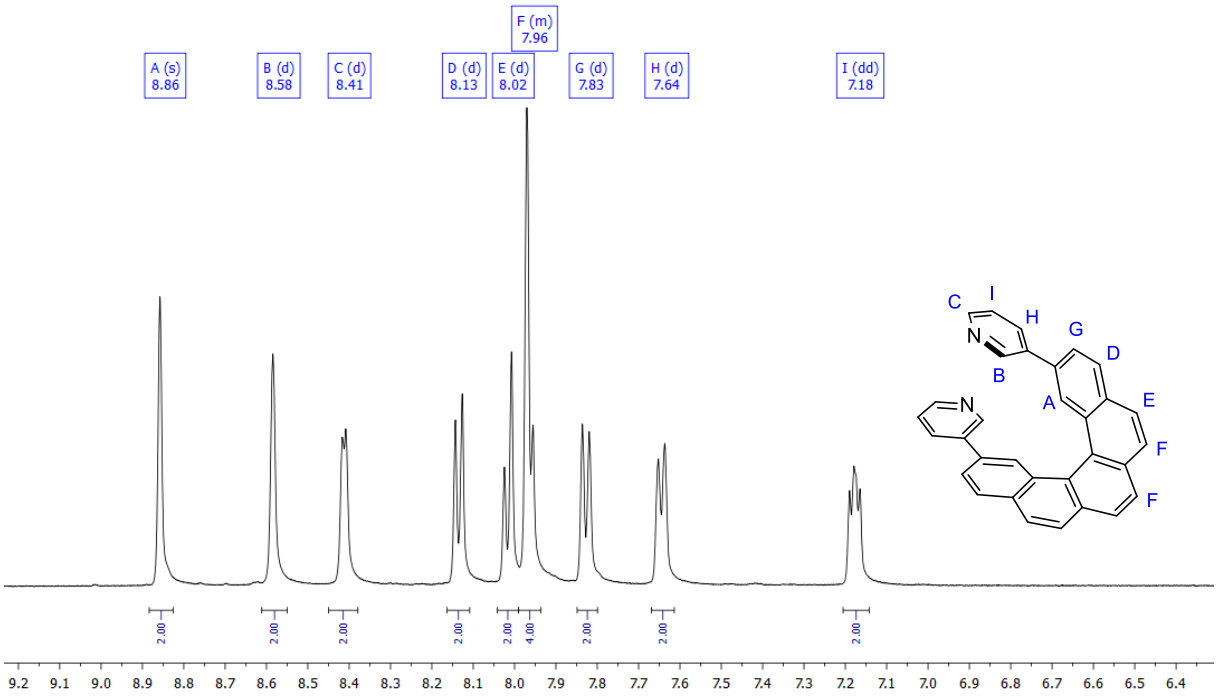

Figure 38: ^{1}H-NMR spectrum and assignment of (*rac*)-**76**.

For the third ligand, the bond lengths were re-examined and re-evaluated. In case of overcrowded vicinity, the donor motifs had to be further distanced from the helical skeleton. To increase the ligand cone angle, an acetylene spacer between the helical shore and the pyridine unit was envisaged. Unexpectedly, triflate (*rac*)-**74** did not react in a Sonogashira reaction under various conditions (**Scheme 102**).

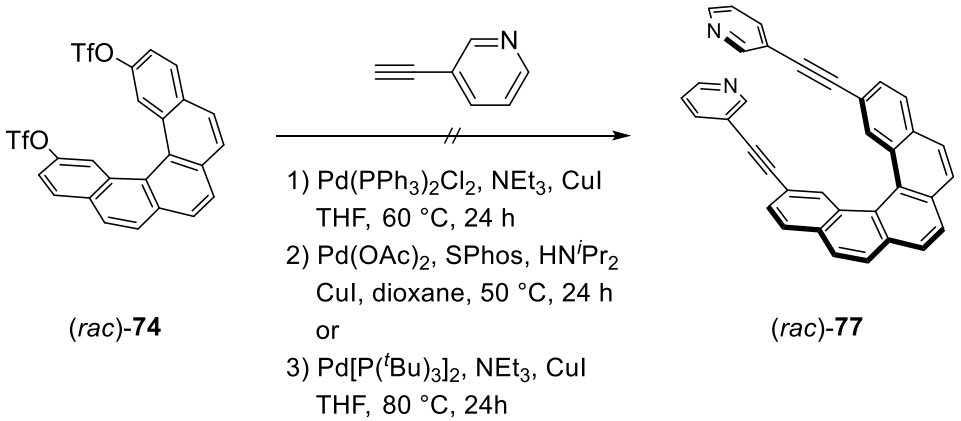

(*rac*)-**74** (*rac*)-**77**

Scheme 102: Sonogashira coupling of (*rac*)-**74** to (*rac*)-**77** under various conditions.

Using the established routine protocol with $Pd(PPh_3)_2Cl_2$, TLC-monitoring indicated an unaltered solution. After column chromatography on silica gel, (*rac*)-**74** was completely recovered. Any attempt to facilitate the oxidative addition with more electron rich ligands failed and the substrate was recovered every time. It was obscure why the

precursors underwent oxidative addition in Suzuki, but not in Sonogashira cross-couplings. But since the former had already been figured out, the acetylene spacer was substituted by a 1,4-phenylene spacer. Indeed, cross-coupling of triflate (*rac*)-**74** under the established Suzuki coupling protocol gave racemic bis(pyridine) (*rac*)-**78** in good yield (**Scheme 103**). The high yield was achieved by omitting chromatographic workup on silica gel. *Via* recrystallization, racemic (*rac*)-**78** was collected in the form of yellow needles and analyzed by ^{1}H-NMR spectroscopy (**Figure 39**) and mass spectrometry.

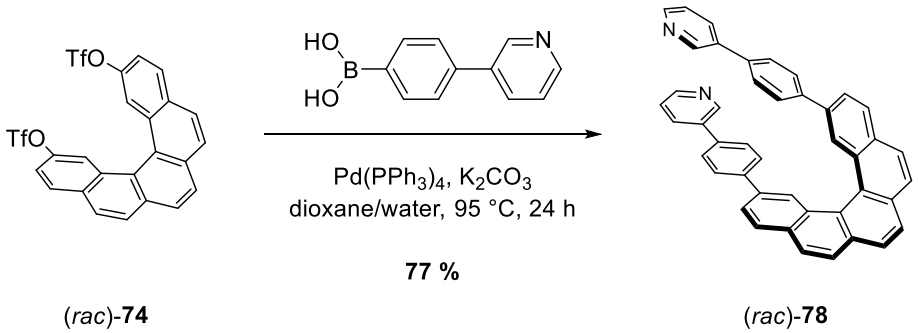

(*rac*)-**74** (*rac*)-**78**

Scheme 103: Suzuki coupling of (*rac*)-**74** to (*rac*)-**78**.

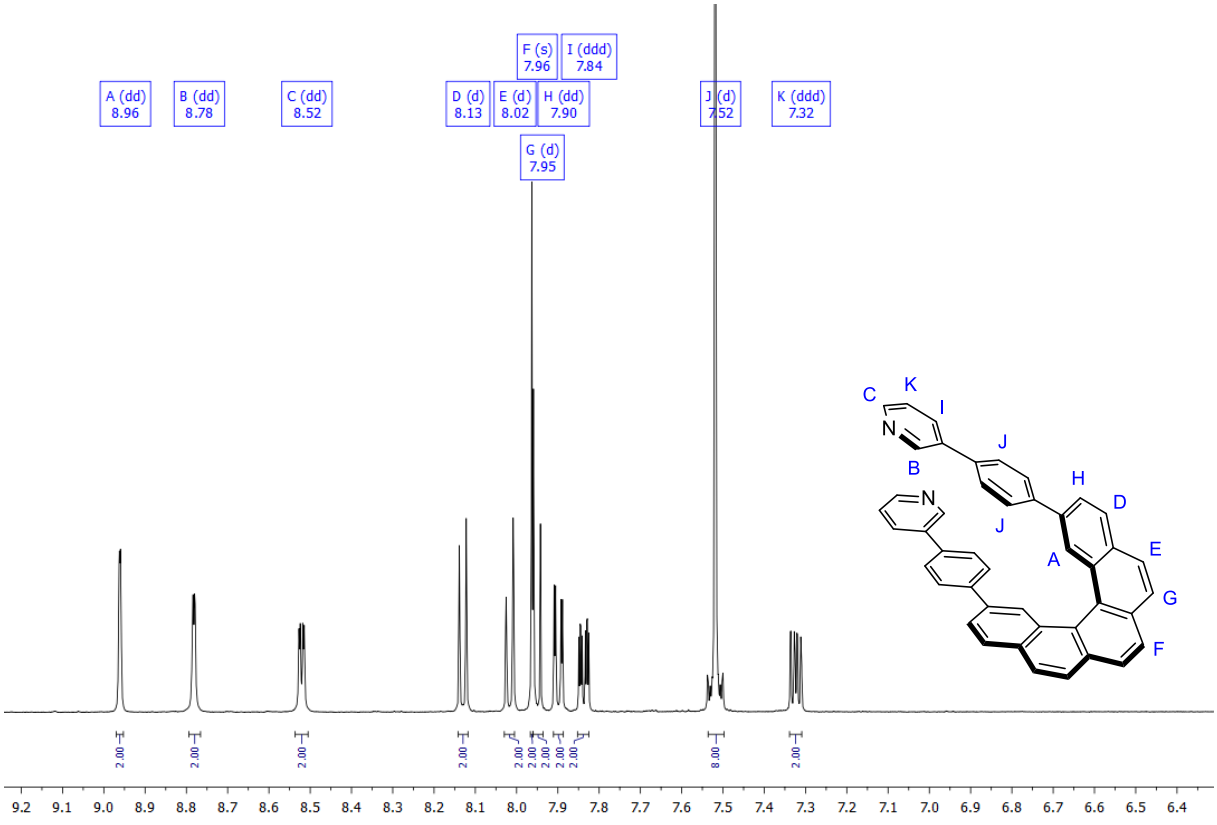

Figure 39: ^{1}H-NMR spectrum and assignment of (*rac*)-**78**.

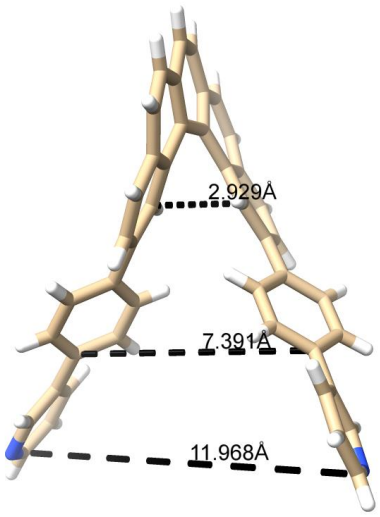

Figure 40: Molecular structure of (*rac*)-**78** as determined by single crystal XRD analysis (carbon in brown, hydrogen in white, nitrogen in blue).

The yellow needles were subjected to XRD analysis, racemic (*rac*)-**78** crystallizes in the monoclinic space group *C*2/*c*. The diameter of the cavity of the [5]helicene backbone remains the same overall, but the gap between the attached aryl units widened. In **78**, the positions previously occupied by nitrogen atoms (in pentahelicene **75**) had a larger distance of 7.4 Å (compared to 7.0 Å in **75**), the outermost carbon atoms have a distance of 12.0 Å (**Figure 40**).

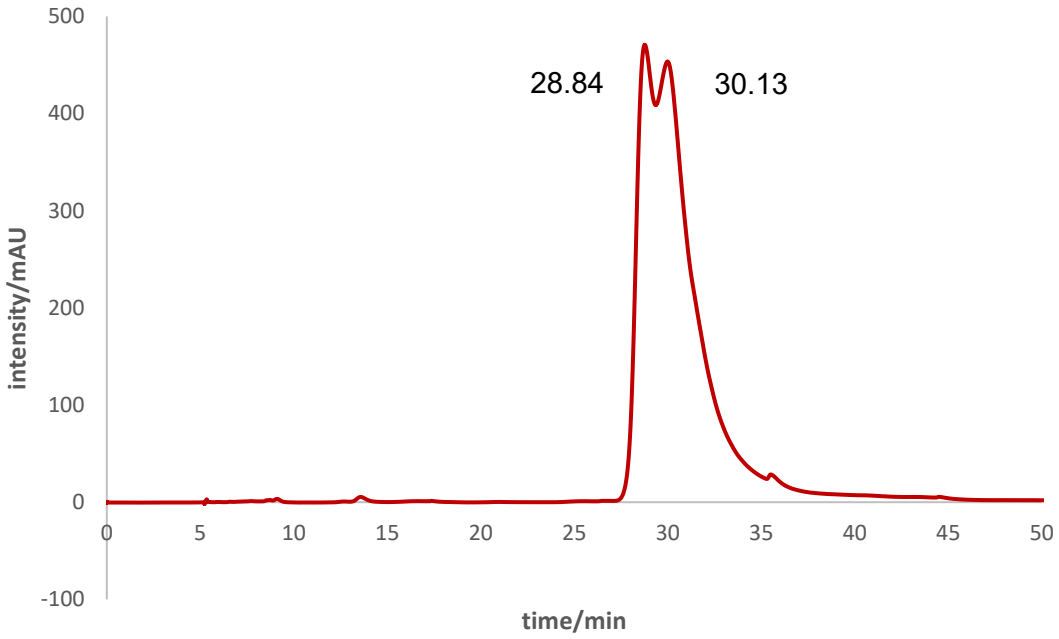

Figure 41: Chiral resolution of (*rac*)-**78** by analytical HPLC (dichloromethane/MeOH = 995:5, *(S,S)-Whelk-O-1* column, 1 mL/min, 235 nm).

Regarding the optical resolution by HPLC, only a slight separation was achieved without lowering the solubility of (*rac*)-**78** too much (**Figure 41**). On the first glance, a recycling HPLC run would theoretically have been feasible, but the long retention times made the cost-benefit ratio way too poor for an actual semipreparative resolution. In light of the dwindling material, a further screening on reverse phase was not made. Nonetheless, for the time being, there was enough material left for complexation experiments.

Based on a 2,13-difunctionalized pentahelicene, a total of three C_2-symmetric bidentate ligands have been synthesized. While the nitrogen donor motif is throughout the same, the resulting donor, bite and cone angles should vary. This should lead to different assemblies around the same metal centers. The 3-pyridine units display a higher amount of flexibility due to the bond rotation of two bridge-head carbon atoms which connect two phenyl units, but have a lower symmetry than the 4-pyridine units which can make analysis of resulting complexes by NMR spectroscopic experiments more difficult.

1,14-Difunctionalized [5]helicene

The route towards 1,14-difunctionalized bidentate ligands started with the optical resolution of racemic 1,14-dimethoxy [5]helicene (*rac*)-**38**. Using the same stationary phase as in the separation of (*rac*)-**20**, the enantiomers of **38** eluted after 1.41 and 2.22 min (**Figure 42**). This resulted in a separation factor of α = 2.03 and a resolution factor of R_s = 2.59.

The semipreparative run was free of any disturbances as well, the overall scale-up gave retention times of t_1 = 6.18 min and t_2 = 7.47 min, a separation factor of α = 1.44 and a resolution factor of R_s = 0.76 (**Figure 43**). The enantiomers were crystallized *via* layering of *n*-hexane on top of their respective solutions in dichloromethane at −10 °C overnight and subjected to XRD analysis. Like (*P*)- and (*M*)-**20**, (*P*)- and (*M*)-**38** crystallize in the orthogonal space group $P2_12_12$. But compared to **20**, **38** has a 0.3 Å larger inner cavity and a 4° higher torsional angle (**Figure 44**). Apparently, **20** has a higher topological similarity towards unfunctionalized parent pentahelicene with which it shares similar dihedral angles and diameters.[2] This is not surprising: The steric impact of the methoxy groups should be much higher in the innermost position which

results in the overall higher values. After analysis of the Flack parameters, the first eluted fraction was assigned to the right-handed enantiomer and the second to the left-handed one. The algebraic signs of the optical rotations validated the suggestions about the absolute configurations.

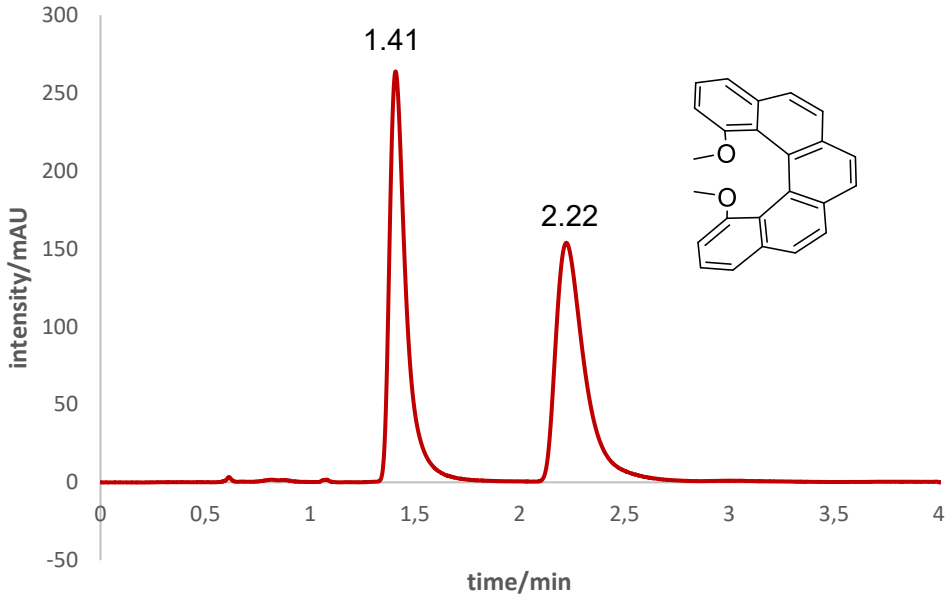

Figure 42: Chiral resolution of (*rac*)-**38** by analytical HPLC (*n*-hexane/^{i}PrOH = 9:1, *Daicel CHIRALPAK IB-U* column, 0.85 mL/min, 235 nm).

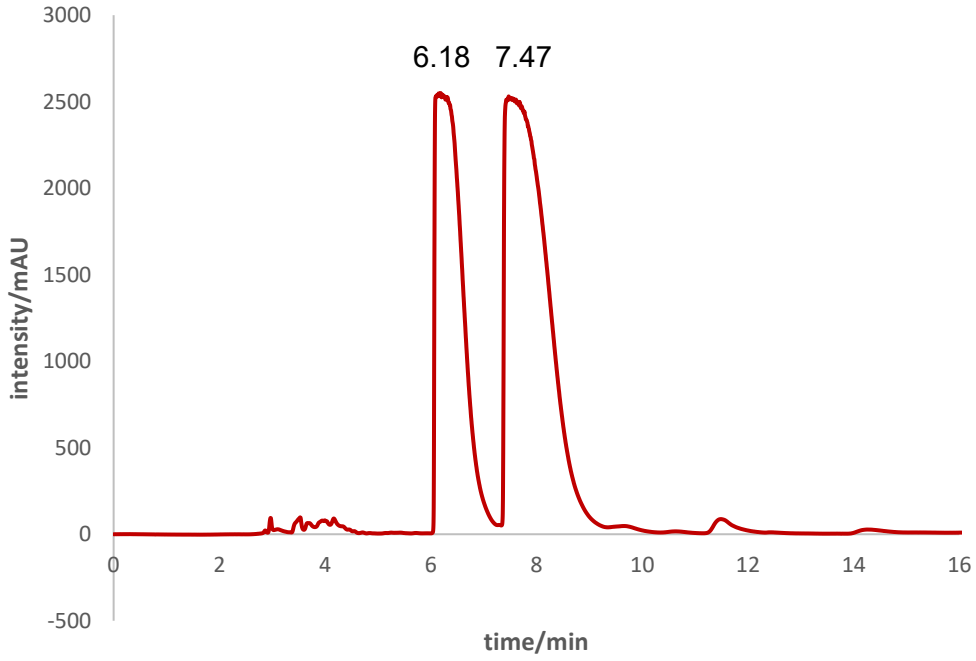

Figure 43: Chiral resolution of (*rac*)-**38** by semipreparative HPLC (*n*-hexane/^{i}PrOH = 95:5, *Daicel CHIRALPAK IB* column, 18 mL/min, 235 nm).

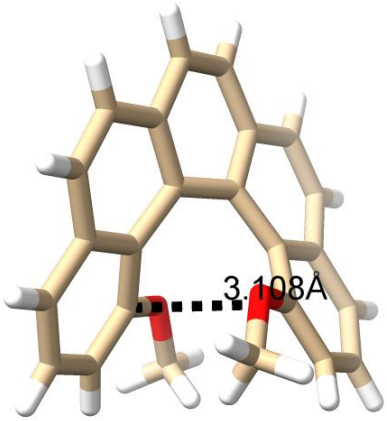

Figure 44: Molecular structure of (*M*)-**38** as determined by single crystal XRD analysis (carbon in brown, hydrogen in white, oxygen in red).

The ECD spectra displayed distinct bands at around λ = 251, 296 and 340 nm for both enantiomers, further emphasizing the lower similarity to parent [5]helicene compared to **20** (**Figure 45**).[247] Last but not least, the calculated spectra had a good agreement with the experimental ones and supported the assignment of the absolute configurations: The first eluting fraction was identified as the (*M*)-enantiomer and *vice versa*. The secured optical resolution was a good fallback option in case future resolutions on later stages would have been unsuccessful.

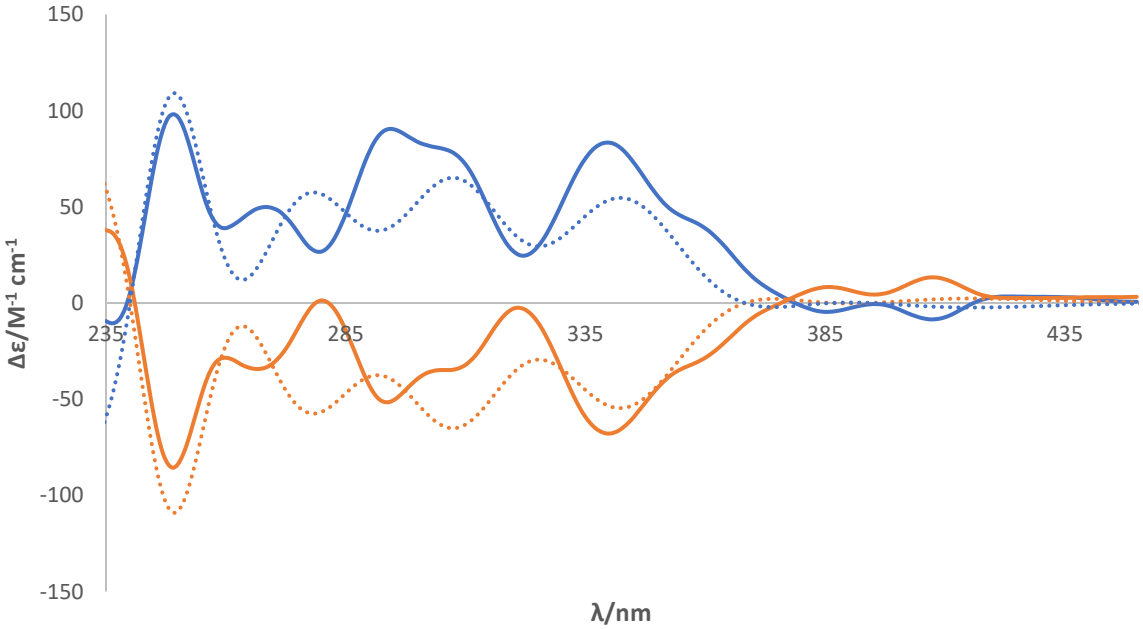

Figure 45: Experimental ECD spectra of (*P*)-**38** (blue solid line, dichloromethane, $c = 4.0\times10^{-4}$ g/L), (*M*)-**38** (orange solid line, dichloromethane, $c = 4.0\times10^{-4}$ g/L), respectively, and the corresponding calculated ECD spectra (dashed lines).

Analogously to the previous pathway, the deprotection of the methoxy groups was targeted next. 1,14-Dimethoxy[5]helicene was treated with a stock solution of boron tribromide in dichloromethane at −78 °C overnight (**Scheme 104**). The workup was remarkably easier compared to the one of regioisomer 2,13-dihydroxy[5]helicene **73**. The running behavior of the compound on a regular silica gel-coated TLC plate showed a suspiciously low polarity and its solubility in dichloromethane was unexpectedly high, whereas the congener **73** was only moderately soluble upon addition of methanol.

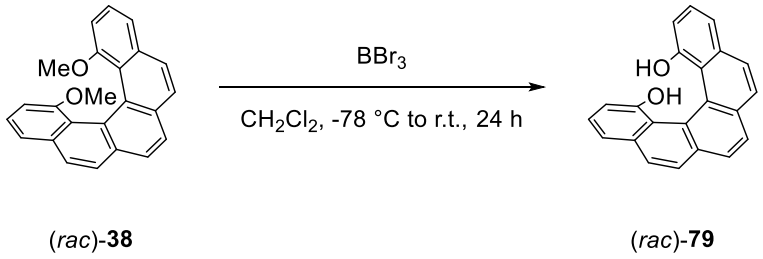

(*rac*)-**38** (*rac*)-**79**

Scheme 104: Deprotection of (*rac*)-**38** with BBr_3.

Nonetheless, the easy purification gave a very clean ^{1}H-NMR spectrum. Since O-H protons are rarely observed *via* proton NMR due to their fast exchange rate, the integral ratios in the spectrum matched those expected for racemic 1,14-dihydroxy[5]helicene (*rac*)-**79** (**Figure 46**).

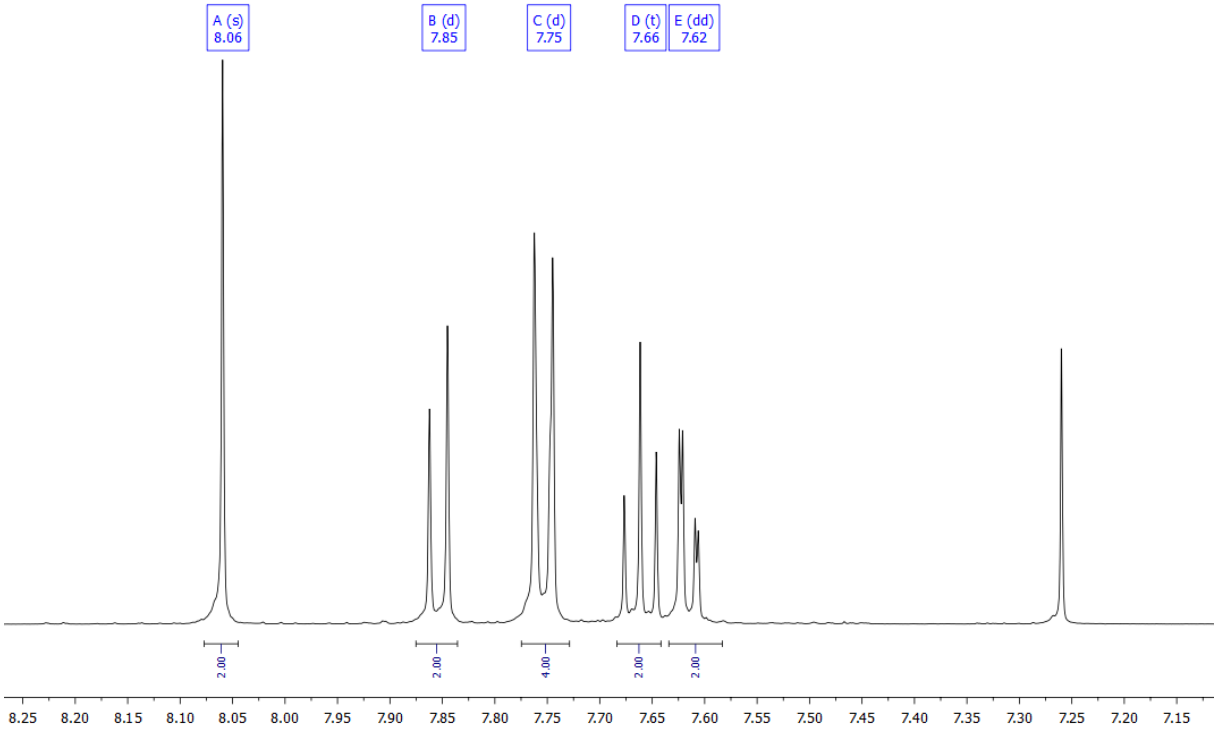

Figure 46: ^{1}H-NMR spectrum after deprotection of (*rac*)-**38** with BBr_3.

The signals of the methoxy protons disappeared and the ^{13}C-NMR spectrum also indicated the formation of (*rac*)-**79**. On the other hand, mass spectrometric analysis did not align with the expected result. EI-mass spectrometry showed a prominent peak with *m*/*z* = 292.0 which would fit to a species with the chemical formula of $C_{22}H_{12}O$. Out of the structures that made logical sense and fitted to all the spectroscopic observations, one resulting from a removal of one methoxy group and subsequent intramolecular ether formation was considered, leading to the bridged helicene **80** (**Figure 47**). Such closed structures are called helicenophanes. *Marinetti* and coworkers used this structure motif in order to ensure configurational stability at room temperature. A chiral tether locked the [5]helicene in its configuration and prevented a racemization at elevated temperatures which occurred in the unfunctionalized equivalent.[9] 10 years later, a tether based on L-(+)-tartaric acid was introduced to a [7]helicene by *Quideau et al*.[10]

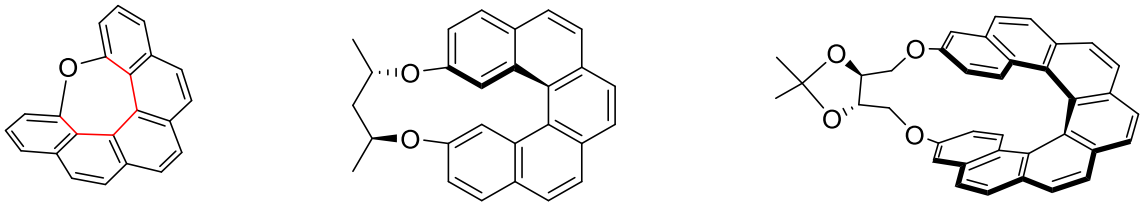

80 (*S*,*S*,*P*) (*S*,*S*,*P*)

Figure 47: Selection of helicenophanes.

But in these examples, the bridges stretch over multiple atoms. The short oxygen tether in **80** makes such an arrangement rather strained und unfavored. A quick GFN2-xTB[177,178] minimized model depicted that the oxygen chain forces the molecule into a bowl shape. This would introduce an internal mirror plane σ_h into the molecule which would also make it achiral. First signs supporting this hypothesis were gathered through analytical HPLC (**Figure 48**). In diverse stationary and mobile phases, not even the slightest separation in the apex of each signal was visible. Combined with a sleek, sharp and slim signal during every run, the observations suggested that only one species was present.

Luckily, single crystals of **80** could be grown by layering of *n*-hexane over its solution in dichloromethane at −10 °C. The crystals took the shapes of plates and needles. XRD analysis confirmed the highly compressed configuration and the achiral nature (**Figure 49**). Depending on its crystal shape, **80** crystallizes either in the orthorhombic

space groups $P2_12_12_1$ or *Pbca*. The average dihedral angle between the inner carbon atoms (marked in red in **Figure 47**) was 22°. The bridging oxygen atom dictates the bowl shape within the molecule and locks it in this configuration.

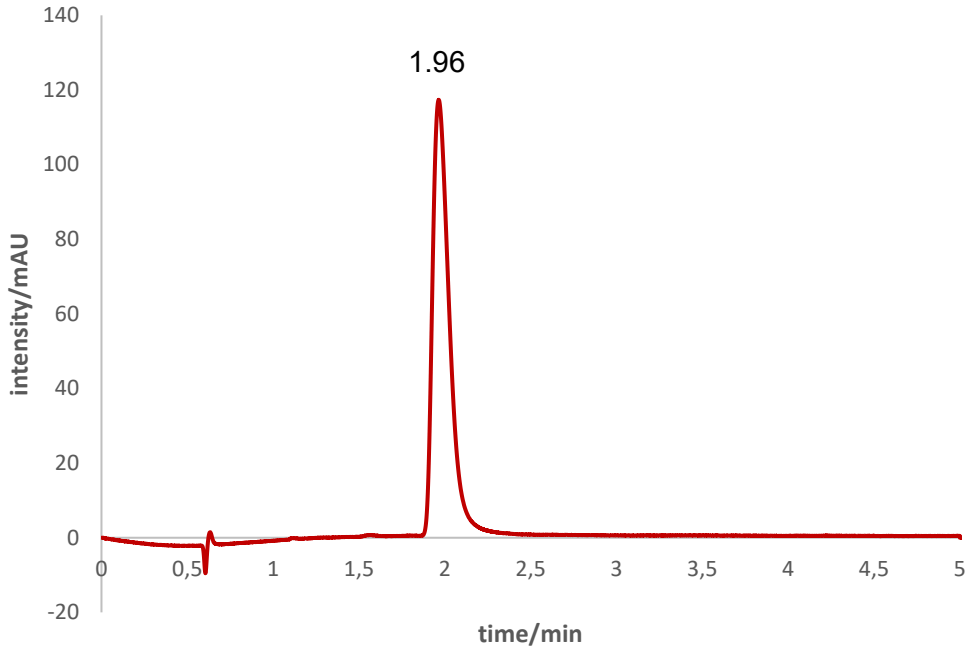

Figure 48: Attempted resolution of putative (*rac*)-**79** by analytical HPLC (*n*-hexane/^{i}PrOH = 95:5, *Daicel CHIRALPAK IB-U* column, 0.85 mL/min, 235 nm).

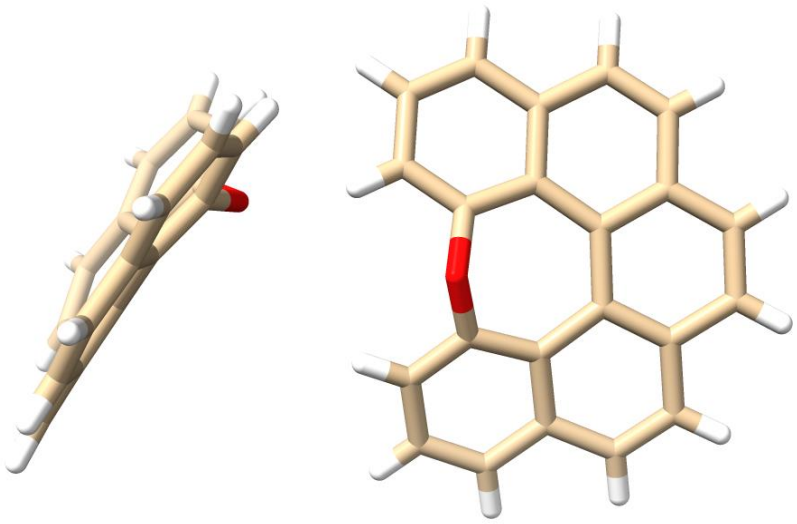

Figure 49: Molecular structures of **80** as determined by single crystal XRD analysis (carbon in brown, hydrogen in white, oxygen in red).

Class-wise, the helicenophane can also be categorized as a benzoxepin. Oxepins are known to be in a dynamic equilibrium with their valence isomers benzene oxide (**Scheme 105**, left).[259] While such a tautomerization was not observed for **80**, it cannot

be entirely be ruled out to a full extent. But opposed to oxepin, forming the epoxide in **80** would involve a double dearomatization which would be energetically unfavored and highly improbable.

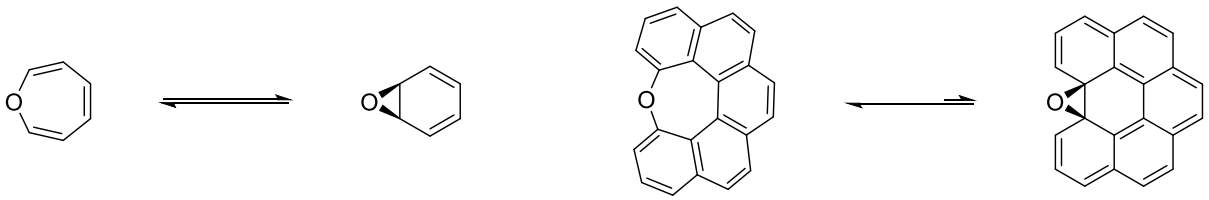

80

Scheme 105: Valence tautomerism for oxepin (left) and **80** (right).

Mechanistically, it was assumed to be a Scholl-type reaction in which the Lewis-acid BBr_3 causes either an arenium ion or a radical cation.[260] Although electron donating groups like methoxy functions can improve reactivity and selectivity in Scholl reactions,[261] the yield of 55 % was still astonishingly high in the face of the fact that the reaction temperature was low and that Scholl reactions typically do not have the highest yields (**Scheme 106**).

Despite the fact that benzoxepin **80** was definitely an interesting and unexpected compound, it was also a dead end in view of the synthetic route. Treating **80** under extreme conditions like refluxing in aqueous HBr over multiple days showed its stability. In order to get back on the right track and gain access to alcohol **79**, the ether functions of **38** had to be cleaved by means preventing the formation of a bridging ether moiety.

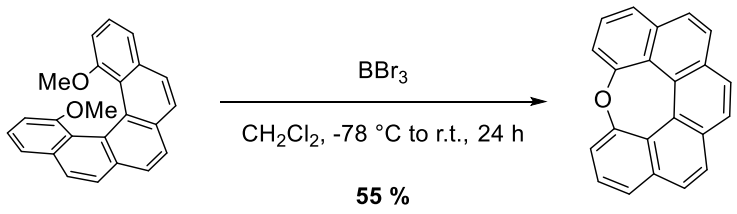

(*rac*)-**38** **80**

Scheme 106: Synthesis of **80** with BBr_3.

In hope of not forming the benzoxepin, the use of Lewis acids was avoided. Ethers can also be cleaved with Brønsted acids. However, refluxing (*rac*)-**38** in a solution of HBr in glacial acetic acid over two days did not cause any change. The substrate was recovered by column chromatography. It was not until a phase transfer catalyst was added that a change was observed. *Starks*' catalyst,[262] a quaternary ammonium salt

which is also advertised as *Aliquat 336*, has been used to accelerate the demethylation of aryl methyl ethers.[263]

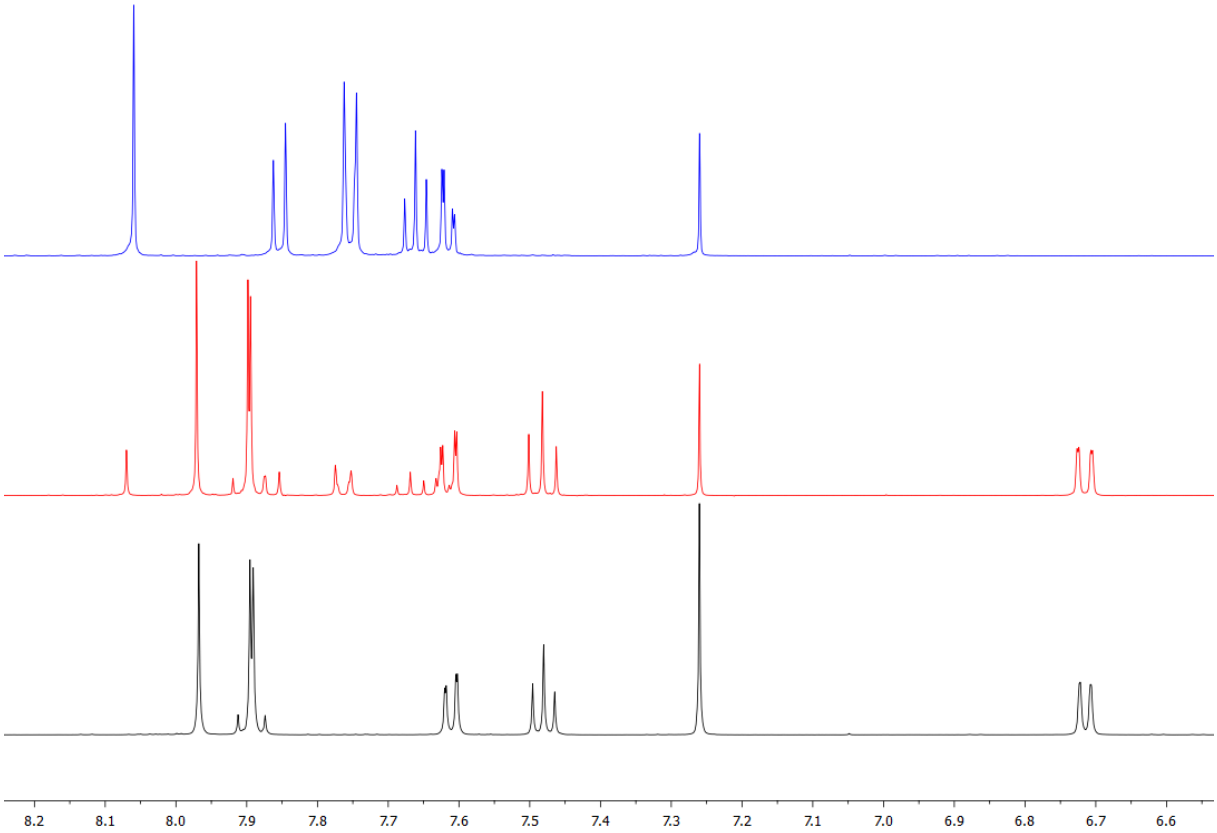

Figure 50: Comparison of ^{1}H-NMR spectra of substrate (*rac*)-**38** (bottom), acidic deprotection of (*rac*)-**38** (middle) and benzoxepin **80** (top).

Indeed, implementing their protocol on helicene (*rac*)-**38** had a noticeable effect, but unfortunately not a positive one. The crude ^{1}H-NMR spectrum showed new signals, but upon stacking of different spectra it was clear that (i) a lot of material remained unreacted and (ii) the new signals corresponded to benzoxepin **80** (**Figure 50**). Evidently, the reaction could also be promoted by Brønsted acids, albeit with far higher temperatures and reaction time. Based on the integral ratios, 18 % of (*rac*)-**38** was converted to **80** over the course of 2 days (**Scheme 107**).

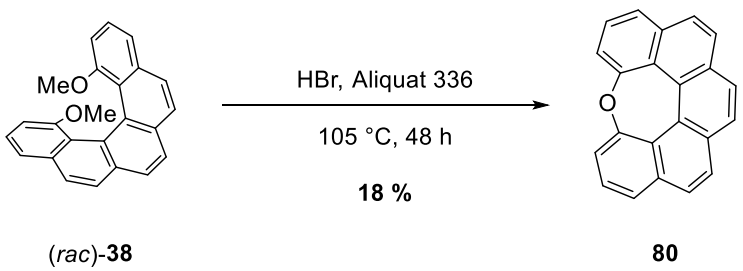

(*rac*)-**38** **80**

Scheme 107: Deprotection of (*rac*)-**38** with HBr.

Due to that, the strategy was re-evaluated and changed altogether. The protection group had to be cleaved under such mild and selective conditions that virtually no other side reaction could have occurred. As the methoxy functions did not meet these criteria, the group was replaced by benzylic ethers. They can selectively be turned to toluene by mild hydrogenation under palladium catalysis. Synthetically, beside the first step in which the protection group is introduced, nothing much changed.

Starting with 2-bromo-3-hydroxybenzaldehyde **30**, the S_N2 reaction with benzyl bromide gave **81** in 76 % yield (**Scheme 108**). The Sonogashira cascade was very straightforward and had expected yields and performances, purification of dialdehyde **84** by recrystallization instead of column chromatography did not cause any material loss. Over 3 steps, the combined yield was 51 %. The nucleophilic addition of the dialdehyde **84** followed by the acylation of the diol **85** on the other hand gave diacetate **86** in only 14 % yield over 2 steps. This was caused by the rather rudimentary workup which prioritized quality of the material over its quantity. In addition, the focus was put on a quick acquirement of the final helicene in order to figure out whether the desired deprotection of the ether was feasible. The Ni^0 facilitated key [2 + 2 + 2] cycloisomerization gave a rather complex ^{1}H-NMR spectrum. This was to be expected: The additional protons from the benzyl group can make the aromatic area around 7 ppm too congested for a meaningful analysis. Without detailed characterization, the isomeric mixture was stirred at 120 °C in silica gel. After purification by column chromatography on silica gel, a much cleaner ^{1}H-NMR spectrum was attained. Despite the additional aromatic protons, the aromatic area was not too convoluted as few signals had intersections (**Figure 51**). APCI-mass spectrometry showed a single prominent signal at m/z = 491.200 which matched with the monoisotopic mass of 1,14-dibenzyloxypentahelicene **88**. Over 2 steps, (*rac*)-**88** was gained in 35 % yield.

Overall, with the exception of the nucleophilic substitution − acylation sequence, the yields are in line with the previous syntheses of [5]helicenes. While the initial reactions partially outperform the ones from previous derivatives, the cyclization sequence performed worse than those towards methoxy[5]helicenes **20**, **38** and **43**. Considering the fact that the reaction has been very volatile so far, with a sample size of 1, an “average” yield of 35 % is statistically insignificant. Still, a lower value can be explained by the fact that the benzyl groups demand way more space than the methoxy groups which negatively affects the cyclization.

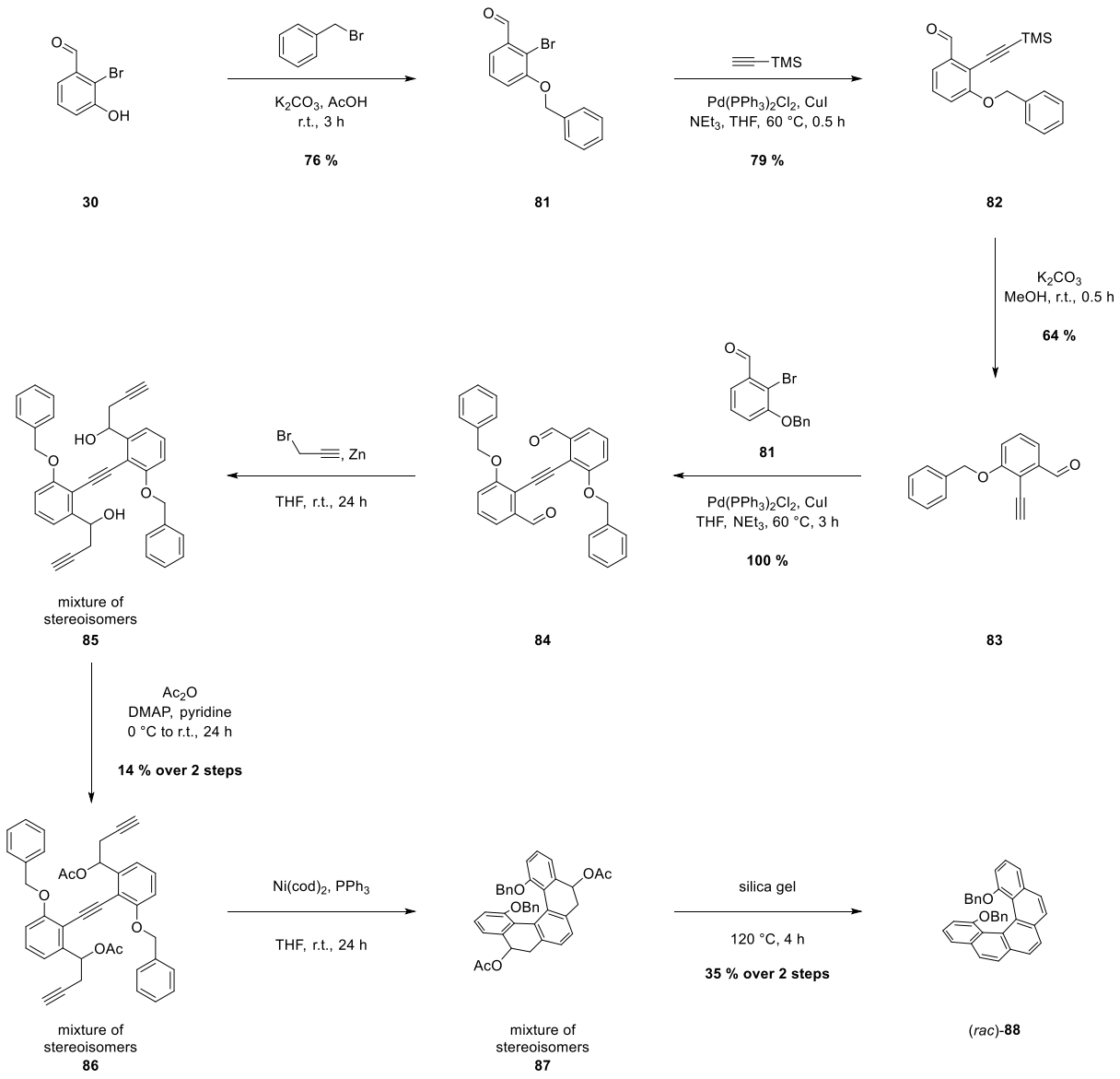

Scheme 108: Synthetic route towards (*rac*)-**88**.

The synthesis of the pentahelicene was then followed by the removal of its benzyl functions. Under an atmosphere of hydrogen gas, the heterogeneous catalytic hydrogenation with palladium on charcoal was carried out in a mixture of dichloromethane and methanol (**Scheme 109**).

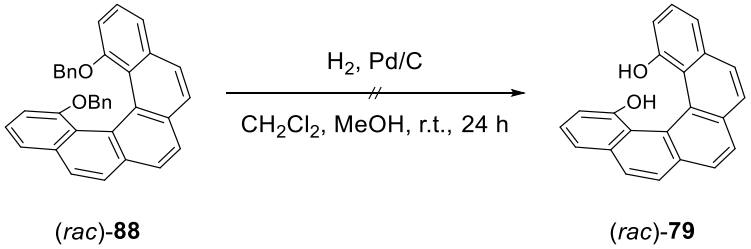

Scheme 109: Deprotection of (*rac*)-**88** with hydrogen.

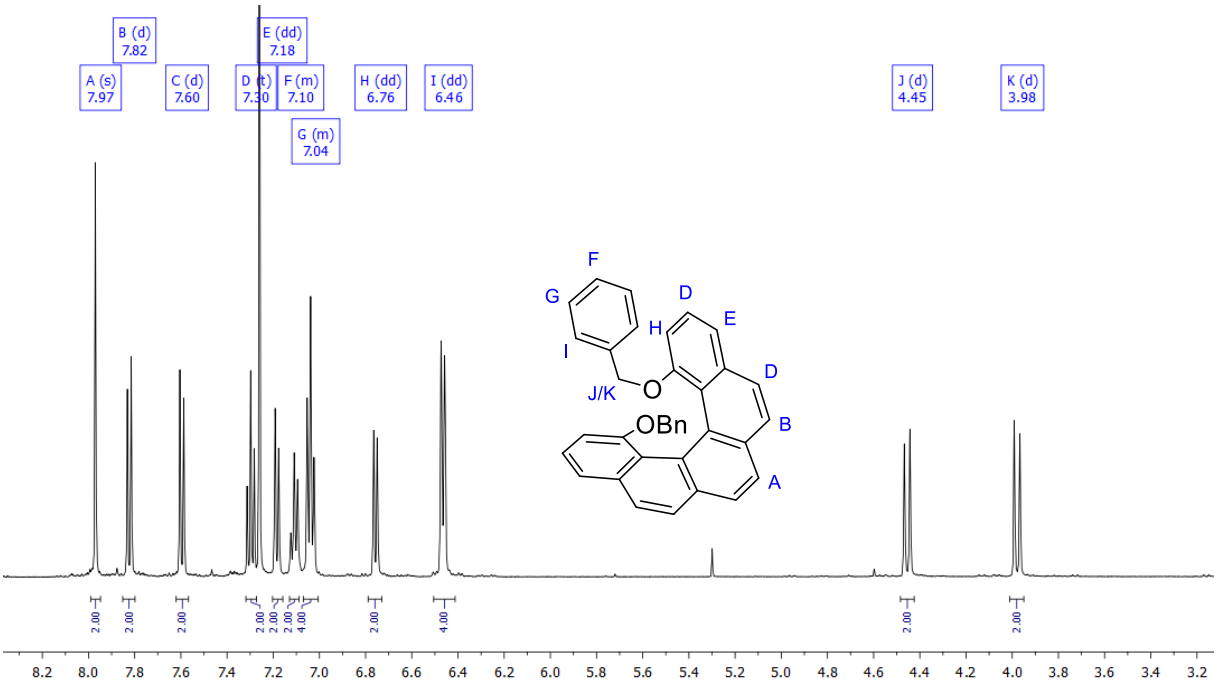

Figure 51: ^{1}H-NMR spectrum and assignment of (*rac*)-**88**.

TLC-monitoring indicated the formation of several species which were difficult to separate by chromatographic means. Two fractions were collected of which one was undoubtedly the substrate. The ^{1}H-NMR spectrum of the other one showed the loss of the benzylic protons around 4 ppm which was a good sign (**Figure 52**).

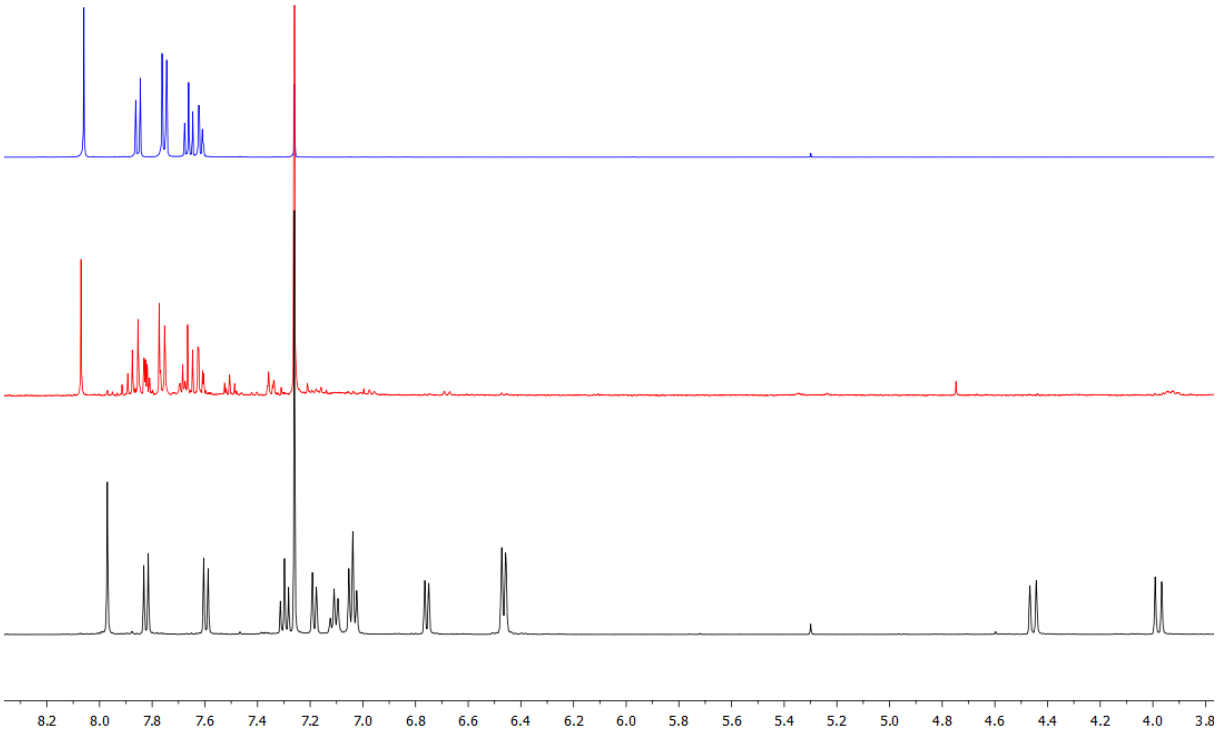

Figure 52: Comparison of ^{1}H-NMR spectra of substrate (*rac*)-**88** (bottom), hydrogenation of (*rac*)-**38** (middle) and benzoxepin **80** (top).

But the spectrum of the semi-pure fraction shared the same signals with the one of benzoxepin **80**. Despite its torsional strain and against chemical intuition, **80** seems to be energetically more favored than expected. In every reaction so far, it has been formed at least to some extent. It seemed that the access to 1,14-dihydroxy[5]helicene **79** is not accomplishable with this strategy. Once the helicene has been formed, the formation to the desired alcohol always leads to the more stable diarylether. A possible workaround could be a deprotection prior to the [2 + 2 + 2] cyclization, but the resilience of hydroxy functions in these reactions can vary.[264]

Therefore, the route towards 1,14-difunctionalized ligands based on pentahelicene was abandoned for the time being. The narrow space in the overcrowded positions 1 and 14 was a major obstacle. Even though these positions are interesting due to the fact that: (i) accommodating for the limited space should induce constrained and extreme conformations and (ii) the racemization barrier should be extraordinarily high, it is questionable whether bulky pyridine functions can be introduced there in the first place. A GFN2-xTB[177,178] minimized model of 1,14-di(pyridin-4-yl)pentahelicene showed that an introduction of two 4-pyridyl units leads to a 15 % increase in the mean dihedral angle, compared to the 2,13-functionalized analogue (**Figure 53**).

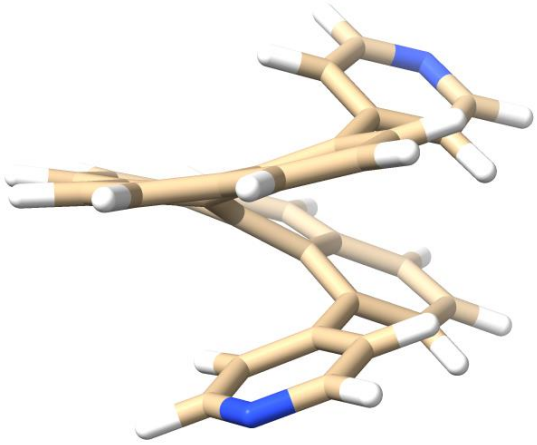

Figure 53: GFN2-xTB[177,178] minimized structure of (*P*)-1,14-di(pyridin-4-yl)pentahelicene (carbon in brown, hydrogen in white, nitrogen in blue).

6.2 [7]Helicene

2,17-Difunctionalized [7]helicene

Because the earliest point at which a chiral resolution made sense was after the removal of the acetates which were attached to the stereogenic carbon centers, a first attempt was not made with the fully aromatic [7]helicene (*rac*)-**55** itself, but with its tetrahydro precursor (*rac*)-**54**. A baseline separation was achieved with separation and resolution factors of α = 1.40 and R_s = 3.56 which again ensured an early resolution within the multistep synthesis towards the desired ligand scaffolds in case these could not be resolved at a later stage (**Figure 54**).

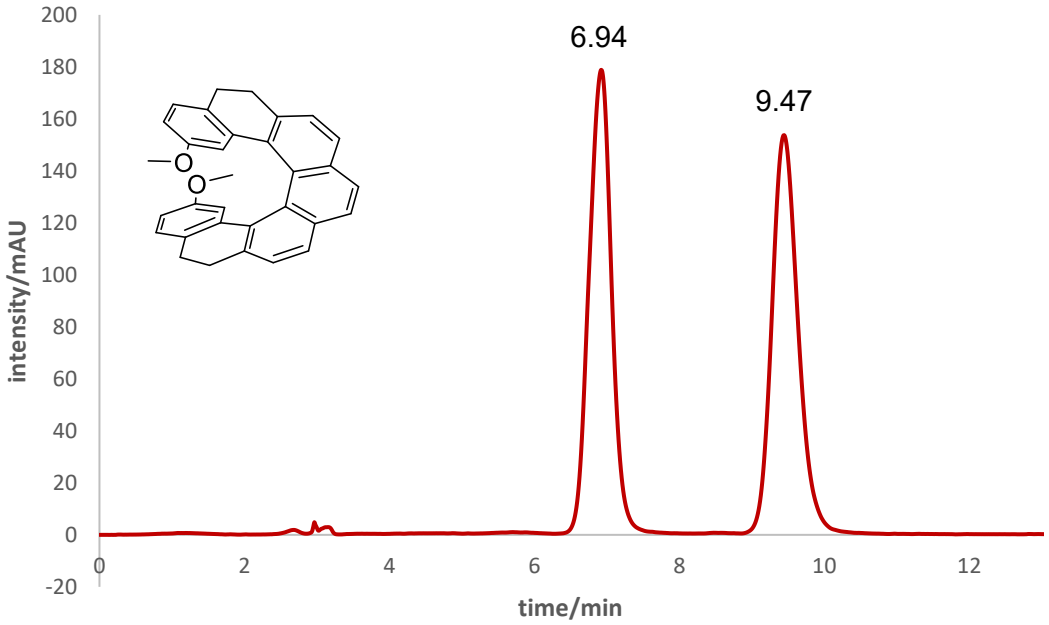

Figure 54: Chiral resolution of (*rac*)-**54** by analytical HPLC (*n*-hexane/dichloromethane = 85:15, *(S,S)-Whelk-O-1* column, 1 mL/min, 235 nm).

Progressing from the fully aromatic 2,17-dimethoxy[7]helicene (*rac*)-**55**, the methoxy groups were removed with BBr_3 in dichloromethane overnight (**Scheme 110**).

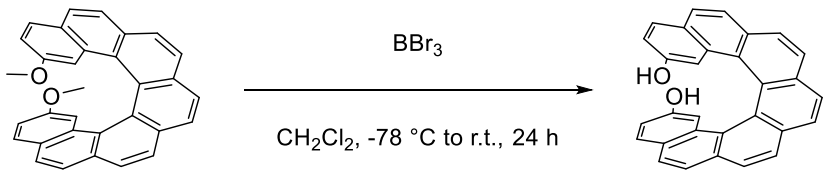

(*rac*)-**55** (*rac*)-**89**

Scheme 110: Deprotection of (*rac*)-**55**.

Just in case, an eye was kept on the formation of a diarylether similar to achiral **80**. Collectively, the unpurified mixture showed a solubility and polarity appropriate for an alcohol. Mass spectrometric analysis revealed just a single signal with the mass of desired diol **89**. At large, 81 % of (*rac*)-**89** was isolated after purification.

The triflation was carried out with Tf_2O in anhydrous pyridine (**Scheme 111**). At the latest from that point on it was clear that diol (*rac*)-**89** had been formed: Since an ether would not undergo a triflation, the presence of (*rac*)-**90** simultaneously proved the presence of its predecessor. Fortunately, the quantitative conversion meant that enough material was available for the upcoming late-stage functionalizations.

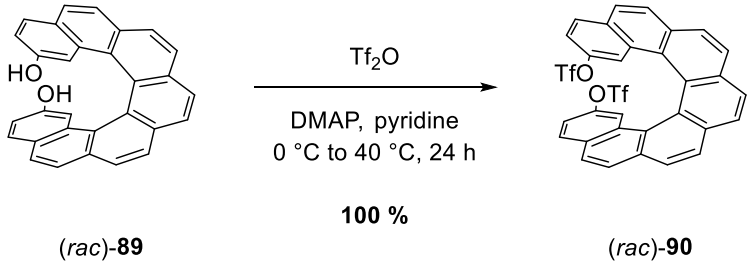

Scheme 111: Triflation of (*rac*)-**89**.

In the same fashion as for [5]helicene, [7]helicene (*rac*)-**90** was first coupled with 4-pyridine boronic acid in order to introduce a donor atom (**Scheme 112**). Refluxing over 24 h led to a yellow precipitate which was believed to be the product. The low solubility made the routine aqueous workup difficult. TLC-analysis showed a species of high polarity which is in accordance with the behavior of its lower homologue based on pentahelicene (*rac*)-**75**.

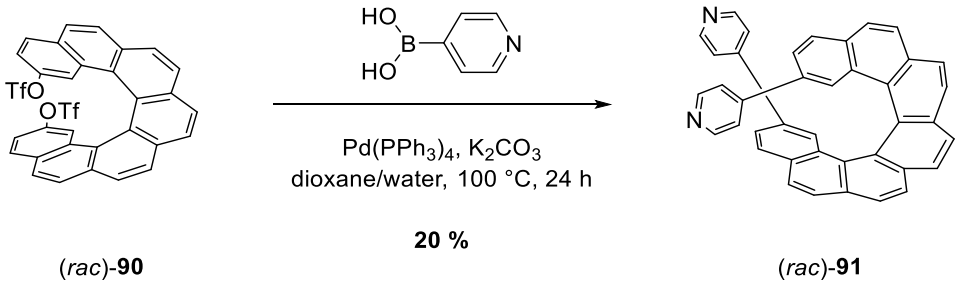

Scheme 112: Suzuki coupling of (*rac*)-**90** to (*rac*)-**91**.

For column chromatography purposes, the same stationary phase and eluent system as for (*rac*)-**75** was implemented. In direct comparison, (*rac*)-**91** had a much lower solubility in these solvents, probably attributed to the higher quota of carbon atoms. Counterintuitively at the same time, (*rac*)-**91** had a much higher polarity. In the end, a

mixture of dichloromethane, ethyl acetate and methanol was required to resolve (*rac*)-**91** on silica gel. These circumstances resulted in a rather poor yield of 20 % which was still enough to do the complexation experiments. The low solubility also related to a ^{1}H-NMR spectrum of low resolution (**Figure 55**), but mass spectrometric experiments proved the formation of (*rac*)-**91**. Due to its low solubility, the substance was not compatible with resolution by HPLC.

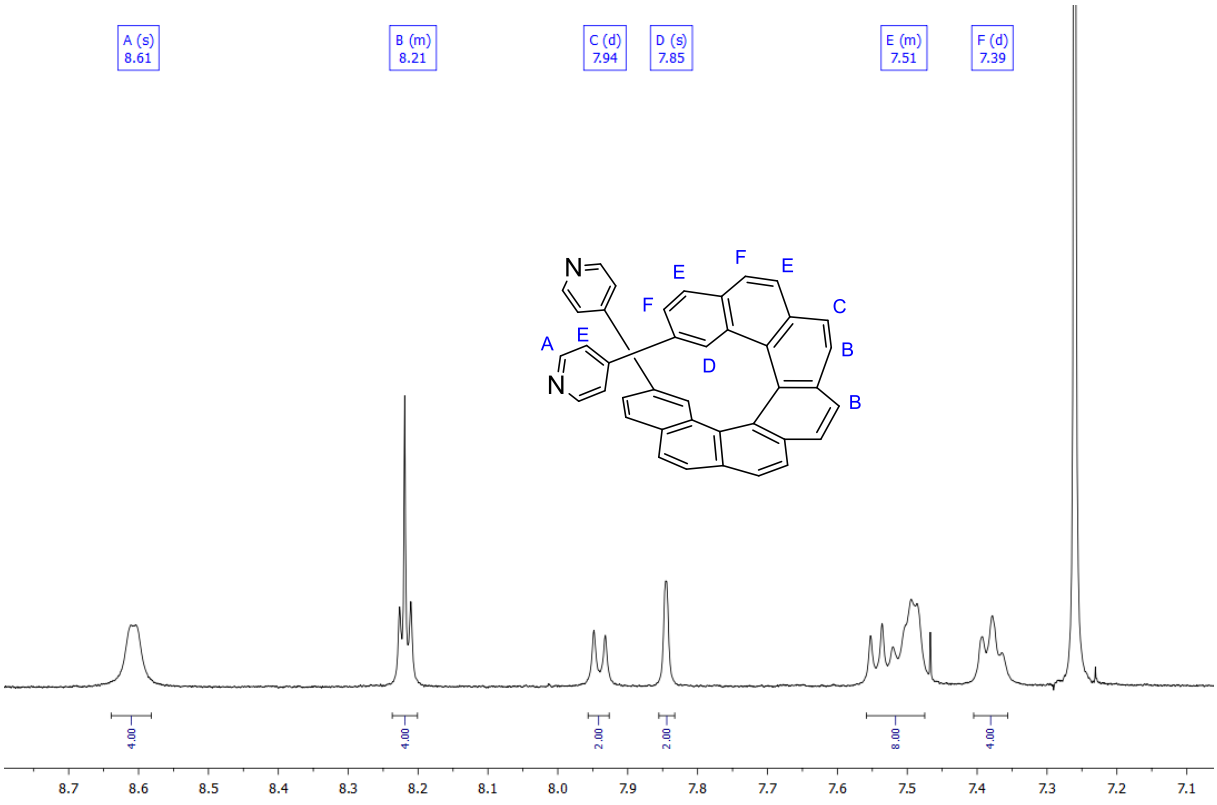

Figure 55: ^{1}H-NMR spectrum and assignment of (*rac*)-**91**.

The second ligand was also planned with an elongation of the lateral side arms in mind. Since the failed Sonogashira reactions inhibited the introduction of an acetylene spacer for the ligands based on [5]helicene, the same was forecasted for [7]helicene and it was opted for a 1,4-phenylene spacer again. Performing the same reaction with a different coupling partner (**Scheme 113**) was accompanied with the same observations, i.e. a yellow precipitate occurred which was believed to be the product. The precipitate shared the same properties with [7]helicene (*rac*)-**91** in the sense that (i) the same amount of a saturated solution of EDTA had to be used for the aqueous workup and (ii) the same combination of solvents as the mobile phase had to be used for chromatographic purposes due to their similar polarities. But based on the even higher ratio of carbon atoms, the solubility of (*rac*)-**92** was worse so that purification by

column chromatography did not properly isolate the desired ligand at first. Repeating the chromatographic purification multiple times brought only slight improvements in purification grade. The semi-pure mixture was recrystallized from ethyl acetate which provided a much cleaner ^{1}H-NMR spectrum. While the low solubility also resulted in a spectrum of lower quality (**Figure 56**), the integrals and multiplicities matched those for (*rac*)-**92**. The multiple purification processes had a toll on the yield, in the end, 16 % of (*rac*)-**92** was isolated.

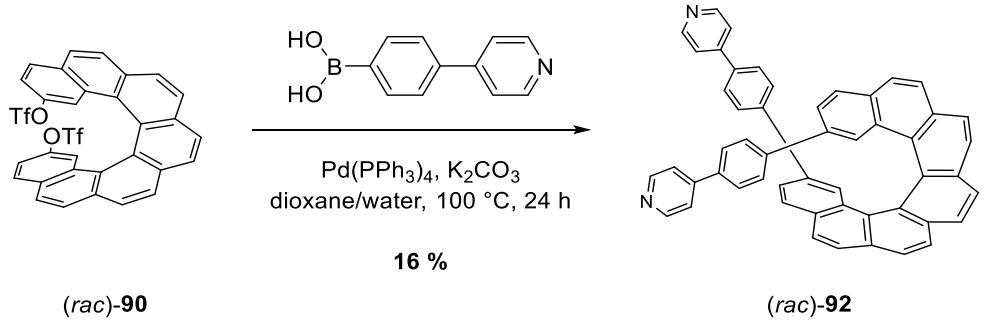

(*rac*)-**90** (*rac*)-**92**

Scheme 113: Suzuki coupling of (*rac*)-**90** to (*rac*)-**92**.

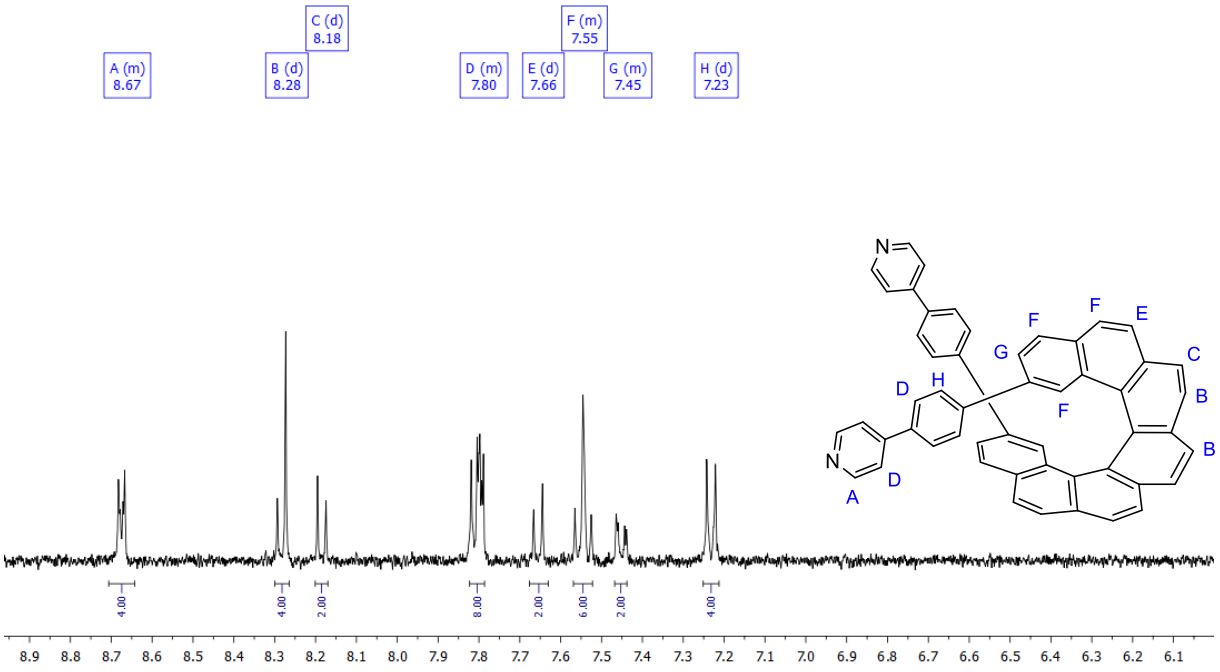

Figure 56: ^{1}H-NMR spectrum and assignment of (*rac*)-**92**.

Mass spectrometric and X-ray diffractometric analysis confirmed the formation of the ligand. (*Rac*)-**92** crystallizes in the monoclinic space group $P2_1/c$, has a cavity with a diameter of 3.0 Å and a wingspan of 21.4 Å measured by the distance between the nitrogen atoms (**Figure 57**). For the same reasons as for (*rac*)-**91**, the idea of a resolution by analytical HPLC was rejected beforehand.

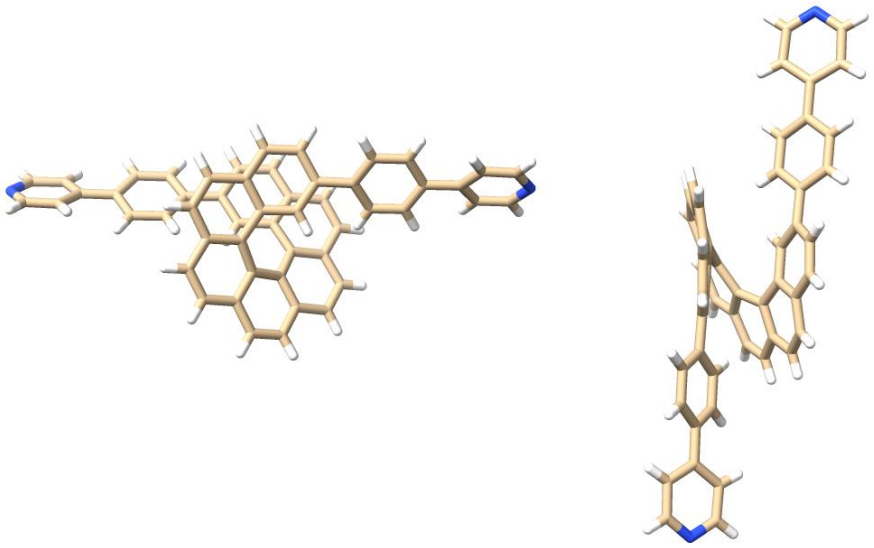

Figure 57: Molecular structures of (*rac*)-**92** as determined by single crystal XRD analysis (carbon in brown, hydrogen in white, nitrogen in blue).

The third and final ligand was prepared with (4-(pyridin-3-yl)phenyl)boronic acid (**Scheme 114**). With the established conditions for the Suzuki coupling of helicenes in this work, the same observations and workup routine were anticipated. Surprisingly, this was not the case this time: The regioisomer had a much higher solubility in common organic solvents than its counterparts (*rac*)-**91** and (*rac*)-**92**. During the reaction, no yellow precipitate was visible throughout the 24 hours (only small amounts of a black precipitate were visible which were attributed to oxidized catalytically inactive palladium species). The aqueous workup required considerably less solution of EDTA. The polarity matched that of compound (*rac*)-**92**, but the chromatographic purification benefitted greatly from the higher solubility. Without crystallization and after a single purification by column chromatography, a clean ^{1}H-NMR spectrum was gained (**Figure 58**). The better resolution of the much sharper signals made their assignment much easier. Mass spectrometric analysis confirmed the presence of (*rac*)-**93**.

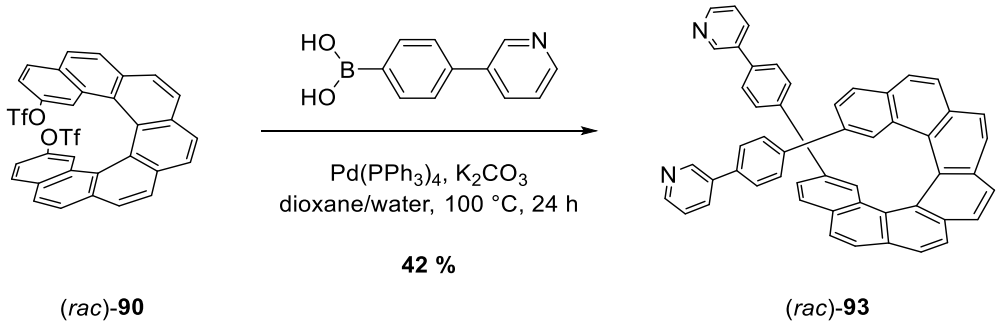

(*rac*)-**90** (*rac*)-**93**

Scheme 114: Suzuki coupling of (*rac*)-**90** to (*rac*)-**93**.

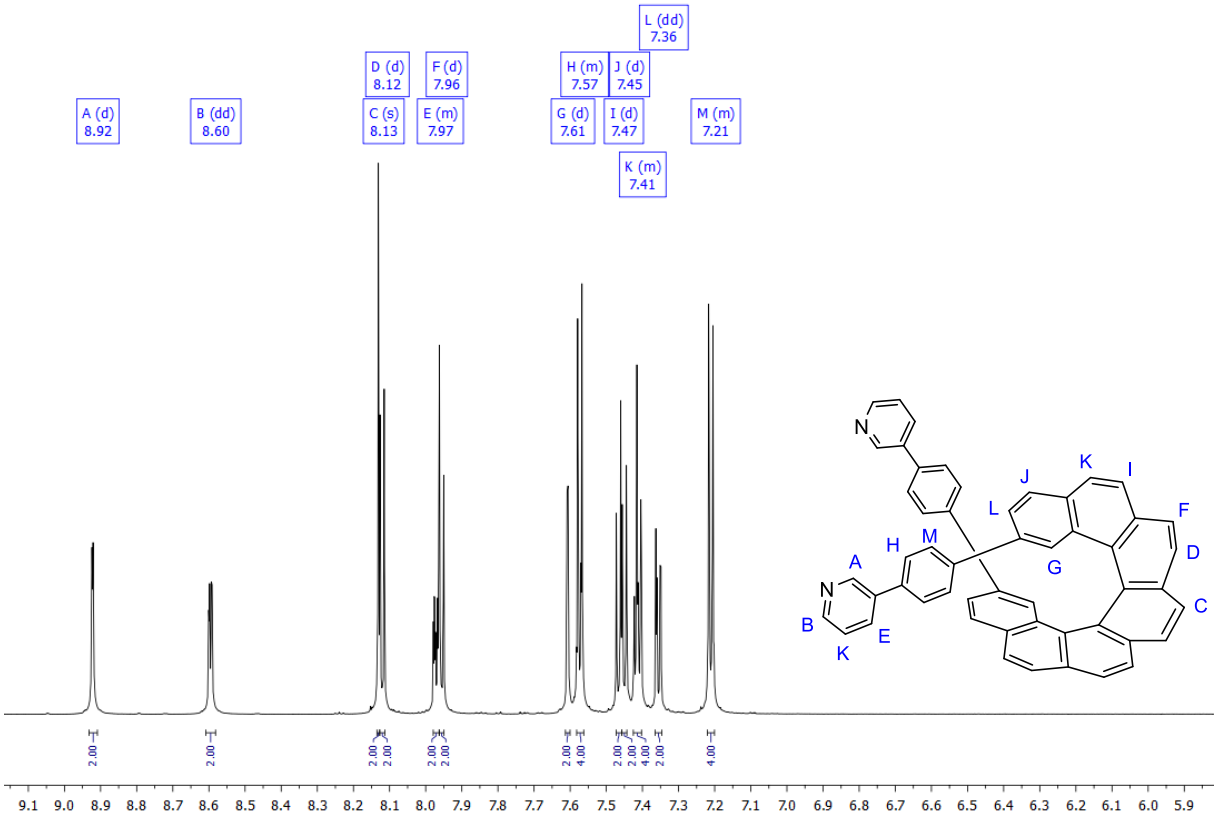

Figure 58: ^{1}H-NMR spectrum and assignment of (*rac*)-**93**.

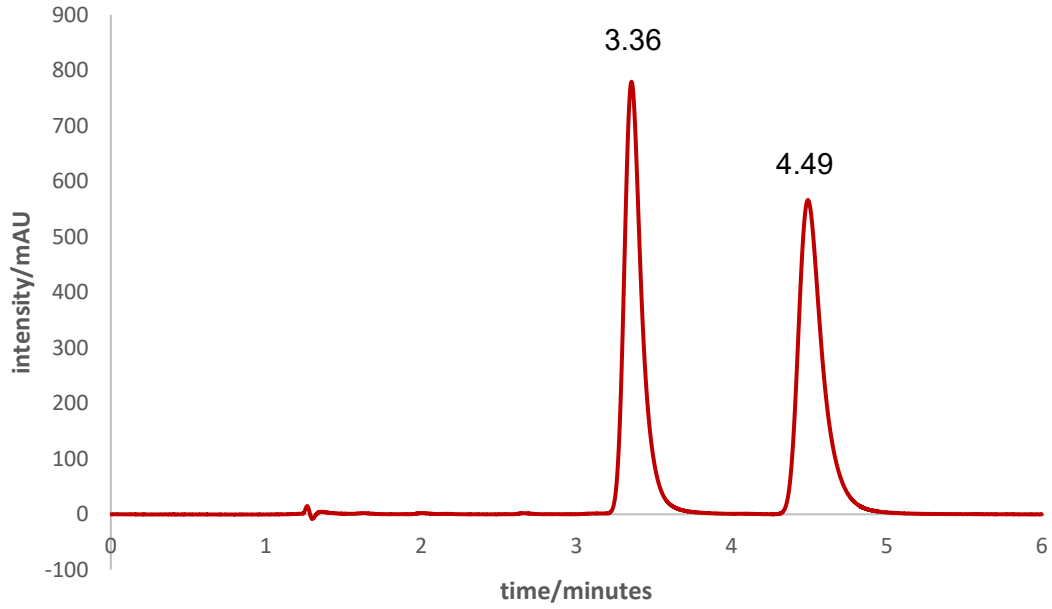

Figure 59: Chiral resolution of (*rac*)-**93** by analytical HPLC (dichloromethane/EtOH = 2:8 + 0.8 vol% DEA, *Daicel CHIRALPAK IC-U* column, 0.43 mL/min, 235 nm).

The higher solubility also meant that an optical resolution was within the realm of possibilities. The racemic mixture was subjected to analytical HPLC. As with the separation of bis(pyridine) (*rac*)-**75**, the basicity of (*rac*)-**93** had to be counteracted with

8 vol% diethylamine, too. With the *Daicel Chiralpak IC-U* column, a good baseline separation with retention times of t_1 = 3.36 min and t_2 = 4.49 min was achieved (**Figure 59**). Overall, the separation took a bit longer than that of (*rac*)-**75**. The retention times corresponded to separation and capacity factors of α = 1.41 and R_s = 3.96. In light of the slightly higher retention times during the analytical HPLC run, it was to be expected that the retention times of the semipreparative HPLC run would also be higher compared to those of (*rac*)-**75**. With retention times of t_1 = 14.63 min and t_2 = 17.66 min, separation and capacity factors of α = 1.25 and R_s = 1.36 were calculated for the semipreparative HPLC run (**Figure 60**).

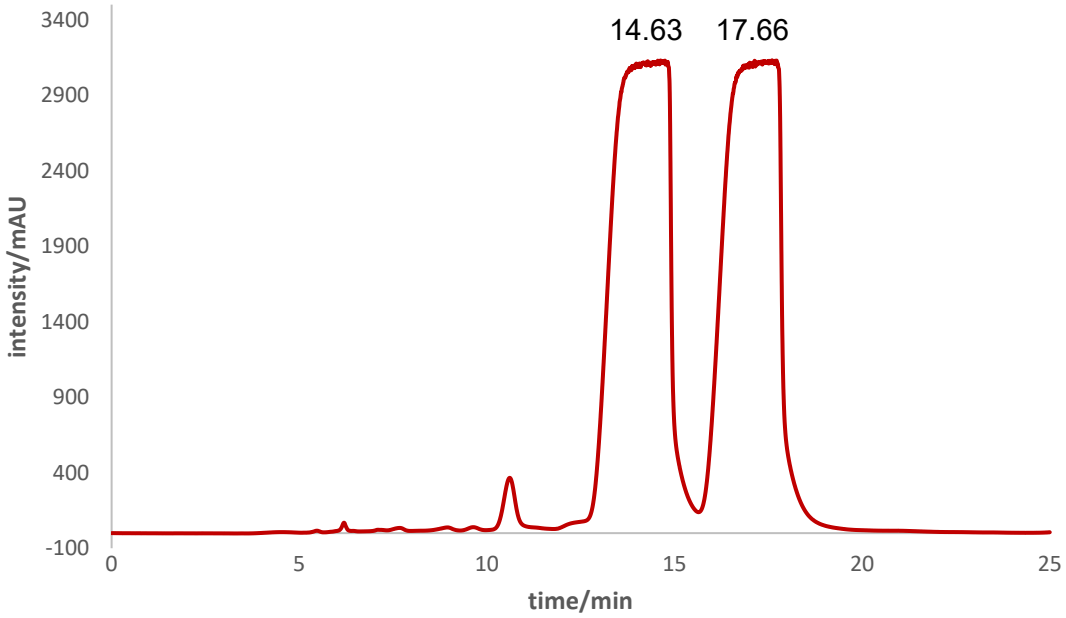

Figure 60: Chiral resolution of (*rac*)-**93** by semipreparative HPLC (dichloromethane//EtOH = 2:8 + 0.8 vol% DEA, *YMC CHIRAL ART Cellulose-SC* column, 10 mL/min, 235 nm).

Needless to say, the enantiomers needed to be characterized in regard of their absolute configurations. The specific rotation of the first eluting enantiomer suggested an (*M*)-configuration due to its negative algebraic sign. ECD spectra were recorded from the solution of each enantiomer in dichloromethane (**Figure 61**). The mirror symmetric spectra showed distinct bands at around λ = 292, 324 and 367 nm. The simulated spectra showed a high level of agreement with the experimental ones and confirmed the first eluting enantiomer to be (*M*)-configurated and the second one to be (*P*)-configurated. Unfortunately, the higher solubility was at the expense of the ability to form crystals. In several organic solvents and within a wide temperature range, no

single crystals could be grown out of (*rac*)-**93**. Structure-wise, (*rac*)-**93** should not be much different than regioisomer (*rac*)-**92**. A GFN2-xTB[177,178] minimized structure indicated that on the whole, distances and torsional angles are in the same range (**Figure 62**). With 3 ligands in hand, the focus was put on the complexation experiments.

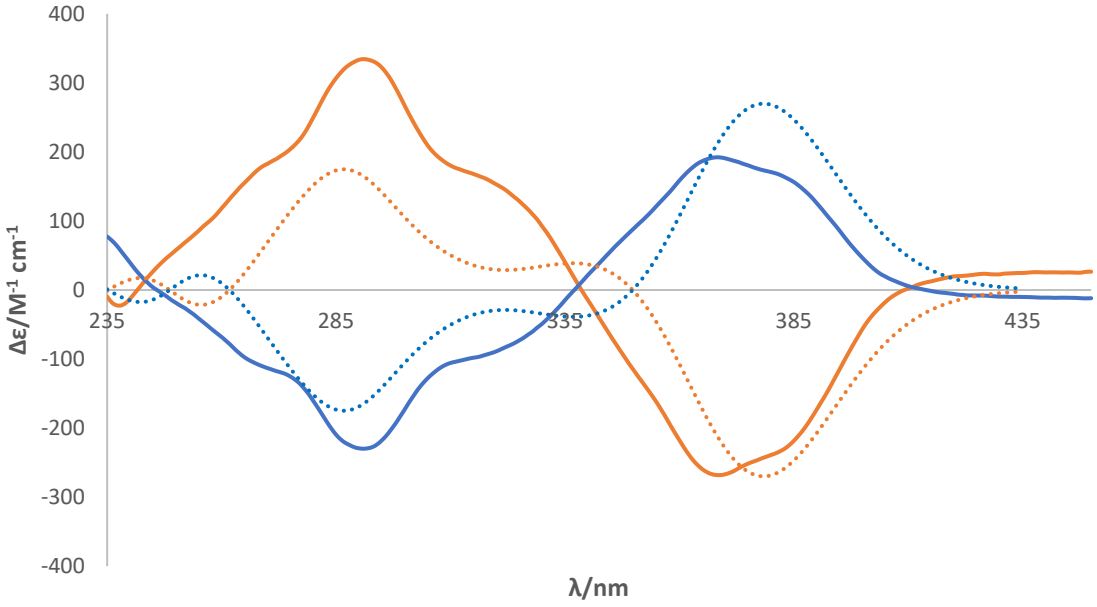

Figure 61: Experimental ECD spectra of (*P*)-**93** (blue solid line, dichloromethane, $c = 3.7\times10^{-3}$ g/L), (*M*)-**93** (orange solid line, dichloromethane, $c = 3.1\times10^{-3}$ g/L), respectively, and the corresponding calculated ECD spectra (dashed lines).

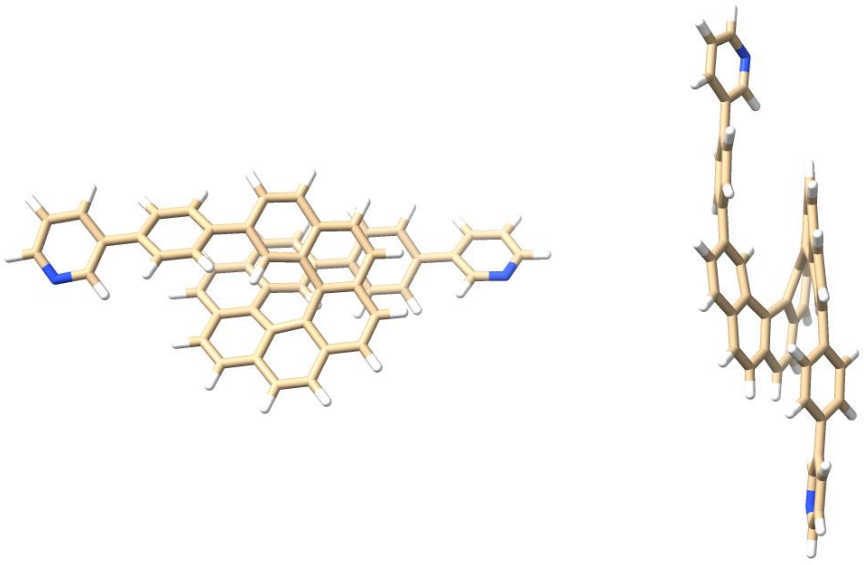

Figure 62: GFN2-xTB[177,178] minimized structures of (*P*)-**93** (carbon in brown, hydrogen in white, nitrogen in blue).

7 Coordination chemistry

7.1 Coordination chemistry of helicenes

As the name suggests, coordination chemistry relies on coordinative interactions between metal acceptors and ligands bearing a donor atom. Thereby, both components are not set in stone, meaning that ligands with different coordinating atoms can be paired with a large variety of metal cations to give structures ranging from one-dimensional, linear rods[265–267] to three-dimensional, Archimedean[268] or Platonic[269] polyhedra.

Incorporating helicenic elements, a mechanical switch has been created by *Crassous* and coworkers. A bis-4-aza[6]helicene with a central bipy unit switched gradually from its transoid to its cisoid form upon titration with $Zn(OAc)_2$, resembling the motion of a molecular hinge (**Scheme 115**). The coordination-induced motion was reversible as the metal center could be removed by *N*,*N*,*N*′,*N*′-tetrakis(2-pyridylmethyl)ethane-1,2-diamine (TPEN).[270]

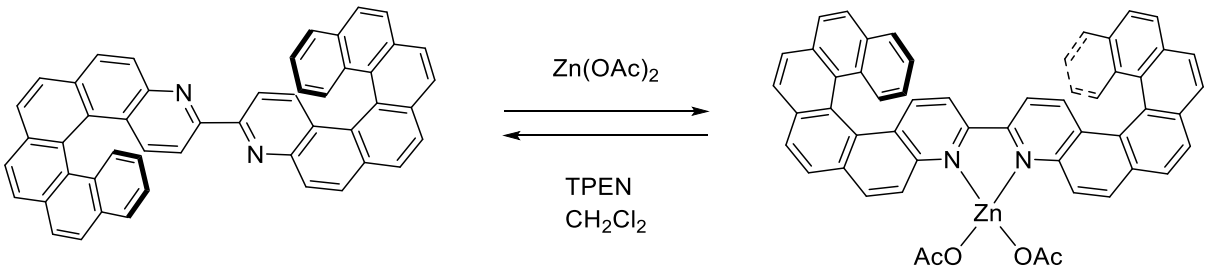

Scheme 115: (De-) coordination-induced motion mimicking a molecular hinge.

Using a bis-helicenic ligand bearing a central terpyridine unit, their group also exploited the same coordination/decoordination strategy to induce a mechanical rotation of both C-C bonds at each side of the central pyridyl unit from a molecular W-shape to a U-shape. Again, the rotation was reversible upon addition of the metal scavenger TPEN.[271] In both cases, the chemical stimuli modified the spectroscopic properties greatly so that the systems acted as chiroptical switches offering multi-output readouts (UV-Vis, ECD, OR, fluorescence, CPL).

The combination of a phthalocyanine and homochiral [7]helicenes gave a polydentate ligand which displayed strong NLO activity upon coordination of Cu(II) and Ni(II) into its inner cavity (**Figure 63**). The complexes were spin-coated on mica substrates and

studied by atomic force microscopy (AFM). A face-to-face columnar stacking of the molecules with their helical axes perpendicular to the surface was observed starting from an approximately 3:1 threshold of ethanol and chloroform, presumably resulting from favorable π-stacking of the aromatic units and van der Waals interactions from the *n*-dodecyl sidechains. When assembled in Langmuir-Blodgett films, stacking occurred with the axes parallel to the air-water interface.[272]

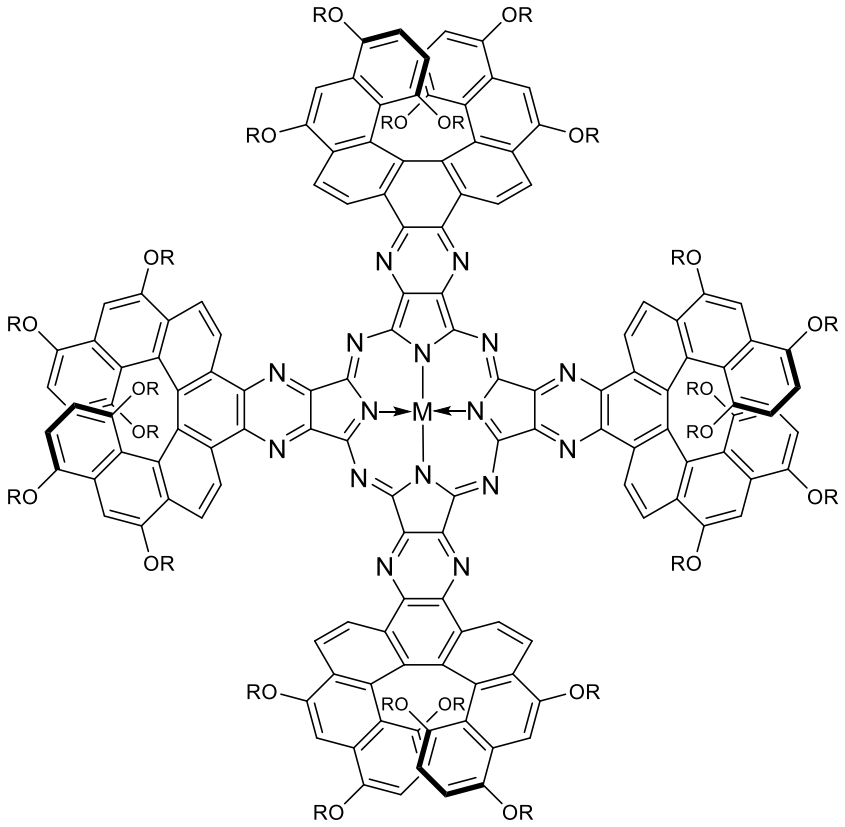

Figure 63: Helical phthalocyanine (M = Cu, Ni; R = $C_{12}H_{25}$).

The disproportional (and at the same time still scarce) occurrence of either monodentate or mononuclear (or both) complexes in literature is not due to the fact that coordination chemistry of helicenes is only limited to these, but rather due to the current lack of comprehensive investigation in this field. Although more challenging and sophisticated, the formation of higher structures comprising polydentate ligands and more than one metal ion should also be possible using helicenes. For this, an elaborate concept has to be created first.

For instance, a molecular square can be constructed with 4 corners dictating a 90° turn and 4 linear edges. Thereby, the metals can provide right angles in linkage which can be difficult to achieve by other means, while the easier realization of 180° angles can

be achieved with organic ligands. Conceptually, this is nothing else than the directional bonding approach which has been developed by *Stang*.[273–276] Based on the alignment of the employed subunits, a prediction for the geometry of the formed product can be made (**Figure 64**). Of course, this guideline can only make tentative predictions. Although these are reasonable, designing such polygons does not necessarily lead to them. For instance, subunits can be more flexible than the Lewis structure suggests.

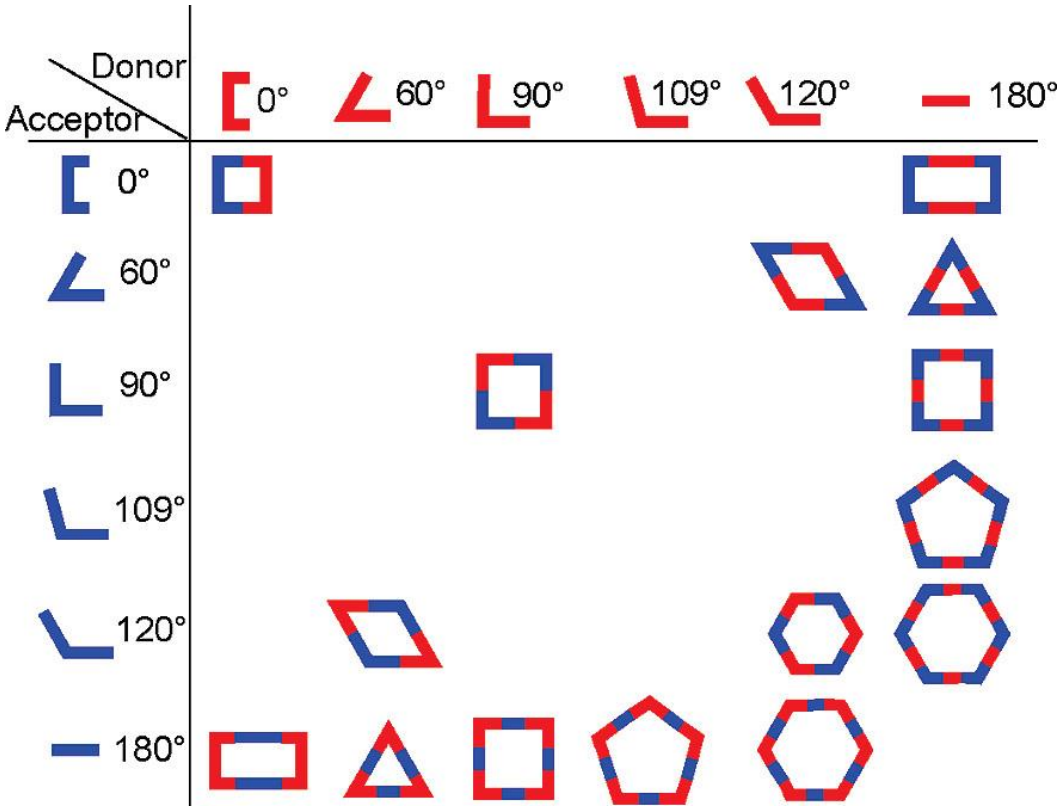

Figure 64: Molecular polygons attainable by systematic combination of ditopic subunits. Reproduced with permission from the *American Chemical Society*.[276]

Based on this rationale, three dimensional structures should also be accessible if the concept is extended. As mentioned before, the creation of three-dimensional architectures based on helicenes is underexplored. While this circumstance certainly correlates with the synthetic effort and the challenging planning, these architectures are highly interesting because they can be arranged with tailored cavities in mind. This gives entry to host-guest chemistry, a field that itself is particularly captivating due to its relevance in catalysis[277] or molecular recognition/separation[278].

7.2 Chiral self-sorting

In a multi-component system, (stereo-) selective considerations have to be discussed. For a self-assembly of a metal with more than one ligand, a distinction can be made between 3 extreme scenarios (**Scheme 116**):

- The metal only binds to one ligand each and forms exclusively homoleptic complexes (narcissistic self-sorting).
- The metal binds to every ligand in every possible way and forms the respective homo- and heteroleptic complexes according to the statistical distribution.
- The metal binds to both ligands and forms heteroleptic complexes deviating from the statistical distribution (social self-sorting).

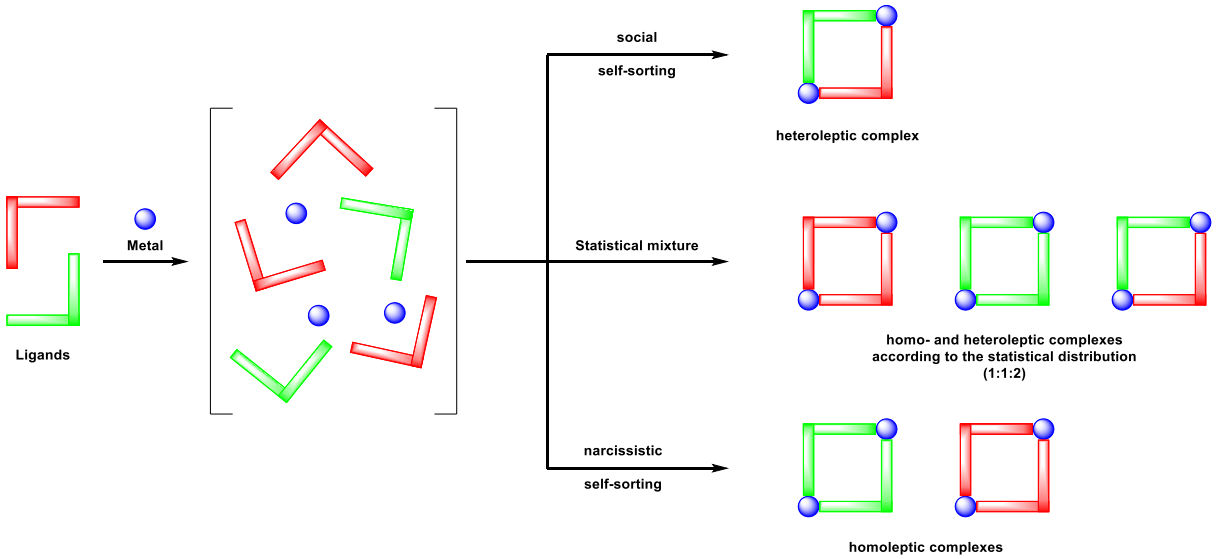

Scheme 116: Different outcomes of self-sorting of metal ions (blue) and two types of ligands (red and green).

The three scenarios mentioned above are just the edge cases. Mixed scenarios involving various degrees of each can lie in between. In fact, every deviation from the statistical probability can be regarded as a form of self-sorting. Numerous circumstantial causes like solvents, counterion etc. can affect this selectivity, therefore it is hardly predictable and not entirely understood. But at the same time, numerous strategies like templates, steric effects, complementarity of size and shape, ligand interactions or control of the metal's coordination sphere have been used to influence the standard distribution.[279–281]

But the definition can not only be applied to homo- and heteroleptic structures involving mixtures of ligands. If the concept is extended and applied to enantioselective or chiral self-sorting, subcategories of the categories mentioned above can be made with homo- and heterochiral complexes. In terms of helicenic self-sorting, there is only one publication in which a self-discrimination has been achieved so far. Using a racemic [6]helicene, coordination with palladium gave a single heterochiral *meso*-cage incorporating both enantiomers exclusively (**Scheme 117**). The presence of the tetracationic $[Pd_2L_4]^{4+}$ species was proven by mass spectrometry and ^{1}H-NMR spectroscopy. A signal splitting occurred which could only be rationalized by a *cis*-arrangement of the respective enantiomers. Interestingly, when an enantiopure [6]helicene with an elongated side arm was used, the solvent determined whether a $[Pd_2L_4]^{4+}$ cage or an interpenetrated $[Pd_4L_8]^{8+}$ dimer formed.[282]

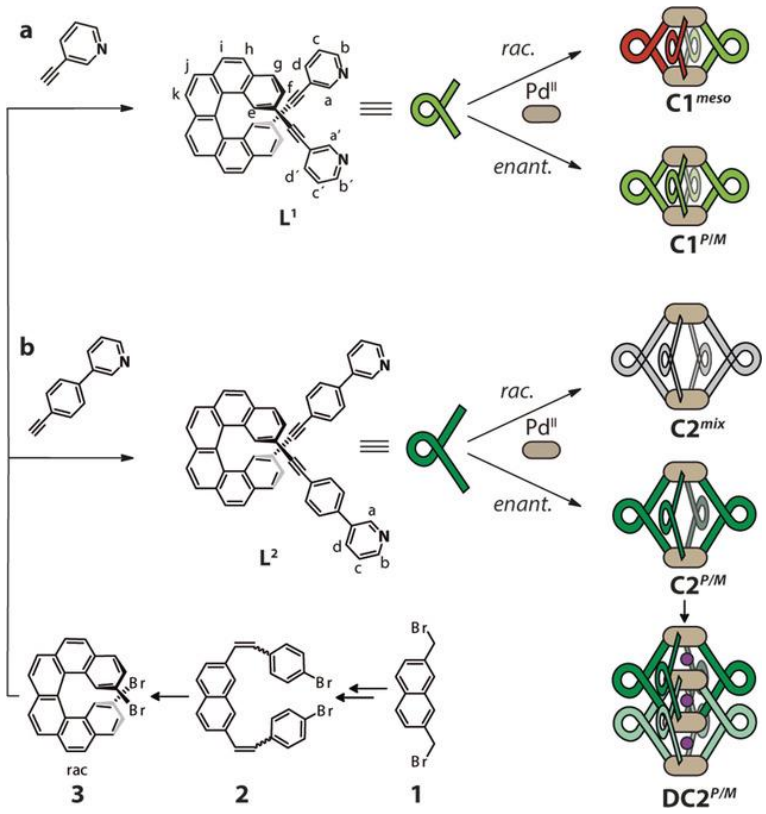

Scheme 117: Helicene-based coordination cages. a) Synthesis of ligand **L^1**, b) synthesis of ligand **L^2**. Depending on the composition and the ligand, different coordination cages are formed. Reproduced with permission from *John Wiley and Sons*.[282]

8 Coordination experiments – setting up the complex

8.1 [5]Helicene

2,13-Difunctionalized [5]helicene

With the incorporation of nitrogen donor atoms into the ligands, supramolecular assemblies with tailored geometries dependent on the employed metal cation were envisaged. The first complexation experiments were carried out with bidentate bis(pyridine) ligand (*rac*)-**75**. Mixing helical ligands with square planar d^8 metals like Pd(II) or Pt(II) has given access to complexes of interesting architectures.[282–285] In hopes of recreating those, (*rac*)-**75** was treated with $Pd(MeCN)_4(BF_4)_2$ in common organic solvents at room temperature. Unexpectedly, the ligand remained mostly free and unattached in these solvents. After 24 h, other signals appeared in the ^{1}H-NMR spectrum of the experiment in dichloromethane (**Figure 65**) which did not really increase or supersede the ligand signals over the course of 3 days of stirring.

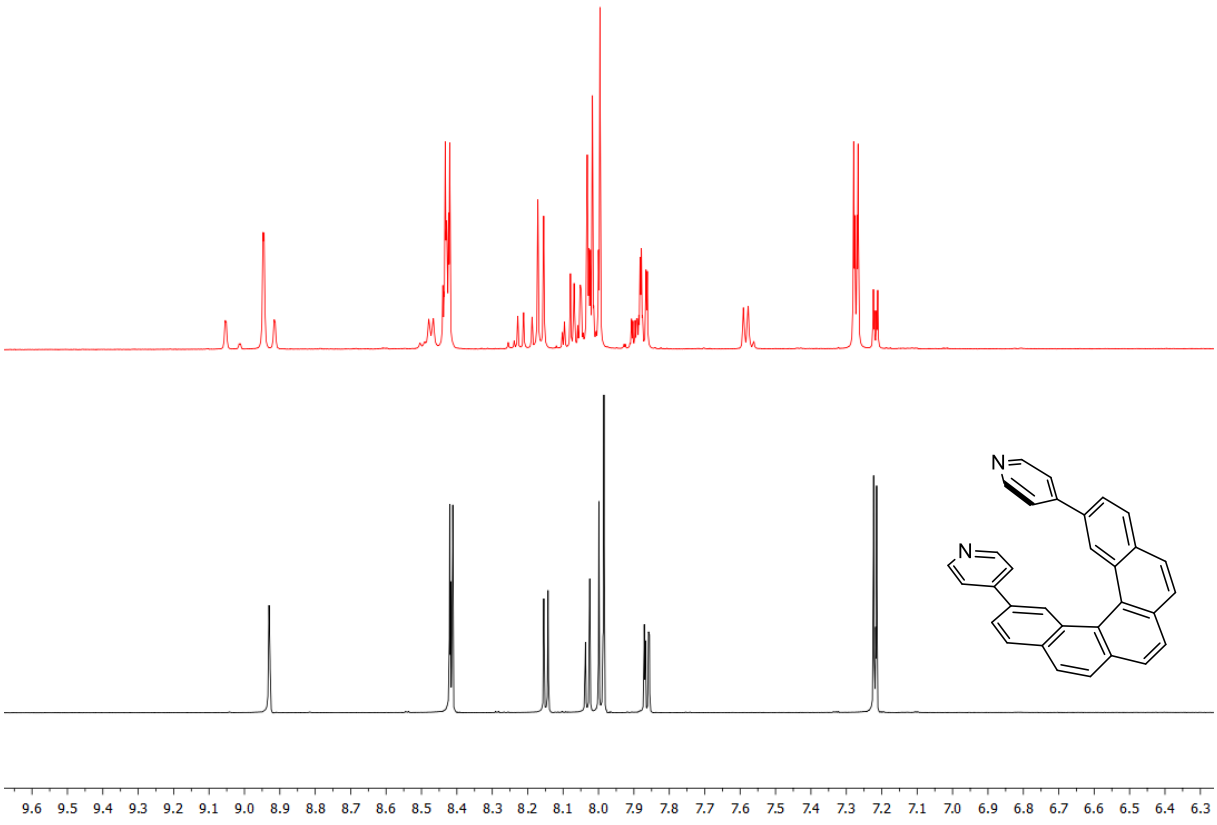

Figure 65: Comparison of ^{1}H-NMR spectra of free ligand (*rac*)-**75** (bottom) and after complexation attempt with $Pd(MeCN)_4(BF_4)_2$ (top).

The 3 new signals around 9 ppm indicate 3 new chemical environments for the protons next to the pyridine nitrogen. These can only be explained by coordination to the metal center. Unfortunately, the new signals around 8 ppm were not pronounced enough to make conclusive statements and mass spectrometric analysis showed no species with a charge higher than +I. Due to the same integral value of the outer signals at 9 ppm, it is possible that they belong to one species with magnetically non-equivalent α-protons (in relation to the pyridine nitrogen), possibly from a heterochiral complex. Alternatively, a complex in which **75** does not act as a chelating, but monodentate ligand, would also have double the amount of signals.

A second complexation attempt was done with Pd(dppp)$(OTf)_2$. Due to the fixed *cis*-attachment of the bidentate dppp ligand, the number of possible architectures were narrowed down to those consisting of di- and tri-ligated metal centers. A di-ligated complex would require an attachment of a single bis(pyridine) ligand **75** in a *cis*-fashion which would force a heavy distortion onto the molecule. Therefore, polynuclear complexes with 3 ligands (1 × dppp + 2 × **75**) on each metal center were anticipated.

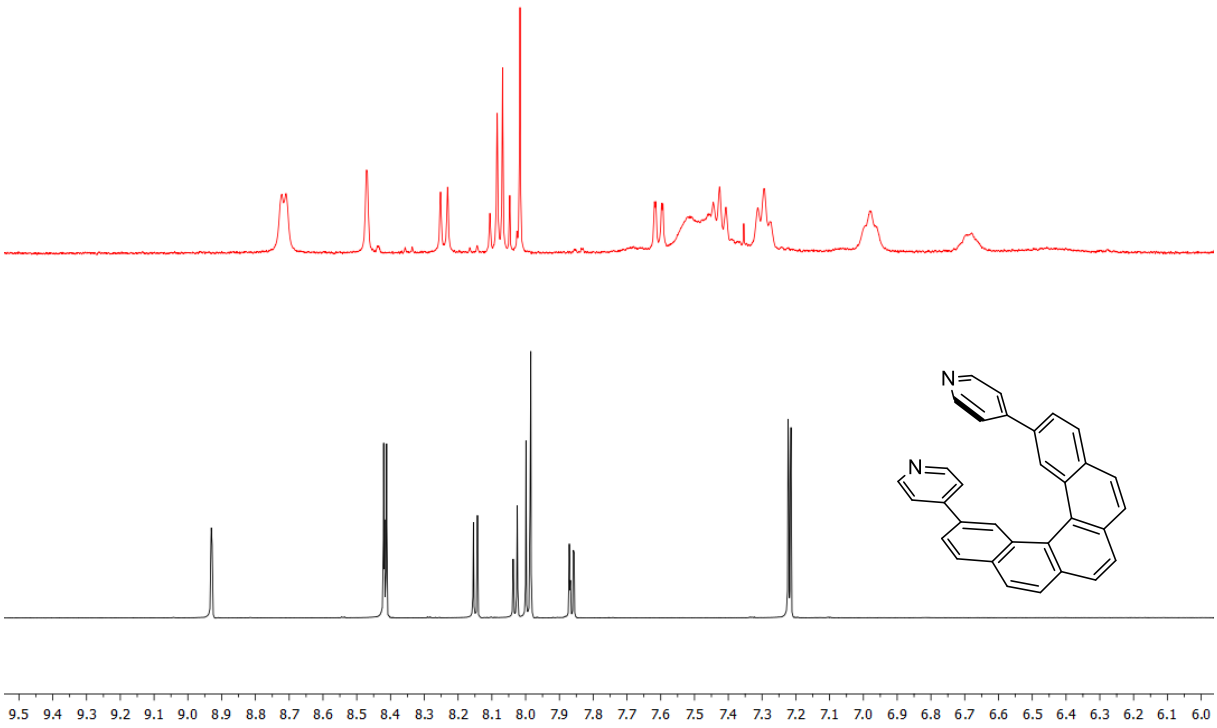

Figure 66: Comparison of ^{1}H-NMR spectra of free ligand (*rac*)-**75** (bottom) and after complexation attempt with Pd(dppp)$(OTf)_2$ (top).

The ^{1}H-NMR spectrum showed a change in chemical shift in comparison to the free ligand (**Figure 66**). However, upon complexation of the nitrogen atom to the palladium

atom, a downfield shift of the α-protons is usually expected due to the lower electron density, which was not the case here.[282] The mass spectrum suggested neither the presence of mono- nor polynuclear complexes. Aside from the signal of **75**, singly charged species of unknown composition and with low intensities were displayed. It was evident that the donor atoms in **75** were too constricted to form complexes of any kind.

The higher rotational freedom of the nitrogen donors in **76** should make complex formation more probable. Mixing the ligand with $Pd(MeCN)_4(BF_4)_2$ overnight led to an ^{1}H-NMR spectrum with scrambled signals which made a proper analysis impossible (**Figure 67**). The isotope pattern of a signal in the mass spectrum showed a doubly charged species with m/z = 485.118. This would fit to a di-ligated mononuclear complex with the composition of $[Pd(\mathbf{76})_2]^{2+}$. The multitude of signals can be rationalized by homochiral complexes consisting of enantiopure **76** and heterochiral complexes consisting of one enantiomer each.

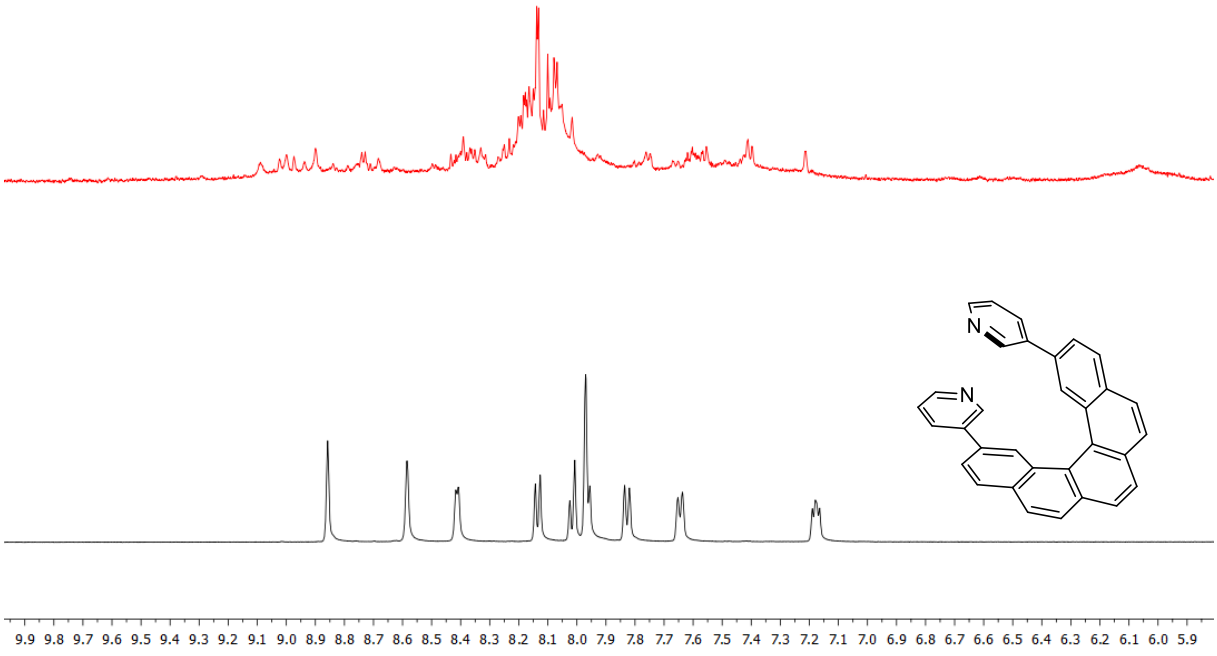

Figure 67: Comparison of ^{1}H-NMR spectra of free ligand (*rac*)-**76** (bottom) and after complexation attempt with $Pd(MeCN)_4(BF_4)_2$ (top).

On top of that, each combination can theoretically adopt a *cis*- or *trans*-configuration with respect to the nitrogen atoms attached on one ligand. This makes a sum of 6 conceivable isomers. It is doubtful whether every isomer has been formed, but based on the ^{1}H-NMR spectrum alone, it cannot be ruled out. Tentative models based on

MMFF[286] molecular mechanics refined geometries indicated that *cis*- and *trans*-configurated complexes were generally feasible, but the GFN2-xTB[177,178] minimized structures showed that both arrangements were not achievable without deviation from the square planar palladium center.

In order to get more insight and figure out whether a *cis*-configuration was experimentally feasible, the complexation experiment was reiterated with Pd(dppp)$(OTf)_2$. As before, the ^{1}H-NMR spectrum showed a change in chemical shifts and new signals, but did not allow any evaluation due to heavy overlap and insufficient resolution (**Figure 68**).

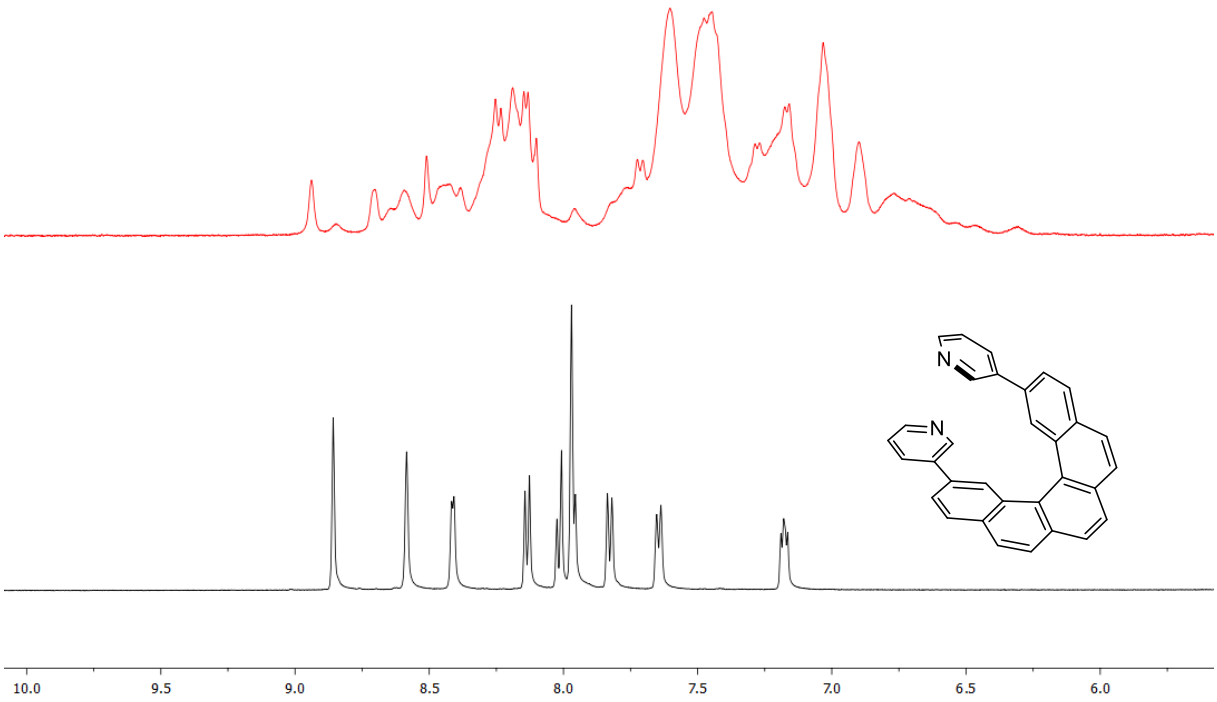

Figure 68: Comparison of ^{1}H-NMR spectra of free ligand (*rac*)-**76** (bottom) and after complexation attempt with Pd(dppp)$(OTf)_2$ (top).

The mass spectrum did not show any noteworthy signals. With this information, a *cis*-arrangement of ligand **76** in the complex $[Pd(\mathbf{76})_2]^{2+}$ can probably be ruled out as well. This would reduce the number of stereoisomers from a maximum of 6 to 3. *Trans*-chelated Pd^{II} complexes occur much less frequently than *cis*-chelated ones because the motif of opposing donor atoms with proper distances is difficult to accomplish synthetically.[287–291] A remarkable example is the *trans*-chelation of a [2.2]paracyclophane derivative which featured chiral self-sorting: When a racemic [2.2]paracyclophane with a bis(pyridine) donor motif was mixed with Pd^{II}, homochiral

PdL_2 complexes were formed exclusively. The experiment showcased a chiral self-sorting in a narcissistic self-recognition manner.[292]

Interestingly, observations affirming the assumption of a possible *trans*-chelation were also made during the complexation attempts of (*rac*)-**76** with $Cu(MeCN)_4BF_4$. While ligand (*rac*)-**75** did not form any complexes with Cu(I)-salts, (*rac*)-**76** coordinated readily with Cu in multiple ways. Initially, the ^{1}H-NMR spectrum after the experiment suggested the sole presence of ligand **76** (**Figure 69**). But in the mass spectrum, every major signal (excluding the ligand signal) proved the coordination of **76** to the metal center (**Figure 70**). In dependance of the coordination number, the preferred coordination geometry of d^{10}-configurated Cu(I) is either linear, trigonal-planar or tetrahedral.[293] With a *m*/*z* = 495.092, a complex in the form of $[Cu(\mathbf{76})]^+$ indicated that **76** formed a *trans*-chelated complex with copper. This configuration shows that **76** is principally capable of *trans*-chelation as assumed in $[Pd(\mathbf{76})_2]^{2+}$. Of course, both comparisons of smaller Cu^I with larger Pd^{II} and mono- with di-ligated complexes are somewhat flawed.

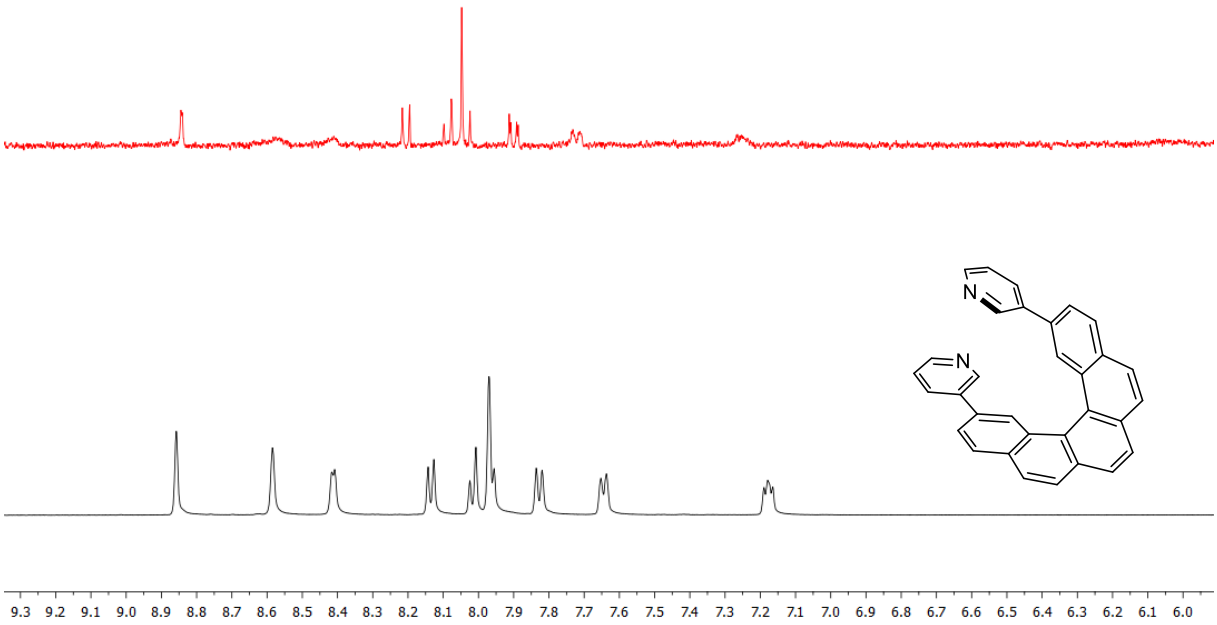

Figure 69: Comparison of ^{1}H-NMR spectra of free ligand (*rac*)-**76** (bottom) and after complexation attempt with $Cu(MeCN)_4BF_4$ (top).

Alongside the mono-ligated complex, a di-ligated complex with a composition of $[Cu(\mathbf{76})(MeCN)]^+$ (presumably resulting in a trigonal planar geometry) and a di-ligated complex with a composition of $[Cu(\mathbf{76})_2]^+$ (presumably resulting in a tetrahedral geometry) were shown. The most interesting signal was the one at *m*/*z* = 1360.422.

This mass would fit to a tri-ligated complex with the composition of [Cu(**76**)$_3$]$^+$. In contrast to Cu(II), Cu(I) usually does not form hexa-coordinated complexes and is rather oxidized to the former. The presence of [Cu(**76**)$_3$]$^+$ could either mean that the bulky ligand **76** can stabilize the metal center in such a way that an octahedral complex is feasible or that not every ligand binds with both donor atoms to the metal center. For example, two ligands can each be bound with a single nitrogen atom to the metal center, leaving the second nitrogen atom uncoordinated. But these arrangements would always lower the symmetry of the complex, leading to a splitting of NMR signals. For illustration, a *C*$_3$-symmetric complex originating from 3 singly bound ligands **76** would have double the amount of signals because of the magnetically non-equivalent protons. Since the protons next to the nitrogen atom should experience the highest change in electron density, a splitting of signals should particularly be visible around 9 ppm. In view of the obtained ^{1}H-NMR spectrum, such a splitting was not observed.

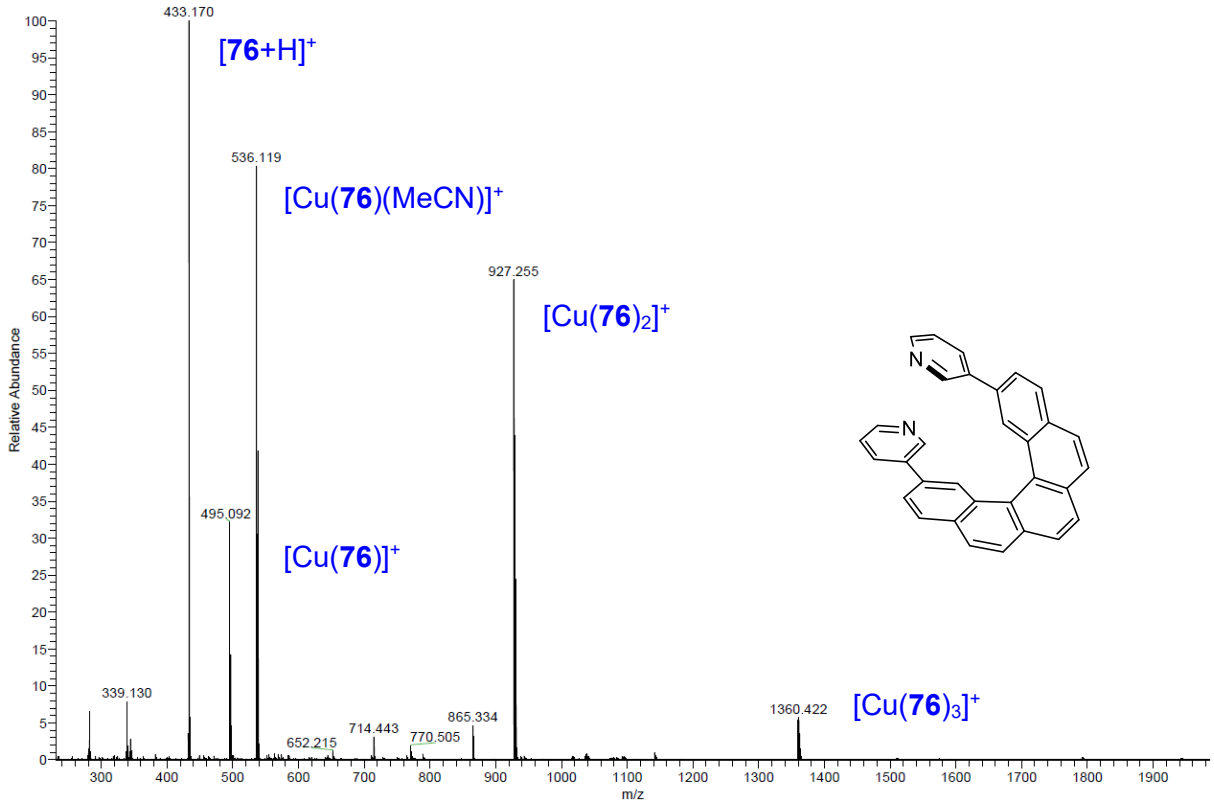

Figure 70: ESI(+)-mass spectrum after complexation attempt of (*rac*)-**76** with Cu(MeCN)$_4$BF$_4$.

Following the last series of experiments, ligand (*rac*)-**78** was treated under the same conditions. Both the ^{1}H-NMR as well as the mass spectrum after mixing (*rac*)-**78** with Pd(MeCN)$_4$(BF4)$_2$ gave no hint to a complex formation. The only discernible signal in the mass spectrum belonged to a triply charged species with *m*/*z* = 870.905

(**Figure 71**). Unfortunately, no anion could be identified that would have reduced the charge of a complex with the constitution of $[Pd_2(\mathbf{78})_4]^{4+}$.

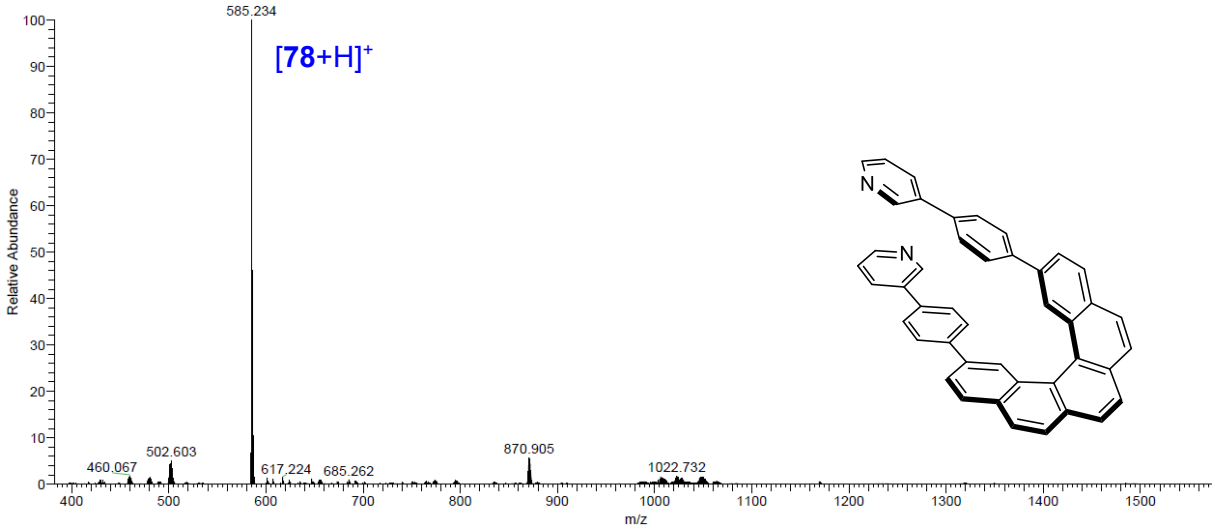

Figure 71: ESI(+)-mass spectrum after complexation attempt of (*rac*)-**78** with $Pd(MeCN)_4(BF_4)_2$.

Likewise, mixing (*rac*)-**78** with $Cu(MeCN)_4BF_4$ did not result in meaningful complexes either. Again, only the presence of the free ligand **78** was indicated. To be fair, the mass spectrum displayed a signal with *m*/*z* = 647.158 which would fit to a mono-ligated complex with the composition of $[Cu(\mathbf{78})]^+$, but the signal was so small that it was negligible (**Figure 72**).

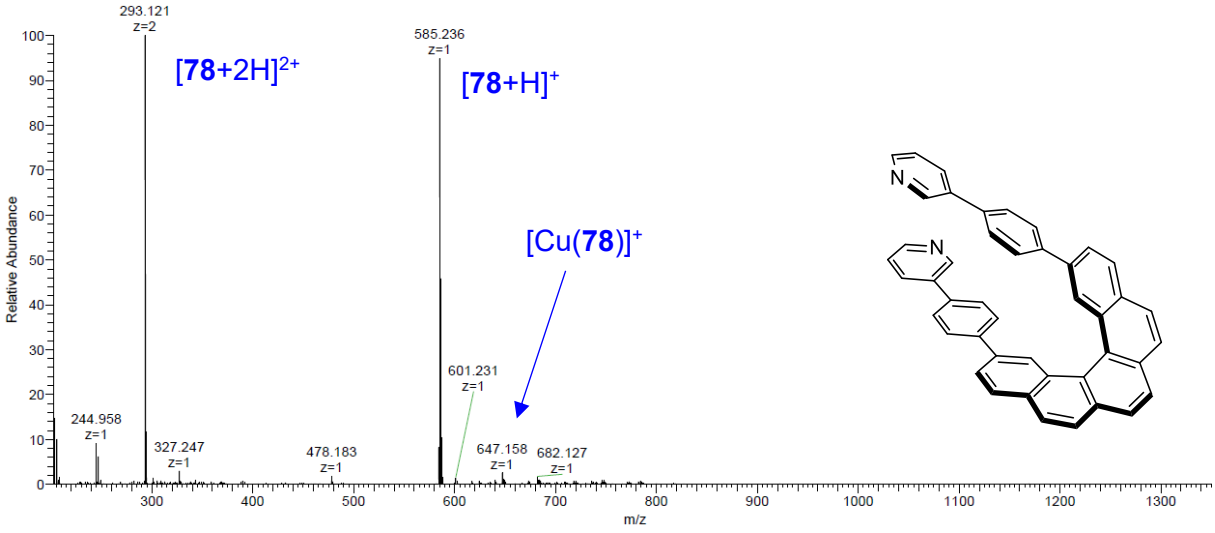

Figure 72: ESI(+)-mass spectrum after complexation attempt of (*rac*)-**78** with $Cu(MeCN)_4BF_4$.

Apparently, the elongation of the side arm bearing the donating nitrogen atom with 1,4-phenylene spacers did not provide any benefits in terms of the ability to form

complexes. Out of the 3 employed ligands, only (*rac*)-**76** was able to form stable complexes with both Pd(II) and Cu(I) to a non-negligible extent.

So far, the 2,13-difunctionalized [5]helicene was not able to form polynuclear complexes. The bond distances and angles are aligned in such a way that the entropic penalty cannot be compensated with favorable enthalpic contributions. All efforts in order to have an impact on this balance were unsuccessful. Conceptually, the possibilities have been exhausted – the adjustment of lengths and angles can only go so far. Without changing the substitution pattern, further customization of the donor angle is not really possible. Of course, an elongation of the side arm to any extent up to infinity is always possible, but certainly not sensible and feasible.

The question whether a 1,14-difunctionalized [5]helicene would have been the turning point from mono- to di- or polynuclear Pd^{II} complexes remains open. Based on the GFN2-xTB[177,178] minimized model (**Figure 53**), a substitution pattern of the positions 1 and 14 would bring the donor atoms not closer, but further apart. Introduction of two 4-pyridyl units would lead to a donor angle of approximately 180°. This would make the compound highly interesting for the generation of grid-like structures. Such components might serve as ideal candidates for the construction of Archimedean or Platonic polyhedra which essentially are molecular frameworks with well-defined inner cavities.

8.2 [7]Helicene

2,17-Difunctionalized [7]helicene

Effectively, a change of the backbone from penta- to heptahelicene is the same as a change in substitution pattern. Regarding ligands based on heptahelicene, as the higher homologue of pentahelicene **75**, ligand **91** was examined first. In terms of its capability to form a complex with Pd(II), (*rac*)-**91** behaved similarly to (*rac*)-**75** in the sense that neither entered a coordinative bond. Even after prolonged stirring at higher temperatures, the ^{1}H-NMR (**Figure 73**) and mass spectrum (**Figure 74**) mainly showed the signals of the substrate. The ^{1}H-NMR showed a slight shift for every signal which was probably caused by the different solvent: While the ^{1}H-NMR of the substrate was recorded in chloroform, the one of the complexation experiment was recorded in DMSO.

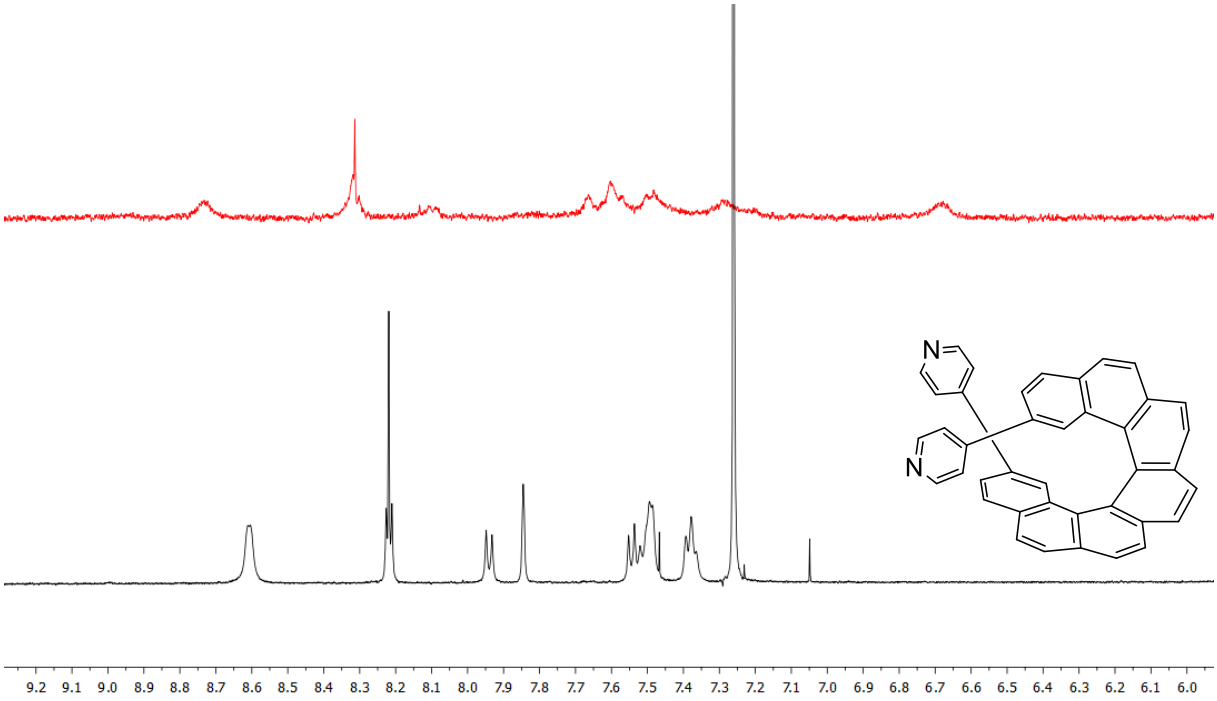

Figure 73: Comparison of ^{1}H-NMR spectra of free ligand (*rac*)-**91** (bottom) and after complexation attempt with $Pd(MeCN)_4(BF_4)_2$ (top).

The mass spectrum had a minor signal with *m*/*z* = 420.144 originating from a doubly charged species. But the mass was too small to be able to assign it to a suitable species incorporating both **75** and Pd(II). The same was true for an even smaller signal at *m*/*z* = 617.257 originating from a singly charged species. Despite the change in

donor angle induced by the switch to a higher homologue, the molecules incorporating 4-pyridinyl side arms were continuously too constricted to form dative bonds with Pd(II). Presumably, it can therefore be concluded that this was rather a problem of bond lengths and not donor angles.

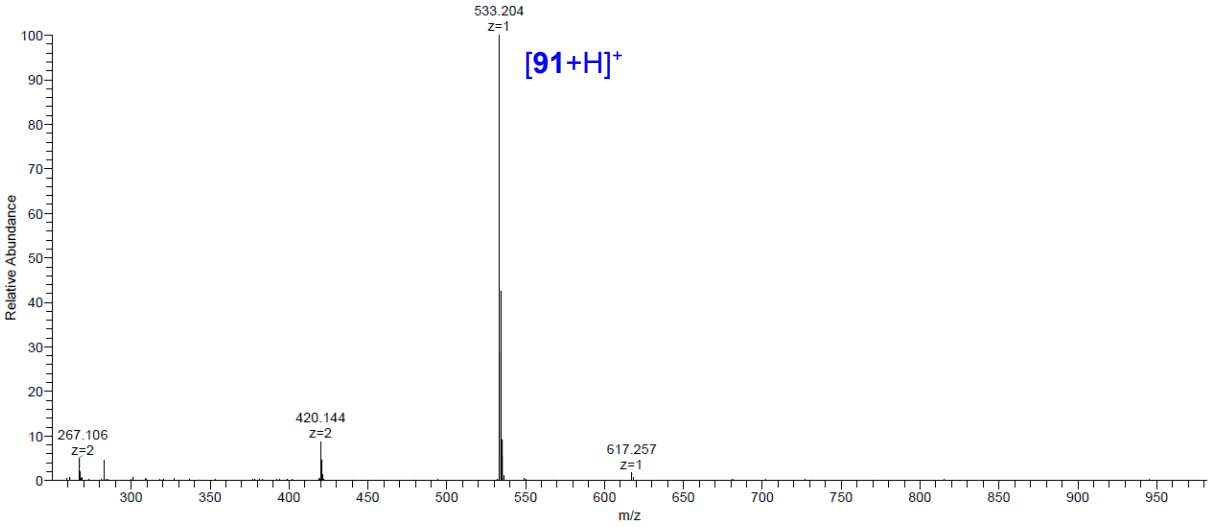

Figure 74: ESI(+)-mass spectrum after complexation attempt of (*rac*)-**91** with $Pd(MeCN)_4(BF_4)_2$.

Ligand **92** can be considered as a modified successor of **91**. The 1,4-phenylene spacer is what distinguishes them, but the donor angle should be the common denominator. From the crystal structure of (*rac*)-**92** it becomes clear that the donor angle is close to 180°. Combined with the fact that the donor atoms point against and not towards each other, the ligand should be suitable as a straight line or an edge in polyhedra. This also means that it cannot be simply paired with any metal. When all coordination sites are open in a metal ion, oligo- or polymeric structures are expected to form. For this to not occur, some sites have to be blocked specifically so that the proceeding perpetual coordination is forced to stop at some point. This can be visualized in the form of a mesh: If the metal ion is d^8-configurated and square planar, coordination with a linear ligand would inevitably lead to an infinite mesh with the metal center as junctions. But if two adjacent entries of each junction are blocked on a molecular level, basically a square can be cut out of the mesh.

Since ligand **92** could be employed as a ditopic rod for a molecular square due to its 180° angle, the metal ions had to ensure a 90° turn in order to be suitable as the corners. The previously used $Pd(dppp)(OTf)_2$ fulfills this purpose and was therefore an obvious first choice. After mixing (*rac*)-**92** with the metal salt in DMSO (**Scheme 118**), the otherwise poorly soluble (*rac*)-**92** disappeared into a clear solution.

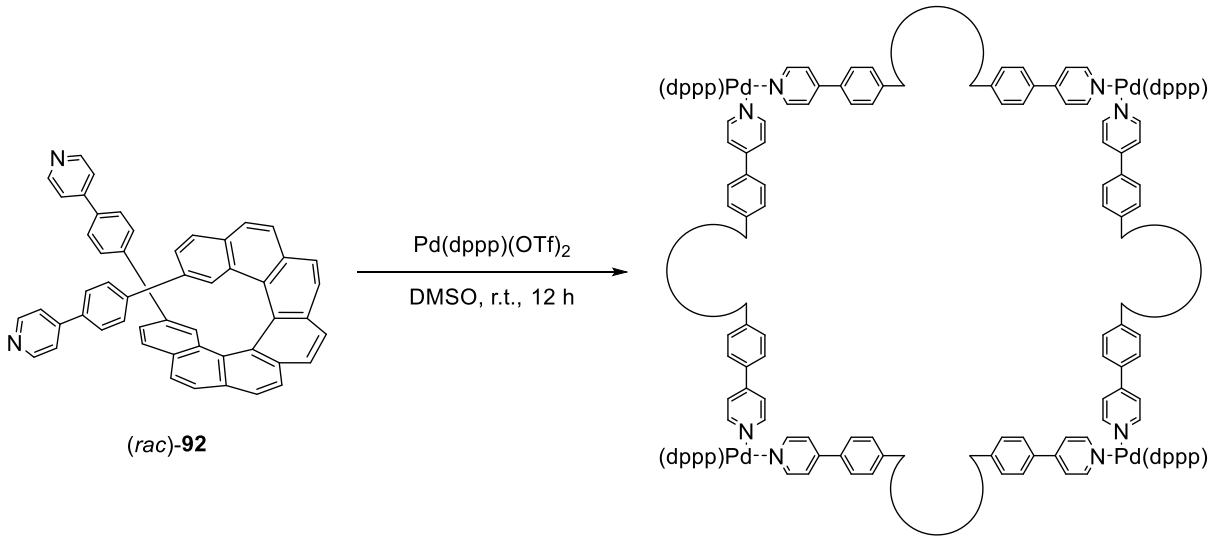

Scheme 118: Complexation attempt of (*rac*)-**92** with Pd(dppp)(OTf)$_2$.

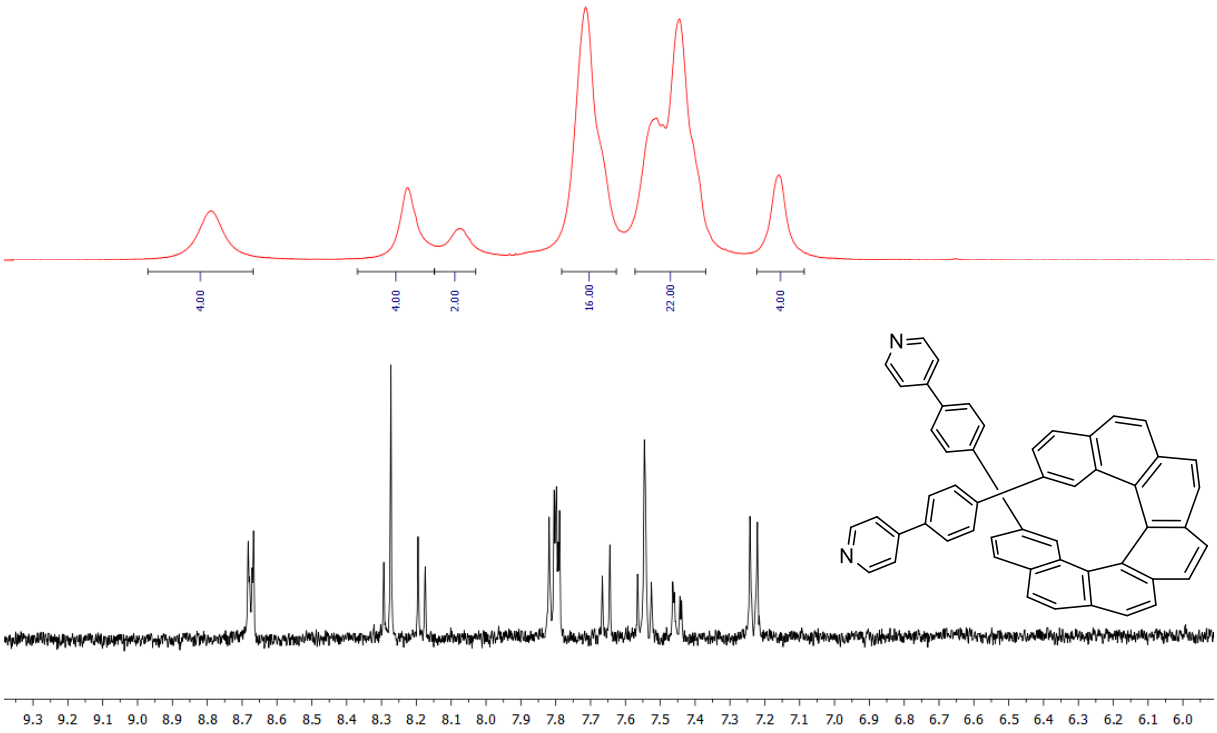

Figure 75: Comparison of ^{1}H-NMR spectra of free ligand (*rac*)-**92** (bottom) and after complexation attempt with Pd(dppp)(OTf)$_2$ (top).

The ^{1}H-NMR spectrum after 1 h had a better resolution and showed broadened signals which speaks for the emergence of a larger structure whose motion is slow on the NMR time scale (**Figure 75**). Moreover, the sum of the integral ratios had a common denominator with the actual number of protons expected for a molecular square (32 aromatic protons for each **92** unit and 20 aromatic protons for each dppp unit, total of

208 aromatic protons). The mixture was stirred for an additional 11 h, but the ^{1}H-NMR spectrum remained unchanged.

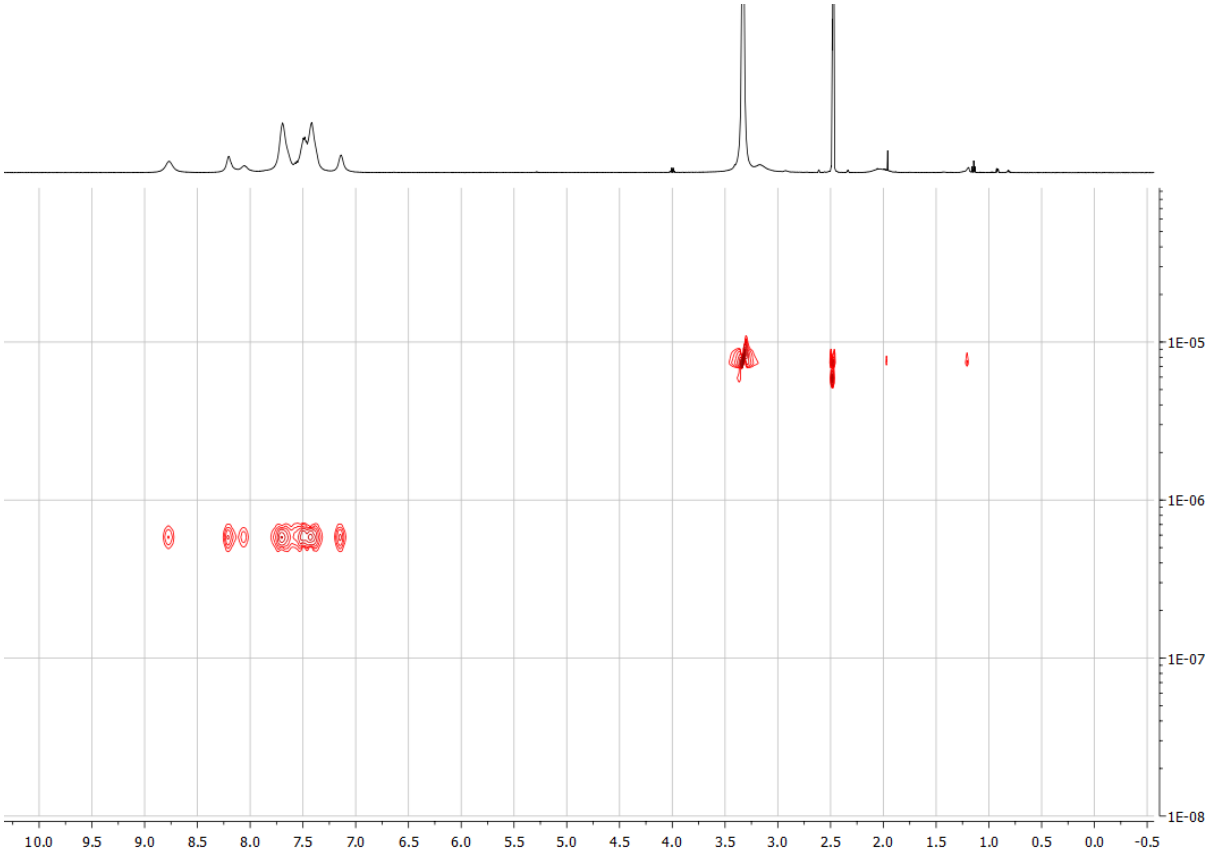

Figure 76: DOSY spectrum after complexation attempt of (*rac*)-**92** with Pd(dppp)(OTf)$_2$.

The solution was also analyzed by diffusion-ordered spectroscopy (DOSY). Therein, the 2D spectrum showed a single diffusion constant *D* for every signal. For that reason, it can be assumed that one species (not including isomers) is present. The diffusion constant was $D = 5.55\times10^{-11}$ m^2 s^{-1} (**Figure 76**). The diffusion constant can be put into relation with the hydrodynamic radius r_H according to the *Stokes-Einstein* equation (4).

$$D = \frac{k_B T}{6\pi\eta r_H} \qquad (4)$$

In this equation, k_B is the *Boltzmann* constant, *T* the absolute temperature and η the viscosity of the fluid. After rearranging the equation, a hydrodynamic radius of r_H = 17.6 Å can be calculated which corresponds to a diameter of 35.2 Å. It should be noted that 6 in the equation is a shape-correction factor for spherical particles of colloidal dimensions so that the equation is strictly speaking only applicable to spheres.[294] Of course, a square is not even in the broadest sense something resembling a sphere, therefore the formula can only be applied with reservations. The

models based on MMFF[286] molecular mechanics refined geometries showed a distance of 35.2 Å between opposing Pd atoms under maintenance of their square planar configuration (**Figure 77**), the GFN2-xTB[177,178] minimized structures repeatedly showed that the arrangement was not achievable without deviation from the square planar palladium center.

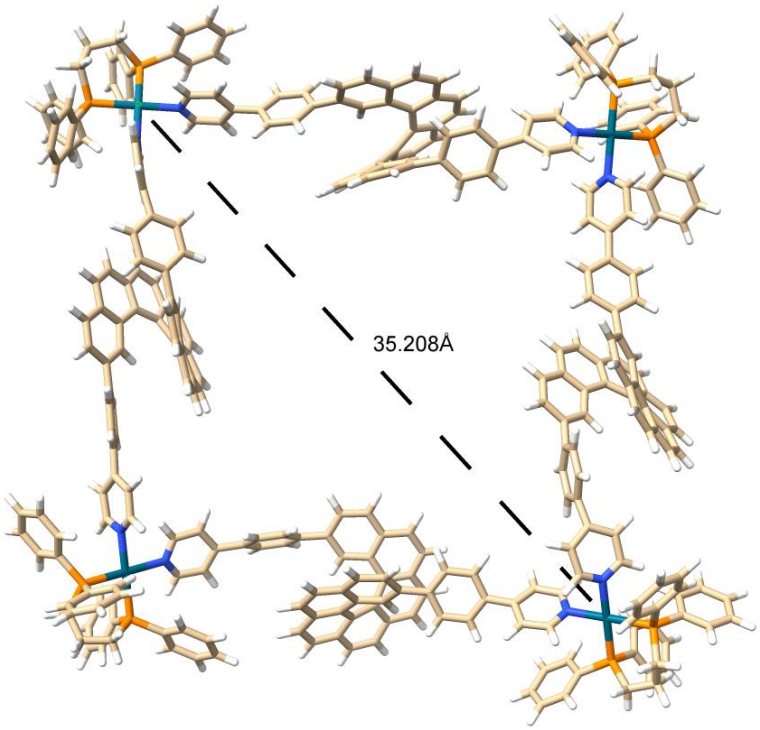

Figure 77: MMFF[286] minimized structure of a molecular square $Pd_4(dppp)_4((M)\text{-}\mathbf{92})_4$ (carbon in brown, hydrogen in white, nitrogen in blue, phosphorus in orange, palladium in cyan).

The mixture was also subjected to mass spectrometric analysis. The largest signal was that of free ligand **92** at *m*/*z* = 685.264 (**Figure 78**). Next to it, there were fragments of the assumed square at regular intervals, although with low intensity. These ranged from one corner in the form of $[Pd(dppp)(\mathbf{92})_2]^{2+}$ up to half a square in the form of $[Pd_2(dppp)_2(\mathbf{92})_2]^{4+}$. Unfortunately, the whole assembly was not found even after zooming in on the spectrum. While complexes with the same metal-to-ligand ratio, but different nuclearity where partially found underneath the major signals (**Figure 79**), no trace of the $Pd_4(dppp)_4(\mathbf{92})_4$ square was found anywhere. It remains unclear whether the square has definitely been formed. While the NMR spectroscopic analysis is in favor of such an arrangement, the mass spectrometric is not. Regarding the mass spectrometric experiments, the complex could theoretically be too labile for ionization or too labile in the gas phase in general.

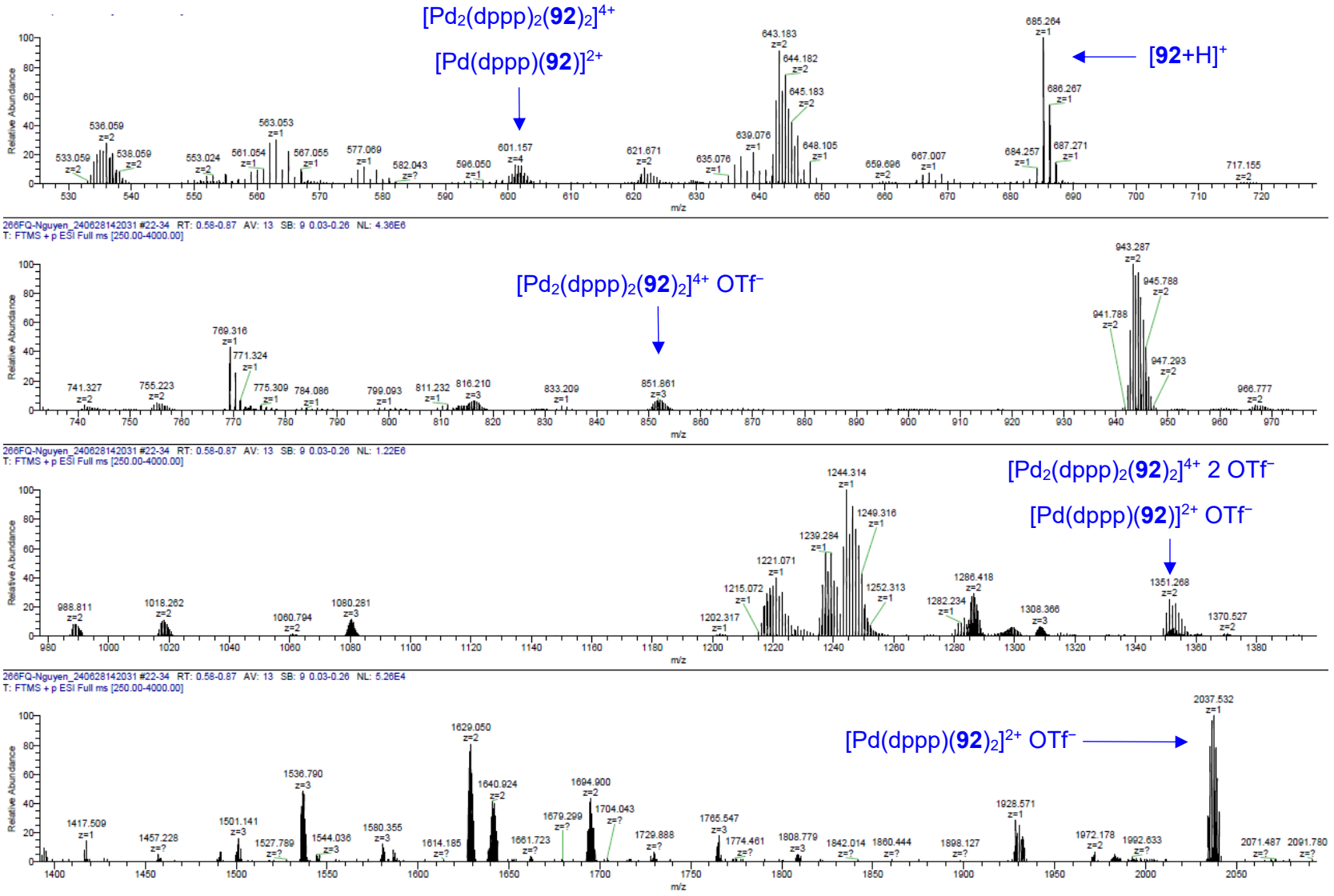

Figure 78: ESI(+)-mass spectrum after complexation attempt of (*rac*)-**92** with Pd(dppp)(OTf)$_2$.

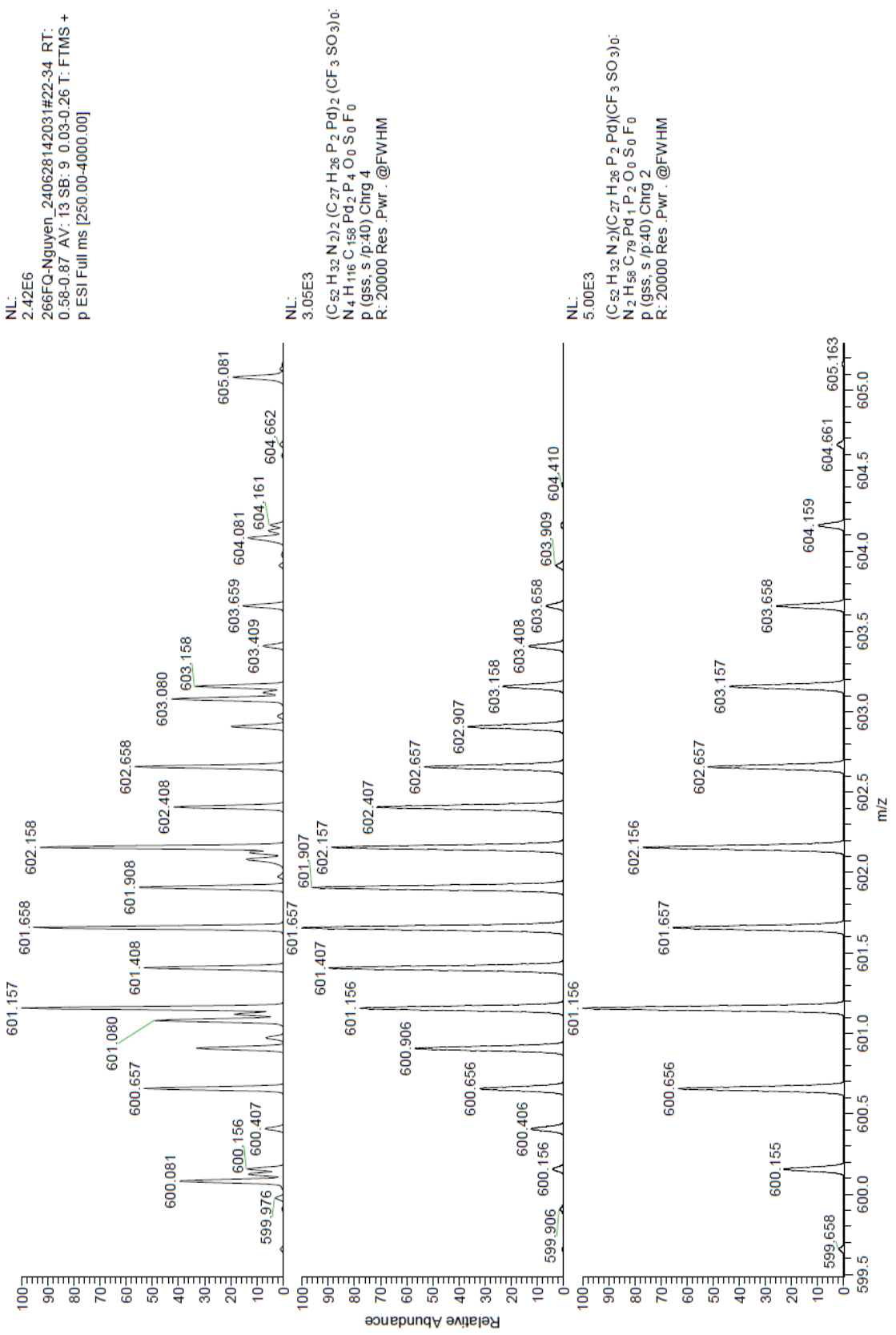

Figure 79: Comparison of the experimental exact masses (top) with the calculated exact masses of $[Pd_2(dppp)_2(\mathbf{92})_2]^{4+}$ (middle) and $[Pd(dppp)(\mathbf{92})]^{2+}$ (bottom).

But if the formation of a molecular square is considered, every possible isomer has to be discussed. Since (*rac*)-**92** consists of 2 enantiomers, a complex incorporating 4 of either can consist of 5 ratios between the (*P*)- and (*M*)-enantiomer (**Table 1**). In case of the complex that incorporates 2 of each, *cis*- and *trans*-configurations also need to be considered. This adds up to a total of 6 theoretically feasible isomers of which 4 are a pair of enantiomers, respectively. This in turn means that at least 4 sets of signals originating from the 4 diastereomers are to be expected in the ^{1}H-NMR.

Table 1: Possible arrangements and symmetry/probability considerations of a molecular square $[Pd_4(dppp)_4)(\mathbf{92})_4]^{8+}$ consisting of (*P*)-**92** (red line) and (*M*)-**92** (blue line). Black dashed lines show axes of rotation C_2, black solid lines show mirror planes σ, black dots show the main axes of rotation which point upwards (C_4 for 4:0 and 0:4, C_2 for 2:2 *trans*).

Ratio (*P*):(*M*)	Permutations	Point group	Probability
4:0	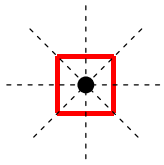	D_4	6.25 %
3:1	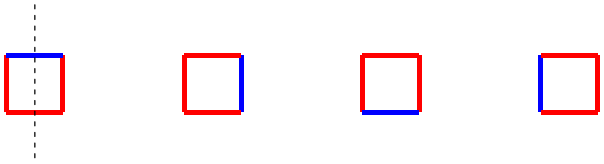	C_2	25.0 %
2:2 *cis*	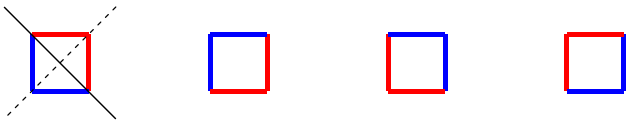	C_{2h}	25.0 %
2:2 *trans*	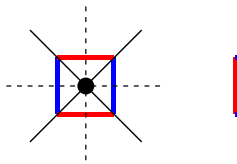	D_{2d}	12.5 %
1:3	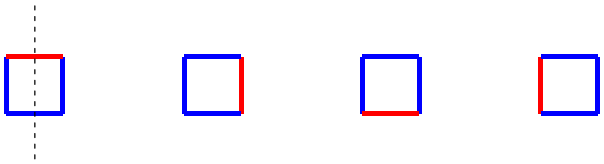	C_2	25.0 %
0:4	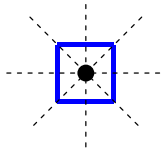	D_4	6.25 %

Statistically, one might assume that each isomer has the same probability. In absence of any driving force towards a species, each enantiomer of **92** would then have a 50 % chance to occupy one of the four edges of the square. With that in mind, each possible square would have the same probability of $p = 0.5^4 = 6.25$ %. But since there are different numbers of permutations for each isomer of the complex, their probabilities vary.

The complex consisting of 4 units of (*P*)-**92** and the one incorporating 4 units of (*M*)-**92** are a pair of enantiomers (ratios 4:0 and 0:4). Since they only have one permutation each, their combined probability is $p = 12.5$ %. The resulting homochiral molecular square belongs to the point group D_4. The highly symmetrical complex should not cause any signal splitting because every ligand can be converted into each other while the C_2 symmetry of each helicene itself is retained which means that each half of each helicene has the same chemical environment.

The other enantiomers are the complexes with a ratio of 3:1 and 1:3. They are part of the C_2 point group. Due to the lower symmetry, these complexes should induce a signal splitting. The resulting square has one rotational axis C_2 which retains the C_2-symmetry of just 2 helicenes within the square and the ligands cannot freely be converted into each other, leading to different chemical environments of former magnetically equivalent protons and a splitting of NMR signals. Each enantiomer has 4 permutations, so their combined probability to form is $p = 50$ %.

In the heterochiral complexes with a 2:2 ratio, a distinction must be made between the *trans*- and the *cis*-isomer. The former falls under the point group D_{2d} which makes it achiral, the presence of 2 rotational axes C_2 and 2 mirror planes σ_d means that the C_2 symmetry of each ligand is retained and that neighboring and opposing ligands can be converted into each other. Because of that, this complex should not cause a signal splitting. Interestingly, the *trans*-isomer has half the probability of forming compared to the *cis*-isomer due to having half as many permutations ($p = 12.5$ %).

But unlike the probability, the symmetry decreases with the *cis*-isomer. The presence of a rotational axis C_2 and a mirror plane σ_h means that the isomer is achiral and belongs to the point group C_{2h}. Although neighboring helicenes can be converted into each other, the presence of just one rotational axis along the corners of the square means that every helicene loses its main C_2 axis. As a result, the halves of each

helicene do not have the same chemical environment any more, leading to a signal splitting of NMR signals.

The actual probabilities need to be examined in order to figure out if self-sorting occurs. The best method to do this would be XRD analysis. Unfortunately, single crystals could not be grown out of the solution. But since any deviation from the statistical probability is a form of self-sorting, an exclusion procedure would be sufficient in order to prove any self-sorting behavior. For instance, if the enantiopure ligand would not form any complex, a deviation from the expected distribution and a social self-sorting process is already proven. Since (*rac*)-**92** was too badly soluble for any optical resolution by HPLC, another pathway was needed. An optical resolution of the precursor followed by its conversion to enantiopure **92** under stereo preservation was considered. As a triflate, substrate (*rac*)-**90** was highly soluble in many common organic solvents and therefore perfectly suitable for an optical resolution by HPLC. With retention times of t_1 = 1.15 min and t_2 = 1.34 min, both fractions eluted very quickly from the *Daicel CHIRALPAK IB-U* column (**Figure 80**). But with a separation and capacity factor of α = 1.36 and R_s = 1.05, the goal of a baseline separation was narrowly missed. Thus, a proper resolution was only feasible with recycling of the fractions and multiple runs (recycling-HPLC).

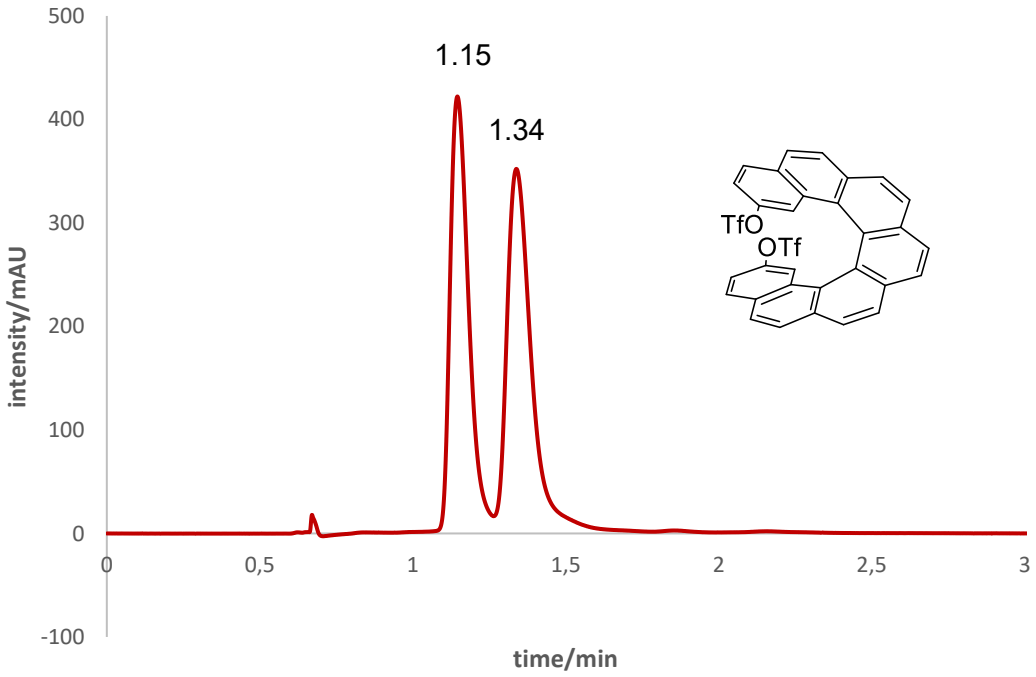

Figure 80: Chiral resolution of (*rac*)-**90** by analytical HPLC (*n*-hexane/^{i}PrOH/EtOH = 98:2:2, *Daicel CHIRALPAK IB-U* column, 0.85 mL/min, 235 nm).

As expected, in the first semipreparative run, a slight separation of the signals could be achieved. A determination of separation and capacity factor at this stage would have been meaningless. Altogether, the fractions had to be recycled and injected 5 times into the system for the separation to be sufficient (**Figure 81**). In combination, this led to retention times of t_1 = 30.42 min and t_2 = 33.15 min, a separation factor of α = 1.10 and a capacity factor of R_s = 0.94.

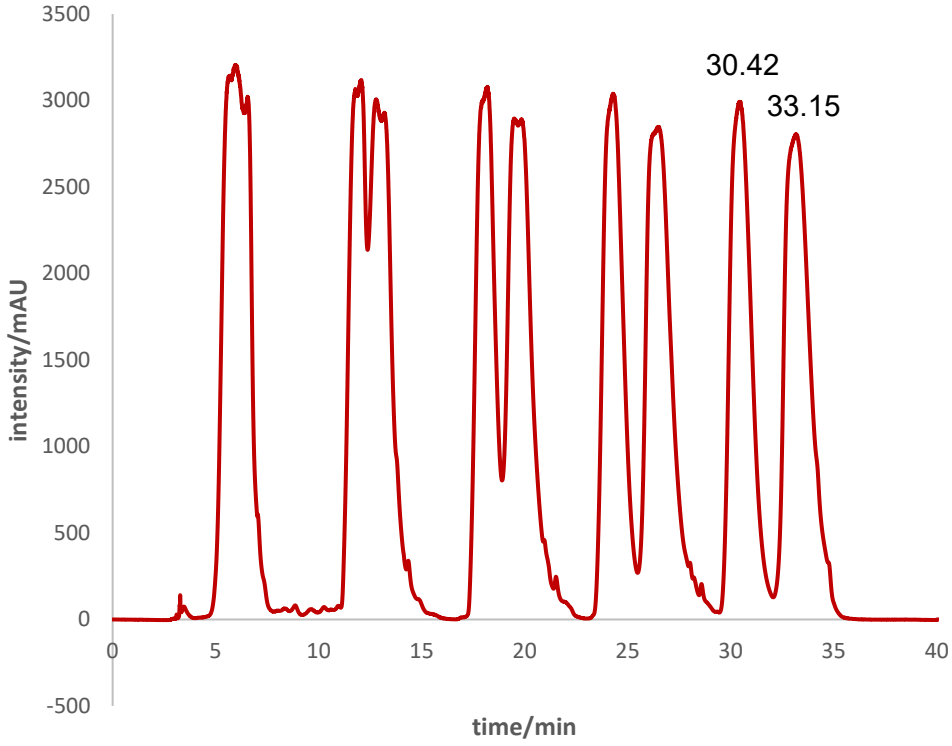

Figure 81: Chiral resolution of (*rac*)-**90** by semipreparative recycling-HPLC (*n*-hexane/^{i}PrOH/EtOH = 98:2:2, *Daicel CHIRALPAK IB* column, 18 mL/min, 235 nm).

Prior to their conversion to **92**, the fractions were characterized regarding their absolute configurations. The algebraic signs from the first to the second fraction went from negative to positive which is in line with every helicene resolved by the *Daicel CHIRALPAK IB* column thus far. The experimental ECD spectra had distinct bands at bands around λ = 270, 265, 340 and 350 nm (**Figure 82**). Based on the simulations, the assignment of the first eluting fraction to the (*M*)-enantiomer (and *vice versa*) was also confirmed. With both enantiomers collected, Suzuki coupling towards **92** was carried out two additional times. After analogous purification procedures, (*P*)- and (*M*)-**92** were obtained in 13 and 12 % yield, respectively (**Scheme 119**) – similar to the transformation of (*rac*)-**90** to (*rac*)-**92**.

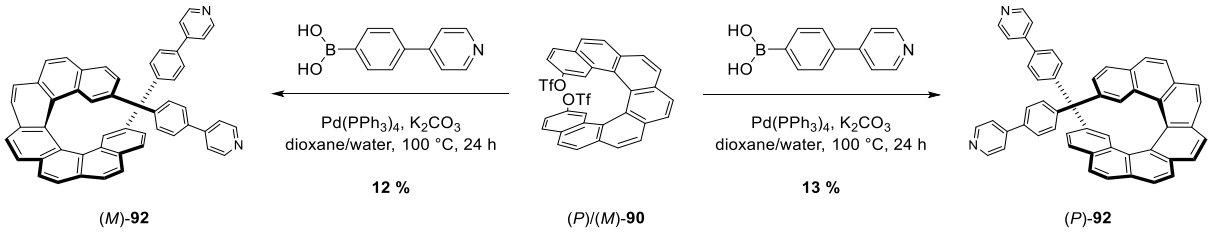

Scheme 119: Suzuki coupling of enantiopure **90** to enantiopure **92**.

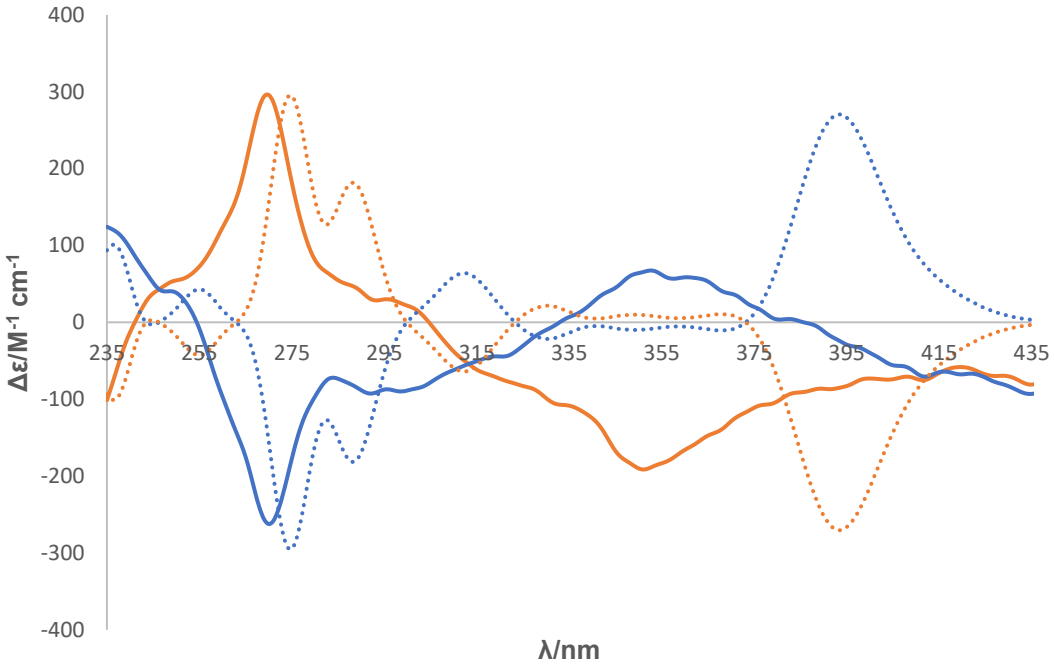

Figure 82: Experimental ECD spectra of (*P*)-**90** (blue solid line, dichloromethane, $c = 5.5\times10^{-4}$ g/L), (*M*)-**90** (orange solid line, dichloromethane, $c = 6.3\times10^{-4}$ g/L), respectively, and the corresponding calculated ECD spectra (dashed lines).

The complexation experiments were reiterated with enantiopure **92**. The ^{1}H-NMR spectra of the experiments with (*P*)- and (*M*)-**92** showed a high resemblance to the one with (*rac*)- **92** (**Figure 83**). The mass spectrometric data also aligned with those of the racemic experiment in the sense that the same fragments were observed. Due to that, it can be assumed that the homochiral complexes were definitely formed in the racemic experiment. But based on this information alone, no statement can be made as to whether heterochiral complexes were formed or not. The nearly identical signals could indicate that no diastereomeric species (which should have different chemical environments for their protons) are present, but (i) it was hard to tell whether the broad signals had a perfect alignment, (ii) signals from any heterochiral species could lie underneath the broad signals in the racemic experiment and (iii) for some homochiral and heterochiral diastereomers, the spectra are nearly identical.[295]

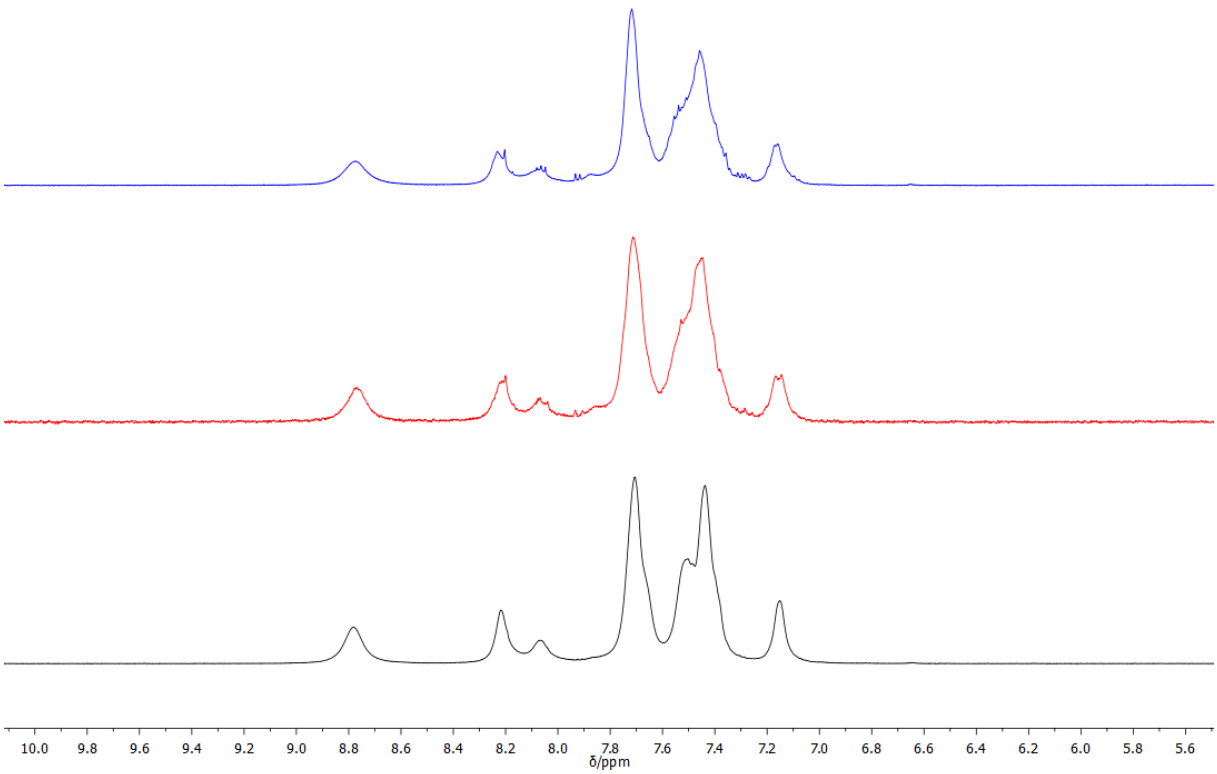

Figure 83: Comparison of ^{1}H-NMR spectra of experiments with (*rac*)-**92** (bottom), (*M*)-**92** (middle) and (*P*)-**92** (top) and Pd(dppp)(OTf)$_2$, respectively.

Last but not least, ligand **93** was also investigated with regard to its coordination behavior. In contrast to ligand **92**, the 3-pyridinyl motif should not result in a 180° donor angle which means that no oligo- or polymeric complexes were necessarily to be expected upon mixing with metal ions having 180° and 90° linkages. Mixing (*rac*)-**93** with Pd(MeCN)$_4$(BF$_4$)$_2$ gave a ^{1}H-NMR spectrum with a multitude of undefined partly overlapping signals (**Figure 84**). Especially the area around 9−10 ppm, where the signals of the 4 protons adjacent to the nitrogen atoms were expected to be, was more crowded than anticipated. The abundance of these signals indicated the presence of more species than the maximum number of different hypothetical homo- and heterochiral Pd$_2$L$_4$ complexes that exist.

In the mass spectrum, the major signals indicated the assembly of a complex in the form of [Pd$_3$(**93**)$_6$]$^{6+}$ (**Figure 85**) which would explain the higher number of signals compared to the 6 isomers of a hypothetical [Pd$_2$(**93**)$_4$]$^{4+}$. Assuming a homoleptic and homochiral trinuclear complex with chemically equal binding sites, there are up to 7 possible arrangements if the maximum occupancy rule is obeyed (**Figure 86**).

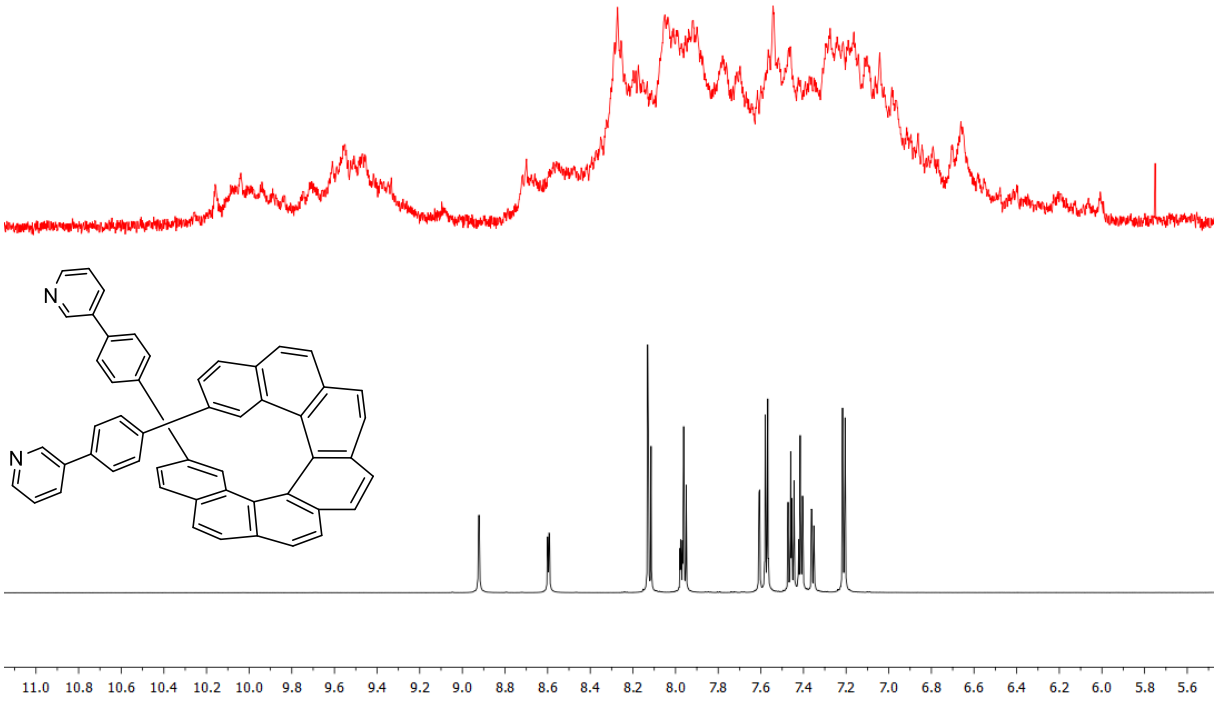

Figure 84: Comparison of ^{1}H-NMR spectra of free ligand (*rac*)-**93** (bottom) and after complexation attempt with $Pd(MeCN)_4(BF_4)_2$ (top).

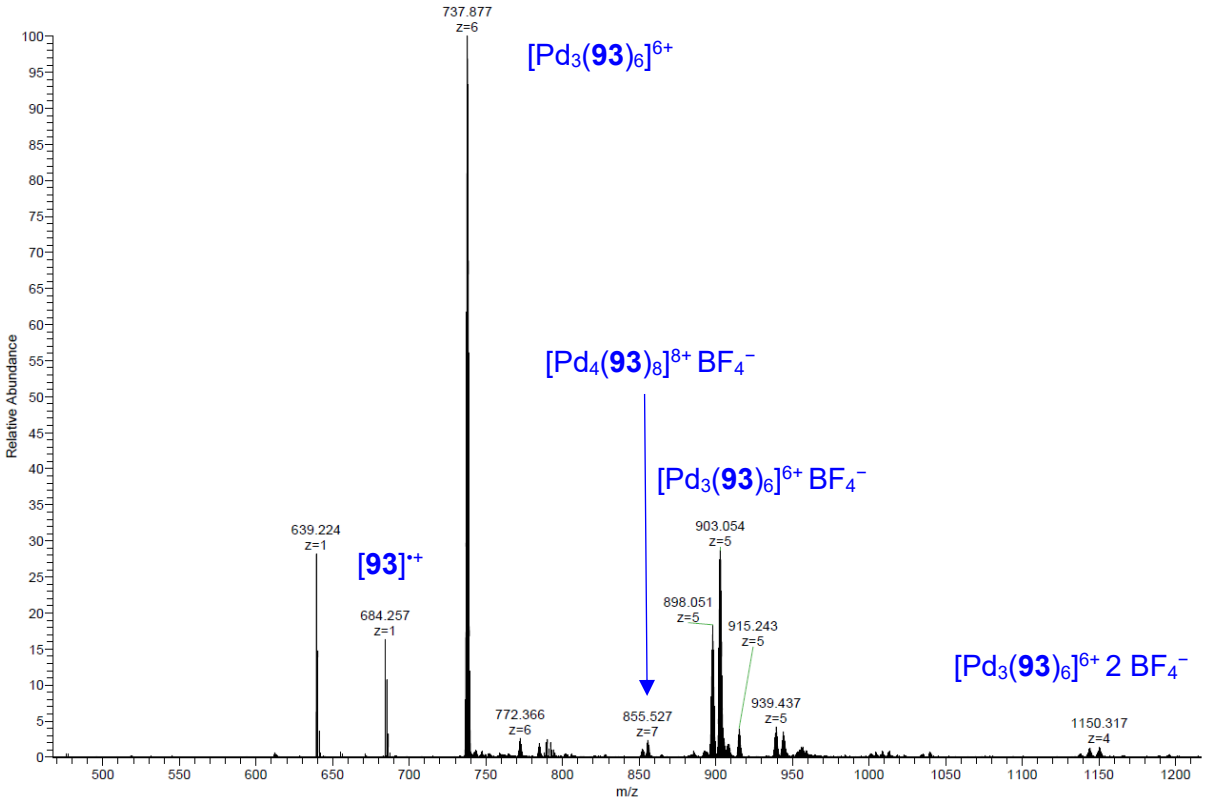

Figure 85: ESI(+)-mass spectrum after complexation attempt of (*rac*)-**93** with $Pd(MeCN)_4(BF_4)_2$.

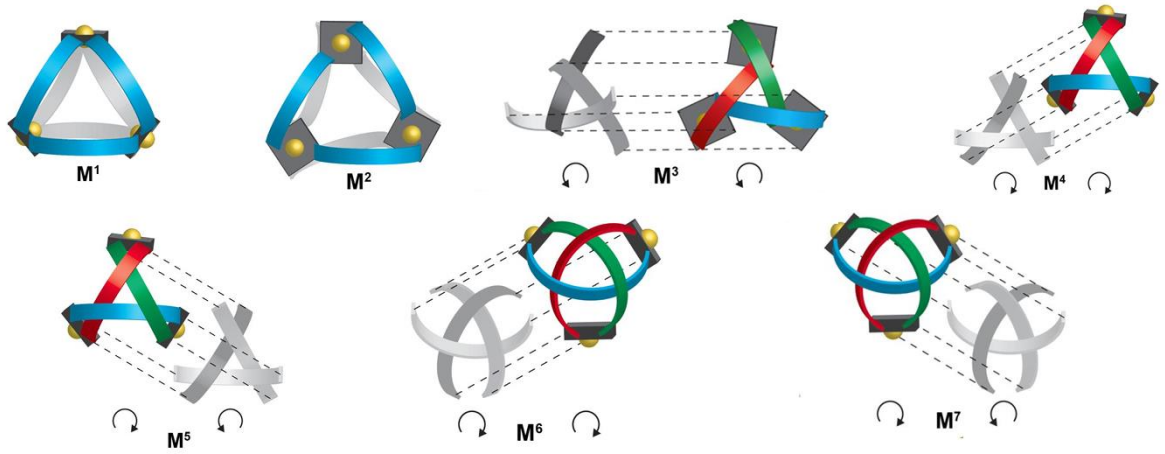

Figure 86: Possible topologies of six bidentate ligands with three square planar metals. Adapted with permission from *John Wiley and Sons*.[296]

Since there are 7 different ratios for (*P*)- and (*M*)-enantiomer in a complex with 6 ligands, there are at least 7 isomers for every model. If different configurations come into play, it could very well go into the double digits. For model **M**^{1} which has the highest symmetry (D_{3h} symmetry), there are 16 possible isomers (**Table 2**). Accordingly, every model with a lower symmetry should have more than 16 isomers.

Table 2: Possible arrangements of (*P*)- and (*M*)-**93** and their probabilities in a $[Pd_3(\mathbf{93})_6]^{6+}$ complex.

Ratio (*P*):(*M*)	∑Permutations	∑Isomers	Probability
0:6	1	≥1	1.5625 %
1:5	6	≥1	9.375 %
2:4	15	≥4	23.4375 %
3:3	20	≥4	31.25 %
4:2	15	≥4	23.4375 %
5:1	6	≥1	9.375 %
6:0	1	≥1	1.5625 %

Of course, it is questionable whether every model is present. While all of them are theoretically constructible with a molecule construction kit, most of them can be ruled out since they would require an extremely flexible and elongated ligand which **93** is not. As an example, all the intertwined models (**M**^{3}–**M**^{7}) are rather unlikely for bulky **93** since atoms and bonds would have to interpenetrate each other (**Figure 87**).

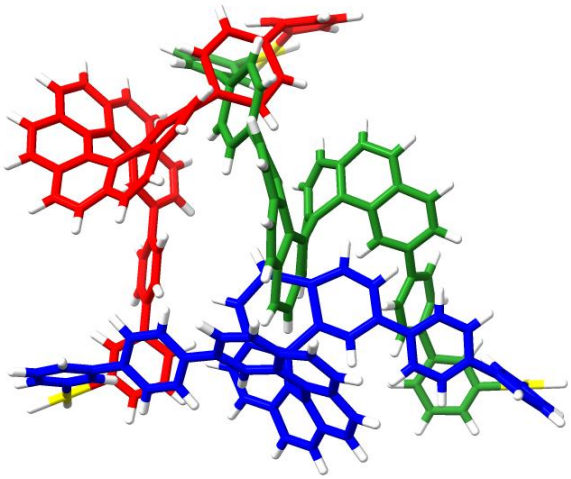

Figure 87: Illustrative structure of upper half of model **M**[7] for reference, lower half omitted for clarity (carbons of respective ligands in blue, red and green; Pd in yellow, hydrogen in white). The ligands would have to interpenetrate each other to make such an arrangement.

Additionally, only the two models **M**[1] and **M**[7] have been reported for the rarely occurring Pd_3L_6 aggregates thus far. Generally, the formation of a cage with a higher nuclearity is entropically disfavored since formation of the smallest possible Pd_nL_{2n} cage requires fewer components to build. But the formation of architectures with more complex topologies can be thermodynamically facilitated by rational ligand design, usage of templates, solvent effects, counter anions and so on. Since there are so many variables which can influence the resulting structure, the formation of more complex ones is often a product of serendipity.

The double-walled triangle **M**[1] is the more common one due to its higher symmetry and simplicity. Each Pd center is bridged by two ligands, the upper and lower halves are identical and interconvertible through a mirror plane σ_h. Only a few reports of such an arrangement have been made.[297–305] In these cases, the driving force towards the trinuclear cage is more or less a fixed donor angle of the nitrogen atoms around 60° which renders the ligands incapable of forming the smaller Pd_2L_4 product.

For model **M**[7], there has ever only been one report.[296] The C_{3h}-symmetric arrangement is characterized by intertwining ligands which form two chiral hemispheres which are also interconvertible though a mirror plane σ_h. But in contrast to model **M**[1], this leads to chemically non-identical donor sites, and thus, a splitting of NMR signals. In the publication, this arrangement was only enabled by an unusually flexible and long ligand (**Scheme 120**). Although a Pd_2L_4 cage would have been

feasible with the same ligand, the driving force towards the trinuclear cage seemed to be attractive interactions like inter-ligand hydrogen bonding and extended π-π interactions within the double trefoil-knotted structure.

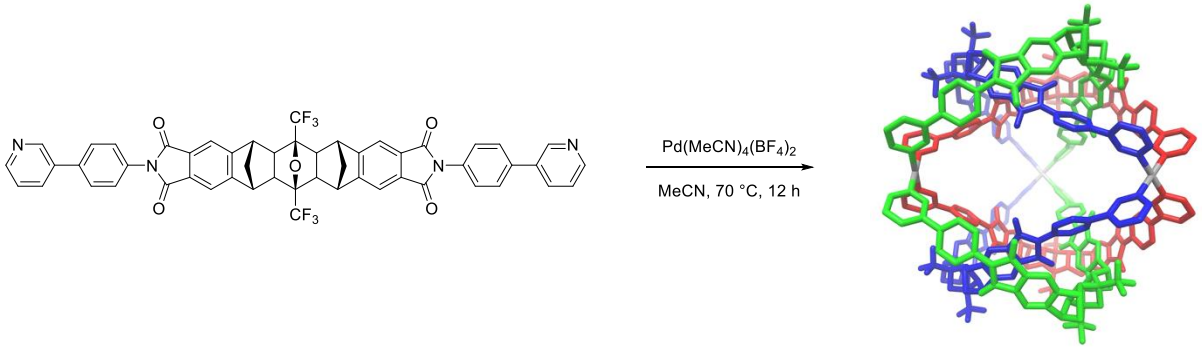

Scheme 120: Intertwined Pd_3L_6 complex. Adapted with permission from *John Wiley and Sons*.[296]

Interestingly, a heptacationic species at $m/z = 855.527$ was shown in the mass spectrum after the complexation attempt of (*rac*)-**93** with $Pd(MeCN)_4(BF_4)_2$ as well. This would match to a tetranuclear complex in the form of $[Pd_4(\mathbf{93})_8](BF_4)$. Actually, the concomitant ability of a ligand to form Pd_3L_6 and Pd_4L_8 complexes simultaneously is not an unprecedented phenomenon as in many of the available publications, the same occurrence was observed as well.[297–301] The fixed donor angle around 60° allows for the formation of both cages so that they often can be in dynamic equilibrium. This equilibrium can be shifted by change in chemical or physical environment (solvent, counterion, temperature, etc.).[306]

Although entropically even more disfavored, Pd_4L_8 complexes are more common than their trinuclear counterpart, but still rare. In regard of possible topologies, the number of models definitely reach the double digits because – apart from intertwined species – oligomeric interlocked catenated species also come into play. As far as possible structures go, mainly three different ones have been reported in literature (**Figure 88**).

Analogously to model $\mathbf{M^1}$, a macrocycle can also be constructed with Pd_4L_8 complexes.[298–301,307–309] Therein, two ligands linearly bridge two metal centers to form a 4-membered ring with a crown-like structure. Although it is the structure with the highest symmetry (D_{4h} symmetry) compared to its competing structures, it is not as dominant as $\mathbf{M^1}$ in terms of empirical occurrence.

The second structure is that of a D_{2d}-symmetric tetrahedron in which the metal ions lie at the corners.[297,310–314] This time, two of the six edges are doubly bridged by two

ligands, whereas the remaining ones are singly bridged by one ligand. Depending on the employed ligands, the tetrahedron can take on a distorted shape so that pseudo-tetrahedra also fall under this category.

Thirdly, catenated species have been assembled in which two Pd_2L_4 cages are interlocked.[315–318] The most prevalent one is a quadruply interlocked double cage of D_4 symmetry which has a linear arrangement of the metal centers. Recently, a new species of C_{2h}-symmetric, triply interlocked cages with a staggered arrangement has been reported which coexisted with the quadruply interlocked cage.[319]

A single report has been made of a doubly bridged bowl with a $(Pd_2L_3)(\mu\text{-}L)_2(Pd_2L_3)$-type of structure in which two edges of the bowl are triply bridged by three ligands, whereas the remaining two edges are singly bridged by one ligand.[320]

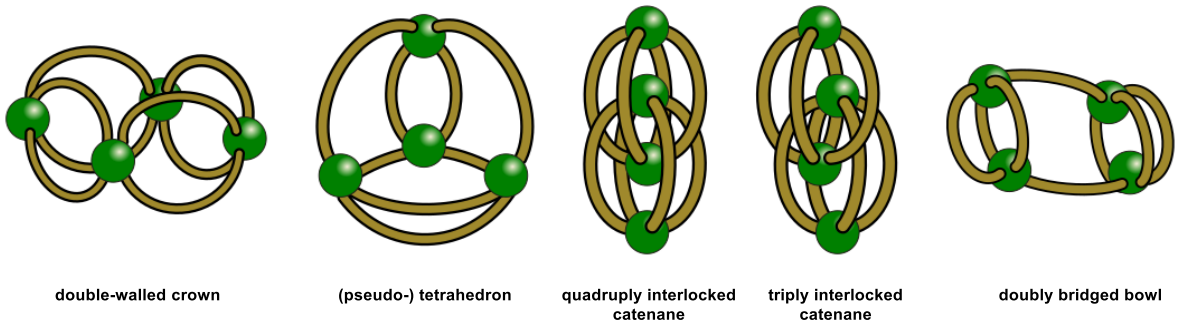

Figure 88: Reported topologies of Pd_4L_8 aggregates (Pd as green spheres, curved ligands as yellow tubes).

Table 3: Possible arrangements of (*P*)- and (*M*)-**93** and their probabilities in a $[Pd_4(\mathbf{93})_8]^{8+}$ complex.

Ratio (*P*):(*M*)	∑Permutations	∑Isomers	Probability
0:8	1	≥1	0.390625 %
1:7	8	≥1	3.125 %
2:6	28	≥6	10.9375 %
3:5	56	≥7	21.875 %
4:4	70	≥13	27.34375 %
5:3	56	≥7	21.875 %
6:2	28	≥6	10.9375 %
7:1	8	≥1	3.125 %
8:0	1	≥1	0.390625 %

Considering the different ratios of enantiomers for **93** and the structure with the highest symmetry, a hypothetical D_{4h}-symmetric crown-shape would already have 43 isomers alone (**Table 3**). Accordingly, every other model has at least 43 possible isomers. In the ^{1}H-NMR spectrum, the proton signals from these structures would come on top of the signals originating from any Pd_3L_6 species which would explain the multitude of observed signals. Disentanglement of these signals alone was impossible since too many factors needed to be paid attention to.

In hopes of differentiating between tri- and tetranuclear species, DOSY-NMR was carried out (**Figure 89**). A precise determination of hydrodynamic radii r_H was not feasible because of the amount of overlapping signals. Nonetheless, the spectrum implied the presence of at least two distinct species with different diffusion constants D which were approximately correlated to hydrodynamic radii between r_H = 12.2−17.6 Å or diameters between 24.4−35.2 Å.

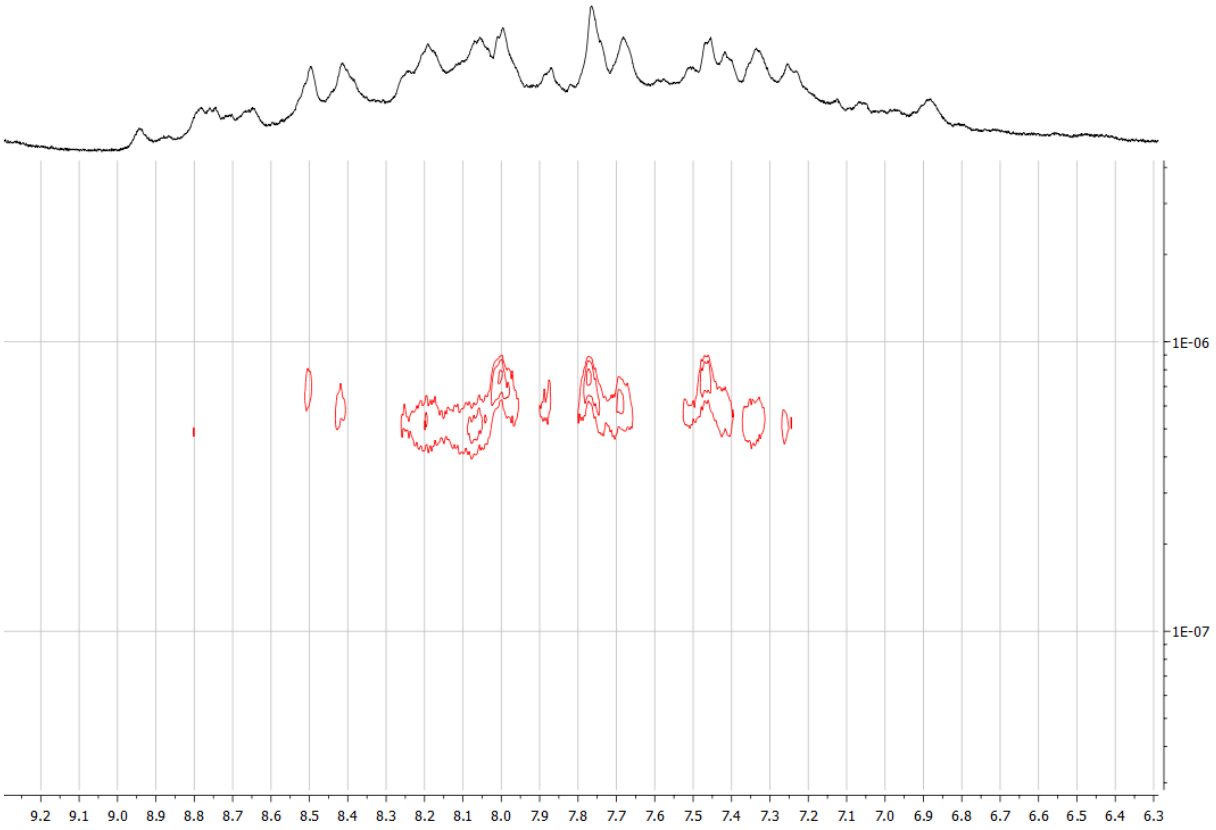

Figure 89: DOSY spectrum after complexation attempt of (*rac*)-**93** with $Pd(MeCN)_4(BF_4)_2$.

The more compact double walled Pd_3(**93**)$_6$ should be much smaller than the double walled Pd_4(**93**)$_8$ which comprises far more atoms. Of course, the presence of double walled species can only be assumed. Different topologies can vary in size which should

have a drastic impact on hydrodynamic radii. Again, all these structures do not really resemble a spherical particle so that deviations are expected. For reference, the models based on MMFF[286] showed diameters of 23.2 Å and 36.6 Å for the double walled Pd_3(**93**)$_6$ and Pd_4(**93**)$_8$, respectively, whereas the GFN2-xTB[177,178] minimized structures repeatedly showed that the arrangement was not achievable without deviation from the square planar palladium center.

As with the molecular square consisting of ligand **92**, a limitation was made by process of elimination. Focusing on all-homochiral complexes should provide more clarity on this matter. The described experiments were reiterated each with (*M*)- and (*P*)-**93**. Among themselves, the respective ^{1}H-NMR spectra were identical, but compared to that of the racemic experiment, they showed fewer signals altogether (**Figure 90**). Especially the area around 9−10 ppm had more pronounced and distinct signals, indicating that far fewer species are involved in the enantiopure experiments. However, the collectivity of the overall signals still indicated the presence of many species of low symmetry.

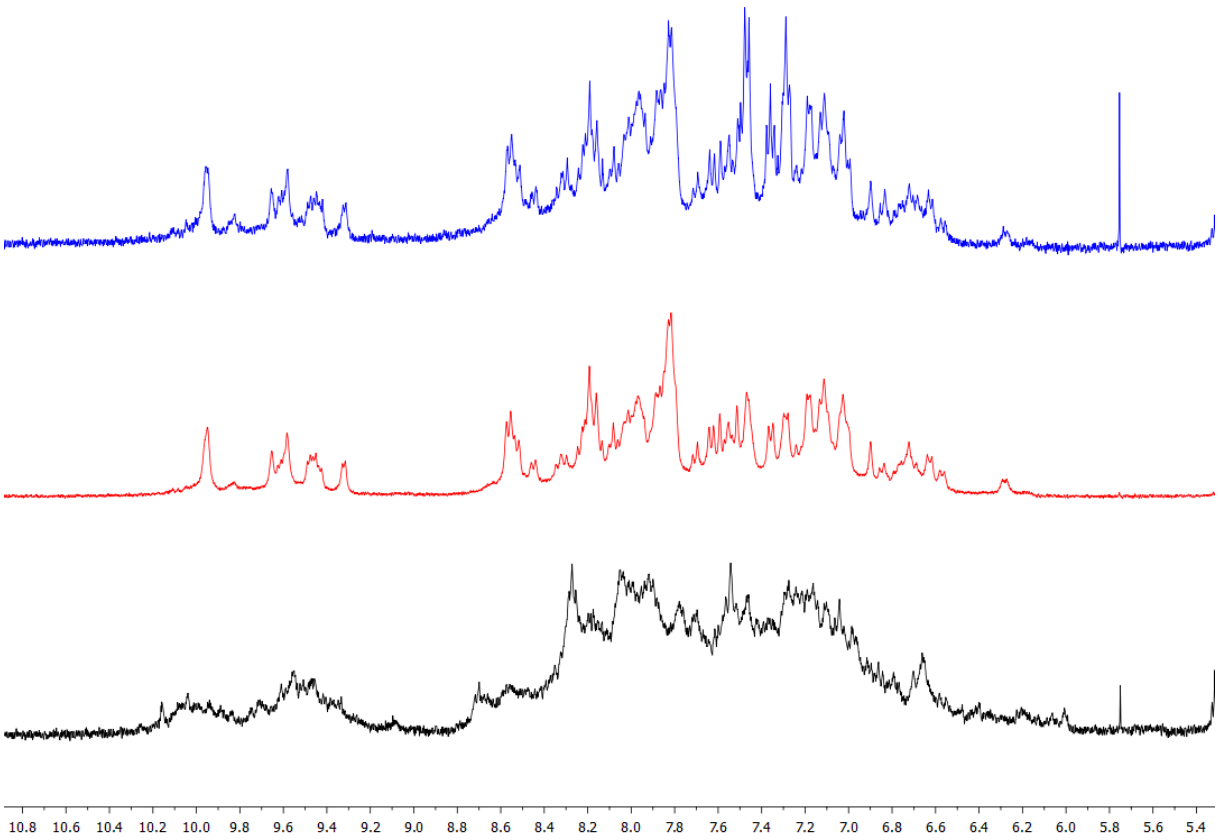

Figure 90: Comparison of ^{1}H-NMR spectra of experiments with (*rac*)-**93** (bottom), (*M*)-**93** (middle) and (*P*)-**93** (top) and $Pd(MeCN)_4(BF_4)_2$, respectively.

Interestingly, the mass spectra indicated neither multicationic species nor signals with the isotope pattern of palladium of high intensity. Interpreting this means that no homochiral species in the form of Pd_3(**93**)$_6$ and Pd_4(**93**)$_8$ had been formed and that these complexes only exist as heterochiral aggregates, indicating a form of social self-sorting during the racemic experiment which would be incredible. In view of the ^{1}H-NMR of the enantiopure experiments it was more plausible that some of the isomers may only exist as heterochiral aggregates (explaining the fewer signals) and that the homochiral aggregates were too labile in the gas phase for the detection by mass spectrometry. In addition, the ^{1}H-NMR spectrum of the racemic experiment does not really imply any highly symmetric structures. However, social self-sorting usually leads to highly symmetric aggregates which incorporate the same amount of each enantiomer as these structures tend to have the best compromise in energetics. A social-self sorting yielding low-symmetry aggregates as suggested for (*rac*)-**93** would be very uncommon. Unfortunately, single crystals for XRD analysis could not be grown so that further statements could not be made.

To get more insight on this matter, enantiopure **93** was treated with Pd(dppp)(OTf)$_2$. Despite the additional aromatic protons from the dppp unit, the aromatic region of the ^{1}H-NMR spectrum was not as crowded as the one of enantiopure **93** and Pd(MeCN)$_4$(BF$_4$)$_2$ (**Figure 91**). Still uneven ratios between the integrals and heavy overlap made the data hard to interpret. On the other hand, the mass spectrum was similar to that of enantiopure **93** and Pd(MeCN)$_4$(BF$_4$)$_2$ as no indications of multicationic species or signals with the isotope pattern of palladium were visible. The major signals were those of [**93**+H]$^+$ and [**93**+2H]$^{2+}$, minor signals of monocationic species could not be assigned to coordination of enantiopure **93** to Pd or any sensible constitutions at all (**Figure 92**). Considering all these data, it was more probable that the enantiopure ligand **93** coordinated to the Pd center in some form and to some extent in order to form aggregates which were not detectable by mass spectrometric experiments. During the racemic experiments, the presence of both enantiomers led to formation of additional isomers which increased the number of signals significantly. Thereby, the exact compositions of the complexes and the ratios of the enantiomers remain unspecified.

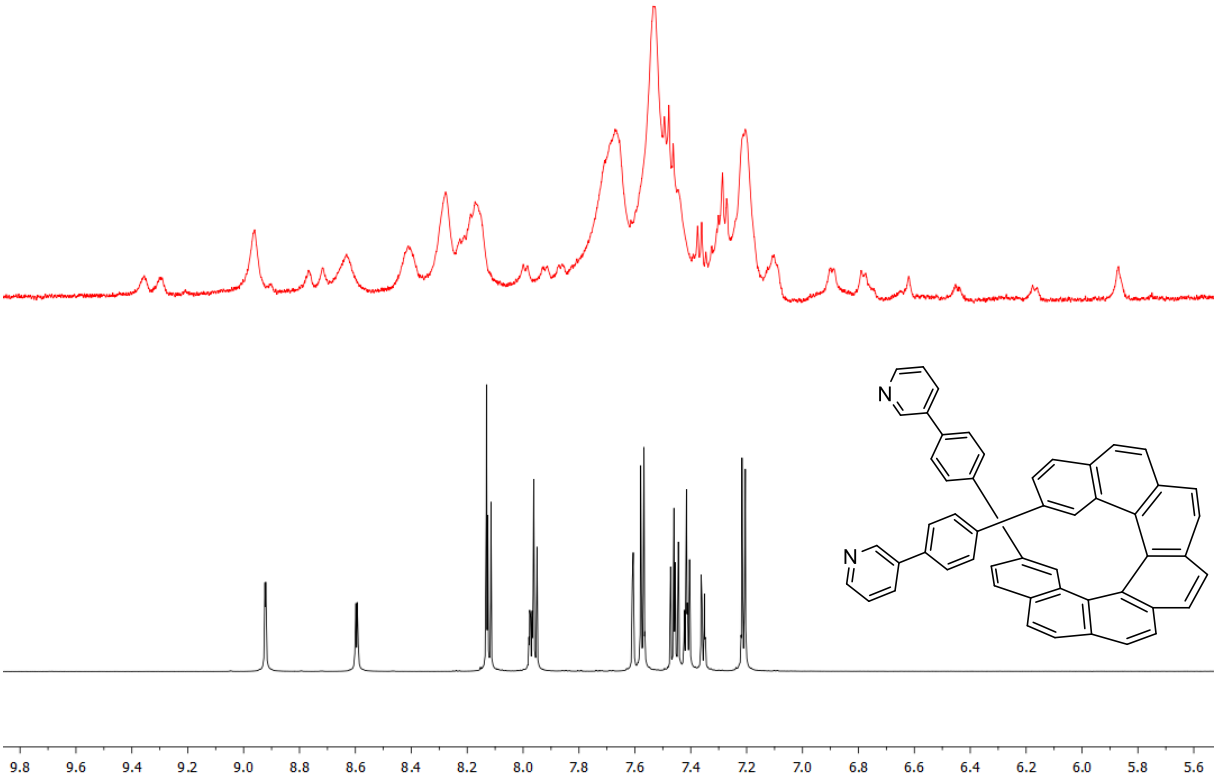

Figure 91: Comparison of ^{1}H-NMR spectra of free ligand (*P*)-**93** (bottom) and after complexation attempt with Pd(dppp)(OTf)$_2$ (top).

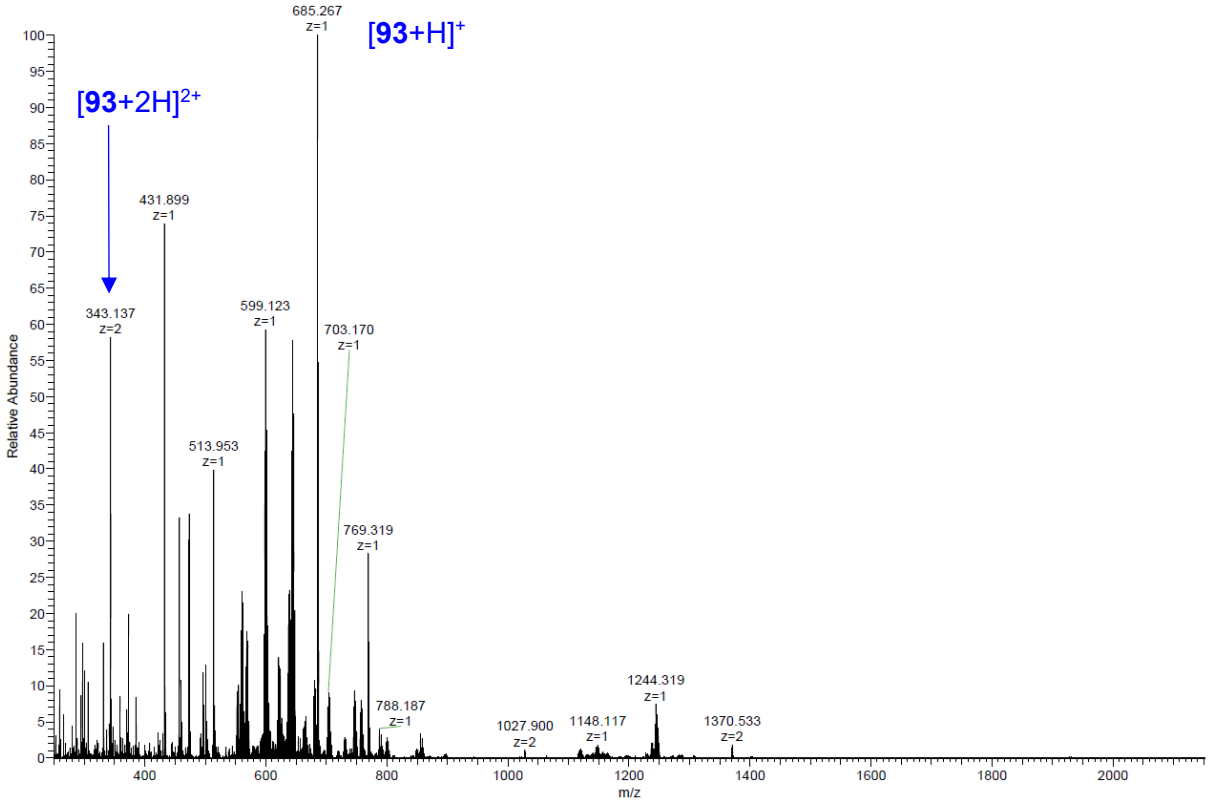

Figure 92: ESI(+)-mass spectrum after complexation attempt of (*P*)-**93** with Pd(dppp)(OTf)$_2$.

Altogether, 2 out of 3 ligands based on [7]helicene were able to form Pd^{II} complexes. The initial ligand (*rac*)-**91** likely failed to coordinate to Pd centers due to the proximity of the donor atoms to the main body which made it impossible for the metal center to approach them. The elongation of the side arms proved to be the solution to this problem as both the elongated **92** and **93** formed complexes with square planar Pd^{II}. Head-to-head, **92** and **93** were able to form aggregates of different compositions. The change from a fixed donor angle of nearly 180° to a variable donor angle around 60° had a drastic impact on possible architectures. No homochiral complexes were found during the experiment with enantiopure **93**. Unfortunately, the data do not allow final and conclusive statements in this regard. It is likely that **93** can form both homo- and heterochiral complexes of different compositions and topologies, from which not all are stable enough for detection by mass spectrometry. On the other hand, ligand **92** was able to form homo- and heterochiral complexes, as proven by both ^{1}H-NMR spectroscopy and mass spectrometry.

9 Conclusions and outlook

The aim of this work was the development of a reliable synthetic route towards functionalized helicenes, their characterization, chiral resolution and application as ligands in supramolecular chemistry.

With the combination of different established synthetic strategies and thoughtful planning as well as the ability to adjust the route at every stage, the first aim was realized and yielded two pathways to functionalized penta-, hexa- and heptahelicenes. The strategy involving the nucleophilic addition of organozinc zinc reagents proved to be the slightly better one as the overall yields were higher. But for hexahelicene, the strategy involving the nucleophilic substitution of organolithium compounds was necessary in order to get hands on the compound. Unfortunately, the isolation of the hexahelicene itself was not successful due to heavy degree of impurity. Still, this is more a problem of the purification process and not of the synthetic route itself. Both strategies are modular and reliable in the sense that a quick change of substitution pattern in the substrate is enough to give access to every region in the innermost bay area. The choice of the methoxy functions as a protection group which were principally masked as a good nucleofuge proved to be profitable: They were resilient towards every reaction condition including the acidic aqueous workups and could readily be cleaved with BBr_3. At the same time, they guaranteed the solubility of the respective species. Even the fully aromatic helicenes which mainly consisted of hydrogen and carbon atoms were highly soluble in common organic solvents like DCM particularly attributed to the 2 extra methoxy functions – the same solubility of the respective hydrocarbons would have been unlikely. The installment of the eventual functional group bearing the donor atom in the very last step increased the versatility even more as the commitment of different functional groups in the substrate itself would effectively branch out the entire route and reduce its predictability. In addition, it can confidently be said that these routes should also grant access to higher homologues like octa- and nonahelicenes *via* simple substrate alteration (**Scheme 121**).

Depending on the selected route, the quickest way to a fully aromatic helicene could be 5 steps long with mostly good yields. At the expense of synthetic rapidity, better yields can be achieved with detours. As a general trend it can be said that the effort increases within the homologous series. The synthesized [5]helicenes required

considerably less effort than their higher homologues. The key [2 + 2 + 2] cycloisomerization remains a key bottleneck for the synthetic route as a large chunk of material goes down the drain due to potential side reactions. Future investigations should therefore focus on its optimization. Adjustments can be made through choice of catalyst or reaction conditions. Regarding the latter, screening for reaction conditions could be conducted in a microwave. As for non-optimizing procedures, a prospect for the enantio- or diastereoselective synthesis can be posed. The change from non-chiral to chiral ligands can not only increase the overall performance, but likewise give enantio- or diastereoenriched products which could save the chiral resolution afterwards. Of course, this can only be realized if *ee* or *de* values of nearly 100 % are achieved. Thus far, values coming even close to 100 % have not been achieved with systems incorporating catalysts based on Co^{I} and Ni^{0}. Optical resolution by HPLC is still unparallelled and the way to go to get enantiopure compounds. Therefore, further research to get total enantio-/diastereoconvergence is required and would be a major breaking point.

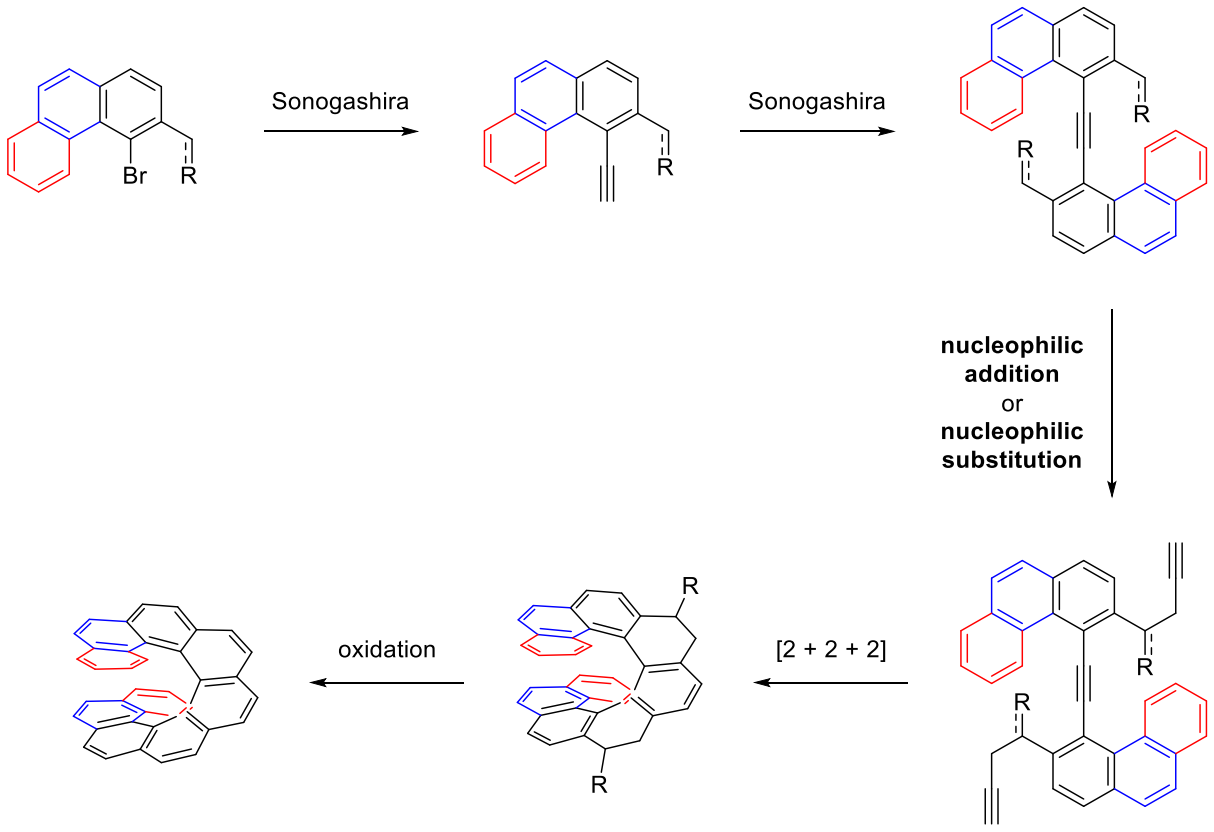

Scheme 121: Modular synthetic route towards functionalized [n]helicenes (n = 5, 6, 7, 8, 9; R = H, Br, O, OH, OAc).

Speaking of, the enhanced solubility stemming from the methoxy groups was also crucial for the chiral resolution by HPLC. Every (tetrahydro-) helicene incorporating methoxy groups could be resolved on a chiral stationary phase. This ensured the access to the enantiomers of the later helicenes. But for the synthesized ligands in this work, this backup plan was luckily never needed. Almost every finished ligand was soluble enough to allow an optical resolution. Just in one case, only one step backwards had to be taken in order to resolve the enantiomers. Heptahelicene (*rac*)-**90** was easily separated into its enantiomers and was the precursor of every ligand based on [7]helicene. The enantiopure **90** was then converted to enantiopure **92**.

In this work, a total of 15 helicenes have been synthesized and largely fully been characterized (**Figure 93**). These range from penta- to hexa- and heptahelicenes. All of them have in common, that only the second innermost positions have been accessed. While for hexa- and heptahelicene this was mostly a problem of available substrates, the same was not true for pentahelicene. Interestingly, the cleavage of varying protection groups under varying reaction conditions always led to a new benzoxepin which was equally bound to the loss of chirality. Contrary to initial beliefs, the unusual conformation is more favored than the expected helical conformation. From a mechanistic point of view, this reaction is particularly interesting: Since the reaction is not necessarily catalyzed by Lewis acids, it does not necessarily seem to go through an arenium ion or radical cation, as is suspected in a Scholl reaction. It could very well also be an S_NAr-type of mechanism involving a Meisenheimer complex or yet another mechanism involving an aryl cation.

Anyway, future research should also focus on the access to positions 1 and 14. One possible solution approach was already mentioned in section 6.1.2. But apart from a deprotection prior to the [2 + 2 + 2] cyclization, a stepwise deprotection using two different protection groups could also lead to desired 1,14-dihydroxy[5]helicene (*rac*)-**79**. For example, a silyl group could be used alongside the methoxy group. Even if these should not lead to (*rac*)-**79**, it would give valuable insights on the mechanistic sequence of the reaction. If everything should fail, a substitution of the methoxy group by another (masked) nucleofuge should definitely work out. Juggling between reactivities of different halides, the methoxy group could be substituted by a bromide so that an iodide should be installed to absorb the initial Sonogashira reaction.

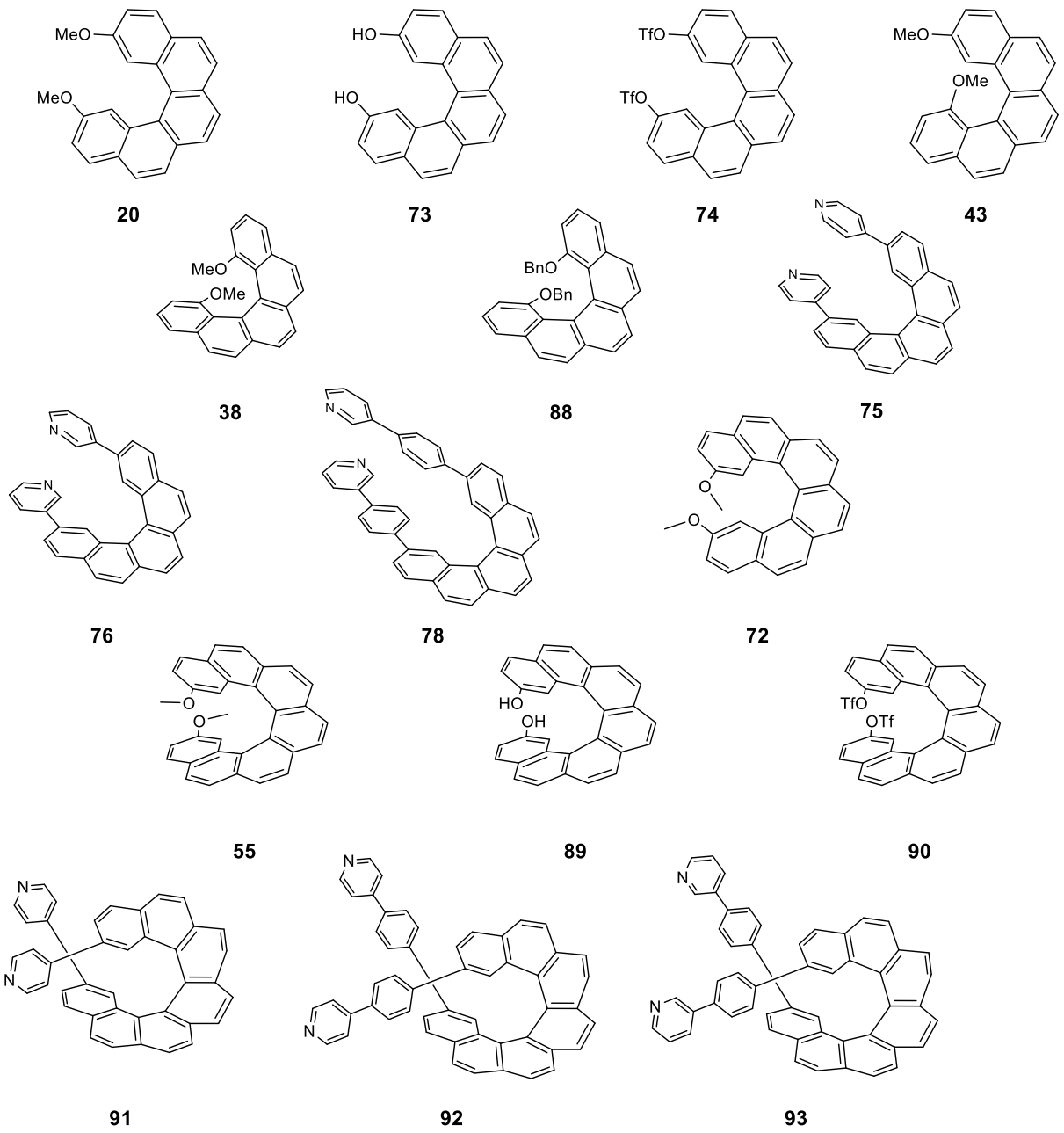

Figure 93: Synthesized helicenes in this work.

Out of the 15 synthesized helicenes, 6 were used as ligands in self-assembly studies aiming at metallosupramolecular aggregates. None of the investigated pentahelicenes were able to form polynuclear complexes. In fact, only ligand (*rac*)-**76** was able to form any complexes with Pd and Cu salts at all. It seems that the positions 2 and 13 in [5]helicene do not give a favorable donor angle for larger aggregates. Future investigations should have the objective to extend the library of helicenic ligands. Since the established strategies allow for the functionalization of the exterior benzene units, the positions 1 and 14, 3 and 12 or 4 and 11 should be investigated in regard of their donor angle and potential self-sorting behavior. Moreover, the retainment of the

C_2 symmetry is not compulsory either. A first step towards an asymmetric ligand was already done with the synthesis of 1,13-dimethoxypentahelicene (*rac*)-**43**. But future ligands can consist of any combinations of the mentioned positions. While the functionalization of the interior benzene units was not addressed in this work, this would still be feasible with the available strategies. For once, during the nucleophilic addition strategy, the hydroxy groups do not necessarily have to be turned to the acetates in order to get good leaving groups for the mild silica gel-assisted aromatization. As seen during the nucleophilic substitution strategy, the latter can be realized by an oxidation with DDQ. By doing so, the hydroxy groups should be transferred up to the helicene so they can also be turned to triflates, giving access to positions 5 and 10. Alternatively, positions 6, 7, 8 and 9 can also be accessed by careful choice of the metalorganic reagent (**Scheme 122**).

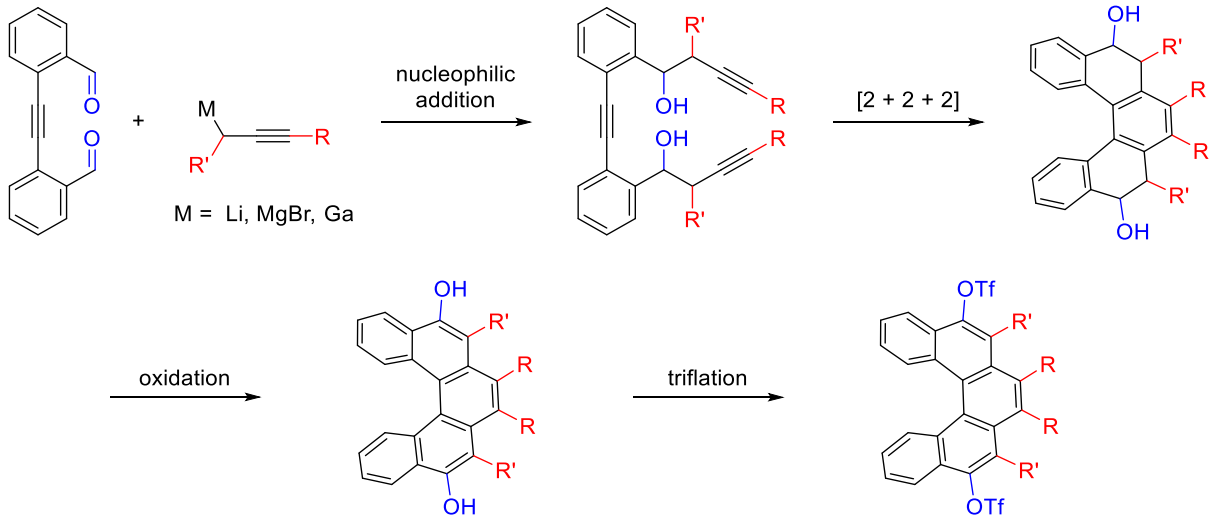

Scheme 122: Access to positions 5 and 10 (blue) or 6, 7, 8 and 9 (red).

Analogously, higher homologues could of course be functionalized in these positions as well. But regardless of the homologue, the donor angle should more or less be the same (especially for positions 7 and 8) for every congener as they all share the same backbone. A meaningful change in donor angle can realistically only be fulfilled by extending the helicene further. So far, [7]helicene showed promising properties in terms of its ability to form polynuclear complexes. Both ligand **92** as well as ligand **93** were able to form di- to tetranuclear complexes with Pd^{II}. The near 180° donor angle in **92** made it a suitable candidate for a molecular square. Unfortunately, the mass spectrometric and NMR spectroscopic data were not sufficient enough to elucidate the reaction to the fullest since the intact square could not be detected with the former. For

that reason, the experiment could be reiterated with *cis*-protected Pt^{II}. Compared to Pd^{II}, complexes consisting of Pt^{II} are usually kinetically more inert which could be a problem for the assembly. But at the same time, these complexes are thermodynamically more stable, and thus, more likely to survive the ionization process during the detection by mass spectrometry. The exact structure and composition could be elucidated with X-ray crystallography so that growing crystals suitable for XRD analysis should be the main concern.

Ligand **93** on the other hand had a variable donor angle which enabled the formation of Pd_3L_6 and Pd_4L_8 species which are rather rare among metallosupramolecular assemblies with tetravalent palladium ions. Still, these often tend to be in equilibrium. Compared to the more often occurring Pd_2L_4 complexes, they have a way higher number of viable topologies. Out of the possible ones, 2 have been reported for Pd_3L_6 aggregates and 5 have been reported for Pd_4L_8 aggregates. It is unclear if one of these or even a new topology is involved in the case of **93**. ^{1}H-NMR spectroscopic analysis did not suggest the formation of only few highly symmetric species. In addition, reiteration with enantiopure **93** implied that some form of chiral-self sorting may have occurred as no homochiral complexes were detected. Again, XRD analysis could provide more insight.

Both **92** and **93** have shown to be applicable ligands for the purpose of metallosupramolecular chemistry. As of yet, there has only been one report for a chiral self-sorting of helicenes. Metallosupramolecular helicene chemistry is still in its infancy and offers a lot of untapped potential, which is why active research should not slow down here. The proposed synthesis routes established in this work should provide the means and tools to extend the library of helicenes further.

But not only viewed from a supramolecular lens the potential of helicenes has been displayed and indicated. Owing to their conjugated aromatic π-system, they offer great potential as organic semiconductors and light-emitting compounds in electronic devices. The ever-growing demand for semiconducting and light-emitting materials is not only a highly attractive field from an economic point of view; the continual increase of their efficiency still remains a scientific challenge. Therefore it is not surprising that they have been used as emissive or hole-transporting components in organic light-emitting diodes (OLEDs).[321,322] But a key advantage over common organic semiconductors in OLEDs is that helicenes are intrinsically chiral so that they benefit

from their additional chiroptical properties. The capability of inducing circularly polarized luminescence can be exploited to manufacture CP-OLEDs which offer benefits on their own. In 2016, *Fuchter* and coworkers used a cyclometalated platinahelicene as a host material for a circularly polarized phosphorescent light-emitting diode.[323] As far as optoelectronic materials are concerned, helicenes have also been investigated in their role in transistors[324,325] or photovoltaics.[326,327] What was true for supramolecular chemistry is certainly true for optoelectronic materials as well: It is an emerging and underdeveloped field. So far, investigations have mainly been done with few helicenes and are far from being competitive with state-of-the-art devices. But at the same time, the condensed opportunities draw prolonged interest which hopefully catalyzes increasing research in the future.

Apart from optoelectronics and supramolecular chemistry, research with helicenes has focused on asymmetric synthesis. Due to their bulkiness, thermodynamic stability and rigidity, they were investigated with regard to their enantiodiscriminating abilities: Phosphorus containing helicenes have been employed as ligands in Rh^{I} catalyzed hydrogenations,[328] Pd^{0} catalyzed Tsuji-Trost reactions[329] or Ir^{I} catalyzed allylic aminations.[4] The helicenes employed in asymmetric synthesis not only differ in size, but also in the installed functional groups: Beside the phosphorus containing helicenes mentioned above, sulphur[330] or nitrogen[331–333] containing ones have also shown to induce chirality (**Figure 94**). Enantiomeric excesses up to 99 % have been achieved, but overall, they cannot compete with mainstream ligands like BINAP yet which should be the main focus after all.

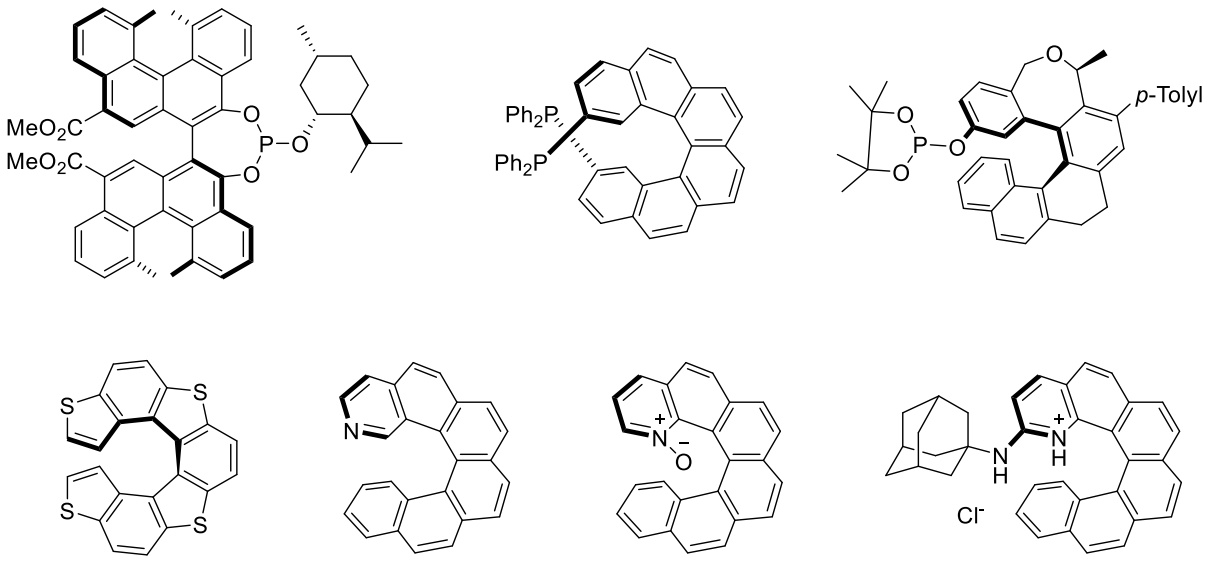

Figure 94: Selection of helicenes used in asymmetric synthesis.

In conclusion, the aim of this work has been accomplished. Out of the 3 leading methods for the synthesis of helicenes, two strategies have been developed using the metal catalyzed [2 + 2 + 2] cycloisomerization. With these, a selection of different helicenes ranging from penta- to heptahelicenes have been synthesized and characterized, using complementary NMR spectroscopic, mass spectrometric, ECD spectroscopic, OR and XRD analytic tools. Last but not least, they were investigated in regard to their self-sorting behavior. The first ground was set with ligands **92** and **93** which formed polynuclear complexes with Pd^{II}. While the exact compositions could not be verified, these examples very clearly show that helicene chemistry is far from being exhaustive and have plenty of room for future investigation. Especially the extensive literature coverage including reviews[122,180,334] and books[27,335] in recent times prove that helicene chemistry has long since left purely curiosity driven research behind.

10 Experimental section

10.1 General procedure

Working under argon atmosphere

Air- and moisture-sensitive reactions were carried out under argon atmosphere using standard Schlenk techniques, glassware was flame-dried at 550 °C with a heat gun under vacuum and cooled under argon.

Reagents and solvents

Reagent grade materials were commercially obtained by *abcr*, *Thermo Fisher Scientific*, *Merck*, *Sigma Aldrich*, *TCI*, *BLDpharm*, *Fluorochem*, *Carl Roth* or *VWR* and used as received without further purification.

Anhydrous dichloromethane and anhydrous tetrahydrofuran were extracted from a solvent purification system (*MS-SPS 800*, *Braun*). Cyclohexane, ethyl acetate and dichloromethane were distilled from their respective technical grade analogue.

The following chemicals were synthesized according to literature protocol: CpCo[P(OEt)$_3$](*trans*-dimethylfumarate),[86] bis(triphenylphosphine)palladium chloride,[336] [1,3-bis(diphenylphosphino)propane]palladium(II) triflate.[337]

Flash chromatography

Flash chromatography was performed on silica gel 60 (0.040−0.063 mm, *Merck*).

Thin-layer chromatography

Analytical thin-layer chromatography (TLC) was performed on silica gel 60 F_{254}-coated aluminum sheets (*Merck*), detection was performed at the wavelengths 254 nm and 366 nm using a UV lamp. The respective retention factors R_f are indicated in the descriptions of the experiments.

NMR-spectroscopy

^{1}H-NMR-, ^{13}C-NMR-, ^{19}F-NMR-, ^{1}H-^{1}H-COSY-, ^{1}H-^{13}C-HSQC-, ^{1}H-^{13}C-HMBC-, ^{1}H-^{1}H-NOESY- and ^{1}H-DOSY-spectra were recorded on a *Bruker Avance I 300 MHz*, a *Bruker Avance I 400 MHz*, a *Bruker Avance I 500 MHz*, a *Bruker Avance III HD*

Ascend 500 MHz or a *Bruker Avance III HD Ascend 700 MHz*. ^{1}H-NMR-spectra were referred and calibrated to residual signals of non-deuterated solvent signals, ^{13}C-NMR-spectra to those of deuterated solvent signals. Chemical shifts δ are indicated in parts per million (ppm), coupling constants J in Hertz (Hz).[338] The following abbreviations are used to indicate the multiplicities of the signals: s (singlet), d (doublet), t (triplet), q (quartet), m (multiplet). For the interpretation of the spectra, the software *MestReNova 8.0.1* (*Mestrelab Research S.L.)* was used. Diffusion constants D were put in relation to the hydrodynamic radius r_{H} according to the *Stokes-Einstein*-equation with the shape-correction factor for spherical particles of colloidal dimensions.[294,339]

$$D = \frac{k_{\mathrm{B}} T}{6\pi\eta r_{\mathrm{H}}} \tag{4}$$

In equation (4), k_{B} is the *Boltzmann* constant, T the absolute temperature and η the viscosity of the fluid.

Mass spectrometry

Mass spectrometric measurements *via* electrospray ionization (ESI), electron ionization (EI) or atmospheric pressure chemical ionization (APCI) were performed on a *MAT 95 XL* (*Thermo Finnigan*), a *MAT 90* (*Thermo Finnigan*), a *micrOTOF-Q* (*Bruker Daltonik*) or an *Orbitrap XL* (*Thermo Fisher Scientific*).

High performance liquid chromatography

Analytical high-performance liquid chromatography (HPLC) was either conducted on a *Prominence LC-20* (*Shimadzu*), consisting of three separate solvent delivery units (2×*LC20-AT*, 1×*LC20-AD*), a degassing unit (*DGU-20A3*), a photo-diode array detector (*SPD-M20A*), a fraction collector (*FRC-10A*), a high-pressure selection valve (*FCV-20AH2*) and a (*S*,*S*)-*Whelk-O-1* (*Gamma Analysentechnik GmbH*) column as the stationary phase; or on a *Knauer AZURA* system equipped with a binary high pressure gradient pump *P 6.1L*, an online degasser, a photodiode array detector *DAD 6.1L* with a deuterium and a halogen lamp and a *CHIRALPAK IB-U* (*Daicel*) or a *CHIRALPAK IC-U* (*Daicel*) column.

High performance liquid chromatography on a (semi-) preparative scale was performed on a *Knauer AZURA* system equipped with a binary high pressure gradient pump

P 6.1L, an online degasser, a multi wavelength detector *MWL 2.1L* with a deuterium lamp, a 16-1 port multi position fraction valve *V2.1S* and a *CHIRALPAK IB* (*Daicel*) or a *CHIRAL ART Cellulose-SC* (*YMC*) column.

Electronic circular dichroism spectroscopy

Electronic circular dichroism spectra were recorded on a *J-810* spectrometer (*Jasco*) equipped with a Peltier element (*PTC-423S*) and an Osram 150 W xenon lamp. Quartz glass cuvettes (*Hellma Analytics*) with a layer thickness of 10 mm were used. For interpretation of the spectra, *Jasco Spectra Manager 1.5* was used.

The measured ellipticity Θ was put in relation to the molar circular dichroism $\Delta\varepsilon$ according to the Beer-Lambert extinction law.

$$\theta = \frac{ln10}{4} \cdot \frac{180°}{\pi} \Delta\varepsilon \cdot c \cdot l \tag{5}$$

In equation (5), *c* is the concentration of the analyte and *l* is the cell pathlength of the cuvette.

Optical rotation

Specific rotation values were measured on an *Anton Paar Model MCP 150* polarimeter with a standard wavelength of 589 nm using a cuvette with a layer thickness of 10 mm.

Microwave assisted reactions

Microwave assisted [2+2+2] cycloisomerizations were performed in a microwave reactor (*CEM Discover SP*).

X-ray crystallography

Single crystals were grown as described in the respective descriptions of the experiments. Single crystal diffraction data were either collected on a *STOE IPDS-2T* diffractometer, equipped with a low temperature device *Oxford Cryostream 700 series* (*Oxford Cryosystems*) using graphite-monochromated MoKα radiation (λ = 0.71073 Å); or a *Bruker D8 Venture* diffractometer, equipped with a low temperature device *Cryostream 800 series* (*Oxford Cryosystems*) using mirror-monochromated CuKα radiation (λ = 1.54184 Å). Intensities were measured by fine-slicing φ- and ω-scans and corrected for background, polarization and Lorentz effects. Semi-empirical

absorption corrections were applied for all data sets following Blessing's method.[340] The structures were solved by intrinsic phasing methods[341] and refined anisotropically by the least-squares procedure implemented in the *ShelX* program system.[342] The hydrogen atoms were included isotropically using the riding model on the bound carbon atoms. Crystallographic data and refinement parameters are shown in descriptions of the experiments.

10.2 Synthetic procedures

Synthesis of ligands

4-Methoxy-2-[(trimethylsilyl)ethynyl]benzaldehyde 14[129]

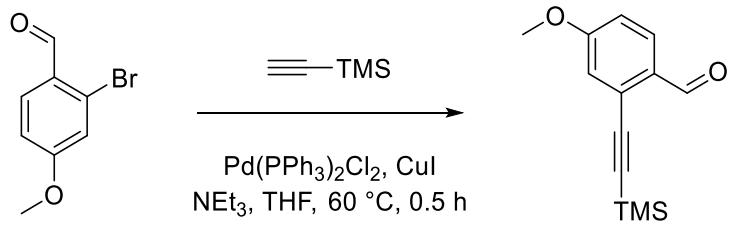

13 **14**

The reaction was carried out under Schlenk conditions. In a Schlenk flask equipped with a magnetic stir bar, 130.55 mg of $PdCl_2(PPh_3)_2$ (4 mol%), 61.98 mg of CuI (7 mol%) and 1.0 g of 2-bromo-4-methoxybenzaldehyde **13** (4.65 mmol, 1.0 equiv.) were dissolved in anhydrous THF (5 mL) and degassed NEt_3 (10 mL). After adding 0.99 mL of trimethylsilylacetylene (6.97 mmol, 1.50 equiv.), the mixture was stirred at 60 °C for 0.5 h. The reaction mixture was poured into a saturated solution of aqueous NH_4Cl (20 mL) and extracted with DCM (3×30 mL). The combined organic portions were washed with brine (150 mL), dried with anhydrous $MgSO_4$ and concentrated under reduced pressure. The crude product was purified by flash chromatography on silica gel (cyclohexane/ethyl acetate = 9:1). Aldehyde **14** was obtained as a yellow oil.

Yield:	900.11 mg (3.87 mmol, 83 %)
Molecular formula:	$C_{13}H_{16}O_2Si$
Molecular weight:	232.35 g/mol
Retention factor:	0.50 (cyclohexane/ethyl acetate = 4:1)

^{1}H-NMR (400 MHz, $CDCl_3$, 298 K):
δ/ppm = 10.40 (d, 1H, *J* = 0.9 Hz), 7.87 (d, 1H, *J* = 8.7 Hz), 7.01 (d, 1H, *J* = 2.5 Hz), 6.94 (ddd, 1H, *J* = 8.7 Hz, *J* = 2.5 Hz, *J* = 0.9 Hz), 3.88 (s, 3H), 0.28 (s, 9H).

The spectral data were in agreement with those previously reported for this compound.[343]

2-Ethynyl-4-methoxybenzaldehyde 15

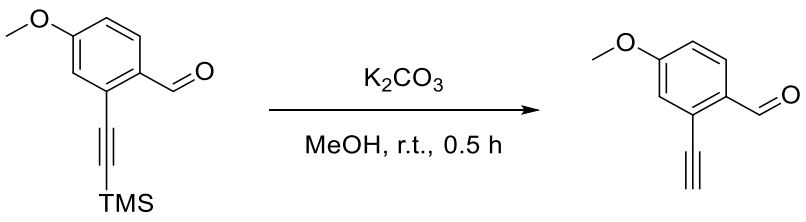

14 **15**

In a round bottomed flask equipped with a magnetic stir bar, 900.0 mg of aldehyde **14** (3.87 mmol, 1.0 equiv.) were dissolved in methanol (20 mL) and 749.49 mg of K_2CO_3 (5.42 mmol, 1.40 equiv.) were added in batches. The mixture was stirred at room temperature for 0.5 h. The reaction mixture was poured into water (20 mL) and extracted with DCM (3×30 mL). The combined organic portions were dried with anhydrous $MgSO_4$ and concentrated under reduced pressure. The crude product was purified by flash chromatography on silica gel (cyclohexane/ethyl acetate = 4:1). Aldehyde **15** was obtained as a white solid.

Yield: 583.25 mg (3.64 mmol, 94 %)

Molecular formula: $C_{10}H_8O_2$

Molecular weight: 160.17 g/mol

Retention factor: 0.34 (cyclohexane/ethyl acetate = 3:1)

^{1}H-NMR (400 MHz, $CDCl_3$, 298 K):
δ/ppm = 10.39 (d, 1H, *J* = 0.8 Hz), 7.90 (d, 1H, *J* = 8.7 Hz), 7.07 (d, 1H, *J* = 2.5 Hz), 6.99 (ddd, 1H, *J* = 8.7 Hz, *J* = 2.5 Hz, *J* = 0.8 Hz), 3.89 (s, 3H), 3.43 (s, 1H).

The spectral data were in agreement with those previously reported for this compound.[344]

2,2'-(Ethyne-1,2-diyl)bis(4-methoxybenzaldehyde) 16

Approach A

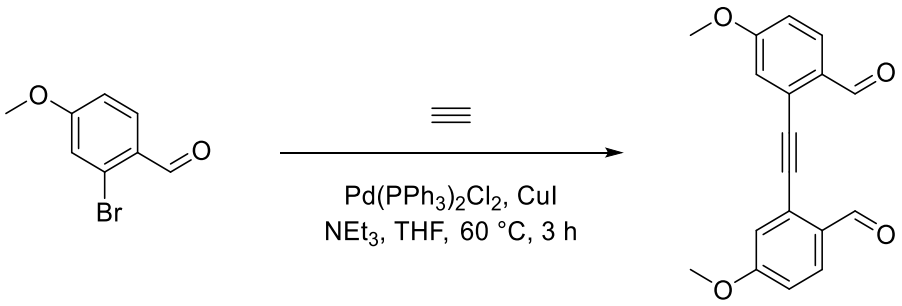

13 **16**

The reaction was carried out under Schlenk conditions. A Schlenk flask equipped with a magnetic stir bar was charged with 2.0 g of 2-bromo-4-methoxybenzaldehyde **13** (9.30 mmol, 1.0 equiv.), 195.84 mg of $PdCl_2(PPh_3)_2$ (3 mol%) and 35.42 mg of CuI (2 mol%). The atmosphere was evacuated and flushed with gaseous acetylene using a balloon. A solution of degassed triethylamine (15 mL) and anhydrous THF (5 mL) was added under stirring at room temperature. Then the mixture was heated to 60 °C and stirred for 3 h. The reaction mixture was poured into an aqueous solution of saturated NH_4Cl (40 mL) and then extracted with dichloromethane (3×30 mL). The combined organic portions were washed with brine (150 mL), dried with anhydrous $MgSO_4$ and concentrated under reduced pressure. The crude product was purified by flash chromatography on silica gel (cyclohexane/ethyl acetate = 9:1 to 1:1) and recrystallized (ethyl acetate) to obtain dialdehyde **16** as a white solid.

Yield:	630.05 mg (2.14 mmol, 46 %)
Molecular formula:	$C_{18}H_{14}O_4$
Molecular weight:	294.31 g/mol
Retention factor:	0.10 (cyclohexane/ethyl acetate = 4:1)
ESI(+)-MS:	*m*/*z* = 333.052 $[M+K]^+$, 317.078 $[M+Na]^+$, 295.096 $[M+H]^+$
HRMS ($C_{18}H_{14}O_4H^+$):	calculated = 295.0965
	found = 295.0963

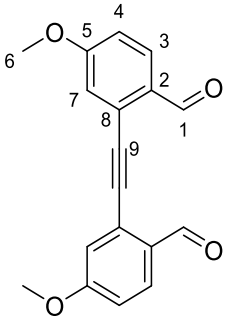

^{1}H-NMR (500 MHz, $CDCl_3$, 298 K):

δ/ppm = 10.47 (d, 2H, H-1, $^{5}J_{1,4}$ = 0.8 Hz), 7.94 (d, 2H, H-3, $^{3}J_{3,4}$ = 8.8 Hz), 7.14 (d, 2H, H-7, $^{4}J_{7,4}$ = 2.5 Hz), 7.03 (ddd, 2H, H-4, $^{3}J_{4,3}$ = 8.8 Hz, $^{4}J_{4,7}$ = 2.5 Hz, $^{5}J_{4,1}$ = 0.8 Hz), 3.93 (s, 6H, H-6).

^{13}C-NMR (500 MHz, $CDCl_3$, 298 K):

δ/ppm = 189.9 (C-1), 164.0 (C-5), 130.3 (C-3), 130.0 (C-2), 127.6 (C-8), 117.7 (C-7), 116.4 (C-4), 91.5 (C-9), 56.0 (C-6).

Approach B

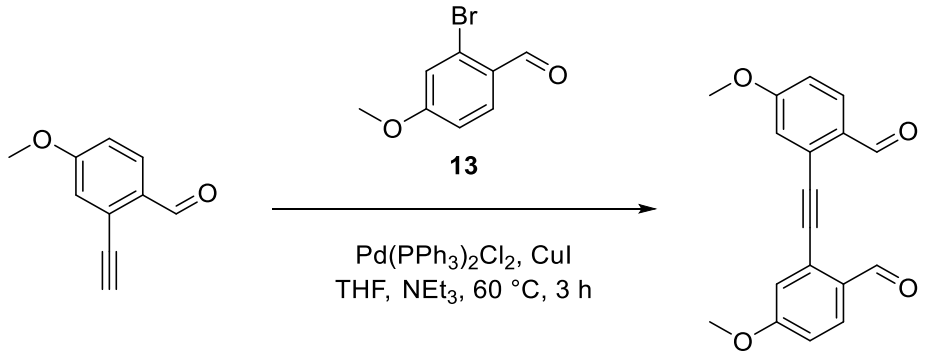

15 **16**

The reaction was carried out under Schlenk conditions. To a Schlenk flask equipped with a magnetic stir bar, 52.58 mg of $PdCl_2(PPh_3)_2$ (4 mol%), 24.96 mg of CuI (7 mol%), 300.0 mg of 2-ethynyl-4-methoxybenzaldehyde **15** (1.87 mmol, 1.0 equiv.) and 443.07 mg of 2-bromo-4-methoxybenzaldehyde **13** (2.06 mmol, 1.10 equiv.) were added. After adding anhydrous THF (5 mL) and degassed NEt_3 (10 mL), the mixture was heated to 60 °C and stirred for 3 h. The reaction mixture was poured into an aqueous solution of saturated NH_4Cl (40 mL) and then extracted with dichloromethane (3×30 mL). The combined organic portions were washed with brine (150 mL), dried with anhydrous $MgSO_4$ and concentrated under reduced pressure. The crude product

was purified by flash chromatography on silica gel (cyclohexane/ethyl acetate = 9:1 to 1:1) and recrystallized (ethyl acetate) to obtain dialdehyde **16** as a white solid.

Yield: 341.23 mg (1.15 mmol, 62 %)

Approach C

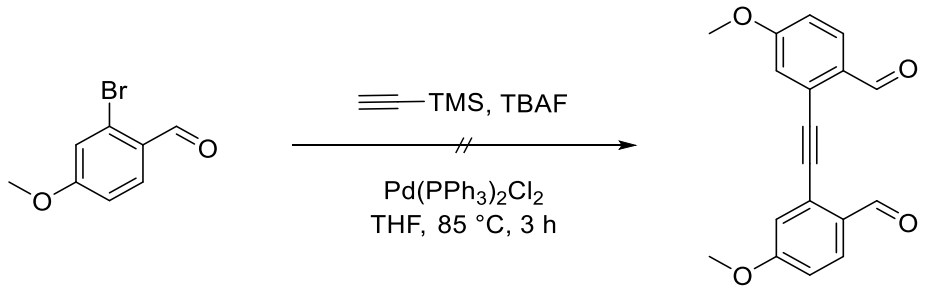

13 **16**

The reaction was carried out under Schlenk conditions. A pressure tube equipped with a magnetic stir bar was charged with 1.0 g of 2-bromo-4-methoxybenzaldehyde **13** (4.65 mmol, 1.0 equiv.) and 163.19 mg of $PdCl_2(PPh_3)_2$ (5 mol%). Using counterflow technique, a stock solution of tetra-*n*-butylammonium fluoride (27.90 mL, 1.0 M in THF, 6.0 equiv.) and 0.66 mL of trimethylsilylacetylene (4.65 mmol, 1.0 equiv.) were added. The pressure tube was closed and the mixture was stirred at 85 °C for 3 h. After cooling to room temperature, the reaction mixture was poured into an aqueous solution of saturated NH_4Cl (40 mL) and then extracted with dichloromethane (3×30 mL). The combined organic portions were washed with brine (150 mL), dried with anhydrous $MgSO_4$ and concentrated under reduced pressure. The residue was subjected to flash chromatography on silica gel (cyclohexane/ethyl acetate = 9:1 to 1:1). The product could not be isolated.

1,1'-[Ethyne-1,2-diylbis(4-methoxy-2,1-phenylene)]bis(but-3-yn-1-ol) 17

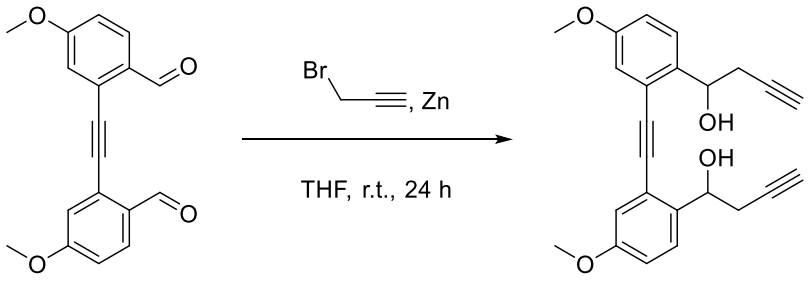

16 **17**

The reaction was carried out under Schlenk conditions. A Schlenk flask equipped with a magnetic stir bar was charged with 666.44 mg of zinc powder (10.19 mmol, 10.0 equiv.). Anhydrous tetrahydrofuran (15 mL) was added, the flask was immersed in a water bath at room temperature and a solution of propargyl bromide (1.14 mL, 80 wt.% in toluene, 10.19 mmol, 10.0 equiv.) was added slowly. The solution was stirred at room temperature for 30 minutes before it was added to the suspension of dialdehyde **16** (300.0 mg, 1.02 mmol, 1.0 equiv.) in anhydrous tetrahydrofuran (10 mL). After 24 h of stirring, the mixture was poured into water (50 mL) and extracted with dichloromethane (3×40 mL), then the combined organic portions were washed with brine (200 mL) and HCl (200 mL, 6 M in water), dried with anhydrous Mg_2SO_4 and concentrated under reduced pressure. The crude product was purified by flash chromatography on silica gel (cyclohexane/ethyl acetate = 5:2 to 1:1) to obtain diol **17** as a yellow solid. The diol could not completely be isolated and had some minor impurities, nonetheless it was used for the subsequent reaction.

Yield:	n/a
Molecular formula:	$C_{24}H_{22}O_4$
Molecular weight:	374.43 g/mol
Retention factor:	0.80 (cyclohexane/ethyl acetate = 4:1)
ESI(+)-MS:	*m*/*z* = 397.140 $[M+Na]^+$
HRMS ($C_{24}H_{22}O_4Na^+$):	calculated = 397.1410
	found = 397.1403

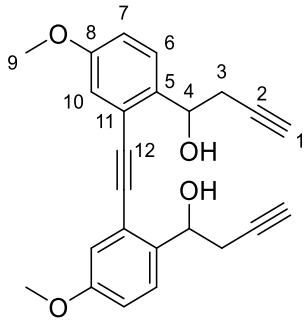

^{1}H-NMR (500 MHz, $CDCl_3$, 298 K):

δ/ppm = 7.52 (d, 2H, H-6, $^{3}J_{6,7}$ = 8.7 Hz), 7.05 (d, 2H, H-10, $^{4}J_{10,7}$ = 2.7 Hz), 6.96 (dd, 2H, H-7, $^{3}J_{7,6}$ = 8.7 Hz, $^{4}J_{7,10}$ = 2.7 Hz), 5.40−5.33 (m, 2H, H-4), 3.84 (s, 6H, H-9), 2.88−2.63 (m, 4H, H-3), 2.11−2.08 (m, 2H, H-1).

^{13}C-NMR (500 MHz, $CDCl_3$, 298 K):

δ/ppm = 158.9 (C-8), 136.5 (C-5), 126.9 (C-6), 121.6 (C-11), 117.1 (C-10), 115.7 (C-7), 91.8 (C-12), 81.0 (C-2), 70.3 (C-4), 70.2 (C-1), 55.6 (C-9), 28.8 (C-3).

[Ethyne-1,2-diylbis(4-methoxy-2,1-phenylene)]bis(but-3-yne-1,1-diyl diacetate

18

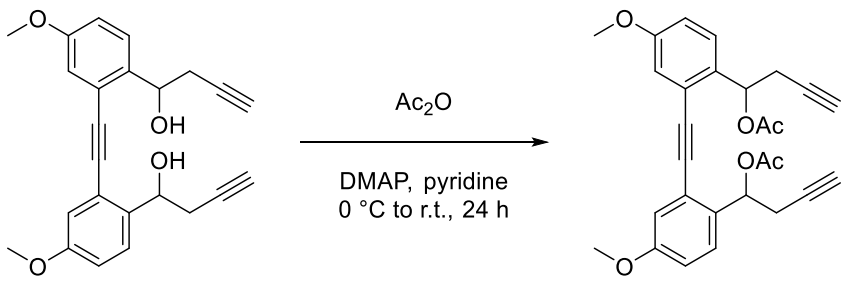

17 **18**

In a round bottomed flask equipped with a magnetic stir bar, a solution of diol **17** (385.0 mg, 1.03 mmol, 1.0 equiv.) and 4-dimethylaminopyridine (15.07 mg, 0.12 mmol, 0.12 equiv.) in anhydrous pyridine (8 mL) was prepared. After adding 1.16 mL of acetic anhydride (12.33 mmol, 12.0 equiv.) at 0 °C while stirring, the reaction mixture was allowed to slowly reach room temperature and stirring was continued at the same temperature for an additional 24 h. The mixture was poured into water (20 mL) and extracted with dichloromethane (3×20 mL), then the combined organic portions were washed with a saturated aqueous solution of $KHCO_3$ (100 mL), dried with anhydrous Mg_2SO_4 and concentrated under reduced pressure. The crude product was purified by flash chromatography on silica gel (cyclohexane/ethyl acetate = 3:1) to afford diacetate **18** as a yellow oil.

Yield:	280.53 mg (0.62 mmol, 61 %) over 2 steps
Molecular formula:	$C_{28}H_{26}O_6$
Molecular weight:	458.51 g/mol
Retention factor:	0.48 (cyclohexane/ethyl acetate = 3:1)

ESI(+)-MS: *m*/*z* = 497.136 $[M+K]^+$, 481.163 $[M+Na]^+$, 476.208 $[M+NH_4]^+$

HRMS ($C_{28}H_{26}O_6Na^+$): calculated = 481.1622

found = 481.1624

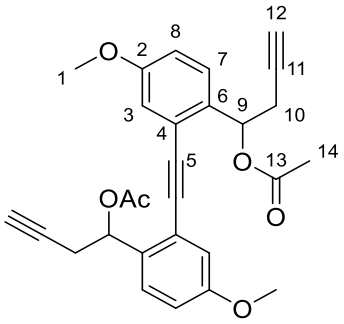

^{1}H-NMR (700 MHz, $CDCl_3$, 298 K):

δ/ppm = 7.42−7.40 (m, 2H, H-7), 7.12−7.10 (m, 2H, H-3), 6.94−6.91 (m, 2H, H-8), 6.39−6.35 (m, 2H, H-9), 3.84 (s, 6H, H-1), 2.95−2.88 (m, 4H, H-10), 2.12 (s, 6H, H-14), 1.99−1.97 (m, 2H, H-12).

^{13}C-NMR (700 MHz, $CDCl_3$, 298 K):

δ/ppm = 169.9 (d, C-13), 159.1 (C-2), 133.0 (d, C-6), 127.5 (d, C-7), 122.4 (d, C-4), 117.0 (d, C-3), 115.8 (C-8), 91.8 (C-5), 79.7 (d, C-11), 71.4 (d, C-9), 70.8 (d, C-12), 55.6 (C-1), 25.8 (C-10), 21.2 (C-14).

2,13-Dimethoxy-5,6,9,10-tetrahydropentahelicene-5,10-diyl diacetate 19

Approach A

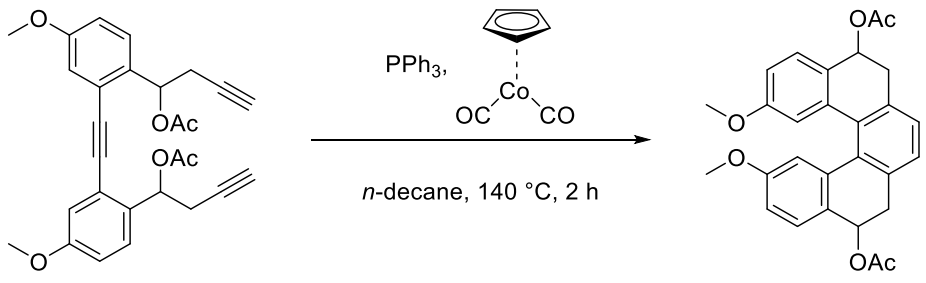

18 **19**

The reaction was carried out under Schlenk conditions. *N*-decane was degassed by 3 freeze-pump-thaw cycles before use. A two-necked flask equipped with a magnetic stir bar was charged with 200.0 mg of triyne **18** (0.43 mmol, 1.0 equiv.) and 228.82 mg of

PPh_3 (0.87 mmol, 2.0 equiv.). Then a solution of $CpCo(CO)_2$ (0.058 mL, 0.44 mmol, 1.0 equiv.) in *n*-decane (20 mL) was added. The reaction mixture was stirred at 140 °C for 2 h and filtered through a plug of silica gel. The solvent was removed under reduced pressure. The crude product was subjected to flash chromatography on silica gel (cyclohexane/ethyl acetate = 5:2) to afford tetrahydro[5]helicene derivative **19** as a complex mixture of stereoisomers. The mixture was used for the subsequent reaction without further analytical characterization.

Yield: n/a

Molecular formula: $C_{28}H_{26}O_6$

Molecular weight: 458.51 g/mol

Retention factor: 0.32 (cyclohexane/ethyl acetate = 5:2)

Approach B

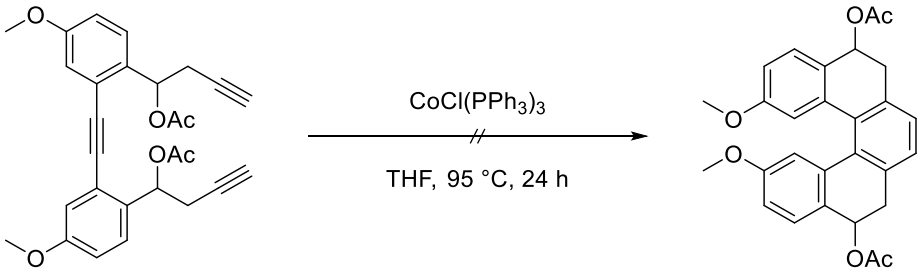

18 **19**

The reaction was carried out under Schlenk conditions. In a Schlenk flask equipped with a magnetic stir bar, $CoCl(PPh_3)_3$ (10 mol%) was suspended in anhydrous THF (1 mL). 130 mg of triyne **18** (0.28 mmol, 1.0 equiv.) were added and the resulting mixture was stirred overnight at 95 °C. The reaction was monitored by TLC. No turnover was observed after that time and the starting material was recovered by column chromatography on silica gel (cyclohexane/ethyl acetate = 4:1).

Approach C

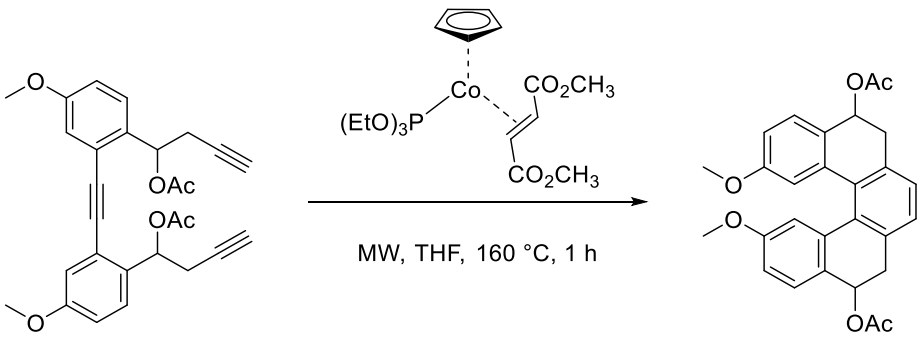

18 **19**

A glass vial equipped with a magnetic stir bar was charged with 100.0 mg of triyne **18** (0.22 mmol, 1.0 equiv.) and 9.47 mg of CpCo[$P(OEt)_3$](*trans*-dimethylfumarate) (10 mol%). After adding anhydrous THF (3 mL) the vial was sealed with a septum-cap and the mixture was degassed by argon bubbling through the septum. After that the mixture was stirred at 160 °C for 1 h under microwave irradiation. The solvent was removed under reduced pressure and the residue was subjected to flash chromatography on silica gel (cyclohexane/ethyl acetate = 5:2) to afford tetrahydro[5]helicene derivative **19** as a complex mixture of stereoisomers. The mixture was used for the subsequent reaction without further analytical characterization.

Yield: n/a

Approach D

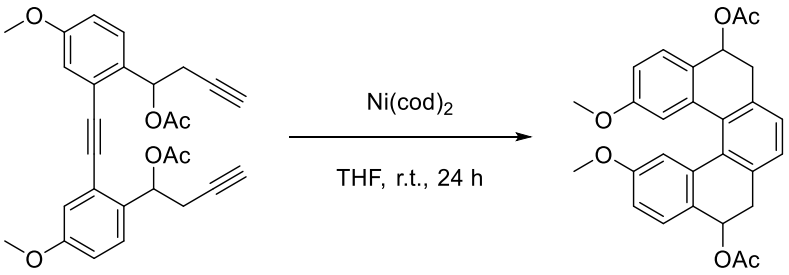

18 **19**

The reaction was carried out under Schlenk conditions. In a Schlenk flask equipped with a magnetic stir bar, 100.0 mg of triyne **18** (0.22 mmol, 1.0 equiv.) were dissolved in anhydrous THF (1 mL). After adding a stock solution of $Ni(cod)_2$ (3.63 mL, 0.06 M in THF, 1.0 equiv.), the mixture was stirred at room temperature for 24 h. The solvent was evaporated under reduced pressure and the residue was subjected to flash

chromatography on silica gel (cyclohexane/ethyl acetate = 5:2) to afford tetrahydro[5]helicene derivative **19** as a complex mixture of stereoisomers. The mixture was used for the subsequent reaction without further analytical characterization.

Yield: n/a

Approach E

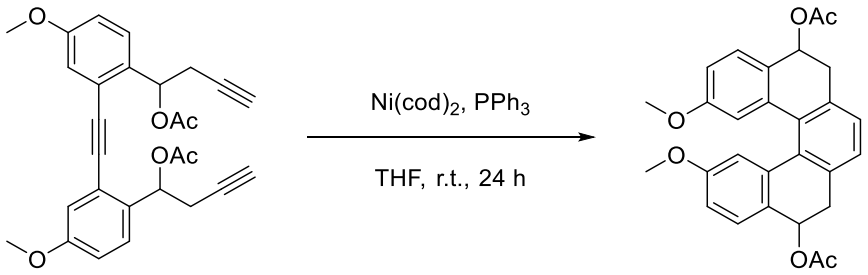

18 **19**

The reaction was carried out under Schlenk conditions. In a Schlenk flask equipped with a magnetic stir bar, 100.0 mg of triyne **18** (0.22 mmol, 1.0 equiv.) and 114.41 mg of PPh_3 (0.44 mmol, 2.0 equiv.) were dissolved in anhydrous THF (1 mL). After adding a stock solution of $Ni(cod)_2$ (3.63 mL, 0.06 M in THF, 1.0 equiv.), the mixture was stirred at room temperature for 24 h. The solvent was evaporated under reduced pressure and the residue was subjected to flash chromatography on silica gel (cyclohexane/ethyl acetate = 5:2) to afford tetrahydro[5]helicene derivative **19** as a complex mixture of stereoisomers. The mixture was used for the subsequent reaction without further analytical characterization.

Yield: n/a

2,13-Dimethoxypentahelicene 20 (see also page 201)

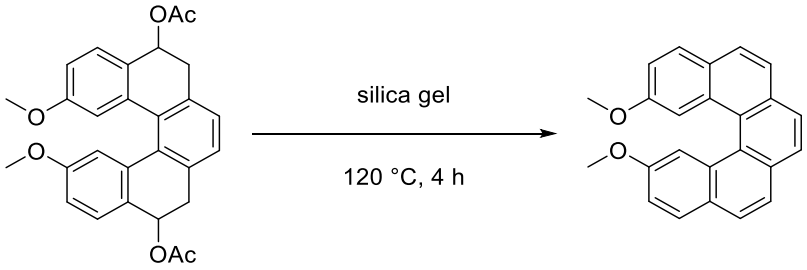

19 **20**

In a round bottomed flask equipped with a magnetic stir bar, a solution of tetrahydro[5]helicene derivative **19** (200.0 mg, 0.43 mmol, 1.0 equiv.) in dichloromethane (5 mL) was prepared. After adding silica gel (500 mg), the solvent was evaporated under reduced pressure and the solvent-free mixture was heated at 120 °C for 4 h under vigorous stirring. The product was extracted from silica gel with dichloromethane (100 mL). Removal of the solvent under reduced pressure gave rise to 2,13-dimethoxy[5]helicene **20** as an amorphous brown solid.

Single crystals for XRD analysis were grown by layering *n*-hexane on top of a solution of racemic or enantiopure **20** in dichloromethane (3:1 or 2:1) overnight at −10 °C.

Yield over 2 steps:	Approach A: 38.52 mg (0.11 mmol, 26 %)
	Approach C: 19.21 mg (0.056 mmol, 26 %)
	Approach D: 22.12 mg (0.065 mmol, 30 %)
	Approach E: 43.01 mg (0.12 mmol, 58 %)
Molecular formula:	$C_{24}H_{18}O_2$
Molecular weight:	338.41 g/mol
Retention factor:	0.5 (cyclohexane/ethyl acetate = 3:1)
EI-MS:	*m*/*z* = 338.1 $[M]^{\bullet+}$, 323.1 $[M\text{-}CH_3]^+$, 308.1 $[M\text{-}C_2H_6]^{\bullet+}$, 276.1 $[M\text{-}C_2H_6O_2]^{\bullet+}$
HRMS ($C_{24}H_{18}O_2^{\bullet+}$):	calculated = 338.1306
	found = 338.1311
Specific optical rotation:	(−)-(*M*)-**20**: $[\alpha]_D^{20} = -1430°$ mL×dm^{-1}×g^{-1} (*c* = 0.92 g/L, dichloromethane)
	(+)-(*P*)-**20**: $[\alpha]_D^{20} = +1440°$ mL×dm^{-1}×g^{-1} (*c* = 1.01 g/L, dichloromethane)
ECD:	(−)-(*M*)-**20**: *λ*/nm (*Δε*/M^{-1}×cm^{-1}) = 247 (−80.9), 273 (+92.0), 321 (−133.7); (*c* = 4.0×10^{-4} g/L, dichloromethane)
	(+)-(*P*)-**20**: *λ*/nm (*Δε*/M^{-1}×cm^{-1}) = 247 (+77.7), 273 (−54.1), 321 (+148.1); (*c* = 4.0×10^{-4} g/L, dichloromethane)

Analytical HPLC: CHIRALPAK IB-U; *n*-hexane/isopropanol (98:2); *f* = 0.85 mL min^{-1}); (–)-(M)-**20**: t_R = 1.38 min; (+)-(P)-**20**: t_R = 2.38 min

Semipreparative HPLC: CHIRALPAK IB; *n*-hexane/isopropanol (98:2); *f* = 18 mL min^{-1}); (–)-(M)-**20**: t_R = 6.37 min, 99.2 % *ee*; (+)-(P)-**20**: t_R = 7.92 min, 99.2 % *ee*

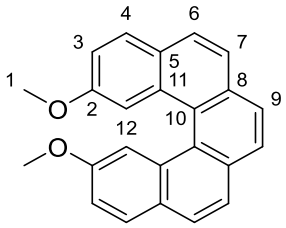

^{1}H-NMR (700 MHz, CD_2Cl_2, 298 K):
δ/ppm = 7.91 (d, 2H, H-6/H-7, $^3J_{6,7}$ = 8.5 Hz), 7.90 (d, 2H, H-4, $^3J_{4,3}$ = 8.7 Hz), 7.90 (s, 2H, H-9), 7.80 (d, 2H, H-6/H-7, $^3J_{6,7}$ = 8.5 Hz), 7.79 (d, 2H, H-12, $^4J_{12,3}$ = 2.5 Hz), 7.19 (dd, 2H, H-3, $^3J_{3,4}$ = 8.7 Hz, $^4J_{3,12}$ = 2.5 Hz), 3.54 (s, 6H, H-1).

^{13}C-NMR (700 MHz, CD_2Cl_2, 298 K):
δ/ppm = 157.0 (C-2), 133.2 (C-10/C-11), 131.8*, 130.0 (C-4/C-9), 128.3 (C-5), 127.9 (C-4/C-9), 127.5 (C-6/C-7), 126.7*, 124.6 (C-6/C-7), 118.2 (C-3), 110.5 (C-12), 55.4 (C-1).

*The signal could not be unambiguously assigned.

Crystallographic data [(*rac*)-**20**]

Empirical formula: $C_{24}H_{18}O_2$; *M* = 338.38 g/mol; *T* = 180.15 K; radiation type: MoKα; *λ* = 0.71073 Å; crystal system: orthorhombic; space group: *Pcbn*; unit cell: *a* = 10.8757(8) Å, *b* = 10.3493(9) Å, *c* = 15.3773(14) Å, *α* = 90°, *β* = 90°, *γ* = 90°, *V* = 1730.8(3) $Å^3$, *Z* = 4, ρ_{calc} = 1.299 g/cm^3; absorption correction = integration; *μ* = 0.081 mm^{-1}; minimum transmission = 0.1010; maximum transmission = 0.4615; *F*(000) = 712.0; crystal color: clear colorless; crystal size = 0.28×0.21×0.14 mm^3; 2*Θ* range for data collection: 5.30°−51.99°; Reflections collected [*R*(int)] = 6887 [0.1578]; Reflections [*I*>2*σ*(*I*)] = 1679; data completeness = 98.0 %; Data/parameters/restraints = 1679/119/0; Goodness-of-fit on F^2 = 0.950; Final *R* indexes [*I*>=2*σ*(*I*)]: R_1 = 0.0672,

wR_2 = 0.1129; Final *R* indexes [all data]: R_1 = 0.1086, wR_2 = 0.1262; Largest diff. peak/hole = 0.22/−0.18 e Å^{-3}.

Crystallographic data [(−)-**20**]

Empirical formula: $C_{24}H_{18}O_2$; *M* = 338.38 g/mol; *T* = 100.0 K; radiation type: CuKα; *λ* = 1.54186 Å; crystal system: orthorhombic; space group: $P2_12_12_1$; unit cell: *a* = 5.1510(3) Å, *b* = 15.9799(9) Å, *c* = 20.4287(19) Å, *α* = 90°, *β* = 90°, *γ* = 90°, *V* = 1681.54(21) Å^3, *Z* = 4, ρ_{calc} = 1.337 g/cm^3; absorption correction = multi-scan; *μ* = 0.660 mm^{-1}; minimum transmission = 0.6492; maximum transmission = 0.9282; *F*(000) = 712.0; crystal color: clear colorless; crystal size = 0.3×0.10×0.05 mm^3; 2*Θ* range for data collection: 8.66°−135.48°; Reflections collected [*R*(int)] = 9716 [0.0814]; Reflections [*I*>2σ(*I*)] = 2924; data completeness = 99.2 %; Data/parameters/restraints = 2924/238/0; Goodness-of-fit on F^2 = 1.026; Final *R* indexes [*I*>=2σ(*I*)]: R_1 = 0.0597, wR_2 = 0.1557; Final *R* indexes [all data]: R_1 = 0.0677, wR_2 = 0.1645; Largest diff. peak/hole = 0.25/−0.34 e Å^{-3}; Flack parameter = 0.6(5)*.

*The high uncertainty originated from a poor quality of the crystal. The assignment of the enantiomer was done based on ECD spectra.

Crystallographic data [(+)-**20**]

Empirical formula: $C_{24}H_{18}O_2$; *M* = 338.38 g/mol; *T* = 100.0 K; radiation type: CuKα; *λ* = 1.54186 Å; crystal system: orthorhombic; space group: $P2_12_12_1$; unit cell: *a* = 5.16009(16) Å, *b* = 15.9555(7) Å, *c* = 20.4345(7) Å, *α* = 90°, *β* = 90°, *γ* = 90°, *V* = 1682.41(11) Å^3, *Z* = 4, ρ_{calc} = 1.336 g/cm^3; absorption correction = multi-scan; *μ* = 0.660 mm^{-1}; minimum transmission = 0.6740; maximum transmission = 0.9081; *F*(000) = 712.0; crystal color: clear colorless; crystal size = 0.45×0.18×0.05 mm^3; 2*Θ* range for data collection: 7.03°−135.34°; Reflections collected [*R*(int)] = 14985 [0.0532]; Reflections [*I*>2σ(*I*)] = 2998; data completeness = 99.0 %; Data/parameters/restraints = 2998/238/0; Goodness-of-fit on F^2 = 1.048; Final *R* indexes [*I*>=2σ(*I*)]: R_1 = 0.0388, wR_2 = 0.1003; Final *R* indexes [all data]: R_1 = 0.0417, wR_2 = 0.1027; Largest diff. peak/hole = 0.16/−0.20 e Å^{-3}; Flack parameter = 0.2(3)*.

*The high uncertainty originated from a poor quality of the crystal. The assignment of the enantiomer was done based on ECD spectra.

2-Iodo-4-methoxy-1-methylbenzene 22[64]

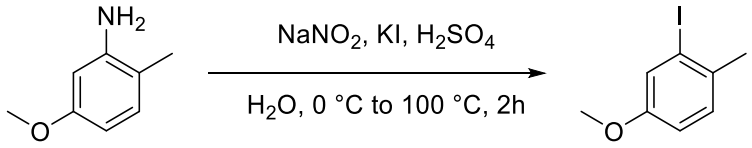

21 **22**

In a round bottomed flask equipped with a magnetic stir bar, a suspension of 5-methoxy-2-methylaniline **21** (5.0 g, 36.45 mmol, 1.0 equiv.) in concentrated sulfuric acid (8 mL) and water (129 mL) was cooled to 0 °C. After adding a solution of sodium nitrite (2.67 g, 38.64 mmol, 1.06 equiv.) in water (8 mL) under stirring while maintaining a temperature between 0−5 °C, the mixture was slowly warmed up to room temperature and treated with 6.05 g of potassium iodide (36.45 mmol, 1.0 equiv.). The reaction mixture was stirred for 1 h at room temperature and an additional hour at 100 °C. The reaction mixture was extracted with dichloromethane (3×50 mL). The combined organic portions were washed with an aqueous saturated solution of $KHCO_3$ (4×200 mL), an aqueous saturated solution of $Na_2S_2O_3$ (5×200 mL) and water (200 mL), dried with anhydrous $MgSO_4$ and concentrated under reduced pressure. The residue was filtered through a plug of silica gel. The solvent was removed under reduced pressure. The crude product was purified by flash chromatography on silica gel (cyclohexane/ethyl acetate = 19:1) to obtain iodide **22** as a yellow oil.

Yield: 4.50 g (18.14 mmol, 49 %)

Molecular formula: C_8H_9OI

Molecular weight: 248.06 g/mol

Retention factor: 0.50 (cyclohexane/ethyl acetate = 4:1)

^{1}H-NMR (400 MHz, $CDCl_3$, 298 K):
δ/ppm = 7.36 (d, 1H, *J* = 2.6 Hz), 7.12 (dd, 1H, *J* = 8.5 Hz, *J* = 0.8 Hz), 6.81 (dd, 1H, *J* = 8.5 Hz, *J* = 2.6 Hz), 3.76 (s, 3H), 2.36 (s, 3H).

The spectral data were in agreement with those previously reported for this compound.[64]

1-(Bromomethyl)-2-iodo-4-methoxybenzene 23[64]

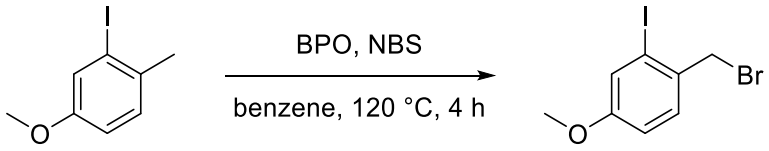

22 **23**

In a round bottomed flask equipped with a magnetic stir bar, a mixture of iodine **22** (4.78 g, 19.25 mmol, 1.0 equiv.), *N*-bromosuccinimide (3.77 g, 21.18 mmol, 1.10 equiv.) and benzoyl peroxide (233.19 mg, 0.96 mmol, 0.05 equiv.) in benzene (20 mL) was stirred at 120 °C for 4 h. The reaction was cooled to room temperature and filtered. The filtrate was washed with an aqueous saturated solution of Na_2SO_3 (100 mL) and extracted with dichloromethane (3×50 mL). The combined organic portions were dried with anhydrous $MgSO_4$ and concentrated under reduced pressure. The crude product was purified by flash chromatography on silica gel (cyclohexane/ethyl acetate = 10:1) to obtain bromide **23** as a yellow solid.

Yield: 4.10 g (12.54 mmol, 65 %)

Molecular formula: C_8H_8OIBr

Molecular weight: 325.88 g/mol

Retention factor: 0.47 (cyclohexane/ethyl acetate = 5:1)

^{1}H-NMR (400 MHz, $CDCl_3$, 298 K):
δ/ppm = 7.39−7.34 (m, 2H), 6.88 (dd, 1H, *J* = 8.5 Hz, *J* = 2.6 Hz), 4.60 (s, 3H), 3.79 (s, 3H).

The spectral data were in agreement with those previously reported for this compound.[64]

2-Iodo-4-methoxy-1-[4-(triisopropylsilyl)-3-butyn-1-yl]benzene 24[64]

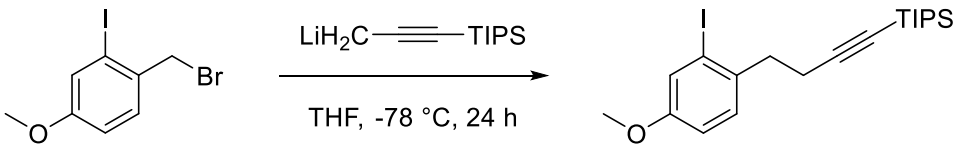

23 **24**

The reaction was carried out under Schlenk conditions. In a Schlenk flask equipped with a magnetic stir bar, 4.11 mL of *n*-butyllithium (2.5 M in *n*-hexane, 10.28 mmol, 1.05 equiv.) were added dropwise to a solution of triisopropyl(prop-1-yn-1-yl)-silane (2.45 mL, 10.37 mmol, 1.06 equiv.) in anhydrous THF (20 mL) at −78 °C under vigorous stirring. After stirring the mixture at −78 °C for 1.5 h, a solution of bromide **23** (3.20 g, 9.79 mmol, 1.0 equiv.) in anhydrous THF (20 mL) was added dropwise. A color change from red over purple and green to yellow was observed. The mixture was stirred at this temperature for 24 h and slowly warmed up to room temperature. The solvent was removed under reduced pressure. The crude product was purified by flash chromatography on silica gel (cyclohexane/ethyl acetate = 20:1) to obtain alkyne **24** as a colorless oil.

Yield:	620.77 mg (1.40 mmol, 14 %)
Molecular formula:	$C_{20}H_{31}OISi$
Molecular weight:	442.46 g/mol
Retention factor:	0.60 (cyclohexane/ethyl acetate = 5:1)

^{1}H-NMR (300 MHz, $CDCl_3$, 298 K):
δ/ppm = 7.35 (d, 1H, *J* = 2.6 Hz), 7.20 (d, 1H, *J* = 8.5 Hz), 6.82 (dd, 1H, *J* = 8.5 Hz, *J* = 2.6 Hz), 3.76 (s, 3H), 2.89 (t, 2H, *J* = 7.2 Hz), 2.53 (t, 2H, *J* = 7.2 Hz), 1.05 (d, 21H, *J* = 3.7 Hz).

The spectral data were in agreement with those previously reported for this compound.[64]

Triisopropyl[4-(4-methoxy-2-((trimethylsilyl)ethynyl)phenyl)but-1-yn-1-yl]silane 25

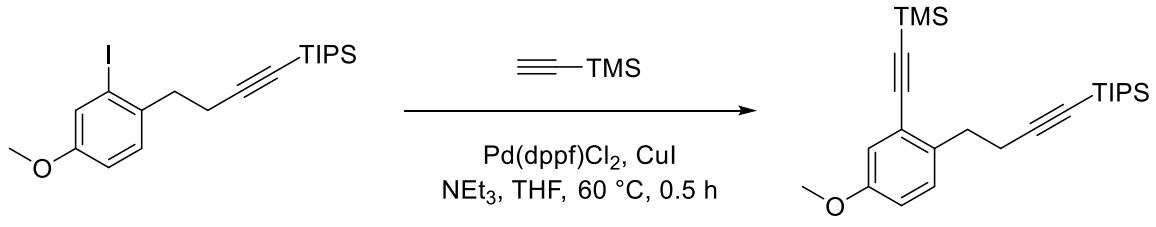

24 **25**

The reaction was carried out under Schlenk conditions. In a Schlenk flask equipped with a magnetic stir bar, 174.64 mg of $PdCl_2$(dppf) (5 mol%), 90.91 mg of CuI (10 mol%) and 2.11 g of alkyne **24** (4.77 mmol, 1.0 equiv.) were dissolved in anhydrous THF (5 mL) and degassed NEt_3 (10 mL). After adding 1.02 mL of trimethylsilylacetylene (7.16 mmol, 1.50 equiv.), the mixture was stirred at 60 °C for 0.5 h. The reaction mixture was poured into a saturated solution of aqueous NH_4Cl (30 mL) and extracted with DCM (3×30 mL). The combined organic portions were washed with brine (100 mL), dried with anhydrous $MgSO_4$ and concentrated under reduced pressure. The crude product was purified by flash chromatography on silica gel (cyclohexane/ethyl acetate = 8:1). Diyne **25** was obtained as a yellow solid.

Yield: 1.80 g (4.36 mmol, 91 %)

Molecular formula: $C_{25}H_{40}OSi_2$

Molecular weight: 412.76 g/mol

Retention factor: 0.65 (cyclohexane/ethyl acetate = 4:1)

APCI-MS: *m*/*z* = 413.269 $[M+H]^+$

HRMS ($C_{25}H_{40}OSi_2H^+$): calculated = 413.2690

found = 413.2692

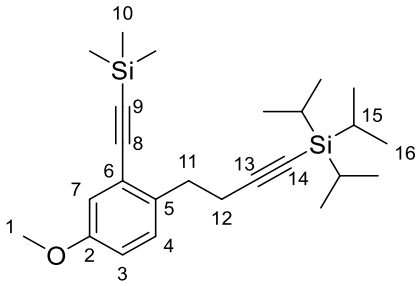

^{1}H-NMR (500 MHz, $CDCl_3$, 298 K):

δ/ppm = 7.15 (d, 1H, H-4, $^3J_{4,3}$ = 8.5 Hz), 6.96 (d, 1H, H-7, $^4J_{7,3}$ = 2.8 Hz), 6.79 (dd, 1H, H-3, $^3J_{3,4}$ = 8.5 Hz, $^4J_{3,7}$ = 2.8 Hz), 3.77 (s, 3H, H-1), 2.95 (t, 2H, H-11, $^3J_{11,12}$ = 7.6 Hz), 2.56 (t, 2H, H-12, $^3J_{12,11}$ = 7.6 Hz), 1.09−0.97 (m, 21H, H-15, H-16), 0.26 (s, 9H, H-10).

^{13}C-NMR (500 MHz, $CDCl_3$, 298 K):

δ/ppm = 157.9 (C-2), 135.7 (C-5), 130.3 (C-4), 123.3 (C-6), 116.7 (C-7), 115.6 (C-3), 108.6 (C-13), 103.7 (C-8), 98.4 (C-9), 80.8 (C-14), 55.5 (C-1), 33.7 (C-11), 21.1 (C-12), 18.8 (C-16), 11.5 (C-15), 0.1 (C-10).

[4-(2-Ethynyl-4-methoxyphenyl)but-1-yn-1-yl]triisopropylsilane 26

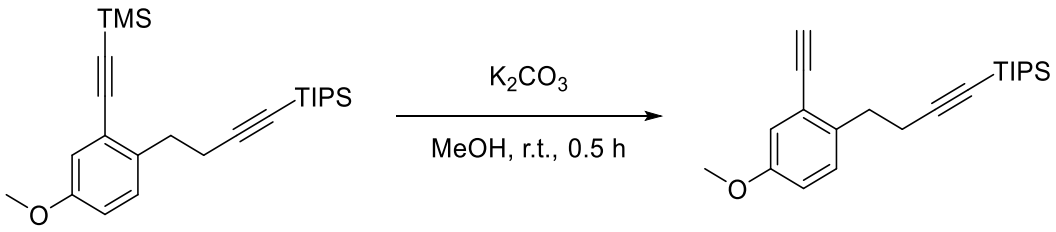

25 **26**

In a round bottomed flask equipped with a magnetic stir bar, 1.80 g of alkyne **25** (4.36 mmol, 1.0 equiv.) were dissolved in methanol (5 mL) and 843.81 mg of K_2CO_3 (6.11 mmol, 1.40 equiv.) were added in batches. The mixture was stirred at room temperature for 0.5 h. The reaction mixture was poured into water (20 mL) and extracted with DCM (3×10 mL). The combined organic portions were dried with anhydrous $MgSO_4$ and concentrated under reduced pressure. The crude product was purified by flash chromatography on silica gel (cyclohexane/ethyl acetate = 4:1) to obtain alkyne **26** as a yellow oil.

Yield:	1.13 g (3.32 mmol, 76 %)
Molecular formula:	$C_{22}H_{32}OSi$
Molecular weight:	340.58 g/mol
Retention factor:	0.55 (cyclohexane/ethyl acetate = 4:1)
ESI(+)-MS:	*m*/*z* = 341.229 $[M+H]^+$
HRMS ($C_{22}H_{32}OSiH^+$):	calculated = 341.2295
	found = 341.2291

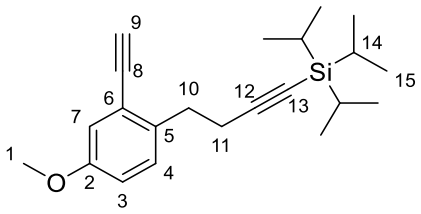

^{1}H-NMR (400 MHz, $CDCl_3$, 298 K):

δ/ppm = 7.20 (d, 1H, H-4, $^{3}J_{4,3}$ = 8.5 Hz), 7.00 (d, 1H, H-7, $^{4}J_{7,3}$ = 2.7 Hz), 6.82 (dd, 1H, H-3, $^{3}J_{3,4}$ = 8.5 Hz, $^{4}J_{3,7}$ = 2.7 Hz), 3.78 (s, 3H, H-1), 3.24 (s, 1H, H-9), 2.96 (t, 2H, H-10, $^{3}J_{10,11}$ = 7.3 Hz), 2.57 (t, 2H, H-11, $^{3}J_{11,10}$ = 7.3 Hz), 1.10−0.95 (m, 21H, H-14, H-15).

^{13}C-NMR (400 MHz, $CDCl_3$, 298 K):

δ/ppm = 157.9 (C-2), 135.7 (C-5), 130.6 (C-4), 122.3 (C-6), 117.5 (C-7), 115.6 (C-3), 108.4 (C-12), 82.2 (C-8), 81.1 (C-9), 80.8 (C-13), 55.5 (C-1), 33.1 (C-10), 21.2 (C-11), 18.8 (C-15), 11.5 (C-14).

1,2-Bis(5-methoxy-2-(4-(triisopropylsilyl)but-3-yn-1-yl)phenyl)ethyne 27

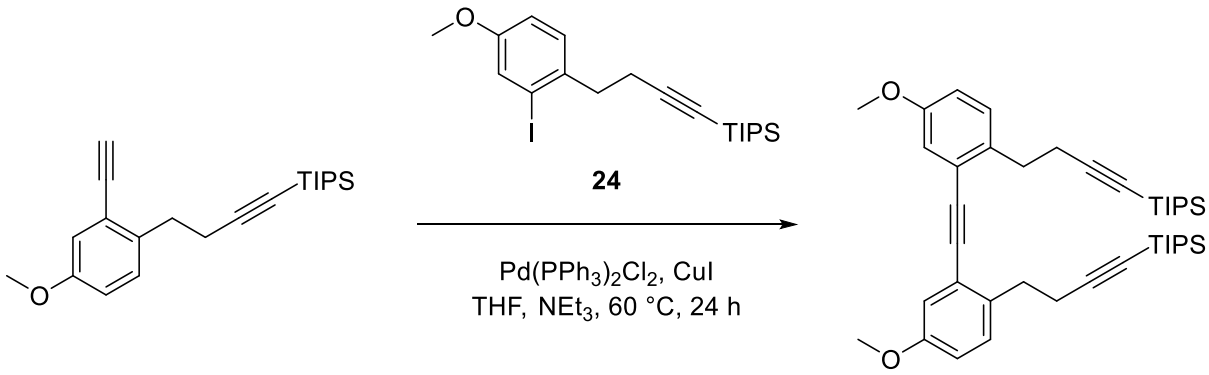

The reaction was carried out under Schlenk conditions. To a Schlenk flask equipped with a magnetic stir bar, 20.61 mg of $PdCl_2(PPh_3)_2$ (2 mol%), 11.18 mg of CuI (4 mol%), 500.0 mg of alkyne **26** (1.47 mmol, 1.0 equiv.) and 650.0 mg of iodide **24** (1.47 mmol, 1.0 equiv.) were added. After adding anhydrous THF (5 mL) and degassed NEt_3 (10 mL), the mixture was heated to 60 °C and stirred for 24 h. The reaction mixture was poured into an aqueous solution of saturated NH_4Cl (40 mL) and then extracted with dichloromethane (3×30 mL). The combined organic portions were washed with brine (150 mL), dried with anhydrous $MgSO_4$ and concentrated under

reduced pressure. The crude product was purified by flash chromatography on silica gel (cyclohexane/ethyl acetate = 10:1) to obtain triyne **27** as a yellow oil.

Yield:	866.68 mg (1.32 mmol, 90 %)
Molecular formula:	$C_{42}H_{62}O_2Si_2$
Molecular weight:	655.13 g/mol
Retention factor:	0.69 (cyclohexane/ethyl acetate = 4:1)
ESI(+)-MS:	*m*/*z* = 655.436 $[M+H]^+$
HRMS ($C_{42}H_{62}O_2Si_2H^+$):	calculated = 655.4361
	found = 655.4359

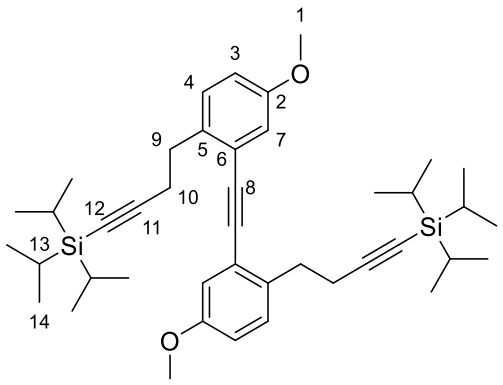

^{1}H-NMR (700 MHz, $CDCl_3$, 298 K):
δ/ppm = 7.23 (d, 2H, H-4, $^3J_{4,3}$ = 8.5 Hz), 7.04 (d, 2H, H-7, $^4J_{7,3}$ = 2.8 Hz), 6.82 (dd, 2H, H-3, $^3J_{3,4}$ = 8.5 Hz, $^4J_{3,7}$ = 2.8 Hz), 3.81 (s, 6H, H-1), 3.02 (t, 4H, H-9, $^3J_{9,10}$ = 7.2 Hz), 2.64 (t, 4H, H-10, $^3J_{10,9}$ = 7.2 Hz), 1.08−0.96 (m, 42H, H-13, H-14).

^{13}C-NMR (700 MHz, $CDCl_3$, 298 K):
δ/ppm = 158.0 (C-2), 134.8 (C-5), 130.6 (C-4), 123.4 (C-6), 117.0 (C-7), 115.1 (C-3), 108.2 (C-11), 91.5 (C-8), 81.2 (C-12), 55.6 (C-1), 33.5 (C-9), 21.5 (C-10), 18.8 (C-14), 11.4 (C-13).

1,2-Bis(2-(but-3-yn-1-yl)-5-methoxyphenyl)ethyne 28

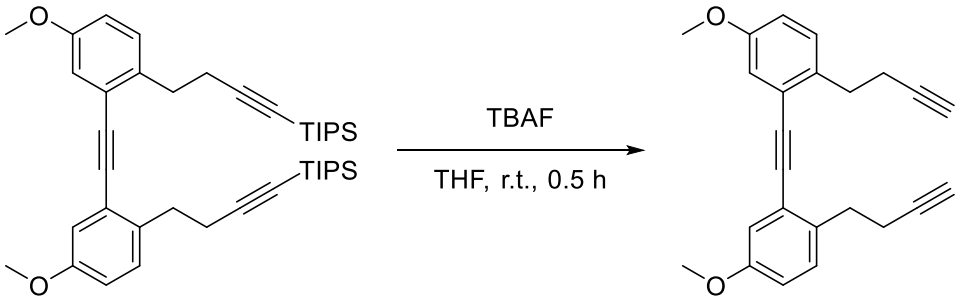

27 **28**

The reaction was carried out under Schlenk conditions. In a Schlenk flask equipped with a magnetic stir bar, 866.68 mg of triyne **27** (1.32 mmol, 1.0 equiv.) were dissolved in anhydrous THF (10 mL). After adding a stock solution of tetra-*n*-butylammonium fluoride (3.31 mL, 1.0 M in THF, 2.50 equiv.), the mixture was stirred at room temperature for 0.5 h. The mixture was poured into a saturated aqueous solution of sodium chloride (20 mL) and extracted with dichloromethane (3×30 mL), then the combined organic portions were dried with anhydrous Mg_2SO_4 and concentrated under reduced pressure. The crude product was purified by flash chromatography on silica gel (cyclohexane/ethyl acetate = 9:1) to afford triyne **28** as a brown solid.

Yield:	387.65 mg (1.13 mmol, 86 %)
Molecular formula:	$C_{24}H_{22}O_2$
Molecular weight:	342.44 g/mol
Retention factor:	0.40 (cyclohexane/ethyl acetate = 4:1)
APCI-MS:	*m*/*z* = 343.169 $[M+H]^+$
HRMS ($C_{24}H_{22}O_2H^+$):	calculated = 343.1693
	found = 343.1689

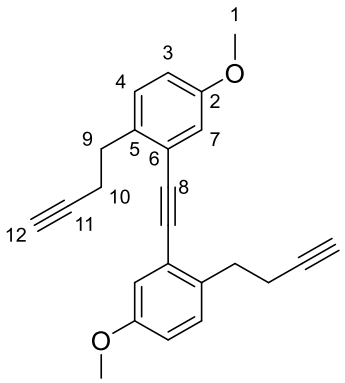

^{1}H-NMR (500 MHz, $CDCl_3$, 298 K):

δ/ppm = 7.21 (d, 2H, H-4, $^{3}J_{4,3}$ = 8.5 Hz), 7.07 (d, 2H, H-7, $^{4}J_{7,3}$ = 2.7 Hz), 6.86 (dd, 2H, H-3, $^{3}J_{3,4}$ = 8.5 Hz, $^{4}J_{3,7}$ = 2.7 Hz), 3.82 (s, 6H, H-1), 3.04 (t, 4H, H-9, $^{3}J_{9,10}$ = 7.5 Hz), 2.57 (td, 4H, H-10, $^{3}J_{10,9}$ = 7.5 Hz, $^{4}J_{10,12}$ = 2.6 Hz), 1.98 (t, 2H, H-12, $^{4}J_{12,10}$ = 2.6 Hz).

^{13}C-NMR (500 MHz, $CDCl_3$, 298 K):

δ/ppm = 158.1 (C-2), 134.6 (C-5), 130.3 (C-4), 123.6 (C-6), 117.1 (C-7), 115.3 (C-3), 91.5 (C-8), 84.0 (C-11), 69.1 (C-12), 55.6 (C-1), 33.2 (C-9), 20.1 (C-10).

2,13-Dimethoxy-5,6,9,10-tetrahydropentahelicene 29

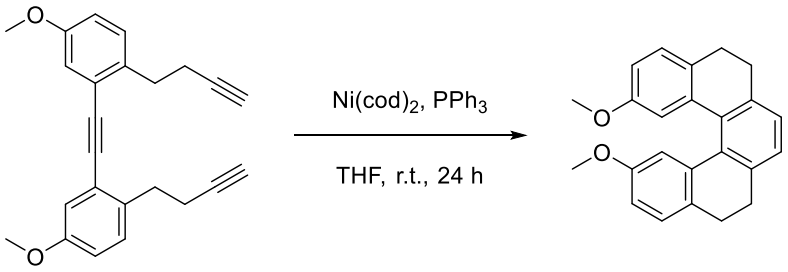

28 **29**

The reaction was carried out under Schlenk conditions. In a Schlenk flask equipped with a magnetic stir bar, 120.0 mg of triyne **28** (0.35 mmol, 1.0 equiv.) and 183.83 mg of PPh_3 (0.70 mmol, 2.0 equiv.) were dissolved in anhydrous THF (5 mL). After adding a stock solution of $Ni(cod)_2$ (5.86 mL, 0.06 M in THF, 1.0 equiv.), the mixture was stirred at room temperature for 24 h. The solvent was evaporated under reduced pressure and the residue was subjected to flash chromatography on silica gel (cyclohexane/ethyl acetate = 8:1) to afford tetrahydro[5]helicene derivative **29** as a yellow solid.

Yield: 45.06 mg (0.13 mmol, 38 %)

Molecular formula: $C_{24}H_{22}O_2$

Molecular weight: 342.44 g/mol

Retention factor: 0.51 (cyclohexane/ethyl acetate = 4:1)

ESI(+)-MS: *m*/*z* = 343.168 $[M+H]^+$

HRMS ($C_{24}H_{22}O_2H^+$): calculated = 343.1693

found = 343.1689

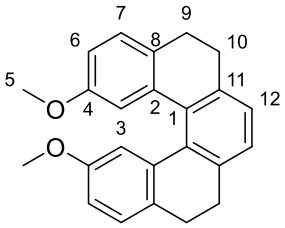

^{1}H-NMR (500 MHz, $CDCl_3$, 298 K):

δ/ppm = 7.16 (d, 2H, H-7, $^3J_{7,6}$ = 8.2 Hz), 7.12 (s, 2H, H-12), 6.81 (d, 2H, H-3, $^4J_{3,6}$ = 2.6 Hz), 6.68 (dd, 2H, H-6, $^3J_{6,7}$ = 8.2 Hz, $^4J_{6,3}$ = 2.6 Hz), 3.43 (s, 6H, H-5), 2.90−2.58 (m, 8H, H-9, H-10).

^{13}C-NMR (500 MHz, $CDCl_3$, 298 K):

δ/ppm = 157.3 (d, C-4), 139.5 (d, C-1), 135.4 (d, C-2), 132.9 (d, C-11), 131.5 (d, C-8), 128.4 (C-7), 126.8 (C-12), 115.3 (d, C-3), 114.0 (d, C-6), 55.2 (d, C-5), 30.7 (d, C-10), 29.0 (d, C-9).

2,13-Dimethoxypentahelicene 20 (see also page 188)

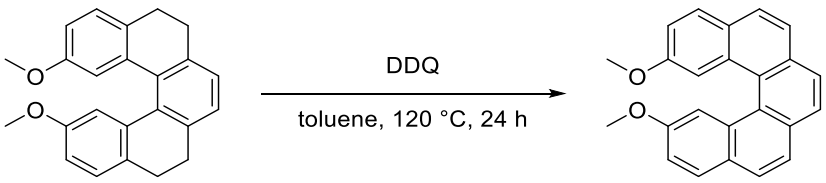

29 **20**

The reaction was carried out under Schlenk conditions. In a two-necked flask equipped with a magnetic stir bar, 100.0 mg of tetrahydro[5]helicene derivative **29** (0.29 mmol, 1.0 equiv.) were dissolved in anhydrous toluene (20 mL). After adding 464.02 mg of 2,3-dichloro-5,6-dicyano-1,4-benzoquinone (2.04 mmol, 7.0 equiv.), the mixture was

stirred at 120 °C for 24 h. The mixture was slowly cooled down to room temperature and filtered over a plug of silica gel. The solvent was evaporated under reduced pressure and the residue was subjected to flash chromatography on silica gel (cyclohexane/ethyl acetate = 99:1) to afford 2,13-dimethoxy[5]helicene **20** as an amorphous brown solid.

Yield: 88.75 mg (0.26 mmol, 90 %)

Molecular formula: $C_{24}H_{18}O_2$

Molecular weight: 338.41 g/mol

Retention factor: 0.5 (cyclohexane/ethyl acetate = 3:1)

^{1}H-NMR (700 MHz, CD_2Cl_2, 298 K):
δ/ppm = 7.91 (d, 2H, H-6/H-7, $^3J_{6,7}$ = 8.5 Hz), 7.90 (d, 2H, H-4, $^3J_{4,3}$ = 8.7 Hz), 7.90 (s, 2H, H-9), 7.80 (d, 2H, H-6/H-7, $^3J_{6,7}$ = 8.5 Hz), 7.79 (d, 2H, H-12, $^4J_{12,3}$ = 2.5 Hz), 7.19 (dd, 2H, H-3, $^3J_{3,4}$ = 8.7 Hz, $^4J_{3,12}$ = 2.5 Hz), 3.54 (s, 6H, H-1).

The spectral data were in agreement with those previously reported for this compound (page 190).

2-Bromo-3-methoxybenzaldehyde 31[345]

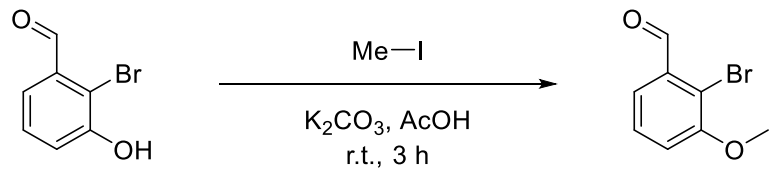

30 **31**

In a round bottomed flask equipped with a magnetic stir bar, 3.78 g of K_2CO_3 (27.36 mmol, 1.10 equiv.) were added to a solution of 2-bromo-3-hydroxy-benzaldehyde **30** (5.0 g, 24.87 mmol, 1.0 equiv.) in acetone (50 mL). After adding 2.01 mL of methyl iodide (32.33 mmol, 1.30 equiv.), the solution was stirred at room temperature for 3 h. The mixture was poured into water (50 mL) and extracted with dichloromethane (3×30 mL). The combined organic portions were dried with anhydrous Mg_2SO_4 and the solvent was evaporated under reduced pressure. The crude product was purified by flash chromatography on silica gel (cyclohexane/ethyl acetate = 3:1) to afford aldehyde **31** as a white solid.

Yield: 4.48 g (20.87 mmol, 83 %)

Molecular formula: $C_8H_7O_2Br$

Molecular weight: 215.05 g/mol

Retention factor: 0.39 (cyclohexane/ethyl acetate = 3:1)

^{1}H-NMR (400 MHz, $CDCl_3$, 298 K):
δ/ppm = 10.45 (d, 1H, *J* = 0.8 Hz), 7.53 (dd, 1H, *J* = 7.8 Hz, *J* = 1.4 Hz), 7.38 (t, 1H, *J* = 7.8 Hz), 7.13 (dd, 1H, *J* = 8.2 Hz, *J* = 1.5 Hz), 3.96 (s, 3H).

The spectral data were in agreement with those previously reported for this compound.[345]

2,2'-(Ethyne-1,2-diyl)bis(3-methoxybenzaldehyde) 32

Approach A

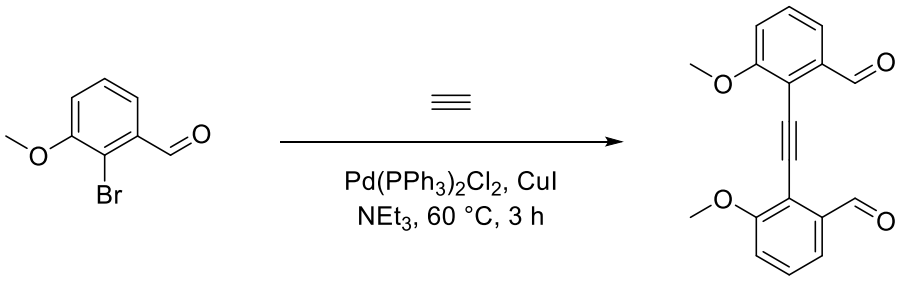

31 **32**

The reaction was carried out under Schlenk conditions. A Schlenk flask equipped with a magnetic stir bar was charged with 4.48 g of 2-bromo-3-methoxybenzaldehyde **31** (20.87 mmol, 1.0 equiv.), 439.47 mg of $PdCl_2(PPh_3)_2$ (3 mol%) and 79.49 mg of CuI (2 mol%). The atmosphere was evacuated and flushed with gaseous acetylene using a balloon. A solution of degassed triethylamine (15 mL) and anhydrous THF (5 mL) was added under stirring at room temperature. Then the mixture was heated to 60 °C and stirred for 3 h. The reaction mixture was poured into an aqueous solution of saturated NH_4Cl (40 mL) and then extracted with dichloromethane (3×30 mL). The combined organic portions were washed with brine (150 mL), dried with anhydrous $MgSO_4$ and concentrated under reduced pressure. The crude product was purified by

flash chromatography on silica gel (cyclohexane/ethyl acetate = 2:1 to 0:1) and recrystallized (ethyl acetate) to obtain dialdehyde **32** as a white solid.

Yield: 300.10 mg (1.02 mmol, 5 %)

Molecular formula: $C_{18}H_{14}O_4$

Molecular weight: 294.31 g/mol

Retention factor: 0.44 (cyclohexane/ethyl acetate = 4:3)

EI-MS: *m*/*z* = 294.0 $[M]^{\bullet+}$, 279.0 $[M\text{-}CH_3]^+$, 264.0 $[M\text{-}C_2H_6]^{\bullet+}$

HRMS ($C_{18}H_{14}O_4^{\bullet+}$): calculated = 294.0892

found = 294.0890

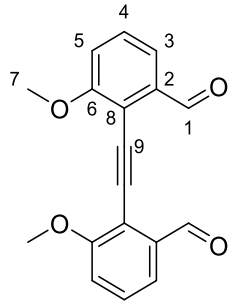

^{1}H-NMR (500 MHz, $CDCl_3$, 298 K):
δ/ppm = 10.75 (d, 2H, H-1, $^5J_{1,4}$ = 0.9 Hz), 7.58 (dd, 2H, H-3, $^3J_{3,4}$ = 7.8 Hz, $^4J_{3,5}$ = 1.0 Hz), 7.44 (td, 2H, H-4, $^3J_{4,3/4,5}$ = 8.0 Hz, $^5J_{4,1}$ = 0.9 Hz), 7.16 (dd, 2H, H-5, $^3J_{5,4}$ = 8.2 Hz, $^4J_{5,3}$ = 1.0 Hz), 3.99 (s, 6H, H-7).

^{13}C-NMR (500 MHz, $CDCl_3$, 298 K):
δ/ppm = 192.5 (C-1), 161.1 (C-6), 137.4 (C-2), 130.1 (C-4), 119.2 (C-3), 116.1 (C-8), 115.7 (C-5), 92.8 (C-9), 56.5 (C-7).

Approach B

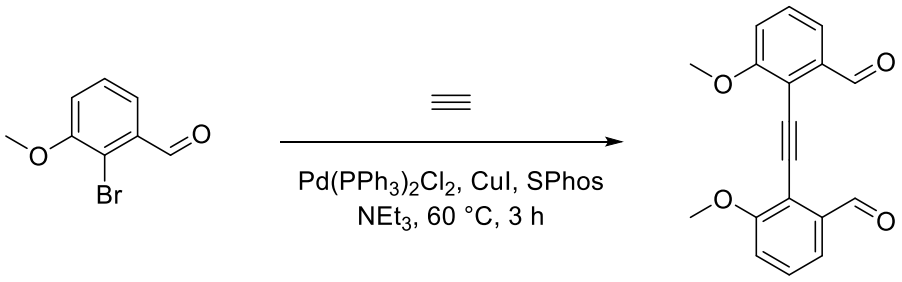

31 **32**

The reaction was carried out under Schlenk conditions. A Schlenk flask equipped with a magnetic stir bar was charged with 1.0 g of 2-bromo-3-methoxybenzaldehyde **31** (4.65 mmol, 1.0 equiv.), 97.92 mg of $PdCl_2(PPh_3)_2$ (3 mol%), 114.55 mg of SPhos (6 mol%) and 17.71 mg of CuI (2 mol%). The atmosphere was evacuated and flushed with gaseous acetylene using a balloon. A solution of degassed triethylamine (15 mL) and anhydrous THF (5 mL) was added under stirring at room temperature. Then the mixture was heated to 60 °C and stirred for 3 h. The reaction mixture was poured into an aqueous solution of saturated NH_4Cl (40 mL) and then extracted with dichloromethane (3×30 mL). The combined organic portions were washed with brine (150 mL), dried with anhydrous $MgSO_4$ and concentrated under reduced pressure. The crude product was purified by flash chromatography on silica gel (cyclohexane/ethyl acetate = 2:1 to 0:1) and recrystallized (ethyl acetate) to obtain dialdehyde **32** as a white solid.

Yield: 150.70 mg (0.51 mmol, 11 %)

Approach C

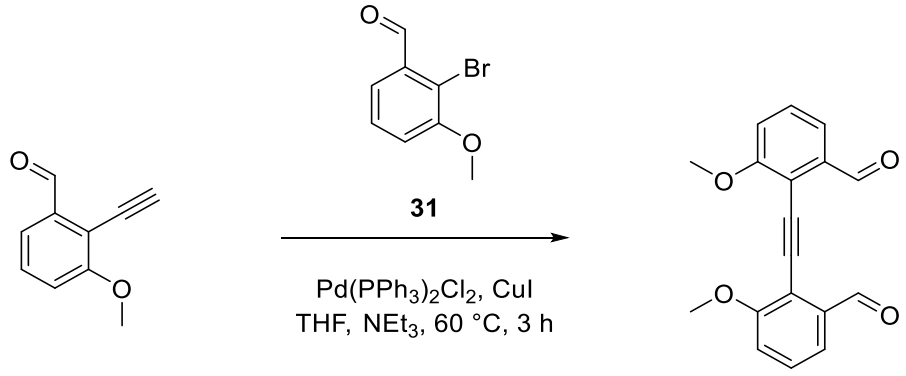

34 **32**

The reaction was carried out under Schlenk conditions. To a Schlenk flask equipped with a magnetic stir bar, 185.81 mg of $PdCl_2(PPh_3)_2$ (2 mol%), 100.83 mg of CuI (4 mol%), 2.12 g of 2-ethynyl-3-methoxybenzaldehyde **34** (13.23 mmol, 1.0 equiv.) and 2.84 g of 2-bromo-3-methoxybenzaldehyde **31** (13.23 mmol, 1.0 equiv.) were added. After adding anhydrous THF (5 mL) and degassed NEt_3 (10 mL), the mixture was heated to 60 °C and stirred for 3 h until the precipitation of a yellow solid was observed. The reaction mixture was concentrated under reduced pressure. The crude product was recrystallized (ethyl acetate) and washed with water (800 mL), acetone (800 mL) and dichloromethane (800 mL) to obtain dialdehyde **32** as yellow needles.

Yield: 2.75 g (9.34 mmol, 71 %)

3-Methoxy-2-[(trimethylsilyl)ethynyl]benzaldehyde 33

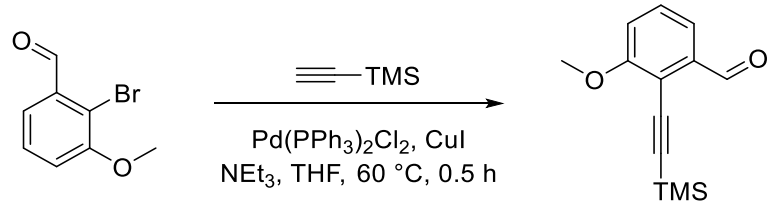

31 **33**

The reaction was carried out under Schlenk conditions. In a Schlenk flask equipped with a magnetic stir bar, 274.17 mg of $PdCl_2(PPh_3)_2$ (2 mol%), 148.77 mg of CuI (4 mol%) and 4.20 g of 2-bromo-3-methoxybenzaldehyde **31** (19.53 mmol, 1.0 equiv.) were dissolved in anhydrous THF (5 mL) and degassed NEt_3 (10 mL). After adding 4.17 mL of trimethylsilylacetylene (29.29 mmol, 1.50 equiv.), the mixture was stirred at 60 °C for 0.5 h. The reaction mixture was poured into a saturated solution of aqueous NH_4Cl (20 mL) and extracted with DCM (3×30 mL). The combined organic portions were washed with brine (150 mL), dried with anhydrous $MgSO_4$ and concentrated under reduced pressure. The crude product was purified by flash chromatography on silica gel (cyclohexane/ethyl acetate = 9:1). Aldehyde **33** was obtained as a yellow oil.

Yield: 4.50 g (19.37 mmol, 99 %)

Molecular formula: $C_{13}H_{16}O_2Si$

Molecular weight: 232.35 g/mol

Retention factor: 0.50 (cyclohexane/ethyl acetate = 4:1)

^{1}H-NMR (500 MHz, $CDCl_3$, 298 K):

δ/ppm = 10.55 (d, 1H, *J* = 0.9 Hz), 7.51 (dd, 1H, *J* = 7.8 Hz, *J* = 1.1 Hz), 7.38 (td, 1H, *J* = 8.0 Hz, *J* = 0.9 Hz), 7.10 (dd, 1H, *J* = 8.2 Hz, *J* = 1.1 Hz), 3.93 (s, 3H), 0.29 (s, 9H).

The spectral data were in agreement with those previously reported for this compound.[346]

2-Ethinyl-3-methoxybenzaldehyde 34

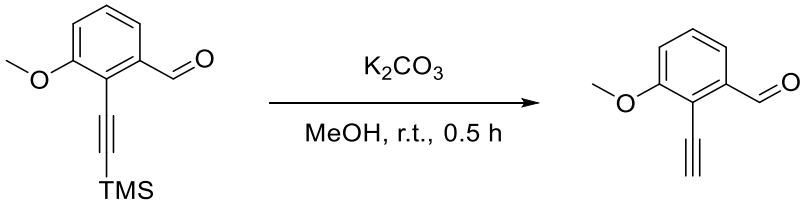

33 **34**

In a round bottomed flask equipped with a magnetic stir bar, 4.50 g of aldehyde **33** (19.37 mmol, 1.0 equiv.) were dissolved in methanol (20 mL) and 3.75 g of K_2CO_3 (27.11 mmol, 1.40 equiv.) were added in batches. The mixture was stirred at room temperature for 0.5 h. The reaction mixture was poured into water (20 mL) and extracted with DCM (3×30 mL). The combined organic portions were dried with anhydrous $MgSO_4$ and concentrated under reduced pressure. The crude product was purified by flash chromatography on silica gel (cyclohexane/ethyl acetate = 10:1). Aldehyde **34** was obtained as a red solid.

Yield: 2.30 g (14.35 mmol, 74 %)

Molecular formula: $C_{10}H_8O_2$

Molecular weight: 160.17 g/mol

Retention factor: 0.45 (cyclohexane/ethyl acetate = 4:1)

^{1}H-NMR (500 MHz, $CDCl_3$, 298 K):

δ/ppm = 10.55 (d, 1H, *J* = 0.9 Hz), 7.54 (dd, 1H, *J* = 7.8 Hz, *J* = 1.1 Hz), 7.44 (td, 1H, *J* = 8.0 Hz, *J* = 0.9 Hz), 7.14 (dd, 1H, *J* = 8.3 Hz, *J* = 1.1 Hz), 3.96 (s, 3H), 3.69 (s, 1H).

The spectral data were in agreement with those previously reported for this compound.[347]

1,1'-[Ethyne-1,2-diylbis(3-methoxy-2,1-phenylene)]bis(but-3-yn-1-ol) 35

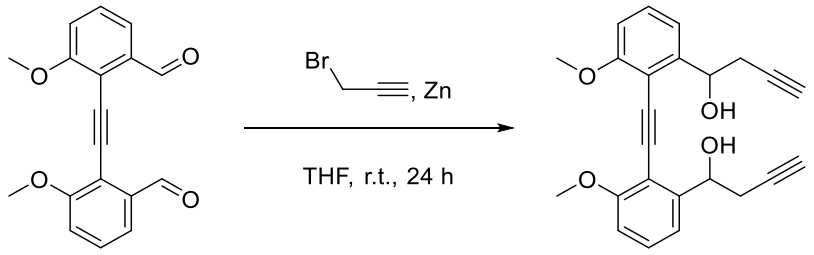

32 **35**

The reaction was carried out under Schlenk conditions. A Schlenk flask equipped with a magnetic stir bar was charged with 444.29 mg of zinc powder (6.80 mmol, 10.0 equiv.). Anhydrous tetrahydrofuran (10 mL) was added, the flask was immersed in a water bath at room temperature and a solution of propargyl bromide (0.76 mL, 80 wt.% in toluene, 6.80 mmol, 10.0 equiv.) was added slowly. The solution was stirred at room temperature for 30 minutes before it was added to the suspension of dialdehyde **32** (200.0 mg, 0.68 mmol, 1.0 equiv.) in anhydrous tetrahydrofuran (10 mL). After 24 h of stirring, the mixture was poured into water (30 mL) and extracted with dichloromethane (3×40 mL), then the combined organic portions were washed with brine (100 mL) and HCl (100 mL, 6 M in water), dried with anhydrous Mg_2SO_4 and concentrated under reduced pressure. The crude product was used for the subsequent reaction without further purification.

Yield: n/a

Molecular formula: $C_{24}H_{22}O_4$

Molecular weight: 374.43 g/mol

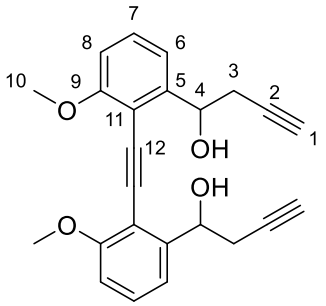

^{1}H-NMR (500 MHz, $CDCl_3$, 298 K):

δ/ppm = 7.34−7.30 (m, 2H, H-7), 7.11−7.07 (m, 2H, H-6), 6.88−6.85 (m, 2H, H-8), 5.22 (dt, 2H, H-4, $^3J_{4,3}$ = 8.7 Hz, $^4J_{4,6}$ = 4.5 Hz), 3.98 (s, 6H, H-10), 3.04−2.80 (m, 4H, H-3), 2.09−2.07 (m, 2H, H-1).

^{13}C-NMR (500 MHz, $CDCl_3$, 298 K):

δ/ppm = 160.6 (d, C-9), 145.8 (d, C-5), 129.8 (d, C-7), 118.8 (d, C-6), 109.8 (d, C-8), 109.7 (C-11), 94.0 (d, C-12), 81.6 (C-2), 72.1 (d, C-4), 70.6 (d, C-1), 56.1 (C-10), 27.7 (d, C-3).

[Ethyne-1,2-diylbis(3-methoxy-2,1-phenylene)]bis(but-3-yne-1,1-diyl) diacetate 36

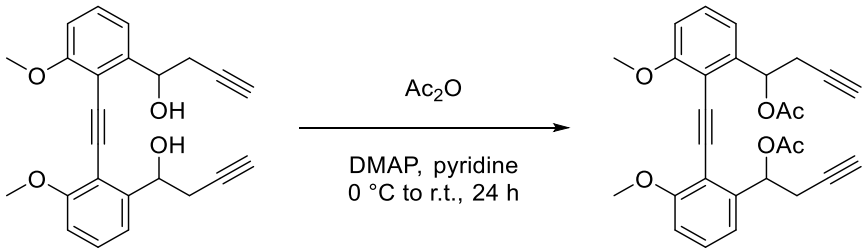

35 **36**

In a round bottomed flask equipped with a magnetic stir bar, a solution of diol **35** (312.0 mg, 0.83 mmol, 1.0 equiv.) and 4-dimethylaminopyridine (12.21 mg, 0.010 mmol, 0.12 equiv.) in anhydrous pyridine (10 mL) was prepared. After adding 0.94 mL of acetic anhydride (10.0 mmol, 12.0 equiv.) at 0 °C while stirring, the reaction mixture was allowed to slowly reach room temperature and stirring was continued at the same temperature for an additional 24 h. The mixture was poured into water (20 mL) and extracted with dichloromethane (3×20 mL), then the combined organic portions were washed with a saturated aqueous solution of $KHCO_3$ (100 mL), dried with anhydrous Mg_2SO_4 and concentrated under reduced pressure. The crude product was purified by flash chromatography on silica gel (cyclohexane/ethyl acetate = 4:1 to 2:1) to afford diacetate **36** as a white solid.

Yield:	225.0 mg (0.49 mmol, 58 %) over 2 steps
Molecular formula:	$C_{28}H_{26}O_6$
Molecular weight:	458.51 g/mol

Retention factor: 0.10 (cyclohexane/ethyl acetate = 4:1)

ESI(+)-MS: *m*/*z* = 497.136 $[M+K]^+$, 481.162 $[M+Na]^+$, 476.207 $[M+NH_4]^+$

HRMS ($C_{28}H_{26}O_6Na^+$): calculated = 481.1622

found = 481.1621

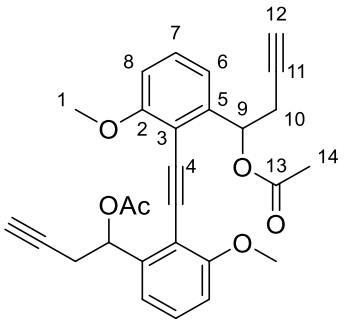

^{1}H-NMR (700 MHz, $CDCl_3$, 298 K):

δ/ppm = 7.32−7.28 (m, 2H, H-7), 7.13−7.09 (m, 2H, H-6), 6.87−6.84 (m, 2H, H-8), 6.54−6.48 (m, 2H, H-9), 3.96 (6H, H-1), 3.09−2.84 (m, 4H, H-10), 2.19−2.17 (m, 6H, H-14), 1.97-1.92 (m, 2H, H-12).

^{13}C-NMR (700 MHz, $CDCl_3$, 298 K):

δ/ppm = 170.0 (d, C-13), 160.5 (d, C-2), 142.2 (d, C-5), 129.4 (d, C-7), 117.7 (d, C-6), 110.7 (d, C-3), 109.9 (d, C-8), 93.3 (d, C-4), 80.3 (d, C-11), 71.8 (d, C-9), 70.3 (d, C-12), 56.1 (d, C-1), 25.3 (d, C-10), 21.3 (d, C-14).

1,14-Dimethoxy-5,6,9,10-tetrahydropentahelicene-5,10-diyl diacetate 37

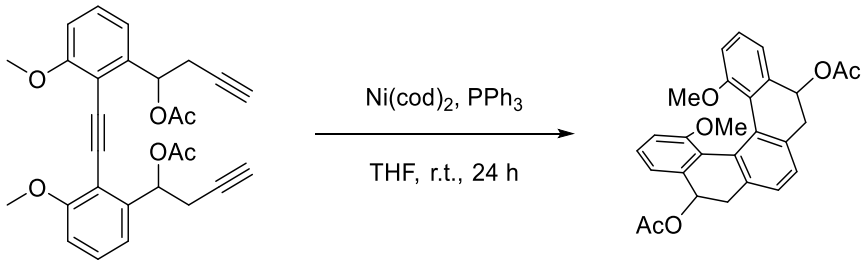

36 **37**

The reaction was carried out under Schlenk conditions. In a Schlenk flask equipped with a magnetic stir bar, 100.0 mg of triyne **36** (0.22 mmol, 1.0 equiv.) and 114.41 mg of PPh_3 (0.44 mmol, 2.0 equiv.) were dissolved in anhydrous THF (1 mL). After adding a stock solution of $Ni(cod)_2$ (3.63 mL, 0.06 M in THF, 1.0 equiv.), the mixture was stirred

at room temperature for 24 h. The solvent was evaporated under reduced pressure and the residue was subjected to flash chromatography on silica gel (cyclohexane/ethyl acetate = 3:1) to afford tetrahydro[5]helicene derivative **37** as a complex mixture of stereoisomers. The mixture was used for the subsequent reaction without further analytical characterization.

Yield:	n/a
Molecular formula:	$C_{28}H_{26}O_6$
Molecular weight:	458.51 g/mol
Retention factor:	0.29 (cyclohexane/ethyl acetate = 4:1)
ESI(+)-MS:	*m*/*z* = 497.135 $[M+K]^+$, 481.162 $[M+Na]^+$, 476.207 $[M+NH_4]^+$
HRMS ($C_{28}H_{26}O_6Na^+$):	calculated = 481.1622
	found = 481.1621

1,14-Dimethoxypentahelicene 38

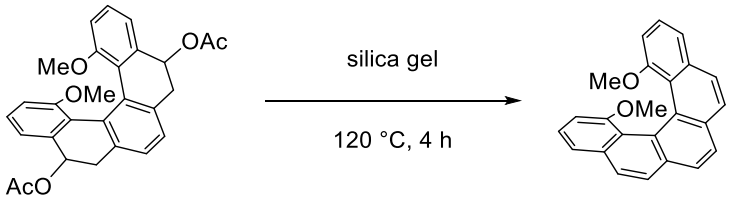

37 **38**

In a round bottomed flask equipped with a magnetic stir bar, a solution of tetrahydro[5]helicene derivative **37** (48.0 mg, 0.10 mmol, 1.0 equiv.) in dichloromethane (5 mL) was prepared. After adding silica gel (200 mg), the solvent was evaporated under reduced pressure and the solvent-free mixture was heated at 120 °C for 4 h under vigorous stirring. The product was extracted from silica gel with dichloromethane (100 mL). Removal of the solvent under reduced pressure gave rise to 1,14-dimethoxy[5]helicene **38** as an amorphous brown solid.

Single crystals for XRD analysis were grown by layering *n*-hexane on top of a solution of enantiopure **38** in dichloromethane (2:1) overnight at −10 °C.

Yield:	35.91 mg (0.11 mmol, 48 %) over 2 steps
Molecular formula:	$C_{24}H_{18}O_2$
Molecular weight:	338.41 g/mol
Retention factor:	0.64 (cyclohexane/ethyl acetate = 1:1)
EI-MS:	*m*/*z* = 338.1 $[M]^{\bullet+}$, 323.1 $[M\text{-}CH_3]^+$, 308.1 $[M\text{-}C_2H_6]^{\bullet+}$, 276.1 $[M\text{-}C_2H_6O_2]^{\bullet+}$
HRMS ($C_{24}H_{18}O_2^{\bullet+}$):	calculated = 338.1306
	found = 338.1308
Specific optical rotation:	(−)-(*M*)-**38**: $[\alpha]_D^{20} = -1644°$ mL×dm^{-1}×g^{-1} (*c* = 1.17 g/L, dichloromethane)
	(+)-(*P*)-**38**: $[\alpha]_D^{20} = +1634°$ mL×dm^{-1}×g^{-1} (*c* = 0.87 g/L, dichloromethane)
ECD:	(−)-(*M*)-**38**: *λ*/nm (*Δε*/M^{-1}×cm^{-1}) = 249 (−85.6), 260 (−28.5), 267 (−34.3), 280 (+1.3), 294 (−51.5), 321 (−2.5), 340 (−67.9); (*c* = 4.0×10^{-4} g/L, dichloromethane)
	(+)-(*P*)-**38**: *λ*/nm (*Δε*/M^{-1}×cm^{-1}) = 249 (+98.1), 260 (+38.9), 267 (+49.4), 280 (+26.8), 294 (+90.5), 321 (+25.2), 340 (+83.4); (*c* = 4.0×10^{-4} g/L, dichloromethane)
Analytical HPLC:	CHIRALPAK IB-U; *n*-hexane/isopropanol (95:5); *f* = 0.85 mL min^{-1}); (–)-(M)-**38**: t_R = 1.41 min; (+)-(P)-**38**: t_R = 2.22 min
Semipreparative HPLC:	CHIRALPAK IB; *n*-hexane/isopropanol (95:5); *f* = 18 mL min^{-1}); (–)-(M)-**38**: t_R = 6.18 min, 99.3 % *ee*; (+)-(P)-**38**: t_R = 7.47 min, 99.3 % *ee*

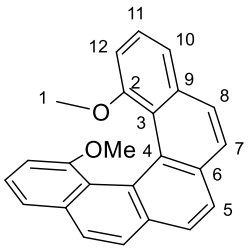

^{1}H-NMR (500 MHz, $CDCl_3$, 298 K):
δ/ppm = 7.97 (s, 2H, H-5), 7.92−7.87 (m, 4H, H-7, H-8), 7.61 (dd, 2H, H-10, $^{3}J_{10,11}$ = 7.9 Hz, $^{4}J_{10,12}$ = 1.2 Hz), 7.48 (t, 2H, H-11, $^{3}J_{11,10}$ = 7.8 Hz, $^{3}J_{11,12}$ = 7.8 Hz), 6.71 (dd, 2H, H-12, $^{3}J_{12,11}$ = 7.8 Hz, $^{4}J_{12,10}$ = 1.2 Hz), 2.86 (s, 6H, H-1).

^{13}C-NMR (500 MHz, $CDCl_3$, 298 K):
δ/ppm = 156.2 (C-2), 132.7 (C-9), 131.5 (C-4), 126.8 (C-6), 126.6 (C-7/C-8), 126.4 (C-7/C-8), 125.7 (C-11), 125.3 (C-5), 124.8 (C-3), 119.8 (C-10), 104.9 (C-12), 53.7 (C-1).

Crystallographic data [(−)-**38**]

Empirical formula: $C_{24}H_{18}O_2$; M = 338.38 g/mol; T = 100.0 K; radiation type: CuKα; λ = 1.54186 Å; crystal system: orthorhombic; space group: $P2_12_12_1$; unit cell: a = 9.3010(4) Å, b = 9.9441(4) Å, c = 18.6907(8) Å, α = 90°, β = 90°, γ = 90°, V = 1728.70(13) Å^3, Z = 4, ρ_{calc} = 1.30 g/cm^3; absorption correction = empirical; μ = 0.643 mm^{-1}; minimum transmission = 0.6605; maximum transmission = 0.7536; F(000) = 712.0; crystal color: clear colorless; crystal size = 0.24×0.16×0.10 mm^3; 2Θ range for data collection: 9.46°−135.42°; Reflections collected [R(int)] = 32887 [0.0296]; Reflections [I>2σ(I)] = 3117; data completeness = 99.5 %; Data/parameters/restraints = 3117/237/0; Goodness-of-fit on F^2 = 1.098; Final R indexes [I>=2σ(I)]: R_1 = 0.0287, wR_2 = 0.0726; Final R indexes [all data]: R_1 = 0.0287, wR_2 = 0.0726; Largest diff. peak/hole = 0.16/−0.24 e Å^{-3}; Flack parameter = 0.03(2).

Crystallographic data [(+)-**38**]

Empirical formula: $C_{24}H_{18}O_2$; M = 338.38 g/mol; T = 100.0 K; radiation type: CuKα; λ = 1.54186 Å; crystal system: orthorhombic; space group: $P2_12_12_1$; unit cell: a = 9.3078(6) Å, b = 9.9410(7) Å, c = 18.6922(13) Å, α = 90°, β = 90°, γ = 90°, V = 1729.6(2) Å^3, Z = 4, ρ_{calc} = 1.30 g/cm^3; absorption correction = empirical; μ = 0.642 mm^{-1}; minimum transmission = 0.6366; maximum transmission = 0.7535; F(000) = 712.0; crystal color: clear colorless; crystal size = 0.31×0.30×0.12 mm^3; 2Θ range for data collection: 9.46°−135.43°; Reflections collected [R(int)] = 19749 [0.0300]; Reflections [I>2σ(I)] = 3092; data completeness = 99.1 %; Data/parameters/restraints = 3092/237/0; Goodness-of-fit on F^2 = 1.124; Final R

indexes [I>=2σ(I)]: R_1 = 0.0313, wR_2 = 0.0777; Final R indexes [all data]: R_1 = 0.0313, wR_2 = 0.0777; Largest diff. peak/hole = 0.16/−0.27 e Å^{-3}; Flack parameter = 0.07(3).

2-[(2-Formyl-5-methoxyphenyl)ethynyl]-3-methoxybenzaldehyde 39

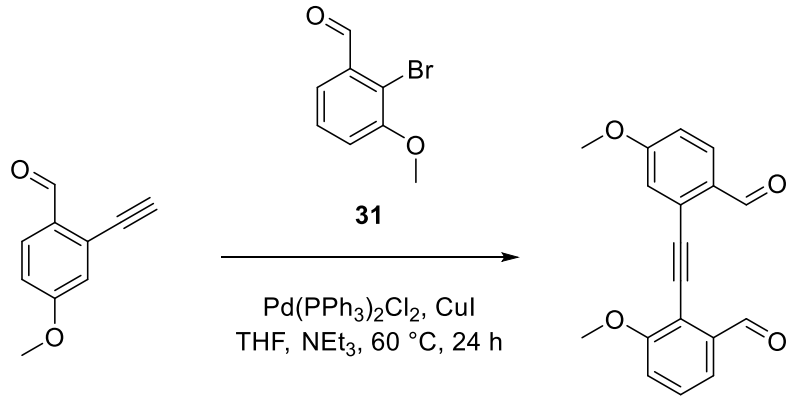

15 **39**

The reaction was carried out under Schlenk conditions. To a Schlenk flask equipped with a magnetic stir bar, 87.64 mg of $PdCl_2(PPh_3)_2$ (4 mol%), 41.61 mg of CuI (7 mol%), 500.0 mg of alkyne **15** (3.12 mmol, 1.0 equiv.) and 738.45 mg of bromide **31** (3.43 mmol, 1.10 equiv.) were added. After adding anhydrous THF (5 mL) and degassed NEt_3 (10 mL), the mixture was heated to 60 °C and stirred for 24 h. The reaction mixture was poured into an aqueous solution of saturated NH_4Cl (40 mL) and then extracted with dichloromethane (3×30 mL). The combined organic portions were washed with brine (150 mL), dried with anhydrous $MgSO_4$ and concentrated under reduced pressure. The crude product was purified by flash chromatography on silica gel (cyclohexane/ethyl acetate = 4:1 to 1:0) to obtain dialdehyde **39** as a white solid.

Yield:	630.04 mg (2.14 mmol, 69 %)
Molecular formula:	$C_{18}H_{14}O_4$
Molecular weight:	294.31 g/mol
Retention factor:	0.31 (cyclohexane/ethyl acetate = 1:1)
ESI(+)-MS:	m/z = 317.078 $[M+Na]^+$, 295.096 $[M-H]^+$
HRMS ($C_{18}H_{14}O_4H^+$):	calculated = 295.0965
	found = 295.0963

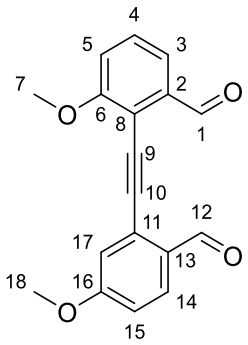

^{1}H-NMR (500 MHz, $CDCl_3$, 298 K):

δ/ppm = 10.63 (d, 1H, H-1, $^{5}J_{1,4}$ = 0.8 Hz), 10.59 (d, 1H, H-12, $^{5}J_{12,15}$ = 0.8 Hz), 7.95 (d, 1H, H-14, $^{3}J_{14,15}$ = 8.7 Hz), 7.58 (dd, 1H, H-3, $^{3}J_{3,4}$ = 7.8 Hz, $^{4}J_{3,5}$ = 1.1 Hz), 7.50−7.45 (m, 1H, H-4), 7.18 (dd, 1H, H-5, $^{3}J_{5,4}$ = 8.2 Hz, $^{4}J_{5,3}$ = 1.1 Hz), 7.13 (d, 1H, H-17, $^{4}J_{17,15}$ = 2.6 Hz), 7.01 (ddd, 1H, H-15, $^{3}J_{15,14}$ = 8.7 Hz, $^{4}J_{15,17}$ = 2.6 Hz, $^{5}J_{15,12}$ = 0.8 Hz), 3.99 (s, 3H, H-7), 3.92 (s, 3H, H-18).

^{13}C-NMR (500 MHz, $CDCl_3$, 298 K):

δ/ppm = 191.4 (C-1), 190.9 (C-12), 163.9 (C-16), 161.4 (C-6), 137.3 (C-2), 130.3 (C-4), 130.1 (C-14), 129.7 (C-13), 128.5 (C-11), 119.8 (C-3), 117.1 (C-17), 116.2 (C-15), 115.8 (C-5), 115.1 (C-8), 96.3 (C-10), 88.0 (C-9), 56.5 (C-7), 56.0 (C-18).

1-[2-((2-(1-Hydroxybut-3-yn-1-yl)-5-methoxyphenyl)ethynyl]-3-methoxyphenyl)but-3-yn-1-ol 40

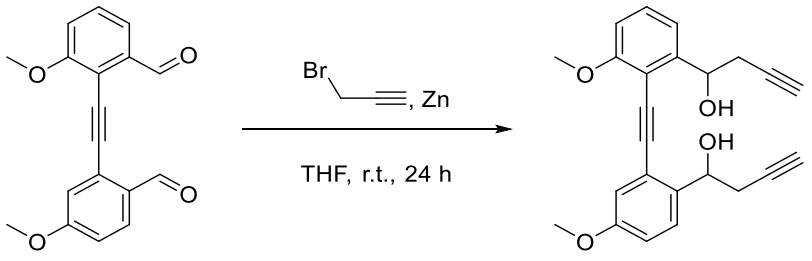

39 **40**

The reaction was carried out under Schlenk conditions. A Schlenk flask equipped with a magnetic stir bar was charged with 444.29 mg of zinc powder (6.80 mmol, 10.0 equiv.). Anhydrous tetrahydrofuran (10 mL) was added, the flask was immersed in a water bath at room temperature and a solution of propargyl bromide (0.76 mL, 80 wt.% in toluene, 6.80 mmol, 10.0 equiv.) was added slowly. The solution was stirred at room temperature for 30 minutes before it was added to the suspension of dialdehyde **39** (200.0 mg, 0.68 mmol, 1.0 equiv.) in anhydrous tetrahydrofuran

(10 mL). After 24 h of stirring, the mixture was poured into water (30 mL) and extracted with dichloromethane (3×40 mL), then the combined organic portions were washed with brine (100 mL) and HCl (100 mL, 6 M in water), dried with anhydrous Mg_2SO_4 and concentrated under reduced pressure. The crude product was used for the subsequent reaction without further purification and analytical characterization.

Yield: n/a

Molecular formula: $C_{24}H_{22}O_4$

Molecular weight: 374.43 g/mol

1-[2-((2-(1-Acetoxybut-3-yn-1-yl)-5-methoxyphenyl)ethynyl]-3-methoxyphenyl)but-3-yn-1-yl acetate 41

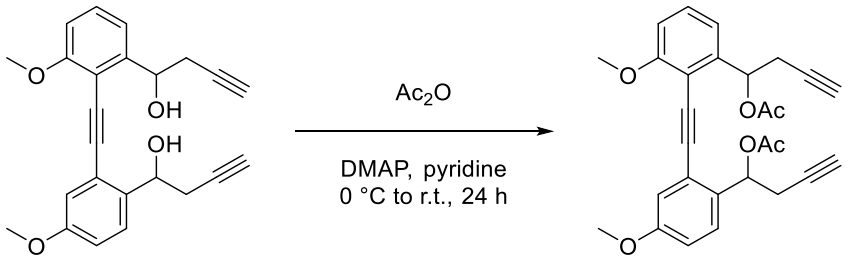

40 **41**

In a round bottomed flask equipped with a magnetic stir bar, a solution of diol **40** (250.0 mg, 0.67 mmol, 1.0 equiv.) and 4-dimethylaminopyridine (9.79 mg, 0.080 mmol, 0.12 equiv.) in anhydrous pyridine (10 mL) was prepared. After adding 0.76 mL of acetic anhydride (8.01 mmol, 12.0 equiv.) at 0 °C while stirring, the reaction mixture was allowed to slowly reach room temperature and stirring was continued at the same temperature for an additional 24 h. The mixture was poured into water (20 mL) and extracted with dichloromethane (3×20 mL), then the combined organic portions were washed with a saturated aqueous solution of $KHCO_3$ (100 mL), dried with anhydrous Mg_2SO_4 and concentrated under reduced pressure. The crude product was purified by flash chromatography on silica gel (cyclohexane/ethyl acetate = 4:1) to afford diacetate **41** as a yellow oil.

Yield: 120.75 mg (0.26 mmol, 39 %) over 2 steps

Molecular formula: $C_{28}H_{26}O_6$

Molecular weight: 458.51 g/mol

Retention factor: 0.22 (cyclohexane/ethyl acetate = 3:1)

ESI(+)-MS: *m*/*z* = 481.162 $[M+Na]^+$, 476.206 $[M+NH_4]^+$

HRMS ($C_{28}H_{26}O_6Na^+$): calculated = 481.1622

found = 481.1619

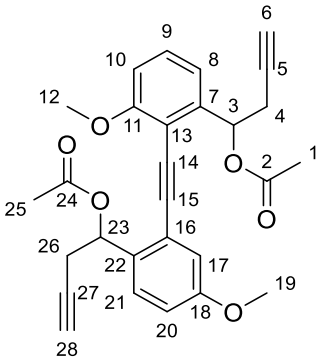

^{1}H-NMR (400 MHz, $CDCl_3$, 298 K):

δ/ppm = 7.44 (dd, 1H, H-21, $^3J_{21,20}$ = 8.7 Hz, $^5J_{21,17}$ = 1.3 Hz), 7.32 (t, 1H, H-9, $^3J_{9,8}$ = 8.1 Hz, $^3J_{9,10}$ = 8.1 Hz), 7.13−7.06 (m, 2H, H-8, H-17), 6.91 (dd, 1H, H-20, $^3J_{20,21}$ = 8.7 Hz, $^4J_{20,17}$ = 2.7 Hz), 6.89−6.85 (m, 1H, H-10), 6.51−6.45 (m, 1H, H-23), 6.42−6.36 (m, 1H, H-3), 3.95 (s, 3H, H-12), 3.83 (s, 3H, H-19), 3.04−2.77 (m, 4H, H-4, H-26), 2.15 (d, 3H, H-1/H-25, $^5J_{1,3}$ = 0.6 Hz/$^5J_{25,23}$ = 0.6 Hz), 2.14 (d, 3H, H-1/H-25, $^5J_{1,3}$ = 0.8 Hz/$^5J_{25,23}$ = 0.8 Hz), 2.01−1.98 (m, 1H, H-6/H28), 1.97−1.95 (m, 1H, H-6/H28).

^{13}C-NMR (400 MHz, $CDCl_3$, 298 K):

δ/ppm = 169.9 (C-2, C-24), 160.9 (C-11), 159.0 (C-18), 142.2 (d, C-7), 133.2 (d, C-22), 129.8 (d, C-9), 127.4 (d, C-21), 122.3 (d, C-16), 117.7 (d, C-8), 116.5 (d, C-17), 115.4 (d, C-20), 110.7 (d, C-13), 110.2 (d, C-10), 96.8 (d, C-15), 88.3 (d, C-14), 80.2 (d, C-27), 79.8 (d, C-5), 71.9 (d, C-3), 71.5 (d, C-23), 70.7 (d, C-28), 70.5 (d, C-6), 56.1 (d, C-12), 55.6 (C-19), 25.8 (d, C-26), 25.4 (d, C-4), 21.3 (C-1/C-25), 21.2 (C-1/C-25).

1,13-Dimethoxy-5,6,9,10-tetrahydropentahelicene-5,10-diyl diacetate 42

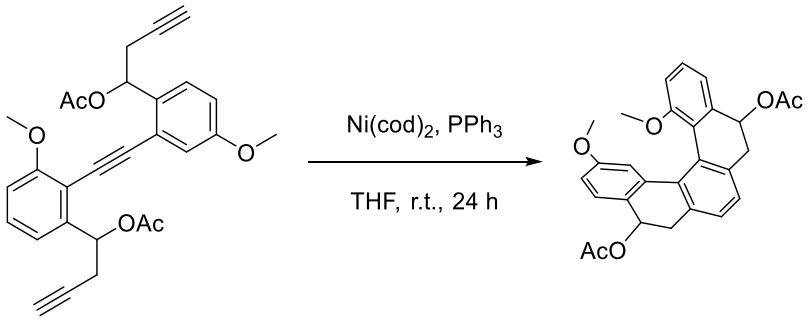

41 **42**

The reaction was carried out under Schlenk conditions. In a Schlenk flask equipped with a magnetic stir bar, 120.0 mg of triyne **41** (0.26 mmol, 1.0 equiv.) and 137.29 mg of PPh_3 (0.52 mmol, 2.0 equiv.) were dissolved in anhydrous THF (5 mL). After adding a stock solution of $Ni(cod)_2$ (4.37 mL, 0.06 M in THF, 1.0 equiv.), the mixture was stirred at room temperature for 24 h. The solvent was evaporated under reduced pressure and the residue was subjected to flash chromatography on silica gel (cyclohexane/ethyl acetate = 4:1) to afford tetrahydrohelicene derivative **42** as a complex mixture of stereoisomers. The mixture was used for the subsequent reaction without further analytical characterization.

Yield: n/a

Molecular formula: $C_{28}H_{26}O_6$

Molecular weight: 458.51 g/mol

Retention factor: 0.20 (cyclohexane/ethyl acetate = 4:1)

1,13-Dimethoxypentahelicene 43

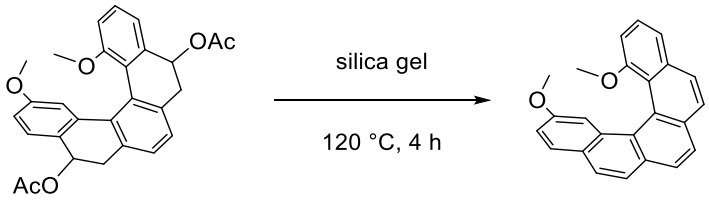

42 **43**

In a round bottomed flask equipped with a magnetic stir bar, a solution of tetrahydro[5]helicene derivative **42** (120.0 mg, 0.26 mmol, 1.0 equiv.) in dichloromethane (5 mL) was prepared. After adding silica gel (200 mg), the solvent was evaporated under reduced pressure and the solvent-free mixture was heated at

120 °C for 4 h under vigorous stirring. The product was extracted from silica gel with dichloromethane (100 mL). Removal of the solvent under reduced pressure gave rise to 1,13-dimethoxypentahelicene **43** as an amorphous yellow solid.

Yield:	60.48 mg (0.18 mmol, 68 %) over 2 steps
Molecular formula:	$C_{24}H_{18}O_2$
Molecular weight:	338.41 g/mol
Retention factor:	0.39 (cyclohexane/ethyl acetate = 4:1)
EI-MS:	m/z = 338.1 $[M]^{\bullet+}$, 276.1 $[M\text{-}C_2H_6O_2]^{\bullet+}$
HRMS ($C_{24}H_{18}O_2^{\bullet+}$):	calculated = 338.1306
	found = 338.1308

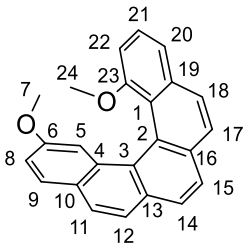

^{1}H-NMR (400 MHz, $CDCl_3$, 298 K):
δ/ppm = 7.95−7.88 (m, 4H, H-14, H-15, H-17, H-18), 7.88−7.83 (m, 2H, H-9, H-11), 7.78 (d, 1H, H-12, $^3J_{12,11}$ = 8.5 Hz), 7.64 (dd, 1H, H-20, $^3J_{20,21}$ = 7.9 Hz, $^4J_{20,22}$ = 1.2 Hz), 7.55 (t, 1H, H-21, $^3J_{21,20}$ = 7.8 Hz, $^3J_{21,22}$ = 7.8 Hz), 7.52 (d, 1H, H-5, $^4J_{5,8}$ = 2.5 Hz), 7.15 (dd, 1H, H-8, $^3J_{8,9}$ = 8.7 Hz, $^4J_{8,5}$ = 2.5 Hz), 6.85 (dd, 1H, H-22, $^3J_{22,21}$ = 7.7 Hz, $^4J_{22,20}$ = 1.2 Hz), 3.40 (s, 3H, H-7), 3.06 (s, 3H, H-24).

^{13}C-NMR (400 MHz, $CDCl_3$, 298 K):
δ/ppm = 157.3 (C-6), 156.7 (C-23), 134.5 (C-4/C-19), 134.4 (C-4/C-19), 132.5*, 131.1 (C-3/C-10), 129.1 (C-9), 128.2*, 127.5*, 127.2*, 126.8 (C-11), 126.7*, 126.6 (C-21), 126.4*, 125.8 (C-3/C-10), 123.8 (C-12), 123.3*, 122.0 (C-1), 120.3 (C-20), 117.5 (C-8), 106.3 (C-22), 104.8 (C-5), 54.7 (C-7), 54.1 (C-24).

*The signal could not be unambiguously assigned.

1-Bromo-3,4-dihydro-7-methoxy-2-naphthalenecarboxaldehyde 45

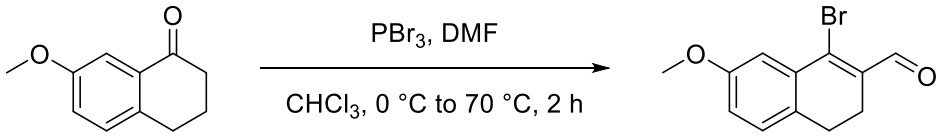

44 **45**

In a round bottomed flask equipped with a magnetic stir bar, 10.19 mL of *N*,*N*-dimethylformamide (131.65 mmol, 2.55 equiv.) were added dropwise to solution of phosphorus tribromide (10.99 mL, 115.76 mmol, 2.55 equiv.) in chloroform (85 mL) at 0 °C and the mixture was stirred at this temperature for 2 h. A solution of 7-methoxytetralone **44** (8.0 g, 45.39 mmol, 1.0 equiv.) in chloroform (15 mL) was added at 0 °C and the mixture was stirred at 70 °C for 2 h. The mixture was slowly cooled down to room temperature, poured into a saturated aqueous solution of $NaHCO_3$ (150 mL) and extracted with dichloromethane (5×40 mL). The combined organic portions were dried with anhydrous Mg_2SO_4 and concentrated under reduced pressure. The crude product was purified by flash chromatography on silica gel (cyclohexane/ethyl acetate = 20:1) to afford bromide **45** as a yellow solid.

Yield: 3.60 g (13.57 mmol, 29 %)

Molecular formula: $C_{12}H_{11}BrO_2$

Molecular weight: 267.12 g/mol

Retention factor: 0.45 (cyclohexane/ethyl acetate = 4:1)

^{1}H-NMR (400 MHz, $CDCl_3$, 298 K):
δ/ppm = 10.25 (s, 1H), 7.46 (d, 1H, *J* = 2.6 Hz), 7.11 (d, 1H, *J* = 8.2 Hz), 6.90 (dd, 1H, *J* = 8.2 Hz, *J* = 2.6 Hz), 3.83 (s, 3H), 2.81−2.74 (m, 2H), 2.65−2.57 (m, 2H).

The spectral data were in agreement with those previously reported for this compound.[348]

1-Bromo-7-methoxy-2-naphthalenecarboxaldehyde 46

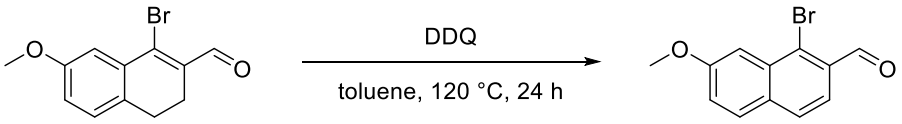

45 **46**

In a two-necked flask equipped with a magnetic stir bar, 3.60 g of bromide **45** (13.57 mmol, 1.0 equiv.) were dissolved in toluene (20 mL). After adding 19.12 g of 2,3-dichloro-5,6-dicyano-1,4-benzoquinone (84.23 mmol, 6.25 equiv.), the mixture was stirred at 120 °C for 24 h. The mixture was slowly cooled down to room temperature, filtered over a plug of silica gel and washed with dichloromethane (500 mL). The solvent was evaporated under reduced pressure and the residue was subjected to flash chromatography on silica gel (cyclohexane/ethyl acetate = 100:1 to 10:3) to obtain aldehyde **46** as a yellow solid.

Yield: 3.15 g (11.88 mmol, 88 %)

Molecular formula: $C_{12}H_9BrO_2$

Molecular weight: 265.11 g/mol

Retention factor: 0.40 (cyclohexane/ethyl acetate = 4:1)

^{1}H-NMR (300 MHz, $CDCl_3$, 298 K):
δ/ppm = 10.66 (s, 1H), 7.82−7.72 (m, 4H), 7.33 (dd, 1H, *J* = 8.9 Hz, *J* = 2.5 Hz), 4.02 (s, 3H).

The spectral data were in agreement with those previously reported for this compound.[171]

Attempts to synthesize 1,1'-(ethyne-1,2-diyl)bis(7-methoxy-2-naphthalenecarboxaldehyde) 47

Approach A

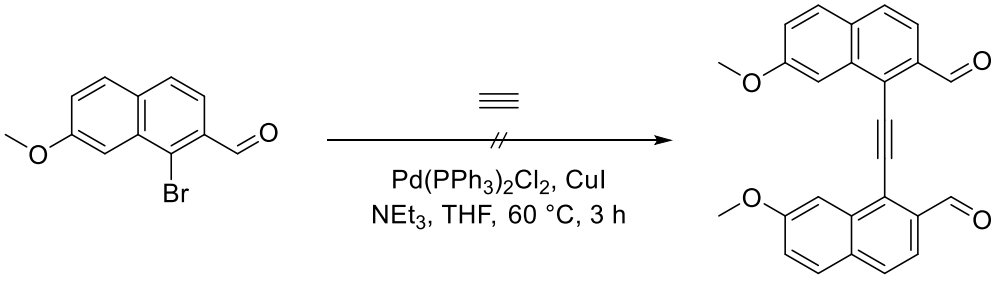

46 **47**

The reaction was carried out under Schlenk conditions. A Schlenk flask equipped with a magnetic stir bar was charged with 200.0 mg of bromide **46** (9.30 mmol, 1.0 equiv.), 21.18 mg of $PdCl_2(PPh_3)_2$ (4 mol%) and 2.87 mg of CuI (2 mol%). The atmosphere was evacuated and flushed with gaseous acetylene using a balloon. A solution of degassed triethylamine (15 mL) and anhydrous THF (5 mL) was added under stirring at room temperature. Then the mixture was heated to 60 °C and stirred for 3 h. The reaction mixture was poured into an aqueous solution of saturated NH_4Cl (40 mL) and then extracted with dichloromethane (3×30 mL). The combined organic portions were washed with brine (150 mL), dried with anhydrous $MgSO_4$ and concentrated under reduced pressure. The residue was subjected to flash chromatography on silica gel (cyclohexane/ethyl acetate = 9:1 to 1:1). The product could not be isolated.

Approach B

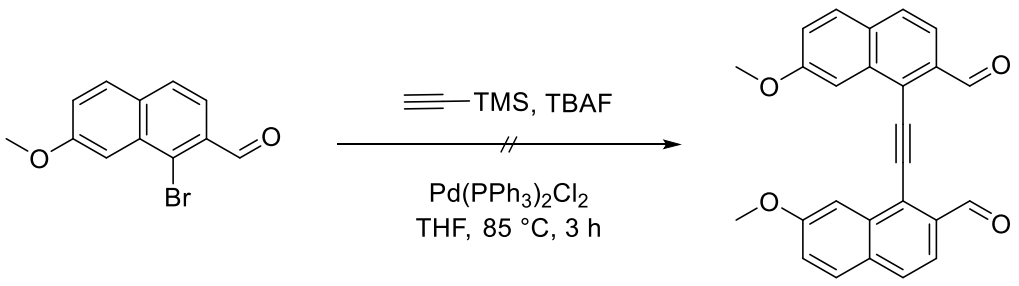

46 **47**

The reaction was carried out under Schlenk conditions. A pressure tube equipped with a magnetic stir bar was charged with 1.0 g of bromide **46** (3.77 mmol, 1.0 equiv.) and 132.37 mg of $PdCl_2(PPh_3)_2$ (5 mol%). Using counterflow technique, a stock solution of

tetra-*n*-butylammonium fluoride (22.63 mL, 1.0 M in THF, 6.0 equiv.) and 0.53 mL of trimethylsilylacetylene (3.77 mmol, 1.0 equiv.) were added. The pressure tube was closed and the mixture was stirred at 85 °C for 3 h. After cooling to room temperature, the reaction mixture was poured into an aqueous solution of saturated NH_4Cl (40 mL) and then extracted with dichloromethane (3×30 mL). The combined organic portions were washed with brine (150 mL), dried with anhydrous $MgSO_4$ and concentrated under reduced pressure. The residue was subjected to flash chromatography on silica gel (cyclohexane/ethyl acetate = 9:1 to 1:1). The product could not be isolated.

Approach C

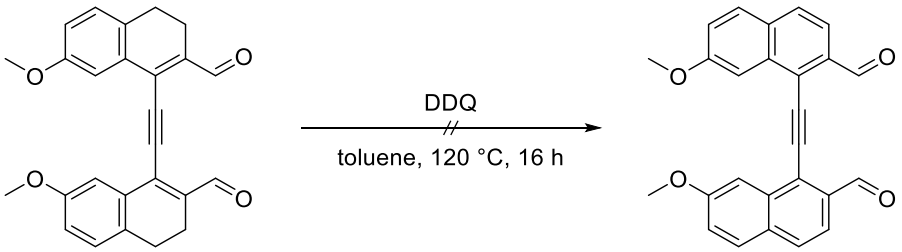

50 **47**

The reaction was carried out under Schlenk conditions. In a two-necked flask equipped with a magnetic stir bar, 100.0 mg of dialdehyde **50** (0.25 mmol, 1.0 equiv.) were dissolved in anhydrous toluene (20 mL). After adding 125.33 mg of 2,3-dichloro-5,6-dicyano-1,4-benzoquinone (0.55 mmol, 2.20 equiv.), the mixture was stirred at 120 °C for 16 h. The mixture was slowly cooled down to room temperature and filtered over a plug of silica gel. The solvent was evaporated under reduced pressure and the residue was subjected to flash chromatography on silica gel (cyclohexane/ethyl acetate = 9:1 to 1:1). The product could not be isolated.

3,4-Dihydro-7-methoxy-1-((trimethylsilyl)ethynyl)-2-naphthalenecarboxaldehyde 48

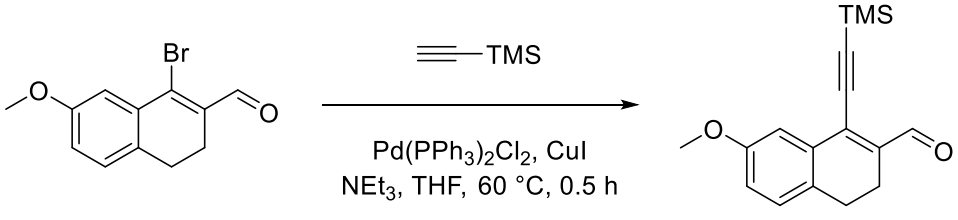

45 **48**

The reaction was carried out under Schlenk conditions. In a Schlenk flask equipped with a magnetic stir bar, 106.42 mg of $PdCl_2(PPh_3)_2$ (3 mol%), 67.37 mg of CuI (7 mol%) and 1.35 g of bromide **45** (5.05 mmol, 1.0 equiv.) were dissolved in anhydrous THF (5 mL) and degassed NEt_3 (10 mL). After adding 1.08 mL of trimethylsilylacetylene (7.58 mmol, 1.50 equiv.), the mixture was stirred at 60 °C for 0.5 h. The reaction mixture was poured into a saturated solution of aqueous NH_4Cl (20 mL) and extracted with DCM (3×30 mL). The combined organic portions were washed with brine (150 mL), dried with anhydrous $MgSO_4$ and concentrated under reduced pressure. The crude product was purified by flash chromatography on silica gel (cyclohexane/ethyl acetate = 9:1). Alkyne **48** was obtained as a yellow solid.

Yield:	1.45 g (5.09 mmol, 100 %)
Molecular formula:	$C_{17}H_{20}O_2Si$
Molecular weight:	284.43 g/mol
Retention factor:	0.40 (cyclohexane/ethyl acetate = 4:1)
APCI-MS:	*m*/*z* = 285.130 $[M+H]^+$
HRMS ($C_{17}H_{20}O_2SiH^+$):	calculated = 285.1305
	found = 285.1301

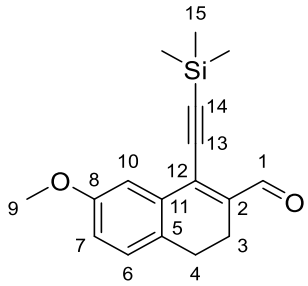

^{1}H-NMR (500 MHz, $CDCl_3$, 298 K):

δ/ppm = 10.40 (s, 1H, H-1), 7.41 (d, 1H, H-10, $^4J_{10,7}$ = 2.7 Hz), 7.11 (d, 1H, H-6, $^3J_{6,7}$ = 8.3 Hz), 6.89 (dd, 1H, H-7, $^3J_{7,6}$ = 8.3 Hz, $^4J_{7,10}$ = 2.7 Hz), 3.85 (s, 3H, H-9), 2.74 (t, 2H, H-4, $^3J_{4,3}$ = 8.1 Hz), 2.57 (t, 2H, H-3, $^3J_{3,4}$ = 8.1 Hz), 0.31 (s, 9H, H-15).

^{13}C-NMR (500 MHz, $CDCl_3$, 298 K):

δ/ppm = 192.7 (C-1), 158.6 (C-8), 141.7 (C-2), 136.0 (C-12), 133.1 (C-11), 129.8 (C-5), 128.7 (C-6), 116.5 (C-7), 112.6 (C-10), 108.0 (C-14), 98.1 (C-13), 55.5 (C-9), 25.9 (C-4), 20.3 (C-3), -0.1 (C-15).

3,4-Dihydro-1-ethynyl-7-methoxy-2-naphthalenecarboxaldehyde 49

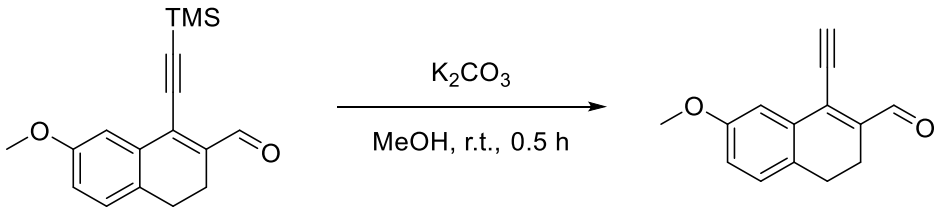

48 **49**

In a round bottomed flask equipped with a magnetic stir bar, 1.45 g of aldehyde **48** (6.24 mmol, 1.0 equiv.) were dissolved in methanol (20 mL) and dichloromethane (20 mL), then 1.21 g of K_2CO_3 (8.73 mmol, 1.40 equiv.) were added in batches. The mixture was stirred at room temperature for 0.5 h. The reaction mixture was poured into water (30 mL) and extracted with DCM (3×30 mL). The combined organic portions were dried with anhydrous $MgSO_4$ and concentrated under reduced pressure. The crude product was purified by flash chromatography on silica gel (cyclohexane/ethyl acetate = 5:1). Aldehyde **49** was obtained as a yellow solid.

Yield:	1.02 g (4.80 mmol, 77 %)
Molecular formula:	$C_{14}H_{12}O_2$
Molecular weight:	212.24 g/mol
Retention factor:	0.55 (cyclohexane/ethyl acetate = 4:1)
ESI(+)-MS:	*m*/*z* = 213.091 $[M+H]^+$
HRMS ($C_{14}H_{12}O_2H^+$):	calculated = 213.0910
	found = 213.0908

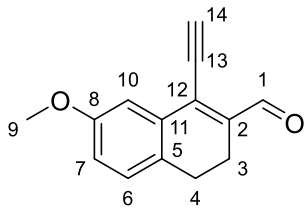

^{1}H-NMR (500 MHz, $CDCl_3$, 298 K):

δ/ppm = 10.40 (s, 1H, H-1), 7.41 (d, 1H, H-10, $^{4}J_{10,7}$ = 2.7 Hz), 7.12 (d, 1H, H-6, $^{3}J_{6,7}$ = 8.2 Hz), 6.90 (dd, 1H, H-7, $^{3}J_{7,6}$ = 8.2 Hz, $^{4}J_{7,10}$ = 2.7 Hz), 3.85 (s, 3H, H-9), 3.70 (s, 1H, H-14), 2.76 (t, 2H, H-4, $^{3}J_{4,3}$ = 8.1 Hz), 2.58 (t, 2H, H-3, $^{3}J_{3,4}$ = 8.1 Hz).

^{13}C-NMR (500 MHz, $CDCl_3$, 298 K):

δ/ppm = 192.3 (C-1), 158.7 (C-8), 142.8 (C-2), 134.9 (C-12), 132.9 (C-11), 129.7 (C-5), 128.8 (C-6), 116.4 (C-7), 112.8 (C-10), 89.0 (C-14), 77.2 (C-13)*, 55.6 (C-9), 25.9 (C-4), 20.4 (C-3).

*The signal was only visible in the HMBC-NMR.

1,1'-(Ethyne-1,2-diyl)bis(3,4-dihydro-7-methoxy-2-naphthalenecarboxaldehyde)

50

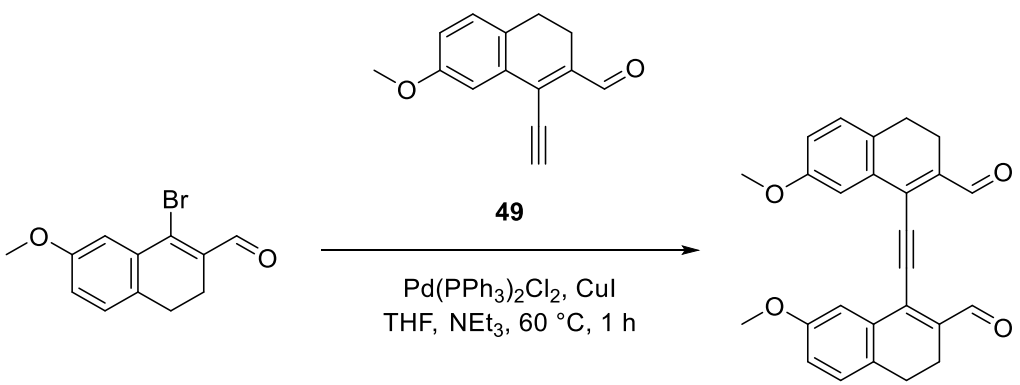

45 **50**

The reaction was carried out under Schlenk conditions. To a Schlenk flask equipped with a magnetic stir bar, 106.42 mg of $PdCl_2(PPh_3)_2$ (3 mol%), 67.37 mg of CuI (7 mol%), 1.35 g of bromide **45** (5.05 mmol, 1.0 equiv.) and 1.07 g of alkyne **49** (5.05 mmol, 1.0 equiv.) were added. After adding anhydrous THF (5 mL) and degassed NEt_3 (10 mL), the mixture was heated to 60 °C and stirred for 1 h until the precipitation of a yellow solid was observed. The reaction mixture was concentrated under reduced pressure. The crude product was recrystallized (ethyl acetate) and

washed with water (500 mL), acetone (500 mL) and dichloromethane (500 mL) to obtain dialdehyde **50** as yellow needles.

Yield:	1.65 g (4.14 mmol, 82 %)
Molecular formula:	$C_{26}H_{22}O_4$
Molecular weight:	398.45 g/mol
Retention factor:	0.40 (cyclohexane/ethyl acetate = 2:1)
ESI(+)-MS:	m/z = 399.158 $[M+H]^+$
HRMS ($C_{26}H_{22}O_4H^+$):	calculated = 399.1591
	found = 399.1581

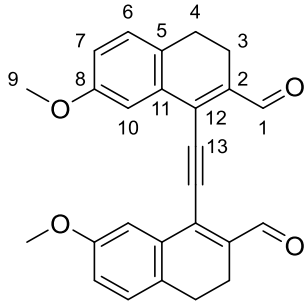

^{1}H-NMR (500 MHz, $CDCl_3$, 298 K):
δ/ppm = 10.51 (s, 2H, H-1), 7.41 (d, 2H, H-10, $^4J_{10,7}$ = 2.6 Hz), 7.17 (d, 2H, H-6, $^3J_{6,7}$ = 8.3 Hz), 6.93 (dd, 2H, H-7, $^3J_{7,6}$ = 8.3 Hz, $^4J_{7,10}$ = 2.6 Hz), 3.81 (s, 6H, H-9), 2.82 (t, 4H, H-4, $^3J_{4,3}$ = 8.0 Hz), 2.67 (t, 4H, H-3, $^3J_{3,4}$ = 8.0 Hz).

^{13}C-NMR (500 MHz, $CDCl_3$, 298 K):
δ/ppm = 191.2 (C-1), 158.9 (C-8), 143.0 (C-2), 134.9 (C-12), 132.9 (C-11), 129.8 (C-5), 129.1 (C-6), 116.8 (C-7), 112.5 (C-10), 94.1 (C-13), 55.6 (C-9), 25.4 (C-4), 20.8 (C-3).

1,1'-(Ethyne-1,2-diylbis(3,4-dihydro-7-methoxy-naphthalene-1,2-diyl))bis(but-3-yn-1-ol) 51

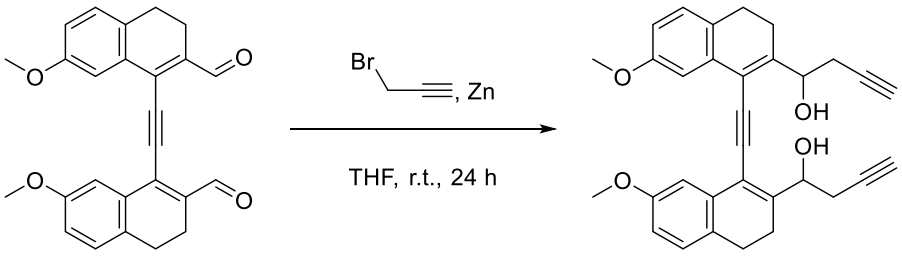

50 **51**

The reaction was carried out under Schlenk conditions. A Schlenk flask equipped with a magnetic stir bar was charged with 656.34 mg of zinc powder (10.03 mmol, 10.0 equiv.). Anhydrous tetrahydrofuran (10 mL) was added, the flask was immersed in a water bath at room temperature and a solution of propargyl bromide (1.11 mL, 80 wt.% in toluene, 10.03 mmol, 10.0 equiv.) was added slowly. The solution was stirred at room temperature for 30 minutes before it was added to the suspension of dialdehyde **50** (400.0 mg, 1.0 mmol, 1.0 equiv.) in anhydrous tetrahydrofuran (10 mL). After 24 h of stirring, the mixture was poured into water (50 mL) and extracted with dichloromethane (3×40 mL), then the combined organic portions were washed with brine (200 mL) and HCl (200 mL, 6 M in water), dried with anhydrous Mg_2SO_4 and concentrated under reduced pressure. The crude product was purified by flash chromatography on silica gel (cyclohexane/ethyl acetate = 1:1) to obtain diol **51** as a yellow oil. The diol could not completely be isolated and had some minor impurities, nonetheless it was used for the subsequent reaction.

Yield:	218.29 mg (0.45 mmol, 45 %)
Molecular formula:	$C_{32}H_{30}O_4$
Molecular weight:	478.58 g/mol
Retention factor:	0.53, 0.48 (cyclohexane/ethyl acetate = 1:1)
ESI(+)-MS:	m/z = 496.247 $[M+NH_4]^+$
HRMS ($C_{32}H_{30}O_4NH_4^+$):	calculated = 496.2482
	found = 496.2472

[Ethyne-1,2-diylbis(3,4-dihydro-7-methoxy-naphthalene-1,2-diyl)]bis(but-3-yne-1,1-diyl) diacetate 52

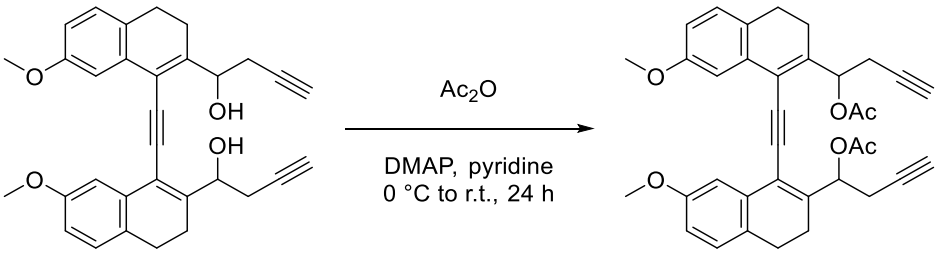

51 **52**

In a round bottomed flask equipped with a magnetic stir bar, a solution of diol **51** (218.29 mg, 0.45 mmol, 1.0 equiv.) and 4-dimethylaminopyridine (6.68 mg, 0.054 mmol, 0.12 equiv.) in anhydrous pyridine (5 mL) was prepared. After adding 0.51 mL of acetic anhydride (5.47 mmol, 12.0 equiv.) at 0 °C while stirring, the reaction mixture was allowed to slowly reach room temperature and stirring was continued at the same temperature for an additional 24 h. The mixture was poured into water (20 mL) and extracted with dichloromethane (3×30 mL), then the combined organic portions were washed with a saturated aqueous solution of $KHCO_3$ (100 mL), dried with anhydrous Mg_2SO_4 and concentrated under reduced pressure. The crude product was purified by flash chromatography on silica gel (cyclohexane/ethyl acetate = 8:1) to afford diacetate **52** as a yellow oil.

Yield:	188.71 mg (0.33 mmol, 73 %)
Molecular formula:	$C_{36}H_{34}O_6$
Molecular weight:	562.66 g/mol
Retention factor:	0.25, 0.30 (cyclohexane/ethyl acetate = 4:1)
ESI(+)-MS:	*m*/*z* = 585.225 $[M+Na]^+$
HRMS ($C_{36}H_{34}O_6Na^+$):	calculated = 585.2253
	found = 585.2250

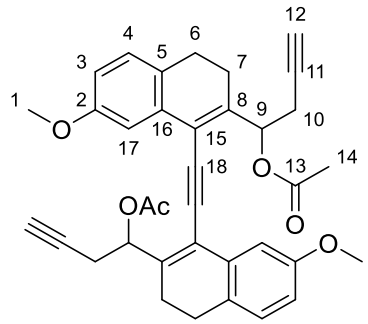

^{1}H-NMR (400 MHz, $CDCl_3$, 298 K):

δ/ppm = 7.37 (d, 2H, H-17, $^{4}J_{17,3}$ = 2.6 Hz), 7.06 (d, 2H, H-4, $^{3}J_{4,3}$ = 8.2 Hz), 6.75 (dd, 2H, H-3, $^{3}J_{3,4}$ = 8.2 Hz, $^{4}J_{3,17}$ = 2.6 Hz), 6.26 (t, 2H, H-9, $^{3}J_{9,10}$ = 6.4 Hz), 3.79 (s, 6H, H-1), 2.89−2.70 (m, 8H, H-6, H-10), 2.62−2.36 (m, 4H, H-7), 2.10 (s, 6H, H-14), 2.02 (t, 2H, H-12, $^{4}J_{12,10}$ = 2.6 Hz).

^{13}C-NMR (400 MHz, $CDCl_3$, 298 K):

δ/ppm = 169.8 (d, C-13), 158.7 (d, C-2), 144.3 (d, C-8), 134.0 (d, C-16), 128.1 (C-4), 127.3 (d, C-5), 119.6 (d, C-15), 113.5 (d, C-3), 111.7 (d, C-17), 92.2 (d, C-18), 79.4 (C-11), 73.3 (d, C-9), 71.1 (d, C-12), 55.6 (d, C-1), 26.6 (d, C-6), 23.5 (d, C-7/C-10), 23.4 (C-7/C-10), 20.9 (C-14).

2,17-Dimethoxy-5,6,7,8,11,12,13,14-octahydroheptahelicene-7,12-diyl diacetate 53

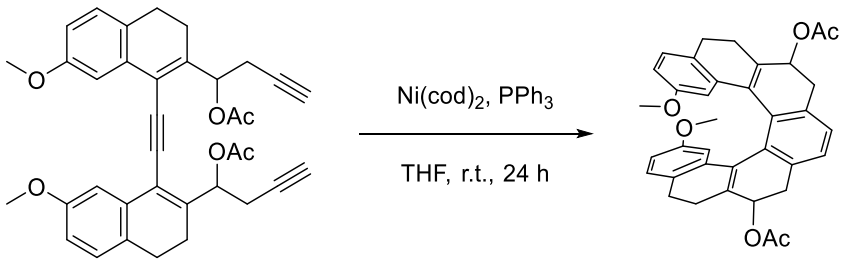

52 **53**

The reaction was carried out under Schlenk conditions. In a Schlenk flask equipped with a magnetic stir bar, 400.0 mg of triyne **52** (0.71 mmol, 1.0 equiv.) and 372.92 mg of PPh_3 (1.42 mmol, 2.0 equiv.) were dissolved in anhydrous THF (10 mL). After adding a stock solution of $Ni(cod)_2$ (11.87 mL, 0.06 M in THF, 1.0 equiv.), the mixture was stirred at room temperature for 24 h. The solvent was evaporated under reduced pressure and the residue was subjected to flash chromatography on silica gel (cyclohexane/ethyl acetate = 8:1) to afford octahydro[7]helicene derivative **53** as a

complex mixture of stereoisomers. The mixture was used for the subsequent reaction without further analytical characterization.

Yield: n/a

Molecular formula: $C_{36}H_{34}O_6$

Molecular weight: 562.66 g/mol

Retention factor: 0.60, 0.50, 0.45 (cyclohexane/ethyl acetate = 4:1)

2,17-Dimethoxy-5,6,13,14-tetrahydroheptahelicene 54

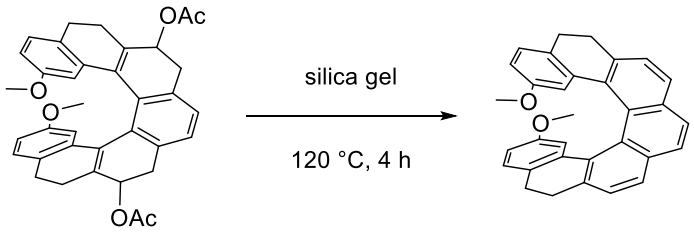

53 **54**

In a round bottomed flask equipped with a magnetic stir bar, a solution of octahydro[7]helicene derivative **53** (50.0 mg, 0.089 mmol, 1.0 equiv.) in dichloromethane (5 mL) was prepared. After adding silica gel (200 mg), the solvent was evaporated under reduced pressure and the solvent-free mixture was heated at 120 °C for 4 h under vigorous stirring. The crude product was extracted from silica gel with dichloromethane (100 mL) and subjected to flash chromatography on silica gel (petroleum ether/ethyl acetate = 100:1) to afford tetrahydro[7]helicene derivative **54** as a yellow solid.

Yield: 30.05 mg (0.067 mmol, 10 %) over 2 steps

Molecular formula: $C_{32}H_{26}O_2$

Molecular weight: 442.55 g/mol

Retention factor: 0.50 (cyclohexane/ethyl acetate = 4:1)

ESI(+)-MS: m/z = 443.200 $[M+H]^+$

HRMS ($C_{32}H_{26}O_2H^+$): calculated = 443.2011

found = 443.2002

Analytical HPLC: (*S*,*S*)-Whelk-O-1; *n*-hexane/dichloromethane (85:15); *f* = 1.0 mL min^{-1}); (–)-(M)-**54**: t_R = 6.94 min; (+)-(P)-**54**: t_R = 9.47 min

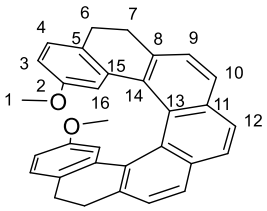

^{1}H-NMR (500 MHz, $CDCl_3$, 298 K):
δ/ppm = 7.65 (d, 2H, H-10, $^3J_{10,9}$ = 7.8 Hz), 7.60 (s, 2H, H-12), 7.34 (d, 2H, H-9, $^3J_{9,10}$ = 7.8 Hz), 6.77 (d, 2H, H-4, $^3J_{4,3}$ = 8.1 Hz), 6.47 (d, 2H, H-16, $^4J_{16,3}$ = 2.6 Hz), 6.44 (dd, 2H, H-3, $^3J_{3,4}$ = 8.1 Hz, $^4J_{3,16}$ = 2.6 Hz), 3.39 (s, 6H, H-1), 2.82−2.76 (m, 2H, H-7), 2.53−2.45 (m, 2H, H-7), 2.44−2.32 (m, 4H, H-6).

^{13}C-NMR (500 MHz, $CDCl_3$, 298 K):
δ/ppm = 157.0 (C-2), 137.5 (C-8), 137.1 (C-15), 135.4 (C-5/C-14), 133.5 (C-11/C-13), 129.8 (C-5/C-14), 128.2 (C-4), 127.3 (C-10), 127.0 (C-9), 126.3 (C-12), 126.2 (C-11/C-13), 112.8 (C-3), 110.7 (C-16), 54.5 (C-1), 30.2 (C-7), 27.4 (C-6).

2,17-Dimethoxyheptahelicene 55

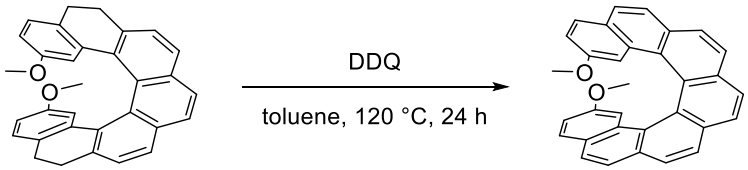

54 **55**

The reaction was carried out under Schlenk conditions. In a two-necked flask equipped with a magnetic stir bar, 115.21 mg of tetrahydro[7]helicene derivative **54** (0.26 mmol, 1.0 equiv.) were dissolved in anhydrous toluene (20 mL). After adding 412.90 mg of 2,3-dichloro-5,6-dicyano-1,4-benzoquinone (1.81 mmol, 7.0 equiv.), the mixture was stirred at 120 °C for 24 h. The mixture was slowly cooled down to room temperature and filtered over a plug of silica gel. The solvent was evaporated under reduced pressure and the residue was subjected to flash chromatography on silica gel

(cyclohexane/ethyl acetate = 100:1 to 10:1) to afford 2,17-dimethoxy[7]helicene **55** as an amorphous yellow solid.

Single crystals for XRD analysis were grown by layering *n*-hexane on top of a solution of racemic **55** in dichloromethane (3:1) overnight at −10 °C.

Yield:	94.84 mg (0.21 mmol, 82 %)
Molecular formula:	$C_{32}H_{22}O_2$
Molecular weight:	438.52 g/mol
Retention factor:	0.45 (cyclohexane/ethyl acetate = 4:1)
APCI-MS:	m/z = 439.169 $[M+H]^+$
HRMS ($C_{32}H_{22}O_2H^+$):	calculated = 439.1693
	found = 439.1687

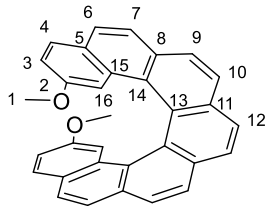

^{1}H-NMR (500 MHz, $CDCl_3$, 298 K):
δ/ppm = 8.07 (s, 2H, H-12), 8.03 (d, 2H, H-10, $^3J_{10,9}$ = 8.2 Hz), 7.92 (d, 2H, H-9, $^3J_{9,10}$ = 8.2 Hz), 7.67 (d, 2H, H-7, $^3J_{7,6}$ = 8.4 Hz), 7.55 (d, 2H, H-6, $^3J_{6,7}$ = 8.4 Hz), 7.29 (d, 2H, H-4, $^3J_{4,3}$ = 8.7 Hz), 6.61 (dd, 2H, H-3, $^3J_{3,4}$ = 8.7 Hz, $^4J_{3,16}$ = 2.5 Hz), 6.51 (d, 2H, H-16, $^4J_{16,3}$ = 2.5 Hz), 3.12 (s, 6H, H-1).

^{13}C-NMR (500 MHz, $CDCl_3$, 298 K):
δ/ppm = 156.7 (C-2), 132.0 (C-11), 131.4 (C-8), 131.0 (C-15), 128.4 (C-4), 128.1 (C-14), 127.5 (C-9), 127.4 (C-6), 127.3 (C-10), 127.1 (C-5), 126.8 (C-12), 125.0 (C-13), 123.2 (C-7), 117.2 (C-3), 104.9 (C-16), 54.0 (C-1).

Crystallographic data [(*rac*)-**55**]

Empirical formula: $C_{32}H_{22}O_2$; M = 438.52 g/mol; T = 100.0 K; radiation type: CuKα; λ = 1.54186 Å; crystal system: monoclinic; space group: $C2/c$; unit cell: a = 32.6415(7) Å, b = 10.10684(12) Å, c = 26.5897(6) Å, α = 90°, β =

90.4944(17)°, γ = 90°, V = 8771.7(3) Å^3, Z = 16, ρ_{calc} = 1.328 g/cm^3; absorption correction = multi-scan; μ = 0.64 mm^{-1}; minimum transmission = 0.6629; maximum transmission = 0.8299; F(000) = 3680.0; crystal color: clear dark yellow; crystal size = 0.32×0.22×0.1 mm^3; 2Θ range for data collection: 6.648°−141.16°; Reflections collected [R(int)] = 107584 [0.0607]; Reflections [I>2σ(I)] = 8369; data completeness = 99.9 %; Data/parameters/restraints = 8369/617/2; Goodness-of-fit on F^2 = 1.058; Final R indexes [I>=2σ(I)]: R_1 = 0.0792, wR_2 = 0.2202; Final R indexes [all data]: R_1 = 0.0868, wR_2 = 0.2269; Largest diff. peak/hole = 0.67/−0.41 e Å^{-3}.

1-[(2-Formyl-5-methoxyphenyl)ethynyl]-7-methoxy-2-naphthaldehyde 56

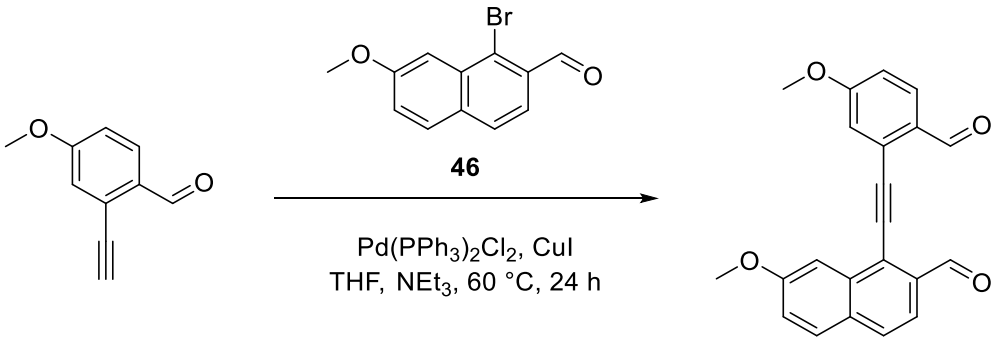

15 **56**

The reaction was carried out under Schlenk conditions. To a Schlenk flask equipped with a magnetic stir bar, 70.11 mg of $PdCl_2(PPh_3)_2$ (4 mol%), 28.53 mg of CuI (6 mol%), 400.0 mg of alkyne **15** (2.49 mmol, 1.0 equiv.) and 728.27 mg of bromide **46** (2.74 mmol, 1.10 equiv.) were added. After adding anhydrous THF (5 mL) and degassed NEt_3 (10 mL), the mixture was heated to 60 °C and stirred for 24 h. The reaction mixture was poured into an aqueous solution of saturated NH_4Cl (40 mL) and then extracted with dichloromethane (3×30 mL). The combined organic portions were washed with brine (150 mL), dried with anhydrous $MgSO_4$ and concentrated under reduced pressure. The crude product was purified by flash chromatography on silica gel (cyclohexane/ethyl acetate = 9:1 to 1:1). The product could not completely be isolated and was used for the subsequent reaction without further purification and analytical characterization.

Yield: 150.05 mg (0.44 mmol, 17 %)

Molecular formula: $C_{22}H_{16}O_4$

Molecular weight: 344.36 g/mol

Retention factor: 0.22 (cyclohexane/ethyl acetate = 3:1)

Attempt to synthesize 1-(1-((2-(1-acetoxybut-3-yn-1-yl)-5-methoxyphenyl)ethynyl)-7-methoxynaphthalen-2-yl)but-3-yn-1-yl acetate 57

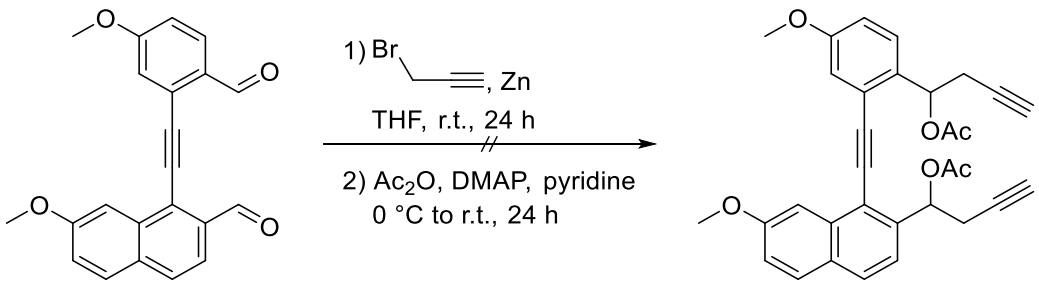

56 **57**

The reaction was carried out under Schlenk conditions. A Schlenk flask equipped with a magnetic stir bar was charged with 284.78 mg of zinc powder (4.36 mmol, 10.0 equiv.). Anhydrous tetrahydrofuran (10 mL) was added, the flask was immersed in a water bath at room temperature and a solution of propargyl bromide (0.48 mL, 80 wt.% in toluene, 4.36 mmol, 10.0 equiv.) was added slowly. The solution was stirred at room temperature for 30 minutes before it was added to the suspension of dialdehyde **56** (150.0 mg, 0.43 mmol, 1.0 equiv.) in anhydrous tetrahydrofuran (5 mL). After 24 h of stirring, 6.39 mg of 4-dimethylaminopyridine (0.052 mmol, 0.12 equiv.), 0.21 mL of anhydrous pyridine (2.61 mmol, 6.0 equiv.) and 0.49 mL of acetic anhydride (5.23 mmol, 12.0 equiv.) were added at 0 °C, the reaction mixture was allowed to slowly reach room temperature and stirring was continued at the same temperature for an additional 24 h. The mixture was poured into water (30 mL) and extracted with dichloromethane (3×20 mL), then the combined organic portions were washed with a saturated aqueous solution of $KHCO_3$ (100 mL), dried with anhydrous Mg_2SO_4 and concentrated under reduced pressure. The residue was subjected to flash chromatography on silica gel (cyclohexane/ethyl acetate = 10:1). The product could not be isolated.

Attempt to synthesize 3,4-dihydro-1-[(2-formyl-5-methoxyphenyl)ethynyl]-7-methoxy-2-naphthalenecarboxaldehyde 58

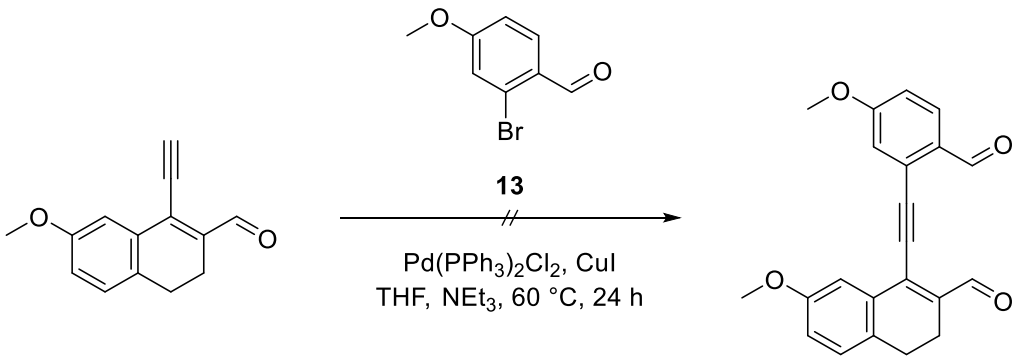

49 **58**

The reaction was carried out under Schlenk conditions. To a Schlenk flask equipped with a magnetic stir bar, 99.20 mg of $PdCl_2(PPh_3)_2$ (3 mol%), 62.80 mg of CuI (7 mol%), 1.0 g of alkyne **49** (4.71 mmol, 1.0 equiv.) and 1.11 g of bromide **13** (5.18 mmol, 1.10 equiv.) were added. After adding anhydrous THF (5 mL) and degassed NEt_3 (10 mL), the mixture was heated to 60 °C and stirred for 24 h. The reaction mixture was poured into an aqueous solution of saturated NH_4Cl (40 mL) and then extracted with dichloromethane (3×30 mL). The combined organic portions were washed with brine (150 mL), dried with anhydrous $MgSO_4$ and concentrated under reduced pressure. The residue was subjected to flash chromatography on silica gel (cyclohexane/ethyl acetate = 9:1). The product could not be isolated.

(1-Bromo-7-methoxynaphthalen-2-yl)methanol 59

Approach A

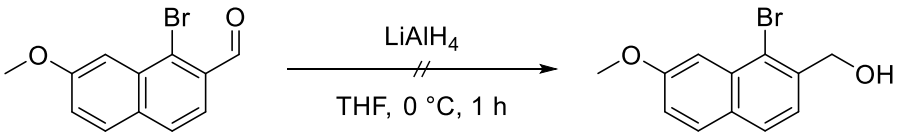

46 **59**

The reaction was carried out under Schlenk conditions. In a Schlenk flask equipped with a magnetic stir bar, a stock solution of lithium aluminium hydride (1.38 mL, 1.0 M in THF, 1.38 mmol, 0.60 equiv.) was added dropwise to a solution of aldehyde **46** (608.0 mg, 2.29 mmol, 1.0 equiv.) in anhydrous THF (10 mL). The reaction mixture was

stirred at 0 °C for 1 h. The reaction mixture was poured into water (20 mL) and extracted with dichloromethane (3×20 mL). The combined organic portions were dried with anhydrous $MgSO_4$ and concentrated under reduced pressure. The residue was subjected to flash chromatography on silica gel (cyclohexane/ethyl acetate = 10:1). The product could not be isolated.

Approach B

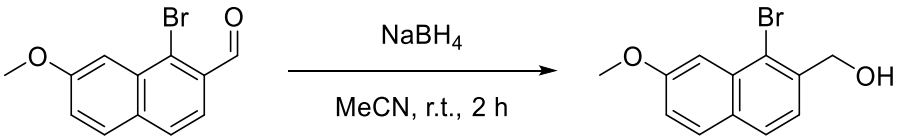

46 **59**

The reaction was carried out under Schlenk conditions. In a Schlenk flask equipped with a magnetic stir bar, 2.50 g of aldehyde **46** (9.43 mmol, 1.0 equiv.) and 713.48 mg of sodium borohydride (18.86 mmol, 2.0 equiv.) were dissolved in anhydrous acetonitrile (20 mL). The reaction mixture was stirred at room temperature for 2 h. The reaction mixture was poured into water (20 mL) and extracted with ethyl acetate (3×20 mL). The combined organic portions were dried with anhydrous $MgSO_4$ and concentrated under reduced pressure. The crude product was purified by flash chromatography on silica gel (cyclohexane/ethyl acetate = 6:1) to obtain alcohol **59** as a white solid.

Yield: 1.72 g (6.42 mmol, 68 %)

Molecular formula: $C_{12}H_{11}BrO_2$

Molecular weight: 267.12 g/mol

Retention factor: 0.20 (cyclohexane/ethyl acetate = 4:1)

^{1}H-NMR (400 MHz, $CDCl_3$, 298 K):
δ/ppm = 7.79−7.71 (m, 2H), 7.59 (d, 1H, *J* = 2.5 Hz), 7.49 (d, 1H, *J* = 8.3 Hz), 7.18 (dd, 1H, *J* = 8.9 Hz, *J* = 2.5 Hz), 4.98 (s, 2H), 3.98 (s, 3H).

The spectral data were in agreement with those previously reported for this compound.[64]

Approach C[64]

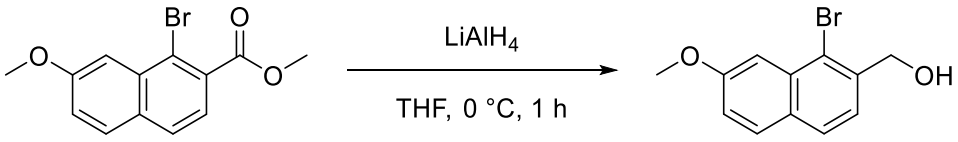

65 **59**

The reaction was carried out under Schlenk conditions. In a Schlenk flask equipped with a magnetic stir bar, a stock solution of lithium aluminium hydride (2.03 mL, 1.0 M in THF, 2.03 mmol, 0.60 equiv.) was added dropwise to a solution of methyl ester **65** (1.0 g, 3.39 mmol, 1.0 equiv.) in anhydrous THF (20 mL). The reaction mixture was stirred at 0 °C for 1 h. The reaction mixture was poured into water (30 mL) and extracted with dichloromethane (3×30 mL). The combined organic portions were dried with anhydrous $MgSO_4$ and concentrated under reduced pressure. The crude product was purified by flash chromatography on silica gel (cyclohexane/ethyl acetate = 10:1) to obtain bromide **59** as a white solid. The product could not completely be isolated and was used for the subsequent reaction without further purification.

Yield: 475.45 mg (1.78 mmol, 52 %)

3,4-Dihydro-7-methoxy-2-naphthalenemethanol 60

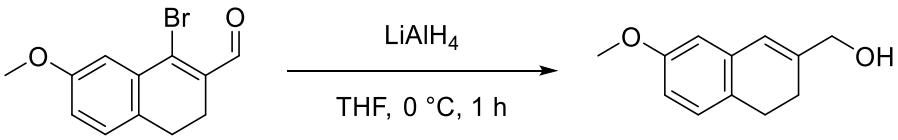

45 **60**

The reaction was carried out under Schlenk conditions. In a Schlenk flask equipped with a magnetic stir bar, a stock solution of lithium aluminium hydride (2.99 mL, 1.0 M in THF, 2.99 mmol, 1.0 equiv.) was added dropwise to a solution of aldehyde **45** (800.0 mg, 2.99 mmol, 1.0 equiv.) in anhydrous THF (10 mL). The reaction mixture was stirred at 0 °C for 1 h. The reaction mixture was poured into water (20 mL) and extracted with dichloromethane (3×20 mL). The combined organic portions were dried with anhydrous $MgSO_4$ and concentrated under reduced pressure. The crude product was purified by flash chromatography on silica gel (cyclohexane/ethyl acetate = 2:1). The product could not completely be isolated and was used for the subsequent reaction without further purification.

Yield: 350.99 mg (1.84 mmol, 61 %)

Molecular formula: $C_{12}H_{14}O_2$

Molecular weight: 190.24 g/mol

Retention factor: 0.43 (cyclohexane/ethyl acetate = 1:2)

EI-MS: *m*/*z* = 190.1 $[M]^{\bullet+}$

3-(Bromomethyl)-1,2-dihydro-6-methoxynaphthalene 61

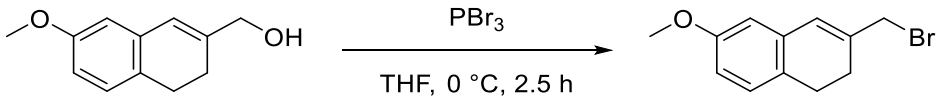

60 **61**

The reaction was carried out under Schlenk conditions. In a Schlenk flask equipped with a magnetic stir bar, 350.0 mg of alcohol **60** (1.84 mmol, 1.0 equiv.) were dissolved in anhydrous THF (10 mL). After adding 0.053 mL of phosphorus tribromide (0.56 mmol, 0.32 equiv.), the reaction mixture was stirred at 0 °C for 2.5 h. The reaction mixture was poured into water (20 mL) and extracted with dichloromethane (3×20 mL). The combined organic portions were dried with anhydrous $MgSO_4$ and concentrated under reduced pressure. The crude product was purified by flash chromatography on silica gel (cyclohexane/ethyl acetate = 6:1) to obtain bromide **61** as a yellow oil.

Yield: 200.51 mg (0.79 mmol, 43 %)

Molecular formula: $C_{12}H_{13}BrO$

Molecular weight: 253.13 g/mol

Retention factor: 0.50 (cyclohexane/ethyl acetate = 4:1)

^{1}H-NMR (500 MHz, $CDCl_3$, 298 K):
δ/ppm = 7.03 (d, 1H, *J* = 8.2 Hz), 6.71 (dd, 1H, *J* = 8.2 Hz, *J* = 2.7 Hz), 6.62 (d, 1H, *J* = 2.7 Hz), 6.53 (s, 1H), 4.16 (s, 2H), 3.78 (s, 3H), 2.80 (t, 2H, *J* = 7.2 Hz), 2.43 (t, 2H, *J* = 7.2 Hz).

The spectral data were in agreement with those previously reported for this compound.[349]

1-Bromo-7-methoxy-2-naphthol 63[182]

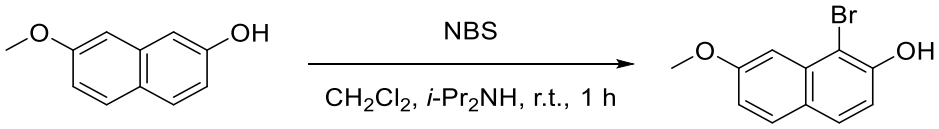

62 **63**

In a round bottomed flask equipped with a magnetic stir bar, 2.0 g of 7-methoxy-2-naphthol **62** (11.48 mmol, 1.0 equiv.) were dissolved in diisopropylamine (0.16 mL) and dichloromethane (10 mL). After adding a solution of *N*-bromosuccinimide (2.04 g, 11.48 mmol, 1.0 equiv.) in dichloromethane (10 mL), the mixture was stirred at room temperature for 1 h. The reaction mixture was poured into water (20 mL) and taken to pH = 1 by addition of concentrated sulfuric acid. The resulting mixture was extracted with dichloromethane (3×10 mL). The combined organic portions were dried with anhydrous $MgSO_4$ and concentrated under reduced pressure. The crude product was purified by flash chromatography on silica gel (cyclohexane/ethyl acetate = 3:1) to obtain bromide **63** as a white solid.

Yield: 2.60 g (10.27 mmol, 89 %)

Molecular formula: $C_{11}H_9O_2Br$

Molecular weight: 253.09 g/mol

Retention factor: 0.36 (cyclohexane/ethyl acetate = 3:1)

^{1}H-NMR (400 MHz, $CDCl_3$, 298 K):
δ/ppm = 7.69−7.64 (m, 2H), 7.32 (d, 1H, *J* = 2.5 Hz), 7.11 (d, 1H, *J* = 8.8 Hz), 7.04 (dd, 1H, *J* = 8.9 Hz, *J* = 2.5 Hz), 5.88 (bs, 1H), 3.97 (s, 3H).

The spectral data were in agreement with those previously reported for this compound.[182]

1-Bromo-7-methoxynaphthalen-2-yl trifluoromethanesulfonate 64[64]

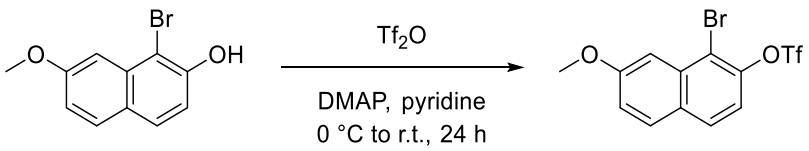

63 **64**

In a round bottomed flask equipped with a magnetic stir bar, a solution of bromide **63** (2.60 g, 10.27 mmol, 1.0 equiv.) and 4-dimethylaminopyridine (62.75 mg, 0.51 mmol, 0.12 equiv.) in anhydrous pyridine (5 mL) was prepared. After adding 2.16 mL of trifluoromethanesulfonic anhydride (12.84 mmol, 1.25 equiv.) at 0 °C while stirring, the reaction mixture was allowed to slowly reach room temperature and stirring was continued for an additional 24 h. The mixture was concentrated under reduced pressure and the crude product was purified by flash chromatography on silica gel (cyclohexane/ethyl acetate = 8:1 to 6:1) to afford triflate **64** as a colorless oil.

Yield: 3.86 g (10.02 mmol, 98 %)

Molecular formula: $C_{12}H_8BrF_3O_4S$

Molecular weight: 385.15 g/mol

Retention factor: 0.44 (cyclohexane/ethyl acetate = 4:1)

^{1}H-NMR (400 MHz, $CDCl_3$, 298 K):
δ/ppm = 7.82−7.76 (m, 2H), 7.56 (d, 1H, *J* = 2.5 Hz), 7.29 (d, 1H, *J* = 8.9 Hz), 7.25 (dd, 1H, *J* = 8.9 Hz, *J* = 2.5 Hz), 3.99 (s, 3H).

The spectral data were in agreement with those previously reported for this compound.[64]

Methyl 1-bromo-7-methoxy-2-naphthalenecarboxylate 65[64]

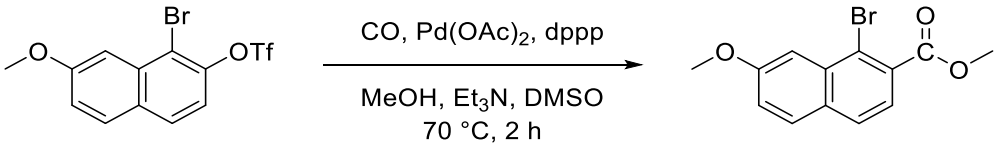

64 **65**

The reaction was carried out under Schlenk conditions. In a Schlenk flask equipped with a magnetic stir bar, 3.86 g of triflate **64** (10.02 mmol, 1.0 equiv.), 112.05 mg of $Pd(OAc)_2$ (5 mol%) and 206.69 mg of dppp (5 mol%) were dissolved in anhydrous DMSO (20 mL), degassed methanol (40 mL) and degassed triethylamine (3 mL). Carbon monoxide, which was generated by careful addition of formic acid to concentrated sulfuric acid, was bubbled through the solution *via* a syringe while the mixture was stirred at 70 °C for 2 h. The reaction mixture was poured into water (100 mL) and extracted with diethyl ether (4×50 mL). The combined organic portions

were dried with anhydrous $MgSO_4$ and concentrated under reduced pressure. The crude product was purified by flash chromatography on silica gel (cyclohexane/ethyl acetate = 8:1) to obtain ester **65** as a white solid.

Yield: 1.97 g (6.67 mmol, 67 %)

Molecular formula: $C_{13}H_{11}BrO_3$

Molecular weight: 295.13 g/mol

Retention factor: 0.50 (cyclohexane/ethyl acetate = 4:1)

^{1}H-NMR (400 MHz, $CDCl_3$, 298 K):
δ/ppm = 7.79−7.71 (m, 3H), 7.54 (d, 1H, *J* = 8.4 Hz), 7.26 (dd, 1H, *J* = 8.9 Hz, *J* = 2.5 Hz), 4.00 (s, 3H), 3.99 (s, 3H).

The spectral data were in agreement with those previously reported for this compound.[64]

1-Bromo-2-(bromomethyl)-7-methoxynaphthalene 66[64]

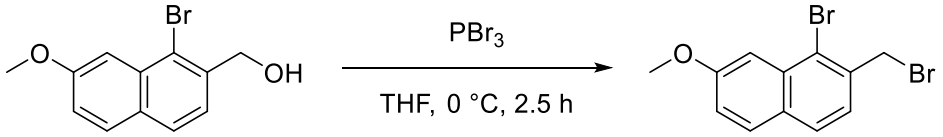

59 **66**

The reaction was carried out under Schlenk conditions. In a Schlenk flask equipped with a magnetic stir bar, 1.72 g of alcohol **59** (6.42 mmol, 1.0 equiv.) were dissolved in anhydrous THF (20 mL). After adding 0.26 mL of phosphorus tribromide (2.76 mmol, 0.43 equiv.), the reaction mixture was stirred at 0 °C for 2.5 h. The reaction mixture was poured into water (20 mL) and extracted with dichloromethane (3×20 mL). The combined organic portions were dried with anhydrous $MgSO_4$ and concentrated under reduced pressure. The crude product was purified by flash chromatography on silica gel (cyclohexane/ethyl acetate = 6:1) to obtain dibromide **66** as a white solid.

Yield: 1.94 g (5.88 mmol, 91 %)

Molecular formula: $C_{12}H_{10}Br_2O$

Molecular weight: 330.01 g/mol

Retention factor: 0.42 (cyclohexane/ethyl acetate = 4:1)

^{1}H-NMR (400 MHz, $CDCl_3$, 298 K):
δ/ppm = 7.75−7.70 (m, 2H), 7.62 (d, 1H, *J* = 2.5 Hz), 7.39 (d, 1H, *J* = 8.4 Hz), 7.19 (dd, 1H, *J* = 8.9 Hz, *J* = 2.5 Hz), 4.85 (s, 2H), 3.98 (s, 3H).

The spectral data were in agreement with those previously reported for this compound.[64]

[4-(1-Bromo-7-methoxynaphthalen-2-yl)but-1-yn-1-yl]triisopropylsilane 67[64]

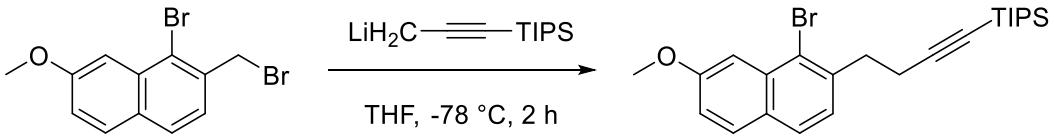

66 **67**

The reaction was carried out under Schlenk conditions. In a Schlenk flask equipped with a magnetic stir bar, 2.47 mL of *n*-butyllithium (2.5 M in *n*-hexane, 6.17 mmol, 1.05 equiv.) were added dropwise to a solution of triisopropyl(prop-1-yn-1-yl)-silane (1.47 mL, 6.23 mmol, 1.06 equiv.) in anhydrous THF (15 mL) at −78 °C under vigorous stirring. After the mixture was stirred at −78 °C for 1.5 h, a solution of dibromide **66** (1.94 g, 5.88 mmol, 1.0 equiv.) in anhydrous THF (10 mL) was added dropwise. A color change from red over purple and green to yellow was observed. The mixture was stirred at this temperature for 2 h and slowly warmed up to room temperature. The solvent was removed under reduced pressure. The crude product was purified by flash chromatography on silica gel (cyclohexane/ethyl acetate = 10:1) to obtain alkyne **67** as a colorless oil.

Yield: 2.18 g (4.90 mmol, 83 %)

Molecular formula: $C_{24}H_{33}BrOSi$

Molecular weight: 445.51 g/mol

Retention factor: 0.62 (cyclohexane/ethyl acetate = 4:1)

^{1}H-NMR (400 MHz, $CDCl_3$, 298 K):
δ/ppm = 7.69 (d, 1H, *J* = 8.9 Hz), 7.64 (d, 1H, *J* = 8.3 Hz), 7.61 (d, 1H, *J* = 2.5 Hz), 7.31 (d, 1H, *J* = 8.2 Hz), 7.14 (dd, 1H, *J* = 8.9 Hz, *J* = 2.5 Hz), 3.98 (s, 3H), 3.20 (t, 2H, *J* = 7.4 Hz), 2.67 (t, 2H, *J* = 7.4 Hz), 1.03 (d, 21H, *J* = 3.7 Hz).

The spectral data were in agreement with those previously reported for this compound.[64]

(4-(1-Iodo-7-methoxynaphthalen-2-yl)but-1-yn-1-yl)triisopropylsilane 68[64]

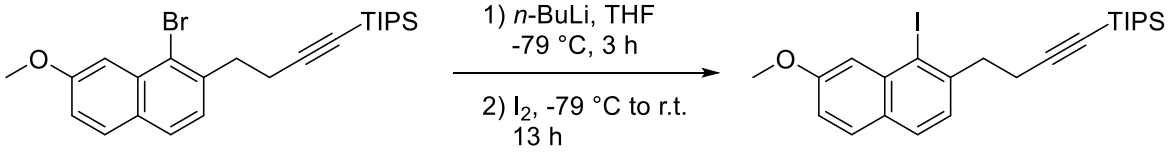

67 **68**

The reaction was carried out under Schlenk conditions. In a Schlenk flask equipped with a magnetic stir bar, 1.97 mL of *n*-butyllithium (2.5 M in *n*-hexane, 4.93 mmol, 1.01 equiv.) were added dropwise to a solution of aryl bromide **67** (2.18 g, 4.88 mmol, 1.0 equiv.) in anhydrous THF (15 mL) at −78 °C under vigorous stirring. After the mixture was stirred at −78 °C for 3 h, a solution of iodine (1.61 g, 6.35 mmol, 1.30 equiv.) in anhydrous THF (10 mL) was added dropwise. The mixture was stirred at this temperature for 1 h and slowly warmed up to room temperature. After stirring for 12 h, the mixture was poured into an aqueous solution of saturated $Na_2S_2O_3$ (100 mL) and extracted with dichloromethane (3×50 mL), then the combined organic portions were dried with anhydrous Mg_2SO_4 and concentrated under reduced pressure. The crude product was purified by flash chromatography on silica gel (cyclohexane/ethyl acetate = 9:1) to afford iodine **68** as a brown oil.

Yield:	1.79 g (3.63 mmol, 74 %)
Molecular formula:	$C_{24}H_{33}IOSi$
Molecular weight:	492.51 g/mol
Retention factor:	0.62 (cyclohexane/ethyl acetate = 4:1)

^{1}H-NMR (400 MHz, $CDCl_3$, 298 K):
δ/ppm = 7.66 (d, 1H, *J* = 8.8 Hz), 7.64 (d, 1H, *J* = 8.2 Hz), 7.58 (d, 1H, *J* = 2.5 Hz), 7.31 (d, 1H, *J* = 8.2 Hz), 7.12 (dd, 1H, *J* = 8.9 Hz, *J* = 2.5 Hz), 3.99 (s, 3H), 3.24 (t, 2H, *J* = 7.4 Hz), 2.65 (t, 2H, *J* = 7.4 Hz), 1.07−0.98 (m, 21H).

The spectral data were in agreement with those previously reported for this compound.[64]

Triisopropyl(4-(7-methoxy-1-((5-methoxy-2-(4-(triisopropylsilyl)but-3-yn-1-yl)phenyl)ethynyl)naphthalen-2-yl)but-1-yn-1-yl)silane 69

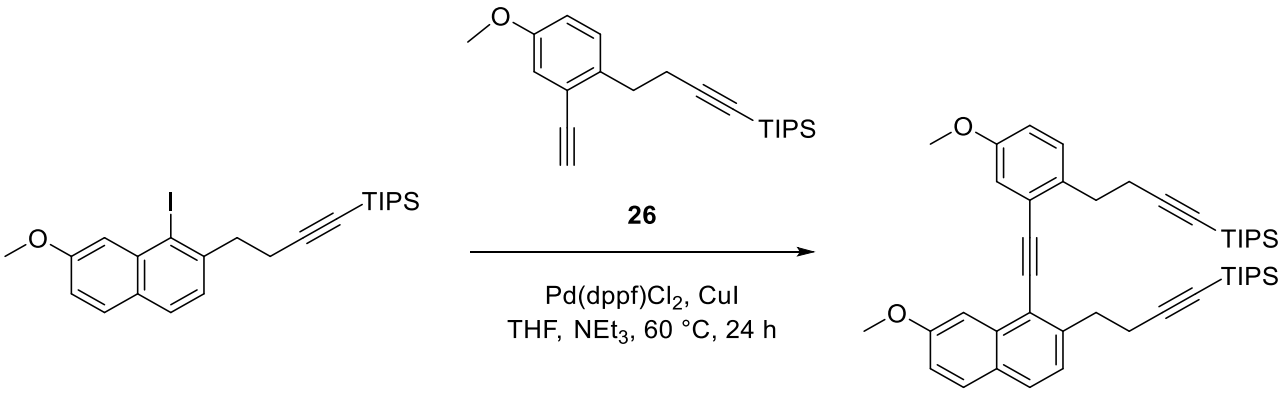

68 **69**

The reaction was carried out under Schlenk conditions. To a Schlenk flask equipped with a magnetic stir bar, 118.16 mg of $PdCl_2$(dppf) (5 mol%), 61.51 mg of CuI (10 mol%), 1.10 g of alkyne **26** (3.23 mmol, 1.0 equiv.) and 1.59 g of iodide **68** (3.23 mmol, 1.0 equiv.) were added. After adding anhydrous THF (5 mL) and degassed NEt_3 (10 mL), the mixture was heated to 60 °C and stirred for 24 h. The reaction mixture was poured into an aqueous solution of saturated NH_4Cl (40 mL) and then extracted with dichloromethane (3×30 mL). The combined organic portions were washed with brine (150 mL), dried with anhydrous $MgSO_4$ and concentrated under reduced pressure. The crude product was purified by flash chromatography on silica gel (cyclohexane/ethyl acetate = 100:1). The product could not completely be isolated and was used for the subsequent reaction without further purification.

Yield: n/a

Molecular formula: $C_{46}H_{64}O_2Si_2$

Molecular weight: 705.18 g/mol

Retention factor: 0.54 (cyclohexane/ethyl acetate = 4:1)

ESI(+)-MS: *m*/*z* = 705.454 $[M+H]^+$

HRMS ($C_{42}H_{64}O_2Si_2H^+$): calculated = 705.4518

found = 705.4526

2-(But-3-yn-1-yl)-1-((2-(but-3-yn-1-yl)-5-methoxyphenyl)ethynyl)-7-methoxynaphthalene 70[64]

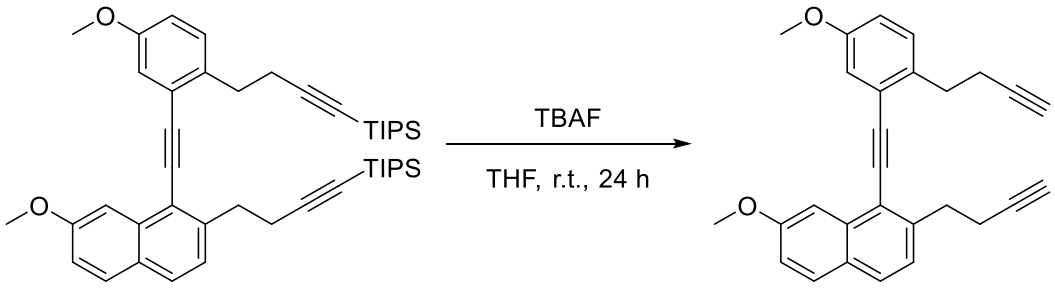

69 **70**

The reaction was carried out under Schlenk conditions. In a Schlenk flask equipped with a magnetic stir bar, 2.39 g of triyne **69** (3.38 mmol, 1.0 equiv.) were dissolved in anhydrous THF (15 mL). After adding a stock solution of tetra-*n*-butylammonium fluoride (8.47 mL, 1.0 M in THF, 2.50 equiv.), the mixture was stirred at room temperature for 24 h. The mixture was poured into a saturated aqueous solution of sodium chloride (30 mL) and extracted with dichloromethane (3×30 mL), then the combined organic portions were dried with anhydrous Mg_2SO_4 and concentrated under reduced pressure. The crude product was purified by flash chromatography on silica gel (cyclohexane/ethyl acetate = 99:1 to 9:1) to afford triyne **70** as a yellow oil.

Yield: 520.17 mg (1.32 mmol, 39 %) over 2 steps

Molecular formula: $C_{28}H_{24}O_2$

Molecular weight: 392.49 g/mol

Retention factor: 0.62 (cyclohexane/ethyl acetate = 4:1)

^{1}H-NMR (400 MHz, $CDCl_3$, 298 K):

δ/ppm = 7.70−7.64 (m, 2H), 7.58 (d, 1H, *J* = 2.5 Hz), 7.28 (d, 1H, *J* = 8.3 Hz), 7.17 (d, 1H, *J* = 8.5 Hz), 7.13 (dd, 1H, *J* = 8.9 Hz, *J* = 2.4 Hz), 7.01 (d, 1H, *J* = 2.8 Hz), 6.86 (dd, 1H, *J* = 8.5 Hz, *J* = 2.8 Hz), 3.99 (s, 3H), 3.78 (s, 3H), 3.25 (t, 2H, *J* = 7.6 Hz),

2.96 (t, 2H, *J* = 7.6 Hz), 2.58 (td, 2H, *J* = 7.5 Hz, *J* = 2.6 Hz), 2.50 (td, 2H, *J* = 7.5 Hz, *J* = 2.6 Hz), 2.01 (t, 1H, *J* = 2.6 Hz), 1.97 (t, 1H, *J* = 2.6 Hz).

The spectral data were in agreement with those previously reported for this compound.[64]

2,15-Dimethoxy-5,6,9,10-tetrahydrohexahelicene 71

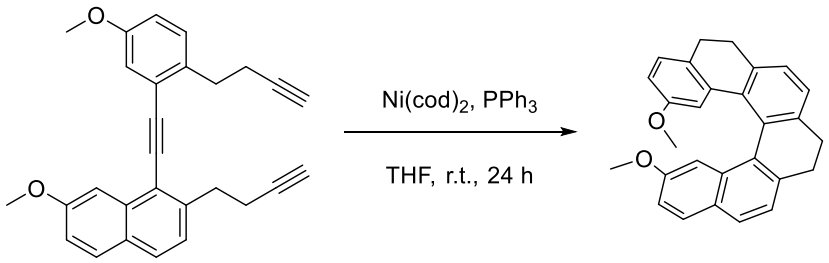

70 **71**

The reaction was carried out under Schlenk conditions. In a Schlenk flask equipped with a magnetic stir bar, 260.0 mg of triyne **70** (0.66 mmol, 1.0 equiv.) and 374.50 mg of PPh_3 (1.32 mmol, 2.0 equiv.) were dissolved in anhydrous THF (5 mL). After adding a stock solution of $Ni(cod)_2$ (11.07 mL, 0.06 M in THF, 1.0 equiv.), the mixture was stirred at room temperature for 24 h. The solvent was evaporated under reduced pressure and the residue was subjected to flash chromatography on silica gel (cyclohexane/ethyl acetate = 10:1). The product could not completely be isolated and was used for the subsequent reaction without further purification and analytical characterization.

Yield: n/a

Molecular formula: $C_{28}H_{24}O_2$

Molecular weight: 392.49 g/mol

Retention factor: 0.62 (cyclohexane/ethyl acetate = 4:1)

2,15-Dimethoxyhexahelicene 72

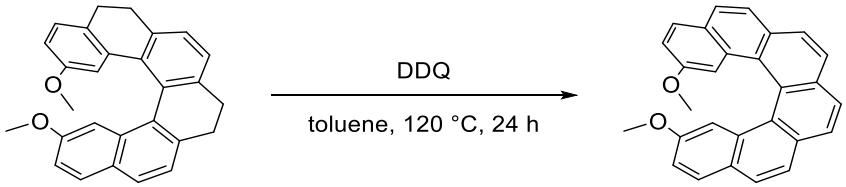

71 **72**

The reaction was carried out under Schlenk conditions. In a two-necked flask equipped with a magnetic stir bar, 100.0 mg of tetrahydro[6]helicene derivative **71** (0.25 mmol, 1.0 equiv.) were dissolved in anhydrous toluene (20 mL). After adding 404.85 mg of 2,3-dichloro-5,6-dicyano-1,4-benzoquinone (1.78 mmol, 7.0 equiv.), the mixture was stirred at 120 °C for 24 h. The mixture was slowly cooled down to room temperature and filtered over a plug of silica gel. The solvent was evaporated under reduced pressure and the residue was subjected to flash chromatography on silica gel (cyclohexane/ethyl acetate = 100:1 to 10:1). The product could not completely be isolated.

Yield:	n/a
Molecular formula:	$C_{28}H_{20}O_2$
Molecular weight:	388.46 g/mol
Retention factor:	0.45 (cyclohexane/ethyl acetate = 4:1)
ESI(+)-MS:	*m*/*z* = 389.153 $[M+H]^+$
HRMS ($C_{28}H_{20}O_2H^+$):	calculated = 389.1536
	found = 389.1536

2,13-Dihydroxypentahelicene 73

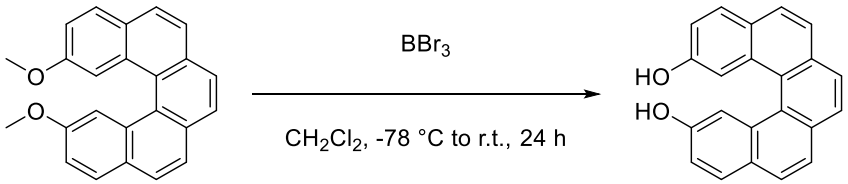

20 **73**

In a round bottomed flask equipped with a magnetic stir bar, a solution of 2,13-dimethoxy[5]helicene **20** (250.0 mg, 0.73 mmol, 1.0 equiv.) in dichloromethane (15 mL) was cooled to −78 °C. A solution of BBr_3 (7.39 mL, 1 M in CH_2Cl_2, 7.39 mmol, 10.0 equiv.) in dichloromethane was added, the mixture was slowly warmed up to room temperature and stirred for 24 h. The reaction mixture was poured into an aqueous solution of saturated $NaHCO_3$ (30 mL) and then extracted with ethyl acetate (3×15 mL). The combined organic portions were washed with water (100 mL), dried with anhydrous $MgSO_4$ and concentrated under reduced pressure. The crude product was purified by flash chromatography on silica gel (cyclohexane/ethyl acetate = 5:1) to obtain 2,13-dihydroxy[5]helicene **73** as a purple solid.

Yield:	165.58 mg (0.53 mmol, 72 %)
Molecular formula:	$C_{22}H_{14}O_2$
Molecular weight:	310.35 g/mol
Retention factor:	0.16 (cyclohexane/ethyl acetate = 5:1)
EI-MS:	*m*/*z* = 310.0 $[M]^{\bullet+}$, 292.0 $[M\text{-}H_2O]^+$
HRMS ($C_{22}H_{14}O_2^{\bullet+}$):	calculated = 310.0994
	found = 310.0989
Analytical HPLC:	(*S*,*S*)-Whelk-O-1; *n*-hexane/isopropanol (10:1); *f* = 1.0 mL min^{-1}); (–)-(M)-**73**: t_R = 6.55 min; (+)-(P)-**73**: t_R = 7.98 min

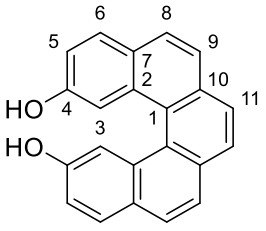

^{1}H-NMR (500 MHz, MeOD, 298 K):

δ/ppm = 7.85−7.80 (m, 8H, H-3, H-6, H-8/H-9, H-11), 7.69 (d, 2H, H-8/H-9, $^{3}J_{8,9}$ = 8.4 Hz), 7.07 (dd, 2H, H-5, $^{3}J_{5,6}$ = 8.7 Hz, $^{4}J_{5,3}$ = 2.4 Hz).

^{13}C-NMR (500 MHz, MeOD, 298 K):

δ/ppm = 155.7 (C-4), 133.9*, 133.3*, 130.5*, 128.5*, 128.2*, 128.1*, 127.4*, 124.3*, 118.5 (C-5), 113.5 (C-3).

*The signal could not be unambiguously assigned.

Pentahelicene-2,13-diyl bis(trifluormethanesulfonate) 74

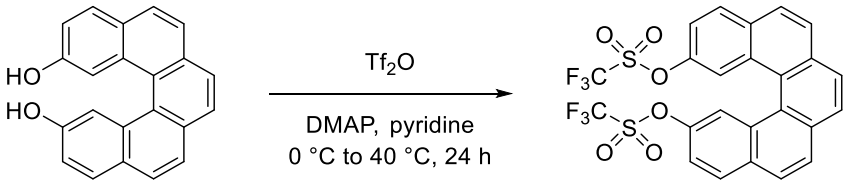

73 **74**

In a round bottomed flask equipped with a magnetic stir bar, a solution of diol **73** (165.0 mg, 0.53 mmol, 1.0 equiv.) and 4-dimethylaminopyridine (3.25 mg, 0.027 mmol, 0.12 equiv.) in anhydrous pyridine (5 mL) was prepared. After adding 0.39 mL of trifluoromethanesulfonic anhydride (2.33 mmol, 4.40 equiv.) at 0 °C while stirring, the reaction mixture was allowed to slowly reach room temperature and stirring was continued at 40 °C for an additional 24 h. The mixture was concentrated under reduced pressure and the crude product was purified by flash chromatography on silica gel (cyclohexane/ethyl acetate = 4:1) to afford triflate **74** as an off-white solid.

Yield:	243.24 mg (0.42 mmol, 80 %)
Molecular formula:	$C_{24}H_{12}F_6O_6S_2$
Molecular weight:	574.46 g/mol
Retention factor:	0.35 (cyclohexane/ethyl acetate = 3:1)
EI-MS:	m/z = 574.0 $[M]^{\bullet+}$
HRMS ($C_{24}H_{12}F_6O_6S_2^{\bullet+}$):	calculated = 573.9979
	found = 573.9972

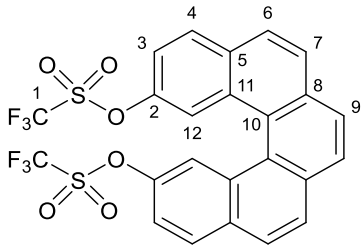

^{1}H-NMR (500 MHz, $CDCl_3$, 298 K):

δ/ppm = 8.29 (d, 2H, H-12, $^{4}J_{12,3}$ = 2.3 Hz), 8.07 (d, 2H, H-4, $^{3}J_{4,3}$ = 8.9 Hz), 8.01−7.94 (m, 6H, H-6, H-7, H-9), 7.45 (dd, 2H, H-3, $^{3}J_{3,4}$ = 8.9 Hz, $^{4}J_{3,12}$ = 2.3 Hz).

^{13}C-NMR (500 MHz, $CDCl_3$, 298 K):

δ/ppm = 146.9 (C-2), 133.2 (C-8/C-10), 132.0 (C-5), 131.1 (C-11), 130.8 (C-4), 128.4 (C-6/C-7/C-9), 127.8 (C-6/C-7/C-9), 127.5 (C-6/C-7/C-9), 126.4 (C-8/C-10), 120.3 (C-12), 119.9 (C-3), 118.1 (q, C-1).

2,13-Di(pyridin-4-yl)pentahelicene 75

Approach A

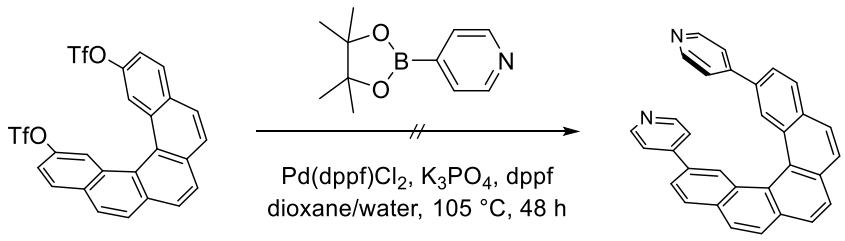

74 **75**

The reaction was carried out under Schlenk conditions. A mixture of 1,4-dioxane and water (10:1) was degassed by 4 freeze-pump-thaw cycles before use. In a Schlenk flask equipped with a magnetic stir bar, 1.08 mg of $PdCl_2$(dppf) (5 mol%), 0.82 mg of dppf (5 mol%), 25.12 mg of potassium phosphate (0.11 mmol, 4.0 equiv.), 18.20 mg of 4-(4,4,5,5-tetramethyl-1,3,2-dioxaborolan-2-yl)pyridine (0.088 mmol, 3.0 equiv.) and 17.0 mg of triflate **74** (0.029 mmol, 1.0 equiv.) were dissolved in a mixture of degassed 1,4-dioxane and water (5 mL). The mixture was stirred at 105 °C for 48 h. The reaction was monitored by TLC. No turnover was observed after that time and the starting material was recovered by column chromatography on silica gel (cyclohexane/ethyl acetate = 4:1).

Approach B

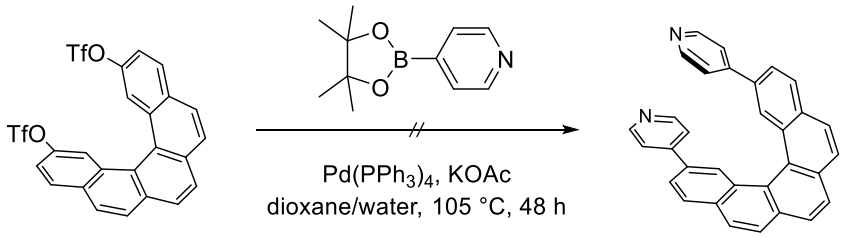

74 **75**

The reaction was carried out under Schlenk conditions. A mixture of 1,4-dioxane and water (10:1) was degassed by 4 freeze-pump-thaw cycles before use. In a Schlenk flask equipped with a magnetic stir bar, 39.58 mg of $Pd(PPh_3)_4$ (8 mol%), 147.96 mg of potassium acetate (1.07 mmol, 2.50 equiv.), 219.53 mg of 4-(4,4,5,5-tetramethyl-1,3,2-dioxaborolan-2-yl)pyridine (1.07 mmol, 2.50 equiv.) and 246.51 mg of triflate **74** (0.42 mmol, 1.0 equiv.) were dissolved in a mixture of degassed 1,4-dioxane and water (15 mL). The mixture was stirred at 105 °C for 48 h. The reaction was monitored by TLC. No turnover was observed after that time and the starting material was recovered by column chromatography on silica gel (cyclohexane/ethyl acetate = 4:1).

Approach C

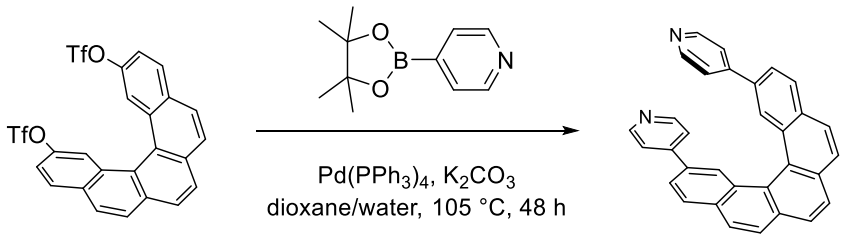

74 **75**

The reaction was carried out under Schlenk conditions. A mixture of 1,4-dioxane and water (4:1) was degassed by 4 freeze-pump-thaw cycles before use. In a Schlenk flask equipped with a magnetic stir bar, 39.10 mg of $Pd(PPh_3)_4$ (8 mol%), 146.15 mg of potassium carbonate (1.05 mmol, 2.50 equiv.), 216.85 mg of 4-(4,4,5,5-tetramethyl-1,3,2-dioxaborolan-2-yl)pyridine (1.05 mmol, 2.50 equiv.) and 243.10 mg of triflate **74** (0.42 mmol, 1.0 equiv.) were dissolved in a mixture of degassed 1,4-dioxane and water (15 mL). The mixture was stirred at 105 °C for 48 h. The reaction mixture was poured into a saturated solution of aqueous EDTA (30 mL) and extracted with DCM (3×30 mL). The combined organic portions were washed with brine (100 mL), dried with anhydrous

$MgSO_4$ and concentrated under reduced pressure. The crude product was purified by flash chromatography on silica gel (cyclohexane/ethyl acetate/triethylamine = 1:1:0.05 to 0:1:0.05). [5]Helicene derivative **75** was obtained as a white solid.

Single crystals for XRD analysis were grown by layering *n*-hexane on top of a solution of enantiopure **75** in dichloromethane (2:1) overnight at −10 °C.

Yield:	100.70 mg (0.23 mmol, 54 %)
Molecular formula:	$C_{32}H_{20}N_2$
Molecular weight:	432.52 g/mol
Retention factor:	0.44 (ethyl acetate)
APCI-MS:	m/z = 433.170 $[M+H]^+$
HRMS ($C_{32}H_{20}N_2H^+$):	calculated = 433.1699
	found = 433.1697
Specific optical rotation:	(−)-(*M*)-**75**: $[\alpha]_D^{20} = -2980°$ mL×dm^{-1}×g^{-1} (*c* = 5.02 g/L, dichloromethane)
	(+)-(*P*)-**75**: $[\alpha]_D^{20} = +2979°$ mL×dm^{-1}×g^{-1} (*c* = 4.97 g/L, dichloromethane)
ECD:	(−)-(*M*)-**75**: λ/nm ($\Delta\varepsilon$/M^{-1}×cm^{-1}) = 254 (+358.9), 270 (+21.3), 293 (+255.8), 330 (−320.0); (*c* = 6.1×10^{-4} g/L, dichloromethane)
	(+)-(*P*)-**75**: λ/nm ($\Delta\varepsilon$/M^{-1}×cm^{-1}) = 254 (−191.8), 270 (+69.1), 293 (−42.1), 330 (+313.4); (*c* = 5.8×10^{-4} g/L, dichloromethane)
Analytical HPLC:	CHIRALPAK IB-U; *n*-hexane/ethanol/diethylamine (70:30:0.03); *f* = 0.85 mL min^{-1}); (–)-(M)-**75**: t_R = 2.47 min; (+)-(P)-**75**: t_R = 3.70 min
Semipreparative HPLC:	CHIRALPAK IB; *n*-hexane/ethanol/diethylamine (70:30:0.03); *f* = 18 mL min^{-1}); (–)-(M)-**75**: t_R = 10.58 min, 90.0 % *ee*; (+)-(P)-**75**: t_R = 13.59 min, 95.0 % *ee*

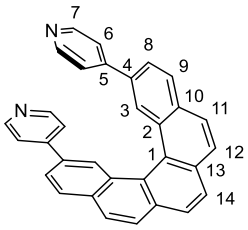

^{1}H-NMR (700 MHz, CD_2Cl_2, 298 K):
δ/ppm = 8.93 (d, 2H, H-3, $^{4}J_{3,8}$ = 1.8 Hz), 8.43−8.40 (m, 4H, H-7), 8.15 (d, 2H, H-9, $^{3}J_{9,8}$ = 8.3 Hz), 8.03 (d, 2H, H-11, $^{3}J_{11,12}$ = 8.4 Hz), 7.99 (d, 2H, H-12, $^{3}J_{12,11}$ = 8.4 Hz), 7.98 (s, 2H, H-14), 7.86 (dd, 2H, H-8, $^{3}J_{8,9}$ = 8.3 Hz, $^{4}J_{8,3}$ = 1.8 Hz), 7.23−7.21 (m, 4H, H-6).

^{13}C-NMR (700 MHz, CD_2Cl_2, 298 K):
δ/ppm = 150.7 (C-7), 148.1 (C-5), 134.6 (C-4), 133.6 (C-10), 133.4 (C-13), 131.2 (C-2), 129.8 (C-9), 128.3 (C-12/C-14), 128.0 (C-12/C-14), 127.8 (C-11), 127.7 (C-3), 127.5 (C-1), 125.4 (C-8), 121.8 (C-6).

Crystallographic data [(−)-**75**]

Empirical formula: $C_{32}H_{20}N_2$; M = 432.51 g/mol; T = 100.0 K; radiation type: CuKα; λ = 1.54186 Å; crystal system: orthorhombic; space group: $P2_12_12_1$; unit cell: a = 6.22994(23) Å, b = 18.5750(9) Å, c = 18.8091(10) Å, α = 90°, β = 90°, γ = 90°, V = 2176.61(17) Å^3, Z = 4, ρ_{calc} = 1.320 g/cm^3; absorption correction = multi-scan; μ = 0.59 mm^{-1}; minimum transmission = 0.6782; maximum transmission = 0.9480; F(000) = 904.0; crystal color: clear colorless; crystal size = 0.3×0.3×0.03 mm^3; 2Θ range for data collection: 6.688°−140.782°; Reflections collected [R(int)] = 18992 [0.0636]; Reflections [I>2σ(I)] = 4127; data completeness = 100 %; Data/parameters/restraints = 4127/307/0; Goodness-of-fit on F^2 = 1.083; Final R indexes [I>=2σ(I)]: R_1 = 0.0559, wR_2 = 0.1398; Final R indexes [all data]: R_1 = 0.0633, wR_2 = 0.1475; Largest diff. peak/hole = 0.22/−0.22 e Å^{-3}; Flack parameter = −0.5(10)*.

*The high uncertainty originated from a poor quality of the crystal. The assignment of the enantiomer was done based on ECD spectra.

Crystallographic data [(+)-**75**]

Empirical formula: $C_{32}H_{20}N_2$; M = 432.51 g/mol; T = 100.0 K; radiation type: CuKα; λ = 1.54186 Å; crystal system: orthorhombic; space group: $P2_12_12_1$; unit cell: a = 6.2349(3) Å, b = 18.5717(8) Å, c = 18.7974(9) Å, α = 90°, β = 90°, γ = 90°, V = 2176.59(17) Å^3, Z = 4, ρ_{calc} = 1.320 g/cm^3; absorption correction = multi-can; μ = 0.59 mm^{-1}; minimum transmission = 0.5050; maximum transmission = 0.9163; F(000) = 904.0; crystal color: clear colorless; crystal size = 0.5×0.06×0.04 mm^3; 2Θ range for data collection: 6.69°−141.226°; Reflections collected [R(int)] = 27403 [0.0896]; Reflections [I>2σ(I)] = 4042; data completeness = 100 %; Data/parameters/restraints = 4042/307/0; Goodness-of-fit on F^2 = 1.091; Final R indexes [I>=2σ(I)]: R_1 = 0.0495, wR_2 = 0.1162; Final R indexes [all data]: R_1 = 0.0647, wR_2 = 0.1333; Largest diff. peak/hole = 0.22/−0.25 e Å^{-3}; Flack parameter = −0.6(5)*.

*The high uncertainty originated from a poor quality of the crystal. The assignment of the enantiomer was done based on ECD spectra.

2,13-Di(pyridin-3-yl)pentahelicene 76

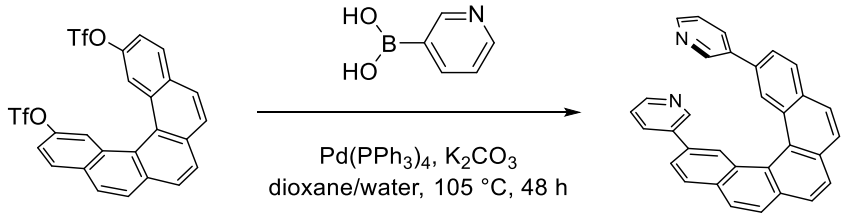

74 **76**

The reaction was carried out under Schlenk conditions. A mixture of 1,4-dioxane and water (4:1) was degassed by 4 freeze-pump-thaw cycles before use. In a Schlenk flask equipped with a magnetic stir bar, 16.09 mg of $Pd(PPh_3)_4$ (8 mol%), 60.14 mg of potassium carbonate (0.43 mmol, 2.50 equiv.), 53.49 mg of 3-pyridinylboronic acid (0.43 mmol, 2.50 equiv.) and 100.0 mg of triflate **74** (0.17 mmol, 1.0 equiv.) were dissolved in a mixture of degassed 1,4-dioxane and water (10 mL). The mixture was stirred at 105 °C for 48 h. The reaction mixture was poured into a saturated solution of aqueous EDTA (20 mL) and extracted with DCM (3×20 mL). The combined organic portions were washed with brine (80 mL), dried with anhydrous $MgSO_4$ and concentrated under reduced pressure. The crude product was purified by flash

chromatography on silica gel (dichloromethane/methanol = 100:1 to 100:3). [5]Helicene derivative **76** was obtained as a white solid.

Yield:	30.44 mg (0.069 mmol, 40 %)
Molecular formula:	$C_{32}H_{20}N_2$
Molecular weight:	432.52 g/mol
Retention factor:	0.52 (dichloromethane/methanol = 10:1)
APCI-MS:	m/z = 433.168 $[M+H]^+$
HRMS ($C_{32}H_{20}N_2H^+$):	calculated = 433.1699
	found = 433.1692

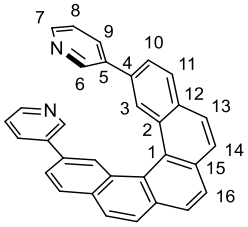

^{1}H-NMR (500 MHz, CD_2Cl_2, 298 K):
δ/ppm = 8.86 (s, 2H, H-3), 8.58 (s, 2H, H-6), 8.41 (d, 2H, H-7, $^3J_{7,8}$ = 4.8 Hz), 8.13 (d, 2H, H-11, $^3J_{11,10}$ = 8.3 Hz), 8.02 (d, 2H, H-13, $^3J_{13,14}$ = 8.6 Hz), 7.99−7.94 (m, 4H, H-14, H-16), 7.83 (d, 2H, H-10, $^3J_{10,11}$ = 8.3 Hz), 7.64 (d, 2H, H-9, $^3J_{9,8}$ = 8.0 Hz), 7.18 (dd, 2H, H-8, $^3J_{8,9}$ = 8.0 Hz, $^3J_{8,7}$ = 4.8 Hz).

^{13}C-NMR (500 MHz, CD_2Cl_2, 298 K):
δ/ppm = 148.9 (C-7), 148.6 (C-6), 136.6 (C-5), 134.5 (C-9), 134.3 (C-4), 133.3 (C-15), 132.9 (C-12), 131.5 (C-2), 129.8 (C-11), 128.2 (C-14/C-16), 127.8 (C-14/C-16), 127.7 (C-3), 127.5 (C-13), 127.4 (C-1), 125.8 (C-10), 124.0 (C-8).

Attempts to synthesize 2,13-bis(pyridin-3-ylethynyl)pentahelicene 77

Approach A

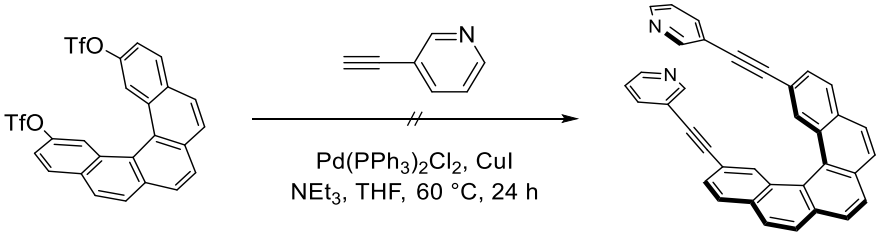

74 **77**

The reaction was carried out under Schlenk conditions. To a Schlenk flask equipped with a magnetic stir bar, 4.88 mg of $PdCl_2(PPh_3)_2$ (4 mol%), 2.32 mg of CuI (7 mol%), 100.0 mg of triflate **74** (0.17 mmol, 1.0 equiv.) and 44.87 mg of 3-ethynylpyridine (0.43 mmol, 2.50 equiv.) were added. After adding anhydrous THF (5 mL) and degassed NEt_3 (5 mL), the mixture was heated to 60 °C and stirred for 24 h. The reaction was monitored by TLC. No turnover was observed after that time and the starting material was recovered by column chromatography on silica gel (cyclohexane/ethyl acetate = 4:1).

Approach B

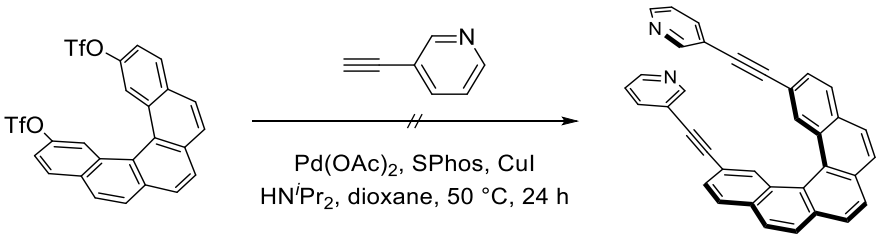

74 **77**

The reaction was carried out under Schlenk conditions. To a Schlenk flask equipped with a magnetic stir bar, 0.97 mg of $Pd(OAc)_2$ (5 mol%), 3.57 mg of SPhos (10 mol%), 0.82 mg of CuI (5 mol%), 50.0 mg of triflate **74** (0.087 mmol, 1.0 equiv.) and 22.44 mg of 3-ethynylpyridine (0.21 mmol, 2.50 equiv.) were added. After adding degassed 1,4-dioxane (5 mL) and degassed diisopropylamine (5 mL), the mixture was heated to 50 °C and stirred for 24 h. The reaction was monitored by TLC. No turnover was observed after that time and the starting material was recovered by column chromatography on silica gel (cyclohexane/ethyl acetate = 4:1).

Approach C

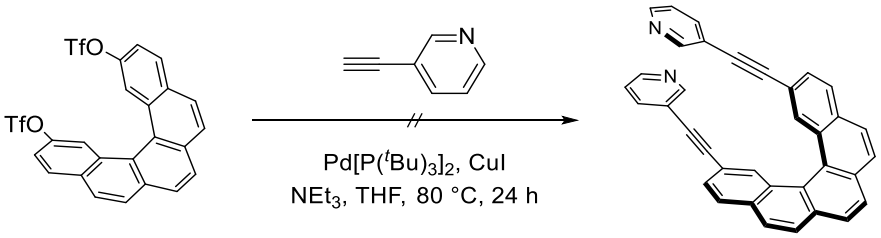

74 **77**

The reaction was carried out under Schlenk conditions. To a Schlenk flask equipped with a magnetic stir bar, 2.66 mg of $Pd[P(^tBu)_3]_2$ (6 mol%), 0.66 mg of CuI (4 mol%), 50.0 mg of triflate **74** (0.087 mmol, 1.0 equiv.) and 22.44 mg of 3-ethynylpyridine (0.21 mmol, 2.50 equiv.) were added. After adding anhydrous THF (5 mL) and degassed NEt_3 (5 mL), the mixture was heated to 80 °C and stirred for 24 h. The reaction was monitored by TLC. No turnover was observed after that time and the starting material was recovered by column chromatography on silica gel (cyclohexane/ethyl acetate = 4:1).

2,13-Bis[4-(pyridin-3-yl)phenyl]pentahelicene 78

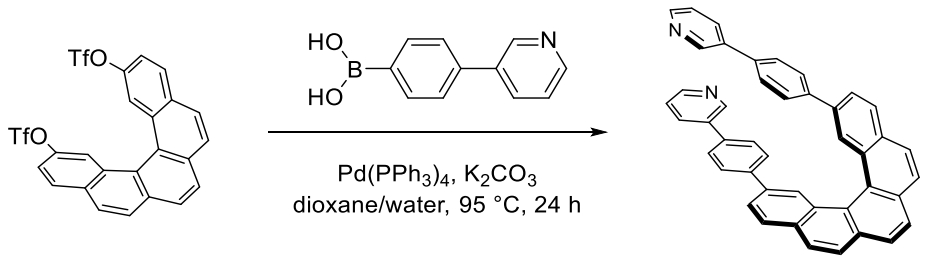

74 **78**

The reaction was carried out under Schlenk conditions. A mixture of 1,4-dioxane and water (4:1) was degassed by 4 freeze-pump-thaw cycles before use. In a Schlenk flask equipped with a magnetic stir bar, 19.31 mg of $Pd(PPh_3)_4$ (8 mol%), 72.17 mg of potassium carbonate (0.52 mmol, 2.50 equiv.), 103.93 mg of (4-(pyridin-3-yl)phenyl)boronic acid (0.52 mmol, 2.50 equiv.) and 120.0 mg of triflate **74** (0.21 mmol, 1.0 equiv.) were dissolved in a mixture of degassed 1,4-dioxane and water (10 mL). The mixture was stirred at 95 °C for 24 h. The reaction mixture was poured into a saturated solution of aqueous EDTA (20 mL) and extracted with DCM (3×20 mL). The combined organic portions were washed with brine (80 mL), dried with anhydrous

$MgSO_4$ and concentrated under reduced pressure. The crude product was recrystallized (ethyl acetate) to obtain [5]helicene derivative **78** as yellow needles.

Yield: 70.02 mg (0.16 mmol, 77 %)

Molecular formula: $C_{44}H_{28}N_2$

Molecular weight: 584.72 g/mol

APCI-MS: m/z = 585.232 $[M+H]^+$

HRMS ($C_{44}H_{28}N_2H^+$): calculated = 585.2325

found = 585.2322

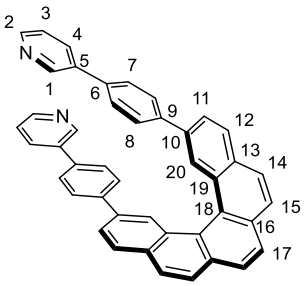

^{1}H-NMR (500 MHz, CD_2Cl_2, 298 K):

δ/ppm = 8.96 (dd, 2H, H-20, $^4J_{20,11}$ = 1.8 Hz, $^5J_{20,12}$ = 0.8 Hz), 8.78 (dd, 2H, H-1, $^4J_{1,4}$ = 2.4 Hz, $^5J_{1,3}$ = 0.9 Hz), 8.52 (dd, 2H, H-2, $^3J_{2,3}$ = 4.8 Hz, $^4J_{2,4}$ = 1.6 Hz), 8.13 (d, 2H, H-12, $^3J_{12,11}$ = 8.4 Hz), 8.02 (d, 2H, H-14, $^3J_{14,15}$ = 8.5 Hz), 7.96 (s, 2H, H,17), 7.95 (d, 2H, H-15, $^3J_{15,14}$ = 8.5 Hz), 7.90 (dd, 2H, H-11, $^3J_{11,12}$ = 8.4 Hz, $^4J_{11,20}$ = 1.8 Hz), 7.84 (ddd, 2H, H-4, $^3J_{4,3}$ = 7.9 Hz, $^4J_{4,1}$ = 2.4 Hz, $^4J_{4,2}$ = 1.6 Hz), 7.54−7.49 (m, 8H, H-7, H-8), 7.32 (ddd, 2H, H-3, $^3J_{3,4}$ = 7.9 Hz, $^3J_{3,2}$ = 4.8 Hz, $^5J_{3,1}$ = 0.9 Hz).

^{13}C-NMR (500 MHz, CD_2Cl_2, 298 K):

δ/ppm = 149.1 (C-2), 148.6 (C-1), 141.1 (C-9), 137.2 (C-6), 136.9 (C-10), 136.3 (C-5), 134.4 (C-4), 133.3 (C-16), 132.7 (C-13), 131.6 (C-19), 129.5 (C-12), 128.2 (C-7/C-8), 128.1 (C-14), 127.9 (C-7/C-8), 127.8 (C-15/C-17), 127.6 (C-18), 127.5 (C-20), 127.2 (C-15/C-17), 125.9 (C-11), 124.0 (C-3).

Crystallographic data [(*rac*)-**78**]

Empirical formula: $C_{44}H_{28}N_2$; M = 584.68 g/mol; T = 100.0 K; radiation type: CuKα; λ = 1.54186 Å; crystal system: monoclinic; space group: $C2/c$; unit cell: a = 31.101(2) Å, b = 5.8274(3) Å, c = 32.690(3) Å, α = 90°, β = 94.046(7)°, γ = 90°,

V = 5910.0(8) Å^3, Z = 8, ρ_{calc} = 1.314 g/cm^3; absorption correction = multi-scan; μ = 0.59 mm^{-1}; minimum transmission = 0.6363; maximum transmission = 0.9479; F(000) = 2448.0; crystal color: clear colorless; crystal size = 0.3×0.04×0.02 mm^3; 2Θ range for data collection: 7.584°−141.056°; Reflections collected [R(int)] = 62455 [0.6434]; Reflections [I>2σ(I)] = 5612; data completeness = 99.9 %; Data/parameters/restraints = 56512/415/0; Goodness-of-fit on F^2 = 1.030; Final R indexes [I>=2σ(I)]: R_1 = 0.1217, wR_2 = 0.2675; Final R indexes [all data]: R_1 = 0.2843, wR_2 = 0.3735; Largest diff. peak/hole = 0.37/−0.43 e Å^{-3}.

Dinaphtho[8,1,2-*def*:2′,1′,8′-*jka*][3]benzoxepin 80

Approach A

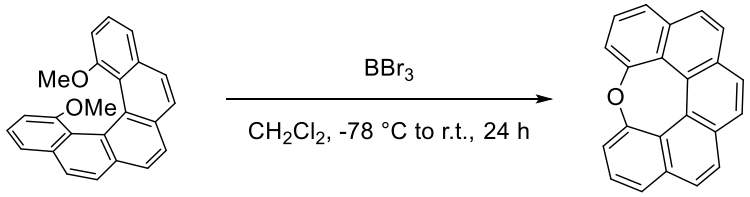

38 **80**

In a round bottomed flask equipped with a magnetic stir bar, a solution of 1,14-dimethoxy[5]helicene **38** (500.0 mg, 1.48 mmol, 1.0 equiv.) in dichloromethane (15 mL) was cooled to −78 °C. A solution of BBr_3 (7.39 mL, 1 M in CH_2Cl_2, 7.39 mmol, 5.0 equiv.) in dichloromethane was added, the mixture was slowly warmed up to room temperature and stirred for 24 h. The reaction mixture was poured into an aqueous solution of saturated $NaHCO_3$ (30 mL) and then extracted with ethyl acetate (3×15 mL). The combined organic portions were washed with water (100 mL), dried with anhydrous $MgSO_4$ and concentrated under reduced pressure. The crude product was purified by flash chromatography on silica gel (cyclohexane/ethyl acetate = 5:1) to obtain Dinaphtho[8,1,2-*def*:2′,1′,8′-*jka*][3]benzoxepin **80** as a yellow solid.

Single crystals for XRD analysis were grown by layering *n*-hexane on top of a solution of **80** in dichloromethane (2:1) overnight at −10 °C. Dinaphtho[8,1,2-*def*:2′,1′,8′-*jka*][3]benzoxepin crystallized as plates and needles.

Yield:	235.79 mg (0.81 mmol, 55 %)
Molecular formula:	$C_{22}H_{12}O$
Molecular weight:	292.33 g/mol

Retention factor: 0.53 (cyclohexane/ethyl acetate = 4:1)

EI-MS: m/z = 292.0 $[M]^{\bullet+}$

HRMS ($C_{22}H_{12}O^{\bullet+}$): calculated = 292.0888

found = 292.0880

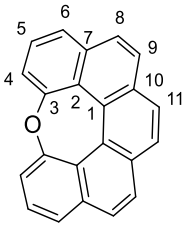

^{1}H-NMR (500 MHz, $CDCl_3$, 298 K):
δ/ppm = 8.06 (s, 2H, H-11), 7.85 (d, 2H, H-9, $^{3}J_{9,8}$ = 8.6 Hz), 7.75 (d, 4H, H-6, H-8, $^{3}J_{6,5}$ = 8.6 Hz, $^{3}J_{8,9}$ = 8.6 Hz), 7.66 (t, 2H, H-5, $^{3}J_{5,6}$ = 7.6 Hz, $^{3}J_{5,4}$ = 7.6 Hz), 7.62 (dd, 2H, H-4, $^{3}J_{4,5}$ = 7.6 Hz, $^{3}J_{4,6}$ = 1.5 Hz).

^{13}C-NMR (500 MHz, $CDCl_3$, 298 K):
δ/ppm = 156.3 (C-3), 134.7 (C-7), 132.7 (C-1), 128.6 (C-9), 128.3 (C-11), 127.9 (C-5), 126.8 (C-2), 126.3 (C-8), 125.1 (C-10), 125.0 (C-6), 118.6 (C-4).

Crystallographic data [**80**] as needles

Empirical formula: $C_{22}H_{12}O$; M = 292.32 g/mol; T = 100.0 K; radiation type: CuKα; λ = 1.54178 Å; crystal system: orthorhombic; space group: $P2_12_12_1$; unit cell: a = 3.9794(2) Å, b = 16.4442(7) Å, c = 20.4271(8) Å, α = 90°, β = 90°, γ = 90°, V = 1336.71(10) Å^3, Z = 4, ρ_{calc} = 1.453 g/cm^3; absorption correction = multi-scan; μ = 0.685 mm^{-1}; minimum transmission = 0.5402; maximum transmission = 0.7536; F(000) = 608.0; crystal color: clear colorless; crystal size = 0.36×0.08×0.04 mm^3; 2Θ range for data collection: 6.9°−135.472°; Reflections collected [R(int)] = 14436 [0.0403]; Reflections [I>2σ(I)] = 2420; data completeness = 99.7 %; Data/parameters/restraints = 2420/208/0; Goodness-of-fit on F^2 = 1.061; Final R indexes [I>=2σ(I)]: R_1 = 0.0260, wR_2 = 0.0646; Final R indexes [all data]: R_1 = 0.0263, wR_2 = 0.0647; Largest diff. peak/hole = 0.22/−0.14 e Å^{-3}.

Crystallographic data [**80**] as plates

Empirical formula: $C_{22}H_{12}O$; M = 292.32 g/mol; T = 100.0 K; radiation type: CuKα; λ = 1.54178 Å; crystal system: orthorhombic; space group: *pbca*; unit cell: a = 10.6248(4) Å, b = 14.7226(5) Å, c = 35.5511(15) Å, α = 90°, β = 90°, γ = 90°, V = 5561.1(4) Å^3, Z = 16, ρ_{calc} = 1.397 g/cm^3; absorption correction = multi-scan; μ = 0.659 mm^{-1}; minimum transmission = 0.3317; maximum transmission = 0.7536; F(000) = 2432.0; crystal color: clear colorless; crystal size = 0.36×0.18×0.04 mm^3; 2Θ range for data collection: 4.972°−135.496°; Reflections collected [R(int)] = 45329 [0.1396]; Reflections [I>2σ(I)] = 5031; data completeness = 99.9 %; Data/parameters/restraints = 5031/415/0; Goodness-of-fit on F^2 = 1.154; Final R indexes [I>=2σ(I)]: R_1 = 0.0826, wR_2 = 0.2034; Final R indexes [all data]: R_1 = 0.1022, wR_2 = 0.2149; Largest diff. peak/hole = 0.32/−0.43 e Å^{-3}.

Approach B

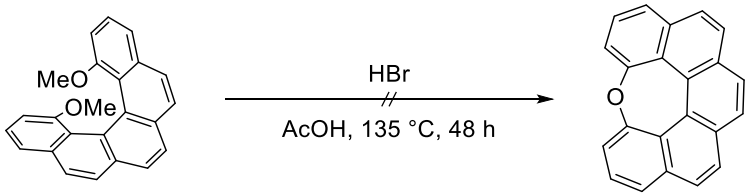

38 **80**

In a round bottomed flask equipped with a magnetic stir bar, 110.0 mg of 1,14-dimethoxy[5]helicene **38** (0.33 mmol, 1.0 equiv.) were suspended in acetic acid (9 mL). After adding a solution of hydrogen bromide (0.60 mL, 33 wt.% in acetic acid, 10.25 equiv.) the mixture was refluxed for 48 h. The reaction was monitored by TLC. No turnover was observed after that time and the starting material was recovered by column chromatography on silica gel (cyclohexane/ethyl acetate = 4:1).

Approach C

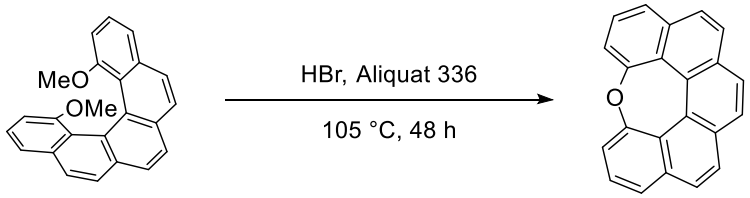

38 **80**

In a round bottomed flask equipped with a magnetic stir bar, 160.0 mg of 1,14-dimethoxy[5]helicene **38** (0.47 mmol, 1.0 equiv.) were added to a solution of Aliquat 336 (0.02 mL, 0.047 mmol, 0.10 equiv.) in hydrogen bromide (20 mL, 8.89 M in water). The solution was refluxed for 48 h. The reaction mixture was poured into water (40 mL) and then extracted with ethyl acetate (3×30 mL). The combined organic portions were washed with brine (2×150 mL), dried with anhydrous $MgSO_4$ and concentrated under reduced pressure. The crude product was purified by flash chromatography on silica gel (cyclohexane/ethyl acetate = 4:1). The product could not completely be isolated.

Yield: 18.0 mg (0.05 mmol, 18 %)

Approach D

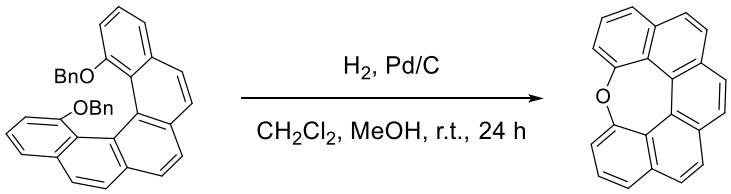

88 **80**

The reaction was carried out under Schlenk conditions. A Schlenk flask equipped with a magnetic stir bar was charged with 55.0 mg of 1,14-di(benzyloxy)pentahelicene **38** (0.11 mmol, 1.0 equiv.) and 11.93 mg of palladium on carbon (10 wt.%, 0.10 equiv.). The atmosphere was evacuated and flushed with hydrogen three times using a balloon. Degassed methanol (3 mL) and degassed dichloromethane (9 mL) were added. After 24 h of stirring at room temperature, the mixture was filtered through a plug of silica gel and extracted with dichloromethane (100 mL). The solvent was removed under reduced pressure. The crude product was purified by flash chromatography on silica gel (cyclohexane/ethyl acetate = 10:1). The product could not be isolated.

Yield: n/a

3-(Benzyloxy)-2-bromobenzaldehyde 81[350]

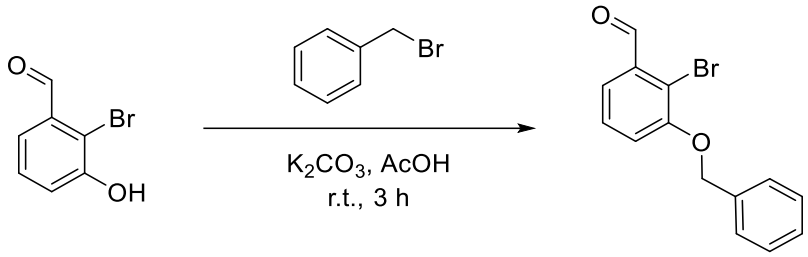

30 **81**

In a round bottomed flask equipped with a magnetic stir bar, 4.12 g of K_2CO_3 (29.84 mmol, 1.20 equiv.) were added to a solution of 2-bromo-3-hydroxy-benzaldehyde **30** (5.0 g, 24.87 mmol, 1.0 equiv.) in acetone (50 mL). After adding 3.84 mL of benzyl bromide (32.33 mmol, 1.30 equiv.), the solution was stirred at 30 °C for 3 h. The mixture was concentrated under reduced pressure, poured into water (50 mL) and extracted with dichloromethane (3×30 mL). The combined organic portions were dried with anhydrous Mg_2SO_4 and the solvent was evaporated under reduced pressure. The crude product was purified by flash chromatography on silica gel (cyclohexane/ethyl acetate = 4:1) to afford aldehyde **81** as a white solid.

Yield: 5.47 g (18.80 mmol, 76 %)

Molecular formula: $C_{14}H_{11}O_2Br$

Molecular weight: 291.14 g/mol

Retention factor: 0.20 (cyclohexane/ethyl acetate = 4:1)

^{1}H-NMR (400 MHz, $CDCl_3$, 298 K):
δ/ppm = 10.46 (d, 1H, *J* = 0.8 Hz), 7.54 (dd, 1H, *J* = 7.7 Hz, *J* = 1.5 Hz), 7.51−7.46 (m, 2H), 7.41 (ddd, 2H, *J* = 8.0 Hz, *J* = 7.1 Hz, *J* = 1.0 Hz), 7.38−7.31 (m, 2H), 7.16 (dd, 1H, *J* = 8.1 Hz, *J* = 1.5 Hz), 5.21 (s, 2H).

The spectral data were in agreement with those previously reported for this compound.[350]

3-(Benzyloxy)-2-[(trimethylsilyl)ethynyl]benzaldehyde 82

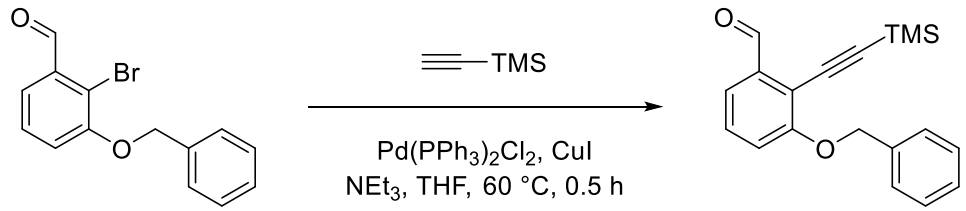

81 **82**

The reaction was carried out under Schlenk conditions. In a Schlenk flask equipped with a magnetic stir bar, 144.65 mg of $PdCl_2(PPh_3)_2$ (2 mol%), 78.49 mg of CuI (4 mol%) and 3.0 g of bromide **81** (10.30 mmol, 1.0 equiv.) were dissolved in anhydrous THF (5 mL) and degassed NEt_3 (10 mL). After adding 2.20 mL of trimethylsilylacetylene (15.46 mmol, 1.50 equiv.), the mixture was stirred at 60 °C for 0.5 h. The reaction mixture was poured into a saturated solution of aqueous NH_4Cl (30 mL) and extracted with DCM (3×30 mL). The combined organic portions were washed with brine (150 mL), dried with anhydrous $MgSO_4$ and concentrated under reduced pressure. The crude product was purified by flash chromatography on silica gel (cyclohexane/ethyl acetate = 9:1). Aldehyde **82** was obtained as a yellow solid.

Yield:	2.50 g (8.11 mmol, 79 %)
Molecular formula:	$C_{19}H_{20}O_2Si$
Molecular weight:	308.45 g/mol
Retention factor:	0.36 (cyclohexane/ethyl acetate = 4:1)
EI-MS:	*m*/*z* = 308.1 $[M]^{\bullet+}$
HRMS ($C_{19}H_{20}O_2Si^{\bullet+}$):	calculated = 308.1233
	found = 307.1149*

*The mass difference of 1 u is likely due to the formation of a benzylic radical.

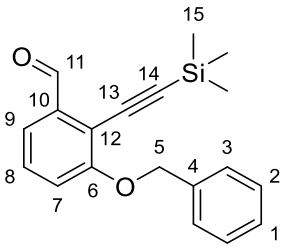

^{1}H-NMR (500 MHz, $CDCl_3$, 298 K):

δ/ppm = 10.58 (d, 1H, H-11, $^{5}J_{11,8}$ = 0.8 Hz), 7.55−7.50 (m, 3H, H-3, H-9), 7.43−7.30 (m, 4H, H-1, H-2, H-8), 7.16 (dd, 1H, H-7, $^{3}J_{7,8}$ = 8.2 Hz, $^{4}J_{7,9}$ = 1.1 Hz), 5.20 (s, 2H, H-5), 0.29 (s, 9H, H-15).

^{13}C-NMR (500 MHz, $CDCl_3$, 298 K):

δ/ppm = 192.2 (C-11), 160.4 (C-6), 137.6 (C-10), 136.5 (C-4), 129.6 (C-8), 128.6 (C-2), 128.1 (C-1), 126.9 (C-3), 119.3 (C-9), 117.8 (C-7), 116.9* (C-12), 107.5* (C-14), 70.8 (C-5), 0.0 (C-15).

*The signal was only visible in the HMBC-NMR, the signal for (C-13) was not visible.

3-(Benzyloxy)-2-ethynylbenzaldehyde 83

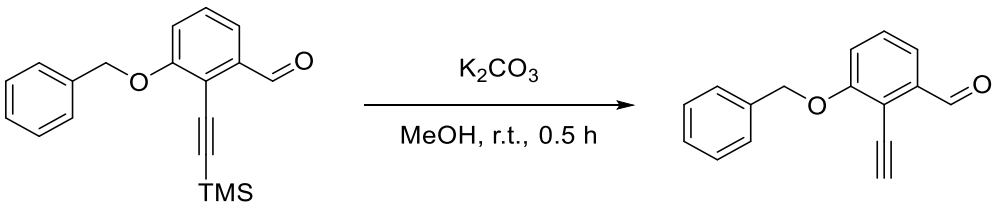

82 **83**

In a round bottomed flask equipped with a magnetic stir bar, 2.50 g of aldehyde **82** (8.11 mmol, 1.0 equiv.) were dissolved in methanol (20 mL) and 1.57 g of K_2CO_3 (11.35 mmol, 1.40 equiv.) were added in batches. The mixture was stirred at room temperature for 0.5 h. The reaction mixture was poured into water (20 mL) and extracted with DCM (3×30 mL). The combined organic portions were dried with anhydrous $MgSO_4$ and concentrated under reduced pressure. The crude product was purified by flash chromatography on silica gel (cyclohexane/ethyl acetate = 4:1) to obtain aldehyde **83**.

Yield: 1.24 g (5.23 mmol, 64 %)

Molecular formula: $C_{16}H_{12}O_2$

Molecular weight: 236.27 g/mol

Retention factor: 0.30 (cyclohexane/ethyl acetate = 4:1)

EI-MS: m/z = 235.0 $[M]^{\bullet+}$

HRMS ($C_{16}H_{12}O_2^{\bullet+}$): calculated = 236.0837

found = 235.0754*

*The mass difference of 1 u is likely due to the formation of a benzylic radical.

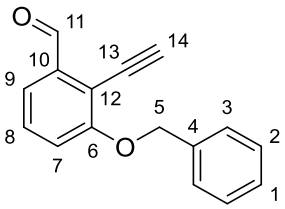

^{1}H-NMR (500 MHz, $CDCl_3$, 298 K):
δ/ppm = 10.56 (d, 1H, H-11, $^5J_{11,8}$ = 0.8 Hz), 7.54 (dd, 1H, H-9, $^3J_{9,8}$ = 7.8 Hz, $^4J_{9,7}$ = 1.1 Hz), 7.48 (ddd, 2H, H-3, $^3J_{3,2}$ = 7.7 Hz, $^4J_{3,1}$ = 1.7 Hz, $^4J_{3,5}$ = 0.8 Hz), 7.43−7.31 (m, 4H, H-1, H-2, H-8), 7.15 (dd, 1H, H-7, $^3J_{7,8}$ = 8.3 Hz, $^4J_{7,9}$ = 1.0 Hz), 5.24 (s, 2H, H-5), 3.70 (s, 1H, H-14).

^{13}C-NMR (500 MHz, $CDCl_3$, 298 K):
δ/ppm = 191.8 (C-11), 160.6 (C-6), 138.1 (C-10), 136.3 (C-4), 129.9 (C-8), 128.8 (C-2), 128.2 (C-1), 127.1 (C-3), 119.6 (C-9), 117.9 (C-7), 115.7 (C-12), 89.0 (C-14), 75.4 (C-13), 71.0 (C-5).

2,2'-(Ethyne-1,2-diyl)bis[3-(benzyloxy)benzaldehyde] 84

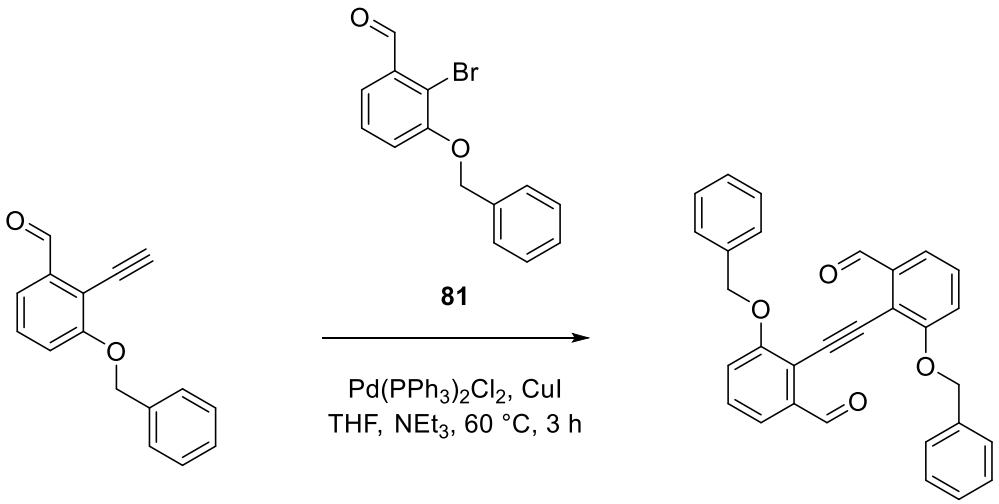

83 **84**

The reaction was carried out under Schlenk conditions. To a Schlenk flask charged with a magnetic stir bar, 59.41 mg of $PdCl_2(PPh_3)_2$ (2 mol%), 32.24 mg of CuI (4 mol%), 1.0 g of alkyne **83** (4.23 mmol, 1.0 equiv.) and 1.23 g of bromide **81** (4.23 mmol, 1.0 equiv.) were added. After adding anhydrous THF (5 mL) and degassed NEt_3 (10 mL), the mixture was heated to 60 °C and stirred for 3 h until the precipitation of a yellow solid was observed. The reaction mixture was concentrated under reduced pressure. The crude product was recrystallized (ethyl acetate) and washed with water (500 mL), acetone (500 mL) and dichloromethane (500 mL) to obtain dialdehyde **84** as yellow needles.

Yield:	1.89 g (4.23 mmol, 100 %)
Molecular formula:	$C_{30}H_{22}O_4$
Molecular weight:	446.50 g/mol
Retention factor:	0.20 (cyclohexane/ethyl acetate = 4:1)
ESI(+)-MS:	*m*/*z* = 485.115 $[M-K]^+$, 469.141 $[M+Na]^+$, 464.186 $[M+NH_4]^+$
HRMS ($C_{30}H_{22}O_4Na^+$):	calculated = 469.1410
	found = 469.1409

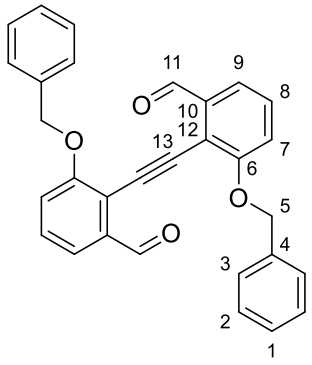

^{1}H-NMR (500 MHz, $CDCl_3$, 298 K):

δ/ppm = 10.62 (d, 2H, H-11, $^{5}J_{11,8}$ = 0.9 Hz), 7.54 (dd, 2H, H-9, $^{3}J_{9,8}$ = 7.7 Hz, $^{4}J_{9,7}$ = 1.1 Hz), 7.44 (dd, 4H, H-3, $^{3}J_{3,2}$ = 7.4 Hz, $^{4}J_{3,1}$ = 1.7 Hz), 7.44−7.31 (m, 8H, H-1, H-2, H-8), 7.18 (dd, 2H, H-7, $^{3}J_{7,8}$ = 8.4 Hz, $^{4}J_{7,9}$ = 1.1 Hz), 5.21 (s, 4H, H-5).

^{13}C-NMR (500 MHz, $CDCl_3$, 298 K):

δ/ppm = 191.9 (C-11), 160.1 (C-6), 137.5 (C-10), 136.0 (C-4), 129.9 (C-8), 129.0 (C-2), 128.4 (C-1), 127.5 (C-3), 119.4 (C-9), 117.3 (C-7), 116.6 (C-12), 92.8 (C-13), 71.2 (C-5).

1,1'-[Ethyne-1,2-diylbis(3-(benzyloxy)-2,1-phenylene)]bis(but-3-yn-1-ol) 85

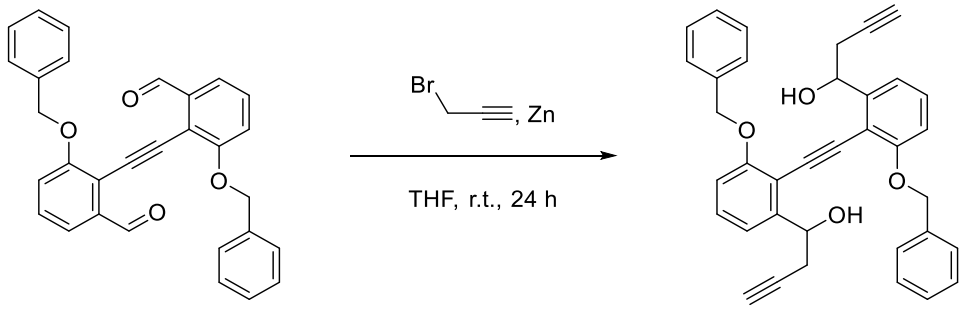

84 **85**

The reaction was carried out under Schlenk conditions. A Schlenk flask equipped with a magnetic stir bar was charged with 732.14 mg of zinc powder (11.20 mmol, 10.0 equiv.). Anhydrous tetrahydrofuran (10 mL) was added, the flask was immersed in a water bath at room temperature and a solution of propargyl bromide (1.24 mL, 80 wt.% in toluene, 11.20 mmol, 10.0 equiv.) was added slowly. The solution was stirred at room temperature for 30 minutes before it was added to the suspension of dialdehyde **84** (500.0 mg, 1.12 mmol, 1.0 equiv.) in anhydrous tetrahydrofuran (10 mL). After 24 h of stirring, the mixture was poured into water (30 mL) and extracted

with dichloromethane (3×40 mL), then the combined organic portions were washed with brine (100 mL) and HCl (100 mL, 6 M in water), dried with anhydrous Mg_2SO_4 and concentrated under reduced pressure. The crude product was used for the subsequent reaction without further purification and analytical characterization.

Yield: n/a

Molecular formula: $C_{36}H_{30}O_4$

Molecular weight: 526.63 g/mol

[Ethyne-1,2-diylbis(3-(benzyloxy)-2,1-phenylene)]bis(but-3-yne-1,1-diyl) diacetate 86

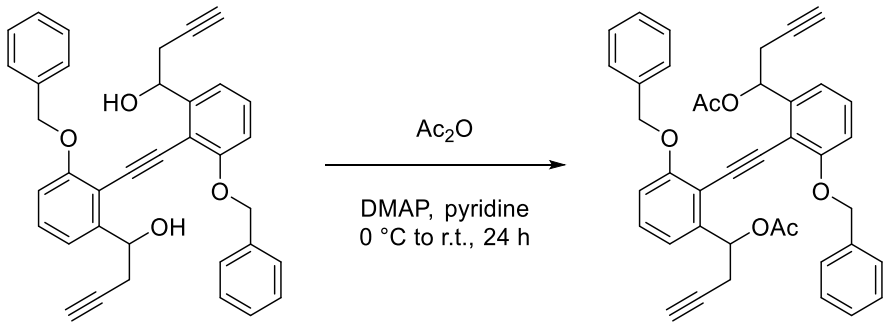

85 **86**

In a round bottomed flask equipped with a magnetic stir bar, a solution of diol **85** (1.2 g, 2.27 mmol, 1.0 equiv.) and 4-dimethylaminopyridine (33.41 mg, 0.27 mmol, 0.12 equiv.) in anhydrous pyridine (20 mL) was prepared. After adding 2.58 mL of acetic anhydride (27.3 mmol, 12.0 equiv.) at 0 °C while stirring, the reaction mixture was allowed to slowly reach room temperature and stirring was continued at the same temperature for an additional 24 h. The mixture was poured into water (20 mL) and extracted with dichloromethane (3×30 mL), then the combined organic portions were washed with a saturated aqueous solution of $KHCO_3$ (100 mL), dried with anhydrous Mg_2SO_4 and concentrated under reduced pressure. The crude product was purified by flash chromatography on silica gel (cyclohexane/ethyl acetate = 4:1) to afford diacetate **86** as a white solid.

Yield: 200.74 mg (0.33 mmol, 14 %) over 2 steps

Molecular formula: $C_{40}H_{34}O_6$

Molecular weight: 610.71 g/mol

Retention factor: 0.16 (cyclohexane/ethyl acetate = 4:1)

EI-MS: *m*/*z* = 610.3 $[M]^{\bullet+}$

HRMS ($C_{40}H_{34}O_6^{\bullet+}$): calculated = 610.2355

found = 610.2352

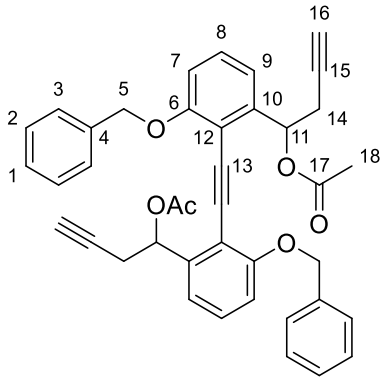

^{1}H-NMR (500 MHz, CD_2Cl_2, 298 K):

δ/ppm = 7.48−7.43 (m, 4H, H-3), 7.39−7.28 (m, 6H, H-1, H-2), 7.24 (t, 2H, H-8, $^{3}J_{8,7}$ = 8.1 Hz, $^{3}J_{8,9}$ = 8.1 Hz), 7.04 (dt, 2H, H-9, $^{3}J_{9,8}$ = 7.8 Hz, $^{4}J_{9,7}$ = 0.8 Hz, $^{4}J_{9,11}$ = 0.8 Hz), 6.88 (dd, 2H, H-7, $^{3}J_{7,8}$ = 8.4 Hz, $^{4}J_{7,9}$ = 1.0 Hz), 6.28 (t, 2H, H-11, $^{3}J_{11,14}$ = 5.2 Hz), 5.25−5.16 (m, 4H, H-5), 2.75 (ddd, 2H, H-14, $^{2}J_{14,14}$ = 17.2 Hz, $^{3}J_{14,11}$ = 5.7 Hz, $^{4}J_{14,16}$ = 2.7 Hz), 2.51 (ddd, 2H, H-14, $^{2}J_{14,14}$ = 17.2 Hz, $^{3}J_{14,11}$ = 4.8 Hz, $^{4}J_{14,16}$ = 2.6 Hz), 2.11 (s, 6H, H-18), 1.89 (t, 2H, H-16, $^{4}J_{16,14}$ = 2.6 Hz).

^{13}C-NMR (500 MHz, CD_2Cl_2, 298 K):

δ/ppm = 170.0 (C-17), 159.8 (C-6), 143.3 (C-10), 137.5 (C-4), 129.7 (C-8), 129.1 (C-2), 128.5 (C-1), 128.3 (C-3), 118.5 (C-9), 111.8 (C-7), 111.2 (C-12), 93.5 (C-13), 80.5 (C-15), 71.7 (C-11), 71.1 (C-5), 71.0 (C-16), 25.3 (C-14), 21.4 (C-18).

1,14-Di(benzyloxy)-5,6,9,10-tetrahydropentahelicene-5,10-diyl diacetate 87

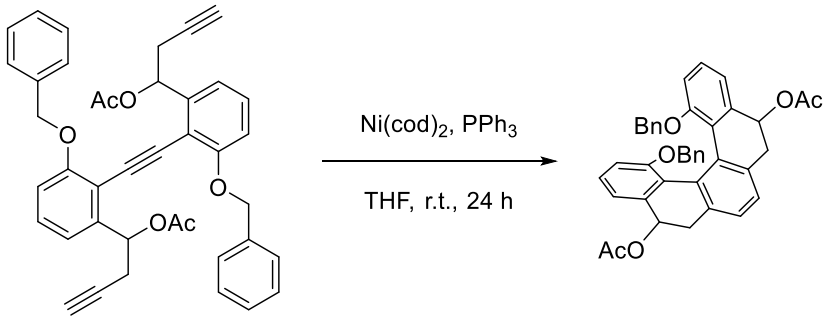

86 **87**

The reaction was carried out under Schlenk conditions. In a Schlenk flask equipped with a magnetic stir bar, 200.0 mg of triyne **86** (0.33 mmol, 1.0 equiv.) and 171.79 mg of PPh_3 (0.65 mmol, 2.0 equiv.) were dissolved in anhydrous THF (3 mL). After adding a stock solution of $Ni(cod)_2$ (5.47 mL, 0.06 M in THF, 1.0 equiv.), the mixture was stirred at room temperature for 24 h. The solvent was evaporated under reduced pressure and the residue was subjected to flash chromatography on silica gel (cyclohexane/ethyl acetate = 4:1) to afford tetrahydro[5]helicene derivative **87** as a complex mixture of stereoisomers. The mixture was used for the subsequent reaction without further analytical characterization.

Yield: n/a

Molecular formula: $C_{40}H_{34}O_6$

Molecular weight: 610.71 g/mol

Retention factor: 0.26 (cyclohexane/ethyl acetate = 4:1)

ESI(+)-MS: *m*/*z* = 633.224 $[M+Na]^+$

HRMS ($C_{40}H_{34}O_6Na^+$): calculated = 633.2248

found = 633.2244

1,14-Di(benzyloxy)pentahelicene 88

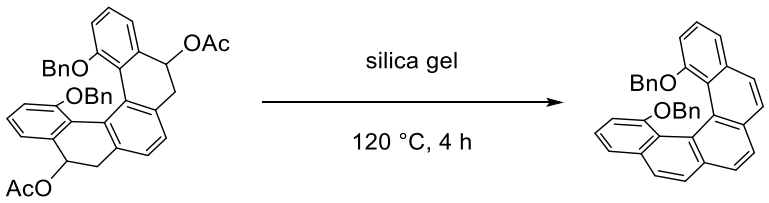

87 **88**

In a round bottomed flask equipped with a magnetic stir bar, a solution of tetrahydrohelicene derivative **87** (48.0 mg, 0.10 mmol, 1.0 equiv.) in dichloromethane (5 mL) was prepared. After adding silica gel (200 mg), the solvent was evaporated under reduced pressure and the solvent-free mixture was heated at 120 °C for 4 h under vigorous stirring. The product was extracted from silica gel with dichloromethane (100 mL). Removal of the solvent under reduced pressure gave rise to 1,14-(dibenzyloxy)[5]helicene **88** as an amorphous brown solid.

Yield: 57.71 mg (0.12 mmol, 35 %) over 2 steps

Molecular formula: $C_{36}H_{26}O_2$

Molecular weight: 490.60 g/mol

APCI-MS: *m*/*z* = 491.200 $[M+H]^+$

HRMS ($C_{36}H_{26}O_2H^+$): calculated = 491.2006

found = 491.2000

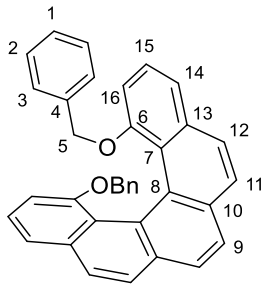

^{1}H-NMR (500 MHz, $CDCl_3$, 298 K):

δ/ppm = 7.97 (s, 2H, H-9), 7.82 (d, 2H, H-11, $^3J_{11,12}$ = 8.4 Hz), 7.60 (d, 2H, H-12, $^3J_{12,11}$ = 8.4 Hz), 7.30 (t, 2H, H-15, $^3J_{15,14}$ = 7.8 Hz, $^3J_{15,16}$ = 7.8 Hz), 7.18 (dd, 2H, H-14, $^3J_{14,15}$ = 7.8 Hz, $^4J_{14,16}$ = 1.3 Hz), 7.14−7.08 (m, 2H, H-1), 7.07−7.00 (m, 4H, H-2), 6.76 (dd, 2H, H-16, $^3J_{16,15}$ = 7.8 Hz, $^4J_{16,14}$ = 1.3 Hz), 6.46 (dd, 4H, H-3, $^3J_{3,2}$ = 7.3 Hz, $^4J_{3,1}$ = 1.7 Hz), 4.45 (d, 2H, H-5, $^2J_{5,5}$ = 12.2 Hz), 3.98 (d, 2H, H-5, $^2J_{5,5}$ = 12.2 Hz).

^{13}C-NMR (500 MHz, $CDCl_3$, 298 K):

δ/ppm = 155.7 (C-6), 136.8 (C-4), 133.2 (C-13), 131.4 (C-10), 127.8 (C-2), 127.3 (C-12), 126.9 (C-1), 126.4 (C-3), 126.2 (C-9), 126.0 (C-11), 125.8 (C-8), 125.4 (C-15), 125.0 (C-7), 120.2 (C-14), 106.6 (C-16), 69.9 (C-5).

2,17-Dihydroxyheptahelicene 89

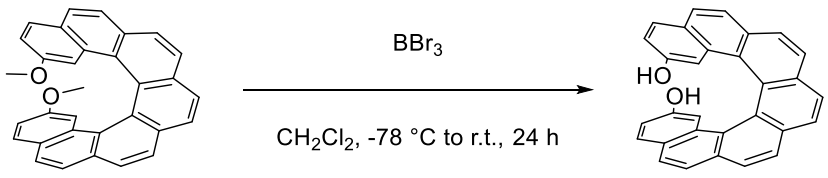

55 **89**

In a round bottomed flask equipped with a magnetic stir bar, a solution of 2,17-dimethoxy[7]helicene **55** (94.73 mg, 0.21 mmol, 1.0 equiv.) in dichloromethane (15 mL) was cooled to −78 °C. A solution of BBr_3 (2.14 mL, 1 M in CH_2Cl_2, 2.14 mmol, 10.0 equiv.) was added, the mixture was slowly warmed up to room temperature and stirred for 24 h. The reaction mixture was poured into an aqueous solution of saturated $NaHCO_3$ (30 mL) and then extracted with ethyl acetate (3×15 mL). The combined organic portions were washed with water (100 mL), dried with anhydrous $MgSO_4$ and concentrated under reduced pressure. The crude product was purified by flash chromatography on silica gel (petroleum ether/ethyl acetate = 4:1) to obtain 2,17-dihydroxy[7]helicene **89** as a yellow solid.

Yield:	71.41 mg (0.17 mmol, 81 %)
Molecular formula:	$C_{30}H_{18}O_2$
Molecular weight:	410.47 g/mol
Retention factor:	0.10 (petroleum ether/ethyl acetate = 4:1)
APCI-MS:	*m*/*z* = 411.138 $[M+H]^+$
HRMS ($C_{30}H_{18}O_2H^+$):	calculated = 411.1380
	found = 411.1377

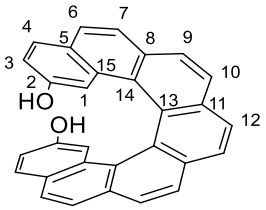

^{1}H-NMR (700 MHz, $CDCl_3$, 298 K):
δ/ppm = 8.05 (s, 2H, H-12), 8.02 (d, 2H, H-10, $^3J_{10,9}$ = 8.1 Hz), 7.95 (d, 2H, H-9, $^3J_{9,10}$ = 8.1 Hz), 7.66 (d, 2H, H-7, $^3J_{7,6}$ = 8.3 Hz), 7.59 (d, 2H, H-6, $^3J_{6,7}$ = 8.3 Hz), 7.31 (d, 2H, H-4, $^3J_{4,3}$ = 8.5 Hz), 6.60 (dd, 2H, H-3, $^3J_{3,4}$ = 8.5 Hz, $^4J_{3,1}$ = 2.5 Hz), 6.47 (d, 2H, H-1, $^4J_{1,3}$ = 2.5 Hz).

^{13}C-NMR (700 MHz, $CDCl_3$, 298 K):

δ/ppm = 152.7 (C-2), 132.1 (C-11), 131.3 (C-8), 130.8 (C-15), 128.8 (C-4), 127.8 (C-14), 127.7 (C-9), 127.5 (C-6), 127.4 (C-10), 127.2 (C-5), 126.9 (C-12), 124.8 (C-13), 123.2 (C-7), 115.9 (C-3), 109.5 (C-1).

Heptahelicene-2,17-diyl bis(trifluormethanesulfonate) 90

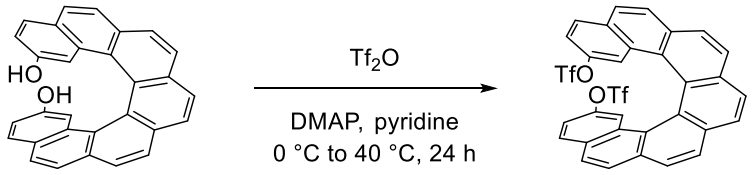

89 **90**

In a round bottomed flask equipped with a magnetic stir bar, a solution of diol **89** (65.98 mg, 0.16 mmol, 1.0 equiv.) and 4-dimethylaminopyridine (0.96 mg, 0.0079 mmol, 0.12 equiv.) in anhydrous pyridine (5 mL) was prepared. After adding 0.23 mL of trifluoromethanesulfonic anhydride (0.69 mmol, 4.40 equiv.) at 0 °C while stirring, the reaction mixture was allowed to slowly reach room temperature and stirring was continued at 40 °C for an additional 24 h. The mixture was concentrated under reduced pressure and the crude product was purified by flash chromatography on silica gel (cyclohexane/ethyl acetate = 4:1) to afford triflate **90** as an off-white solid.

Yield:	110.24 mg (0.16 mmol, 100 %)
Molecular formula:	$C_{32}H_{16}F_6O_6S_2$
Molecular weight:	674.58 g/mol
Retention factor:	0.45 (cyclohexane/ethyl acetate = 4:1)
APCI-MS:	*m*/*z* = 674.029 $[M]^{\bullet+}$
HRMS ($C_{32}H_{16}F_6O_6S_2^{\bullet+}$):	calculated = 674.0287
	found = 674.0284

Specific optical rotation: (−)-(*M*)-**90**: $[\alpha]_D^{20} = -1888°$ mL×dm^{-1}×g^{-1}* (*c* ≈ 0.63 g/L, dichloromethane)

(+)-(*P*)-**90**: $[\alpha]_D^{20} = +2036°$ mL×dm^{-1}×g^{-1}* (*c* ≈ 0.55 g/L, dichloromethane)

*The difference observed is likely due to deviations in concentrations caused by the volatility of dichloromethane.

ECD: (−)-(*M*)-**90**: *λ*/nm (*Δε*/M^{-1}×cm^{-1}) = 250 (+54.6), 270 (+295.8), 293 (+28.5), 317 (−66.7), 351 (−191.5), 400 (−73.1); (*c* = 6.3×10^{-4} g/L, dichloromethane)

(+)-(*P*)-**90**: *λ*/nm (*Δε*/M^{-1}×cm^{-1}) = 250 (+38.5), 270 (−262.3), 293 (−91.7), 317 (−46.3), 351 (+65.4), 400 (−39.6); (*c* = 5.5×10^{-4} g/L, dichloromethane)

Analytical HPLC: CHIRALPAK IB-U; *n*-hexane/isopropanol/ethanol (98:2:2); *f* = 0.85 mL min^{-1}); (–)-(M)-**90**: t_R = 1.15 min; (+)-(P)-**90**: t_R = 1.34 min

Semipreparative HPLC: CHIRALPAK IB; *n*-hexane/ethanol (98:2); *f* = 18 mL min^{-1}); (–)-(M)-**90**: t_R = 30.42 min, >98 % *ee*; (+)-(P)-**90**: t_R = 33.15 min, 96.0 % *ee*

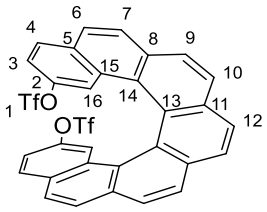

^{1}H-NMR (500 MHz, $CDCl_3$, 298 K):

δ/ppm = 8.13 (s, 2H, H-12), 8.12 (d, 2H, H-10, $^3J_{10,9}$ = 8.2 Hz), 8.02 (d, 2H, H-9, $^3J_{9,10}$ = 8.2 Hz), 7.89 (d, 2H, H-7, $^3J_{7,6}$ = 8.5 Hz), 7.62 (d, 2H, H-6, $^3J_{6,7}$ = 8.5 Hz), 7.45 (d, 2H, H-4, $^3J_{4,3}$ = 8.8 Hz), 7.00 (d, 2H, H-16, $^4J_{16,3}$ = 2.5 Hz) 6.86 (dd, 2H, H-3, $^3J_{3,4}$ = 8.8 Hz, $^4J_{3,16}$ = 2.5 Hz).

^{13}C-NMR (500 MHz, $CDCl_3$, 298 K):

δ/ppm = 146.4 (C-2), 132.7 (C-11), 131.9 (C-8), 131.0 (C-5), 129.8 (C-15), 129.2 (C-4), 128.5 (C-10/C-12), 127.9 (C-10/C-12), 127.8 (C-9), 127.7 (C-7), 127.3 (C-14), 126.7 (C-6), 124.1 (C-13), 118.5 (C-3), 116.8 (C-16).*

*C-1 is not visible in the ^{13}C-spectrum.

2,17-Di(pyridin-4-yl)heptahelicene 91

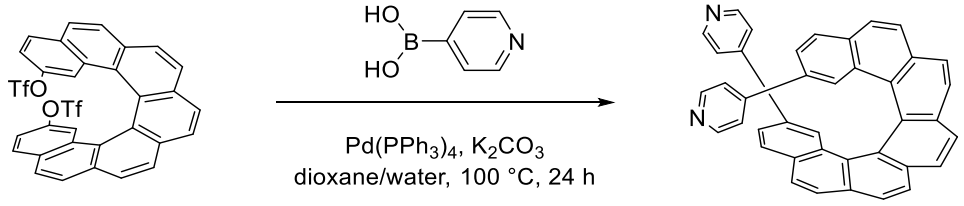

90 **91**

The reaction was carried out under Schlenk conditions. A mixture of 1,4-dioxane and water (4:1) was degassed by 3 freeze-pump-thaw cycles before use. In a Schlenk flask equipped with a magnetic stir bar, 16.44 mg of $Pd(PPh_3)_4$ (8 mol%), 61.46 mg of potassium carbonate (0.44 mmol, 2.50 equiv.), 54.66 mg of 4-pyridinylboronic acid (0.44 mmol, 2.50 equiv.) and 120.0 mg of triflate **90** (0.17 mmol, 1.0 equiv.) were dissolved in a mixture of degassed 1,4-dioxane and water (20 mL). The mixture was stirred at 100 °C for 24 h. The reaction mixture was poured into a saturated solution of aqueous EDTA (20 mL) and extracted with DCM (3×20 mL). The combined organic portions were washed with brine (80 mL), dried with anhydrous $MgSO_4$ and concentrated under reduced pressure. The crude product was purified by flash chromatography on silica gel (dichloromethane/ethyl acetate/methanol = 1:1:0 to 50:50:4). [7]Helicene derivative **91** was obtained as a yellow solid.

Yield:	20.39 mg (0.036 mmol, 20 %)
Molecular formula:	$C_{40}H_{24}N_2$
Molecular weight:	532.64 g/mol
Retention factor:	0.08 (ethyl acetate)
ESI(+)-MS:	*m*/*z* = 533.202 $[M+H]^+$, 267.105 $[M+2H]^{2+}$

HRMS ($C_{40}H_{24}N_2H^+$): calculated = 533.2012

found = 533.2018

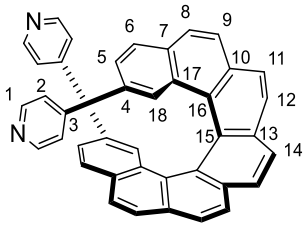

^{1}H-NMR (500 MHz, $CDCl_3$, 298 K):

δ/ppm = 8.61 (s, 4H, H-1), 8.24−8.20 (m, 4H, H-12, H-14), 7.94 (d, 2H, H-11, $^3J_{11,12}$ = 8.1 Hz), 7.85 (s, 2H, H-18), 7.57−7.46 (m, 8H, H-2, H-6, H-9), 7.41−7.34 (m, 4H, H-5, H-8).

^{13}C-NMR (500 MHz, $CDCl_3$, 298 K):

δ/ppm = 140.4 (C-1), 133.9 (C-3), 133.3*, 131.8*, 129.4*, 129.2*, 129.1*, 129.0*, 128.9*, 128.4*, 127.9*, 127.5*, 126.7*, 125.9*, 125.0*, 124.5*, 123.0 (C-2/C-5).

*The signal could not be unambiguously assigned.

2,17-Bis[4-(pyridin-4-yl)phenyl]heptahelicene 92

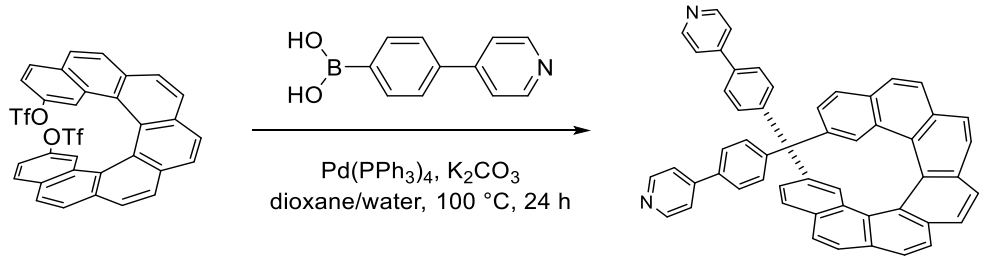

90 **92**

The reaction was carried out under Schlenk conditions. A mixture of 1,4-dioxane and water (4:1) was degassed by 3 freeze-pump-thaw cycles before use. In a Schlenk flask equipped with a magnetic stir bar, 16.44 mg of $Pd(PPh_3)_4$ (8 mol%), 61.46 mg of potassium carbonate (0.44 mmol, 2.50 equiv.), 88.50 mg of (4-(pyridin-4-yl)phenyl)boronic acid (0.44 mmol, 2.50 equiv.) and 120.0 mg of triflate **90** (0.17 mmol, 1.0 equiv.) were dissolved in a mixture of degassed 1,4-dioxane and water (20 mL). The mixture was stirred at 100 °C for 24 h. The reaction mixture was poured into a saturated solution of aqueous EDTA (20 mL) and extracted with DCM (3×20 mL). The

combined organic portions were washed with brine (80 mL), dried with anhydrous $MgSO_4$ and concentrated under reduced pressure. The crude product was purified by flash chromatography on silica gel (dichloromethane/ethyl acetate/methanol = 1:1:0 to 50:50:2) and recrystallized (ethyl acetate/methanol = 20:1). [7]Helicene derivative **92** was obtained as yellow needles.

Yield:	20.92 mg (0.029 mmol, 16 %)
Molecular formula:	$C_{52}H_{32}N_2$
Molecular weight:	684.84 g/mol
Retention factor:	0.05 (dichloromethane/ethyl acetate = 1:1)
ESI(+)-MS:	*m*/*z* = 685.266 $[M+H]^+$, 343.136 $[M+2H]^{2+}$
HRMS ($C_{52}H_{32}N_2H_2^{2+}$):	calculated = 343.1356
	found = 343.1363
Specific optical rotation:	(−)-(*M*)-**92**: $[\alpha]_D^{20} = -1176°$ mL×dm^{-1}×g^{-1}* (*c* = 1.7×10^{-2} g/L, DMSO)
	(+)-(*P*)-**92**: $[\alpha]_D^{20} = +1000°$ mL×dm^{-1}×g^{-1}* (*c* = 5.0×10^{-2} g/L, DMSO)

*Due to the low solubility of the substance, the solutions had a lower concentration than is usually required for measurements of optical rotations. For that reason, the obtained values carry a considerable uncertainty.

ECD:	(−)-(*M*)-**92**: *λ*/nm (*Δε*/M^{-1}×cm^{-1}) = 300 (+13.5), 311 (+12.1), 328 (+16.3), 370 (−101.2), 386 (−89.9); (*c* = 1.7×10^{-2} g/L, dimethylsulfoxid)
	(+)-(*P*)-**92**: *λ*/nm (*Δε*/M^{-1}×cm^{-1}) = 300 (+0.5), 311 (+0.3), 328 (−2.1), 370 (+86.0), 386 (+79.1); (*c* = 3.0×10^{-2} g/L, dimethylsulfoxid)

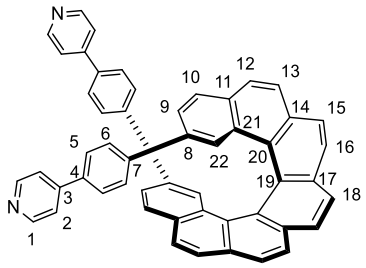

^{1}H-NMR (400 MHz, DMSO-d6, 298 K):

δ/ppm = 8.69−8.66 (m, 4H, H-1), 8.30−8.26 (m, 4H, H-16, H-18), 8.18 (d, 2H, H-15, $^{3}J_{15,16}$ = 8.2 Hz), 7.83−7.78 (m, 8H, H-2, H-5), 7.66 (d, 2H, H-13, $^{3}J_{13,12}$ = 8.6 Hz), 7.57−7.52 (m, 6H, H-10, H-12, H-22), 7.45 (dd, 2H, H-9, $^{3}J_{9,10}$ = 8.2 Hz, $^{4}J_{9,22}$ = 1.9 Hz), 7.23 (d, 4H, H-6, $^{3}J_{6,5}$ = 8.4 Hz).

^{13}C-NMR (400 MHz, DMSO-d6, 298 K):

No spectrum could be measured due to low solubility of the compound.

Crystallographic data [(*rac*)-**92**]

Empirical formula: $C_{52}H_{32}N_2C_2H_8O_2$; M = 748.88 g/mol; T = 100.0 K; radiation type: CuKα; λ = 1.54186 Å; crystal system: monoclinic; space group: $P2_1/c$; unit cell: a = 14.8051(7) Å, b = 13.9724(4) Å, c = 18.4223(9) Å, α = 90°, β = 92.683(4)°, γ = 90°, V = 3806.7(3) Å^3, Z = 4, ρ_{calc} = 1.307 g/cm^3; absorption correction = multi-scan; μ = 0.613 mm^{-1}; minimum transmission = 0.6981; maximum transmission = 0.9056; F(000) = 1576.0; crystal color: clear light yellow pale; crystal size = 0.5×0.15×0.04 mm^3; 2Θ range for data collection: 5.976°−141.298°; Reflections collected [R(int)] = 36967 [0.0881]; Reflections [I>2σ(I)] = 7166; data completeness = 99.3 %; Data/parameters/restraints = 7166/527/0; Goodness-of-fit on F^2 = 1.059; Final R indexes [I>=2σ(I)]: R_1 = 0.0797, wR_2 = 0.2123; Final R indexes [all data]: R_1 = 0.1219, wR_2 = 0.2521; Largest diff. peak/hole = 0.49/−0.36 e Å^{-3}.

2,17-Bis[4-(pyridin-3-yl)phenyl]heptahelicene 93

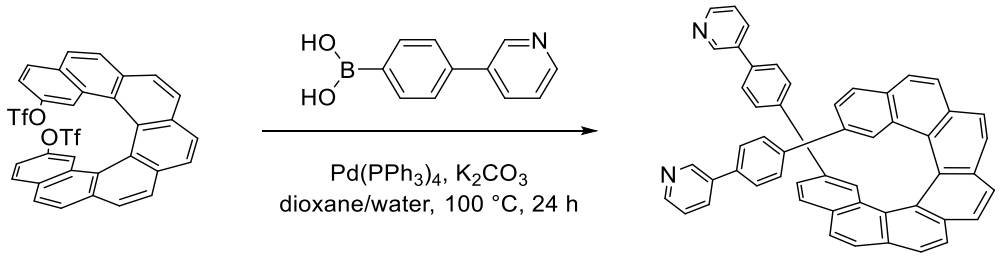

90 **93**

The reaction was carried out under Schlenk conditions. A mixture of 1,4-dioxane and water (4:1) was degassed by 4 freeze-pump-thaw cycles before use. In a Schlenk flask equipped with a magnetic stir bar, 15.07 mg of $Pd(PPh_3)_4$ (8 mol%), 56.34 mg of potassium carbonate (0.40 mmol, 2.50 equiv.), 81.13 mg of (4-(pyridin-3-yl)phenyl)boronic acid (0.40 mmol, 2.50 equiv.) and 110.0 mg of triflate **90** (0.16 mmol, 1.0 equiv.) were dissolved in a mixture of degassed 1,4-dioxane and water (20 mL). The mixture was stirred at 100 °C for 24 h. The reaction mixture was poured into a saturated solution of aqueous EDTA (20 mL) and extracted with DCM (3×20 mL). The combined organic portions were washed with brine (80 mL), dried with anhydrous $MgSO_4$ and concentrated under reduced pressure. The crude product was purified by flash chromatography on silica gel (dichloromethane/ethyl acetate/methanol = 1:1:0 to 50:50:2), [7]helicene derivative **93** was obtained as a yellow solid.

Yield:	47.68 mg (0.069 mmol, 42 %)
Molecular formula:	$C_{52}H_{32}N_2$
Molecular weight:	684.84 g/mol
Retention factor:	0.05 (dichloromethane/ethyl acetate = 1:1)
ESI(+)-MS:	*m*/*z* = 685.263 $[M+H]^+$, 343.135 $[M+2H]^{2+}$
HRMS ($C_{52}H_{32}N_2H^+$):	calculated = 685.2638
	found = 685.2634

Specific optical rotation: (−)-(*M*)-**93**: $[\alpha]_D^{20} = -3660°$ mL×dm^{-1}×g^{-1}* (*c* = 10.0 g/L, dichloromethane)

(+)-(*P*)-**93**: $[\alpha]_D^{20} = +3720°$ mL×dm^{-1}×g^{-1}* (*c* = 10.01 g/L, dichloromethane)

*The difference observed is likely due to deviations in concentrations caused by the volatility of dichloromethane.

ECD: (−)-(*M*)-**93**: *λ*/nm (*Δε*/M^{-1}×cm^{-1}) = 269 (+179.3), 293 (+331.5), 310 (+180.4), 368 (−267.8), 379 (−241.5); (*c* = 3.1×10^{-3} g/L, dichloromethane)

(+)-(*P*)-**93**: *λ*/nm (*Δε*/M^{-1}×cm^{-1}) = 269 (−110.6), 293 (−227.4), 310 (−105.6), 368 (+192.2), 379 (+172.5); (*c* = 3.7×10^{-3} g/L, dichloromethane)

Analytical HPLC: CHIRALPAK IC-U; dichloromethane/ethanol/diethylamine (20:80:0.08); *f* = 0.43 mL min^{-1}); (–)-(M)-**93**: t_R = 3.66 min; (+)-(P)-**93**: t_R = 4.49 min

Semipreparative HPLC: YMC CHIRAL ART Cellulose-SC; dichloromethane/ethanol/diethylamine (20:80:0.08); *f* = 10 mL min^{-1}); (–)-(M)-**93**: t_R = 14.63 min, >99 % *ee*; (+)-(P)-**93**: t_R = 17.66 min, 98 % *ee*

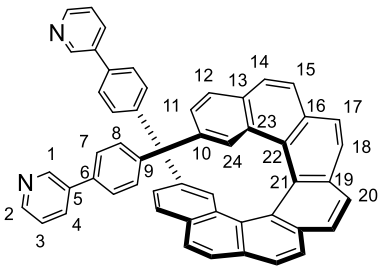

^{1}H-NMR (700 MHz, CD_2Cl_2, 298 K):

δ/ppm = 8.92 (dd, 2H, H-1, $^4J_{1,4}$ = 2.4 Hz, $^5J_{1,3}$ = 0.9 Hz), 8.60 (dd, 2H, H-2, $^3J_{2,3}$ = 4.8 Hz, $^4J_{2,4}$ = 1.6 Hz), 8.13 (s, 2H, H-20), 8.12 (d, 2H, H-18, $^3J_{18,17}$ = 8.2 Hz), 7.97 (ddd, 2H, H-4, $^3J_{4,3}$ = 7.7 Hz, $^4J_{4,1}$ = 2.4 Hz, $^4J_{4,2}$ = 1.6 Hz), 7.96 (d, 2H, H-17,

$^{3}J_{17,18}$ = 8.2 Hz), 7.61 (d, 2H, H-24, $^{4}J_{24,11}$ = 1.7 Hz), 7.59−7.56 (m, 4H, H-7), 7.47 (d, 2H, H-15, $^{3}J_{15,14}$ = 8.4 Hz), 7.45 (d, 2H, H-12, $^{3}J_{12,11}$ = 8.2 Hz), 7.43−7.40 (m, 4H, H-3, H-14), 7.36 (dd, 2H, H-11, $^{3}J_{11,12}$ = 8.2 Hz, $^{4}J_{11,24}$ = 1.7 Hz), 7.23−7.19 (m, 4H, H-8).

^{13}C-NMR (700 MHz, CD_2Cl_2, 298 K):
δ/ppm = 149.1 (C-2), 148.7 (C-1), 140.3 (C-9), 136.8 (C-6), 136.6 (C-5), 135.6 (C-10), 134.5 (C-4), 132.8 (C-19), 132.1 (C-16), 131.9 (C-13), 130.0 (C-23), 128.8 (C-22), 128.0 (C-17), 127.96 (C-12), 127.94 (C-18/C-20), 127.8 (C-8), 127.5 (C-18/C-20), 127.4 (C-14), 127.3 (C-7), 126.6 (C-15), 125.6 (C-21), 124.3 (C-11), 124.1 (C-3), 123.9 (C-24).

Complexation experiments

$[Pd(76)_2](BF_4)_2$

In a microwave tube equipped with a magnetic stir bar, 1.77 mg of (*rac*)-**76** (4.09 µmol, 1.0 equiv.) were dissolved in CD_3CN (0.4 mL). A stock solution of $Pd(MeCN)_4(BF_4)_2$ (225 µL, 10.0 mM in CD_3CN, 0.55 equiv.) was added. The tube was closed with a screw cap and the solution was stirred at room temperature overnight.

ESI(+)-MS: *m*/*z* = 1057.240 $\{[Pd(\mathbf{76})_2](BF_4)\}^+$, 989.234 $\{[Pd(\mathbf{76})_2]F\}^+$, 485.118 $[Pd(\mathbf{76})_2]^{2+}$, 433.172 $[\mathbf{76}+H]^+$

^{1}H-NMR (500 MHz, CD_3CN, 298 K):

The signals could not be assigned due to the heavy amount of overlapping multiplets.

$[Cu(76)](BF_4)$, $[Cu(76)(MeCN)](BF_4)$, $[Cu(76)_2](BF_4)$, $[Cu(76)_3](BF_4)$

The reaction was carried out under Schlenk conditions. In a microwave tube equipped with a magnetic stir bar, 1.12 mg of (*rac*)-**76** (2.58 µmol, 1.0 equiv.) were dissolved in CD_3CN (0.39 mL). A stock solution of $Cu(MeCN)_4(BF_4)$ (129 µL, 10.0 mM in CD_3CN, 0.50 equiv.) was added. The tube was closed with a screw cap and the solution was stirred at room temperature overnight.

ESI(+)-MS: *m*/*z* = 1360.422 $[Cu(\mathbf{76})_3]^+$, 927.255 $[Cu(\mathbf{76})_2]^+$, 536.119 $[Cu(\mathbf{76})(MeCN)]^+$, 495.092 $[Cu(\mathbf{76})]^+$, 433.170 $[\mathbf{76}+H]^+$

^{1}H-NMR (400 MHz, CD_3CN, 298 K):

δ/ppm = 8.84 (s, 2H), 8.58 (bs, 2H), 8.41 (bs, 2H), 8.21 (d, 2H, ^3J = 8.3 Hz), 8.09 (d, 2H, ^3J = 8.6 Hz), 8.06−8.02 (m, 4H), 7.90 (dd, 2H, ^3J = 8.4 Hz, ^4J = 1.8 Hz), 7.74−7.70 (m, 2H), 7.26 (bs, 2H).

$[Pd_2(dppp)_2(92)_2](OTF)_4$, $[Pd_2(dppp)(92)_2](OTf)_2$

In a microwave tube equipped with a magnetic stir bar, 5.0 mg of (*P*)-**92**, (*M*)-**92** or (*rac*)-**92** (7.30 µmol, 1.0 equiv.) were dissolved in DMSO-d6 (0.30 mL). A stock solution of $Pd(dppp)(OTf)_2$ (730 µL, 10.0 mM in DMSO-d6, 1.0 equiv.) was added. The tube was closed with a screw cap and the solution was stirred at room temperature overnight.

ESI(+)-MS: *m*/*z* = 2037.532 {[Pd(dppp)(**92**)$_2$](OTf)}$^+$, 1351.268 {[Pd$_2$(dppp)$_2$(**92**)$_2$](OTf)$_2$}$^{2+}$, 851.861 {[Pd$_2$(dppp)$_2$(**92**)$_2$](OTf)}$^{3+}$, 685.264 [**92**+H]$^+$, 601.157 [Pd$_2$(dppp)$_2$(**92**)$_2$]$^{4+}$

^{1}H-NMR (400 MHz, CD_3CN, 298 K):

δ/ppm = 8.74 (bs, 16H), 8.23 (bs, 16H), 8.08 (bs, 8H), 7.71 (bs, 64H), 7.60−7.35 (m, 88H), 7.17 (bs, 16H), 3.20 (bs, 24H).

[Pd$_3$(93)$_6$](BF$_4$)$_6$, [Pd$_4$(93)$_8$](BF$_4$)$_8$

In a microwave tube equipped with a magnetic stir bar, 4.50 mg of (*P*)-**93**, (*M*)-**93** or (*rac*)-**93** (6.57 µmol, 1.0 equiv.) were dissolved in DMSO-d6 (0.45 mL). A stock solution of Pd(MeCN)$_4$(BF$_4$)$_2$ (328 µL, 10.0 mM in DMSO-d6, 1.0 equiv.) was added. The tube was closed with a screw cap and the solution was stirred at 50 °C overnight.

ESI(+)-MS: *m*/*z* = 1150.317 {[Pd$_3$(**93**)$_6$](BF$_4$)$_2$}$^{4+}$, 903.054 {[Pd$_3$(**93**)$_6$](BF$_4$)}$^{5+}$, 855.527 {[Pd$_4$(**93**)$_8$](BF$_4$)}$^{7+}$, 737.877 [Pd$_3$(**93**)$_6$]$^{6+}$, 684.257 [**93**]$^{\bullet+}$

^{1}H-NMR (400 MHz, CD_3CN, 298 K):

The signals could not be assigned due to the heavy amount of overlapping multiplets.

11 Abbreviations

acac	Acetylacetone
AFM	Atomic force microscopy
APCI	Atmospheric pressure chemical ionization
b	Broad
BINAP	[2,2′-Bis(diphenylphosphino)-1,1′-binaphthyl]
BINOL	1,1′-Bi-2-naphthol
BINPHAT	Bis(tetrachlorobenzenediolato)mono([1,1‘]binaphthalenyl-2,2‘diolato)phosphate(V)
BPO	Benzoyl peroxide
BuLi	Butyllithium
C-PCM	Conductor-like polarizable continuum model
CA	*Candida antarctica*
CA	Cycloaddition
CAN	Cerium ammonium nitrate
CD	Cyclodextrin
CE	Capillary eletrophoresis
cod	1,5-Cyclooctadiene
COSY	Correlation spectroscopy
CP	Circularly polarized
CPL	Circularly polarized luminescence
CSP	Chiral stationary phase
DCM	Dichloromethane
DDQ	2,3-Dichloro-5,6-dicyano-1,4-benzoquinone
de	Diastereomeric excess
DEA	Diethylamine
DFT	Density functional theory
Diff.	Difference
DKR	Dynamic kinetic resolution
DMAP	4-Dimethylaminopyridine

DME	Dimethoxyethane
DMF	Dimethylformamide
DMSO	Dimethyl sulfoxide
DNA	Deoxyribonucleic acid
DOSY	Diffusion-ordered spectroscopy
dppf	1,1′-Bis(diphenylphosphino)ferrocene
dppp	1,3-Bis(diphenylphosphino)propane
ECD	Electronic circular dichroism
EDL	Electrodeless discharge lamps
EDTA	Ethylenediaminetetraacetic acid
ee	Enantiomeric excess
e.g.	*exempli gratia*
EI	Electron ionization
EOF	Electro-osmotic flow
equiv.	Equivalents
ESI	Electrospray ionization
HMBQ	Heteronuclear multiple-bond correlation
HPLC	High-performance liquid chromatography
HRMS	High-resolution mass spectrometry
HSQC	Heteronuclear single quantum coherence
i.e.	*id est*
IUPAC	International Union of Pure and Applied Chemistry
KHMDS	Potassium hexamethyldisilazide
l	Left
L	Ligand
LAH	Lithium aluminium hydride
LED	Light-emitting diode
MMFF	Merck molecular force field
MW	Microwaves
mol%	Mole percent
NBS	*N*-Bromosuccinimide

NHC	*N*-Heterocyclic carbene
NLO	Nonlinear optics
NMR	Nuclear magnetic resonance
NOESY	Nuclear Overhauser enhancement spectroscopy
OR	Optical rotation
pin	Pinacol
ppm	Parts per million
PS	*Pseudomonas cepacian*
r	Right
rac	Racemic
RCM	Ring closing metathesis
ROESY	Rotating frame Overhauser enhancement spectroscopy
r.t.	Room temperature
TAPA	2-(2,4,5,7-Tetranitro-9-fluorenylideneaminooxy)propionic acid
TBAF	Tetra-*n*-butylammonium fluoride
THF	Tetrahydrofuran
TIPS	Triisopropylsilyl
TLC	Thin-layer chromatography
TMS	Trimethylsilyl
TPEN	*N*,*N*,*N*′,*N*′-Tetrakis(2-pyridylmethyl)ethane-1,2-diamine
UV	Ultraviolet
VCD	Vibrational circular dichroism
Vis	Visible
wt.%	Weight percent
XRD	X-ray diffraction

12 Bibliography

[1] M. S. Newman, D. Lednicer, *J. Am. Chem. Soc.* **1956**, *78*, 4765–4770.
[2] P. Ravat, R. Hinkelmann, D. Steinebrunner, A. Prescimone, I. Bodoky, M. Juríček, *Org. Lett.* **2017**, *19*, 3707–3710.
[3] P. Ravat, *Chem. Eur. J.* **2021**, *27*, 3957–3967.
[4] Z. Krausová, P. Sehnal, B. P. Bondzic, S. Chercheja, P. Eilbracht, I. G. Stará, D. Šaman, I. Starý, *Eur. J. Org. Chem.* **2011**, 3849–3857.
[5] K. Yavari, P. Aillard, Y. Zhang, F. Nuter, P. Retailleau, A. Voituriez, A. Marinetti, *Angew. Chem. Int. Ed.* **2014**, *53*, 861–865.
[6] J. Malinčík, S. Gaikwad, J. P. Mora-Fuentes, M.-A. Boillat, A. Prescimone, D. Häussinger, A. G. Campaña, T. Šolomek, *Angew. Chem. Int. Ed.* **2022**, *61*, e202208591.
[7] F. Aribot, A. Merle, P. Dechambenoit, H. Bock, A. Artigas, N. Vanthuyne, Y. Carissan, D. Hagebaum-Reignier, Y. Coquerel, F. Durola, *Angew. Chem. Int. Ed.* **2023**, *62*, e202304058.
[8] P. Izquierdo-García, J. M. Fernández-García, S. Medina Rivero, M. Šámal, J. Rybáček, L. Bednárová, S. Ramírez-Barroso, F. J. Ramírez, R. Rodríguez, J. Perles, D. García-Fresnadillo, J. Crassous, J. Casado, I. G. Stará, N. Martín, *J. Am. Chem. Soc.* **2023**, *145*, 11599–11610.
[9] R. E. Abed, B. B. Hassine, J.-P. Genêt, M. Gorsane, J. Madec, L. Ricard, A. Marinetti, *Synthesis* **2004**, 2513–2516.
[10] K. Antien, L. Pouységu, D. Deffieux, S. Massip, P. A. Peixoto, S. Quideau, *Chem. Eur. J.* **2019**, *25*, 2852–2858.
[11] L. Pospíšil, F. Teplý, M. Gál, L. Adriaenssens, M. Horáček, L. Severa, *Phys. Chem. Chem. Phys.* **2010**, *12*, 1550–1556.
[12] J. Hirano, S. Miyoshi, E. Yashima, T. Ikai, H. Shinokubo, N. Fukui, *Chem. Commun.* **2024**, *60*, 6035–6038.
[13] R. Amemiya, M. Yamaguchi, *Org. Biomol. Chem.* **2008**, *6*, 26–35.
[14] S. Grimme, S. D. Peyerimhoff, *Chem. Phys.* **1996**, *204*, 411–417.
[15] R. H. Martin, M. J. Marchant, *Tetrahedron* **1974**, *30*, 347–349.
[16] R. H. Martin, M. J. Marchant, *Tetrahedron Lett.* **1972**, *13*, 3707–3708.
[17] J. Barroso, J. L. Cabellos, S. Pan, F. Murillo, X. Zarate, M. A. Fernandez-Herrera, G. Merino, *Chem. Commun.* **2017**, *54*, 188–191.
[18] H. J. Lindner, *Tetrahedron* **1975**, *31*, 281–284.
[19] W. Oppolzer, *Tetrahedron* **1987**, *43*, 1969–2004.
[20] R. Yoshioka, H. Hiramatsu, K. Okamura, I. Tsujioka, S. Yamada, *J. Chem. Soc. Perkin Trans. 2* **2000**, 2121–2128.
[21] T. Yuan, M. Chen, X. Sun, J. Guan, F. Zhu, K. Tang, Z. Zhang, Q. Liu, X. Chen, *Appl. Clay Sci.* **2022**, *224*, 106521.
[22] M. Lupi, M. Onori, S. Menichetti, S. Abbate, G. Longhi, C. Viglianisi, *Molecules* **2022**, *27*, 1160.
[23] C. Nuckolls, T. J. Katz, L. Castellanos, *J. Am. Chem. Soc.* **1996**, *118*, 3767–3768.
[24] K. Usui, K. Yamamoto, T. Shimizu, M. Okazumi, B. Mei, Y. Demizu, M. Kurihara, H. Suemune, *J. Org. Chem.* **2015**, *80*, 6502–6508.
[25] R. B. Woodward, R. Hoffmann, *Angew. Chem. Int. Ed.* **1969**, *8*, 781–853.
[26] T. J. H. M. Cuppen, W. H. Laarhoven, *J. Am. Chem. Soc.* **1972**, *94*, 5914–5915.

[27] J. Storch, J. Žádný, V. Církva, M. Jakubec, J. Hrbáč, J. Vacek, in *Helicenes: Synthesis, Properties and Applications* (Eds.: J. Crassous, I. G. Stará, I. Starý), Wiley-VCH, Weinheim, **2022**, pp. 2–3.
[28] V. Církva, P. Jakubík, T. Strašák, J. Hrbáč, J. Sýkora, I. Císařová, J. Vacek, J. Žádný, J. Storch, *J. Org. Chem.* **2019**, *84*, 1980–1993.
[29] R. K. Mohamed, S. Mondal, J. V. Guerrera, T. M. Eaton, T. E. Albrecht-Schmitt, M. Shatruk, I. V. Alabugin, *Angew. Chem. Int. Ed.* **2016**, *55*, 12054–12058.
[30] M. Daigle, A. Picard-Lafond, E. Soligo, J.-F. Morin, *Angew. Chem. Int. Ed.* **2016**, *55*, 2042–2047.
[31] M. Hori, J.-D. Guo, T. Yanagi, K. Nogi, T. Sasamori, H. Yorimitsu, *Angew. Chem. Int. Ed.* **2018**, *57*, 4663–4667.
[32] H. Saito, A. Uchida, S. Watanabe, *J. Org. Chem.* **2017**, *82*, 5663–5668.
[33] M. Scholz, M. Mühlstädt, F. Dietz, *Tetrahedron Lett.* **1967**, *8*, 665–668.
[34] J. Storch, J. Žádný, V. Církva, M. Jakubec, J. Hrbáč, J. Vacek, in *Helicenes: Synthesis, Properties and Applications* (Eds.: J. Crassous, I. G. Stará, I. Starý), Wiley-VCH, Weinheim, **2022**, p. 5.
[35] M. Jakubec, I. Ghosh, J. Storch, B. König, *Chem. Eur. J.* **2020**, *26*, 543–547.
[36] V. Cirkva, S. Relich, *Curr. Org. Chem.* **2011**, *15*, 248–264.
[37] M. T. Reetz, S. Sostmann, *Tetrahedron* **2001**, *57*, 2515–2520.
[38] S. Arai, M. Ishikura, T. Yamagishi, *J. Chem. Soc. Perkin Trans. 1* **1998**, 1561–1568.
[39] K. Mori, T. Murase, M. Fujita, *Angew. Chem. Int. Ed.* **2015**, *54*, 6847–6851.
[40] F. Dietz, M. Scholz, *Tetrahedron* **1968**, *24*, 6845–6849.
[41] R. H. Martin, M. Flammang-Barbieux, J. P. Cosyn, M. Gelbcke, *Tetrahedron Lett.* **1968**, *9*, 3507–3510.
[42] J. Roose, S. Achermann, O. Dumele, F. Diederich, *Eur. J. Org. Chem.* **2013**, 3223–3231.
[43] M. Kos, J. Žádný, J. Storch, V. Církva, P. Cuřínová, J. Sýkora, I. Císařová, F. Kuriakose, I. V. Alabugin, *Int. J. Mol. Sci.* **2020**, *21*, 5868.
[44] T. Murase, T. Suto, H. Suzuki, *Chem. Asian J.* **2017**, *12*, 726–729.
[45] W. Xu, L. Wu, M. Fang, Z. Ma, Z. Shan, C. Li, H. Wang, *J. Org. Chem.* **2017**, *82*, 11192–11197.
[46] K. Yavari, S. Moussa, B. Ben Hassine, P. Retailleau, A. Voituriez, A. Marinetti, *Angew. Chem. Int. Ed.* **2012**, *51*, 6748–6752.
[47] R. Chakrabortty, S. Ghosh, V. Ganesh, *Eur. J. Org. Chem.* **2024**, *27*, e202400801.
[48] S. Sakai, T. Udagawa, S. Kato, K. Nakada, *J. Phys. Org. Chem.* **2013**, *26*, 517–522.
[49] O. Donoso-Tauda, A. Aizman, C. A. Escobar, J. C. Santos, *Chem. Phys. Lett.* **2009**, *469*, 219–223.
[50] M. Berthelot, *Liebigs Ann.* **1866**, *139*, 272–282.
[51] W. Reppe, O. Schlichting, K. Klager, T. Toepel, *Liebigs Ann.* **1948**, *560*, 1–92.
[52] G. Domínguez, J. Pérez-Castells, *Chem. Soc. Rev.* **2011**, *40*, 3430–3444.
[53] A. Roglans, A. Pla-Quintana, M. Solà, *Chem. Rev.* **2021**, *121*, 1894–1979.
[54] G. Domínguez, J. Pérez-Castells, *Chem. Eur. J.* **2016**, *22*, 6720–6739.
[55] Y. Satoh, Y. Obora, *Eur. J. Org. Chem.* **2015**, 5041–5054.
[56] M. R. Shaaban, R. El-Sayed, A. H. M. Elwahy, *Tetrahedron* **2011**, *67*, 6095–6130.
[57] Y. Obora, Y. Satoh, Y. Ishii, *J. Org. Chem.* **2010**, *75*, 6046–6049.
[58] Y. Satoh, Y. Obora, *J. Org. Chem.* **2011**, *76*, 8569–8573.

[59] K. Tanaka, N. Fukawa, T. Suda, K. Noguchi, *Angew. Chem. Int. Ed.* **2009**, *48*, 5470–5473.
[60] Y. Kimura, N. Fukawa, Y. Miyauchi, K. Noguchi, K. Tanaka, *Angew. Chem. Int. Ed.* **2014**, *53*, 8480–8483.
[61] P. Aillard, P. Retailleau, A. Voituriez, A. Marinetti, *Chem. Commun.* **2014**, *50*, 2199–2201.
[62] G. R. Kiel, H. M. Bergman, A. E. Samkian, N. J. Schuster, R. C. Handford, A. J. Rothenberger, R. Gomez-Bombarelli, C. Nuckolls, T. D. Tilley, *J. Am. Chem. Soc.* **2022**, *144*, 23421–23427.
[63] I. G. Stará, I. Starý, *Acc. Chem. Res.* **2020**, *53*, 144–158.
[64] F. Teplý, I. G. Stará, I. Starý, A. Kollárovič, D. Luštinec, Z. Krausová, D. Šaman, P. Fiedler, *Eur. J. Org. Chem.* **2007**, 4244–4250.
[65] J. Nejedlý, M. Šámal, J. Rybáček, M. Tobrmanová, F. Szydlo, C. Coudret, M. Neumeier, J. Vacek, J. Vacek Chocholoušová, M. Buděšínský, D. Šaman, L. Bednárová, L. Sieger, I. G. Stará, I. Starý, *Angew. Chem. Int. Ed.* **2017**, *56*, 5839–5843.
[66] J. Klívar, A. Jančařík, D. Šaman, R. Pohl, P. Fiedler, L. Bednárová, I. Starý, I. G. Stará, *Chem. Eur. J.* **2016**, *22*, 14401–14405.
[67] S. Chercheja, J. Klívar, A. Jančařík, J. Rybáček, S. Salzl, J. Tarábek, L. Pospíšil, J. Vacek Chocholoušová, J. Vacek, R. Pohl, I. Císařová, I. Starý, I. G. Stará, *Chem. Eur. J.* **2014**, *20*, 8477–8482.
[68] K. Yamamoto, H. Nagae, H. Tsurugi, K. Mashima, *Dalton Trans.* **2016**, *45*, 17072–17081.
[69] J. Míšek, F. Teplý, I. G. Stará, M. Tichý, D. Šaman, I. Císařová, P. Vojtíšek, I. Starý, *Angew. Chem. Int. Ed.* **2008**, *47*, 3188–3191.
[70] A. Bensalah-Ledoux, D. Pitrat, T. Reynaldo, M. Srebro-Hooper, B. Moore II, J. Autschbach, J. Crassous, S. Guy, L. Guy, *Chem. Eur. J.* **2016**, *22*, 3333–3346.
[71] L. Fang, M. Li, W.-B. Lin, Y. Shen, C.-F. Chen, *Asian J. Org. Chem.* **2018**, *7*, 2518–2526.
[72] I. G. Stará, I. Starý, A. Kollárovič, F. Teplý, Š. Vyskočil, D. Šaman, *Tetrahedron Lett.* **1999**, *40*, 1993–1996.
[73] F. Teplý, I. G. Stará, I. Starý, A. Kollárovič, D. Šaman, Š. Vyskočil, P. Fiedler, *J. Org. Chem.* **2003**, *68*, 5193–5197.
[74] J. Rybáček, G. Huerta-Angeles, A. Kollárovič, I. G. Stará, I. Starý, P. Rahe, M. Nimmrich, A. Kühnle, *Eur. J. Org. Chem.* **2011**, 853–860.
[75] L. Pallova, E. S. Gauthier, L. Abella, M. Jean, N. Vanthuyne, V. Dorcet, L. Vendier, J. Autschbach, J. Crassous, S. Bastin, V. César, *Chem. Eur. J.* **2021**, *27*, 7722–7730.
[76] M. Šámal, S. Chercheja, J. Rybáček, J. Vacek Chocholoušová, J. Vacek, L. Bednárová, D. Šaman, I. G. Stará, I. Starý, *J. Am. Chem. Soc.* **2015**, *137*, 8469–8474.
[77] O. Songis, J. Míšek, M. B. Schmid, A. Kollárovič, I. G. Stará, D. Šaman, I. Císařová, I. Starý, *J. Org. Chem.* **2010**, *75*, 6889–6899.
[78] D. Schweinfurth, M. Zalibera, M. Kathan, C. Shen, M. Mazzolini, N. Trapp, J. Crassous, G. Gescheidt, F. Diederich, *J. Am. Chem. Soc.* **2014**, *136*, 13045–13052.
[79] A. Jančařík, J. Rybáček, K. Cocq, J. Vacek Chocholoušová, J. Vacek, R. Pohl, L. Bednárová, P. Fiedler, I. Císařová, I. G. Stará, I. Starý, *Angew. Chem. Int. Ed.* **2013**, *52*, 9970–9975.
[80] P. Aillard, P. Retailleau, A. Voituriez, A. Marinetti, *Chem. Eur. J.* **2015**, *21*, 11989–11993.

[81] J. Klívar, M. Šámal, A. Jančařík, J. Vacek, L. Bednárová, M. Buděšínský, P. Fiedler, I. Starý, I. G. Stará, *Eur. J. Org. Chem.* **2018**, 5164–5178.
[82] I. G. Sánchez, M. Šámal, J. Nejedlý, M. Karras, J. Klívar, J. Rybáček, M. Buděšínský, L. Bednárová, B. Seidlerová, I. G. Stará, I. Starý, *Chem. Commun.* **2017**, *53*, 4370–4373.
[83] T. Shibata, T. Uchiyama, Y. Yoshinami, S. Takayasu, K. Tsuchikama, K. Endo, *Chem. Commun.* **2012**, *48*, 1311–1313.
[84] K. Murayama, Y. Oike, S. Furumi, M. Takeuchi, K. Noguchi, K. Tanaka, *Eur. J. Org. Chem.* **2015**, 1409–1414.
[85] I. G. Stará, I. Starý, in *Helicenes: Synthesis, Properties and Applications* (Eds.: J. Crassous, I. G. Stará, I. Starý), Wiley-VCH, Weinheim, **2022**, pp. 56–57.
[86] I. Thiel, A. Spannenberg, M. Hapke, *ChemCatChem* **2013**, *5*, 2865–2868.
[87] F. Fischer, M. Hapke, *Eur. J. Org. Chem.* **2018**, 3193–3201.
[88] G. A. Ville, K. P. C. Vollhardt, M. J. Winter, *Organometallics* **1984**, *3*, 1177–1187.
[89] K. Tanaka, A. Kamisawa, T. Suda, K. Noguchi, M. Hirano, *J. Am. Chem. Soc.* **2007**, *129*, 12078–12079.
[90] Y. Honjo, Y. Shibata, K. Tanaka, *Chem. Eur. J.* **2019**, *25*, 9427–9432.
[91] H. A. Weidlich, *Ber. Dtsch. Chem. Ges.* **1938**, *71*, 1203–1209.
[92] M. S. Newman, *J. Am. Chem. Soc.* **1940**, *62*, 1683–1687.
[93] L. Liu, T. J. Katz, *Tetrahedron Lett.* **1990**, *31*, 3983–3986.
[94] N. D. Willmore, L. Liu, T. J. Katz, *Angew. Chem. Int. Ed.* **1992**, *31*, 1093–1095.
[95] L. Minuti, A. Taticchi, A. Marrocchi, E. Gacs-Baitz, R. Galeazzi, *Eur. J. Org. Chem.* **1999**, 3155–3163.
[96] C. Nuckolls, T. J. Katz, T. Verbiest, S. V. Elshocht, H.-G. Kuball, S. Kiesewalter, A. J. Lovinger, A. Persoons, *J. Am. Chem. Soc.* **1998**, *120*, 8656–8660.
[97] F. Russig, *J. Prakt. Chem.* **1900**, *62*, 30–60.
[98] H. Laatsch, *Liebigs Ann.* **1980**, 140–157.
[99] M. Abe, K. Ohmori, K. Suzuki, T. Yamamoto, *J. Polym. Sci.* **2010**, *48*, 1844–1848.
[100] K. Ohmori, M. Kitamura, K. Suzuki, *Angew. Chem. Int. Ed.* **1999**, *38*, 1226–1229.
[101] F. Dubois, M. Gingras, *Tetrahedron Lett.* **1998**, *39*, 5039–5040.
[102] K. Tanaka, H. Suzuki, H. Osuga, *J. Org. Chem.* **1997**, *62*, 4465–4470.
[103] S. K. Collins, A. Grandbois, M. P. Vachon, J. Côté, *Angew. Chem. Int. Ed.* **2006**, *45*, 2923–2926.
[104] A. Kina, H. Miki, Y.-H. Cho, T. Hayashi, *Adv. Synth. Catal.* **2004**, *346*, 1728–1732.
[105] D. C. Harrowven, M. I. T. Nunn, D. R. Fenwick, *Tetrahedron Lett.* **2002**, *43*, 3189–3191.
[106] D. C. Harrowven, I. L. Guy, L. Nanson, *Angew. Chem. Int. Ed.* **2006**, *45*, 2242–2245.
[107] K. Fuchibe, H. Jyono, M. Fujiwara, T. Kudo, M. Yokota, J. Ichikawa, *Chem. Eur. J.* **2011**, *17*, 12175–12185.
[108] J. Ichikawa, M. Yokota, T. Kudo, S. Umezaki, *Angew. Chem. Int. Ed.* **2008**, *47*, 4870–4873.
[109] L. Kötzner, M. J. Webber, A. Martínez, C. De Fusco, B. List, *Angew. Chem. Int. Ed.* **2014**, *53*, 5202–5205.
[110] I. G. Stara, I. Stary, M. Tichy, J. Zavada, V. Hanus, *J. Am. Chem. Soc.* **1994**, *116*, 5084–5088.
[111] D. Bogaert-Verhogen, R. H. Martin, *Tetrahedron Lett.* **1967**, *8*, 3045–3048.

[112] D. J. Morrison, T. K. Trefz, W. E. Piers, R. McDonald, M. Parvez, *J. Org. Chem.* **2005**, *70*, 5309–5312.
[113] Y. Nakakuki, T. Hirose, H. Sotome, H. Miyasaka, K. Matsuda, *J. Am. Chem. Soc.* **2018**, *140*, 4317–4326.
[114] Y. Zhu, Z. Xia, Z. Cai, Z. Yuan, N. Jiang, T. Li, Y. Wang, X. Guo, Z. Li, S. Ma, D. Zhong, Y. Li, J. Wang, *J. Am. Chem. Soc.* **2018**, *140*, 4222–4226.
[115] Y. Hu, X.-Y. Wang, P.-X. Peng, X.-C. Wang, X.-Y. Cao, X. Feng, K. Müllen, A. Narita, *Angew. Chem. Int. Ed.* **2017**, *56*, 3374–3378.
[116] T. Fujikawa, Y. Segawa, K. Itami, *J. Am. Chem. Soc.* **2016**, *138*, 3587–3595.
[117] T. Fujikawa, Y. Segawa, K. Itami, *J. Am. Chem. Soc.* **2015**, *137*, 7763–7768.
[118] Y. Ogawa, T. Ueno, M. Karikomi, K. Seki, K. Haga, T. Uyehara, *Tetrahedron Lett.* **2002**, *43*, 7827–7829.
[119] M. Jakubec, S. Hansen-Troøyen, I. Císařová, J. Sýkora, J. Storch, *Org. Lett.* **2020**, *22*, 3905–3910.
[120] J.-D. Chen, H.-Y. Lu, C.-F. Chen, *Chem. Eur. J.* **2010**, *16*, 11843–11846.
[121] K. Nakano, Y. Hidehira, K. Takahashi, T. Hiyama, K. Nozaki, *Angew. Chem. Int. Ed.* **2005**, *44*, 7136–7138.
[122] M. Gingras, *Chem. Soc. Rev.* **2013**, *42*, 968–1006.
[123] J. W. Diesveld, J. H. Borkent, W. H. Laarhoven, *Recl. Trav. Chim. Pays-Bas* **1980**, *99*, 391–394.
[124] D. Nečas, R. P. Kaiser, J. Ulč, *Eur. J. Org. Chem.* **2016**, 5647–5652.
[125] R. P. Kaiser, J. Ulč, I. Císařová, D. Nečas, *RSC Adv.* **2017**, *8*, 580–583.
[126] E. Kaneko, Y. Matsumoto, K. Kamikawa, *Chem. Eur. J.* **2013**, *19*, 11837–11841.
[127] L. Zhao, R. I. Kaiser, B. Xu, U. Ablikim, W. Lu, M. Ahmed, M. M. Evseev, E. K. Bashkirov, V. N. Azyazov, M. V. Zagidullin, A. N. Morozov, A. H. Howlader, S. F. Wnuk, A. M. Mebel, D. Joshi, G. Veber, F. R. Fischer, *Nat. Commun.* **2019**, *10*, 1510.
[128] C.H. Goedicke, H. Stegemeyer, *Tetrahedron Lett.* **1970**, *11*, 937–940.
[129] L. Wang, L. Liu, W. Chang, J. Li, *J. Org. Chem.* **2018**, *83*, 7799–7813.
[130] J. Nejedlý, M. Šámal, J. Rybáček, I. G. Sánchez, V. Houska, T. Warzecha, J. Vacek, L. Sieger, M. Buděšínský, L. Bednárová, P. Fiedler, I. Císařová, I. Starý, I. G. Stará, *J. Org. Chem.* **2020**, *85*, 248–276.
[131] P. H. Lee, H. Kim, K. Lee, *Adv. Synth. Catal.* **2005**, *347*, 1219–1222.
[132] M. Weiner, G. Vogel, R. West, *Inorg. Chem.* **1962**, *1*, 654–658.
[133] T. Kottke, D. Stalke, *Angew. Chem. Int. Ed.* **1993**, *32*, 580–582.
[134] T. F. Bates, M. T. Clarke, R. D. Thomas, *J. Am. Chem. Soc.* **1988**, *110*, 5109–5112.
[135] K. Bergander, R. He, N. Chandrakumar, O. Eppers, H. Günther, *Tetrahedron* **1994**, *50*, 5861–5868.
[136] W. Bauer, W. R. Winchester, P. von R. Schleyer, *Organometallics* **1987**, *6*, 2371–2379.
[137] L. W. Bieber, M. F. da Silva, R. C. da Costa, L. O. S. Silva, *Tetrahedron Lett.* **1998**, *39*, 3655–3658.
[138] C. C. K. Keh, C. Wei, C.-J. Li, *J. Am. Chem. Soc.* **2003**, *125*, 4062–4063.
[139] F. Zhou, C.-J. Li, *Nat. Commun.* **2014**, *5*, 4254.
[140] K. P. C. Vollhardt, *Acc. Chem. Res.* **1977**, *10*, 1–8.
[141] R. L. Funk, K. P. C. Vollhardt, *J. Am. Chem. Soc.* **1980**, *102*, 5253–5261.
[142] R. L. Hillard III, K. P. C. Vollhardt, *Angew. Chem. Int. Ed.* **1975**, *14*, 712–713.
[143] R. L. Hillard III, K. P. C. Vollhardt, *J. Am. Chem. Soc.* **1977**, *99*, 4058–4069.
[144] D. J. Paymode, C. V. Ramana, *ACS Omega* **2017**, *2*, 5591–5600.
[145] A. A. More, C. V. Ramana, *J. Org. Chem.* **2016**, *81*, 3400–3406.

[146] C. Yuan, C.-T. Chang, A. Axelrod, D. Siegel, *J. Am. Chem. Soc.* **2010**, *132*, 5924–5925.
[147] C. Yuan, C.-T. Chang, D. Siegel, *J. Org. Chem.* **2013**, *78*, 5647–5668.
[148] C. Kesenheimer, A. Kalogerakis, A. Meißner, U. Groth, *Chem. Eur. J.* **2010**, *16*, 8805–8821.
[149] R. Grigg, R. Scott, P. Stevenson, *Tetrahedron Lett.* **1982**, *23*, 2691–2692.
[150] R. Grigg, R. Scott, P. Stevenson, *J. Chem. Soc. Perkin Trans. 1* **1988**, 1365–1369.
[151] L. Adriaenssens, L. Severa, T. Šálová, I. Císařová, R. Pohl, D. Šaman, S. V. Rocha, N. S. Finney, L. Pospíšil, P. Slavíček, F. Teplý, *Chem. Eur. J.* **2009**, *15*, 1072–1076.
[152] M. R. Crittall, N. W. G. Fairhurst, D. R. Carbery, *Chem. Commun.* **2012**, *48*, 11181–11183.
[153] K. P. Angermund, P. Betz, H. Butenschön, *Chem. Ber.* **1993**, *126*, 713–724.
[154] P. Jungk, F. Fischer, I. Thiel, M. Hapke, *J. Org. Chem.* **2015**, *80*, 9781–9793.
[155] J. A. Osborn, F. H. Jardine, J. F. Young, G. Wilkinson, *J. Chem. Soc. A* **1966**, 1711–1732.
[156] S. L. Baysdon, L. S. Liebeskind, *Organometallics* **1982**, *1*, 771–775.
[157] A. Geny, N. Agenet, L. Iannazzo, M. Malacria, C. Aubert, V. Gandon, *Angew. Chem. Int. Ed.* **2009**, *48*, 1810–1813.
[158] J. Žádný, A. Jančařík, A. Andronova, M. Šámal, J. Vacek Chocholoušová, J. Vacek, R. Pohl, D. Šaman, I. Císařová, I. G. Stará, I. Starý, *Angew. Chem. Int. Ed.* **2012**, *51*, 5857–5861.
[159] M. Buchta, J. Rybáček, A. Jančařík, A. A. Kudale, M. Buděšínský, J. V. Chocholoušová, J. Vacek, L. Bednárová, I. Císařová, G. J. Bodwell, I. Starý, I. G. Stará, *Chem. Eur. J.* **2015**, *21*, 8910–8917.
[160] T. W. Greene, P. G. Wuts, in: *Greene's Protective Groups in Organic Synthesis*, John Wiley & Sons, New York, **1999**, p. 114.
[161] H. Hock, W. Susemichl, *Ber. Dtsch. Chem. Ges.* **1933**, *66*, 61–68.
[162] P.-C. Kuo, Y.-C. Li, T.-S. Wu, *J. Tradit. Complement. Med.* **2012**, *2*, 249–266.
[163] W. E. Childers, M. A. Abou-Gharbia, *ACS Med. Chem. Lett.* **2021**, *12*, 961–968.
[164] L. Lai, L. Gao, M. Liu, Y. Guo, D. Cheng, M. Jiang, F. Chen, *J. Flow Chem.* **2023**, *13*, 375–383.
[165] W. Nerinckx, M. Vandewalle, *Tetrahedron Asymmetry* **1990**, *1*, 265–276.
[166] M. E. Freed, J. R. Potoski, G. L. Conklin, S. C. Bell, *J. Med. Chem.* **1976**, *19*, 560–562.
[167] M. E. Freed, J. R. Potoski, E. H. Freed, G. L. Conklin, J. L. Malis, *J. Med. Chem.* **1973**, *16*, 595–599.
[168] K. Yamamoto, M. Okazumi, H. Suemune, K. Usui, *Org. Lett.* **2013**, *15*, 1806–1809.
[169] P. Sarkar, A. Ahmed, J. K. Ray, *Tetrahedron Lett.* **2020**, *61*, 151701.
[170] D. Guo, J. Zhang, B. Zhang, J. Wang, *Org. Lett.* **2018**, *20*, 6284–6288.
[171] T. Cadart, D. Nečas, R. P. Kaiser, L. Favereau, I. Císařová, R. Gyepes, J. Hodačová, K. Kalíková, L. Bednárová, J. Crassous, M. Kotora, *Chem. Eur. J.* **2021**, *27*, 11279–11284.
[172] M. Lehr, T. Paschelke, V. Bendt, A. Petersen, L. Pietsch, P. Harders, A. J. McConnell, *Eur. J. Org. Chem.* **2021**, 2728–2735.
[173] Y. Liang, Y.-X. Xie, J.-H. Li, *J. Org. Chem.* **2006**, *71*, 379–381.
[174] P. Siemsen, R. C. Livingston, F. Diederich, *Angew. Chem. Int. Ed.* **2000**, *39*, 2632–2657.
[175] R. R. Tykwinski, *Angew. Chem. Int. Ed.* **2003**, *42*, 1566–1568.

[176] A. F. Littke, G. C. Fu, *Angew. Chem. Int. Ed.* **2002**, *41*, 4176–4211.
[177] C. Bannwarth, S. Ehlert, S. Grimme, *J. Chem. Theory Comput.* **2019**, *15*, 1652–1671.
[178] C. Bannwarth, E. Caldeweyher, S. Ehlert, A. Hansen, P. Pracht, J. Seibert, S. Spicher, S. Grimme, *Wiley Interdiscip. Rev. Comput. Mol. Sci.* **2021**, *11*, e1493.
[179] M. Joly, N. Defay, R. H. Martin, J. P. Declerq, G. Germain, B. Soubrier-Payen, M. Van Meerssche, *Helv. Chim. Acta* **1977**, *60*, 537–560.
[180] Y. Shen, C.-F. Chen, *Chem. Rev.* **2012**, *112*, 1463–1535.
[181] D. A. Lightner, D. T. Hefelfinger, T. W. Powers, G. W. Frank, K. N. Trueblood, *J. Am. Chem. Soc.* **1972**, *94*, 3492–3497.
[182] J. Caeiro, D. Peña, A. Cobas, D. Pérez, E. Guitián, *Adv. Synth. Catal.* **2006**, *348*, 2466–2474.
[183] R. E. Dolle, S. J. Schmidt, L. I. Kruse, *J. Chem. Soc. Chem. Commun.* **1987**, 904–905.
[184] J. S. Morgan, *J. Chem. Soc. Trans.* **1916**, *109*, 274–283.
[185] L. M. Chapman, B. Adams, L. T. Kliman, A. Makriyannis, C. L. Hamblett, *Tetrahedron Lett.* **2010**, *51*, 1517–1522.
[186] C. Zhu, H. Chu, G. Li, S. Ma, J. Zhang, *J. Am. Chem. Soc.* **2019**, *141*, 19246–19251.
[187] R. E. Colborn, K. P. C. Vollhardt, *J. Am. Chem. Soc.* **1986**, *108*, 5470–5477.
[188] H. Kagan, A. Moradpour, J. F. Nicoud, G. Balavoine, G. Tsoucaris, *J. Am. Chem. Soc.* **1971**, *93*, 2353–2354.
[189] A. Moradpour, H. Kagan, M. Baes, G. Morren, R. H. Martin, *Tetrahedron* **1975**, *31*, 2139–2143.
[190] W. J. Bernstein, M. Calvin, O. Buchardt, *J. Am. Chem. Soc.* **1972**, *94*, 494–498.
[191] T. L. Davis, J. Jr. Ackerman, *J. Am. Chem. Soc.* **1945**, *67*, 486–489.
[192] T. L. Davis, R. Heggie, *J. Am. Chem. Soc.* **1935**, *57*, 1622–1624.
[193] K. L. Stevenson, J. F. Verdieck, *J. Am. Chem. Soc.* **1968**, *90*, 2974–2975.
[194] K. A. Muszkat, E. Fischer, *J. Chem. Soc. B* **1967**, 662–678.
[195] W. H. Laarhoven, T. J. H. M. Cuppen, *J. Chem. Soc. Chem. Commun.* **1977**, 47.
[196] W. H. Laarhoven, T. J. H. M. Cuppen, *J. Chem. Soc. Perkin Trans. 2* **1978**, 315–318.
[197] M. Nakazaki, K. Yamamoto, K. Fujiwara, M. Maeda, *J. Chem. Soc. Chem. Commun.* **1979**, 1086–1087.
[198] M. Hibert, G. Solladie, *J. Org. Chem.* **1980**, *45*, 5393–5394.
[199] J. Tribout, R. H. Martin, M. Doyle, H. Wynberg, *Tetrahedron Lett.* **1972**, *13*, 2839–2842.
[200] I. G. Stará, I. Starý, A. Kollárovič, F. Teplý, D. Šaman, M. Tichý, *J. Org. Chem.* **1998**, *63*, 4046–4050.
[201] B. Heller, M. Hapke, C. Fischer, A. Andronova, I. Starý, I. G. Stará, *J. Organomet. Chem.* **2013**, *723*, 98–102.
[202] R. L. Halterman, K. P. C. Vollhardt, *Organometallics* **1988**, *7*, 883–892.
[203] S. Kinoshita, R. Yamano, Y. Shibata, Y. Tanaka, K. Hanada, T. Matsumoto, K. Miyamoto, A. Muranaka, M. Uchiyama, K. Tanaka, *Angew. Chem. Int. Ed.* **2020**, *59*, 11020–11027.
[204] Y. Sawada, S. Furumi, A. Takai, M. Takeuchi, K. Noguchi, K. Tanaka, *J. Am. Chem. Soc.* **2012**, *134*, 4080–4083.
[205] K. Murayama, Y. Shibata, H. Sugiyama, H. Uekusa, K. Tanaka, *J. Org. Chem.* **2017**, *82*, 1136–1144.
[206] R. Yamano, Y. Shibata, K. Tanaka, *Chem. Eur. J.* **2018**, *24*, 6364–6370.

[207] A. Yubuta, T. Hosokawa, M. Gon, K. Tanaka, Y. Chujo, A. Tsurusaki, K. Kamikawa, *J. Am. Chem. Soc.* **2020**, *142*, 10025–10033.
[208] M. C. Carreño, R. Hernández-Sánchez, J. Mahugo, A. Urbano, *J. Org. Chem.* **1999**, *64*, 1387–1390.
[209] M. C. Carreño, S. García-Cerrada, A. Urbano, *J. Am. Chem. Soc.* **2001**, *123*, 7929–7930.
[210] A. Urbano, M. C. Carreño, *Org. Biomol. Chem.* **2013**, *11*, 699–708.
[211] A. Latorre, A. Urbano, M. C. Carreño, *Chem. Commun.* **2009**, 6652–6654.
[212] M. D. Curtis, J. Cao, J. W. Kampf, *J. Am. Chem. Soc.* **2004**, *126*, 4318–4328.
[213] A. Grandbois, S. K. Collins, *Chem. Eur. J.* **2008**, *14*, 9323–9329.
[214] M. Miyasaka, A. Rajca, M. Pink, S. Rajca, *J. Am. Chem. Soc.* **2005**, *127*, 13806–13807.
[215] M. Gingras, F. Dubois, *Tetrahedron Lett.* **1999**, *40*, 1309–1312.
[216] R. H. Martin, M. J. Marchant, *Tetrahedron* **1974**, *30*, 343–345.
[217] R. H. Martin, *Angew. Chem. Int. Ed.* **1974**, *13*, 649–660.
[218] M. S. Newman, W. B. Lutz, D. Lednicer, *J. Am. Chem. Soc.* **1955**, *77*, 3420–3421.
[219] M. S. Newman, C. H. Chen, *J. Org. Chem.* **1972**, *37*, 1312–1314.
[220] M. Yamaguchi, H. Okubo, M. Hirama, *Chem. Commun.* **1996**, 1771–1772.
[221] J. P. Gao, X. S. Meng, T. P. Bender, S. MacKinnon, V. Grand, Z. Y. Wang, *Chem. Commun.* **1999**, 1281–1282.
[222] K. Tanaka, Y. Shogase, H. Osuga, H. Suzuki, K. Nakamura, *Tetrahedron Lett.* **1995**, *36*, 1675–1678.
[223] D. Koval, L. Severa, L. Adriaenssens, J. Vávra, F. Teplý, V. Kašička, *Electrophoresis* **2011**, *32*, 2683–2692.
[224] C. Herse, D. Bas, F. C. Krebs, T. Bürgi, J. Weber, T. Wesolowski, B. W. Laursen, J. Lacour, *Angew. Chem. Int. Ed.* **2003**, *42*, 3162–3166.
[225] B. Laleu, P. Mobian, C. Herse, B. W. Laursen, G. Hopfgartner, G. Bernardinelli, J. Lacour, *Angew. Chem. Int. Ed.* **2005**, *44*, 1879–1883.
[226] T. Thongpanchang, K. Paruch, T. J. Katz, A. L. Rheingold, K.-C. Lam, L. Liable-Sands, *J. Org. Chem.* **2000**, *65*, 1850–1856.
[227] K. E. S. Phillips, T. J. Katz, S. Jockusch, A. J. Lovinger, N. J. Turro, *J. Am. Chem. Soc.* **2001**, *123*, 11899–11907.
[228] F. Mikeš, G. Boshart, E. Gil-Av, *J. Chem. Soc. Chem. Commun.* **1976**, 99–100.
[229] H. Nakagawa, H. Tanaka, K. Yamada, H. Kawazura, *J. Phys. Chem.* **1982**, *86*, 2311–2314.
[230] B. L. Karger, L. V. Berry, *Clin. Chem.* **1971**, *17*, 757–764.
[231] W. H. Pirkle, T. C. Pochapsky, *Chem. Rev.* **1989**, *89*, 347–362.
[232] Y. H. Kim, A. Tishbee, E. Gil-Av, *J. Am. Chem. Soc.* **1980**, *102*, 5915–5917.
[233] F. Mikeš, G. Boshart, *J. Chromatogr. A* **1978**, *149*, 455–464.
[234] W. J. C. Prinsen, W. H. Laarhoven, *J. Chromatogr. A* **1987**, *393*, 377–390.
[235] F. Mikeš, G. Boshart, E. Gil-Av, *J. Chromatogr. A* **1976**, *122*, 205–221.
[236] M. Gingras, G. Félix, R. Peresutti, *Chem. Soc. Rev.* **2013**, *42*, 1007–1050.
[237] M. C. Carreño, M. González-López, A. Urbano, *Chem. Commun.* **2005**, 611–613.
[238] M. E. Tiritan, Q. B. Cass, A. Del Alamo, S. A. Matlin, S. J. Grieb, *Chirality* **1998**, *10*, 573–577.
[239] S. A. Matlin, V. E. Stacey, W. J. Lough, *J. Chromatogr. A* **1988**, *450*, 157–162.
[240] N. C. Kneten, N. J. Krause, T. O. Carmichael, O. E. Weigang, *J. Am. Chem. Soc.* **1962**, *84*, 1738–1739.

[241] M. C. Carreño, S. García-Cerrada, A. Urbano, *Chem. Eur. J.* **2003**, *9*, 4118–4131.
[242] I. G. Stará, Z. Alexandrová, F. Teplý, P. Sehnal, I. Starý, D. Šaman, M. Buděšínský, J. Cvačka, *Org. Lett.* **2005**, *7*, 2547–2550.
[243] J. M. Seco, E. Quiñoá, R. Riguera, *Chem. Rev.* **2004**, *104*, 17–118.
[244] J. A. Dale, H. S. Mosher, *J. Am. Chem. Soc.* **1973**, *95*, 512–519.
[245] T. R. Hoye, C. S. Jeffrey, F. Shao, *Nat. Protoc.* **2007**, *2*, 2451–2458.
[246] F. Furche, R. Ahlrichs, C. Wachsmann, E. Weber, A. Sobanski, F. Vögtle, S. Grimme, *J. Am. Chem. Soc.* **2000**, *122*, 1717–1724.
[247] Y. Nakai, T. Mori, Y. Inoue, *J. Phys. Chem. A* **2012**, *116*, 7372–7385.
[248] K. Dhbaibi, L. Favereau, J. Crassous, *Chem. Rev.* **2019**, *119*, 8846–8953.
[249] S. Parsons, *Tetrahedron Asymmetry* **2017**, *28*, 1304–1313.
[250] H. D. Flack, *Acta Crystallogr. A* **1983**, *39*, 876–881.
[251] P. H. Fuoss, P. Eisenberger, W. K. Warburton, A. Bienenstock, *Phys. Rev. Lett.* **1981**, *46*, 1537–1540.
[252] H. D. Flack, G. Bernardinelli, *J. Appl. Crystallogr.* **2000**, *33*, 1143–1148.
[253] Z. Domínguez, R. López-Rodríguez, E. Álvarez, S. Abbate, G. Longhi, U. Pischel, A. Ros, *Chem. Eur. J.* **2018**, *24*, 12660–12668.
[254] C. Bannwarth, S. Grimme, *Comput. Theor. Chem.* **2014**, *1040–1041*, 45–53.
[255] M. de Wergifosse, S. Grimme, *J. Chem. Phys.* **2019**, *150*, 094112.
[256] S. Kümmel, *Adv. Energy Mater.* **2017**, *7*, 1700440.
[257] D. Mester, M. Kállay, *J. Chem. Theory Comput.* **2022**, *18*, 1646–1662.
[258] X. Wu, X. Xie, A. Troisi, *J. Mater. Chem. C* **2024**, *12*, 18886–18892.
[259] E. Vogel, H. Günther, *Angew. Chem. Int. Ed.* **1967**, *6*, 385–401.
[260] M. Grzybowski, K. Skonieczny, H. Butenschön, D. T. Gryko, *Angew. Chem. Int. Ed.* **2013**, *52*, 9900–9930.
[261] B. T. King, J. Kroulík, C. R. Robertson, P. Rempala, C. L. Hilton, J. D. Korinek, L. M. Gortari, *J. Org. Chem.* **2007**, *72*, 2279–2288.
[262] C. M. Starks, *J. Am. Chem. Soc.* **1971**, *93*, 195–199.
[263] S. B. Waghmode, G. Mahale, V. P. Patil, K. Renalson, D. Singh, *Synth. Commun.* **2013**, *43*, 3272–3280.
[264] I. G. Stará, I. Starý, in *Helicenes: Synthesis, Properties and Applications* (Eds.: J. Crassous, I. G. Stará, I. Starý), Wiley-VCH, Weinheim, **2022**, p. 76.
[265] R. G. Vranka, E. L. Amma, *Inorg. Chem.* **1966**, *5*, 1020–1025.
[266] A. J. Blake, N. R. Champness, M. Crew, S. Parsons, *New J. Chem.* **1999**, *23*, 13–15.
[267] A. J. Blake, G. Baum, N. R. Champness, S. S. M. Chung, P. A. Cooke, D. Fenske, A. N. Khlobystov, D. A. Lemenovskii, W.-S. Li, M. Schröder, *J. Chem. Soc. Dalton Trans.* **2000**, 4285–4291.
[268] Q.-F. Sun, J. Iwasa, D. Ogawa, Y. Ishido, S. Sato, T. Ozeki, Y. Sei, K. Yamaguchi, M. Fujita, *Science* **2010**, *328*, 1144–1147.
[269] B. Olenyuk, M. D. Levin, J. A. Whiteford, J. E. Shield, P. J. Stang, *J. Am. Chem. Soc.* **1999**, *121*, 10434–10435.
[270] H. Isla, N. Saleh, J.-K. Ou-Yang, K. Dhbaibi, M. Jean, M. Dziurka, L. Favereau, N. Vanthuyne, L. Toupet, B. Jamoussi, M. Srebro-Hooper, J. Crassous, *J. Org. Chem.* **2019**, *84*, 5383–5393.
[271] H. Isla, M. Srebro-Hooper, M. Jean, N. Vanthuyne, T. Roisnel, J. L. Lunkley, G. Muller, J. A. G. Williams, J. Autschbach, J. Crassous, *Chem. Commun.* **2016**, *52*, 5932–5935.
[272] J. M. Fox, T. J. Katz, S. Van Elshocht, T. Verbiest, M. Kauranen, A. Persoons, T. Thongpanchang, T. Krauss, L. Brus, *J. Am. Chem. Soc.* **1999**, *121*, 3453–3459.

[273] P. J. Stang, B. Olenyuk, *Acc. Chem. Res.* **1997**, *30*, 502–518.
[274] S. Leininger, B. Olenyuk, P. J. Stang, *Chem. Rev.* **2000**, *100*, 853–908.
[275] B. Olenyuk, A. Fechtenkötter, P. J. Stang, *J. Chem. Soc. Dalton Trans.* **1998**, 1707–1728.
[276] R. Chakrabarty, P. S. Mukherjee, P. J. Stang, *Chem. Rev.* **2011**, *111*, 6810–6918.
[277] Y. Fang, J. A. Powell, E. Li, Q. Wang, Z. Perry, A. Kirchon, X. Yang, Z. Xiao, C. Zhu, L. Zhang, F. Huang, H.-C. Zhou, *Chem. Soc. Rev.* **2019**, *48*, 4707–4730.
[278] D. Zhang, T. K. Ronson, Y.-Q. Zou, J. R. Nitschke, *Nat. Rev. Chem.* **2021**, *5*, 168–182.
[279] A. J. McConnell, *Chem. Soc. Rev.* **2022**, *51*, 2957–2971.
[280] W. M. Bloch, G. H. Clever, *Chem. Commun.* **2017**, *53*, 8506–8516.
[281] L. R. Holloway, P. M. Bogie, R. J. Hooley, *Dalton Trans.* **2017**, *46*, 14719–14723.
[282] T. R. Schulte, J. J. Holstein, G. H. Clever, *Angew. Chem. Int. Ed.* **2019**, *58*, 5562–5566.
[283] D. Mendola, N. Saleh, N. Vanthuyne, C. Roussel, L. Toupet, F. Castiglione, T. Caronna, A. Mele, J. Crassous, *Angew. Chem. Int. Ed.* **2014**, *53*, 5786–5790.
[284] S. Graule, M. Rudolph, N. Vanthuyne, J. Autschbach, C. Roussel, J. Crassous, R. Réau, *J. Am. Chem. Soc.* **2009**, *131*, 3183–3185.
[285] C. Shen, E. Anger, M. Srebro, N. Vanthuyne, K. K. Deol, T. D. Jefferson, G. Muller, J. A. G. Williams, L. Toupet, C. Roussel, J. Autschbach, R. Réau, J. Crassous, *Chem. Sci.* **2014**, *5*, 1915–1927.
[286] T. A. Halgren, *J. Comput. Chem.* **1996**, *17*, 490–519.
[287] Y.-Z. Hu, C. Chamchoumis, J. S. Grebowicz, R. P. Thummel, *Inorg. Chem.* **2002**, *41*, 2296–2300.
[288] S. Shotwell, H. L. Ricks, J. G. M. Morton, M. Laskoski, J. Fiscus, M. D. Smith, K. D. Shimizu, H.-C. zur Loye, U. H. F. Bunz, *J. Organomet. Chem.* **2003**, *671*, 43–51.
[289] E. Bosch, C. L. Barnes, N. L. Brennan, G. L. Eakins, B. E. Breyfogle, *J. Org. Chem.* **2008**, *73*, 3931–3934.
[290] M. Jung, Y. Suzaki, T. Saito, K. Shimada, K. Osakada, *Polyhedron* **2012**, *40*, 168–174.
[291] F. A. Pereira, T. Fallows, M. Frank, A. Chen, G. H. Clever, *Z. Anorg. Allg. Chem.* **2013**, *639*, 1598–1605.
[292] G. Meyer-Eppler, F. Topić, G. Schnakenburg, K. Rissanen, A. Lützen, *Eur. J. Inorg. Chem.* **2014**, 2495–2501.
[293] S. Banthia, A. Samanta, *Polyhedron* **2006**, *25*, 2269–2276.
[294] A. Macchioni, G. Ciancaleoni, C. Zuccaccia, D. Zuccaccia, *Chem. Soc. Rev.* **2008**, *37*, 479–489.
[295] C. Gütz, R. Hovorka, C. Stobe, N. Struch, F. Topić, G. Schnakenburg, K. Rissanen, A. Lützen, *Eur. J. Org. Chem.* **2014**, 206–216.
[296] D. M. Engelhard, S. Freye, K. Grohe, M. John, G. H. Clever, *Angew. Chem. Int. Ed.* **2012**, *51*, 4747–4750.
[297] D. K. Chand, K. Biradha, M. Kawano, S. Sakamoto, K. Yamaguchi, M. Fujita, *Chem. Asian J.* **2006**, *1*, 82–90.
[298] S. Kai, T. Tateishi, T. Kojima, S. Takahashi, S. Hiraoka, *Inorg. Chem.* **2018**, *57*, 13083–13086.
[299] K. Suzuki, M. Kawano, M. Fujita, *Angew. Chem. Int. Ed.* **2007**, *46*, 2819–2822.
[300] T. Zhang, L.-P. Zhou, X.-Q. Guo, L.-X. Cai, Q.-F. Sun, *Nat. Commun.* **2017**, *8*, 15898.
[301] M. Han, Y. Luo, B. Damaschke, L. Gómez, X. Ribas, A. Jose, P. Peretzki, M. Seibt, G. H. Clever, *Angew. Chem. Int. Ed.* **2016**, *55*, 445–449.

[302] D. R. Martir, L. Delforce, D. B. Cordes, A. M. Z. Slawin, S. L. Warriner, D. Jacquemin, E. Zysman-Colman, *Inorg. Chem. Front.* **2019**, *7*, 232–238.
[303] O. Jurček, P. Bonakdarzadeh, E. Kalenius, J. M. Linnanto, M. Groessl, R. Knochenmuss, J. A. Ihalainen, K. Rissanen, *Angew. Chem. Int. Ed.* **2015**, *54*, 15462–15467.
[304] L. M. Mesquita, J. Anhäuser, D. Bellaire, S. Becker, A. Lützen, S. Kubik, *Org. Lett.* **2019**, *21*, 6442–6446.
[305] Y. Gu, E. A. Alt, H. Wang, X. Li, A. P. Willard, J. A. Johnson, *Nature* **2018**, *560*, 65–69.
[306] A. Kumar, R. Banerjee, E. Zangrando, P. S. Mukherjee, *Inorg. Chem.* **2022**, *61*, 2368–2377.
[307] D. K. Chand, M. Fujita, K. Biradha, S. Sakamoto, K. Yamaguchi, *Dalton Trans.* **2003**, 2750–2756.
[308] S. Park, D. Kim, D. Kim, D. Kim, O.-S. Jung, *Chem. Commun.* **2021**, *57*, 2919–2922.
[309] H. Yu, Z. Guo, N. Han, J. Shi, X. Jiang, Q. Bai, Z. Zhang, P. Wang, M. Wang, *Cell Rep. Phys. Sci.* **2023**, *4*, 101631.
[310] R.-J. Li, A. Marcus, F. Fadaei-Tirani, K. Severin, *Chem. Commun.* **2021**, *57*, 10023–10026.
[311] M. R. Black, S. Bhattacharyya, S. P. Argent, B. S. Pilgrim, *J. Am. Chem. Soc.* **2024**, *146*, 28233–28241.
[312] J. A. Findlay, K. M. Patil, M. G. Gardiner, H. I. MacDermott-Opeskin, M. L. O'Mara, P. E. Kruger, D. Preston, *Chem. Asian J.* **2022**, *17*, e202200093.
[313] A. Walther, I. Regeni, J. J. Holstein, G. H. Clever, *J. Am. Chem. Soc.* **2023**, *145*, 25365–25371.
[314] C. Klein, C. Gütz, M. Bogner, F. Topić, K. Rissanen, A. Lützen, *Angew. Chem. Int. Ed.* **2014**, *53*, 3739–3742.
[315] J. I. Virtue, S. Tsoukatos, M. R. Johnston, W. M. Bloch, *Chem. Sci.* **2024**, *15*, 19119–19125.
[316] Q.-Y. Hong, B. Huang, M.-X. Wu, J.-Y. Jiang, H.-B. Yang, X.-L. Zhao, G. H. Clever, X. Shi, *Nat. Commun.* **2025**, *16*, 2484.
[317] M. Fukuda, R. Sekiya, R. Kuroda, *Angew. Chem. Int. Ed.* **2008**, *47*, 706–710.
[318] R. Zhu, J. Lübben, B. Dittrich, G. H. Clever, *Angew. Chem. Int. Ed.* **2015**, *54*, 2796–2800.
[319] P. Montes-Tolentino, A. S. Mikherdov, C. Drechsler, J. J. Holstein, G. H. Clever, *Angew. Chem. Int. Ed.* **2025**, *64*, e202423810.
[320] S. Sudan, F. Fadaei-Tirani, R. Scopelliti, K. E. Ebbert, G. H. Clever, K. Severin, *Angew. Chem. Int. Ed.* **2022**, *61*, e202201823.
[321] S. Sahasithiwat, T. Mophuang, L. Menbangpung, S. Kamtonwong, T. Sooksimuang, *Synth. Met.* **2010**, *160*, 1148–1152.
[322] S. Jhulki, A. K. Mishra, T. J. Chow, J. N. Moorthy, *Chem. Eur. J.* **2016**, *22*, 9375–9386.
[323] J. R. Brandt, X. Wang, Y. Yang, A. J. Campbell, M. J. Fuchter, *J. Am. Chem. Soc.* **2016**, *138*, 9743–9746.
[324] C. Kim, T. J. Marks, A. Facchetti, M. Schiavo, A. Bossi, S. Maiorana, E. Licandro, F. Todescato, S. Toffanin, M. Muccini, C. Graiff, A. Tiripicchio, *Org. Electron.* **2009**, *10*, 1511–1520.
[325] S. Xiao, S. J. Kang, Y. Wu, S. Ahn, J. B. Kim, Y.-L. Loo, T. Siegrist, M. L. Steigerwald, H. Li, C. Nuckolls, *Chem. Sci.* **2013**, *4*, 2018–2023.
[326] Y.-S. Lin, S. Y. Abate, K.-W. Lai, C.-W. Chu, Y.-D. Lin, Y.-T. Tao, S.-S. Sun, *ACS Appl. Mater. Interfaces* **2018**, *10*, 41439–41449.

[327] P. Josse, L. Favereau, C. Shen, S. Dabos-Seignon, P. Blanchard, C. Cabanetos, J. Crassous, *Chem. Eur. J.* **2017**, *23*, 6277–6281.
[328] D. Nakano, M. Yamaguchi, *Tetrahedron Lett.* **2003**, *44*, 4969–4971.
[329] M. T. Reetz, S. Sostmann, *J. Organomet. Chem.* **2000**, *603*, 105–109.
[330] T. Kawasaki, K. Suzuki, E. Licandro, A. Bossi, S. Maiorana, K. Soai, *Tetrahedron Asymmetry* **2006**, *17*, 2050–2053.
[331] A. Matsumoto, K. Yonemitsu, H. Ozaki, J. Míšek, I. Starý, I. G. Stará, K. Soai, *Org. Biomol. Chem.* **2017**, *15*, 1321–1324.
[332] N. Takenaka, R. S. Sarangthem, B. Captain, *Angew. Chem. Int. Ed.* **2008**, *47*, 9708–9710.
[333] N. Takenaka, J. Chen, B. Captain, R. S. Sarangthem, A. Chandrakumar, *J. Am. Chem. Soc.* **2010**, *132*, 4536–4537.
[334] H. Yang, H.-X. Feng, L. Zhou, *Eur. J. Org. Chem.* **2024**, *27*, e202400671.
[335] C.-F. Chen, Y. Shen, *Helicene Chemistry: From Synthesis to Applications*, Springer, Berlin, **2017**.
[336] M. Korb, S. A. Moggach, P. J. Low, *Chem. Commun.* **2021**, *57*, 4251–4254.
[337] G. Berton, T. Lorenzetto, G. Borsato, P. Sgarbossa, C. Santo, F. Visentin, F. Fabris, A. Scarso, *Tetrahedron Lett.* **2019**, *60*, 151202.
[338] G. R. Fulmer, A. J. M. Miller, N. H. Sherden, H. E. Gottlieb, A. Nudelman, B. M. Stoltz, J. E. Bercaw, K. I. Goldberg, *Organometallics* **2010**, *29*, 2176–2179.
[339] L. Avram, Y. Cohen, *Chem. Soc. Rev.* **2014**, *44*, 586–602.
[340] R. H. Blessing, *Acta Crystallogr. A* **1995**, *51*, 33–38.
[341] Rigaku Oxford Diffraction, (2017), CrysAlisPro Software system, version 1.171.38.43, Rigaku Corporation, Oxford, UK.
[342] G. M. Sheldrick, *Acta Crystallogr. C* **2015**, *71*, 3–8.
[343] A. Camacho-Davila, L. S. R. Gamage, Z. Wang, J. W. Herndon, *Tetrahedron* **2010**, *66*, 4954–4960.
[344] J. Suffert, E. Abraham, S. Raeppel, R. Brückner, *Liebigs Ann.* **1996**, *1996*, 447–456.
[345] H. Niu, T. E. Strecker, J. L. Gerberich, J. W. I. Campbell, D. Saha, D. Mondal, E. Hamel, D. J. Chaplin, R. P. Mason, M. L. Trawick, K. G. Pinney, *J. Med. Chem.* **2019**, *62*, 5594–5615.
[346] F. Yang, X. Liu, X. Shi, Y. Wang, G. Hu, S. Lin, X. Jiao, P. Xie, *Tetrahedron* **2019**, *75*, 3101–3107.
[347] W. Debrouwer, R. A. J. Seigneur, T. S. A. Heugebaert, C. V. Stevens, *Chem. Commun.* **2014**, *51*, 729–732.
[348] R. Jana, I. Chatterjee, S. Samanta, J. K. Ray, *Org. Lett.* **2008**, *10*, 4795–4797.
[349] A. K. Adak, A. Mandal, S. K. Manna, S. K. Mondal, A. Jana, D. Ghosh, D. Kundu, S. Samanta, J. K. Ray, *Synth. Commun.* **2016**, *46*, 452–459.
[350] S. Zhu, Z. Ye, M.-J. Chen, L. Wang, Y.-Z. Wang, K.-N. Zhang, W.-B. Li, H.-M. Ding, Z. Li, J. Zhang, *Nat. Commun.* **2023**, *14*, 7611.

13 Appendix

13.1 List of molecules

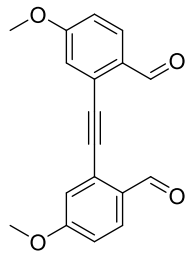

16

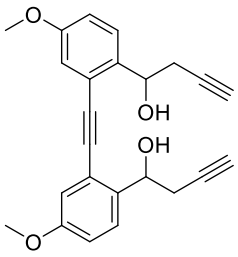

17

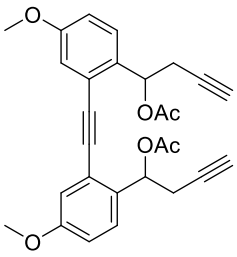

18

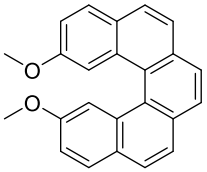

20

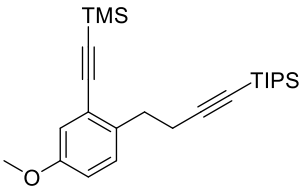

25

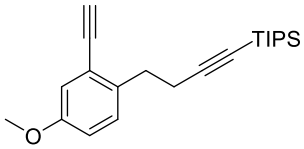

26

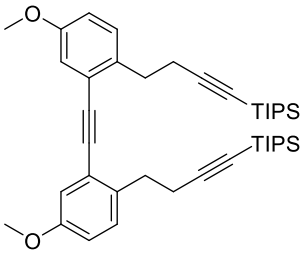

27

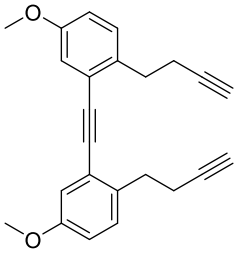

28

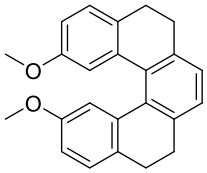

29

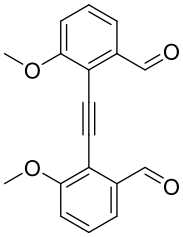

32

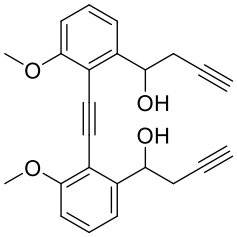

35

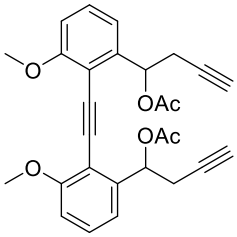

36

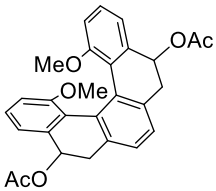

37

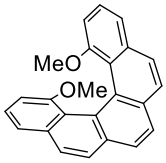

38

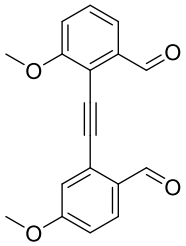

39

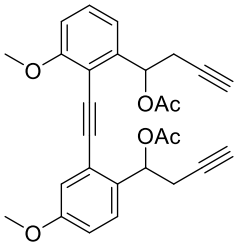

41

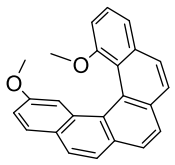

43

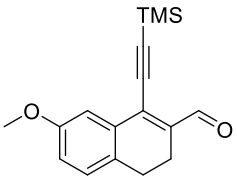

48

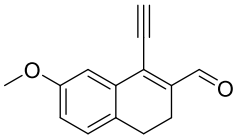

49

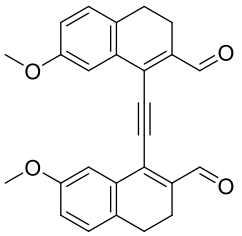

50

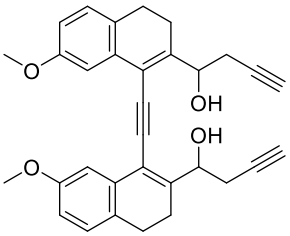

51

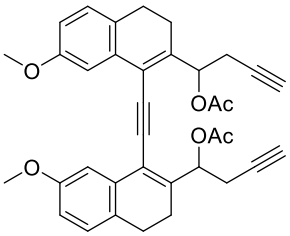

52

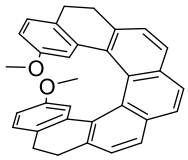

54

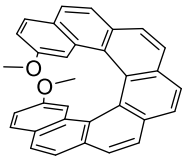

55

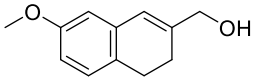

60

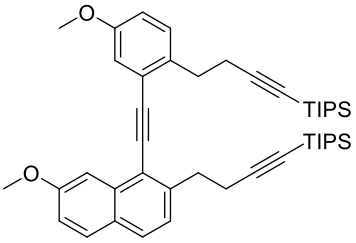

69

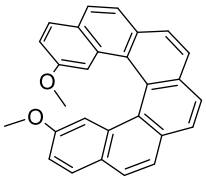

72

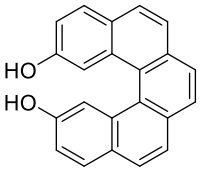

73

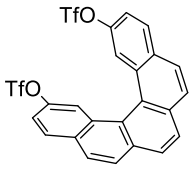

74

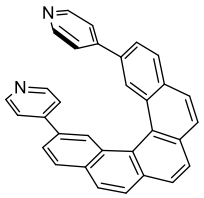

75

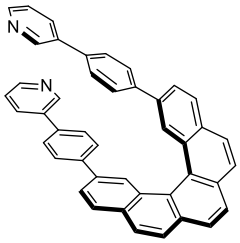

78

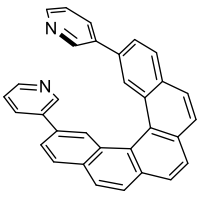

76

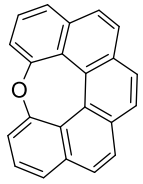

80

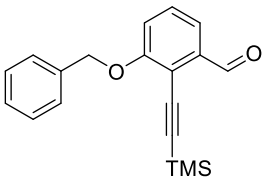

82

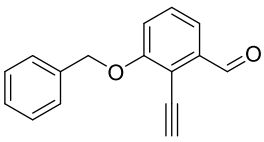

83

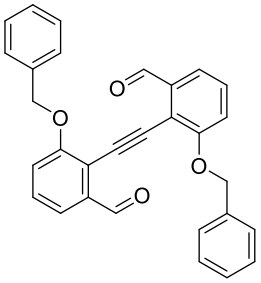

84

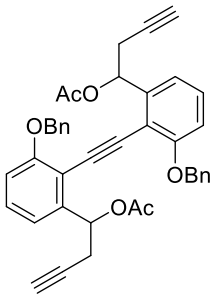

86

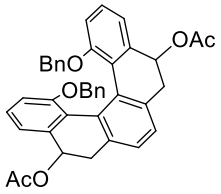

87

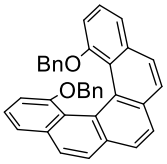

88

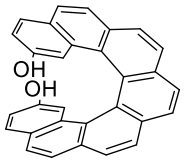

89

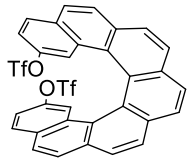

90

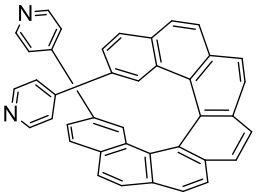

91

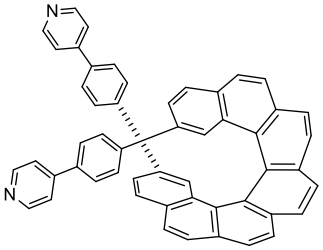

92

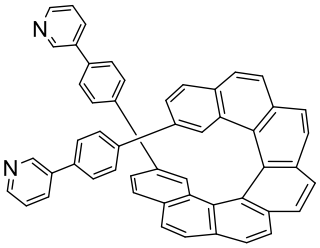

93

13.2 NMR spectra

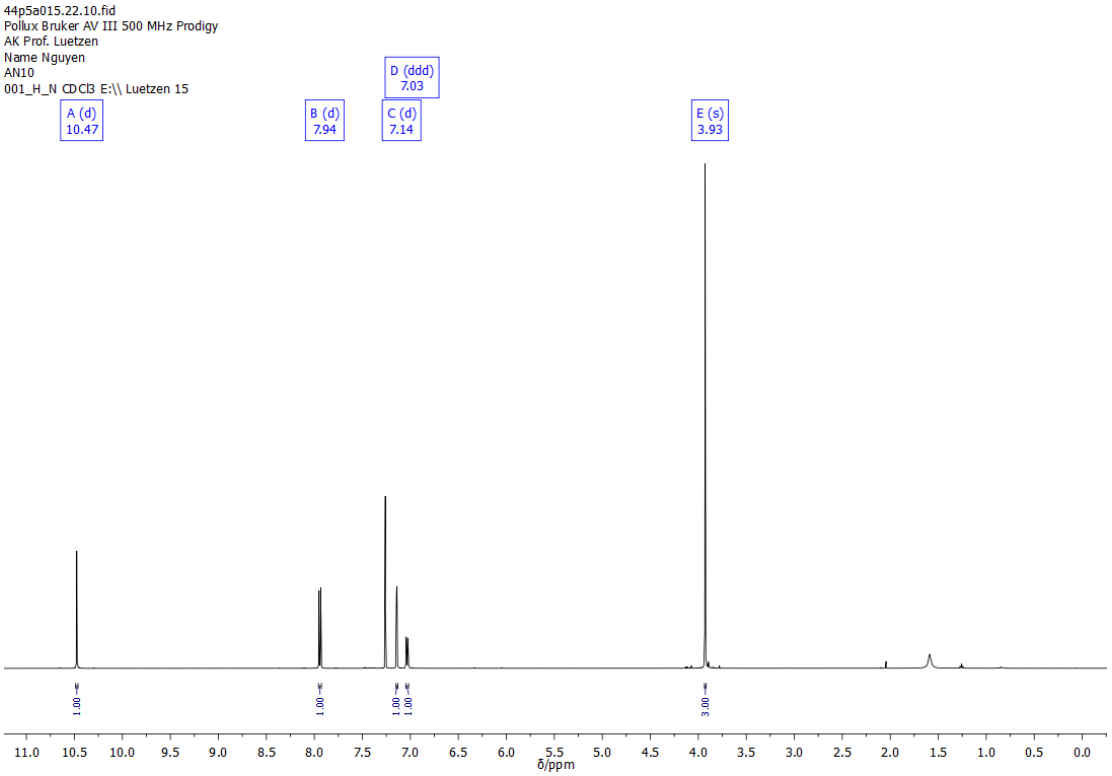

Figure 95: ^{1}H-NMR spectrum of **16** in $CDCl_3$.

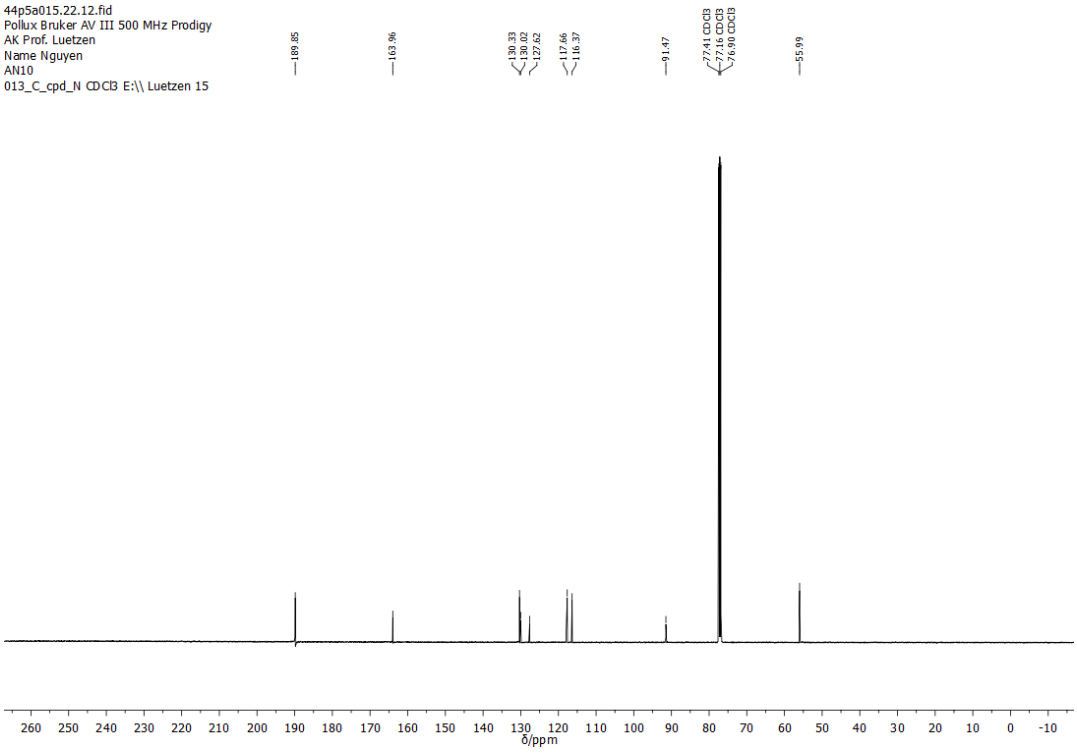

Figure 96: ^{13}C-NMR spectrum of **16** in $CDCl_3$.

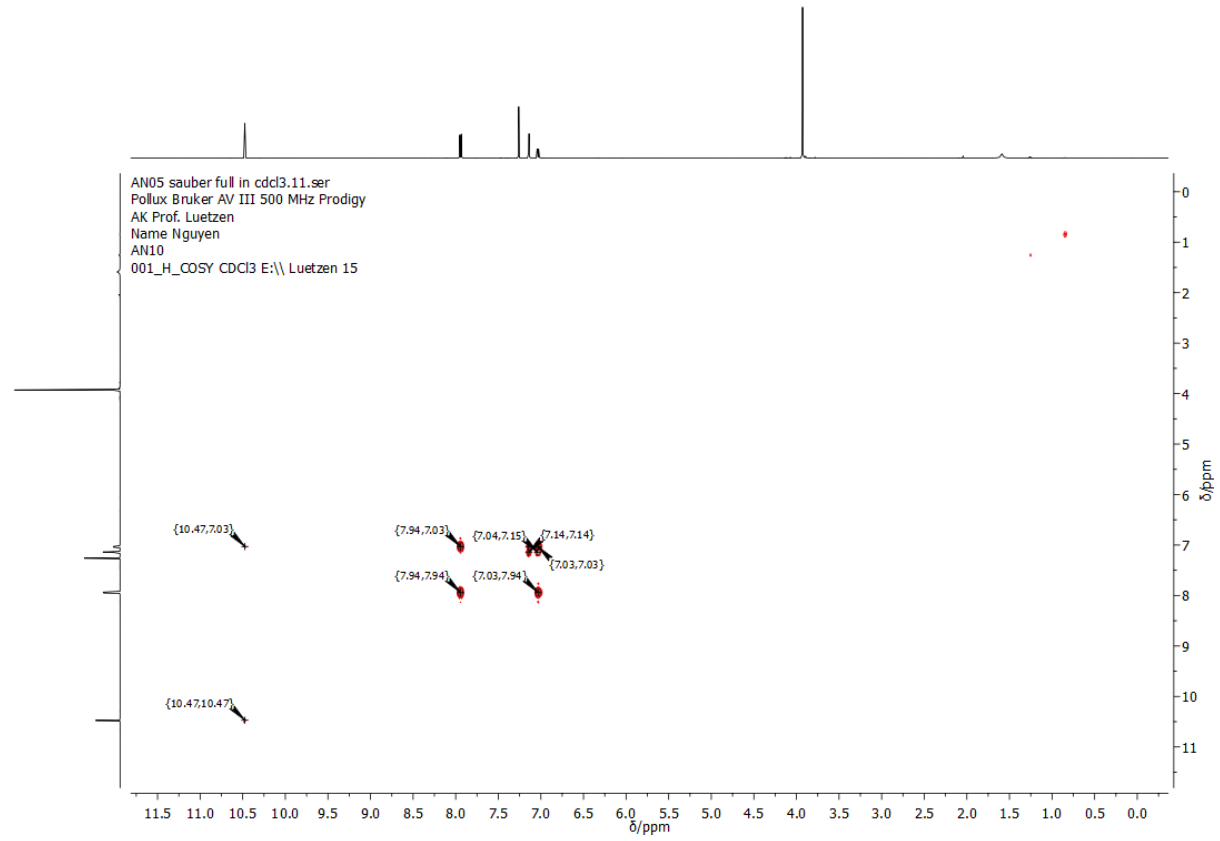

Figure 97: COSY-NMR spectrum of **16** in $CDCl_3$.

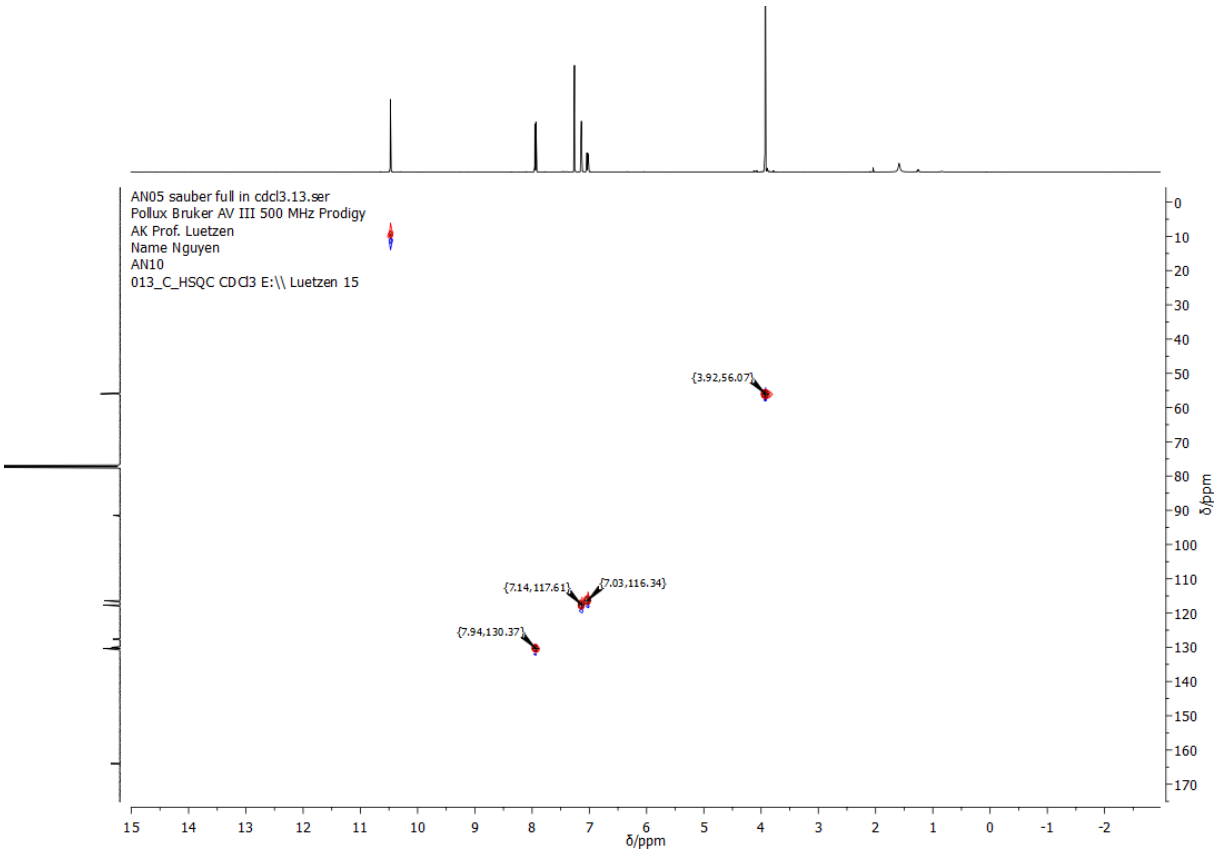

Figure 98: HSQC-NMR spectrum of **16** in $CDCl_3$.

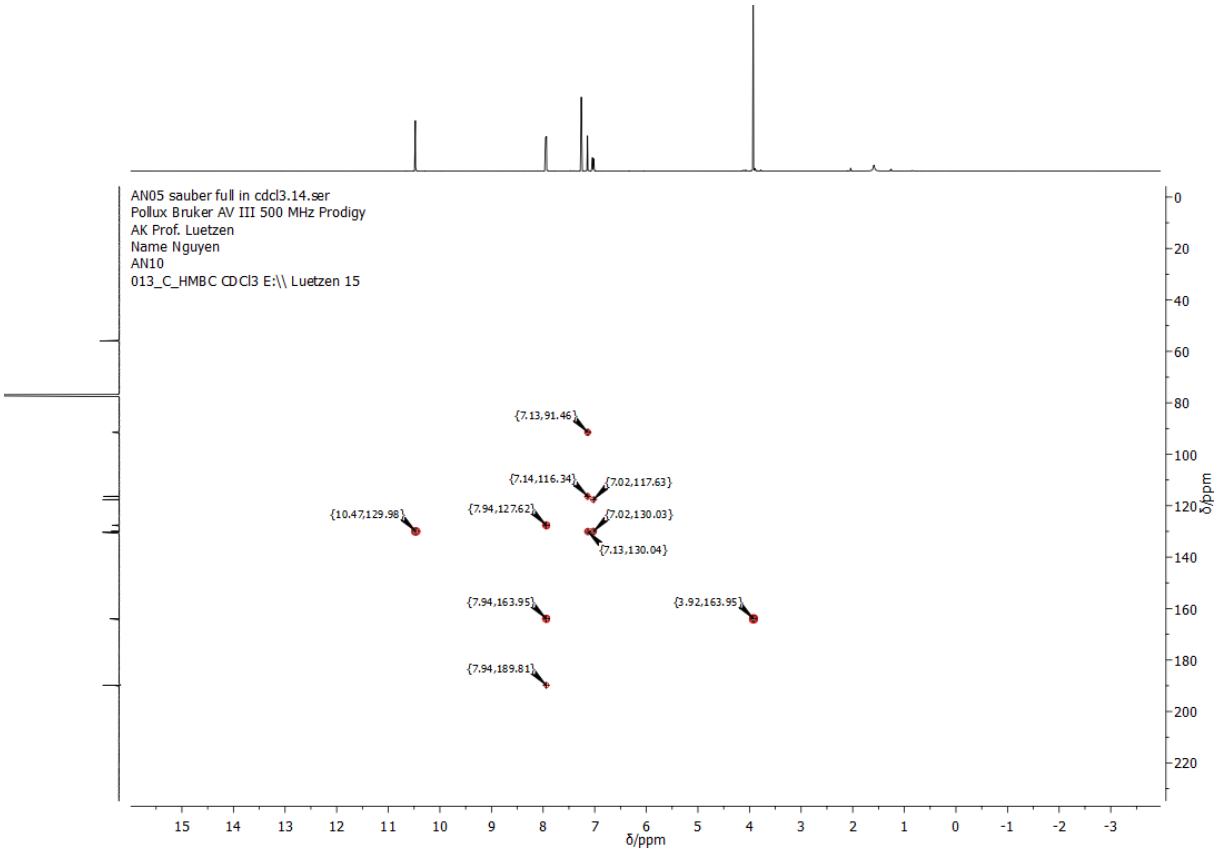

Figure 99: HMBC-NMR spectrum of **16** in $CDCl_3$.

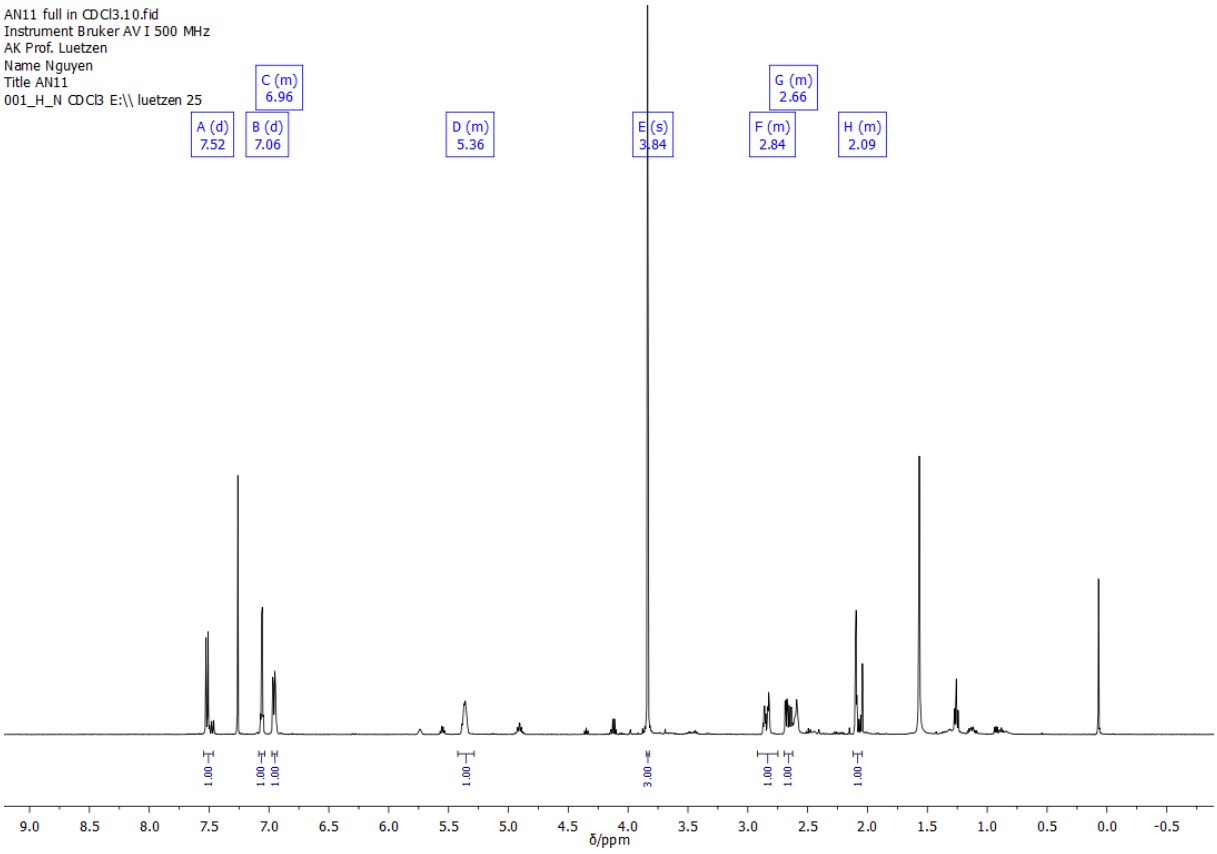

Figure 100: ^{1}H-NMR spectrum of **17** in $CDCl_3$.

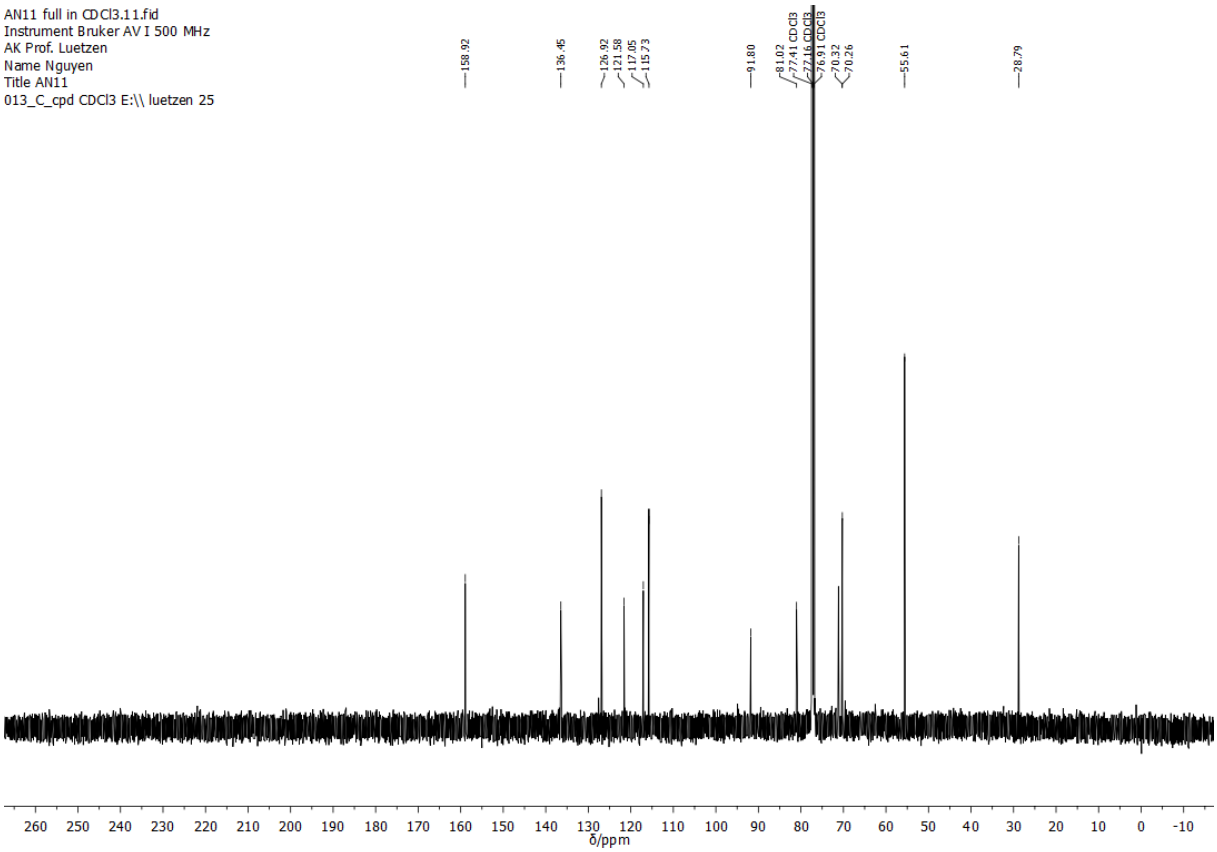

Figure 101: ^{13}C-NMR spectrum of **17** in $CDCl_3$.

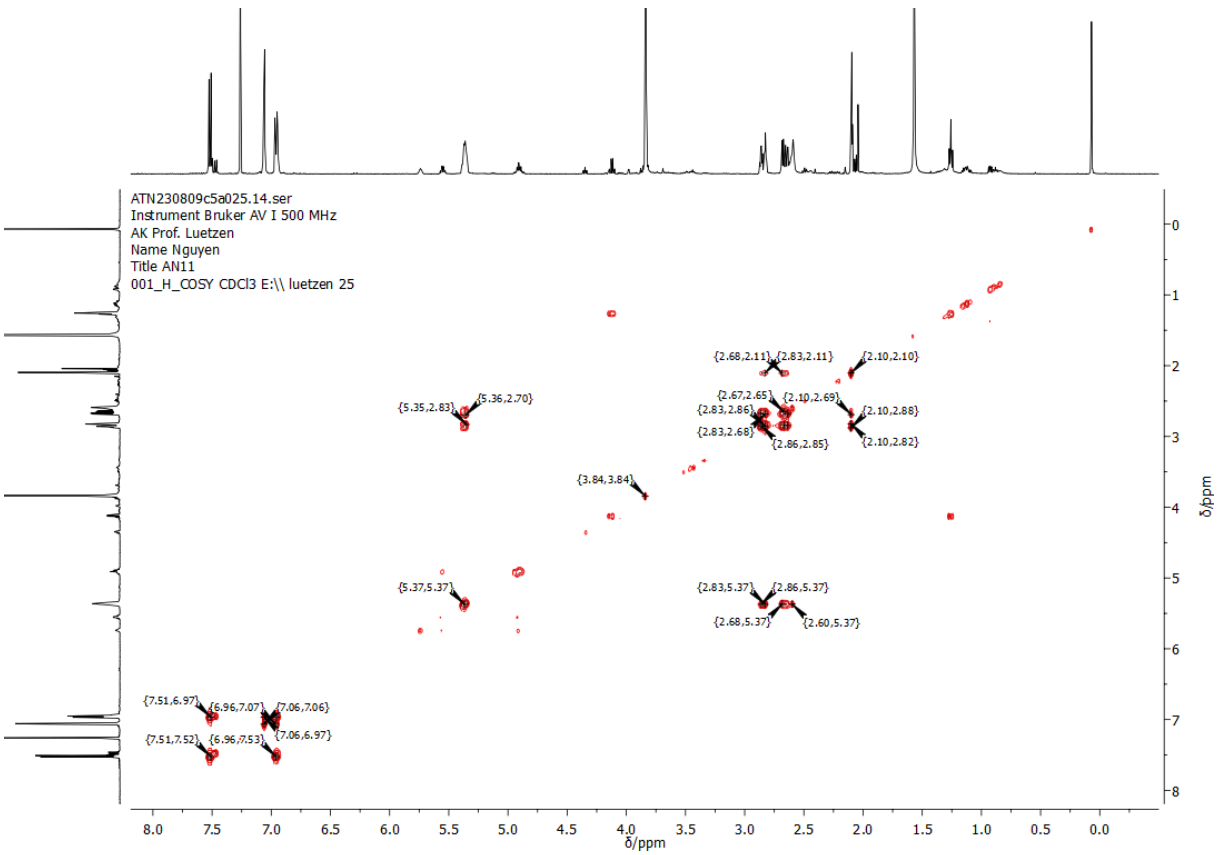

Figure 102: COSY-NMR spectrum of **17** in $CDCl_3$.

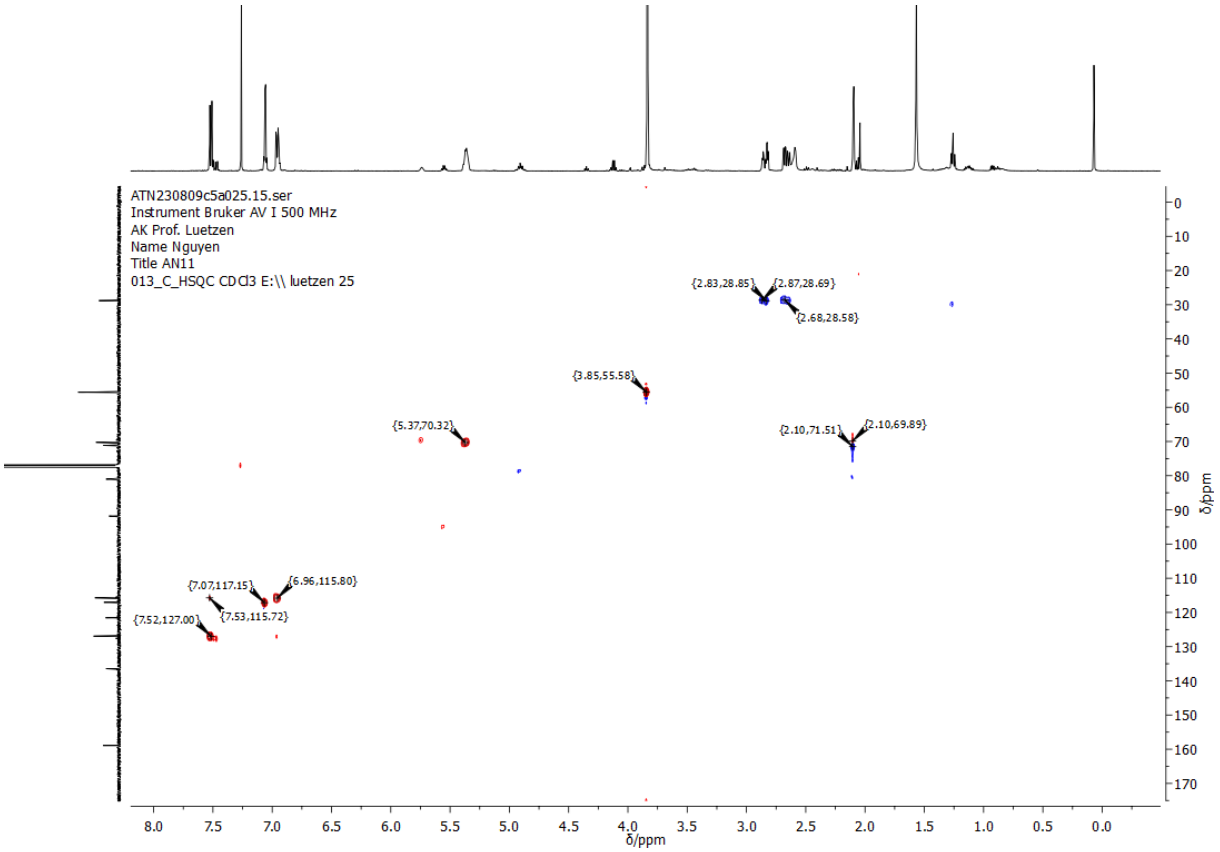

Figure 103: HSQC-NMR spectrum of **17** in $CDCl_3$.

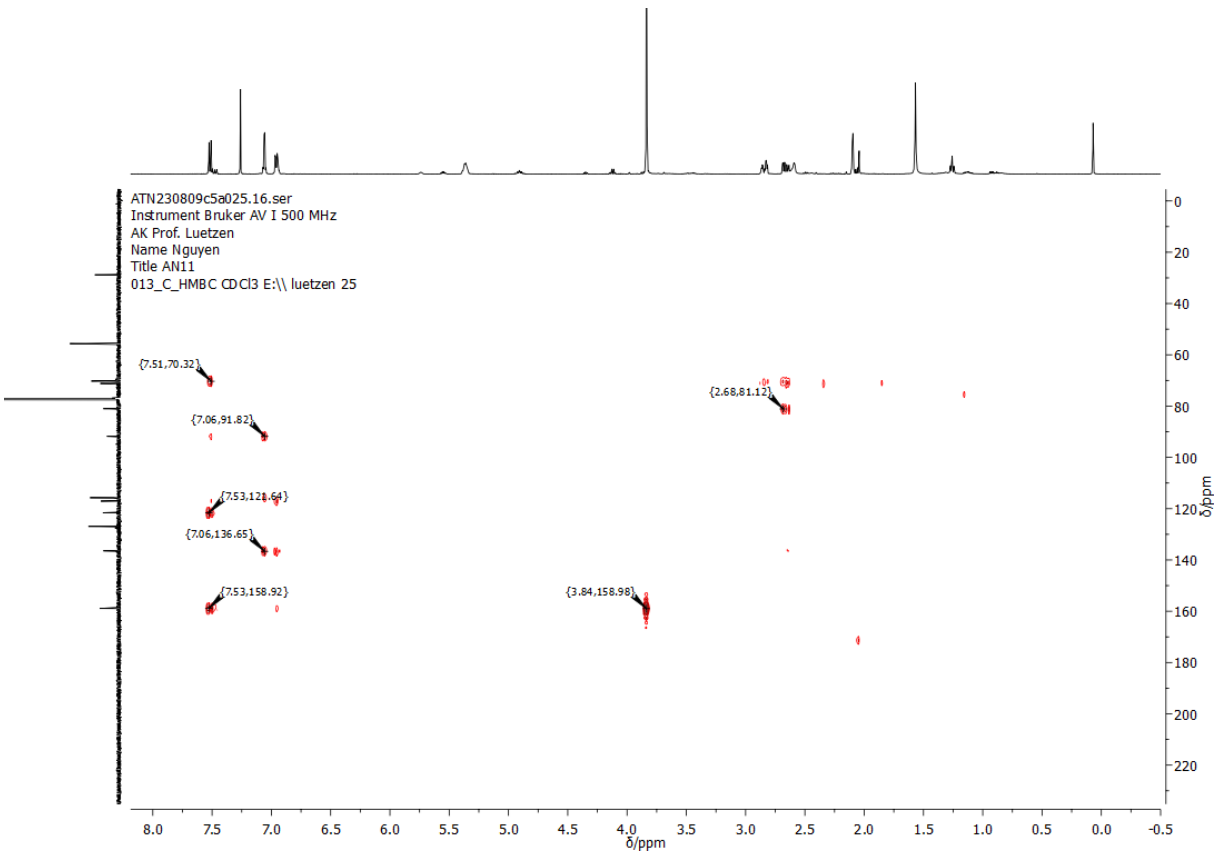

Figure 104: HMBC-NMR spectrum of **17** in $CDCl_3$.

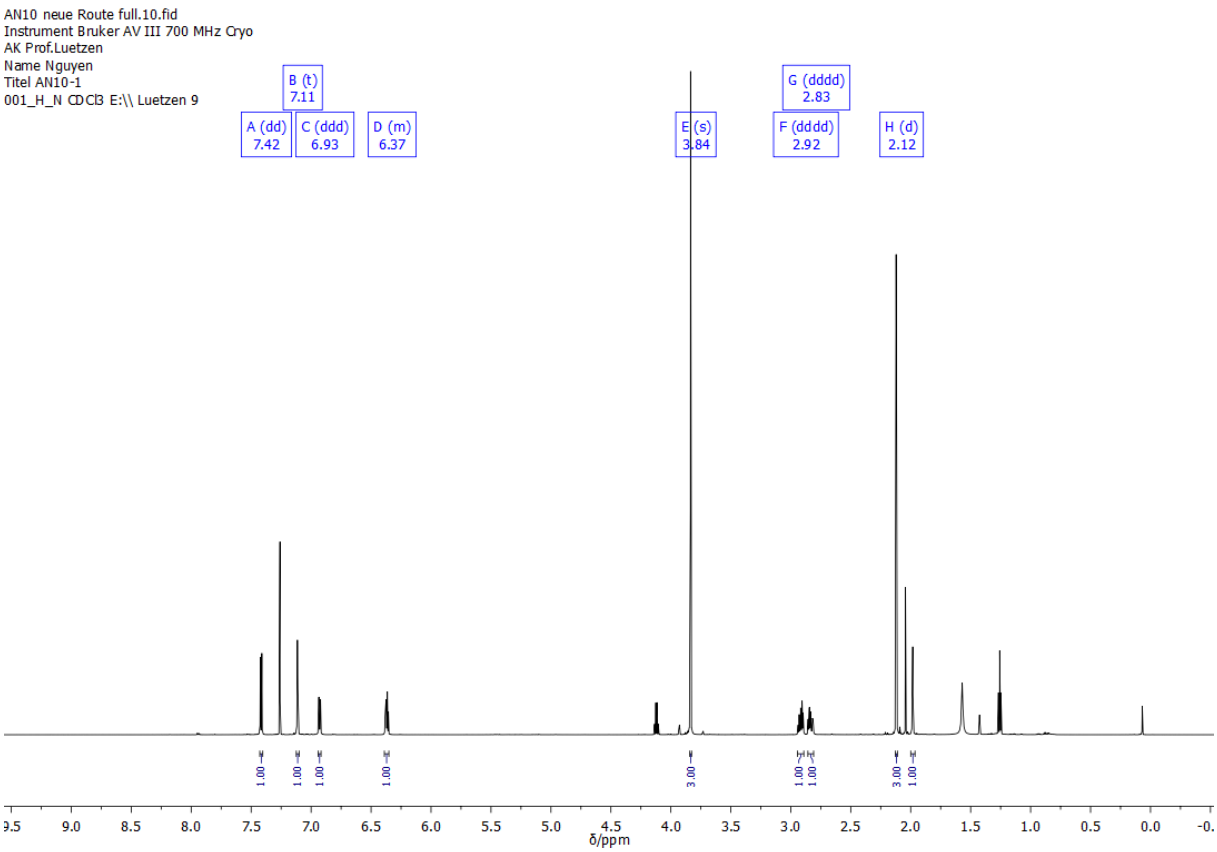

Figure 105: ^{1}H-NMR spectrum of **18** in $CDCl_3$.

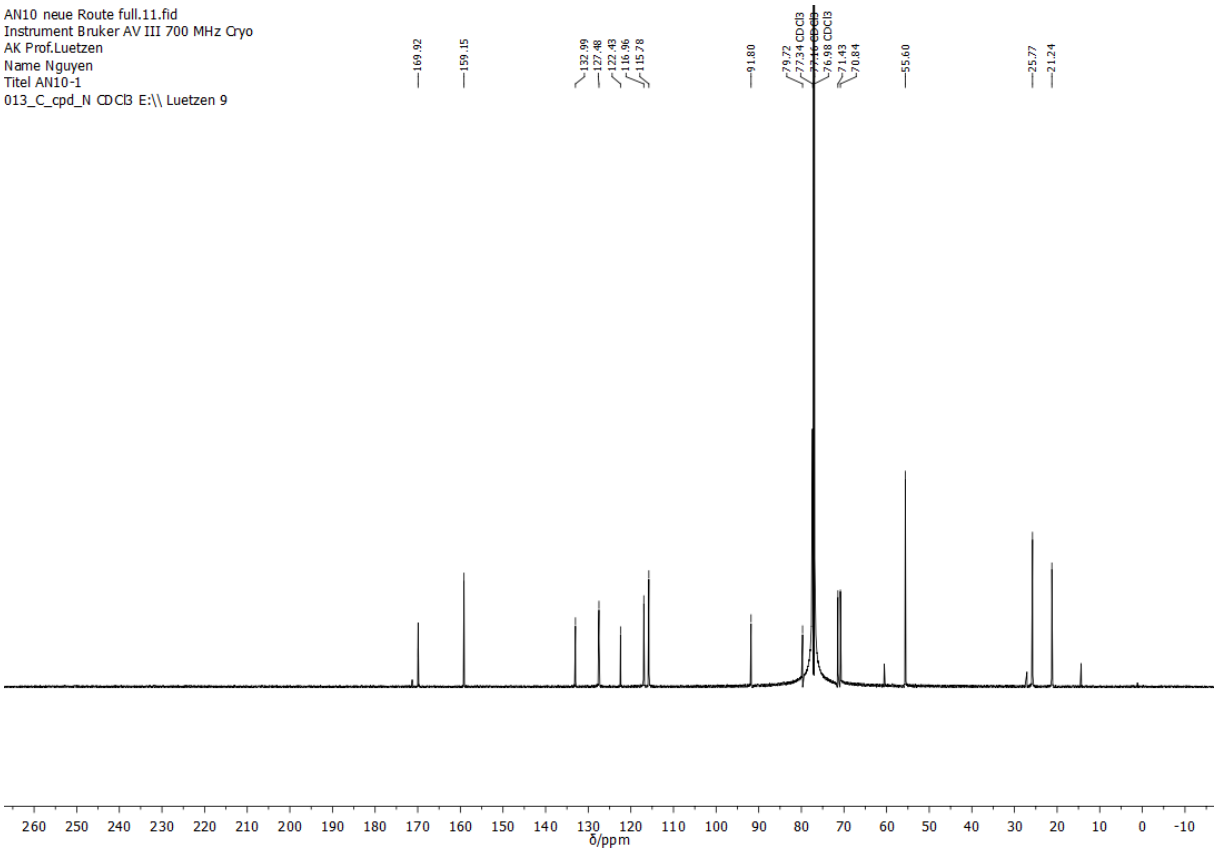

Figure 106: ^{13}C-NMR spectrum of **18** in $CDCl_3$.

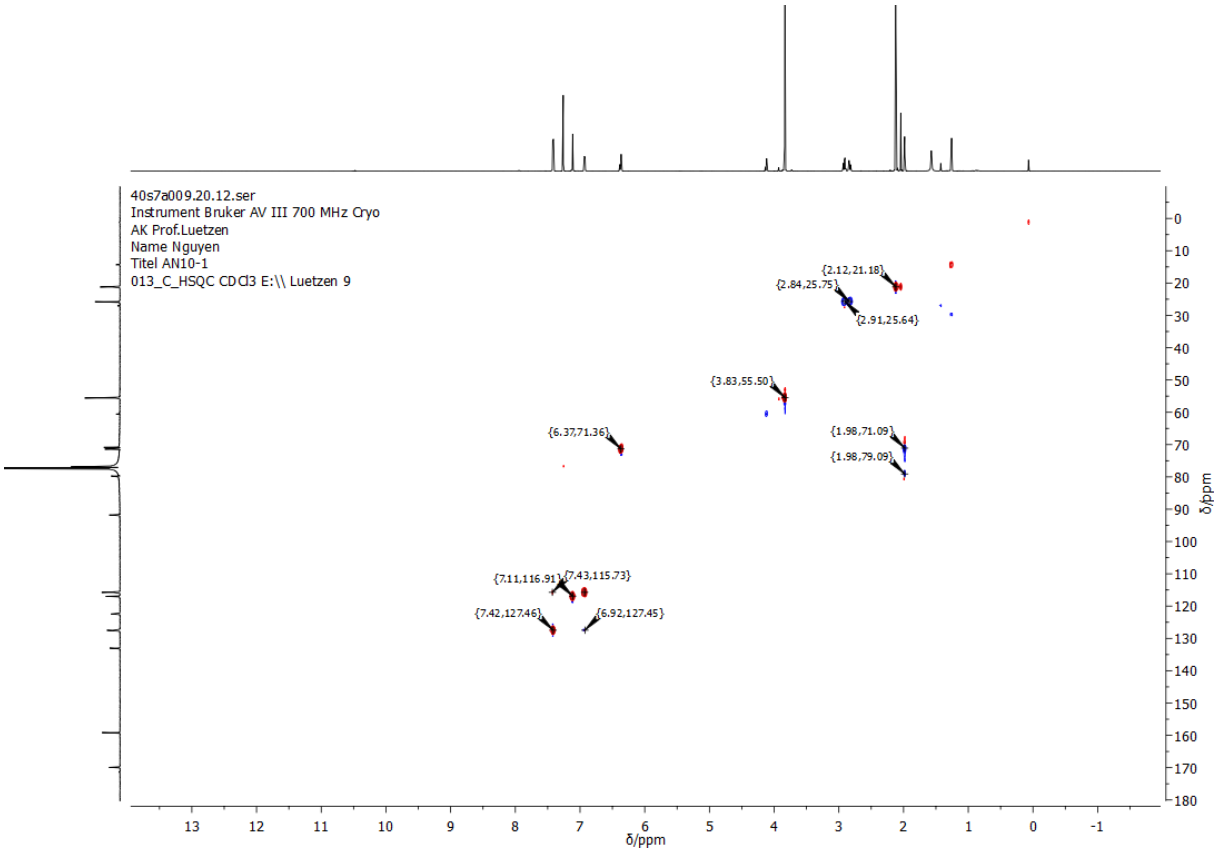

Figure 107: HSQC-NMR spectrum of **18** in $CDCl_3$.

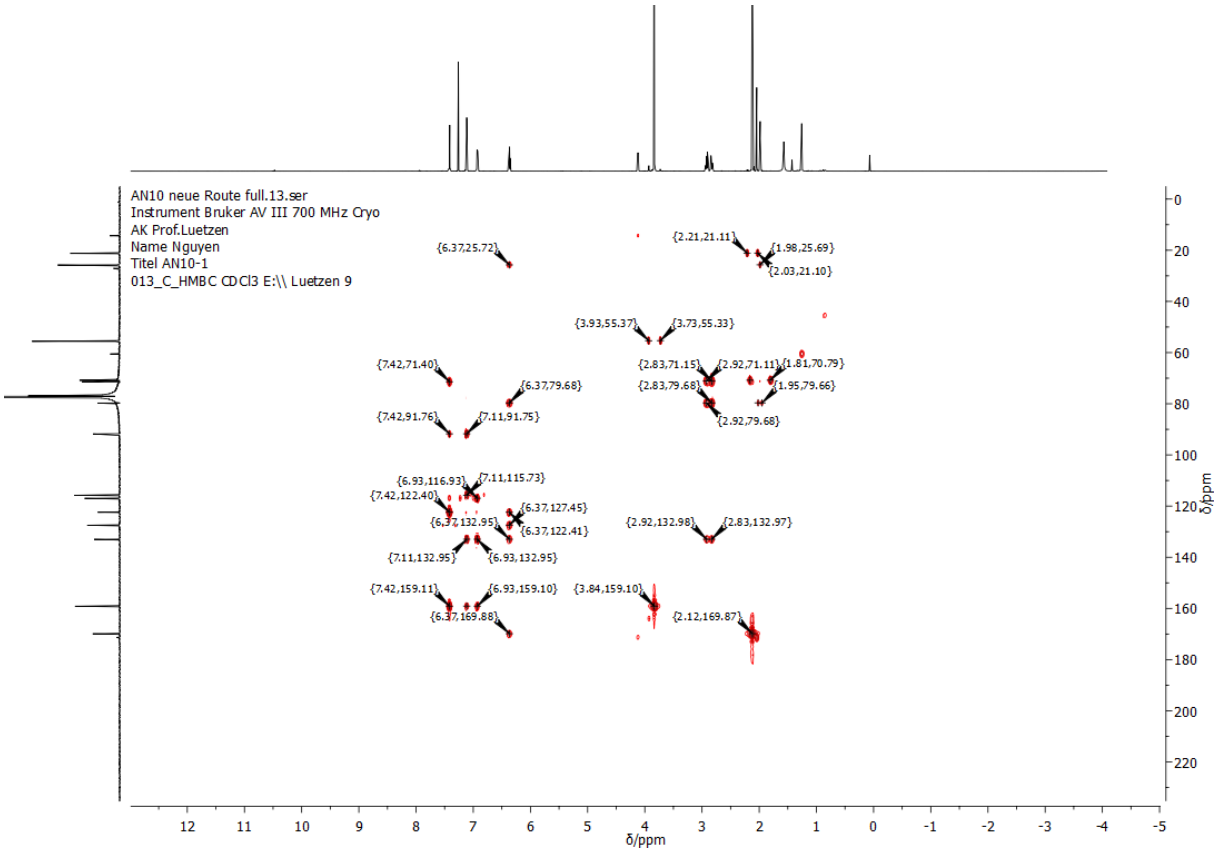

Figure 108: HMBC-NMR spectrum of **18** in $CDCl_3$.

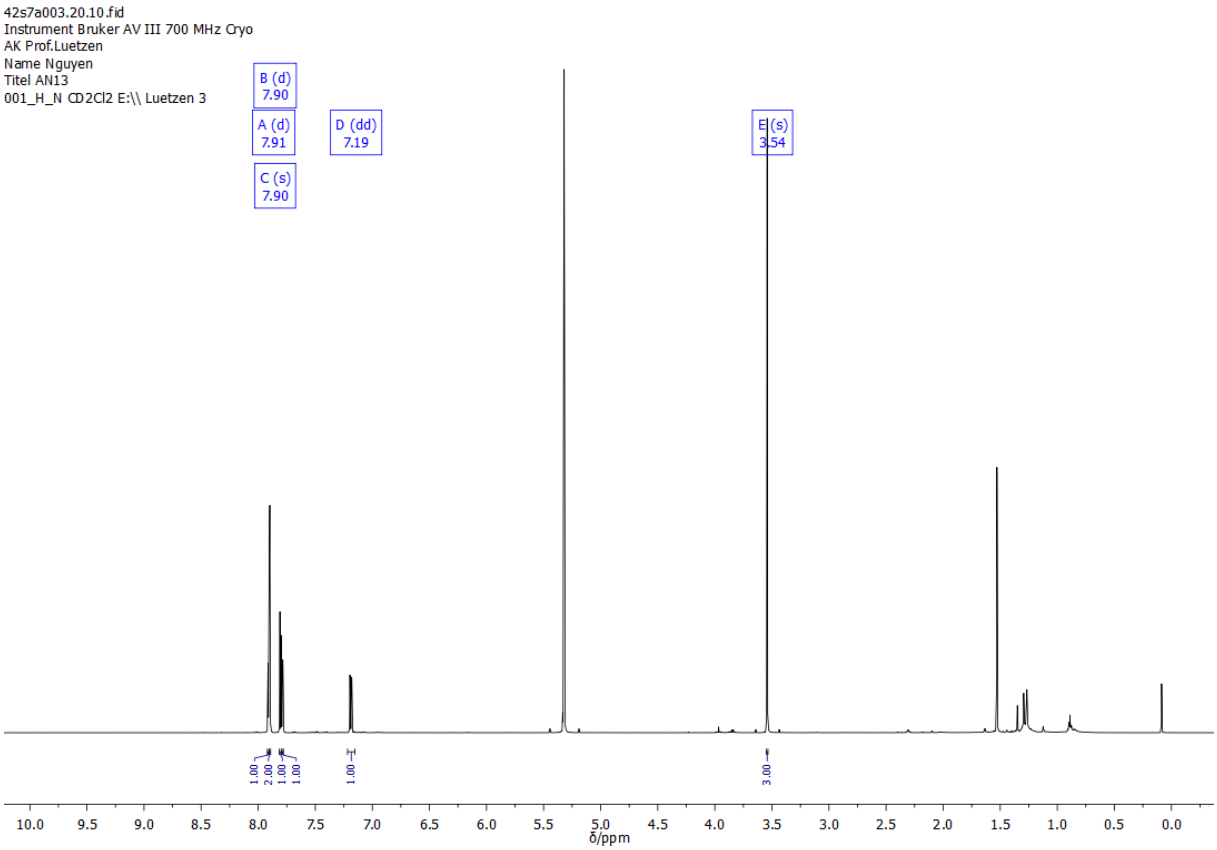

Figure 109: ^{1}H-NMR spectrum of **20** in CD_2Cl_2.

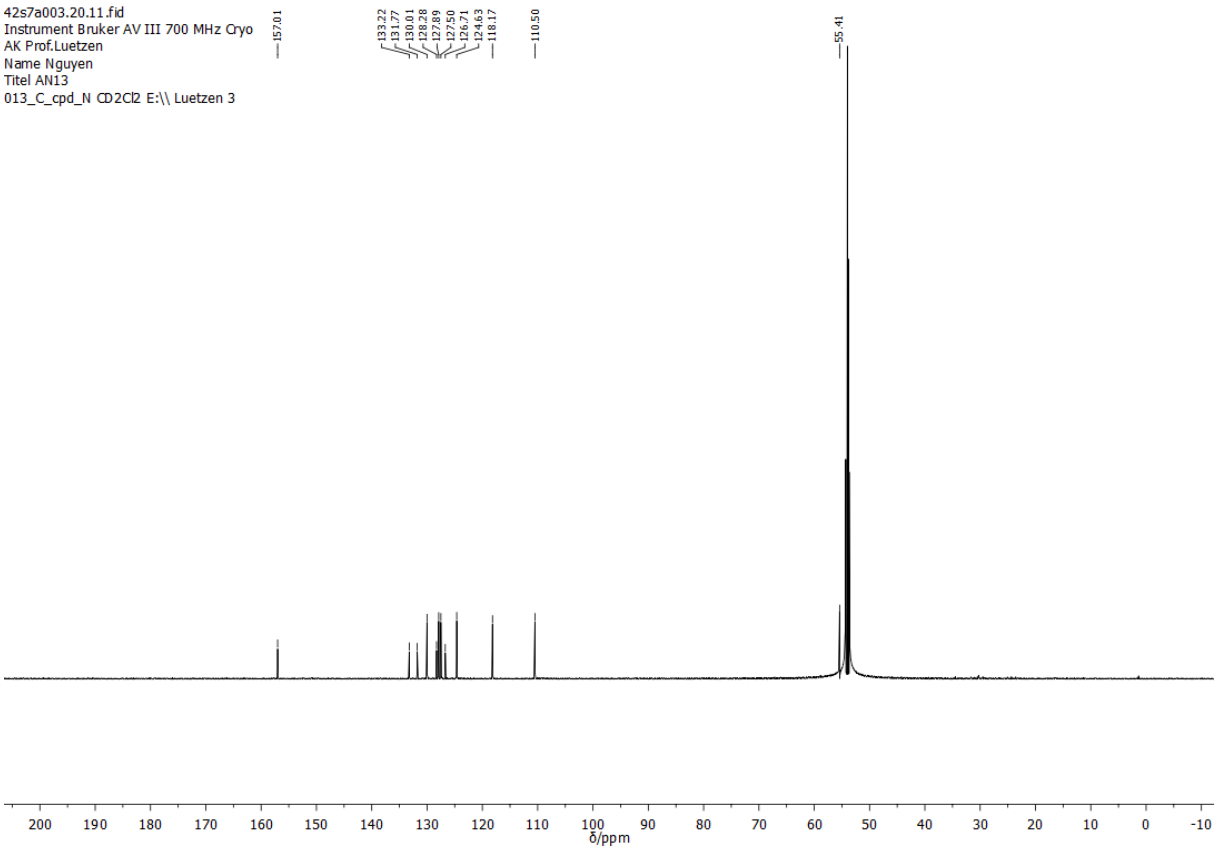

Figure 110: ^{13}C-NMR spectrum of **20** in CD_2Cl_2.

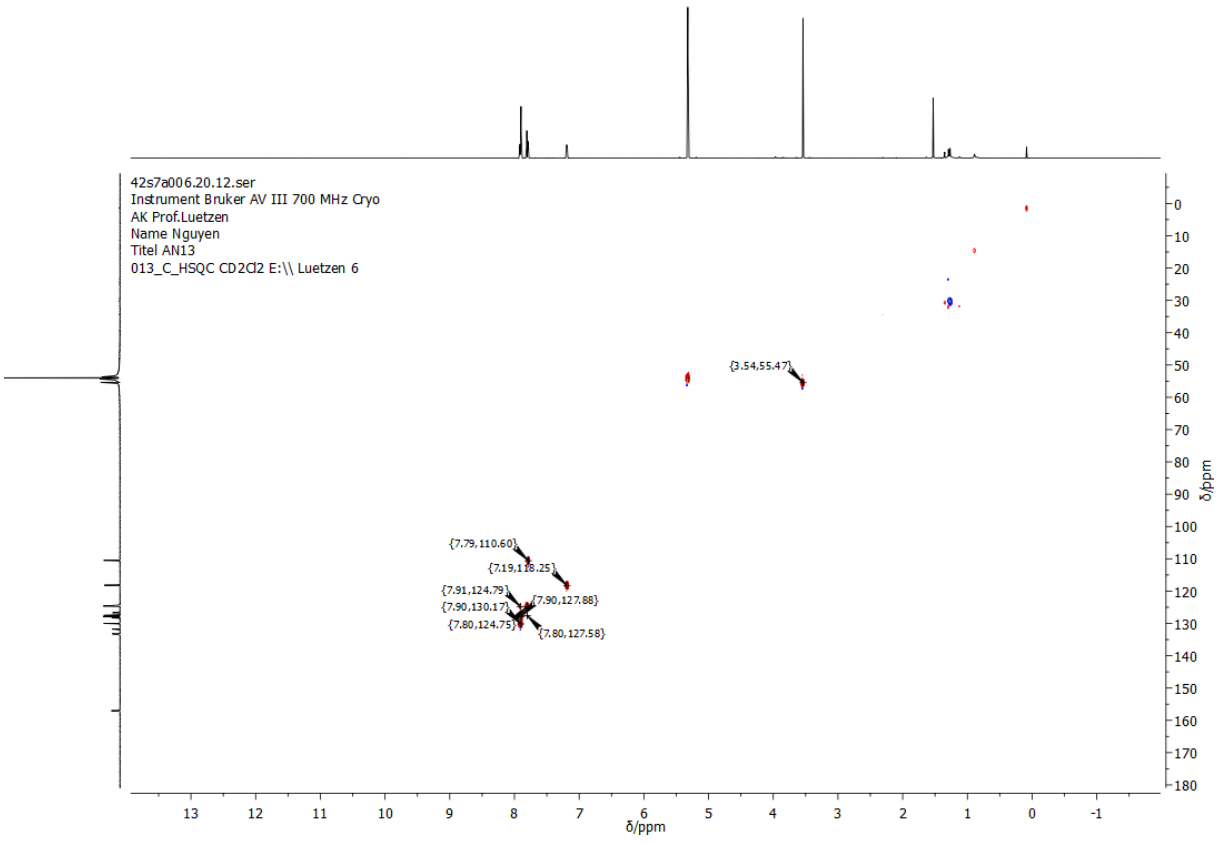

Figure 111: HSQC-NMR spectrum of **20** in CD_2Cl_2.

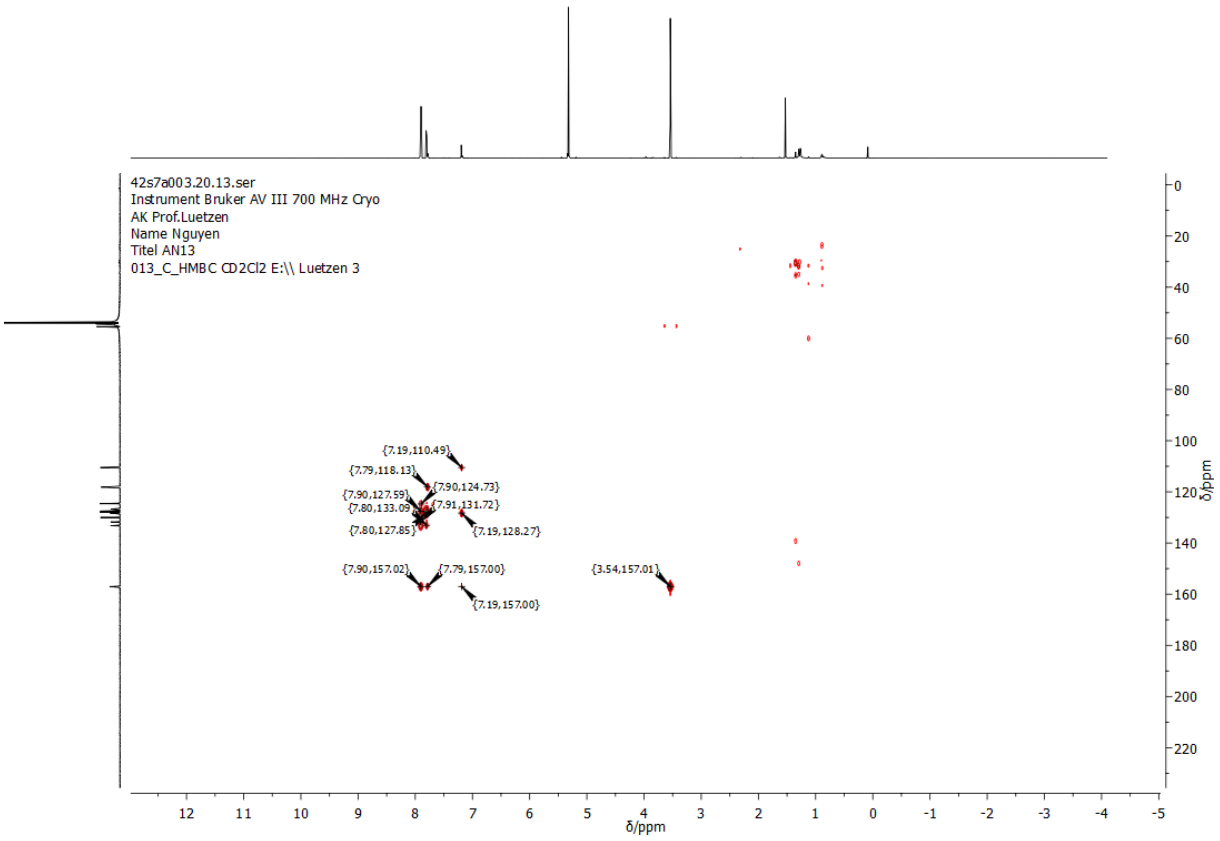

Figure 112: HMBC-NMR spectrum of **20** in CD_2Cl_2.

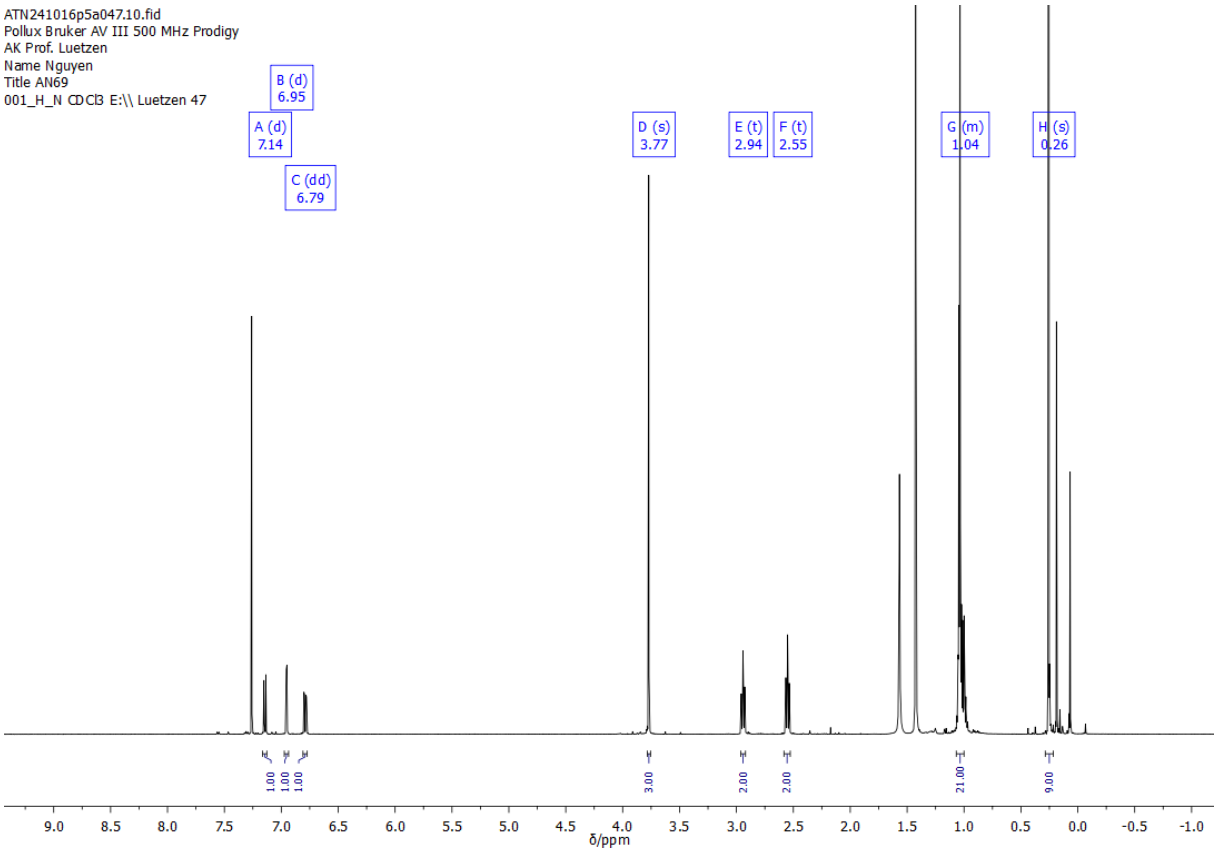

Figure 113: ^{1}H-NMR spectrum of **25** in $CDCl_3$.

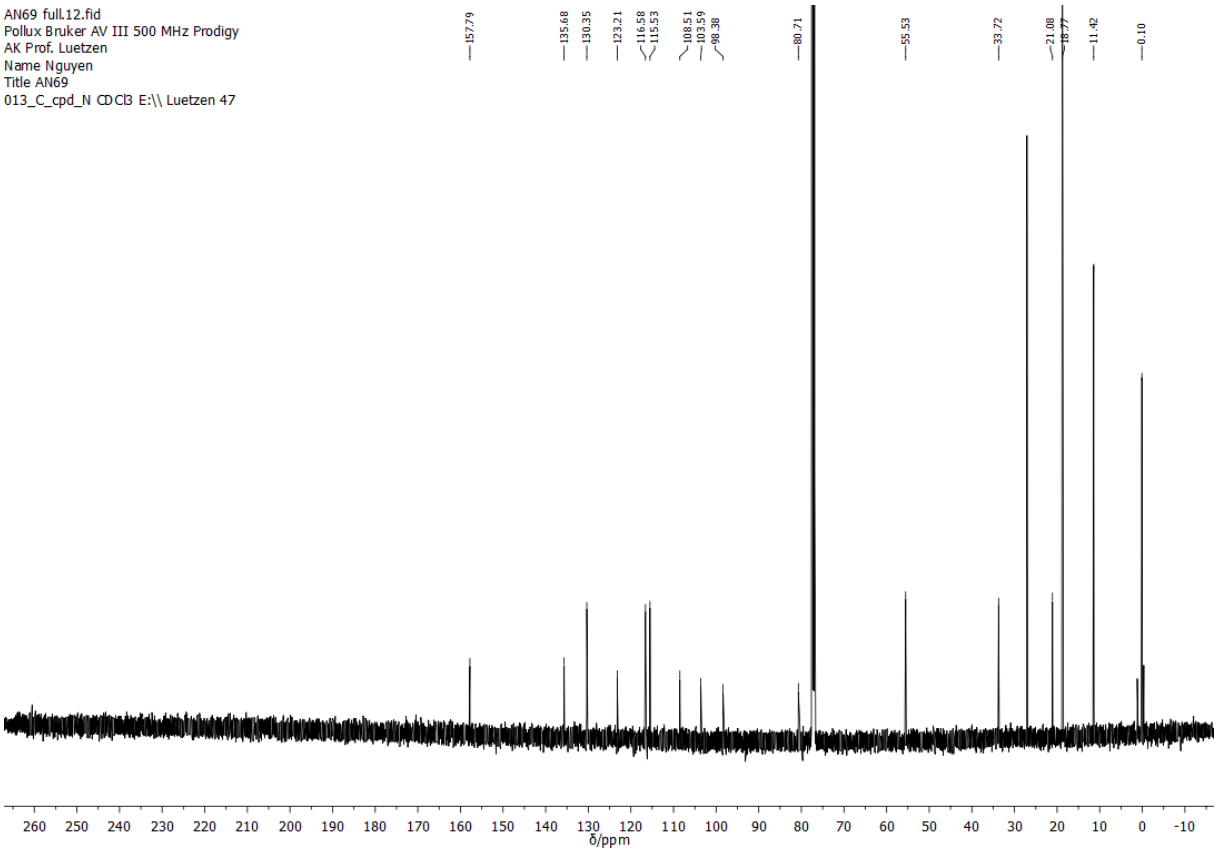

Figure 114: ^{13}C-NMR spectrum of **25** in $CDCl_3$.

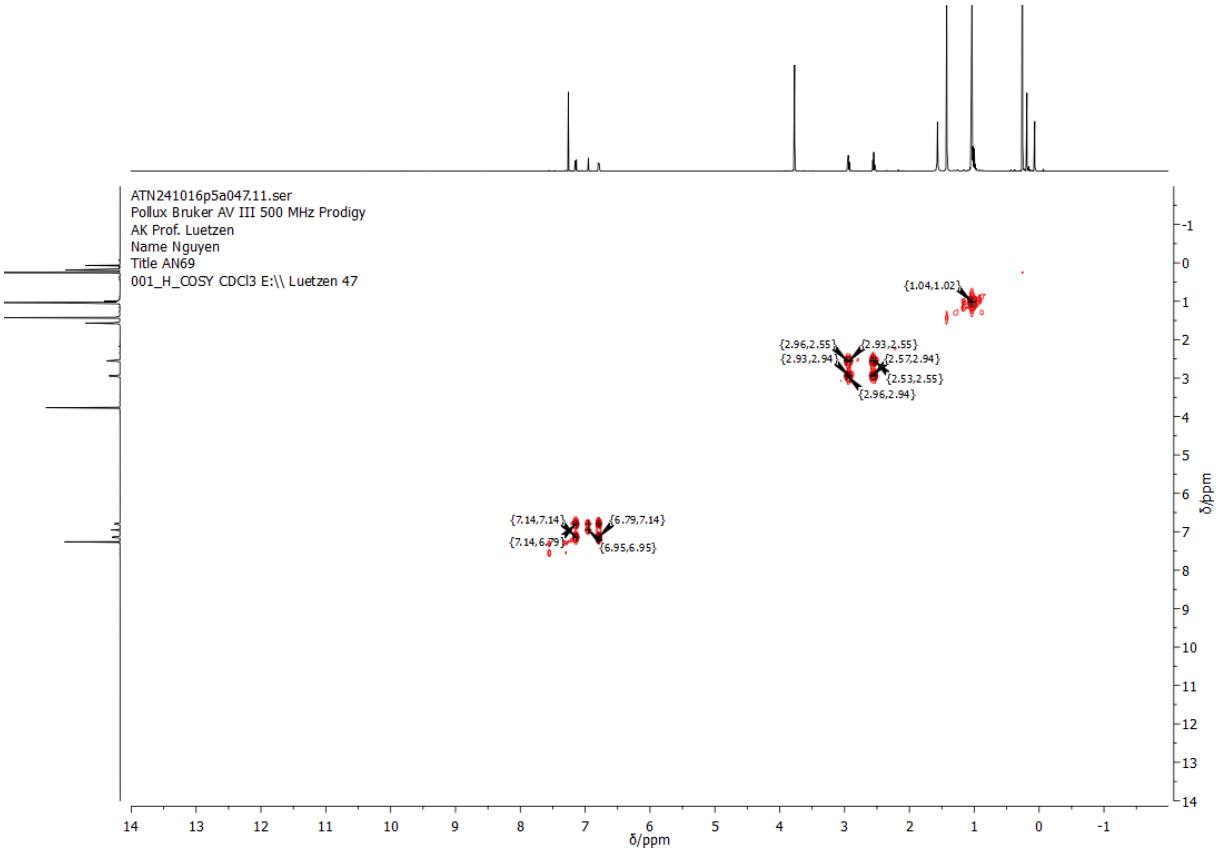

Figure 115: COSY-NMR spectrum of **25** in $CDCl_3$.

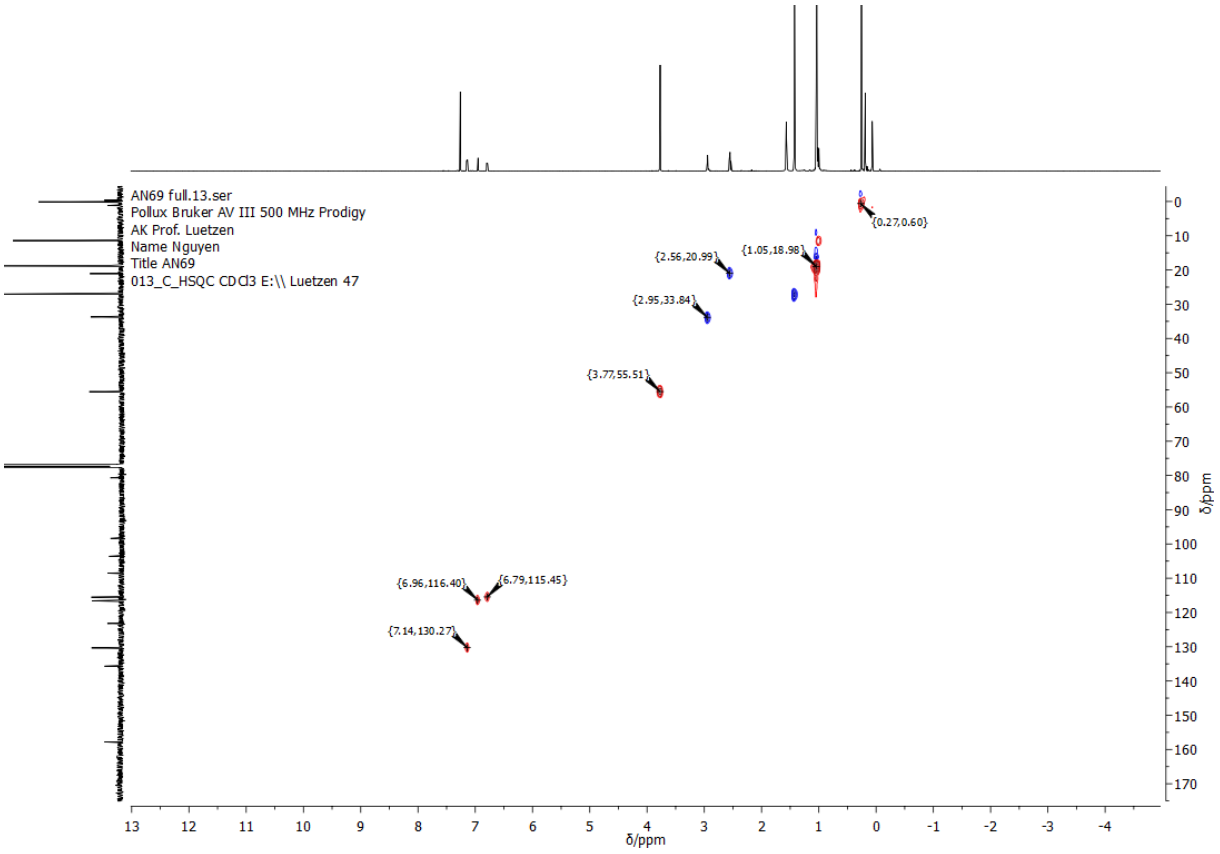

Figure 116: HSQC-NMR spectrum of **25** in $CDCl_3$.

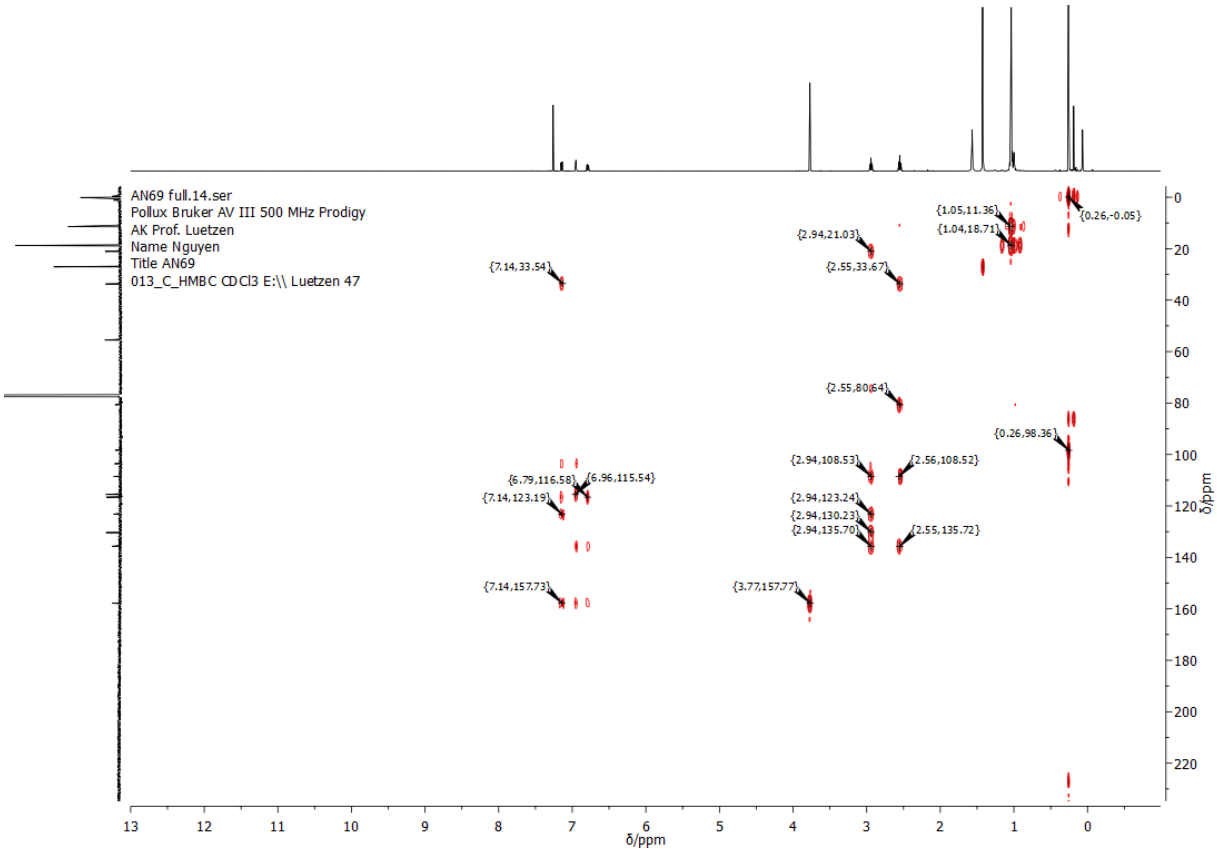

Figure 117: HMBC-NMR spectrum of **25** in $CDCl_3$.

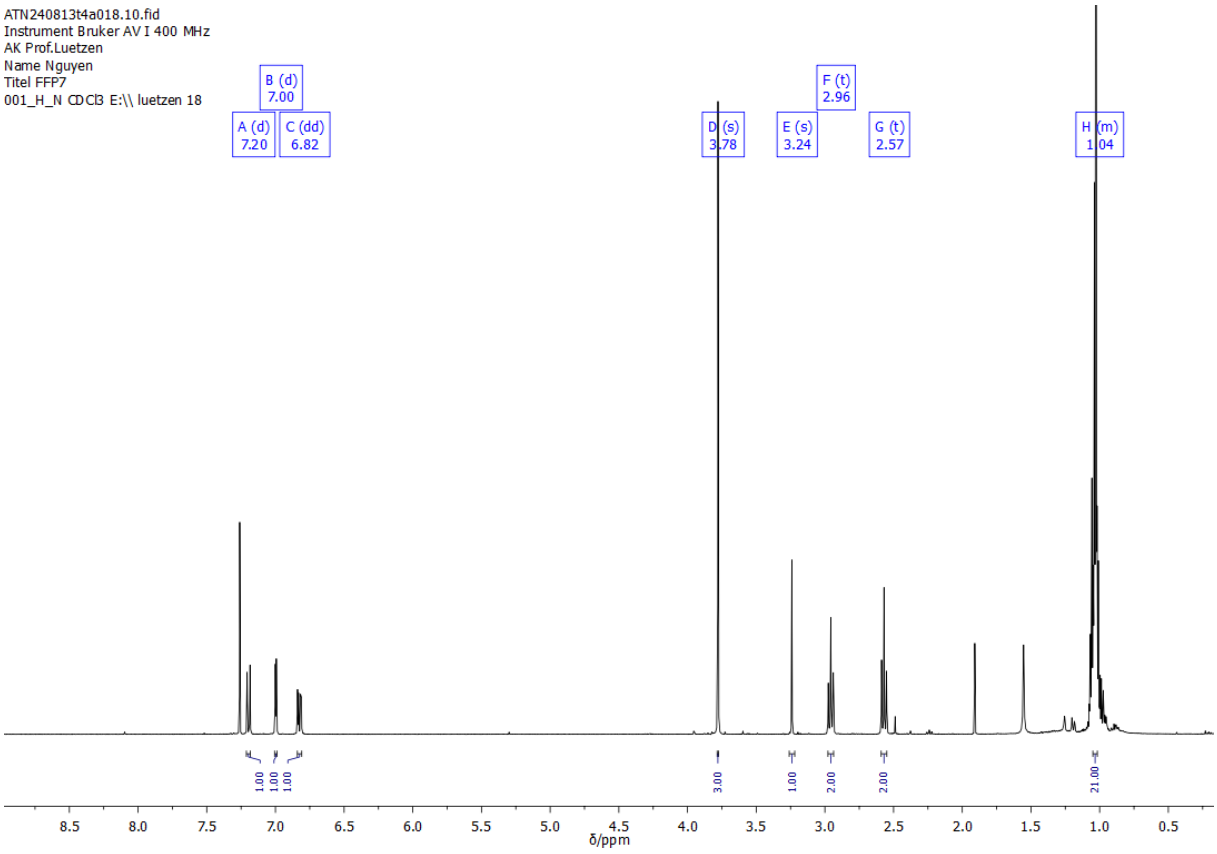

Figure 118: ^{1}H-NMR spectrum of **26** in $CDCl_3$.

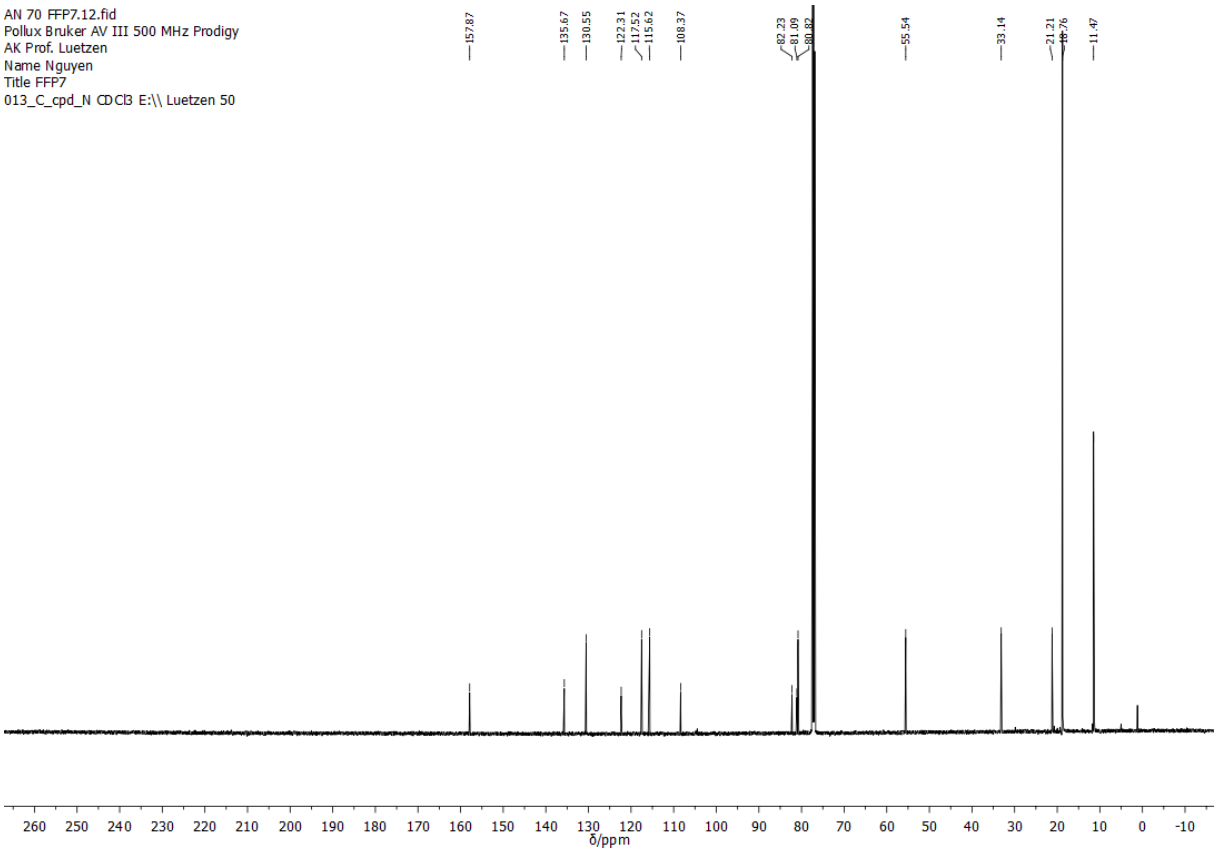

Figure 119: ^{13}C-NMR spectrum of **26** in $CDCl_3$.

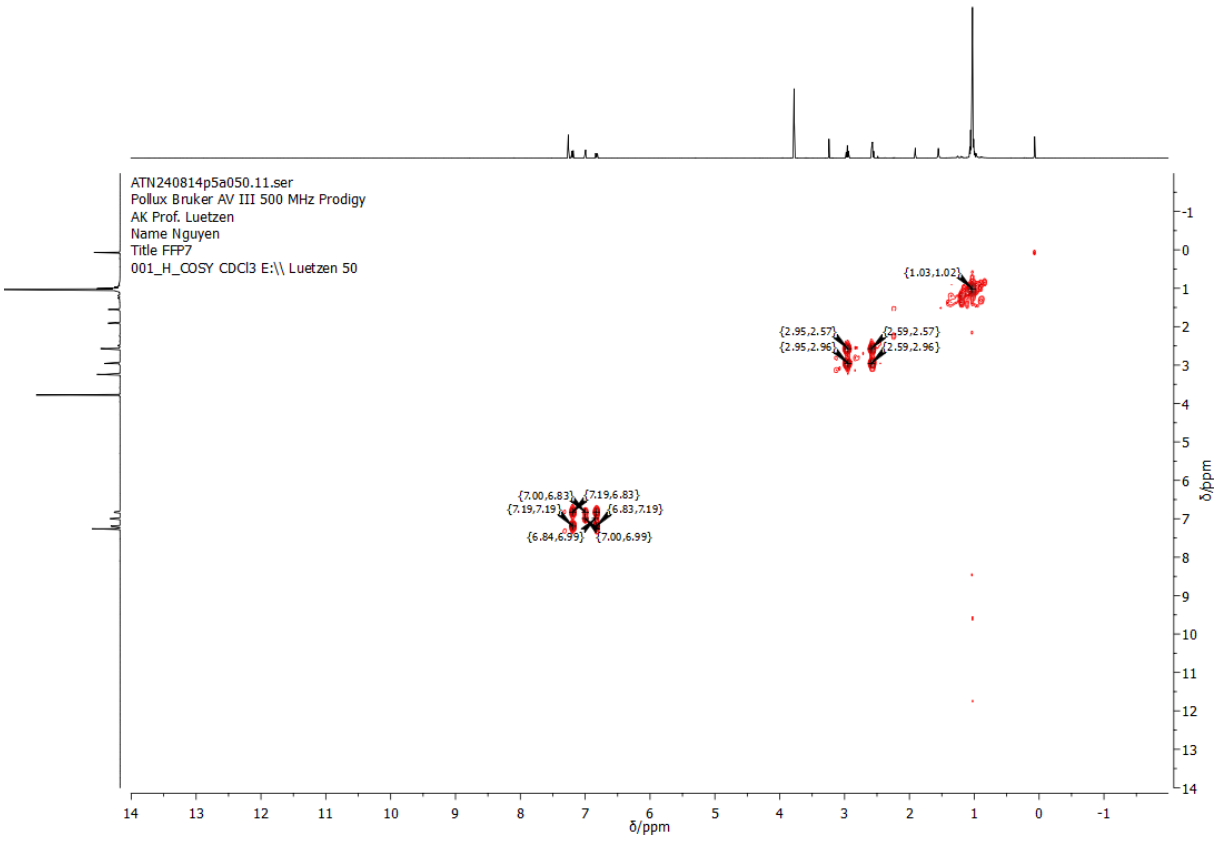

Figure 120: COSY-NMR spectrum of **26** in $CDCl_3$.

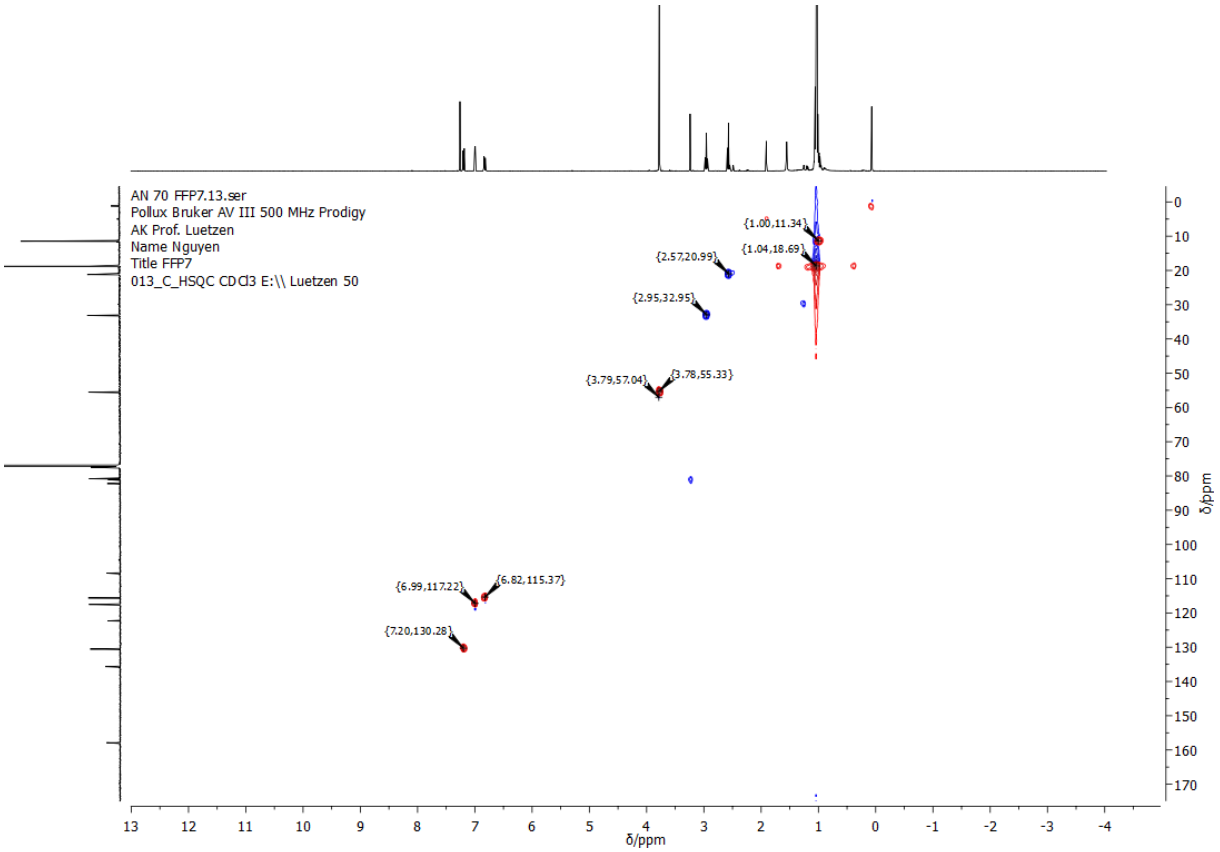

Figure 121: HSQC-NMR spectrum of **26** in $CDCl_3$.

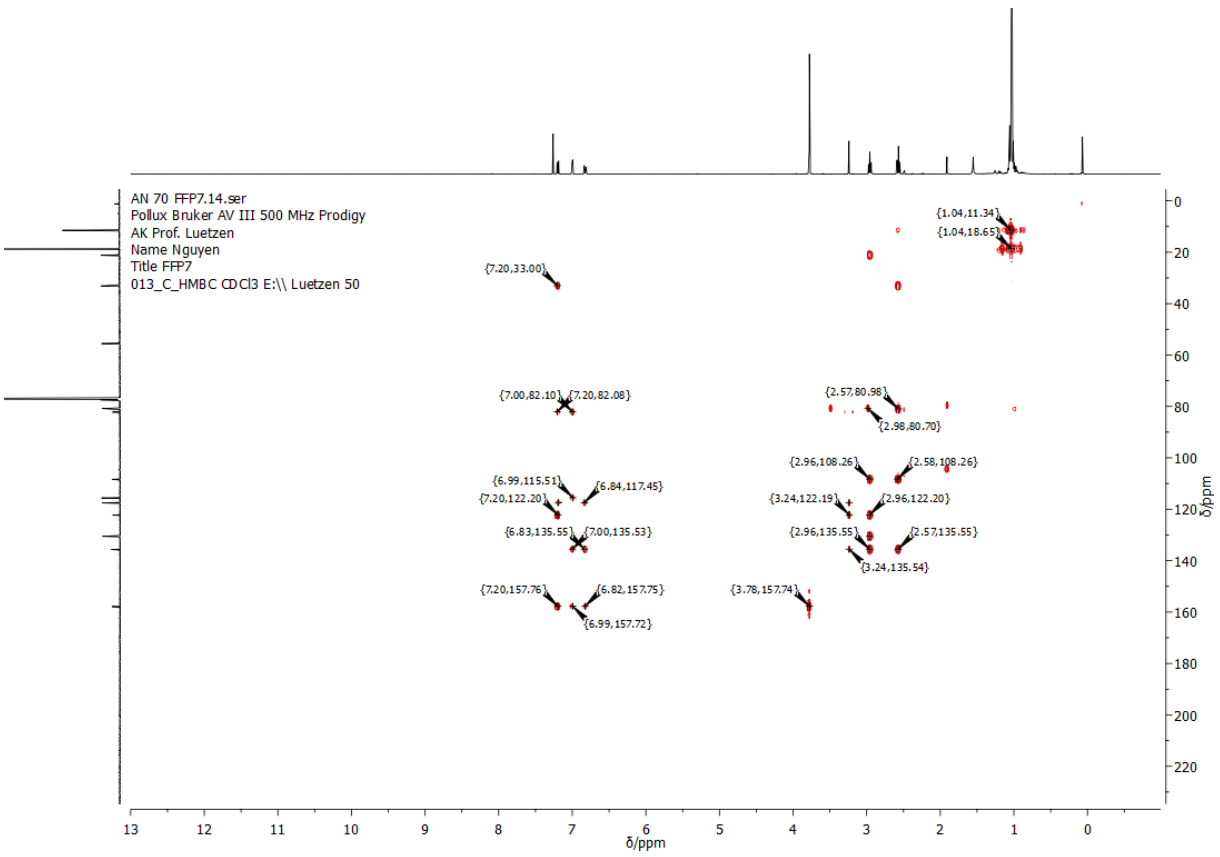

Figure 122: HMBC-NMR spectrum of **26** in $CDCl_3$.

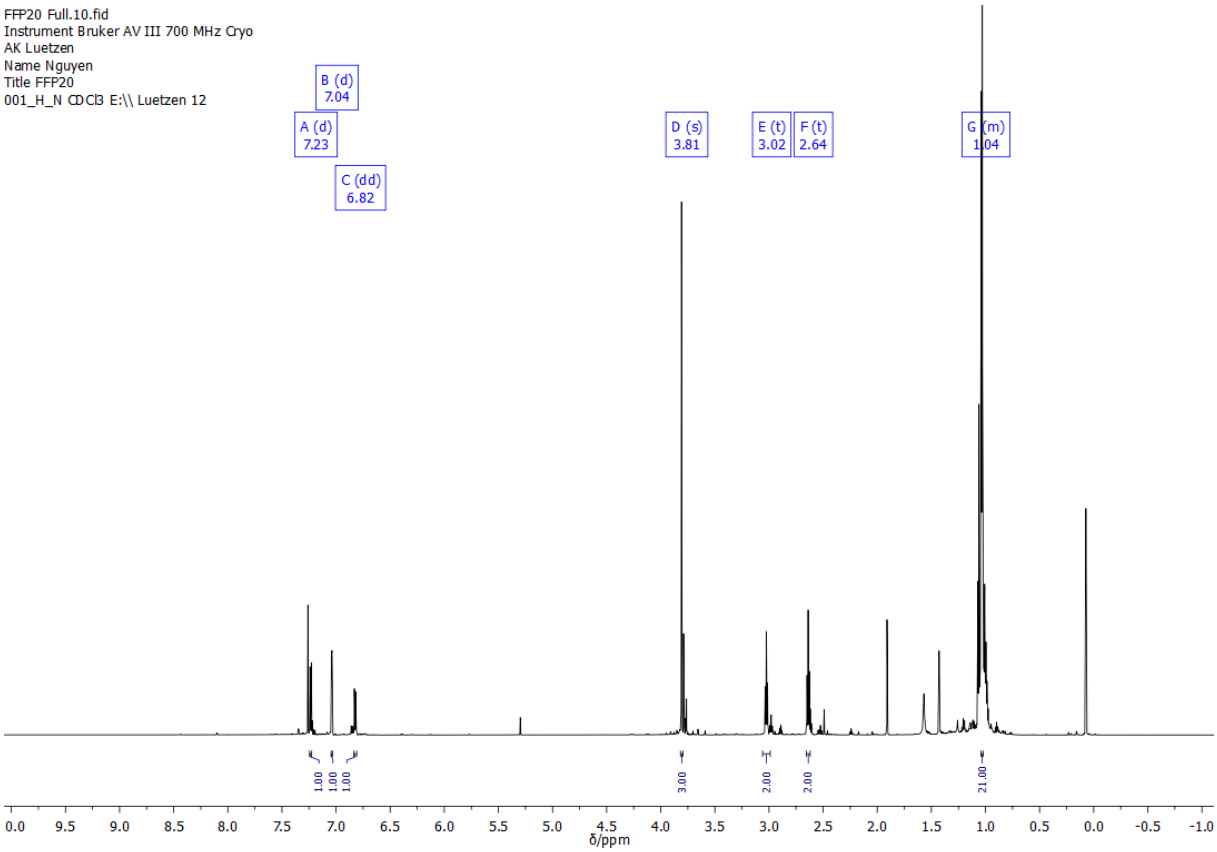

Figure 123: ^{1}H-NMR spectrum of **27** in $CDCl_3$.

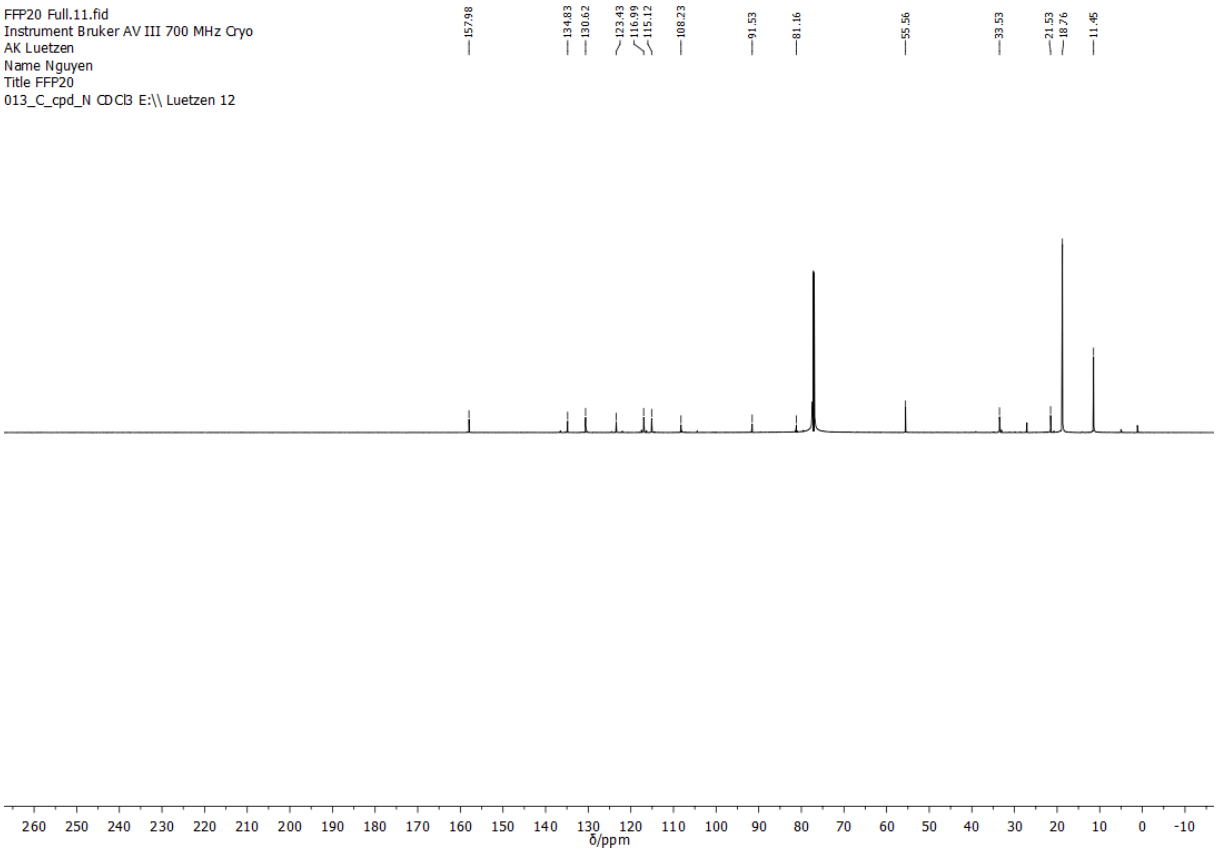

Figure 124: ^{13}C-NMR spectrum of **27** in $CDCl_3$.

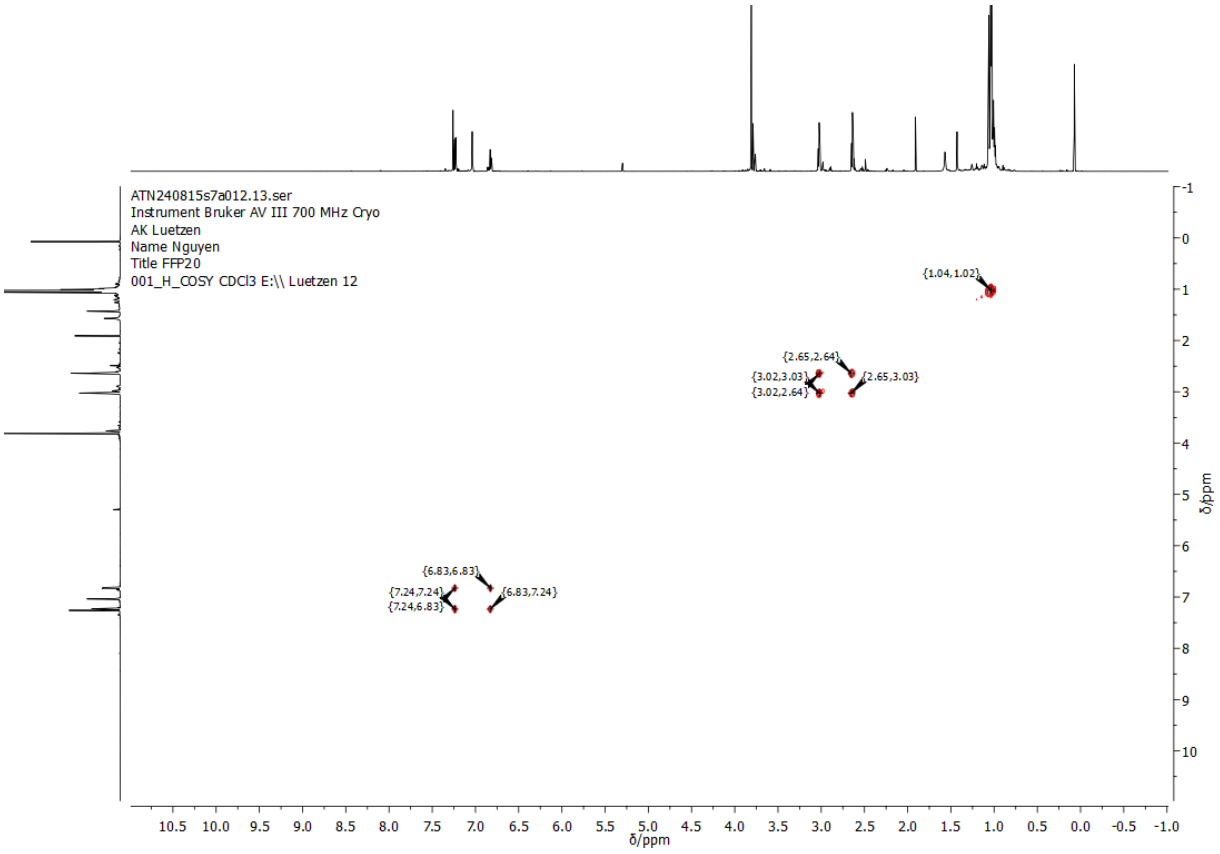

Figure 125: COSY-NMR spectrum of **27** in $CDCl_3$.

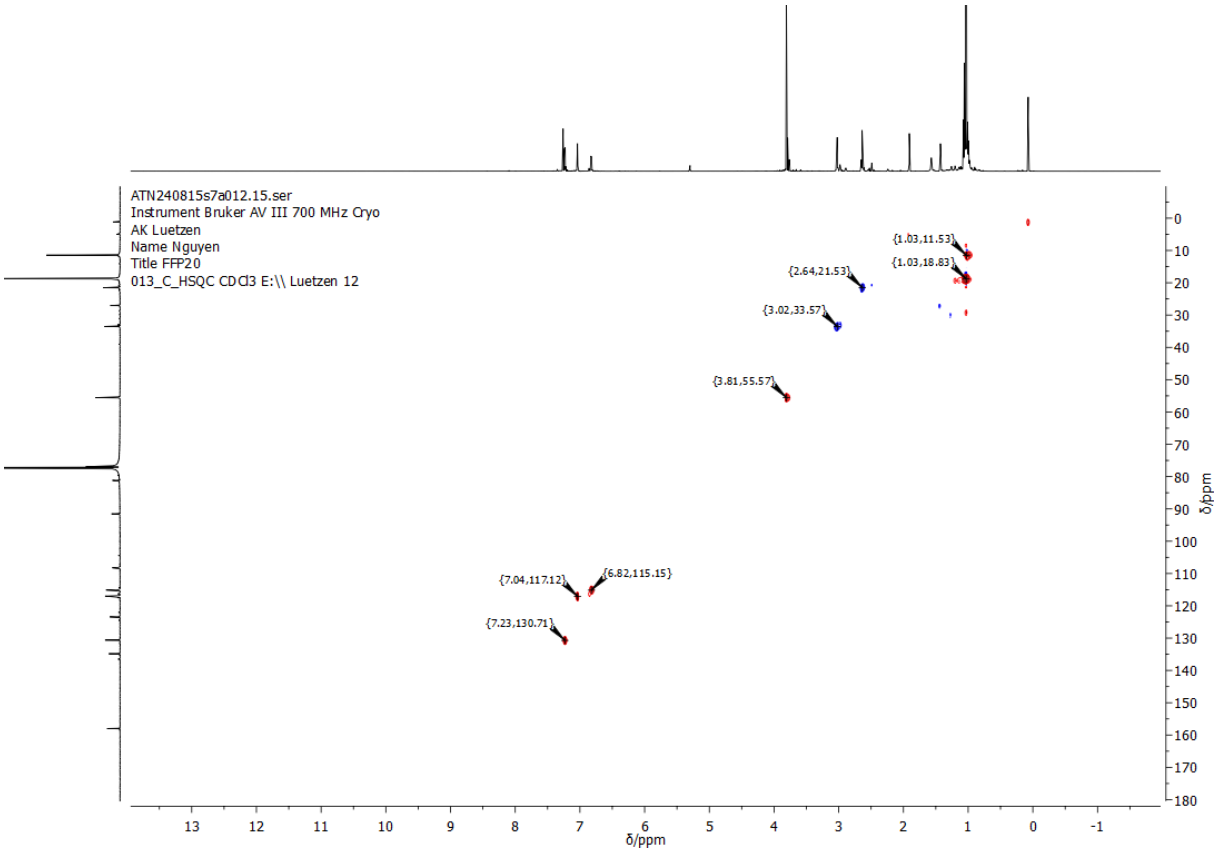

Figure 126: HSQC-NMR spectrum of **27** in $CDCl_3$.

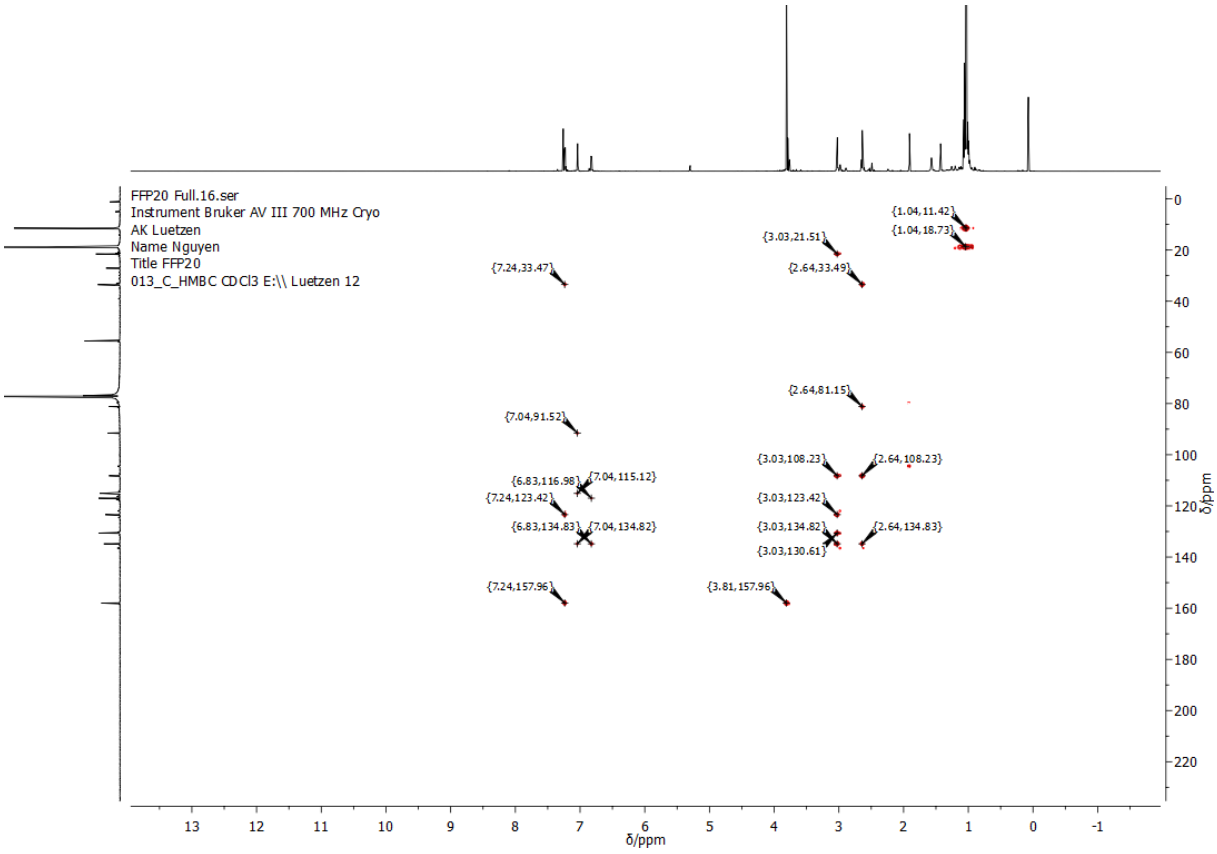

Figure 127: HMBC-NMR spectrum of **27** in $CDCl_3$.

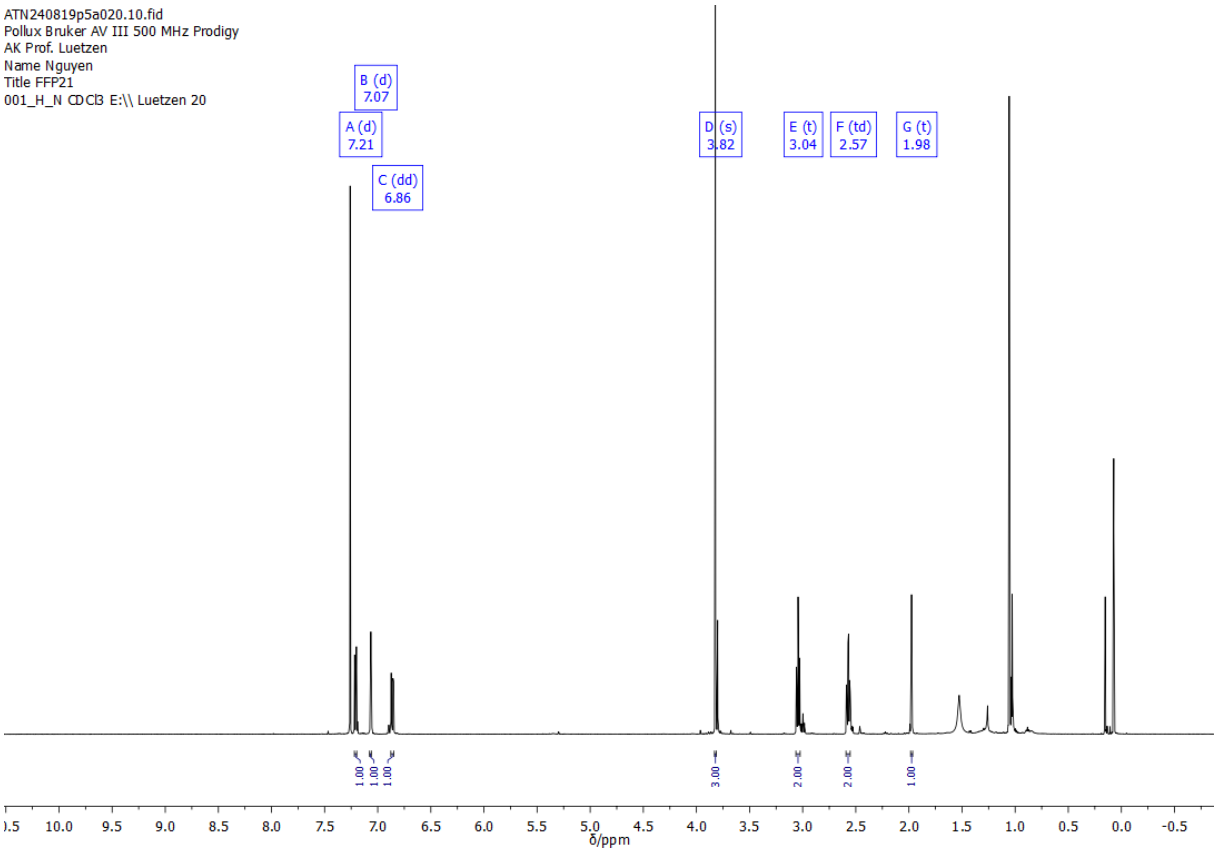

Figure 128: ^{1}H-NMR spectrum of **28** in $CDCl_3$.

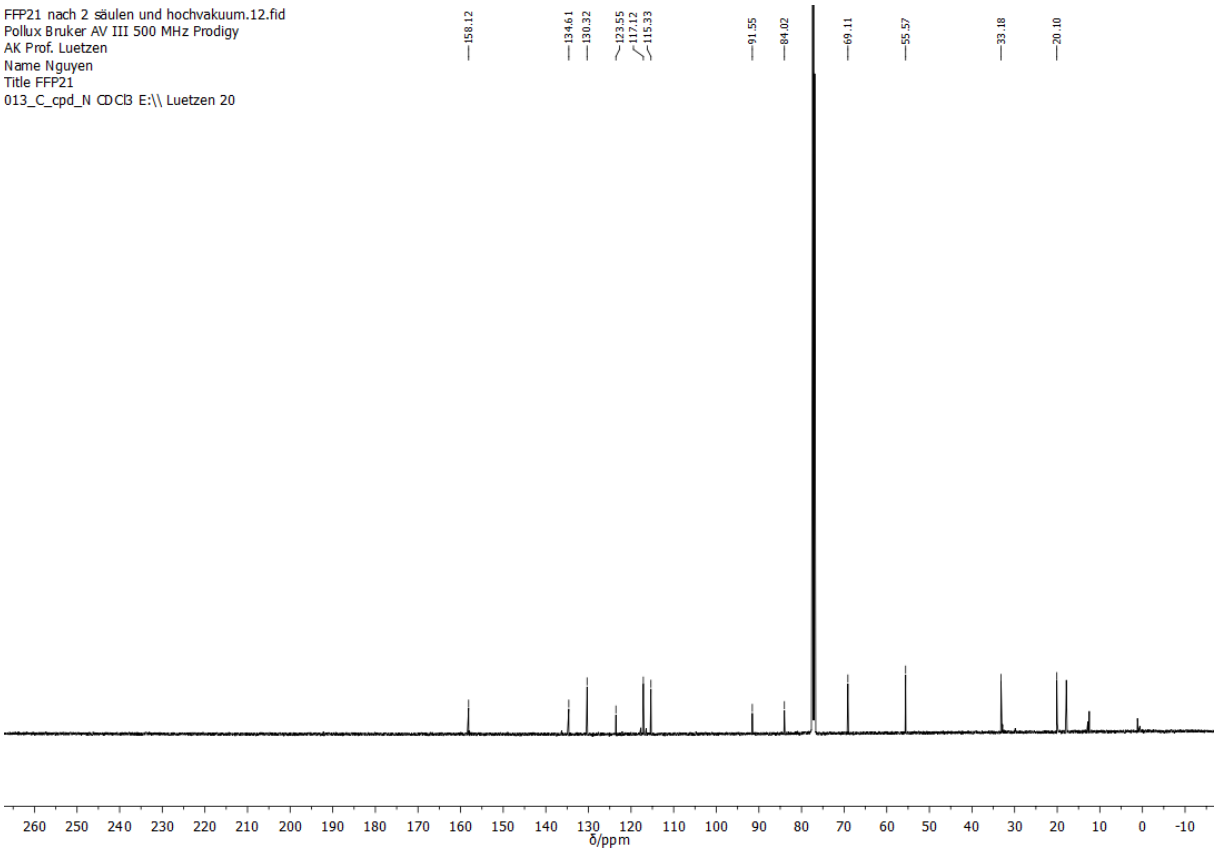

Figure 129: ^{13}C-NMR spectrum of **28** in $CDCl_3$.

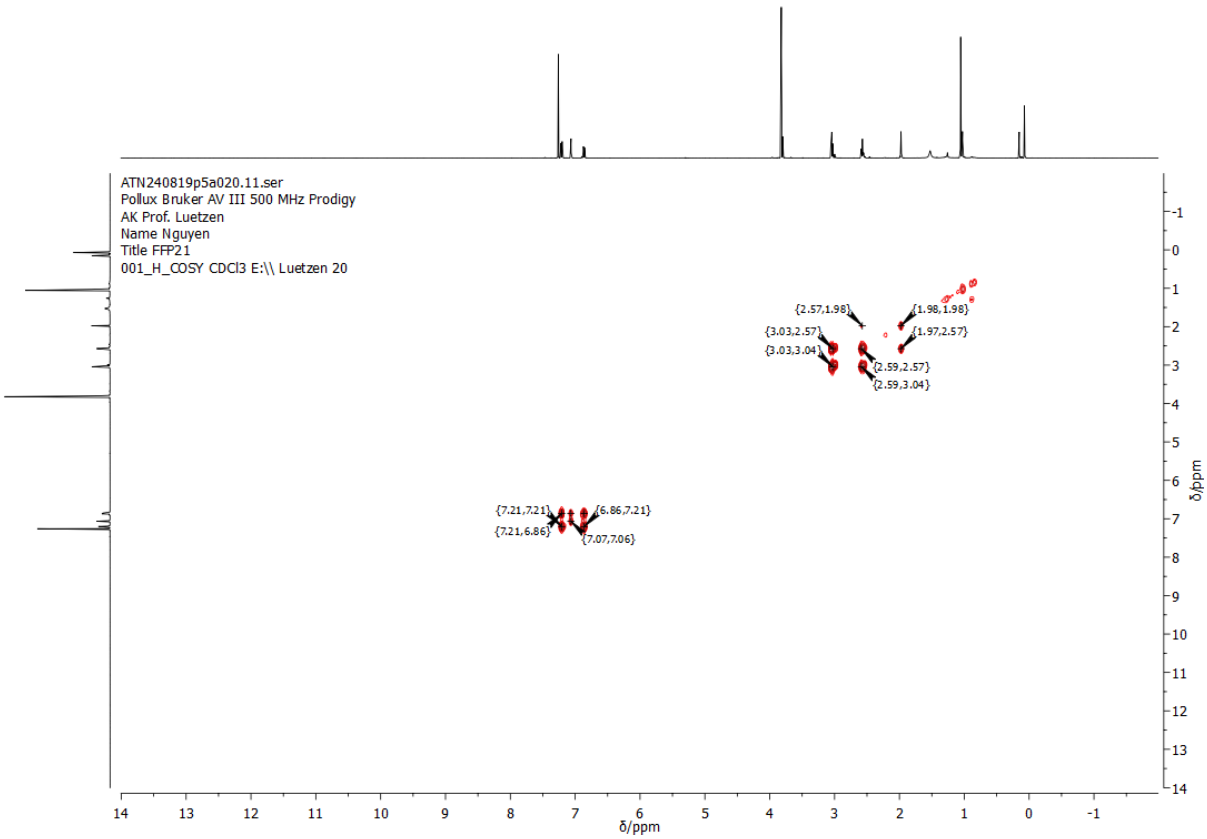

Figure 130: COSY-NMR spectrum of **28** in $CDCl_3$.

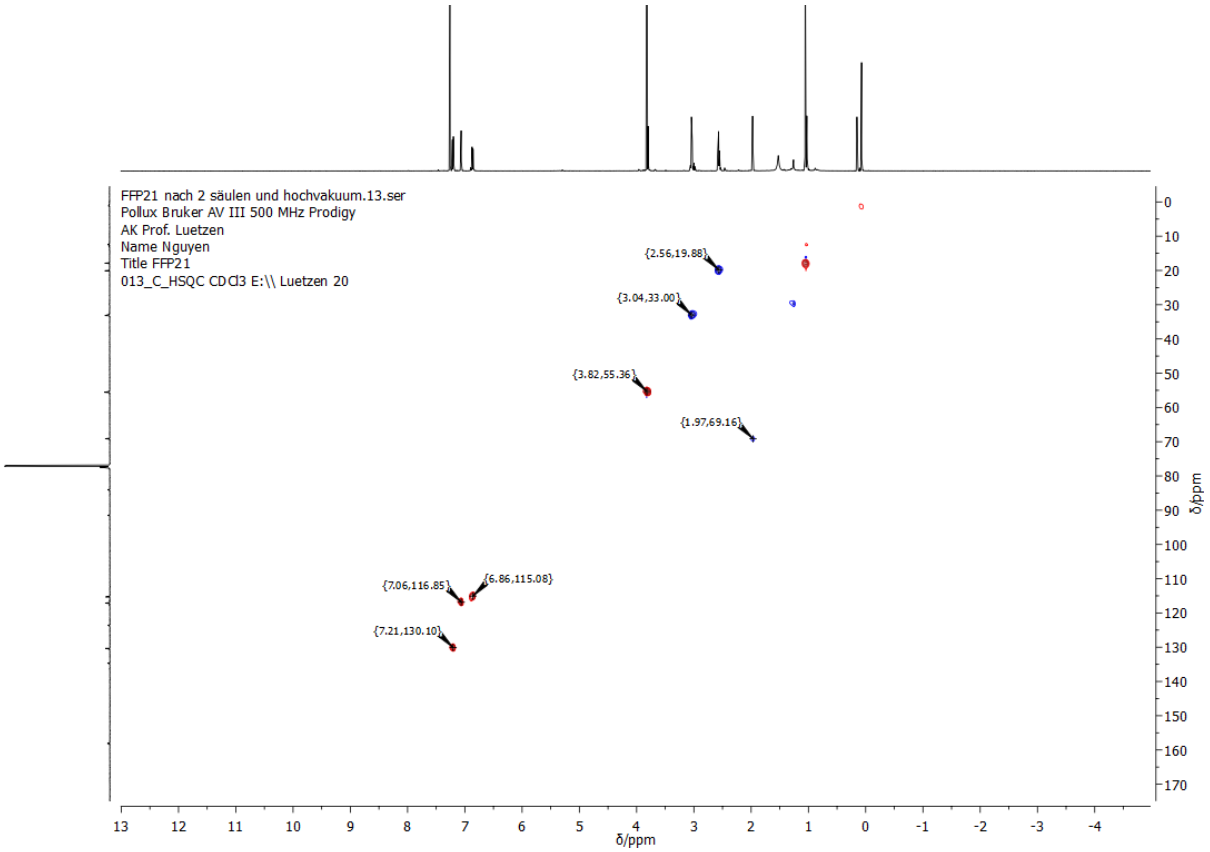

Figure 131: HSQC-NMR spectrum of **28** in $CDCl_3$.

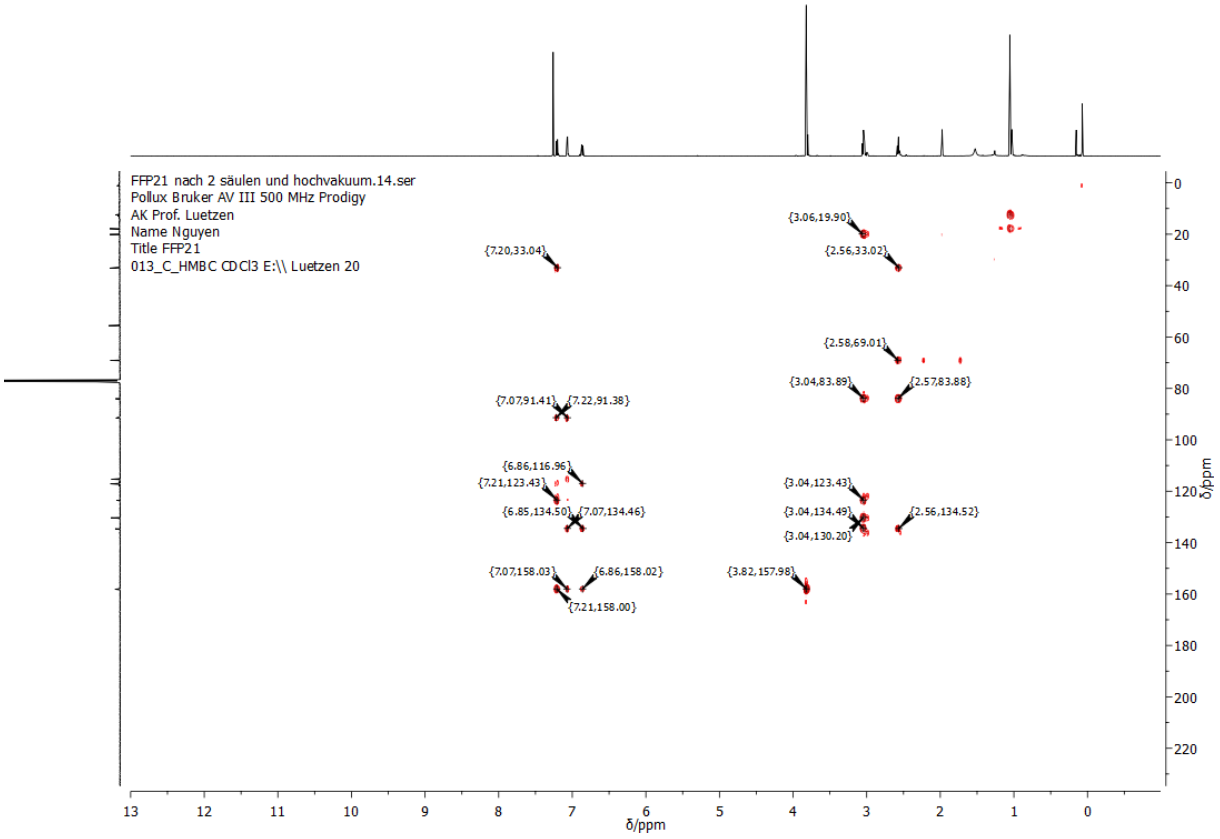

Figure 132: HMBC-NMR spectrum of **28** in $CDCl_3$.

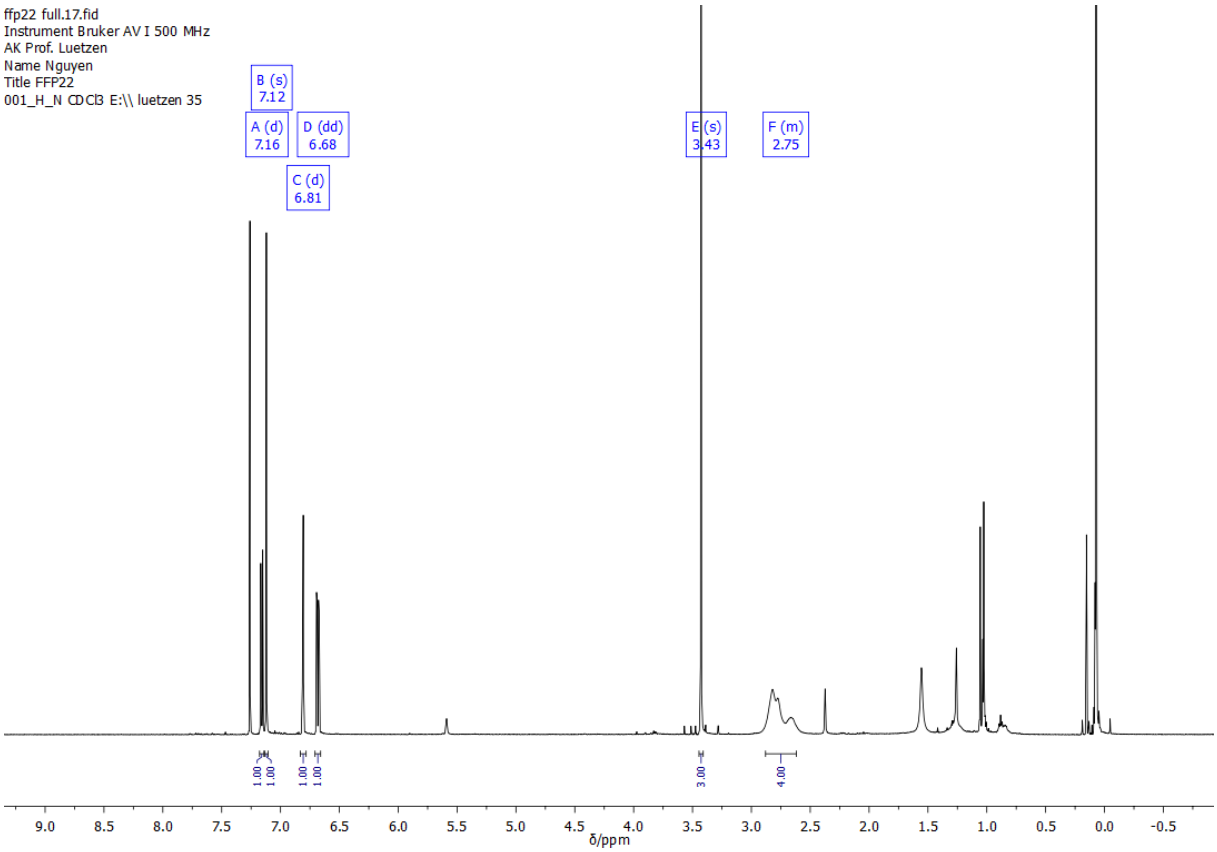

Figure 133: ^{1}H-NMR spectrum of **29** in $CDCl_3$.

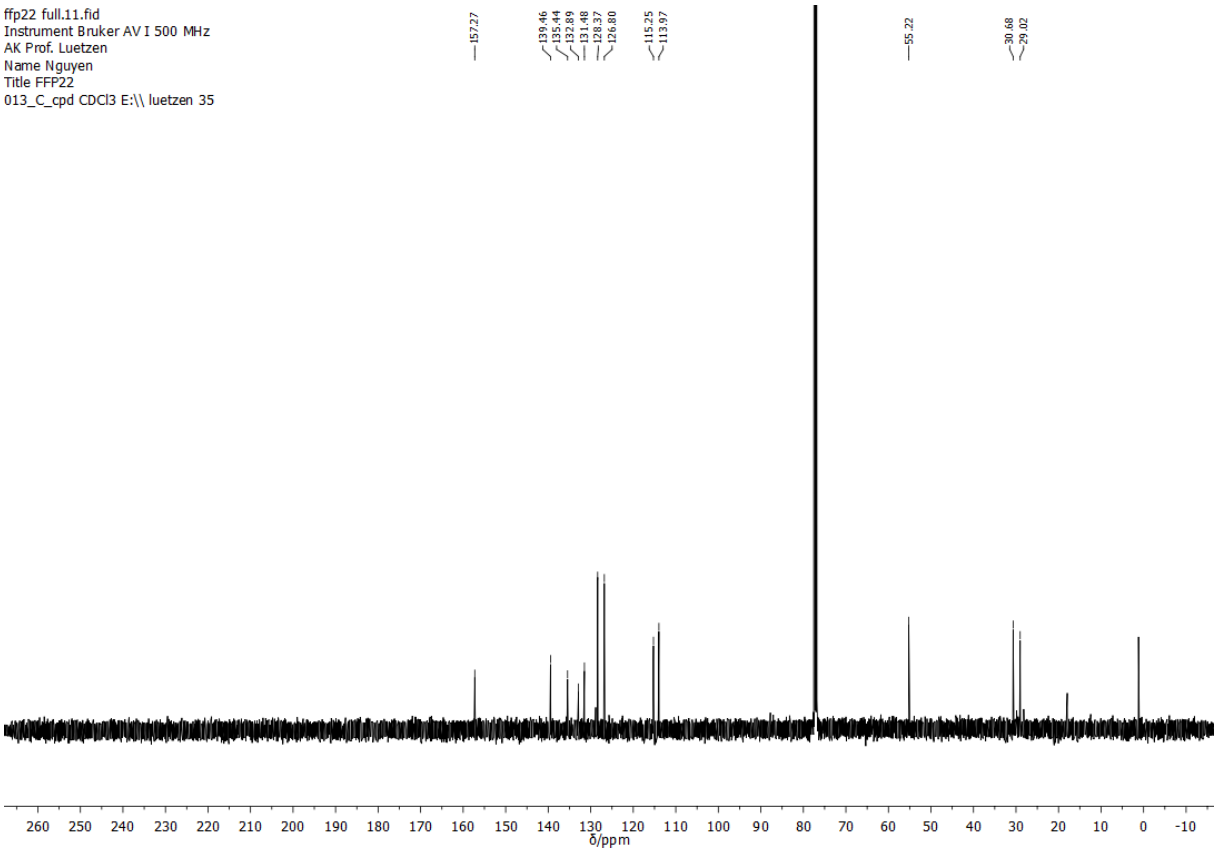

Figure 134: ^{13}C-NMR spectrum of **29** in $CDCl_3$.

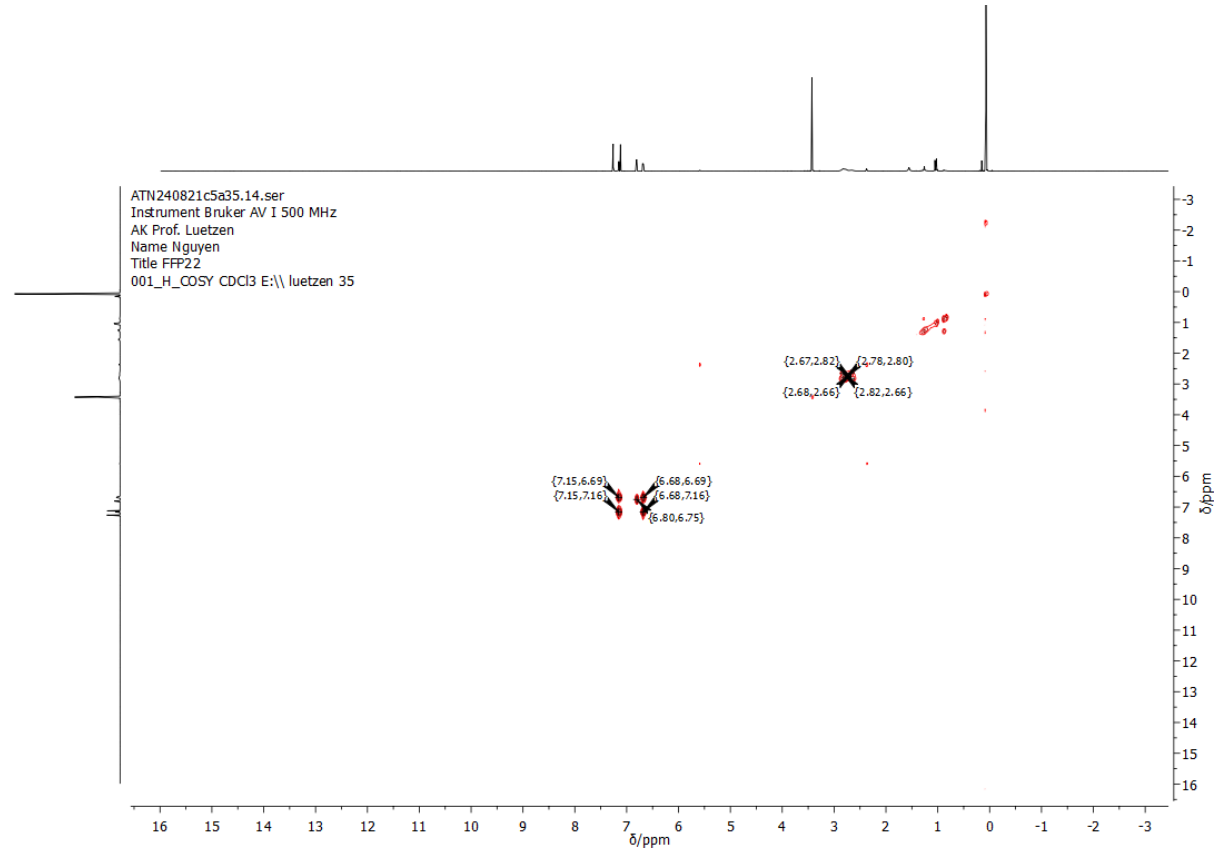

Figure 135: COSY-NMR spectrum of **29** in $CDCl_3$.

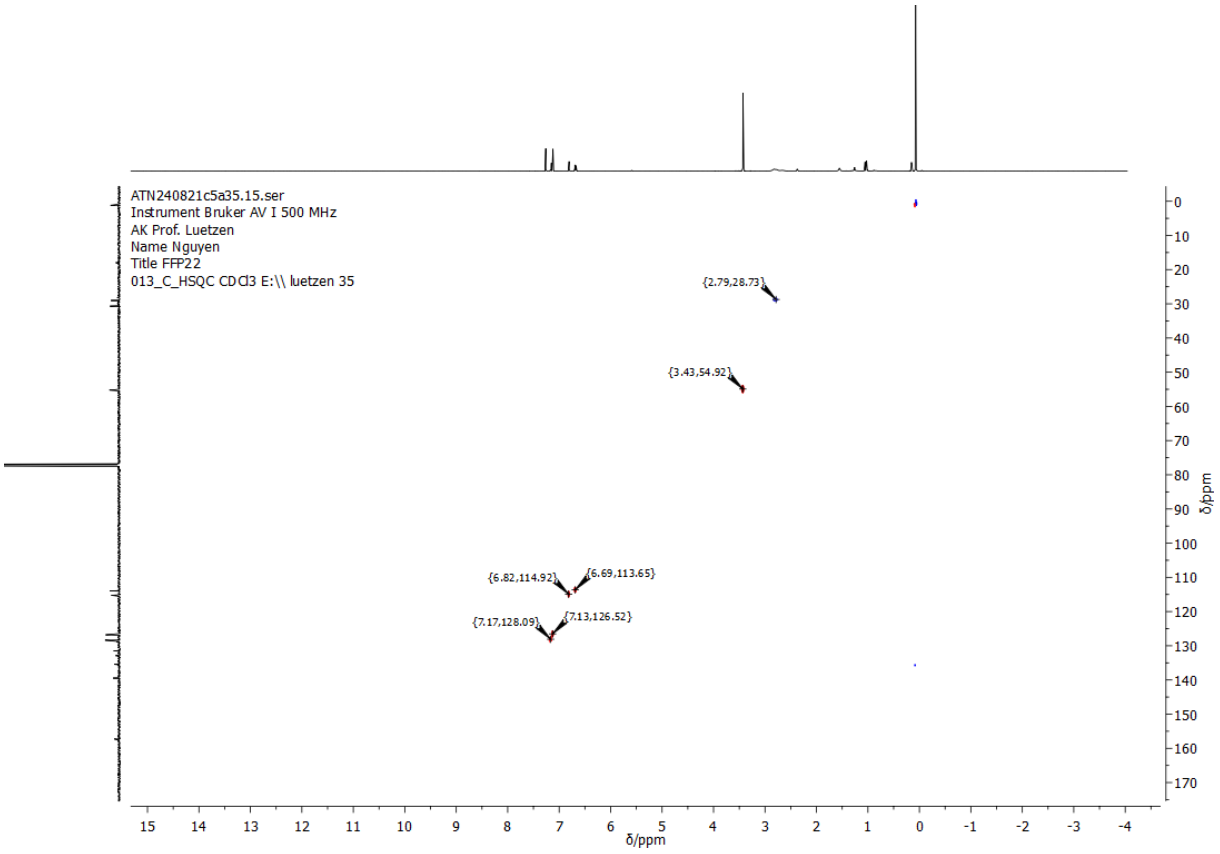

Figure 136: HSQC-NMR spectrum of **29** in $CDCl_3$.

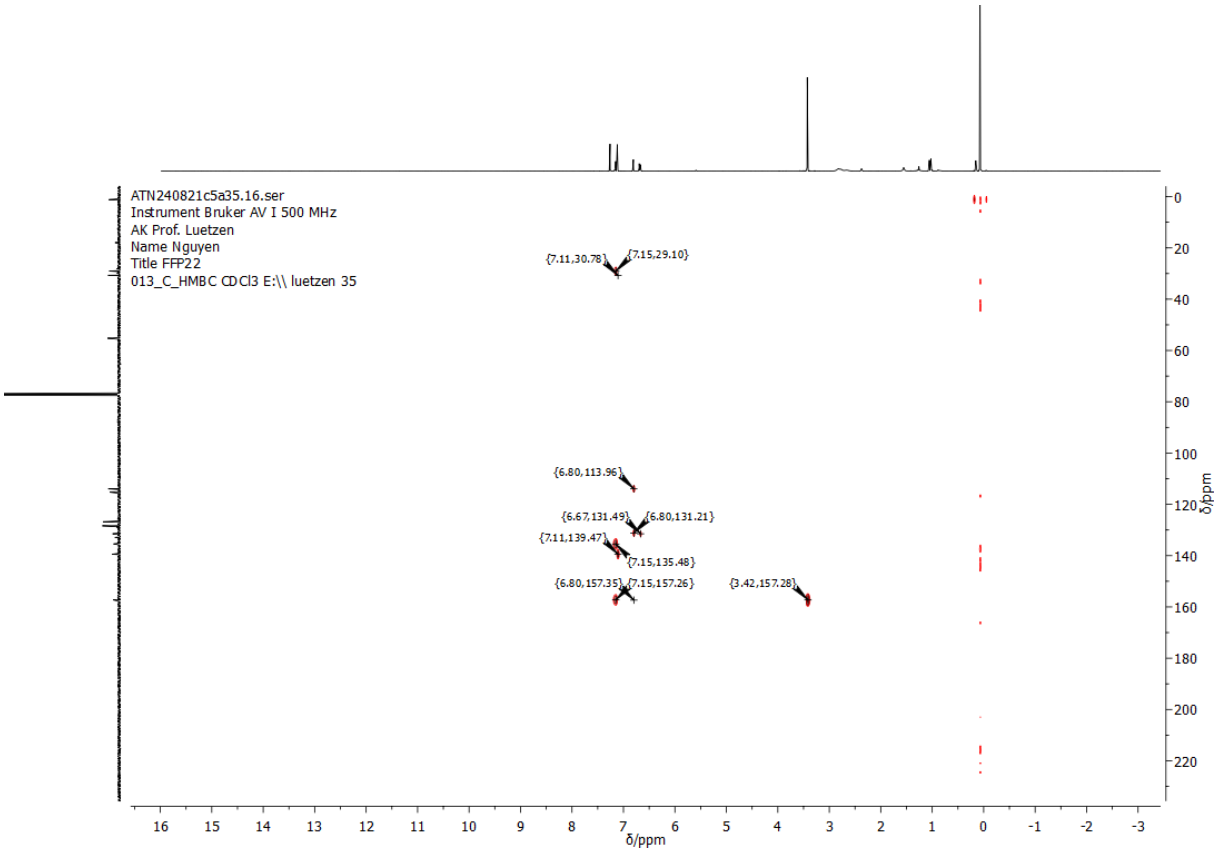

Figure 137: HMBC-NMR spectrum of **29** in $CDCl_3$.

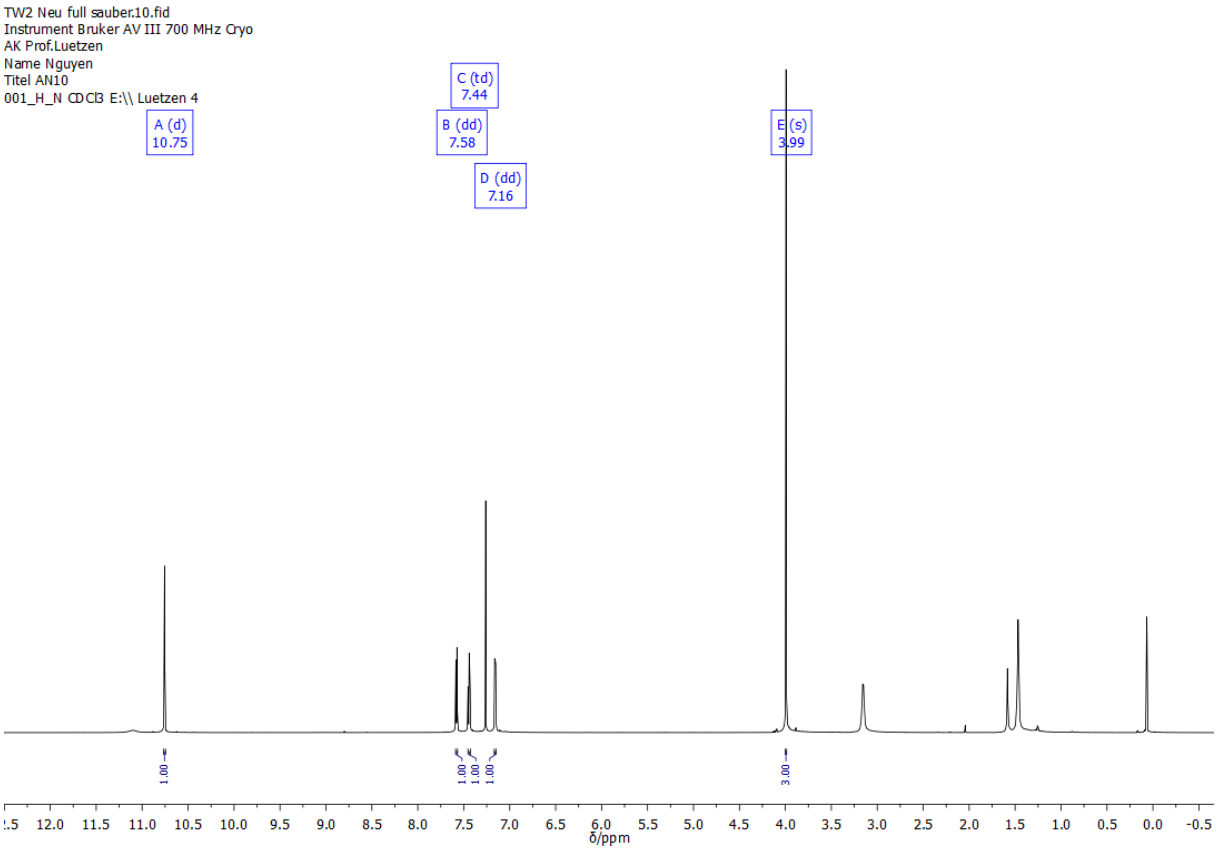

Figure 138: ^{1}H-NMR spectrum of **32** in $CDCl_3$.

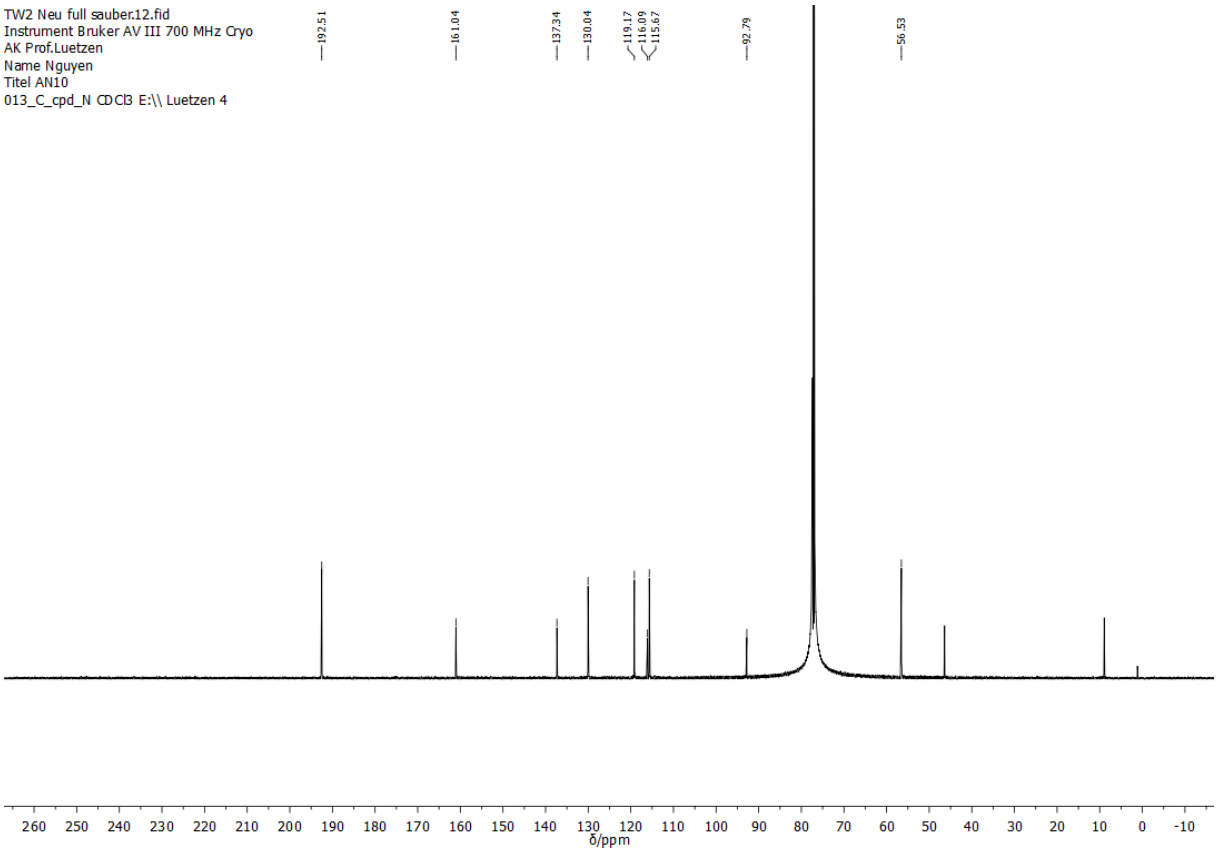

Figure 139: ^{13}C-NMR spectrum of **32** in $CDCl_3$.

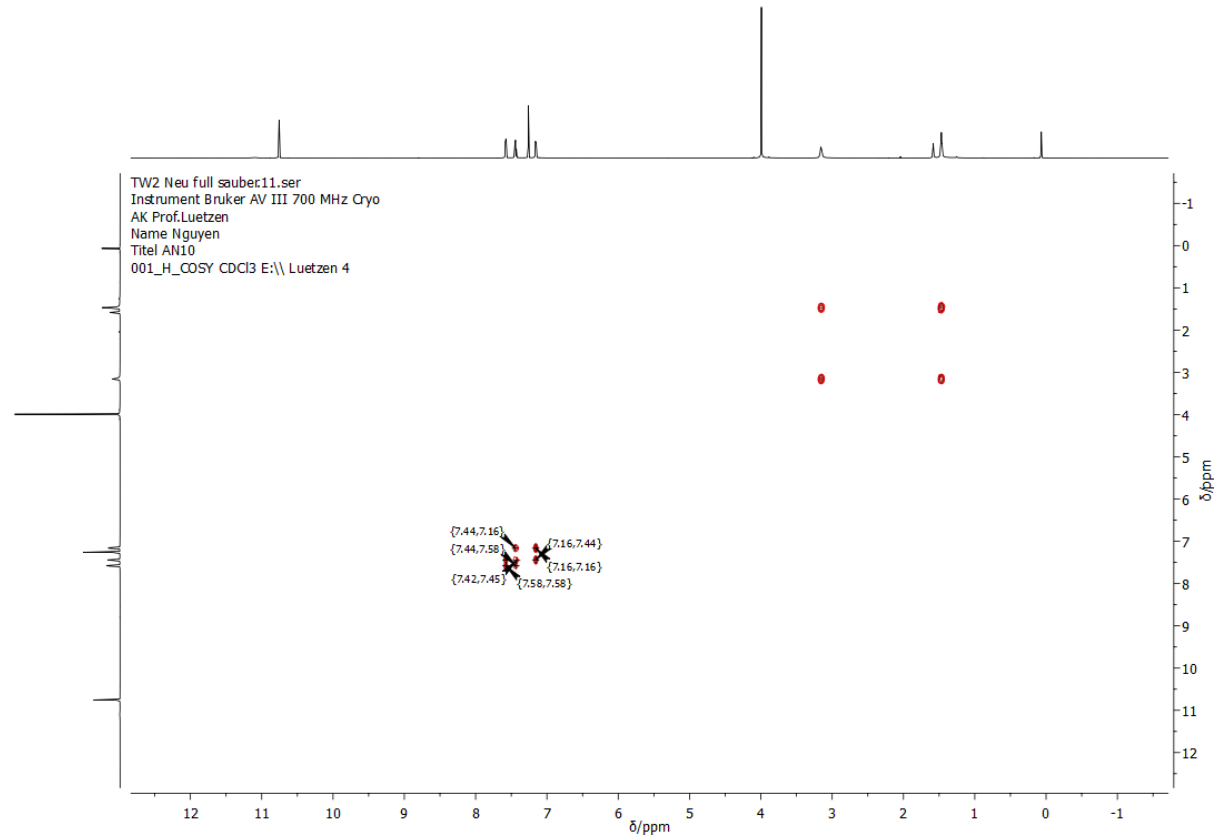

Figure 140: COSY-NMR spectrum of **32** in $CDCl_3$.

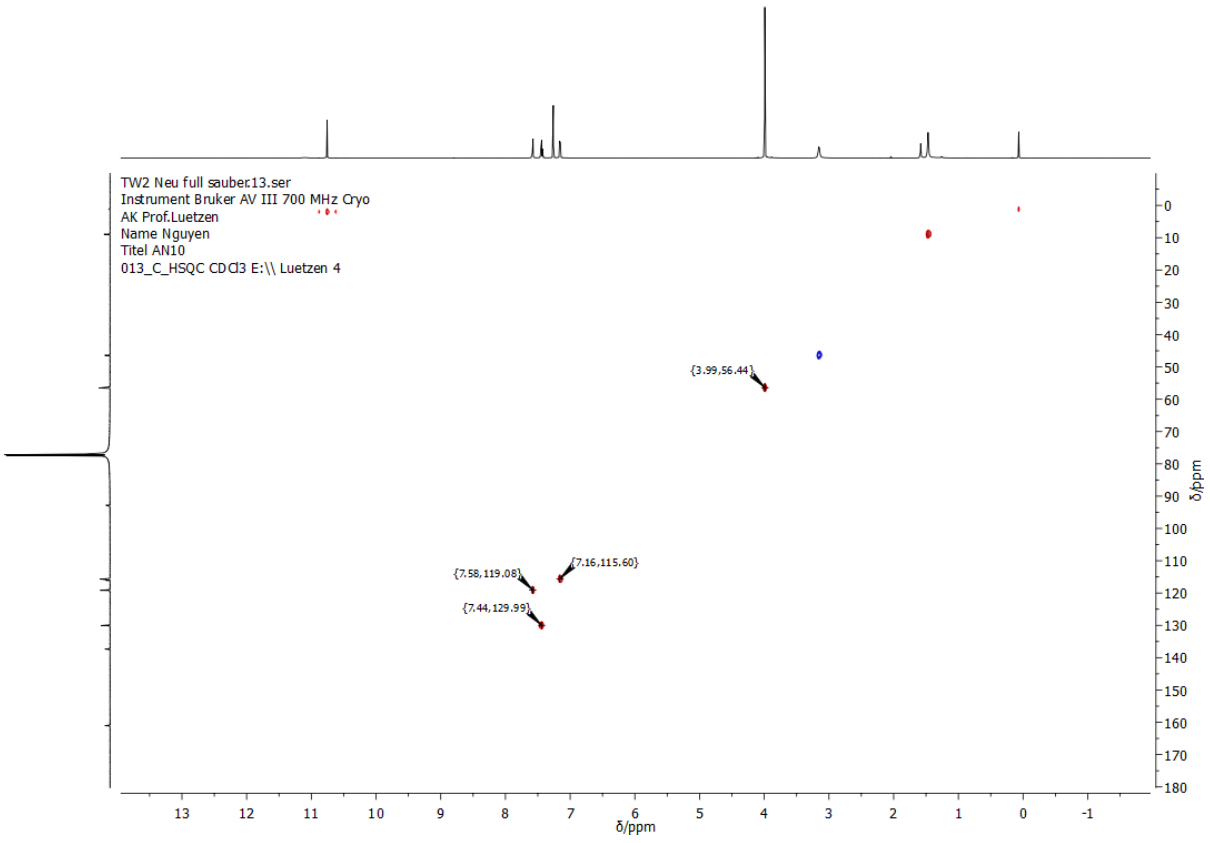

Figure 141: HSQC-NMR spectrum of **32** in $CDCl_3$.

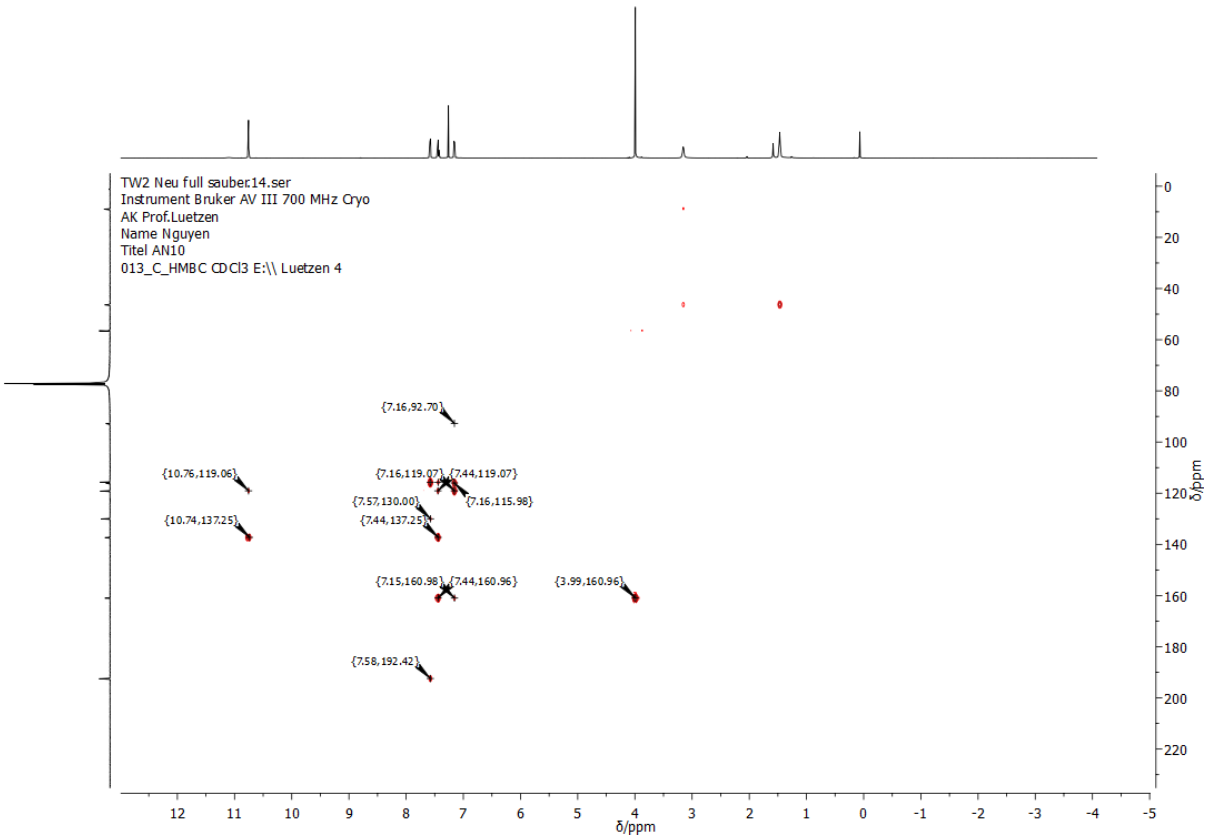

Figure 142: HMBC-NMR spectrum of **32** in $CDCl_3$.

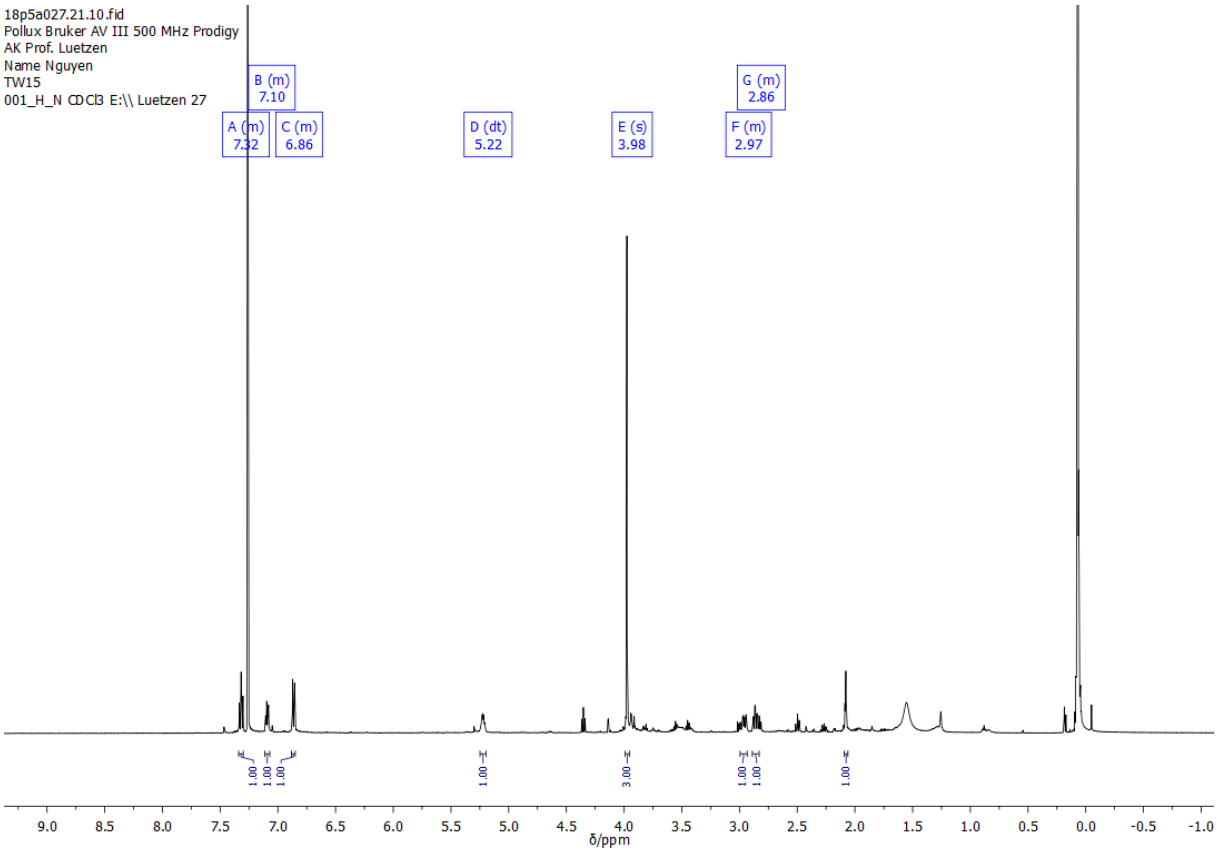

Figure 143: ^{1}H-NMR spectrum of **35** in $CDCl_3$.

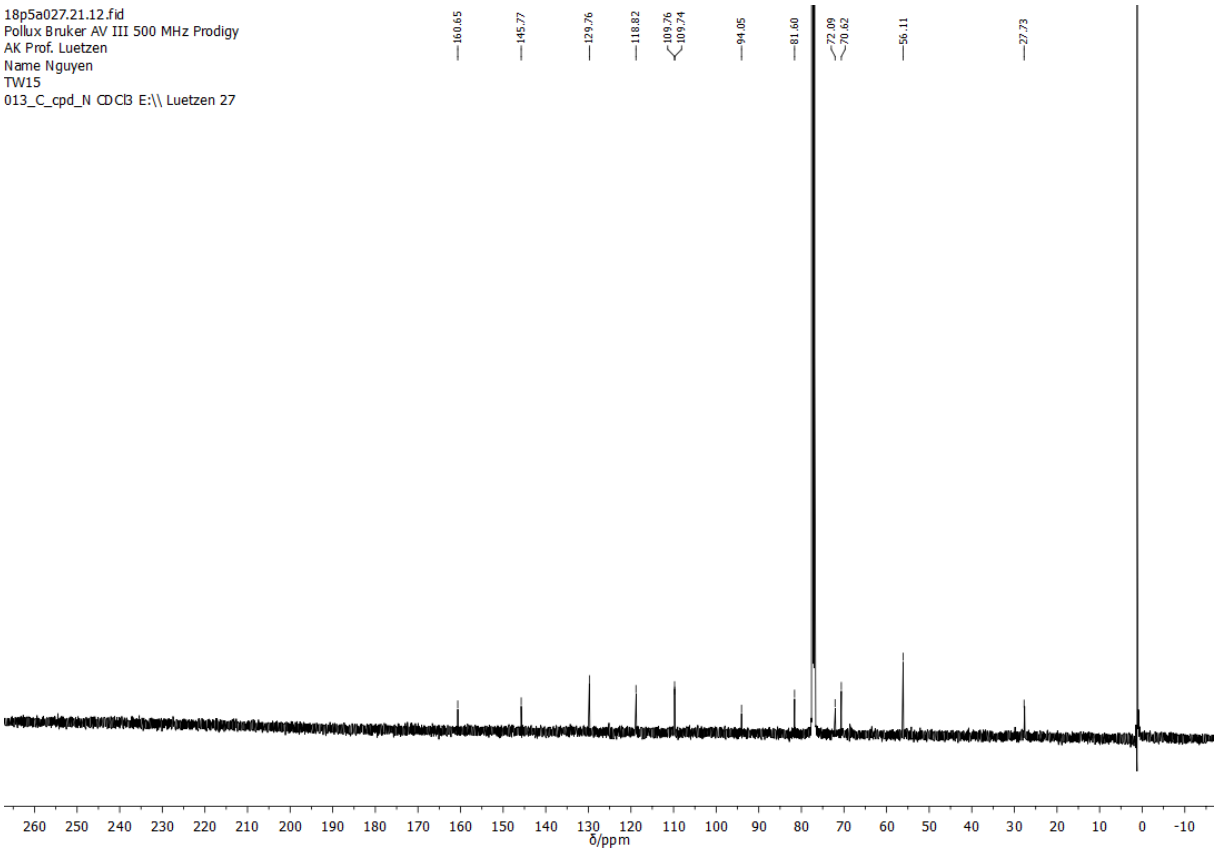

Figure 144: ^{13}C-NMR spectrum of **35** in $CDCl_3$.

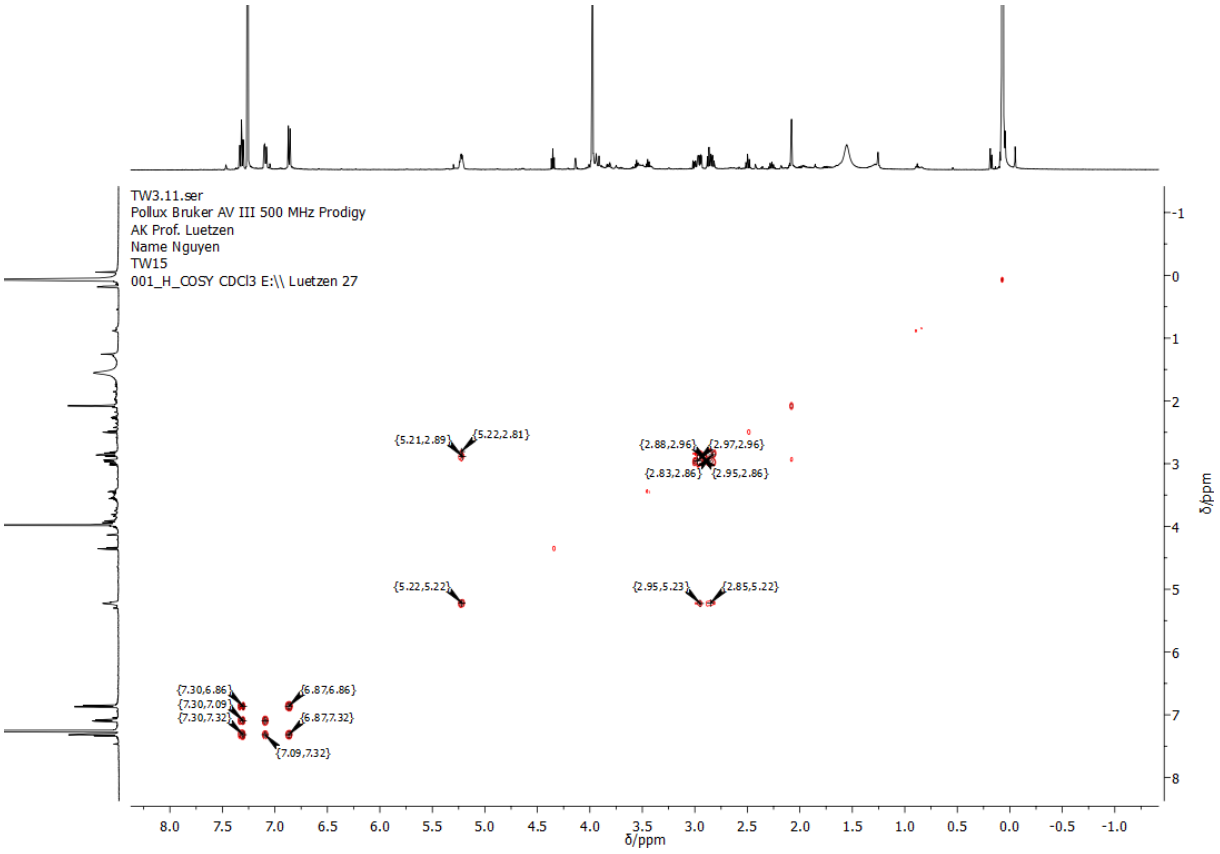

Figure 145: COSY-NMR spectrum of **35** in $CDCl_3$.

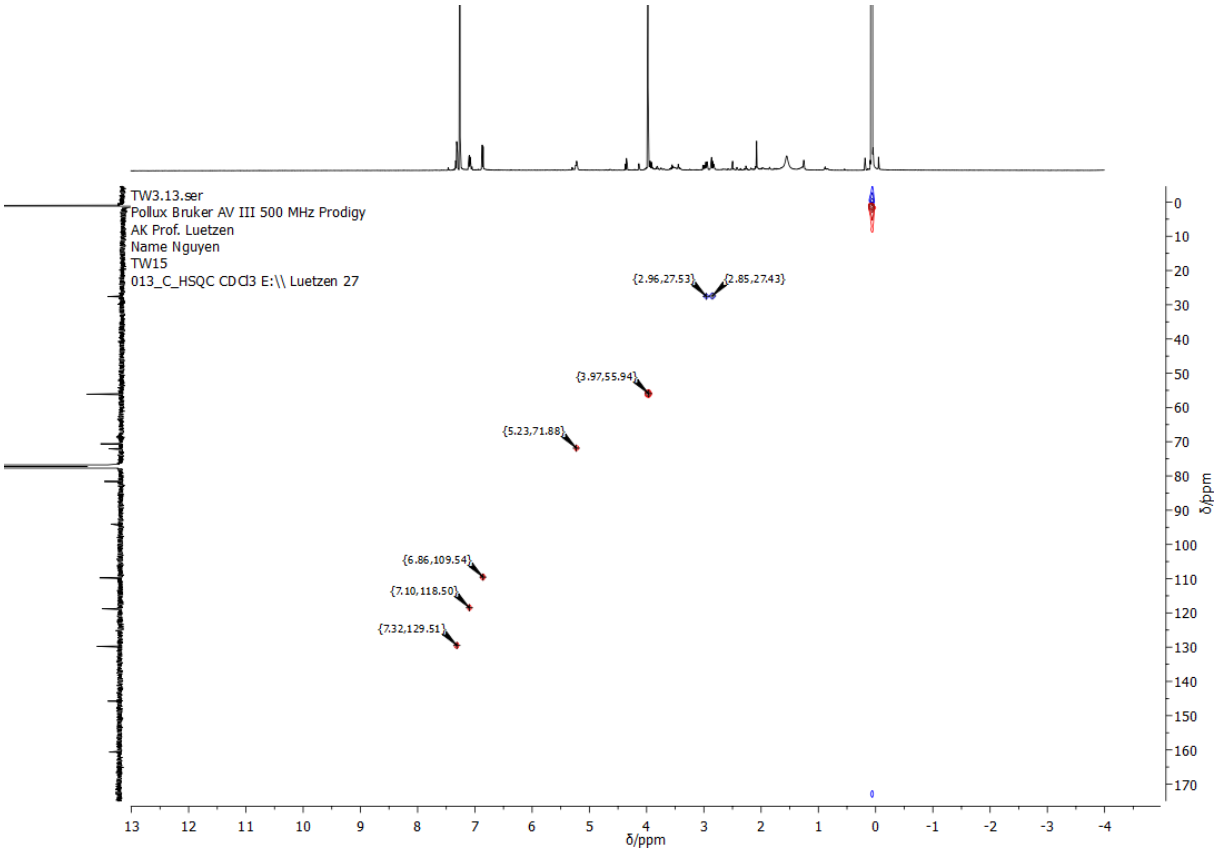

Figure 146: HSQC-NMR spectrum of **35** in $CDCl_3$.

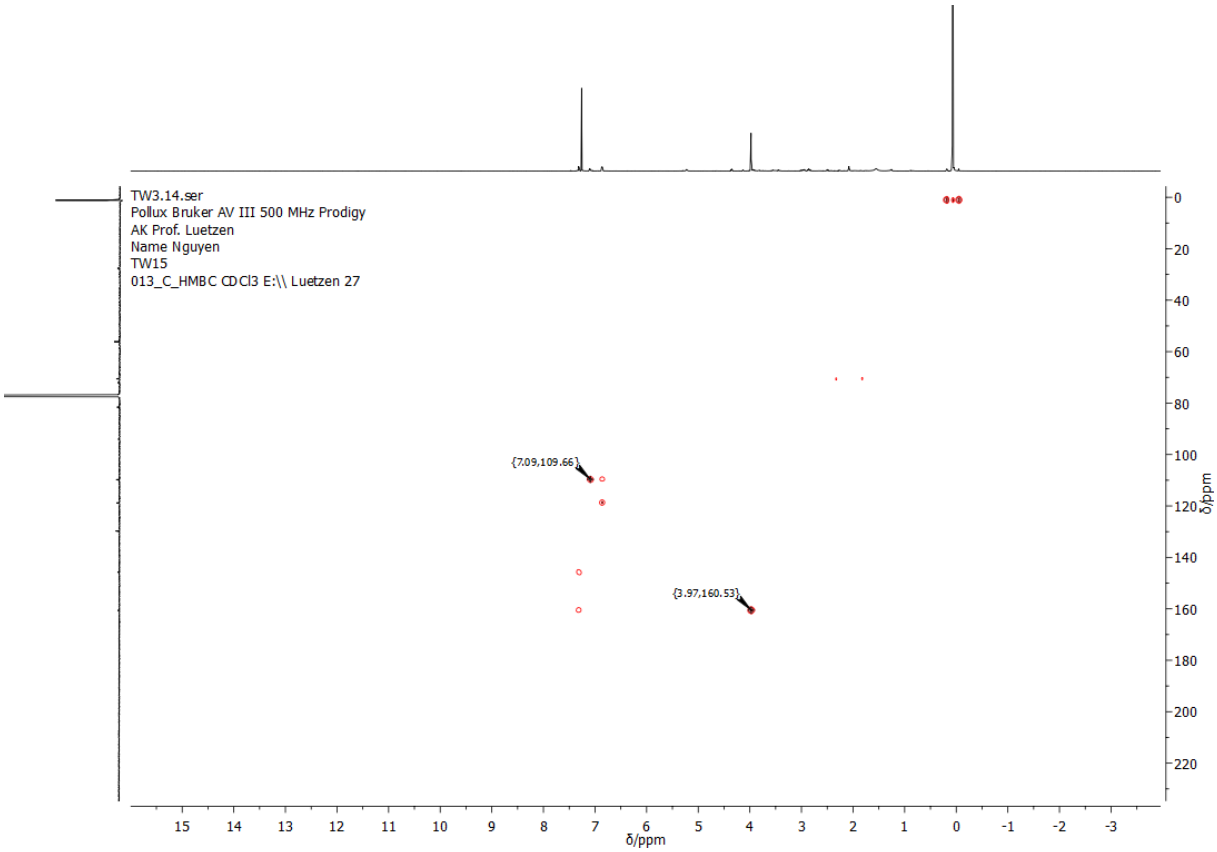

Figure 147: HMBC-NMR spectrum of **35** in $CDCl_3$.

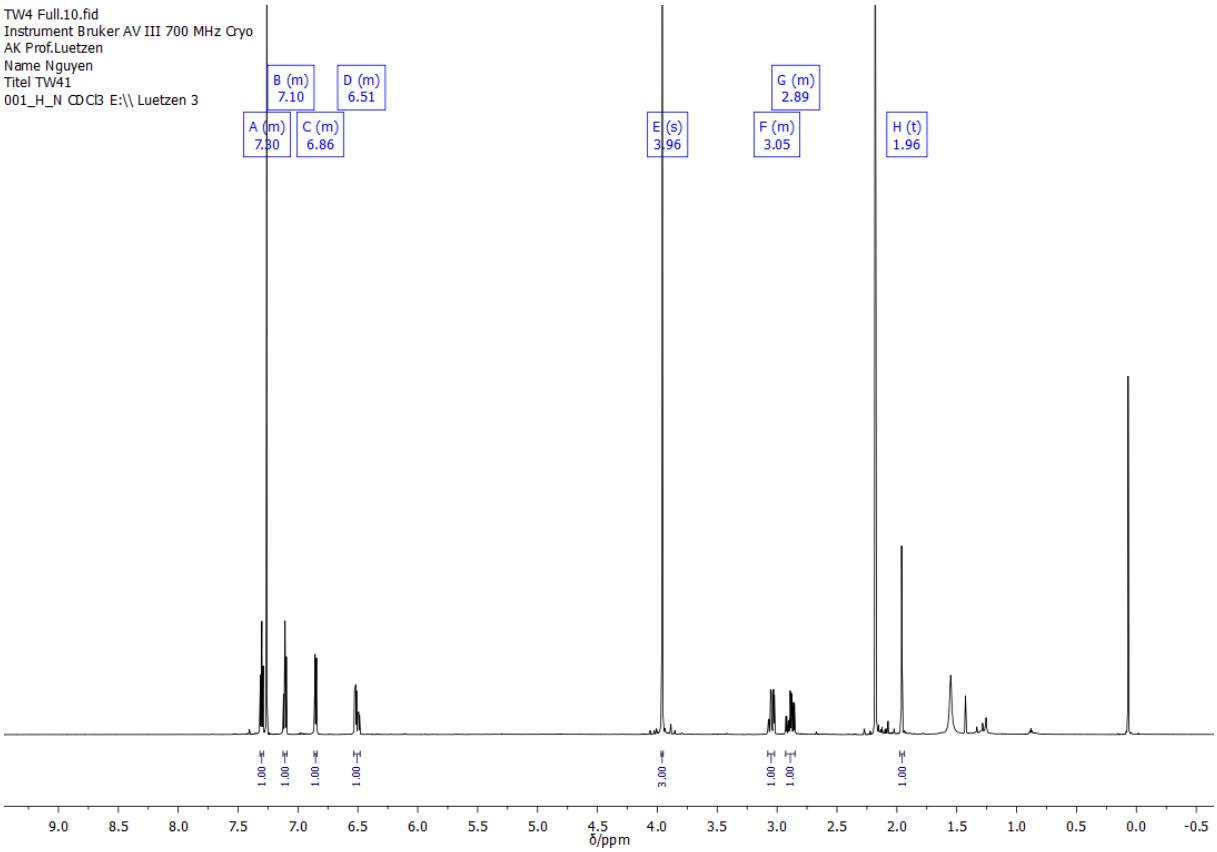

Figure 148: ^{1}H-NMR spectrum of **36** in $CDCl_3$.

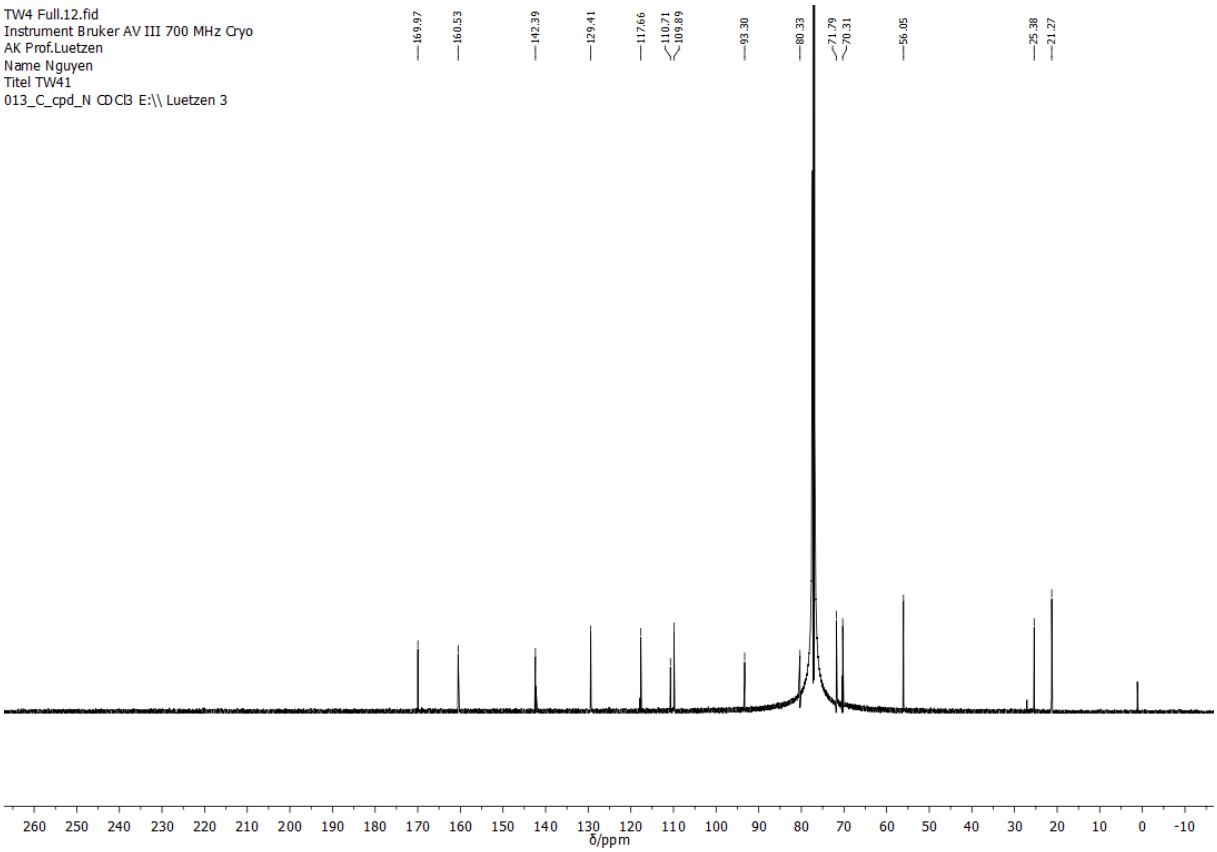

Figure 149: ^{13}C-NMR spectrum of **36** in $CDCl_3$.

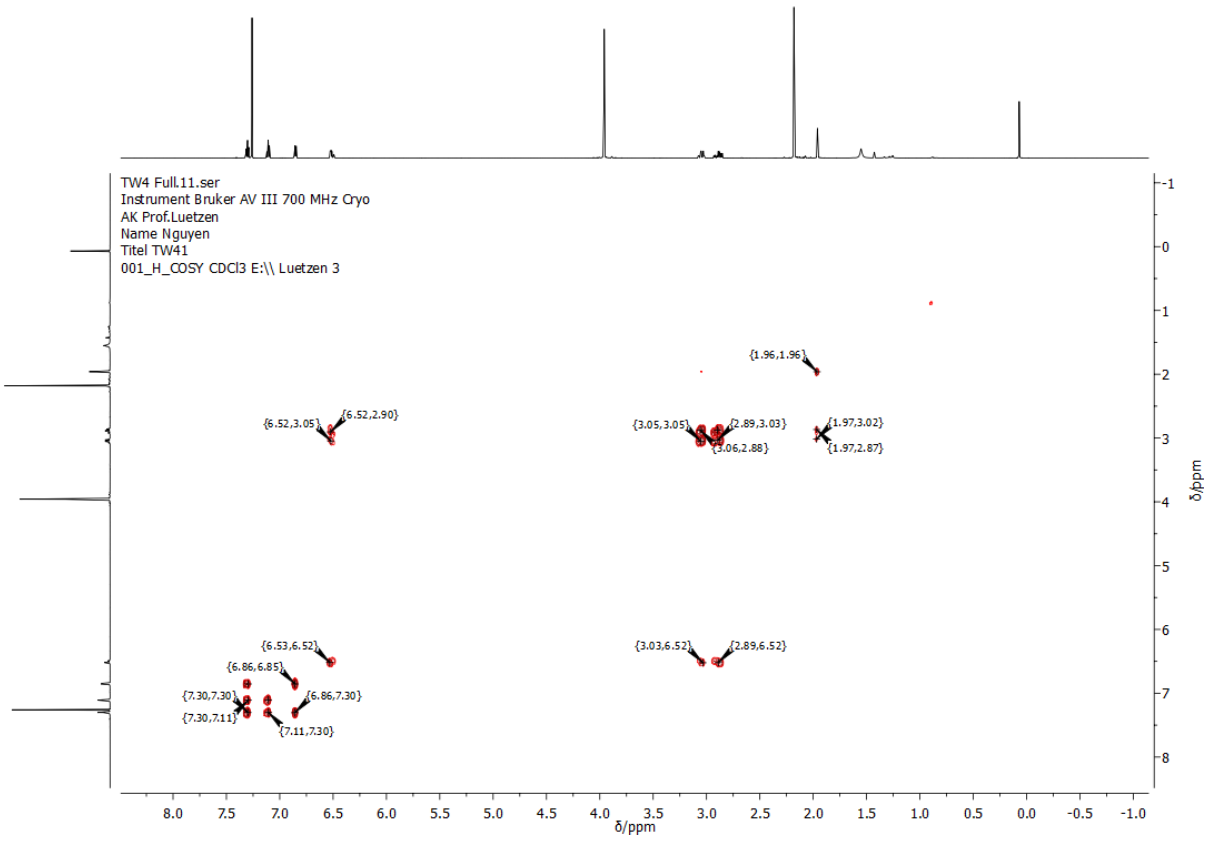

Figure 150: COSY-NMR spectrum of **36** in $CDCl_3$.

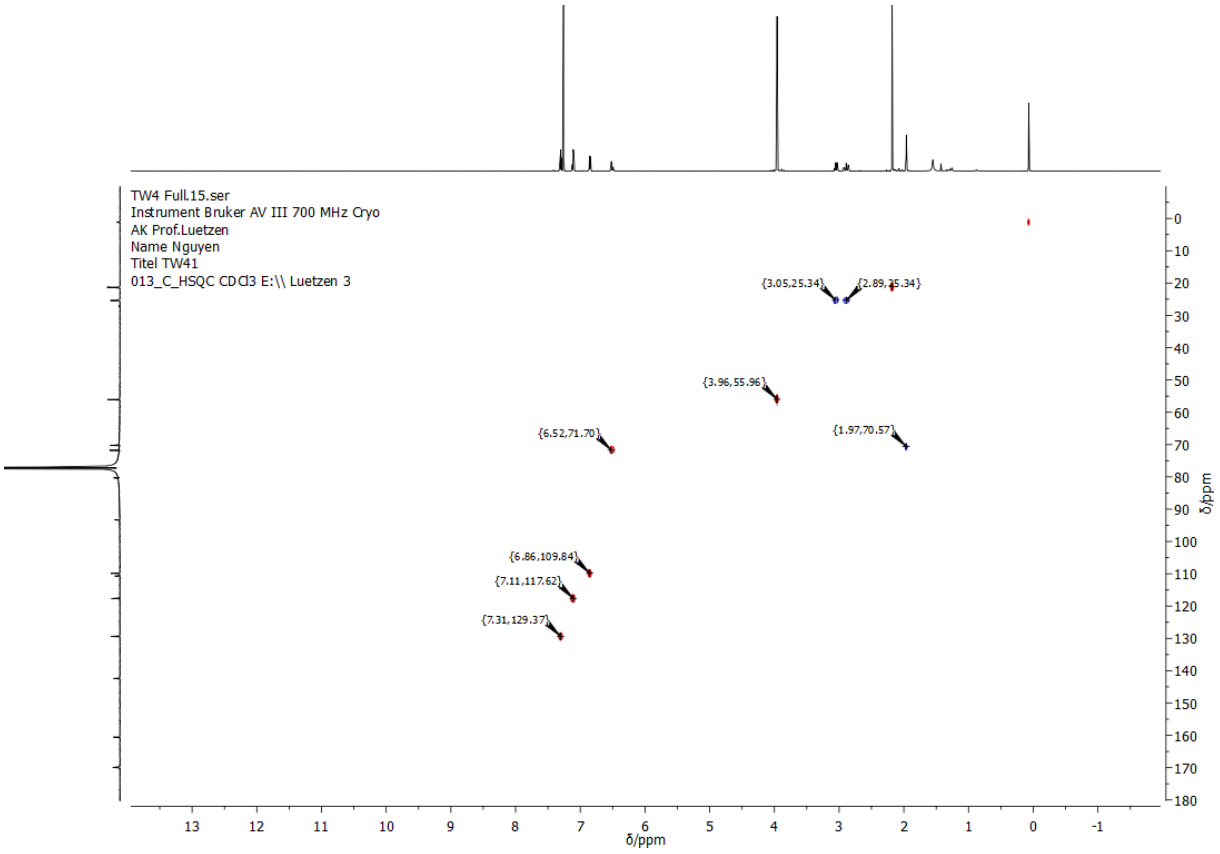

Figure 151: HSQC-NMR spectrum of **36** in $CDCl_3$.

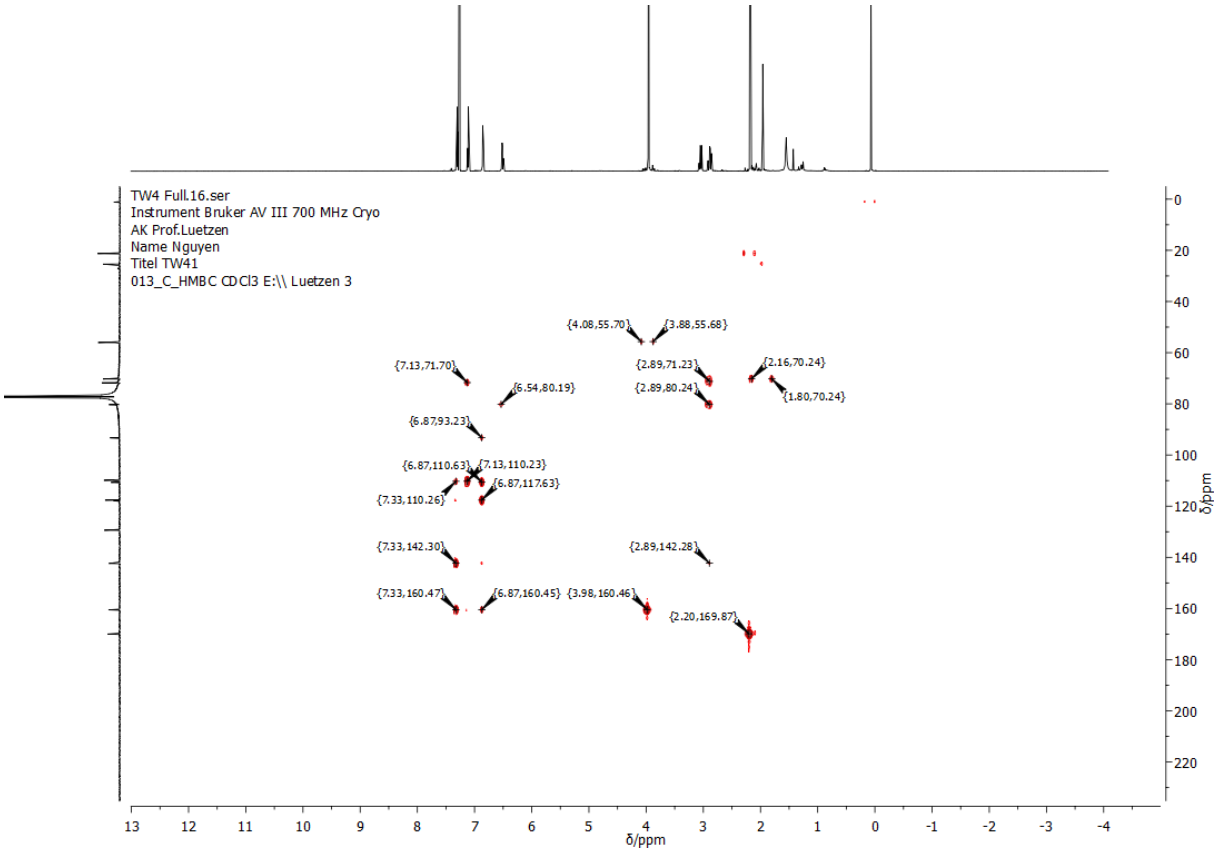

Figure 152: HMBC-NMR spectrum of **36** in $CDCl_3$.

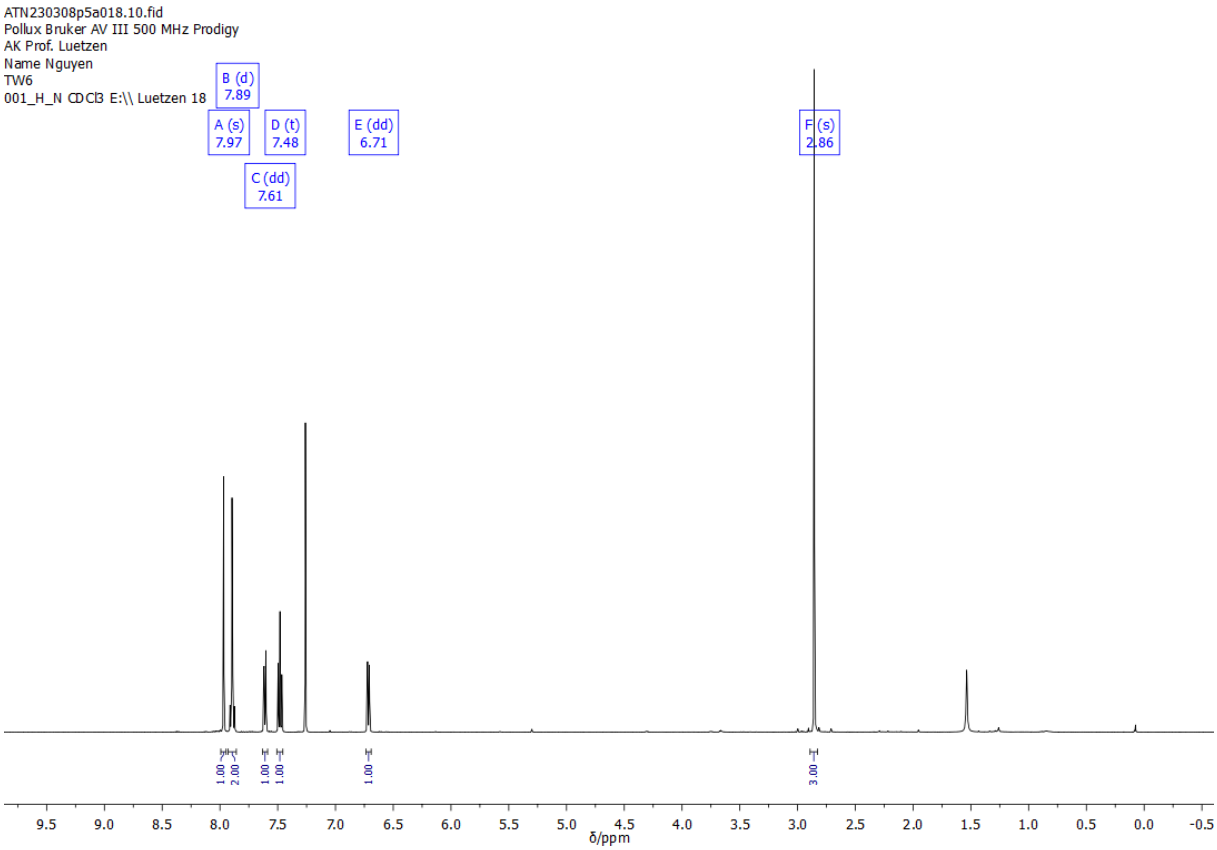

Figure 153: ^{1}H-NMR spectrum of **38** in $CDCl_3$.

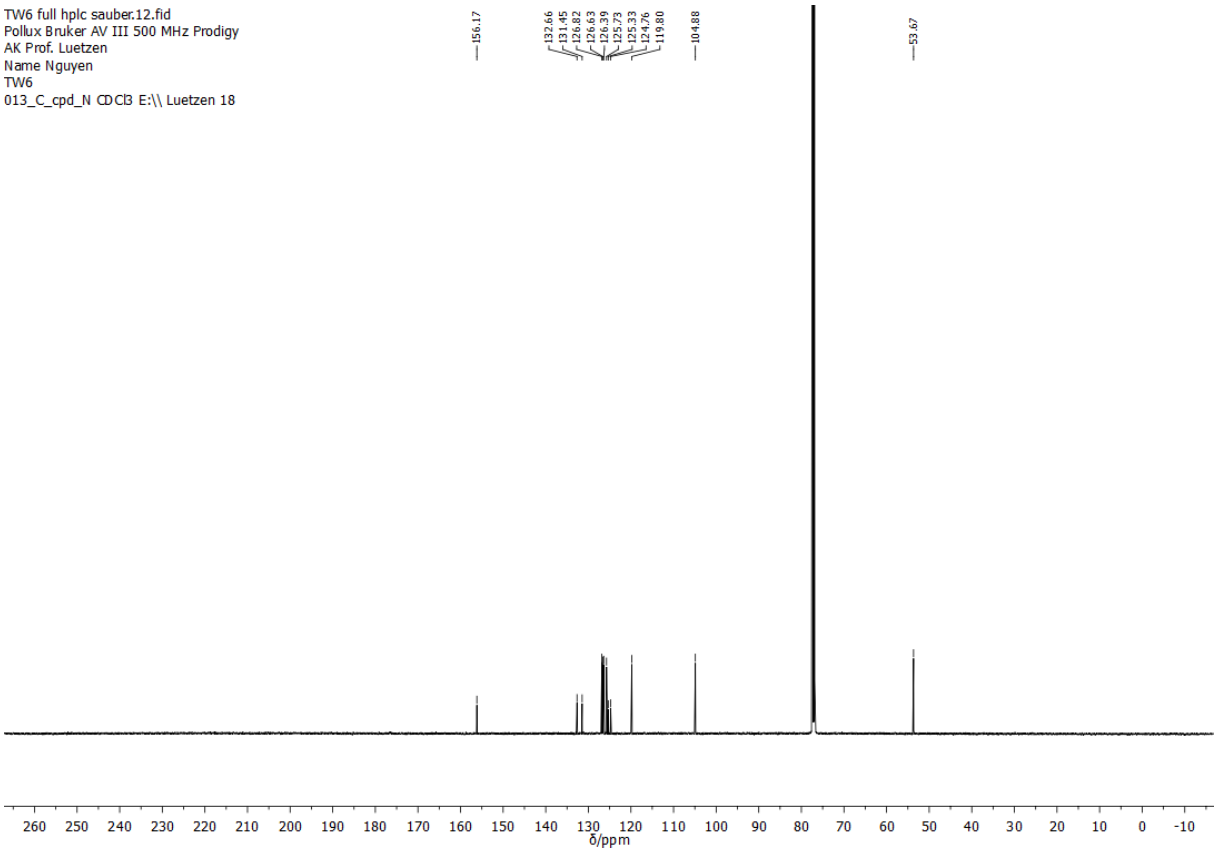

Figure 154: ^{13}C-NMR spectrum of **38** in $CDCl_3$.

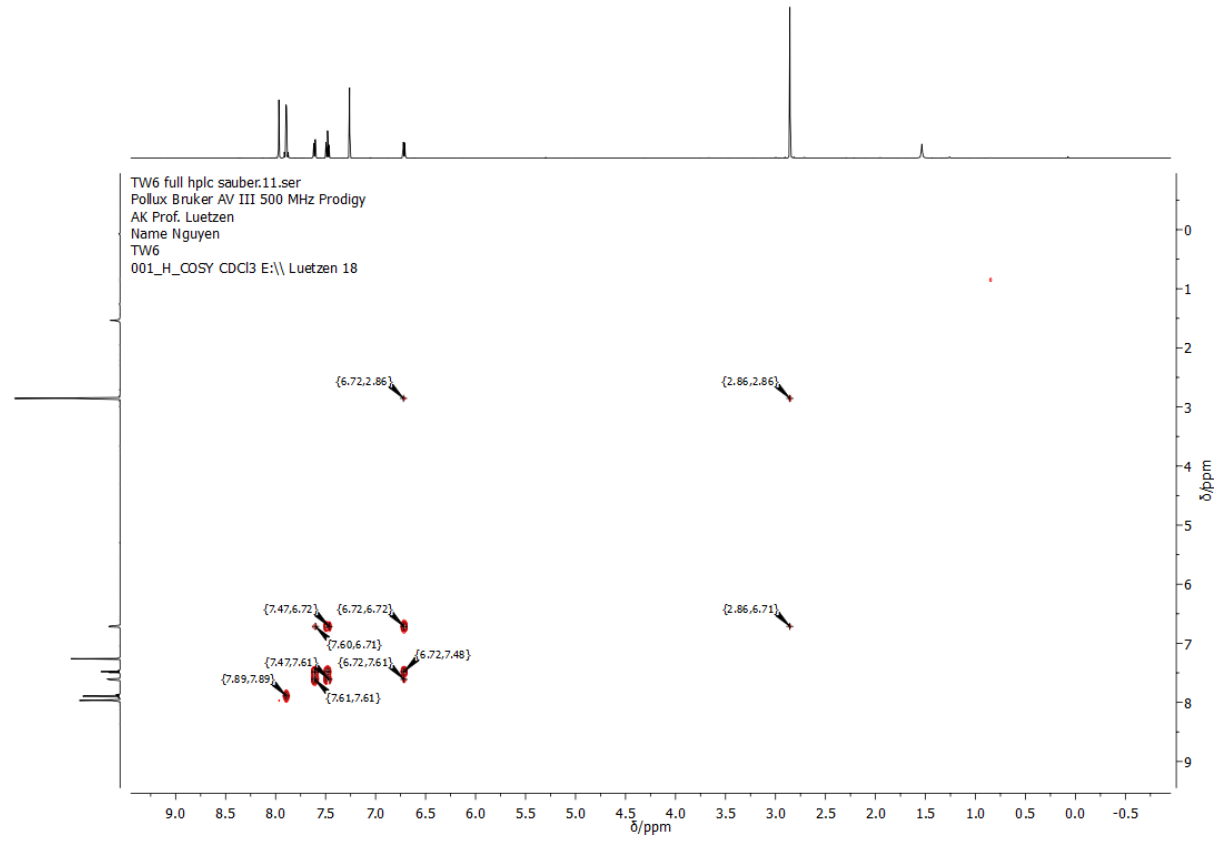

Figure 155: COSY-NMR spectrum of **38** in $CDCl_3$.

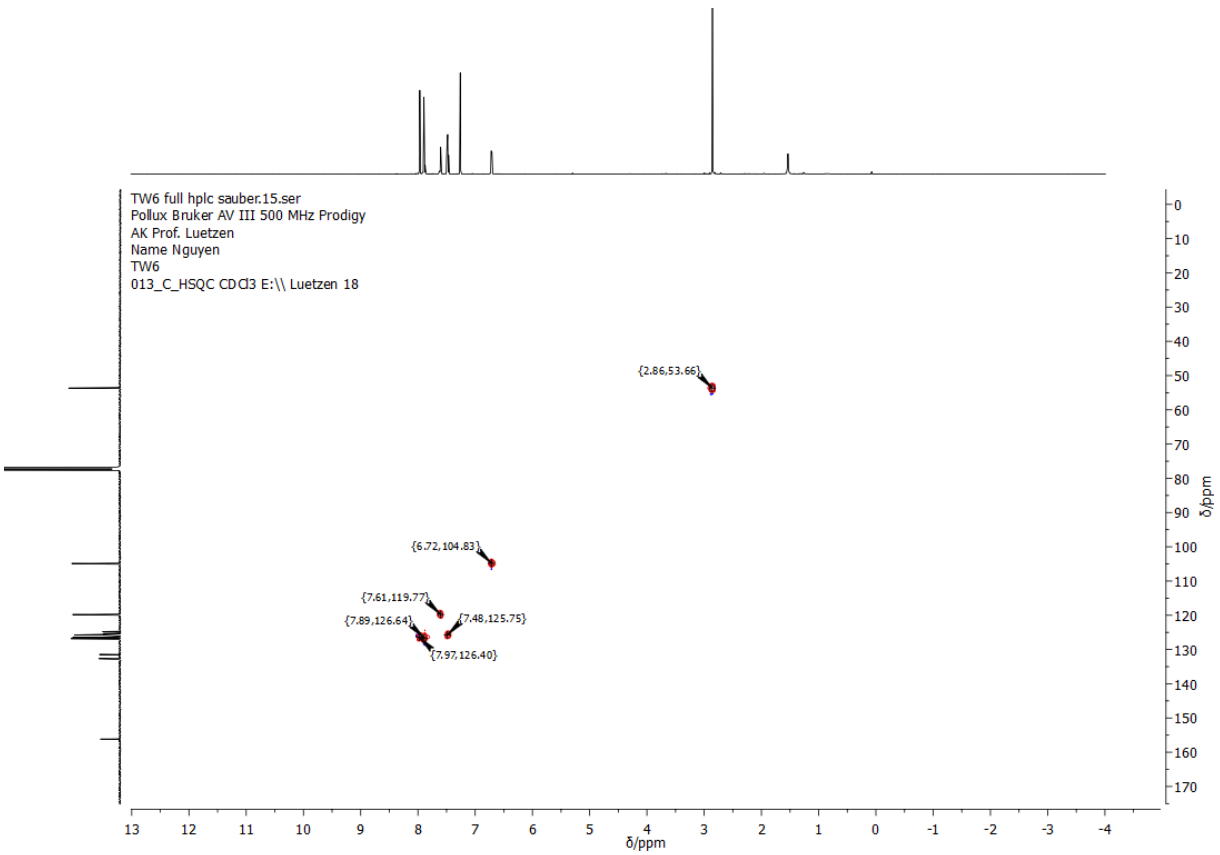

Figure 156: HSQC-NMR spectrum of **38** in $CDCl_3$.

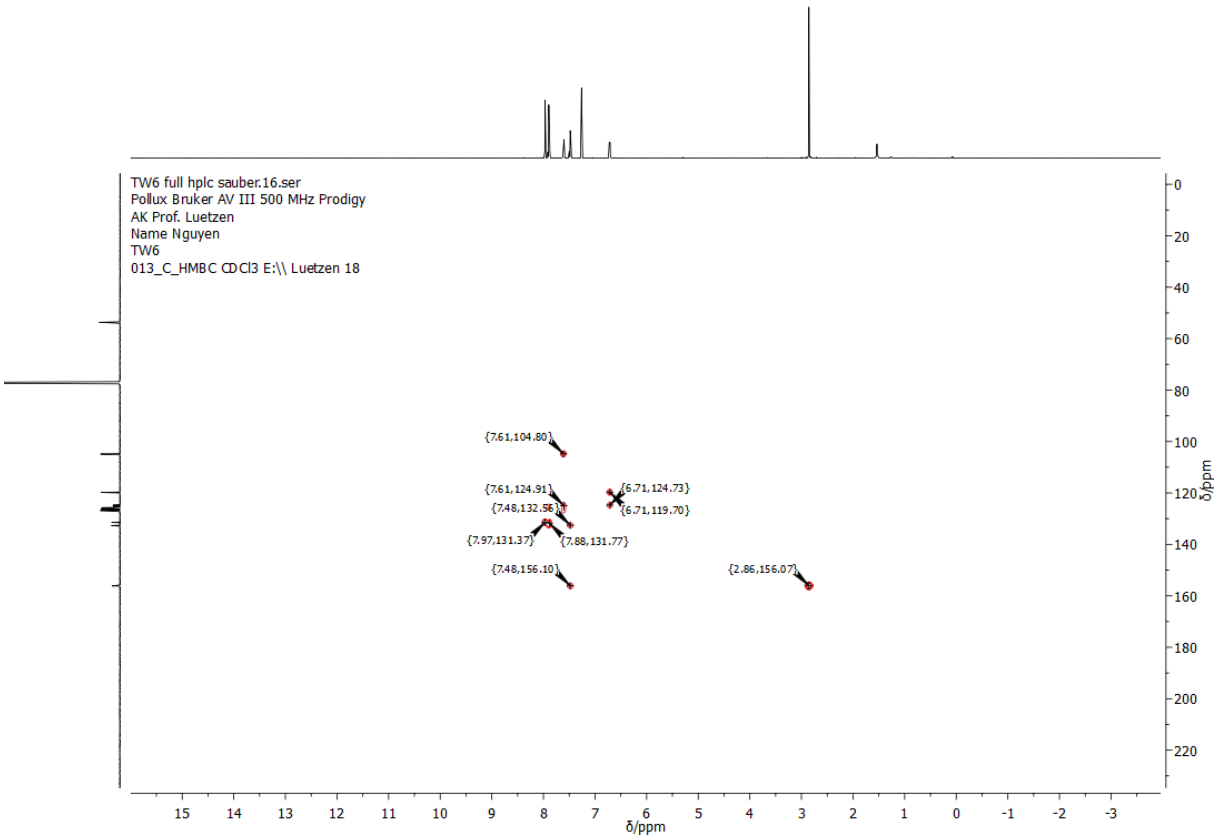

Figure 157: HMBC-NMR spectrum of **38** in $CDCl_3$.

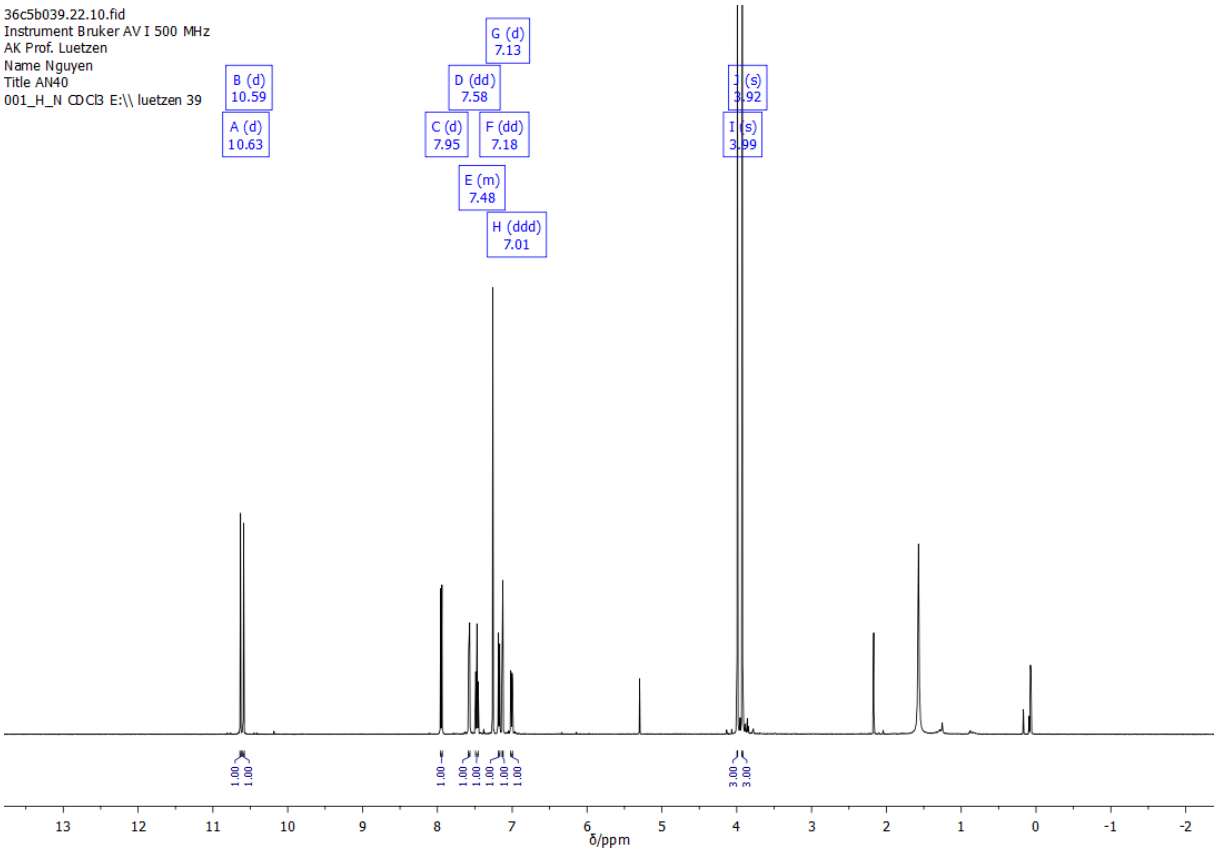

Figure 158: ^{1}H-NMR spectrum of **39** in $CDCl_3$.

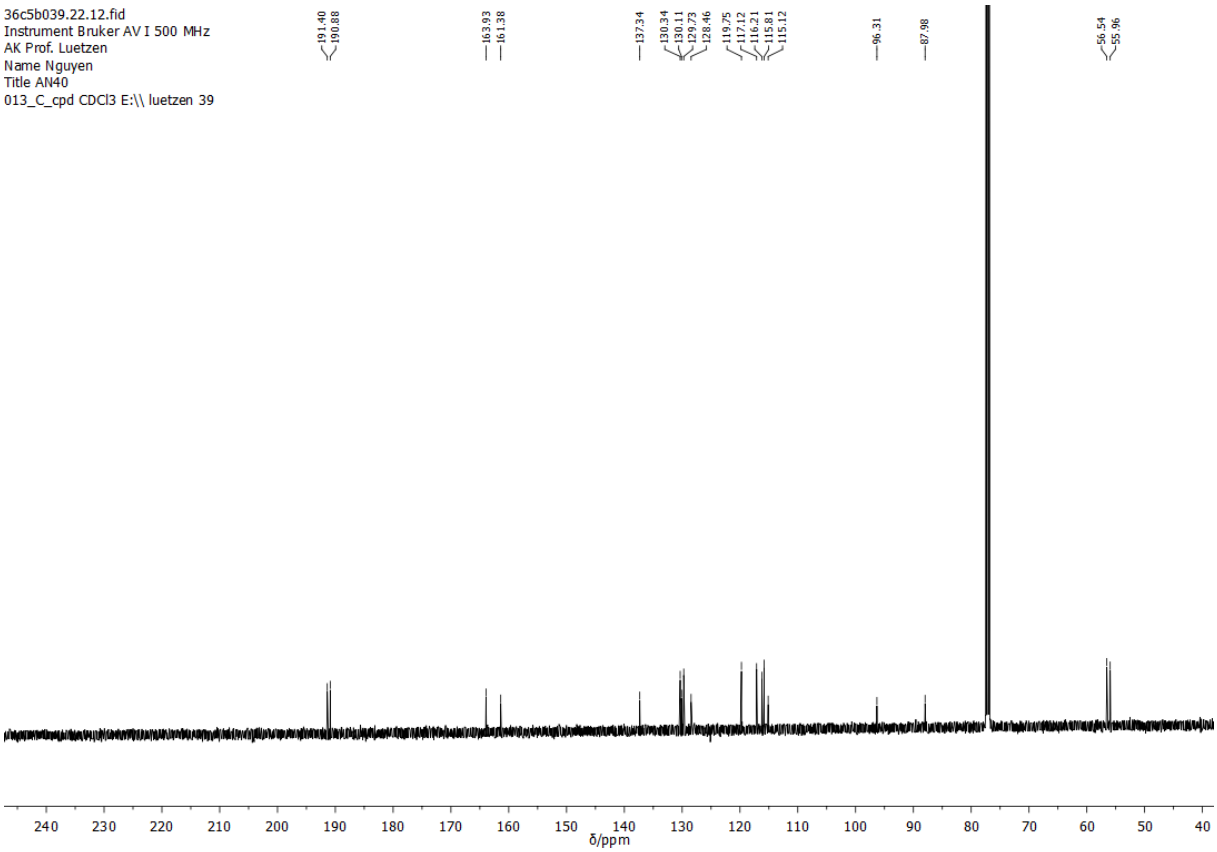

Figure 159: ^{13}C-NMR spectrum of **39** in $CDCl_3$.

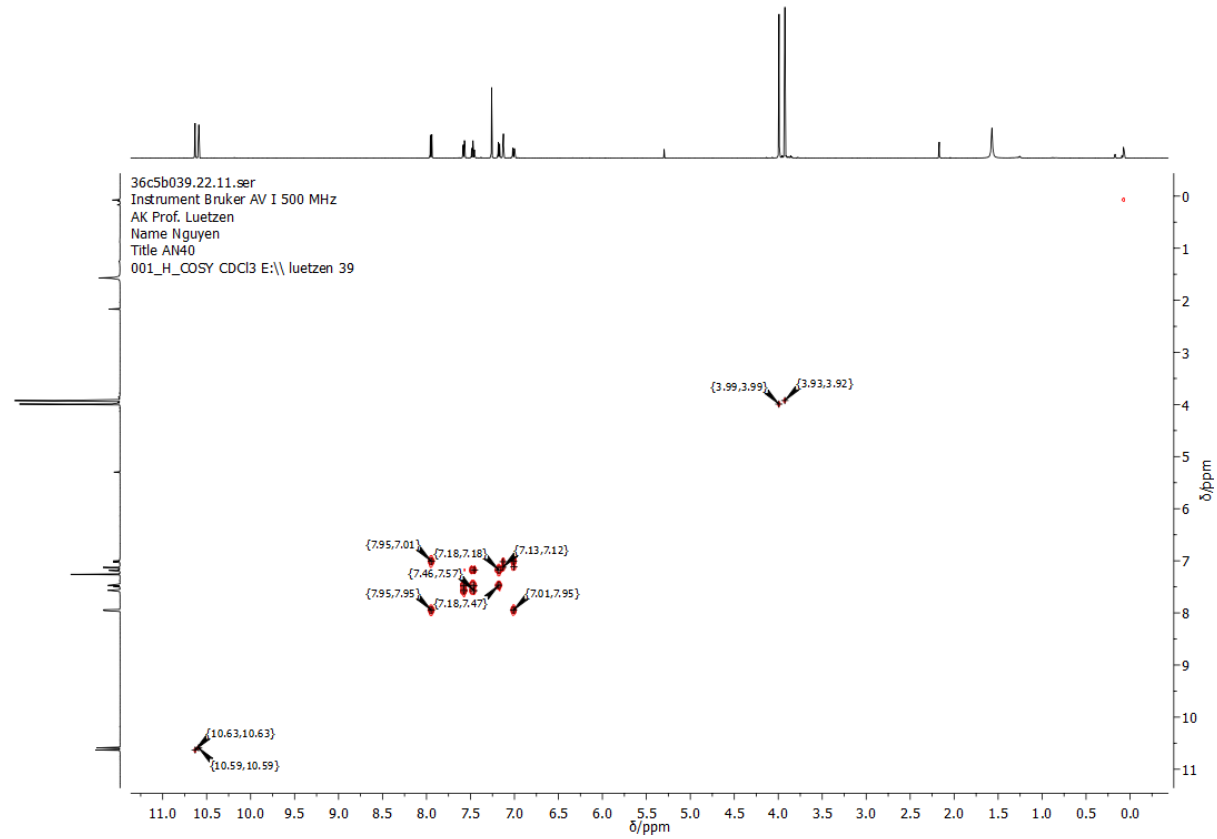

Figure 160: COSY-NMR spectrum of **39** in $CDCl_3$.

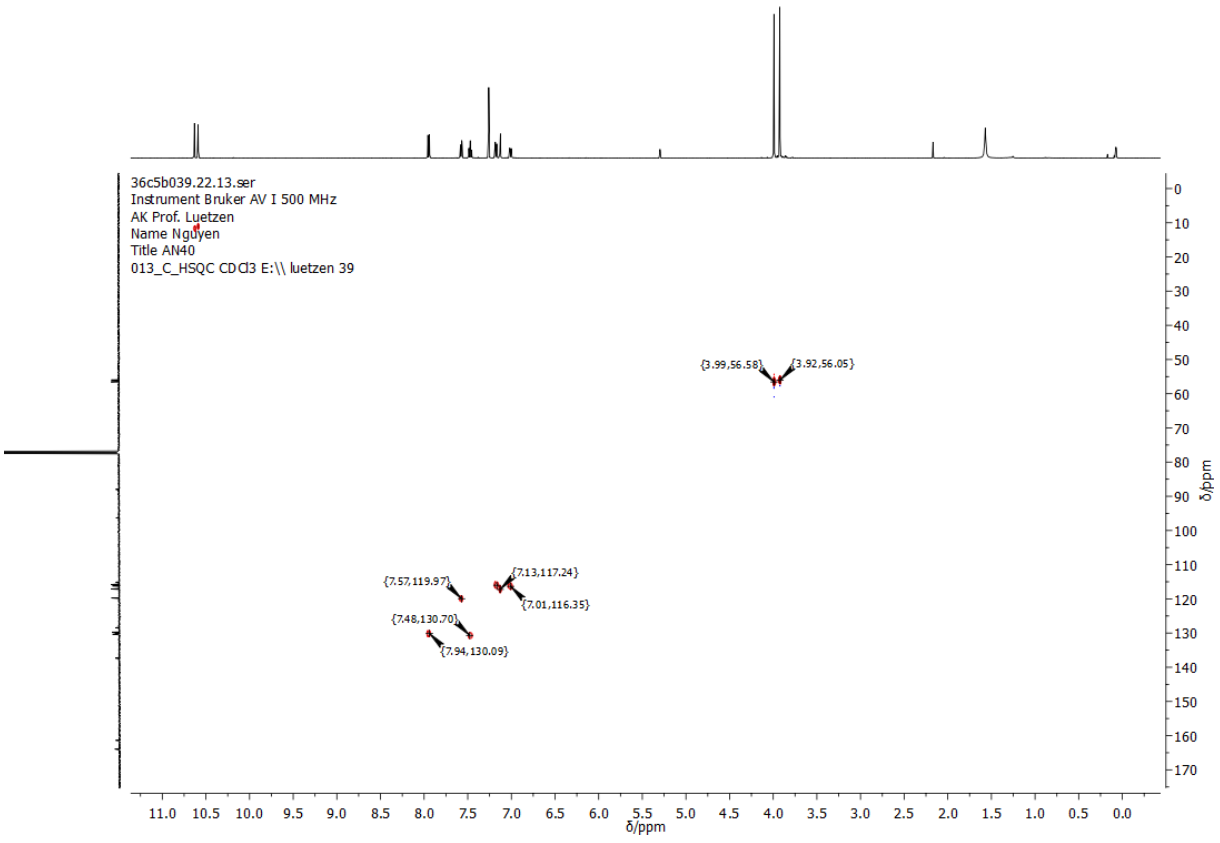

Figure 161: HSQC-NMR spectrum of **39** in $CDCl_3$.

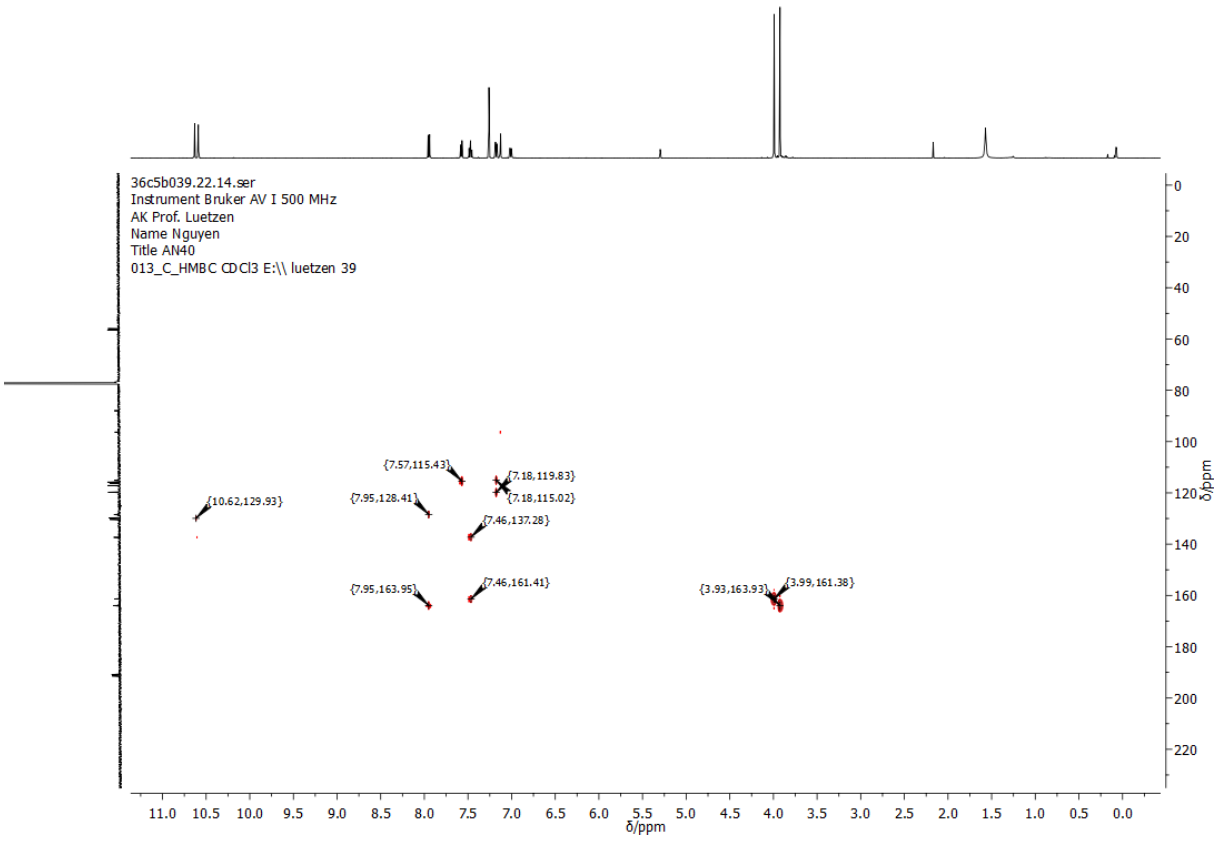

Figure 162: HMBC-NMR spectrum of **39** in $CDCl_3$.

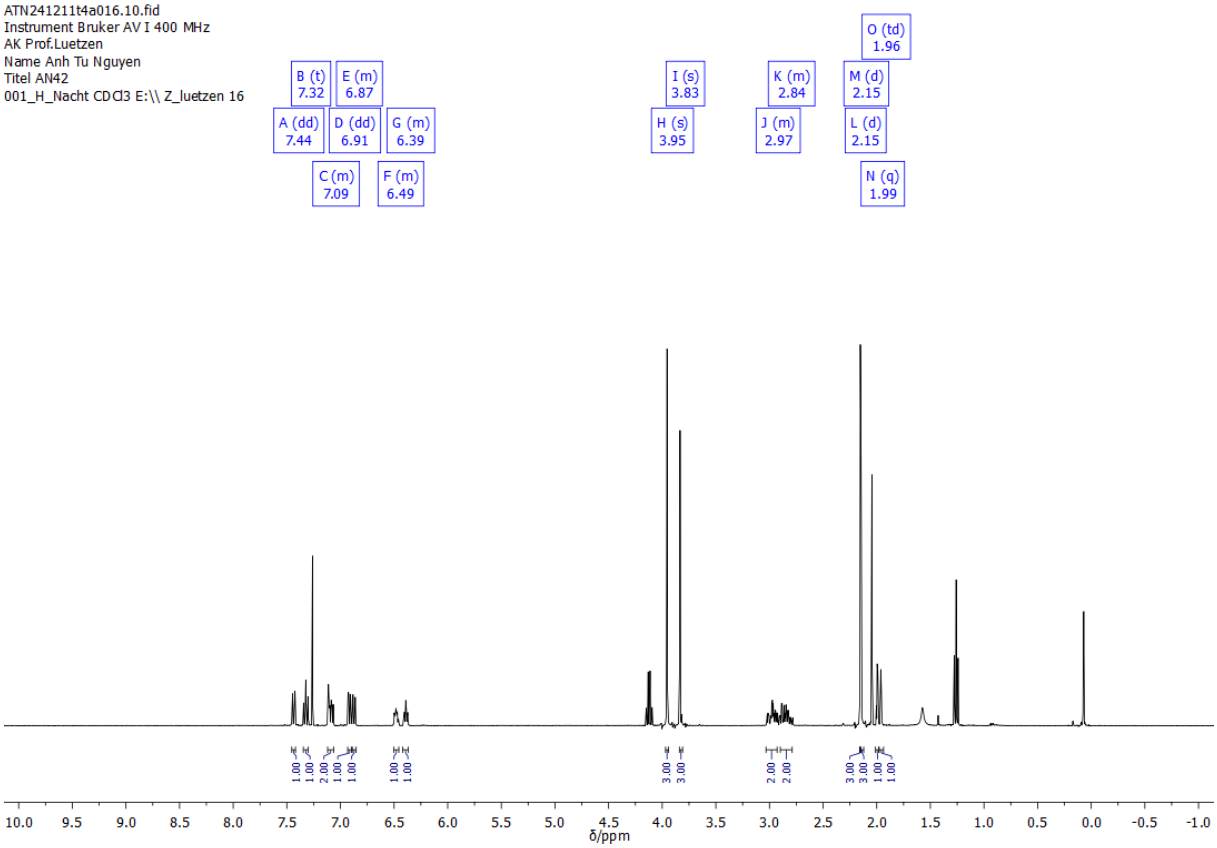

Figure 163: ^{1}H-NMR spectrum of **41** in $CDCl_3$.

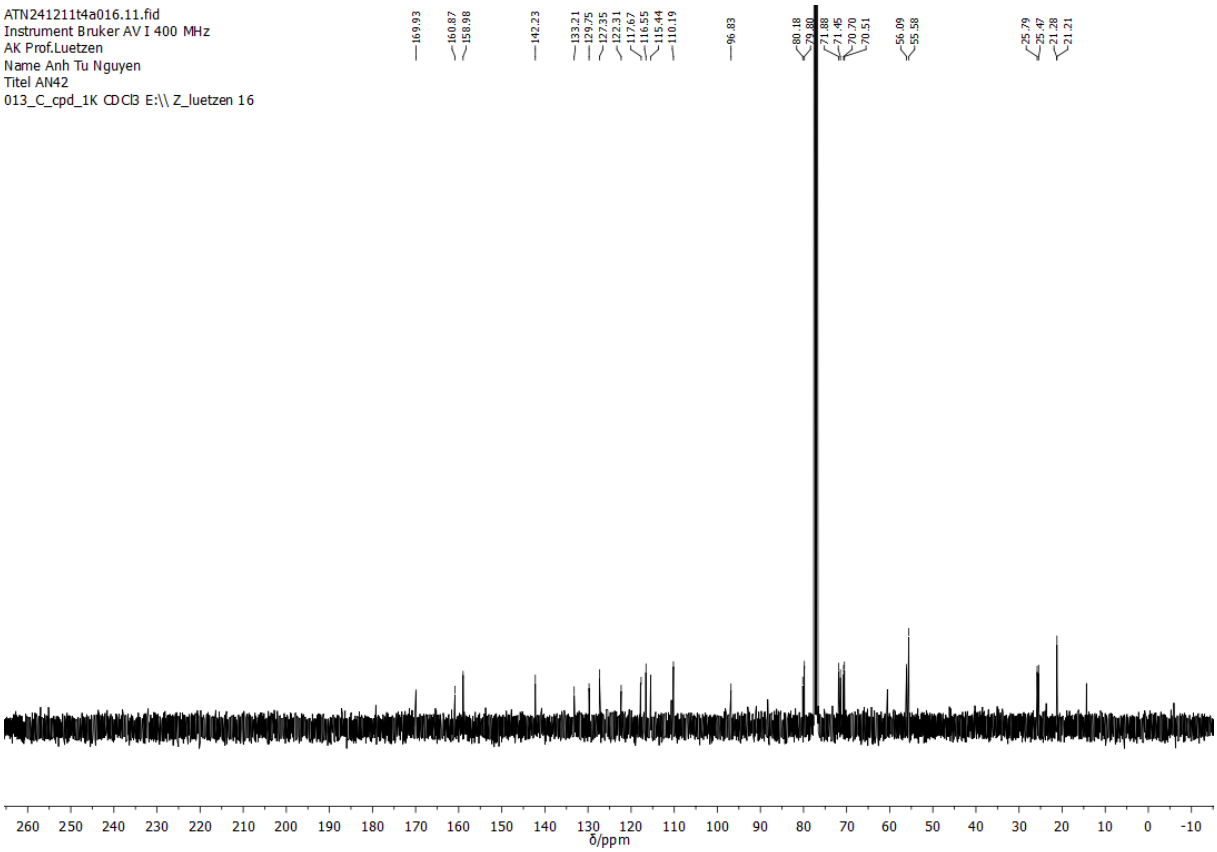

Figure 164: ^{13}C-NMR spectrum of **41** in $CDCl_3$.

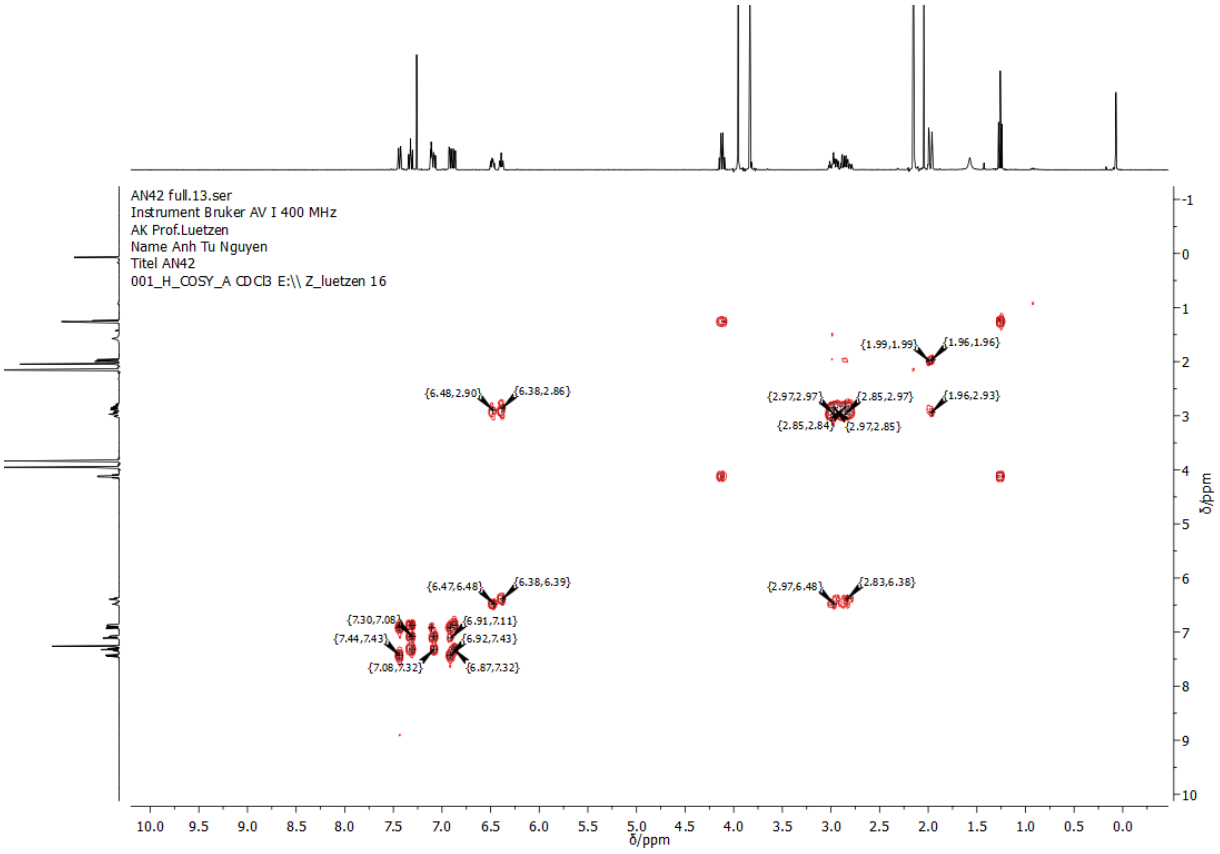

Figure 165: COSY-NMR spectrum of **41** in $CDCl_3$.

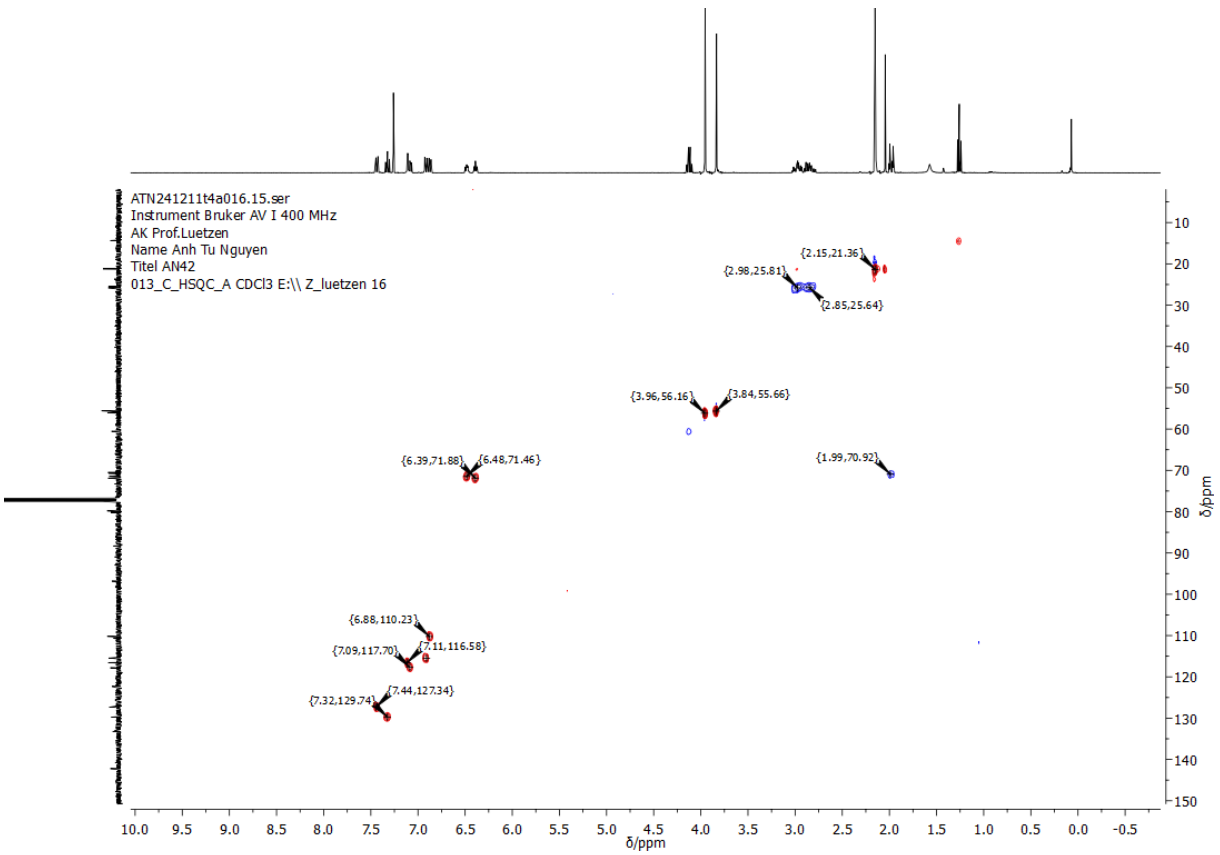

Figure 166: HSQC-NMR spectrum of **41** in $CDCl_3$.

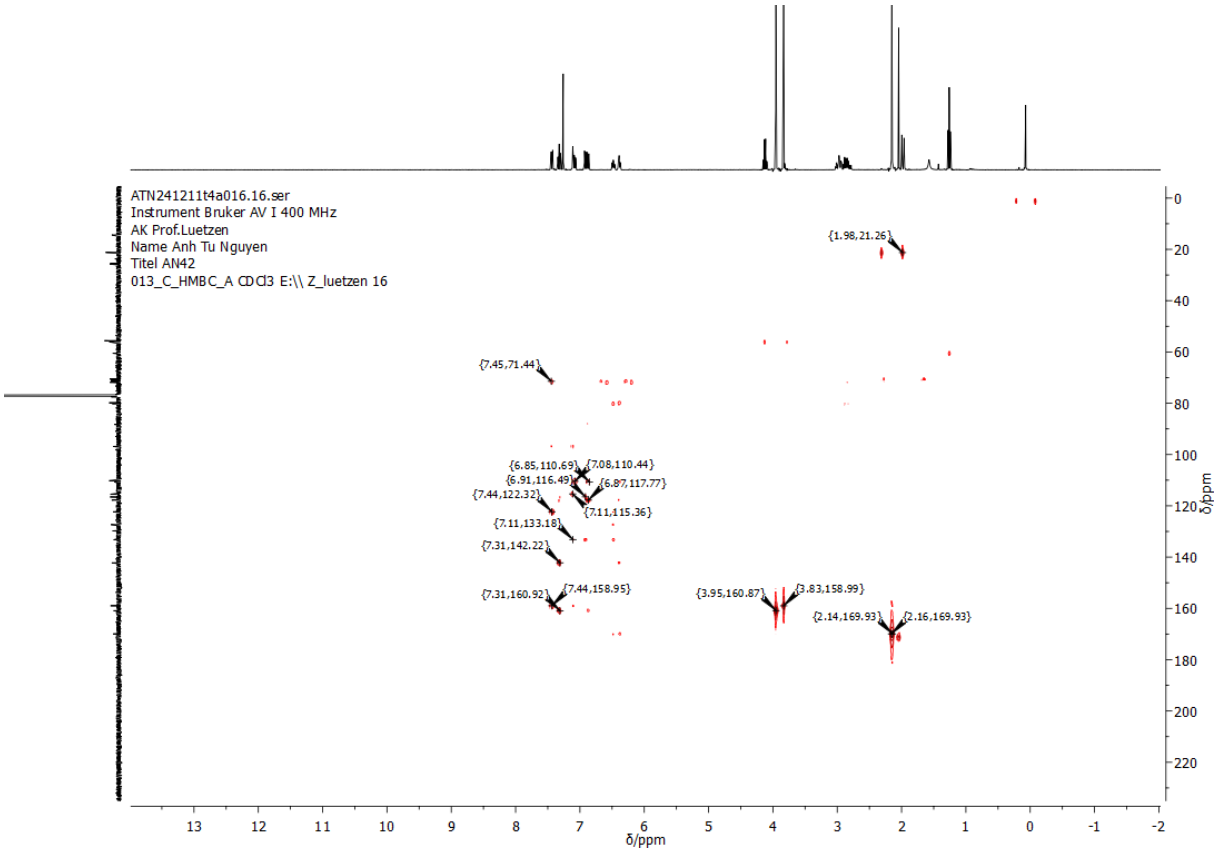

Figure 167: HMBC-NMR spectrum of **41** in $CDCl_3$.

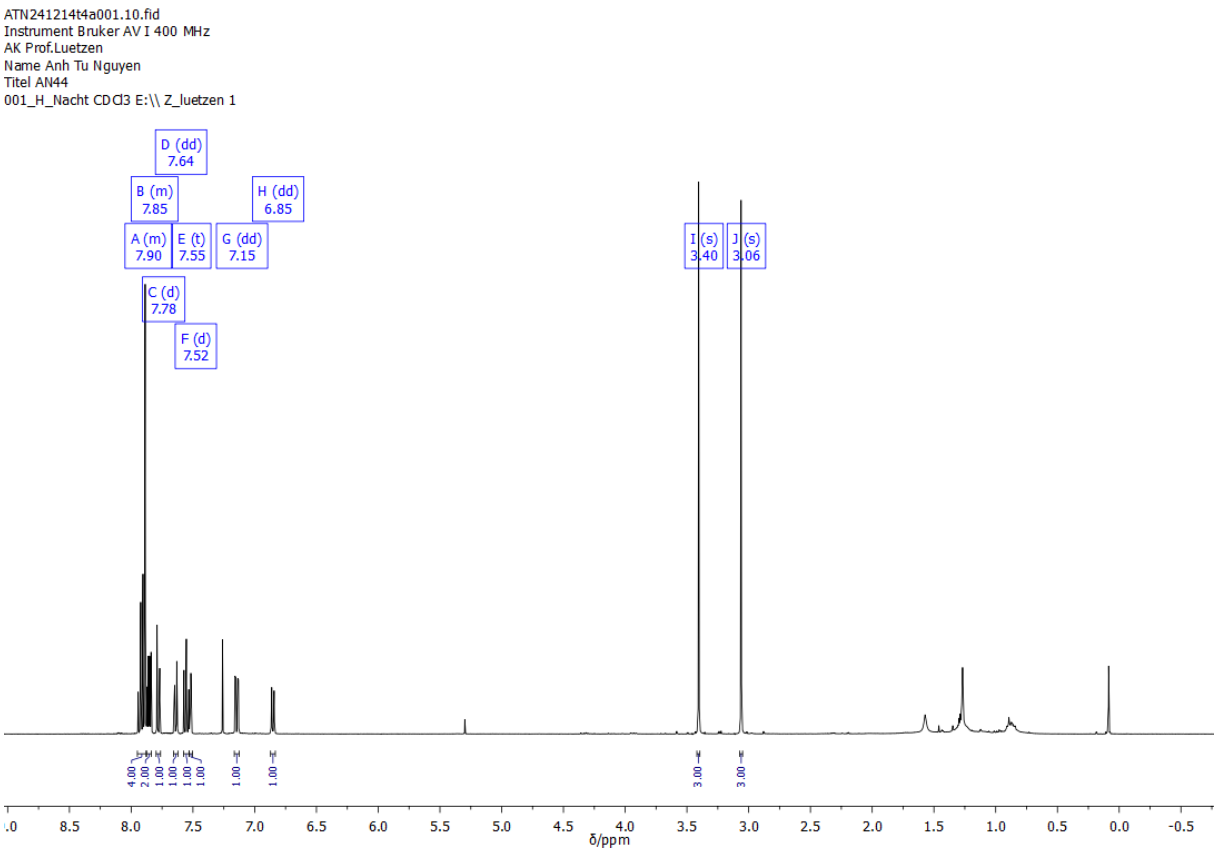

Figure 168: ^{1}H-NMR spectrum of **43** in $CDCl_3$.

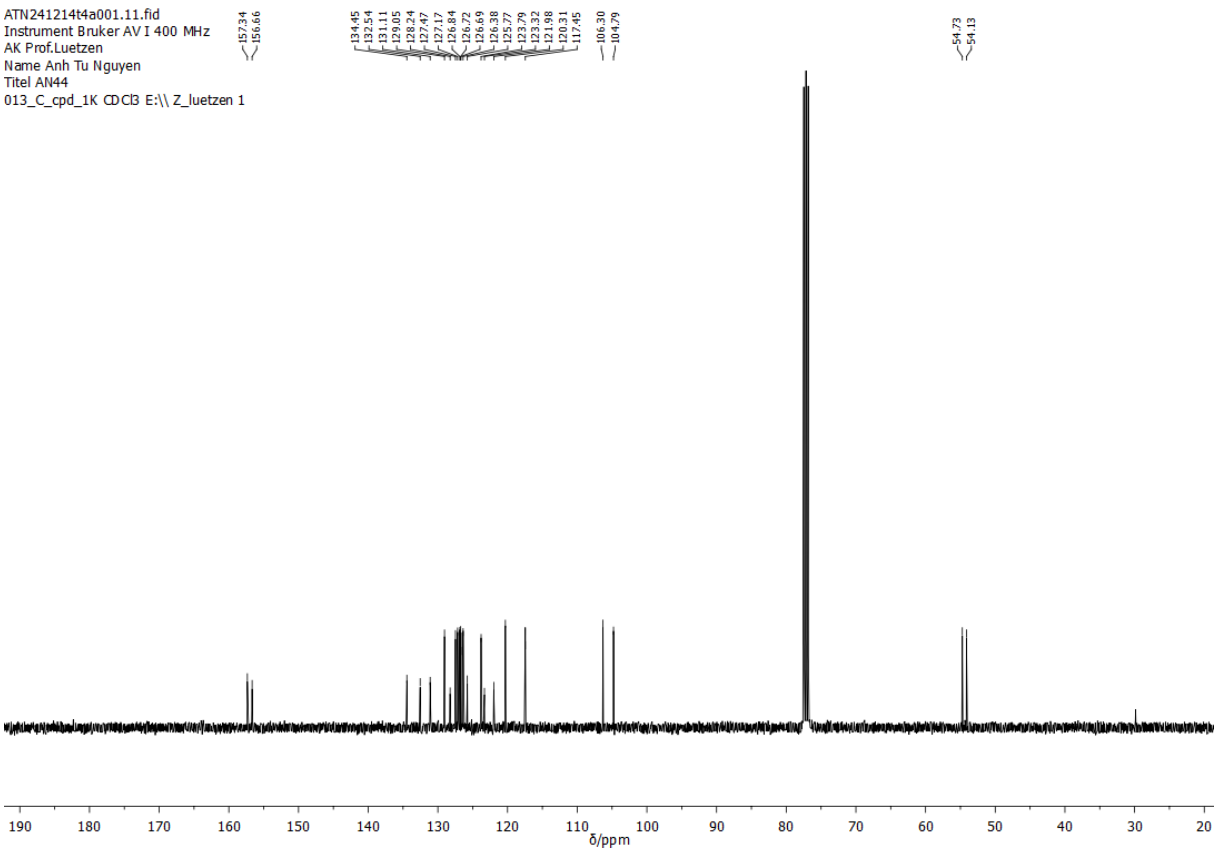

Figure 169: ^{13}C-NMR spectrum of **43** in $CDCl_3$.

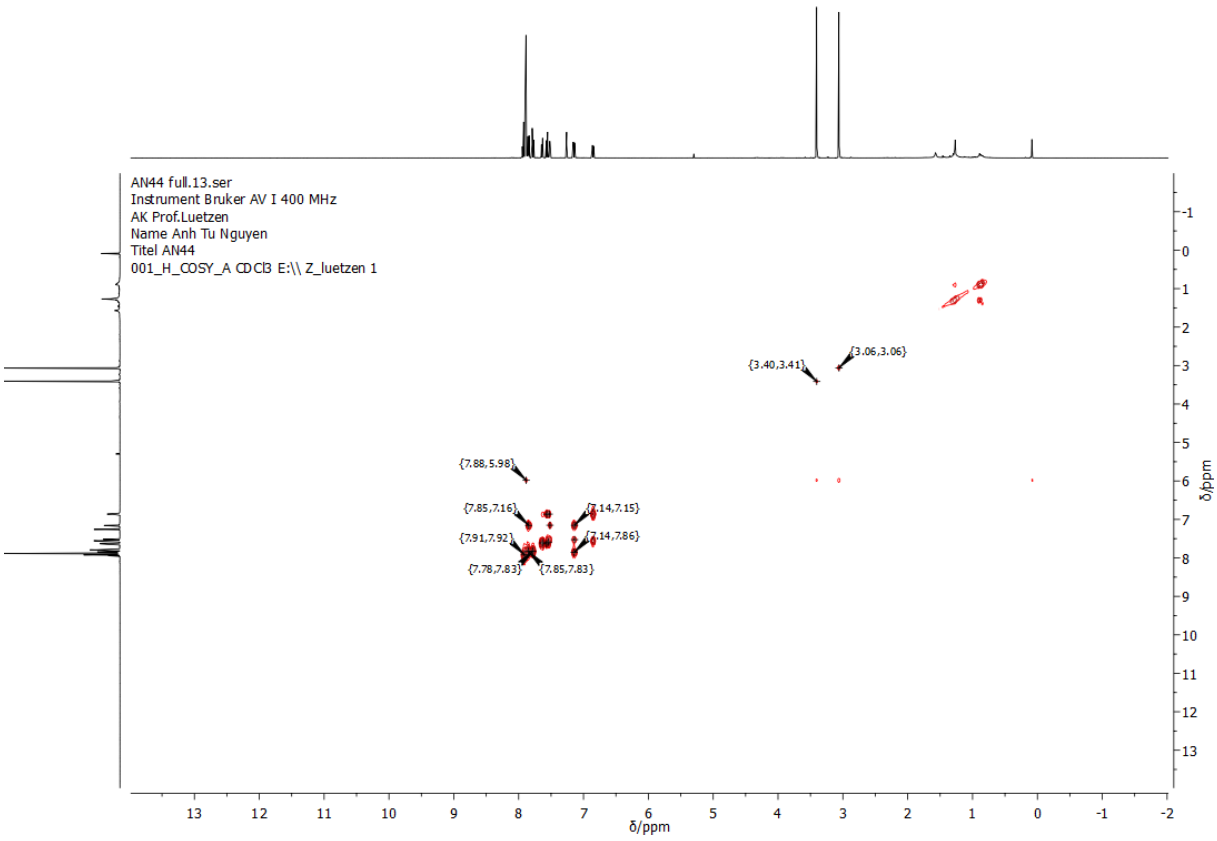

Figure 170: COSY-NMR spectrum of **43** in $CDCl_3$.

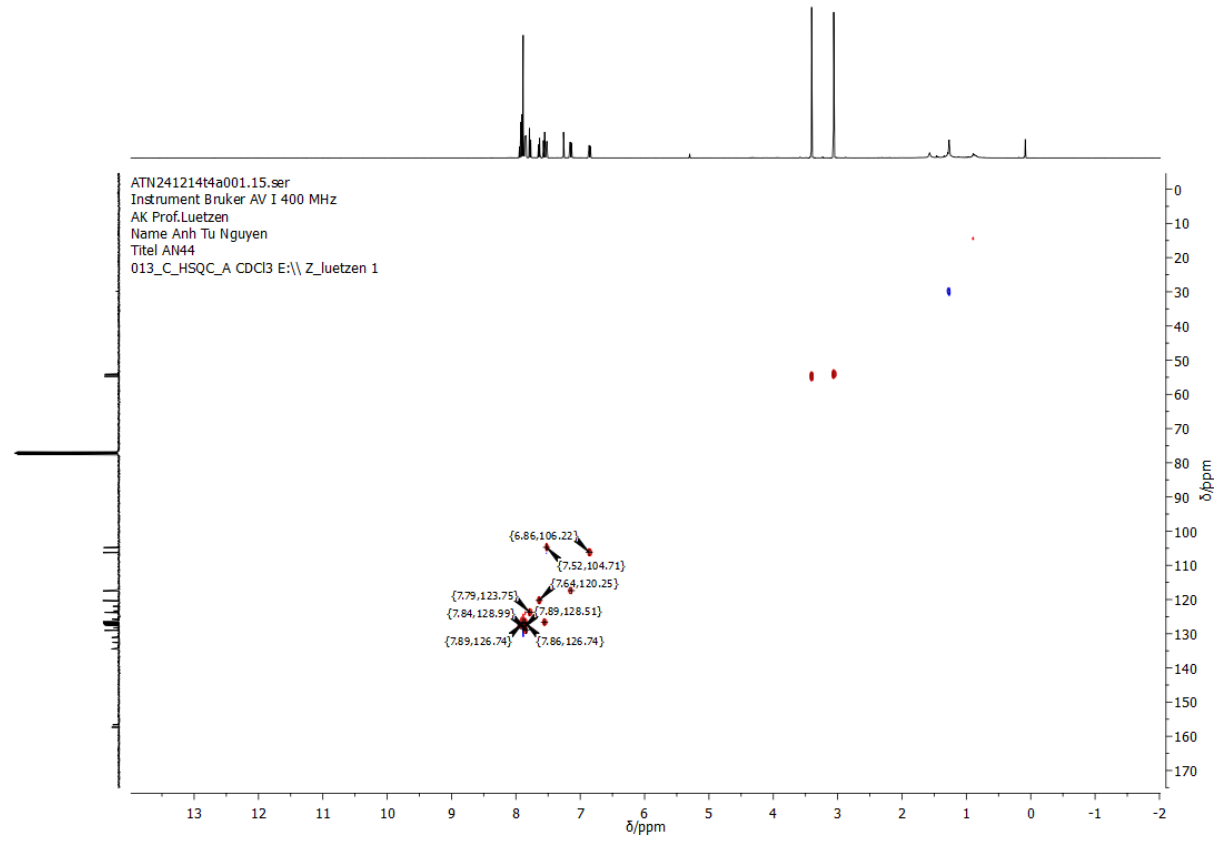

Figure 171: HSQC-NMR spectrum of **43** in $CDCl_3$.

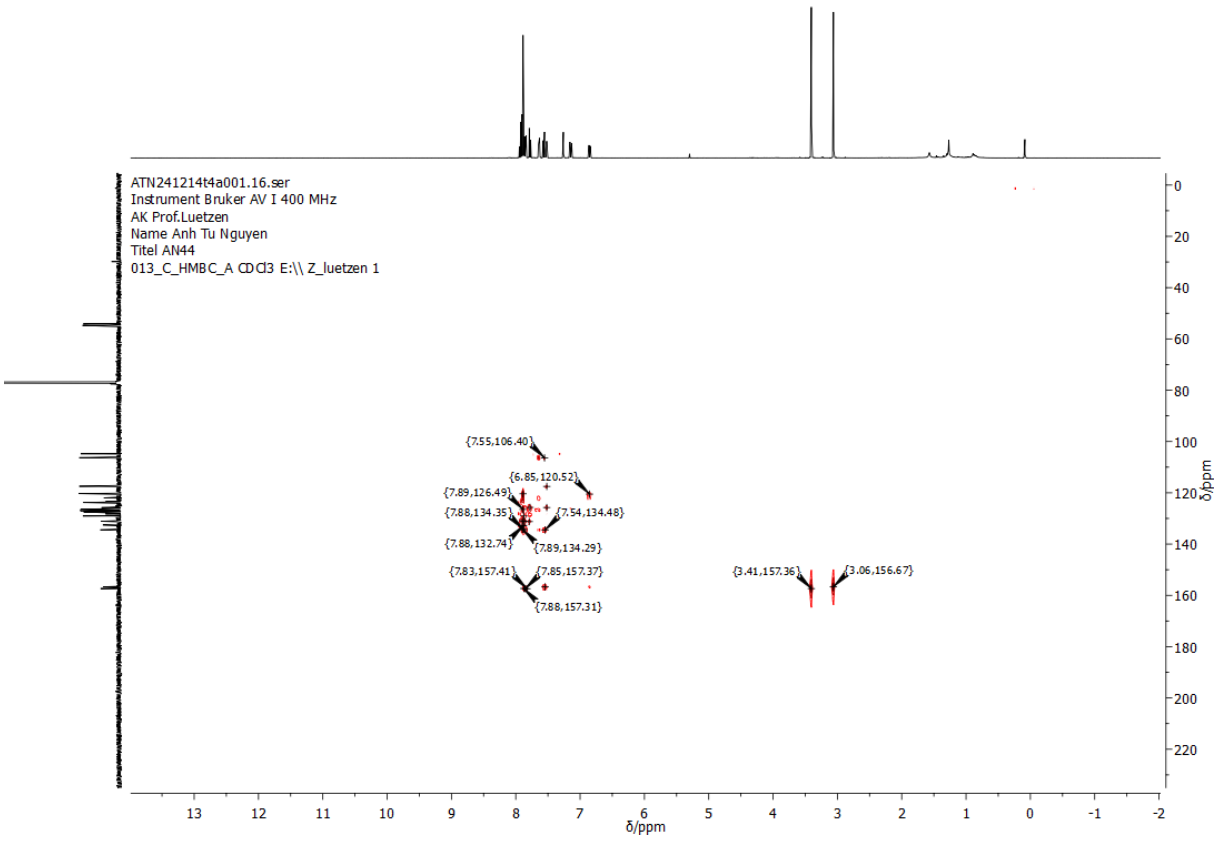

Figure 172: HMBC-NMR spectrum of **43** in $CDCl_3$.

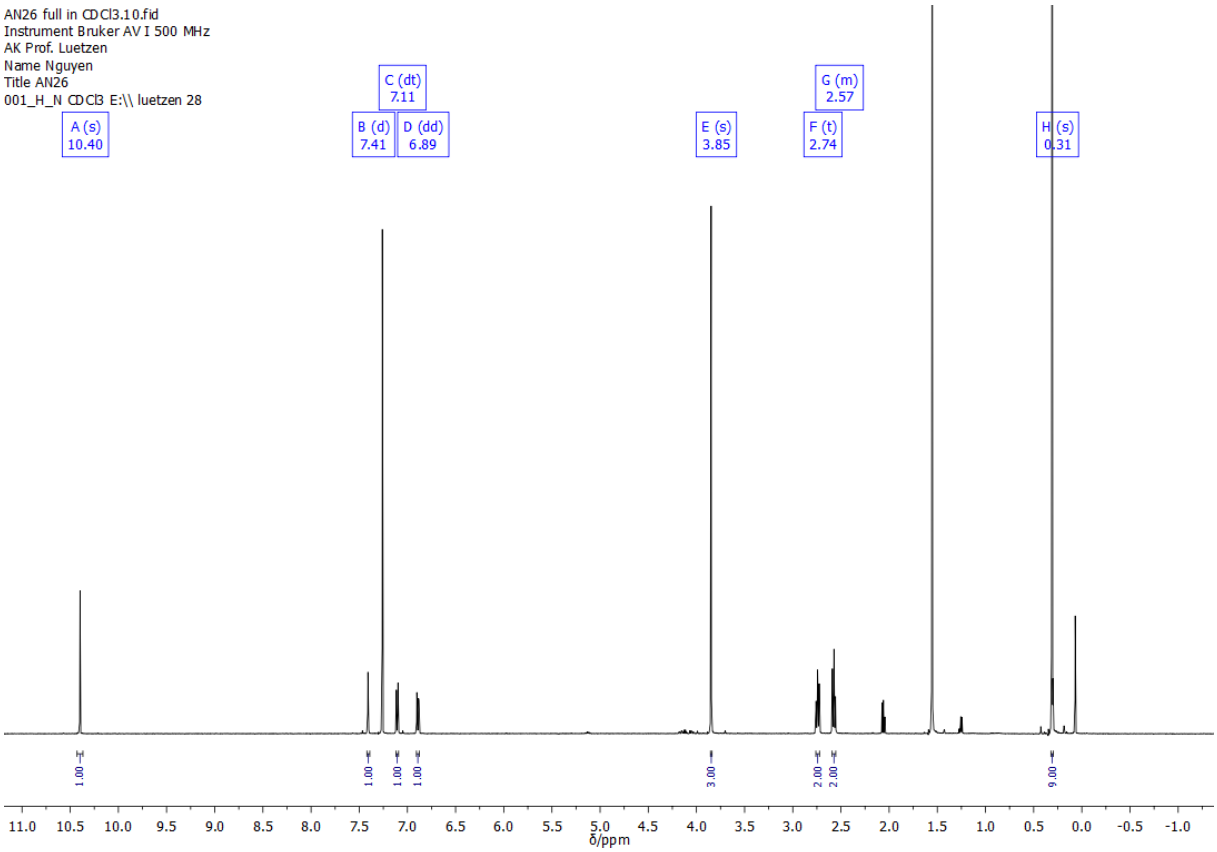

Figure 173: ^{1}H-NMR spectrum of **48** in $CDCl_3$.

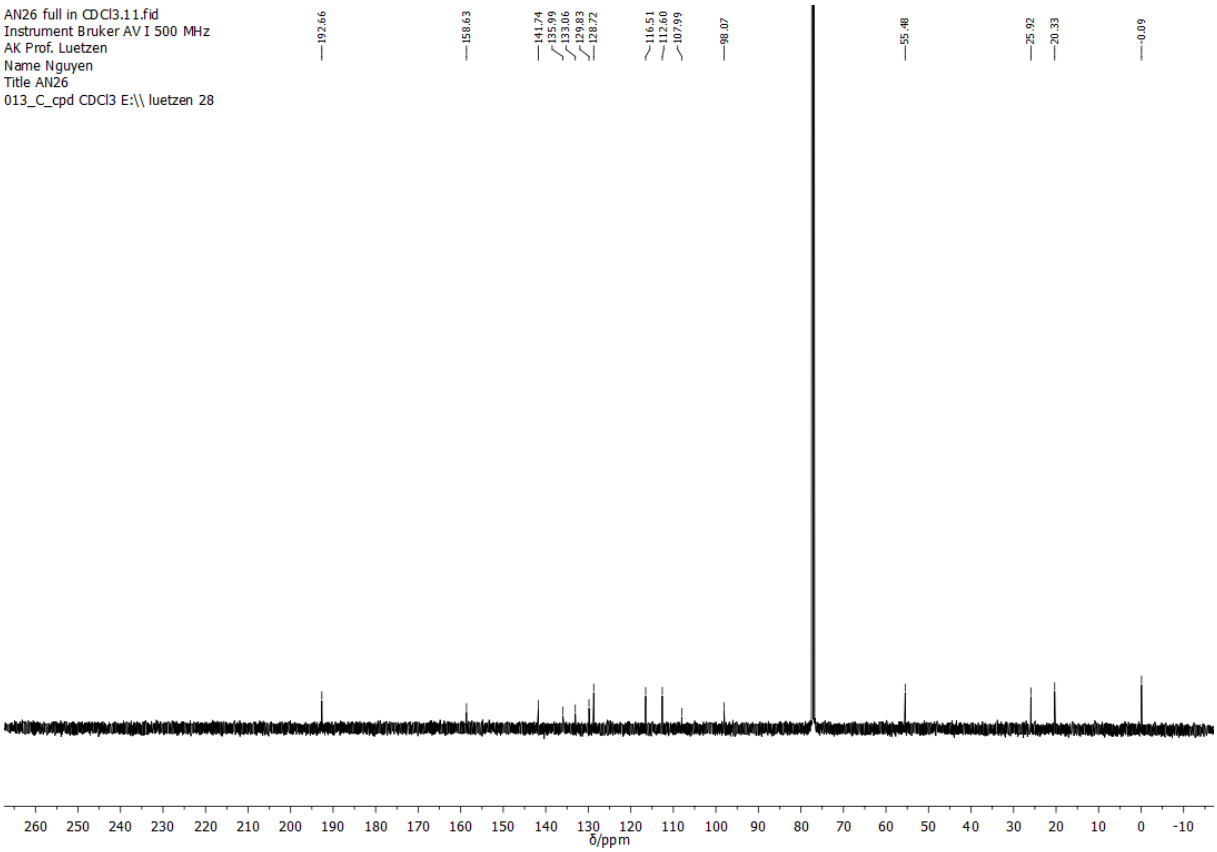

Figure 174: ^{13}C-NMR spectrum of **48** in $CDCl_3$.

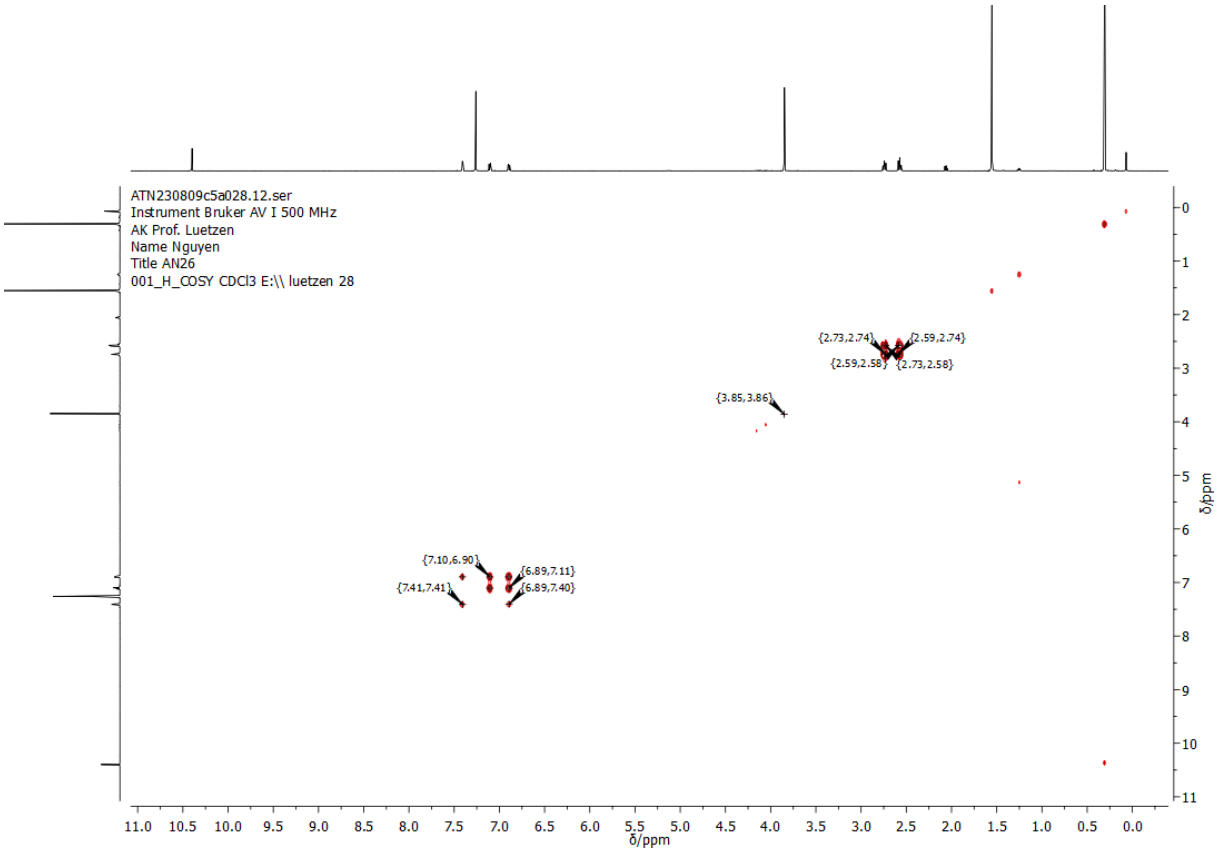

Figure 175: COSY-NMR spectrum of **48** in $CDCl_3$.

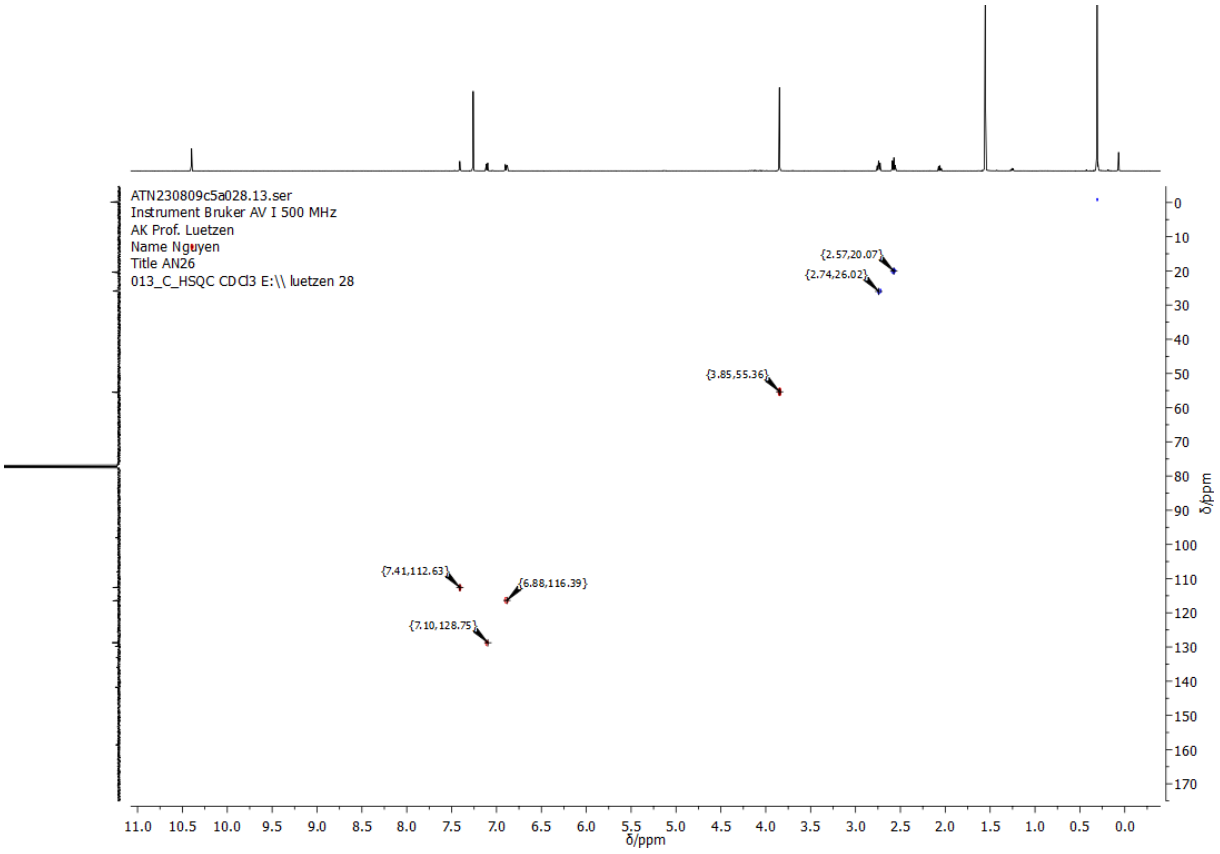

Figure 176: HSQC-NMR spectrum of **48** in $CDCl_3$.

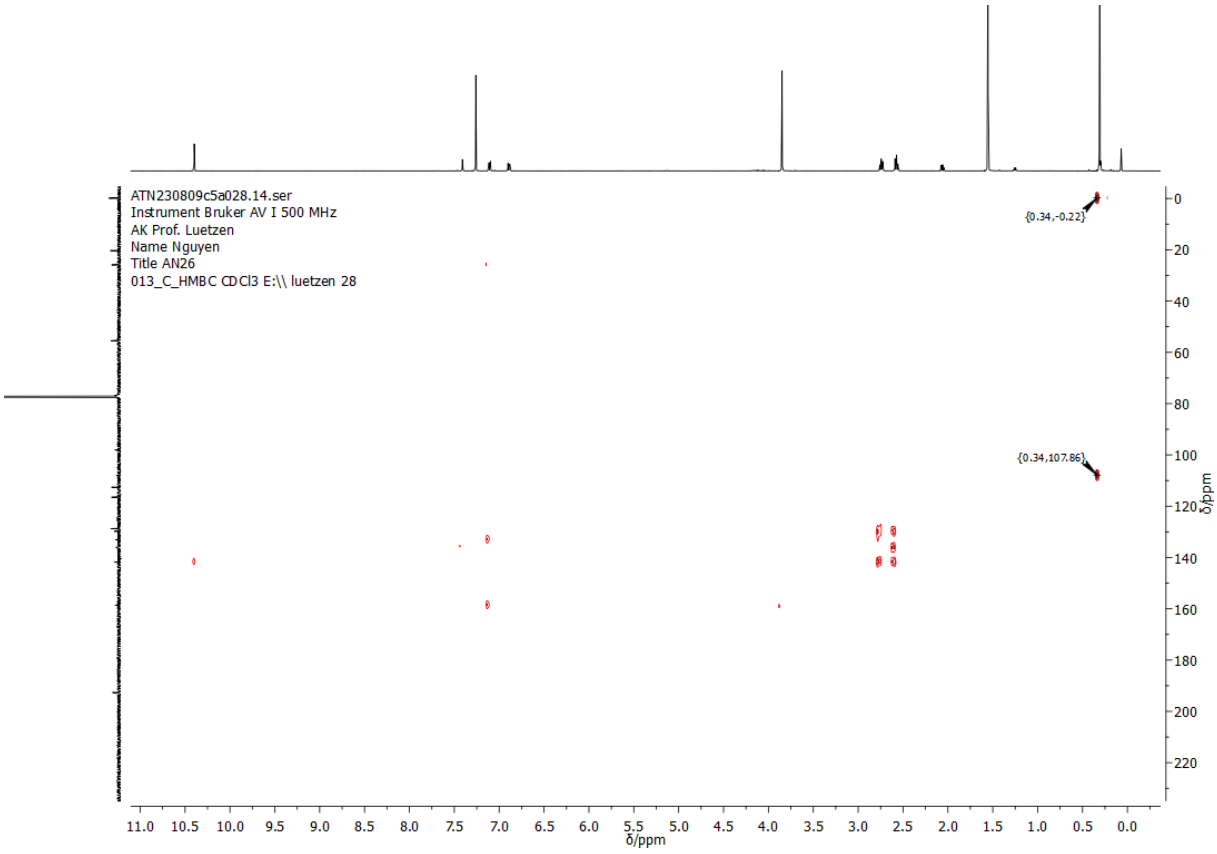

Figure 177: HMBC-NMR spectrum of **48** in $CDCl_3$.

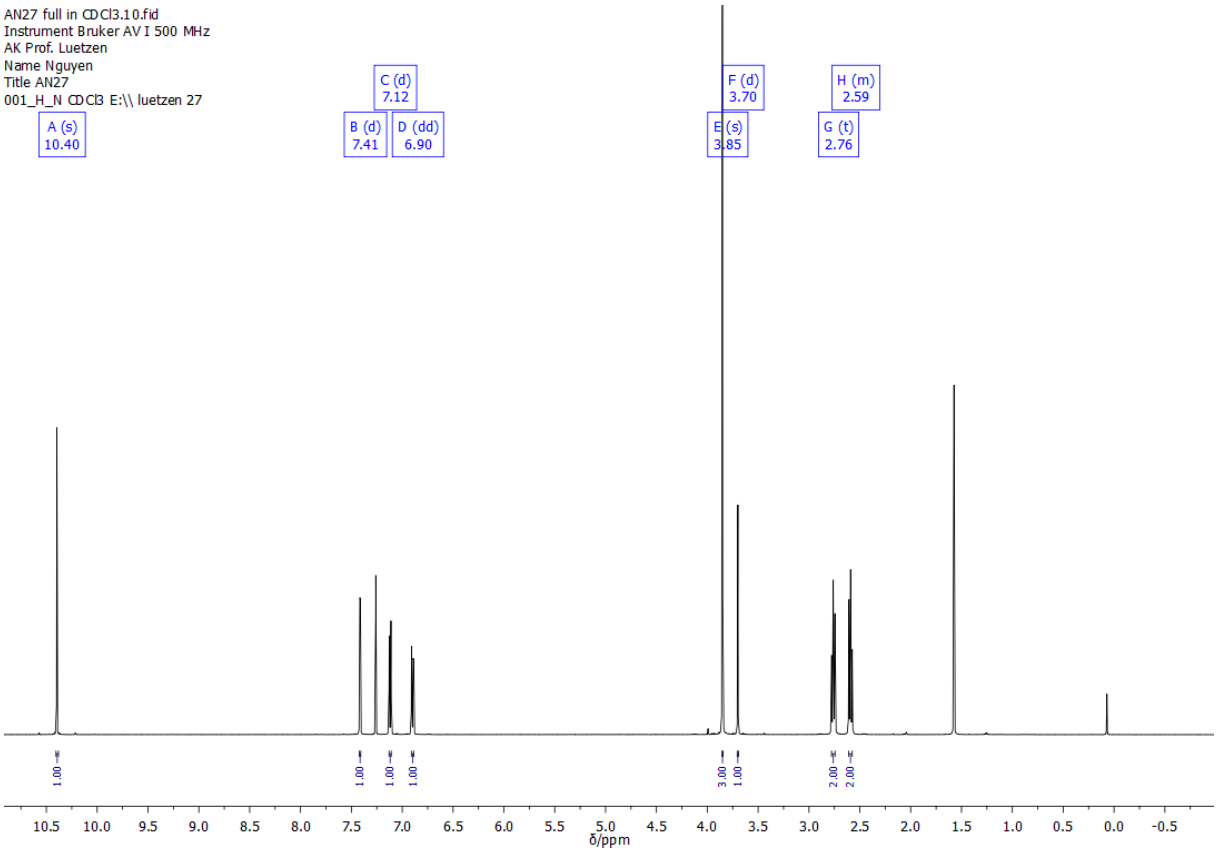

Figure 178: ^{1}H-NMR spectrum of **49** in $CDCl_3$.

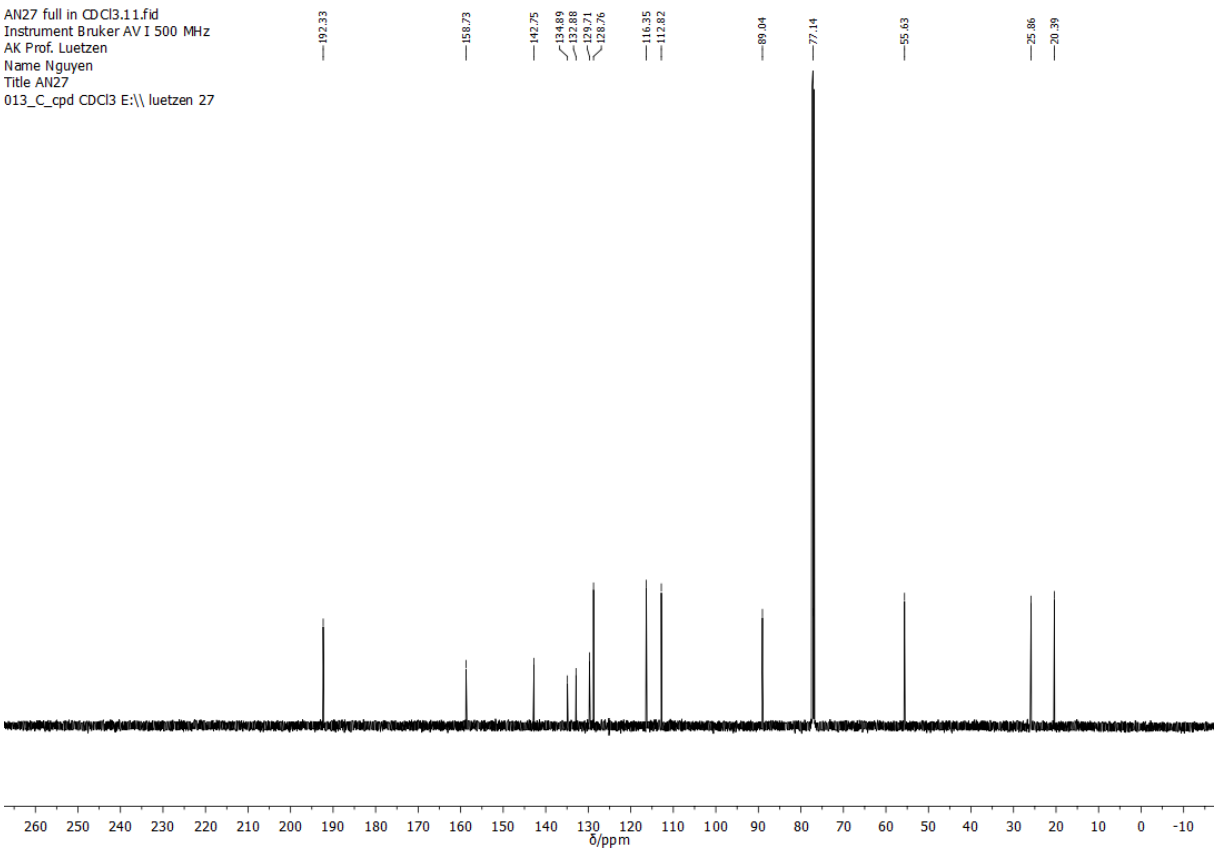

Figure 179: ^{13}C-NMR spectrum of **49** in $CDCl_3$.

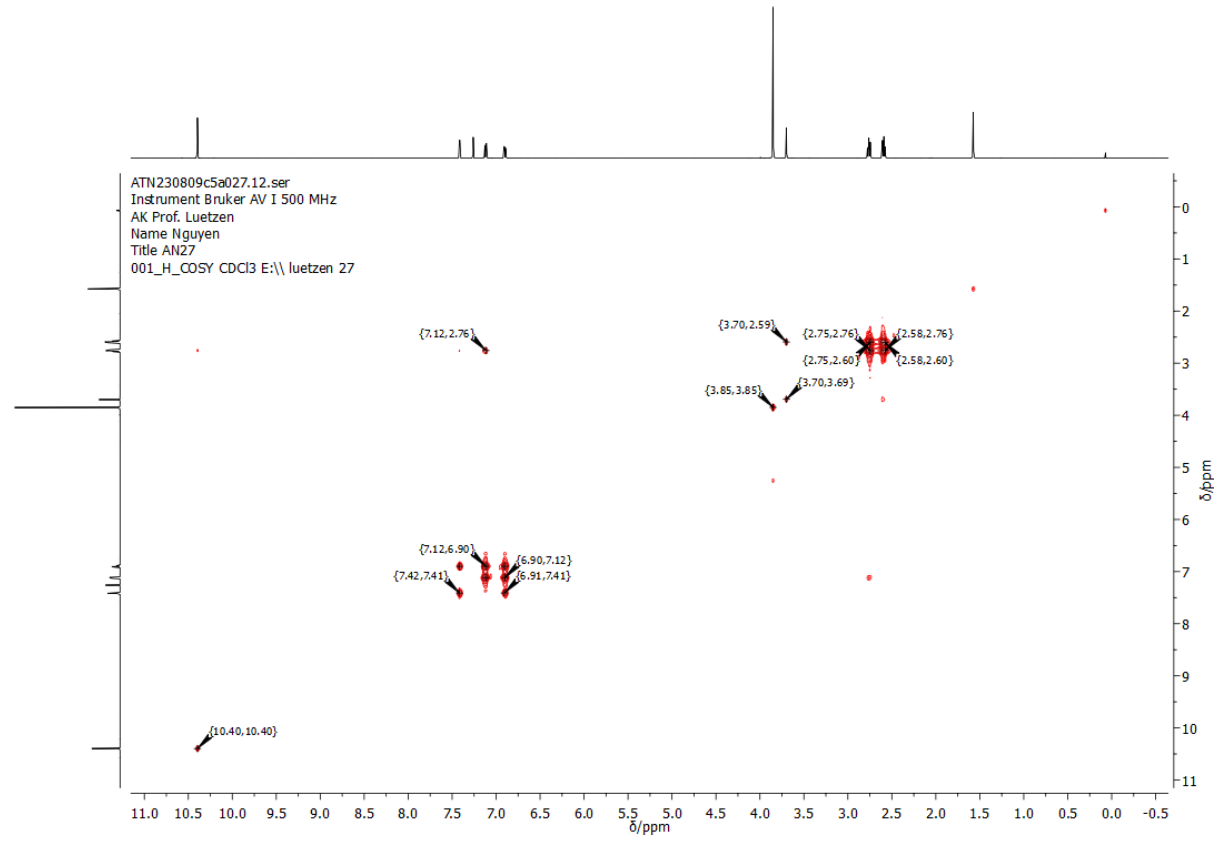

Figure 180: COSY-NMR spectrum of **49** in $CDCl_3$.

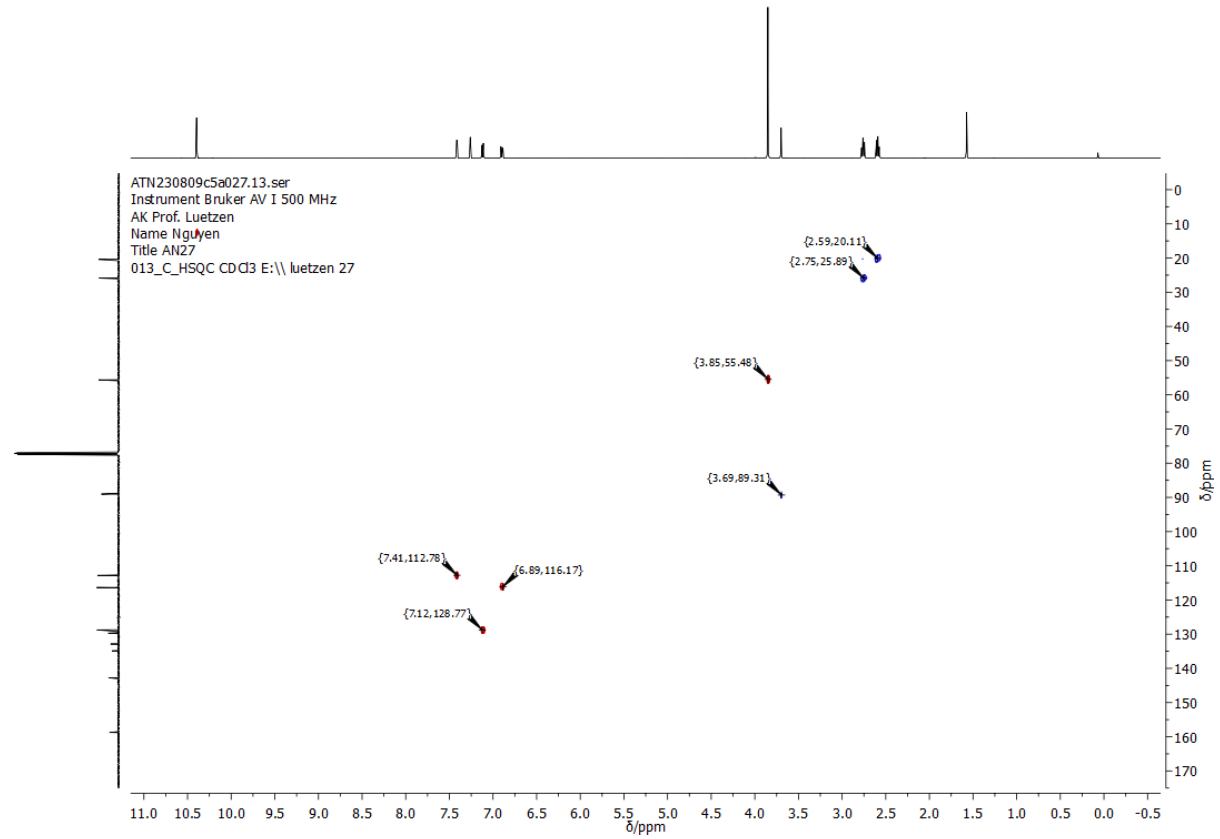

Figure 181: HSQC-NMR spectrum of **49** in $CDCl_3$.

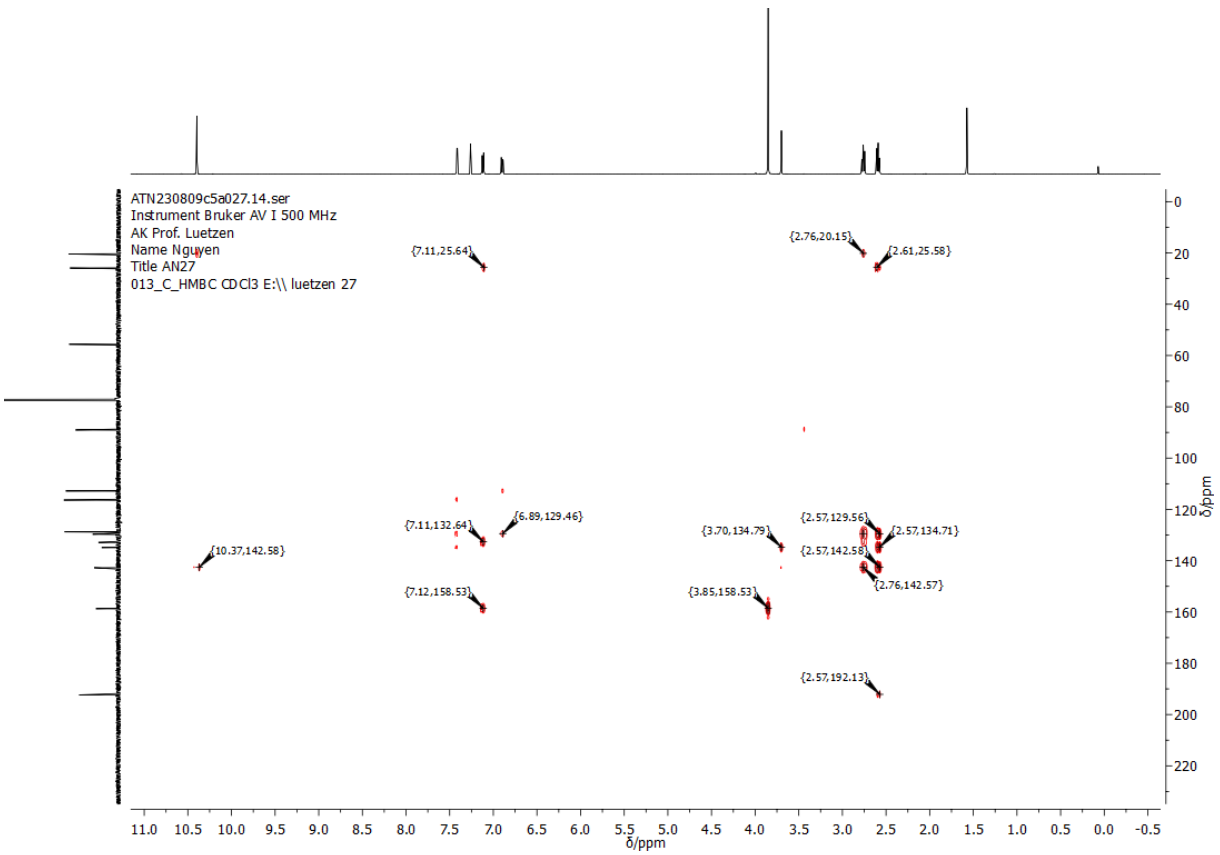

Figure 182: HMBC-NMR spectrum of **49** in $CDCl_3$.

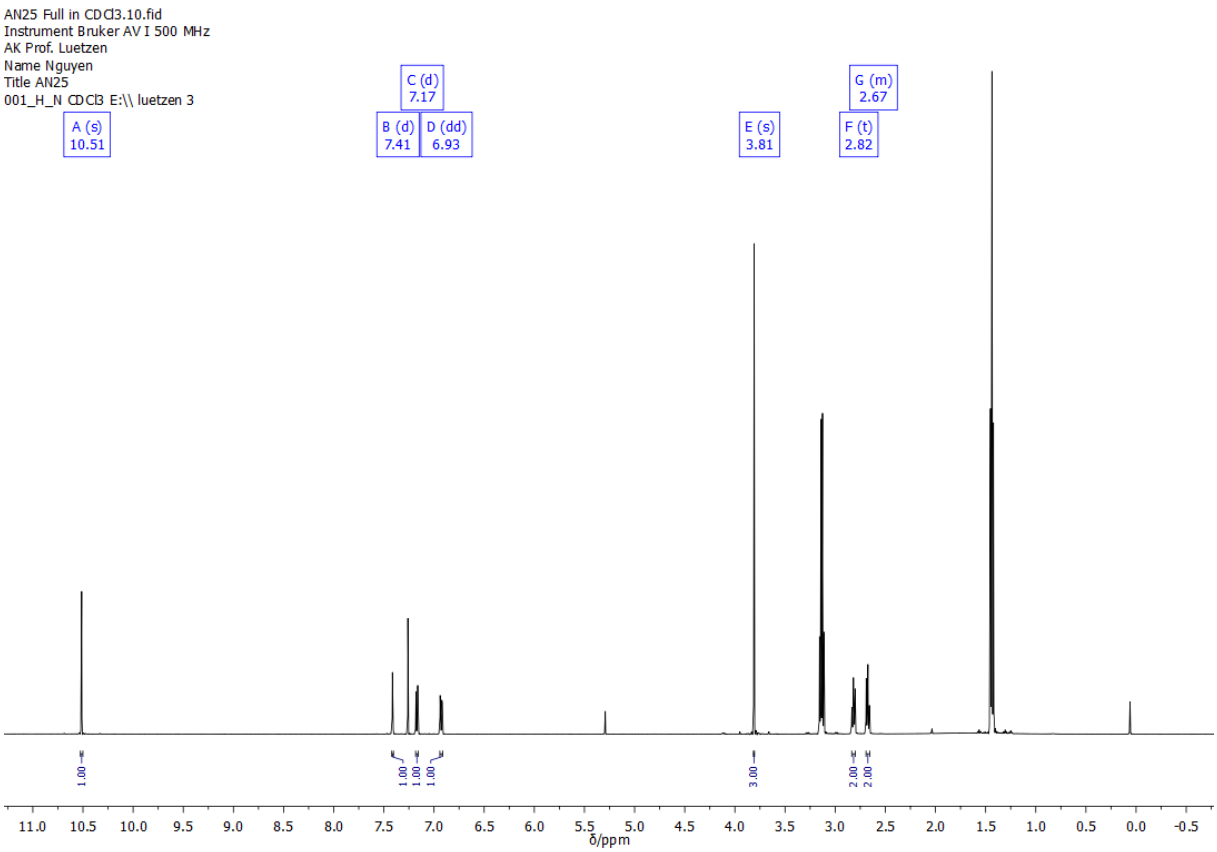

Figure 183: ^{1}H-NMR spectrum of **50** in $CDCl_3$.

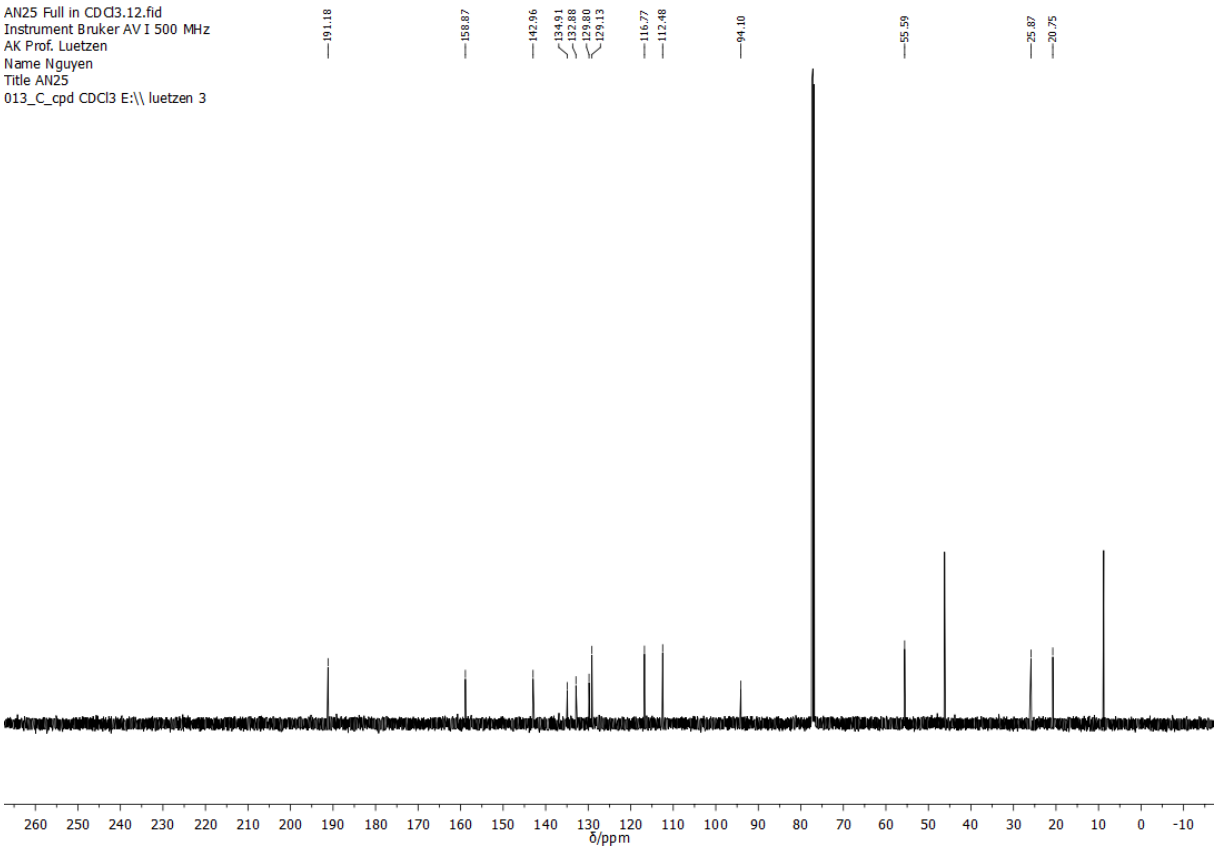

Figure 184: ^{13}C-NMR spectrum of **50** in $CDCl_3$.

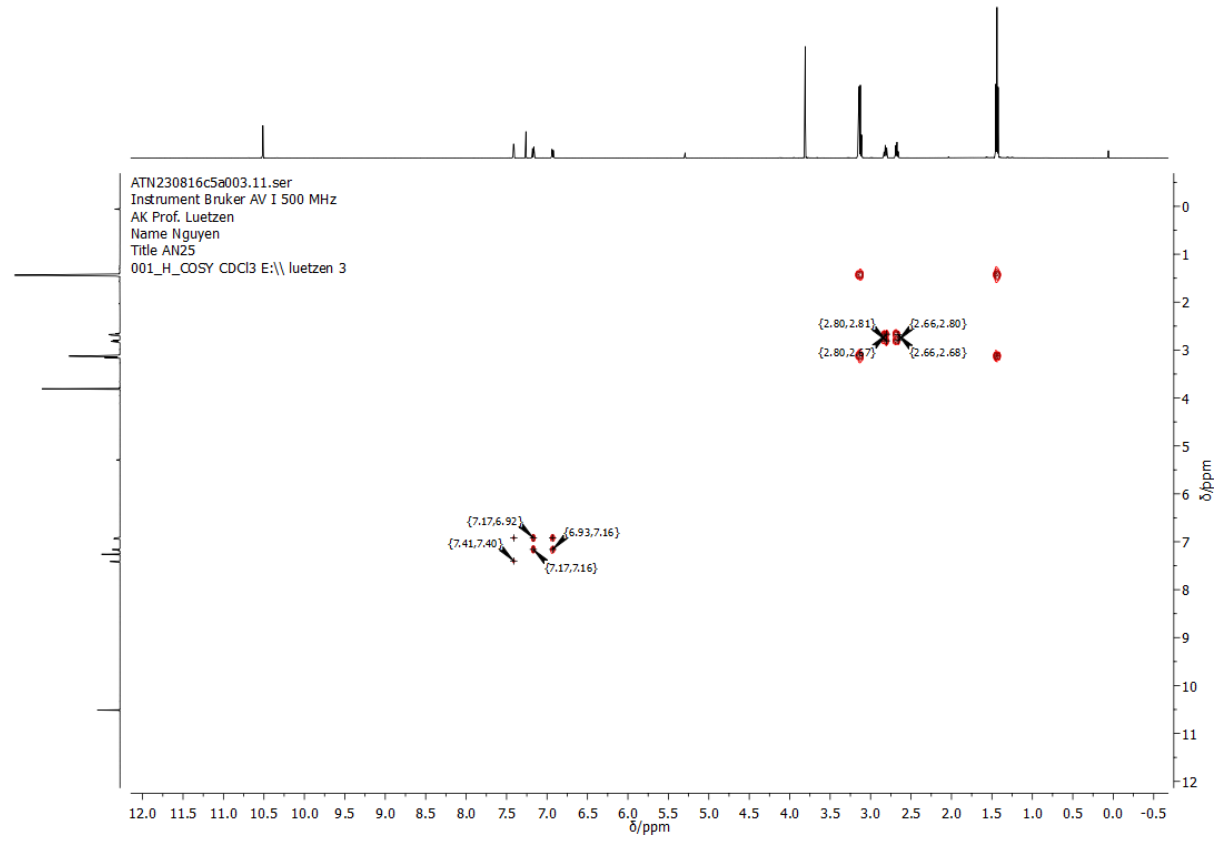

Figure 185: COSY-NMR spectrum of **50** in $CDCl_3$.

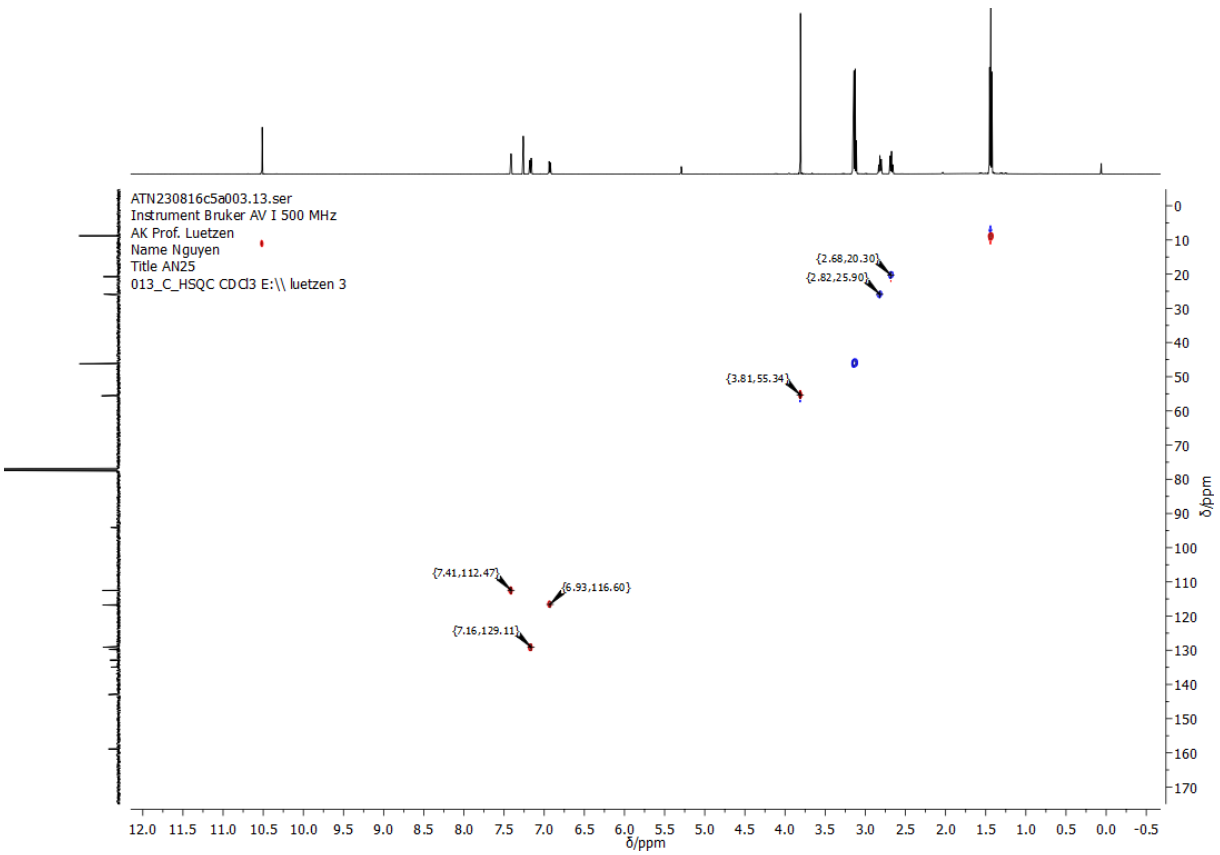

Figure 186: HSQC-NMR spectrum of **50** in $CDCl_3$.

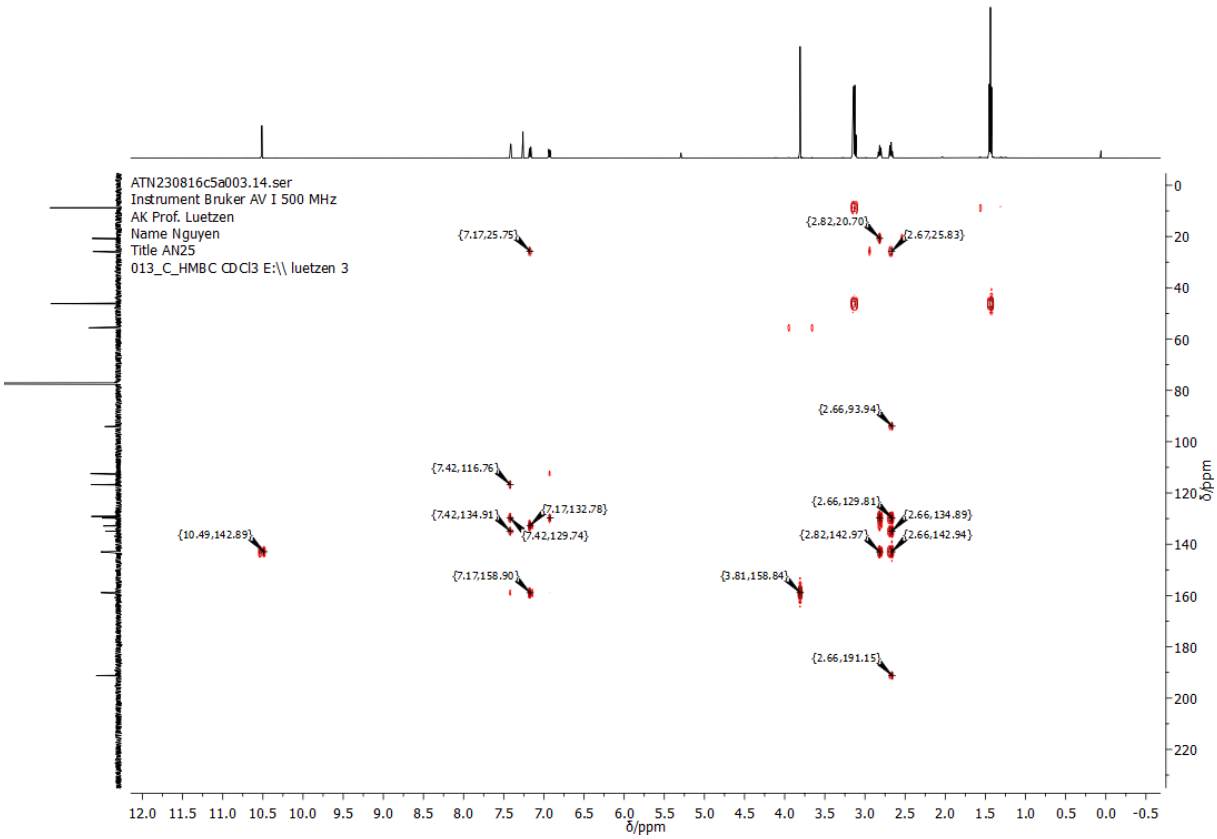

Figure 187: HMBC-NMR spectrum of **50** in $CDCl_3$.

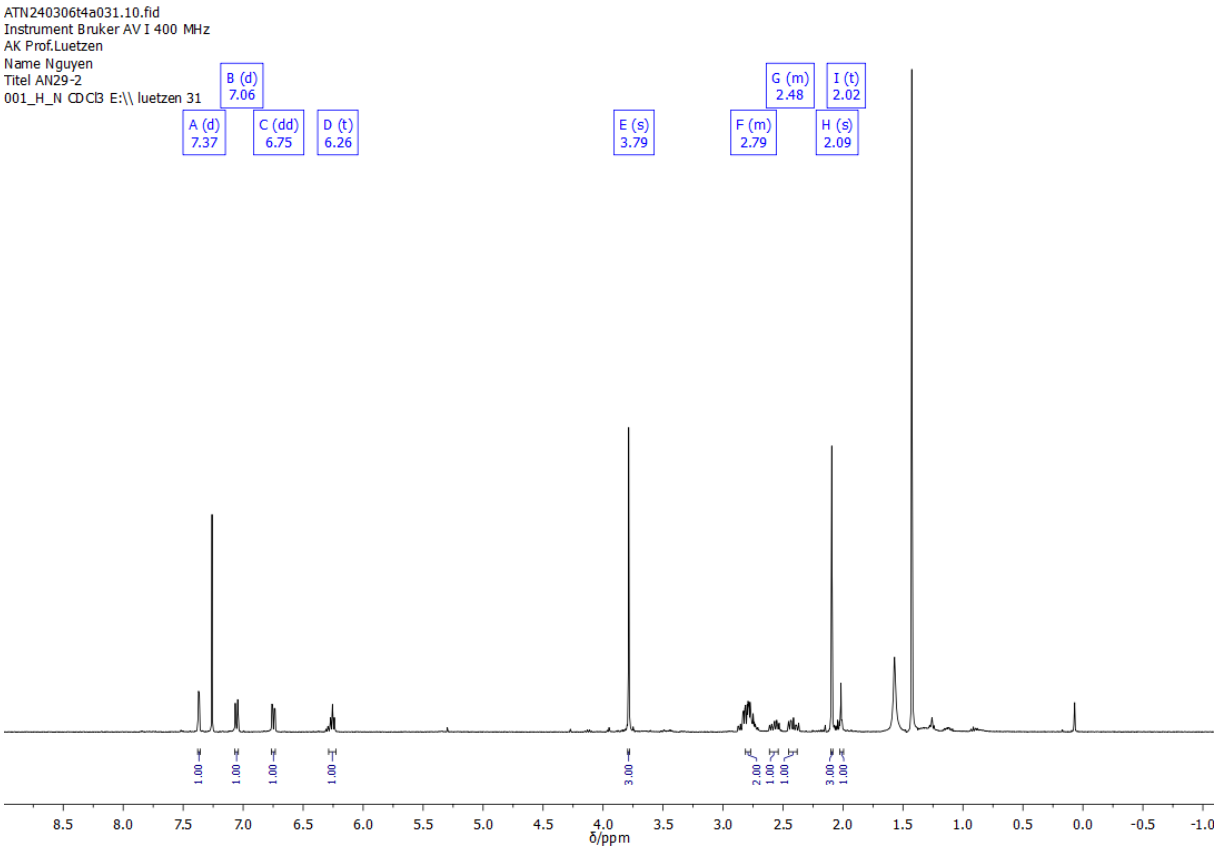

Figure 188: ^{1}H-NMR spectrum of **52** in $CDCl_3$.

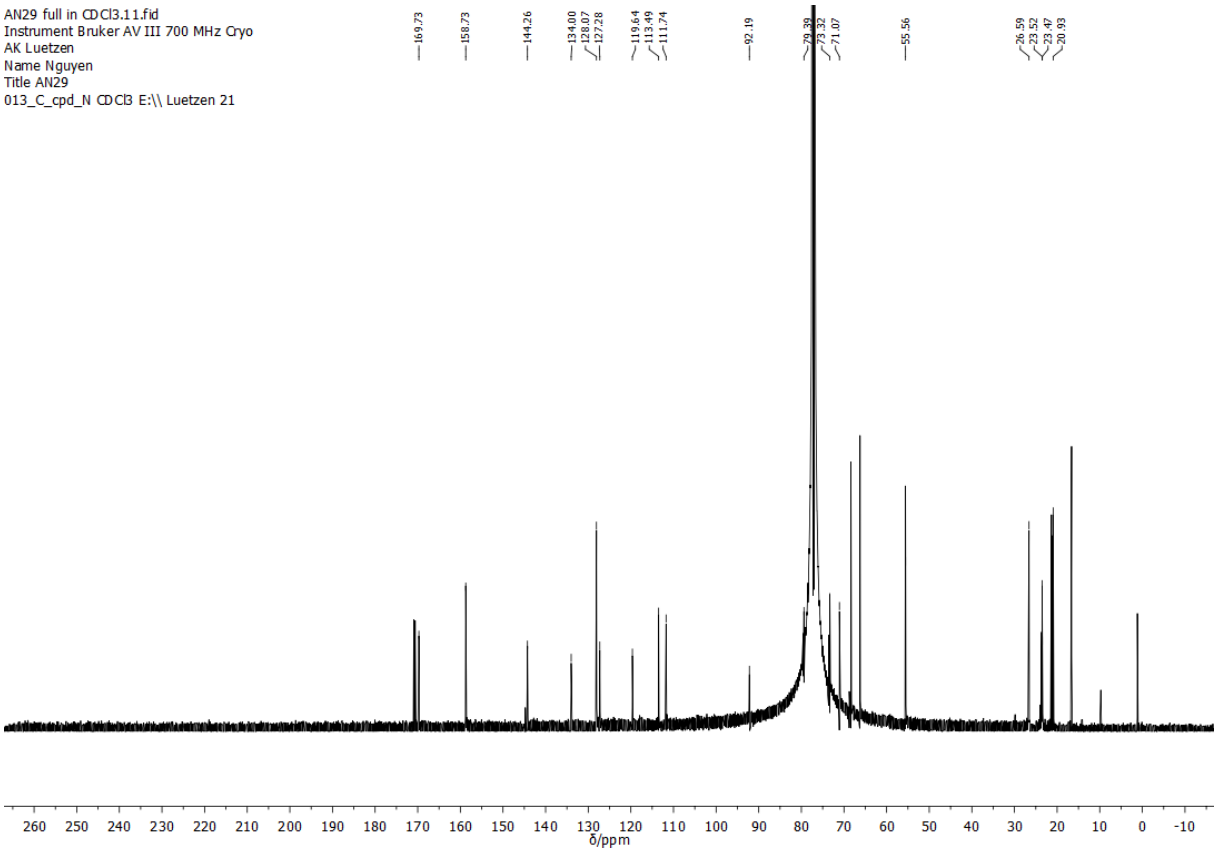

Figure 189: ^{13}C-NMR spectrum of **52** in $CDCl_3$.

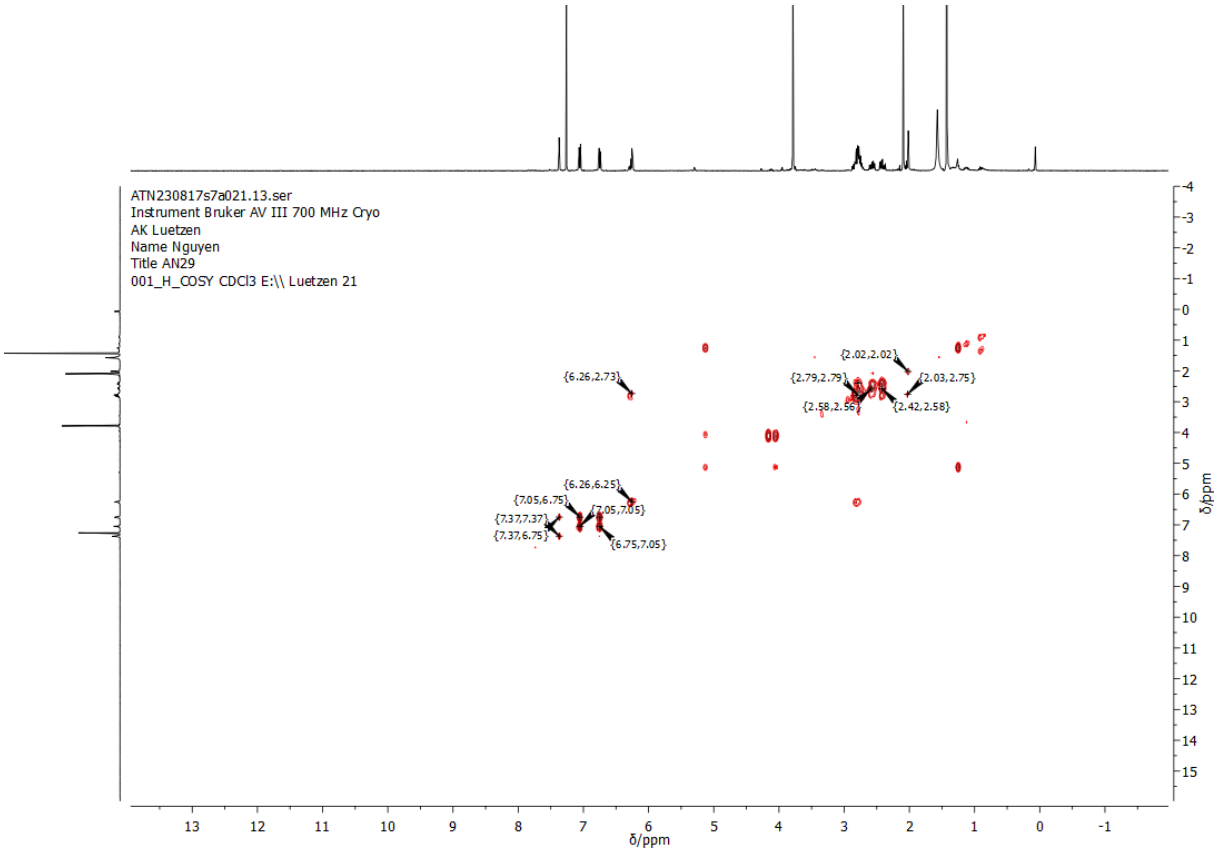

Figure 190: COSY-NMR spectrum of **52** in $CDCl_3$.

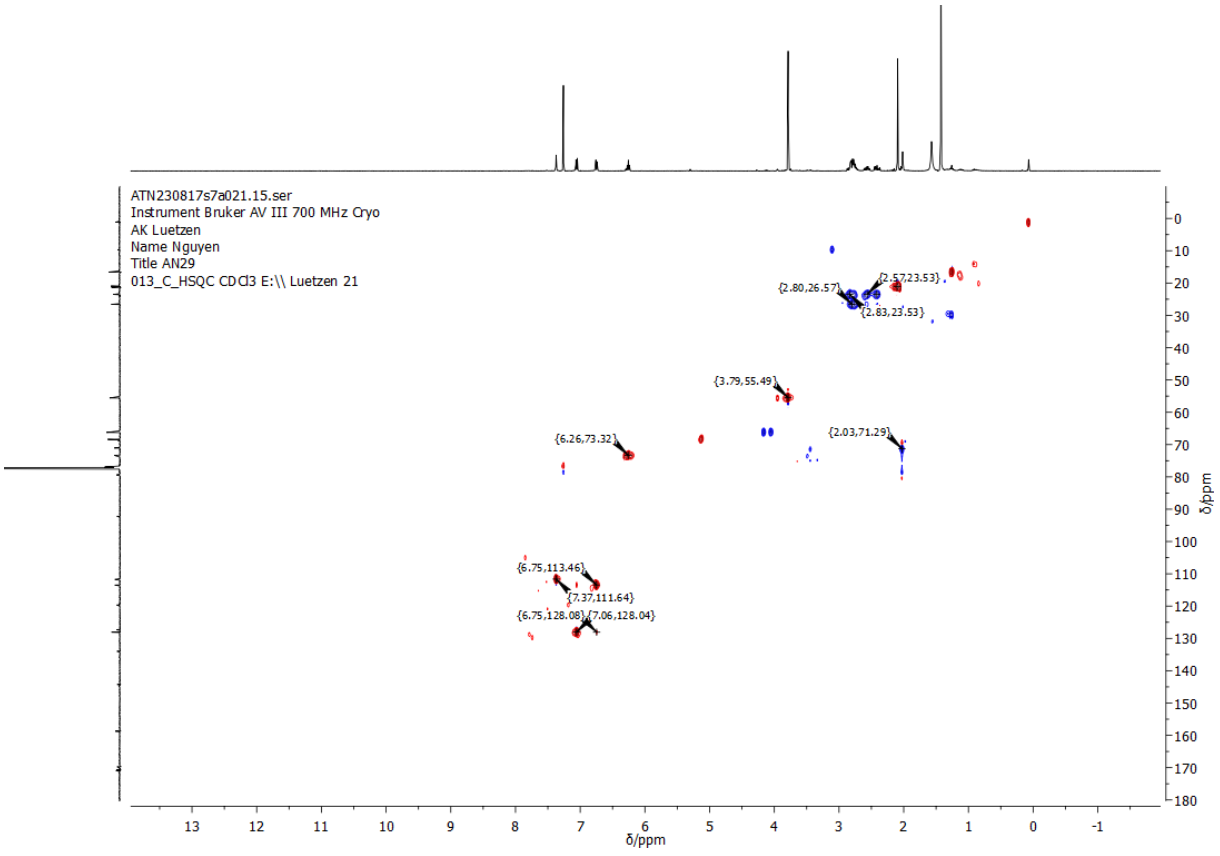

Figure 191: HSQC-NMR spectrum of **52** in $CDCl_3$.

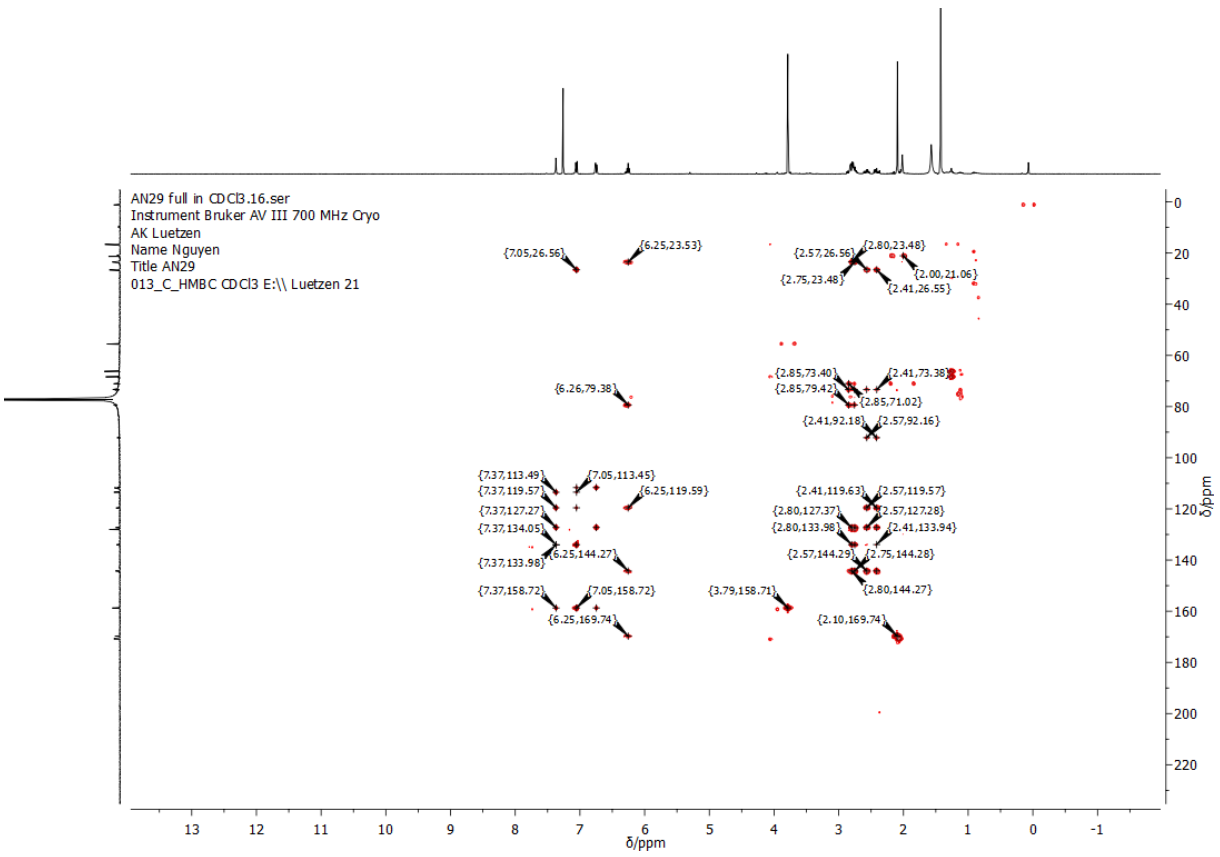

Figure 192: HMBC-NMR spectrum of **52** in $CDCl_3$.

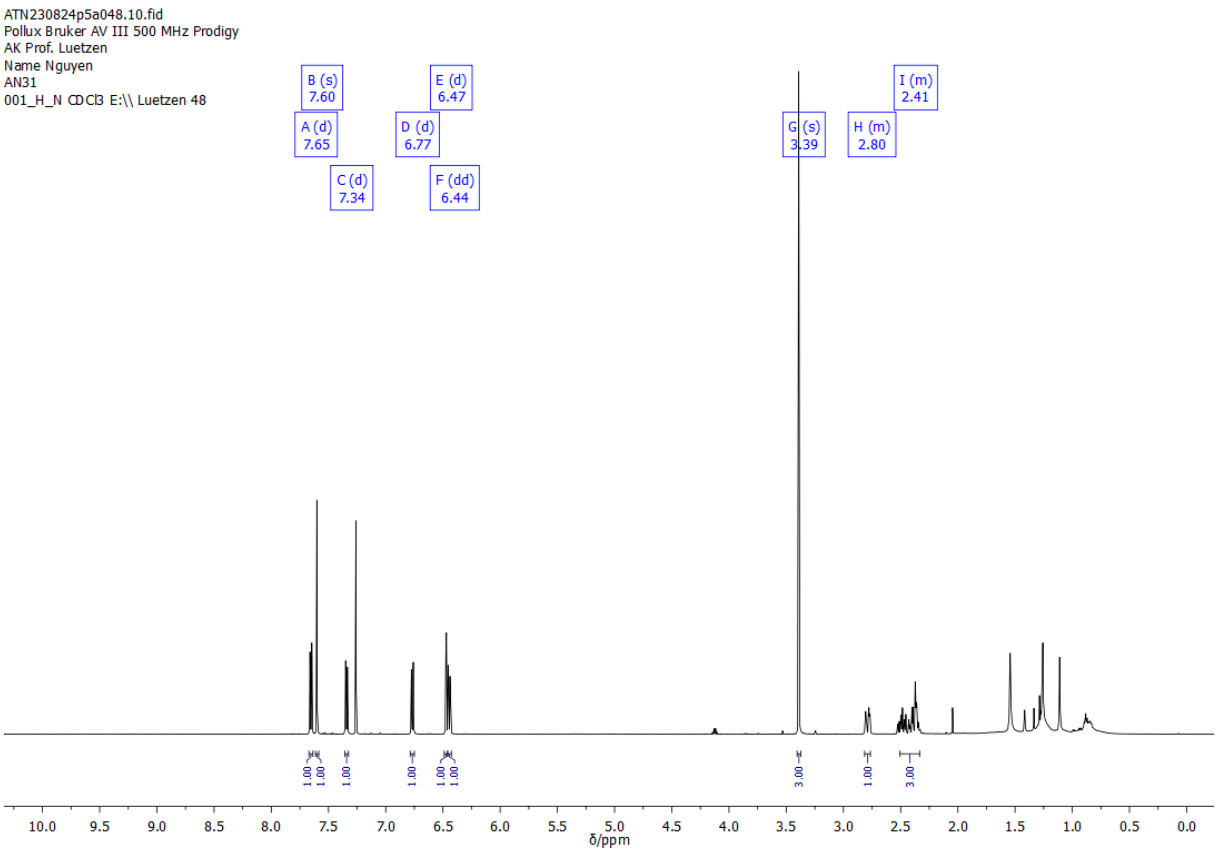

Figure 193: ^{1}H-NMR spectrum of **54** in $CDCl_3$.

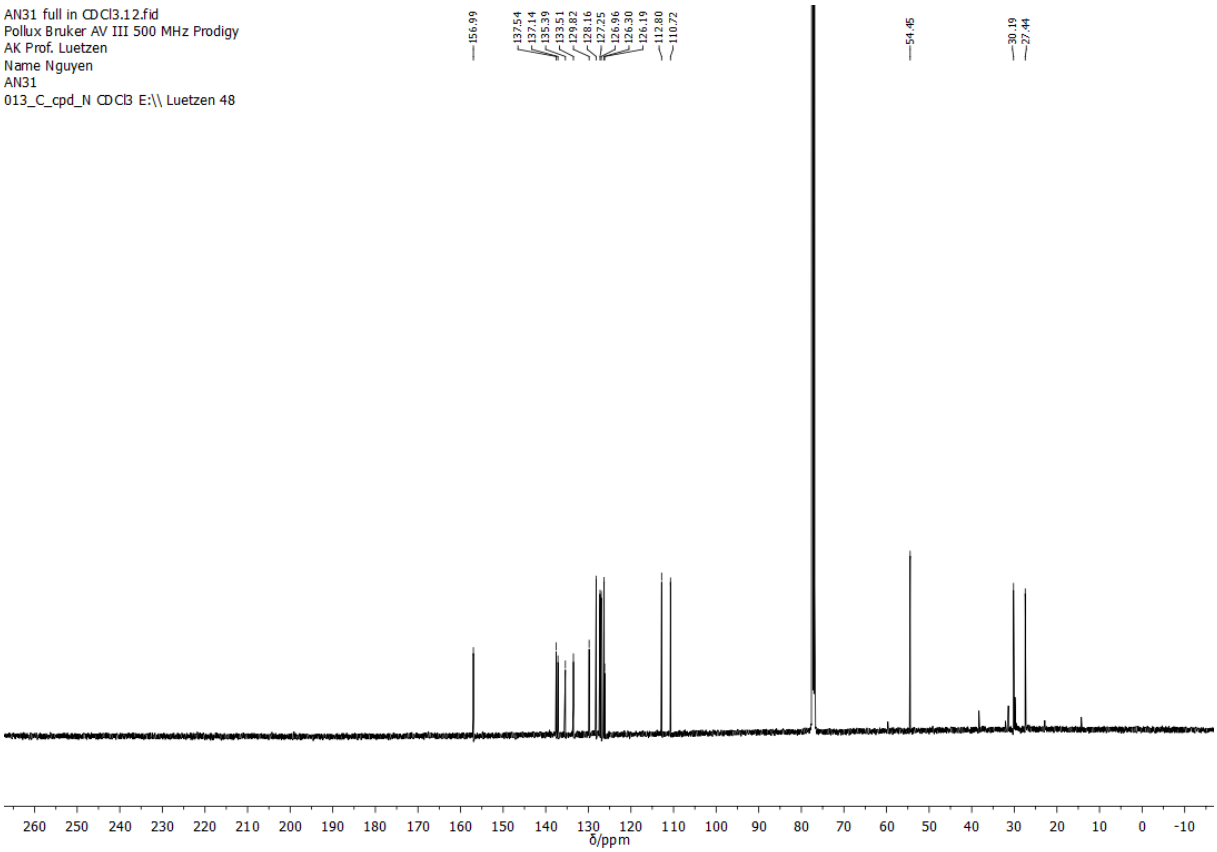

Figure 194: ^{13}C-NMR spectrum of **54** in $CDCl_3$.

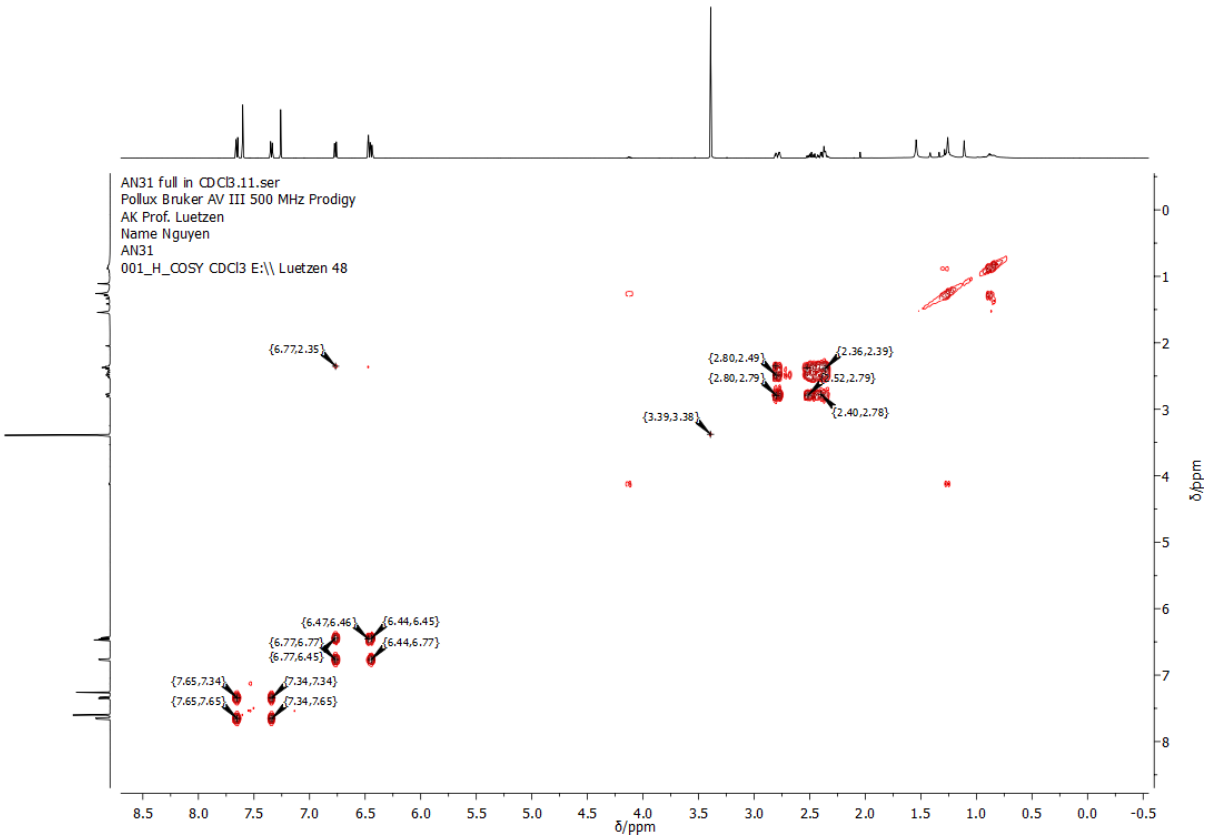

Figure 195: COSY-NMR spectrum of **54** in $CDCl_3$.

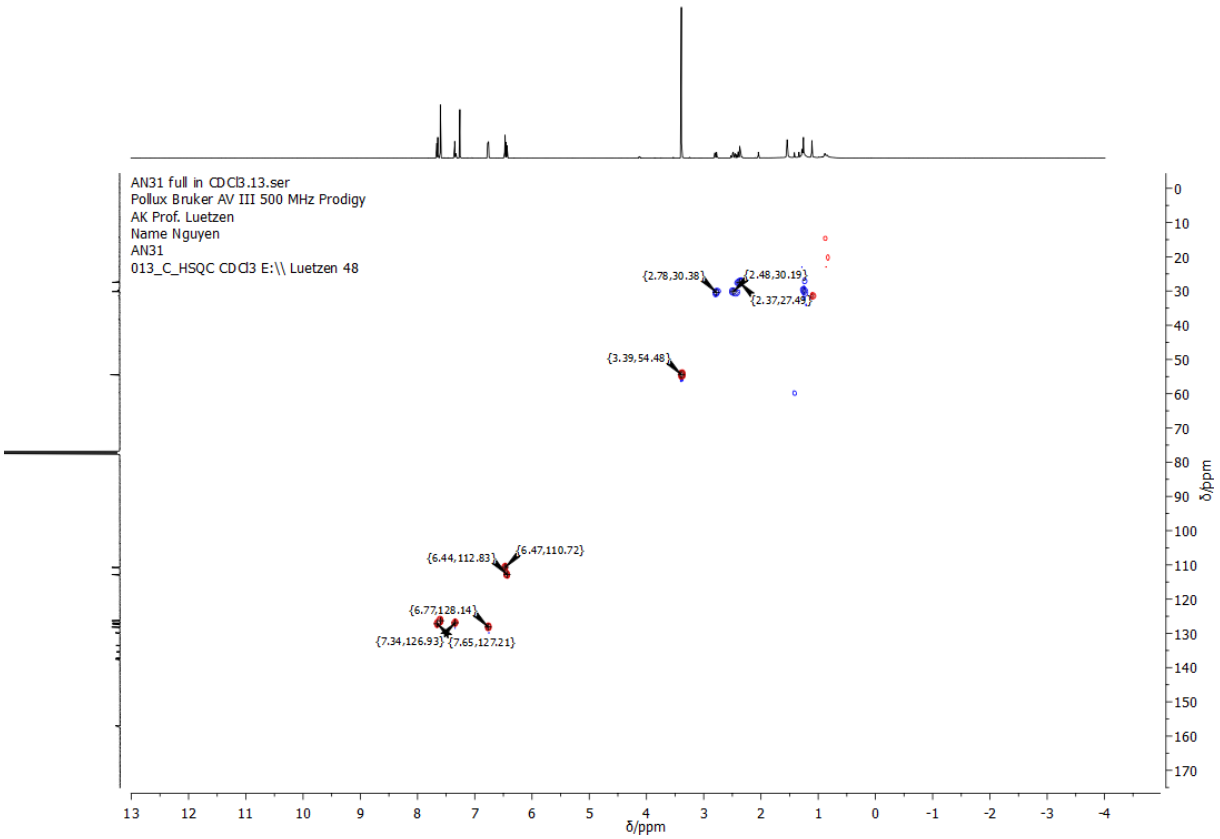

Figure 196: HSQC-NMR spectrum of **54** in $CDCl_3$.

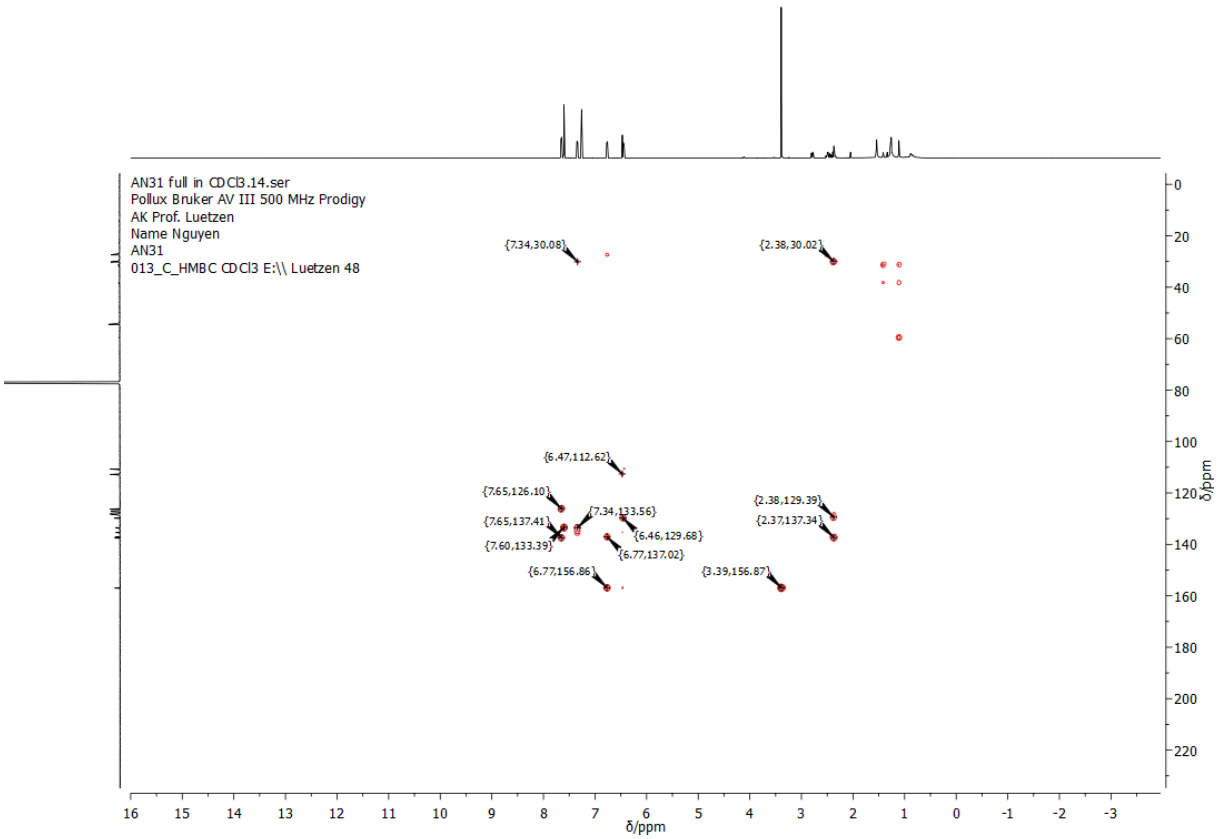

Figure 197: HMBC-NMR spectrum of **54** in $CDCl_3$.

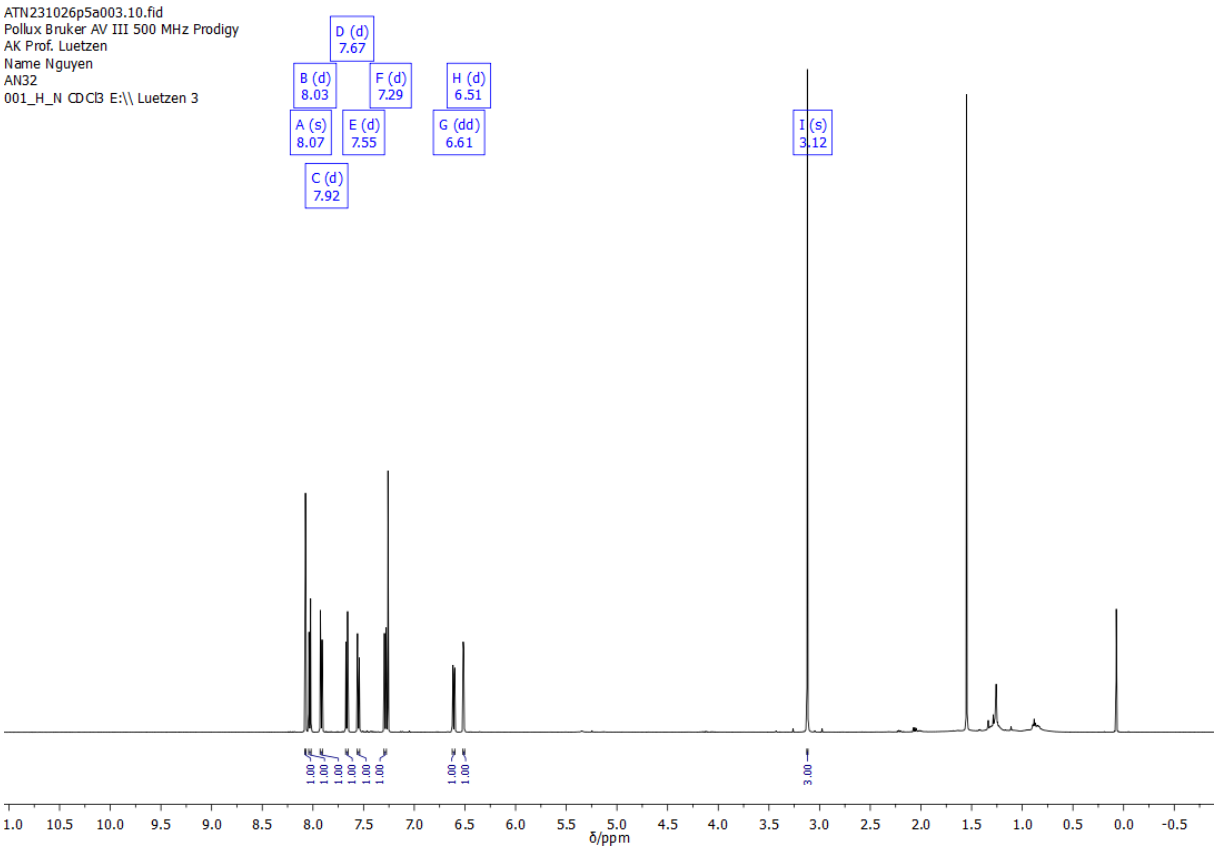

Figure 198: ^{1}H-NMR spectrum of **55** in $CDCl_3$.

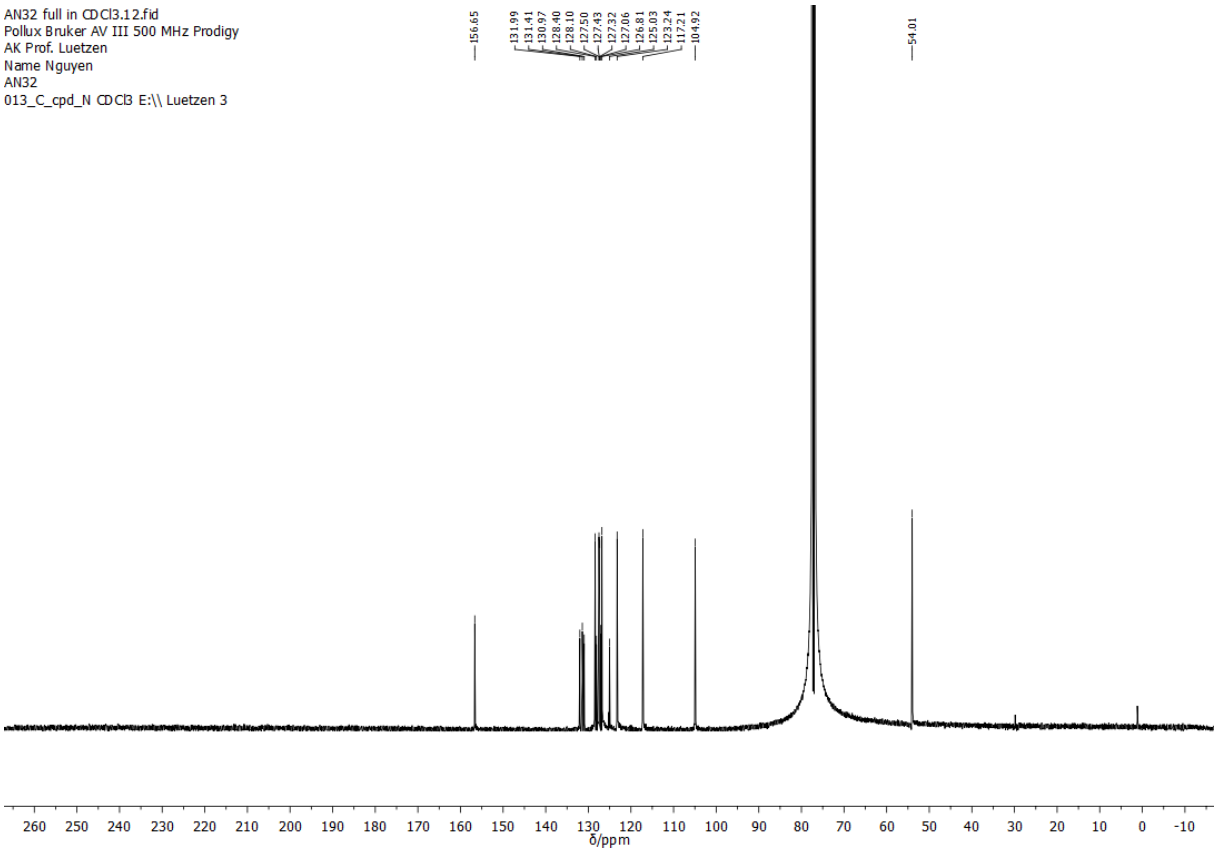

Figure 199: ^{13}C-NMR spectrum of **55** in $CDCl_3$.

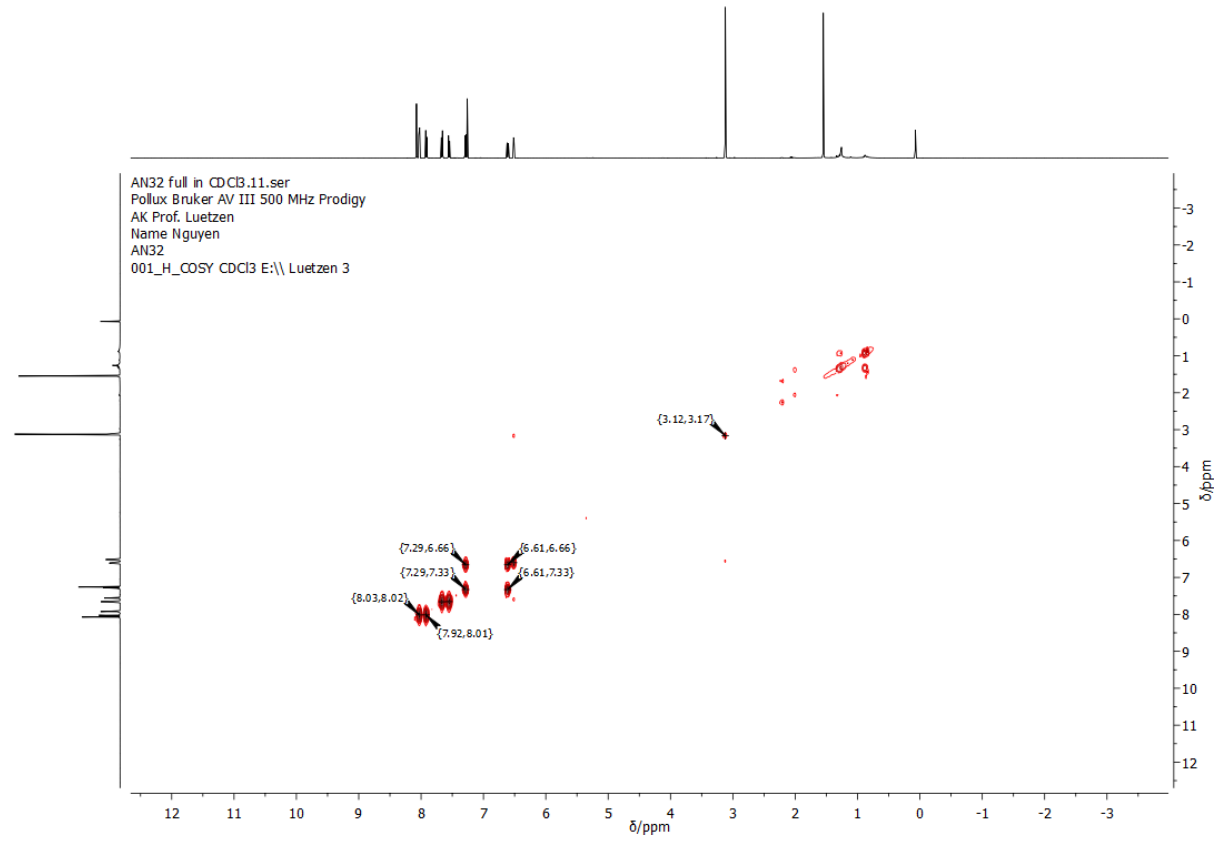

Figure 200: COSY-NMR spectrum of **55** in $CDCl_3$.

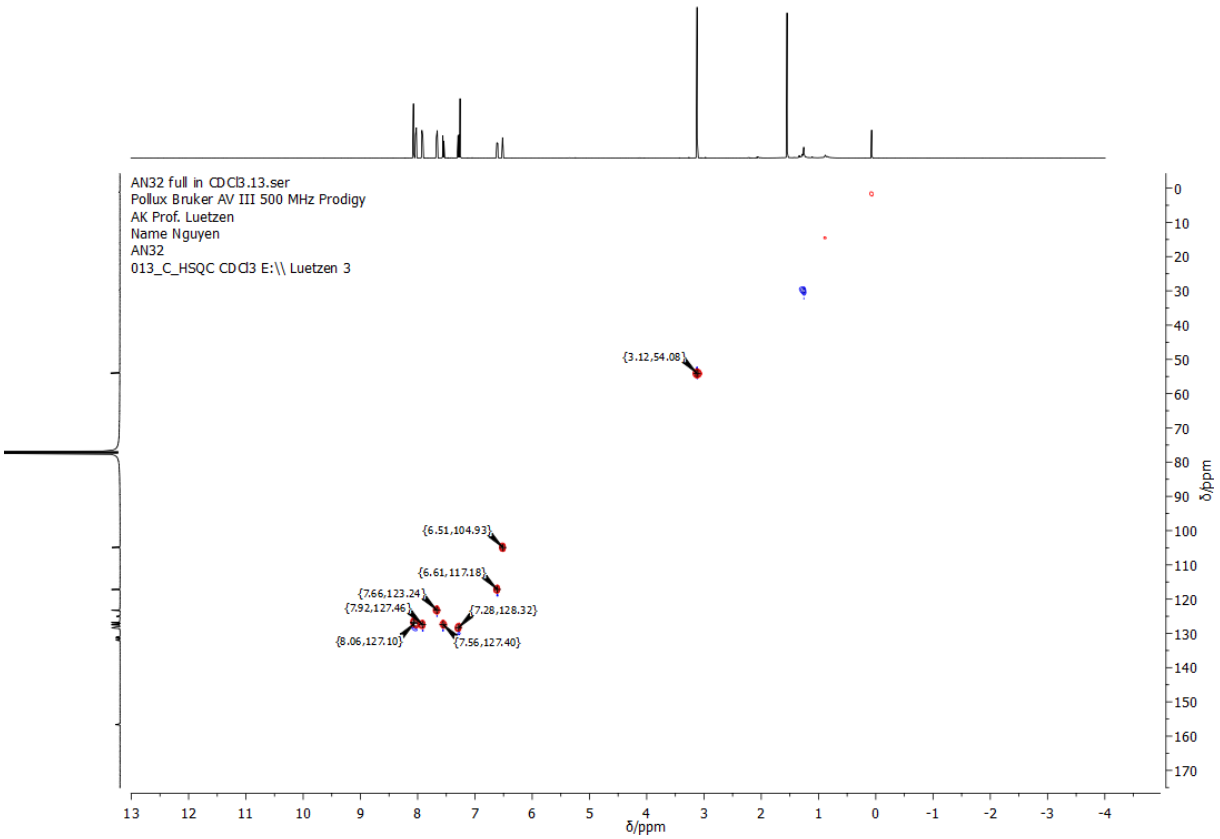

Figure 201: HSQC-NMR spectrum of **55** in $CDCl_3$.

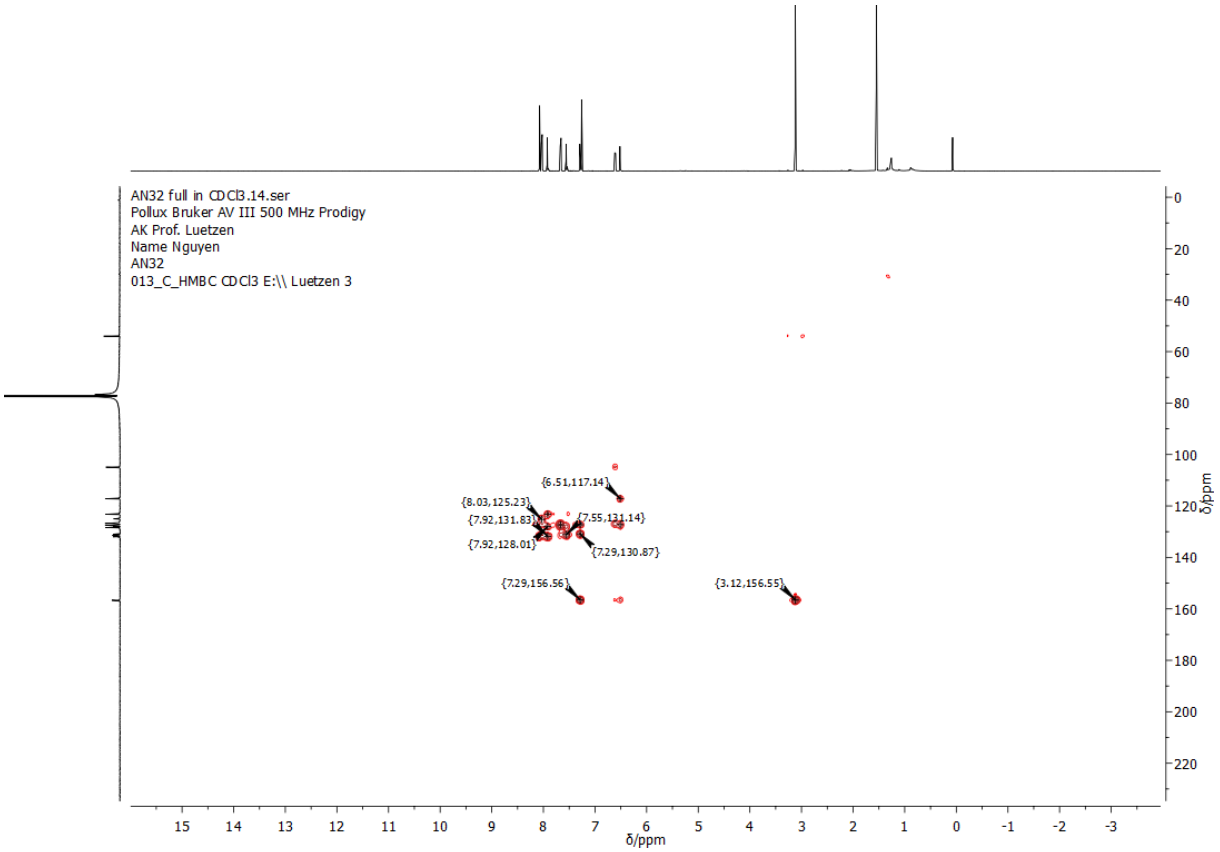

Figure 202: HMBC-NMR spectrum of **55** in $CDCl_3$.

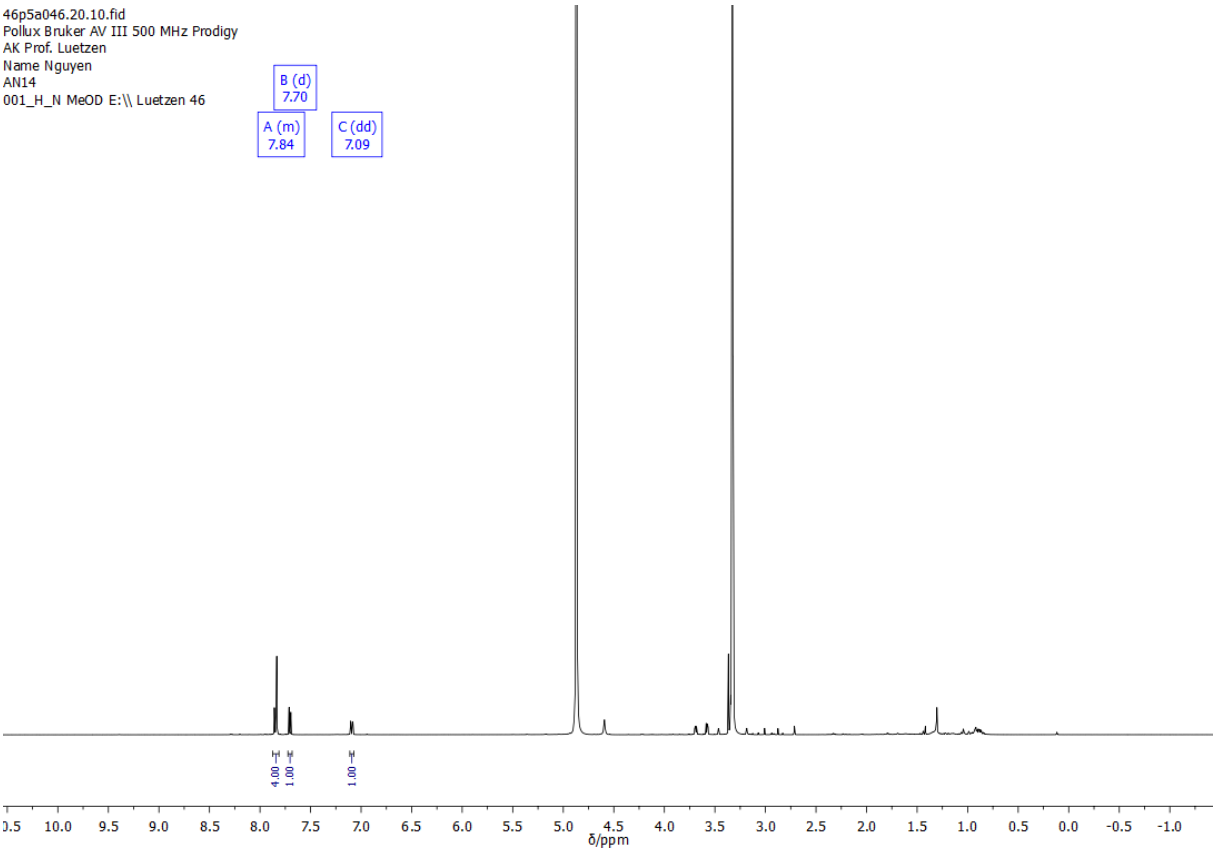

Figure 203: [1]H-NMR spectrum of **73** in MeOD.

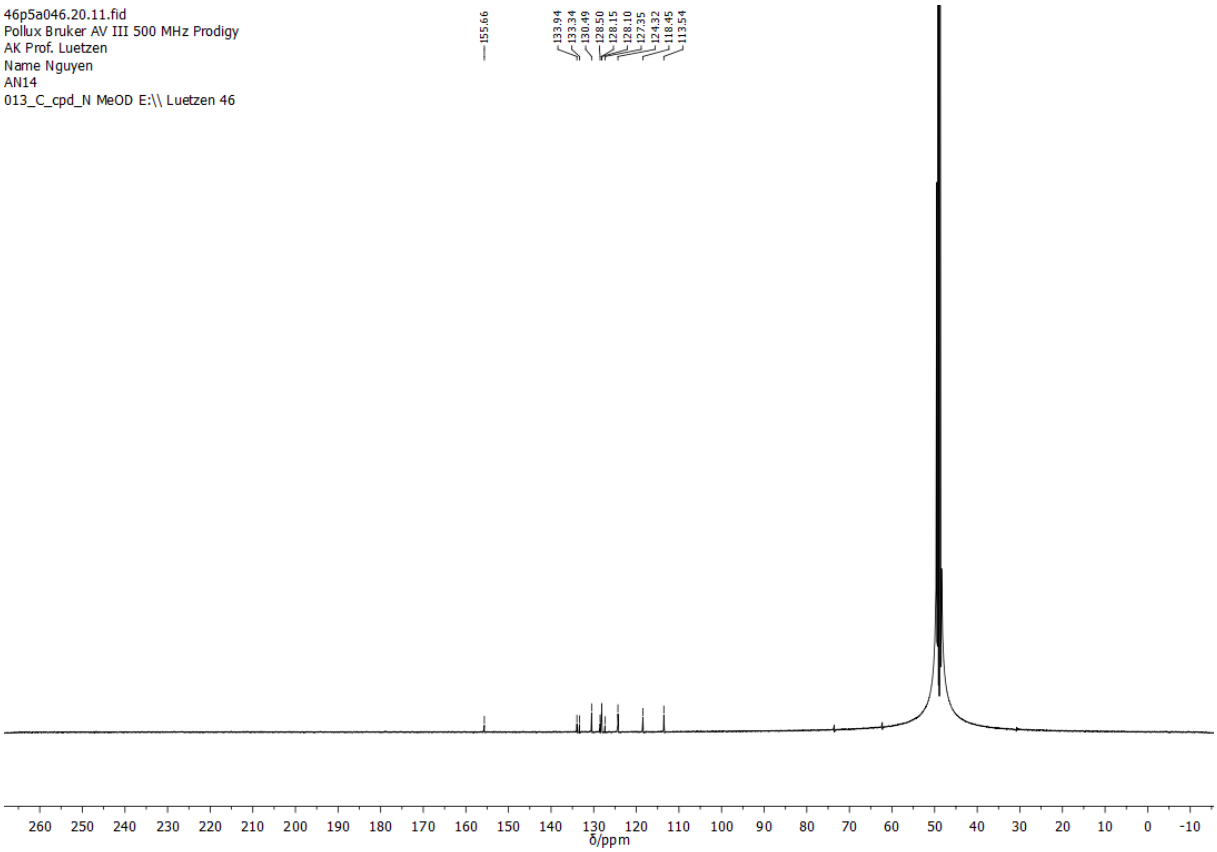

Figure 204: [13]C-NMR spectrum of **73** in MeOD.

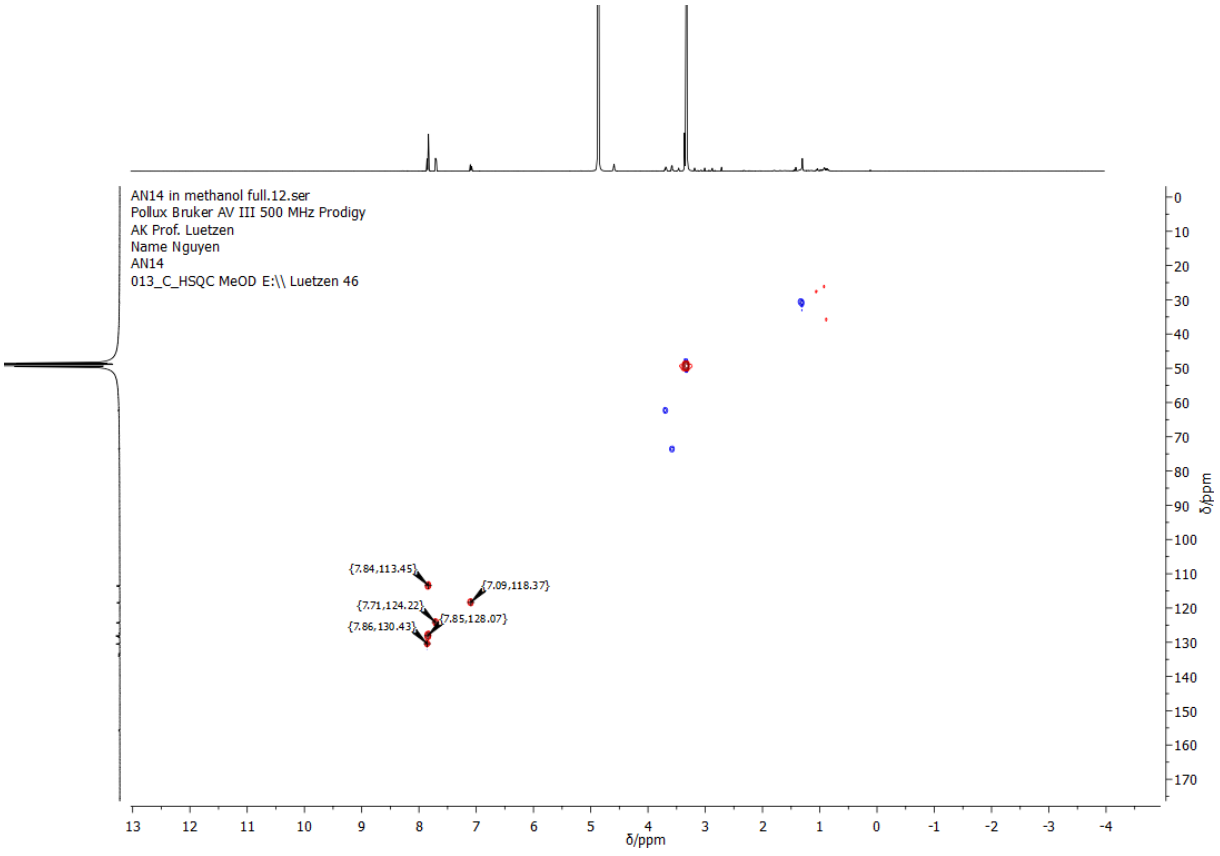

Figure 205: HSQC-NMR spectrum of **73** in MeOD.

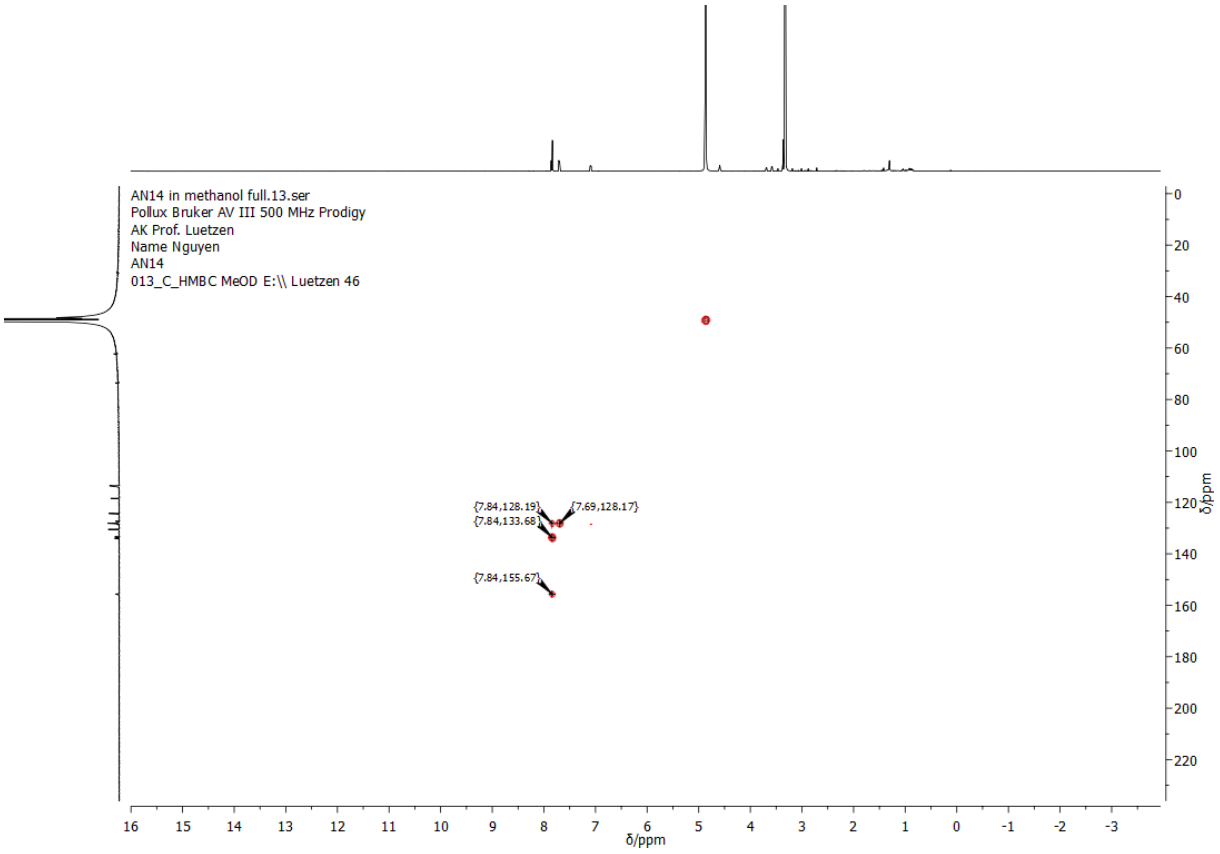

Figure 206: HMBC-NMR spectrum of **73** in MeOD.

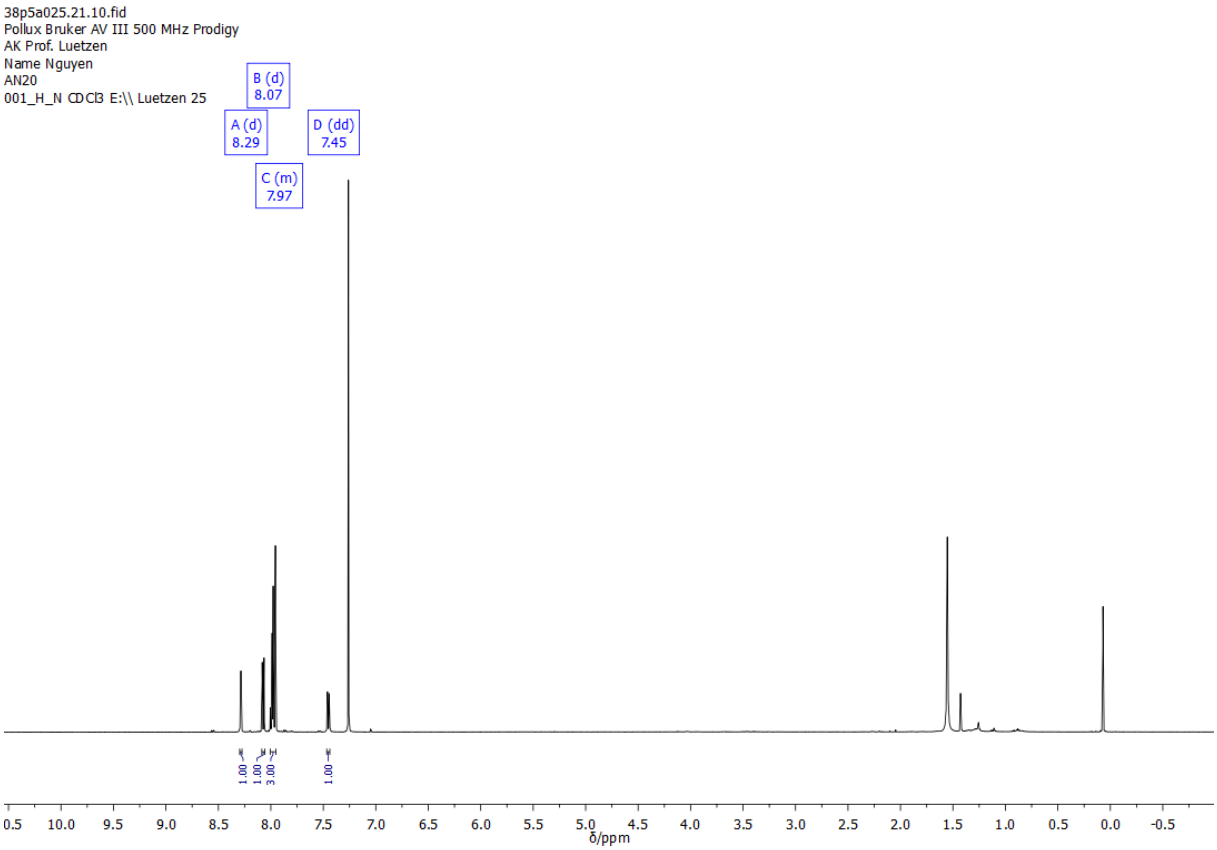

Figure 207: ^{1}H-NMR spectrum of **74** in $CDCl_3$.

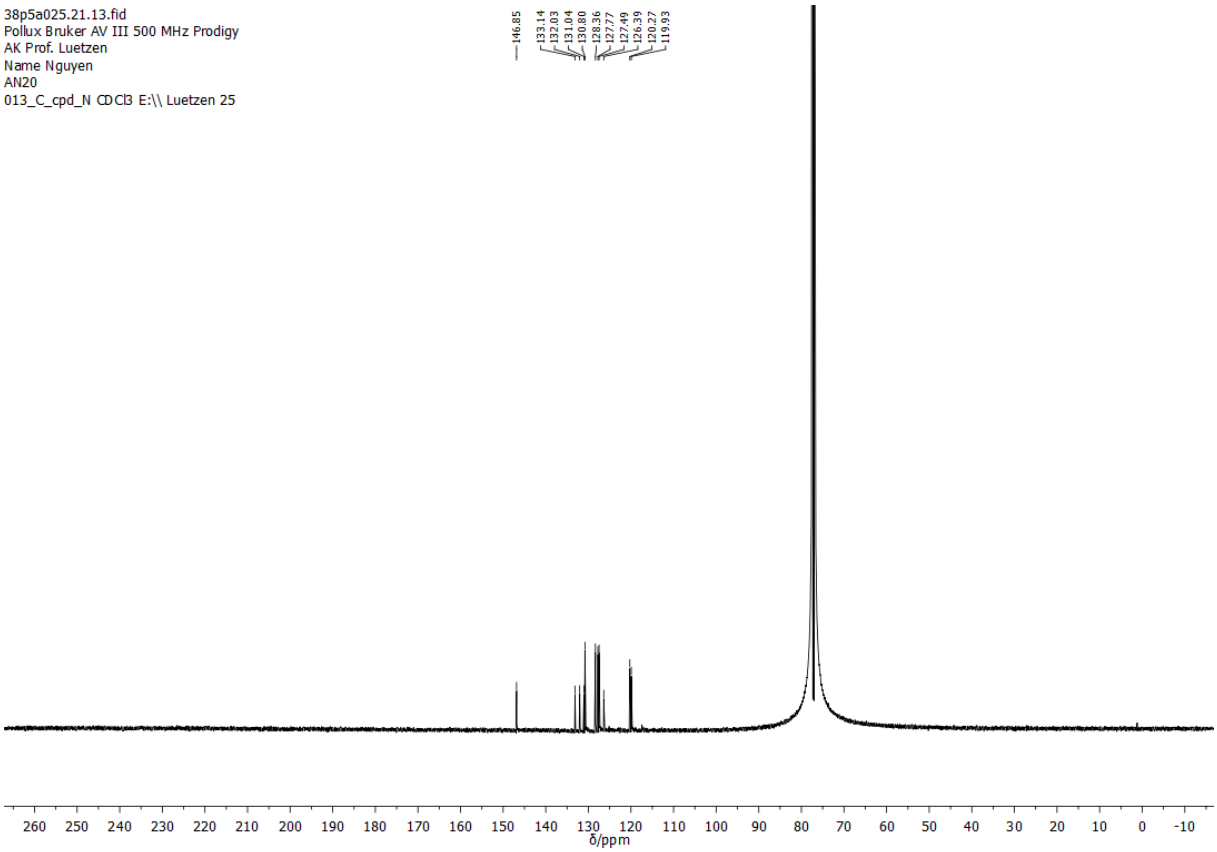

Figure 208: ^{13}C-NMR spectrum of **74** in $CDCl_3$.

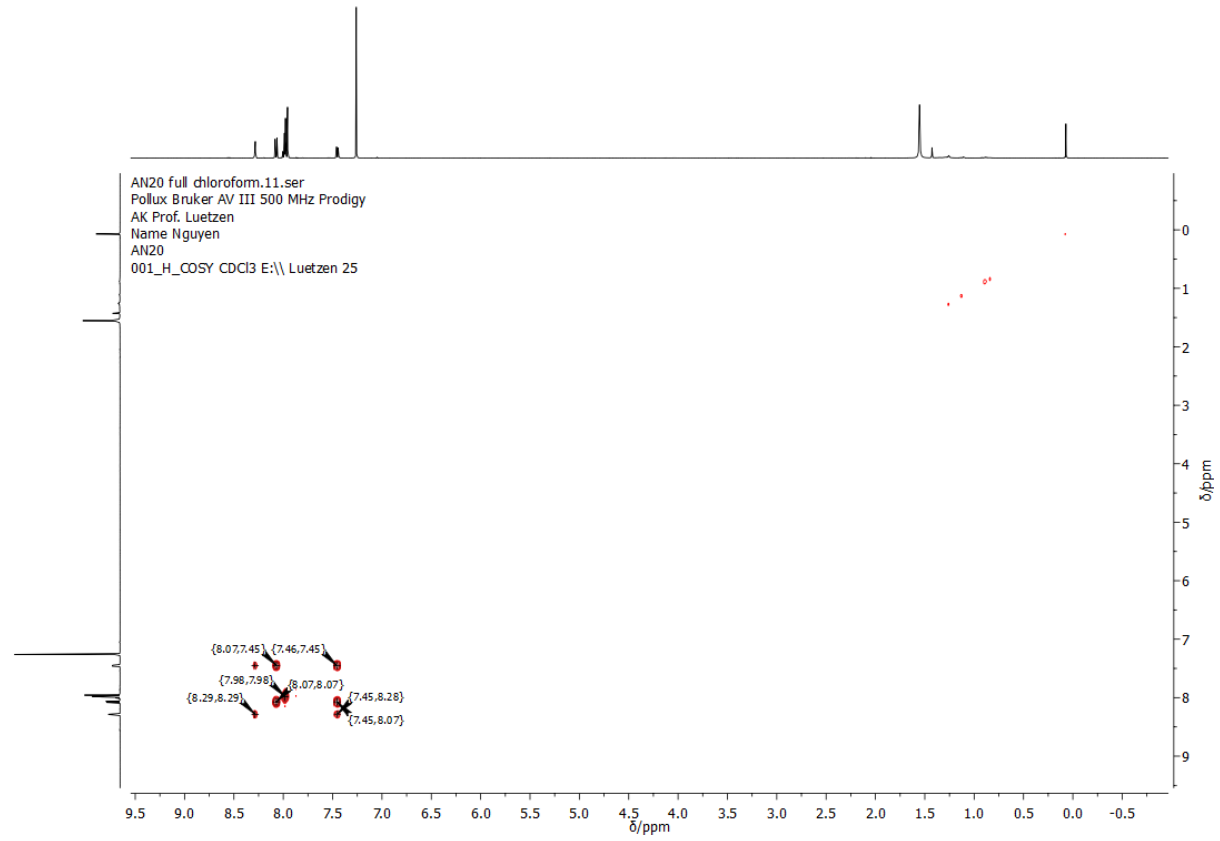

Figure 209: COSY-NMR spectrum of **74** in $CDCl_3$.

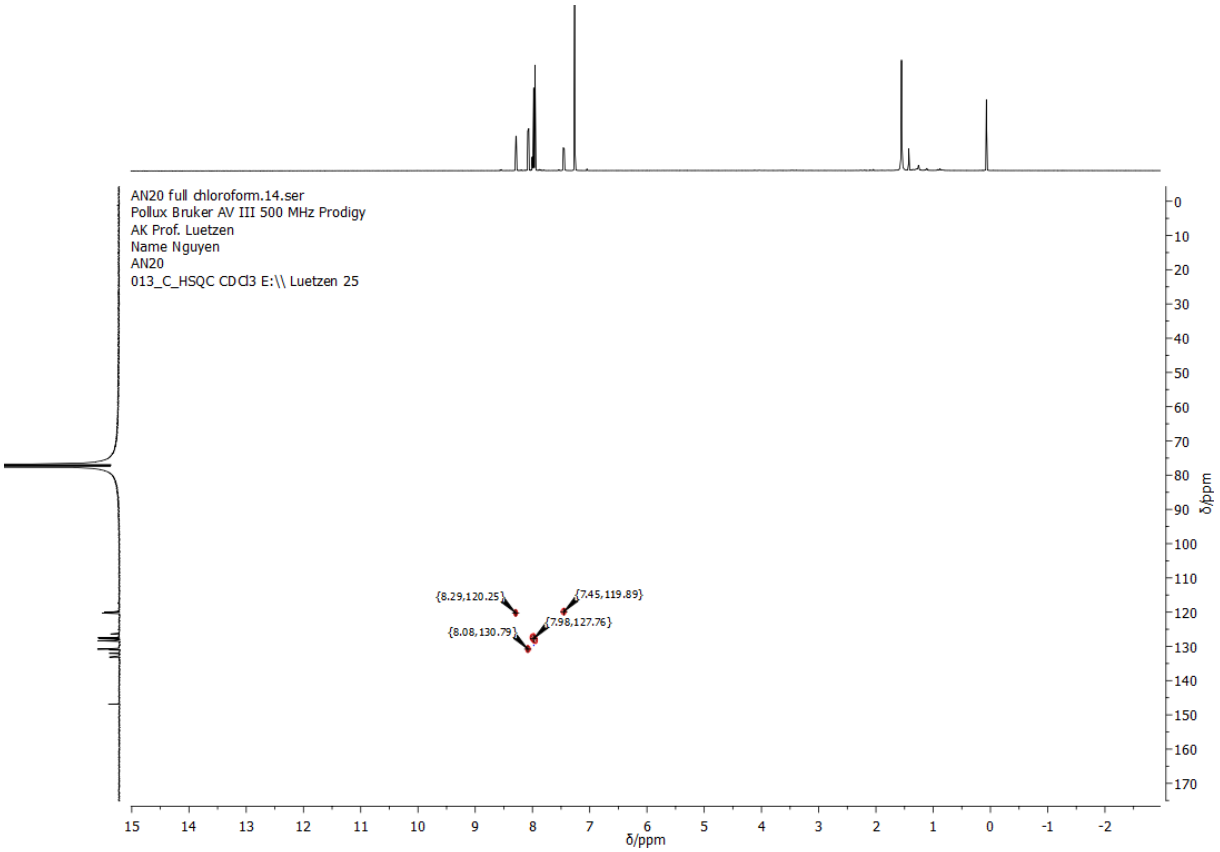

Figure 210: HSQC-NMR spectrum of **74** in $CDCl_3$.

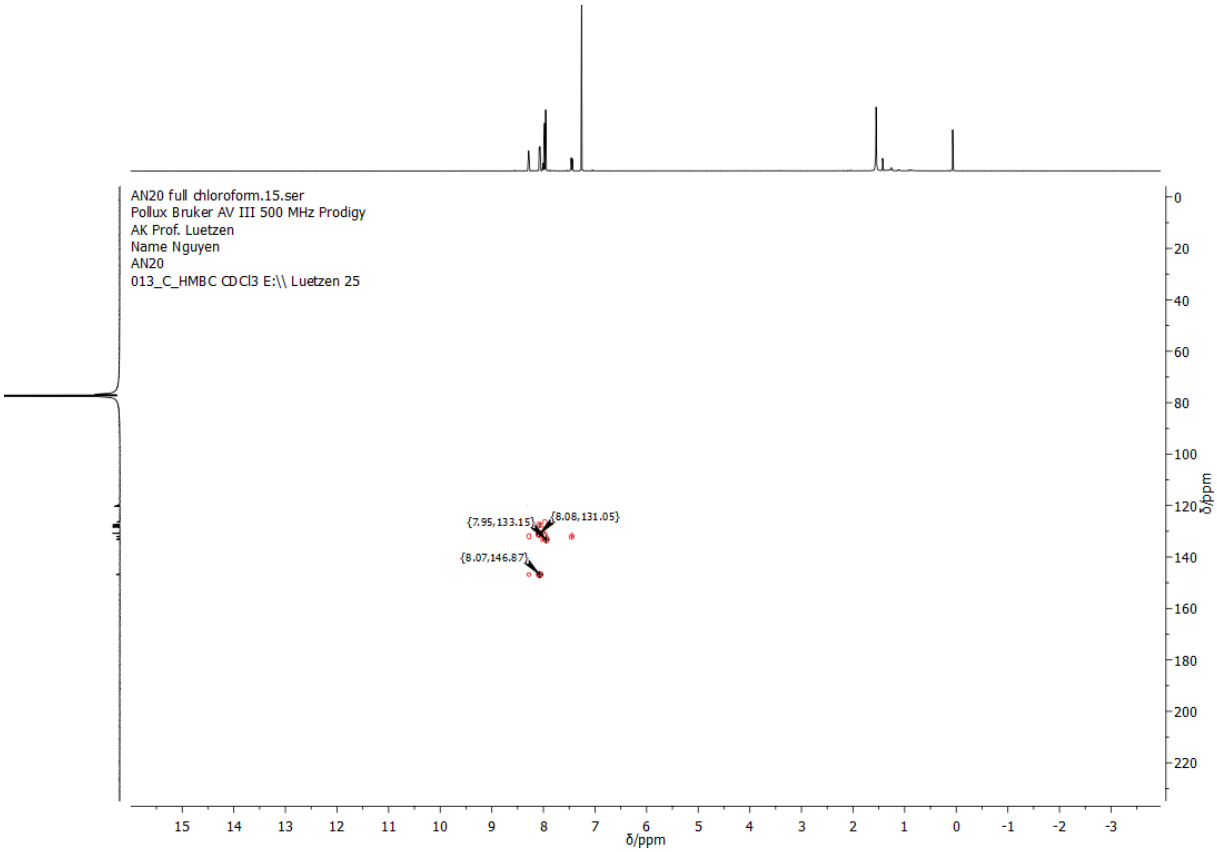

Figure 211: HMBC-NMR spectrum of **74** in $CDCl_3$.

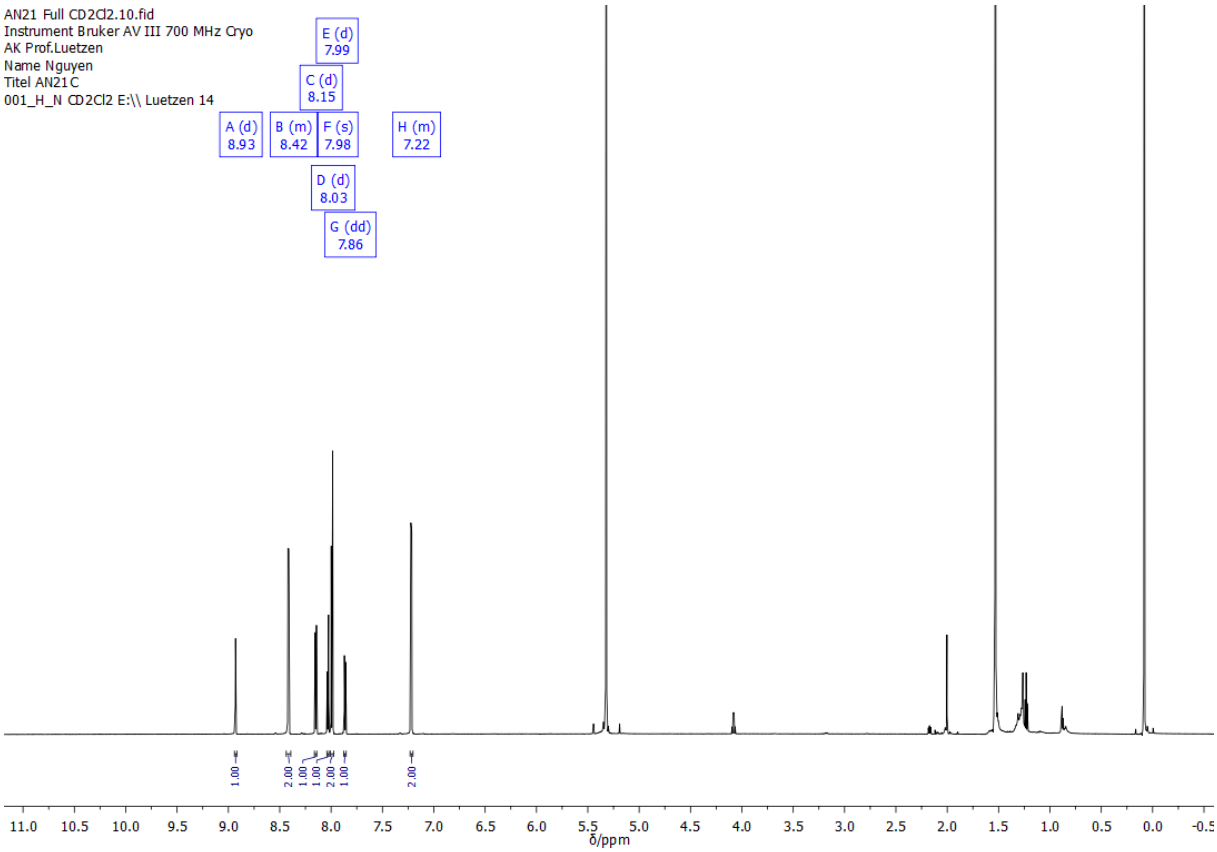

Figure 212: ^{1}H-NMR spectrum of **75** in CD_2Cl_2.

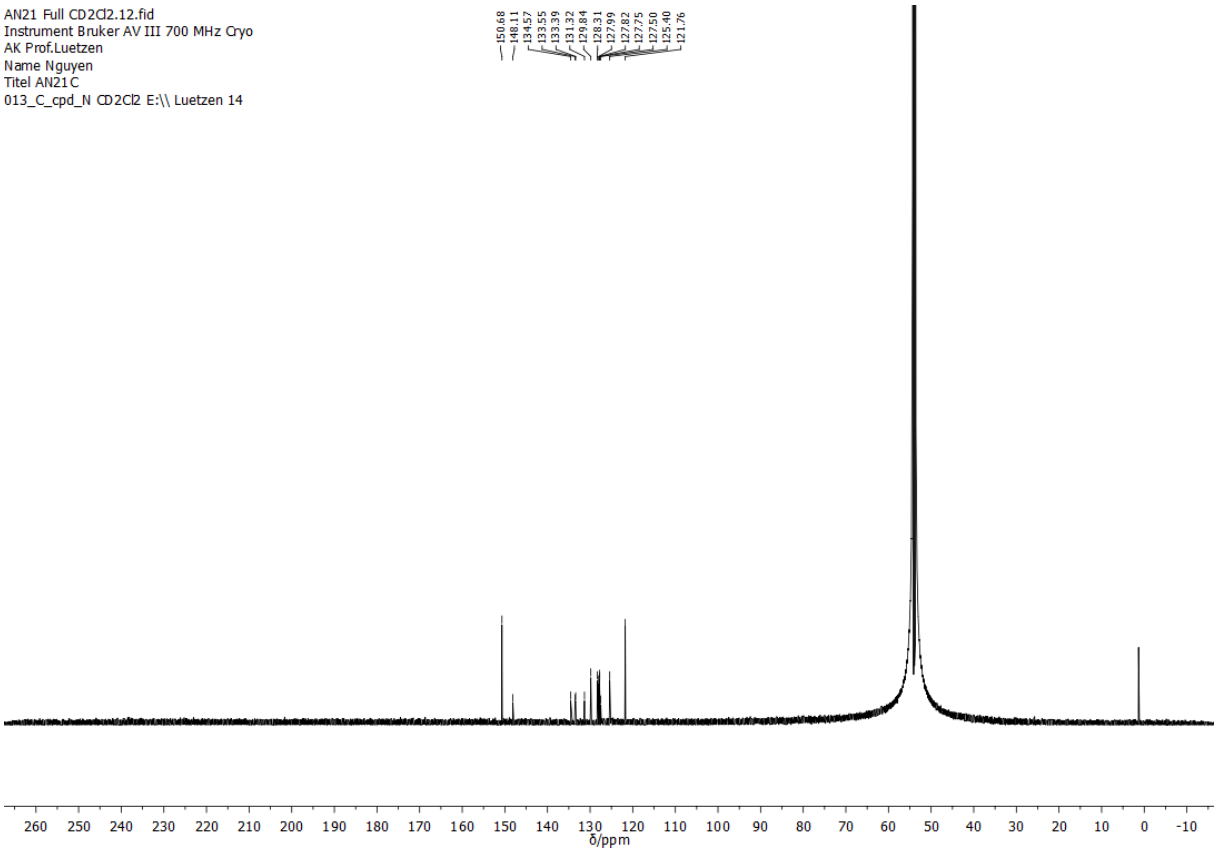

Figure 213: ^{13}C-NMR spectrum of **75** in CD_2Cl_2.

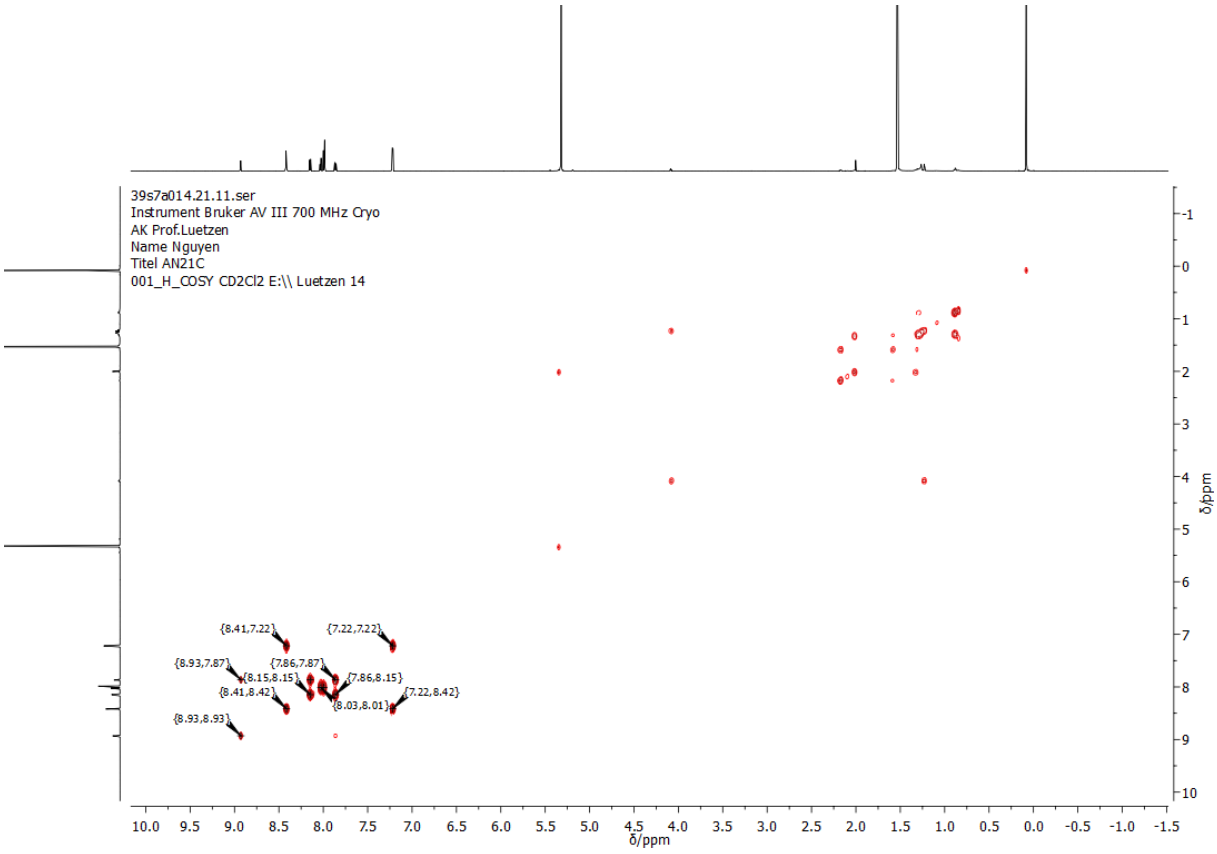

Figure 214: COSY-NMR spectrum of **75** in CD_2Cl_2.

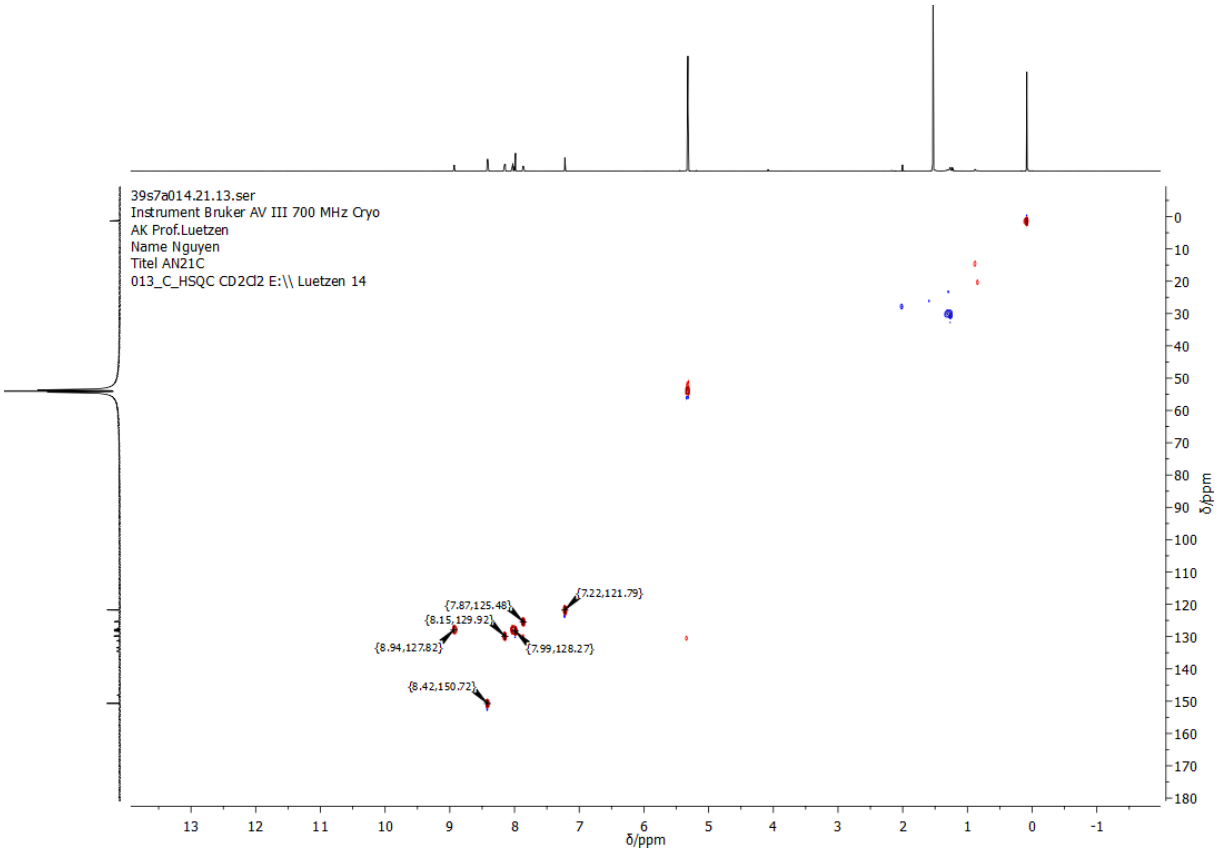

Figure 215: HSQC-NMR spectrum of **75** in CD_2Cl_2.

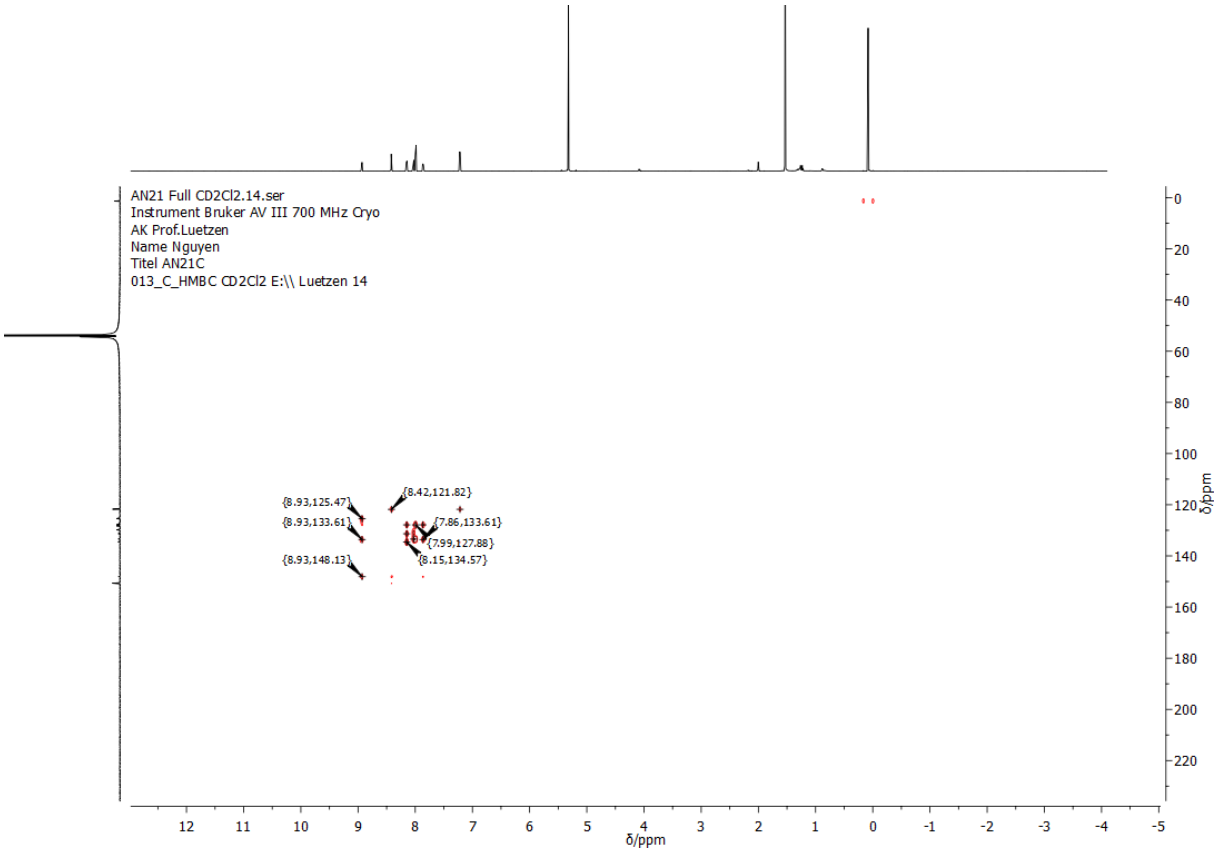

Figure 216: HMBC-NMR spectrum of **75** in CD_2Cl_2.

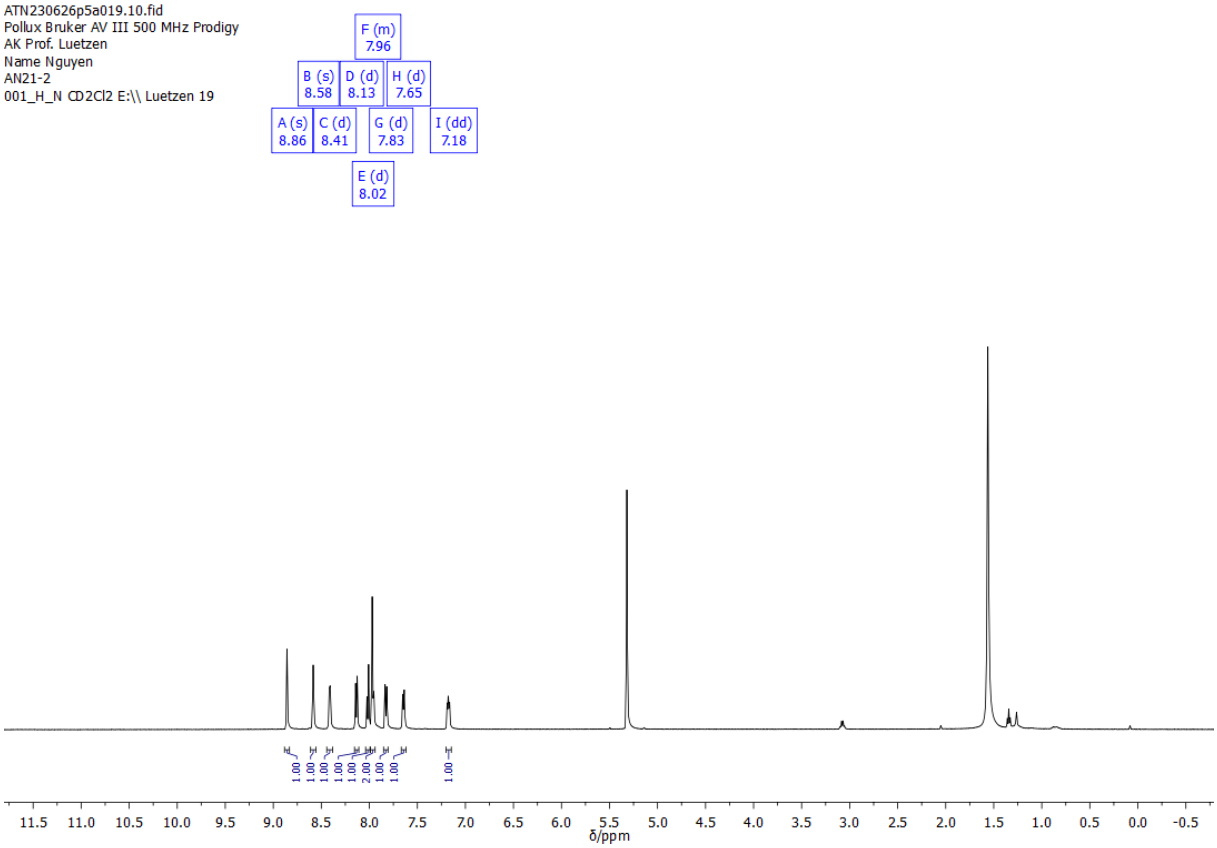

Figure 217: ^{1}H-NMR spectrum of **76** in CD_2Cl_2.

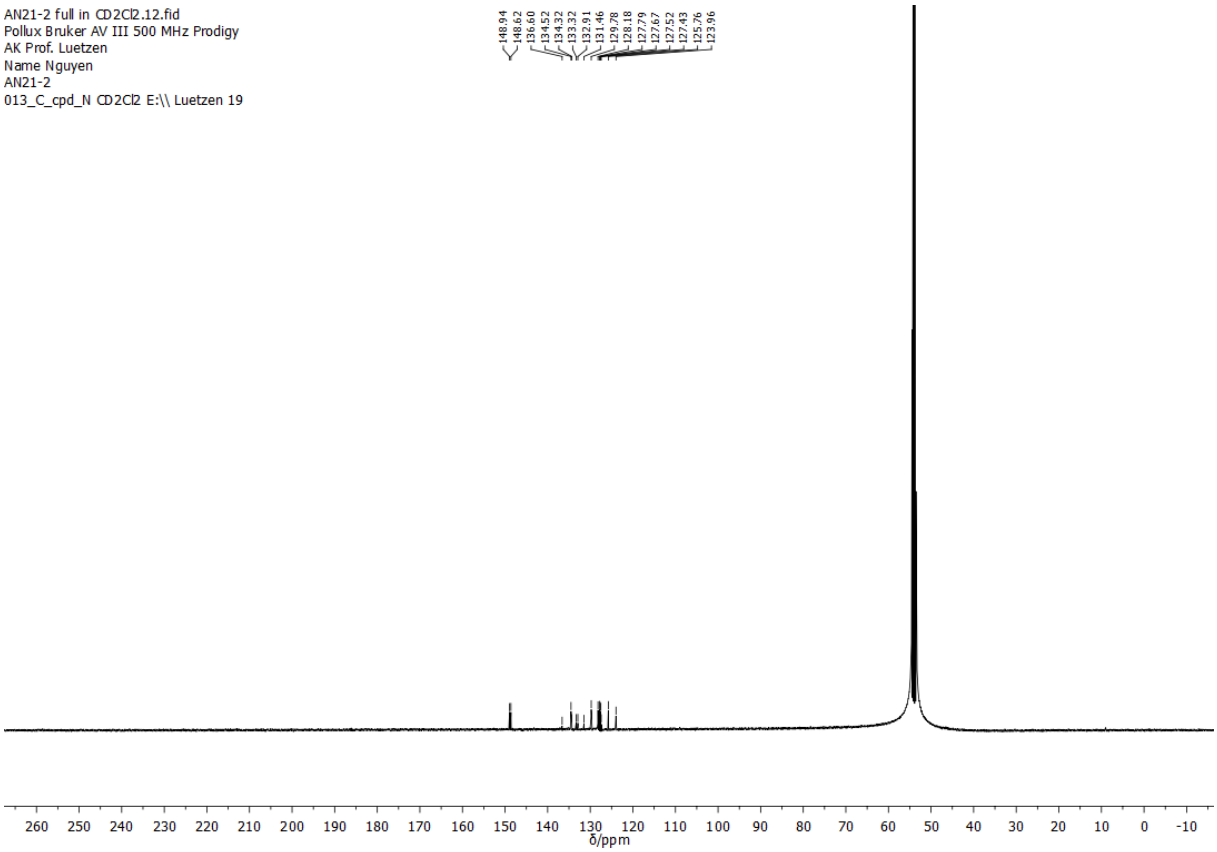

Figure 218: ^{13}C-NMR spectrum of **76** in CD_2Cl_2.

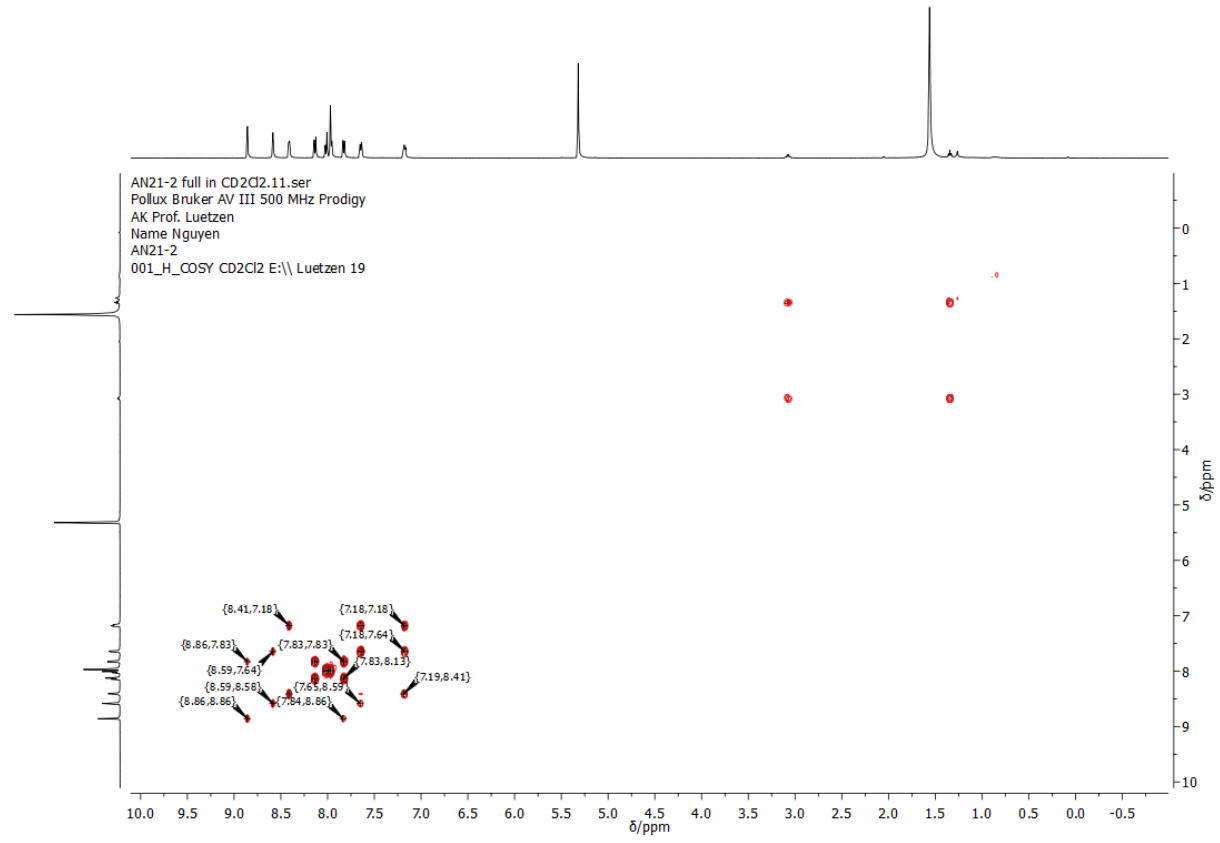

Figure 219: COSY-NMR spectrum of **76** in CD_2Cl_2.

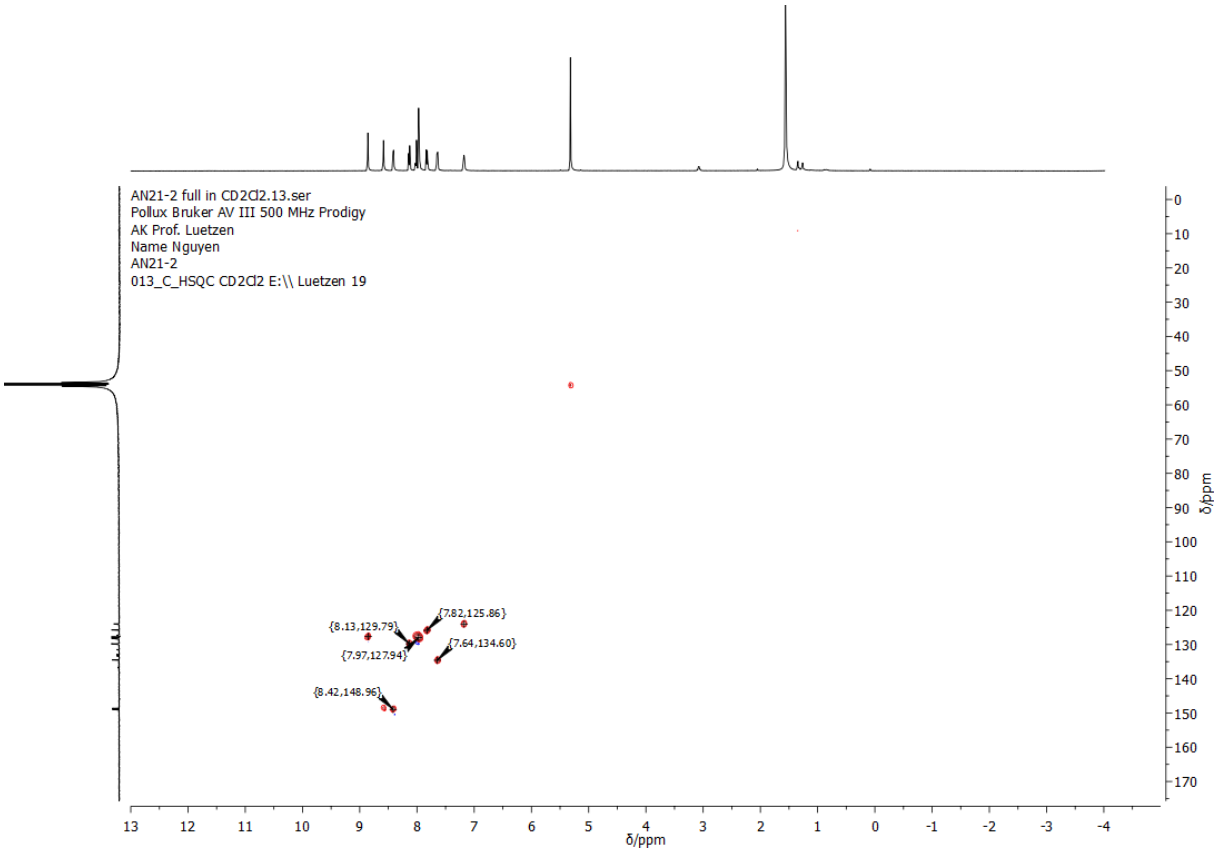

Figure 220: HSQC-NMR spectrum of **76** in CD_2Cl_2.

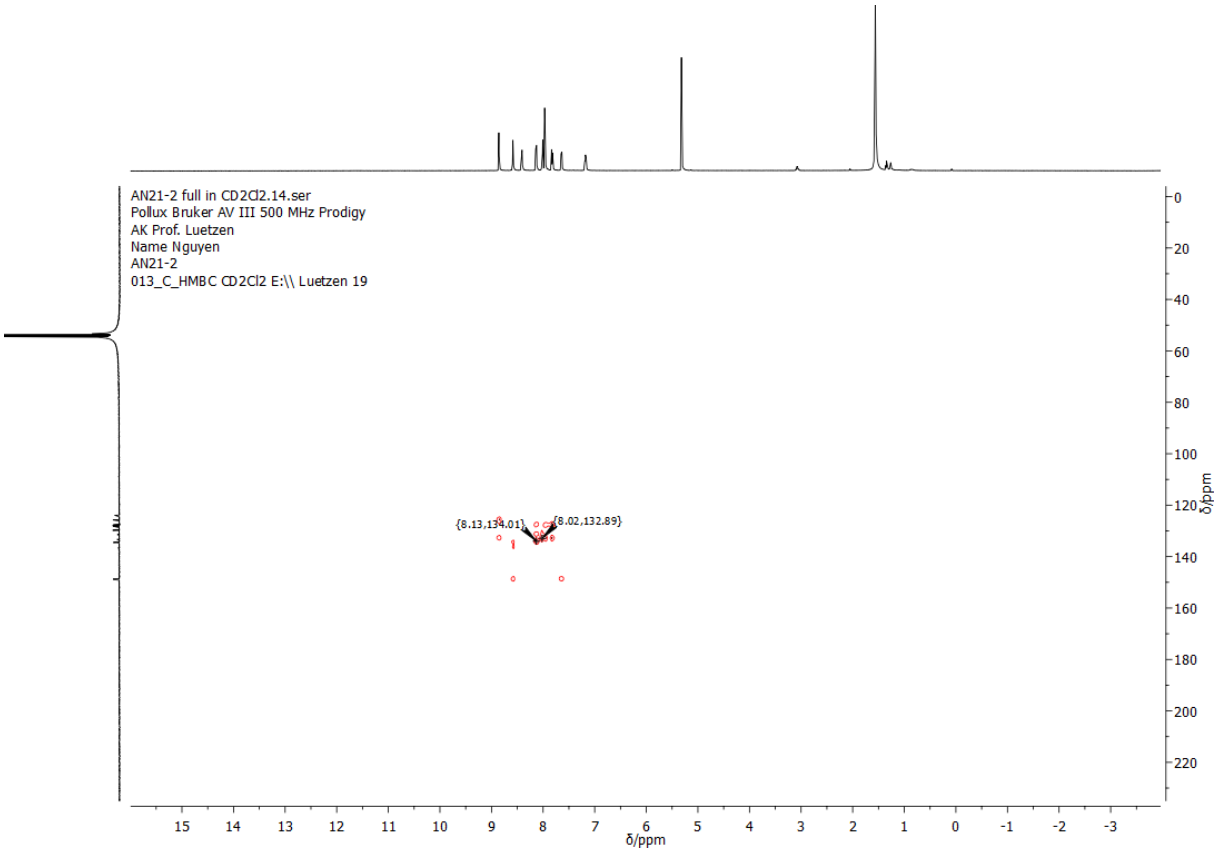

Figure 221: HMBC-NMR spectrum of **76** in CD_2Cl_2.

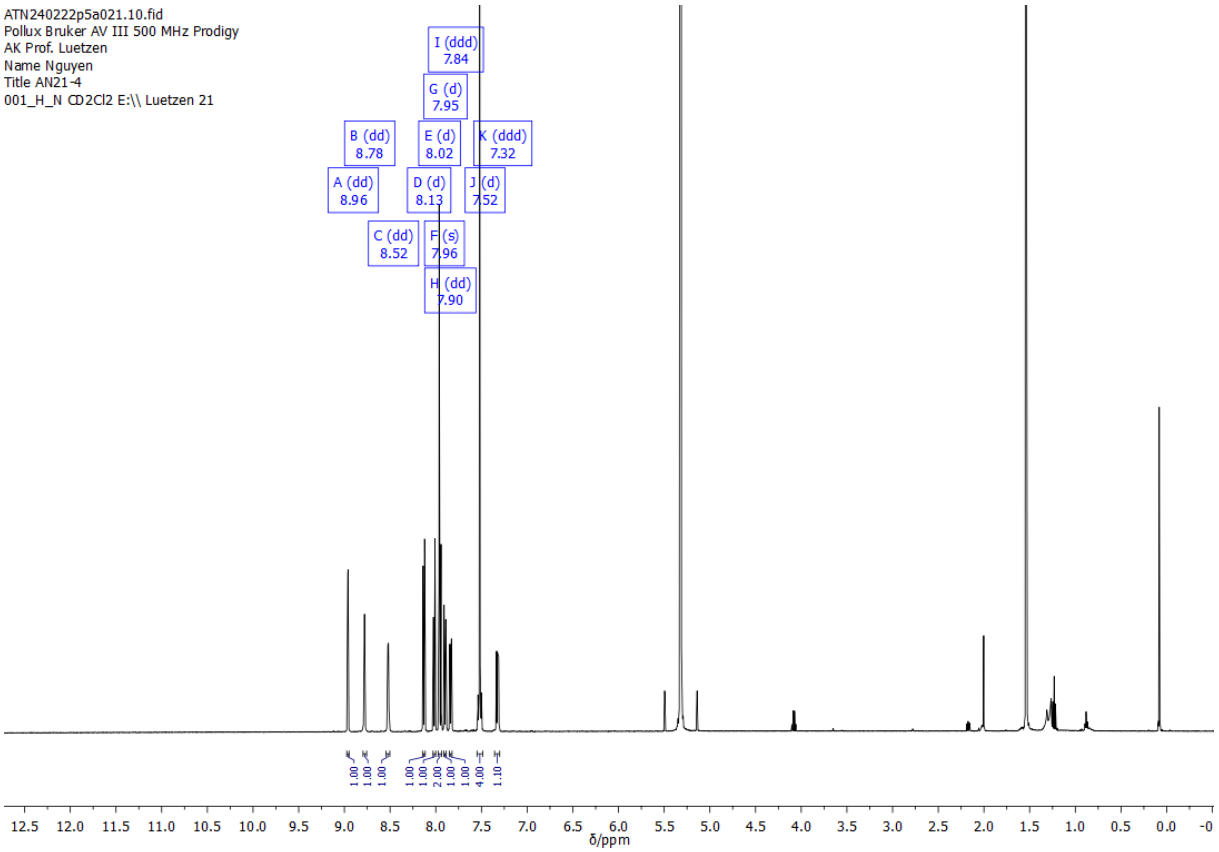

Figure 222: ^{1}H-NMR spectrum of **78** in CD_2Cl_2.

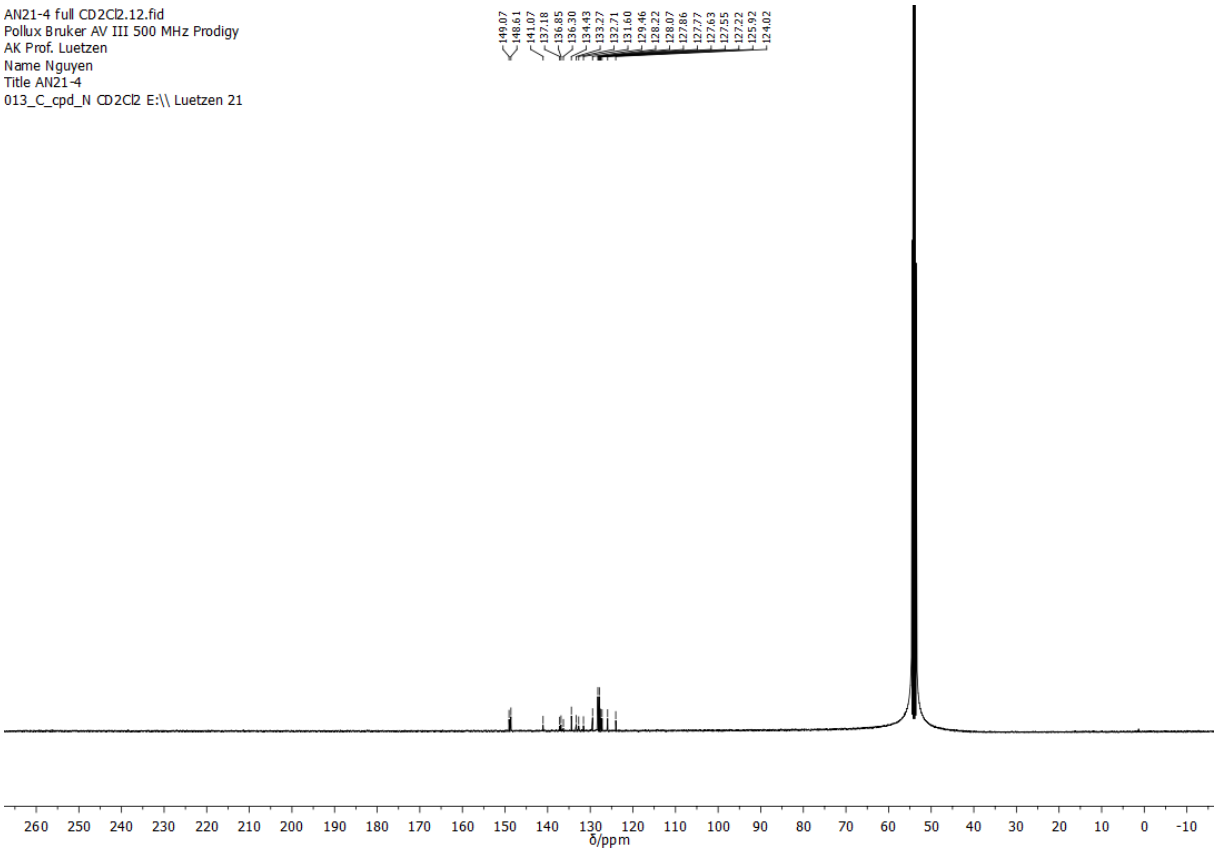

Figure 223: ^{13}C-NMR spectrum of **78** in CD_2Cl_2.

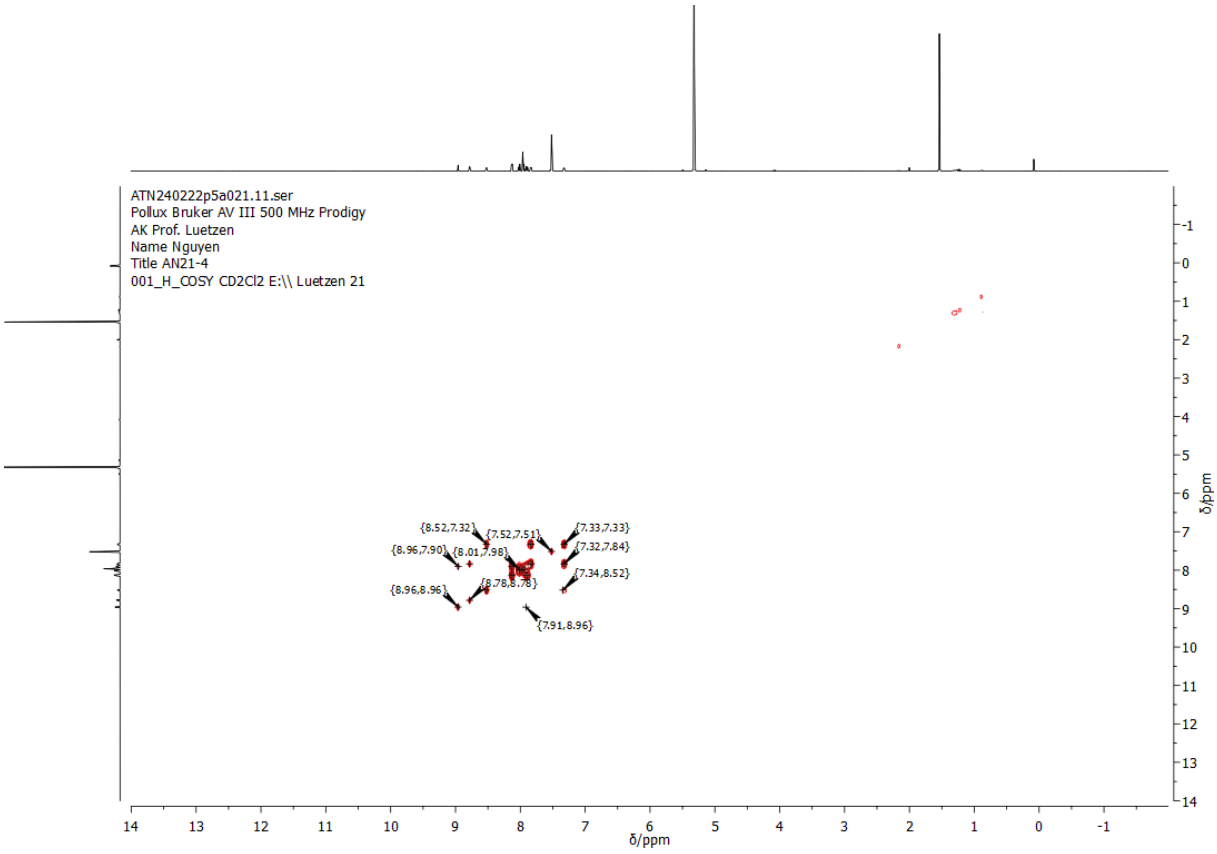

Figure 224: COSY-NMR spectrum of **78** in CD_2Cl_2.

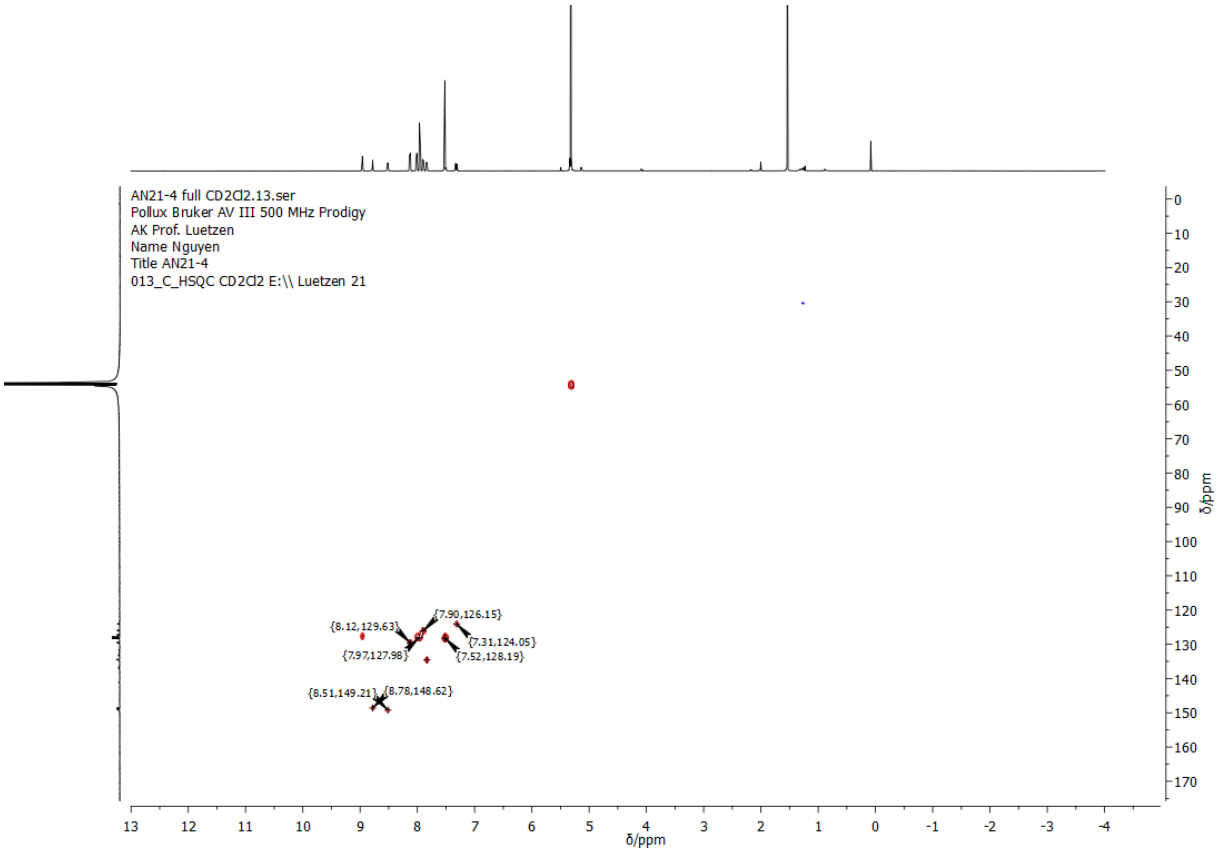

Figure 225: HSQC-NMR spectrum of **78** in CD_2Cl_2.

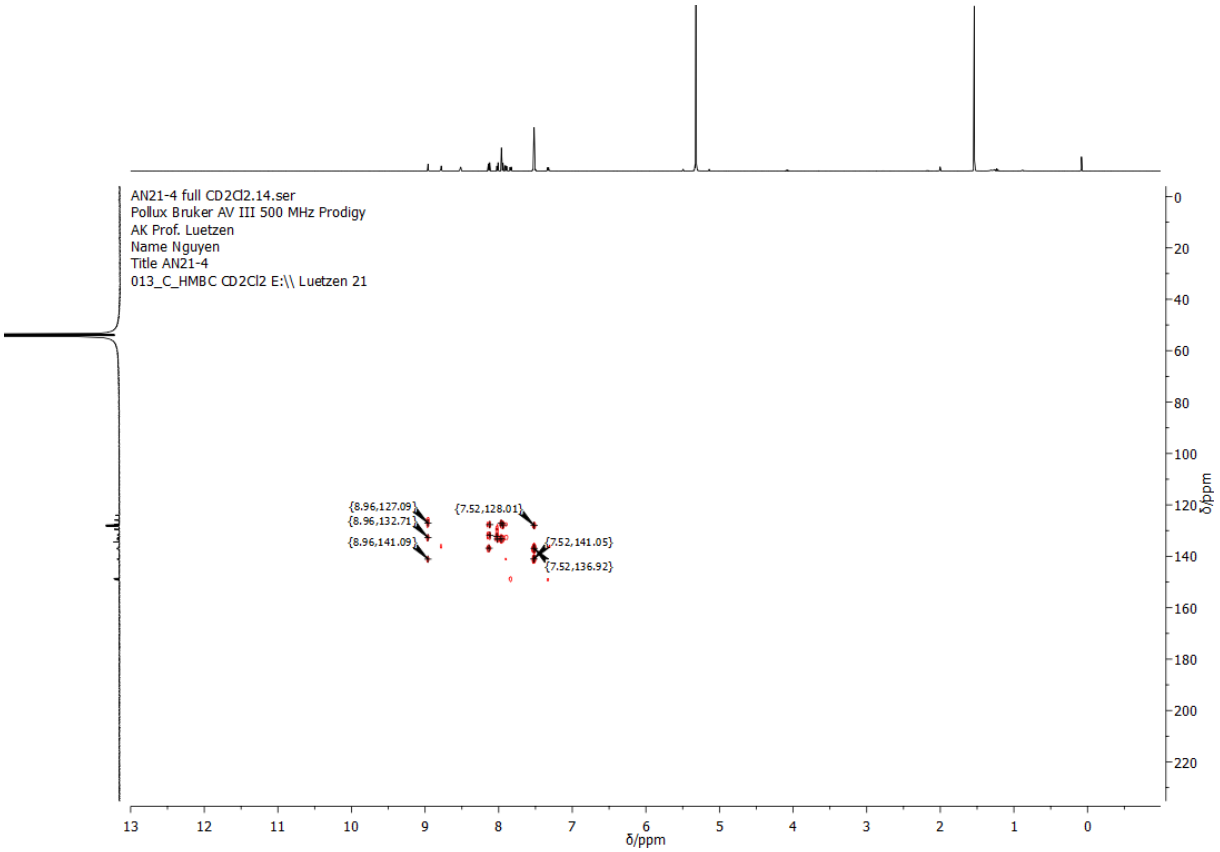

Figure 226: HMBC-NMR spectrum of **78** in CD_2Cl_2.

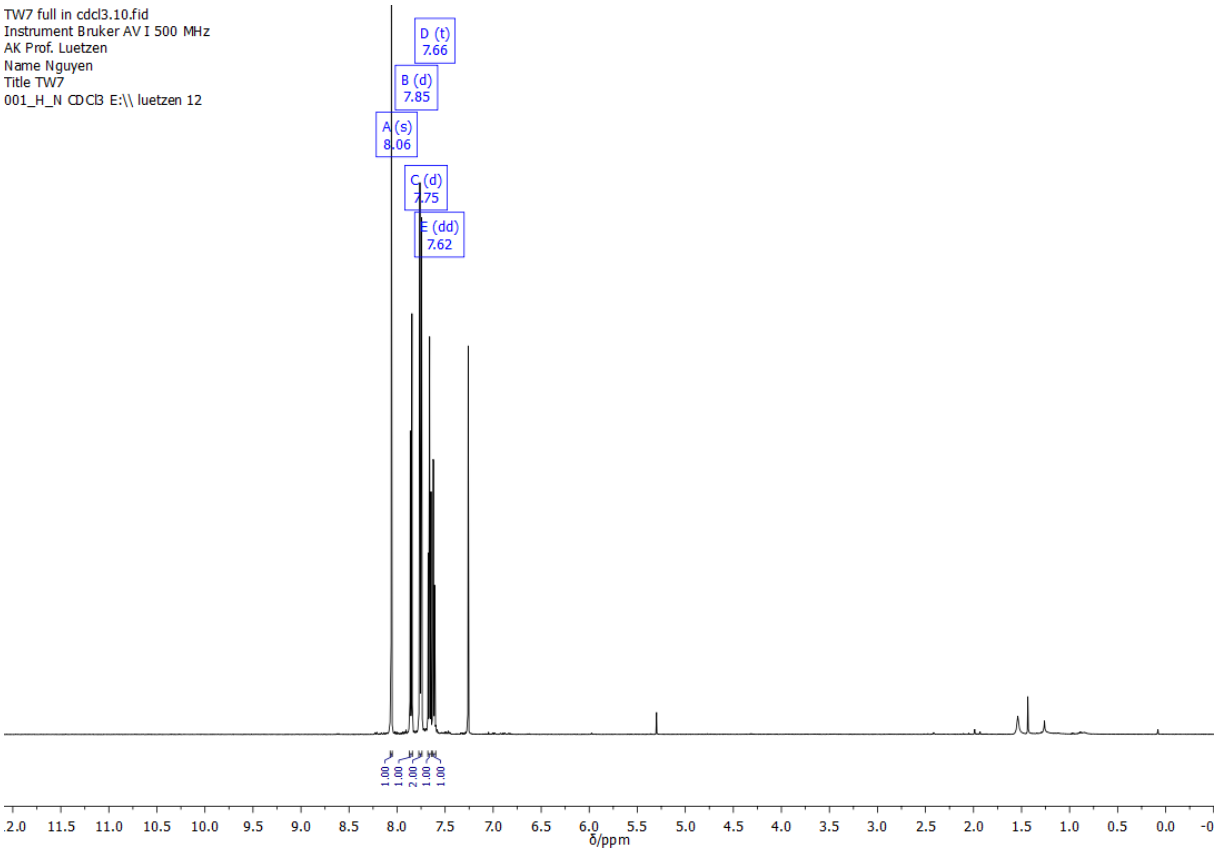

Figure 227: ^{1}H-NMR spectrum of **80** in $CDCl_3$.

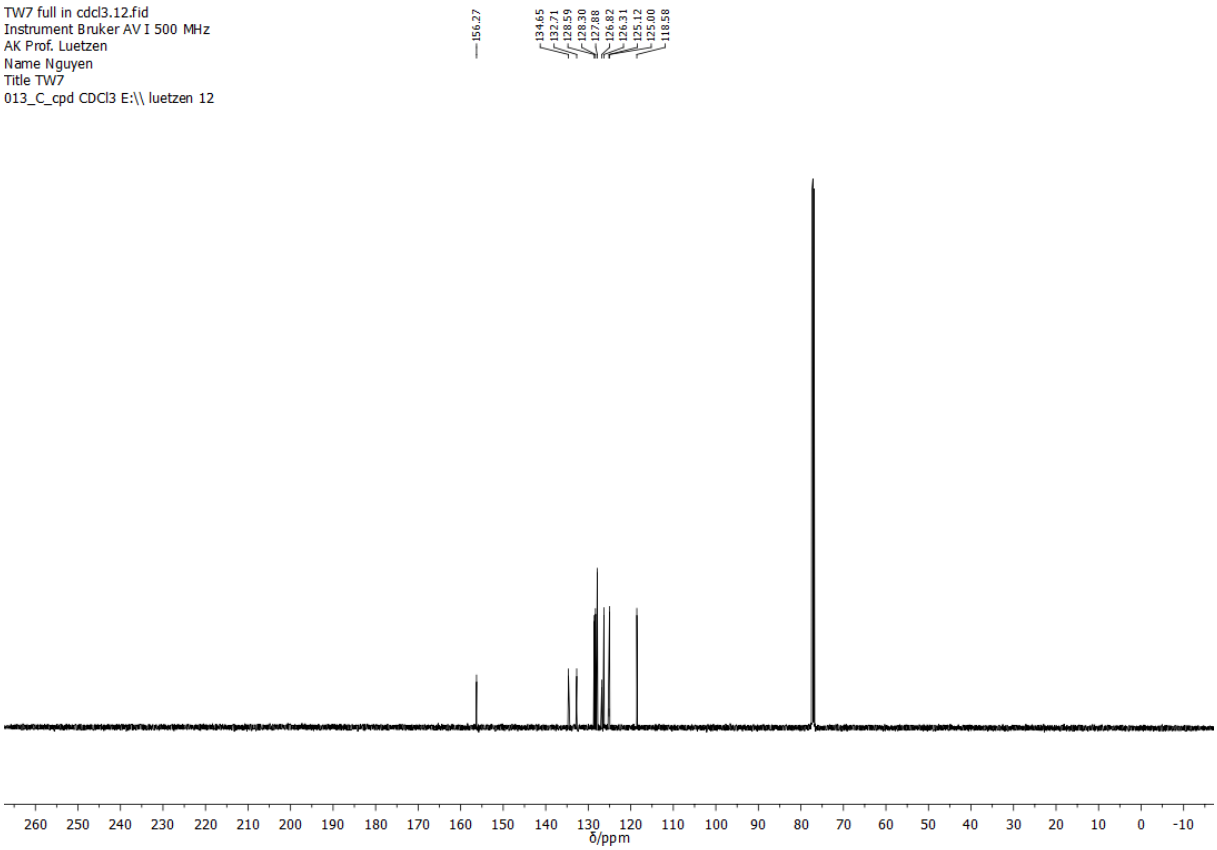

Figure 228: ^{13}C-NMR spectrum of **80** in $CDCl_3$.

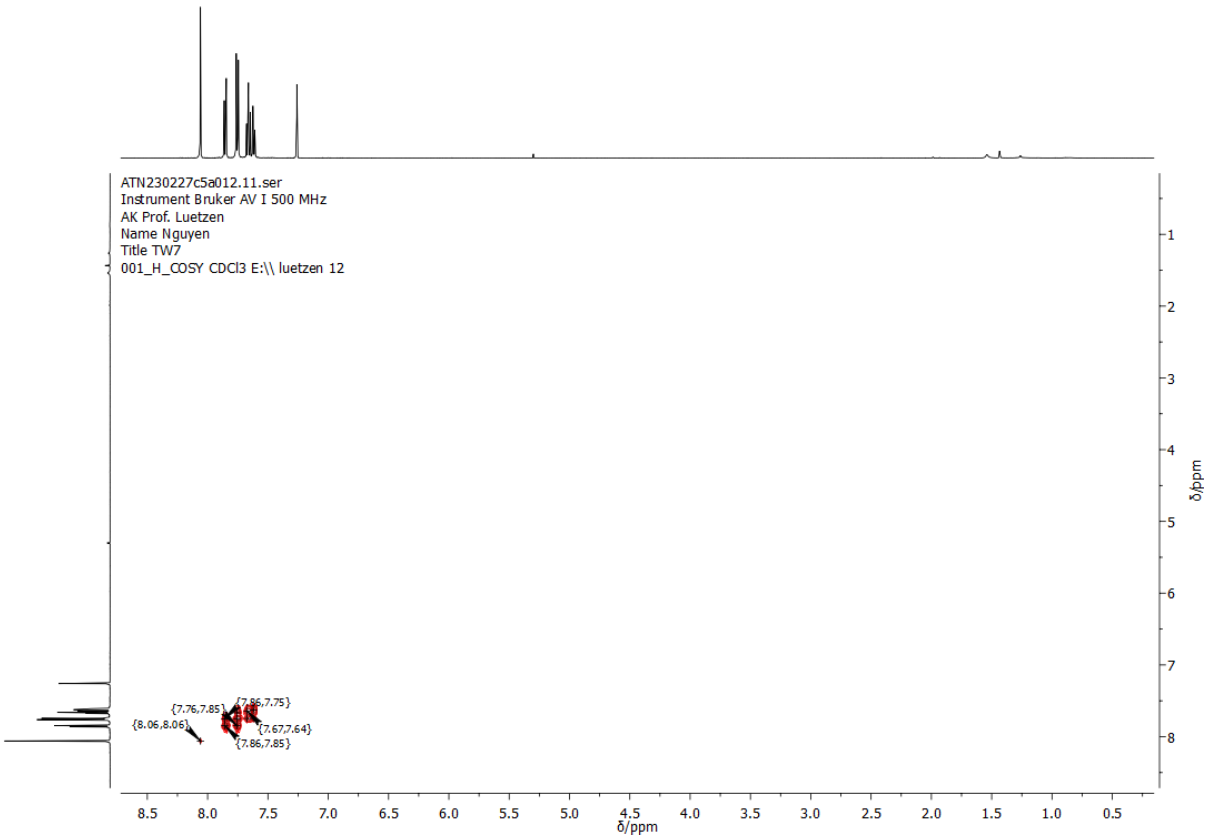

Figure 229: COSY-NMR spectrum of **80** in $CDCl_3$.

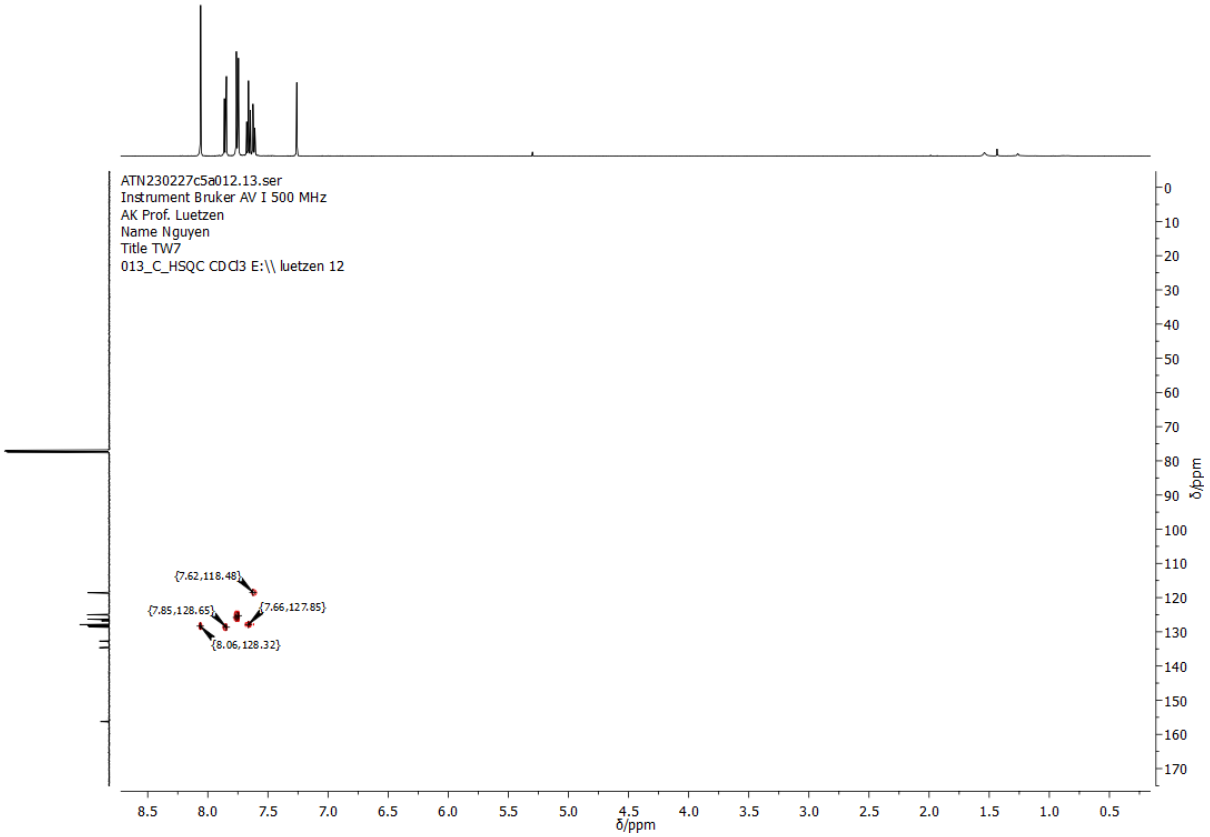

Figure 230: HSQC-NMR spectrum of **80** in $CDCl_3$.

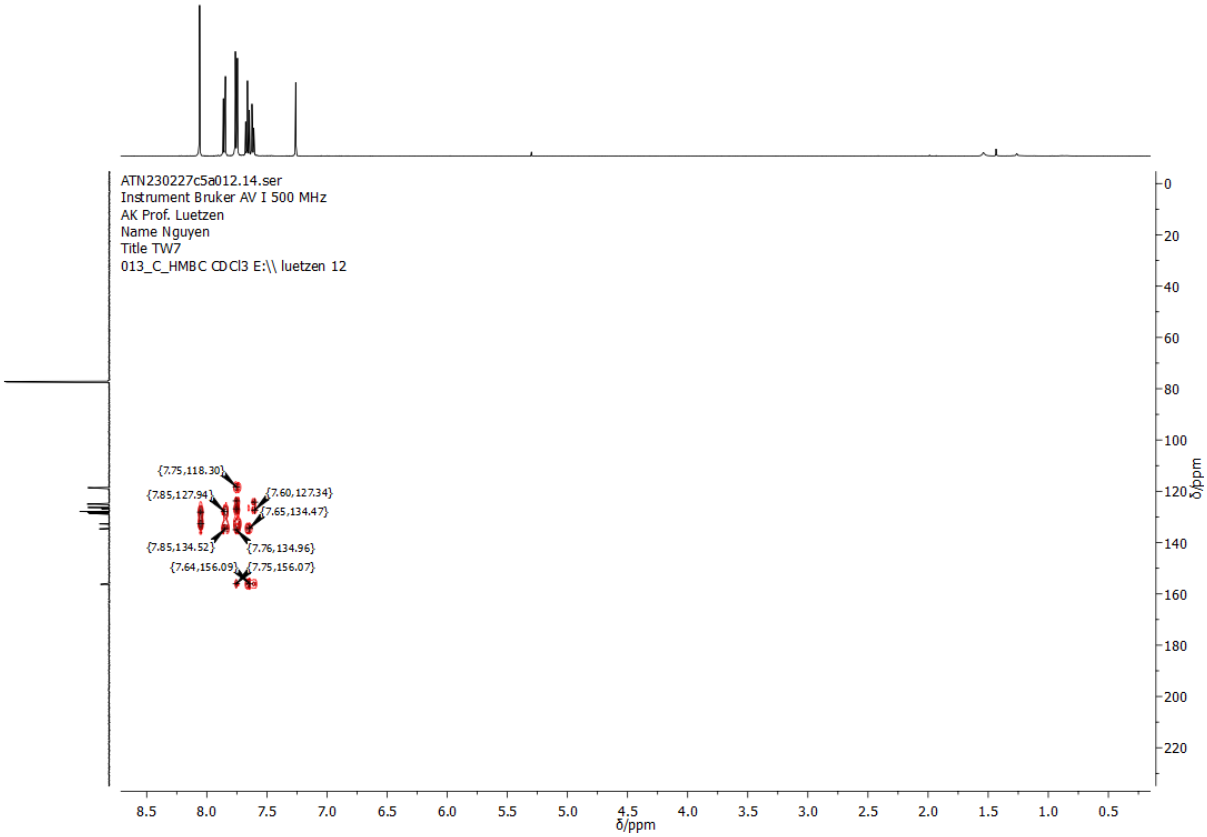

Figure 231: HMBC-NMR spectrum of **80** in $CDCl_3$.

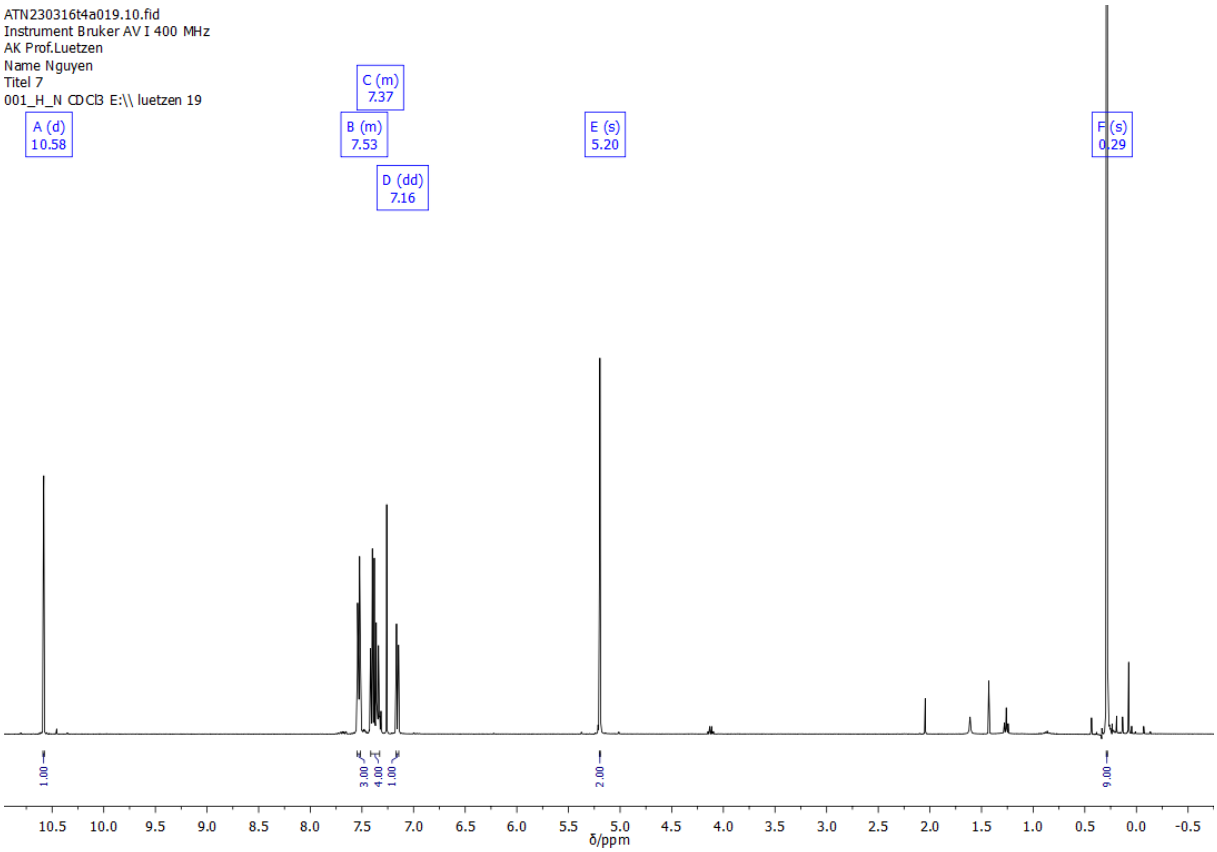

Figure 232: ^{1}H-NMR spectrum of **82** in $CDCl_3$.

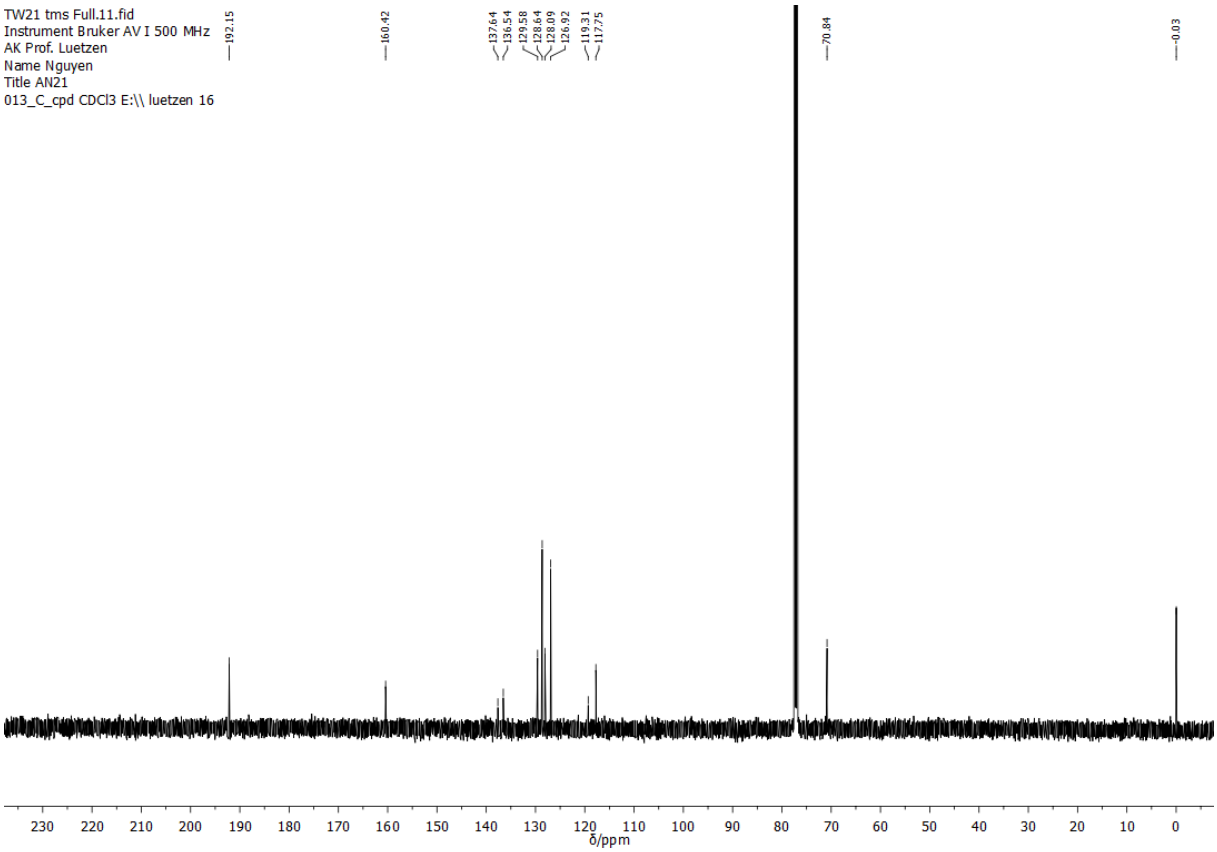

Figure 233: ^{13}C-NMR spectrum of **82** in $CDCl_3$.

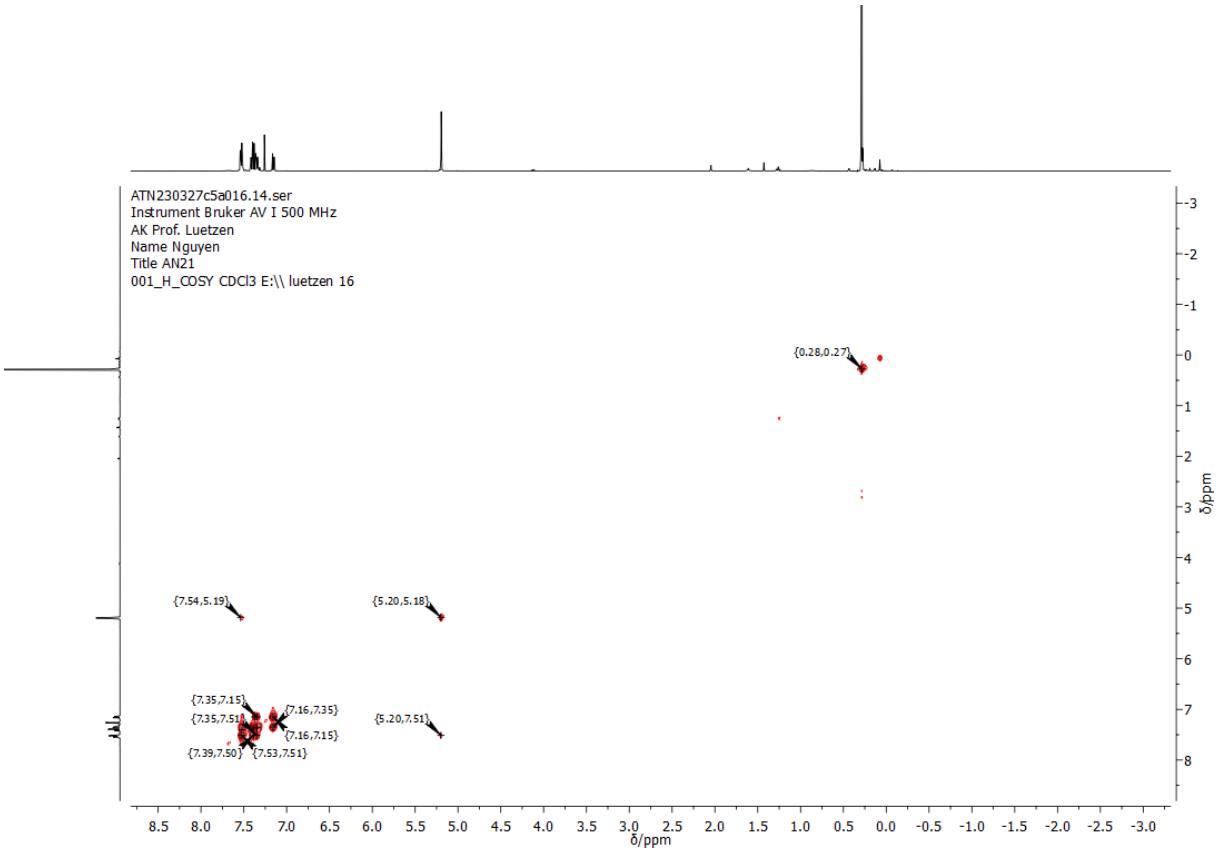

Figure 234: COSY-NMR spectrum of **82** in $CDCl_3$.

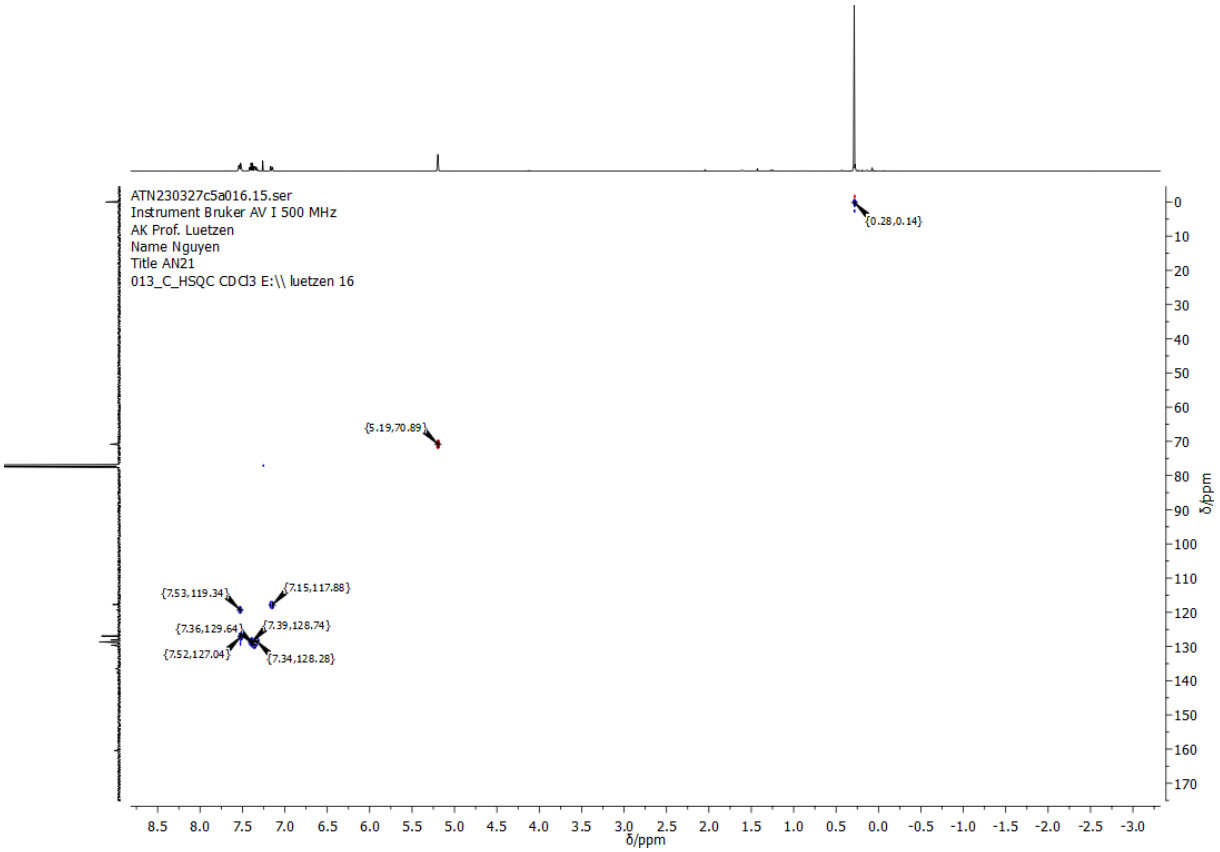

Figure 235: HSQC-NMR spectrum of **82** in $CDCl_3$.

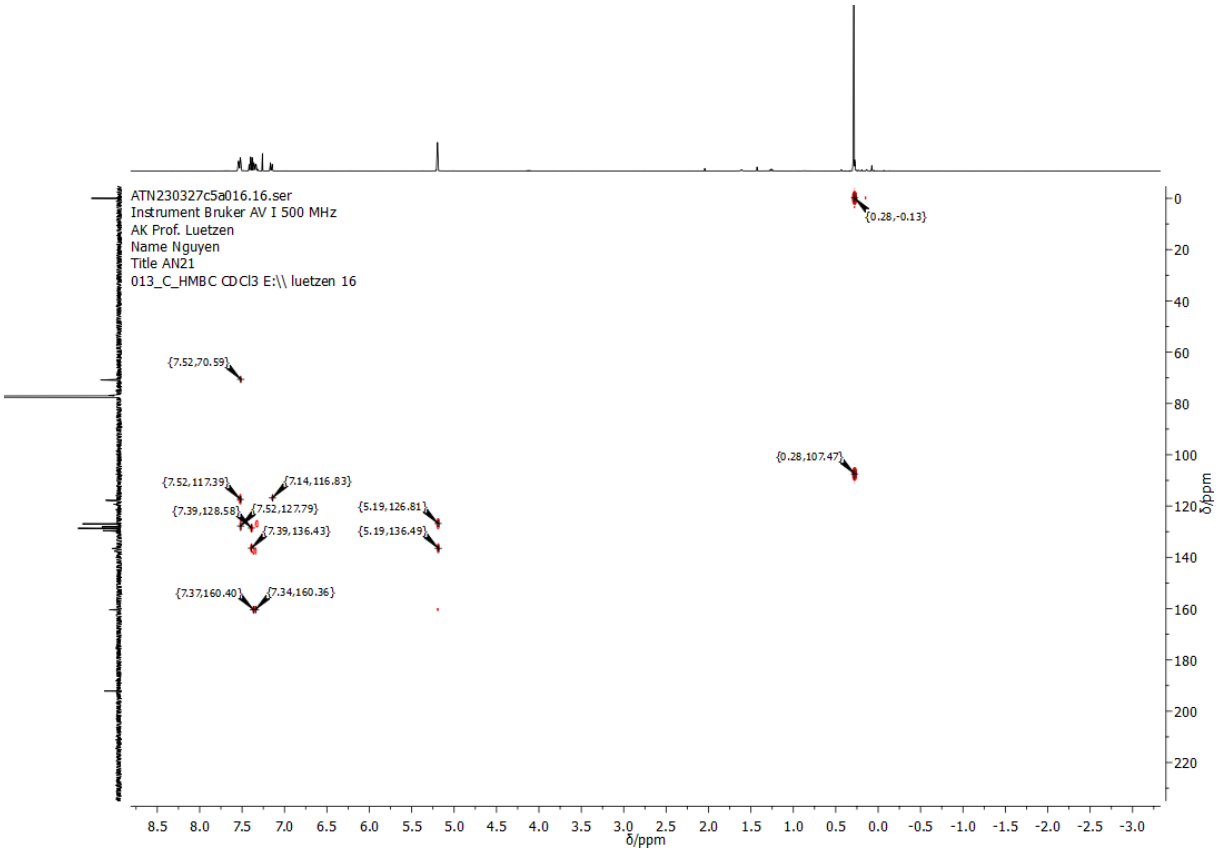

Figure 236: HMBC-NMR spectrum of **82** in $CDCl_3$.

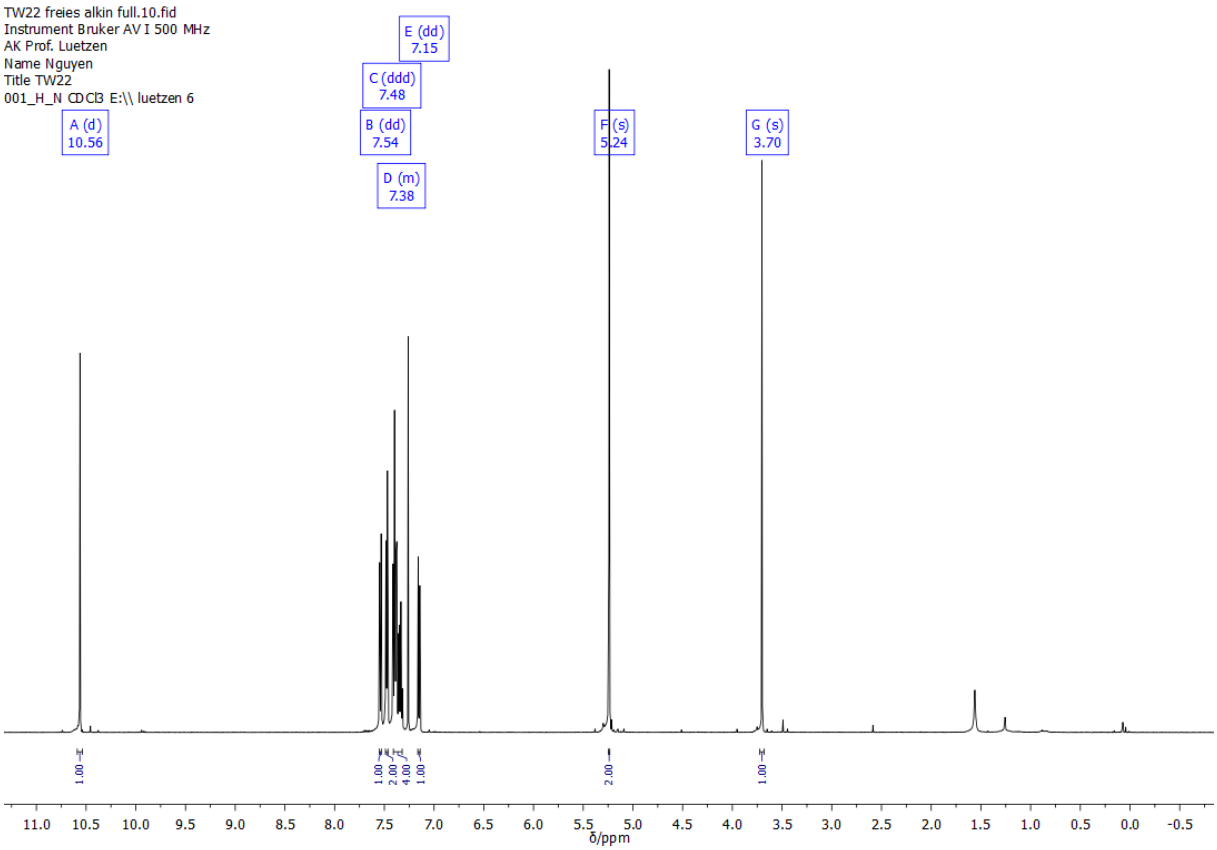

Figure 237: ^{1}H-NMR spectrum of **83** in $CDCl_3$.

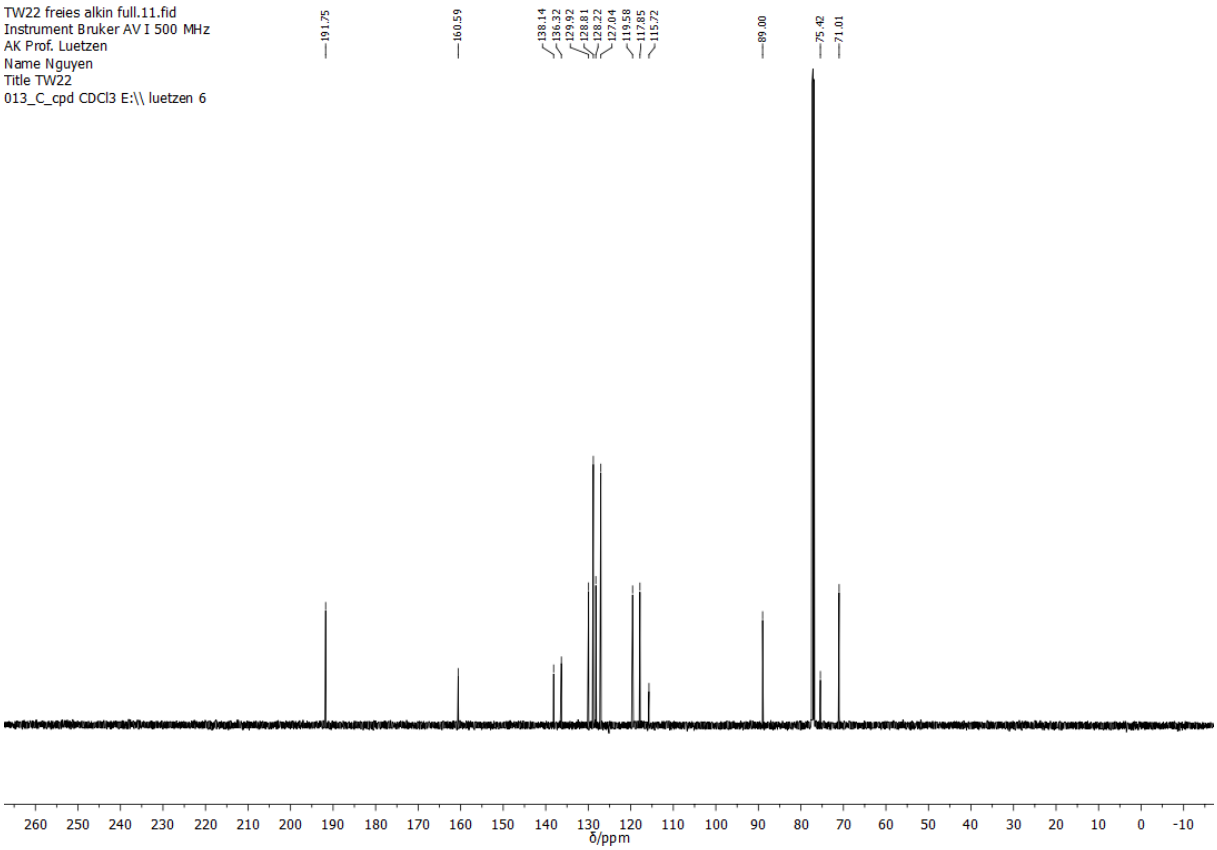

Figure 238: ^{13}C-NMR spectrum of **83** in $CDCl_3$.

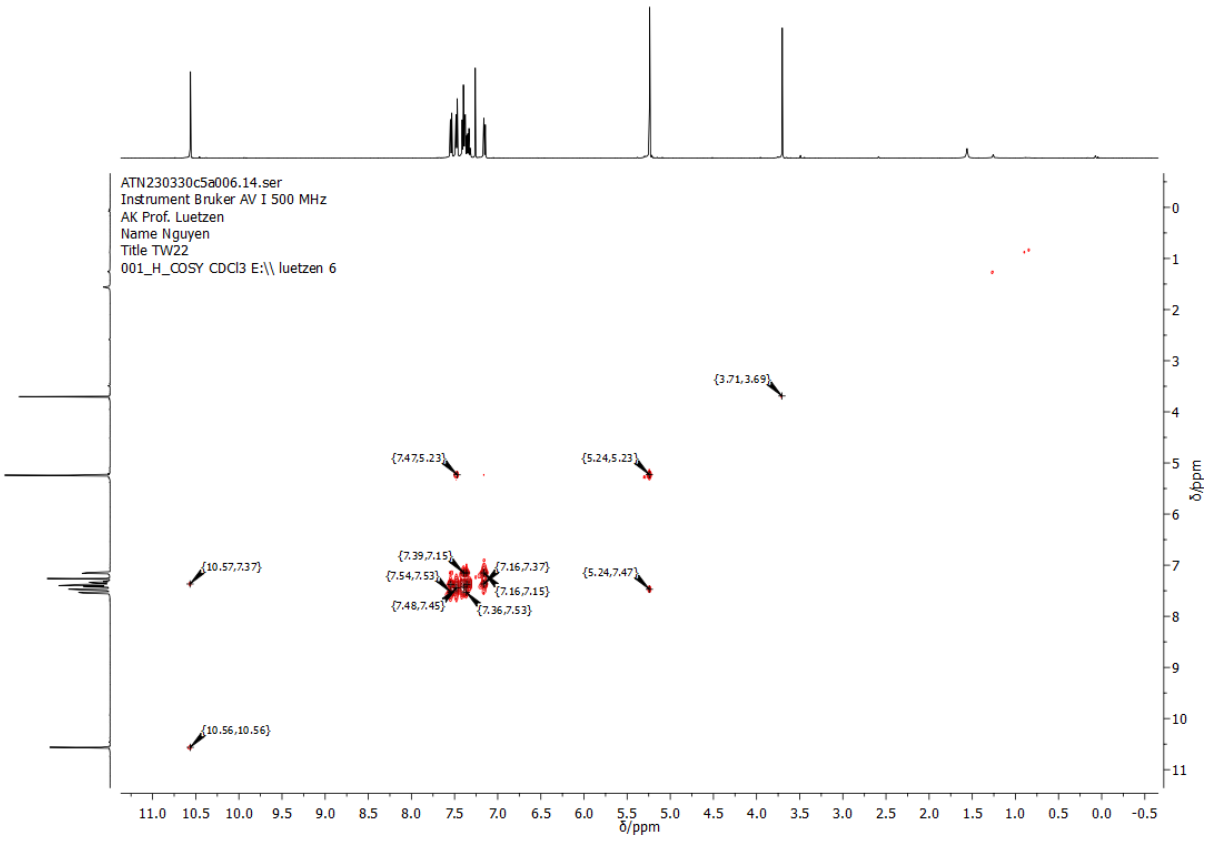

Figure 239: COSY-NMR spectrum of **83** in $CDCl_3$.

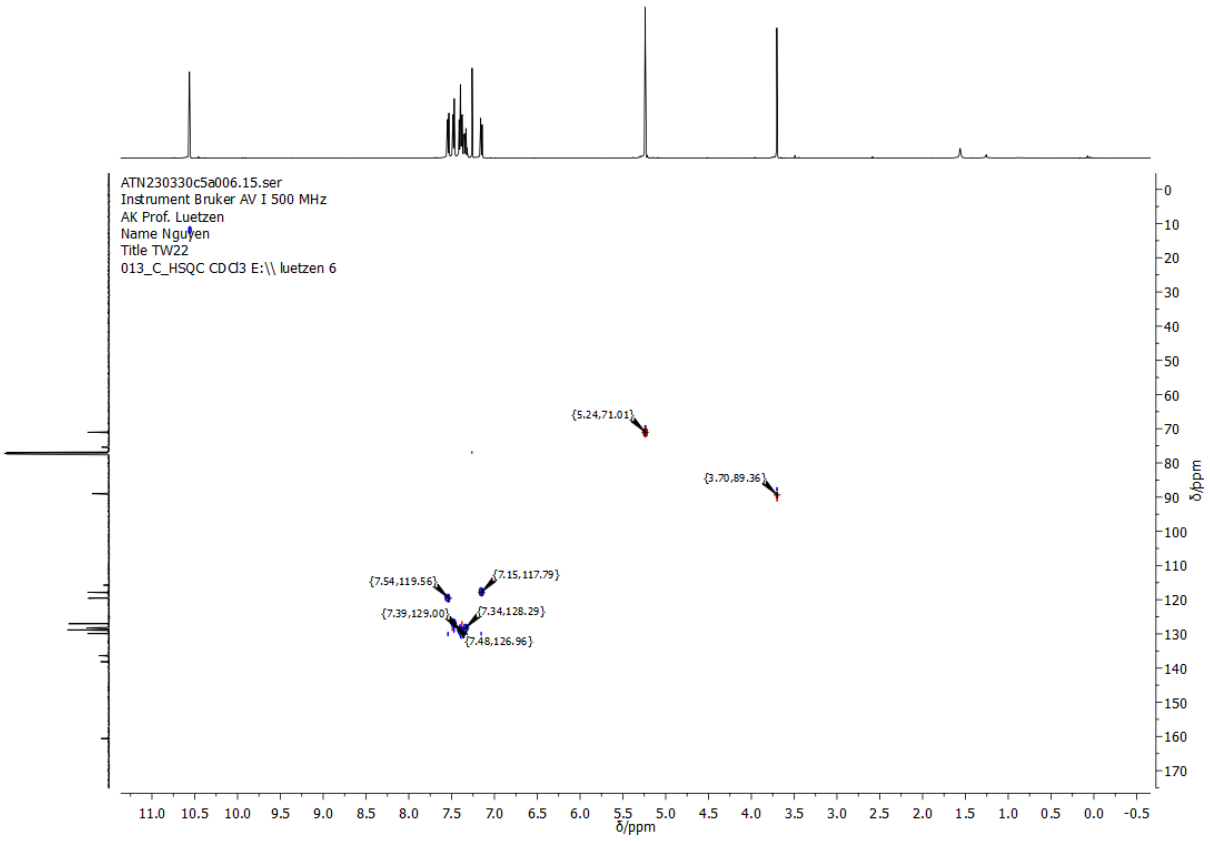

Figure 240: HSQC-NMR spectrum of **83** in $CDCl_3$.

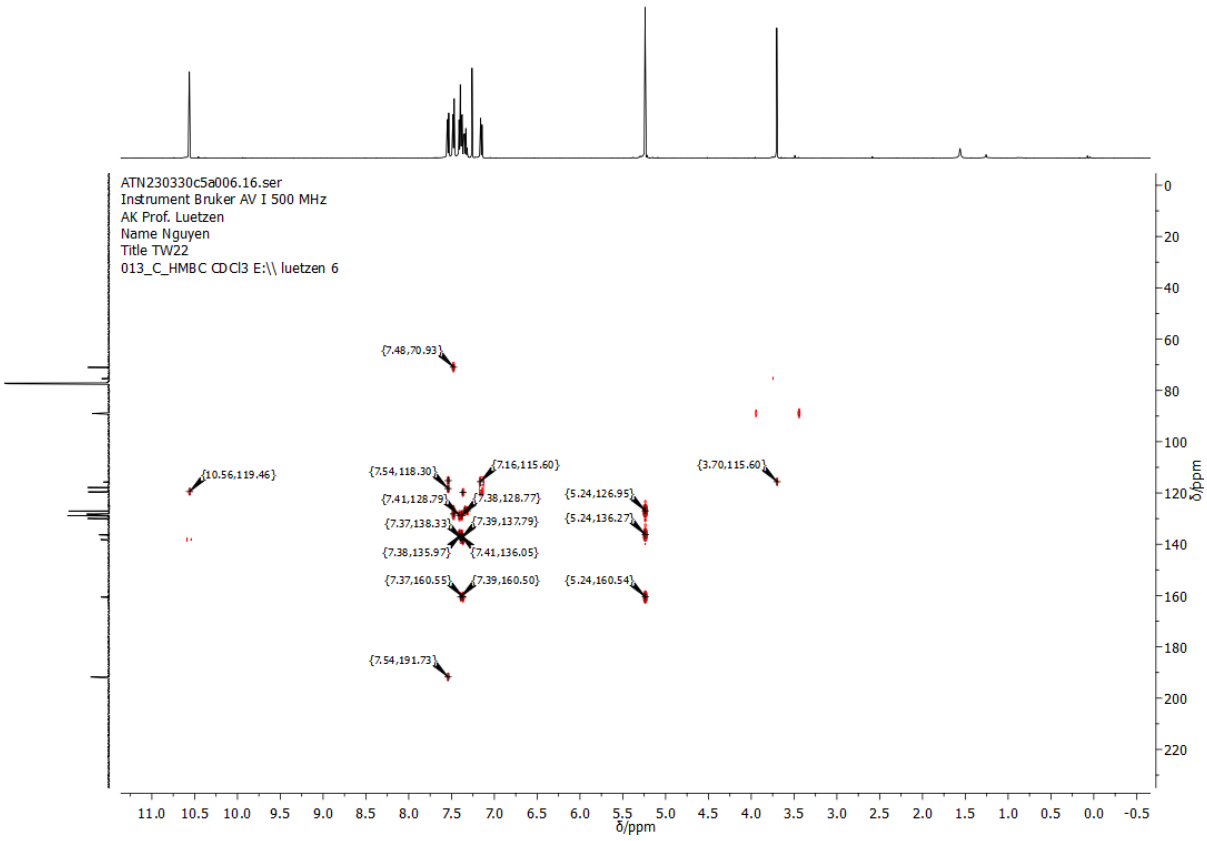

Figure 241: HMBC-NMR spectrum of **83** in $CDCl_3$.

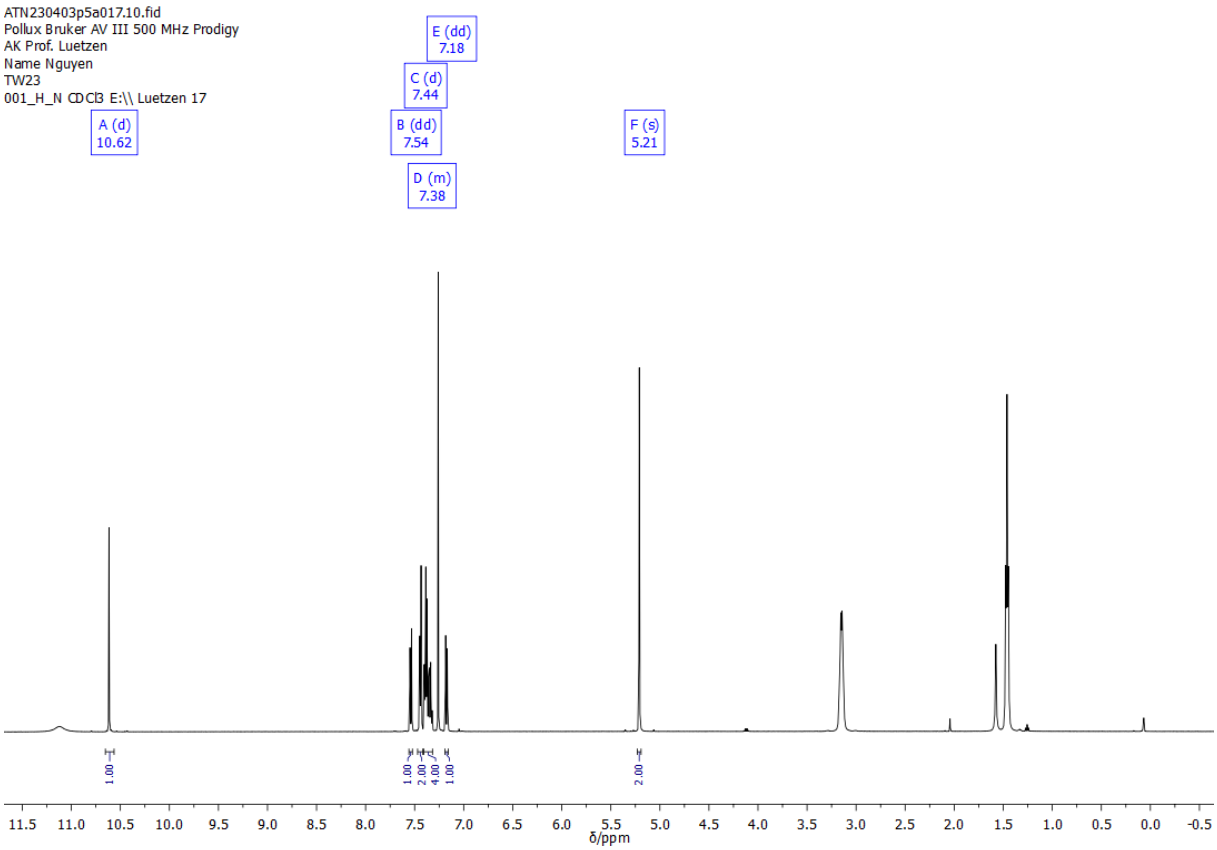

Figure 242: ^{1}H-NMR spectrum of **84** in $CDCl_3$.

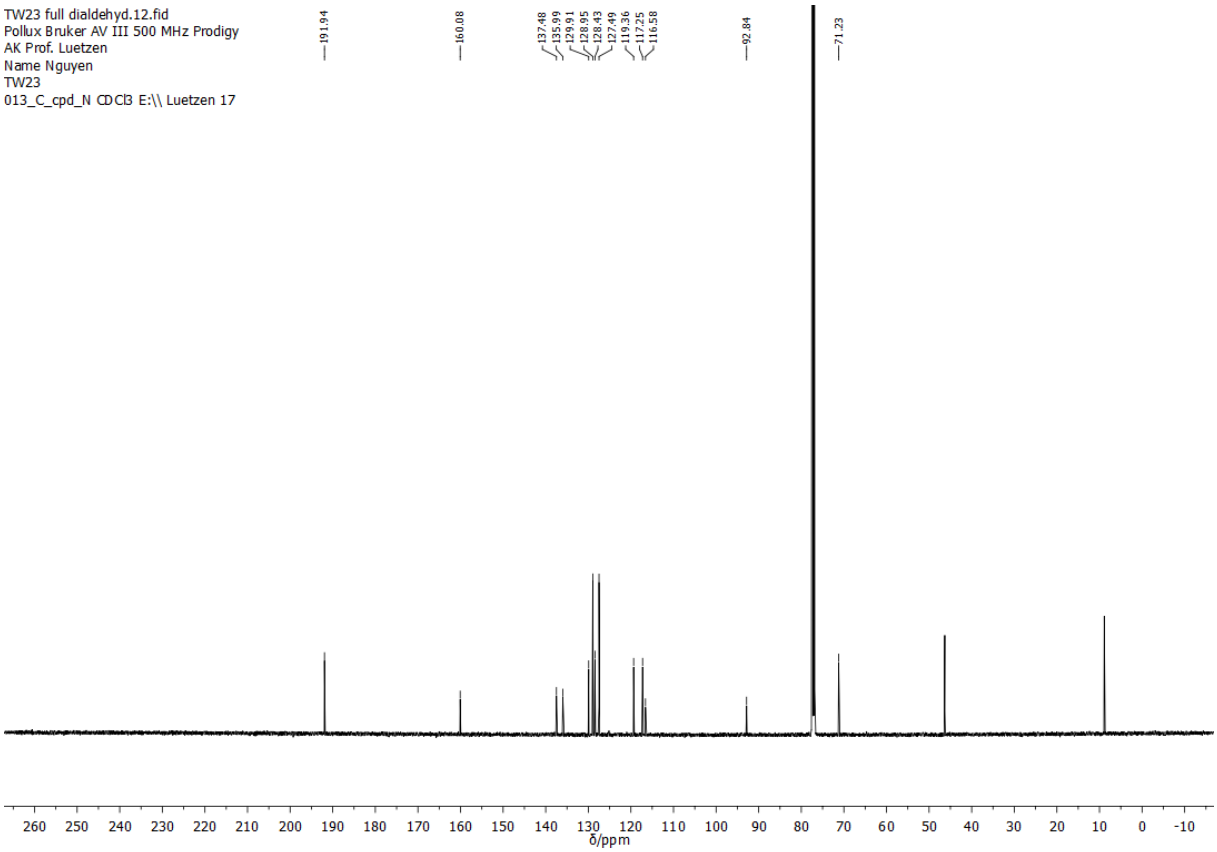

Figure 243: ^{13}C-NMR spectrum of **84** in $CDCl_3$.

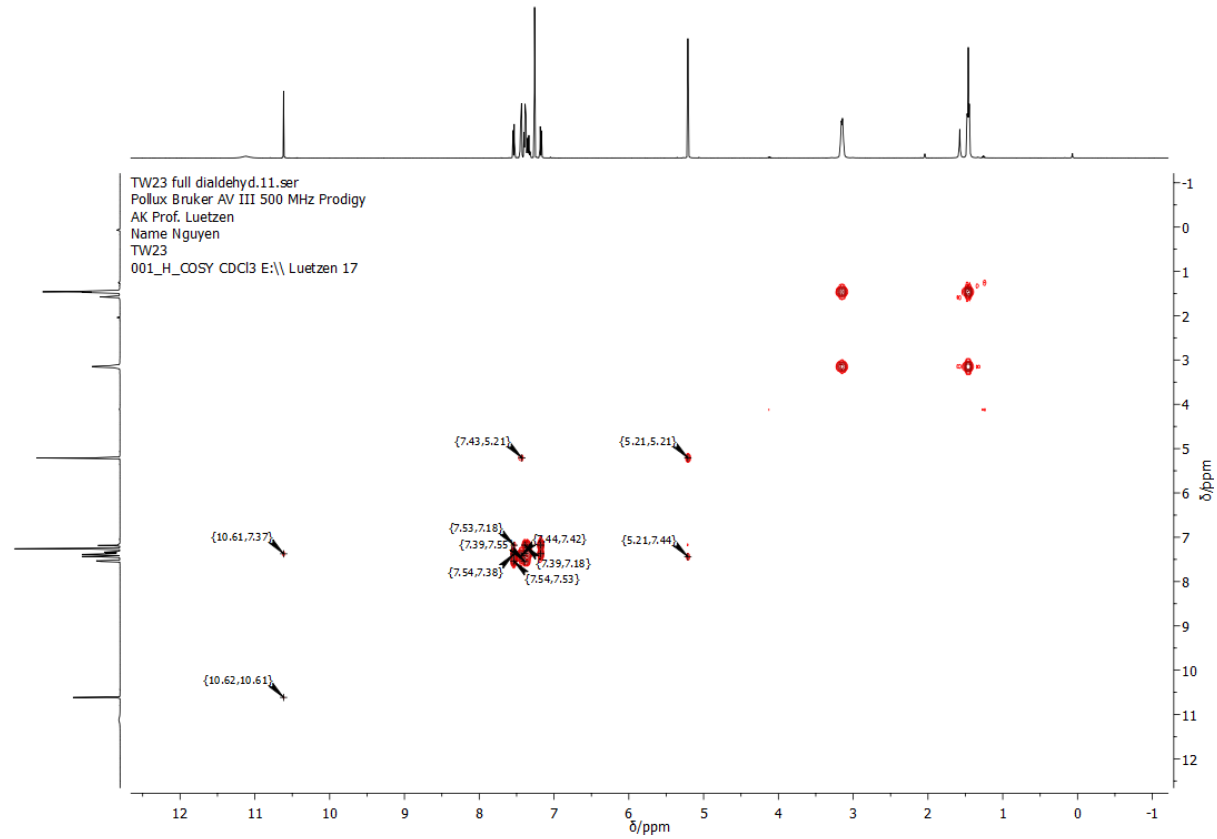

Figure 244: COSY-NMR spectrum of **84** in $CDCl_3$.

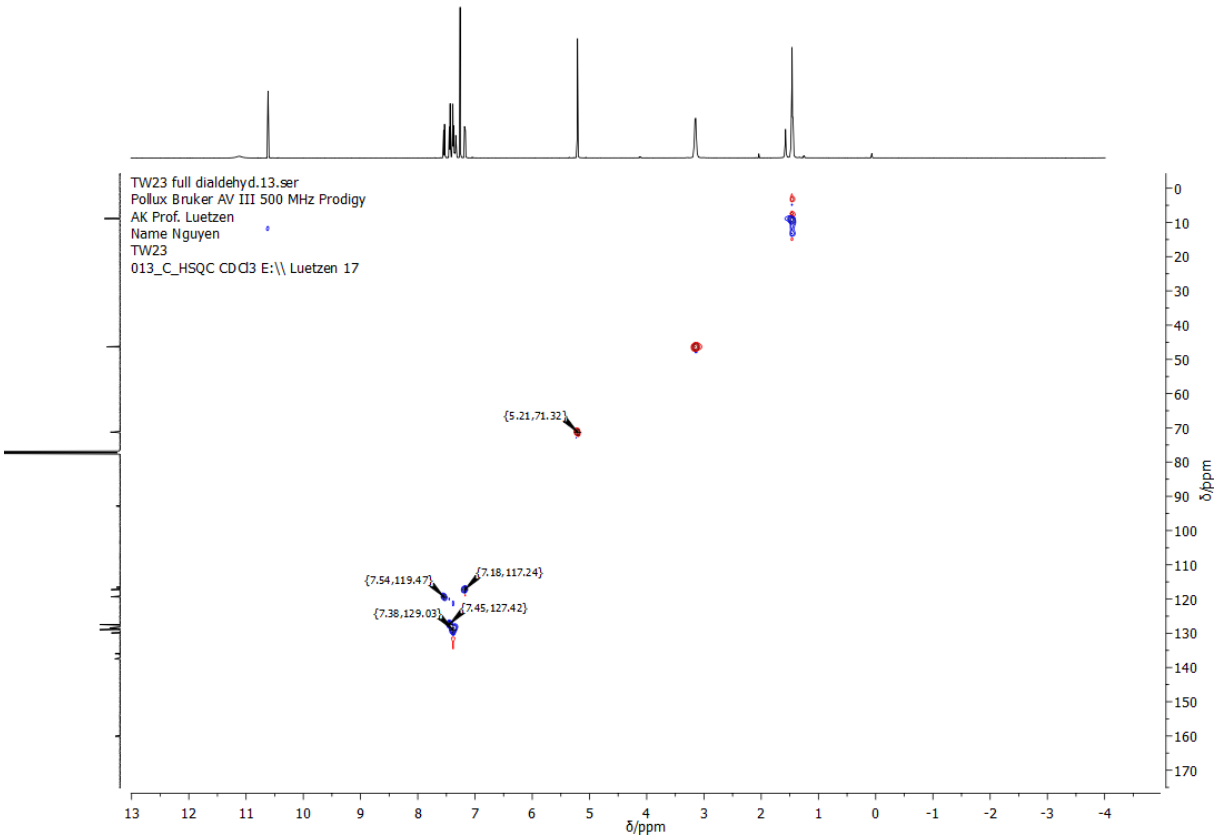

Figure 245: HSQC-NMR spectrum of **84** in $CDCl_3$.

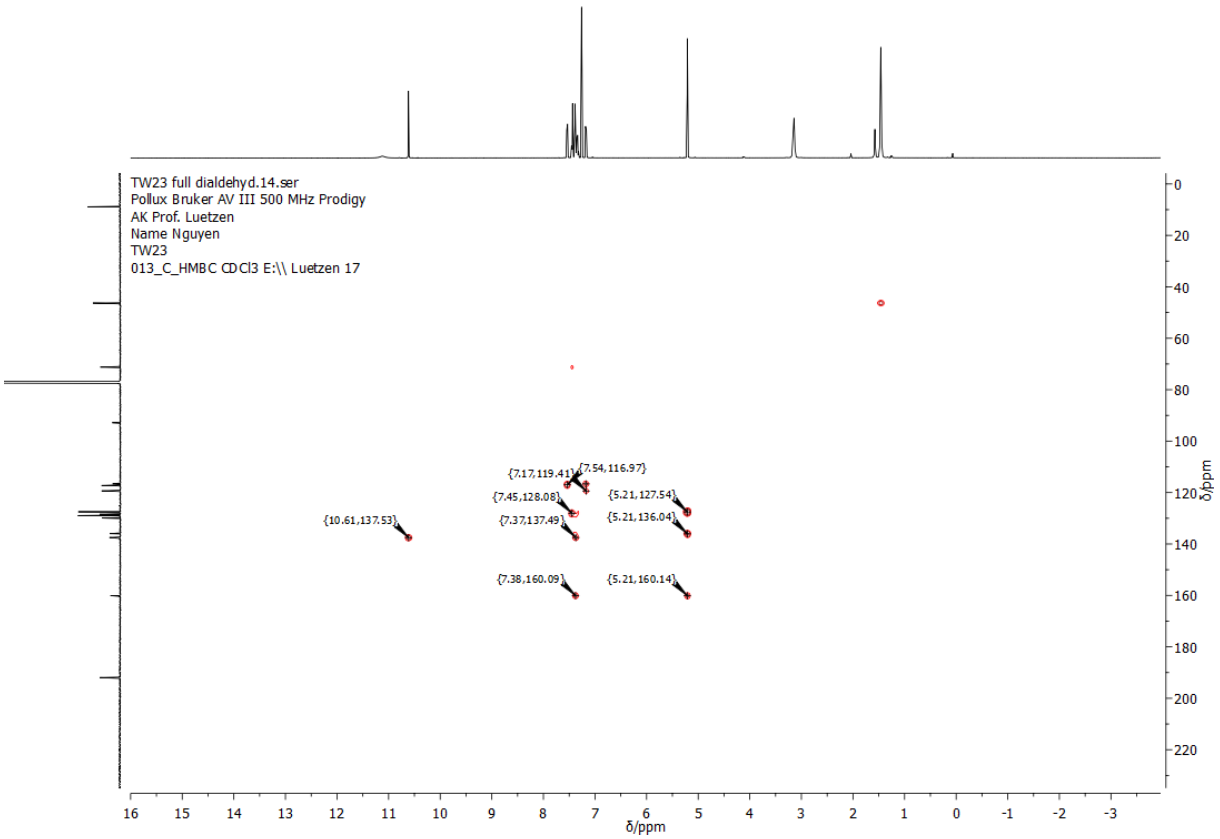

Figure 246: HMBC-NMR spectrum of **84** in $CDCl_3$.

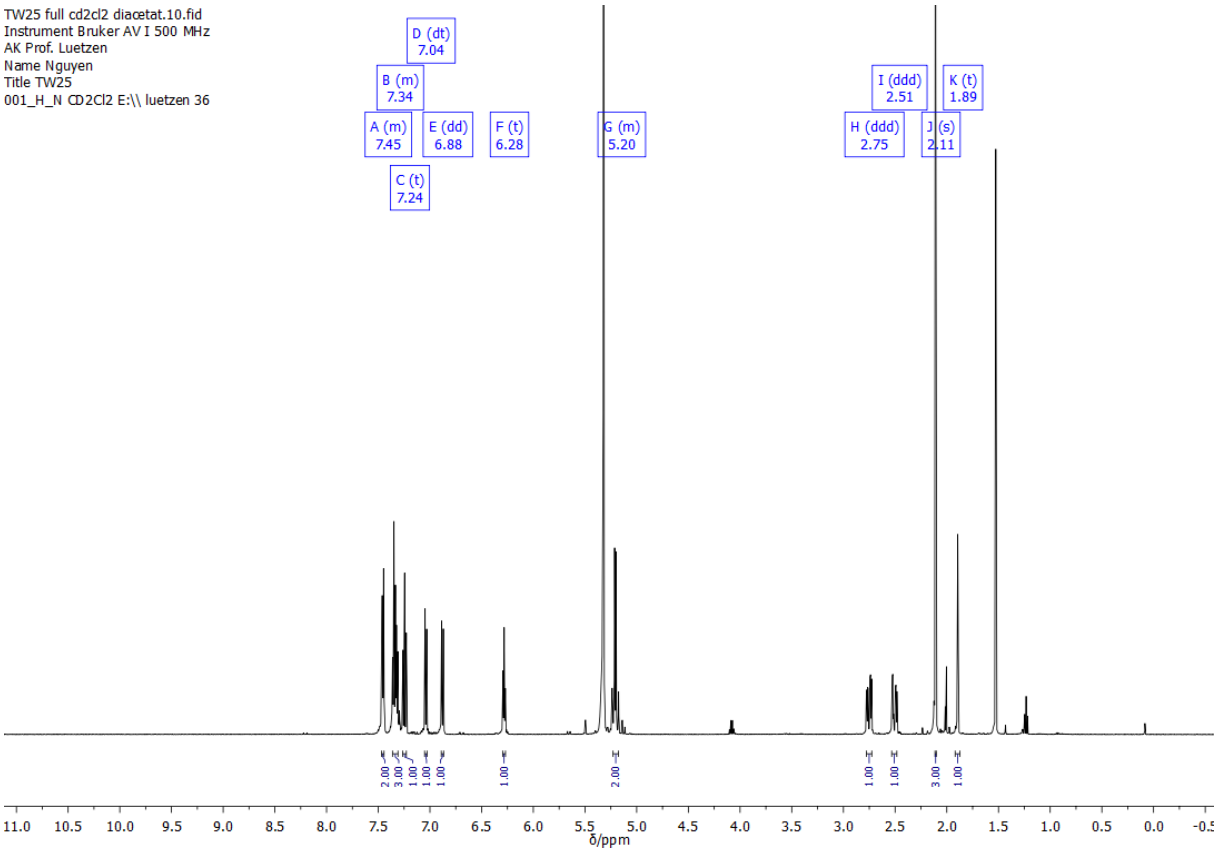

Figure 247: ^{1}H-NMR spectrum of **86** in CD_2Cl_2.

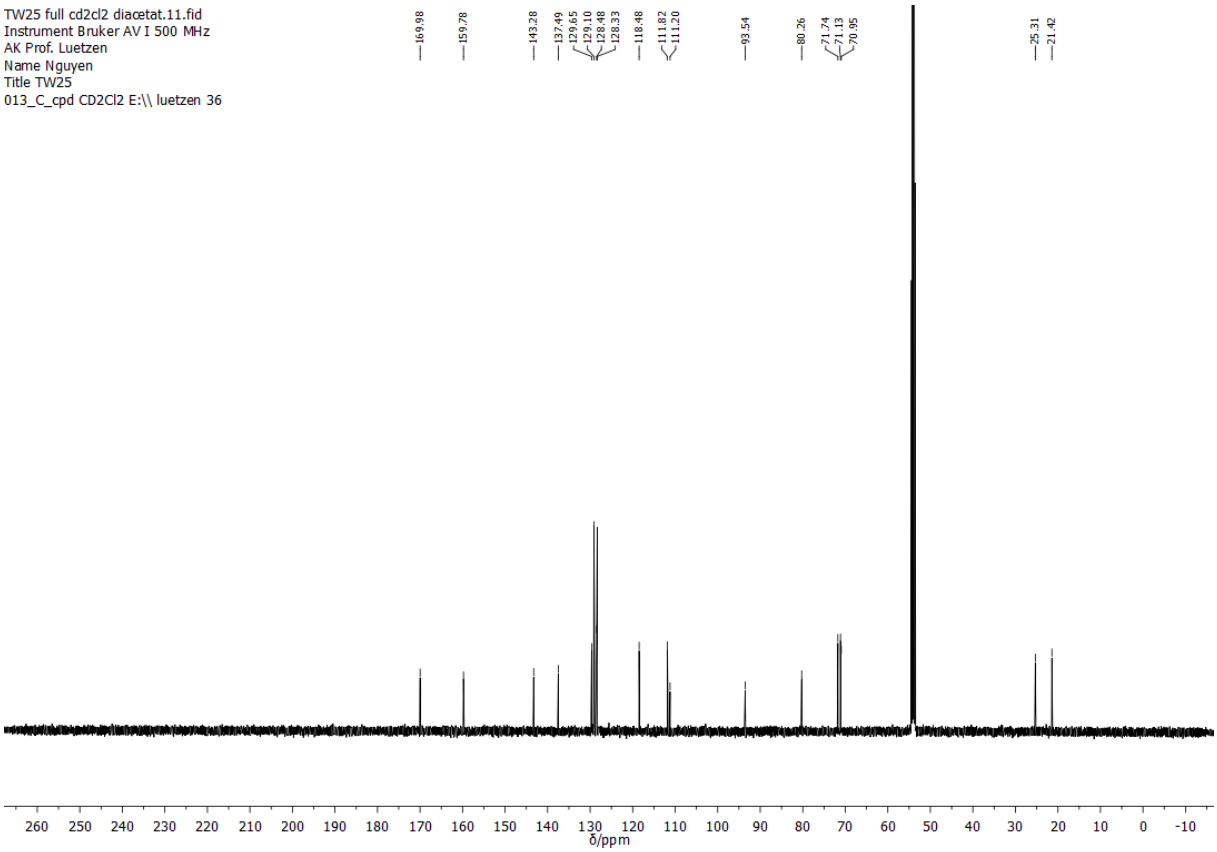

Figure 248: ^{13}C-NMR spectrum of **86** in CD_2Cl_2.

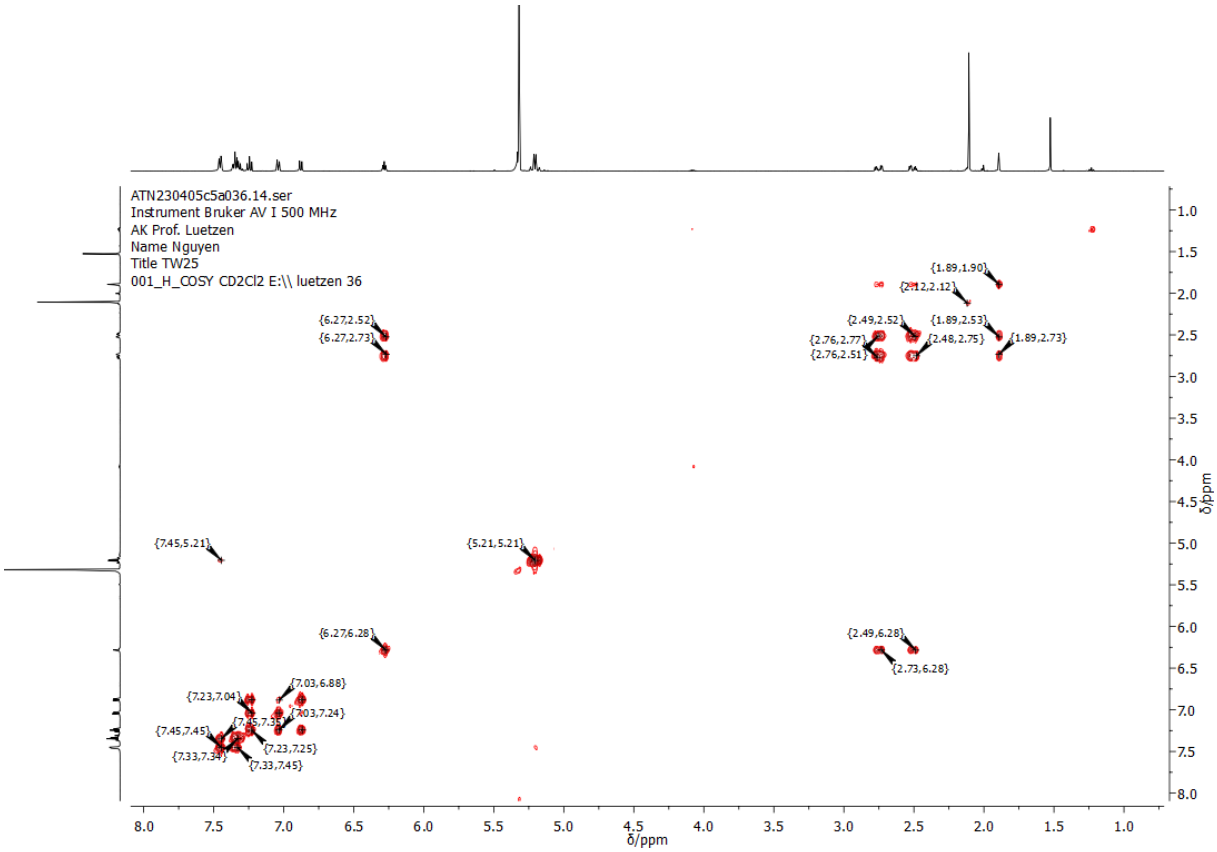

Figure 249: COSY-NMR spectrum of **86** in CD_2Cl_2.

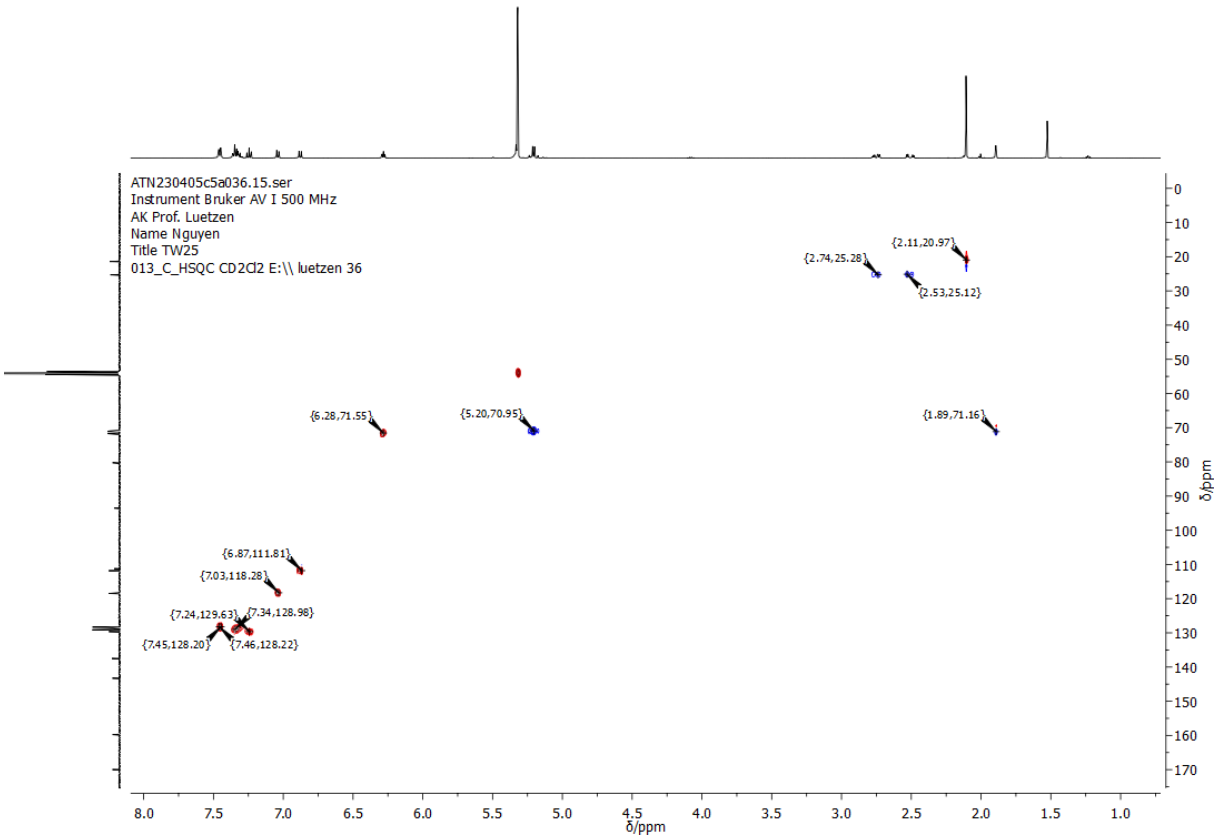

Figure 250: HSQC-NMR spectrum of **86** in CD_2Cl_2.

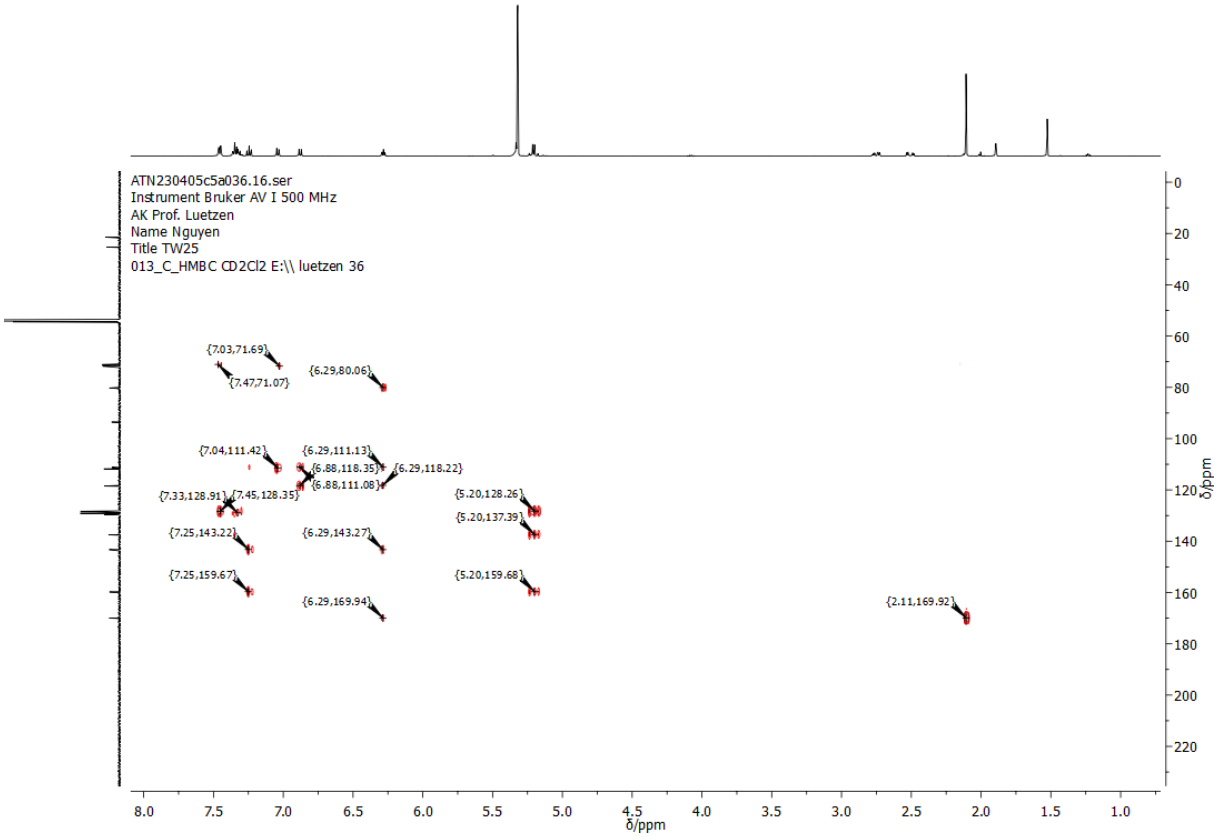

Figure 251: HMBC-NMR spectrum of **86** in CD_2Cl_2.

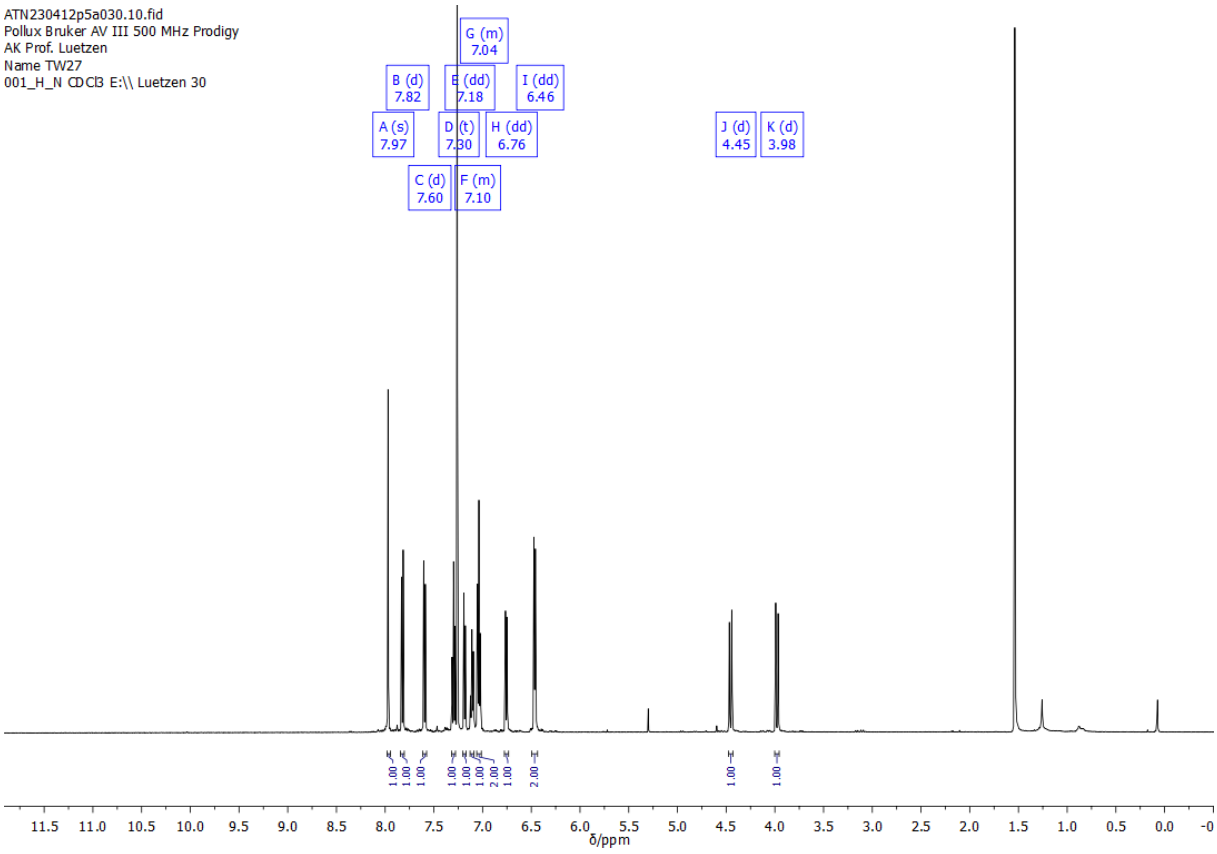

Figure 252: ^{1}H-NMR spectrum of **88** in $CDCl_3$.

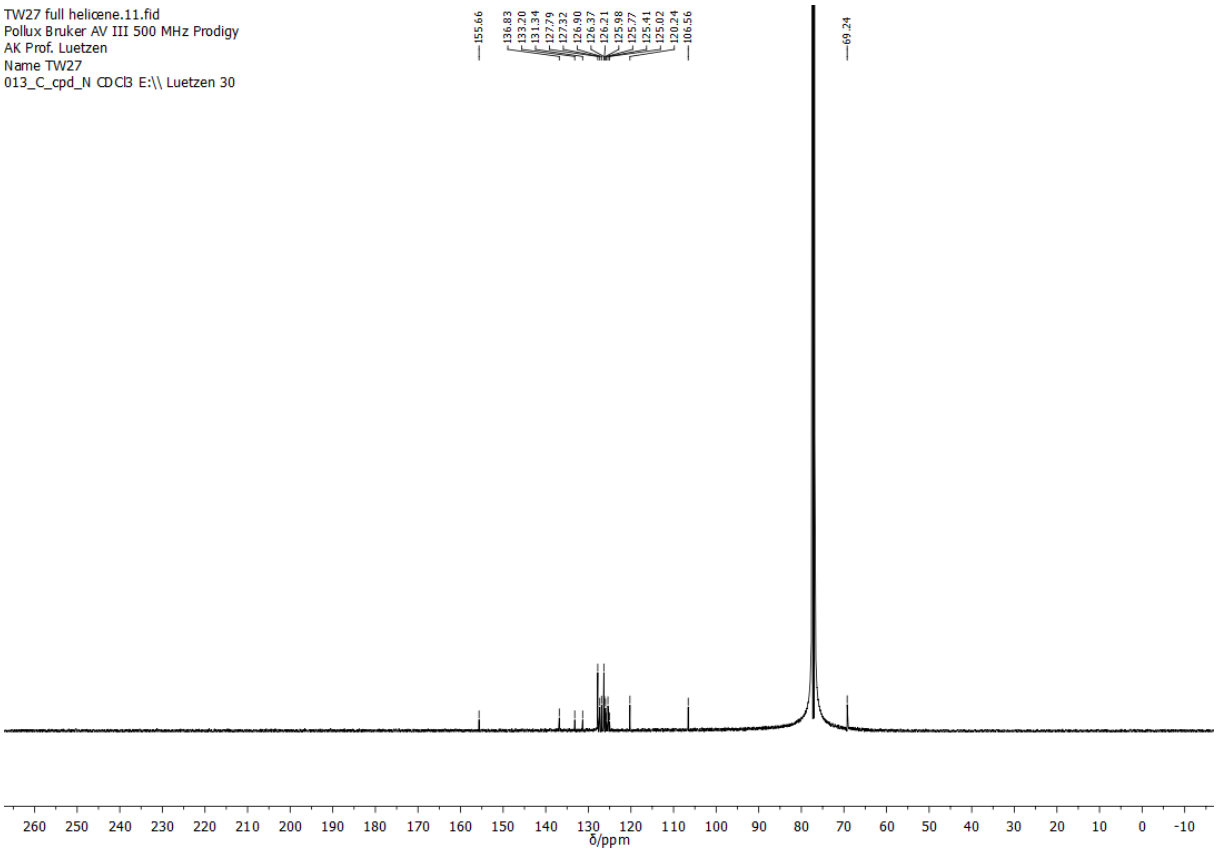

Figure 253: ^{13}C-NMR spectrum of **88** in $CDCl_3$.

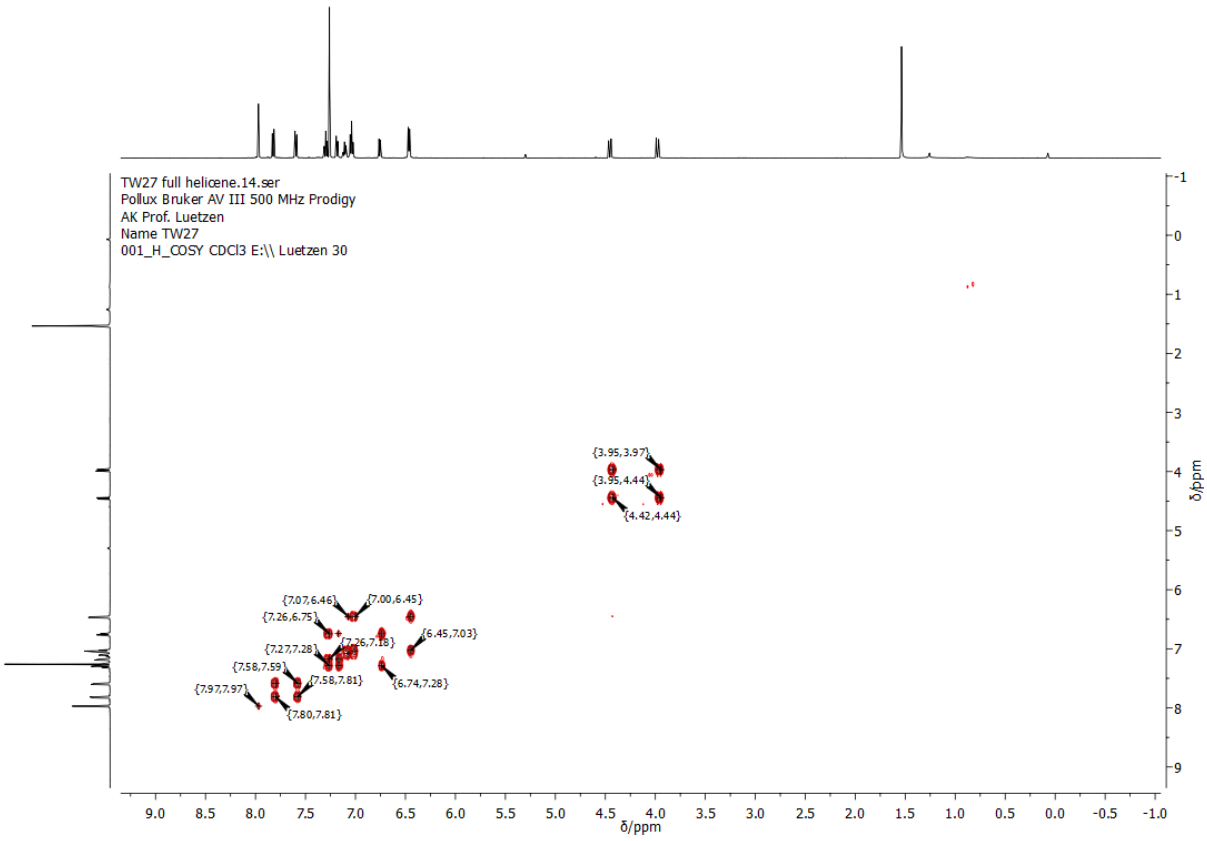

Figure 254: COSY-NMR spectrum of **88** in $CDCl_3$.

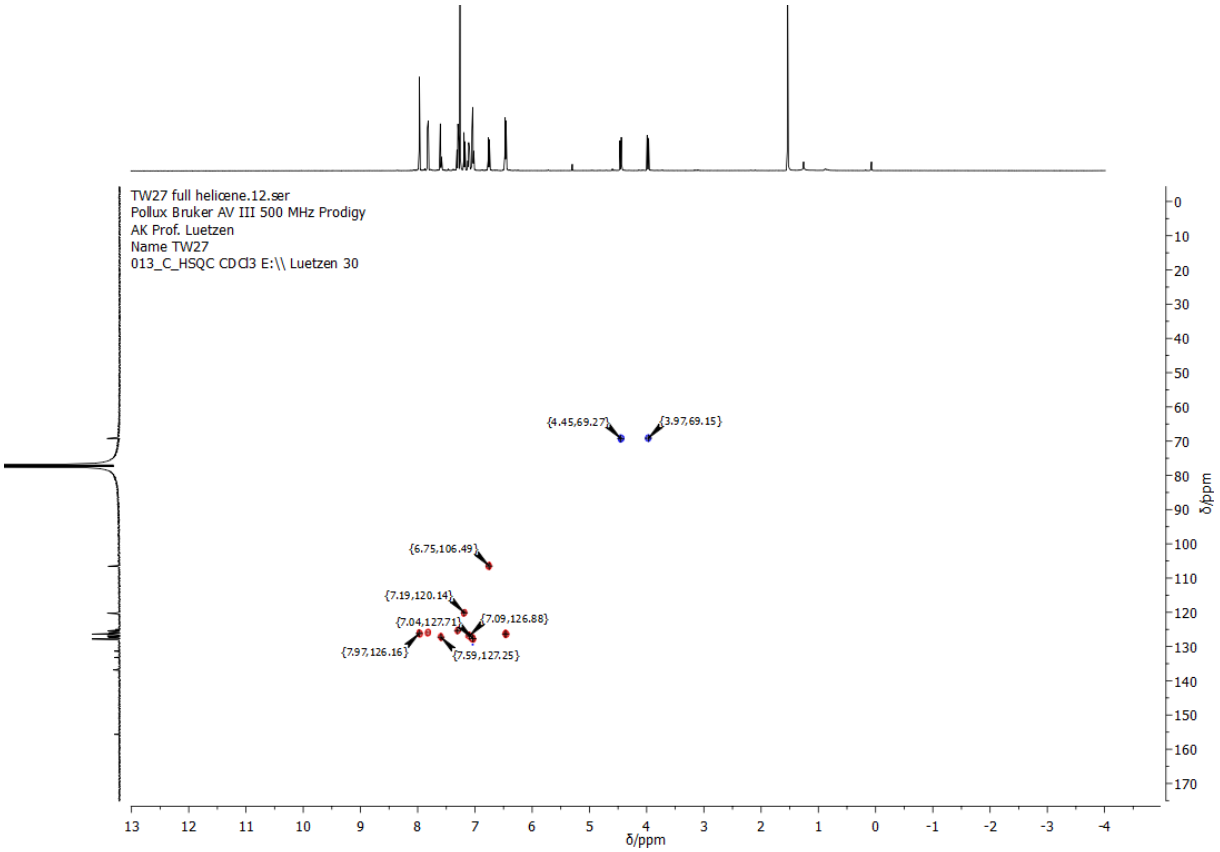

Figure 255: HSQC-NMR spectrum of **88** in $CDCl_3$.

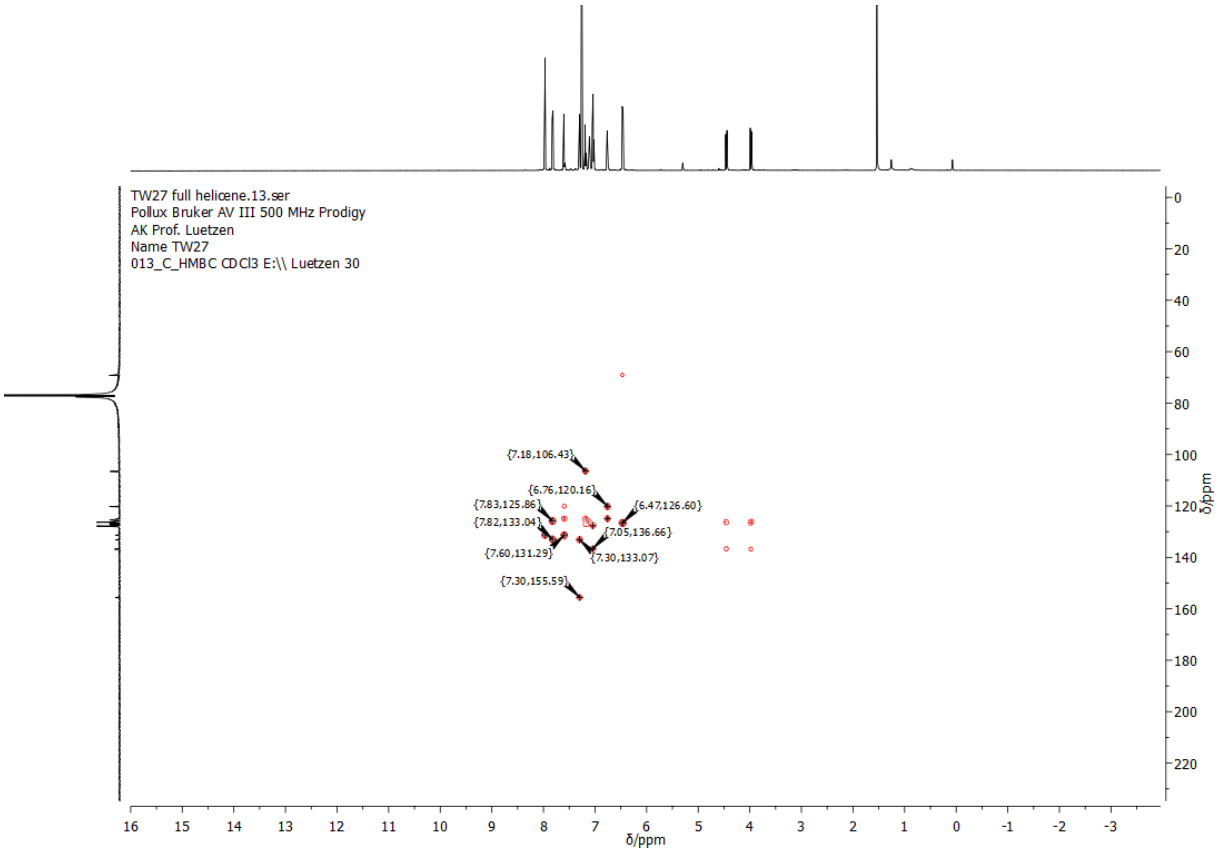

Figure 256: HMBC-NMR spectrum of **88** in $CDCl_3$.

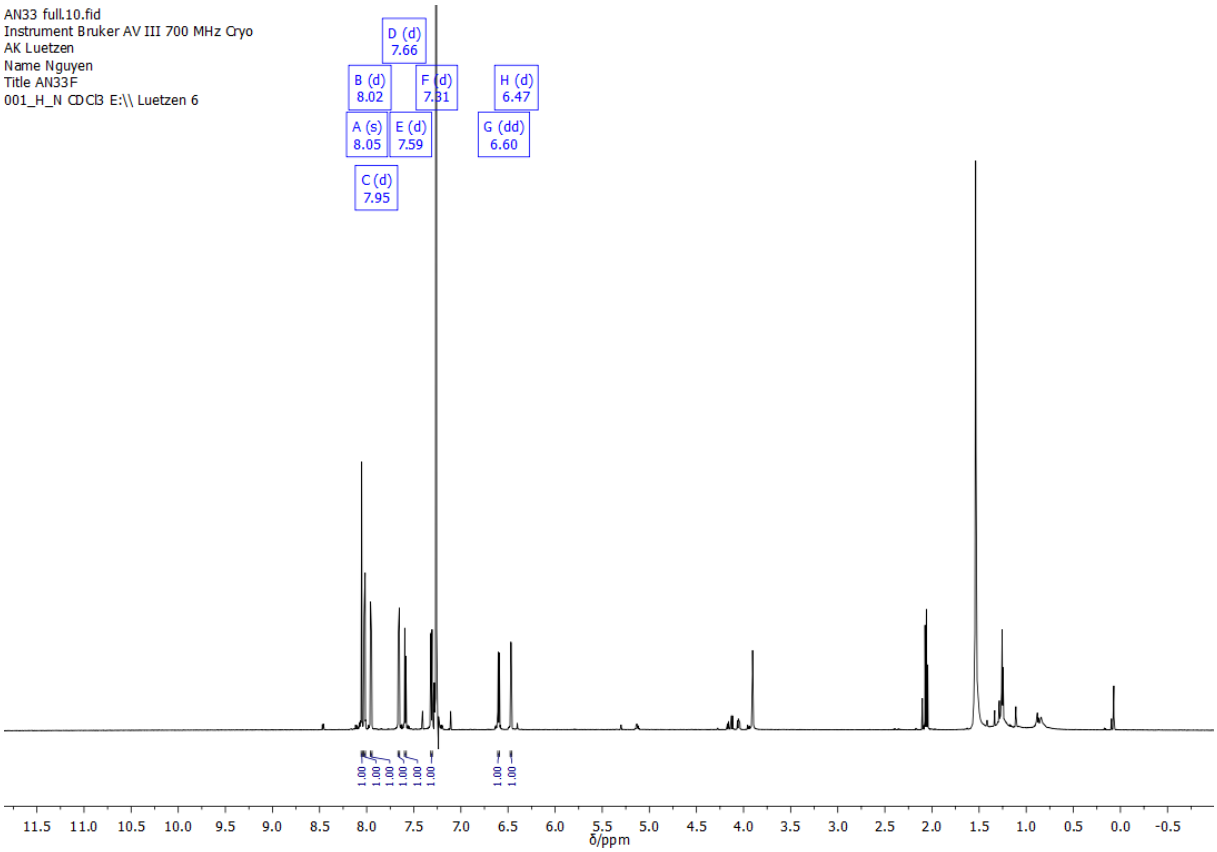

Figure 257: ^{1}H-NMR spectrum of **89** in $CDCl_3$.

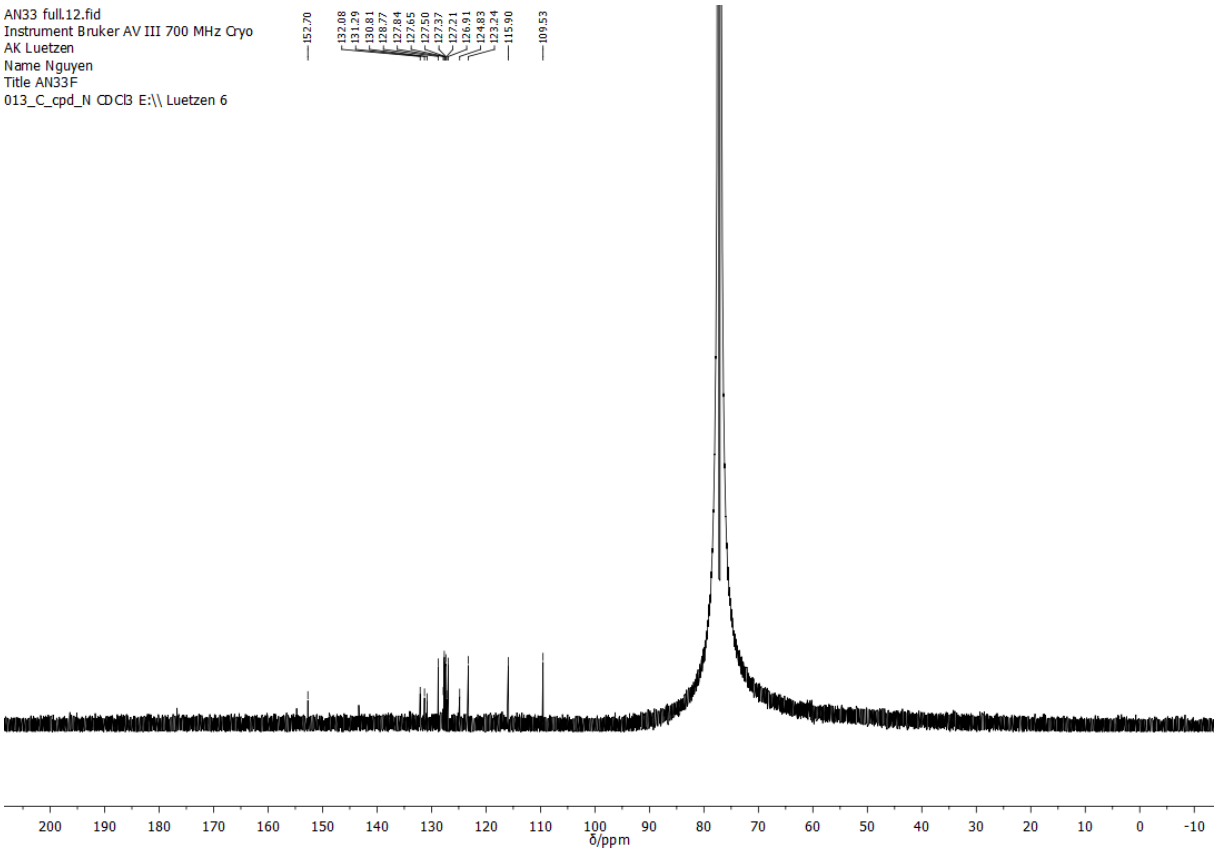

Figure 258: ^{13}C-NMR spectrum of **89** in $CDCl_3$.

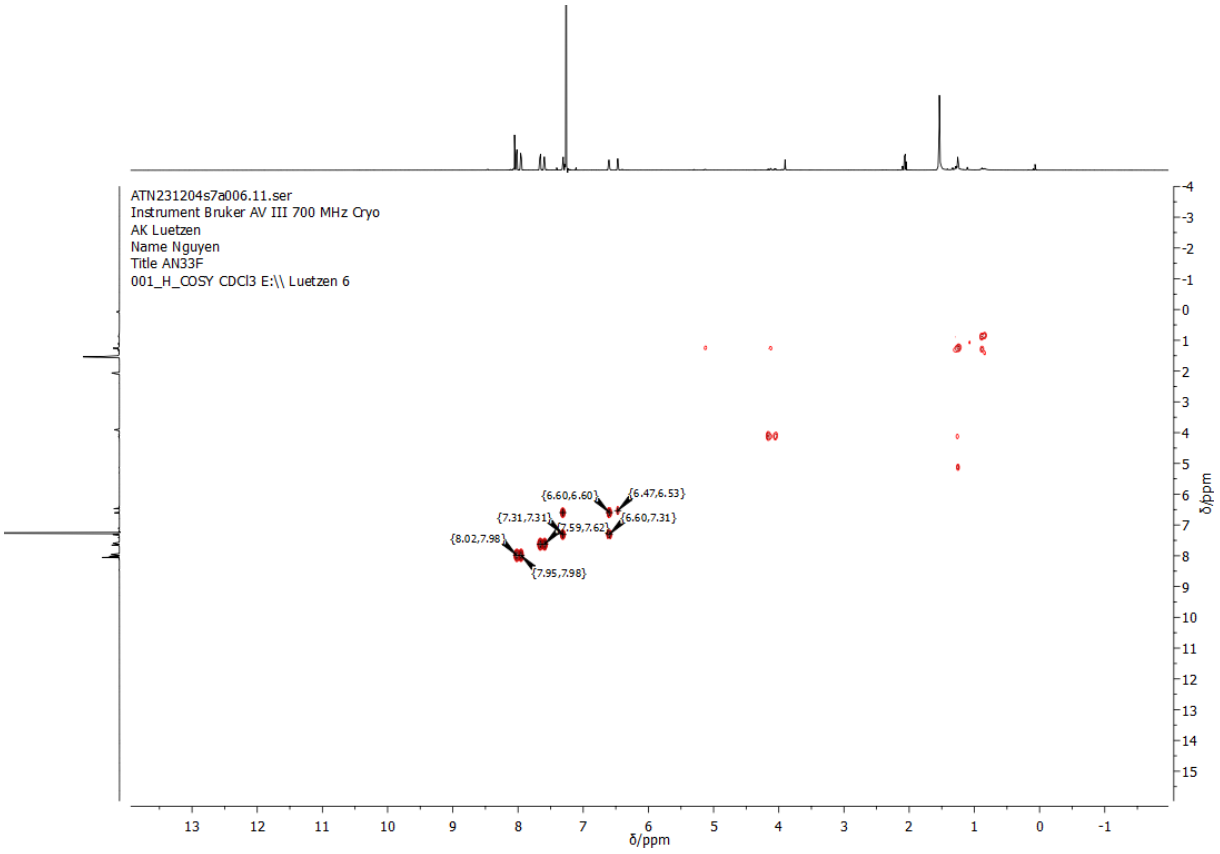

Figure 259: COSY-NMR spectrum of **89** in $CDCl_3$.

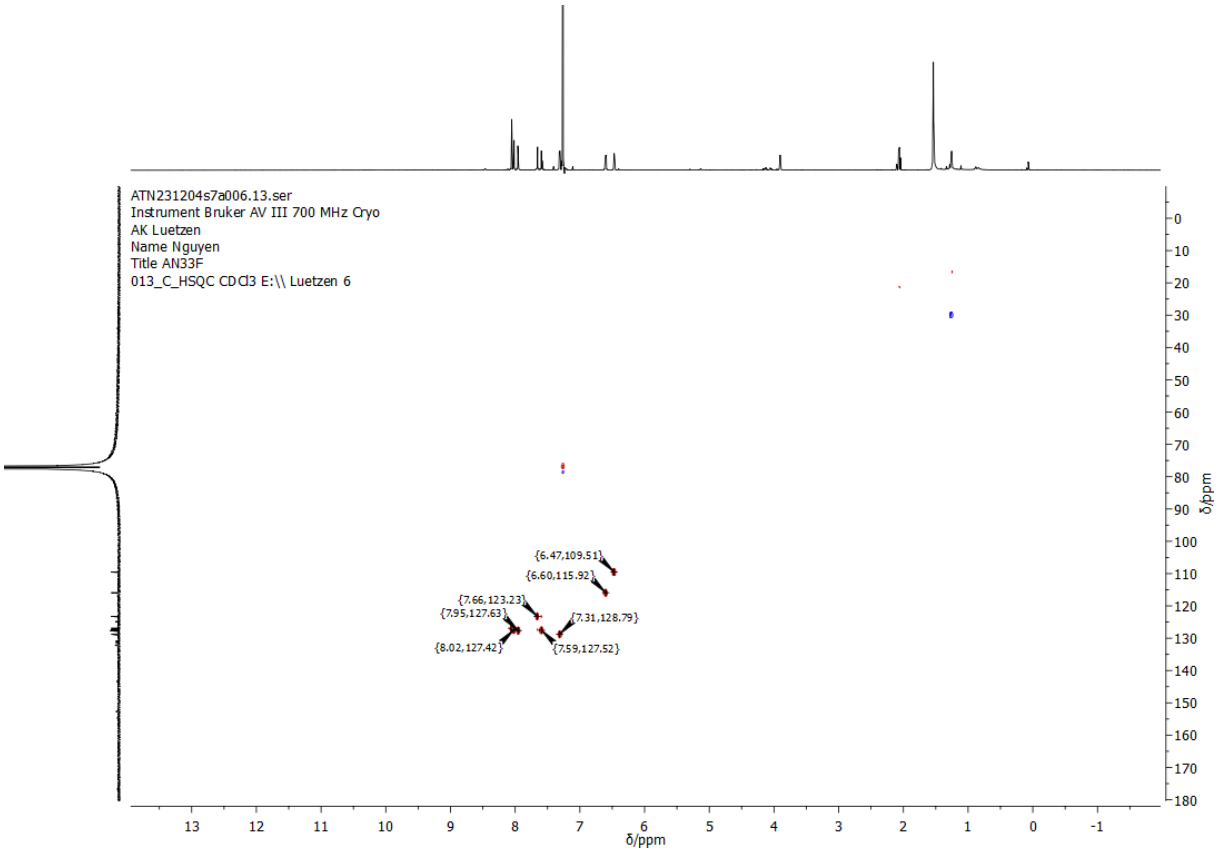

Figure 260: HSQC-NMR spectrum of **89** in $CDCl_3$.

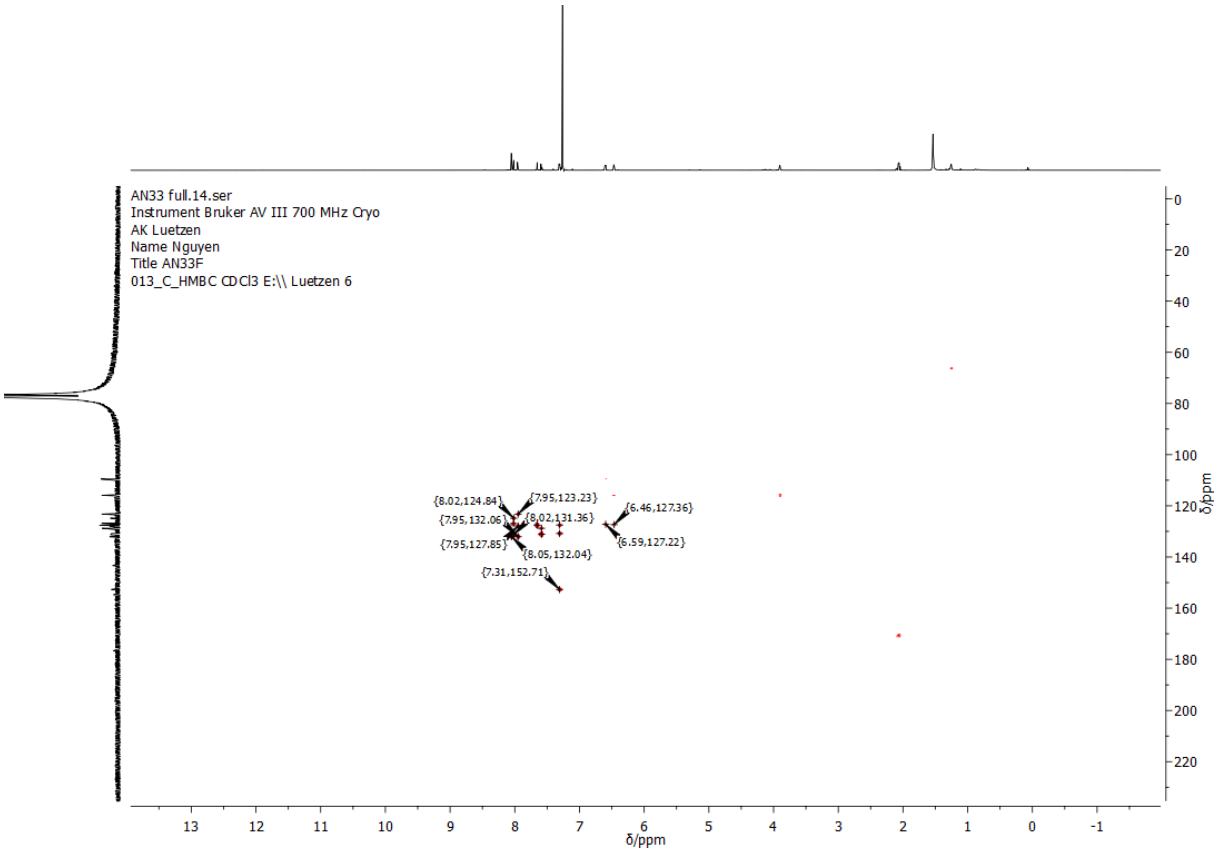

Figure 261: HMBC-NMR spectrum of **89** in $CDCl_3$.

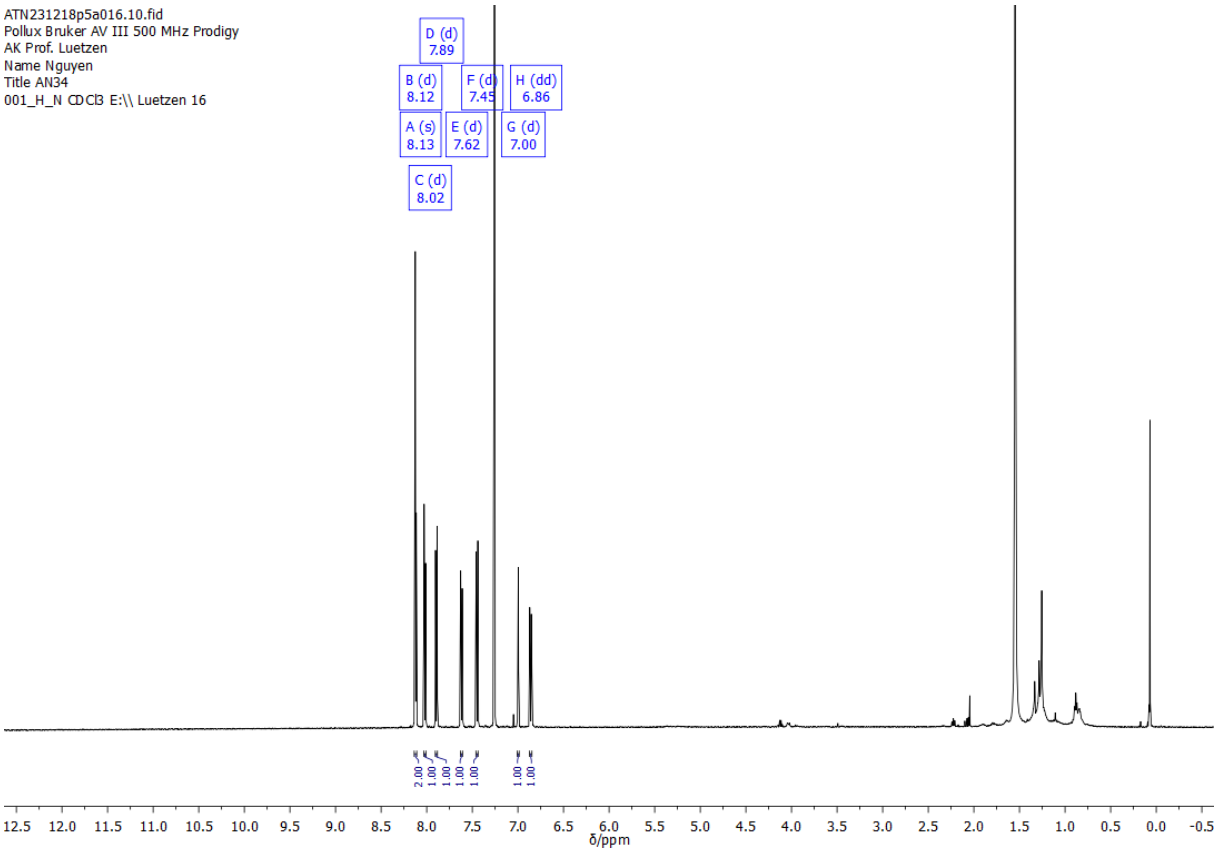

Figure 262: ^{1}H-NMR spectrum of **90** in $CDCl_3$.

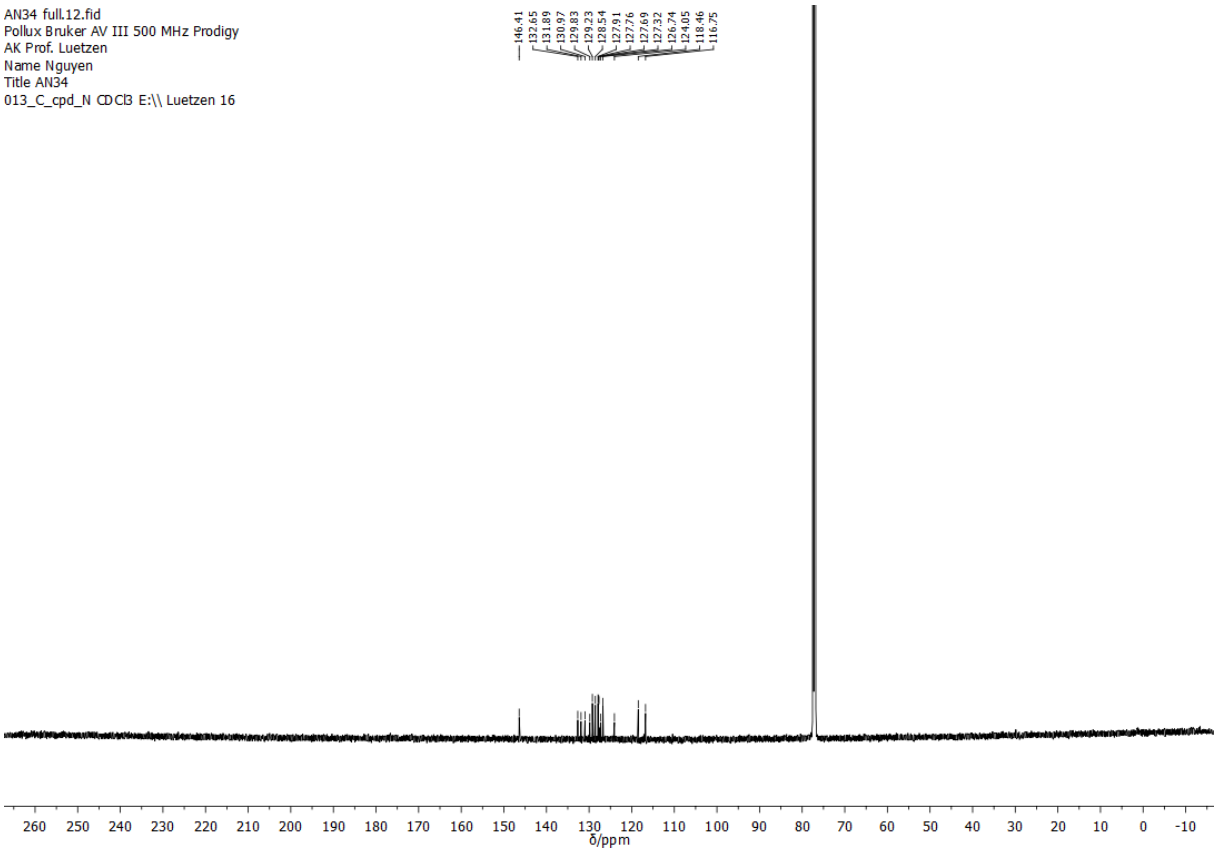

Figure 263: ^{13}C-NMR spectrum of **90** in $CDCl_3$.

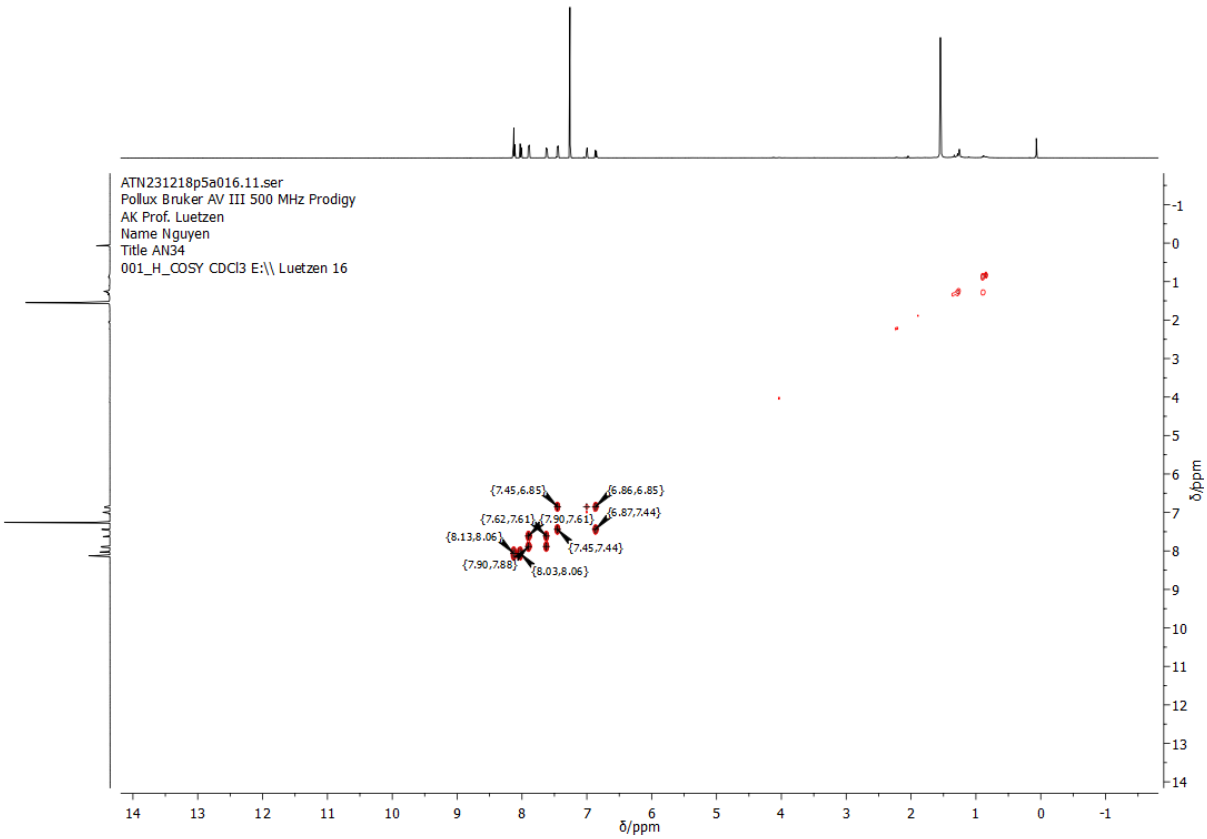

Figure 264: COSY-NMR spectrum of **90** in $CDCl_3$.

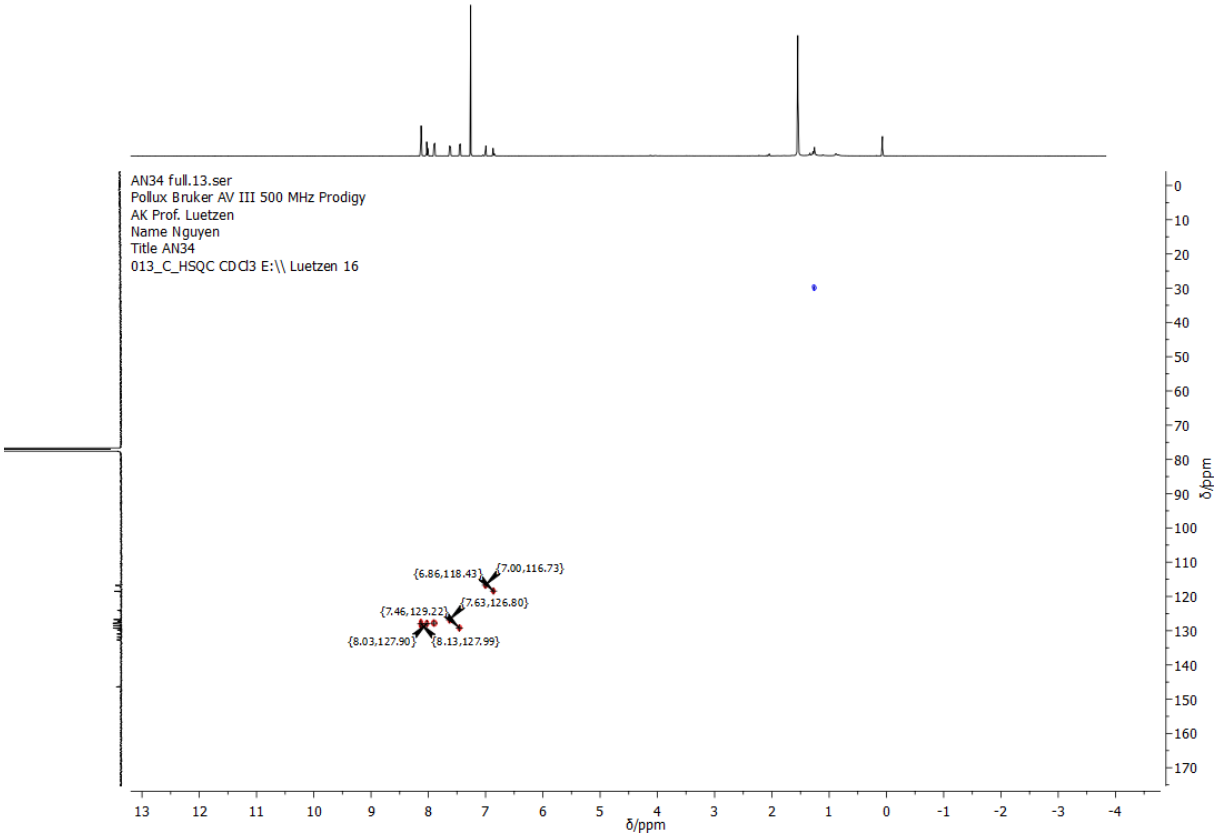

Figure 265: HSQC-NMR spectrum of **90** in $CDCl_3$.

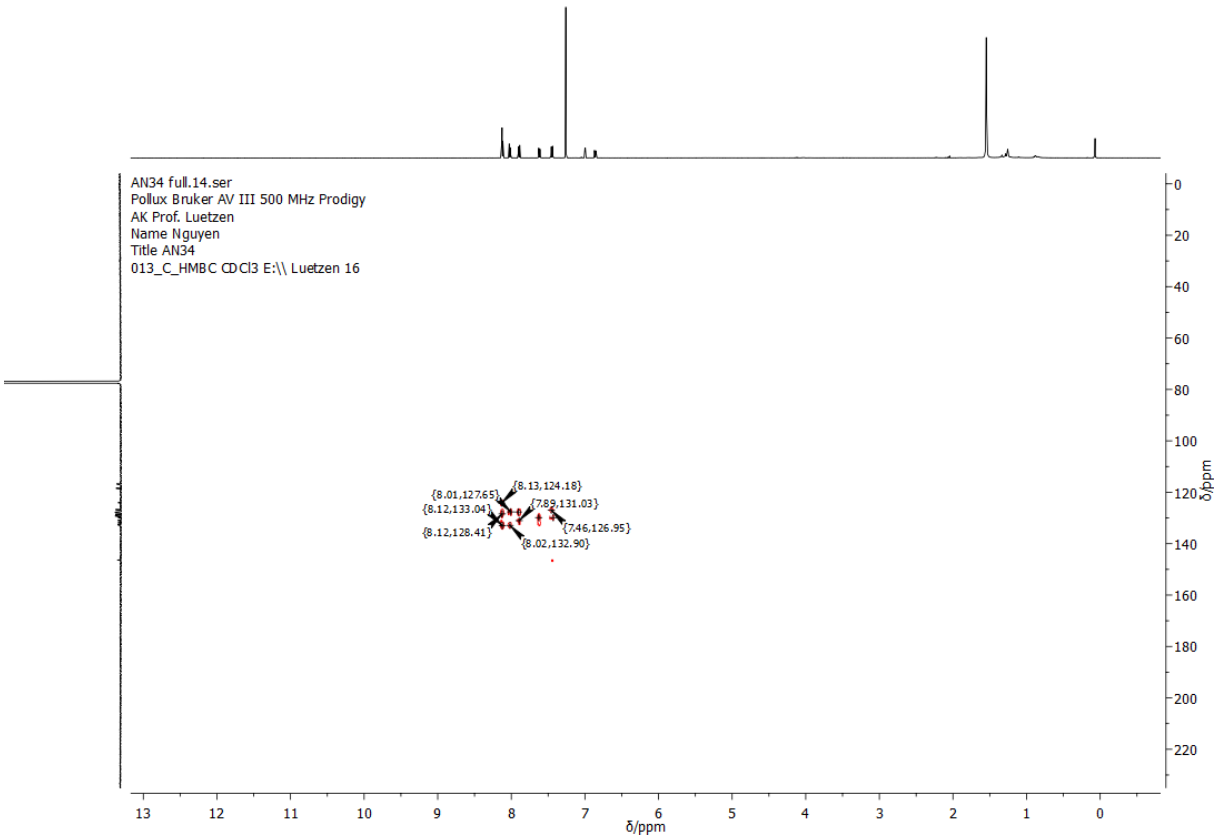

Figure 266: HMBC-NMR spectrum of **90** in $CDCl_3$.

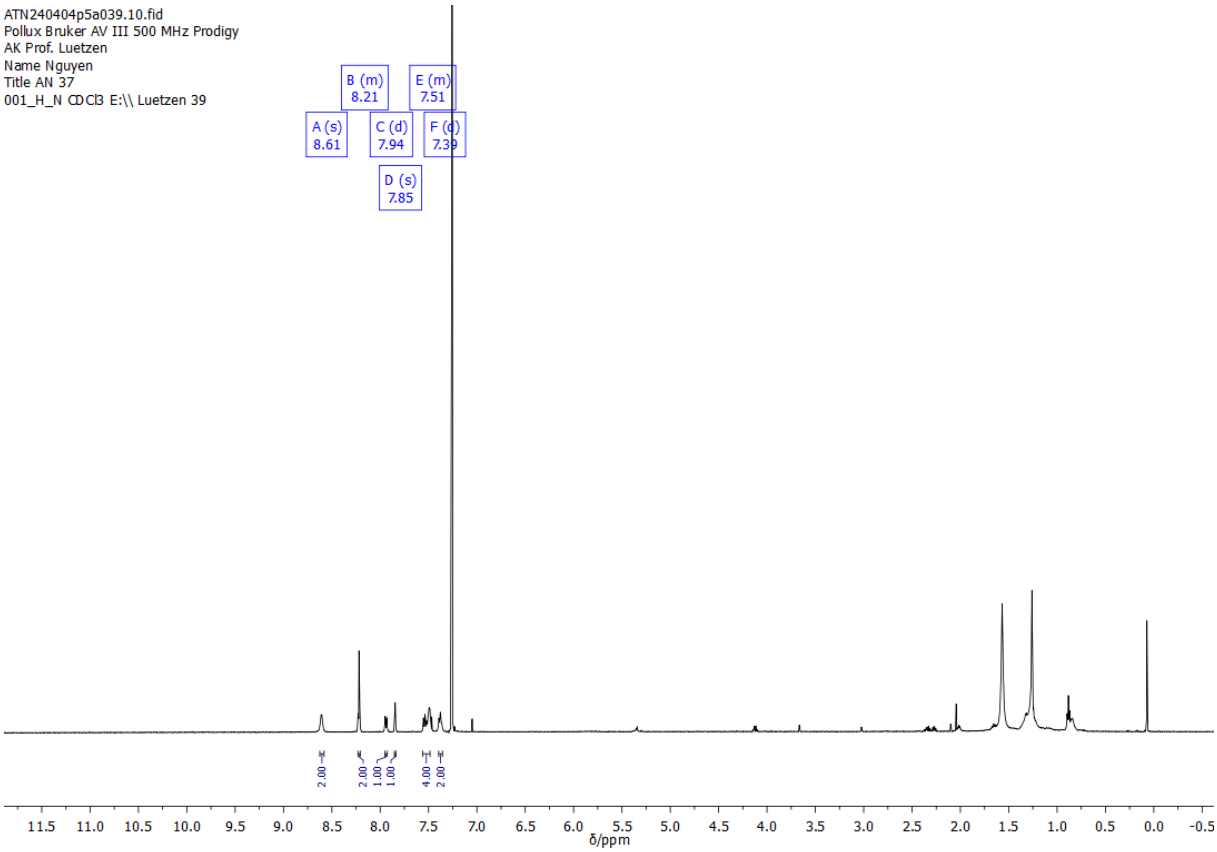

Figure 267: ^{1}H-NMR spectrum of **91** in $CDCl_3$.

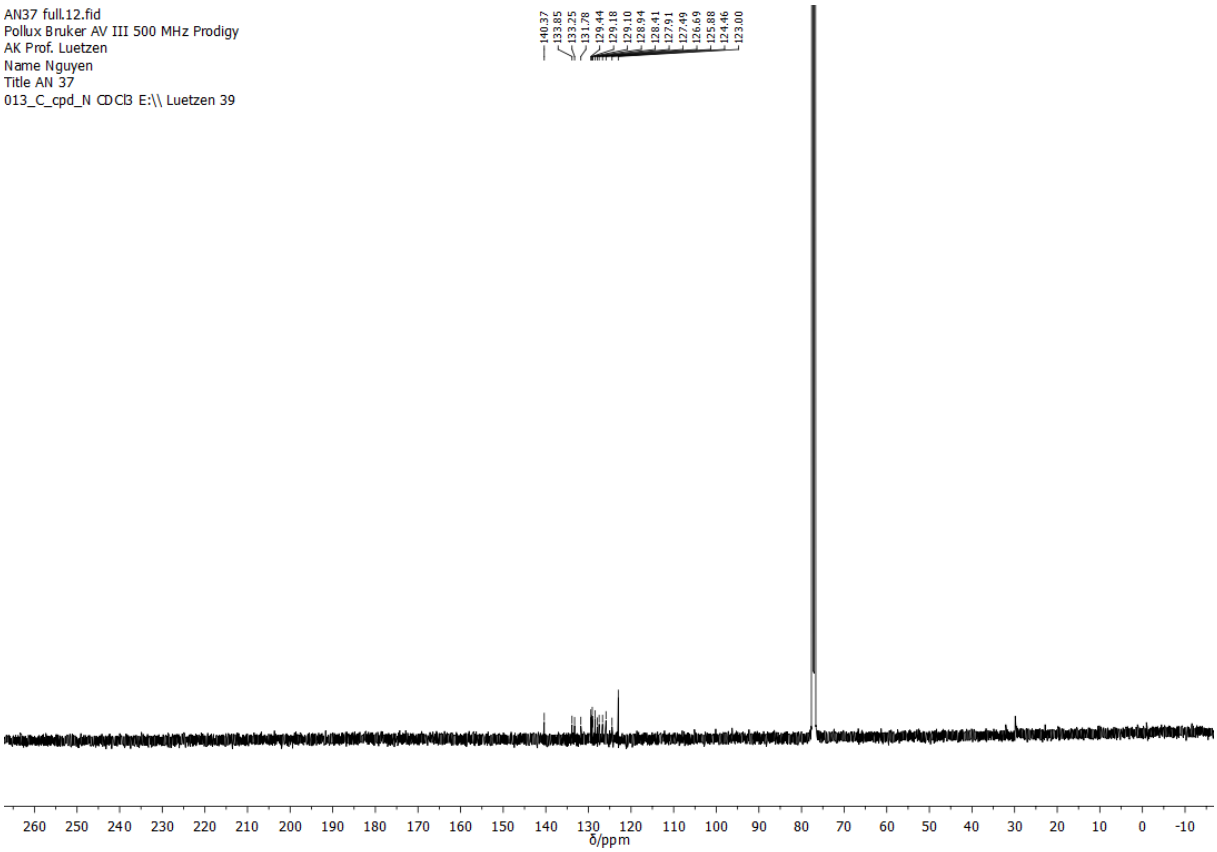

Figure 268: ^{13}C-NMR spectrum of **91** in $CDCl_3$.

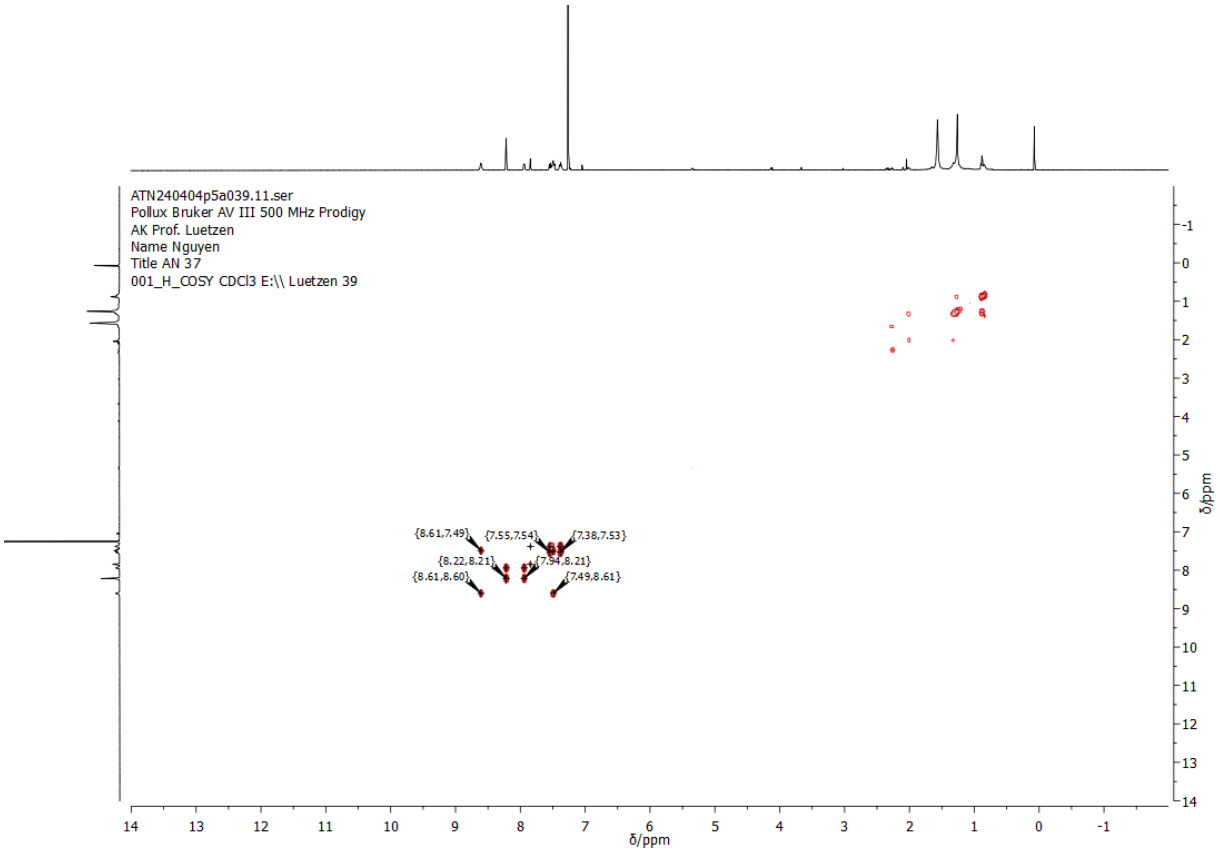

Figure 269: COSY-NMR spectrum of **91** in $CDCl_3$.

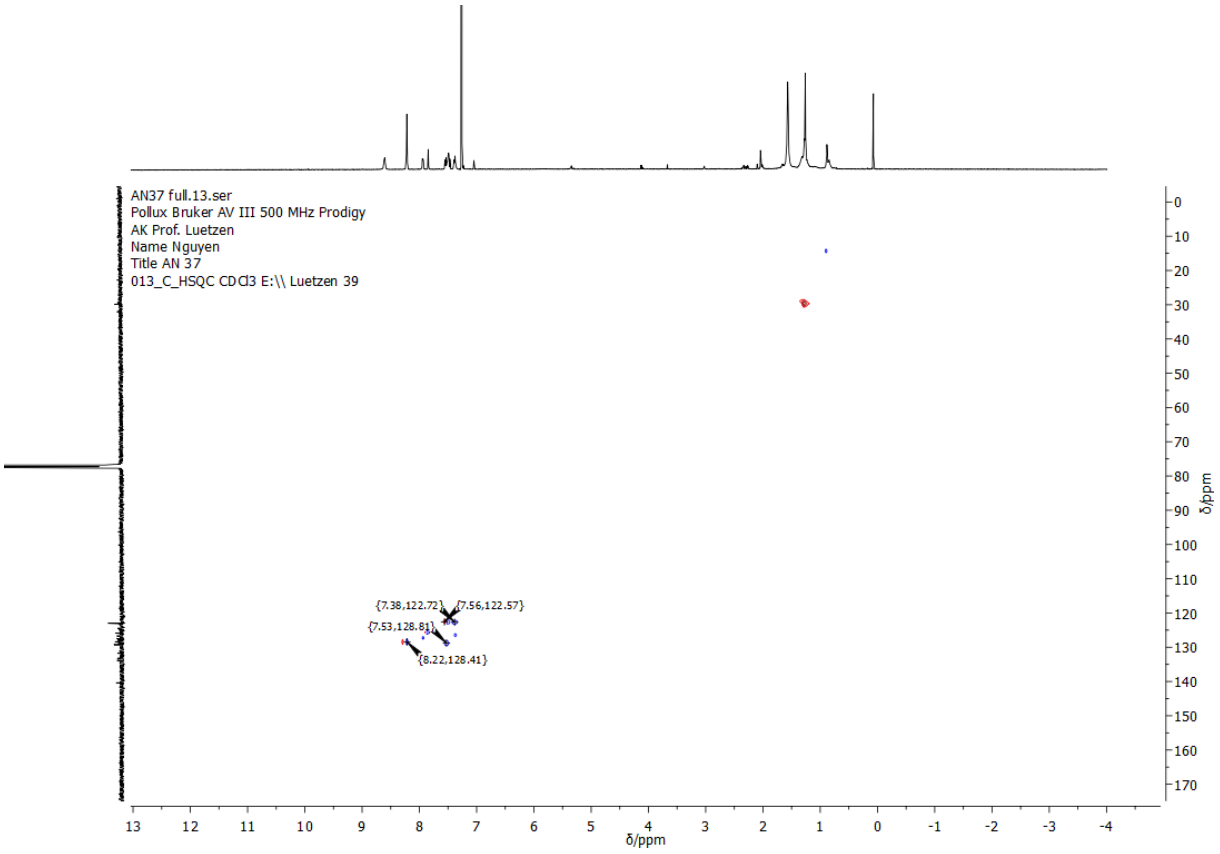

Figure 270: HSQC-NMR spectrum of **91** in $CDCl_3$.

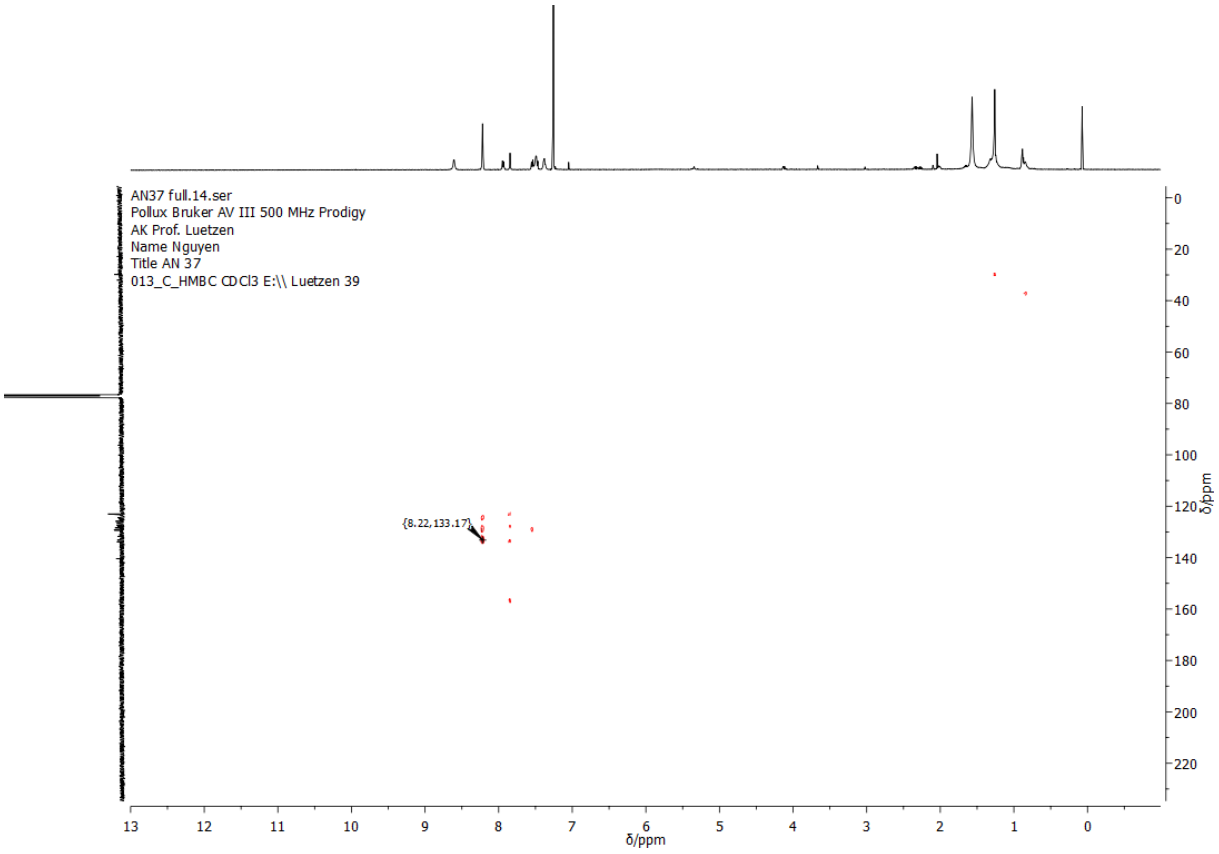

Figure 271: HMBC-NMR spectrum of **91** in $CDCl_3$.

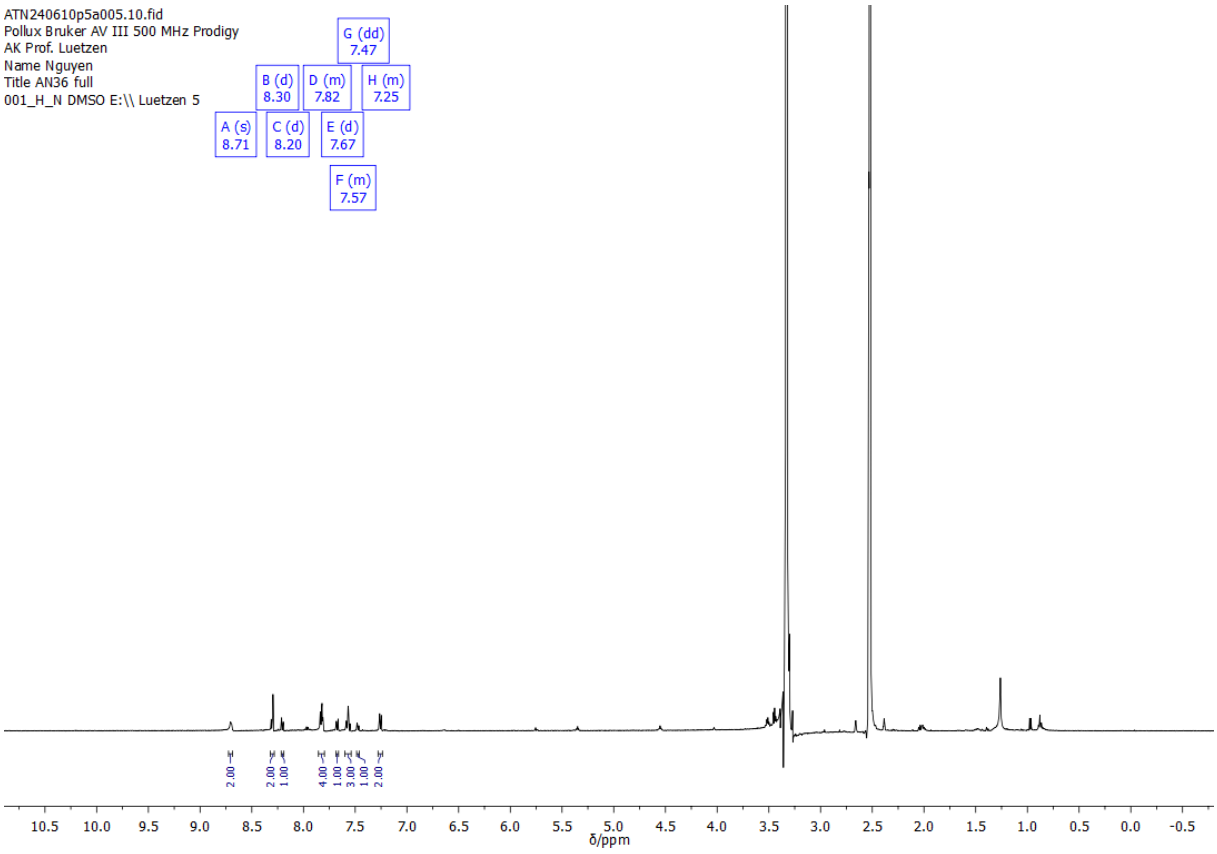

Figure 272: ^{1}H-NMR spectrum of **92** in DMSO-d6.

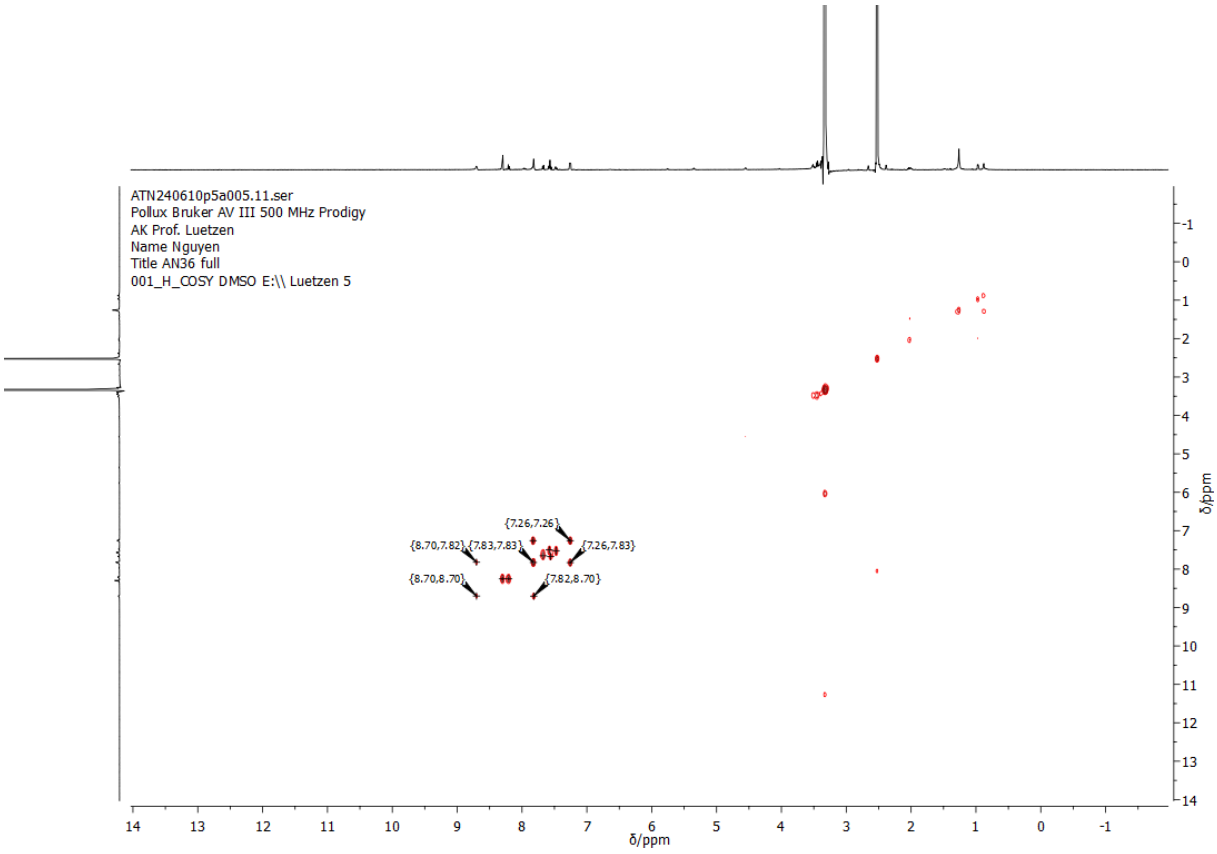

Figure 273: COSY-NMR spectrum of **92** in DMSO-d6.

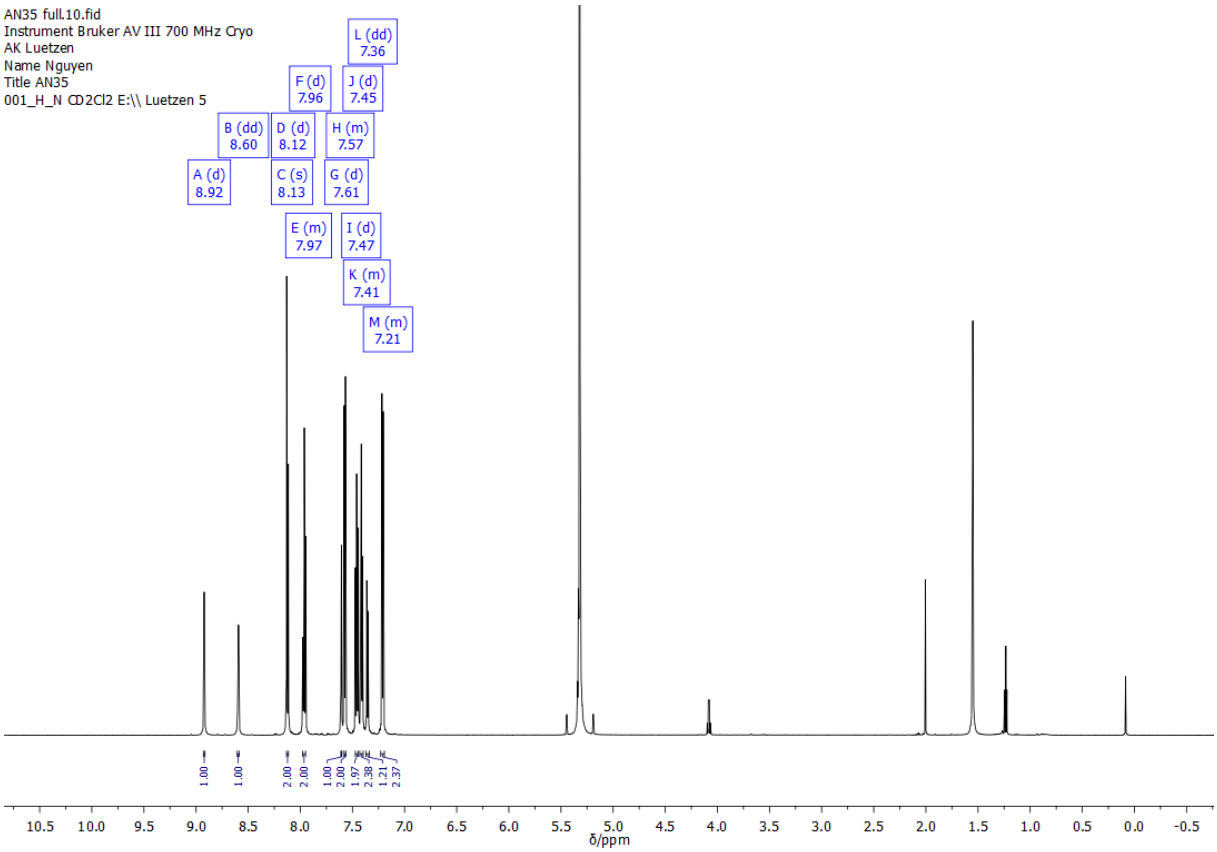

Figure 274: ^{1}H-NMR spectrum of **93** in CD_2Cl_2.

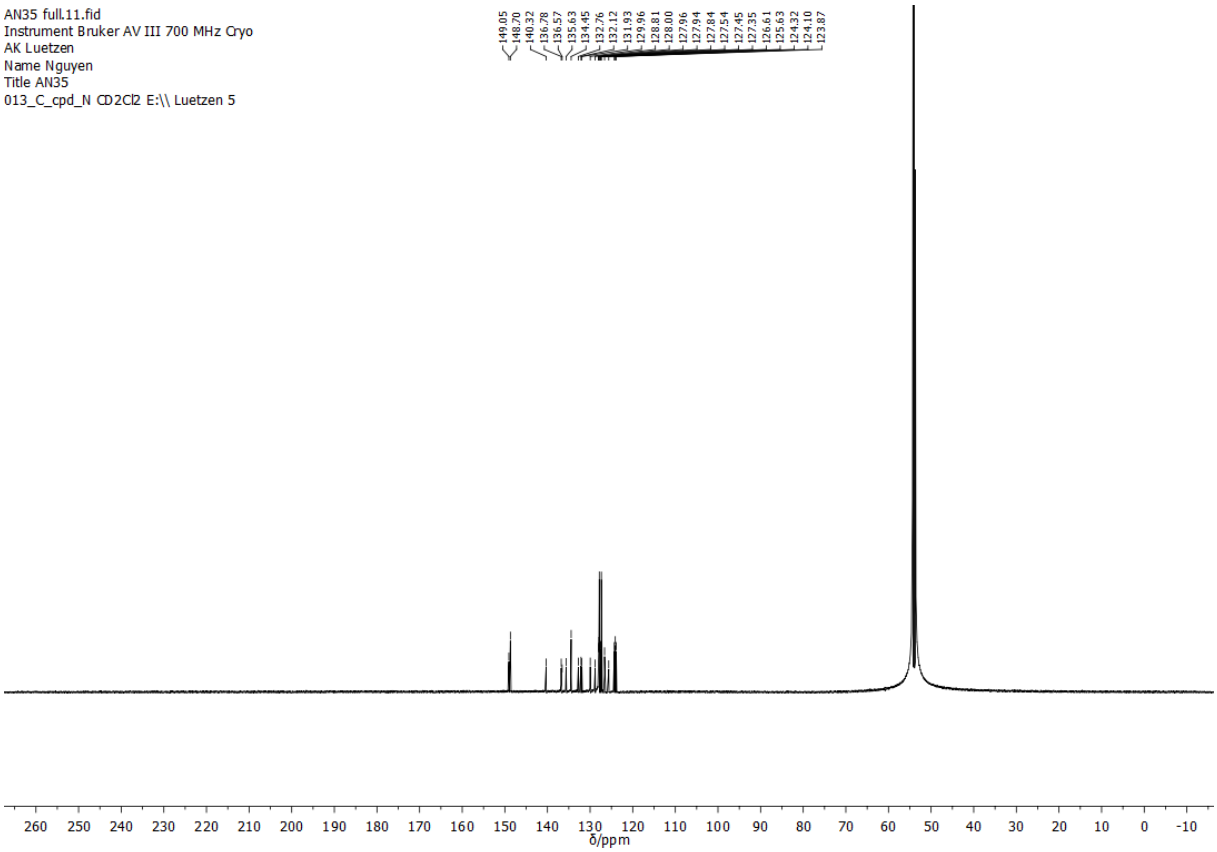

Figure 275: ^{13}C-NMR spectrum of **93** in CD_2Cl_2.

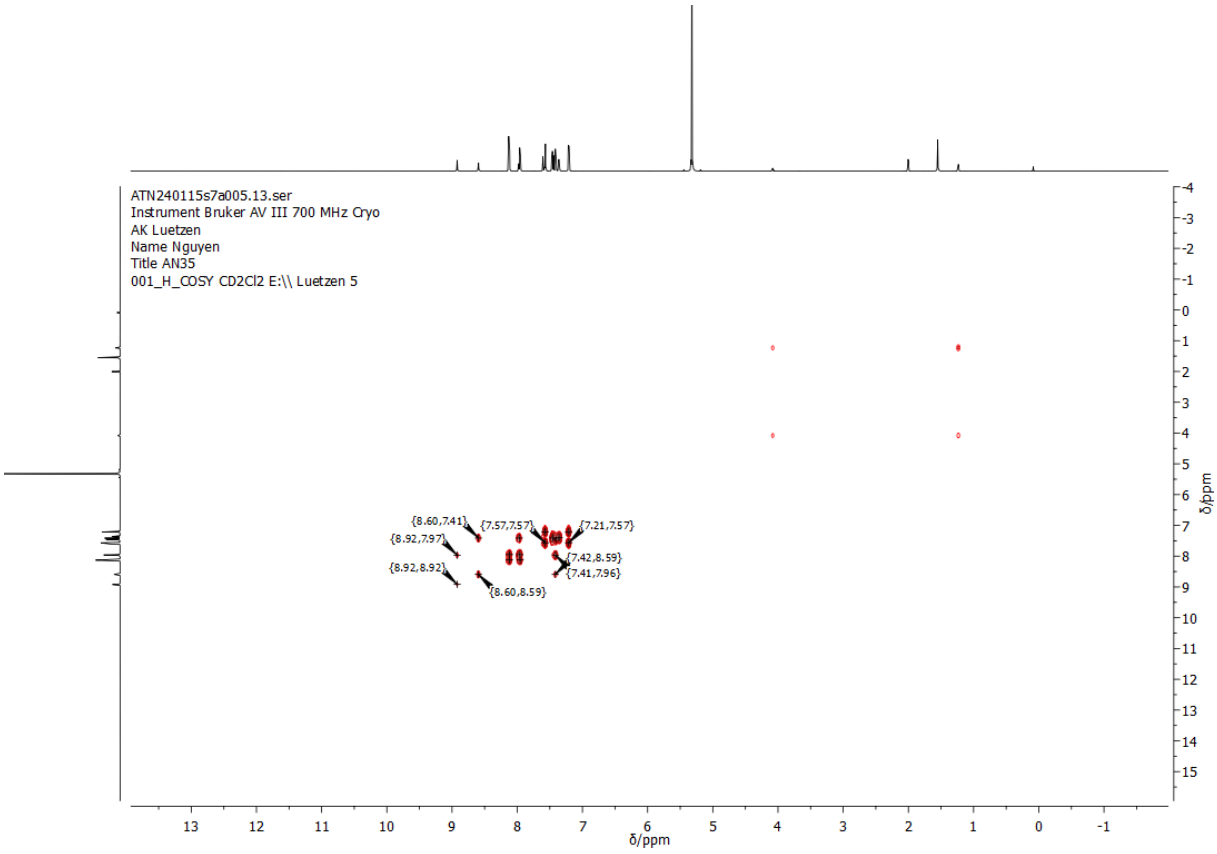

Figure 276: COSY-NMR spectrum of **93** in CD_2Cl_2.

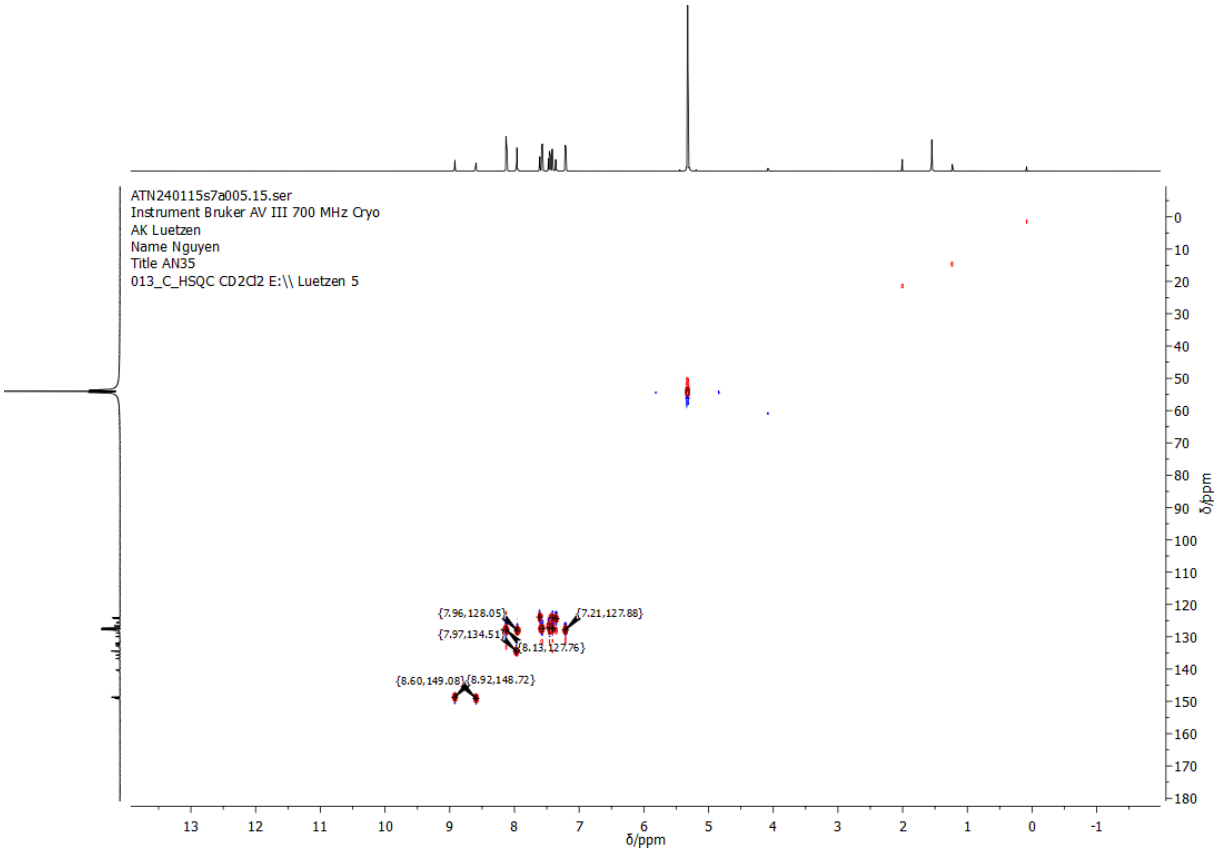

Figure 277: HSQC-NMR spectrum of **93** in CD_2Cl_2.

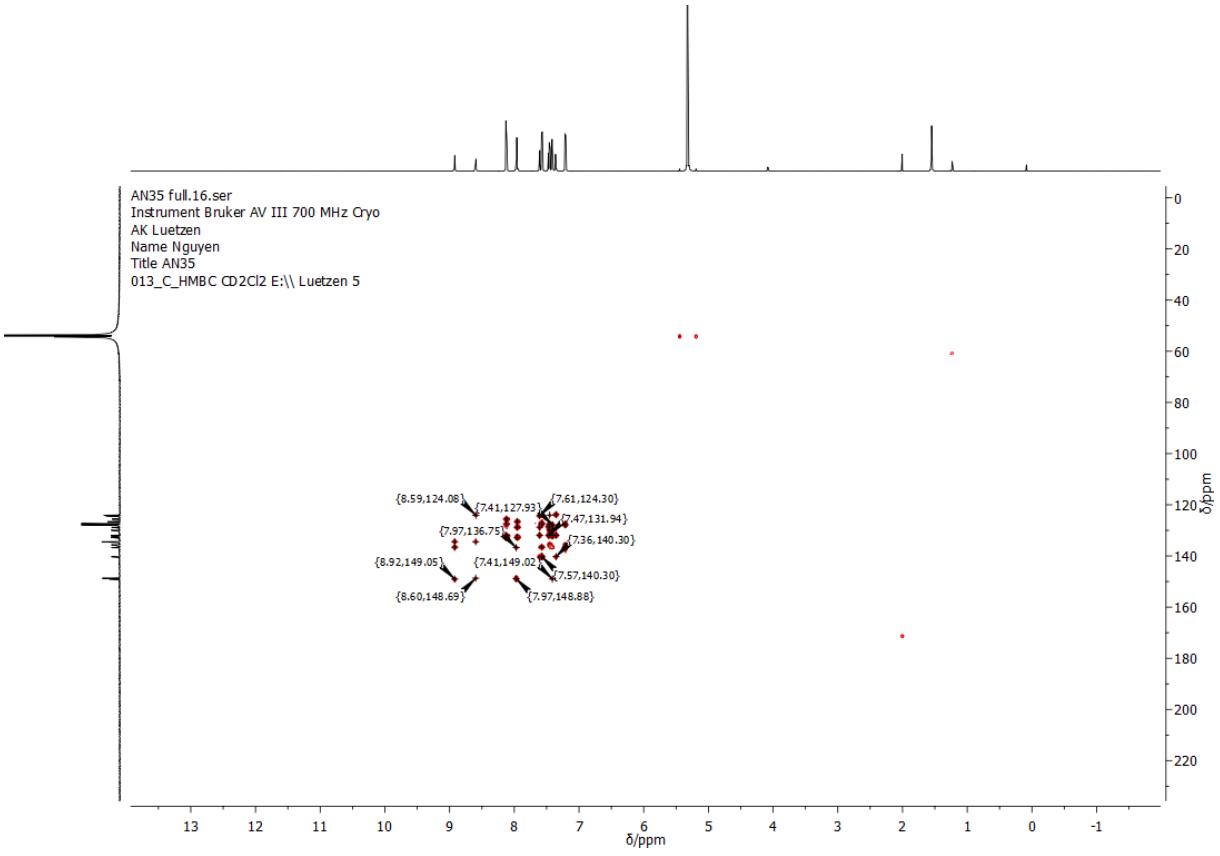

Figure 278: HMBC-NMR spectrum of **93** in CD_2Cl_2.

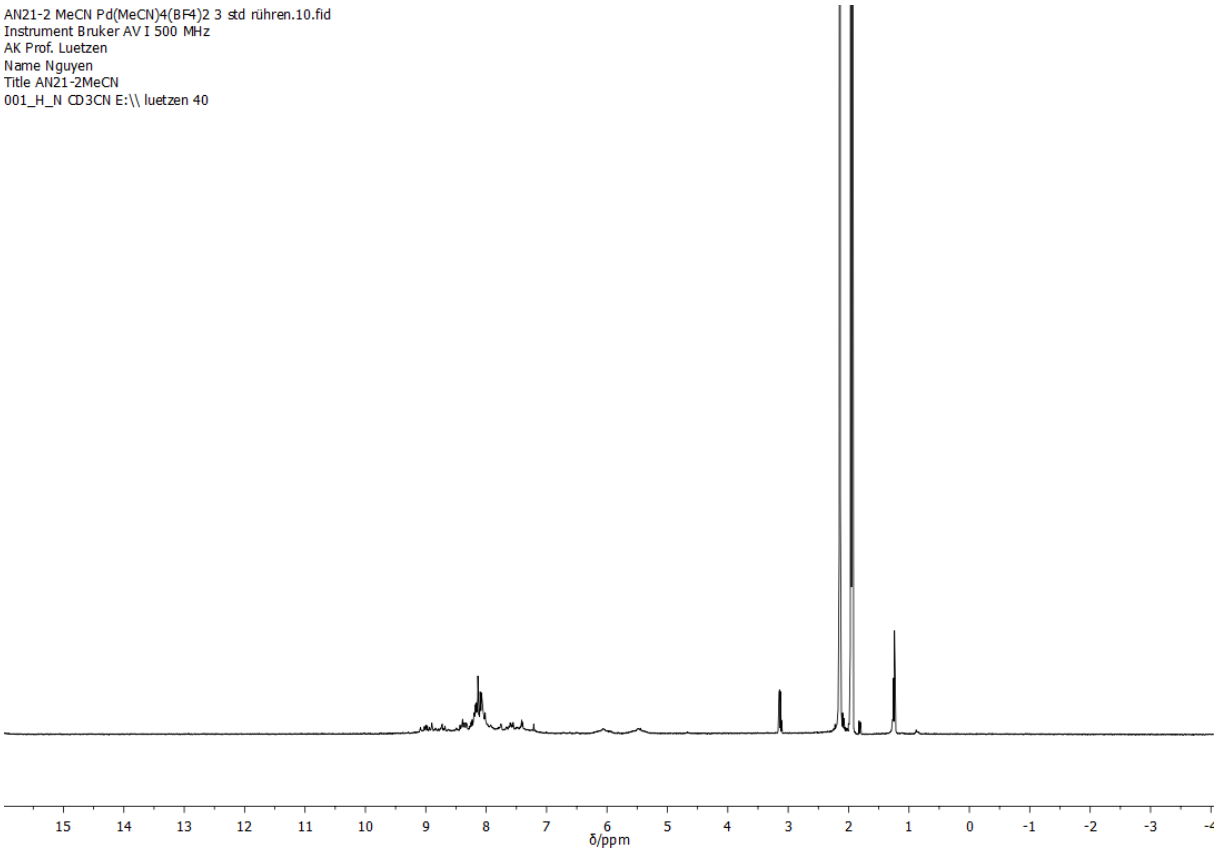

Figure 279: ^{1}H-NMR spectrum of complexation of **76** with $Pd(MeCN)_4(BF_4)_2$ in CD_3CN.

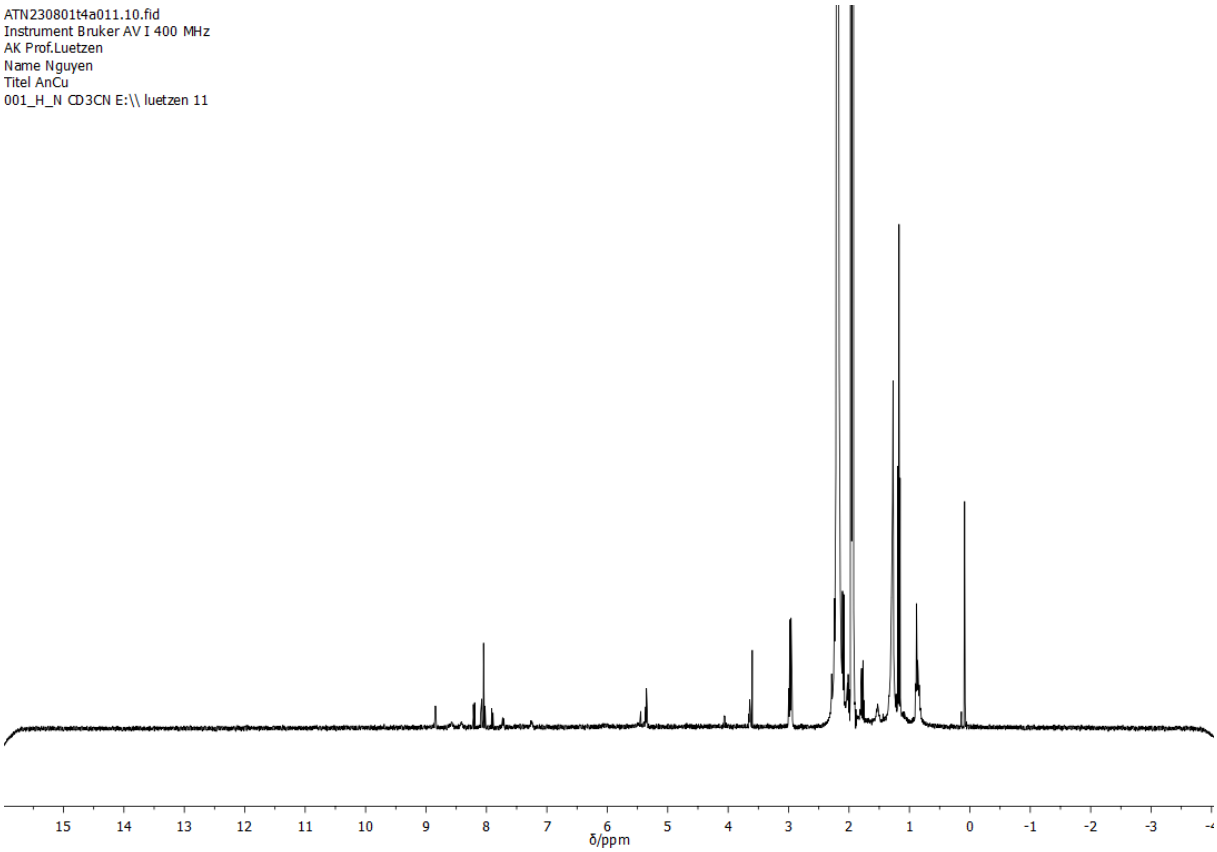

Figure 280: ^{1}H-NMR spectrum of complexation of **76** with $Cu(MeCN)_4(BF_4)$ in CD_3CN.

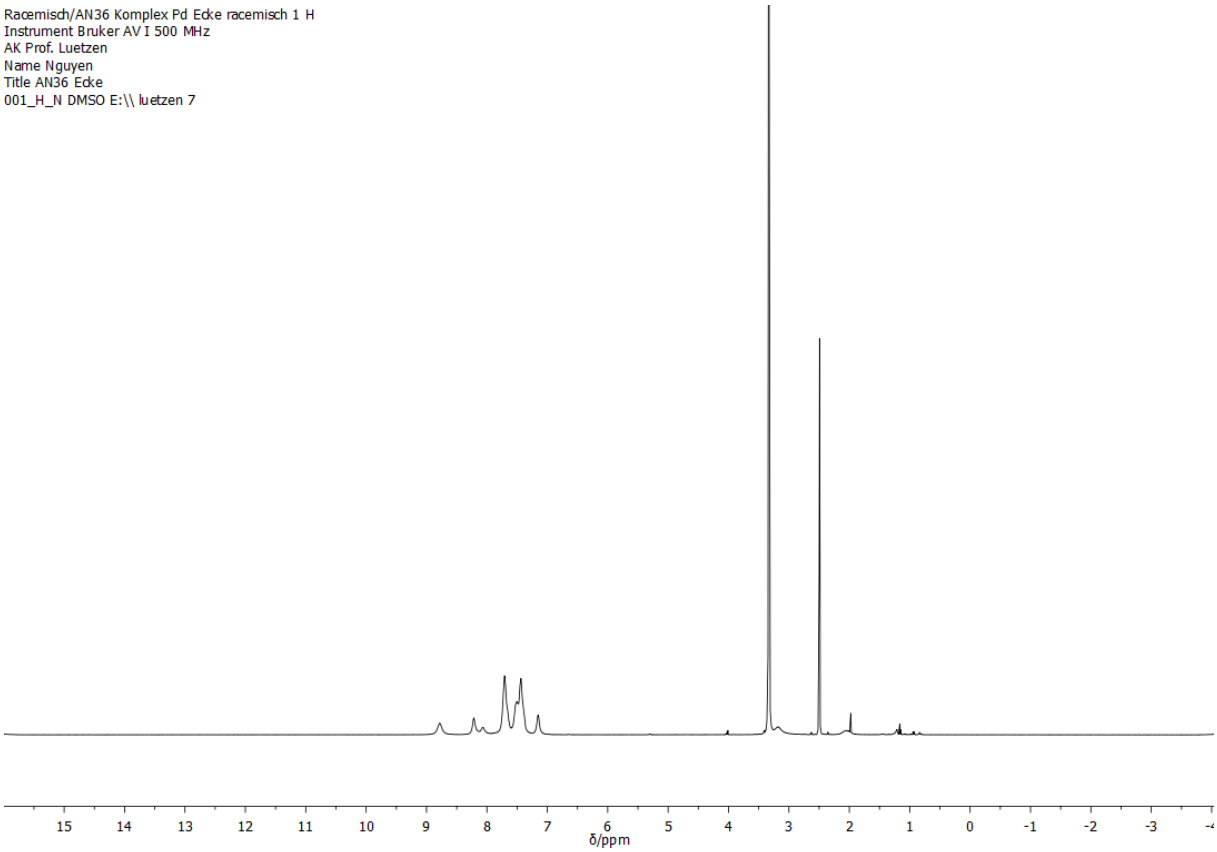

Figure 281: ^{1}H-NMR spectrum of complexation of (*rac*)-**92** with Pd(dppp)(OTf)$_2$ in DMSO-d6.

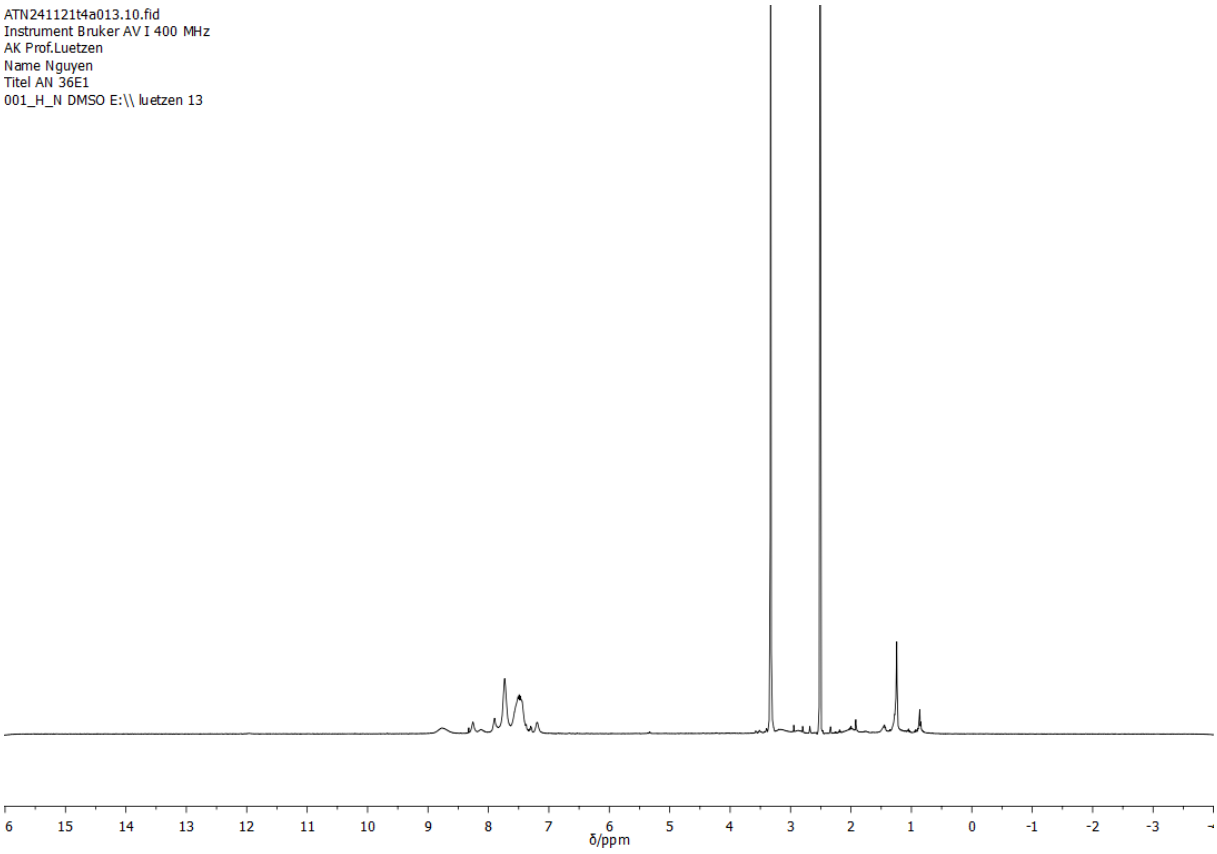

Figure 282: ^{1}H-NMR spectrum of complexation of (*M*)-**92** with Pd(dppp)(OTf)$_2$ in DMSO-d6.

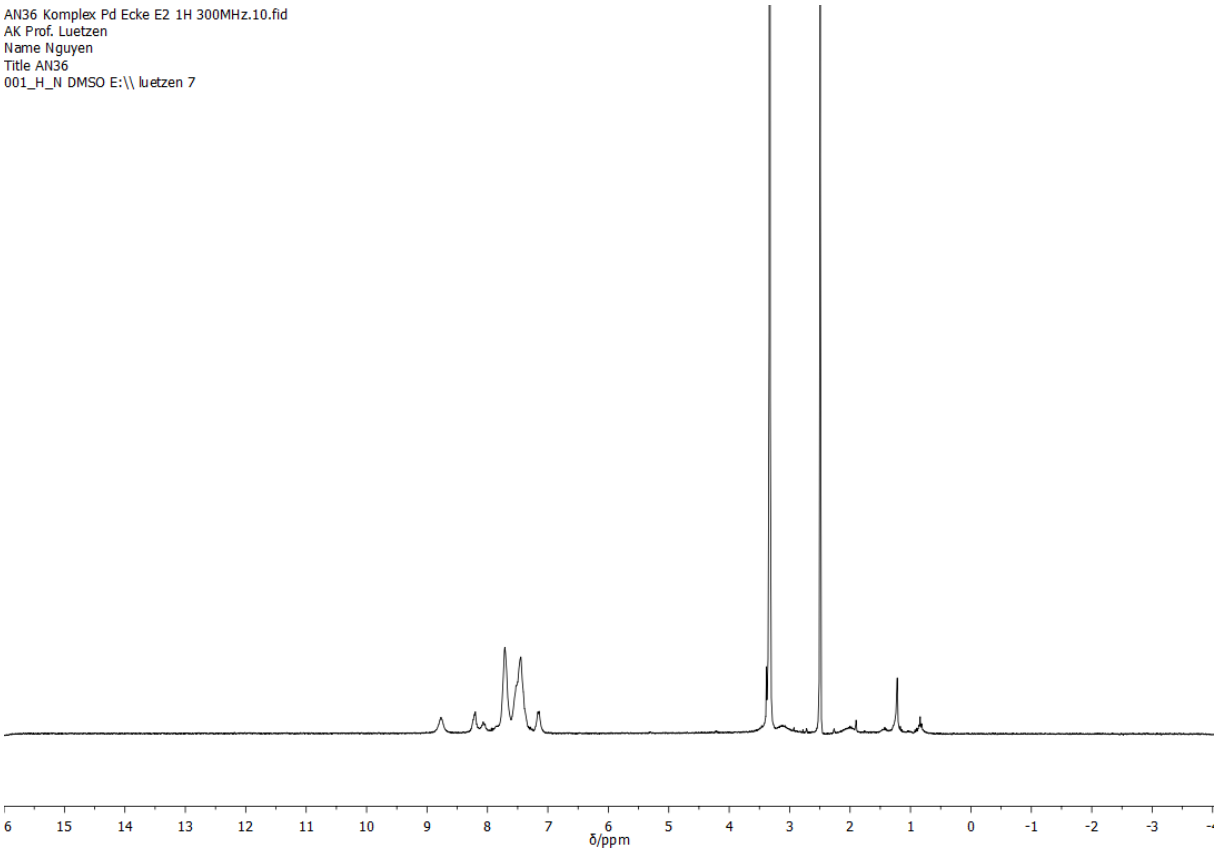

Figure 283: ^{1}H-NMR spectrum of complexation of (*P*)-**92** with Pd(dppp)(OTf)$_2$ in DMSO-d6.

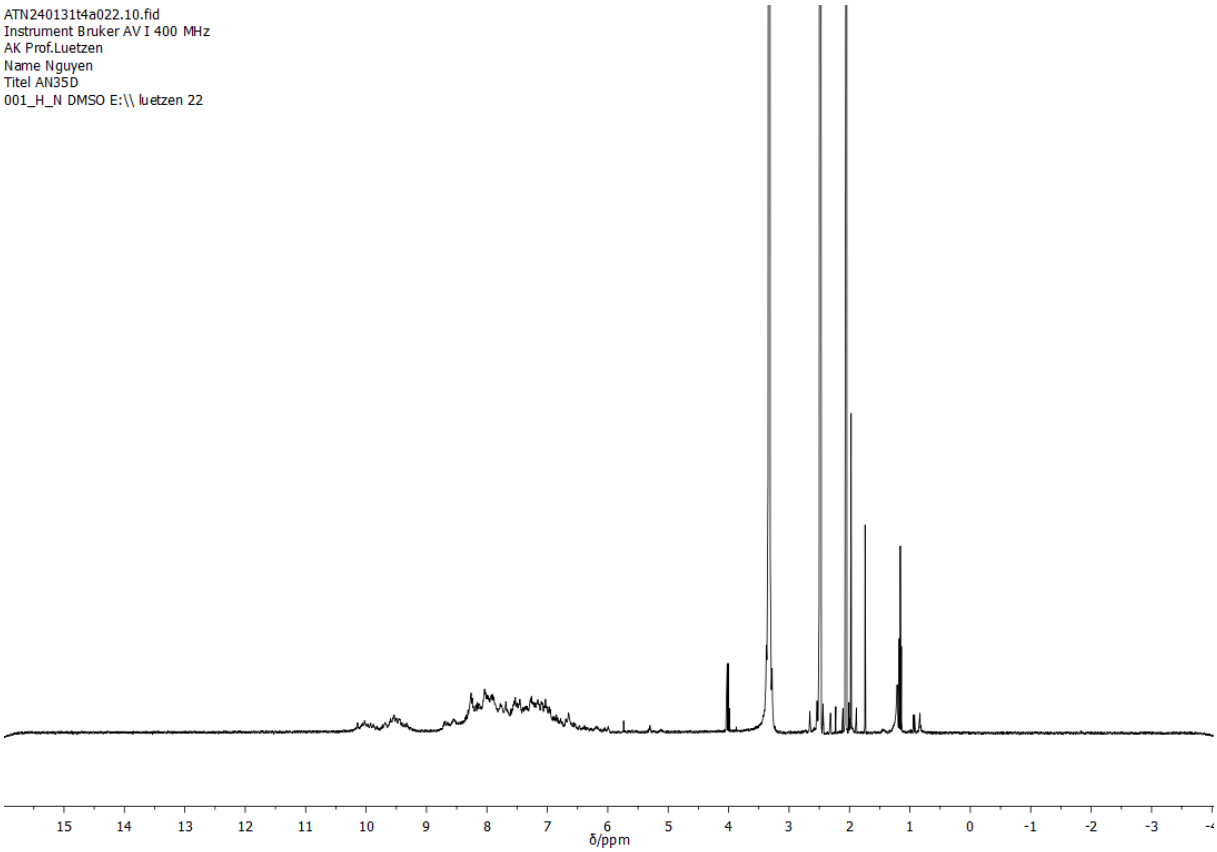

Figure 284: ^{1}H-NMR spectrum of complexation of (*rac*)-**93** with Pd(MeCN)$_4$(BF$_4$)$_2$ in DMSO-d6.

13.3 Mass spectra

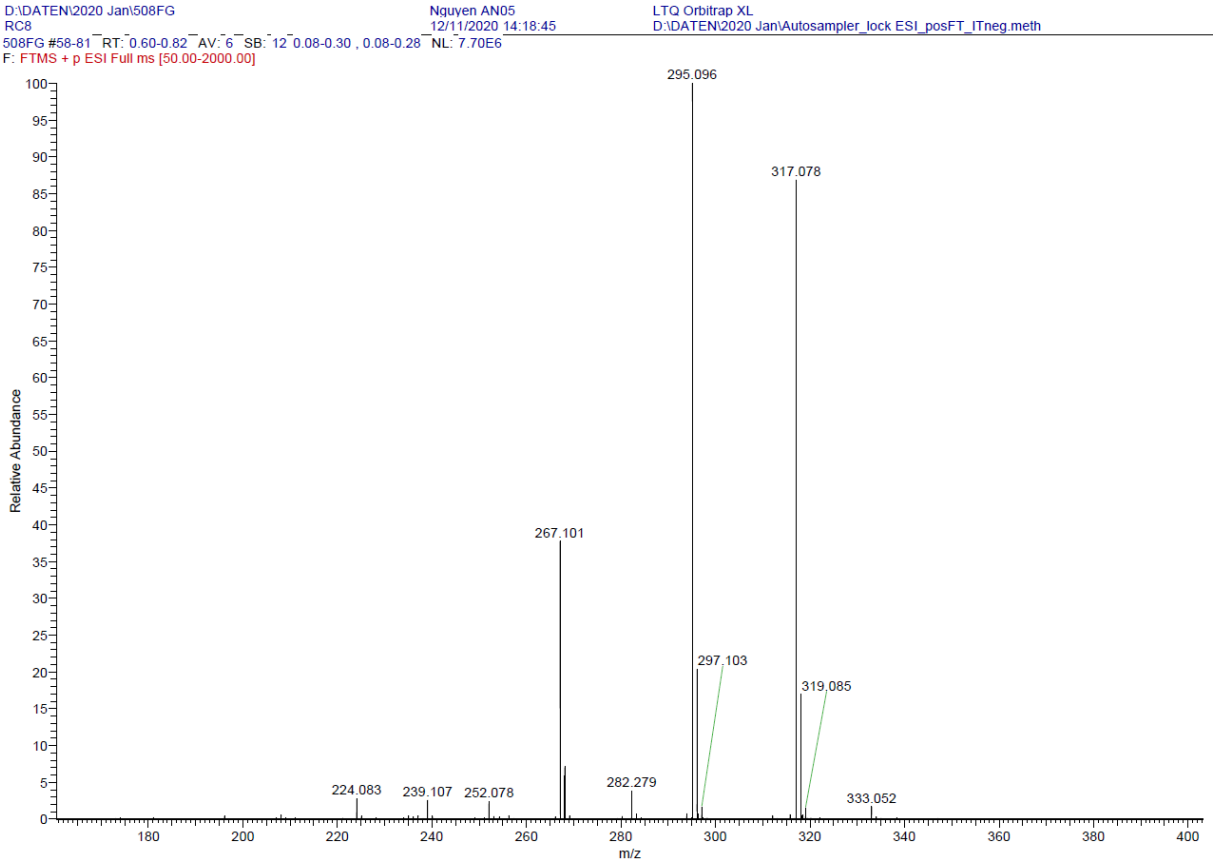

Figure 285: ESI(+)-mass spectrum of **16**.

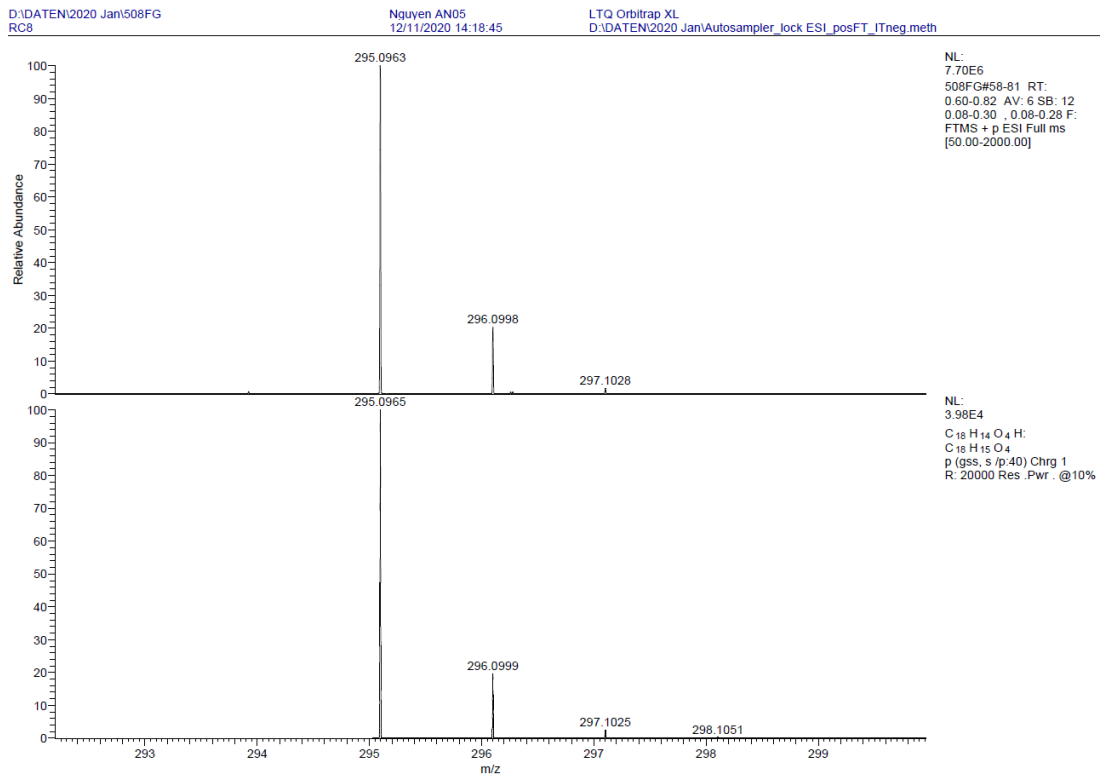

Figure 286: Experimental exact mass (top) and calculated exact mass (bottom) of **16**.

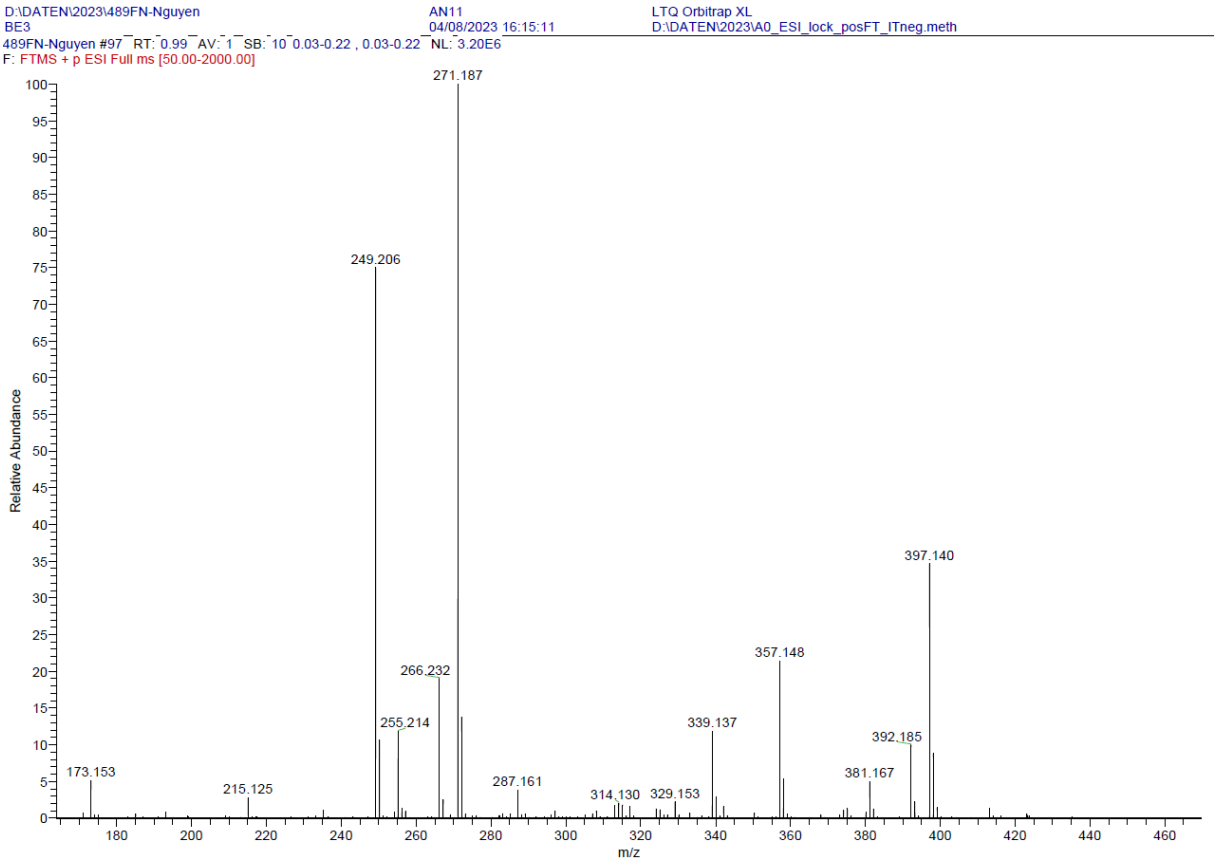

Figure 287: ESI(+)-mass spectrum of **17**.

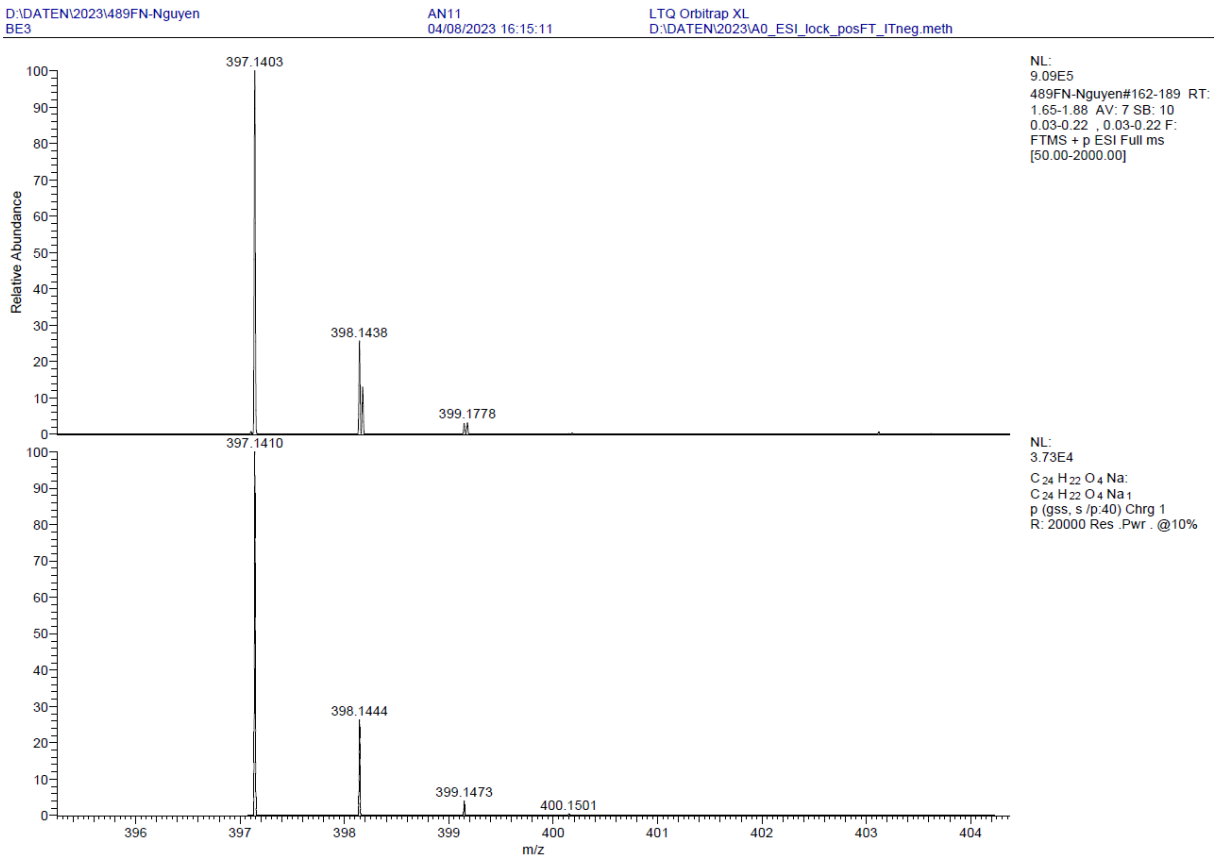

Figure 288: Experimental exact mass (top) and calculated exact mass (bottom) of **17**.

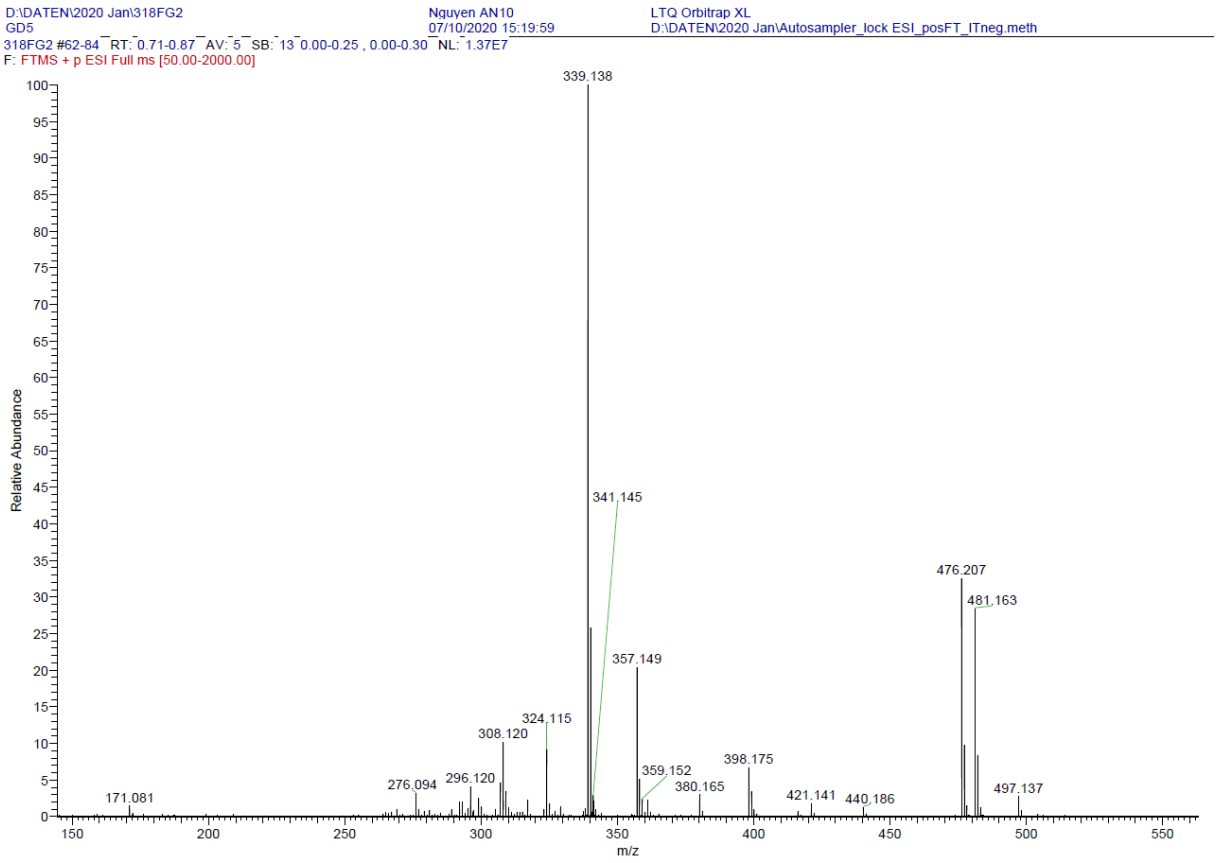

Figure 289: ESI(+)-mass spectrum of **18**.

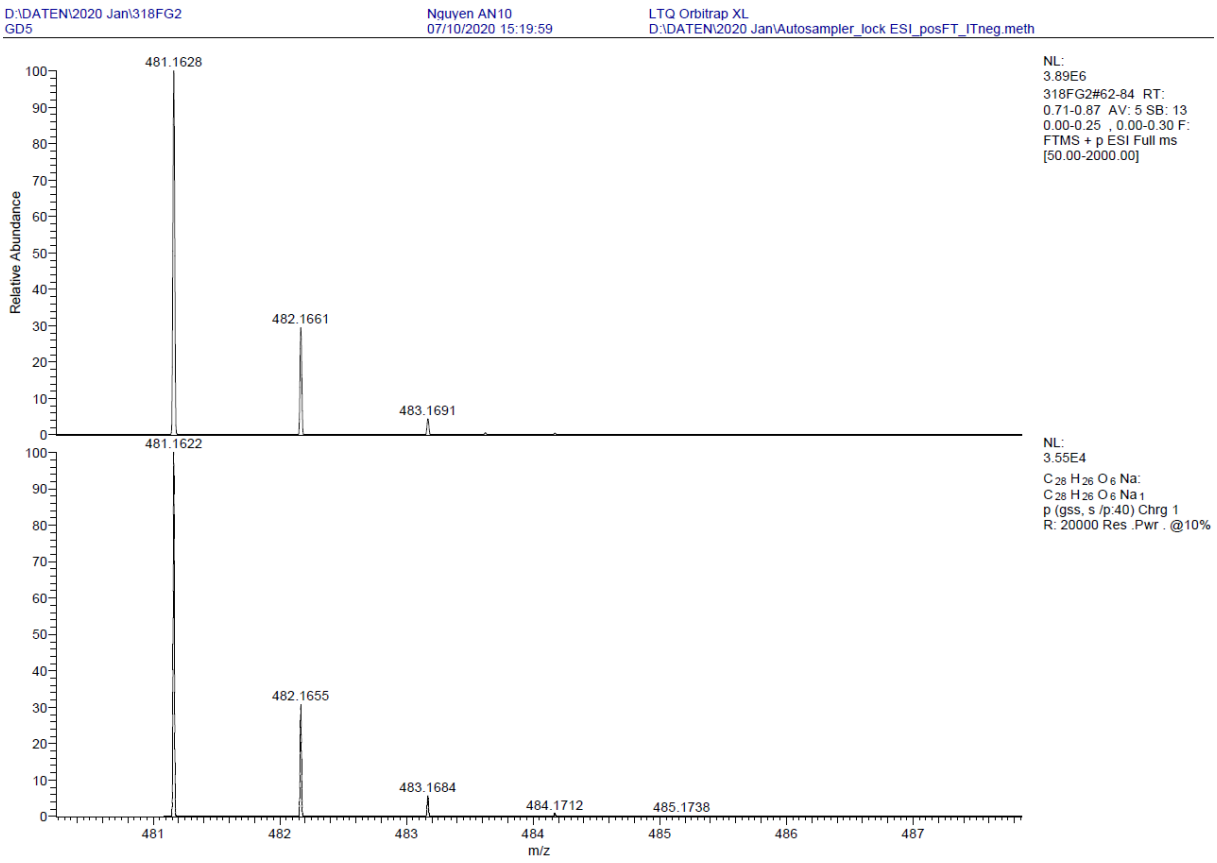

Figure 290: Experimental exact mass (top) and calculated exact mass (bottom) of **18**.

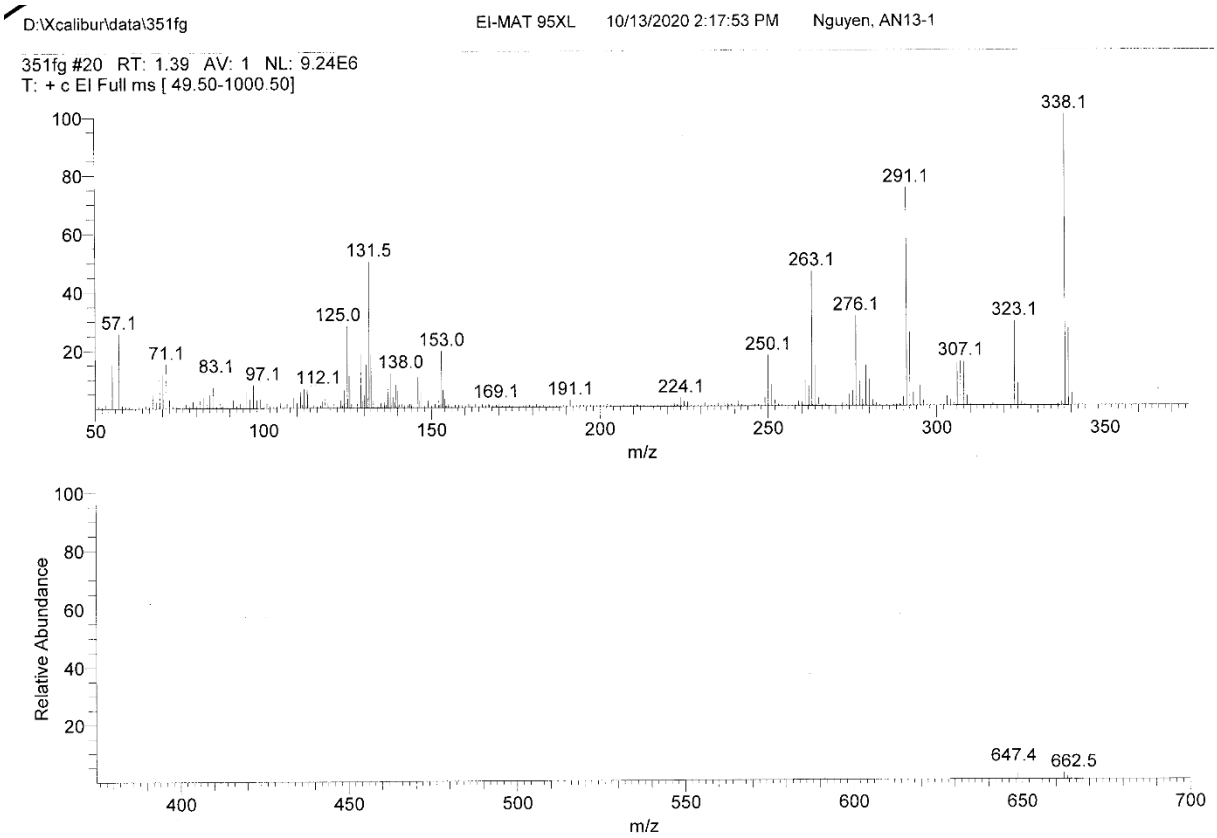

Figure 291: EI-mass spectrum of **20**.

UCLR USER LIST FILE (4x500): 538f1 SAVE

1:	338.13129	0.00000	0.00000	0.00000
2:	338.13128	0.00000	0.00000	0.00000
3:	338.13117	0.00000	0.00000	0.00000
4:	338.13126	0.00000	0.00000	0.00000
5:	338.13081	0.00000	0.00000	0.00000
6:	338.13099	0.00000	0.00000	0.00000
7:	338.13090	0.00000	0.00000	0.00000
8:	338.13091	0.00000	0.00000	0.00000
9:	338.13163	0.00000	0.00000	0.00000
10:	338.13079	0.00000	0.00000	0.00000
11:	0.00000	0.00000	0.00000	0.00000
12:	0.00000	0.00000	0.00000	0.00000
13:	0.00000	0.00000	0.00000	0.00000
14:	0.00000	0.00000	0.00000	0.00000
15:	0.00000	0.00000	0.00000	0.00000
16:	0.00000	0.00000	0.00000	0.00000
17:	0.00000	0.00000	0.00000	0.00000
18:	0.00000	0.00000	0.00000	0.00000
19:	0.00000	0.00000	0.00000	0.00000
20:	0.00000	0.00000	0.00000	0.00000
LINK	NONE	NONE	NONE	NONE
SIZE	10.00000	0.00000	0.00000	0.00000
MEAN	338.13110	0.00000	0.00000	0.00000
SUM	3381.31103	0.00000	0.00000	0.00000
S.D.	0.00027	0.00000	0.00000	0.00000
MAX	338.13163	0.00000	0.00000	0.00000
MIN	338.13079	0.00000	0.00000	0.00000

ULIST: _

Thu Nov 3 14:38:07 2022 ICL version 10.621 5.July 1999 mat95 MAT 95

Figure 292: Experimental exact mass of **20**.

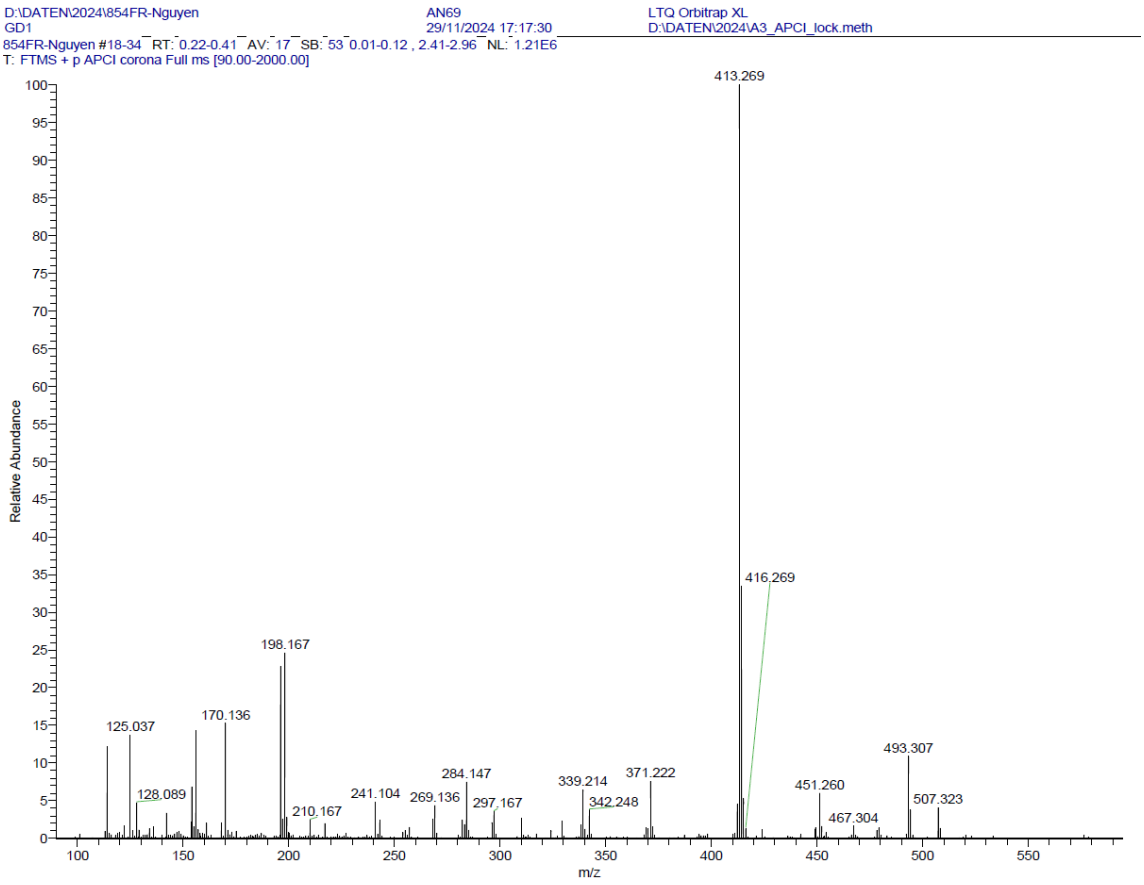

Figure 293: APCI-mass spectrum of **25**.

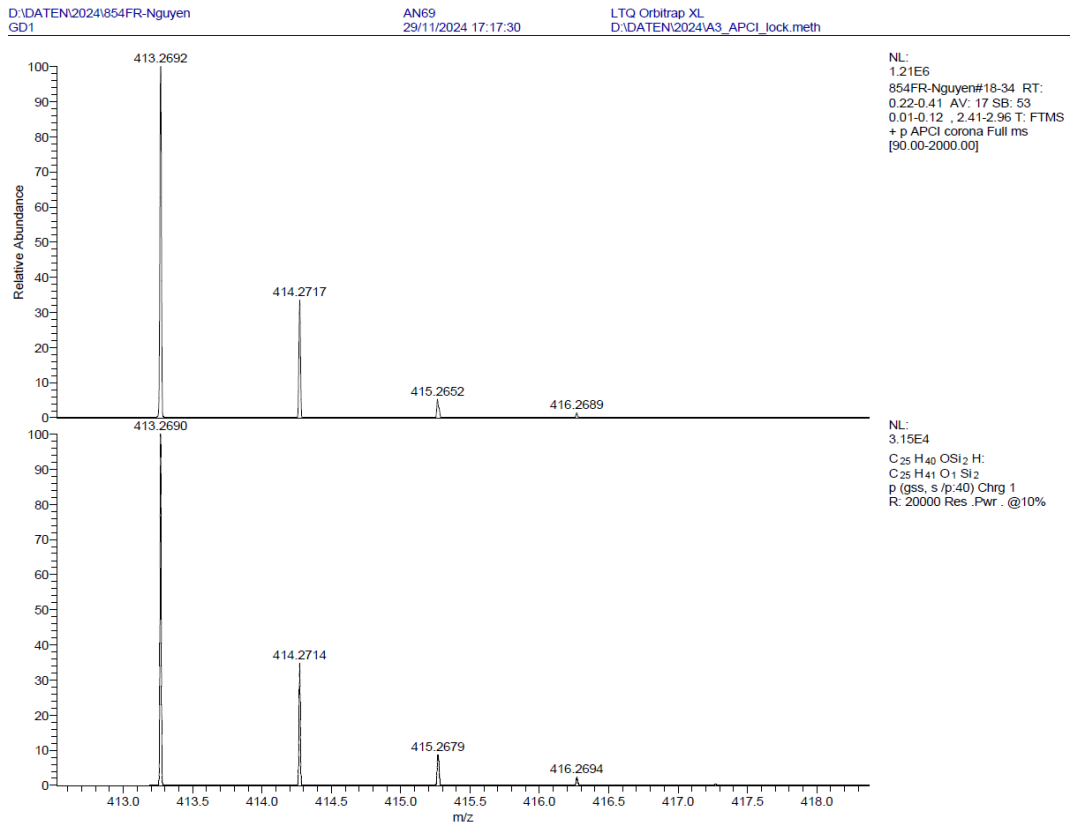

Figure 294: Experimental exact mass (top) and calculated exact mass (bottom) of **25**.

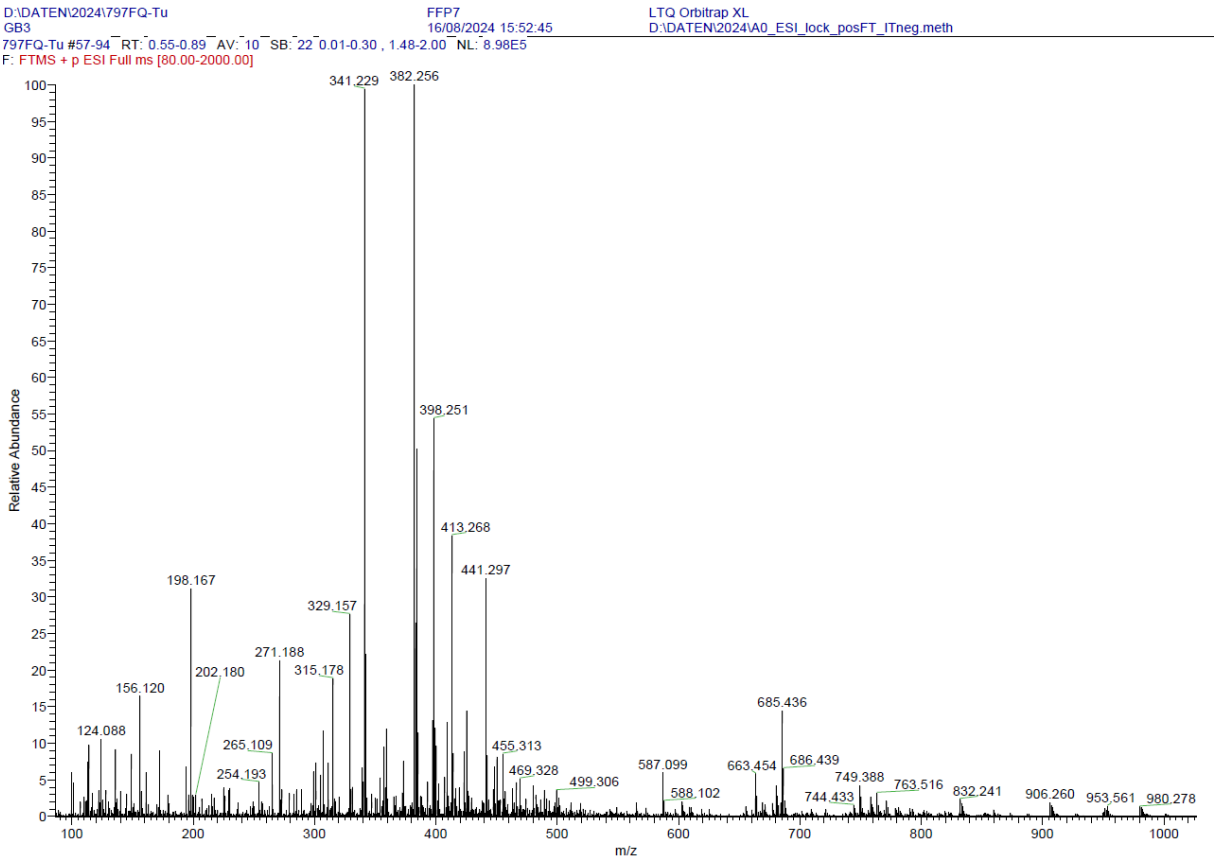

Figure 295: ESI(+)-mass spectrum of **26**.

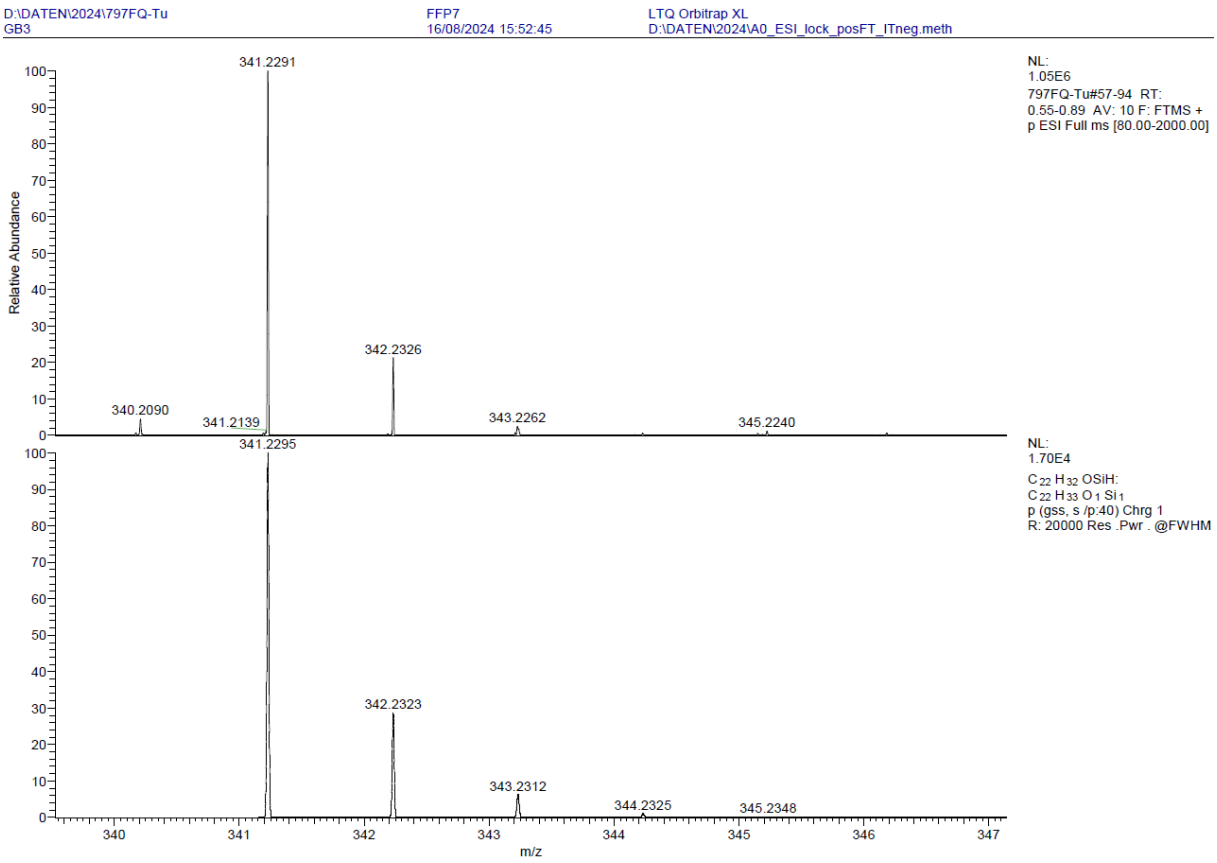

Figure 296: Experimental exact mass (top) and calculated exact mass (bottom) of **26**.

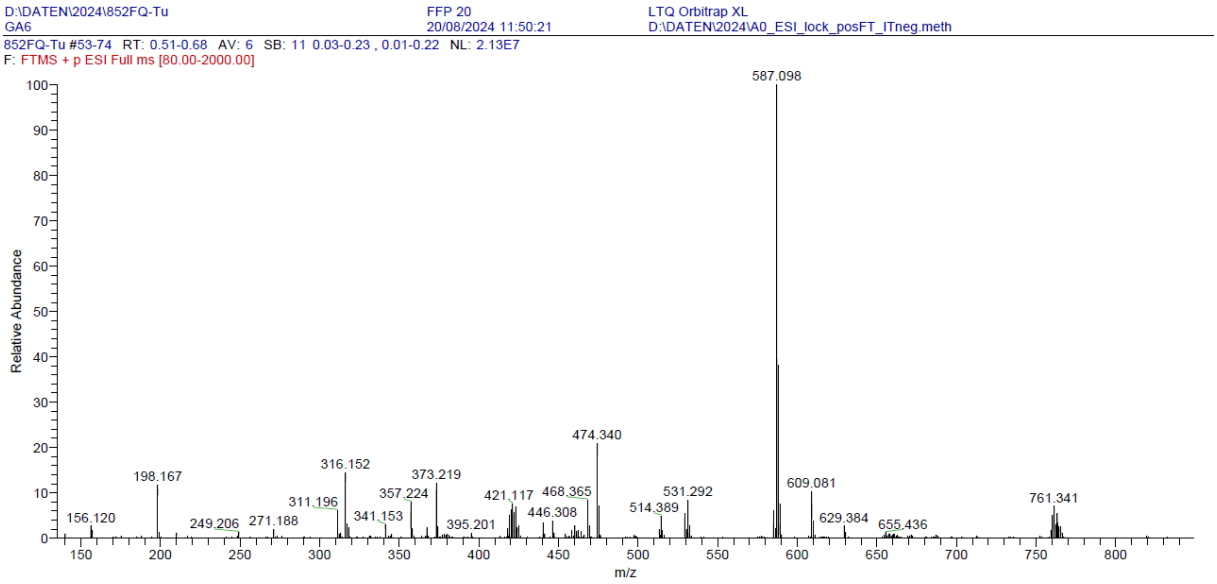

Figure 297: ESI(+)-mass spectrum of **27**.

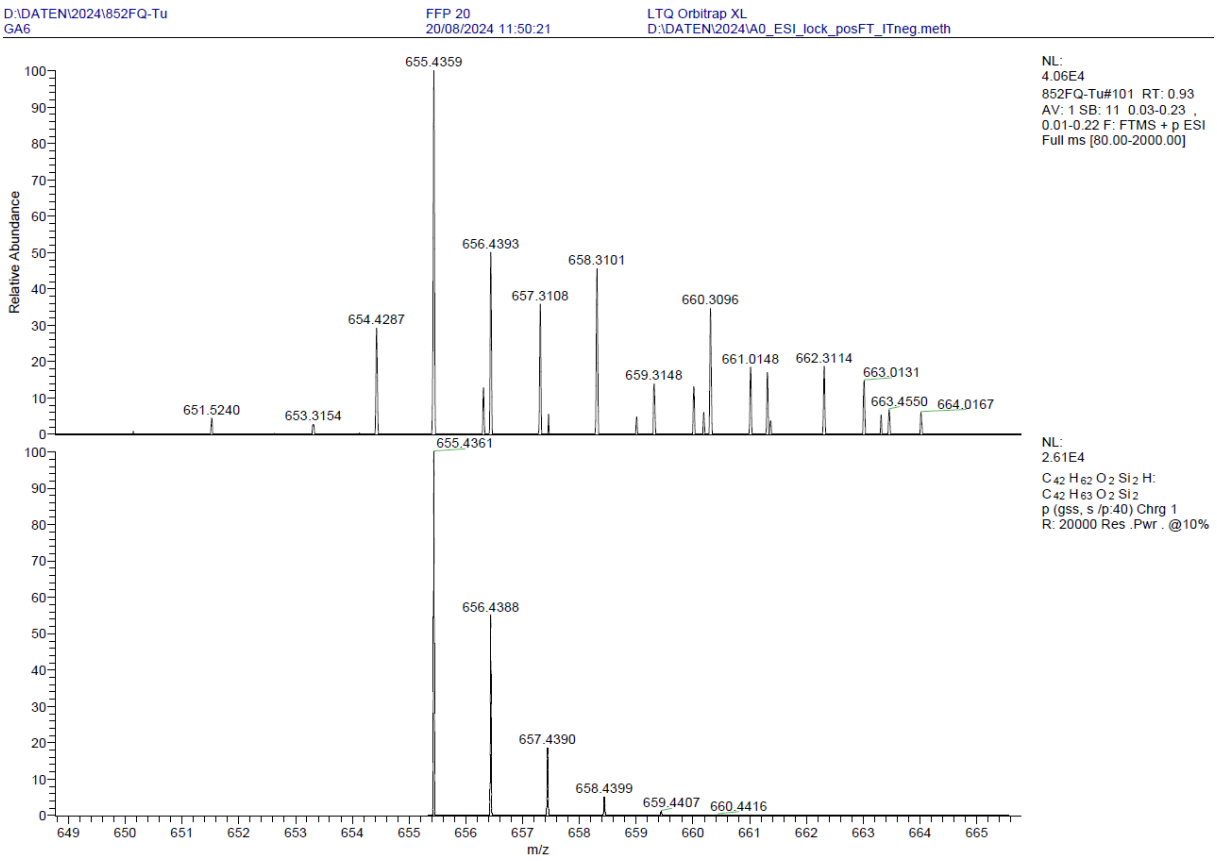

Figure 298: Experimental exact mass (top) and calculated exact mass (bottom) of **27**.

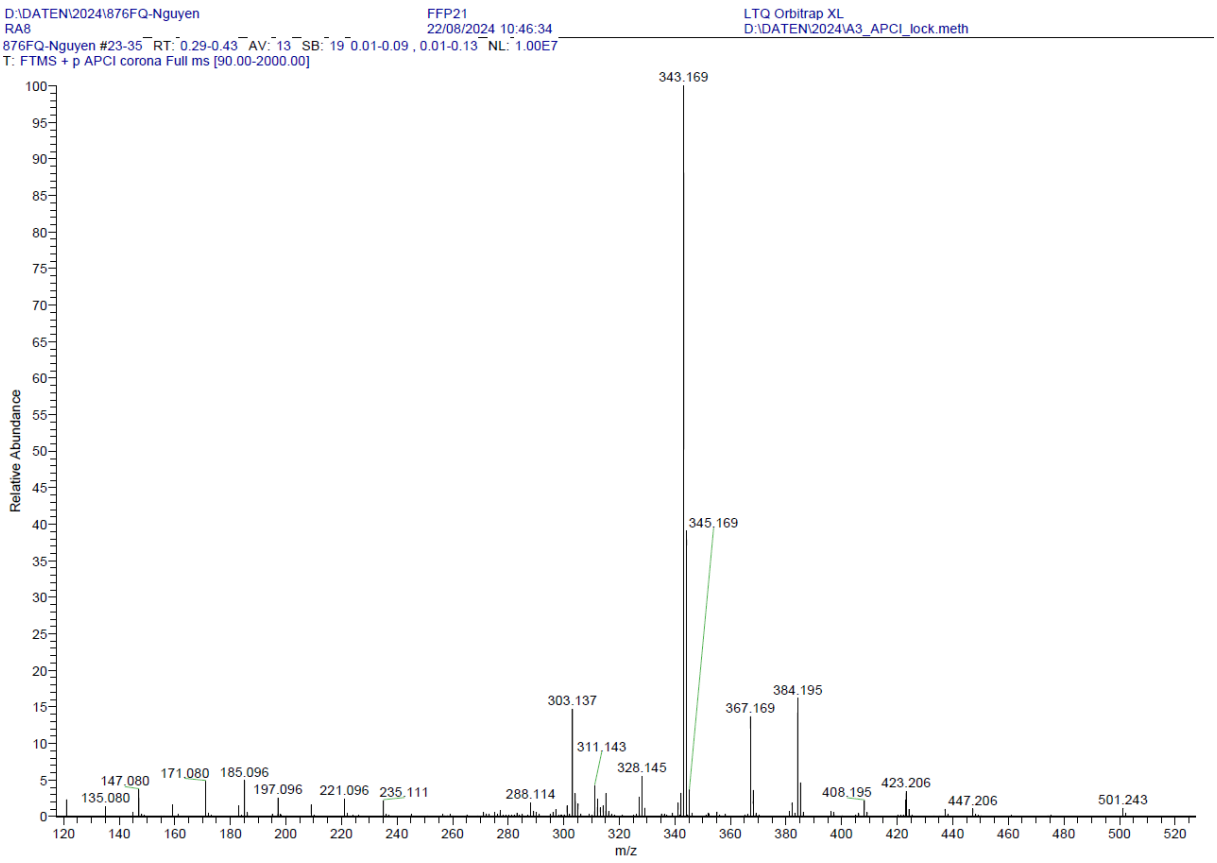

Figure 299: APCI-mass spectrum of **28**.

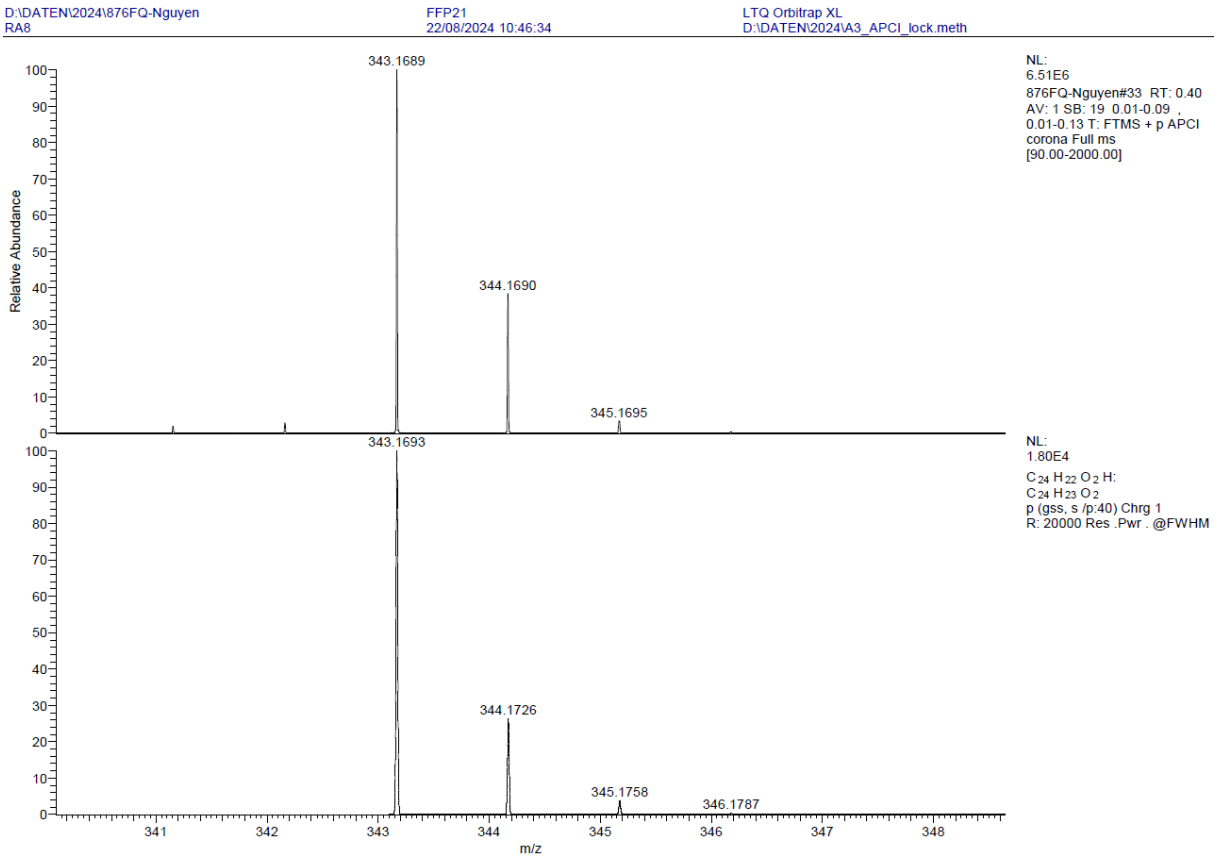

Figure 300: Experimental exact mass (top) and calculated exact mass (bottom) of **28**.

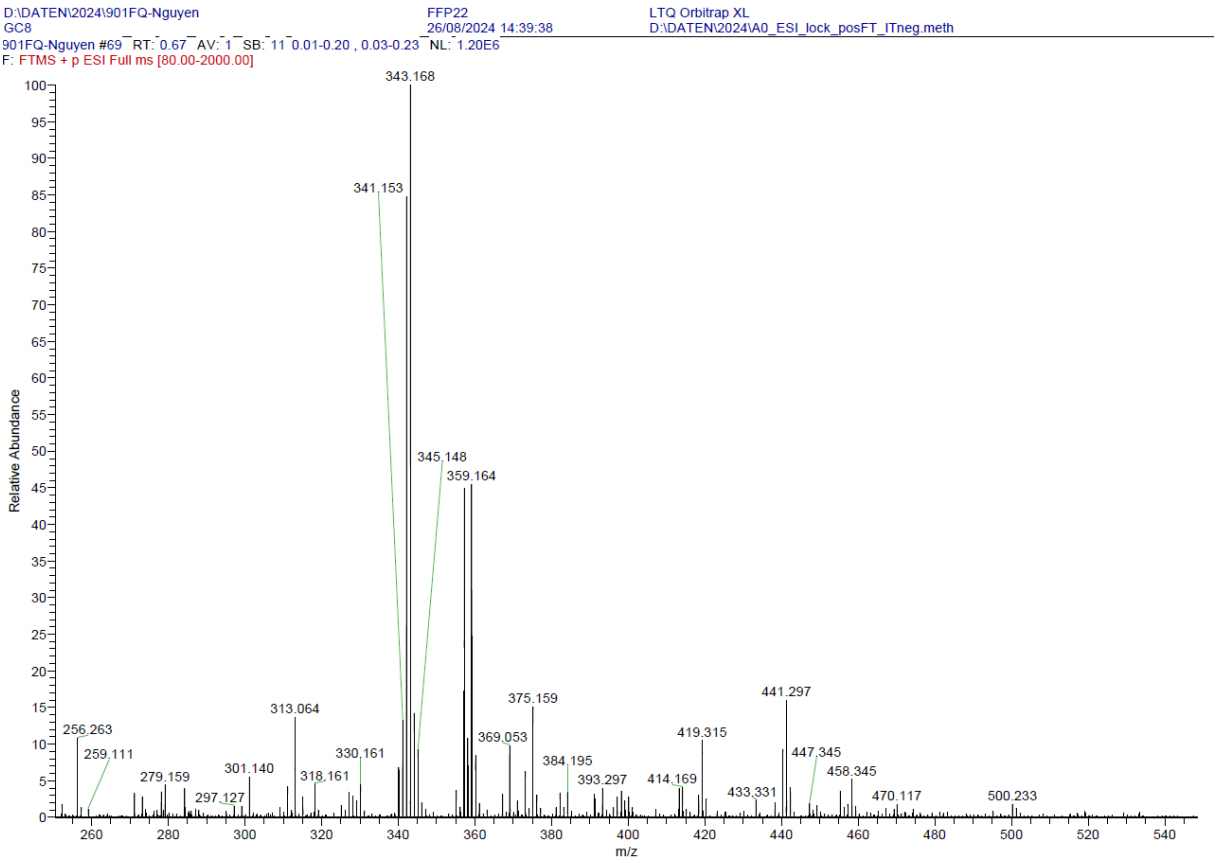

Figure 301: ESI(+)-mass spectrum of **29**.

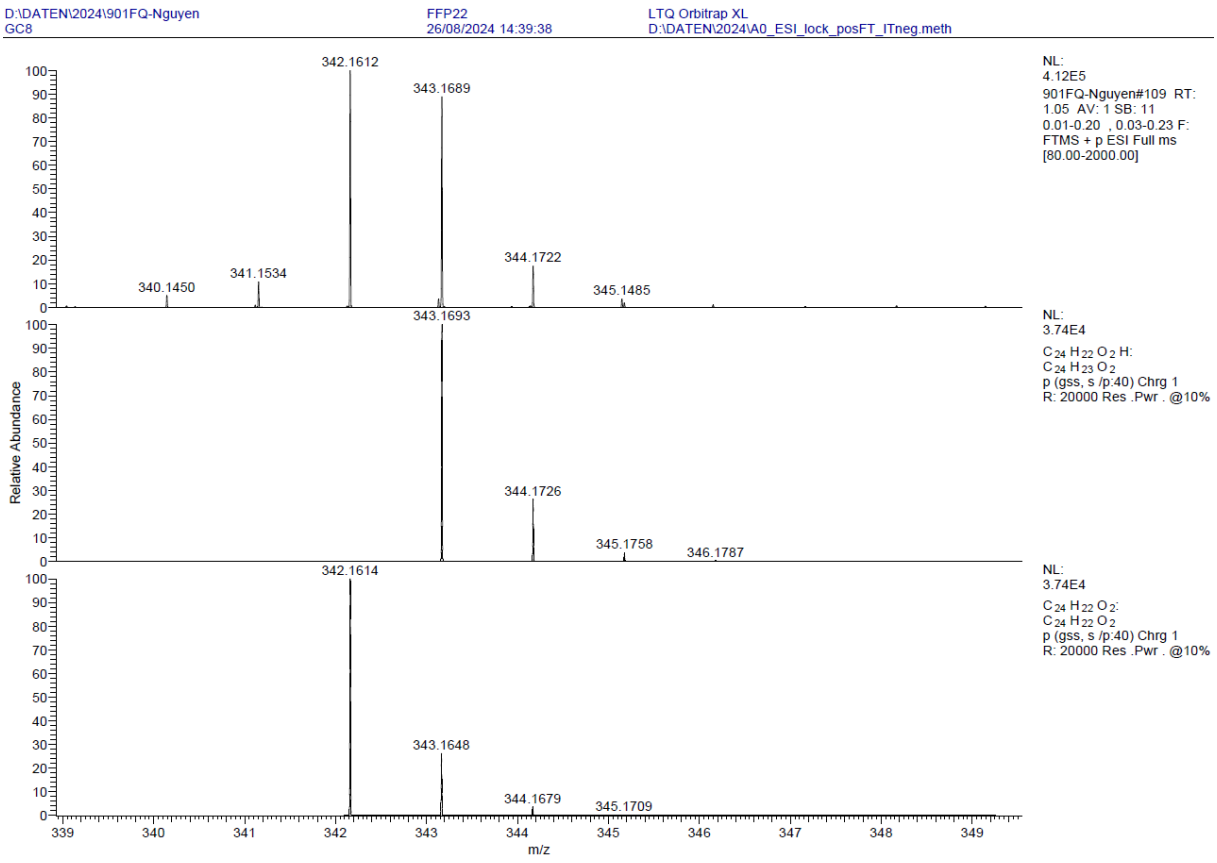

Figure 302: Experimental exact mass (top) and calculated exact masses (middle, bottom) of **29**.

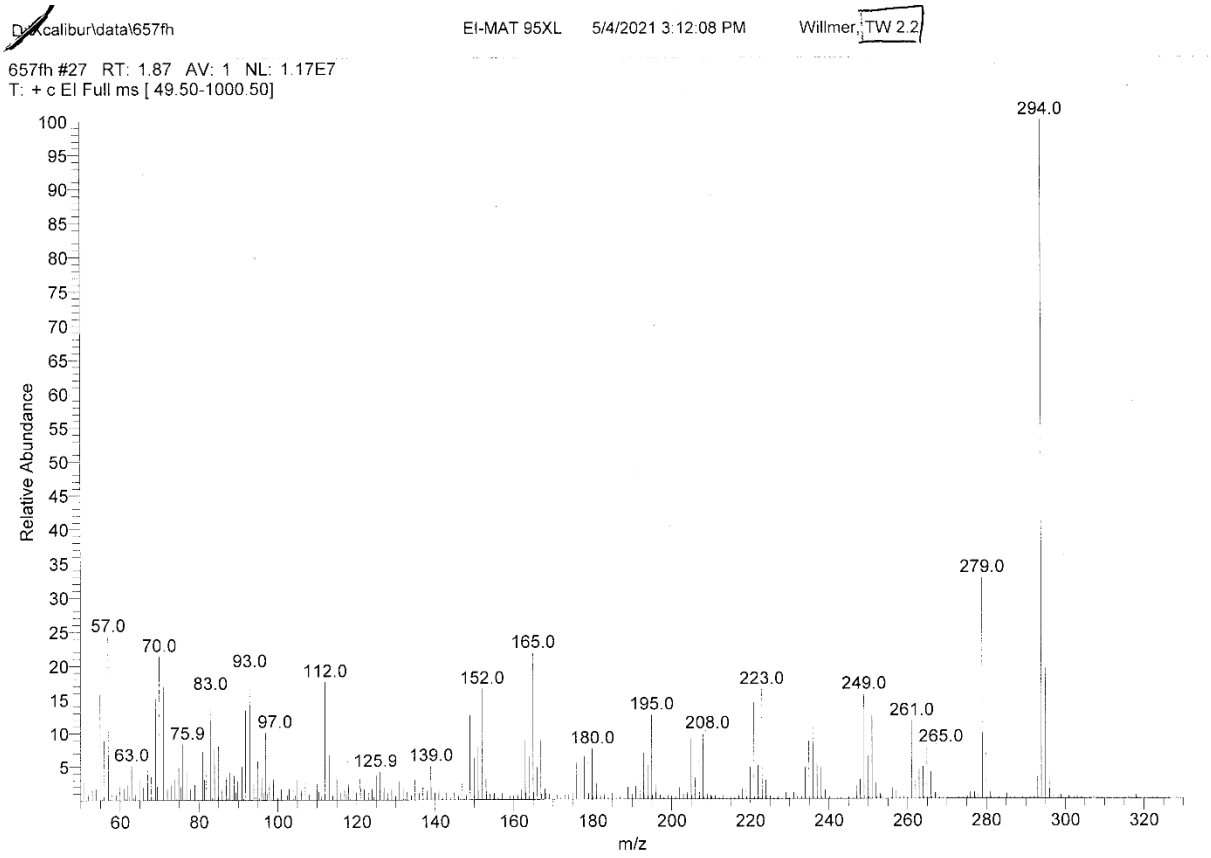

Figure 303: EI-mass spectrum of **32**.

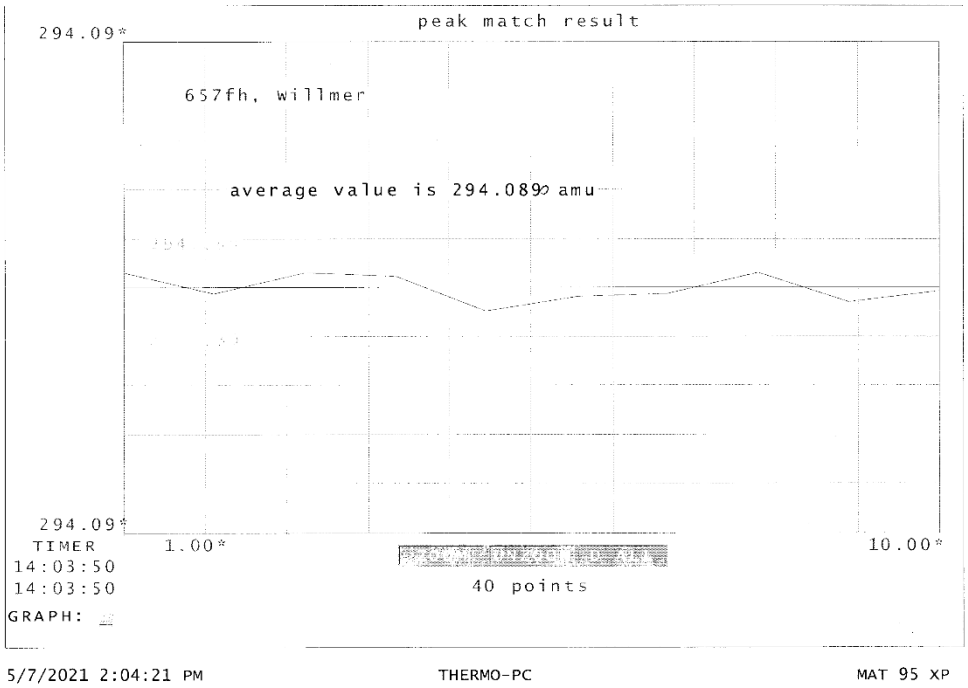

Figure 304: Experimental exact mass of **32**.

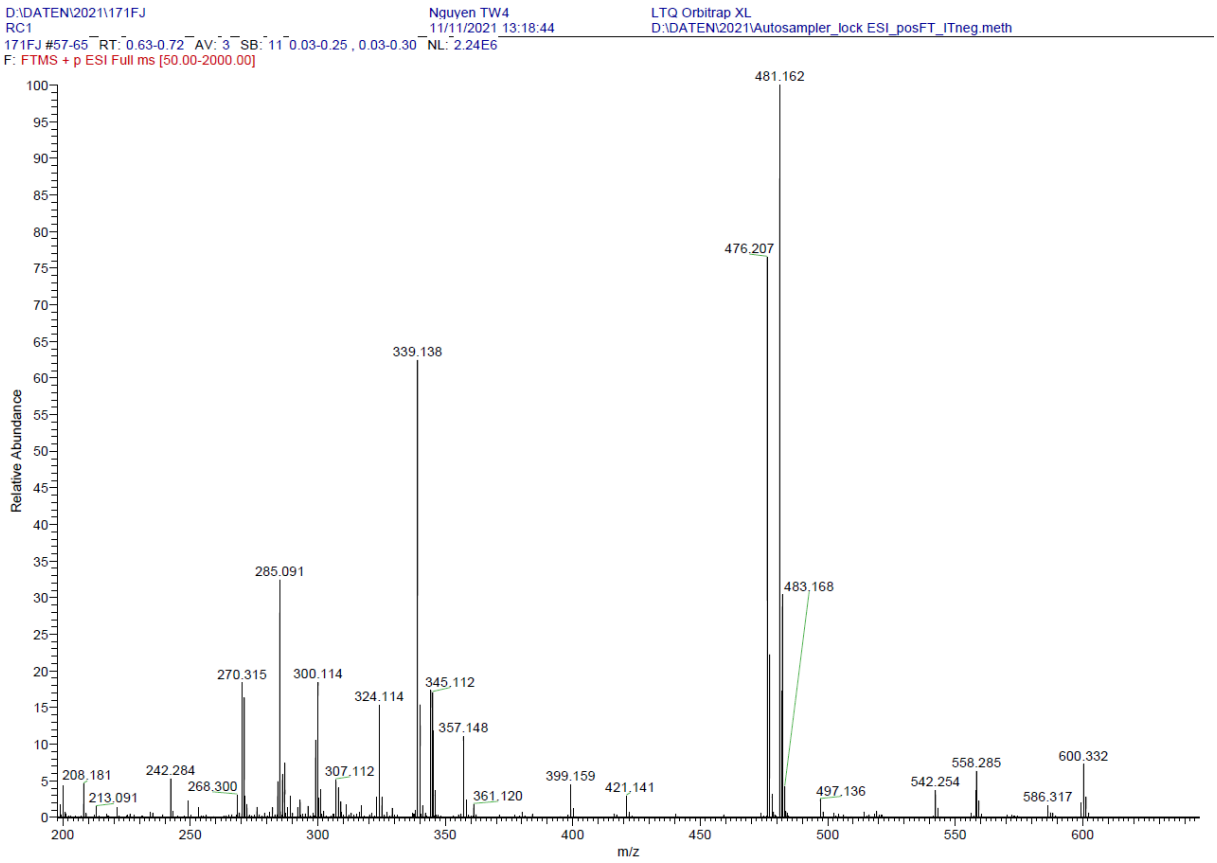

Figure 305: ESI(+)-mass spectrum of **36**.

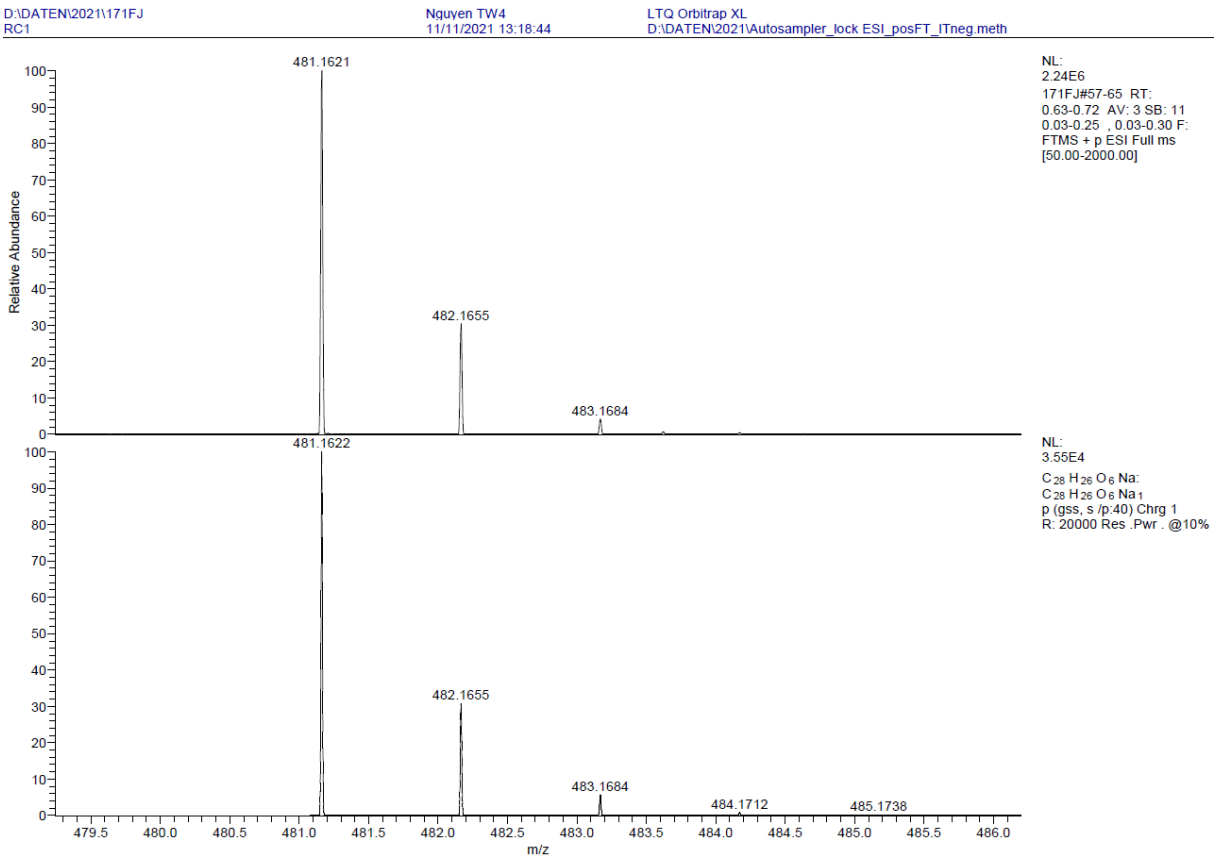

Figure 306: Experimental exact mass (top) and calculated exact mass (bottom) of **36**.

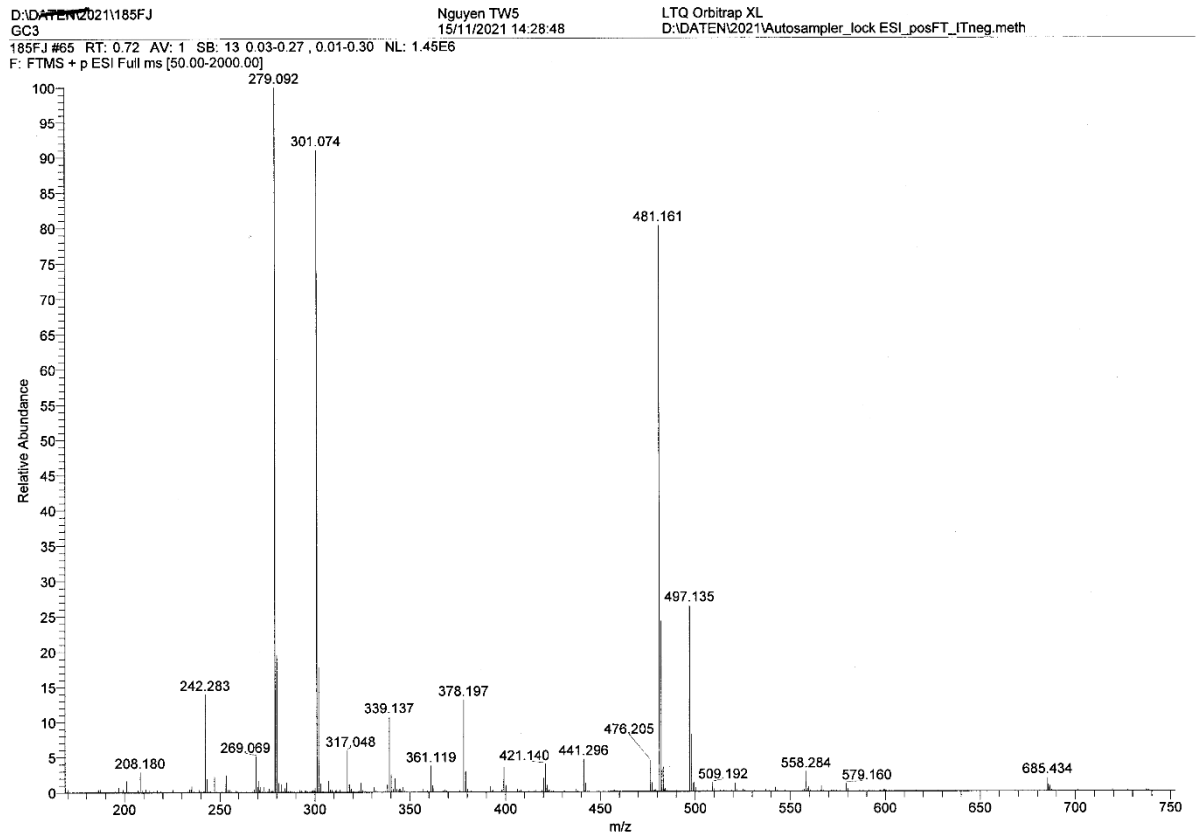

Figure 307: ESI(+)-mass spectrum of **37**.

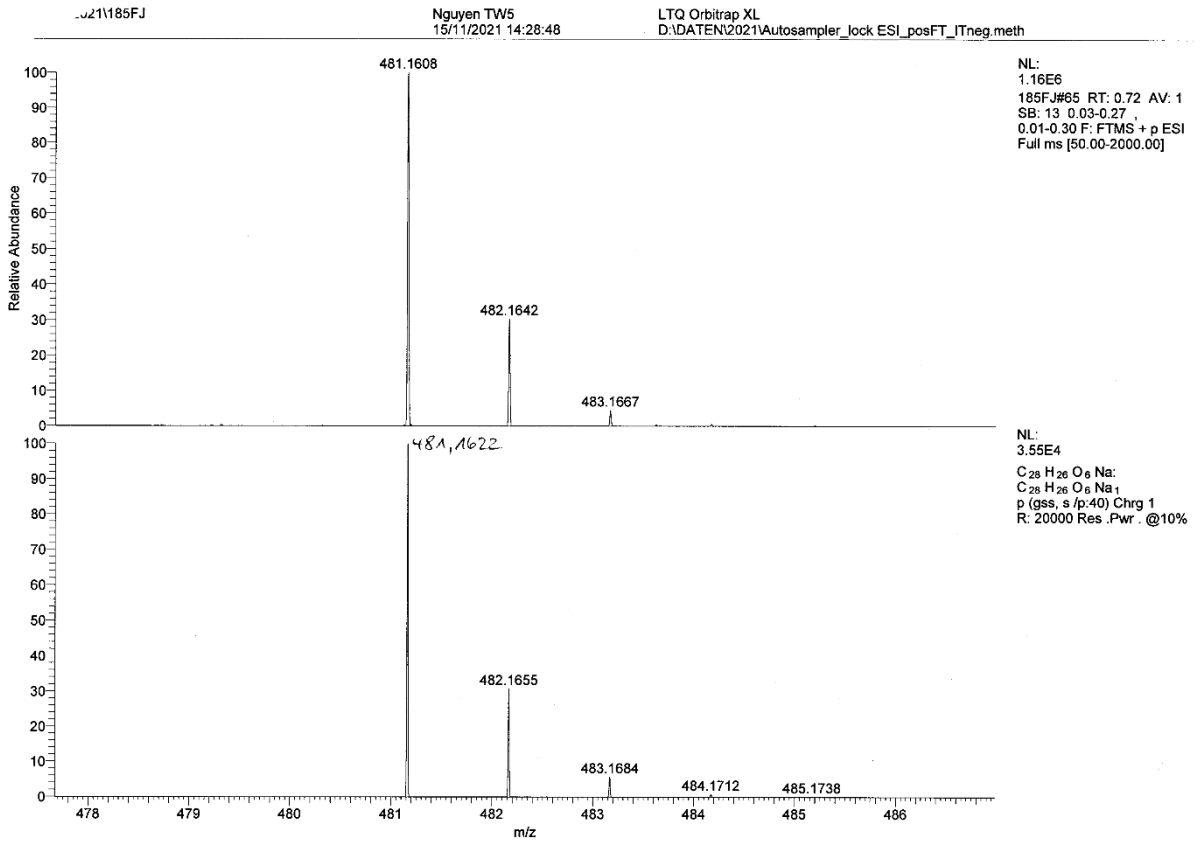

Figure 308: Experimental exact mass (top) and calculated exact mass (bottom) of **37**.

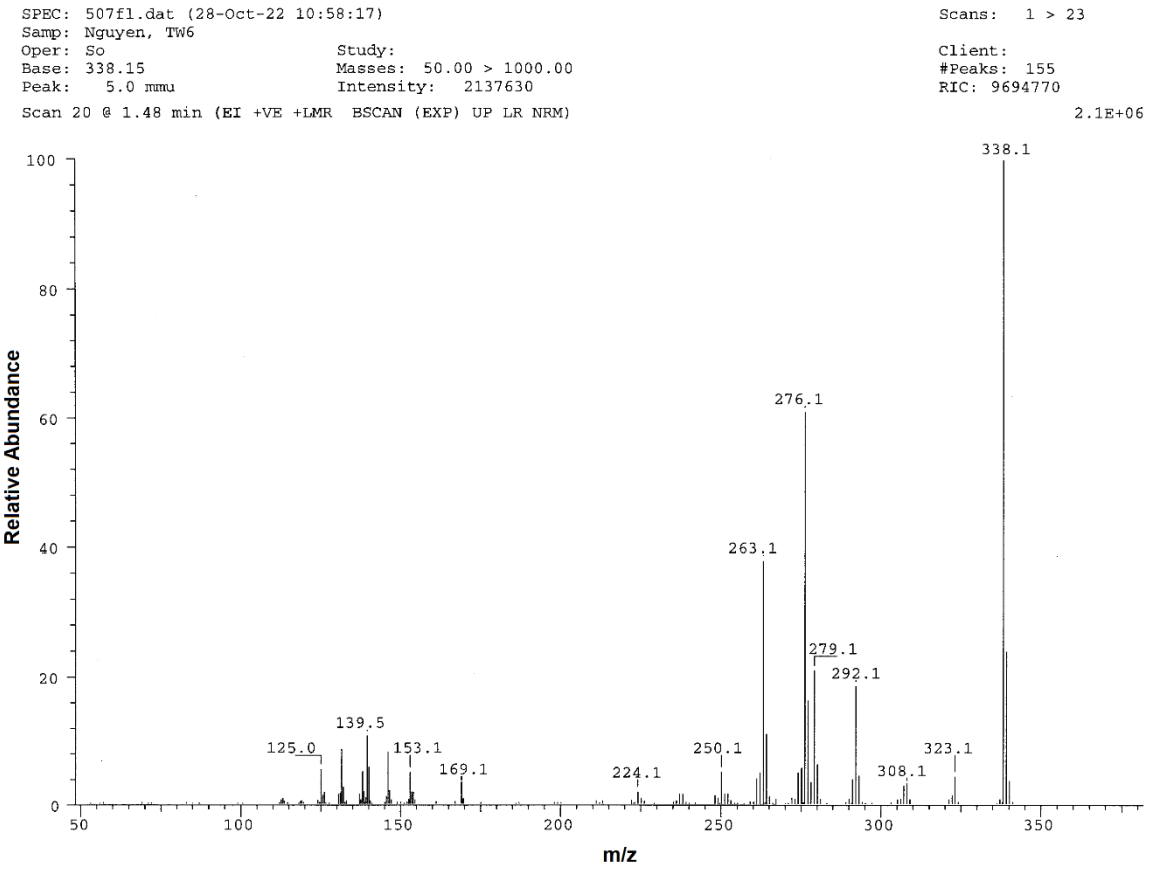

Figure 309: EI-mass spectrum of **38**.

UCLR	USER LIST FILE (4x500): 507f1			SAVE
1:	338.13127	0.00000	0.00000	0.00000
2:	338.13160	0.00000	0.00000	0.00000
3:	338.13148	0.00000	0.00000	0.00000
4:	338.13121	0.00000	0.00000	0.00000
5:	338.13123	0.00000	0.00000	0.00000
6:	338.12958	0.00000	0.00000	0.00000
7:	338.13117	0.00000	0.00000	0.00000
8:	338.13057	0.00000	0.00000	0.00000
9:	338.12978	0.00000	0.00000	0.00000
10:	338.13013	0.00000	0.00000	0.00000
11:	0.00000	0.00000	0.00000	0.00000
12:	0.00000	0.00000	0.00000	0.00000
13:	0.00000	0.00000	0.00000	0.00000
14:	0.00000	0.00000	0.00000	0.00000
15:	0.00000	0.00000	0.00000	0.00000
16:	0.00000	0.00000	0.00000	0.00000
17:	0.00000	0.00000	0.00000	0.00000
18:	0.00000	0.00000	0.00000	0.00000
19:	0.00000	0.00000	0.00000	0.00000
20:	0.00000	0.00000	0.00000	0.00000
LINK	NONE	NONE	NONE	NONE
SIZE	10.00000	0.00000	0.00000	0.00000
MEAN	338.13080	0.00000	0.00000	0.00000
SUM	3381.30803	0.00000	0.00000	0.00000
S.D.	0.00073	0.00000	0.00000	0.00000
MAX	338.13160	0.00000	0.00000	0.00000
MIN	338.12958	0.00000	0.00000	0.00000

ULIST: _

Fri Oct 28 15:04:34 2022 ICL version 10.621 5.July 1999 mat95 NAT 95

Figure 310: Experimental exact mass of **38**.

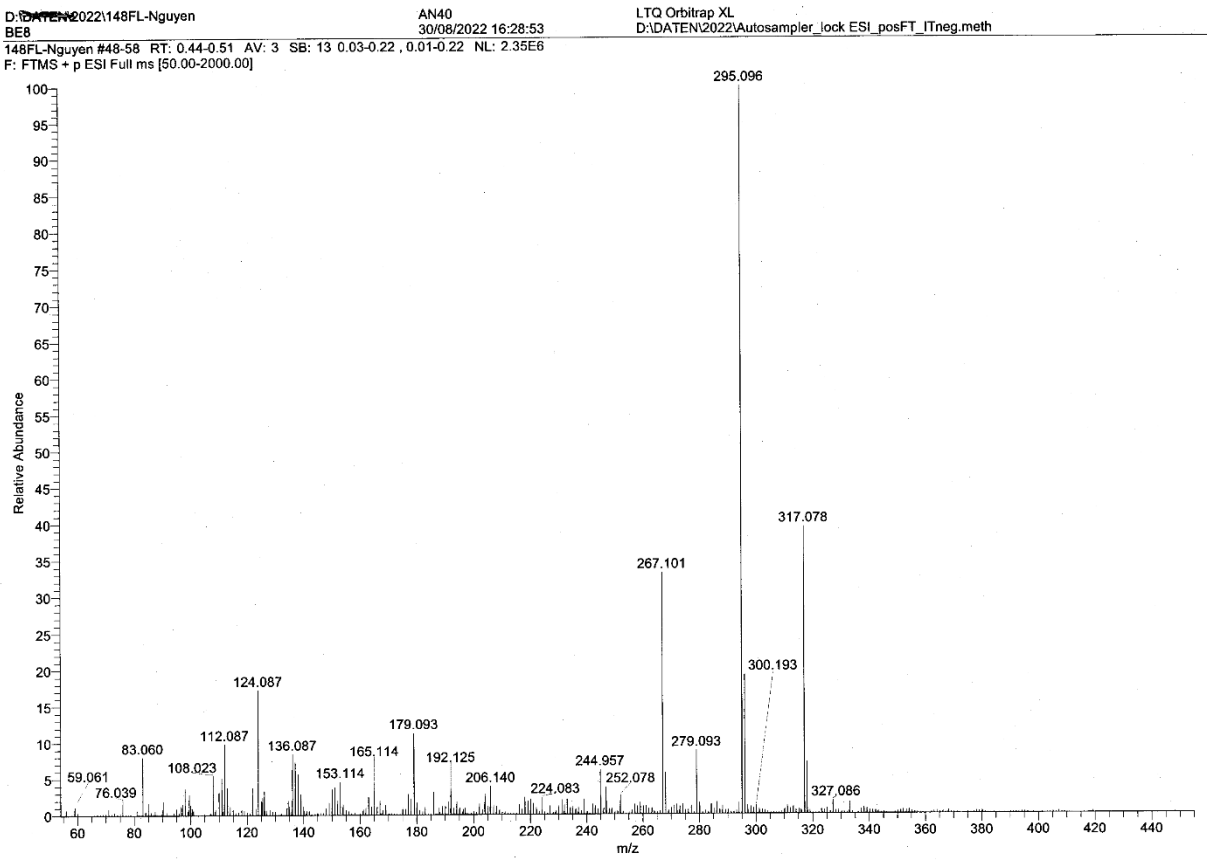

Figure 311: ESI(+)-mass spectrum of **39**.

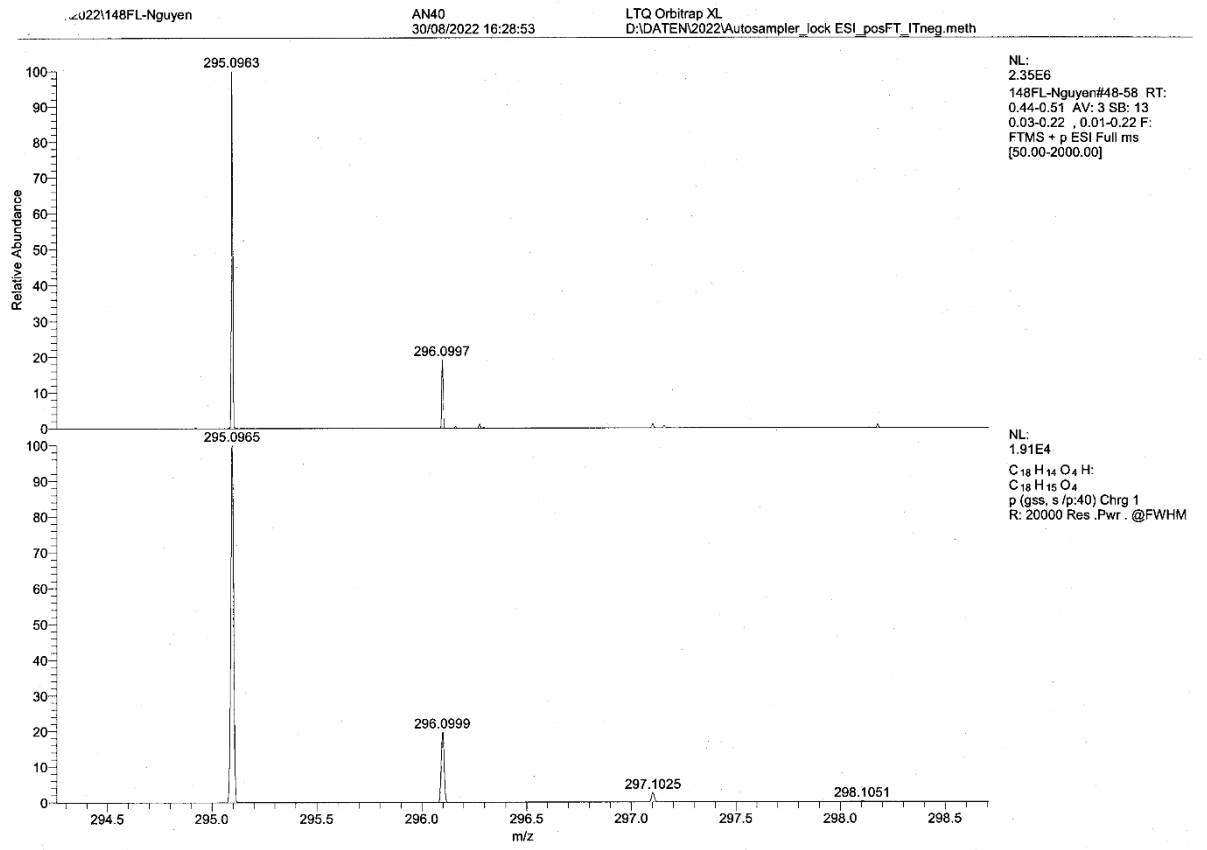

Figure 312: Experimental exact mass (top) and calculated exact mass (bottom) of **39**.

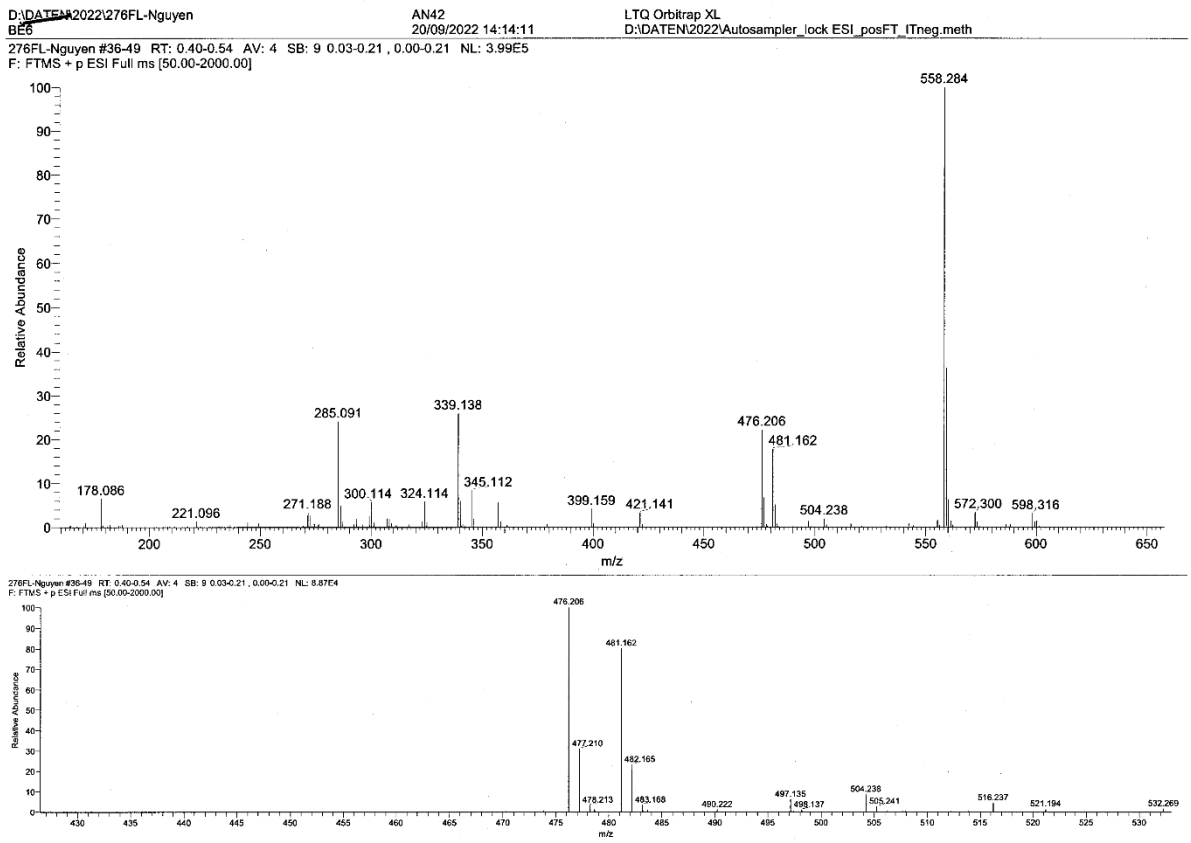

Figure 313: ESI(+)-mass spectrum of **41**.

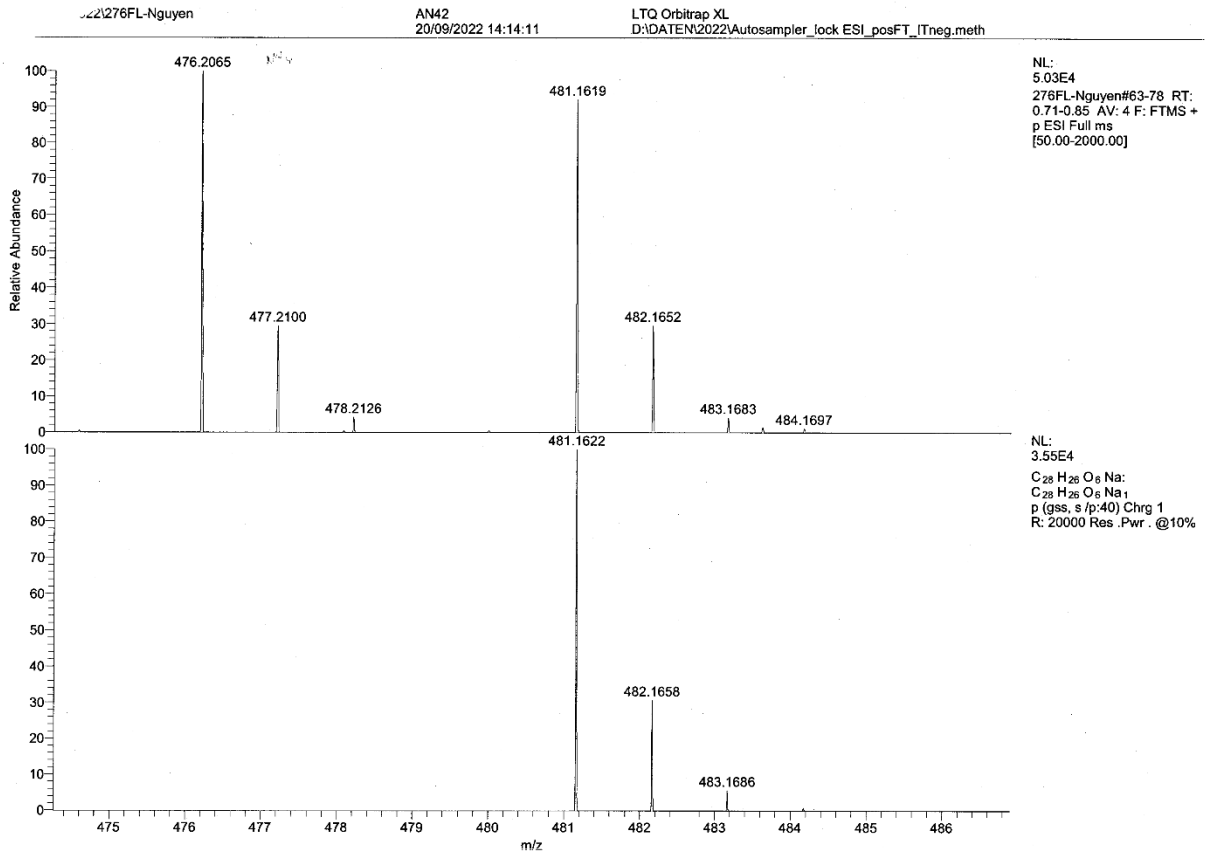

Figure 314: Experimental exact mass (top) and calculated exact mass (bottom) of **41**.

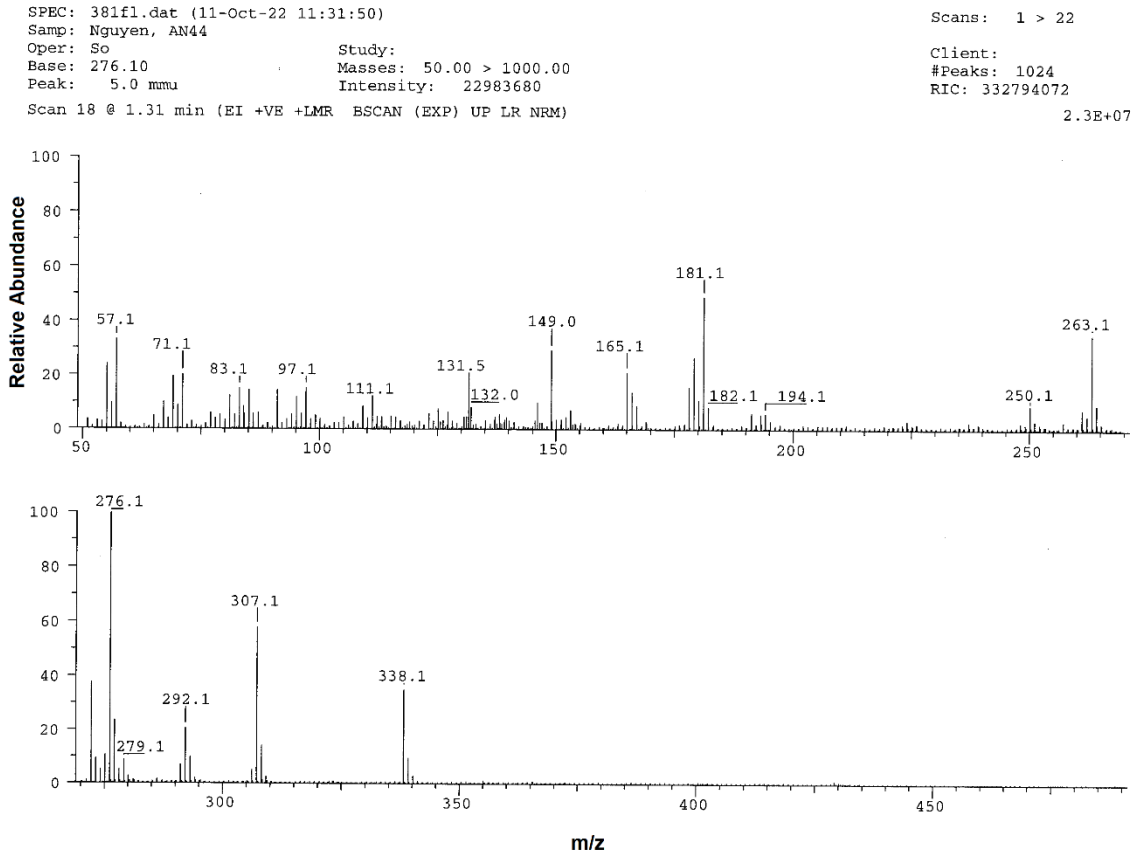

Figure 315: EI-mass spectrum of **43**.

UCLR USER LIST FILE (4x500): 381f1 SAVE

1:	338.13113	0.00000	0.00000	0.00000
2:	338.13105	0.00000	0.00000	0.00000
3:	338.13138	0.00000	0.00000	0.00000
4:	338.13074	0.00000	0.00000	0.00000
5:	338.13130	0.00000	0.00000	0.00000
6:	338.13020	0.00000	0.00000	0.00000
7:	338.13117	0.00000	0.00000	0.00000
8:	338.13091	0.00000	0.00000	0.00000
9:	338.13047	0.00000	0.00000	0.00000
10:	338.13059	0.00000	0.00000	0.00000
11:	0.00000	0.00000	0.00000	0.00000
12:	0.00000	0.00000	0.00000	0.00000
13:	0.00000	0.00000	0.00000	0.00000
14:	0.00000	0.00000	0.00000	0.00000
15:	0.00000	0.00000	0.00000	0.00000
16:	0.00000	0.00000	0.00000	0.00000
17:	0.00000	0.00000	0.00000	0.00000
18:	0.00000	0.00000	0.00000	0.00000
19:	0.00000	0.00000	0.00000	0.00000
20:	0.00000	0.00000	0.00000	0.00000
LINK	NONE	NONE	NONE	NONE
SIZE	10.00000	0.00000	0.00000	0.00000
MEAN	338.13089	0.00000	0.00000	0.00000
SUM	3381.30893	0.00000	0.00000	0.00000
S.D.	0.00039	0.00000	0.00000	0.00000
MAX	338.13138	0.00000	0.00000	0.00000
MIN	338.13020	0.00000	0.00000	0.00000

ULIST: _

Tue Oct 11 16:35:59 2022 ICL version 10.621 5.July 1999 mat95 MAT 95

Figure 316: Experimental exact mass of **43**.

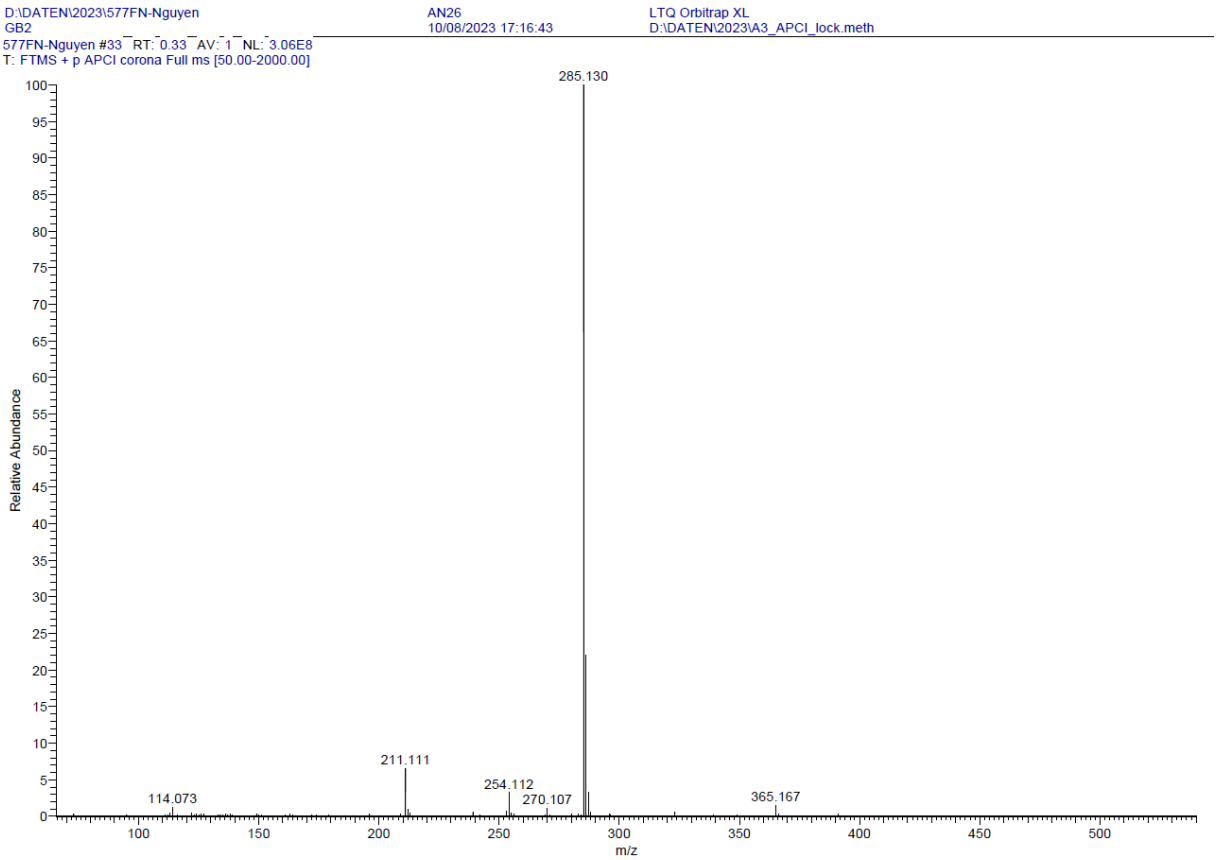

Figure 317: APCI-mass spectrum of **48**.

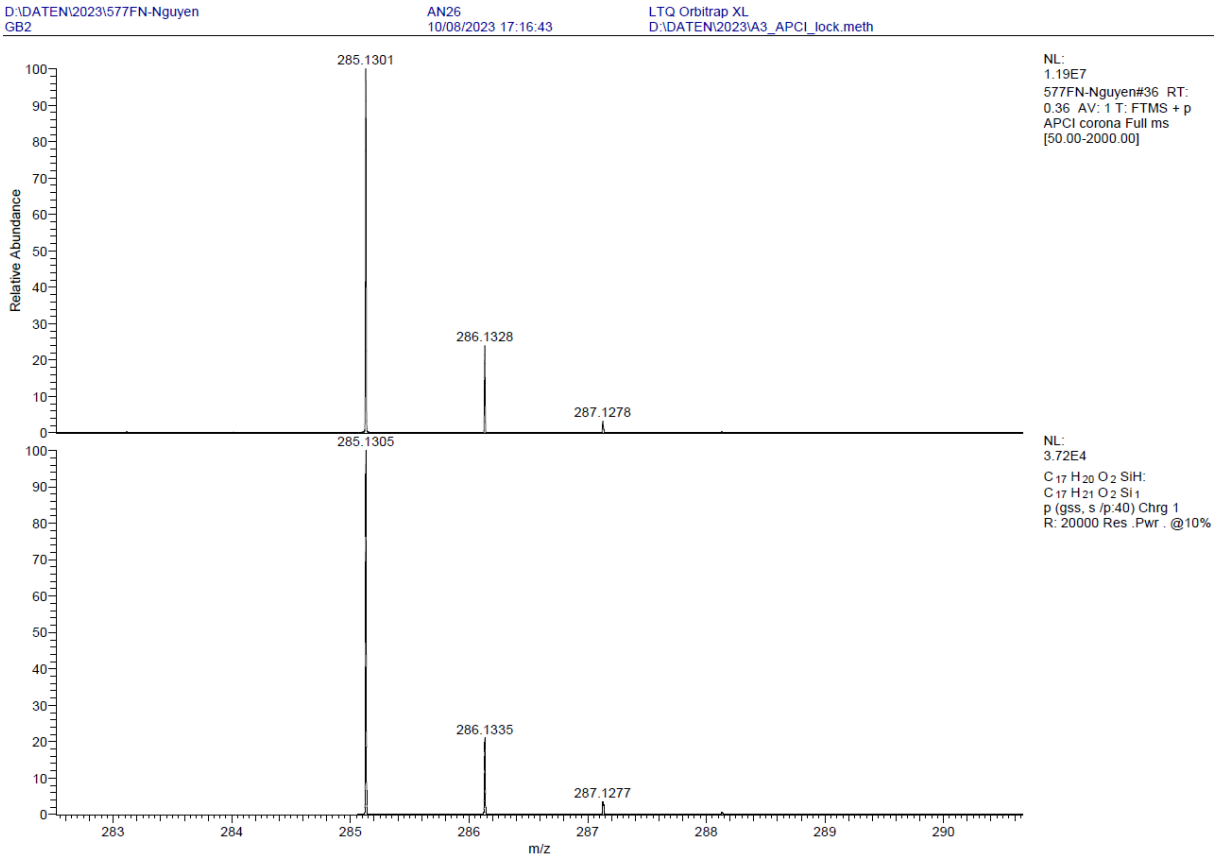

Figure 318: Experimental exact mass (top) and calculated exact mass (bottom) of **48**.

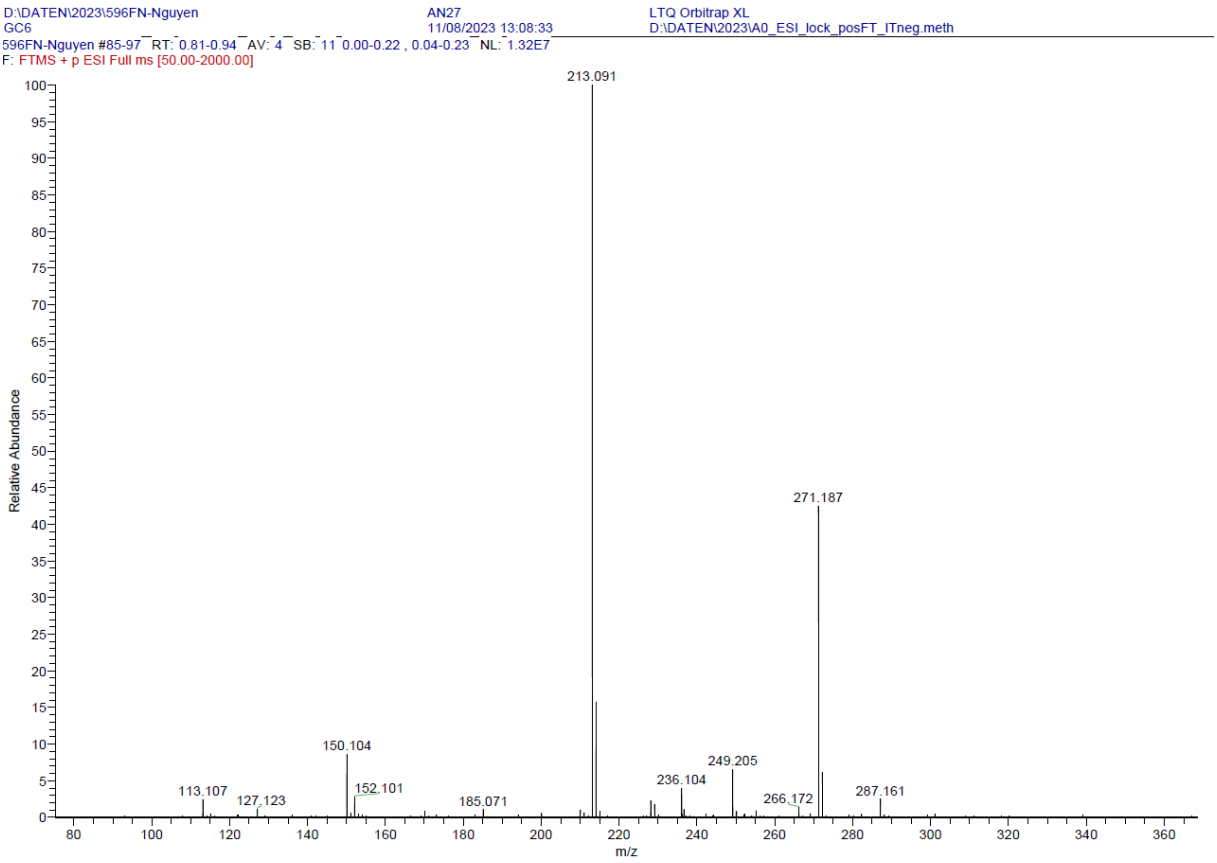

Figure 319: ESI(+)-mass spectrum of **49**.

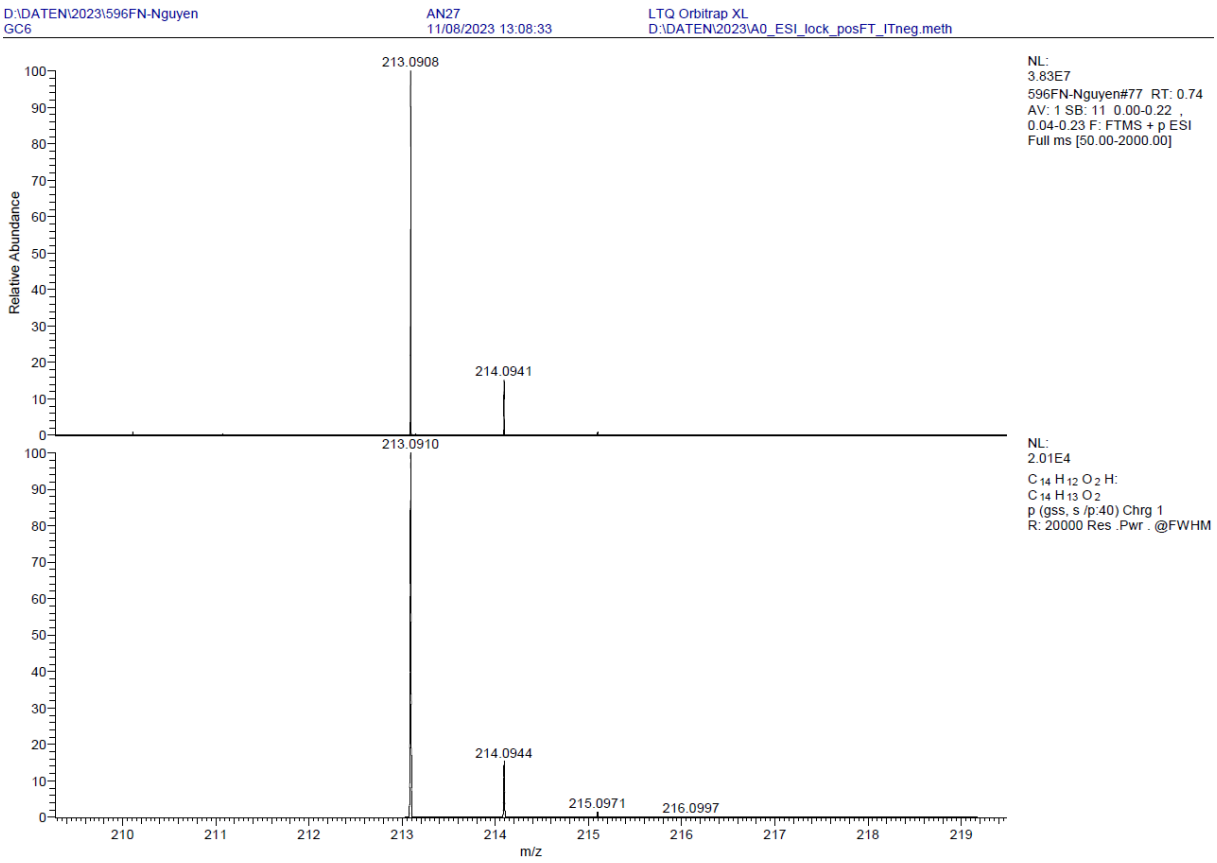

Figure 320: Experimental exact mass (top) and calculated exact mass (bottom) of **49**.

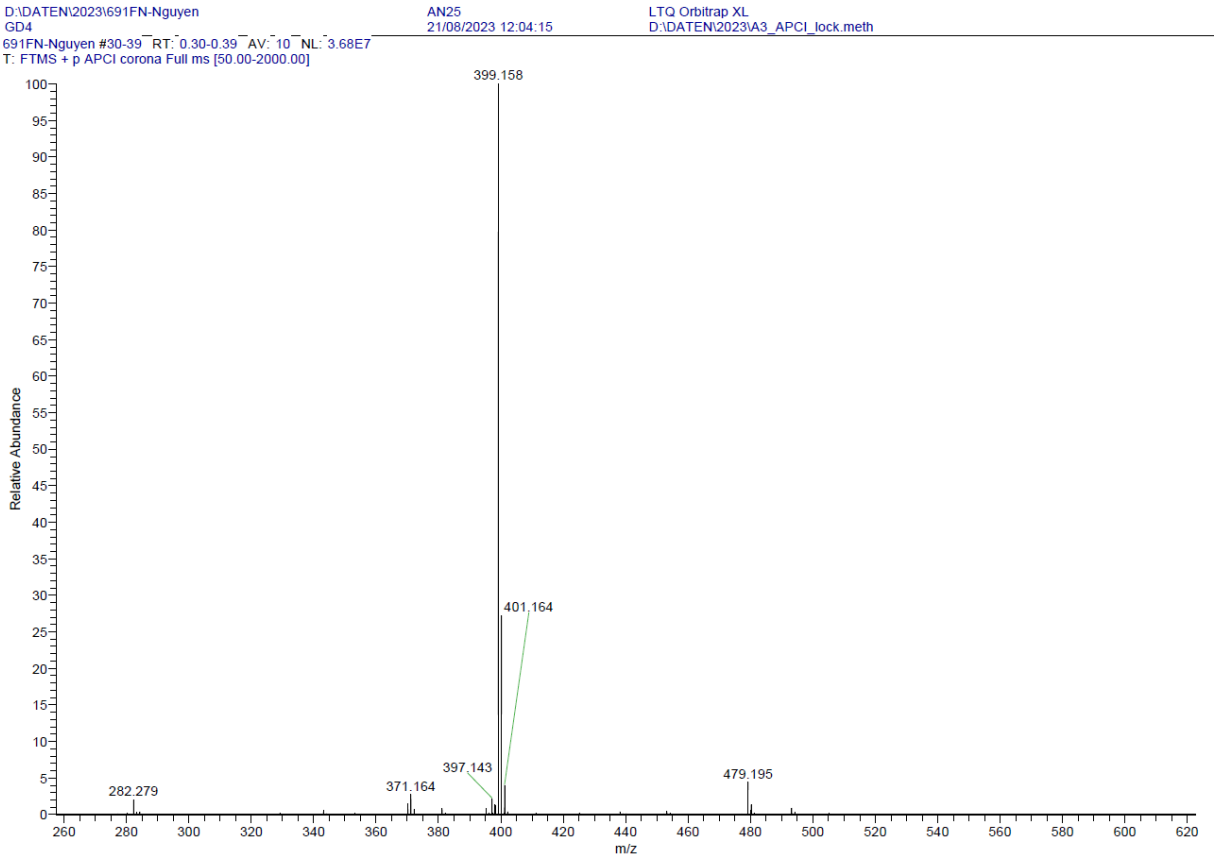

Figure 321: APCI-mass spectrum of **50**.

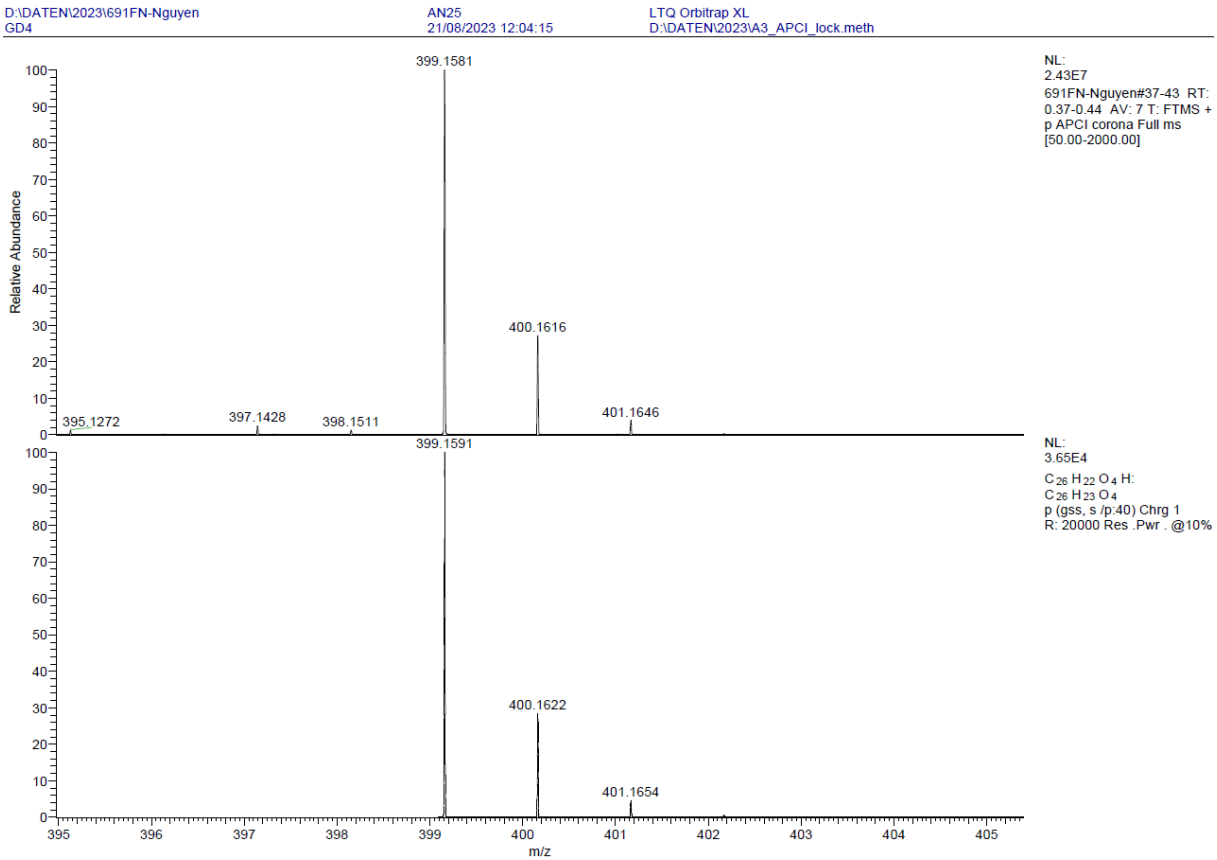

Figure 322: Experimental exact mass (top) and calculated exact mass (bottom) of **50**.

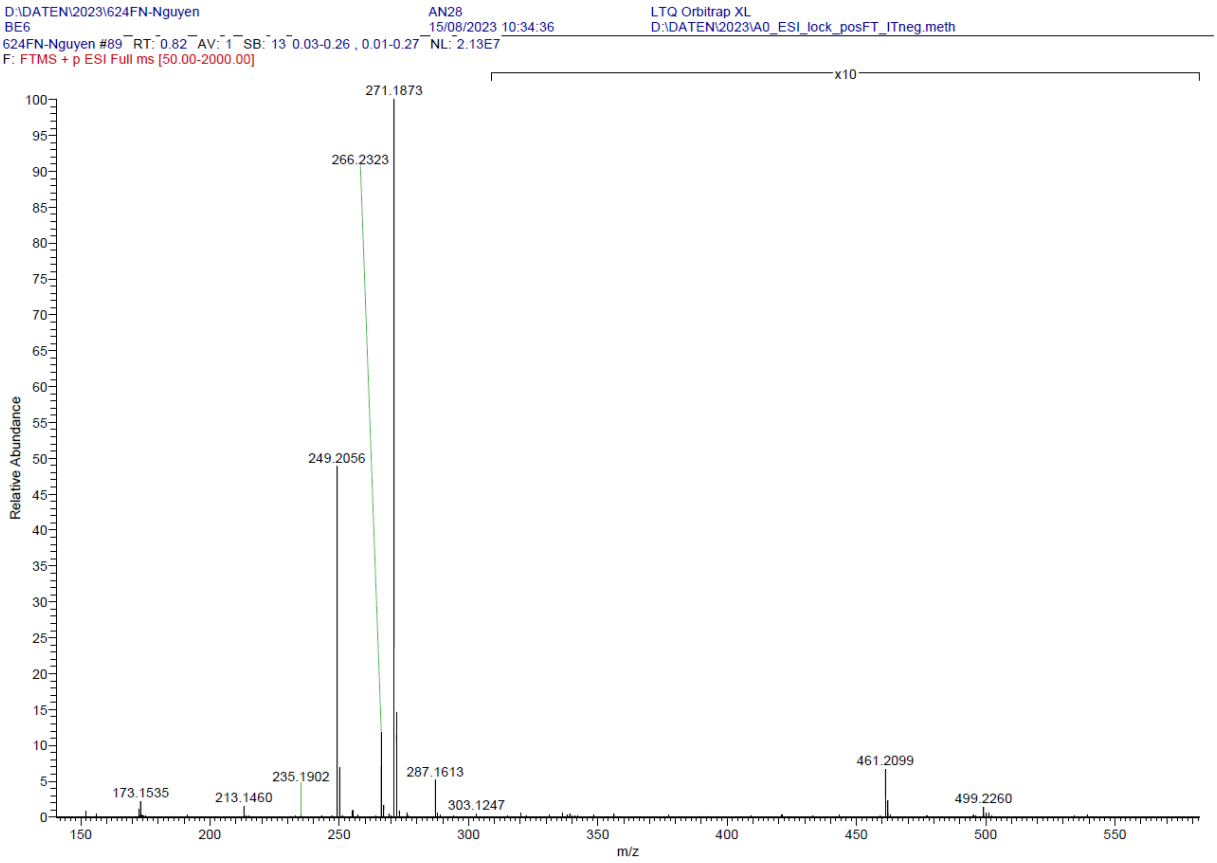

Figure 323: ESI(+)-mass spectrum of **51**.

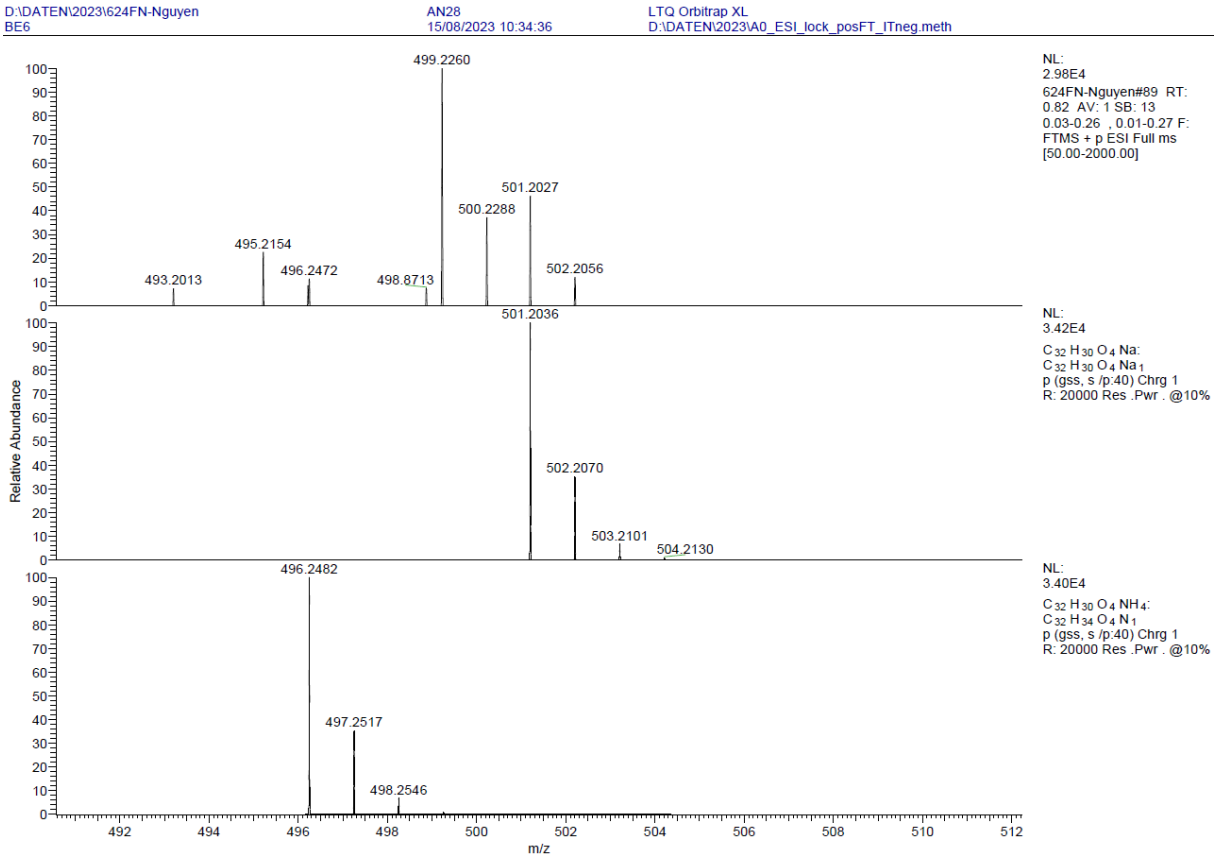

Figure 324: Experimental exact mass (top) and calculated exact masses (middle, bottom) of **51**.

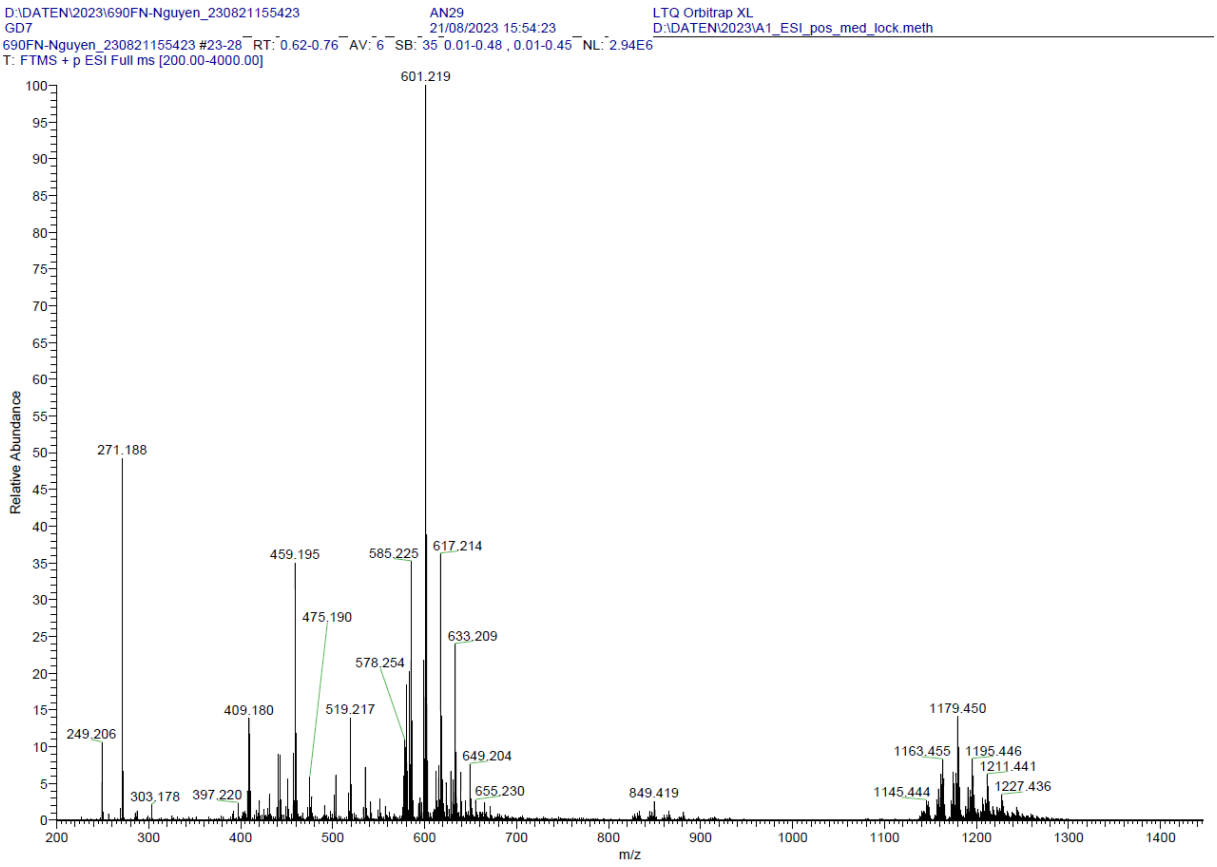

Figure 325: ESI(+)-mass spectrum of **52**.

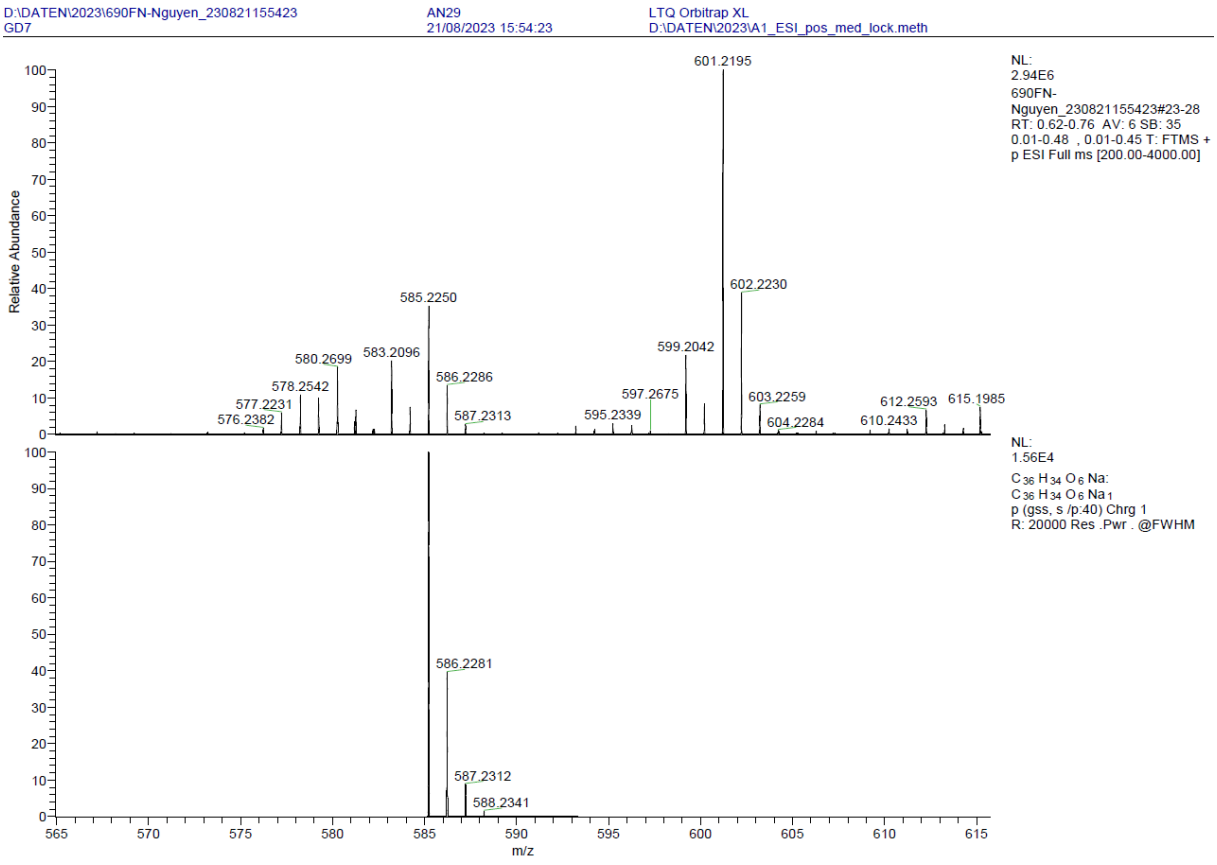

Figure 326: Experimental exact mass (top) and calculated exact mass (bottom) of **52**.

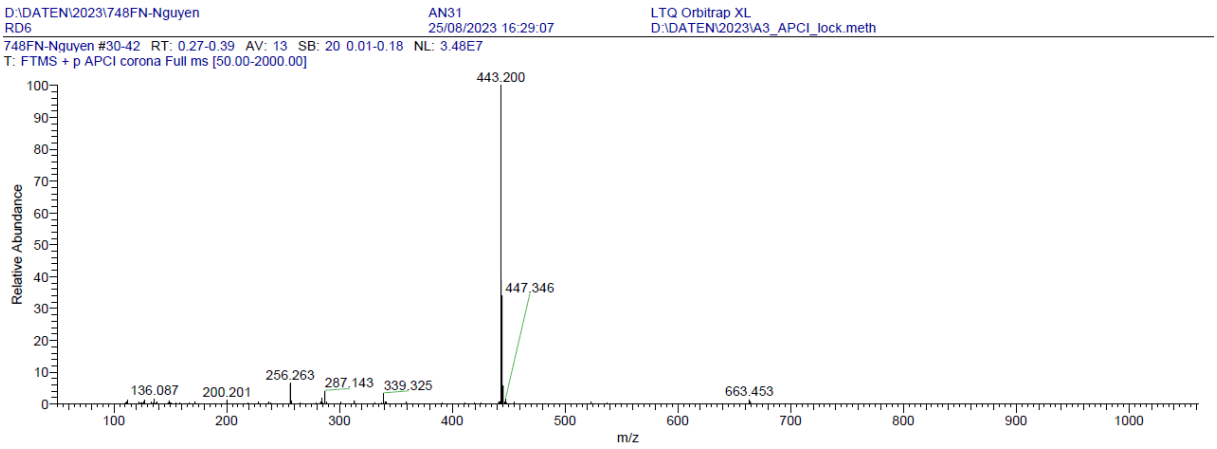

Figure 327: APCI-mass spectrum of **54**.

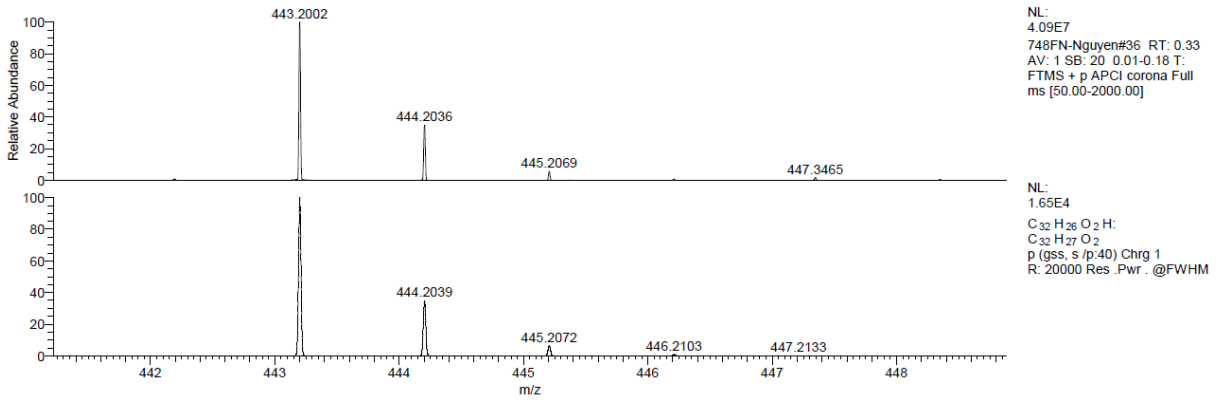

Figure 328: Experimental exact mass (top) and calculated exact mass (bottom) of **54**.

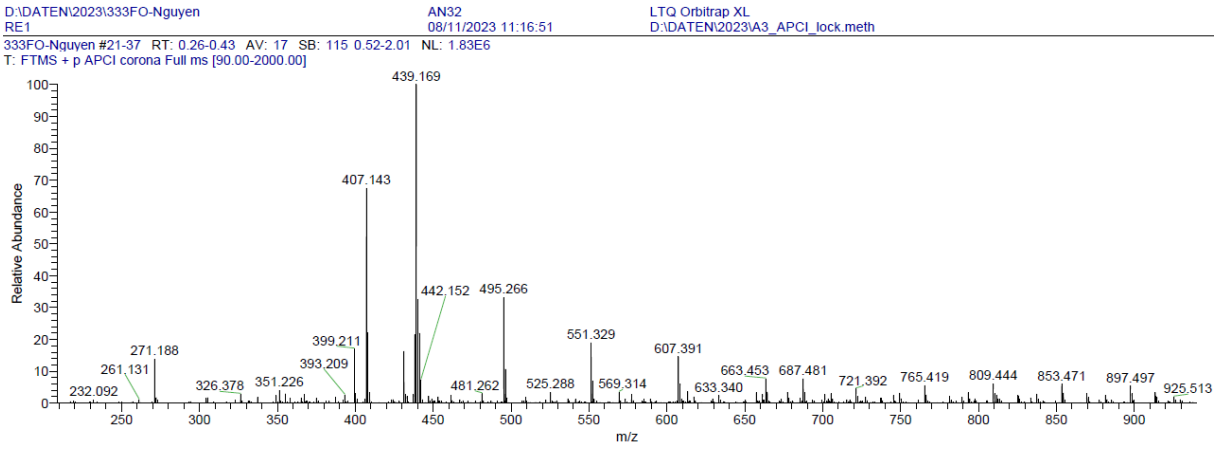

Figure 329: APCI-mass spectrum of **55**.

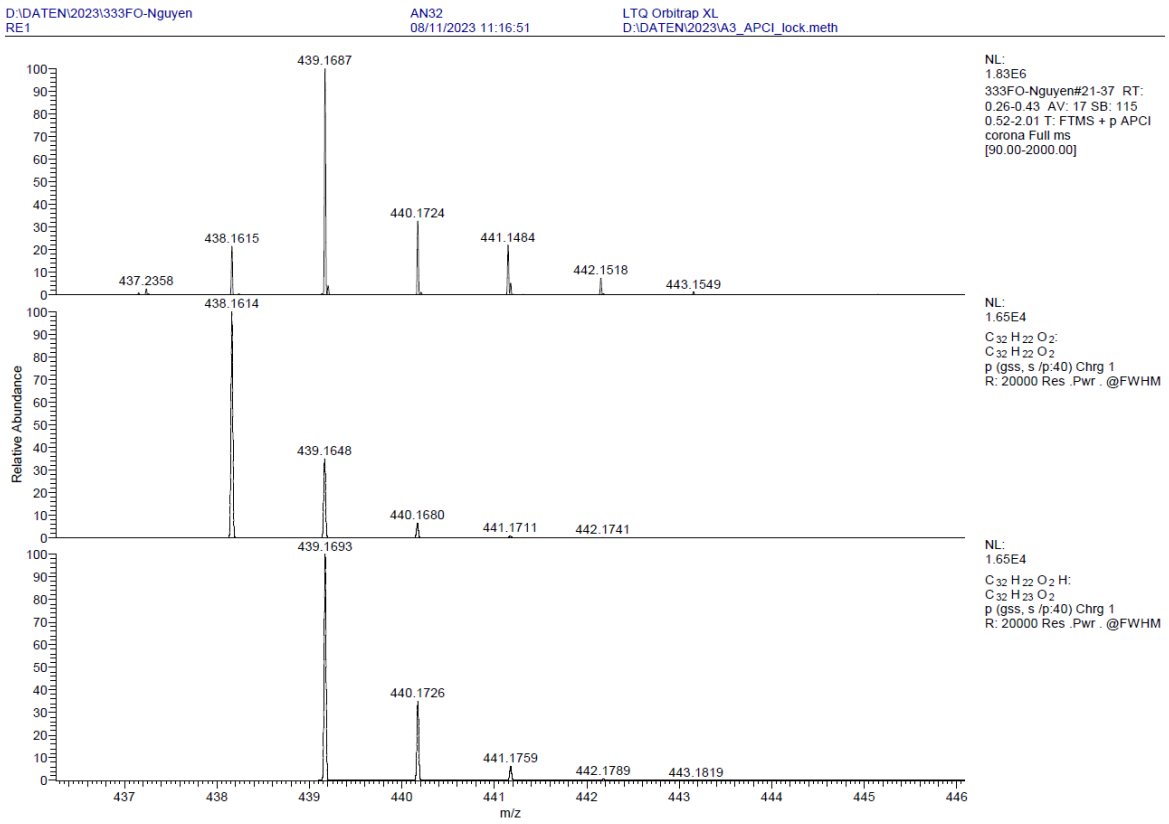

Figure 330: Experimental exact mass (top) and calculated exact masses (middle, bottom) of **55**.

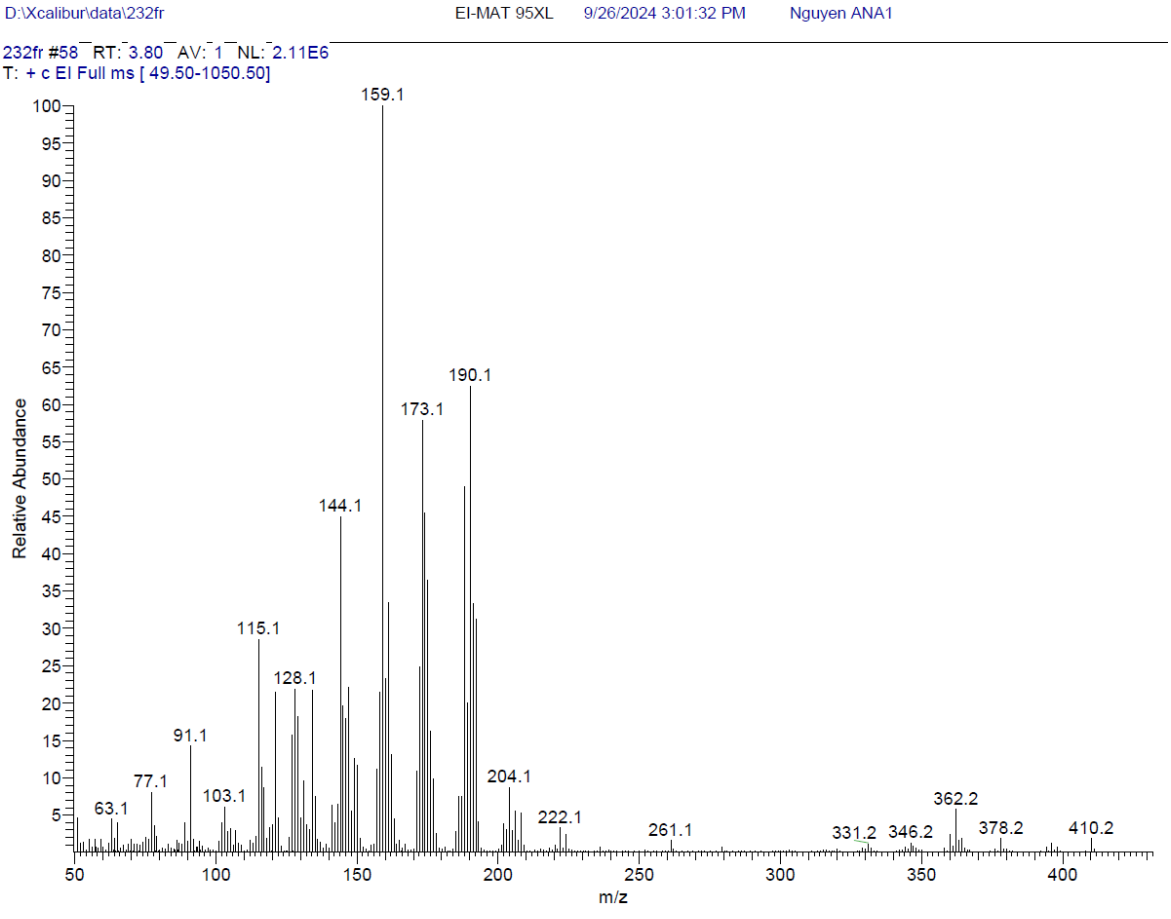

Figure 331: EI-mass spectrum of **60**.

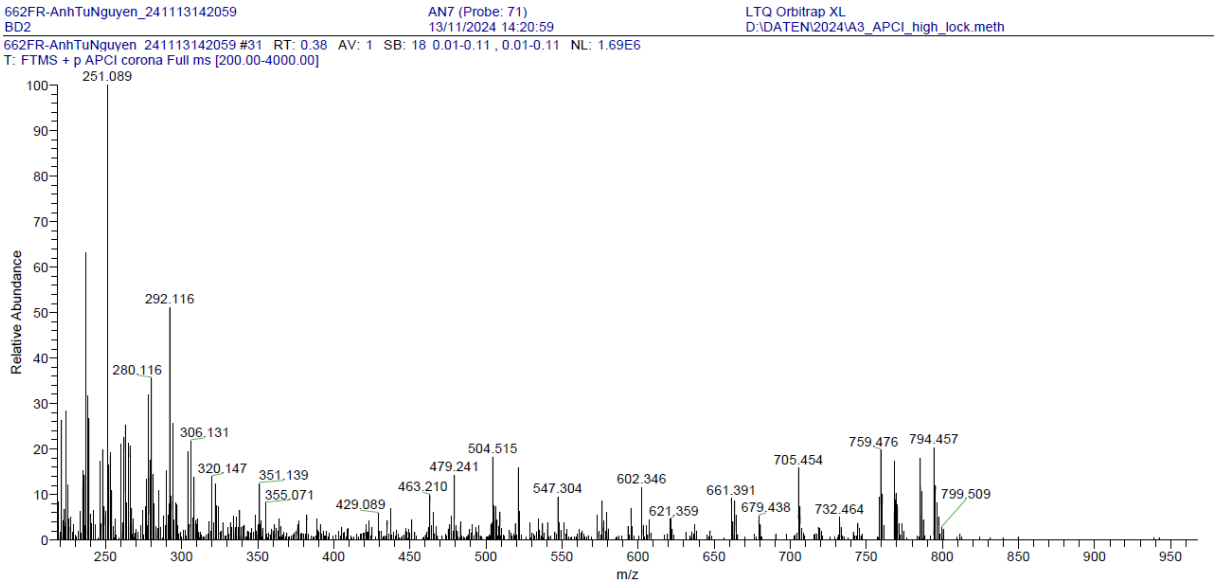

Figure 332: APCI-mass spectrum of **69**.

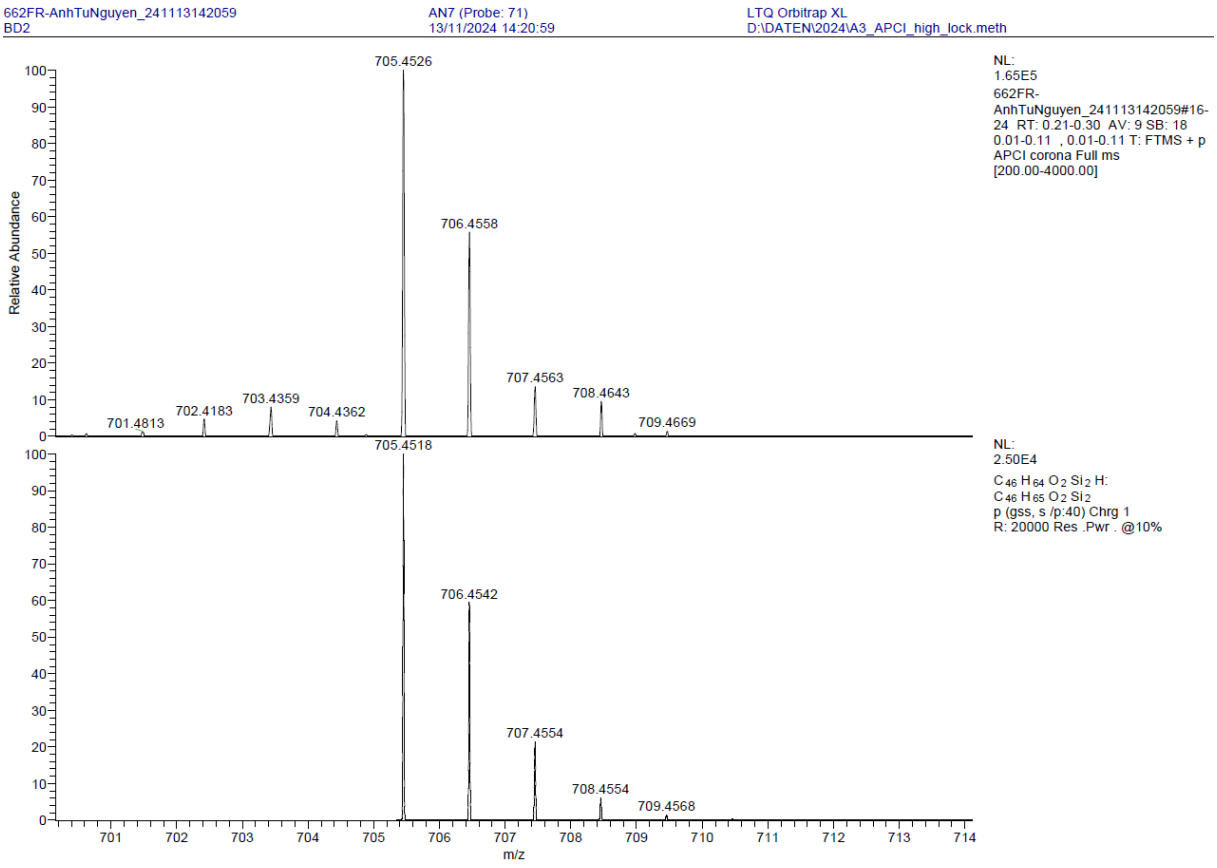

Figure 333: Experimental exact mass (top) and calculated exact mass (bottom) of **69**.

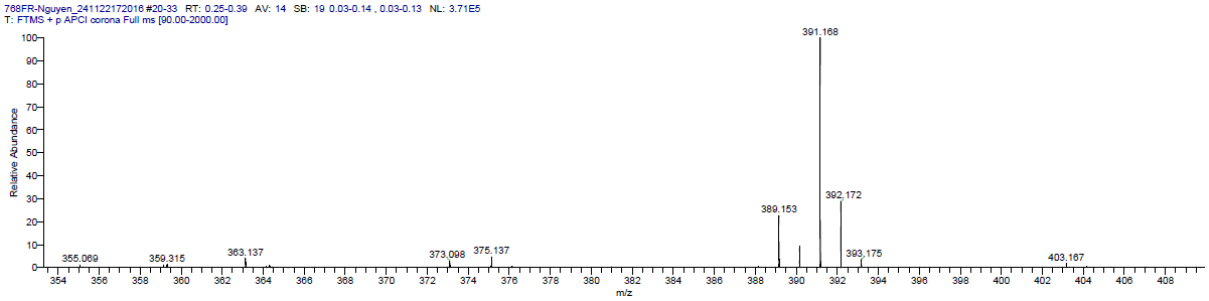

Figure 334: APCI-mass spectrum of **72**.

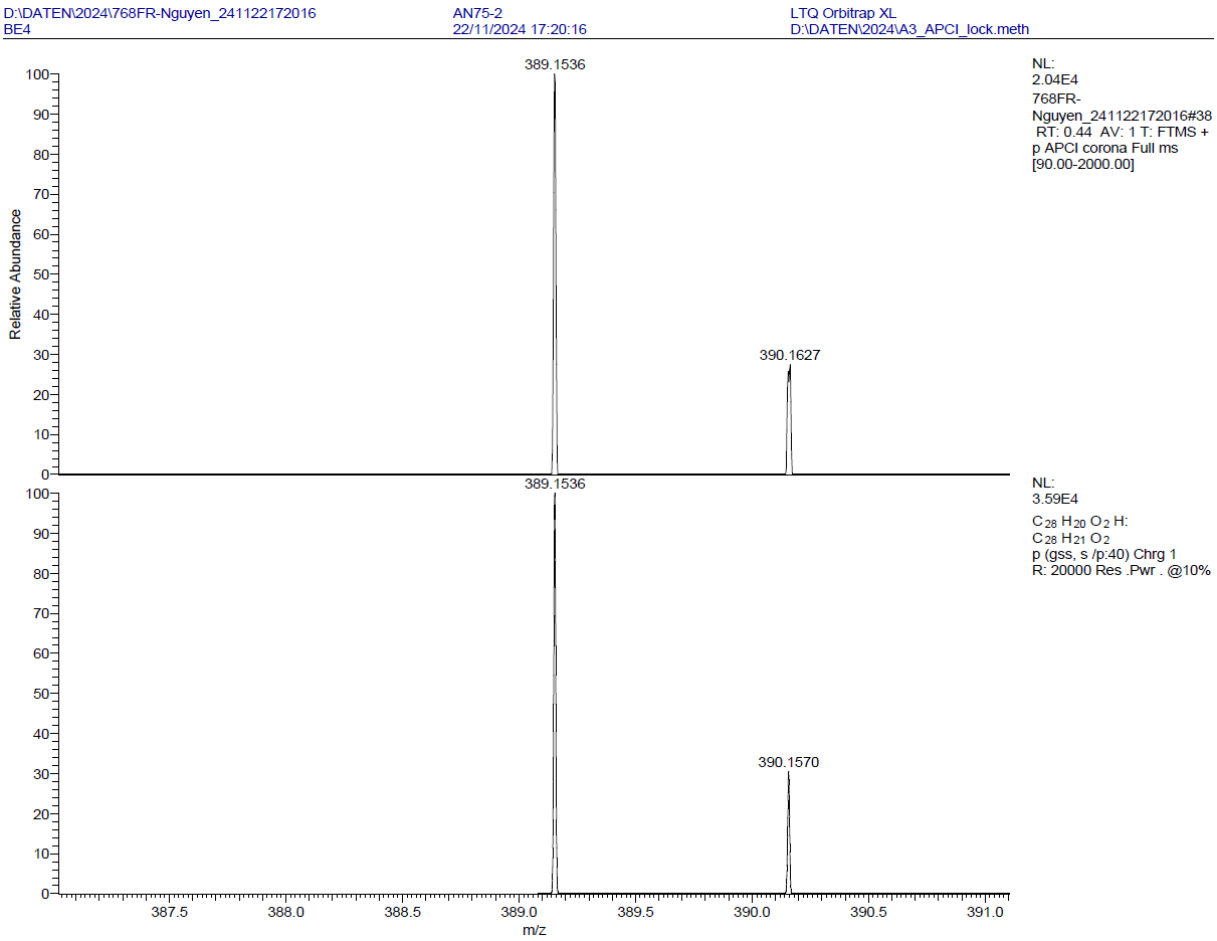

Figure 335: Experimental exact mass (top) and calculated exact mass (bottom) of **72**.

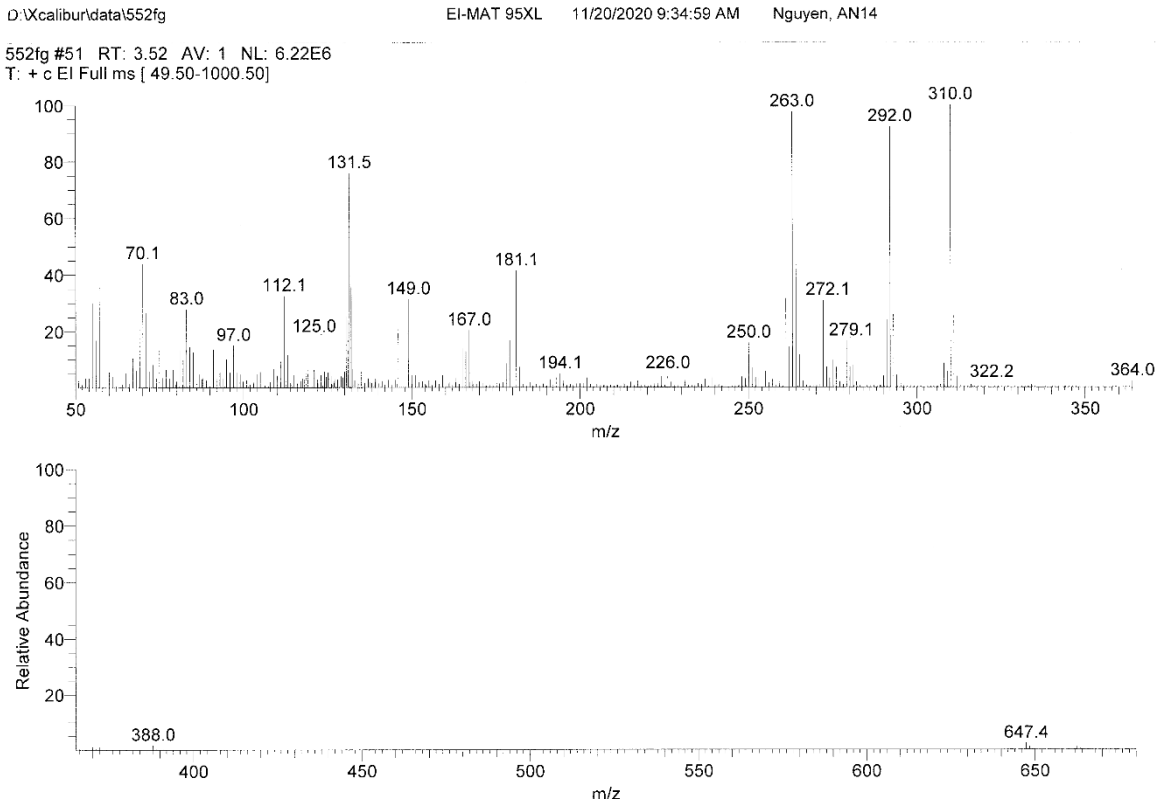

Figure 336: EI-mass spectrum of **73**.

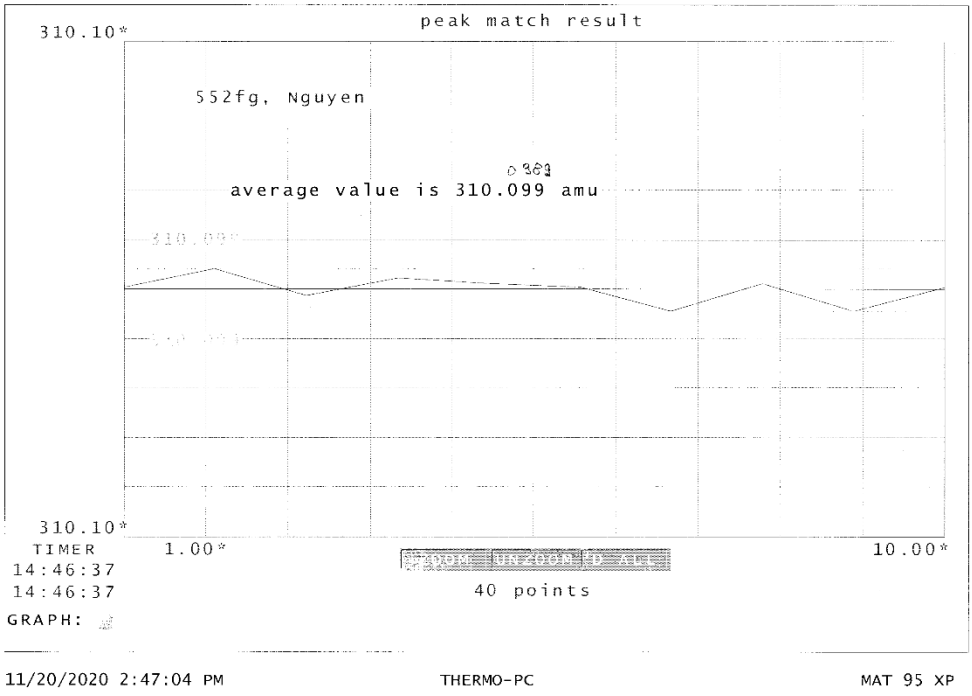

Figure 337: Experimental exact mass of **73**.

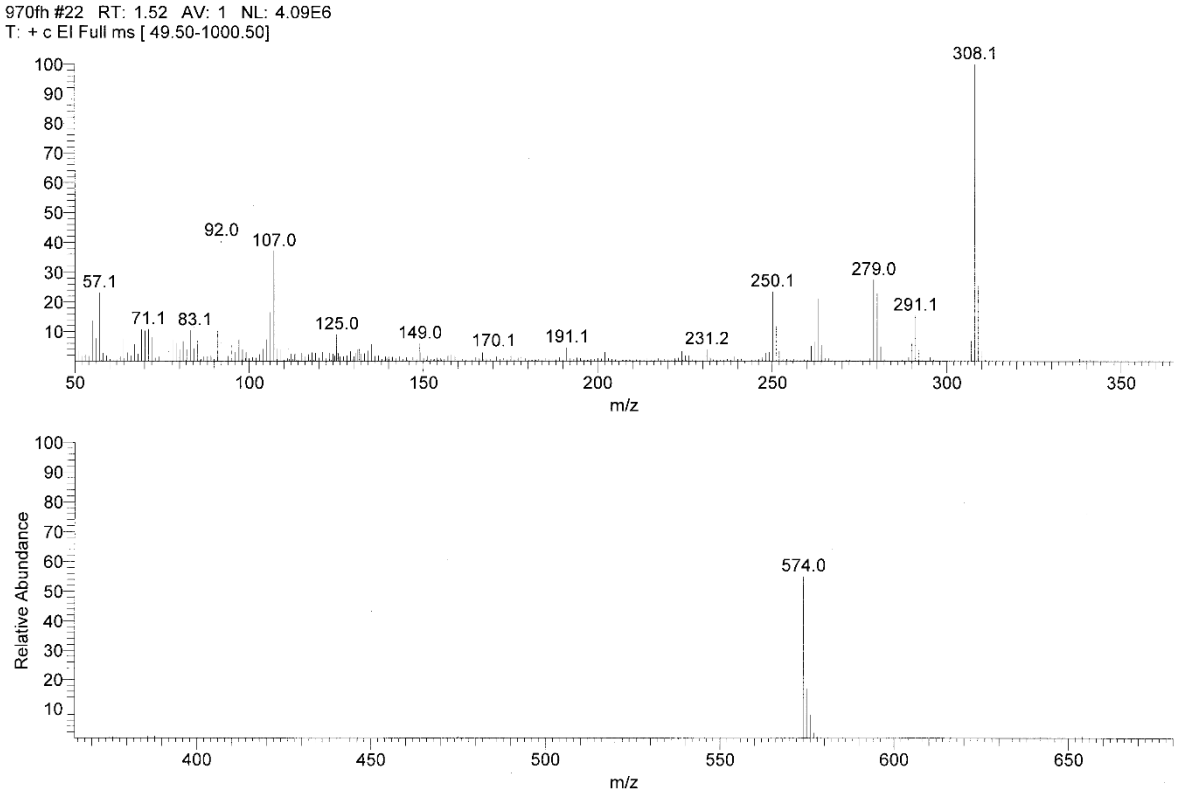

Figure 338: EI-mass spectrum of **74**.

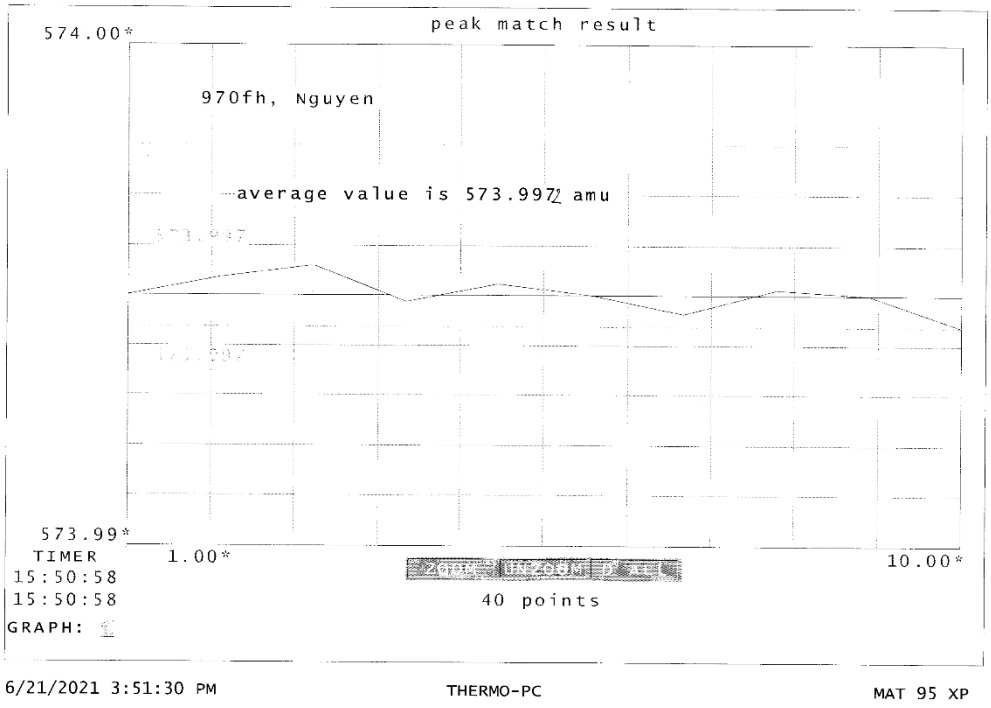

Figure 339: Experimental exact mass of **74**.

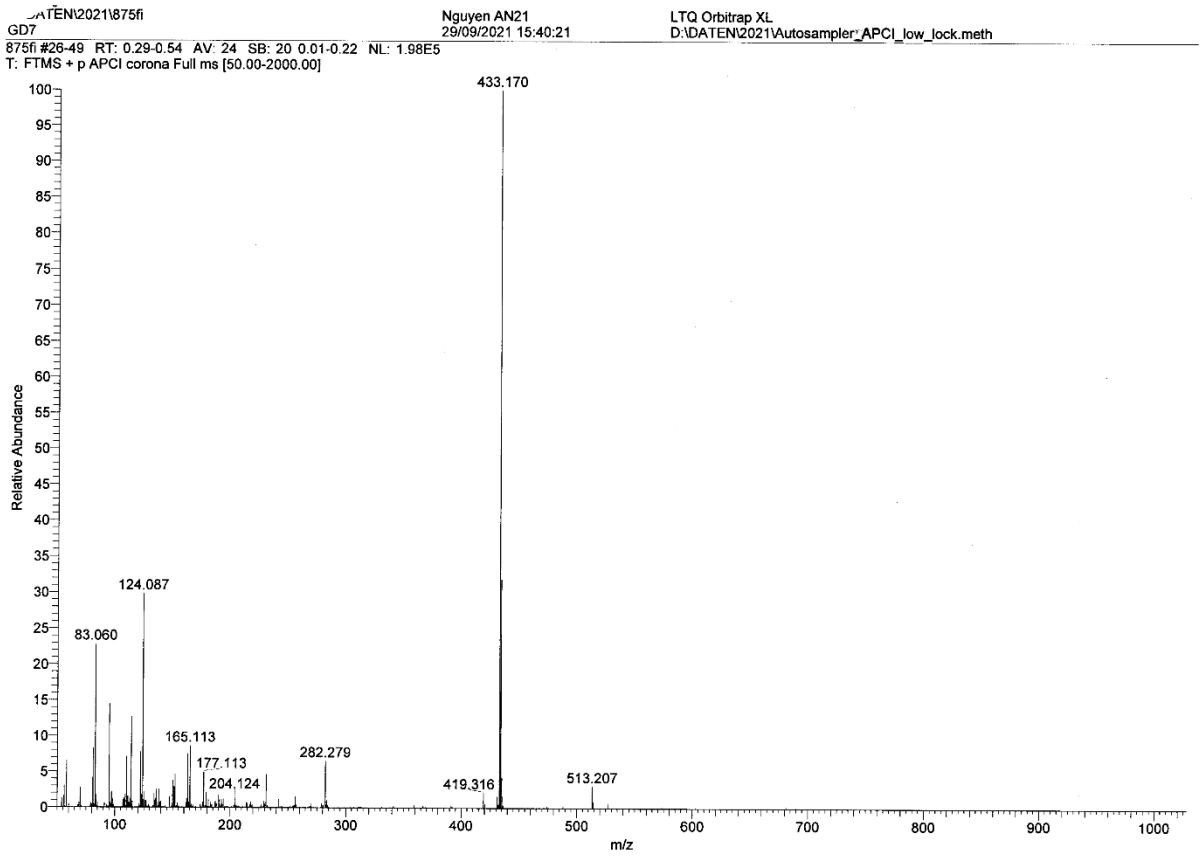

Figure 340: APCI-mass spectrum of **75**.

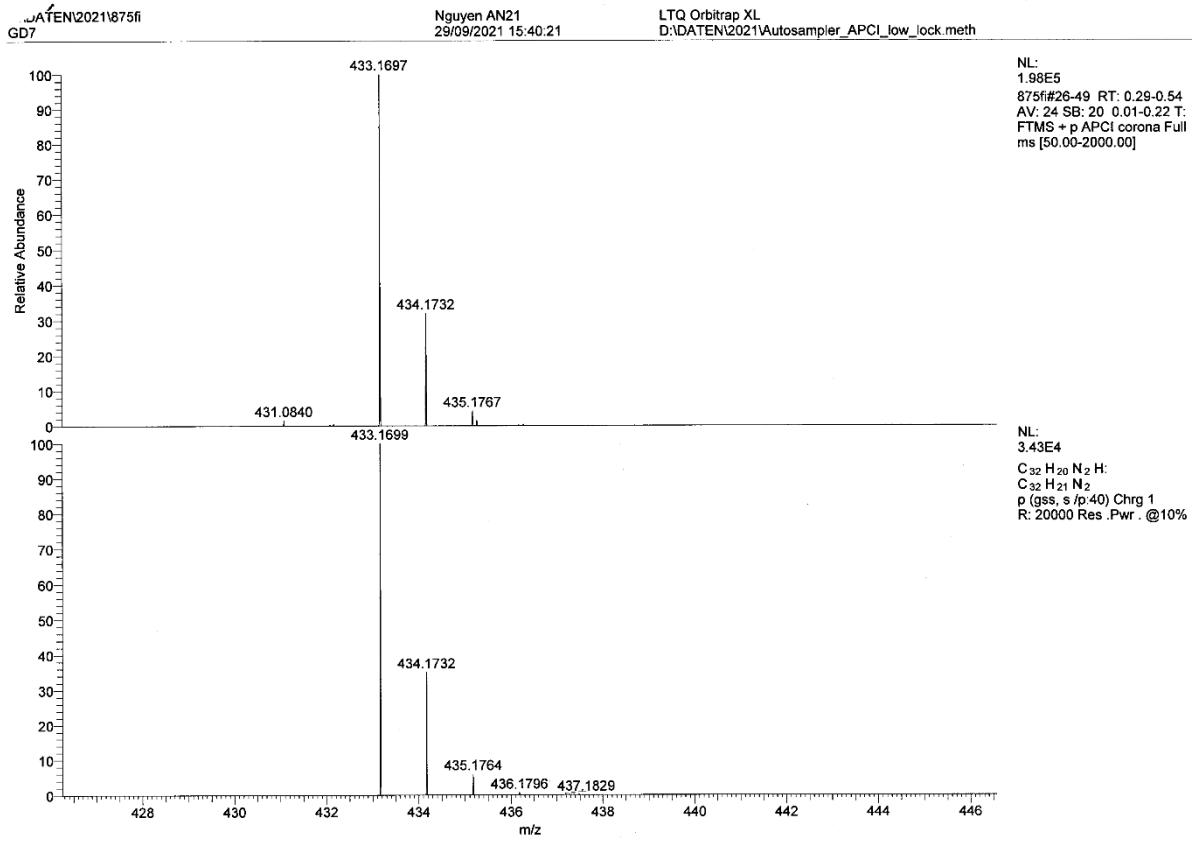

Figure 341: Experimental exact mass (top) and calculated exact mass (bottom) of **75**.

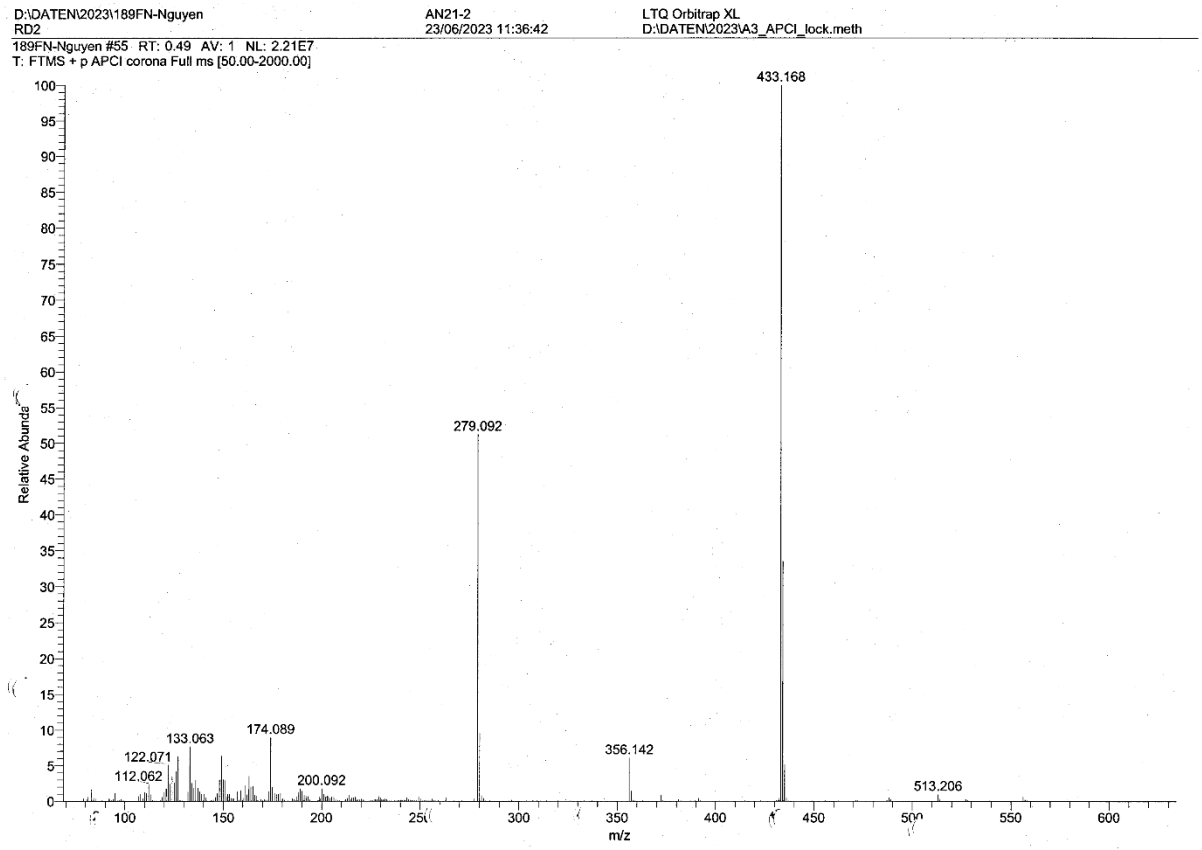

Figure 342: APCI-mass spectrum of **76**.

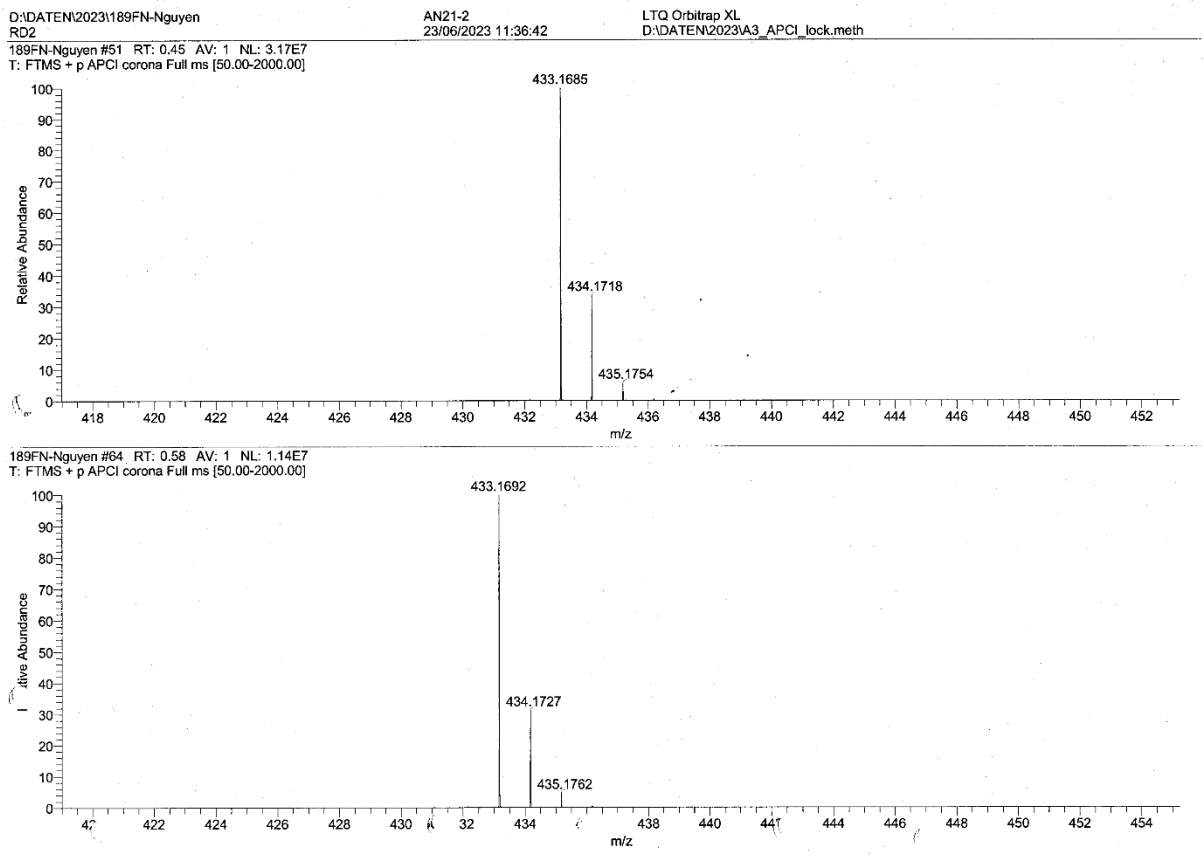

Figure 343: Experimental exact mass (top) and calculated exact mass (bottom) of **76**.

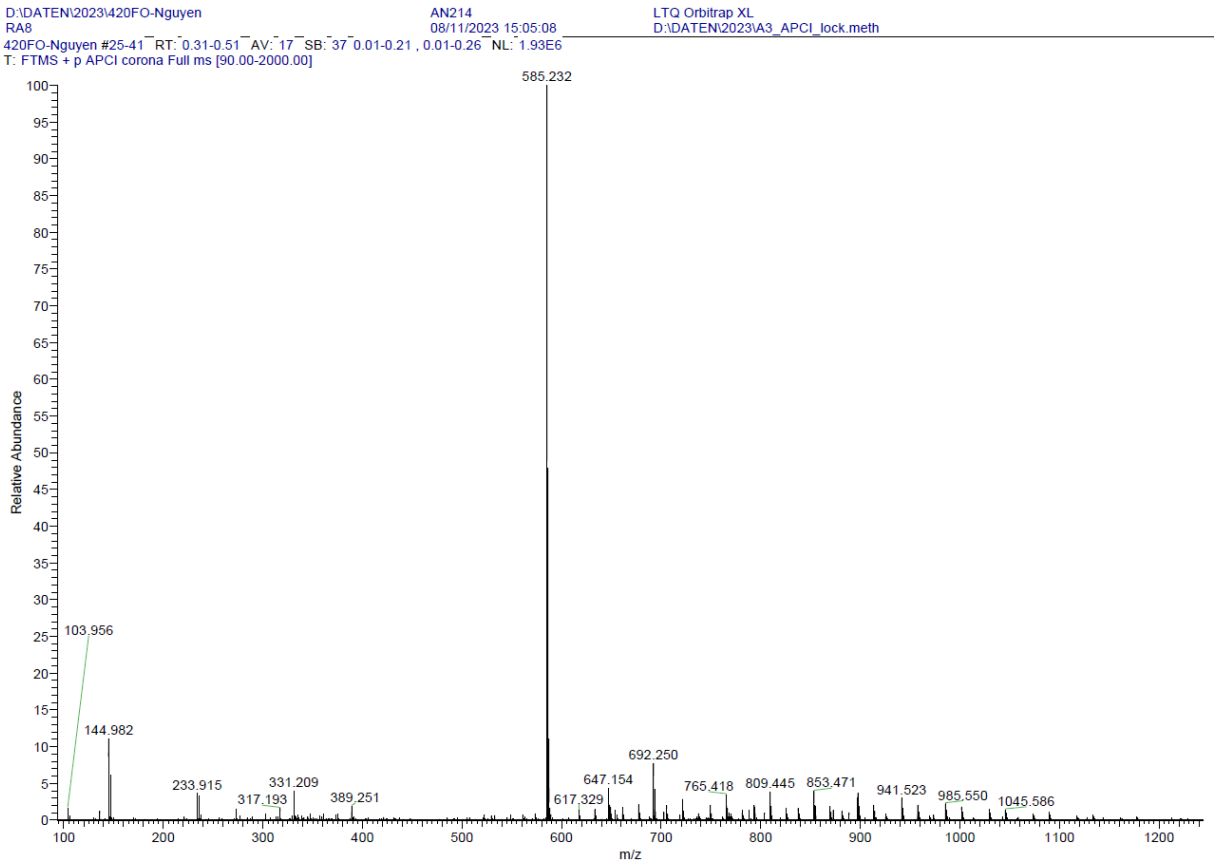

Figure 344: APCI-mass spectrum of **78**.

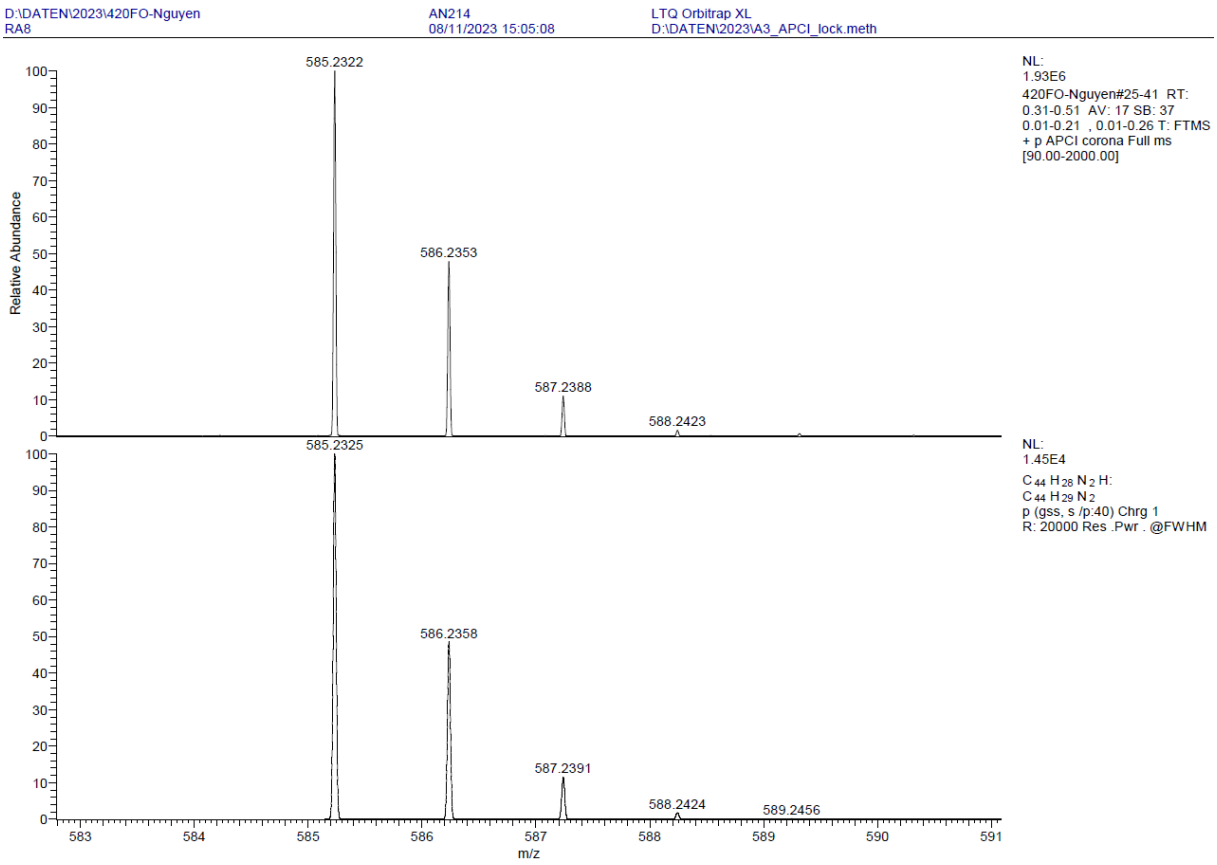

Figure 345: Experimental exact mass (top) and calculated exact mass (bottom) of **78**.

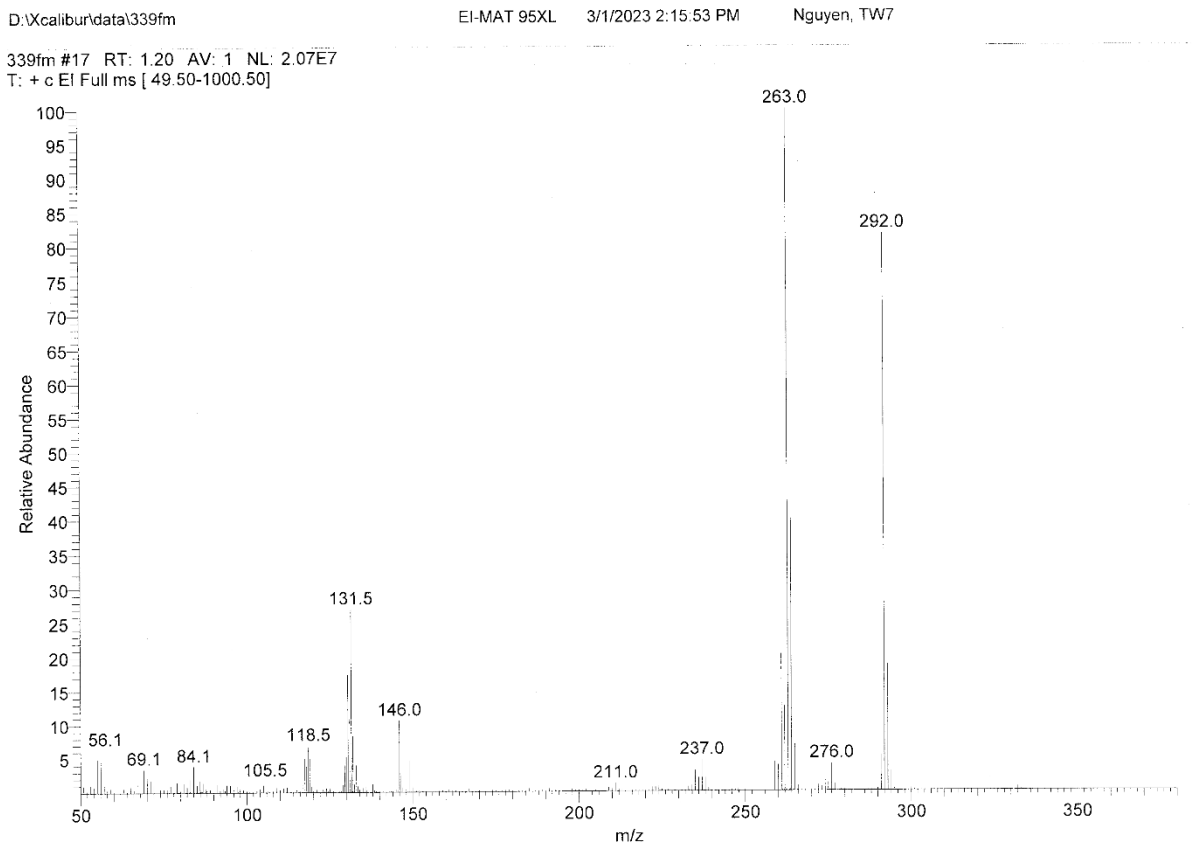

Figure 346: EI-mass spectrum of **80**.

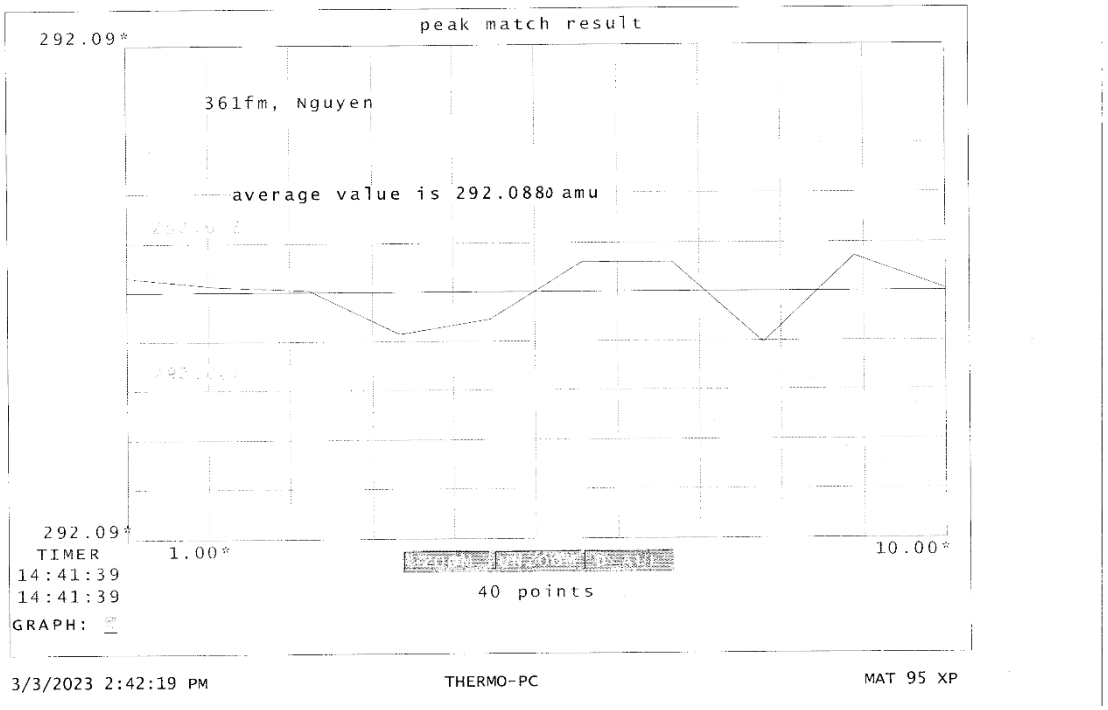

Figure 347: Experimental exact mass of **80**.

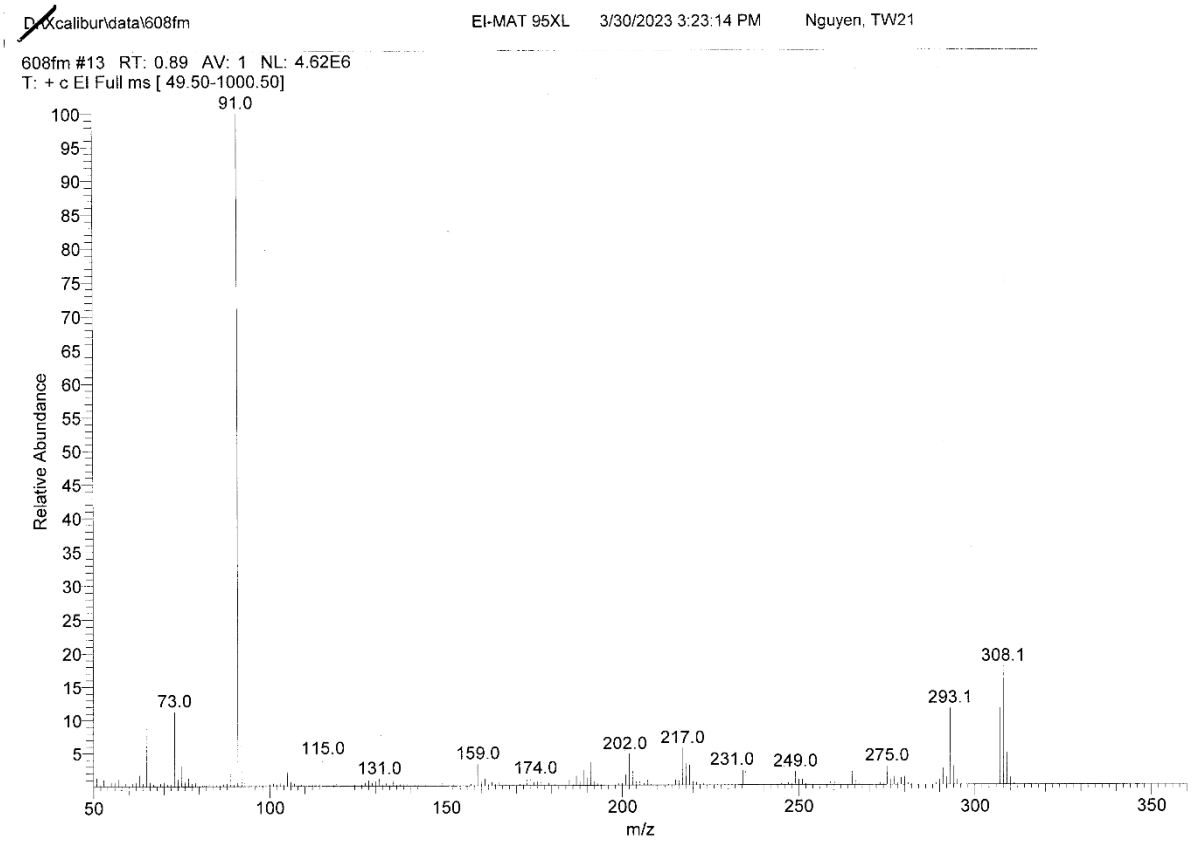

Figure 348: EI-mass spectrum of **82**.

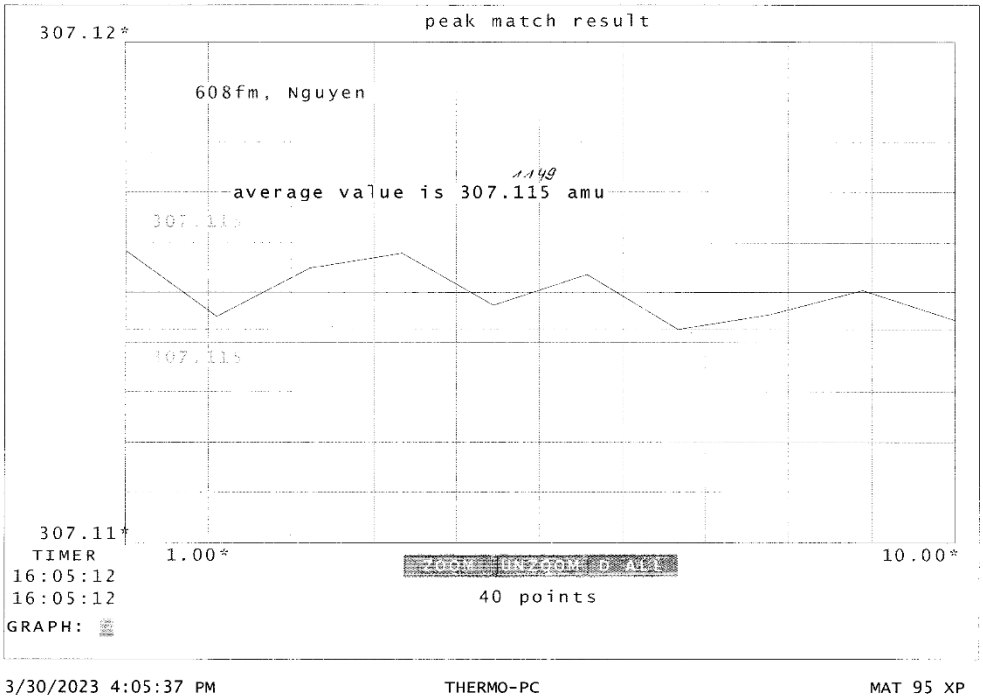

Figure 349: Experimental exact mass of **82**.

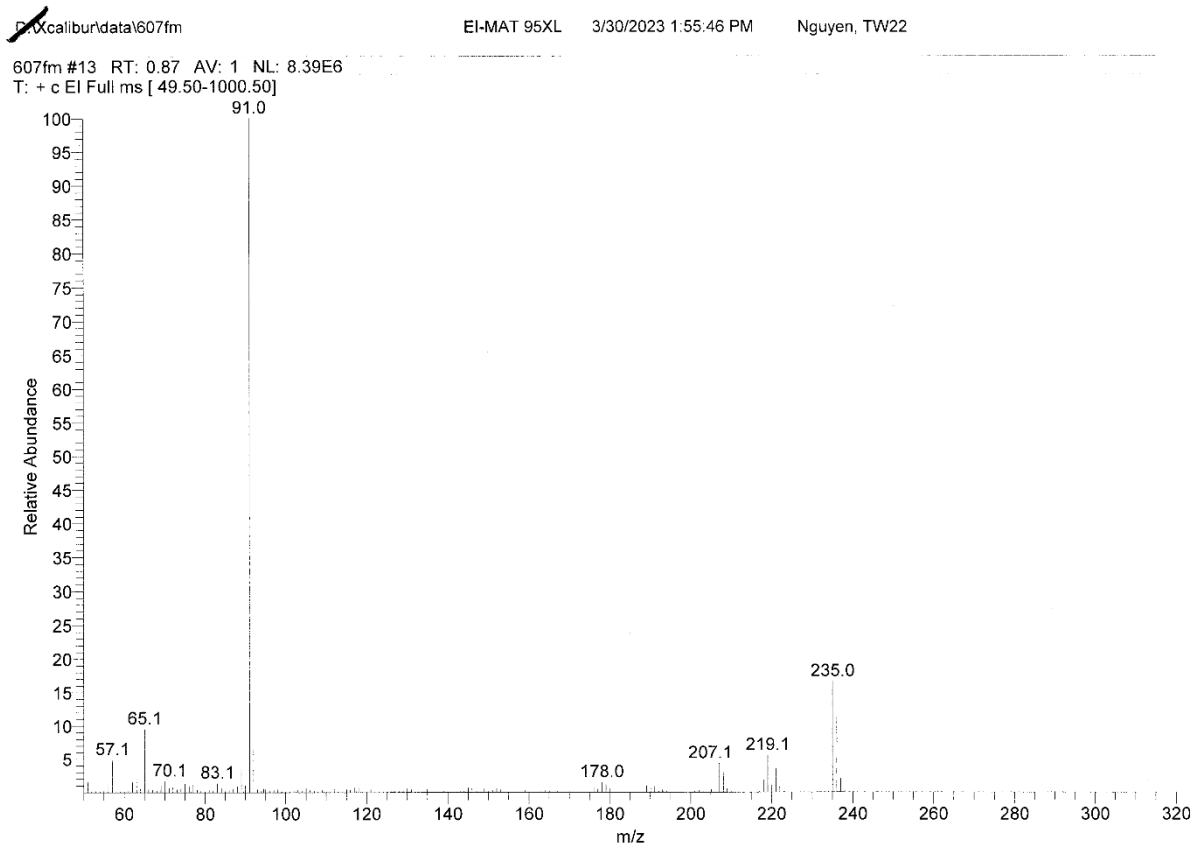

Figure 350: EI-mass spectrum of **83**.

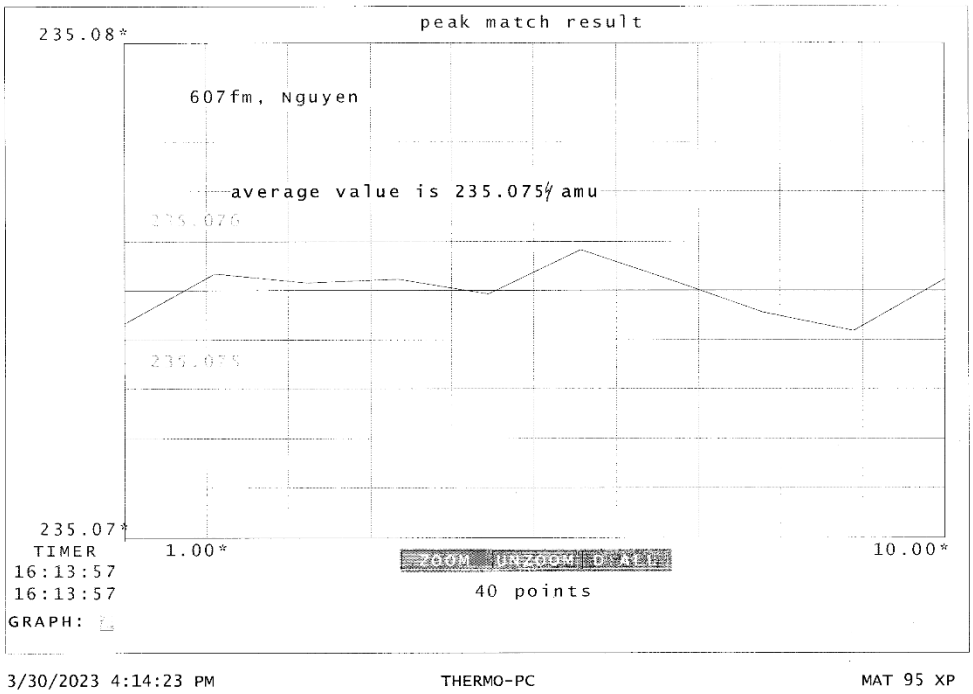

Figure 351: Experimental exact mass of **83**.

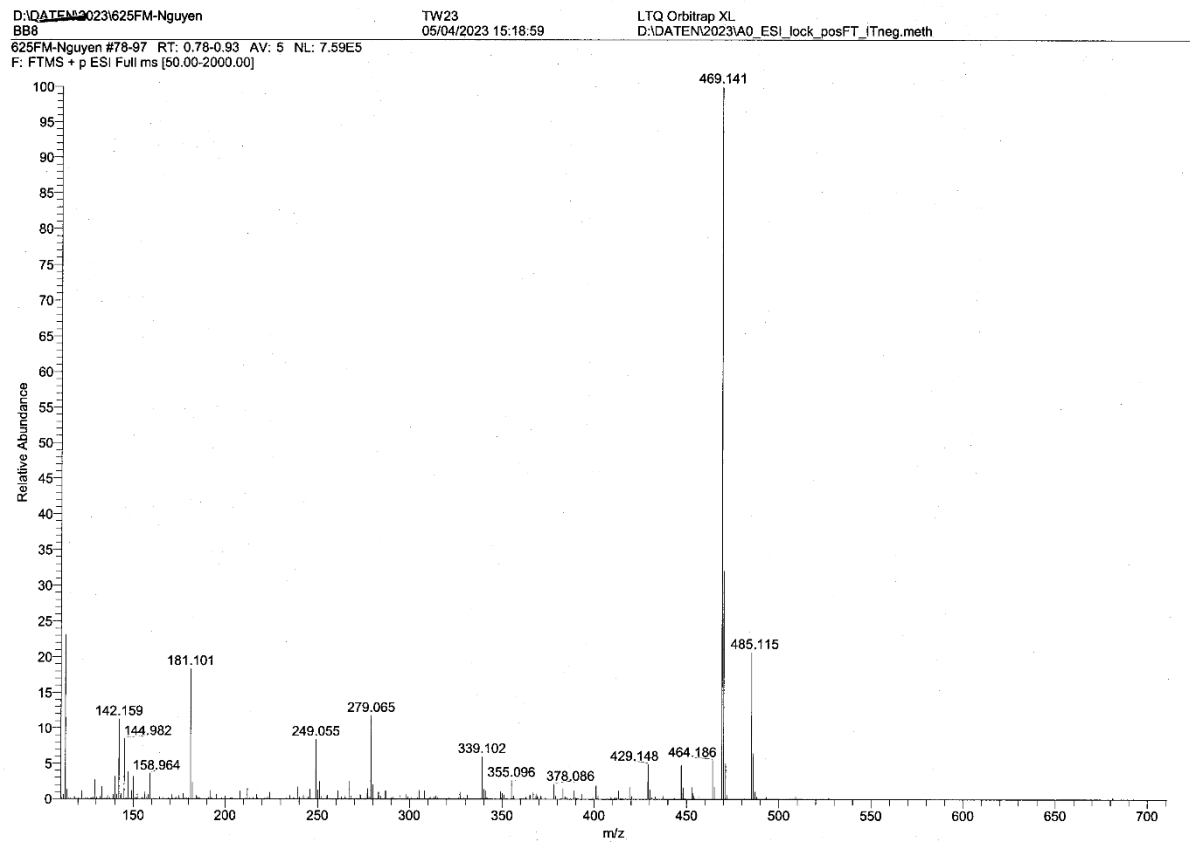

Figure 352: ESI(+)-mass spectrum of **84**.

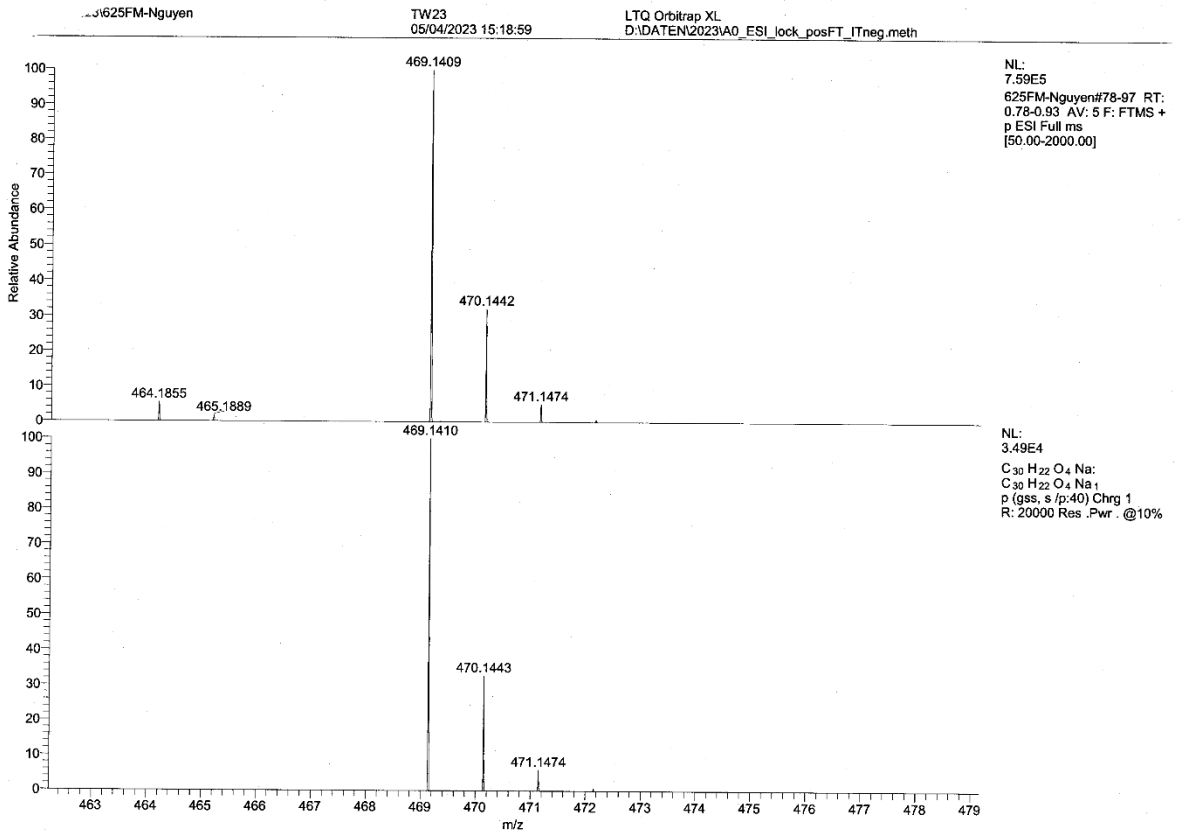

Figure 353: Experimental exact mass (top) and calculated exact mass (bottom) of **84**.

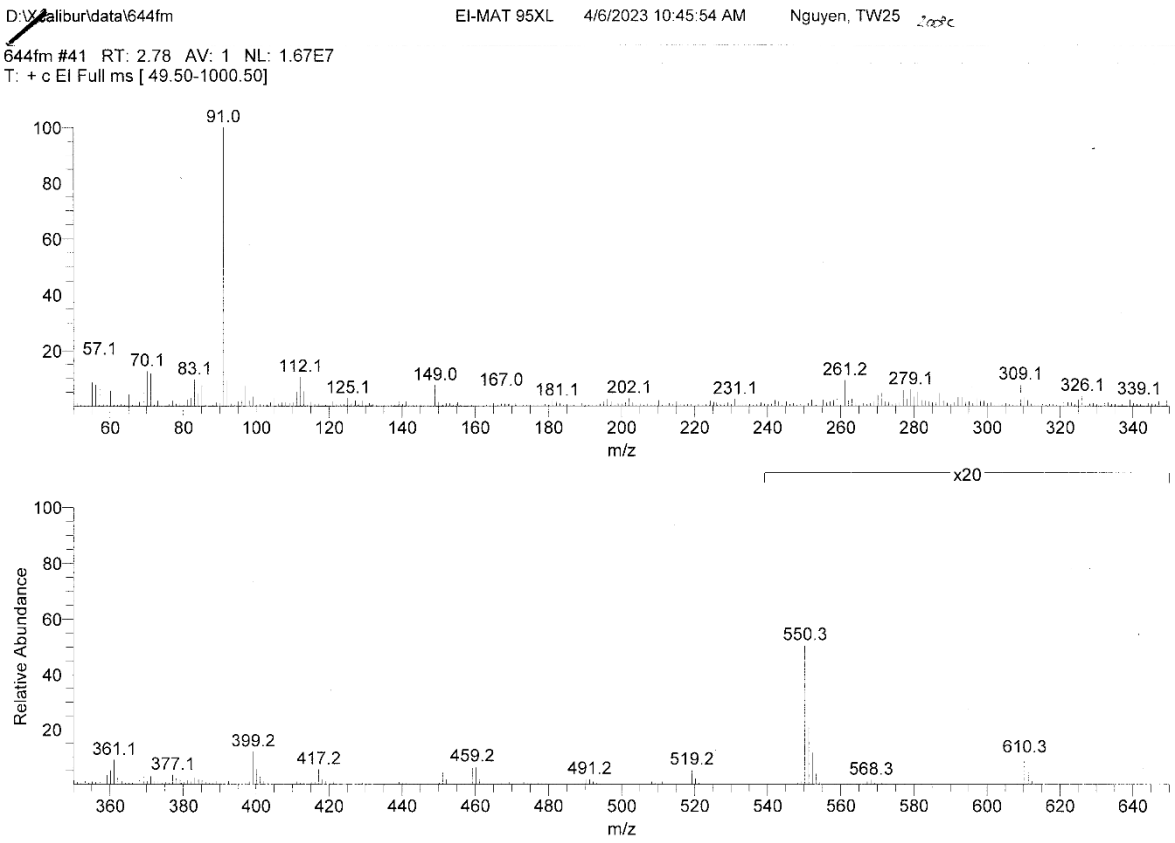

Figure 354: EI-mass spectrum of **86**.

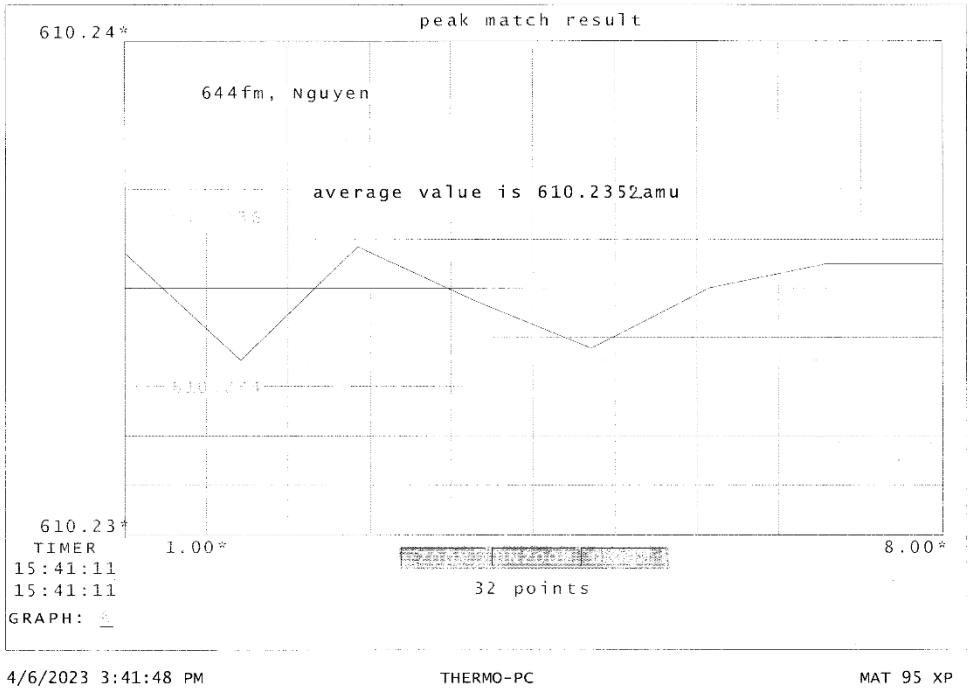

Figure 355: Experimental exact mass of **86**.

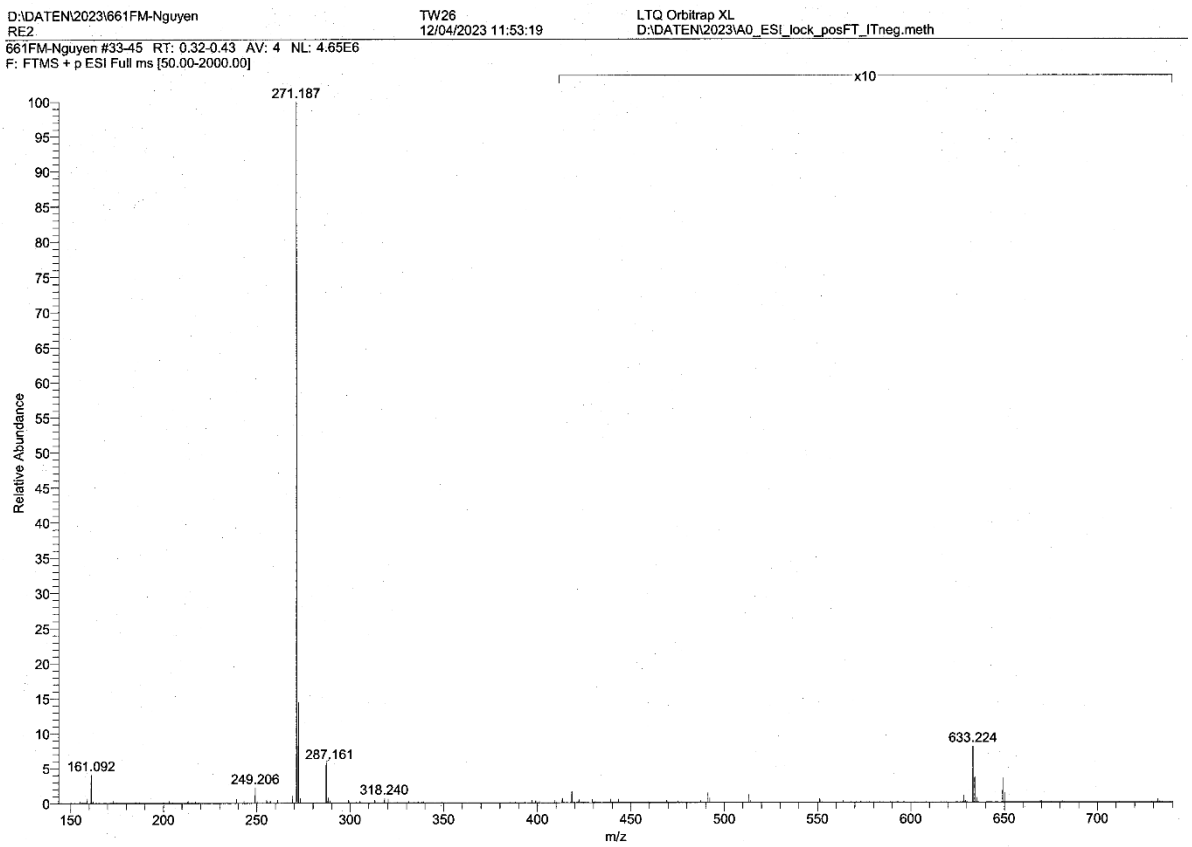

Figure 356: ESI(+)-mass spectrum of **87**.

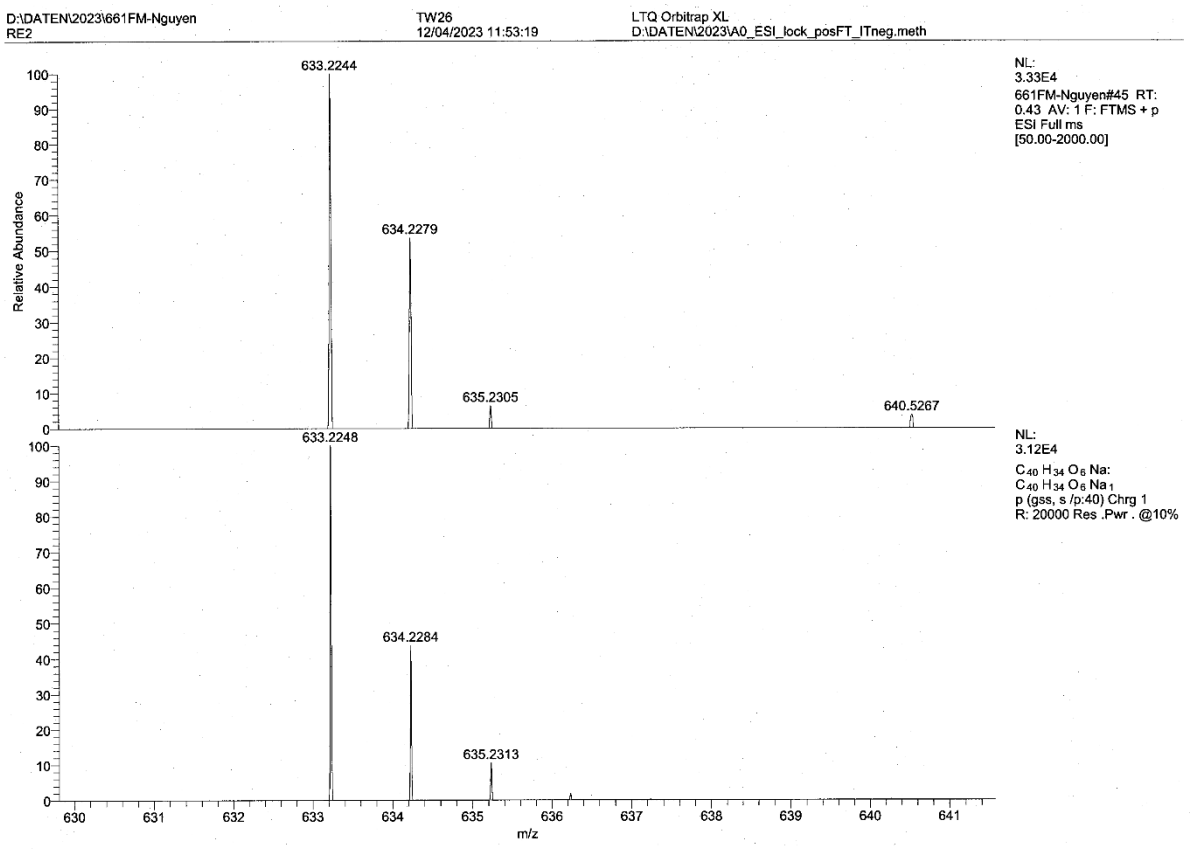

Figure 357: Experimental exact mass (top) and calculated exact mass (bottom) of **87**.

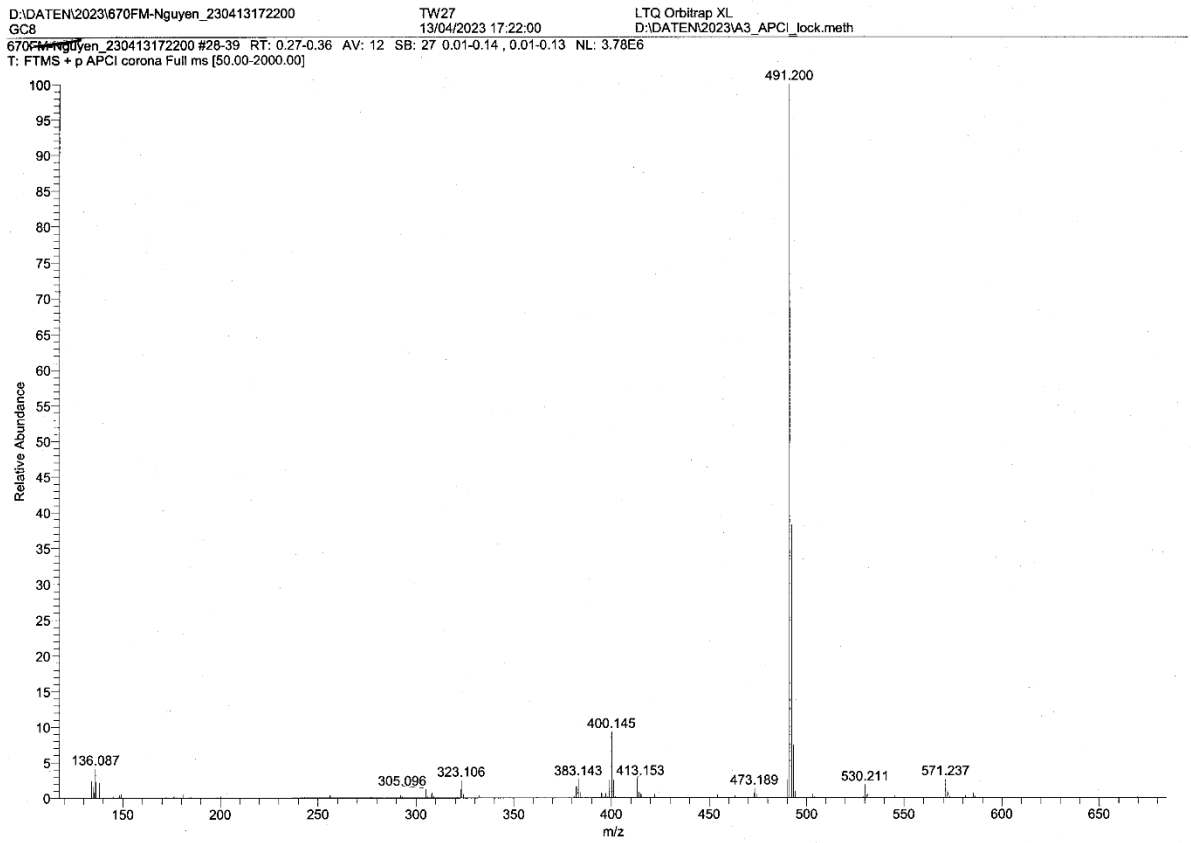

Figure 358: APCI-mass spectrum of **88**.

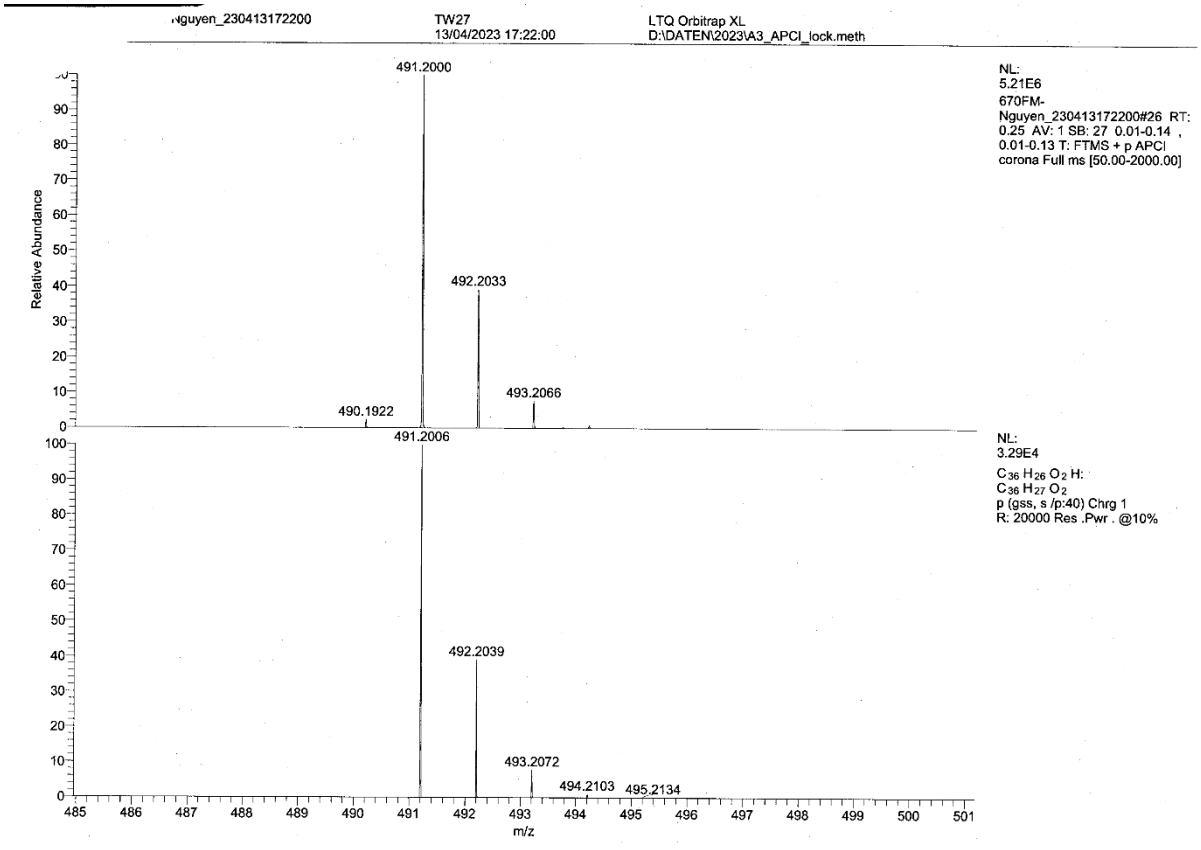

Figure 359: Experimental exact mass (top) and calculated exact mass (bottom) of **88**.

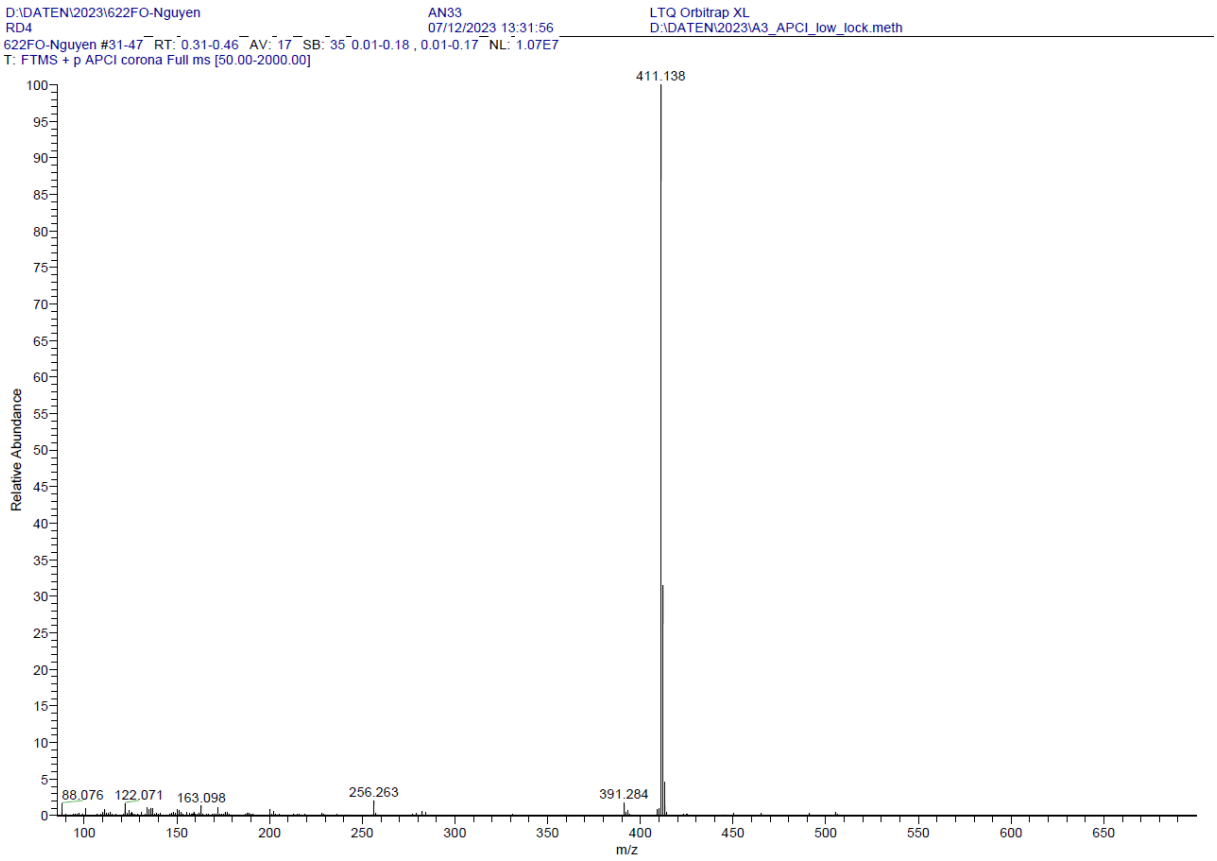

Figure 360: APCI-mass spectrum of **89**.

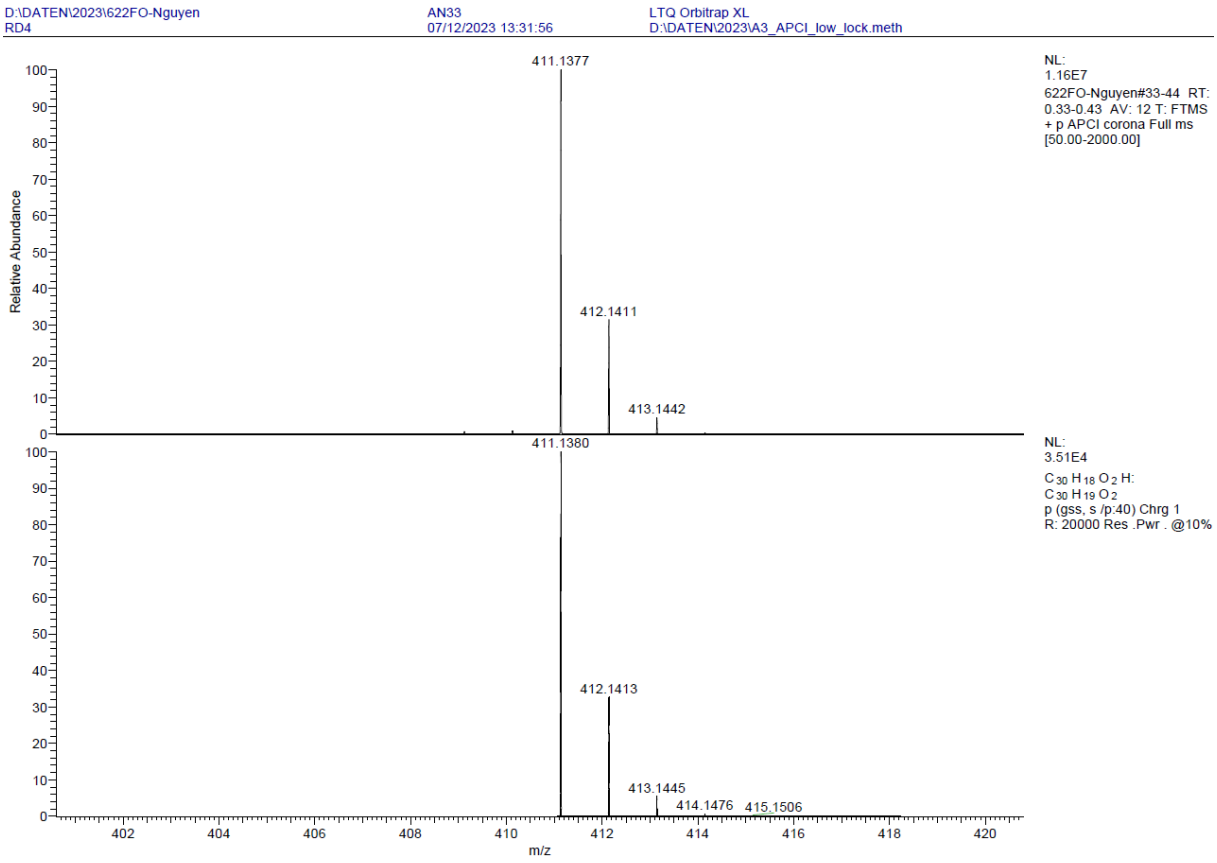

Figure 361: Experimental exact mass (top) and calculated exact mass (bottom) of **89**.

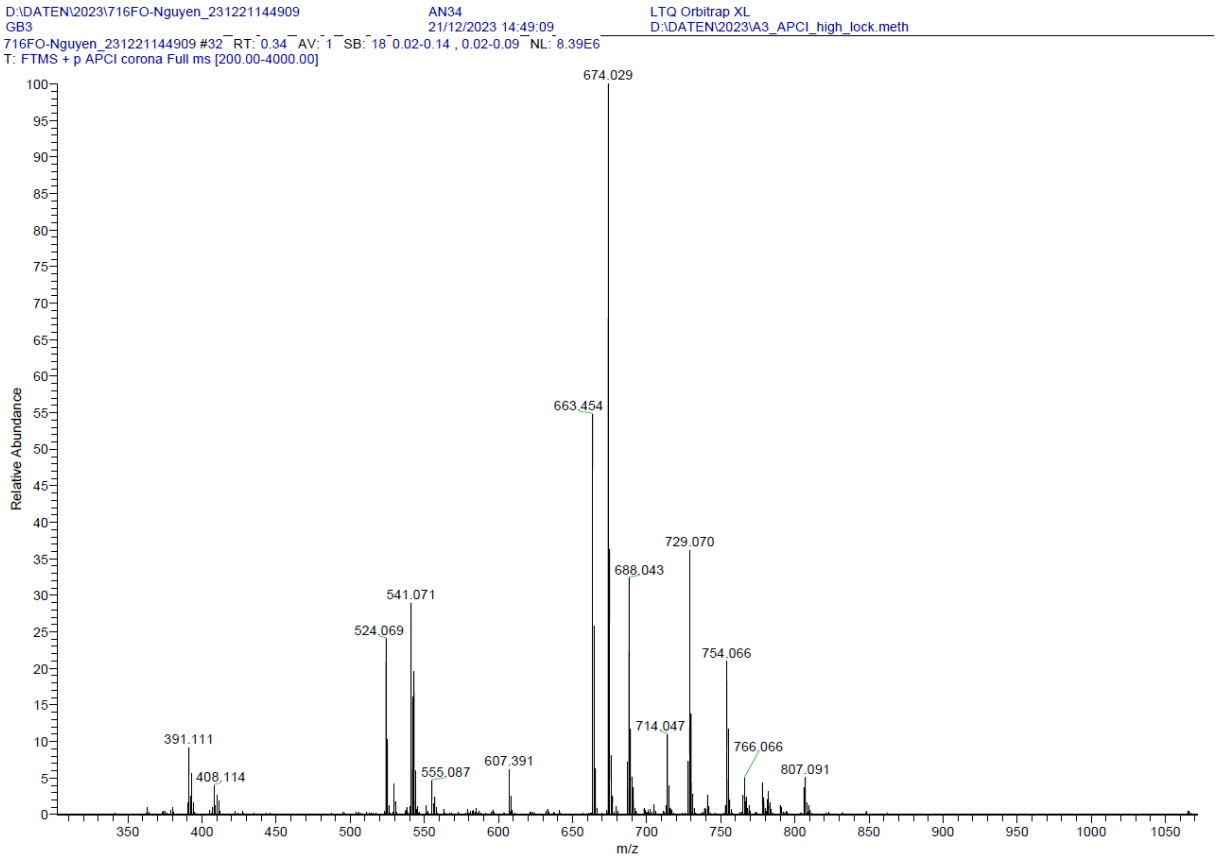

Figure 362: APCI-mass spectrum of **90**.

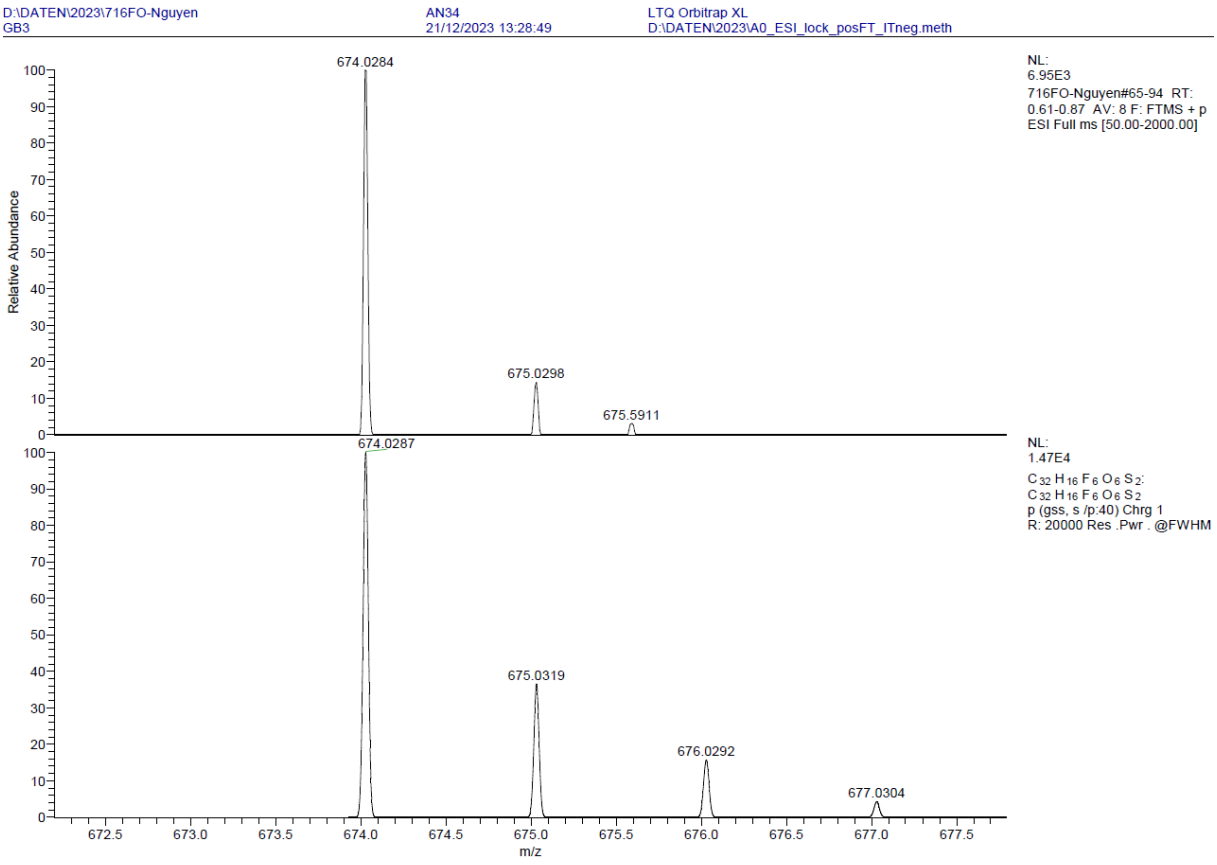

Figure 363: Experimental exact mass (top) and calculated exact mass (bottom) of **90**.

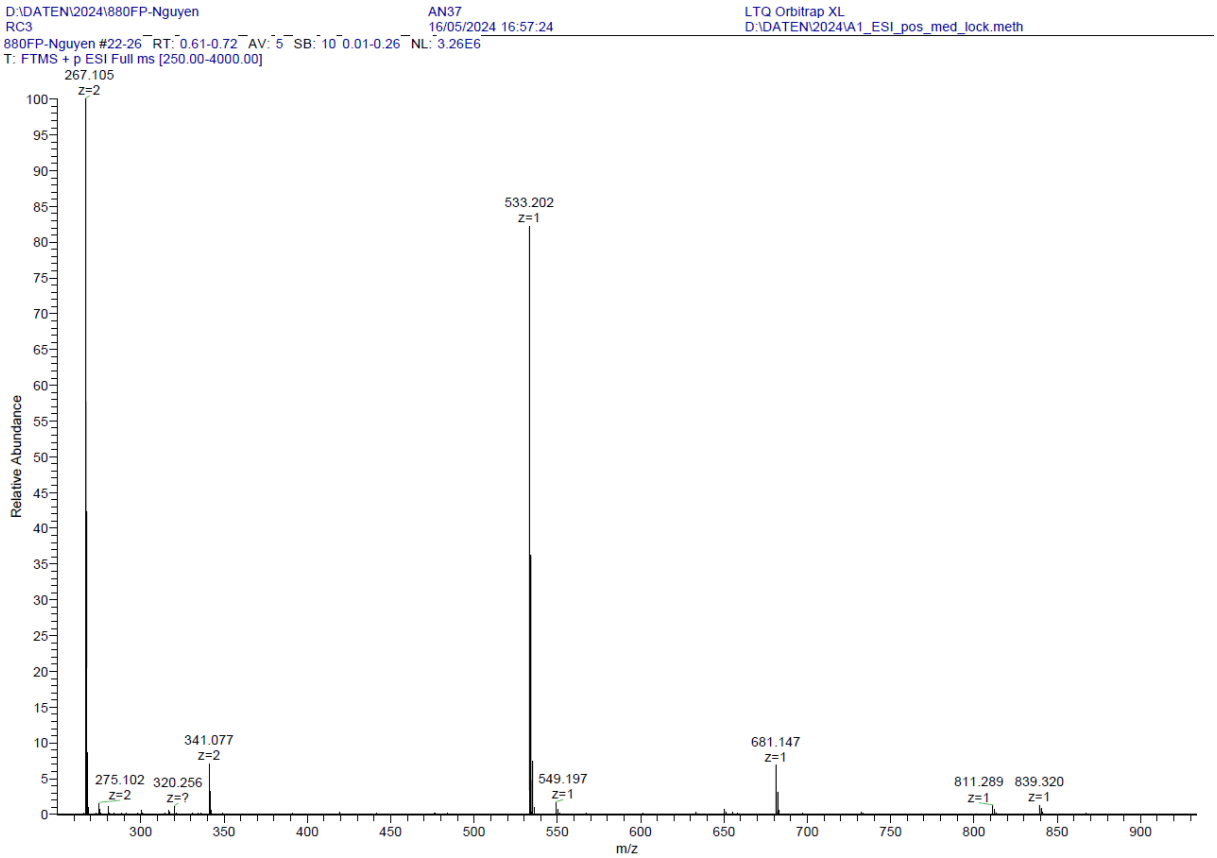

Figure 364: ESI(+)-mass spectrum of **91**.

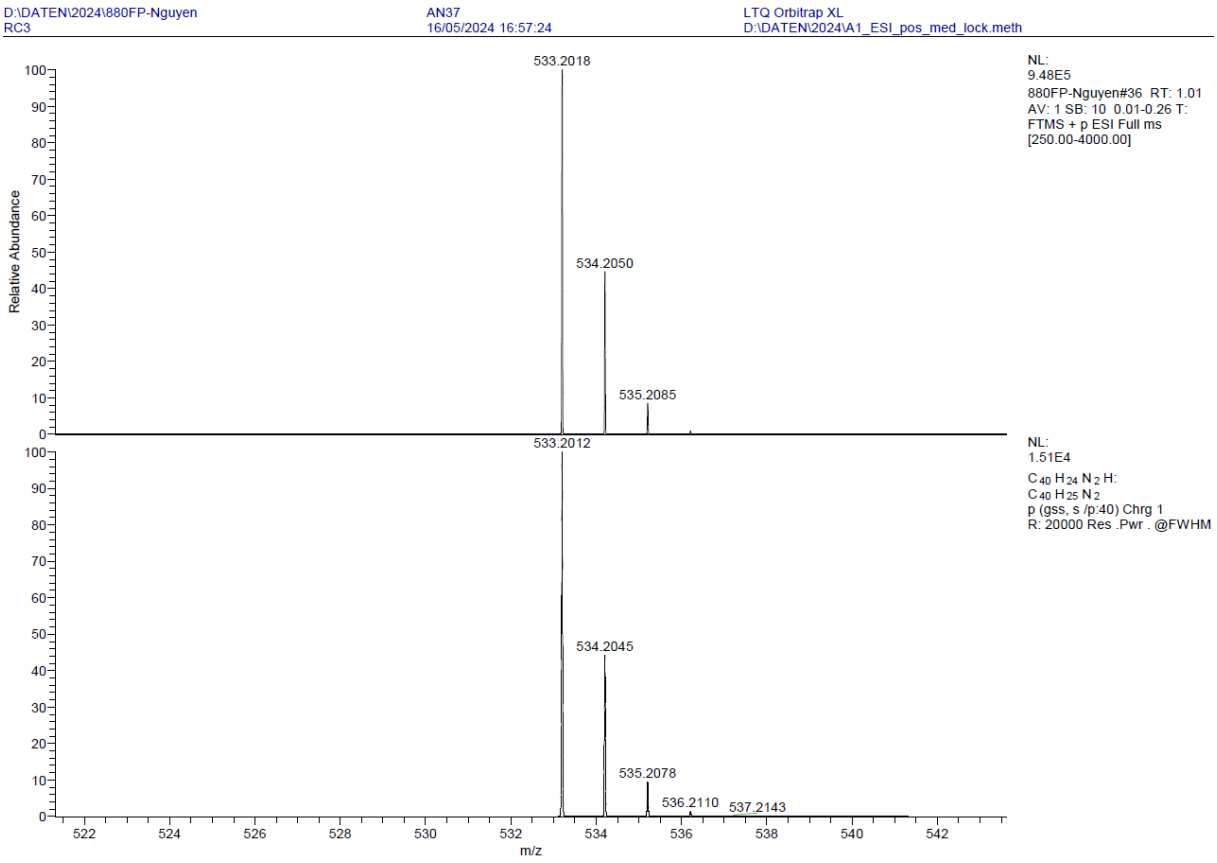

Figure 365: Experimental exact mass (top) and calculated exact mass (bottom) of **91**.

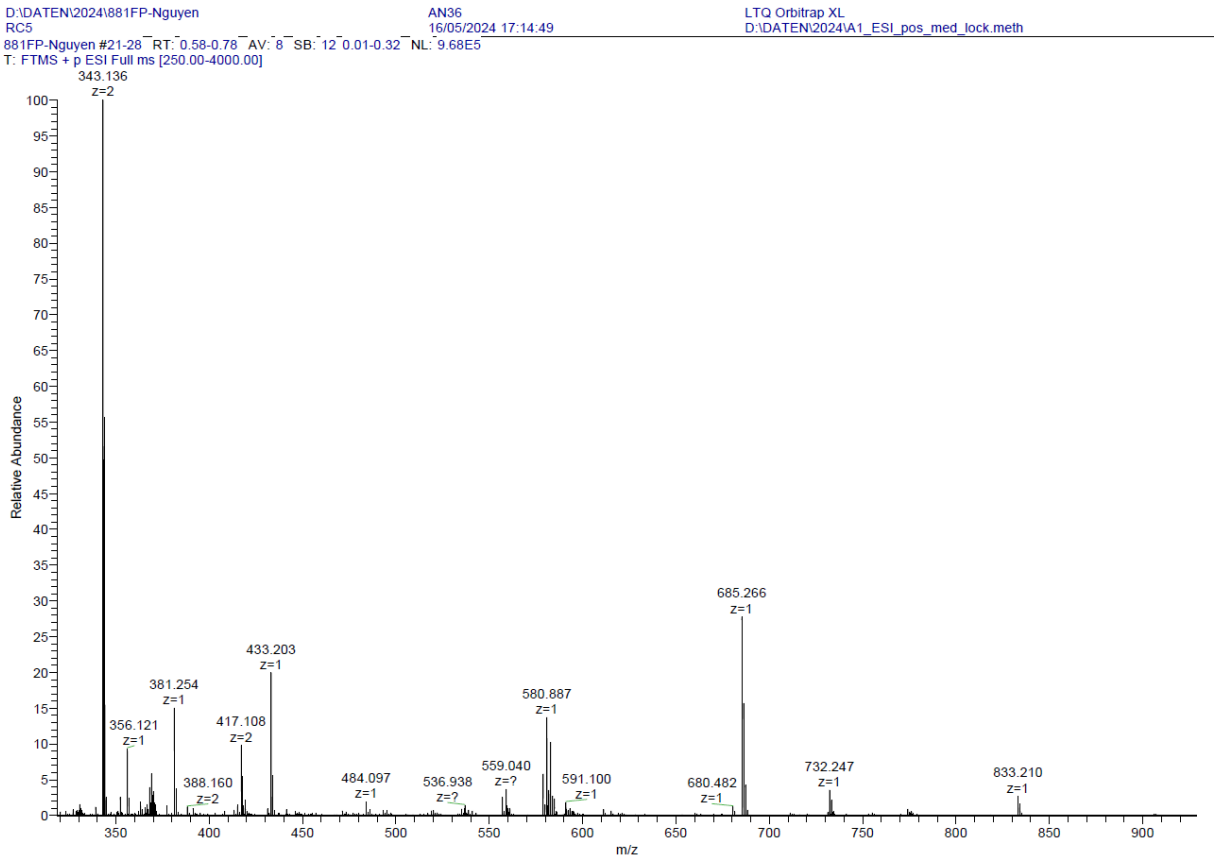

Figure 366: ESI(+)-mass spectrum of **92**.

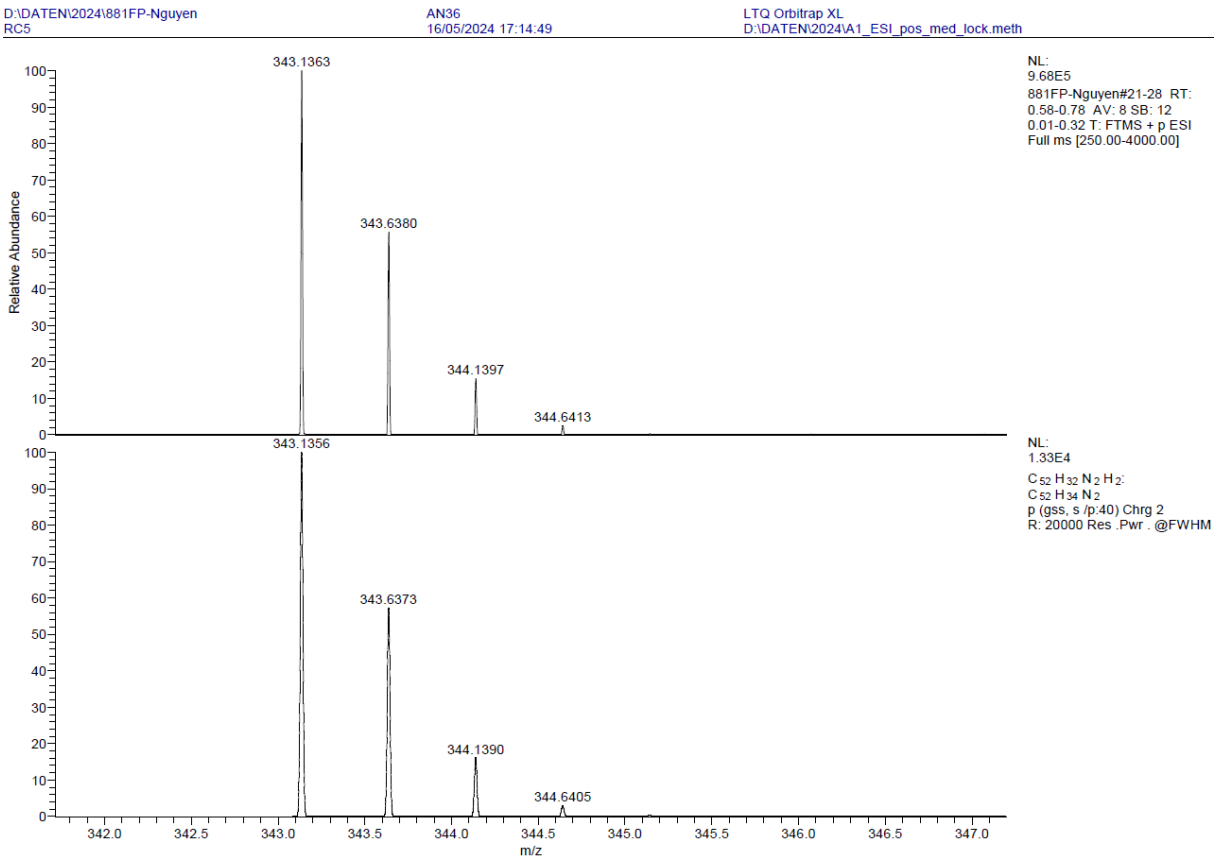

Figure 367: Experimental exact mass (top) and calculated exact mass (bottom) of **92**.

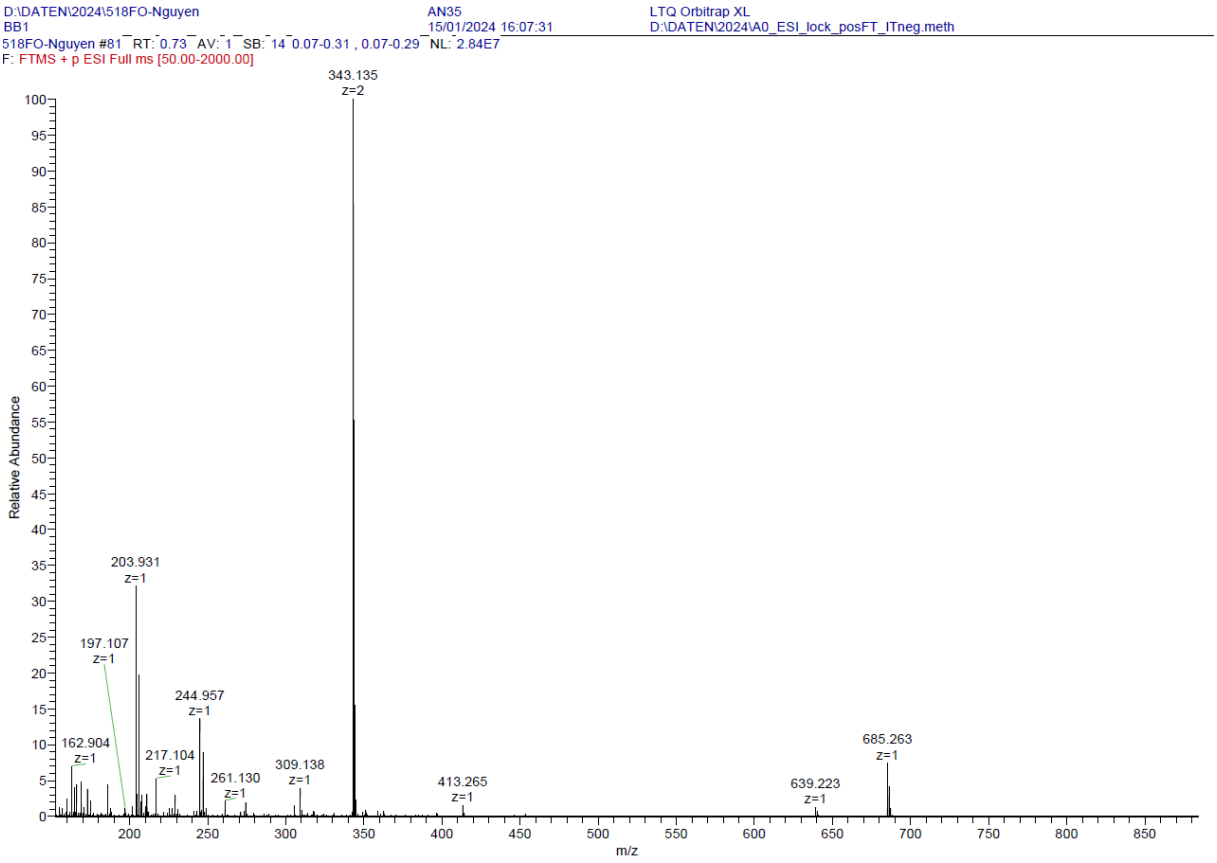

Figure 368: ESI(+)-mass spectrum of **93**.

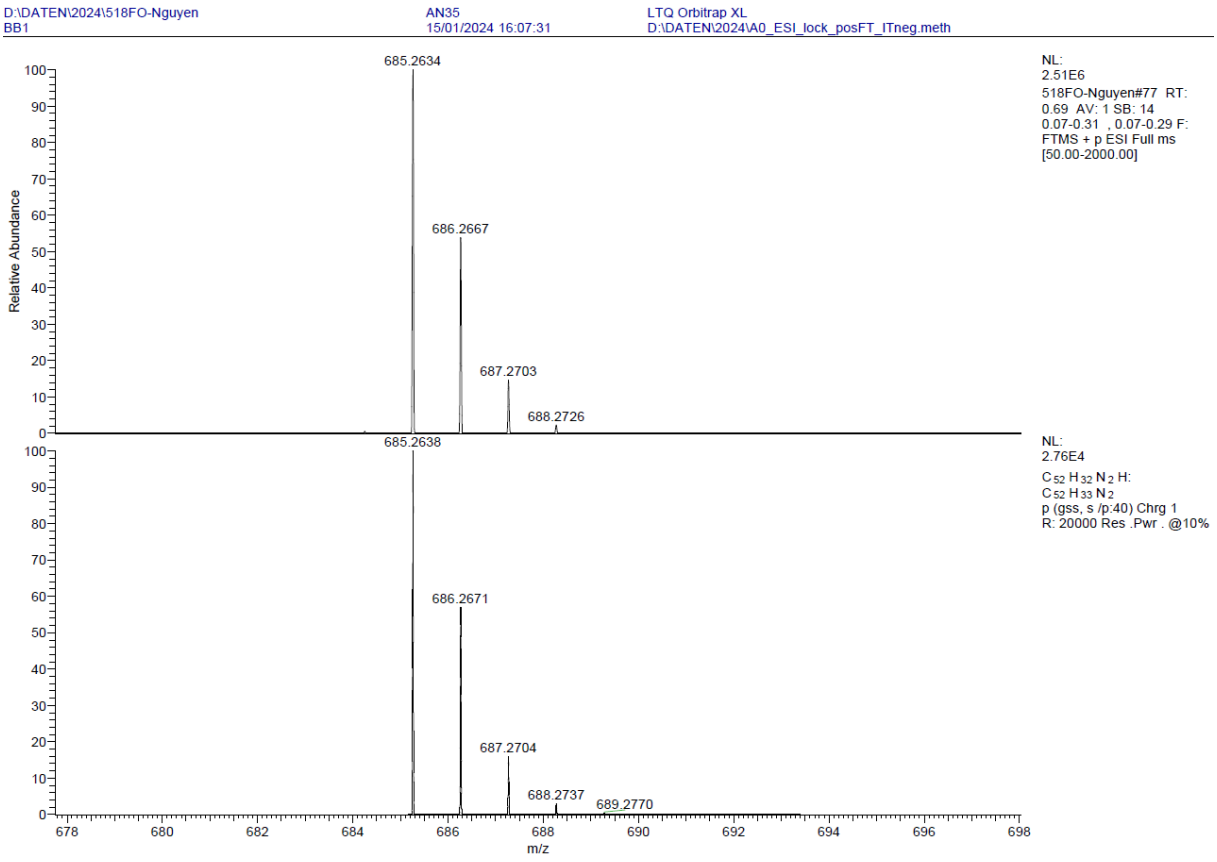

Figure 369: Experimental exact mass (top) and calculated exact mass (bottom) of **93**.

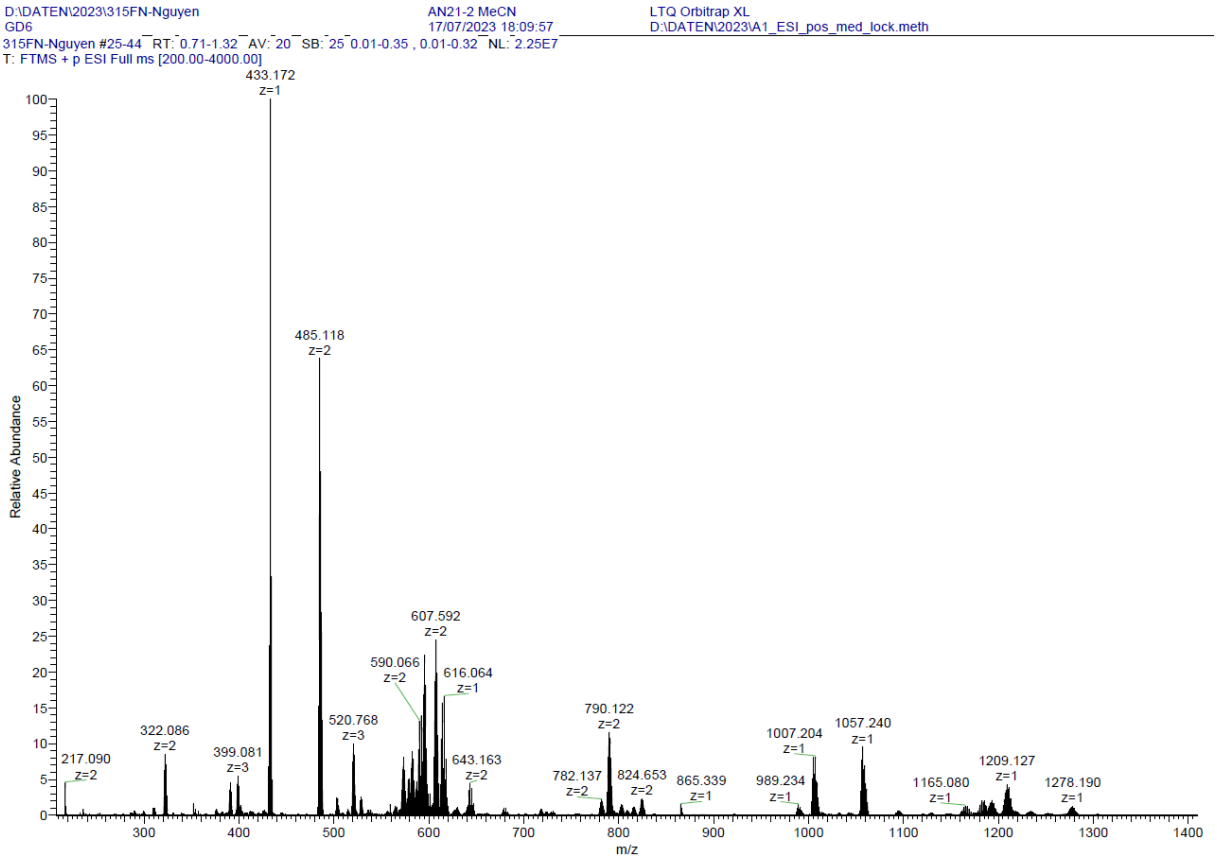

Figure 370: ESI(+)-mass spectrum of complexation of **76** with $Pd(MeCN)_4(BF_4)_2$.

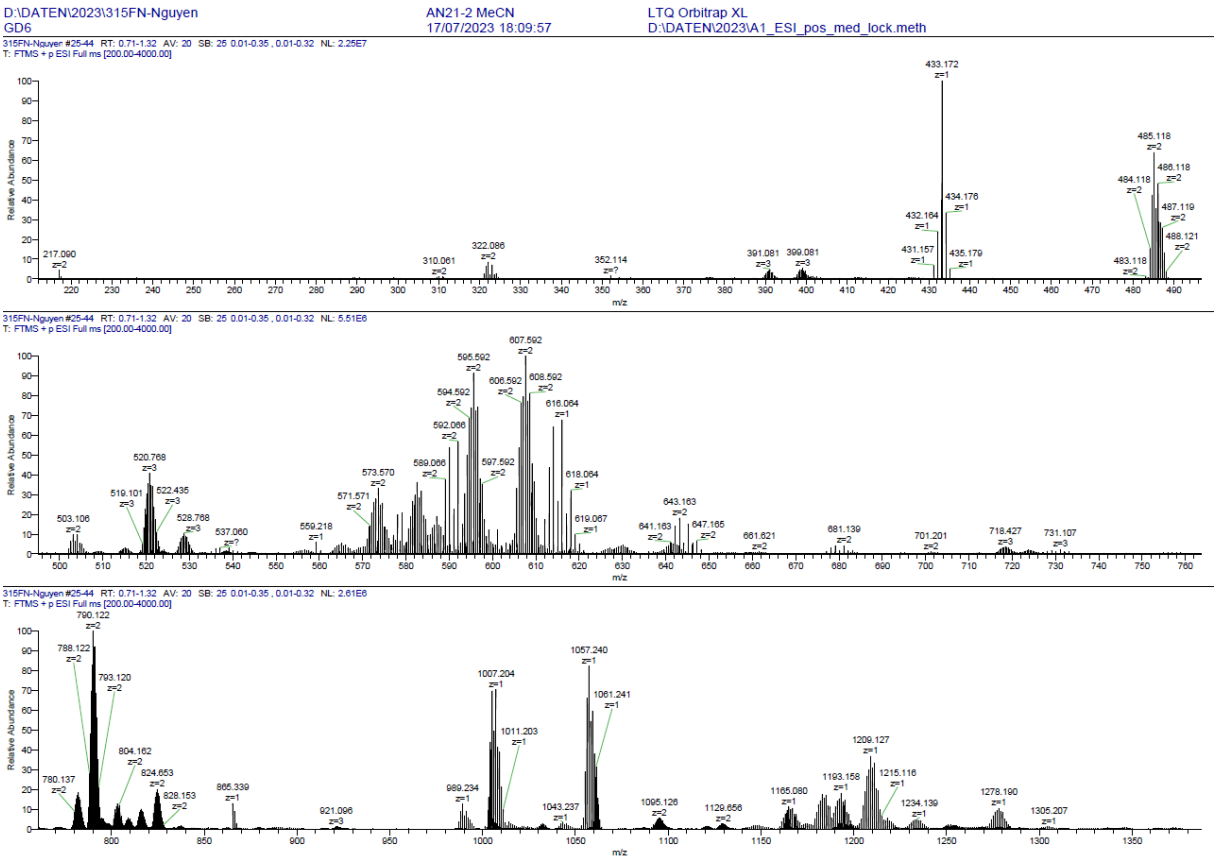

Figure 371: Excerpts of ESI(+)-mass spectrum of complexation of **76** with $Pd(MeCN)_4(BF_4)_2$.

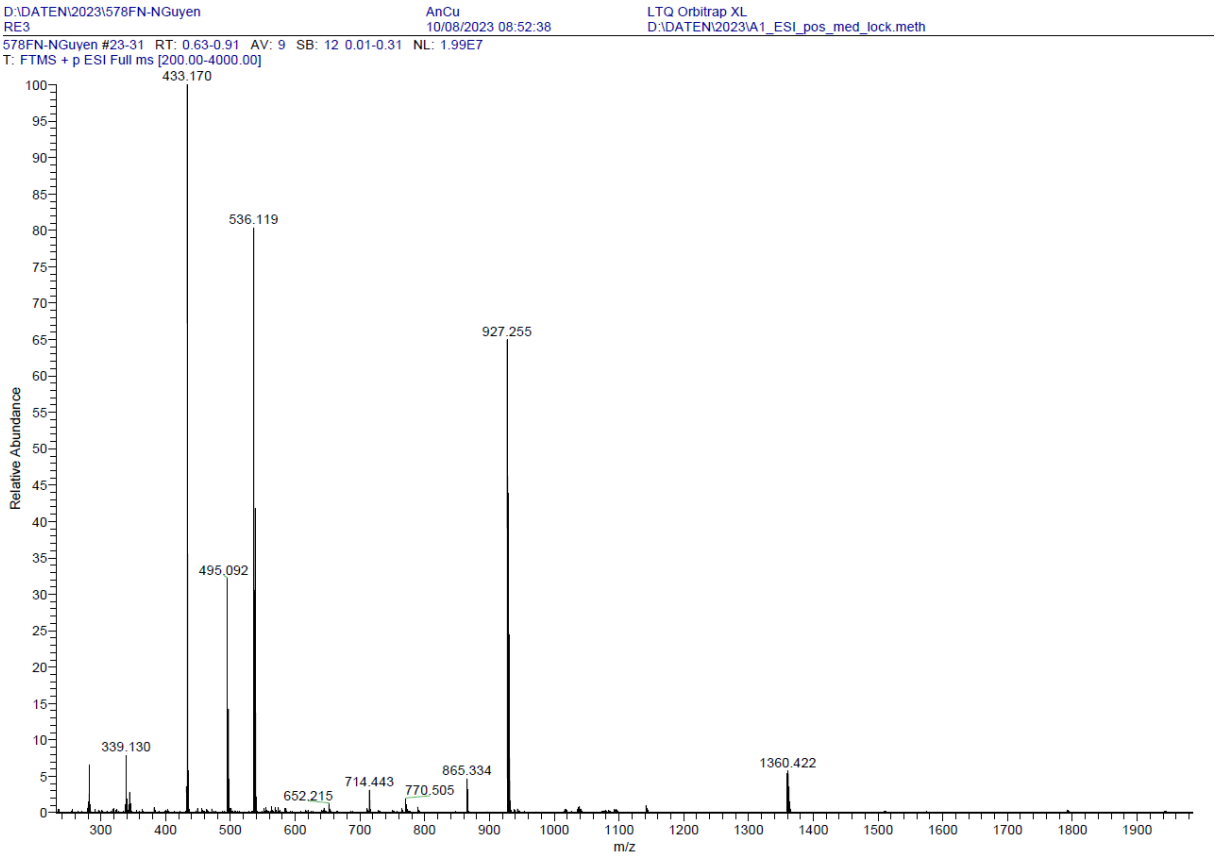

Figure 372: ESI(+)-mass spectrum of complexation of **76** with $Cu(MeCN)_4(BF_4)$.

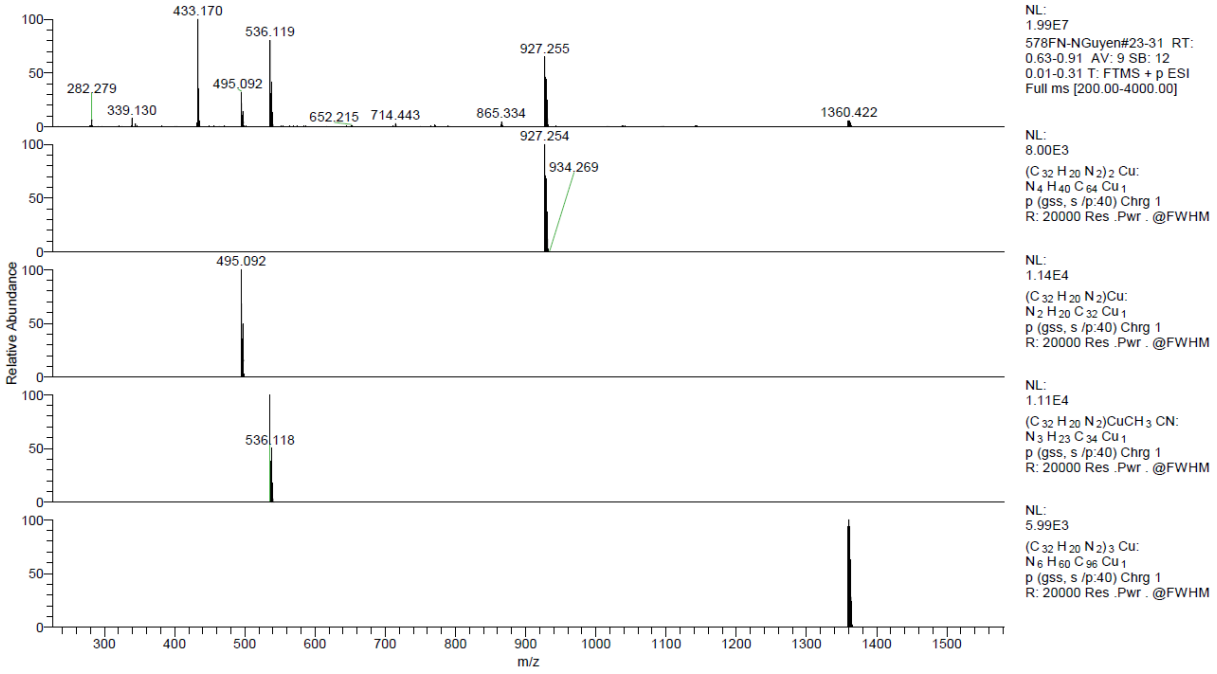

Figure 373: Experimental exact mass (top) and calculated exact masses (bottom four) of complexation of **76** with $Cu(MeCN)_4(BF_4)$.

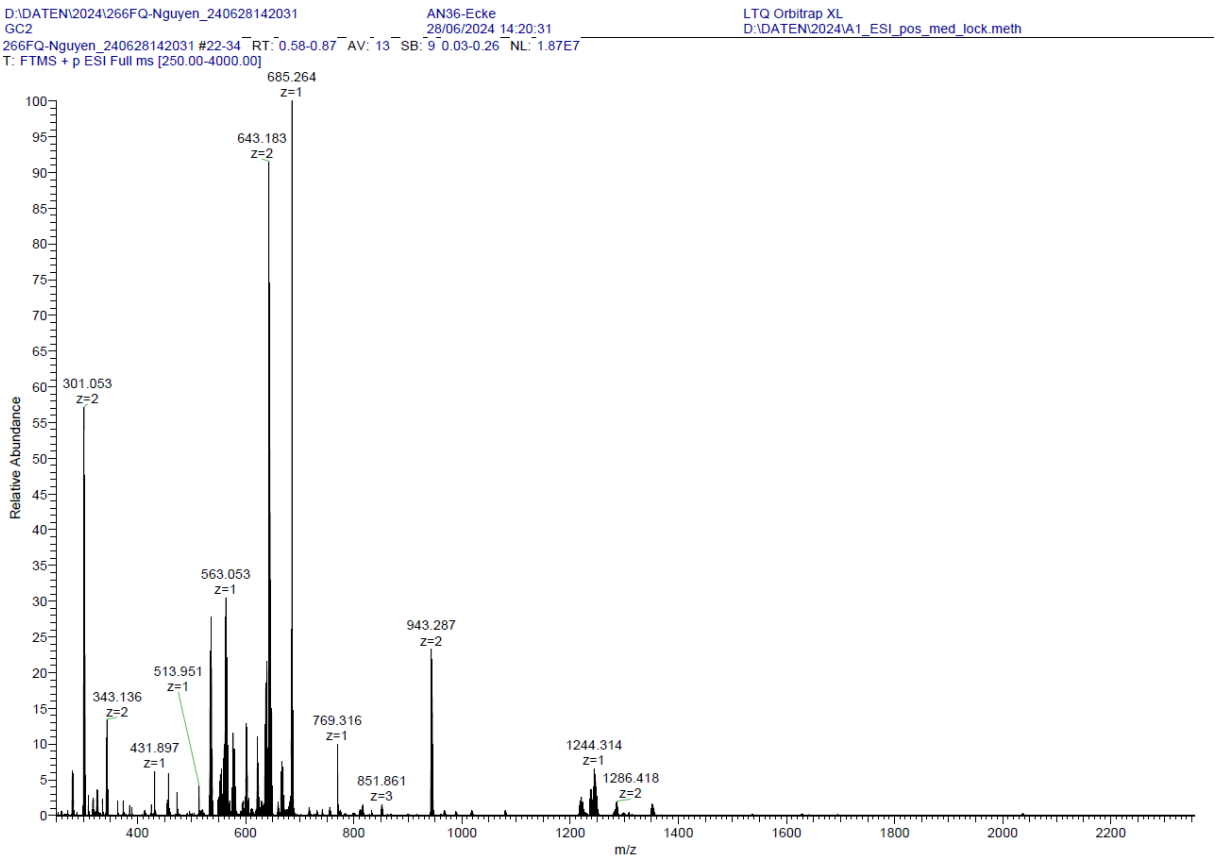

Figure 374: ESI(+)-mass spectrum of complexation of (*rac*)-**92** with Pd(dppp)(OTf)$_2$.

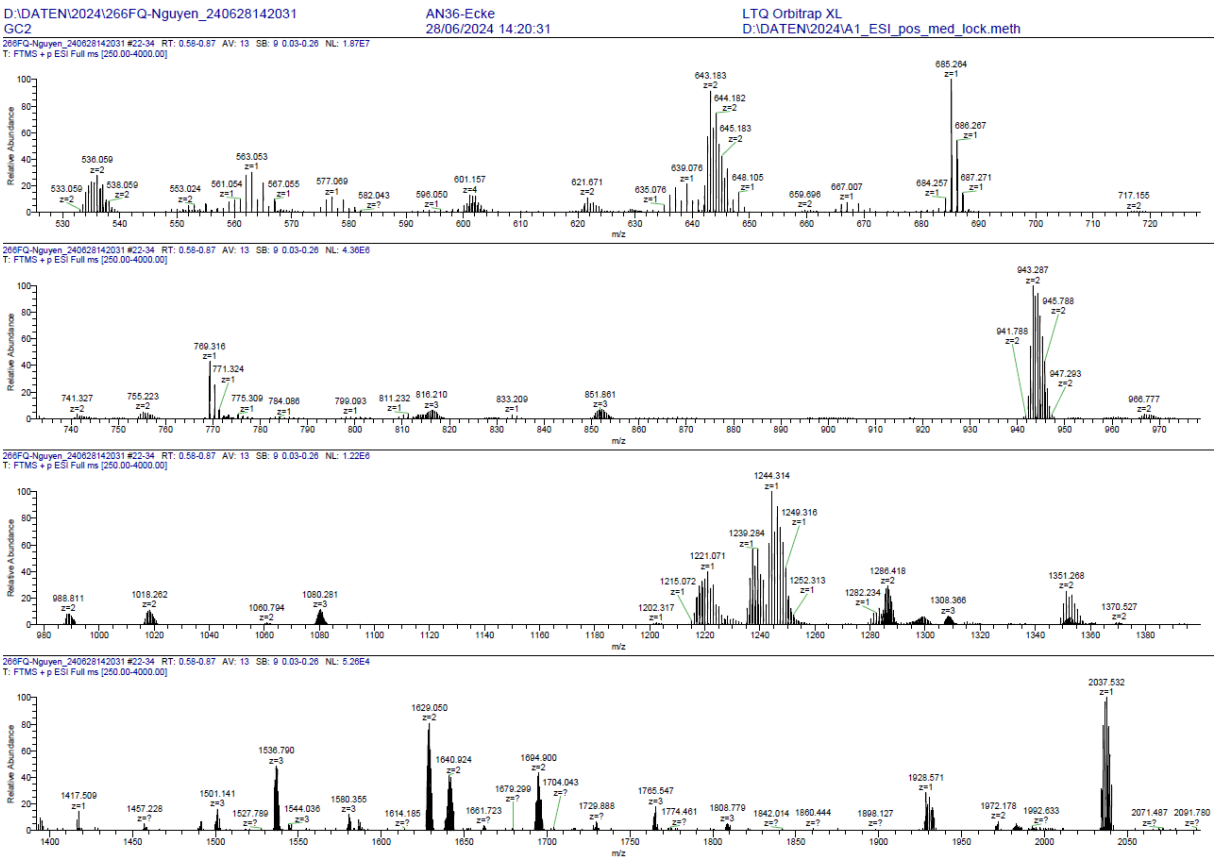

Figure 375: Excerpts of ESI(+)-mass spectrum of complexation of (*rac*)-**92** with Pd(dppp)(OTf)$_2$.

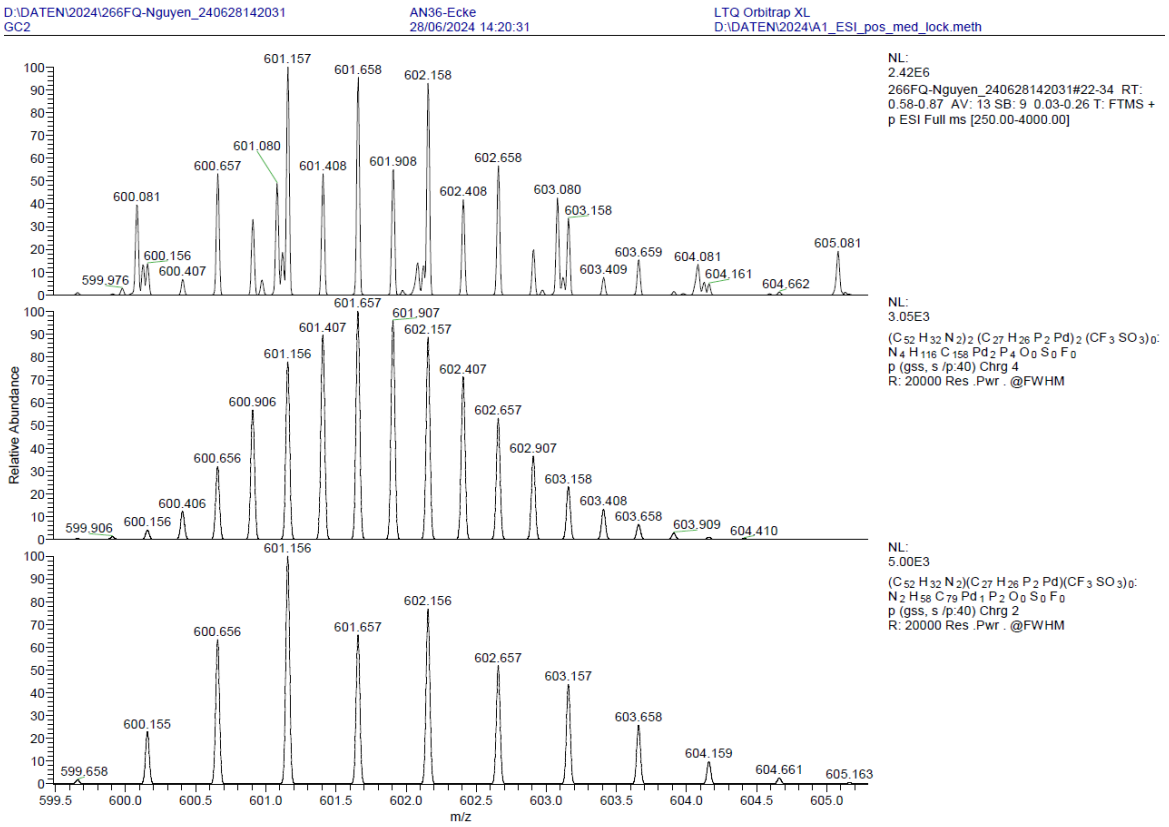

Figure 376: Experimental exact mass (top) and calculated exact masses (middle, bottom) of complexation of (*rac*)-**92** with Pd(dppp)(OTf)$_2$.

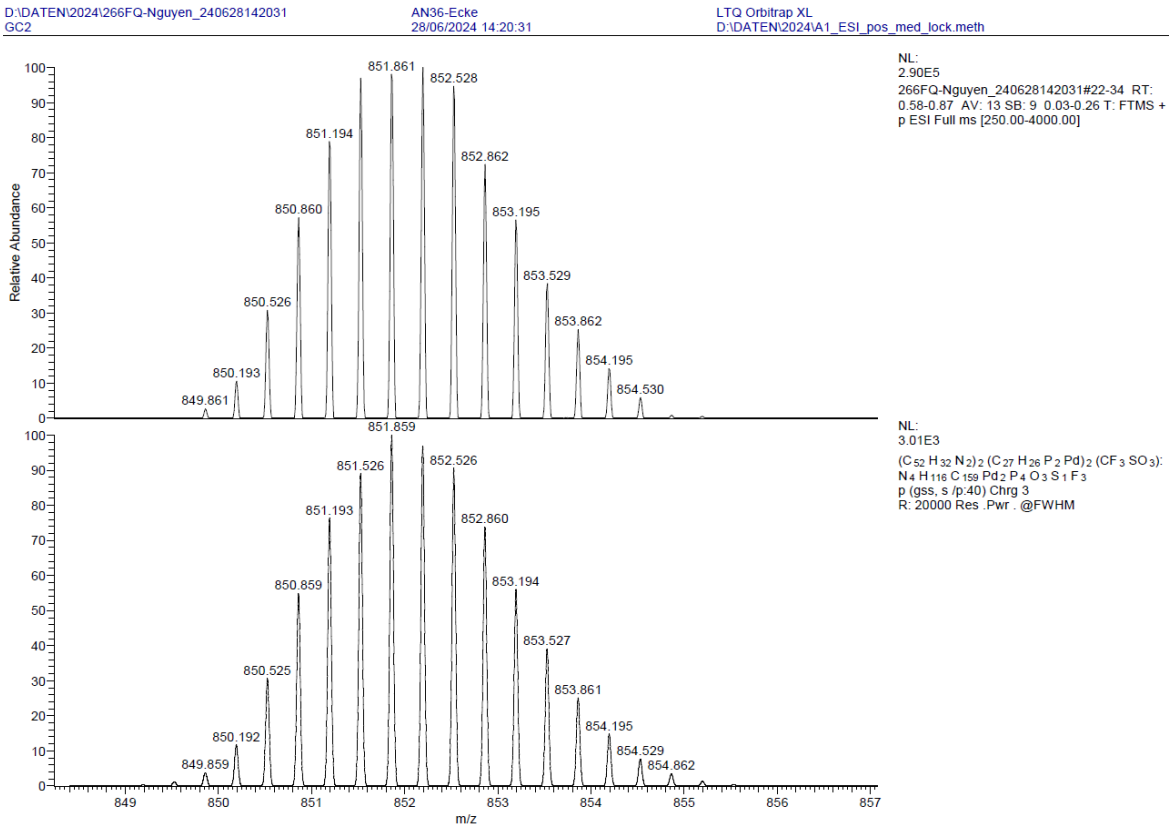

Figure 377: Experimental exact mass (top) and calculated exact mass (bottom) of complexation of (*rac*)-**92** with Pd(dppp)(OTf)$_2$.

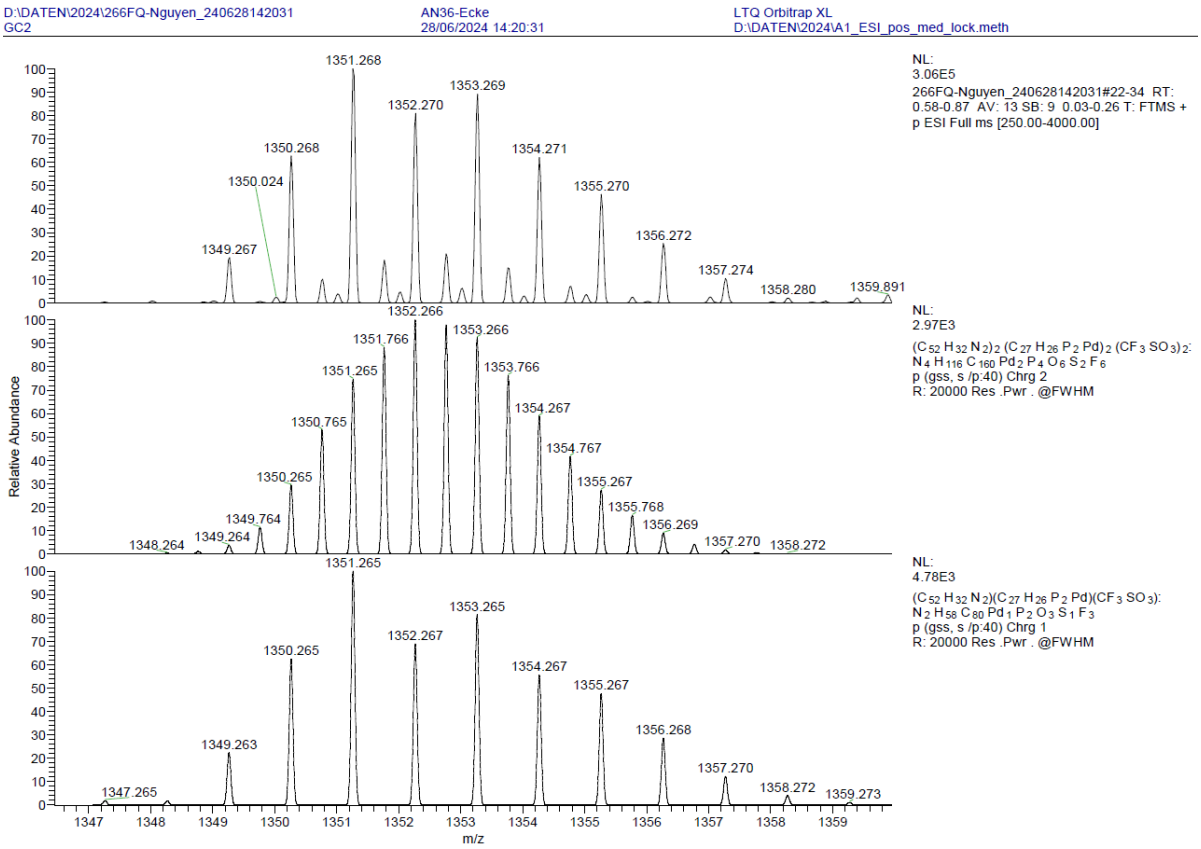

Figure 378: Experimental exact mass (top) and calculated exact masses (middle, bottom) of complexation of (*rac*)-**92** with Pd(dppp)(OTf)$_2$.

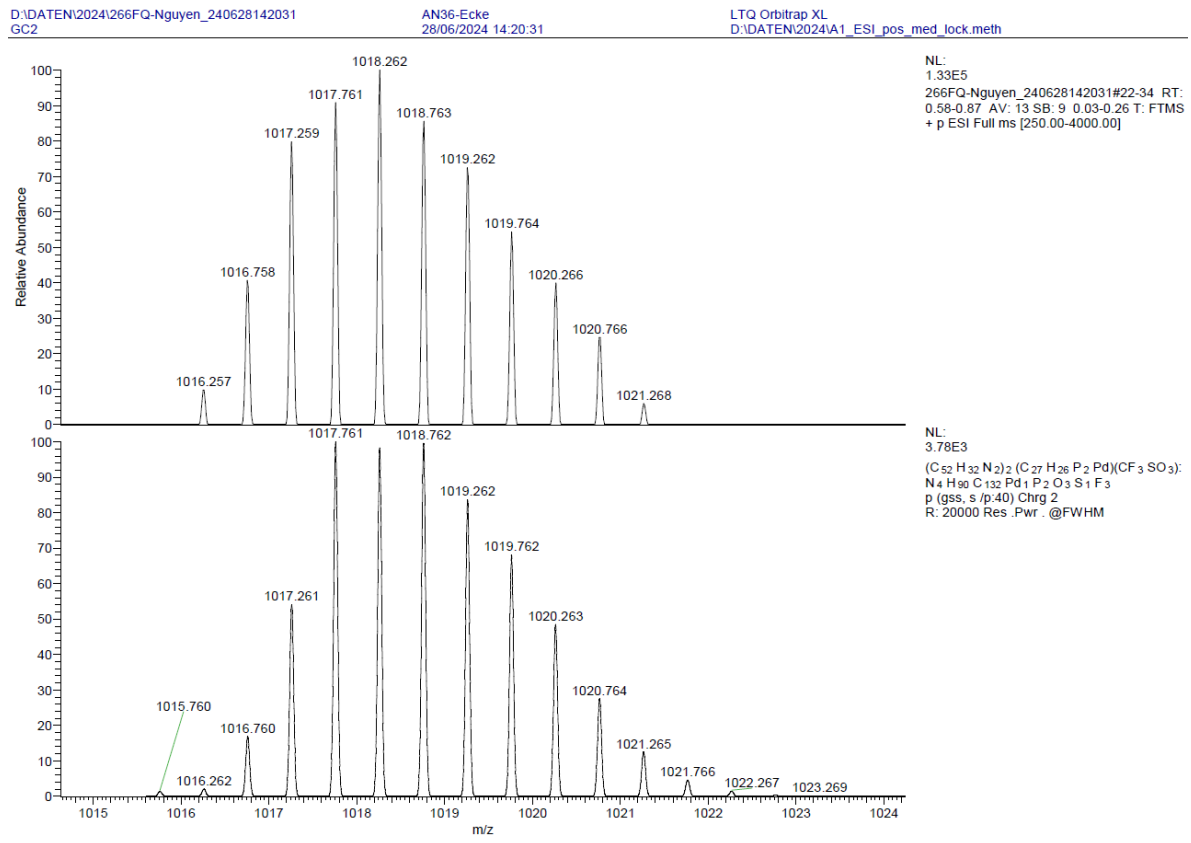

Figure 379: Experimental exact mass (top) and calculated exact mass (bottom) of complexation of (*rac*)-**92** with Pd(dppp)(OTf)$_2$.

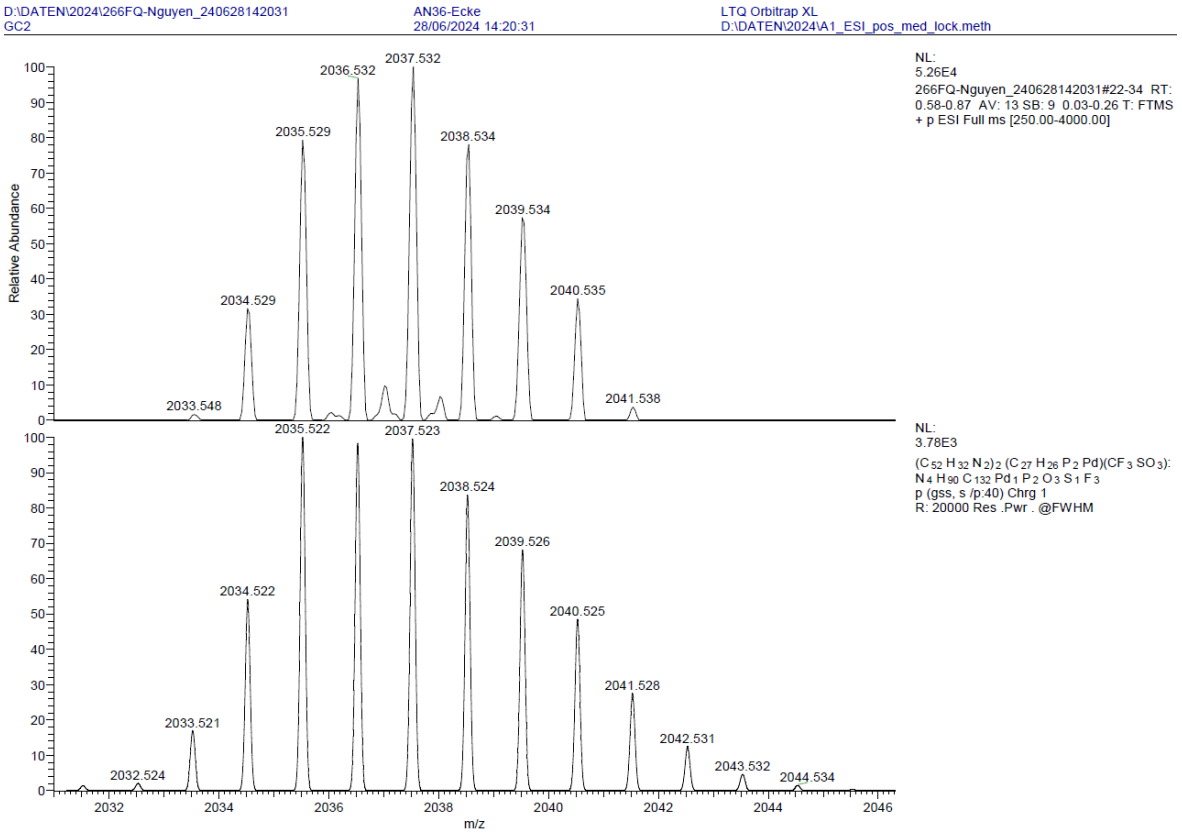

Figure 380: Experimental exact mass (top) and calculated exact mass (bottom) of complexation of (*rac*)-**92** with Pd(dppp)(OTf)$_2$.

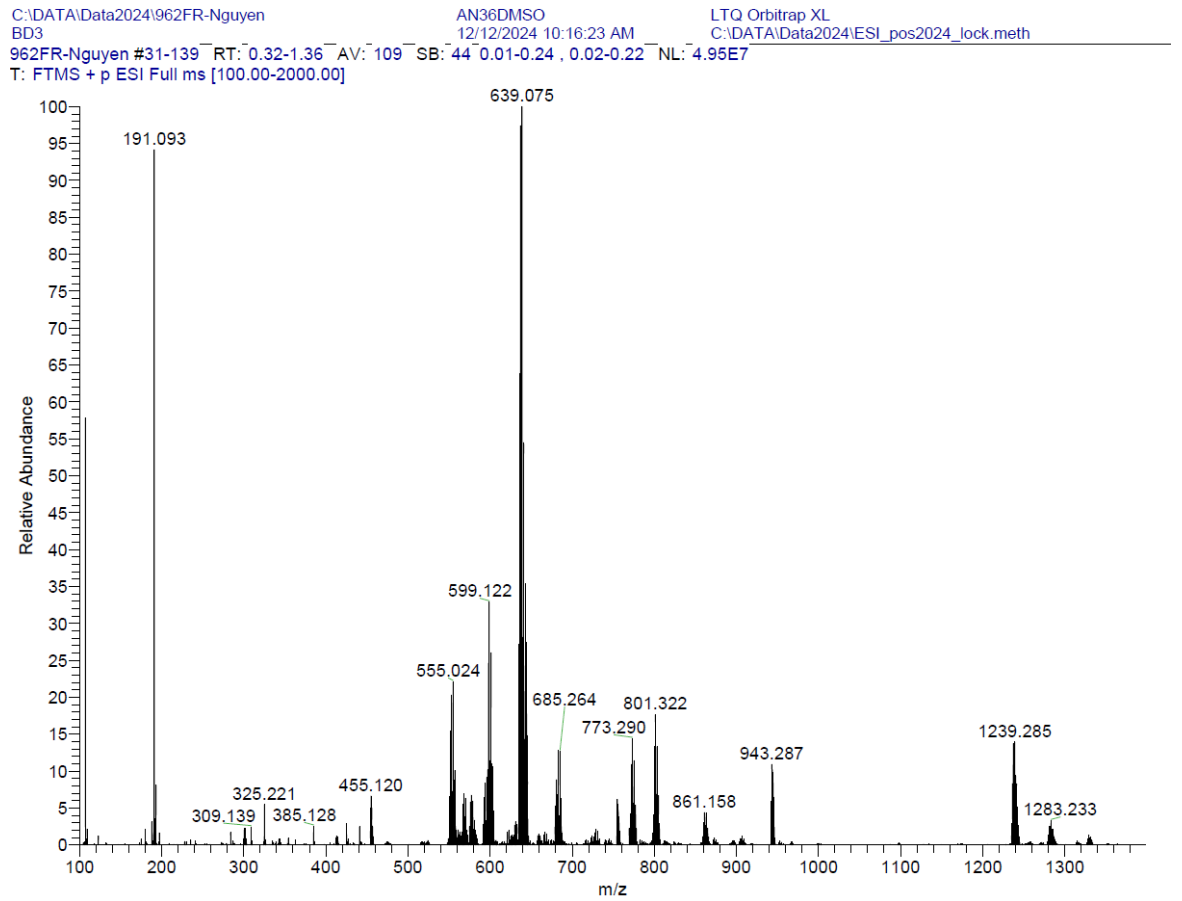

Figure 381: ESI(+)-mass spectrum of complexation of (*M*)-**92** with Pd(dppp)(OTf)$_2$.

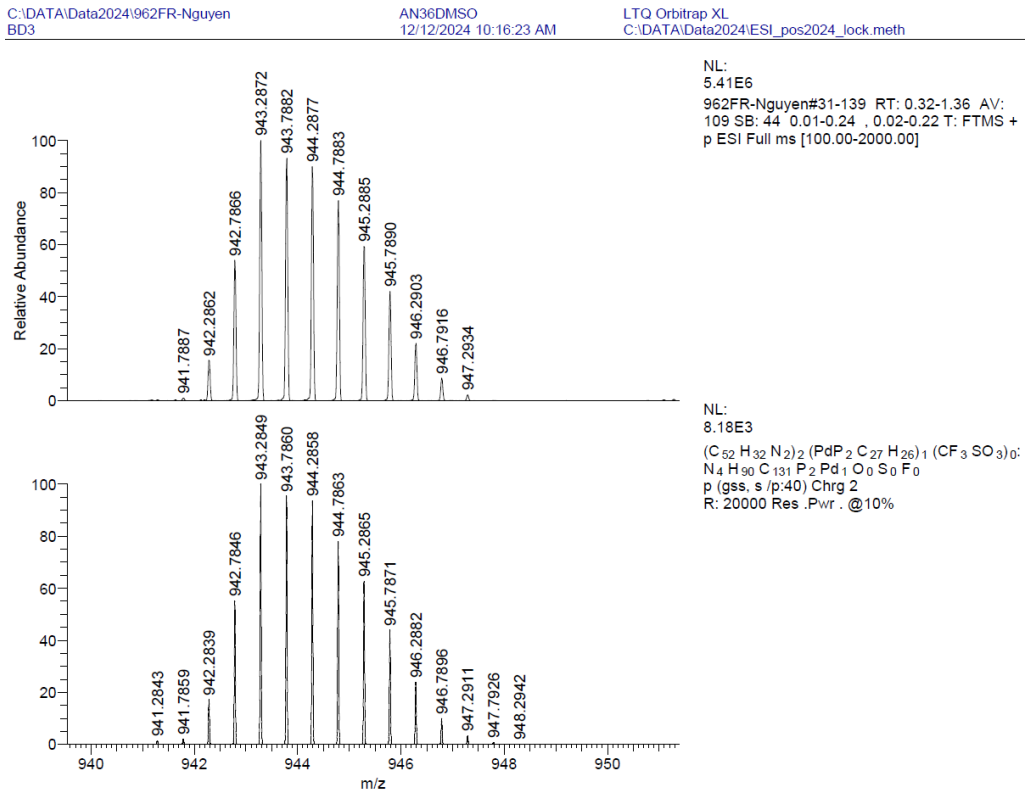

Figure 382: Experimental exact mass (top) and calculated exact mass (bottom) of complexation of (*M*)-**92** with Pd(dppp)(OTf)$_2$.

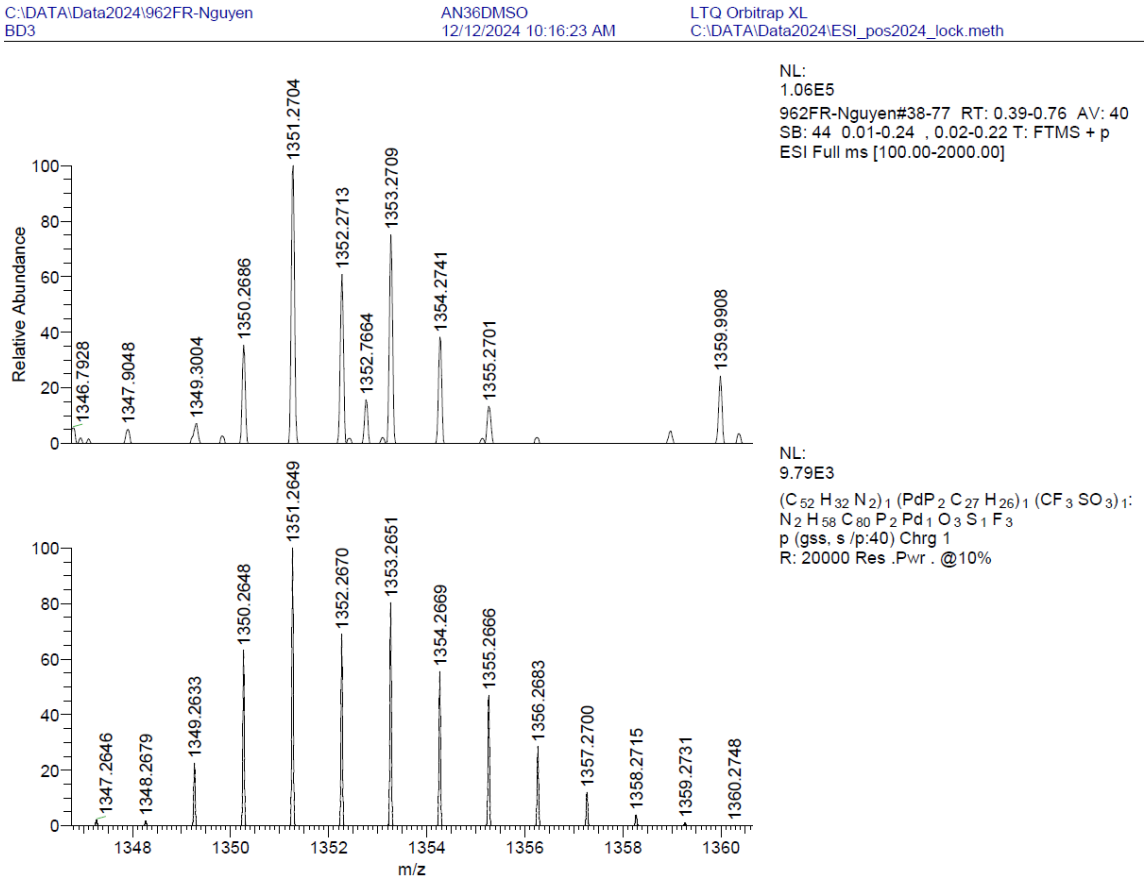

Figure 383: Experimental exact mass (top) and calculated exact mass (bottom) of complexation of (*M*)-**92** with Pd(dppp)(OTf)$_2$.

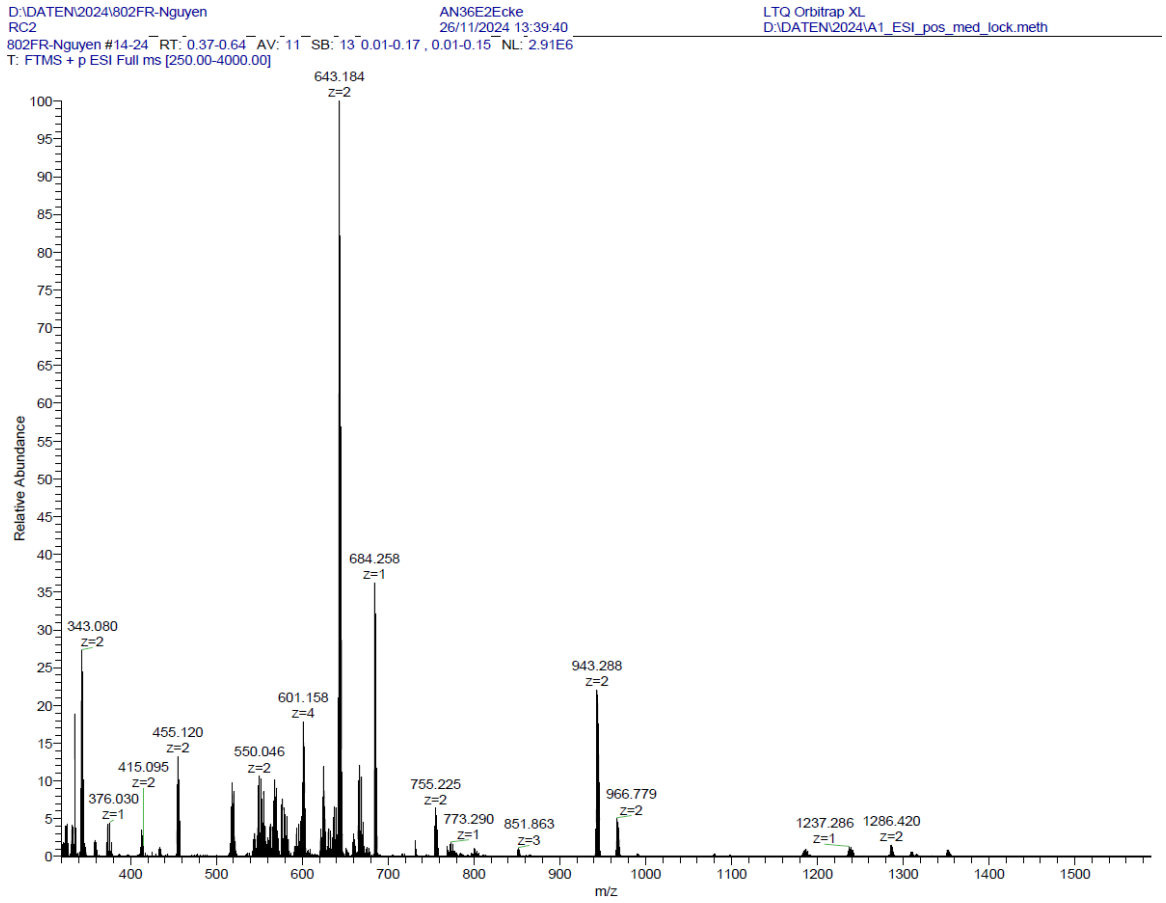

Figure 384: ESI(+)-mass spectrum of complexation of (*P*)-**92** with Pd(dppp)(OTf)$_2$.

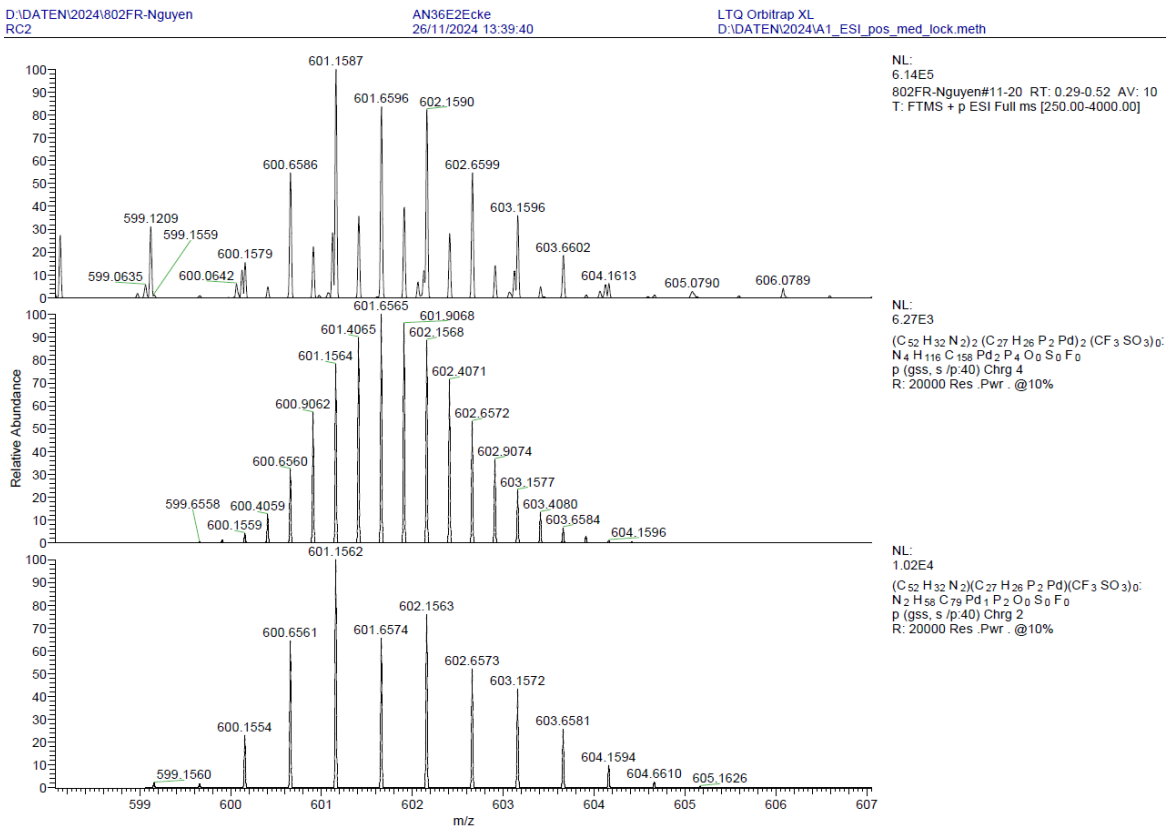

Figure 385: Experimental exact mass (top) and calculated exact masses (middle, bottom) of complexation of (*P*)-**92** with Pd(dppp)(OTf)$_2$.

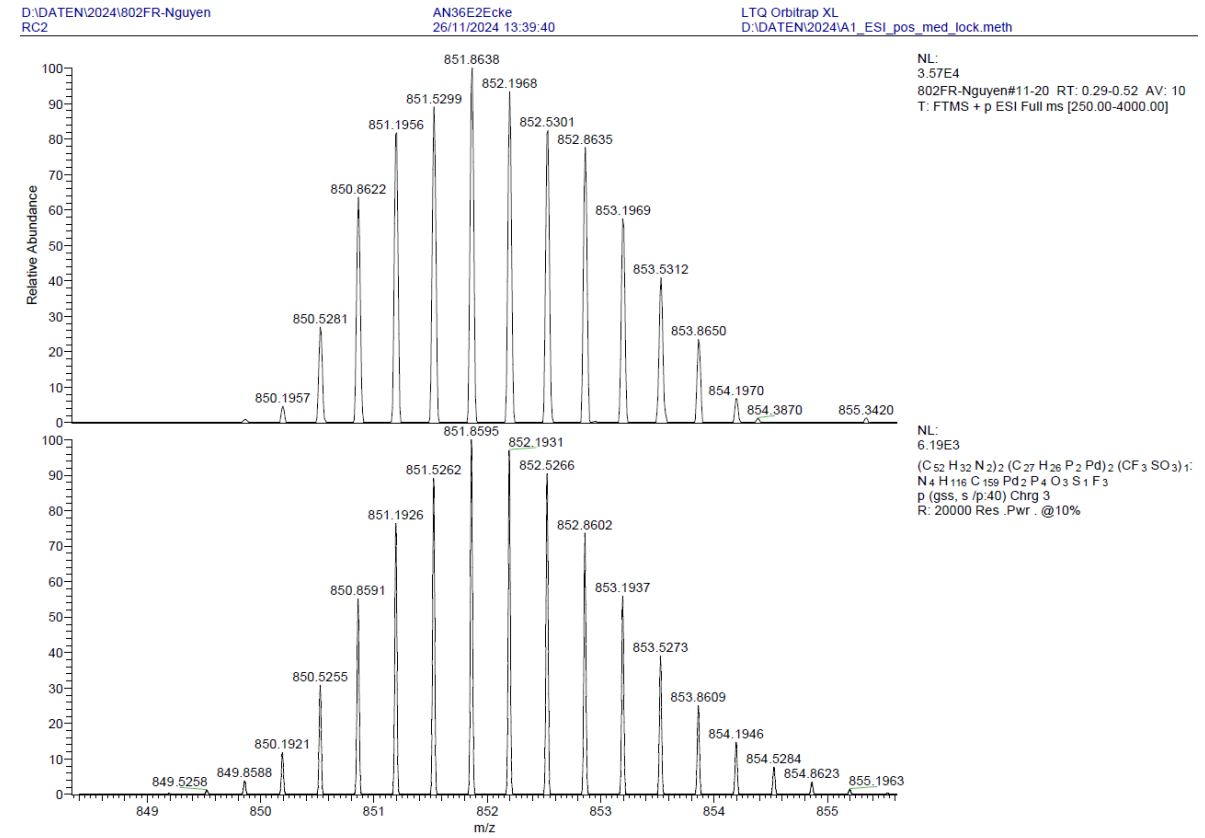

Figure 386: Experimental exact mass (top) and calculated exact mass (bottom) of complexation of (*P*)-**92** with Pd(dppp)(OTf)$_2$.

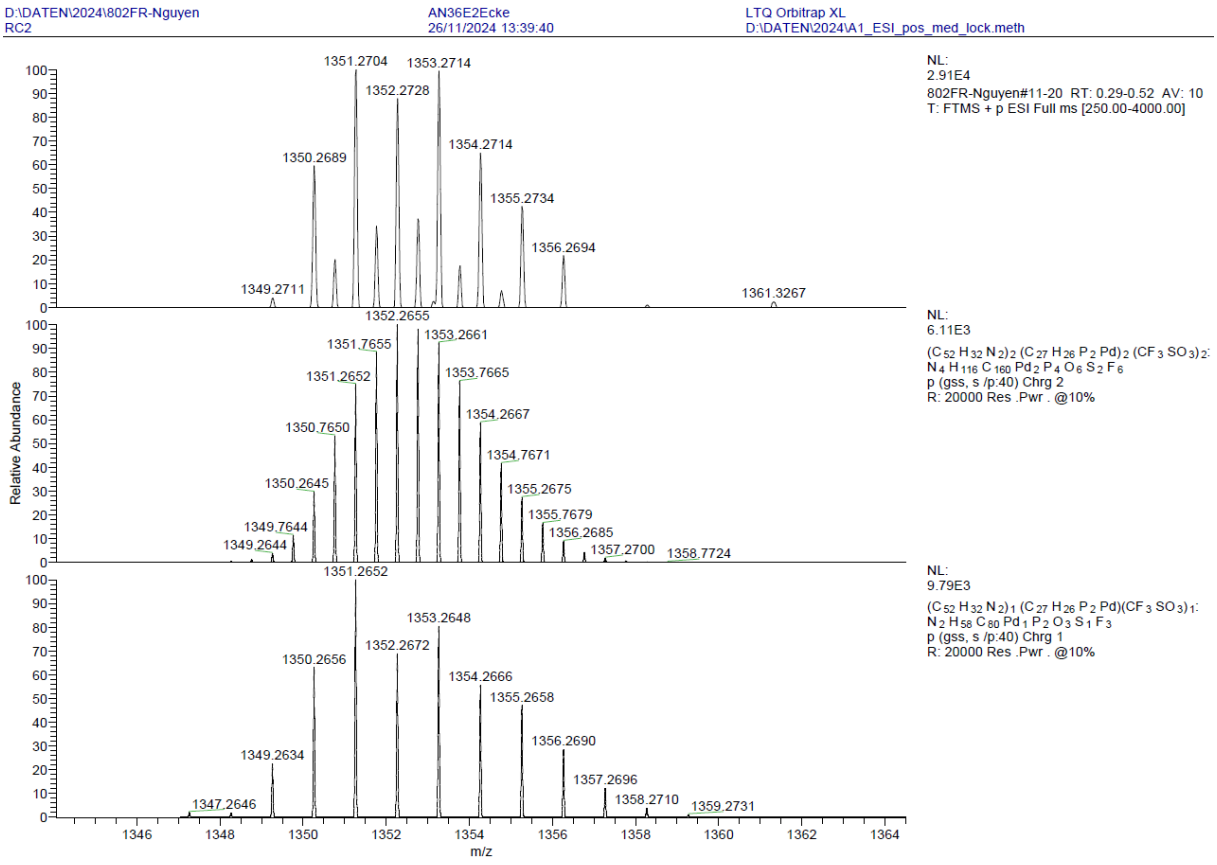

Figure 387: Experimental exact mass (top) and calculated exact masses (middle, bottom) of complexation of (*P*)-**92** with Pd(dppp)(OTf)$_2$.

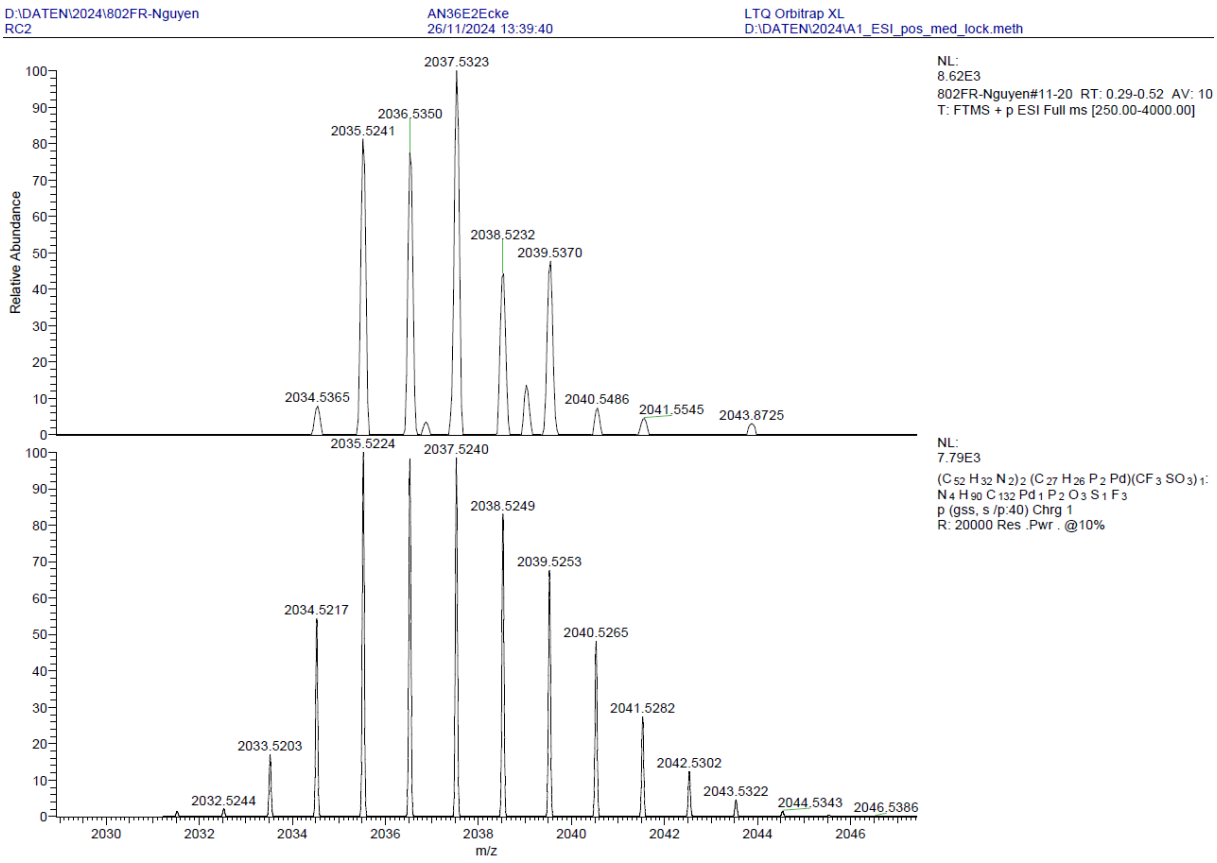

Figure 388: Experimental exact mass (top) and calculated exact mass (bottom) of complexation of (*P*)-**92** with Pd(dppp)(OTf)$_2$.

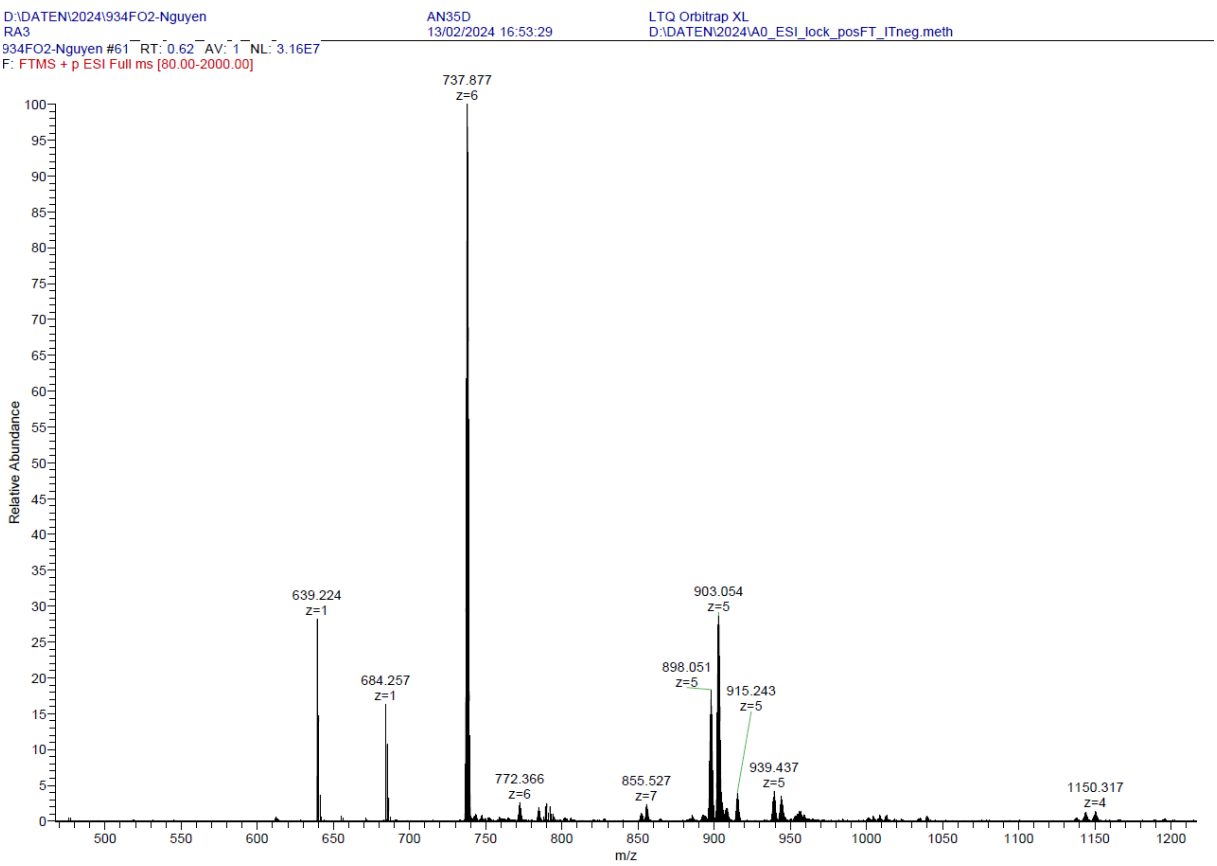

Figure 389: ESI(+)-mass spectrum of complexation of (*rac*)-**93** with Pd(MeCN)$_4$(BF$_4$)$_2$.

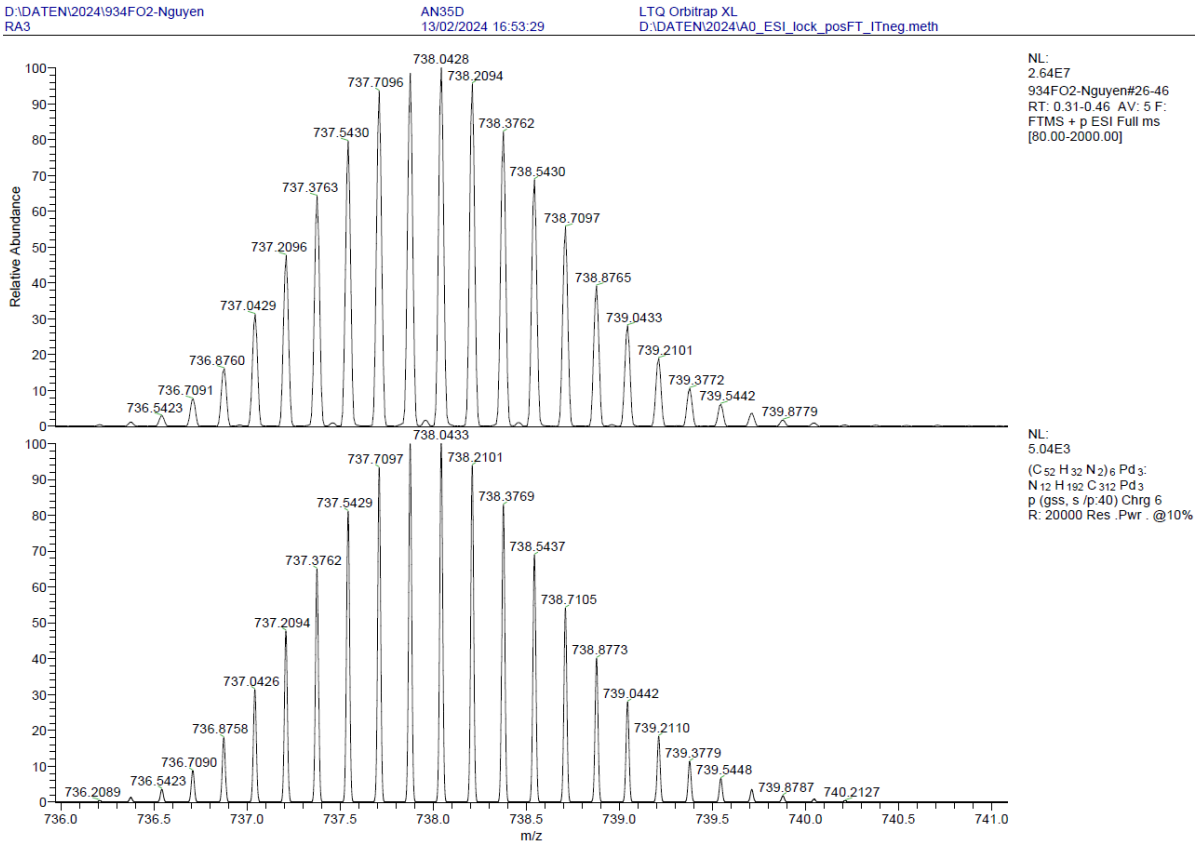

Figure 390: Experimental exact mass (top) and calculated exact mass (bottom) of complexation of (*rac*)-**93** with $Pd(MeCN)_4(BF_4)_2$.

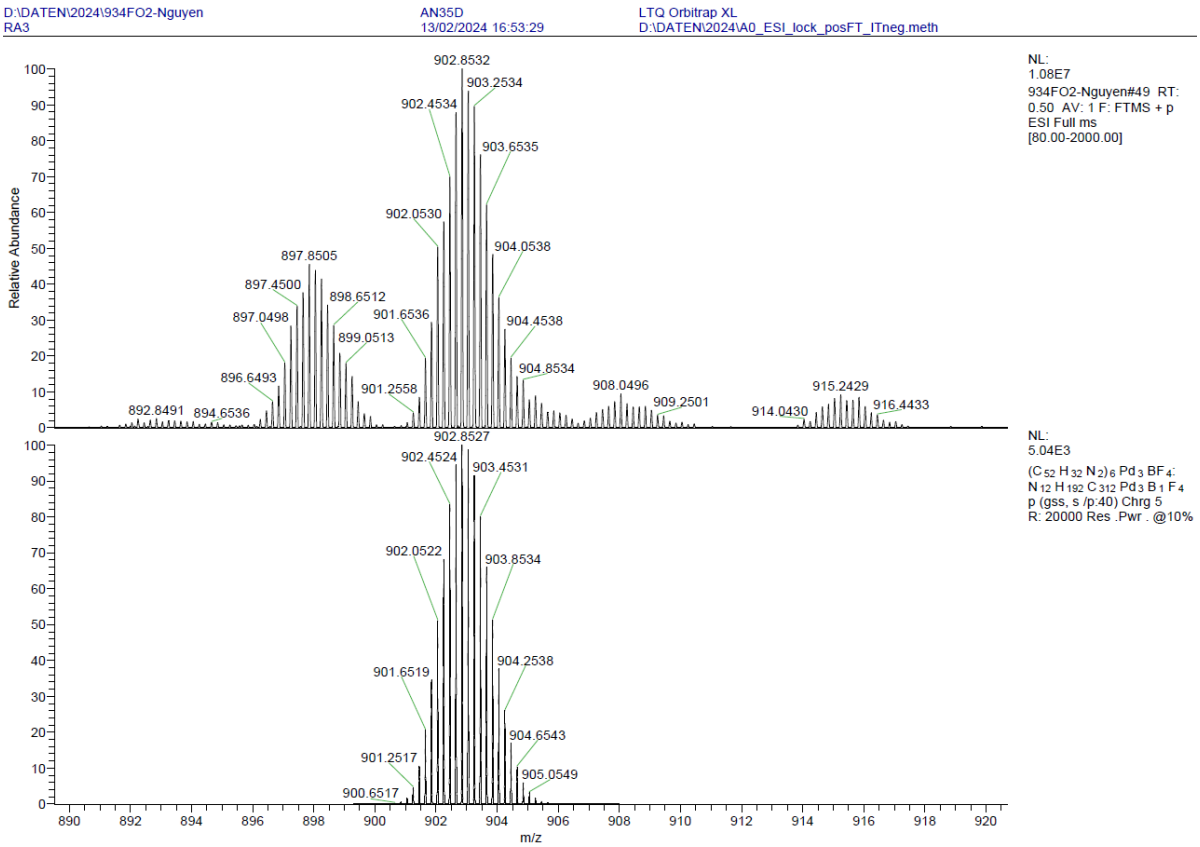

Figure 391: Experimental exact mass (top) and calculated exact mass (bottom) of complexation of (*rac*)-**93** with $Pd(MeCN)_4(BF_4)_2$.